QA: QA

MDL-MGR-GS-000003 REV 01

November 2004

Development of Earthquake Ground Motion Input for Preclosure Seismic Design and Postclosure Performance Assessment of a Geologic Repository at Yucca Mountain, NV

NOTICE OF OPEN CHANGE DOCUMENTS - THIS DOCUMENT IS IMPACTED BY THE LISTED CHANGE DOCUMENT AND CANNOT BE USED WITHOUT IT.

---

1) ACN-001, DATED 11/29/2005

Prepared for:
U.S. Department of Energy
Office of Civilian Radioactive Waste Management
Office of Repository Development
1551 Hillshire Drive
Las Vegas, Nevada 89134-6321

Prepared by:
Bechtel SAIC Company, LLC
1180 Town Center Drive
Las Vegas, Nevada 89144

Under Contract Number
DE-AC28-01RW12101

DISCLAIMER

This report was prepared as an account of work sponsored by an agency of the United States Government. Neither the United States Government nor any agency thereof, nor any of their employees, nor any of their contractors, subcontractors or their employees, makes any warranty, express or implied, or assumes any legal liability or responsibility for the accuracy, completeness, or any third party's use or the results of such use of any information, apparatus, product, or process disclosed, or represents that its use would not infringe privately owned rights. Reference herein to any specific commercial product, process, or service by trade name, trademark, manufacturer, or otherwise, does not necessarily constitute or imply its endorsement, recommendation, or favoring by the United States Government or any agency thereof or its contractors or subcontractors. The views and opinions of authors expressed herein do not necessarily state or reflect those of the United States Government or any agency thereof.

QA: QA

Development of Earthquake Ground Motion Input for Preclosure Seismic Design and Postclosure Performance Assessment of a Geologic Repository at Yucca Mountain, NV

MDL-MGR-GS-000003 REV 01

November 2004

OCRWM	MODEL SIGNATURE PAGE/CHANGE HISTORY	Page iii 1. Total Pages: ~~1007~~ 742

1022 11-9-04

2. Type of Mathematical Model

☒ Process Model ☐ Abstraction Model ☐ System Model

Describe Intended Use of Model

The ground motion site-response model represents the effect on seismic response spectra, peak ground motion, and strains and curvatures of the upper about 300 m of rock and soil at Yucca Mountain. Ground motion input to the model is based on the results of a probabilistic seismic hazard analysis for Yucca Mountain. The model determines the site-response in a manner that maintains the hazard level of the input ground motion. For preclosure analyses, output of the model is used to determine seismic design response spectra, strain-compatible soil properties, and corresponding time histories for surface facility sites. Seismic design response spectra and time histories are also determined for the waste emplacement level. In addition, model output is used to determine the variation of strains, curvatures, and peak ground motions with depth. For postclosure analyses, output of the model is used to determine time histories and peak ground velocities at the waste emplacement level.

3. Title

Development of Earthquake Ground Motion Input for Preclosure Seismic Design and Postclosure Performance Assessment of a Geologic Repository at Yucca Mountain, NV

4. DI (including Rev. No., if applicable):

MDL-MGR-GS-000003 REV 01

5. Total Appendices	6. No. of Pages in Each Appendix
2	I - 4, II - 300 11-9-04 ~~1 (electronic) - 1 CD; 2 (electronic) - 1 CD~~

	Printed Name	Signature	Date
7. Originator	Ivan Wong	Ivan D. Wong	5 Nov 2004
8. Independent Technical Reviewer	Joseph Litehiser	Joseph Litehiser JL	11/05/04
9. Checker	Robert Youngs	Robert R. Youngs	11/05/04
10. QER	Kenneth Gilkerson	Kenneth McGill for	11/05/04
11. Responsible Manager/Lead	Richard Pernisi	Richard Pernisi	11/5/04
12. Responsible Manager	Jerry King	Jerry King	11/5/04

13. Remarks

The following persons contributed to the preparation of Rev 01 of this report:

Ivan Wong, Patricia Thomas, Walter Silva, Richard Quittmeyer, Gabriel Toro, Mark Dober, Chaiwat Law Pattanapong, Shobhna Upadhyaya, Segaran Logeswaran, Susan Olig, and Fabia Terra.

Rev 01 of the report incorporates changes documented in Errata 1, which addressed Condition Report 1960. Rev 01 also addresses errors documented in Condition Reports 1685, 2674 and 2823, and Software Problem Report SDN013620030407. In all cases, the impact of the error is negligible and results are used "as is." Condition Report 2084 is also addressed in Rev 01.

Limitations on Use of Model: Depending on the model inputs used, the site-response model can produce ground motion results that the rocks at Yucca Mountain probably cannot sustain. For input consisting of high levels of ground motion (i.e. ground motions with very low annual probabilities of exceedance), the model produces shear strains that exceed the strength of the rock and would cause it to fail. While these ground motions can be used to assess the sensitivity of the response of waste emplacement drifts and engineered barrier system components to such high levels of ground motion, ultimately results should be evaluated for ground motions that are credible for Yucca Mountain. To support the identification of credible ground motions, analysis report ANL-MGR-GS-000004 (Peak Ground Velocities for Seismic Events at Yucca Mountain, Nevada) addresses the issue of bounding horizontal peak ground velocities at Yucca Mountain with a low annual probability of exceedance.

The site-response model is also limited in that it does not explicitly represent two- or three-dimensional ground motion effects. Such effects are implicitly included because the ground motion attenuation relations used in ground motion interpretations for the probabilistic seismic hazard analysis are based on strong ground motion recordings that include two- and three-dimensional effects.

Change History	
14. Revision No.	15. Description of Change
00	Initial issue. For vibratory ground motion, supersedes B00000000-01727-5700-00018 ("Seismic Design Basis Inputs for a High-Level Waste Repository at Yucca Mountain, Nevada").
00 Errata 1	Errata to address Condition Report 1960 concerning calculation of seismic ray angles of incidence.
01	Revision to incorporate additional results. Namely, ground motion inputs with annual probabilities of exceedance of 10^{-3}, 10^{-4}, and 10^{-5}. In addition, revised results for the surface facilities area (Points D & E) with an annual probability of exceedance of 5×10^{-4} are provided. These revised results reflect the elimination of an assumption that engineered fill will be placed at the surface. This revision also presents strain-compatible soil properties for the surface facilities area and the variation of strains, curvatures, and peak ground motions as a function of depth for Yucca Mountain for annual probabilities of exceedance of 10^{-3}, 5×10^{-4}, 10^{-4}. Results for a site to the north of the Exile Hill splay fault (Point F) are provided for comparison to results at Points D & E, which are the seismic design inputs for preclosure analyses. Model validation is enhanced by inclusion of validation results for a site at which large strains were achieved. The report is also revised to follow the current versions of applicable procedures.

ACKNOWLEDGMENTS

The following individuals, listed alphabetically, provided significant technical contribution to the development of this document: Rajendram Arulnathan, Mark Dober, Chaiwat Law Pattanapong, Richard Lee, Segaran Logeswaran, Susan Olig, Richard Quittmeyer, Walter Silva, Patricia Thomas, Gabriel Toro, Shobhna Upadhyaya, Ivan Wong, and Robert Youngs. The co-Principal Investigators were Ivan Wong, Patricia Thomas, and Walter Silva. Mark Dober, Chaiwat Law Pattanapong, Segaran Logeswaran, and Shobhna Upadhyaya performed the ground motion calculations. Richard Lee and Rajendram Arulnathan assisted in the model validation. Gabriel Toro developed the site-specific probabilistic representation of the seismic velocity profiles. Susan Olig managed the software quality assurance aspects for the study. Richard Quittmeyer, and Carl Stepp assisted in the writing of the AMR.

EXECUTIVE SUMMARY

This report describes a site-response model and its implementation for developing earthquake ground motion input for preclosure seismic design and postclosure assessment of the proposed geologic repository at Yucca Mountain, Nevada. The model implements a random-vibration theory (RVT), one-dimensional (1D) equivalent-linear approach to calculate site response effects on ground motions. The model provides results in terms of spectral acceleration including peak ground acceleration, peak ground velocity, and dynamically-induced strains as a function of depth. In addition to documenting and validating this model for use in the Yucca Mountain Project, this report also describes the development of model inputs, implementation of the model, its results, and the development of earthquake time history inputs based on the model results.

The purpose of the site-response ground motion model is to incorporate the effects on earthquake ground motions of (1) the approximately 300 m of rock above the emplacement levels beneath Yucca Mountain and (2) soil and rock beneath the site of the Surface Facilities Area. A previously performed probabilistic seismic hazard analysis (PSHA) (CRWMS M&O 1998a [DIRS 103731]) estimated ground motions at a reference rock outcrop for the Yucca Mountain site (Point A), but those results do not include these site response effects. Thus, the additional step of applying the site-response ground motion model is required to develop ground motion inputs that are used for preclosure and postclosure purposes.

The RVT-based equivalent-linear site response model involves a computational method (i.e., equivalent-linear) that has been widely employed to evaluate 1D site response using vertically propagating plane shear (S)-waves. Departures of soil response from a linear constitutive relation are treated in an approximate manner through the use of the equivalent-linear approach. Idriss and Seed (1968 [DIRS 163520]) introduced this approach, in its present form. Basically, the approach approximates a second-order nonlinear equation, over a limited range of its variables, by a linear equation. Formally this is done in such a way that the average of the difference between the two systems is minimized. This is done in an ad-hoc manner for ground response modeling by defining an effective strain that is taken to exist for the duration of the excitation. Shear modulus reduction and hysteretic damping curves are then used to define new parameters for each layer based on the effective strain computations. The linear response calculation is repeated, new effective strains evaluated, and iterations performed until the changes in parameters are below an established tolerance level.

The RASCALS code used in this study is an implementation of the equivalent-linear formulation. The RASCALS code is an RVT-based equivalent-linear approach, which propagates an outcrop (control motion) power spectral density through a 1D soil column. RVT is used to predict peak time domain values of shear strain based upon the shear-strain power spectrum. In this approach, the control motion power spectrum is propagated through the 1D rock/soil profile using plane-wave propagators. Both P-SV (vertically polarized S-wave) and SH (horizontally polarized S-wave) waves are incorporated into the analysis and have specified angles of incidence.

Three methods were used to validate the RVT equivalent-linear site response model for use in these analyses:

1. Corroboration of model results with data acquired from the laboratory, field experiments, analog studies, or other relevant observations, not previously used to develop or calibrate the model.

2. Corroboration of results with alternative mathematical models.

3. Technical review by individuals independent of the development, checking, and interdisciplinary review of the model documentation.

Four approaches to validate the RVT-based equivalent-linear site response model or its components based on the above Methods (1) and (2), are described in this report:

1. A comparison of response spectra computed using time domain and RVT approaches. This validation is only of the RVT component of the site response model.

2. Comparison of the predictions of recorded ground motions up to peak shear strains of 1.0% using the RVT-based equivalent-linear and three established nonlinear approaches.

3. Validation of use of the site response model in a linear mode to predict vertical ground motions.

4. A comprehensive comparison of predictions involving the site response model with recorded earthquake data from 16 earthquakes recorded at more than 500 sites.

Three reviewers selected by the Chief Science Office carried out Method (3). Their review is also summarized in this report. An evaluation of the site-specific applicability of the site response model to Yucca Mountain is also presented in this report.

Geological/geotechnical inputs to the site-response ground motion model consist of small-strain seismic velocities, densities, nonlinear dynamic material properties, and the angles of incidence of the control motions. For the Repository Block, two base case shear-wave and compressional-wave velocity profiles are used to represent uncertainty in the mean profile. For the Surface Facilities Area, where uncertainty in the mean profile is less, a single base case profile (for both shear-wave and compressional-wave velocity) is used. (In this study, the Surface Facilities Area is the area southwest of the Exile Hill splay fault.) The base case profiles are used, along with information on the statistical correlation of layer thicknesses and layer velocities, to develop a suite of random velocity profiles that are used as model input. Similarly for the nonlinear dynamic properties of site materials, multiple base case curves of normalized shear modulus reduction and damping, as a function of cyclic shear strain, are developed to represent uncertainty in the mean values of these properties. Two sets of curves are developed each for the tuff and alluvium at the site. For input to the site response model, the curves for all materials are randomized to represent random variability in properties within and across the site. The velocity profiles and dynamic material property curves were developed based upon a geotechnical, geological, and geophysical program performed in 2000 to 2001.

The starting point for the site response modeling is the output of the PSHA. For a given annual frequency of ground motion exceedance, the seismic hazard results are used to derive an acceleration response spectrum with a uniform probability of being exceeded, the uniform hazard spectrum (UHS). The UHS is the ground motion used as input (the control motion) to the site-response model. Results for peak ground velocity are also determined.

The approach used herein in developing site-specific ground motions follows one (called 2B) recommended in NUREG/CR-6728 (McGuire et al. 2001 [DIRS 157510], Section 6.1). The PSHA results for a given annual frequency of exceedance are deaggregated to identify controlling earthquakes. Two controlling earthquakes are determined from the deaggregated hazard at structural frequencies of 1 to 2 Hz and at 5 to 10 Hz. Response spectra for the controlling earthquakes are scaled to match the UHS at 1 to 2 Hz and 5 to 10 Hz and these form the "reference earthquake" response spectra. The reference earthquake response spectra form the basis for development of the site-specific ground motions (Regulatory Guide 1.165, 1997 [DIRS 119139], Regulatory Position 4). Non-linear site-response may be sensitive to earthquake magnitude (spectral composition of the control motion). Because this sensitivity may not be sufficiently captured by the range of magnitudes for the reference earthquakes, three "deaggregation" earthquakes are defined to account for the range of magnitudes contributing to the hazard in the 1 to 2 Hz and 5 to 10 Hz structural frequency ranges. These earthquakes nominally represent the 5^{th}, mean, and 95^{th} fractile magnitudes and associated distances determined from the hazard deaggregation. These deaggregation earthquakes form the input, or control motion, for the site-response ground motion model. Thus, for both horizontal and vertical ground motion modeling, the methodology employs six control motion response spectra as inputs. A weighted average is taken of the model outputs for each set of deaggregation earthquakes with the results for the mean magnitude getting the highest weight.

Response spectral (5%-damped) and peak particle velocity transfer functions from the PSHA reference rock outcrop (Point A) to repository locations of interest are developed. For each combination of deaggregation earthquake, base case velocity profile, and base case dynamic material properties, multiple runs using the site response model are carried out using randomized parameter values to determine the effect of input parameter variation across the site. The model results are then appropriately combined to determine the final output (e.g., response spectra, peak ground velocities or accelerations, strain-compatible soil properties). For horizontal component motions, the transfer function is applied to the enveloped reference earthquake motions (response spectra and UHS or peak particle velocities) to determine the final motions. For vertical motions, the transfer function is applied to a spectrum derived from the horizontal spectrum using vertical-to-horizontal ratios, as a function of frequency, appropriate for the Yucca Mountain Site. Based on these outputs, further analysis is carried out to develop time histories.

Based on the UHS at Point A and the site response model, ground motion inputs for preclosure analyses are determined for the planned waste emplacement drifts (Point B; about 335 m depth). Preclosure inputs also are determined for the Surface Facilities Area (Point D/E). For this site, three conditions are modeled: 35 ft of alluvium covering rock and a 110-ft-thick layer of alluvium covering rock (Point D). In addition, a thin layer of alluvium (15 ft), which represents the area adjacent to Exile Hill is modeled (Point E). Ground motion inputs for postclosure analyses are determined only for the waste emplacement level.

BSC (2004b [DIRS 170564]) describes the preclosure seismic design methodology for a repository at Yucca Mountain. The report presents a risk-informed methodology for establishing design basis hazard levels for systems, structures, and components determined to be important to safety. Two design basis ground motion levels (DBGM-1 and DBGM-2) are used. DBGM-1 has a mean annual frequency of exceedance of $1x10^{-3}$, while DBGM-2 has a mean annual frequency of exceedance of $5x10^{-4}$. BSC (2004b [DIRS 170564], Section 3.3) also describes analyses to evaluate seismic margin. Beyond-design-basis ground motion analyses and high-confidence-of-low-probability-of-failure analyses will be carried out, as appropriate. For these analyses, beyond design basis ground motions with a mean annual frequency of exceedance of $1x10^{-4}$ are used. Thus, in this report, design ground motions (response spectra, time histories, strain-compatible soil properties, and strains, curvatures, and peak ground motion values as a function of depth) are presented for annual frequencies of exceedance of 10^{-3}, $5x10^{-4}$, and 10^{-4}.

For postclosure analyses, the focus is on model results for ground motion annual exceedance frequencies between 10^{-4} and 10^{-8}. These ground motions are larger than those used for preclosure design and address the regulatory requirement to consider events with a 10^{-4} chance of occurring in 10,000 years. In this report, suites of 17 sets of three-component time histories, either scaled to peak ground velocity, spectrally conditioned and scaled to peak ground velocity, or spectrally matched, are presented for mean annual exceedance frequencies of 10^{-5}, 10^{-6}, and 10^{-7} in support of the Total Systems Performance Assessment for the License Application. Table E-1 summarizes the products of site response modeling and associated analyses for preclosure seismic design and postclosure performance assessment.

Control motions used as input to the site response model are based on results of the PSHA. . In a topical report submitted to the NRC, the DOE described the approach for performing a PSHA for the Yucca Mountain Site (YMP 1997b [DIRS 100522]). The approach specifically captures variabilities in features, processes, models, and model parameters as required by 10 CFR 63.114(a)(b)(c) [DIRS 156605] and expresses the variabilities in the hazard results. The variabilities in the input parameters are modeled for hazard computation using unbounded distributions and are captured in the hazard results by integrating over all input distributions. The integrated variability in the inputs, which is expressed in the hazard results as a probability distribution, becomes increasingly large and increasingly asymmetric with increasingly low annual frequency of exceedance. As a consequence, ground motion values corresponding to very low mean annual exceedance frequencies are larger than can be considered to be physically reasonable or even possible. That is, they would imply dynamic strains that would exceed the strength of the rock. This outcome simply expresses the state of the scientific community's variability in the estimation of PSHA input parameters and, consequently, the probability of exceeding ground motion values at low annual exceedance frequencies. It carries no implication that ground motions corresponding to the mean probability of exceedance at such low annual frequencies should be considered physically attainable.

To address this issue, a separate analysis to estimate peak horizontal velocities with a very low annual frequency of being exceeded ($\sim 10^{-7}$) was performed that considers the maximum strain level sustainable by the rock at Yucca Mountain. The resulting probability distribution provides a bound on peak horizontal velocities at the repository waste emplacement level for use in the seismic consequence abstraction and the TSPA (BSC 2004c [DIRS 170137]).

Table E-1. Seismic Design and Postclosure Assessment Ground Motions

	Annual Exceedance Frequency	Site	Design Response Spectrum	Time Histories	Mean PGA[1] (g)		Mean PGV (cm/sec)	
					Horizontal	Vertical	Horizontal	Vertical
Preclosure	10^{-3}	Surface Facilities	Horizontal and Vertical	5 3-component sets spectrally matched to Point D/E	0.37	0.29		
	$5x10^{-4}$	Surface Facilities	Horizontal and Vertical	5 3-component sets spectrally matched to Point D/E	0.58	0.52		
	10^{-4}	Surface Facilities	Horizontal and Vertical	1 3-component set spectrally matched to Point D/E	1.19	1.49		
	10^{-3}	Emplacement Level	Horizontal and Vertical	1 3-component set spectrally matched to Point B	0.13	0.12		
	$5x10^{-4}$	Emplacement Level	Horizontal and Vertical	3-component set spectrally matched to Point B	0.19	0.23		
	10^{-4}	Emplacement Level	Horizontal and Vertical	3-component set spectrally matched to Point B	0.43	0.61	40	48
Postclosure	10^{-5}	Emplacement Level	NA	17 3-component sets spectrally conditioned to Point B			105	137
	10^{-6}	Emplacement Level	NA	17 3-component sets scaled to PGV 17 3-component sets spectrally conditioned to Point A and scaled to PGV			244	236
	10^{-7}	Emplacement Level	NA	17 3-component sets spectrally conditioned to Point A and scaled to PGV 17 3-component sets spectrally conditioned to Point B and scaled to PGV			535	625

Source: DTN: MO0410SDSTMHIS.005 [DIRS 172237], MO0407SDARS104.001 [DIRS 170683], MO0303DPGVB106.002 [DIRS 162712], MO0210PGVPB107.000 [DIRS 162713], MO0306SDSAVDTH.000 [DIRS 164033], MO0410SDSDE103.002 [DIRS 172236], MO0410WHBDF104.002 [DIRS 172238], MO0405SDSTPNTB.001 [DIRS 169851], MO0404PGVRL104.000 [DIRS 170437], MO0402AVDTM105.001 [DIRS 168890], MO0401SEPPGVRL.022 [DIRS 169099], MO0312SEPRSRLB.019 [DIRS 170427], MO0407TMHIS104.003 [DIRS 170599], MO0301TMHIS106.001 [DIRS 161868]

NOTES: [1] PGA = peak ground acceleration

CONTENTS

Page

CONTENTS (Continued)

Page

CONTENTS (Continued)

Page

INTENTIONALLY LEFT BLANK

FIGURES

Page

FIGURES (Continued)

Page

FIGURES (Continued)

Page

FIGURES (Continued)

Page

FIGURES (Continued)

Page

FIGURES (Continued)

Page

FIGURES (Continued)

Page

FIGURES (Continued)

Page

FIGURES (Continued)

Page

FIGURES (Continued)

Page

FIGURES (Continued)

Page

FIGURES (Continued)

Page

FIGURES (Continued)

Page

FIGURES (Continued)

Page

FIGURES (Continued)

Page

FIGURES (Continued)

Page

FIGURES (Continued)

Page

FIGURES (Continued)

Page

FIGURES (Continued)

Page

INTENTIONALLY LEFT BLANK

TABLES

Page

TABLES (Continued)

Page

TABLES (Continued)

Page

TABLES (Continued)

Page

TABLES (Continued)

Page

INTENTIONALLY LEFT BLANK

ACRONYMS, ABBREVIATIONS, AND SYMBOLS

1D, 2D, 3D	one-, two-, three-dimensional
ACC	Accession Number
BC	base case
BNL	Brookhaven National Laboratory
BSC	Bechtel-SAIC Company, LLC
CEUS	central and eastern U.S.
CFR	Code of Federal Regulations
cgs	centimeter-gram-sec
cm	centimeter(s)
COV	coefficient of variation
CRWMS M&O	Civilian Radioactive Waste Management System Management and Operating (Contractor)
DEA	Deaggregation Earthquake
DIR	Document Input Reference (sheet)
DOE	U.S. Department of Energy
DTN	Data Tracking Number
e	void ratio
EBS	Engineered Barrier System
ENA	Eastern North America
ε	number of standard deviations above the mean ground motion
ESF	Exploratory Studies Facility
FEPs	features, events, and processes
ft	feet
ft/sec	feet per second
g	gravitational acceleration (980 cm/sec^2) or gram(s)
g/cc	gram(s) per cubic centimeter
G	shear modulus
G_{max}	low-strain (maximum) shear modulus
G_S	specific gravity
HSHH	incident vertical and inclined SH-wave
HSVH	incident vertical and inclined SV-wave
Hz	Hertz
IED	Interface Engineering Drawing
κ	kappa
km	kilometer
LMA	lower mean alluvium (curve)

ACRONYMS, ABBREVIATIONS, AND SYMBOLS (Continued)

LMT	lower mean tuff (curve)
LSST	Large-Scale Seismic Test
m	meter(s)
m/sec	meter(s) per second
M	mode magnitude
MH	high magnitude DEA
ML	low magnitude DEA
MM	mean magnitude DEA
M_{max}	maximum magnitude
M	moment magnitude
M*	modal magnitude
NRC	U.S. Nuclear Regulatory Commission
NWTRB	Nuclear Waste Technical Review Board
σ	standard deviation
P	compression (wave)
PA	performance assessment
pcf	pounds per cubic foot
PI	plasticity index
PE&A	Pacific Engineering and Analysis
PGA	peak ground acceleration
PGV	peak ground velocity
PSD	Power Spectral Density
PSHA	probabilistic seismic hazard analysis
PSRV	pseudo-velocity response spectrum
PSV	pseudo-velocity
QA	quality assurance
QARD	Quality Assurance Requirements and Description
Q(f)	frequency-independent damping
Q_P	frequency-independent P-wave damping
Q_S	frequency-independent S-wave damping
R	distance
RCTS	resonant column and torsional shear
RE	reference earthquake
REI	Risk Engineering Incorporated
rms	root-mean-square
RQD	Rock Quality Designation
RVT	random-vibration theory
R*	modal distance

ACRONYMS, ABBREVIATIONS, AND SYMBOLS (Continued)

S	shear (wave)
Sa	spectral acceleration
SH	horizontally-polarized shear (wave)
SV	vertically-polarized shear (wave)
SAF	spectral amplification function
SASW	spectral-analysis-of-surface-waves (surveys)
sec	second
SPT	Standard Penetration Test
SRP	Standard Review Plan
SSI	soil structure interaction
SSCs	structures, systems, and components
TBV	to be verified
TDMS	Technical Data Management System
TIC	Technical Information Center
Tmbt1	pre-Rainier Mesa Tuff bedded tuff
Tmr	Rainer Mesa Tuff of the Timber Mountain Group
Tpbt4	pre-Tiva Canyon Tuff bedded tuff
Tpbt5	pre-Tuff unit "x" bedded tuffs (also known as post-Tiva Canyon Tuff bedded tuff)
Tpcpln	Tiva Canyon Tuff: crystal-poor member, lower nonlithophysal zone
Tpcpmn	Tiva Canyon Tuff: crystal-poor, middle nonlithophysal zone
Tpcpul	Tiva Canyon Tuff: crystal-poor member, upper lithophysal zone
Tpcpv	Tiva Canyon Tuff: vitric zone
Tpcrn	Tiva Canyon Tuff: crystal-rich, nonlithophysal zone
Tpcrv	Tiva Canyon Tuff: crystal-rich, vitric zone
Tpcrl	Tiva Canyon Tuff: crystal-rich, lithophysal zone
Tpki	Tuff unit "x"
Tpy	Yucca Mountain tuff
TSPA-LA	total system performance assessment for the License Application
TSPA-SR	total system performance assessment for the Site Recommendation
TWP	Technical Work Plan
UHS	uniform hazard spectrum
UNE	underground nuclear explosion
UMA	upper mean alluvium (curve)
UMT	upper mean tuff
UR	upper range velocity
URS	URS Corporation
USBR	U.S. Bureau of Reclamation
USGS	U.S. Geological Survey
UTA	University of Texas at Austin
ν	Poisson's ratio
V/H	vertical-to-horizontal

ACRONYMS, ABBREVIATIONS, AND SYMBOLS (Continued)

V_P	compression-wave velocity
VPV	incident vertical and inclined P-wave
V_S	shear-wave velocity
VSP	Vertical Seismic Profiling
VSVV	incident vertical and inclined SV-wave
WHB	waste handling buildings
WNA	Western North America
WUS	western U.S.
YMP	Yucca Mountain Site Characterization Project

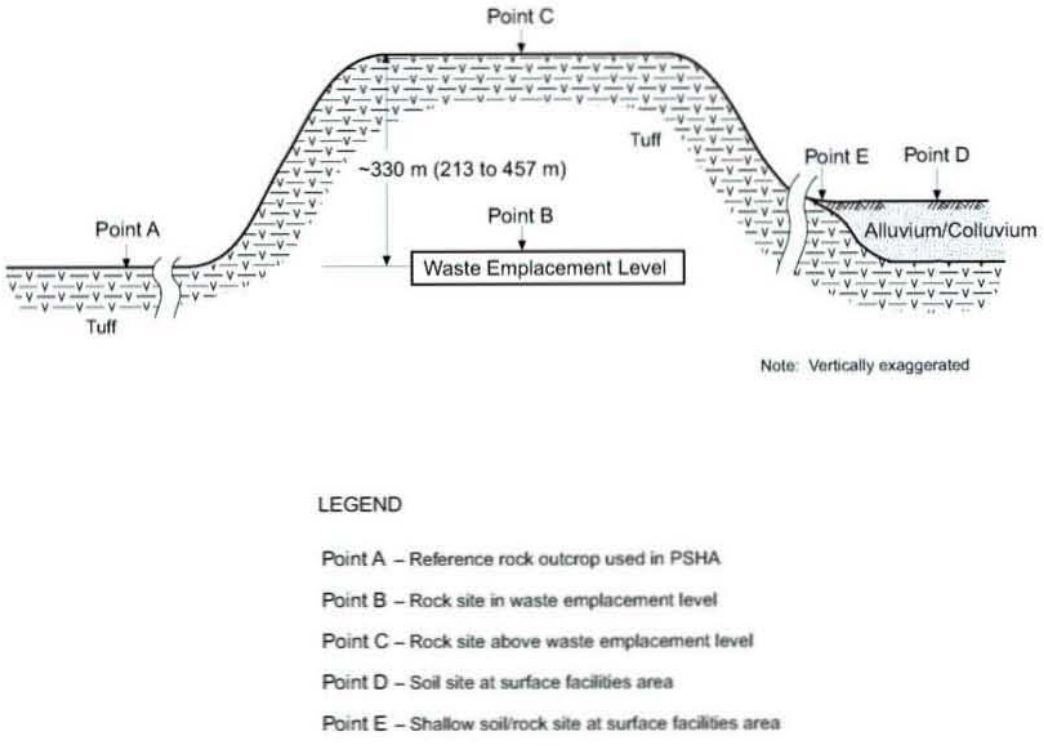

Figure 1-1. Schematic Representation of the Locations for which Seismic Input Ground Motions are Developed

Ground motion inputs for preclosure analyses are determined for an underground location at the depth of planned waste emplacement drifts (nominally 300 m depth) (Figure 1-1, Point B). Preclosure inputs are also determined for the planned site of surface facilities. This area, southwest of the Exile Hill fault splay, is referred herein as the "Surface Facilities Area". This is the area that has been geotechnically characterized and where the preclosure seismic design ground motions have been calculated. For the Surface Facilities Area, two conditions are modeled: a thin layer of alluvium covering rock (Figure 1-1, Point E) and a thicker layer of alluvium covering rock (Figure 1-1, Point D). Points D and E are located within the Surface Facilities Area. Originally, surface facilities were to be located in the area south of the fault, but due to changes in design and facility placement, some facilities are now planned to be located north of the fault. To examine the differences north and south of the fault, ground motions for a location north of the fault (Point F) have been computed based on the available data. A geotechnical program to characterize the area northeast of the Exile Hill splay fault began in June 2004.

Ground motion inputs for postclosure analyses are determined for the waste emplacement level (Point B) only. Ground motions for a rock outcrop at the surface of Yucca Mountain (Figure 1-1, Point C) are not required and, thus, are not addressed in this report.

The relation of this study to other preclosure and postclosure seismic-related work is shown on Figure 1-2. The ground motion hazard results from the PSHA provide the basis for inputs to a site response analysis. Preclosure ground motions derived from the site response analysis are used for design of the surface facilities and in soil-structure interaction analyses for the waste handling buildings. They are also used for preclosure subsurface facility design and analyses and to support preclosure waste package design and analyses.

For postclosure, peak ground velocity values determined from the site-response analysis for the waste emplacement level are used to develop time histories (seismograms) that form input to a model of drift degradation under seismic loads producing rockfall (Figure 1-2). The time histories are also used to carry out dynamic seismic structural response calculations of the drip shield and waste package system. For the drip shield, damage from seismically induced rockfall also is considered. In the seismic consequence abstraction, residual stress results from the structural response calculations are interpreted in terms of the percentage of the component (drip shield, waste package) damaged as a function of peak horizontal ground velocity (Figure 1-2). The seismic consequence abstraction also uses peak horizontal ground velocities to determine a seismic hazard curve for the waste emplacement level.

Reports that document inputs to the modeling and analyses, and those that document use of the results, are listed below:

OCRWM Project Reports Documenting Inputs:

- *Characterize Framework for Seismicity and Structural Deformation at Yucca Mountain, Nevada*. ANL-CRW-GS-000003 REV 00 [Errata 001]. (BSC 2004j [DIRS 168030])

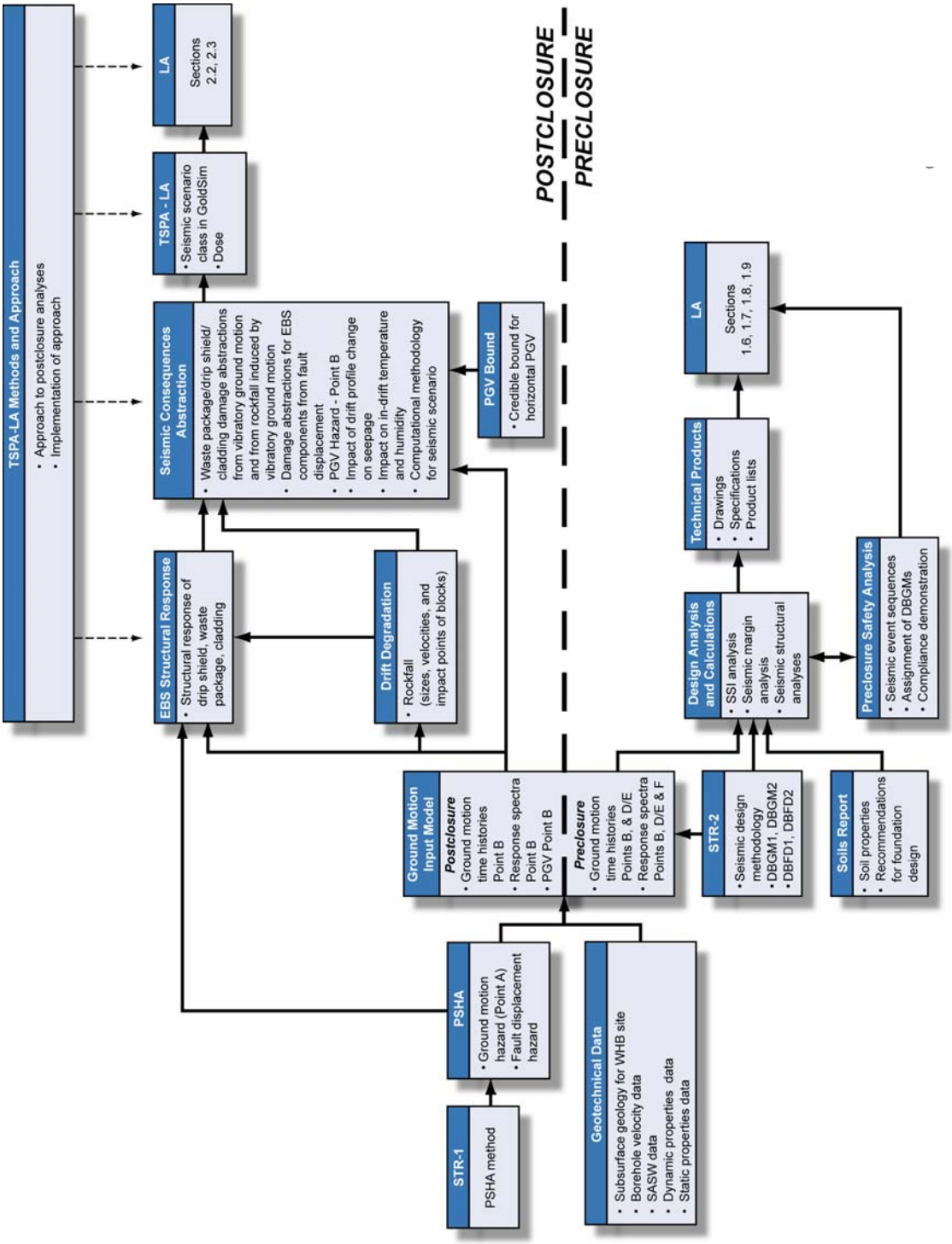

Figure 1-2. Documentation of Seismic Analyses

- *Surface Geophysics. Volume I of Synthesis of Borehole and Surface Geophysical Studies at Yucca Mountain, Nevada and Vicinity*. (Majer et al. 1996b [DIRS 104685], Section IV)

- *Geotechnical Data for a Potential Waste Handling Building and for Ground Motion Analyses for the Yucca Mountain Site Characterization Project*. ANL-MGR-GE-000003 REV 00. (BSC 2002a [DIRS 157829])

- *Geologic Framework Model (GFM2000)*. MDL-NBS-GS-000002 REV 02. (BSC 2004n [DIRS 170029])

- *Characterize Eruptive Processes at Yucca Mountain, Nevada.* ANL-MGR-GS-000002, Rev. 02. (BSC 2004k [DIRS 169980], Section 6.3.1.3, Table 7-1)

- *Preclosure Seismic Design Methodology for a Geologic Repository at Yucca Mountain*. TDR-WHS-MD-000004 REV 01. (BSC 2004b [DIRS 170564])

OCRWM Project Reports Documenting Use of Results:

- *Drift Degradation Analysis*, ANL-EBS-MD-000027.

- *Features, Events, and Processes: Disruptive Events*, ANL-WIS-MD-000005.

- *Structural Calculations of Waste Package Exposed to Vibratory Ground Motion*, 000-00C-WIS0-01400-000-00.

- *Additional Structural Calculations of Waste Package Exposed to Vibratory Ground Motion*, 000-00C-WIS0-01700-000-00.

- *Seismic Consequence Abstraction*, MDL-WIS-PA-000003.

- *Peak Ground Velocities for Seismic Events at Yucca Mountain, Nevada*, ANL-MGR-GS-000004.

In a topical report submitted to the U. S. Nuclear Regulatory Commission (NRC), the Department of Energy (DOE) identified two levels of seismic ground motion hazard appropriate for preclosure ground motion inputs (YMP 1997a [DIRS 100521], Section 3.1). These levels were defined for SSCs associated with Category 1 and Category 2 design basis events as defined in 10 Code of Federal Regulations (CFR) 60.2. With the issuance of 10 CFR 63 the concept of event sequences was introduced and preclosure performance objectives were defined in terms of them (10 CFR 63.111). In light of this change, DOE has revised its preclosure seismic design methodology to include two levels of Design Basis Ground Motion (DBGM-1 and DBGM-2) (BSC 2004b [DIRS 170564]). DBGM-1 and DBGM-2 are associated with annual frequencies of being exceeded (hazard levels) of 1×10^{-3} and 5×10^{-4}, respectively. In addition, the revised methodology includes high-confidence-of-low-probability-of-failure seismic margins analyses and some analyses for "beyond design basis ground motion" (e.g., ground motions with a 1×10^{-4} annual frequency of being exceeded).

In this report, results (5%-damped design response spectra, three-component sets of time histories matched to the seismic design response spectra, and strain-compatible soil properties) are provided for the 1×10^{-3}, 1×10^{-4}, and 5×10^{-4} hazard levels. (Note, that unless specified otherwise, all response spectra discussed and/or described in this report are 5%-damped.)

For postclosure analyses, the focus is on model results for ground motion hazard levels between 10^{-4} and 10^{-8}. These ground motions are larger than those used for preclosure design and address the regulatory requirement to consider events with a 10^{-4} chance of occurring in 10,000 years (10 CFR 63.114(d) 2002 [DIRS 156605]). In this report, 17 three-component sets of time histories are presented for annual exceedance frequencies of 10^{-5}, 10^{-6}, and 10^{-7} in support of TSPA.

This report also describes an evaluation of ground motions from maximum magnitude earthquakes associated with potential intrusion of basalt dikes at Yucca Mountain. Development of these ground motion inputs is treated deterministically. Results can be used to assess criticality issues related to possible dike intrusion.

1.1 SCOPE OF WORK

There are no standards that are applicable to the development of seismic inputs for Yucca Mountain (Section 4.3). The products of this study, however, address, in whole or in part, requirements of 10 CFR 63 and the Yucca Mountain Review Plan, Final Report (NRC 2003 [DIRS 163274]), as identified in Section 4.2. The site response analysis followed the guidance provided in Regulatory Guide 1.165 (1997 [DIRS 119139], Appendix C) and NUREG/CR-6728 (McGuire et al. 2001 [DIRS 157510], Section 6) with some exceptions as noted in the report. The Technical Work Plan (TWP), *Development of Seismic Design Inputs, Preparation of a Seismic Topical Report and Evaluation of Disruptive Events Features, Events, and Processes,* TWP-MGR-GS-000001, Revision 03 ICN 02 (BSC 2004a [DIRS 171850], Section 1.2), describes the scope of work performed. Planned tasks listed in the TWP that are documented, in whole or in part, in this report consist of:

- Develop velocity profiles, nonlinear dynamic material properties curves, density profiles, and velocity correlation statistics based on geotechnical investigations at the site and other available information.

- Extend the PSHA calculations to higher ground motions (lower annual frequencies of exceedance) to support TSPA-LA.

- Carry out seismic hazard deaggregation for appropriate annual exceedance frequencies: 10^{-3}, $5x10^{-4}$, 10^{-4}, 10^{-5}, 10^{-6}, and 10^{-7}.

- Develop seismic design inputs for required annual frequencies of exceedance and for appropriate sites (e.g., emplacement level, surface) to support preclosure and postclosure analyses.

- Prepare a seismic design inputs model report documenting the seismic design inputs supporting initial preclosure design and TSPA-LA.

The TWP also describes the planned approach to model validation. Previously published results that compare output of the modeling approach to observed data and to the output of alternative modeling approaches are described in Section 7. Section 7 also describes the results of an independent technical review of the model. This review forms a component of the overall model validation approach to reach the desired level of model confidence (Section 7.2). The validation of the model was completed in Revision 00 of this report (BSC 2003d [DIRS 166274]). In this Revision 01, additional confirmation analyses are documented that increase confidence in the validation of the model at higher shear strains. In particular, the model confirmation is for shear strains near 1%, which exceed the shear strains generated by the ground motions calculated for annual frequencies of exceedance at 10^{-6} and 10^{-7}. The model validation carried out and described in Section 7 is a Level III validation.

1.2 BACKGROUND

Preliminary ground motion inputs were first developed for the Yucca Mountain site in CRWMS M&O (1998b [DIRS 156499]). These inputs were for the emplacement drift level and for a rock outcrop at the surface. Inputs for the surface facilities site were not developed because the site geology had not yet been sufficiently characterized. Subsequent efforts resulted in an initial characterization of the surface facilities site and led to updated preliminary inputs. These preliminary inputs provided the basis for analyses supporting the site recommendation (CRWMS M&O 2000 [DIRS 151288], BSC 2001a [DIRS 155187]). A more extensive characterization of the geotechnical properties of the Repository Block and surface facilities site was carried out in 2000 and 2001 (BSC 2002a [DIRS 157829]). Results from these investigations form the basis for the current modeling and analyses efforts.

1.3 MODEL LIMITATIONS

A mathematical model is a mathematical representation of a conceptual model (system, process, or phenomenon) that is based on established scientific and engineering principles and from which the approximate behavior of a system, process, or phenomenon can be calculated within determinable limits of uncertainty. A limitation of models is that a mathematical representation is used that only approximates a physical process and cannot capture its every detail. There are also limitations to the inputs that are required by the model. These limitations, which are generally due to the availability and uncertainties of data, are discussed in Section 6.2.

In addition to general limitations that pertain to models, the RVT equivalent-linear site-response modeling approach is limited in that it considers the ground motion process as one-dimensional (1D). The modeling approach employs plane-wave propagation through a 1D profile of layers with associated velocities and material properties. Two-dimensional (2D) and three-dimensional (3D) effects on ground motions (e.g., effects from dipping interfaces or topography) are not explicitly included in the model.

Although 2D and 3D effects are not explicitly included, predicted response spectra using the 1D equivalent-linear approach have been favorably compared against actual earthquake data in studies worldwide by numerous investigators since the inception of the model in 1968 (e.g., Electric Power Research Institute [EPRI] 1993b [DIRS 103320], Appendix 6B; see also Section 7.3.2.4). The approach is widely used in the earthquake engineering community and is accepted

by the NRC. Because of the extensive experience of the engineering community with the 1D equivalent-linear modeling approach for site response, it has been adopted for use in this study. Also, based on the available velocity data, a 1D model appears to adequately represent the velocity structure in the Repository Block and beneath the surface facilities site. Further discussion of model limitations is contained in Section 6.1.14.

Because of the assessed epistemic uncertainty in ground motion and the characterization of ground motion variability with unbounded lognormal distributions in the PSHA, as lower and lower annual frequencies of exceedance are considered, the calculated ground motions get larger, eventually reaching levels that are not credible. It is assumed that the mean ground motions at these low annual exceedance frequencies are valid for the purposes of this study. In developing time histories to support calculations of the dynamic response of engineered barrier system (EBS) components (drift, drip shield, waste package), the levels of ground motion determined in the PSHA were used without consideration of whether they could be realized at Yucca Mountain, as they reflect the state of uncertainty in the estimation of ground motion probability estimates. Thus, some of the time histories representing ground motion with annual frequencies of exceedance smaller than 10^{-5} (Section 6.3.2.3) may not be credible in that the levels of ground motion cannot be sustained at Yucca Mountain. Nevertheless, they were used to evaluate the performance of EBS components as if those levels of ground motion could be achieved to determine the sensitivity of response calculations to such ground motions. The EBS component damage functions based on those results, therefore, to some degree represent damage from ground motions that are higher than can be realized at Yucca Mountain. A realistic and reasonable bound on peak horizontal ground velocity at the waste emplacement level (BSC 2004c [DIRS 170137]) is incorporated into the sampling process for TSPA. Thus, only those portions of the damage functions resulting from credible ground motions are ultimately used.

1.4 ORGANIZATION OF THIS REPORT

The organization of this report conforms to the format specified in AP-SIII.10Q, *Models*. Section 1 describes the purpose and background of the study, the scope of work, and a brief description of the model used in the analyses and its limitations. Section 2 describes the applicability of the Quality Assurance (QA) Program. Computer software and models used to support quality-affecting work are discussed in Section 3. Inputs and their sources, identified and documented in accordance with AP-3.15Q, *Managing Technical Products Inputs*, are described in Section 4. Section 5 documents the lack of data assumptions made to perform the modeling and analyses. Section 6 describes the RVT-based equivalent-linear site response model and the model inputs. Modeling, analyses, and results are also described in detail in this section. Section 7 presents the model validation. Finally, Section 8 summarizes the conclusions of the study and Section 9 lists the inputs and references including documents cited, data, and software.

INTENTIONALLY LEFT BLANK

2. QUALITY ASSURANCE

Development of this model report and supporting modeling activities and analyses have been determined to be subject to the Yucca Mountain Project's quality assurance program (BSC 2004a [DIRS 171850], Section 8.1). Approved quality assurance procedures identified in the TWP (BSC 2004a [DIRS 171850], Section 4.1) have been used to conduct and document the activities described in this report. The TWP also identifies the methods used to control the electronic management of data during the activities and these were implemented in this study (BSC 2004a [DIRS 171850], Section 8.1). Methods identified in the TWP were followed without variance. This modeling activity does not involve items or natural barriers identified on the Q-List (YMP 2001 [DIRS 154817]); a Safety Category designation in accordance with AP-2.22Q (Classification Analyses and Maintenance of the Q-List) is not applicable.

INTENTIONALLY LEFT BLANK

3. USE OF SOFTWARE

A new suite of procedures controlling the use and qualification of computer software became effective since the previous version of this report. As a result, use of computer programs to develop ground motion inputs for Yucca Mountain was controlled in accordance with AP-SI.1Q prior to 23 March 2004, and with LP-SI.11Q-BSC since 23 March 2004. Programs were baselined prior to 23 March 2004 and were qualified in accordance with AP-SI-1Q. The programs were used consistently with their intended use and within their range of validation in accordance with the respective effective procedure. Limitations of use and outputs are described in respective associated software qualification documents. The input for the computer programs and the resulting output are documented in scientific notebooks supporting the effort (Wong and Toro 2003 [DIRS 163848]; Toro 2003 [DIRS 163720], 2004 [DIRS 172034]; Wong and Silva 2003 [DIRS 163201], 2004a [DIRS 170443], 2004d [DIRS 172075]). The computer programs used in these modeling and analysis activities are listed alphabetically in Table 3-1. These programs were selected for three reasons: (1) they provide the technical functions needed and were already available on the Software Baseline (e.g., FRISK88 v. 2.0, EARTHVISION v. 5.1); (2) they are the only software available to calculate ground motions for the velocity/layer thickness correlation analysis used at Yucca Mountain (e.g., RASCALS, RASCALP, and RANPAR); (3) they are necessary pre- or post-processing programs that are used in more efficient batch-processing of large volumes of files, and/or they are uniquely compatible with the operating environments and format requirements of the above main programs (all other programs listed in Table 3-1). No software was used prior to qualification to develop preliminary outputs for this model report.

Table 3-1. Software Used

Software Name	Reference	Software Tracking Number	Computer Type
BASE4 v. 4.0	Pacific Engineering and Analysis 2002a [DIRS 163293]	10940-4.0-00	IBM PC-compatible
CMB_FRAC v. 2.0	Risk Engineering, Inc. 2002a [DIRS 163294]	10464-2.0-00	HP-735
CORBB v. 1.0	Pacific Engineering and Analysis 2002b [DIRS 163295]	10941-1.0-00	IBM PC-compatible
DESIGN_EVENTS v. 1.0	Risk Engineering, Inc. 2002b [DIRS 163302]	10362-1.0-00	IBM PC-compatible
DUR v. 1.0	Pacific Engineering and Analysis 2003a [DIRS 163303]	10942-1.0-00	IBM PC-compatible
EARTHVISION V5.1	Dynamic Graphics 2000 [DIRS 167994]	10174-5.1-00	Silicon Graphics Indigo R4000
FRISK88 v. 2.0	Risk Engineering, Inc. 2000a [DIRS 163365]	10139-2.0-00	HP-735
INTEG1 v. 1.0	Pacific Engineering and Analysis 2002c [DIRS 163304]	10943-1.0-00	IBM PC-compatible
INTERPOL v. 1.0	Pacific Engineering and Analysis 2002d [DIRS 163305]	10944-1.0-00	IBM PC-compatible
LAYERING v. 1.0	Risk Engineering, Inc. 2002c [DIRS 163307]	10648-1.0-00	IBM PC-compatible

Software Name	Reference	Software Tracking Number	Computer Type
LOGNORM v. 1.0	Pacific Engineering and Analysis 2002e [DIRS 163308]	10384-1.0-00	IBM PC-compatible
LOGNORM v. 1.01	Pacific Engineering and Analysis 2004 [DIRS 170313]	10384-1.01-00	IBM PC-compatible
MAXMIN v. 1.0	Pacific Engineering and Analysis 2002f [DIRS 163309]	10945-1.0-00	IBM PC-compatible
MEAN v. 1.1	Risk Engineering, Inc. 2002d [DIRS 163310]	10463-1.1-00	HP-735
MRE88 v. 1.0	Risk Engineering, Inc. 2000d [DIRS 163312]	10140-1.0-00	HP-735
NORM v. 1.01	Pacific Engineering and Analysis 2002g [DIRS 163313]	10386-1.01-00	IBM PC-compatible
PARINP v. 1.1	Pacific Engineering and Analysis 2002h [DIRS 163314]	10387-1.1-00	IBM PC-compatible
POST88 v. 1.0	Risk Engineering, Inc. 2000b [DIRS 163361]	10136-1.0-00	HP-735
PREP88 v. 1.0	Risk Engineering, Inc. 2000c [DIRS 163362]	10138-1.0-00	HP-735
RANPAR v. 2.0	Pacific Engineering and Analysis 2002i [DIRS 163315]	10486-2.0-00	IBM PC-compatible
RANPAR v. 2.1	Pacific Engineering and Analysis 2003d [DIRS 170442]	10486-2.1-00	IBM PC-compatible
RASCALP v. 2.01	Pacific Engineering and Analysis 2002j [DIRS 163367]	10388-2.01-00	IBM PC-compatible
RASCALP v. 2.02	Pacific Engineering and Analysis 2002k [DIRS 163316]	10388-2.02-00	IBM PC-compatible
RASCALS v. 5.4	Pacific Engineering and Analysis 2002l [DIRS 163317]	10389-5.4-00	IBM PC-compatible
REPLOT v. 1.0	Pacific Engineering and Analysis 2003b [DIRS 163318]	10949-1.0-00	IBM PC-compatible
SCALE1 v. 1.0	Pacific Engineering and Analysis 2002m [DIRS 163319]	10946-1.0-00	IBM PC-compatible
SMRATIO v. 1.0	Pacific Engineering and Analysis 2002n [DIRS 163320]	10917-1.0-00	IBM PC-compatible
SPCTLR v. 1.0	Pacific Engineering and Analysis 2003c [DIRS 163321]	10947-1.0-00	IBM PC-compatible
SPMEAN v. 1.0	Pacific Engineering and Analysis 2002o [DIRS 163322]	10918-1.0-00	IBM PC-compatible
VEL_SIMUL v. 1.0	Risk Engineering, Inc. 2002e [DIRS 163323]	10647-1.0-00	IBM PC-compatible
VEL_STAT v. 1.0	Risk Engineering, Inc. 2002f [DIRS 163324]	10646-1.0-00	IBM PC-compatible
VELAVG v. 1.0	Pacific Engineering and Analysis 2002p [DIRS 163325]	10390-1.0-00	IBM PC-compatible
XYMULT v. 1.0	Pacific Engineering and Analysis 2002q [DIRS 163326]	10919-1.0-00	IBM PC-compatible

Software has been used in this study to develop inputs to the site-response ground motion model, to implement the model itself, and to develop ground motion inputs based on model results. Brief descriptions of the programs used in this study follow; more detailed information on the programs is found in the software qualification documentation associated with each program.

The programs PREP88, FRISK88, POST88, CMB_FRAC, and MEAN are used to compute PSHA results for additional ground motion levels (lower annual exceedance frequencies) needed for postclosure analyses. The programs are also used to develop uniform hazard spectra.

The programs FRISK88, PREP88, and MRE88 are used to deaggregate seismic hazard results such that the contributions from different earthquake magnitudes, distances, and ground motion variability ranges can be observed. Deaggregation results are used to identify the dominant contributors to ground motion hazard, which form the basis for ground motions that are input to the site-response model.

DESIGN_EVENTS is used to generate spectra for the dominant contributors to ground motion hazard. These spectra form the input to the site-response model. DESIGN_EVENTS is also used to determine ground motions for maximum magnitude earthquakes associated with possible basalt-dike intrusions.

The programs LAYERING, VEL_STAT and VEL_SIMUL are used to analyze the correlations between profile layer thicknesses and velocities. The resulting correlations are used to generate random velocity profiles that represent the variability in velocity observed at the site.

RASCALS implements the RVT-based equivalent-linear site-response model approach. The program computes a source Fourier amplitude spectrum, and acceleration and velocity response spectra using RVT techniques. The program is used to determine spectral amplification functions that describe the ground motion response of the site, which are then applied to the response spectra for the control motions. A multi-layer rock/soil profile is used as input. The program also is used to generate synthetic time histories. Shear strains and curvatures also are computed by RASCALS. RASCALP is the P-wave version of RASCALS.

The program RANPAR produces input and parameter files for RASCALS and RASCALP using a randomization approach selected by the user.

VELAVG reads in a number of velocity profiles (either depth to top of layer and velocity or thickness and velocity), interpolates to a finer depth grid if necessary, computes log statistics using LOGNORM, and recombines layers of the average, 84^{th}, and 16^{th} percentile profiles if velocities are within an input range parameter.

LOGNORM calculates mean and standard deviation of tabular data contained in a set of files. The distribution is assumed to be log-normal. Weights are applied to each curve. NORM also calculates mean and standard deviation for tabular data assuming a normal distribution. Weights also are applied to each curve.

PARINP reads in a given set of parameter files and computes the number of layers and depth for input with either NORM or LOGNORM.

The programs BASE4, CORBB, DUR, INTEG1, INTERPOL, MAXMIN, REPLOT, SCALE1, SMRATIO, SPCTLR, SPMEAN, and XYMULT are post-processing routines that support the development of model outputs and ground motion inputs developed from them. BASE4 performs time domain baseline correction of acceleration time histories and also integrates the corrected records to produce velocity and displacement time histories. CORBB computes correlation coefficients between two time histories. DUR computes Arias Intensity (Kramer 1996 [DIRS 103337], page 82) versus duration of an acceleration time history. INTEG1 performs time domain integration of an acceleration time history to produce velocity and displacement time histories. INTERPOL is used to interpolate an expanded set of points for a user-defined curve such as a response spectrum. MAXMIN determines the maximum and minimum values from a series of input data, such as a time history, and the points at which they occur. REPLOT generates graphical representations of data. SCALE1 scales data values such as acceleration time histories. SMRATIO divides columns of data and is used to determine the ratio between response spectra to obtain a transfer function. SPCTLR computes the response spectra of multiple time histories at specified dampings. SPMEAN determines the mean, minimum, and maximum of the data in a series of input files and is used to envelop seismic transfer functions or response spectra. XYMULT multiplies two columns of data together such as multiplying a response spectrum by a transfer function.

EARTHVISION is used to determine the range of thickness of overburden above the waste emplacement area. This result is used in developing randomized velocity profiles for input to the site response model.

Two commercial-off-the-shelf programs, Microsoft Excel and MathCad, were used to support the work. Microsoft Excel 2000 was used in the development of velocity profiles forming input to the model, in revising vertical uniform hazard spectra, in carrying out ray-tracing calculations, and in determining peak ground velocity and scaled peak ground velocity values. Microsoft Excel 97 was used to compare normalized layer thickness from a velocity and thickness correlation analysis with gamma and lognormal distributions. MathCad 2000 was used to develop ground motion incidence angles that are an input to the model. MathCad 7 was used to develop response spectra for some reference and deaggregation earthquakes and to determine weights for deaggregation earthquakes in cases for which the 95^{th}-percentile magnitude was adjusted to better represent the range of magnitudes contributing to ground motion hazard. Documentation of the use of these commercial-off-the-shelf software programs, including algorithms, inputs, outputs, and other information, is contained in Appendix I.

In addition to the software used in modeling and analysis activities, several other programs are mentioned in Sections 6.1 and 7. The program SHAKE is discussed as an alternative method of implementing an equivalent-linear site-response model. The programs DESRA-2C, SUMDES, and TESS are described because of their use in EPRI (1993b [DIRS 103320], Appendix 6.B), which is cited in support of model validation. SUMDES and TESS were also used in a study to confirm model validation. None of these programs were used in the modeling and analysis activities to develop seismic inputs supporting design and performance assessment at Yucca Mountain.

4. INPUTS

This section describes the input data and other inputs used in the site-response ground motion model. The section also lists project requirements and criteria that pertain to the work discussed in this report. Finally the section notes codes and standards that are relevant to the work.

4.1 DIRECT INPUT

This subsection identifies input data that are used in the models and analyses detailed in this report.

4.1.1 Qualified Input Data

Qualified input data used in analyses and modeling described in this report are identified in Table 4-1.

Table 4-1. Qualified Input Data

Input Data	Data Source	Data Tracking Number, Design Data, or Value
Results of the Yucca Mountain Probabilistic Seismic Hazard Analysis (PSHA)	BSC (2004j [DIRS 168030]) CRWMS M&O (1998a [DIRS 103731])	MO0401MWDRPSHA.000[1] [DIRS 166962]
Velocity Seismic Profile Results from Boreholes NRG-6,WT-2,RF-4,RF-7/7A,SD-12,G-2 & G-4	Majer et al. (1996b [DIRS 104685], Section IV)	LB0306VSP95DAT.001 [DIRS 164559]
Downhole Velocity Measurements at the WHB Site (Shear and Compression Wave Velocity Profiles from boreholes RF#13, 14, 15, 16, 18, 19, 20, 21, 22, 23, 24, 25, 26, 28, & 29) (WHB = Waste Handling Building)	BSC (2002a [DIRS 157829], Section 6.2.5)	MO0111DVDWHBSC.001 [DIRS 157296]
Downhole Velocity Measurements at the WHB Site (Shear and Compression Wave Velocity Profiles from boreholes RF#13 & RF#17)	BSC (2002a [DIRS 157829], Section 6.2.5)	MO0110DVDBOREH.000 [DIRS 157295]
Downhole Velocity Measurements from the Top of Yucca Mountain (Shear and Compression Wave Velocity Profiles from boreholes UZ-N66, UZ-N94, UZ-N71, UZ-N75, UZ-N64, UZ-N27, & UZ-N46)	BSC (2002a [DIRS 157829], Section 6.4.3)	MO0202DVDWHBSC.002 [DIRS 158078]
SASW Velocity Data from the WHB Site Characterization Area (SASW = Spectral Analysis of Surface Waves)	BSC (2002a [DIRS 157829], Section 6.2.7)	MO0110SASWWHBS.000 [DIRS 157969]
SASW Velocity Data from the Top of Yucca Mountain (2000)	BSC (2002a [DIRS 157829], Section 6.4.2)	MO0203SEPSASWD.000 [DIRS 158084]

[1] DTN MO0401MWDRPSHA.000 [DIRS 166962] supersedes MO0004MWDRIFM3.002 [DIRS 149092], which was cited in Revision 00 of this report. The original DTN was superseded to add to the data a file containing the coordinates of the locations at which ground motion and fault displacement hazard were computed. None of the original data associated with DTN MO0004MWDRIFM3.002 [DIRS 149092] was altered. Note that supporting scientific notebooks refer to the superseded DTN (MO0004MWDRIFM3.002 [DIRS 149092]).

Input Data	Data Source	Data Tracking Number, Design Data, or Value
SASW Velocity Data from the Top of Yucca Mountain (2001)	BSC (2002a [DIRS 157829], Section 6.4.2)	MO0110SASWVDYM.000 [DIRS 158076]
Borehole Suspension Data for the WHB Site Characterization Area	BSC (2002a [DIRS 157829], Section 6.2.6)	MO0204SEPBSWHB.001 [DIRS 158088]
Borehole Suspension Data for RF#13 at WHB Site Characterization Area	CRWMS M&O (1999 [DIRS 109209], Section 4.4, Appendix O)	MO0204SEISDWHB.001 [DIRS 158086]
Geotechnical Borehole Logs at the WHB site from RF#13, 14, 15, 16, 17, 18, 19, 20, 21, 22, 23, 24, 25, 26, 28 & 29	BSC (2002a [DIRS 157829], Sections 6.2.2, 6.2.3, and 6.6.2)	GS030783114233.001 [DIRS 164561]
Laboratory Dynamic Rock/Soil Testing Results from UE-25 RF#13	CRWMS M&O (1999 [DIRS 109209], Section 5.2 and Appendix Q)	MO9905LABDYNRS.000 [DIRS 103792]
SASW Velocity Data from Rock Sites on Yucca Mountain and in the ESF	BSC (2002a [DIRS 157829], Sections 6.3.2 and 6.4.2)	MO0206SASWROCK.000 [DIRS 159081]
Dynamic Laboratory Test Results from the WHB Site, Fran Ridge Borrow Area and the ESF Tunnel	BSC (2002a [DIRS 157829], Sections 6.2.10. 6.3.3, and 6.5.3)	MO0203DHRSSWHB.001 [DIRS 158082]
USBR Soil Classification and Relative Density Laboratory Data	BSC (2002a [DIRS 157829], Section 6.2.9)	GS020483114233.004 [DIRS 158242]
Rock Bulk Density Data	Not applicable	SNL01A05059301.002 [DIRS 150042], SNL02030193001.004 [DIRS 108415], SNL01A05059301.005 [DIRS 109002], SNL02030193001.012 [DIRS 108416], SNL02030193001.019 [DIRS 108431], SNL02030193001.020 [DIRS 108432], SNL02030193001.021 [DIRS 108433]
Gamma-Gamma Density Measurements	BSC (2002a [DIRS 157829], Section 6.2.8)	MO0204SEPGAMDM.000 [DIRS 158125]
Underground layout configuration – outline and elevation	BSC (2004d [DIRS 164519])	800-IED-WIS0-00101-000-00A
Gradation Analysis Test Results for Test Pit Bag Samples from the Waste Handling Building Site Characterization Area	BSC (2002a [DIRS 157829], Section 6.2.9)	GS020783114233.005 [DIRS 159542]
Geologic Framework Model (GFM2000)	BSC (2004n [DIRS 170029])	MO0012MWDGFM02.002 [DIRS 153777]
Physical Parameters of Basalt Magma and Eruption Phenomena	BSC (2004k [DIRS 169980])	LA0407DK831811.001 [DIRS 170768]
Value of site attenuation parameter kappa used in the PSHA for Yucca Mountain	BSC (2004j [DIRS 168030], Section 6.3.3.1.1)	0.02 sec

These data are used in developing model inputs, as described in Section 6.2. Section 6.2 also provides details on how data uncertainties are handled in modeling and analysis activities. Results of the PSHA are used to extend ground motion hazard curves to lower annual frequencies of being exceeded (Section 6.2.2.2). These results then feed the development of ground motion inputs, or control motions, to the site-response ground motion model (Sections 6.2.2.3 to 6.2.2.5). Seismic velocity data from the Repository Block and the Surface Facilities Area are used to determine velocity versus depth profiles (Section 6.2.3). They also are used to assess the correlation of velocities and thicknesses for profile layers (Section 6.2.3.6). Borehole geotechnical logs provide information on the depth of alluvium at the Surface Facilities Area (Section 6.2.3.4). Results of laboratory testing of the dynamic properties of site materials are used to characterize the behavior of shear modulus and damping as a function of shear strain (Section 6.2.4). Other laboratory data are used to assess the density of materials at the site (Section 6.2.3.7). In cases for which only some of the data associated with a given data tracking number (DTN) are used, the specific data used and a justification are provided in the appropriate subsection of Section 6.2. The outline of the waste emplacement area is used to identify velocity data that are relevant to characterizing the Repository Block (Section 6.2.3.2.5). Gradation analysis of soil samples is used to develop dynamic material property curves (Section 6.2.4.3). The topographic component of the Geologic Framework Model is used along with the elevation of the waste emplacement area to determine the range of overburden thickness for site response modeling (Section 6.2.3.5). The value of site attenuation (kappa) for Yucca Mountain is used to determine revised vertical spectra (Section 6.2.2.6.3). Physical parameters of basalt magma and eruption phenomena, specifically maximum magnitudes for basalt-dike-related earthquakes, are used in Section 6.5 to evaluate ground motions from such events.

4.1.2 Input Data Considered Qualified for Use Within This Report

In addition to qualified input data, the modeling and analyses described in this report also use other non site-specific data as input. These data are considered qualified for use within this report as justified below in accordance with AP-SIII.10Q, Section 5.2.1(k). Input data considered qualified for use in this report are summarized in Table 4-2.

Table 4-2. Input Data Considered Qualified for Use Within This Report

Input	Source
Crustal velocity profile underlying the reference rock outcrop used in the PSHA	Schneider et al. (1996 [DIRS 103270], Table 5.2)
Nominal values of the site attenuation parameter kappa for the western U.S. and the central and eastern U.S.	McGuire et al. (2001 [DIRS 157510], Section 4.8, Table 4-2)
Depth distribution of earthquakes in the western U.S.	McGuire et al. (2001 [DIRS 157510], Table 6.2)
Recommended vertical/horizontal spectral ratios for the western U.S. and for the central and eastern U.S.	McGuire et al. (2001 [DIRS 157510], Tables 4-4 and 4-5, Figures 4-36 and 4-39)
Generic western U.S. rock velocity profile	Silva et al. (1996 [DIRS 110474], Figure 3.8)
Catalog of time histories for analyses	McGuire et al. (2001, Appendix B)
Generic curves for shear modulus reduction and damping as a function of cyclic shear strain and typical range of modulus reduction curves for gravels	EPRI (1993b [DIRS 103320], Appendix 7, Figure 7.A-3, Section 7.A.5)

The regional crustal velocity profile in the Yucca Mountain region used to compute incidence angles for control motions (Section 6.2.2.5.1) was developed by Schneider et al. (1996 [DIRS 103270]). It is based on vertical seismic profiling (VSP) data from selected holes atop Yucca Mountain (Majer et al. 1996a [DIRS 106330]), refraction data from Mooney and Schapper (1995 [DIRS 106384]), and a crustal model used by the U.S. Geological Survey (USGS) for earthquake locations (Harmsen 1993 [DIRS 105106], Appendix F). In a project carried out by the USGS, the crustal velocity profile was used by a group of six nationally-known ground motion modeling experts to simulate ground motions for Yucca Mountain using assumed scenario earthquakes (Schneider et al. 1996 [DIRS 103270]). Prior to its use, the velocity profile was reviewed by the modelers and other project participants. The report describing the Scenario Ground Motion Project underwent technical review under the USGS Yucca Mountain QA Program. The profile was subsequently used in the Yucca Mountain PSHA Project by seven ground motion experts (CRWMS M&O 1998a [DIRS 103731]). These seven experts are some of the top ground motion experts in the U.S. The PSHA was guided by a review panel of internationally-known experts and monitored by the NRC. The PSHA Project was also documented in a peer-reviewed journal paper (Stepp et al. 2001 [DIRS 158656]).

Values of kappa for the western (WUS) and central/eastern U.S. (CEUS) are used to determine revised vertical spectra (Section 6.2.2.6.3). The values of kappa for the western and central/eastern U.S. are adopted from NUREG/CR-6728 (McGuire et al. 2001 [DIRS 157510], Section 4.8, Table 4-2), which provides guidelines for revising the regulatory guidance on ground motions for nuclear facilities. The report was authored by three internationally-known individuals in earthquake engineering and seismology assisted by several engineers and seismologists of equal stature. The study was guided along by a Review Panel of experts, tops in their areas of expertise. The report was reviewed by members of the NRC staff as part of the publication process (McGuire et al. 2001 [DIRS 157510], page xlv). The kappa values came originally from the work of Silva and Darragh (1995 [DIRS 105398]), which was supported by the Electric Power Research Institute. . The two values were derived from the analysis of 414 strong motion records. Much of this database is available from the Pacific Earthquake Engineering Research Center's website (http://peer.Berkeley.edu/). The kappa values have been cited or used in studies published in peer-reviewed journals (e.g., Atkinson and Silva 1997 [DIRS 163171]).

The depth distribution of earthquakes in the western U.S. is used to compute incidence angles for control motions serving as model input (Section 6.2.2.5.1). The depth distribution of earthquakes in the western U.S. has been well documented by numerous peer-reviewed scientific journal papers. Example papers that specifically include Nevada are Rogers et al. (1991 [DIRS 106702], pages 166-168) and Smith and Bruhn 1984 [DIRS 170607]). This depth distribution or similar distributions were used by the 18 seismic source experts in the PSHA Project (CRWMS M&O 1998a [DIRS 103731]). The best-estimate, lower and upper-bound point source focal depths are based on an analysis of the western U.S. depth distributions. These values or similar values have been used in several urban, regional, and state hazard maps developed by URS Corporation supported by the U.S. Geological Survey and FEMA (e.g., Wong et al. 2004 [DIRS 170544]). The values have been adopted from Table 6-2 in NUREG/CR 6728, the report discussed above (McGuire et al. 2001 [DIRS 157510]).

Values of recommended vertical-to-horizontal (V/H) spectral ratios are used to determine revised vertical spectra (Section 6.2.2.6.3). The recommended vertical/horizontal spectral ratios for the WUS and CEUS are adopted from Tables 4-4 and 4-5 in NUREG/CR6728 (McGuire et al. 2001 [DIRS 157510]). As described above, this was guided along by a Review Panel of experts, and the report was reviewed by members of the NRC staff. The V/H ratios for the western U.S. are derived by evaluating three state-of-the-art ground motion attenuation relationships. The CEUS ratios are calculated using the well-known stochastic point-source numerical ground motion technique (Silva et al. 1996 [DIRS 110474]). The ratios were also evaluated with respect to the available but sparse CEUS strong motion database. Since these V/H ratios have been made publicly available, they have been used in the earthquake engineering practice.

A generic western U.S. rock velocity profile is used in developing a transfer function applied to western U.S. strong ground motion recordings in the process of spectrally conditioning the time histories to Point A or Point B spectral shape (Section 6.3.2.3.1). The generic western U.S. rock profile was developed from the extensive Pacific Engineering and Analysis database of velocity profiles. The database consists of *in situ* velocity measurements made generally from strong motion instrumentation sites in the U.S. The generic western U.S. profile is presented in the report by Silva et al. (1996 [DIRS 110474]) as described above, which summarizes studies supported by DOE through the Brookhaven National Laboratory. The generic profile has been used by other researchers (e.g., Schneider et al. 1993 [DIRS 110467]).

Response spectral calculations are combined with selected recorded strong ground motion data from a catalog of time histories to produce site-specific time histories for Yucca Mountain locations of interest (Section 6.3.2). These time histories are adopted from NUREG/CR 6728 (McGuire et al. 2001 [DIRS 157510], Appendix B), which has been sponsored and reviewed by the NRC staff and published as a NRC contractor report.

Generic curves for shear modulus reduction and damping as a function of cyclic shear strain are used in developing site-specific curves for Yucca Mountain (Section 6.2.4). These generic curves have been developed by a group of internationally-known experts in geotechnical engineering and reviewed by a panel of experts. The generic curves from EPRI (1993b [DIRS 103320]) have been used by the earthquake engineering community in hundreds of studies, many of which have been published in peer-reviewed journals (e.g., Schneider et al. 1993 [DIRS 110467]).

4.2 CRITERIA

Project requirements are identified in *Project Requirements Document* (TER-MGR-MD-000001) (Canori and Leitner 2003 [DIRS 166275]). The requirements that pertain to this model report and their links to 10 CFR 63 are summarized in Table 4-3.

Table 4-3. Project Requirements Pertaining to the Site-Specific Ground Motion Model

Requirement Number	Title	10 CFR 63 Link
PRD-002/T-004	Content of Application	10 CFR 63.21
PRD-002/T-011	Purpose and Nature of Findings	10 CFR 63.101
PRD-002/P-029	Concepts	10 CFR 63.102
PRD-002/T-012	Performance Objectives for the Geologic Repository Operations Area Through Permanent Closure	10 CFR 63.111
PRD-002/T-013	Requirements for Pre-Closure Safety Analysis of the Geologic Repository Operations Area	10 CFR 63.112
PRD-002/T-015	Requirements for Performance Assessment	10 CFR 63.114

This report addresses criterion PRD-002/T-004 by describing ground motions from earthquakes in the Yucca Mountain region that potentially affect the design of the geologic repository operations area and performance of the geologic repository. It thus provides information needed for a complete description of the site. The results also support characterization of features, events, and processes (FEPs) that might affect performance of a geologic repository. In addition, the report describes how the results of the PSHA for Yucca Mountain, which employed expert elicitation to assess inputs for hazard calculation, are used to develop seismic ground motion inputs.

This report addresses criterion PRD-002/T-011 by describing the technical basis for the range of parameters and variability distributions used in developing seismic inputs for analyses supporting the assessment of performance of a geologic repository.

This report addresses criterion PRD-002/P-029 by providing ground motion inputs that characterize one of the potential hazards and the initiating events that must be evaluated in the Preclosure Safety Analysis. It also addresses this criterion by describing seismic ground motion inputs that are appropriate for analyses supporting assessment of the postclosure performance of a geologic repository at Yucca Mountain, including determination of those features, events, and processes expected to materially affect compliance with postclosure performance objectives. The inputs are based on the results of the PSHA for Yucca Mountain and, thus, reflect the range of earthquakes for the Yucca Mountain site.

This report addresses criterion PRD-002/T-012 by providing ground motion inputs that allow design to take into account seismic-initiated Category 1 and Category 2 event sequences in a manner such that preclosure performance objectives are met.

This report addresses criterion PRD-002/T-013 by providing the site-specific preclosure ground motions needed to analyze naturally occurring hazards at the geologic repository operations area.

This report addresses criterion PRD-002/T-015 by describing ground motion inputs that form part of the information on disruptive initiating events that are used to evaluate the performance of the geologic repository at Yucca Mountain. The report also describes the uncertainties and variability in parameter values that provide input to the development of ground motion inputs and the alternative models evaluated. In addition, the report describes ground motions that can initiate or contribute to events having at least one chance in 10,000 of occurring over

10,000 years. It thus provides information that is used to determine whether features, events, and processes should be included or excluded from the performance assessment and to evaluate seismic effects on the degradation, deterioration, or alteration processes of engineered barriers in the performance assessment. Finally, the report addresses this criterion by providing the technical basis for the site response ground motion model and describes the validation of that model.

Criteria are also provided by the *Yucca Mountain Review Plan, Final Report* (NRC 2003 [DIRS 163274]). Relevant acceptance criteria from this document are:

Acceptance criteria listed in Section 1.5.3 of NRC (2003 [DIRS 163274]) are based on meeting requirements of 10 CFR 63.21(b)(5) [DIRS 156605], which relate to description of site characterization work:

> *1. The "General Information" section of the license application contains an adequate description of site characterization activities.*
>
> *2. The "General Information" section of the license applications contains an adequate description of site characterization results.*

This report addresses Part 1 of criterion 1 and Parts 1 and 2 of criterion 2 by providing ground motion inputs with various annual frequencies of being exceeded that form part of the description of site characterization activities and results.

Acceptance criteria listed in Section 2.1.1.5.1.3 are based on meeting requirements of 10 CFR 63.111(a)(1), (a)(2), (b)(1), (c)(1), and (c)(2) [DIRS 156605], which relate to consequence analysis methodology and meeting radiation protection requirements for normal operations and Category 1 event sequences:

> *1. Consequence analyses adequately assess normal operations and Category 1 event sequences, as well as factors that allow an event sequence to propagate within the Geologic Repository Operations Area.*
>
> *2. Consequence calculations adequately assess the consequences to workers and members of the public from normal operations and Category 1 event sequences.*
>
> *3. The Dose to Workers and Members of the Public From Normal Operations and Category 1 Event Sequences is Within the Limits Specified in 10 CFR 63.111 (a) [DIRS 156605].*

This report provides information that contributes to addressing Part 1 of criterion 1, Parts 1 and 3 of criterion 2, and Part 1 of criterion 3 by providing ground motion inputs for annual frequencies of exceedance of 10^{-3}, 5×10^{-4}, and 10^{-4}.

Acceptance criteria listed in Section 2.1.1.5.2.3 of NRC (2003 [DIRS 163274]) are based on meeting requirements of 10 CFR 63.111(b)(2) and (c) [DIRS 156605], which relate to meeting radiation protection requirements for Category 2 event sequences:

> *1. Consequence analyses include Category 2 event sequences as well as factors that allow an event sequence to propagate within the geologic repository operations area.*
>
> *2. Consequence calculations adequately assess the consequences to members of the public from Category 2 event sequences.*
>
> *3. The dose to hypothetical members of the public from category 2 event sequences is within the limits specified in 10 CFR 63.111(b)(2) [DIRS 156605].*

This report provides information that contributes to addressing Part 1 of criterion 1, Parts 1 and 3 of criterion 2, and Part 1 of criterion 3 by providing ground motion inputs for annual frequencies of exceedance of 10^{-3}, 5×10^{-4}, and 10^{-4}.

Acceptance criteria listed in Section 2.1.1.1.3 of NRC (2003 [DIRS 163274]) are based on meeting requirements of 10 CFR 63.112(c) [DIRS 156605], which relate to the site description as it pertains to Preclosure Safety Analysis:

> *5. The license application contains descriptions of the site geology and seismology adequate to permit evaluation of the preclosure safety analysis and the Geologic Repository Operations Area design.*

This report addresses Part 6 of criterion 5 by providing ground motion inputs forming part of the description of the geology and seismology of the site in support of the preclosure safety analysis and design of the geologic repository operations area. The ground motion inputs are based on results of acceptable methodologies for evaluating seismic hazards at the site.

Acceptance criteria listed in Section 2.1.1.3.3 of NRC (2003 [DIRS 163274]) are based on meeting requirements of 10 CFR 63.112(b) and (d) [DIRS 156605], which relate to identification of hazards and initiating events for preclosure safety analysis:

> *1. Technical basis and assumptions for methods for identification of hazards and initiating events are adequate.*
>
> *2. Site data and system information are appropriately used in identification of hazards and initiating events.*
>
> *3. Determination of frequency or probability of occurrence of hazards and initiating events is acceptable.*
>
> *4. Adequate technical bases for the inclusion and exclusion of hazards and initiating events are provided.*

This report addresses Parts 1, 2, 3, and 4 of criterion 1, Part 1 of criterion 2, Parts 1 and 3 of criterion 3, and Parts 1 and 2 of criterion 4 by providing the technical basis and assumptions for ground motion inputs developed to support design of the geologic repository operations area and the preclosure safety analysis. It describes how site data and other information were appropriately used in developing the inputs, including consideration of uncertainties. It describes how the ground motion inputs are consistent with the ground motion hazard determined by the PSHA for Yucca Mountain. The ground motion inputs provide part of the technical basis for including or excluding ground motion hazards and ground motion initiated events.

Acceptance criteria listed in Section 2.1.1.7.3.2 of NRC (2003 [DIRS 163274]) are based on meeting requirements of 10 CFR 63.112 [DIRS 156605](f), which relate to design of structures, systems, and components important to safety and safety controls:

1. *Geologic repository operations area design methodologies are adequate.*

This report addresses Part 4 of criterion 1 by providing ground motion information that takes into account current guidance and recommendations (e.g., McGuire et al. 2001 [DIRS 157510]) resulting in information that is appropriate for seismic design and for performance assessment.

Acceptance criteria listed in Section 2.2.1.2.2.3 of NRC (2003 [DIRS 163274]) are based on meeting requirements of 10 CFR 63.114 [DIRS 156605](d), which relate to identification of events with probabilities greater than 10^{-8} per year:

1. *Events are adequately defined.*

2. *Probability estimates for future events are supported by appropriate technical bases.*

3. *Probability model support is adequate.*

4. *Probability model parameters have been adequately established.*

5. *Uncertainty in event probability is adequately evaluated.*

This report addresses Parts 1 and 2 of criterion 1, Part 1 of criterion 2, Part 1 of criterion 3, Part 1 of criterion 4, and Part 1 of criterion 5 by describing ground motion inputs that are used to determine frequencies of ground motion initiated events related to the performance of the engineered barrier system and excavated drifts. The ground motion inputs are derived from the ground motion hazard determined by the PSHA for Yucca Mountain. Use of annual mean hazard incorporates uncertainty in the annual frequency of ground motion being exceeded. The report also describes the site response ground motion model and its validation. In addition, the report discusses how inputs to the model were determined and how uncertainties are incorporated and propagated through the analysis.

Acceptance criteria in Section 2.2.1.3.2.3 of NRC (2003 [DIRS 163274]) are based on meeting the requirements of 10 CFR 63.114(a)-(c) and (e)-(g) [DIRS 156605], which relate to mechanical disruption of engineered barriers:

> *2. Data are sufficient for model justification.*
>
> *3. Data uncertainty is characterized and propagated through the model abstraction.*

This report addresses Parts 1 and 3 of criterion 2 and Parts 1, 2, and 3 of criterion 3 by describing the use of data to develop inputs to the site-response analysis and how data uncertainty is incorporated into the analysis. The data uncertainties are incorporated into the site-response model and are propagated to the ground motion time histories, which are used in modeling mechanical disruption of engineered barriers to determine disruptive events for TSPA input.

The *Yucca Mountain Review Plan, Final Report* (NRC 2003 [DIRS 163274]) also provides information on the review methods that are used to assess whether the acceptance criteria have been met. Review methods specifically relevant to the analyses and modeling described in this report are:

Section 2.2.1.2.2.2

Review Method 1 Event Definition

Evaluate whether the definitions for events (potentially beneficial or disruptive), applicable to the Yucca Mountain repository, are unambiguous; probabilities are estimated for the specific event; and event definitions are used consistently and appropriately in probability models.

Confirm that probabilities of intrusive and extrusive igneous events are calculated separately. Verify that definitions of faulting and earthquakes are derived from the historical record, paleoseismic studies, or geological analyses. Confirm that criticality events, for the purpose of initial screening of the features, events, and processes list, are calculated separately, only by location of the criticality event (e.g., in-package, near-field, and far-field).

Review Method 2 Probability Estimates

. . . Verify that probability estimates for future faulting and seismic events have considered past patterns of these events in the Yucca Mountain region. Examine the adequacy and sufficiency of characterization and documentation of past faulting and seismicity in the Yucca Mountain region, since 2 million years ago. This should include characterization of uncertainties in the age, timing, magnitude (i.e., displacements), distribution, size, location, and style of faulting and seismicity. Evaluate whether interpretations of faulting and seismicity from surficial and underground mapping, interpretations of geophysical data, or analog investigations are internally consistent and geologically feasible, so reasonable projections can be made about the probability of future faulting and earthquake-induced ground vibrations at the site.

Review Method 4 Probability Model Parameters

Verify whether the parameters used to calculate the probability of events, applicable to the Yucca Mountain repository, are reasonable, based on data from the Yucca Mountain region or analogous natural systems, and/or design and engineering characteristics of the proposed Yucca Mountain repository system.

. . . Verify whether parameter values used in probabilistic seismic and fault-displacement hazard assessments are adequately supported by Yucca Mountain region faulting and earthquake data or appropriate analogs, so the effects of faulting and seismicity are appropriately factored into repository performance. Verify that parameters are consistent with the range of faulting characteristics and seismicity observed in the Yucca Mountain region, or with parameters derived from representative analogs, and ascertain that the parameters account for variability in data precision and accuracy. For example, confirm that the U.S. Department of Energy adequately evaluated uncertainties in faulting or earthquake activity (i.e., recurrence). Confirm that the U.S. Department of Energy has established reasonable and consistent correlations between parameters, where appropriate. Where sufficient data do not exist, confirm that parameter values and conceptual models are based on appropriate use of other sources, such as expert elicitation, using NUREG–1563 (Kotra et al., 1996 [DIRS 100909]).

Review Method 5 Uncertainty in Event Probability

. . . Verify that probabilities used in the evaluation of faulting and seismicity effects on repository performance include both infrequent seismic and faulting events with relatively large-magnitude ground motions and fault displacements, and the cumulative effects of repeated ground motions or fault displacements from more frequent and lower-magnitude seismic or faulting events.

4.3 CODES, STANDARDS, AND REGULATIONS

There are no codes, standards, or regulations, other than those identified in Section 4.2, pertaining to the work described in this report. However, the following documents published by the NRC provide guidance for developing seismic inputs using the site-response ground motion model. In Section 6 of this report, use of these recommendations and guidance is noted.

- Regulatory Guide 1.165 (1997 [DIRS 119139]), *Identification and Characterization of Seismic Sources and Determination of Safe Shutdown Earthquake Ground Motion*, provides guidance for developing reference earthquakes based on the deaggregation of the probabilistic seismic hazard for Yucca Mountain. This guidance is generally followed, with deviations from the guidance identified and justified.

- NUREG/CR-6728 (McGuire et al. 2001 [DIRS 157510], Sections 4, 5, and 6), *Technical Basis for Revision of Regulatory Guidance on Design Ground Motions: Hazard- and Risk-Consistent Ground Motion Spectra Guidelines*, provides recommendations for developing seismic inputs. Recommendations followed in the work documented in this report include those for determining hazard-consistent response spectra at a soil site (Approach 2B), incorporating magnitude effects on nonlinear site response, developing vertical-component response spectra that are consistent with the horizontal component

and factors affecting vertical-to-horizontal spectral ratios, and spectral matching of seismic time histories.

- NUREG-0800, Section 3.7.1 (NRC 1989a [DIRS 165110]) and Section 3.7.2 (1989b [DIRS 165111]), *Standard Review Plan for the Review of Safety Analysis Reports for Nuclear Power Plants, Design of Structures, Components, Equipment, and Systems.* Section 3.7.1 provides guidance for spectral matching to determine time histories consistent with developed response spectra. Section 3.7.2 provides guidance on soil-structure interaction analyses and development of strain-compatible soil properties to support such analyses.

5. ASSUMPTIONS

No assumptions were made, in the absence of direct confirming data or evidence, to perform the modeling and analyses described in this report. Data limitations are described in Section 6.2.

INTENTIONALLY LEFT BLANK

6. MODEL DISCUSSION

This section describes the site response ground motion model employed for the Yucca Mountain Project. Preclosure design ground motion inputs (5%-damped response spectra and time histories) are required for two locations at the repository: at the depth of the waste emplacement drifts and at the soil sites of the repository surface facilities. Postclosure ground motions (time histories) also are required at the depth of the waste emplacement drifts. In addition, 3D dynamic strains and curvatures, peak ground acceleration and velocity are required as a function of depth between the surface and the waste repository level. Consequently, the effects of site response must be accounted for in the design of the waste repository.

An overview of site effects on earthquake ground motions, history of the engineering approach and issues related to the determination of site effects is contained in EPRI (1993a [DIRS 103319], Section 6). Near-surface rock and soil materials generally cause an increase of seismic wave amplitude due to a decrease in material velocity near the surface. In an elastic system, the wave amplitude increases with decreasing wave velocity and this increase can be compensated by material damping in the layers. Resonance also occurs in soil and rock layers and between the surface and the soil/bedrock interface and resonance frequency and amplitude are affected by material damping.

Linear 1D modeling of site response for weak ground motions has had a long history of success. At low shear strain levels (less than 10^{-2}%), linear constitutive relationships have been demonstrated to be appropriate to model site response in both soil and rock (Seed and Idriss 1970 [DIRS 103324], Rogers et al. 1979 [DIRS 163653], Joyner et al. 1976 [DIRS 163522], Hays et al. 1979 [DIRS 163515], Johnson and Silva 1981 [DIRS 110447], Joyner et al. 1981 [DIRS 157285], Rogers et al. 1984 [DIRS 163652], Tucker and King 1984 [DIRS 163181], Chang et al. 1986 [DIRS 163449]). Modeling strong ground motions requires assessments of material property strain dependency. Laboratory measurements of soil and rock samples exhibit nonlinear behavior under loading conditions (clearly for strains greater than about 10^{-2}%). Strain dependency of soil sample material properties is universally observed and repeatable in the laboratory. Field evidence of material nonlinearity is evident in the modeling of site response from strong ground motion (EPRI 1988 [DIRS 107489; Silva et al. 1989 [DIRS 163187]; Chang et al. 1990 [DIRS 163450]; EPRI 1993b [DIRS 103320], Appendix 6.B; Silva et al. 1996 [DIRS 110474]).

This section describes the site-response ground motion model, including its conceptual and mathematical basis. The section also addresses alternative conceptual models for site-response calculation. The section describes the development of model inputs, how uncertainties in the inputs are incorporated, and how the site response results are used to develop earthquake ground motion inputs (response spectra, strain-compatible soil properties, time histories) that are needed for preclosure design analyses and for postclosure performance analyses. The section also addresses the relation between the developed ground motion inputs and seismic-related features, events, and processes. Finally, ground motions from potential basalt-dike related maximum magnitude earthquakes are described.

6.1 RVT-BASED EQUIVALENT-LINEAR SITE RESPONSE APPROACH

To compute the ground motion inputs for preclosure and postclosure analyses, the results of the PSHA (i.e., the motions at Point A) are modified using a site response model. The conventional approach to estimating the effects of local shallow rock and soil on strong ground motions involves development of a set (1-, 2-, or 3-component) of time histories compatible with the specified outcrop response spectra to serve as control (or input) motions. The control motions are then used to drive a nonlinear computational formulation to transmit the motions through the site profile. Simplified analyses generally assume vertically propagating shear (S)-waves for horizontal components and vertically propagating compression (P)-waves for vertical motions.

Control motions at the reference rock outcrop level (Point A) are specified using ground motion predictions based on the attenuation models employed in the hazard assessment. Earthquake magnitudes and distances needed to develop the control motions are taken from the hazard deaggregation at the appropriate rate of exceedance. Source-to-site paths and angles of incidence at the control motion depth are established using ray tracing techniques.

6.1.1 Model Description

The computational formulation that has been most widely employed to evaluate 1D site response assumes vertically-propagating plane S-waves. Departures of soil response from a linear constitutive relation are treated in an approximate manner through the use of the equivalent-linear formulation .

The equivalent-linear formulation, in its present form, was introduced by Idriss and Seed (1968 [DIRS 163520]). It is a particular application of the general equivalent-linear theory developed by Iwan (1967 [DIRS 110379]). Basically, the approach is to approximate a second-order nonlinear equation, over a limited range of its variables, by a linear equation. Formally this is done in such a way that the average of the difference between the two systems is minimized. This was done in an ad-hoc manner for ground motion response modeling by defining an effective strain that is assumed to exist for the duration of the excitation. This value is typically taken as 65% of the peak time-domain strain calculated at the midpoint of each layer, using a linear analysis. Shear modulus reduction and hysteretic damping curves are then used to define new parameters for each layer based on the effective strain computations. The linear response calculation is repeated, new effective strains evaluated, and iterations continue until the changes in parameters are below an established tolerance level. Generally a few iterations are sufficient to achieve a strain-compatible linear solution.

This stepwise analysis approach was formalized into a 1D, vertically propagating S-wave code called SHAKE (Schnabel et al. 1972 [DIRS 103323]). Subsequently, this code has become the most widely used and validated analysis package for 1D site response calculations.

The advantages of the equivalent-linear formulation are that parameterization of complex nonlinear soil models is avoided and the mathematical simplicity of a linear analysis is preserved. (Limitations are discussed in Section 6.1.14.) A truly nonlinear approach requires the specification of the shapes of hysteresis curves and their cyclic dependencies through an increased number of material parameters. In the equivalent-linear methodology the soil data are

utilized directly and, because at each iteration the problem is linear and the material properties are frequency independent, the damping is rate independent and hysteresis loops close.

Careful validation exercises between equivalent-linear and fully nonlinear formulations using recorded motions (peak horizontal acceleration) from 0.05 to 0.5 g showed little difference in results (Sections 7.3.2 and 7.3.5). Both formulations compared favorably to recorded motions suggesting both the adequacies of the vertically propagating S-wave model and the approximate equivalent-linear formulation. While the assumptions of vertically propagating S-waves and equivalent-linear soil response represent approximations to actual conditions, their combination has achieved demonstrated success in modeling observations of site effects and represent a stable, mature, and reliable means of estimating the effects of site conditions on strong ground motions (Schnabel et al. 1972 [DIRS 103323]; EPRI 1988 [DIRS 107489]; Schneider et al. 1993 [DIRS 110467]; EPRI 1993b [DIRS 103320], Appendix 6.B).

A consequence of the equivalent-linear formulation is the preservation of the superposition principle. For linear systems this principle permits, among other things, spectral decomposition and frequency-domain solutions such as the propagator matrix solution scheme (Haskell 1960 [DIRS 163513], Schnabel et al. 1972 [DIRS 103323], Silva 1976 [DIRS 103326]) for efficient frequency-domain solutions of the wave equation. The superposition principle then permits a spectral recomposition of the wavefields (sum over frequencies) through an inverse Fourier or Laplace transform. A nonsubtle result of this is that the deconvolution process, that of propagating the control motion down rather than up, results in a unique solution (EPRI 1988 [DIRS 107489], Section 3). That is, for a given motion at the surface, within an equivalent-linear framework there is only one input motion (solution). In reality, of course, if the soils are behaving in a nonlinear fashion and have degraded, many different input motions at the base of the soil could have resulted in a similar surface response.

Both the RASCALS code (including RASCALP, the P-wave version of the code), which has been implemented in this study, and the SHAKE code represent an implementation of the equivalent-linear formulation of Seed and Idriss (1969 [DIRS 163655]) applied to 1D site response analyses. The RASCALS code is an RVT-based equivalent-linear approach, which propagates an outcrop (control motion) power spectral density through a 1D soil column. RVT is used to predict peak time domain values of shear strain based upon the shear-strain power spectrum. In this approach, the control motion power spectrum is propagated through the 1D rock/soil profile using the plane-wave propagators of Silva (1976 [DIRS 103326]). Both P-SV (vertically polarized S-wave) and SH (horizontally polarized S-wave) waves are included in the analysis and have specified angles of incidence.

6.1.2 Documentation

The most thorough documentation of the RASCALS site response methodology is contained in EPRI (1993b [DIRS 103320], Appendix 6B) and Silva et al. (1996 [DIRS 110474]). Additional related or supporting documentation is found in Silva (1976 [DIRS 103326]) for wave propagation in a layered anelastic medium, Schnabel et al. (1972 [DIRS 103323]) for the equivalent-linear formulation and Boore (1983 [DIRS 103317]) for the RVT methodology.

6.1.3 Uncertainties

As discussed in Section 6.1.8.2, the mathematical formulation used in the site response model is exact in its computation of motions for a given set of input parameters. Accuracy of results in the context of how well the model captures observed effects of site conditions on strong ground motions are assessed in the model validation (Section 7). Limitations and appropriateness of the model are discussed in Section 6.1.14.

The uncertainties of the input into the site response model are discussed in Section 6.2.

6.1.4 Consideration of Alternative Conceptual Models

Alternative models considered for site response analyses include fully nonlinear as well as 2D and 3D models (see the discussion given below and in Section 7). The advantage of the equivalent-linear formulation over fully nonlinear formulations is that parameterization of complex nonlinear soil or rock models is avoided and the mathematical simplicity of a linear analysis is preserved. A truly nonlinear computation requires the specification of the shapes of hysteresis curves and their cyclic dependencies through an increased number of material parameters.

2D and 3D formulations accommodate explicit treatment of lateral variability in dynamic material properties as well as topographic effects. Implementation of these formulations require detailed knowledge of vertical and lateral variations of material properties and result in a site response that is spatially varying. Additionally the wavefields developed within 2D and 3D models depend strongly upon the azimuth and depth of the source, contributing to the variability of the site response. Demands on site characterization, treatment of random variability (within a 2D or 3D deterministic variation) in dynamic material properties, and the effects of source azimuth on response have made it difficult to consider 2D and 3D analyses in an unambiguous manner for engineering design. While it is accepted that 2D and 3D effects are present at all sites to some extent, validations have demonstrated that simple 1D models accommodate the significant and stable features of site response (Silva et al. 1996 [DIRS 110474], Silva et al. 1990 [DIRS 163660], Section 7). Site-specific variations from simple 1D response due to laterally varying dynamic material properties over the site are accommodated through multiple 1D analyses using randomized parameters (Sections 6.2.3.5 and 6.2.4.5). Accommodation of random 2D and 3D variations in dynamic material properties for generic site conditions is present in the rock outcrop UHS as computed in the PSHA (see Section 6.1.6 for additional discussion).

6.1.4.1 Equivalent-Linear (SHAKE)

The equivalent-linear model SHAKE is similar in many ways to RASCALS. SHAKE is described in Schnabel et al. (1972 [DIRS 103323]) as follows: Program SHAKE computes the responses in a system of homogenous, viscoelastic layers of infinite horizontal extent subjected to vertically traveling S-waves. The program is based on the continuous solution to the wave equation adapted for use with transient motions through the Fast Fourier Transform algorithm (Cooley and Tukey 1965 [DIRS 163452]). The nonlinearity of the shear modulus and damping is accounted for by the use of equivalent-linear soil properties (Idriss and Seed 1968 [DIRS

163520], Seed and Idriss 1970 [DIRS 103324]) using an iterative process to obtain values for modulus and damping compatible with the effective strains in each layer.

6.1.4.2 Nonlinear Approaches

The two main components of nonlinear analyses are a solution (integration) scheme for the wave equation and a nonlinear material model. Nonlinear wave propagation techniques utilize finite-element schemes (Day 1982a [DIRS 164685], 1982b [DIRS 164684]), implicit or explicit finite-difference schemes (Joyner and Chen 1975 [DIRS 163521]), or the method of characteristics (Streeter et al. 1974 [DIRS 163661]). One approach incorporates a general nonlinear soil model into an explicit finite difference approach that retains second-order terms (EPRI 1978 [DIRS 163669], EPRI 1981 [DIRS 163607]).

Nonlinear soil models that have been primarily developed from laboratory test results and utilized in dynamic analyses, include the Ramberg-Osgood model (Streeter et al. 1974 [DIRS 163661]), an elasto-plastic model (Richart 1975 [DIRS 163651]), Iwan-type model (Joyner and Chen 1975 [DIRS 163521], Taylor and Larkin 1978 [DIRS 163663], EPRI 1978 [DIRS 163669]), and the hyperbolic model (Hardin and Drnevich 1972b [DIRS 163511], Pyke 1979 [DIRS 163612]).

Each of the nonlinear models mentioned has certain limitations and advantages in describing the response of soils to the type of loading produced by seismic disturbances. An effort has been made in some models to predict permanent deformations, while others have included pore pressure buildup and dissipation. Strain dependency of material properties from laboratory data is universally observed.

Section 7 summarizes comparisons of several nonlinear modeling codes including DESRA, SUMDES, and TESS, with RASCALS (EPRI 1993b [DIRS 103320], Appendix 6.B). Comparisons are made of these formulations in modeling strong ground motion at sites where nonlinear soil behavior was clearly observed. Based on these comparisons, it is concluded that the 1D equivalent-linear formulation accurately predicts the effects of site conditions on strong ground motions for most applications.

6.1.5 Description of Input

Inputs to the model, as implemented in the software codes RASCALS and RASCALP, are as follows:

- Location of input and output motions within the site profile.
- Input (control) motions characterized by earthquake response spectra and corresponding power spectra.
- Incidence angles of input motion.
- A representation of the rock and soil at the site, consisting of homogeneous layers with specified thickness, seismic velocity, and density.

- A representation of the dynamic material properties of the rock and soil at the site, consisting of strain-dependent shear modulus and damping for each layer.

Section 6.2 describes the development of specific values for these inputs. Specifically, control motions and incidence angles are discussed in Section 6.2.2, velocity profiles and densities in Section 6.2.3, and dynamic material properties in Section 6.2.4. Use of these inputs in subsequent modeling and analyses is described in Section 6.3.

6.1.6 Assumptions, Idealizations, and Simplifications

The RVT-based equivalent-linear site-response model uses two key simplifications to represent the physical processes of ground motion propagation and nonlinear dynamic behavior of site materials.

- Seismic wave propagation is treated as a 1D problem. The soil/rock medium making up the site is represented as a series of horizontally infinite plane layers. Dynamic material properties are constant within each layer and smooth gradient depth profiles are characterized by a sequence of thin layers. shear-wave velocity (V_S), compression-wave velocity (V_P), density, thickness, and strain-dependent shear modulus and damping values define the properties for each layer.

By definition, the use of a 1D simplification means that 2D and 3D effects, such as from dipping structure and topography, are not explicitly addressed as part of the site response. However, consistent with the current state-of-practice, 2D and 3D effects are implicitly included in the modeling through the control motions derived from the PSHA results. Empirical ground motion attenuation relations formed a key input to the ground motion component of the PSHA. These relations reflect the 1D, 2D and 3D site effects associated with the recorded data on which they are based. The attenuation relations do not explicitly address such 2D and 3D effects separately, but rather include them as part of the random variation of ground motion. Thus, evaluations by the PSHA ground motion experts included 2D/3D effects as part of the random or aleatory component of ground motion variability.

- Nonlinear behavior of the site medium under dynamic loading is treated with an equivalent-linear approximation. This formulation relies on the ability of the approximation to capture the effects of material nonlinearity on peak values of motions (Section 6.1.3).

The adequacy of these approximations in developing site response spectra is discussed in Section 6.1.14 and is addressed in Section 7.

While some or all of these factors are generally present in observations of site response, the 1D model for site response has been demonstrated to be a valid approach for determining median site response. The motivation for validation exercises involving several site conditions is to capture unmodeled effects. The unmodeled effects that are random are captured in estimates of model uncertainty and those that are pervasive are captured in the estimates of model bias (Section 7).

The effective strain of 65% of the peak time domain strain adopted as the standard value used in SHAKE is also used in RASCALS. Other assumptions associated with the RVT equivalent-linear site response model as implemented in these analyses are discussed in subsequent sections of this report (e.g., Section 6.1.8.1).

6.1.7 Initial and/or Boundary Conditions

Initial conditions are the low-strain material properties of the soil/rock column including V_S and V_P, corresponding low-strain damping, and density. These material properties are defined through site geotechnical and geophysical investigations discussed in Section 6.2.

Actual boundary conditions used in the mathematical formulation (Section 6.1.8) are continuity of displacements as well as shear and normal stresses at layer boundaries and vanishing of shear stress at a free surface (Aki and Richards 1980 [DIRS 150723], Section 5.2.1).

6.1.7.1 Development of Control Motions

Control motions (power spectral density) must be calculated for input into the site response analysis that are representative of the earthquake magnitude and distance dominating the hazard at the desired rate of exceedance. The basis for the control motions are the magnitude and distances specified by the hazard deaggregation and their response spectral shape based on the ground motion attenuation models used in the PSHA. For each control motion, spectral matching is used to develop the input power spectrum. Spectral matching as implemented in this study is a procedure by which the power spectral density is developed based on the suite of input parameters (e.g., magnitude and distance). This computed power spectral density and the corresponding response spectrum are spectrally matched to the given target response spectrum. The control motion is then input at the appropriate profile depth consistent with the outcrop layer velocity used in the development of the PSHA.

6.1.8 Mathematical Formulation

The following describes the mathematical formulation of the RVT equivalent-linear site response model.

6.1.8.1 Propagation of Plane Waves

Plane-wave propagator matrices (Silva 1976 [DIRS 103326]) are used to propagate seismic energy through the profile. Silva (1976 [DIRS 103326]) extended the Haskell-Thompson matrix method to include the effect of anelasticity in an exact fashion. The methodology incorporates any number of layers, for P-SV and SH plane waves at arbitrary incidence angles. Damping is incorporated in each layer without approximation.

Following Silva (1976 [DIRS 103326]), the most general form of a linear constitutive relation is Boltzman's superposition principle, which, written in terms of the tensorial relaxation function $r(t)$, is

$$P_{ij}(t) = \int_{-\infty}^{t} r_{ijkl}(t-\tau)\, d\varepsilon_{kl}(\tau)$$
$$= r_{ijkl}(t) * d\varepsilon_{kl}(t) \qquad \text{(Eq. 1)}$$

where $P_{ij}(t)$ and $\varepsilon_{ij}(t)$ are the time-dependent stress and strain tensors and the symbol * denotes the Stieltjes convolution.

Assuming the medium to be isotropic and homogeneous, Eq. (1) may be broken up into bulk and shear components and written as

$$P_{ij}(t) = 2\mu(t) * d\varepsilon_{ij}(t) \qquad i \neq j$$
$$P_{kk}(t) = 3\kappa(t) * d\varepsilon_{kk}(t) \qquad \text{(Eq. 2)}$$

where $\mu(t)$ and $\kappa(t)$ are the relaxation functions in shear and bulk. Assuming that the particle displacements u_i are infinitesimal, the strain can be written

$$\varepsilon_{ij} = \tfrac{1}{2}[u_{i,j} + u_{j,i}] \qquad \text{(Eq. 3)}$$

and, neglecting body forces, the linear momentum equation is

$$P_{ij,j}(t) = \rho \ddot{u}_i \qquad \text{(Eq. 4)}$$

where ρ is the medium density. Substituting Eq. (2) into Eq. (4) yields the equation of motion.

$$[\kappa(t) + \tfrac{4}{3}\mu(t)] * [\nabla(\nabla \cdot d\mathbf{u})] - [\mu(t) * [\nabla \times (\nabla \times d\mathbf{u})] = \rho \ddot{\mathbf{u}}. \qquad \text{(Eq. 5)}$$

Since the convolutions make the time-domain representation quite intractable, it is customary to take the Fourier transform of Eq. (5). Restated in terms of transformed variables, Eq. (5) becomes

$$[\bar{\kappa} + \tfrac{4}{3}\bar{\mu}]\nabla(\nabla \cdot \bar{\mathbf{u}}) - [\bar{\mu}]\nabla \times (\nabla \times \bar{\mathbf{u}}) = -\rho\omega^2 \bar{\mathbf{u}} \qquad \text{(Eq. 6)}$$

Where

$$\bar{\kappa} = i\omega \int_{-\infty}^{\infty} \kappa(t) e^{-i\omega t}\, dt, \qquad \bar{\mu} = i\omega \int_{-\infty}^{\infty} \mu(t) e^{-i\omega t}\, dt$$
$$\bar{\mathbf{u}} = \int_{-\infty}^{\infty} \mathbf{u} e^{i\omega t}\, dt. \qquad \text{(Eq. 7)}$$

At this point it is convenient to introduce the transformed P-wave and S-wave displacement potentials in terms of Helmholtz's relation

$$\bar{\mathbf{u}} = \nabla\bar{\phi} + \nabla \times \bar{\boldsymbol{\psi}}, \qquad \nabla \cdot \bar{\boldsymbol{\psi}} \equiv 0. \qquad \text{(Eq. 8)}$$

Substituting Eq. (8) into Eq. (6) results in the Helmholtz equations for the *P* and *S* potentials $\bar{\phi}$ and $\bar{\psi}$.

$$[\nabla^2 + K_P^2]\bar{\phi} = 0, \qquad [\nabla^2 + K_S^2]\bar{\psi} = 0 \tag{Eq. 9}$$

where

$$K_P^2 = \frac{\omega^2}{\bar{\alpha}^2} = \omega^2 \frac{\rho}{\bar{\kappa}(\omega) + \frac{4}{3}\bar{\mu}(\omega)}$$
$$K_S^2 = \frac{\omega^2}{\bar{\beta}^2} = \omega^2 \frac{\rho}{\bar{\mu}(\omega)}. \tag{Eq. 10}$$

Note that the terms $\bar{\alpha}^2$ and $\bar{\beta}^2$ are in general frequency-dependent in both real and imaginary parts.

6.1.8.2 Medium Parameterization

Consider, for demonstration purposes, the case of S-waves. A general solution for $\bar{\psi}$ in Eq. (9) is

$$\bar{\psi} = \bar{\psi}(\omega) \exp(-i\mathbf{K}_S \cdot \mathbf{X}) \tag{Eq. 11}$$

where $\mathbf{K}_S$ is a complex vector with the real and imaginary parts having different directions in general.

$$\mathbf{K}_S = \mathbf{P}_S - i\mathbf{A}_S \tag{Eq. 12}$$
$$K_S^2 = \mathbf{K}_S \cdot \mathbf{K}_S = |P_S|^2 - |A_S|^2 - i2\mathbf{P}_S \cdot \mathbf{A}_S \tag{Eq. 13}$$
$$\mathbf{P}_S \cdot \mathbf{A}_S = |\mathbf{P}_S| \, |\mathbf{A}_S| \cos(\gamma_s). \tag{Eq. 14}$$

$\mathbf{P}_S$ is the propagation vector such that $\omega/|\mathbf{P}_S|$ is the phase velocity and $\mathbf{A}_S$ the attenuation vector such that $\exp(-\mathbf{A}_S \cdot \mathbf{X})$ represents the spatial decay of the potential. The nonzero γ_s gives rise to the inhomogeneous waves (Borcherdt 1973 [DIRS 163176], Buchen 1971 [DIRS 163348], Lockett 1962 [DIRS 163528]) whose amplitude varies (monotonically) along a wave front. It becomes necessary now to specify the three parameters $|\mathbf{P}_S|$, $|\mathbf{A}_S|$, and γ_s in terms of material properties and medium geometry.

Writing the transformed shear modulus $\bar{\mu}(\omega)$ in Eq. (10) in terms of a real part, $\bar{\mu}_R(\omega)$, and an imaginary part, $\bar{\mu}_I(\omega)$, the quality factor Q_S for S-waves is defined as

$$Q_S^{-1} = \frac{\bar{\mu}_I(\omega)}{\bar{\mu}_R(\omega)} = \frac{1}{2\pi} \frac{\Delta E}{E} \tag{Eq. 15}$$

where E is the peak energy density stored and ΔE is the energy lost, both per cycle (Borcherdt 1973 [DIRS 163176]). K_S^2 may be written in the following form

$$K_S^2 = \frac{\omega^2}{v_s^2} \frac{2}{1+\sqrt{1+Q_S^{-2}}} \left(1 - \frac{i}{Q_S}\right) \quad \text{(Eq. 16)}$$

where v_s is the homogeneous wave velocity of the medium. Using Eq. (16) to invert Eq. (13) and Eq. (14), convenient expressions for $|\mathbf{P}_S|$ and $|\mathbf{A}_S|$ are derived

$$|\mathbf{P}_S|^2 = \frac{\omega^2}{v_s^2} \frac{1}{1+\sqrt{1+Q_S^{-2}}} (1+\sqrt{1+Q_S^{-2}\cos^{-2}(\gamma_s)}) \quad \text{(Eq. 17)}$$

$$|\mathbf{A}_S|^2 = \frac{\omega^2}{v_s^2} \frac{1}{1+\sqrt{1+Q_S^{-2}}} (-1+\sqrt{1+Q_S^{-2}\cos^{-2}(\gamma_s)}) \quad \text{(Eq. 18)}$$

with similar expressions for P waves using the P parameters. In the low-loss approximation for homogeneous waves ($\gamma_s = 0$, $Q_s >> 1$) Eq. (18) reduces to the expression

$$|\mathbf{A}| = \frac{\omega}{2 v_s Q_S}. \quad \text{(Eq. 19)}$$

When dealing with highly dissipative materials, the vectoral nature of **A** must be considered. The problem is that for a given incident wave (direction of both **P** and **A** specified) onto a plane boundary between two viscoelastic media, the direction of both P and A must be determined for the P and SV reflected and transmitted waves. These directions can be uniquely determined by applying the usual boundary conditions at a welded interface (or free surface for half-space problems). This results in an extended form of Snell's law in that A_x as well as P_x must be continuous (Borcherdt 1973 [DIRS 163176], Lockett 1962 [DIRS 163528]).

6.1.8.3 Extensions of the Haskell-Thompson Formulation for Layered Media

The following development follows closely that of Haskell (1953 [DIRS 151232], 1962 [DIRS 163514]), although displacement potentials are used here. Referring to Figure 6.1-1 for coordinate reference, the solutions to Eq. (9) can be written in the form

$$\bar{\phi} = [A_p \exp(iK_{Pz}Z) + B_p \exp(-iK_{Pz}Z)] \exp(-iK_{Px}X)$$

$$\bar{\psi} = \bar{\psi}_v = [A_S \exp(iK_{Sz}Z) + B_S \exp(-iK_{Sz}Z)] \exp(-iK_{Sx}X) \quad \text{(Eq. 20)}$$

where A, B are complex and, in general, frequency-dependent amplitudes. From Eq. (12)

$$K_z = P_z - iA_z; \quad K_x = P_x - iA_x. \quad \text{(Eq. 21)}$$

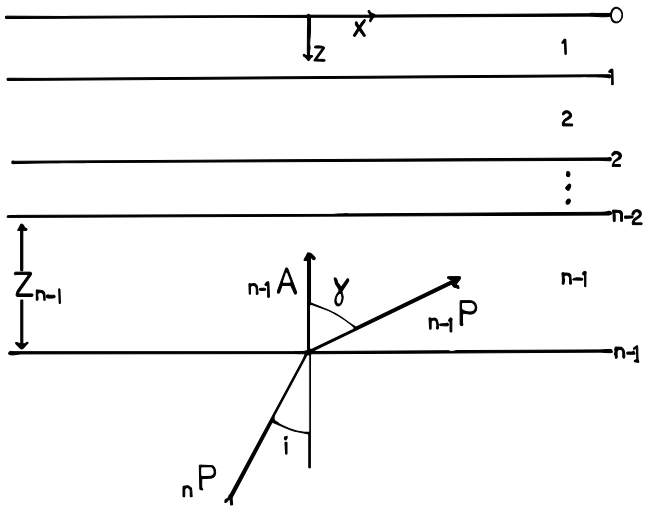

Source: Silva 1976 [DIRS 103326], Figure 1

NOTE: The problem is uniquely specified given V_P, V_S, Q_P, Q_S, ρ, and Z for each layer and given ${}_nA_{P,S}$ (incident *P*- or *S*-wave potential amplitude) in the elastic half-space. For an anelastic half-space, the direction of the incident-wave attenuation vector must also be specified.

Figure 6.1-1. Illustration of Layered Half-Space and P-Wave Propagation

In the simple case, it is considered that $A_x \equiv 0$ (incident elastic wave), and from the boundary conditions A_x must be zero everywhere. Thus K_x remains a real quantity. If the incident medium were anelastic, the incident attenuation direction would have to be specified along with the propagation direction, and then A_z in each layer would adjust itself to be consistent with a continuous A_x and a specified $\boldsymbol{K}^2_{P,S}$ for that layer (see Eq. 16). Choosing A_P and A_S as upgoing potentials (negative z direction) for each layer

$$K_z = \text{principal value } (K^2 - K_x^2)^{1/2}. \qquad \text{(Eq. 22)}$$

Using Eq. (2), (4), (8), and (20), the displacements and stresses for layer m can be put in the following matrix form

$$\begin{bmatrix} u \\ w \\ P_{zx} \\ P_{zz} \end{bmatrix}_m = \begin{bmatrix} -iK_{Px}C_P & K_{Sz}S_S & K_{Px}S_P & -iK_{Sz}C_S \\ -K_{Pz}S_P & -iK_{Sx}C_S & iK_{Pz}C_P & K_{Sx}S_S \\ i2\bar{\mu}K_{Px}K_{Pz}S_P & -\bar{\mu}\Omega C_S & 2\bar{\mu}K_{Pz}K_{Px}C_P & -i\bar{\mu}\Omega S_S \\ \bar{\mu}\Omega C_P & i2\bar{\mu}K_{Sz}K_{Px}S_S & i\bar{\mu}\Omega S_P & 2\bar{\mu}K_{Sz}K_{Sx}C_S \end{bmatrix}_m \times \begin{bmatrix} A_P + B_P \\ A_S + B_S \\ A_P - B_P \\ A_S - B_S \end{bmatrix}_m \qquad \text{(Eq. 23)}$$

where

$$C_P = \mathrm{Cos}\,(K_{Pz} Z_m) \qquad C_S = \mathrm{Cos}\,(K_{Sz} Z_m)$$
$$S_P = \mathrm{Sin}\,(K_{Pz} Z_m) \qquad S_S = \mathrm{Sin}\,(K_{Sz} Z_m).$$
$$\Omega = K_{Px}^2 - K_{Sz}^2 \qquad \text{(Eq. 24)}$$

The result can be conveniently written as

$$X_m = D_m(Z_m) C_m. \qquad \text{(Eq. 25)}$$

Thus Z_m (layer thickness) is the phase factor that propagates the potentials across the mth layer and that D_m may be thought of as a form of propagator matrix with C_m the coefficient matrix. With this in mind and with the idea of eliminating C_m, it can be written (Haskell 1953 [DIRS 151232])

$$X_{m-1} = D_m(0) C_m; \qquad C_m = D_m^{-1}(0) X_{m-1}. \qquad \text{(Eq. 26)}$$

Then applying the usual boundary conditions

$$\begin{aligned} X_m &= (D_m(Z_m) D_m^{-1}(0))(D_{m-1}(Z_{m-1}) D_{m-1}^{-1}(0)) X_{m-2} \\ &= a_m a_{m-1} \ldots a_1 X_0. \end{aligned} \qquad \text{(Eq. 27)}$$

and for $n - 1$ layers where layer n is anelastic half-space and interface 0 is a free surface

$$\begin{aligned} C_n &= D_n^{-1}(0) a_{n-1} a_{n-2} \ldots a_1 X_0 \\ &= J X_0 \end{aligned} \qquad \text{(Eq. 28)}$$

with the following matrix elements.

$$(-{}_m K_S^2) D_m(0)^{-1} = \begin{bmatrix} -2iK_{Px} & 0 & 0 & 1/\bar{\mu} \\ 0 & -i2K_{Px} & -1/\bar{\mu} & 0 \\ 0 & -i\Omega/K_{Pz} & -K_{Px}/(\bar{\mu} K_{Pz}) & 0 \\ i\Omega/K_{Sz} & 0 & 0 & -K_{Px}/(\bar{\mu} K_{Sz}) \end{bmatrix}_m \qquad \text{(Eq. 29)}$$

$$X_0 = \begin{bmatrix} u_0 \\ w_0 \\ 0 \\ 0 \end{bmatrix} \qquad C_n = \begin{bmatrix} A_P + B_P \\ A_S + B_S \\ A_P - B_P \\ A_S - B_S \end{bmatrix} \qquad \text{(Eq. 30)}$$

The elements of

$$(-{}_mK_S{}^2)a_m$$

are given by

$$\begin{aligned}
a_{11} &= \Omega C_S - 2K_{Px}^2 C_P \\
a_{12} &= -iK_{Px}[2K_{Sz}S_S + (\Omega/K_{Pz})S_p] \\
a_{13} &= -\bar{\mu}^{-1}[K_{Sz}S_S + (K_{Px}^2/K_{Pz})S_p] \\
a_{14} &= -iK_{Px}\bar{\mu}^{-1}[C_P - C_S] \\
a_{21} &= iK_{Px}[2K_{Pz}S_P + (\Omega/K_{Sz})S_S] \\
a_{22} &= \Omega C_P - 2K_{Px}^2 C_S \\
a_{23} &= a_{14} \\
a_{24} &= -\bar{\mu}^{-1}[K_{Pz}S_P + (K_{Px}^2/K_{Sz})S_S] \\
a_{31} &= \bar{\mu}[4K_{Px}^2 K_{Pz}S_P + (\Omega^2/K_{Sz})S_S] \\
a_{32} &= -i2\bar{\mu}K_{Px}\Omega[C_P - C_S] \\
a_{33} &= a_{11} \\
a_{34} &= a_{21} \\
a_{41} &= a_{32} \\
a_{42} &= \bar{\mu}[4K_{Px}^2 K_{Sz}S_S + (\Omega^2/K_{Pz})S_P] \\
a_{43} &= a_{12} \\
a_{44} &= a_{22}.
\end{aligned} \qquad \text{(Eq. 31)}$$

C_n therefore becomes the input matrix and choosing $A_{P,S}$ in the upgoing (– z) direction and considering incident P, Eq. (28) can be inverted to give the surface displacements u_o and w_o in terms of the incident potential ($_nA_p$), K_x, and the layering.

$$\begin{aligned}
u_0 &= -2[J_{22} + J_{42}]_n A_p/R \\
w_0 &= 2[J_{21} + J_{41}]_n A_p/R \\
R &= [J_{21} + J_{41}][J_{12} + J_{32}] - [J_{22} + J_{42}][J_{11} + J_{31}].
\end{aligned} \qquad \text{(Eq. 32)}$$

6.1.8.4 Application of RVT

In order to compute peak time-domain values, i.e., peak acceleration, peak particle velocity, and oscillator response, RVT is used to relate root-mean-square (rms) computations to peak value estimates. Boore (1983 [DIRS 103317]) and Boore and Joyner (1984 [DIRS 163174]) present an excellent development of the RVT methodology as applied to the stochastic ground motion model.

As illustrated by Boore (1983 [DIRS 103317]), the RVT formulation is computationally efficient for obtaining estimates of peak ground motion parameters corresponding to a specified amplitude spectrum. The amplitude spectrum is generally based on the Brune (1970 [DIRS 103315]) source spectrum, which represents part of the deterministically derived amplitude spectrum. In addition to the seismic moment and source spectrum, the amplitude spectrum also contains path and site factors.

The RVT approach to estimate peak motions is based on the analysis of stationary time series. Relationships between the expected peak motions in a stationary time series are related to moments of the energy density spectrum and the number of extrema in the time interval. The approach involves computing the rms value by integrating the power spectrum from zero frequency to the Nyquist frequency and applying Parseval's relation. Extreme value theory is then used to estimate the expected ratio of the peak value to the rms value of a specified duration of the stochastic time history. The duration is taken as the inverse of the source corner frequency (Boore 1983 [DIRS 103317]). This approach was used by Boore (1983 [DIRS 103317]) and Hanks and McGuire (1981 [DIRS 163510]) to estimate peak ground acceleration and other peak time domain values. Boore (1983 [DIRS 103317]) has shown that RVT is a good approximation except for simulations where N, the number of extrema in a time interval T, is very small or when successive peaks are highly correlated. For these cases, analytical and empirical (Boore and Joyner 1984 [DIRS 163174], Boore 2003 [DIRS 163706]) correction factors have been developed to provide estimates of oscillator response. A combination of both types of correction factors are used in RASCALS.

To compute the soil and rock response, an RVT-based equivalent-linear formulation is used, in which an outcrop power spectral density is propagated through a 1D column. RVT is used to predict peak time domain values. In this sense, the approach is analogous to SHAKE (Schnabel et al. 1972 [DIRS 103323]) except that peak shear strains in SHAKE are measured in the time domain. The purely frequency domain approach obviates the need for a time domain control motion and eliminates the need for a suite of analyses based on different input motions. This arises because each time domain analysis may be viewed as one realization of a random process. In this case, several realizations of the random process must be sampled to have a statistically stable estimate of site response. The realizations are usually performed by employing different control motions whose response spectra match a specified target. In contrast, stable estimates of site response can be rapidly computed using RVT permitting statistically significant estimates of uncertainties based on parametric variations.

6.1.9 Average Horizontal Component from Vertical and Inclined SH-Waves

Determination of the average horizontal-component ground motion requires a careful description of the control motions, which include magnitude, distance, and power spectrum. The controlling or dominant source contributing to the hazard at high (5-10 Hz) and low (1-2 Hz) frequencies at the desired annual frequency of ground motion exceedance are provided by the hazard deaggregations. Ray tracing is used to establish incidence angles of S-waves for each of these controlling earthquakes. Two independent site response analyses are conducted using the equivalent-linear analysis to develop motions due to incident SH-waves: (1) vertically propagating SH-waves and (2) inclined SH-waves. The envelope motion in these two cases is used as the horizontal-component for SH-waves.

6.1.10 Average Horizontal Component from Inclined SV-Waves

In addition to the horizontal-component contribution from incident vertical and inclined SH-waves, described above, additional energy in the form of inclined P-SV-waves contributes to the horizontal component of motion. An equivalent-linear analysis is completed for inclined incident SV-waves. The maximum horizontal component motion is taken as the envelope of the SH- and SV-wave spectral evaluations.

It is expected that the dominant contribution to the horizontal component is captured through vertically propagating SH-waves. Analysis of strong motions recorded at two vertical soil arrays indicated that approximately 75% of the ground motion power can be modeled by vertically propagating S-waves. The remaining energy may be due to scattered waves and P-waves (EPRI 1988 [DIRS 107489], page 5-1).

6.1.11 Vertical Component from Vertical and Inclined P-Waves and Inclined SV-Waves

To model vertical motions, incident vertical and inclined P- and SV-waves are used at the control motion point. Similar to the analysis of the horizontal component, the controlling earthquakes at the desired annual frequency of ground motion exceedance are established from the hazard deaggregations. Ray tracing is used to establish incidence angles of P- and SV-waves for each of these earthquakes. For each of the deaggregation earthquakes, a linear analysis is performed with incident inclined P-SV waves using low-strain, V_P and V_S (Section 6.3.1.1). P-wave damping is assumed to be equal to low strain S-wave damping (Johnson and Silva 1981 [DIRS 110447]; EPRI 1993b [DIRS 103320], Appendix 6.B; Silva 1997 [DIRS 163747]). The vertical and horizontal motions are treated in separate analyses.

6.1.12 Model Testing, Sensitivities, and Calibration Activities

Testing and application of the 1D equivalent-linear model is referenced and documented in Sections 6.1.1 and Section 7. These testing activities have been thorough and make use of the available strong motion data. Site-specific strong ground motion data for these activities is unavailable. Thus, validation is based on data recorded at other locations. Monitoring of potential strong ground motion at Yucca Mountain, however, has been initiated (e.g., von Seggern 2004 [DIRS 170522]).

Site response sensitivity to variations in Repository Block velocity profile and ranges of strain-dependent material properties have been conducted and are documented in Wong and Silva (2004a [DIRS 170443], page 25, Supplemental Record 3).

6.1.13 Use of Output

Preclosure seismic ground motion inputs are developed for two locations: the rock interface at the depth of the waste emplacement drifts (Point B) and the soil site of the repository surface facilities (Point D/E) (Section 6.2.2.1). Acceleration response spectra are developed for both horizontal and vertical components and for hazard mean annual exceedance rates appropriate for preclosure analysis (e.g., 5×10^{-4}). In addition, time histories (2 horizontal and 1 vertical components) consistent with the spectra are calculated as well as 3D dynamic strains and curvatures, peak ground acceleration, and peak particle velocity as functions of depth between

the surface and the waste repository level. Strain-compatible soil properties are also estimated at Point D/E.

In support of the postclosure analyses, time histories are developed that are consistent with the emplacement level spectra for mean annual exceedance rates of 10^{-5}, 10^{-6}, and 10^{-7}. The time histories support the performance assessments of the engineered barrier system components as part of the Total System Performance Assessment.

6.1.14 Limitations

The two fundamental simplifications of the RVT site response model used in these analyses, plane horizontal layers (1D) and equivalent-linear approximation to nonlinear dynamic material response (Section 6.1.6), are its two limitations. For conditions under which lateral variations in dynamic material properties control strong motions, the 1D model may not be appropriate. Generally these conditions involve deep basins with sources located outside of the basins (large source-to-site distances), and at low frequencies (≤ 0.5 Hz) (Campbell 1981 [DIRS 102191], Joyner 2000 [DIRS 164134], Boore 2001 [DIRS 163993]). For these cases, surface waves may dominate the low frequencies, resulting in long duration wavetrains. Experience has shown that conventional site response analyses assuming vertically-propagating S-waves accommodates much of the amplification due to surface waves. Seed et al. (1988 [DIRS 163924]) were successful in modeling ground motions from the 1985 moment magnitude (**M**) 7.9 Mexico City earthquake using a simple 1D model. Additional analyses by Chávez-García et al. (1995 [DIRS 164971]) indicate that the 1985 ground motions were dominated by surface waves. The data collected from the geotechnical investigations to date (BSC 2002a [DIRS 157829]) do not indicate significant 2D or 3D velocity variations at the Surface Facilities Area or the Repository Block. The 1D limitation is not considered an issue of concern for Yucca Mountain because the conditions there are not conducive to the generation of surface waves. Also the site response analyses are performed to develop appropriate spectral levels and not durations.

The limitation involving the equivalent-linear approximation is generally cast in the form of acceptable levels of cyclic shear strain. In assessing the ability of the equivalent-linear approximation to appropriately accommodate the effects of material nonlinearity on peak acceleration, peak particle velocity, and peak oscillator response (5%-damped response spectra), maximum cyclic shear strains are considered the key indicator. Current validations of the equivalent-linear approximation have successfully modeled response spectra computed from motions recorded at soil sites, which have experienced large enough shear strains, mean peak of 1.00%, to fail (liquefy) (Section 7; Silva et al. 1999 [DIRS 164081]). For the analyses documented in this report, postclosure ground motions with an annual exceedance frequency of 10^{-7} produce mean shear strains ranging from 0.27% to 1.09%, reflecting uncertainty in knowledge of the site material properties (BSC 2004c [DIRS 170137], Table 6-3).

6.2 MODEL INPUTS

Inputs to the site-response computational model consist of control motion response spectra, small-strain velocities, densities, nonlinear dynamic material properties, and the angles of incidence of the control motions. This subsection describes the development of these inputs and how input uncertainties are treated.

6.2.1 Overview of Approach to Develop Earthquake Ground Motion Input

This subsection provides an overview of the methodology to develop ground motion inputs for use in analyses supporting preclosure design and postclosure performance assessment. A detailed description follows in subsequent sections. The site-response ground motion model forms one element in the overall methodology. An understanding of the overall methodology provides the context for the discussion of model inputs in the following sections.

The approach used for developing site-specific ground motions that are conditional on a probabilistically determined control (rock outcrop) motion follows the guidance contained in NUREG/CR-6728 (McGuire et al. 2001 [DIRS 157510], Section 6.1 [Approach 2B]). The approach conservatively maintains the hazard level of the control motions while incorporating variability in site-specific dynamic material properties. The approach captures the effects that magnitude (spectral shape) has on the degree of nonlinearity in site response by using a suite of scaled spectral shapes as control motions. The spectral shapes reflect the range in earthquake magnitudes contributing to both the low frequency (1-2 Hz) and high frequency (5-10 Hz) portions of the Point A UHS. The site response model is used to develop transfer functions for response spectra and peak particle velocities from the reference rock outcrop (Point A), where the UHS is defined, to repository locations underground and at the surface. The model also determines values of strains and curvatures as functions of depth.

The PSHA provides mean estimates of the hazard where this is defined as the annual probability of exceedance or numerically equivalent, the annual mean frequency of exceedance for a given amplitude of a ground motion parameter. The starting point for the methodology is the output of the PSHA expressed as seismic hazard curves for various measures of ground motion (CRWMS M&O 1998a [DIRS 103731], Section 7.3). Results are provided for spectral acceleration at structural frequencies of 0.3, 0.5, 1, 2, 5, 10, 20, and 100 Hz (peak ground acceleration). Results for peak ground velocity are also provided.

For a given mean annual frequency of ground motion exceedance, the seismic hazard results are used to derive a response spectrum with a uniform mean annual frequency of being exceeded, the UHS. The UHS forms the basis for the ground motion used as input (the control motion) to the site-response model.

There are no codes, standards, or regulations that govern the development of earthquake ground motions in this study (Sections 1.1 and 4.3). However, generally following the guidance provided in Regulatory Guide 1.165 (1997 [DIRS 119139], Appendix C), the PSHA results for a given mean annual frequency of exceedance are deaggregated to identify controlling earthquakes. Two controlling earthquakes are determined from the deaggregated hazard at structural frequencies of 1 to 2 Hz and at 5 to 10 Hz. Response spectra for the controlling

earthquakes are computed using the suite of attenuation models used in the PSHA and scaled to match the UHS amplitude at 1 to 2 Hz and 5 to 10 Hz; these scaled spectra form the "reference earthquake" response spectra.

The reference earthquake response spectra form the basis for development of the site-specific motions (Regulatory Guide 1.165 1997 [DIRS 119139], Regulatory Position 4). Response spectral (5%-damped) and peak particle velocity transfer functions from the PSHA reference rock outcrop (Point A) to repository locations of interest (Points B, D, and E) are developed. For horizontal component motions, the horizontal transfer functions are applied to the enveloped reference earthquake motions (response spectra and peak particle velocities) to determine the final motions. For vertical motions, the vertical transfer functions are applied to the vertical enveloped reference earthquake motions (see Section 6.2.2.4).

Non-linear site-response may be sensitive to earthquake magnitude (spectral composition of the control motion). Because this sensitivity may not be sufficiently captured in the mean of the range of magnitudes reflected in the reference earthquakes, three deaggregation earthquakes (DEAs) are obtained to account for the range of magnitudes contributing to the hazard in the 1 to 2 Hz and 5 to 10 Hz structural frequency ranges (McGuire et al. 2001 [DIRS 157510], Section 6.1, Approach 2B). These DEAs nominally represent the 5^{th}, mean, and 95^{th} fractile magnitudes and associated distances determined from the hazard deaggregation. These DEAs form the input, or control motion, for the site-response ground motion model. Thus, the methodology employs six control motion response spectra as inputs. A weighted average is taken of the model outputs for each set of DEAs with the results for the mean magnitude getting the largest weight.

Other site-specific inputs required for the site response model include seismic velocity profiles, material densities, and nonlinear dynamic material properties for the emplacement area (Repository Block) and surface facilities. For the Repository Block, two base case V_S and two V_P profiles are used to represent uncertainty in the mean profile (see Section 6.2.3.3). For the surface facilities site, where uncertainty in the mean profile is less, a single base case profile is used (see Section 6.2.3.4). The base case profiles are used, along with information on the statistical correlation of layer thicknesses and layer velocities, to develop a suite of random velocity profiles that are used as model input. Similarly for the nonlinear dynamic properties of site materials, multiple base case curves of normalized shear modulus reduction and damping, as a function of cyclic shear strain, are developed to represent epistemic uncertainty in the mean values of these properties. Two sets of curves are developed each for the tuff and alluvium materials at the site. For input to the model, the curves are randomized to represent random variability in properties within and across the site.

Finally, the model incorporates a range of control motion incidence angles, the angle at which the ground motion impinges upon the site model from below. Incidence angles are determined consistent with the local velocity structure and hazard deaggregation results (i.e., magnitude, distance, and corresponding source depth given in Section 6.2.2.5.1), which provide the distance at which a given DEA occurs.

The methodology to develop ground motion inputs for analyses supporting design and performance assessment involves exercising the site-response model multiple times to capture the effects of variability. For each combination of DEA, base case velocity profile, and base

case dynamic material properties, multiple model runs are carried out using randomized parameter values to capture the effect of input parameter uncertainty and variation across the site. The model results are then appropriately combined to determine the final output (e.g., response spectra, peak ground velocities or accelerations, strain-compatible soil properties). Based on these outputs, further analyses are carried out to develop time histories, if required.

The remaining subsections of Section 6.2 address in more detail the development of model inputs that are used in the computation. Section 6.3 describes the results of the computations and additional analyses to develop time histories.

6.2.1.1 Definitions of Uncertainty, Variability, and Randomness

A goal of approaches to model ground motion numerically (including site response models) is a quantitative assessment of prediction variability (Silva et al. 1996 [DIRS 110474], Section 5.1). A desirable approach to achieving this goal is in a manner that lends itself to characterizing the variability associated with model results. For a ground motion model, variability in results is due to a combination of modeling variability and parametric variability. Modeling variability is a measure of how well the model works (how accurately it predicts ground motions) when specific parameter values are known. Modeling variability is determined through validation exercises in which model predictions are compared to recorded motions (see Section 7.3.4). This variability can be due to source, path, and site factors for which the model does not account (e.g., linear site response does not completely accommodate nonlinear effects). Parametric variability results from a viable range of values for model parameters (e.g., soil profile, normalized shear modulus, and damping curves). It is the sensitivity of a model to a viable range of values for model parameters. The total variability, modeling plus parametric, represents the variance associated with the ground motion estimation and, because it is expressed as fractile levels, is as important as median estimates.

Both the *modeling* and *parametric* variabilities may have components of randomness (aleatory variability) and uncertainty (epistemic variability). Table 6.2-1 summarizes the four components of total variability in the context of ground motion estimates (Silva et al. 1996 [DIRS 110474], Table 5.1). Uncertainty is that portion of both modeling and parametric variability that, in principle, can be reduced as additional information (knowledge) becomes available, whereas randomness represents the intrinsic or irreducible component of variability for a given model or suite of parameters. The uncertainty component reflects a lack of knowledge and may be reduced as more data are analyzed. In the context of the PSHA, uncertainty is characterized by weighted alternatives in logic trees. Randomness (aleatory variability) is integrated in the hazard calculation. The terminology shown in Table 6.2-1 is followed in this report.

Table 6.2-1. Contributions to Total Variability in Ground Motion Models

	Modeling Variability	**Parametric Variability**
Uncertainty *(also Epistemic Uncertainty)*	Modeling Uncertainty: Variability in estimated motions resulting from particular model assumptions, simplifications and/or fixed parameter values. *Can be reduced by adjusting or "calibrating" model to better fit observed earthquake response.*	Parametric Uncertainty: Variability in estimated motions resulting from incomplete data needed to characterize parameters. *Can be reduced by collection of additional information, which better constrains parameters.*
	Modeling Variability	**Parametric Variability**
Randomness *(also Aleatory Variability)*	Modeling Randomness: Variability in estimated motions resulting from discrepancies between model and actual complex physical processes. *Cannot be reduced for a given model form.*	Parametric Randomness: Variability in estimated motions resulting from inherent randomness of parameters values. *Cannot be reduced a priori* by collection of additional information.*

Source: Silva et al. 1996 [DIRS 110474], Table 5.1

NOTE: *Some parameters (e.g., source characteristics) may be well defined after an earthquake.

6.2.2 Computation of Reference Rock Outcrop Spectra

As a result of the PSHA for vibratory ground motion, which was based on the expert elicitation of 18 seismic source characterization experts and 7 ground motion experts, the probabilistic hazard has been calculated for Yucca Mountain (CRWMS M&O 1998a [DIRS 103731]). The probabilistic methodology allows the frequency of earthquake occurrences to be incorporated, and allows uncertainties and randomness to be quantified in a consistent manner in the final hazard results. The probabilistic methodology is consistent with the requirement of total system performance assessment and with the design process. The methodology is described in detail in *Methodology to Assess Fault Displacement and Vibratory Ground Motion Hazards at Yucca Mountain* (YMP 1997b [DIRS 100522]).

In the PSHA Project, the hazard was specified at a defined hard-rock free-field site condition (Point A, Figure 1-1) (CRWMS M&O 1998a [DIRS 103731], Sections 5.3.1.2 and 5.7.1). Rock properties for Point A were those that available data indicated existed at a nominal 300-m depth, the approximate depth of the repository waste emplacement horizon. The mean V_S at Point A is 1900 m/sec. This value was derived from a Yucca Mountain velocity profile with the top 300 m removed (Schneider et al. 1996 [DIRS 103270], Section 5).

A fixed reference hard-rock site condition was used because a detailed geotechnical site characterization had not been completed at the time of the PSHA ground motion characterization (CRWMS M&O 1998a [DIRS 103731], Section 5.3.1.2). By defining the ground motion at Point A, subsequent detailed geotechnical site information would be incorporated through analyses using the site response model without having to conduct another elicitation of the ground motion experts. In particular, response of the tuff as well as soil materials would be incorporated into the analyses as site characterization results became available.

In the PSHA, because the site response calculations include damping in the top 300 m, the effects of this damping needed to be removed from the Point A ground motions. This was accomplished by defining a value of the site attenuation parameter, kappa, for Point A. Kappa for surface sites in the vicinity of Yucca Mountain was determined to be 0.022 sec based on data given in Su et al. (1996 [DIRS 100087], Table 4). For the PSHA, a value of 0.02 sec was used in the analysis (CRWMS M&O 1998a [DIRS 103731], Section 5.3.1.2). Damping in tuff was measured as part of the preliminary site characterization and it was found that the low-strain damping in the top 300 m corresponded to a kappa of 0.0014 sec (CRWMS M&O 1998a [DIRS 103731], Section 5.3.1.2). Therefore, to avoid double-counting the damping in the top 300 m, the surface kappa value of 0.02 sec was reduced by 0.0014 sec to give a kappa at Point A of 0.0186 sec. This kappa value is a defined property of hard-rock outcrop (Point A). The precision of the Point A value of kappa is an artifact of the calculation that was made; it is not meant to imply that kappa is known with that precision.

Control motion response spectra to be used as input to the site-response ground motion model are determined for each ground motion hazard level of interest. That is, control motions are needed for each annual frequency of ground motion exceedance for which inputs are to be developed. In this report, control motion response spectra are developed for annual exceedance frequencies of 10^{-3}, 5×10^{-4}, 10^{-4}, 10^{-5}, 10^{-6}, and 10^{-7}. As described in Section 6.2.1, for each hazard level development of the control motion response spectra consists of the following steps:

- Determine the UHS based on the results of the PSHA
- On the basis of a deaggregation of the PSHA results, determine reference earthquakes whose response spectra represents the UHS
- Also on the basis of PSHA deaggregation results, define DEAs to represent the range of magnitudes associated with each reference earthquake.

These steps are described in more detail below. In addition, a task to extend the PSHA hazard results to lower annual frequencies of exceedance is also discussed.

6.2.2.1 Locations of Computed Ground Motions

Using the ground motion derived at Point A (Figure 1-1), ground motions were calculated at Point B, the waste emplacement level and Points D and E, the surface facilities site. The computed ground motions at Point B are developed to apply anywhere within the proposed emplacement area for which the base case velocity models were determined. Point D refers to any location within the Surface Facilities Area (i.e., that portion of the waste handling building site characterization area southwest of the Exile Hill fault splay, see Section 6.2.3.2.2) where the thickness of alluvium/colluvium is at least about 15 ft. The area on the west side of the Surface Facilities Area adjacent to Exile Hill is designated as Point E (Figure 1-1). Point E represents those portions of the Surface Facilities Area for which alluvium is approximately 15 ft thick or less. Ground motions are also evaluated for a site northeast of the Exile Hill splay fault (Point F) and compared to those for Points D and E.

6.2.2.2 Calculation of Hazard

Input to develop the control motion response spectra consists of the PSHA results. This input is summarized in Table 6.2-2.

Table 6.2-2. Input Data to Extend Ground Motion Hazard Results

Input Data	Data Source	Data Tracking Number
Results of the Yucca Mountain Probabilistic Seismic Hazard Analysis (PSHA)	BSC 2004j [DIRS 168030]	MO0401MWDRPSHA.000[2] [DIRS 166962]

The PSHA expert interpretations (CRWMS M&O 1998a [DIRS 103731], BSC 2004j [DIRS 168030]) form the basis for the current work to extend the PSHA hazard curves to lower annual exceedance frequencies. The mean results from the original calculations do not in all cases extend to low enough annual exceedance frequencies to meet the needs for ground motion inputs supporting postclosure analyses.

The analysis to extend the PSHA results to lower annual exceedance frequencies followed the same methodology as documented in BSC 2004j [DIRS 168030], Section 6.5.1). The following software programs were used to carry out the analysis:

- MEAN V1.1 (Software Tracking Number 10463-1.1-00) (Risk Engineering 2002d [DIRS 163310])
- CMB_FRAC V2.0 (Software Tracking Number 10464-2.0-00) (Risk Engineering 2002a [DIRS 163294])
- FRISK88 V2.0 (Software Tracking Number 10139-2.0-00 (Risk Engineering 2000a [DIRS 163365])
- PREP88 V1.0 (Software Tracking Number 10138-1.0-00 (Risk Engineering 2000c [DIRS 163362])
- POST88 V1.0 (Software Tracking Number 10136-1.0-00 (Risk Engineering 2000b [DIRS 163361])

Inputs were taken from DTN MO0401MWDRPSHA.000 [DIRS 166962][2] and consist of files in subdirectories .shaking/aar/inputs, .shaking/asm/inputs, .shaking/dfs/inputs, .shaking/rya/inputs, .shaking/sbk/iputs, and .shaking/sdo/inputs. Details of the analysis are documented in Scientific Notebook SN-M&O-SCI-038-V1 (Toro 2003 [DIRS 163720], pages 13-31 and associated supplemental records). Hazard curves were developed for spectral acceleration at structural frequencies of 0.3, 0.5, 1, 2, 5, 10, 20, and 100 Hz and peak ground velocity. Mean, median, and

[2,3] DTN MO0401MWDRPSHA.000 [DIRS 166962] supersedes MO0004MWDRIFM3.002 [DIRS 149092], which was cited in Revision 00 of this report. The original DTN was superseded to add to the data a file containing the coordinates of the locations at which ground motion and fault displacement hazard were computed. None of the original data associated with DTN MO0004MWDRIFM3.002 [DIRS 149092] was altered. Note that supporting scientific notebooks refer to the superseded DTN (MO0004MWDRIFM3.002 [DIRS 149092]).

fractile hazard curves for Point A are shown on Figures 6.2-1 through 6.2-4 for peak horizontal acceleration, 10 Hz and 1 Hz horizontal spectral acceleration, and peak horizontal velocity, respectively. The hazard was calculated for the random component of the horizontal ground motions (CRWMS M&O 1998a [DIRS 103731], Appendix F). Complete results were submitted to the Technical Data Management System (TDMS) and have DTN MO03061E9PSHA1.000 [DIRS 163721].

OCRWM Project Condition Report 1685 documents that the incorrect version of FRISK88 was used in carrying out the original PSHA calculations for one areal source zone for one expert team for one ground motion measure (10 Hz spectral acceleration). An unqualified (no version number) version was used in place of the baselined version 2.0. Sensitivity studies were carried out to evaluate the impact of the use of incorrect software disclosing that the mean hazard used to compute the UHS (see DTN MO0401MWDRPSHA.000 [DIRS 166962]) differs by at most 0.9%. In addition, Software Defect Notification SDN13620030407 documents an error in FRISK88 v. 2.0 that offsets hazard calculations for areal source zones. Sensitivity studies carried out to evaluate the impact of this error show the corrected total mean hazard used to compute the UHS is higher then the original hazard by 5.2% or less (BSC 2003c [DIRS 170500]). These differences in the UHS output are negligible when compared to the variability and uncertainty incorporated into the overall analysis and modeling. Thus, the original results obtained using the incorrect input are used in the analyses documented in this report.

6.2.2.3 Uniform Hazard Spectra

To develop the UHS for a given annual frequency of exceedance, the results of the analysis described in Section 6.2.2.2 (DTN MO03061E9PSHA1.000 [DIRS 163721]) are used along with results from MO0401MWDRPSHA.000 [DIRS 166962][3]. The spectral accelerations with the desired annual exceedance frequency for each structural frequency (0.3 to 100 Hz) are used to calculate a spectrum. Details of the analysis are documented in Scientific Notebook SN-M&O-SCI-038-V1 (Toro 2003 [DIRS 163720], pages 31-34, 56, 92) and Scientific Notebook SN-M&O-SCI-038-V2 (Toro 2004 [DIRS 172034], pages 29-33). Mean horizontal and vertical UHS are shown on Figures 6.2-5 through 6.2-16 for annual exceedance frequencies of 10^{-3}, 5×10^{-4}, 10^{-4}, 10^{-5}, 10^{-6}, and 10^{-7}, respectively. Results were submitted to the TDMS as summarized in Table 6.2-3.

Table 6.2-3. Summary of Data Tracking Numbers for UHS

Description	Data Tracking Number
UHS for Annual Exceedance Frequency of 10^{-3}	MO0211REDES103.000 [DIRS 170424]
UHS for Annual Exceedance Frequency of 5×10^{-4}	MO0208UNHZ5X10.000 [DIRS 163722]
UHS for Annual Exceedance Frequency of 10^{-4}	MO0211DERES104.000 [DIRS 170423]
UHS for Annual Exceedance Frequency of 10^{-5}	MO0308UNHAZ105.000 [DIRS 170425]
UHS for Annual Exceedance Frequency of 10^{-6}	MO0206UNHAZ106.001 [DIRS 163723]
UHS for Annual Exceedance Frequency of 10^{-7}	MO0209UNHAZ107.000 [DIRS 163724]

6.2.2.4 Reference Earthquakes

Reference earthquakes (REs) are determined from ground motion hazard deaggregation and the attenuation models used in the PSHA. Input to the analysis consists of the results of the ground motion hazard analysis described in Section 6.2.2.2 (DTNs MO0401MWDRPSHA.000 [DIRS 166962] and MO03061E9PSHA1.000 [DIRS 163721]). Guidance found in Regulatory Guide 1.165 (1997 [DIRS 119139]) was also generally followed. However, rather than deaggregating the hazard for the structural frequency range of 1 to 2.5 Hz, deaggregation was carried out for the range of 1 to 2 Hz. This modification to the guidance in Regulatory Guide 1.165 (1997 [DIRS 119139], Appendix C) was made because PSHA results are provided for a structural frequency of 2 Hz, not 2.5 Hz. This difference is considered negligible.

Also, rather than using the mean magnitude and distance as specified in Regulatory Guide 1.165 (1997 [DIRS 119139], Appendix C), the modal magnitude and distance are used to define the REs. The mode better represents the events that dominate the hazard for a given annual exceedance frequency (McGuire 1995 [DIRS 107483], page 1281), however, a moderate difference between the mode and mean has only a small effect on the RE spectral shape. In addition, because the RE spectrum is scaled to the UHS in the appropriate structural frequency range, use of the mode instead of the mean has a negligible effect on the amplitude of the RE spectrum at the key structural frequencies.

The RE analysis used the following software:

- PREP88 V1.0 (Software Tracking Number 10138-1.0-00) (Risk Engineering 2000c [DIRS 163362])
- FRISK88 V2.0 (Software Tracking Number 10139-2.0-00) (Risk Engineering 2000a [DIRS 163365])
- MRE88 V1.0 (Software Tracking Number 10140-1.0-00) (Risk Engineering 2000d [DIRS 163312])
- DESIGN_EVENTS V1.0 (Software Tracking Number 10362-1.0-00) (Risk Engineering 2002b [DIRS 163302])

In addition, the commercial-off-the-shelf software MathCad V7.0 was used. Details of the use of commercial-off-the-shelf software are provided in Appendix I. Details of the analysis are documented in Scientific Notebook SN-M&O-SCI-038-V1 (Toro 2003 [DIRS 163720]), pages 31-119 and Scientific Notebook SN-M&O-SCI-038-V2 (Toro 2004 [DIRS 172034], pages 33-36).

The deaggregation of ground motion hazard is the process of determining the contributions of combinations of modal magnitude (M*), distance (R*), and ground motion deviation (ε) to the annual frequency of exceeding a given ground motion amplitude (McGuire 1995 [DIRS 107483]). For this purpose, ε is the difference between the logarithm of the ground motion amplitude and the mean logarithm of ground motion (for that M and R), measured in units of the standard deviation σ of log (ground motion). Deaggregation is performed as a part of the ground

motion hazard calculations by storing (in M, R and ε bins) the contributions to annual frequency of exceedance. Plots of M, R, and ε indicate which combinations of these parameters contribute most, and which contribute least, to the hazard for a given ground motion amplitude. M, R, and ε combinations contribute differently depending on the annual frequency of exceedance and on the structural frequency of the ground motion measure.

The ground motion hazard was deaggregated at ground motion amplitudes corresponding to the annual exceedance frequencies of 10^{-3}, $5x10^{-4}$, 10^{-4}, 10^{-5}, 10^{-6}, and 10^{-7}. This deaggregation was done at response frequencies 10, 5, 2, and 1 Hz, and results for 5 and 10 Hz were averaged, as were results for 1 and 2 Hz.

Figures 6.2-17 to 6.2-22 show the relative contributions by M, R, and ε for the average of 5 to 10 Hz horizontal motions. The predominant contribution at these higher frequency motions comes from magnitudes in the **M** 5.0 to 6.5 range and distances less than 15 km. These close-in moderate-sized earthquakes have their sources in the local faults and background seismicity (CRWMS M&O 1998a [DIRS 103731], Section 7.3).

Figures 6.2-23 to 6.2-28 show the equivalent contributions for the average of 1 to 2 Hz horizontal motions. These plots show a larger contribution, relative to the results for 5 to 10 Hz, coming from large events (approximate **M** 7 to 7.5) at distances of about 50 km. The sources for these events are the Death Valley-Furnace Creek faults, which have a higher slip rate than do the local faults (CRWMS M&O 1998a [DIRS 103731], Section 7.3).

REs (characterized by M and R) were determined with the use of the deaggregation of horizontal ground motion hazard. Response spectra (computed using the attenuation models used in the PSHA) for the REs (M and R) at 1-2 Hz and 5-10 Hz are scaled to match the UHS at these response frequency bands. Modal magnitudes and distances derived from the joint deaggregation are provided in Table 6.2-4. At 1-2 Hz, the deaggregation also was done for the regional sources alone, which are a secondary contributor to the 1-2 Hz hazard. For 10^{-4}, 10^{-5}, 10^{-6}, and 10^{-7} annual exceedance frequencies, these larger magnitude earthquakes are used in the computation of RE spectra because they have a broader spectral shape at low frequencies. Therefore, scale factors were not computed for the smaller magnitude earthquakes. For 10^{-3}, $5x10^{-4}$, and 10^{-4} annual exceedance frequencies, the 1-2 Hz modal magnitudes were adjusted downward due to spectral shape considerations. The 5-10 Hz magnitudes were adjusted upward slightly to provide more frequency content at intermediate frequencies. These M and R adjustments broaden the spectra for the REs and allow two REs to represent all frequencies of the UHS. The RE spectral values were computed using these RE magnitudes and distances and an epsilon of zero along with the horizontal and vertical attenuation relationships from the PSHA.

For the 1-2 Hz case, the RE spectra were scaled to the 1.4 Hz (the geometric mean of 1 and 2 Hz) ground motion and for the 5-10 Hz case, the RE spectra were scaled to the 7.1 Hz (the geometric mean of 5 and 10 Hz) ground motion. An additional constraint was applied such that the maximum of the two RE spectra was not less than 95% of the corresponding UHS at any frequency. In some cases (all 1-2 Hz vertical RE spectra; e.g., see Figure 6.2-30), the scaled RE spectrum was adjusted up to maintain the 95% constraint. REs for vertical motions were taken to be identical to those for horizontal motion for consistency. Because the REs are derived from

the results of the PSHA, they incorporate both aleatory (randomness) and epistemic (uncertainty) variability in ground motion hazard at Yucca Mountain. REs at annual exceedance frequencies of 10^{-3}, $5x10^{-4}$, 10^{-4}, 10^{-5}, 10^{-6}, and 10^{-7} are shown along with the corresponding UHS on Figures 6.2-29 to 6.2-40. Results were submitted to the TDMS as summarized in Table 6.2-5.

Table 6.2-4. Summary of Deaggregation for Selection of Reference Earthquakes

10^{-3} Annual Exceedance Frequency

	M*	R*	RE Magnitude and Distance	Horizontal Scale Factor	Vertical Scale Factor
5-10 Hz	5.15	8.75	**M** 6.3, 5 km	0.572	0.543
1–2 Hz	7.35	51.25	**M** 6.9, 52 km	3.830	4.880
1-2 Hz Regional Sources	7.35	51.25			
1-2 Hz Local Sources	5.85	3.75			

Source: Toro 2003 [DIRS 163720], pages 116 and 117, SR 186, DTN: MO0211REDES103.000 [DIRS 170424]

$5x10^{-4}$ Annual Exceedance Frequency

	M*	R*	RE Magnitude and Distance	Horizontal Scale Factor	Vertical Scale Factor
5-10 Hz	5.15	8.75	**M** 6.3, 5 km	0.843	0.812
1–2 Hz	7.35	51.25	**M** 7.0, 51 km	4.820	5.361
1-2 Hz Regional Sources	7.35	51.24			

Source: Toro 2003 [DIRS 163720], page 60, SR 105, DTN: MO0208UNHZ5X10.000 [DIRS 163722]

10^{-4} Annual Exceedance Frequency

	M*	R*	RE Magnitude and Distance	Horizontal Scale Factor	Vertical Scale Factor
5-10 Hz	6.2	3.75	**M** 6.3, 5 km	1.835	1.855
1–2 Hz	7.7	51.3	**M** 7.7, 52 km	5.613	6.824
1-2 Hz Regional Sources	7.7	51.3			

Source: Toro 2003 [DIRS 163720], page 112, SR 169 and 171, DTN: MO0211DERES104.000 [DIRS 170423]

10^{-5} Annual Exceedance Frequency

	M*	R*	RE Magnitude and Distance	Horizontal Scale Factor	Vertical Scale Factor
5-10 Hz	6.25	3.75	**M** 6.4, 4 km	4.261	4.624
1–2 Hz	6.25	3.75	**M** 7.7, 51 km	13.735	15.531
1-2 Hz Regional Sources	7.35	51.25			

Source: Toro 2004 [DIRS 172034], page 31, SR 34 and 39, DTN: MO0308UNHAZ105.000 [DIRS 170425]

10^{-6} Annual Exceedance Frequency

	M*	R*	RE Magnitude and Distance	Horizontal Scale Factor	Vertical Scale Factor
5-10 Hz	6.15	1.25	**M** 6.5, 1 km	8.030	8.675
1–2 Hz	6.65	1.25	**M** 7.7, 51 km	30.600	47.640
1-2 Hz Regional Sources	7.65	51.25			

Source: Toro 2003 [DIRS 163720], page 38, SR 63 and 70, DTN: MO0206UNHAZ106.001 [DIRS 163723]

10^{-7} Annual Exceedance Frequency

	M*	R*	RE Magnitude and Distance	Horizontal Scale Factor	Vertical Scale Factor
5-10 Hz	6.15	1.25	**M** 6.5, 1 km	16.843	18.583
1–2 Hz	6.65	1.25	**M** 7.7, 51 km	64.225	72.809
1-2 Hz Regional Sources	7.65	51.25			

Source: Toro 2003 [DIRS 163720], page 95, SR 141 and 159, DTN: MO0209UNHAZ107.000 [DIRS 163724]

Table 6.2-5. Summary of Data Tracking Numbers for REs

Description	DTN
REs for Annual Exceedance Frequency of 10^{-3}	MO0211REDES103.000 [DIRS 170424]
REs for Annual Exceedance Frequency of $5x10^{-4}$	MO0208UNHZ5X10.000 [DIRS 163722]
REs for Annual Exceedance Frequency of 10^{-4}	MO0211DERES104.000 [DIRS 170423]
REs for Annual Exceedance Frequency of 10^{-5}	MO0308UNHAZ105.000 [DIRS 170425]
REs for Annual Exceedance Frequency of 10^{-6}	MO0206UNHAZ106.001 [DIRS 163723]
REs for Annual Exceedance Frequency of 10^{-7}	MO0209UNHAZ107.000 [DIRS 163724]

In addition to deaggregating the PSHA results to determine reference earthquakes, deaggregation was also carried out with respect to PGV to support development of time histories for postclosure analyses (Section 6.3.2). Recorded accelerograms to use as a basis for developing the postclosure time histories are selected such that their distribution in magnitude and epicentral distance is similar to the range of magnitudes and distances contributing to the PGV hazard at the annual exceedance frequency of interest. A summary of the PGV magnitude and distance deaggregation is provided in Table 6.2-6. Results were submitted to the TDMS and have DTNs MO0309PGVDEAGG.000 [DIRS 170426], MO0208PGVDEAG6.001 [DIRS 164203] and MO0210PGVD1E07.000 [DIRS 164205] for annual exceedance frequencies of 10^{-5}, 10^{-6} and 10^{-7}, respectively.

Table 6.2-6. Summary of Peak Ground Velocity (PGV) Deaggregation

	10^{-5} Annual Exceedance Frequency		10^{-6} Annual Exceedance Frequency		10^{-7} Annual Exceedance Frequency	
	Moment Magnitude	Distance (km)	Moment Magnitude	Distance (km)	Moment Magnitude	Distance (km)
Modal	6.55	3.75	6.65	1.25	6.7	1.3
Mean	6.44	13.36	6.47	8.62	6.5	5.7
5th percentile	Not computed[1]	Not computed[1]	5.65	1.3	5.9	1.3
Median (50th percentile)	6.45	3.75	6.45	3.75	6.6	3.8
95th percentile	Not computed[1]	Not computed[1]	7.25	51.3	7.2	13.8

Source: DTNs: MO0309PGVDEAGG.000 [DIRS 170426], MO0208PGVDEAG6.001 [DIRS 164203], MO0210PGVD1E07.000 [DIRS 164205]

NOTE: [1] 5th and 95th percentile values were not computed for 10-5 annual exceedance frequency. Instead the entire probability distribution was provided in DTN: MO0309PGVDEAGG.000 [DIRS 170426].

6.2.2.5 Deaggregation Earthquakes

While the magnitude of each RE is the most likely magnitude controlling response in the given structural frequency range, the UHS reflects a range of magnitudes. This section describes the development of DEAs to include the effects of the range of earthquake magnitude reflected in the UHS on modeling of nonlinear ground motion effects. Nonlinear site response may depend on the spectral content (and thus magnitude) of the earthquakes generating the ground motion.

Input to the DEA analysis consists of the results of the analysis described in Section 6.2.2.2 (DTNs MO0401MWDRPSHA.000 [DIRS 166962] and MO03061E9PSHA1.000 [DIRS 163721]). The guidance for Approach 2B in NUREG/CR-6728 (McGuire et al. 2001 [DIRS 157510], Section 6) were generally followed. The analysis used the following software:

- PREP88 V1.0 (Software Tracking Number 10138-1.0-00) (Risk Engineering 2000c [DIRS 163362])
- FRISK88 V2.0 (Software Tracking Number 10139-2.0-00) (Risk Engineering 2000a [DIRS 163365])
- MRE88 V1.0 (Software Tracking Number 10140-1.0-00) (Risk Engineering 2000d [DIRS 163312])
- DESIGN_EVENTS V1.0 (Software Tracking Number 10362-1.0-00) (Risk Engineering 2002b [DIRS 163302])

In addition, the commercial-off-the-shelf program MathCad V7.0 was used. Details of this use of commercial-off-the-shelf software are provided in Appendix I. Details of the analysis, including use of commercial-off-the-shelf software, are documented in Scientific Notebook SN-M&O-SCI-038-V1 (Toro 2003 [DIRS 163720], pages 31-119 and Scientific Notebook SN-M&O-SCI-038-V2 (Toro 2004 [DIRS 172034], pages 29-36).

For a given annual ground motion exceedance frequency and structural response frequency range (low frequency, 1 to 2 Hz; high frequency, 5 to 10 Hz), three DEAs are developed based on the magnitude, distance, and epsilon deaggregation of the PSHA hazard and the suite of attenuation models used in the PSHA. Three control motions (MM, ML, MH) were defined as having magnitudes corresponding nominally to the mean, 5th, and 95th percentile of the distribution of events contributing to the hazard (with respect to magnitude only). (The differences between the mean and median magnitudes was at most 0.1 unit.) For 10^{-4} annual exceedance frequency, the 1-2 Hz horizontal ML, MM, and MH magnitudes (5.4, 6.4, and 7.8) and their associated weights are adjustments from the 5th percentile, mean, and 95th percentile magnitudes (5.35, 6.4, and 7.6) and weights. These adjustments were made to provide a better representation of the large magnitude earthquakes on regional sources and to represent intermediate response frequencies (2-5 Hz). The associated weights were computed by conserving the mean and sigma of the magnitude distribution. The same adjustment of magnitudes for horizontal DEAs was made for 10^{-5}, 10^{-6} and 10^{-7} annual exceedance frequencies. The corresponding distances were obtained by deaggregating the hazard with respect to distance only and selecting the mean, 5th, and 95 percentile distances. Weighting factors were developed depending on the percentile values

(assuming a normal distribution) used (Toro 2003 [DIRS 163720], SR 94, 110, 143, 144, 146, 160, 176, and 189) and are shown in Tables 6.2-8 and 6.2-9. (Note that the weights in some cases do not sum exactly to unity because of numerical rounding. This difference is not significant for the analysis.) Mean epsilons (at 1-2 Hz and 5-10 Hz) were used with the magnitudes and distances in the horizontal and vertical attenuation models to compute DEA spectra. Response spectra for the DEAs are scaled to match the UHS in the appropriate frequency range (1 to 2 Hz or 5 to 10 Hz).

As was noted earlier in Section 6.2.2.4, the scaled RE spectra for certain cases were greater than the UHS value for the appropriate frequency range and thus the corresponding DEA spectra, which are scaled to the UHS response amplitude may fall below the RE for the appropriate response frequency range. DEA magnitude, distance, and epsilon values for vertical motion were taken to be identical to those for horizontal motion, for consistency. The corresponding DEA response spectra for the vertical component, however, used the vertical attenuation models used in the PSHA. Results were submitted to the TDMS as summarized in Table 6.2-7. The three DEAs replace the RE (1-2 Hz, 5-10 Hz, horizontal and vertical component) as the input control motions to the site-response ground motion model. Note that the RE spectra are used in a later step of the procedure as discussed below. Model results for each DEA are combined to provide a weighted-average result. Because the DEAs are derived from the results of the PSHA, they incorporate the uncertainty in ground motion hazard at Yucca Mountain.

Table 6.2-7. Summary of Data Tracking Numbers for DEAs

Description	DTN
DEA for Annual Exceedance Frequency of 10^{-3}	MO0211REDES103.000 [DIRS 170424]
DEA for Annual Exceedance Frequency of $5x10^{-4}$	MO0208UNHZ5X10.000 [DIRS 163722]
DEA for Annual Exceedance Frequency of 10^{-4}	MO0211DERES104.000 [DIRS 170423]
DEA for Annual Exceedance Frequency of 10^{-5}	MO0308UNHAZ105.000 [DIRS 170425]
DEA for Annual Exceedance Frequency of 10^{-6}	MO0206UNHAZ106.001 [DIRS 163723]
DEA for Annual Exceedance Frequency of 10^{-7}	MO0209UNHAZ107.000 [DIRS 163724]

Magnitude, distance, ε, and a scale factor of these earthquakes are shown in Tables 6.2-8 and 6.2-9 for horizontal and vertical components, respectively. Note that as the annual exceedance frequency decreases, the scale factor used to match the DEA spectra to the UHS at each frequency band increases. This reflects the fact that the UHS at low annual exceedance frequencies is controlled by the tails of the distributions in the attenuation relationships used in the PSHA. The ε values listed in Tables 6.2-8 and 6.2-9 (which are associated with the corresponding magnitude and distance deaggregation) increase from 1.1 for the 0^{-3} to 2.81 for 10^{-7} annual exceedance frequency. The Point A outcrop spectra for these earthquakes are shown on Figures 6.2-41 through 6.2-44 for 10^{-3} annual exceedance frequency, Figures 6.2-45 through 6.2-48 for $5x10^{-4}$ annual exceedance frequency, Figures 6.2-49 through 6.2-52 for 10^{-4} annual exceedance frequency, Figures 6.2-53 through 6.2-56 for 10^{-5} annual exceedance frequency, Figures 6.2-57 through 6.2-60 for 10^{-6} annual exceedance frequency, and Figures 6.2-61 through 6.2-64 for 10^{-7} annual exceedance frequency. The spectral shapes of the DEAs differ significantly while conforming to the UHS at the target frequency range. The DEAs are not used to compute seismic design response spectra directly. DEAs are used only to compute spectral

amplification factors (SAF) (Section 6.3.1.1.2). For horizontal motions, these SAF are then applied to the envelope of the Point A horizontal RE spectra and horizontal UHS to develop the corresponding suite of site-response spectra representing the uncertainty in the analysis. A horizontal design or target spectrum is determined by enveloping the suite of site-response spectra. For vertical motions, instead of the envelope of the Point A vertical RE spectra and vertical UHS (Section 6.2.2.6.3), a revised vertical spectrum is used that is determined from the envelope of the horizontal RE spectra and UHS and vertical to horizontal (V/H) ratios as discussed in Section 6.2.2.6. Magnitude dependence of the site response is incorporated into the SAF.

For each of the DEA spectra developed based on the parameters listed in Tables 6.2-8 and 6.2-9, a corresponding power spectrum (i.e., control motion) is generated as input for the site response analysis. These input control motions are generated by the spectral matching procedure (see Section 6.1.7.1) based on the deaggregation results for the PSHA. The target spectra for the spectral matching procedure are defined based on the parameters given in Tables 6.2-8 and 6.2-9 and the corresponding attenuation relationships used in the PSHA.

Table 6.2-8a. Magnitude, Distance, Epsilon, and Scale Factor on Horizontal Ground Motions of DEAs at an Annual Exceedance Frequency of 10^{-3}

1-2 Hz

Case	ML	MM	MH
Weight[1]	0.18	0.64	0.18
M	5.3	6.4	7.6
R (km)	3.8	35	76
Epsilon[1]	1.1	1.1	1.1
Scale Factor[1]	0.826	1.797	1.318

Source: DTN: MO0211REDES103.000 [DIRS 170424]

[1]Toro 2003 [DIRS 163720], Supplemental Record (SR) 189, page 2

NOTE: To convert kilometers to miles, multiply by 0.62137

5-10 Hz

Case	ML	MM	MH
Weight[1]	0.18	0.64	0.18
M	5.1	5.9	7.3
R (km)	3.8	19	54
Epsilon[1]	1.1	1.1	1.1
Scale Factor[1]	0.594	1.276	2.284

Source: DTN: MO0211REDES103.000 [DIRS 170424]

[1]Toro 2003 [DIRS 163720], SR 189, page 2

NOTE: To convert kilometers to miles, multiply by 0.62137

Table 6.2-8b. Magnitude, Distance, Epsilon, and Scale Factor on Horizontal Ground Motions of DEAs at an Annual Exceedance Frequency of $5x10^{-4}$

1-2 Hz

Case	ML	MM	MH
Weight[1]	0.18	0.64	0.18
M	5.3	6.4	7.6
R (km)	1.3	18.8	71.3
Epsilon[1]	1.6	1.6	1.6
Scale Factor[1]	0.653	0.736	1.215

Source: DTN: MO0208UNHZ5X10.000 [DIRS 163722]
[1]Toro 2003 [DIRS 163720], SR 110, page 1
NOTE: To convert kilometers to miles, multiply by 0.62137

5-10 Hz

Case	ML	MM	MH
Weight[1]	0.18	0.64	0.18
M	5.1	5.9	7.1
R (km)	1.3	9.0	51.3
Epsilon[1]	1.3	1.3	1.3
Scale Factor[1]	0.643	0.685	3.123

Source: DTN: MO0208UNHZ5X10.000 [DIRS 163722]
[1]Toro 2003 [DIRS 163720], SR 110, page 2
NOTE: To convert kilometers to miles, multiply by 0.62137

Table 6.2-8c. Magnitude, Distance, Epsilon, and Scale Factor on Horizontal Ground Motions of DEAs at an Annual Exceedance Frequency of 10^{-4}

1-2 Hz

Case	ML	MM	MH
Weight[1]	0.18	0.69	0.13
M	5.4	6.4	7.8
R (km)	5	20	74
Epsilon[1]	2.1	2.1	2.1
Scale Factor[1]	1.12	1.133	1.571

Source: DTN: MO0211DERES104.000 [DIRS 170423]
[1]Toro 2003 [DIRS 163720], SR 176, page 2
NOTE: To convert kilometers to miles, multiply by 0.62137

5-10 Hz

Case	ML	MM	MH
Weight[1]	0.18	0.64	0.18
M	5.2	6	7
R (km)	5	10	15
Epsilon[1]	0.9	0.9	0.9
Scale Factor[1]	2.308	1.972	1.85

Source: DTN: MO0211DERES104.000 [DIRS 170423]
[1]Toro 2003 [DIRS 163720], SR 176, page 2
NOTE: To convert kilometers to miles, multiply by 0.62137

Table 6.2-8d. Magnitude, Distance, Epsilon, and Scale Factor on Horizontal Ground Motions of DEAs at an Annual Exceedance Frequency of 10^{-5}

1-2 Hz

Case	ML	MM	MH
Weight	0.163	0.733	0.104
M	5.5	6.4	7.8
R (km)	1.5	15	70
Epsilon	2.26	2.26	2.26
Scale Factor	1.628	1.881	3.337

Source: DTN: MO0308UNHAZ105.000 [DIRS 170425]
NOTE: To convert kilometers to miles, multiply by 0.62137

5-10 Hz

Case	ML	MM	MH
Weight	0.18	0.64	0.18
M	5.3	6.1	7
R (km)	1.3	7	14
Epsilon	2	2	2
Scale Factor	1.909	1.714	2.259

Source: DTN: MO0308UNHAZ105.000 [DIRS 170425]
NOTE: To convert kilometers to miles, multiply by 0.62137

Table 6.2-8e. Magnitude, Distance, Epsilon, and Scale Factor on Horizontal Ground Motions of DEAs at an Annual Exceedance Frequency of 10^{-6}

1-2 Hz

Case	ML	MM	MH
Weight[1]	0.0834	0.8452	0.0715
M	5.2	6.4	7.8
R (km)	1.3	3.8	59.0
Epsilon[1]	2.56	2.56	2.56
Scale Factor[1]	3.884	1.591	5.136

Source: DTN: MO0206UNHAZ106.001 [DIRS 163723]
[1]Toro 2003 [DIRS 163720], SR 94, page 7
NOTE: To convert kilometers to miles, multiply by 0.62137

5-10 Hz

Case	ML	MM	MH
Weight[1]	0.18	0.64	0.18
M	5.4	6.2	7.0
R (km)	1.3	3.8	11.0
Epsilon[1]	2.69	2.69	2.69
Scale Factor[1]	2.506	1.817	2.597

Source: DTN: MO0206UNHAZ106.001 [DIRS 163723]
[1]Toro 2003 [DIRS 163720], SR 94, page 5
NOTE: To convert kilometers to miles, multiply by 0.62137

Table 6.2-8f. Magnitude, Distance, Epsilon, and Scale Factor on Horizontal Ground Motions of DEAs at an Annual Exceedance Frequency of 10^{-7}

1-2 Hz

Case	ML	MM	MH
Weight	0.0475	0.8833	0.0693
M	5.2	6.4	7.8
R (km)	1.3	3.8	51.0
Epsilon[2]	2.81	2.81	2.81
Scale Factor[2]	6.721	2.799	8.112

Source: DTN: MO0209UNHAZ107.000 [DIRS 163724]
[1]Toro 2003 [DIRS 163720], SR 144, page 2
[2]Toro 2003 [DIRS 163720], SR 146, page 4
NOTE: To convert kilometers to miles, multiply by 0.62137

5-10 Hz

Case	ML	MM	MH
Weight	0.18	0.64	0.18
M	5.5	6.3	7.0
R (km)	1.3	1.3	8.8
Epsilon	2.53	2.53	2.53
Scale Factor	5.545	3.563	4.973

Source: DTN: MO0209UNHAZ107.000 [DIRS 163724]
Toro 2003 [DIRS 163720], SR 143, page 2
NOTE: To convert kilometers to miles, multiply by 0.62137

Table 6.2-9a. Magnitude, Distance, Epsilon, and Scale Factor on Vertical Ground Motions of DEAs at 10^{-3} Annual Exceedance Frequency

1-2 Hz

Case	ML	MM	MH
Weight[1]	0.18	0.64	0.18
M	5.3	6.4	7.6
R (km)	3.8	35	76
Epsilon[1]	1.1	1.1	1.1
Scale Factor[1]	0.962	2.046	1.515

Source: DTN: MO0211REDES103.000 [DIRS 170424]
[1]Toro 2003 [DIRS 163720], SR 189, page 3
NOTE: To convert kilometers to miles, multiply by 0.62137

5-10 Hz

Case	ML	MM	MH
Weight[1]	0.18	0.64	0.18
M	5.1	5.9	7.3
R (km)	3.8	19	54
Epsilon[1]	1.1	1.1	1.1
Scale Factor[1]	0.625	1.35	2.48

Source: DTN: MO0211REDES103.000 [DIRS 170424]
[1]Toro 2003 [DIRS 163720], SR 189, page 3
NOTE: To convert kilometers to miles, multiply by 0.62137

Table 6.2-9b. Magnitude, Distance, Epsilon, and Scale Factor on Vertical Ground Motions of DEAs at $5x10^{-4}$ Annual Exceedance Frequency

1-2 Hz

Case	ML	MM	MH
Weight[1]	0.18	0.64	0.18
M	5.3	6.4	7.6
R (km)	1.3	18.8	71.3
Epsilon[1]	1.6	1.6	1.6
Scale Factor[1]	0.799	0.832	1.442

Source: DTN: MO0208UNHZ5X10.000 [DIRS 163722]
[1]Toro 2003 [DIRS 163720], SR 110, page 5
NOTE: To convert kilometers to miles, multiply by 0.62137

5-10 Hz

Case	ML	MM	MH
Weight[1]	0.18	0.64	0.18
M	5.1	5.9	7.1
R (km)	1.3	9.0	51.3
Epsilon[1]	1.3	1.3	1.3
Scale Factor[1]	0.693	0.699	3.475

Source: DTN: MO0208UNHZ5X10.000 [DIRS 163722]
[1]Source: Toro 2003 [DIRS 163720], SR 110, page 6
NOTE: To convert kilometers to miles, multiply by 0.62137

Table 6.2-9c. Magnitude, Distance, Epsilon, and Scale Factor on Vertical Ground Motions of DEAs at 10^{-4} Annual Exceedance Frequency

1-2 Hz

Case	ML	MM	MH
Weight[1]	0.18	0.69	0.13
M	5.4	6.4	7.8
R (km)	5	20	74
Epsilon[1]	2.1	2.1	2.1
Scale Factor[1]	1.416	1.337	1.927

Source: DTN: MO0211DERES104.000 [DIRS 170423]
[1]Toro 2003 [DIRS 163720], SR 176, page 3
NOTE: To convert kilometers to miles, multiply by 0.62137

5-10 Hz

Case	ML	MM	MH
Weight[1]	0.18	0.64	0.18
M	5.2	6	7
R (km)	5	10	15
Epsilon[1]	0.9	0.9	0.9
Scale Factor[1]	2.645	2.091	1.699

Source: DTN: MO0211DERES104.000 [DIRS 170423]
[1]Toro 2003 [DIRS 163720], SR 176, page 3
NOTE: To convert kilometers to miles, multiply by 0.62137

Table 6.2-9d. Magnitude, Distance, Epsilon, and Scale Factor on Vertical Ground Motions of DEAs at 10^{-5} Annual Exceedance Frequency

1-2 Hz

Case	ML	MM	MH
Weight	0.163	0.733	0.104
M	5.5	6.4	7.8
R (km)	1.5	15	70
Epsilon	2.26	2.26	2.26
Scale Factor	2.13	2.247	4.188

Source: DTN: MO0308UNHAZ105.000 [DIRS 170425]

NOTE: To convert kilometers to miles, multiply by 0.62137

5-10 Hz

Case	ML	MM	MH
Weight	0.18	0.64	0.18
M	5.3	6.1	7
R (km)	1.3	7	14
Epsilon	2	2	2
Scale Factor	2.144	1.75	2.025

Source: DTN: MO0308UNHAZ105.000 [DIRS 170425]

NOTE: To convert kilometers to miles, multiply by 0.62137

Table 6.2-9e. Magnitude, Distance, Epsilon, and Scale Factor on Vertical Ground Motions of DEAs at 10^{-6} Annual Exceedance Frequency

1-2 Hz

Case	ML	MM	MH
Weight[1]	0.0834	0.8452	0.0715
M	5.2	6.4	7.8
R (km)	1.3	3.8	59.0
Epsilon[1]	2.56	2.56	2.56
Scale Factor[1]	5.285	1.917	6.433

Source: DTN: MO0206UNHAZ106.001 [DIRS 163723]

[1]Toro2003 [DIRS 163720], SR 94, page 8

NOTE: To convert kilometers to miles, multiply by 0.62137

5-10 Hz

Case	ML	MM	MH
Weight[1]	0.18	0.64	0.18
M	5.4	6.2	7.0
R (km)	1.3	3.8	11.0
Epsilon[1]	2.69	2.69	2.69
Scale Factor[1]	2.873	1.901	2.304

Source: DTN: MO0206UNHAZ106.001 [DIRS 163723]
[1]Toro 2003 [DIRS 163720], SR 94, page 6
NOTE: To convert kilometers to miles, multiply by 0.62137

Table 6.2-9f. Magnitude, Distance, Epsilon, and Scal e Factor on Vertical Ground Motions of DEAs at 10^{-7} Annual Exceedance Frequency

1-2 Hz

Case	ML	MM	MH
Weight[1]	0.0475	0.8833	0.0693
M	5.2	6.4	7.8
R (km)	1.3	3.8	51.0
Epsilon[1]	2.81	2.81	2.81
Scale Factor[1]	9.23	3.40	10.03

Source: DTN: MO0209UNHAZ107.000 [DIRS 163724]
[1]Toro 2003 [DIRS 163720], SR 160, page 2
NOTE: To convert kilometers to miles, multiply by 0.62137

5-10 Hz

Case	ML	MM	MH
Weight[1]	0.18	0.64	0.18
M	5.5	6.3	7.0
R (km)	1.3	1.3	8.8
Epsilon[1]	2.53	2.53	2.53
Scale Factor[1]	6.46	3.78	4.46

Source: DTN: MO0209UNHAZ107.000 [DIRS 163724]
[1]Toro 2003 [DIRS 163720], SR 160, page 2
NOTE: To convert kilometers to miles, multiply by 0.62137

6.2.2.5.1 Incidence Angles

Appropriate body-wave incidence angles (as measured from the vertical) for each DEA control motion are estimated using source distance and depth. Ray-tracing methods (Ou and Herrmann, 1990 [DIRS 170648]) were used to determine P- and S-wave incidence angles at Point A. The crustal model used in the ray-tracing (Table 6.2-10) is based on a crustal velocity profile for Yucca Mountain from Schneider et al. (1996 [DIRS 103270], Section 5). This profile was also used in the development of ground motion attenuation relations in the PSHA (CRWMS M&O 1998a [DIRS 103731], Section 5.3.2). For consistency with the reference rock outcrop (Point A)

in the PSHA, the top four layers in the Schneider et al. (1996 [DIRS 103270]) model are removed and replaced with a 0.70 km thick V_S 1.9 km/sec layer.

Table 6.2-10. Crustal Velocity Profiles at Point A Used in Ray-Tracing

Thickness (km)	V_S (km/sec)	V_P (km/sec)	Density (cgs)
0.70	1.9	3.2	2.4
0.60	2.1	3.6	2.4
1.50	2.9	5.0	2.5
2.20	3.4	5.8	2.7
10.70	3.5	6.2	2.8
16.00	3.8	6.5	2.9
Half-space	4.6	7.8	3.3

Source: Schneider et al. (1996 [DIRS 103270], Table 5.2)

NOTES: Top layer thickness has been modified to 0.70 km (Wong and Silva 2004d [DIRS 172075], page 28).

To convert kilometers to miles, multiply by 0.62137
To convert kilometers per second to feet per second, multiply by 3281

A point source depth of 7.5 km, the middle of the seismogenic crust in the western U.S. (WUS), was used for earthquakes greater than **M** 5.5. For events **M** ≤ 5.5, a point-source depth of 5.0 km was used. These point-source depths are derived from observations of WUS crustal seismicity (e.g., McGuire et al. 2001 [DIRS 157510], Table 6-2) and are generally consistent with evaluations of the thickness of the seismogenic crust that were made during the PSHA for Yucca Mountain. For the PSHA, expert teams assigned the most weight to a seismogenic crustal thickness of 12 to 18 km (CRWMS M&O 1998a [DIRS 103731], Table 4-1). The expert teams assigned a mean depth of seismicity generally in the range of 8 to 9 km.

P- and S-wave incidence angles are given in Tables 6.2-11 to 6.2-16. Incidence angles for SV- and SH-waves differ because the SV-wave angles are limited by the critical angle due to coupling with P-waves. Mathcad 2000 and Microsoft Excel 2000 were used to compute incidence angles (see Appendix I).

OCRWM Project Condition Report 1960 documents that an incorrect value for the top layer thickness in the crustal model was used in carrying out the analysis/modeling. Sensitivity studies were carried out to evaluate the impact of the use of incorrect layer thickness and show that the calculated incidence angles differ on average for all the various cases by less than 0.20 degree. The sensitivity studies are documented in Wong and Silva (2004d [DIRS 172075], page 28). Differences in the calculated ground motions are expected to be negligible when compared to the variability and uncertainty incorporated into the overall analysis and modeling. Thus, the results obtained using the incorrect input are considered to be valid and used in this study.

Table 6.2-11. Incidence Angles for Control Motions at 10^{-3} Annual Exceedance Frequency

Wave Type	Component	Frequency Range	Incidence Angle (Degrees)			
			DEA-ML	DEA-MM	DEA-MH	RE
SH	Horizontal	1-2	21.54	32.58	32.84	32.77
SH	Horizontal	5-10	21.54	31.44	32.78	25.17
SV	Horizontal	1-2	(15.75)	(15.75)	(15.75)	(15.75)
SV	Horizontal	5-10	(15.75)	(15.75)	(15.75)	(15.75)
SV	Vertical	1-2	(15.75)	(15.75)	(15.75)	(15.75)
SV	Vertical	5-10	(15.75)	(15.75)	(15.75)	(15.75)
P	Vertical	1-2	21.05	26.55	26.55	26.55
P	Vertical	5-10	21.05	26.55	26.55	24.57

Source: Wong and Silva 2004a [DIRS 170443], page 126, SR 118

NOTE: Values in parentheses signify critical angles

Table 6.2-12. Incidence Angles for Control Motions at $5x10^{-4}$ Annual Exceedance Frequency

Wave Type	Component	Frequency Range	Incidence Angle (Degrees)			
			DEA-ML	DEA-MM	DEA-MH	RE
SH	Horizontal	1-2	8.91	31.41	32.83	32.76
SH	Horizontal	5-10	8.91	26.27	32.77	18.91
SV	Horizontal	1-2	8.91	(15.75)	(15.75)	(15.75)
SV	Horizontal	5-10	8.91	(15.75)	(15.75)	(15.75)
SV	Vertical	1-2	8.91	(15.75)	(15.75)	(15.75)
SV	Vertical	5-10	8.91	(15.75)	(15.75)	(15.75)
P	Vertical	1-2	8.71	26.55	26.55	26.55
P	Vertical	5-10	8.71	25.29	26.55	18.27

Source: Wong and Silva 2004a [DIRS 170443], page 126, SR 118

NOTE: Values in parentheses signify critical angles

Table 6.2-13. Incidence Angles for Control Motions at 10^{-4} Annual Exceedance Frequency

Wave Type	Component	Frequency Range	Incidence Angle (Degrees)			
			DEA-ML	DEA-MM	DEA-MH	RE
SH	Horizontal	1-2	25.17	31.61	32.83	32.77
SH	Horizontal	5-10	25.17	27.35	30.40	25.80
SV	Horizontal	1-2	(15.75)	(15.75)	(15.75)	(15.75)
SV	Horizontal	5-10	(15.75)	(15.75)	(15.75)	(15.75)
SV	Vertical	1-2	(15.75)	(15.75)	(15.75)	(15.75)
SV	Vertical	5-10	(15.75)	(15.75)	(15.75)	(15.75)
P	Vertical	1-2	24.57	26.55	26.55	26.55
P	Vertical	5-10	24.57	26.29	26.55	24.57

Source: Wong and Silva 2004a [DIRS 170443], page 126, SR 118

Note: Values in parentheses signify critical angles

Table 6.2-14. Incidence Angles for Control Motions at 10^{-5} Annual Exceedance Frequency

Wave Type	Component	Frequency Range	Incidence Angle (Degrees)			
			DEA-ML	DEA-MM	DEA-MH	RE
SH	Horizontal	1-2	10.17	30.40	32.83	32.76
SH	Horizontal	5-10	8.91	23.33	30.00	16.01
SV	Horizontal	1-2	10.17	(15.75)	(15.75)	(15.75)
SV	Horizontal	5-10	8.91	(15.75)	(15.75)	16.01
SV	Vertical	1-2	10.17	(15.75)	15.75	(15.75)
SV	Vertical	5-10	8.91	(15.75)	(15.75)	16.01
P	Vertical	1-2	9.96	26.55	26.55	26.55
P	Vertical	5-10	8.71	22.49	26.55	15.48

Source: Wong and Silva 2004a [DIRS 170443], page 126, SR 118

Note: Values in parentheses signify critical angles

Table 6.2-15. Incidence Angles for Control Motions at 10^{-6} Annual Exceedance Frequency

Wave Type	Component	Frequency Range	Incidence Angle (Degrees)			
			DEA-ML	DEA-MM	DEA-MH	RE
SH	Horizontal	1-2	8.91	15.37	32.80	32.76
SH	Horizontal	5-10	8.91	15.37	28.22	4.47
SV	Horizontal	1-2	8.91	15.37	(15.75)	(15.75)
SV	Horizontal	5-10	8.91	15.37	(15.75)	4.47
SV	Vertical	1-2	8.91	15.37	(15.75)	(15.75)
SV	Vertical	5-10	8.91	15.37	(15.75)	4.47
P	Vertical	1-2	8.71	14.86	26.55	26.55
P	Vertical	5-10	8.71	14.86	26.55	4.33

Source: Wong and Silva 2004a [DIRS 170443], page 126, SR 118
NOTE: Values in parentheses signify critical angles

Table 6.2-16. Incidence Angles for Control Motions at 10^{-7} Annual Exceedance Frequency

Wave Type	Component	Frequency Range	Incidence Angle (Degrees)			
			DEA-ML	DEA-MM	DEA-MH	RE
SH	Horizontal	1-2	8.91	15.37	32.76	32.76
SH	Horizontal	5-10	8.91	5.78	26.03	4.47
SV	Horizontal	1-2	8.91	15.37	(15.75)	(15.75)
SV	Horizontal	5-10	8.91	5.78	(15.75)	4.47
SV	Vertical	1-2	8.91	15.37	(15.75)	(15.75)
SV	Vertical	5-10	8.91	5.78	(15.75)	4.47
P	Vertical	1-2	8.71	14.86	26.55	26.55
P	Vertical	5-10	8.71	5.60	25.06	4.33

Source: Wong and Silva 2004a [DIRS 170443], page 126, Supplemental Record 118
NOTE: Values in parentheses signify critical angles

6.2.2.6 Calculation of Vertical Uniform Hazard Spectra

Examination of the vertical and horizontal UHS for Point A derived from the Yucca Mountain PSHA (Figures 6.2-5 to 6.2-16) reveals four characteristics that are inconsistent with trends recently observed in empirical data and with the results of numerical modeling evaluations of V/H ratios (McGuire et al. 2001 [DIRS 157510], Section 4.7). First, at nearly all structural frequencies and annual exceedance frequencies, the horizontal component is greater than the vertical component. Second, the vertical and horizontal spectra peak at approximately the same frequency. Third, the vertical UHS exhibits a dip centered at approximately 1 Hz that affects the overall UHS shape between about 0.5 Hz and 1.5 Hz. The dip becomes increasingly distinctive with decreasing annual rates of ground motion exceedance. Finally, V/H spectral ratios do not increase significantly at higher structural frequencies with decreasing annual exceedance frequencies.

These characteristics are inconsistent with observations from earthquakes of comparable distance and magnitude to those that dominate the hazard at Yucca Mountain (McGuire, et al., 2001 [DIRS 157510], Tables B-1 and B-3). McGuire et al. (2001 [DIRS 157510], Section 4.7), have evaluated the available recordings and have recommended an approach for obtaining V/H spectral ratios based on scaling horizontal UHS spectra. This approach is used to develop revised vertical-component spectra, as described in Section 6.2.2.6.3. The vertical-component spectra developed in these analyses exhibit properties observed in empirical data and incorporate site-specific adjustments that are appropriate for Yucca Mountain. Transfer functions developed from application of the site-response model are applied to the revised vertical spectra rather than the original vertical UHS.

6.2.2.6.1 Trends in Observed Horizontal and Vertical Component Motions

Recordings of large earthquakes at close distance to the fault rupture show that the vertical component of motion exceeds the horizontal component at short periods. To illustrate this effect, Figures 6.2-65 to 6.2-68 show 5%-damped pseudo-absolute response spectra for four earthquakes recorded on rock sites: site S1 for the 1985 **M** 6.8 Nahanni earthquake, the Karakyr site for the 1976 **M** 6.8 Gazli earthquake, the Lucerne site for the 1992 **M** 7.3 Landers earthquake, and the Pacoima Dam (downstream toe) record for the 1994 **M** 6.7 Northridge earthquake (McGuire et al. 2001 [DIRS 157510], Tables B-1 and B-3). The sites range from 1 to 8 km distance from the rupture. These spectra show the vertical component exceeding the horizontal components at periods less than about 0.1 sec. At long periods, greater than about 1 to 5 seconds, the vertical amplitude is comparable to either the lower or both of the horizontal components.

Comparison of observed vertical and horizontal response spectra also shows vertical component motion peaks at a shorter structural period than the horizontal component. For example, Silva (1997 [DIRS 163747]) examined vertical and horizontal component WUS empirical spectral shapes, for a magnitude range of **M** 6.0 to 7+, and two distance bins: 0 to 10 km and 10 to 50 km. Figure 6.2-69 shows median horizontal and vertical shapes for events recorded on rock sites. The vertical spectral shapes (dashed lines) show more short-period energy than the horizontal shapes (solid and dotted lines) and about the same level of maximum spectral amplification. The vertical shapes have a maximum spectral amplification or peak near 0.1 sec

whereas the shapes for the horizontal component peak near 0.2 sec. This difference can be explained through differences in damping with the vertical component showing significantly less damping than the horizontal. The lack of any significant distance dependency in this shift in peak spectral amplification between the vertical and horizontal components suggests that the difference in damping is occurring in the shallow portion of the path. This shallow crustal damping is generally modeled as a frequency-independent exponential damping term with the parameter "kappa" controlling the rate of decay (Anderson and Hough 1984 [DIRS 128813]).

Response spectral shapes depend strongly on kappa, shifting to shorter periods as kappa decreases (Silva and Darragh 1995 [DIRS 105398]). To illustrate this effect, Figure 6.2-70 shows response spectral shapes computed using a point-source representation with kappa values ranging from 0.006 sec to 0.160 sec. The shift in shape with kappa is easily seen and a peak near 0.2 sec period is consistent with a kappa value of about 0.04 sec while a factor of two shift in the peak to about 0.1 sec period corresponds to a similar shift in kappa value to about 0.02 sec.

Analyses of vertical and horizontal-component response spectral shapes for both rock and soil sites at varying magnitudes and distances showed significantly less damping at both rock and soil sites for vertical motions (Silva 1997 [DIRS 163747]). These analyses also suggested that site response to vertical motions is largely linear. In contrast, horizontal motions for earthquakes of **M** 6.0 to 7.0+ and at source distances within 10 km showed a broad-band shift in spectral shape to longer periods consistent with an increase in damping due to nonlinear site response. To support this observation, median WUS empirical V/H response spectra ratios are shown on Figure 6.2-71 for a suite of distances for both soil and rock conditions. The larger V/H ratio at short period between the soil and rock site conditions is attributable to the increase in nonlinear site response for the horizontal component relative to the vertical component (Silva 1997 [DIRS 163747]).

Systematic differences are also observed between WUS and CEUS response spectra. The only large magnitude earthquake considered representative of the CEUS and that generated close-in strong motion records is the 1985 **M** 6.8 Nahanni earthquake. It was recorded at three hard rock sites within 20 km of the source. These recordings, along with smaller magnitude CEUS hard rock recordings, clearly show that spectral content differs between WUS and CEUS horizontal rock motions. This feature is illustrated on Figure 6.2-72, which contrasts WUS (WNA) and CEUS (ENA) horizontal-component rock site response spectral shapes for **M** ~6.4 and **M** ~4.0. The difference in short-period spectral content between WUS and CEUS is significant and consistent between different magnitude earthquakes and is attributed to differences in kappa (Silva and Darragh 1995 [DIRS 105398]). Differences in kappa affect hard-rock vertical spectral shapes as well.

To further evaluate V/H ratios for CEUS hard rock conditions, the stochastic point-source numerical ground motion approach has been used to predict both rock and soil horizontal and vertical motions (Silva 1997 [DIRS 163747]). Similar predictions for WUS V/H ratios showed generally favorable agreement with empirical V/H ratios. At longer periods ($T > 0.3$ sec) results showed generally higher V/H ratios for CEUS hard rock sites (average kappa 0.006 sec; McGuire et al. 2001 [DIRS 157510], Section 4.8) compared to WUS soft rock sites (average kappa 0.040 sec; McGuire et al. 2001 [DIRS 157510], Section 4.8). At short periods, the peak in

the V/H ratio is shifted to higher frequencies for hard rock (CEUS) conditions (Silva 1997 [DIRS 163747]). These results are due to the lower kappa for the hard rock site.

6.2.2.6.2 Comparison of Vertical and Horizontal UHS to Observations

Examination of the UHS determined from the PSHA results (Section 6.2.2.3) for annual exceedance frequencies of 10^{-3}, $5x10^{-4}$, 10^{-4}, 10^{-5}, 10^{-6}, and 10^{-7} (Figure 6.2-73) reveals characteristics that are inconsistent with the observed trends described in Section 6.2.2.6.1. First, for a given annual exceedance frequency, the horizontal and vertical UHS peak at approximately the same frequency. This is in contrast to observations and numerical modeling that indicate the peak of the vertical spectrum should be shifted to higher frequencies relative to the horizontal spectrum. Second, V/H spectral ratios do not increase significantly at higher structural frequencies with decreasing annual frequencies of exceedance. This observation is counter to the trends seen in the empirical data in which closer, larger earthquakes (corresponding generally to lower rates of exceedance) exhibit larger vertical relative to horizontal motions at higher frequencies. Finally, the vertical UHS exhibit a dip at about a structural frequency of 1 Hz (e.g., Figure 6.2-38), which is not seen in observed spectral shapes. The expression of this dip appears to get stronger at lower annual exceedance frequencies. Thus, the relation between the horizontal and vertical UHS derived from the PSHA for Yucca Mountain is inconsistent with empirical observations and with recent developments in understanding the factors that drive V/H spectral ratios.

6.2.2.6.3 Revised Vertical Point A Spectra and Vertical Peak Ground Velocity

To address the issues identified in Section 6.2.2.6.2, an alternative approach is employed to develop revised Point A vertical spectra that are used in developing response spectra at Points B, D, and E. This approach is based on recommendations presented in NUREG/CR 6728 (McGuire et al. 2001 [DIRS 157510], Section 4.7) and results in more suitable V/H spectral ratios for Yucca Mountain.

The recommendations depend on site conditions (classified as WUS, CEUS, intermediate) and ground motion loading levels. For WUS site conditions, the recommendations are based on empirical relationships developed from earthquakes that have occurred in the WUS and similar tectonic regimes. For the CEUS site conditions, because recorded data are sparse even when data from similar tectonic regimes are included, the recommendations are based largely on results of numerical modeling. For site conditions that are intermediate between the site conditions in the WUS and CEUS, such as at Yucca Mountain, a weighted average is used. Site conditions are parameterized by kappa.

Figure 6.2-74 illustrates the NUREG/CR-6728 (McGuire et al. 2001 [DIRS 157510], Figure 4-36) V/H ratios for loading levels of < 0.2g, 0.2-0.5g and > 0.5g for WUS soft rock conditions. Figure 6.2-75 illustrates the V/H ratios for similar loading levels for CEUS rock (hard-rock conditions). For application to Yucca Mountain site conditions, the WUS and CEUS ratios are weighted based on a comparison of the Yucca Mountain site-specific kappa to nominal kappa values for WUS and CEUS conditions (McGuire et al. 2001 [DIRS 157510], Section 4.8). At Yucca Mountain kappa is 0.02 sec (Section 6.2.2; BSC 2004j [DIRS 168030], Section 6.3.3.1.1). For WUS and CEUS average rock, kappa values are 0.040 and 0.006 sec, respectively (McGuire

et al. 2001 [DIRS 157510], Section 4.8). Thus for Yucca Mountain, the WUS and CEUS V/H ratios are weighted by 0.412 and 0.588, respectively.

Using these weights and the WUS and CEUS V/H ratios for the <0.2 g loading level (McGuire et al. 2001 [DIRS 157510], Tables 4-4 and 4-5), reference rock outcrop (Point A) spectral V/H ratios for an annual exceedance frequency of 10^{-3} are evaluated. Figure 6.2-76 shows the 10^{-3} UHS V/H ratios together with NUREG/CR-6728 (McGuire et al. 2001 [DIRS 157510], Tables 4-4 and 4-5) recommended V/H for CEUS and WUS rock site conditions. The revised YMP V/H ratio, derived using the weighted combination of the WUS and CEUS V/H ratios, is also shown on Figure 6.2-76. At this relatively high rate of exceedance, note that the revised V/H ratio is generally greater (by as much as 20-30%) than the V/H ratio derived from the PSHA results.

Similarly, Figures 6.2-77 through 6.2-81 illustrate the revised V/H ratios for $5x10^{-4}$, 10^{-4}, 10^{-5}, 10^{-6} and 10^{-7} annual exceedance frequencies, respectively, using the WUS and CEUS V/H ratios for the $0.2<g<0.5$ loading levels for the $5x10^{-4}$ case and >0.5g loading level for the 10^{-4}, 10^{-5}, 10^{-6}, and 10^{-7} cases (McGuire et al. 2001 [DIRS 157510], Tables 4-4 and 4-5). As discussed in Section 6.3.1, the site-response transfer function is applied to the envelope of the Point A 1-2 Hz RE, 5-10 Hz RE, and the UHS, not solely the UHS. To obtain the revised Point A vertical envelope, the V/H ratios are applied to the envelope of the horizontal 1-2 Hz RE, 5-10 Hz RE, and UHS. The Point A horizontal envelope (1-2 Hz RE, 5-10 Hz RE, and UHS), original vertical envelope (1-2 Hz RE, 5-10 Hz RE, and UHS), and revised vertical envelope are shown on Figures 6.2-82 to 6.2-87. In summary, the revised V/H ratios are judged to be conservative (McGuire et al. 2001 [DIRS 157510], pages 4-18 and 4-19).

The vertical peak ground velocities corresponding to the revised vertical spectra at each annual exceedance frequency level are provided in Table 6.2-17. These revised PGV values for Point A are computed using the RASCALS program. Given the revised Point A vertical spectra, RASCALS is used to compute the corresponding PGV values for each spectrum. Details of this analysis is given in scientific notebook SN-M&O-SCI-037-V2 (Wong and Silva 2004a [DIRS 170443], page 45). These revised vertical PGVs for Point A are used in the site response analyses to compute PGVs at Point B (see Sections 6.3.1.4.1 and 6.3.1.4.2).

Table 6.2-17. Point A Peak Ground Velocities and Revised Vertical Peak Ground Velocities

Annual Exceedance Frequency	Point A Horizontal PGV	Point A Vertical PGV	Revised Point A Vertical PGV[1]
10^{-4}	48.3 cm/sec	24.9 cm/sec	46.6 cm/sec
10^{-5}	126.6 cm/sec	63.1 cm/sec	116.4 cm/sec
10^{-6}	301 cm/sec	156 cm/sec	224 cm/sec
10^{-7}	655 cm/sec	340 cm/sec	572 cm/sec

DTNs: MO0404PGVAPSHA.000 [DIRS 170436], MO0309PGVDEAGG.000 [DIRS 170426], MO0208PGVDEAG6.001 [DIRS 164203], MO0210PGVD1E07.000 [DIRS 164205]

Source: [1]Wong and Silva 2004d [DIRS 172075], page 45.

Inputs to the above analysis consist of the horizontal UHS (Section 6.2.2.3, Table 6.2-3), kappa value for the Yucca Mountain site (BSC 2004j [DIRS 168030], Section 6.3.3.1.1) and for WUS and CEUS site conditions (McGuire et al. 2001 [DIRS 157510], Section 4.8), and recommended V/H spectral ratios for WUS and CEUS site conditions (McGuire et al. 2001 [DIRS 157510], Figures 4-36 and 4-39). The commercial-off-the-shelf software program Microsoft Excel 2000 was used to carry out the analysis as documented in Appendix I. Details of the analysis are documented in scientific notebook SN-M&O-SCI-037-V2 (Wong and Silva 2004a [DIRS 170443], pages 31-32, 42, 48, 62, 80 and supplemental records 9, 14, 36, 41, 67, and 90).

6.2.2.7 Treatment of Uncertainty in Control Motions

The Point A ground motions incorporate the uncertainty in the PSHA (BSC 2004j [DIRS 168030], Section 6.5.2; CRWMS M&O 1998a [DIRS 103731], Sections 4.1.1 and 5.6). The DEA spectra used as control motions are based directly on the PSHA results.

Uncertainty was characterized in the PSHA through an expert elicitation process. Teams of experts (for seismic source and fault displacement characterization) and individual experts (for ground motion characterization) developed multiple alternative interpretations to represent the uncertainties in the inputs to the hazard calculation. They assigned weights to the viable alternative interpretations according to the assessed credibility of each given the current state of knowledge and the degree to which each alternative was supported by the available data. In computing the seismic hazard, integration is carried out over random variabilities for weighted alternative hazard input scenarios (i.e., alternative pathways through the experts' logic trees) to produce a single hazard curve and its associated weight. Uncertainty is propagated through the analysis by calculating hazard curves for all weighted alternative input scenarios. The distribution of hazard is then summarized in terms of mean, median, and fractiles of the weighted curves. In accordance with BSC (2004b [DIRS 170564], Section 3.1) and Brocoum (2001 [DIRS 159576]), mean hazard results are used to develop ground motion inputs for preclosure and postclosure analyses.

Because of the characterization of ground motion inputs for the PSHA, including the use of unbounded probability distributions, the mean ground motion hazard reaches a level that is not credible for the Yucca Mountain site as low annual frequencies of exceedance are considered. That is, the ground motions reach a level that would produce shear strains in the rock at Yucca Mountain that would cause the rock to fail pervasively, which is not observed. In the modeling and analysis described in this report, however, the ground motions determined by the PSHA are used without modification. A bound to ground motion at Yucca Mountain (BSC 2004c [DIRS 170137]) is applied at a later stage in the postclosure seismic process, as part of the seismic consequence abstraction (BSC 2004m [DIRS 169183]).

To develop the final vertical-component motions for locations of interest, V/H ratios are applied to the Point A horizontal enveloped UHS (see Section 6.3.1.1.2). The vertical ground motions thus reflect the uncertainties of the horizontal PSHA results on which they are based as no additional uncertainty from the application of the V/H ratios was included in the analysis.

6.2.2.8 Potential Conservatisms in the Revised Vertical Motions

In the context of probabilistically-based seismic demands (i.e., the performance-based approach), desired conservatism is properly defined by the hazard levels (annual frequencies of exceedance) appropriate for assuring that seismic design or performance assessment safety criteria provided by the regulation are achieved. To maintain the exceedance level of the hazard results, site response as well as structural analyses and performance assessment are mean based, preserving the integrity of a performance-based approach. However, some conservatism enters the process and is reflected in the mean, primarily through the incorporation of large associated epistemic uncertainty. Development of site-specific vertical motions incorporates conservative assessments of epistemic uncertainty together with the random variability in material properties and dynamic response of the materials into the seismic demand motions.

Because vertical motions rarely control design, limited past effort has gone into the study of recorded vertical motions and development of site-specific vertical motions. Typically vertical motions for design are taken as some fraction (0.7 to 1.0) of horizontal design motions. For this project, because the importance to design and performance assessment was not known *a-priori*, more careful consideration was given to developing site-specific vertical ground motions than is commonly done. The approaches used reflect the less knowledge and maturity for determining vertical motions compared to horizontal motions, with the consequence that some conservatism enters the development process.

This conservatism enters in two places: 1) the soft and hard rock design V/H ratios (McGuire et al. 2001 [DIRS 157510], Section 4.7) used to develop site-specific V/H ratios and the use of envelopes of horizontal reference earthquake response spectra and 2) the UHS (1 to 2 Hz RE, 5 to 10 Hz RE, UHS) to which the V/H ratios are applied. In developing the soft and hard rock V/H ratios, magnitude and distance dependencies (Silva 1997 [DIRS 163747]) were cast in the form of expected horizontal peak acceleration values, for ease of implementation. In this process of reducing V/H ratio dependencies from two continuous explanatory variables (magnitude and distance) to a single three-level variable for engineering applications, some conservatism enters. The degree of conservatism in this process depends on the expected horizontal peak acceleration value with respect to the three levels (0 to 0.2g, 0.2g to 0.5g, > 0.5g) in the hard and soft rock design V/H ratios (McGuire et al. 2001 [DIRS 157510], Section 4.7). Horizontal peak accelerations that are just above the boundaries are likely to have the largest conservatism in the V/H ratios while horizontal peak accelerations just below boundaries may have little or no conservatism. It is judged that the maximum conservatism does not exceed 10 to 20%.

The second conservatism is driven by a strict implementation of Regulatory Guide 1.165 (1997 [DIRS 119139]) procedures for the enveloping of reference earthquake spectra to define Safe Shutdown Earthquake ground motions. This enveloping process, which is applied in developing site-specific ground motions (both horizontal and vertical) for Yucca Mountain, propagates through all subsequent analyses and effectively lowers the probability levels of the design motions over some frequency ranges. As stated in NUREG-CR/6728 (McGuire et al. 2001 [DIRS 157510]), the UHS, provided attenuation relations appropriate for the region were used, correctly reflects the ground motion hazard of the site and should be considered as representing the appropriate control motion for deriving seismic design motions as well as the appropriate motions for postclosure performance analysis.

6.2.3 Development of Seismic Velocity Profiles

Major inputs into the site response model are the V_S and V_P profiles for the Repository Block and the Surface Facilities Area. Beginning in the spring of 2000, a geotechnical, geologic, and geophysical program of investigations was undertaken to characterize the velocity structure and the nonlinear dynamic material properties of the Repository Block above the waste emplacement level (Figure 6.2-88) and beneath the area termed the waste handling buildings site characterization area (referred hereon as the WHB Area; Figure 6.2-89) (BSC 2002a [DIRS 157829]). The WHB Area was originally anticipated to encompass the area where waste is handled. These new data supplement pre-existing data obtained during previous investigations (e.g., CRWMS M&O 1999 [DIRS 109209]). The following provides an overview of the geology of the Repository Block and WHB Area, a summary of the investigations that were performed in 2000-2001, the development of V_S, V_P, and density profiles, and the probabilistic representation used to randomize the base case V_S and V_P profiles. Uncertainties in the model input and their limitations are also discussed.

The outline of the proposed waste emplacement area has changed over time. For site recommendation work, the base case repository layout consisted of emplacement drifts situated to the west of the main drift of the Exploratory Studies Facility (ESF). The emplacement area extended from about the latitude of the ESF south ramp to 2 km north of the ESF north ramp (DOE 2001 [DIRS 153849], Section 2.3.1.1, Figure 2-38). This area, referred to as the "upper block," was the focus of geotechnical investigations to characterize the Repository Block. Subsequent to the site recommendation, ideas concerning the repository layout have evolved with the objectives of reducing uncertainties in a License Application and supporting a flexible design with respect to waste types and receipt rates (BSC 2002b [DIRS 157756], p. vii). BSC (2002b [DIRS 157756], Figures 4-5 and 5-4) suggest a repository outline that includes much of the base case outline used for site recommendation evaluations and expands the outline to include additional area to the east (Figure 6.2-90). The repository footprint follows the BSC (2002b [DIRS 157756]) recommendations, except that the easternmost panel, Panel 4, is not included (Figure 6.2-90). Also, the current layout has re-numbered the panels to reflect a revised order for excavation.

Because some of the outline of the proposed waste emplacement area was not well covered by the 2000-2001 geotechnical investigations (Figure 6.2-90), Vertical Seismic Profiling (VSP) data collected in 1995 in the southern portion of the lower block (Majer et al. 1996b [DIRS 104685], Section IV) were evaluated (Figure 6.2-90) and are discussed in Section 6.2.3.2.5. This data limitation resulted, in part, in the use of two base case profiles for the repository block (Section 6.2.3.3.1).

6.2.3.1 Inputs for Development of Seismic Velocity Profiles

Input data used in the analysis to develop seismic velocity profiles are listed in Table 6.2-18. Most of these data were acquired during investigations in 2000 and 2001. One set of data (DTN LB0306VSP95DAT.001 [DIRS 164559]) was acquired earlier. The scope and techniques used in these investigations are summarized in the subsections below. For some input data, not all the data associated with a DTN is used in the velocity profile analyses. In these cases, the discussion below includes justification for the data that are excluded.

In addition to the input data listed in Table 6.2-18, design data on the extent of the repository outline are also used in the analyses. These data are taken from 800-IED-WIS0-00101-000-00A (BSC 2004d [DIRS 164519]).

Table 6.2-18. Input Data for Development of Seismic Velocity Profiles

Input Data	Data Source	Data Tracking Number
Velocity Seismic Profile Results from Boreholes NRG-6, WT-2, RF-4, RF-7/7A, SD-12, G-2 & G-4	Majer et al. (1996b [DIRS 104685], Section IV)	LB0306VSP95DAT.001 [DIRS 164559]
Downhole Velocity Measurements at the WHB Site (Shear and Compression Wave Velocity Profiles from boreholes RF#13, 14, 15, 16, 17, 18, 19, 20, 21, 22, 23, 24, 25, 26, 28, & 29)	BSC (2002a [DIRS 157829], Section 6.2.5)	MO0111DVDWHBSC.001 [DIRS 157296]
Downhole Velocity Measurements at the WHB Site (Shear and Compression Wave Velocity Profiles from boreholes RF#13 & 17)	BSC (2002a [DIRS 157829], Section 6.2.5)	MO0110DVDBOREH.000 [DIRS 157295]
Downhole Velocity Measurements from the Top of Yucca Mountain (Shear and Compression Wave Velocity Profiles from boreholes UZ-N66, UZ-N94, UZ-N71, UZ-N75, UZ-N64, UZ-N27, & UZ-N46)	BSC (2002a [DIRS 157829], Section 6.4.3)	MO0202DVDWHBSC.002 [DIRS 158078]
SASW Velocity Data from the WHB Site Characterization Area (SASW = Spectral Analysis of Surface Waves)	BSC (2002a [DIRS 157829], Section 6.2.7)	MO0110SASWWHBS.000 [DIRS 157969]
SASW Velocity Data from the Top of Yucca Mountain (2000)	BSC (2002a [DIRS 157829], Section 6.4.2)	MO0203SEPSASWD.000 [DIRS 158084]
SASW Velocity Data from the Top of Yucca Mountain (2001)	BSC (2002a [DIRS 157829], Section 6.4.2)	MO0110SASWVDYM.000 [DIRS 158076]
SASW Velocity Data from Rock Sites on Yucca Mountain and in the ESF	BSC (2002a [DIRS 157829], Sections 6.3.2 and 6.4.2)	MO0206SASWROCK.000 [DIRS 159081]
Borehole Suspension Data for the WHB Site Characterization Area	BSC (2002a [DIRS 157829], Section 6.2.6)	MO0204SEPBSWHB.001 [DIRS 158088]
Borehole Suspension Data for RF#13 at WHB Site Characterization Area	CRWMS M&O (1999 [DIRS 109209], Section 4.4, Appendix O)	MO0204SEISDWHB.001 [DIRS 158086]
Geotechnical Borehole Logs from RF#13, 14, 15, 16, 17, 18, 19, 20, 21, 22, 23, 24, 25, 26, 28 & 29	BSC (2002a [DIRS 157829], Sections 6.2.2, 6.2.3, and 6.6.2)	GS030783114233.001 [DIRS 164561]

6.2.3.2 Overview of 2000-2001 Geotechnical Site Investigations

This section provides an overview of geotechnical site investigations carried out in 2000 and 2001 (BSC 2002a [DIRS 157829], Section 6.1). During the geotechnical investigations, field and geotechnical laboratory data were acquired for three distinct geographic areas: the WHB Area, the North Ramp and Main Drift of the Exploratory Studies Facility (ESF), and the Repository Block. Borehole RF#13, which was drilled in 1998 (CRWMS M&O 1999 [DIRS 109209]), was re-occupied to perform velocity surveys. Data that were acquired in 2000 and 2001 within the WHB Area consist of:

- Geologic data from fifteen new boreholes. The new boreholes are designated UE-25 RF#14 through UE-25 RF#26 and UE-25 RF#28 through UE-25 RF#29 (Figure 6.2-92).

- V_S and V_P profiles from downhole seismic surveys at boreholes RF#13 through RF#29.

- V_S and V_P profiles from suspension seismic surveys at boreholes RF#13 through RF#29.

- Caliper and gamma-gamma wireline surveys in boreholes RF#16, RF#18, RF#20, RF#21, RF#22, RF#24, and RF#28.

- V_S profiles from spectral-analysis-of-surface-waves (SASW) surveys SASW-1 to SASW-36 and D-12.

- Geologic data, photographs and in-place density measurements in the alluvium encountered in test pits TP-WHB-1 to TP-WHB-4.

- Maximum density, minimum density, specific gravity, particle-size distribution, in-place density, natural water content, and relative density corresponding to in-place density tests that were performed in test pits.

- Resonant column and torsional shear (RCTS) test results for samples of tuff and alluvium (includes density, water content, shear-wave velocity, and shear modulus and material damping ratio as a function of shear strain and confining pressure).

Data that were acquired in 2000 and 2001 along the North Ramp and Main Drift of the ESF consist of:

- V_S profiles from SASW surveys T-1 to T-5.
- RCTS test results for samples of bedrock taken in the ESF North Ramp.

Crosshole seismic surveys were attempted but did not yield useable results because the piezoelectric seismic source was unable to generate sufficient energy in the shallow soft rock surrounding the ESF.

Data that were acquired in 2000 and 2001 for the Repository Block consist of:

- SASW surveys C-1 to C-7, S-1 to S-12, D-1 to D-11, and R-1 to R-3.

- Downhole seismic surveys using existing boreholes UZ-N27, UZ-N33, UZ-N46, UZ-N64, UZ-N66, UZ-N71, UZ-N75, and UZ-N94.

Exploratory drilling in the WHB Area began in June 2000 and concluded in November 2000 at the locations shown on Figure 6.2-92. The drilling program was developed to gain an understanding of the subsurface geologic conditions and provide access for downhole geophysical methods. Fifteen new boreholes were drilled, seven "deep" boreholes (> 400 ft deep) and eight "shallow" boreholes (Table 6.2-19). The borehole depths were selected with the objective that deep boreholes would extend 100 feet into bedrock with a V_S of at least 5,000 ft/sec and shallow boreholes would extend 50 feet into the densely welded Tiva Canyon

Tuff. Because the V_S in the deep boreholes will not be known until after the holes had been drilled and cased, the depths at which 5,000 ft/sec rock would be found in each borehole were estimated based on earlier downhole seismic survey results from borehole RF#13. A target was established of about 20 to 30 feet into the Tiva Canyon Tuff crystal-poor middle nonlithophysal zone (Tpcpmn).

Table 6.2-19. WHB Site Characterization Area Borehole Locations, Total Depth, and Drilling Method

Designation	Northing	Easting	Surface Elevation (ft.)	Total Depth (ft.)	Drilling Method
RF#13*	N765,500	E570,720	3671.0	350.1	Core
RF#14	N765,309	E571,065	3651.5	550.0	Core
RF#15	N765,774	E570,225	3681.0	330.0	Core
RF#16	N765,056	E570,473	3672.0	452.8	Core
RF#17	N766,076	E571,042	3672.4	667.8	Core
RF#18	N764,522	E570,627	3640.3	493.6	Mud Rotary
RF#19	N765,880	E571,384	3661.8	645.2	Mud Rotary
RF#20	N765,637	E570,797	3671.3	160.0	Mud Rotary
RF#21	N765,899	E570,739	3673.0	192.2	Mud Rotary
RF#22	N766,206	E570,793	3679.2	540.6	Mud Rotary/core
RF#23	N765,311	E570,465	3674.0	159.1	Mud Rotary
RF#24	N766,344	E570,542	3684.5	268.0	Mud Rotary
RF#25	N765,968	E570,626	3676.5	159.0	Mud Rotary
RF#26	N765,248	E570,580	3670.8	264.9	Mud Rotary
RF#28	N765,510	E570,105	3680.6	99.8	Mud Rotary
RF#29	N766,018	E570,836	3672.7	430.0	Mud Rotary

Source: DTN: GS030783114233.001 [DIRS 164561]

NOTE: * RF#13 was drilled in 1998 (CRWMS M&O 1999 [DIRS 109209], Appendix L)

Geologic data acquired in the boreholes included depth (below ground surface) of lithostratigraphic subunit contacts; depth and dip of faults and other structural features; rock hardness, welding, and fracture density; percent core recovery, and Rock Quality Designation (RQD). Given the difficulty of collecting useful information regarding geotechnical properties in alluvial material with a significant gravel and cobble content, it was elected to core through the alluvium in the four core boreholes. This method allowed collection of representative, though disturbed, samples of the alluvium and a better understanding of the nature of caliche cementation in the alluvial material. The boreholes were cased with PVC to allow various geophysical surveys to be conducted.

6.2.3.2.1 Geology of Repository Block and WHB Area

The following summary is extracted from BSC (2002a [DIRS 157829], Section 6.6) and the *Yucca Mountain Site Description* (BSC 2004i [DIRS 169734]). Yucca Mountain and the WHB Area lie within the central southern part of Nevada within the Great Basin, which is part of the Basin and Range structural/physiographic province. Pre-Tertiary rocks, consisting of a thick

sequence of Proterozoic and Paleozoic sedimentary rocks, underlie approximately 3,300 to 9,800 ft of Miocene volcanic rock in the Yucca Mountain area.

Yucca Mountain is an irregularly shaped upland, 4 to 6 mi. wide and about 22 mi. long. The crest of Yucca Mountain is at an average elevation of about 4,900 ft (Figure 6.2-91). Elevation of the ground surface in the region ranges from about 3,000 ft southeast of the site, in the lower reaches of Forty Mile Wash, to over 6,000 ft about 4 mi. to the north, in the area of the Timber Mountain caldera. Near the site of the proposed surface facilities, relief is approximately 250 ft, ranging from about elevation 3,850 ft at the crest of Exile Hill, to the west, to about elevation 3,600 ft at the center of Midway Valley, to the east (The WHB Area is located just to the east of Exile Hill on Figure 6.2-88).

Yucca Mountain consists of stacked layers of tuffs (Figure 6.2-93), approximately 15 to 7.5 million years old, that formed by eruptions of volcanic ash from the north (BSC 2002a [DIRS 157829], Section 6.6). Individual layers of volcanic tuff, therefore, get progressively thinner from north to south. Most of the rocks are welded and nonwelded ash flow tuffs. As the ash settled, it was subjected to various degrees of compaction and fusion, depending on the temperature and pressure. When the temperature was high enough, ash was compressed and fused to produce a welded tuff, a hard, dense, brick-like rock with little open pore space in the rock matrix. Nonwelded tuffs occur between the layers of welded tuff. These tuffs are compacted and consolidated at lower temperatures, are less dense and brittle, and have a higher porosity. The composition of the rocks at Yucca Mountain ranges from rhyolite to dacite or latite.

Three main volcanic tuff layers are present at the planned repository at Yucca Mountain: the Tiva Canyon Tuff welded tuff at the surface, the Topopah Springs Tuff welded tuff at the planned level of waste emplacement and intervening nonwelded tuff units. As a result of faulting over the last 13 million years, these layers are all tilted to the east with dips ranging from about 5 to 20 degrees. The layer of nonwelded tuff that underlies the Tiva Canyon welded tuff consists of the Pah Canyon Tuff and Yucca Mountain Tuff. Below these nonwelded tuffs is the Topopah Springs Tuff, which is the host rock for the planned repository tunnels. The Topopah Spring Tuff has a maximum thickness of about 1,230 ft near Yucca Mountain. Using information from boreholes and the ESF tunnel exposures of the unit, further subdivision of four layers within this unit has been developed. An important distinguishing characteristic of these layers is the presence or absence of lithophysae or small to large bubble-like holes or voids within the rock mass that formed 13 million years ago as this ash flow tuff cooled. Like the Tiva Canyon Tuff above, this unit is commonly fractured.

The WHB Area is situated mainly in Midway Valley along the east side of Exile Hill, though a small part of the area laps onto Exile Hill (BSC 2002a [DIRS 157829], Section 6.6.1). Exile Hill is a horst, bounded on its west side by the Bow Ridge fault and on its east side by the Exile Hill fault. Exile Hill consists of Tiva Canyon Tuff that is surrounded and partially covered by Quaternary alluvium/colluvium. The upper Tertiary and Quaternary sediments that fill Midway Valley consist mostly of alluvial deposits (fluvial and colluvial sediments) and some thin eolian deposits. Over most of the WHB Area the alluvium is covered by an artificial fill known as the North Portal pad or by the adjacent muck piles. The North Portal pad is about 800 to 1,200 by 600 to 700 ft in size and slopes roughly 2 degrees to the east, from approximately elevation

3,685 ft at the base of Exile Hill to 3,670 ft. The North Portal pad fill was constructed of colluvium and bedrock from shallow excavations at the toe of Exile Hill and for the ESF's north portal, alluvium from distant borrow pits, and tunnel muck.

Figure 6.2-92 is a plan view map showing the location of boreholes, interpreted geologic structures (faults as indicated by thin, thick, and dashed red lines), and cross-sections locations (BSC 2002a [DIRS 157829], Section 6.6.2). Cross section, A-A′ through the center of the WHB Area (Figure 6.2-93) illustrates the subsurface geologic interpretation developed for the site. Section A-A' is cut approximately parallel to the dip of the volcanic stratigraphy. The alluvium varies in thickness from zero on the western edge of the WHB Area along the base of Exile Hill to over 100 ft in the part of the area located east of the muck pile. Alluvial materials in the WHB Area consist of interbedded caliche-cemented and non-cemented, poorly sorted gravel with some fines, cobbles and boulders.

Under the alluvium are welded and non-welded volcanic rock units of the Timber Mountain and Paintbrush groups (BSC 2002a [DIRS 157829], Section 6.6.2). Figure 6.2-94 provides a lithostratigraphic column for relevant units of these groups. Non-welded units beneath the site include the pre-Rainier Mesa Tuff bedded tuffs (Tmbt1) of the Timber Mountain Group, and the Tuff unit "x" (Tpki) and pre-Tuff unit "x" bedded tuffs (Tpbt5) of the Paintbrush Group. Beneath these non-welded units is the Tiva Canyon Tuff, which is generally densely welded. The Tiva Canyon Tuff has been divided into two members; the younger crystal-rich member (Tpcr) and the older crystal-poor member (Tpcp). These members are further divided into zones, for example, the Tiva Canyon Tuff crystal-rich nonlithophysal zone (Tpcrn) (Buesch et al. 1996 [DIRS 100106]). To simplify the distinction between the welded and nonwelded Tiva Canyon Tuff and the post-Tiva Canyon Tuff bedded tuffs, the vitric and lithophysal zones (Tpcrv and Tpcrl) of the crystal-rich member of the Tiva Canyon Tuff have been included with the crystal-rich nonlithophysal zone (Tpcrn) in this report. The general orientation of bedding beneath the WHB Area is northeast-striking and southeast-dipping, which is slightly different than the orientation of bedding mapped on Exile Hill.

The most prominent structural feature encountered during the geotechnical program is a north-northwest-trending, east-northeast-dipping normal fault that cuts across the WHB Area, passing near boreholes RF#14 and RF#29 (Figure 6.2-92). This fault, informally referred to in this report as the "Exile Hill fault splay," is shown as the bolder (wider) fault trace. The fault is not considered to be seismogenic since it does not displace the overlying alluvium based on the borehole investigations (BSC 2002a [DIRS 157829]). The master fault, the Exile Hill fault also was not considered to be an active fault in the PSHA (CRWMS M&O 1998a [DIRS 103731], Section 4).

The largest displacement associated with the Exile Hill fault splay is on the northern edge of the WHB Area. Between boreholes RF#22 and RF#24 (Figure 6.2-92) there is approximately 300 feet of down-to-the-northeast separation, dropping the non-welded pre-Rainier Mesa Tuff bedded tuffs (Tmbt1) on the northeast against the densely welded Tiva Canyon Tuff on the southwest. This vertical displacement along the Exile Hill fault splay has, in effect, subdivided the WHB Area into two distinct domains. Southwest of this fault, the top of the welded Tiva Canyon Tuff is relatively near the surface, ranging from zero to a maximum of about 190 ft below natural grade. A substantially greater thickness of the post-Tiva Canyon Tuff nonwelded

bedded tuffs (Tptb5, Tpki, Tmbt1) occurs beneath the alluvium on the northeast side of the Exile Hill fault splay relative to the southwest side. The offset diminishes along the strike of the fault to the southeast with 65 feet of down-to-the-east separation near borehole RF#14.

In addition to the Exile Hill fault splay, the interpretation of subsurface conditions includes several other faults that cut the volcanic bedrock within the WHB Area. These other faults are shown on Figure 6.2-92 as the thinner fault traces on either side of the Exile Hill fault splay. Most, but not all, of these faults strike north-northeasterly and exhibit a mixture of down-to-the-west and down-to-the-east normal displacement.

6.2.3.2.2 Downhole Velocity Surveys

Downhole velocity surveys were performed in the WHB Area and within the upper block of the emplacement area, primarily on the crest of Yucca Mountain.

Downhole Surveys in the WHB Area

This section describes the collection, analyses, and estimates of S- and P-wave velocities in 16 boreholes in the WHB Area through the use of downhole seismic velocity surveys (BSC 2002a [DIRS 157829], Section 6.2.5). Techniques and equipment used to acquire the data by means of the standard downhole technique are described in BSC (2002a [DIRS 157829], Section 6.2.5). Downhole measurements were also conducted in 1999 in borehole RF#13 (CRWMS M&O 1999 [DIRS 109209], Section 4.3). These data, however, were superseded by new surveys in RF#13 during the 2000-2001 geotechnical investigations and are not considered further.

Downhole velocity surveys were performed in the boreholes listed in Table 6.2-20. Borehole locations are shown on Figure 6.2-92. Figures 6.2-95 and 6.2-96 are velocity-depth plots for V_S and V_P, respectively, for the surveys.

Table 6.2-20. Boreholes Used for Downhole Surveys at WHB Area

Borehole	Depth of Survey (ft)
RF#13	345
RF#14	520
RF#15	320
RF#16	445
RF#17	620
RF#18	485
RF#19	640
RF#20	155
RF#21	185
RF#22	505
RF#23	155
RF#24	260
RF#25	155

Borehole	Depth of Survey (ft)
RF#26	260
RF#28	96
RF#29	405

Source: BSC 2002a [DIRS 157829], Table 7

The conventional downhole survey method was used in which travel times of signals from an impulsive source of energy at the surface are measured to various depths in the borehole. The corresponding plot of travel time versus depth is then converted to velocity versus depth by computing slopes of the interpreted major straight-line segments of the plotted data. A vehicle-on-a-beam traction source located about 10 ft from the collar of the hole was used to generate S-waves. P-waves were generated by vertical hammer blows to a steel striker plate on the ground, also located close to the collar of the hole.

Examination and comparison of the tabulated values of V_S and V_P reveals that the depths to the interfaces between layers based on the respective velocities are not always coincident, i.e., the V_S and V_P boundaries may not agree. This may be caused by the S- and P-wave signals not always following the same path from source to receiver.

Overall, V_S increases with depth in the top 100 ft. The variability in velocities spans a range of ± 1,000 ft/s except at the velocity contrasts observed in boreholes RF#13 and RF#15 at a depth of about 230 ft, at 305 ft in borehole RF#14, and 375 ft in borehole RF#16 (Figure 6.2-95). Similar trends are observed in the V_P profiles (Figure 6.2-96). Variability is smaller for V_P except for the strong contrasts observed in some of the boreholes, e.g., at a depth of 130 and 210 ft in borehole RF#15. Boundaries between velocity layers do not correlate strongly with lithologic units suggesting that changes in density control these changes rather than material type.

To support development of velocity profiles for the WHB Area, profile statistics were developed for the alluvium and tuff separately. Mean, median, and 16th and 84th percentile profiles were determined. For a given depth, the distribution of V_S or V_P was taken to be lognormally distributed. Statistically the mean $\left[\overline{V}\right]$, median $\left[V_{50}\right]$, and 16th $\left[V_{16}\right]$, and 84th $\left[V_{84}\right]$ percentile profiles were determined based on the following equations:

$$
\begin{aligned}
V_{50}(d) &= e^{\left[\overline{\ln V}(d)\right]} \\
\overline{V}(d) &= e^{\left[\overline{\ln V}(d)+\frac{\sigma_{\ln}^2(d)}{2}\right]} = V_{50}(d)\, e^{\left[\frac{\sigma_{\ln}^2(d)}{2}\right]} \\
V_{16}(d) &= e^{\left[\overline{\ln V}(d)-\sigma_{\ln}(d)\right]} = V_{50}(d) e^{-\sigma_{\ln}(d)} \\
V_{84}(d) &= e^{\left[\overline{\ln V}(d)+\sigma_{\ln}(d)\right]} = V_{50}(d) e^{+\sigma_{\ln}(d)}
\end{aligned}
\qquad \text{Eq. (33)}
$$

where d is depth, $\overline{\ln V}(d)$ is the mean of the natural logarithm of the velocities, and $\sigma_{\ln}$ (d) is the standard deviation of the velocities in natural logarithm units. For a lognormal distribution, the geometric mean is equivalent to the median.

Equation 33 was applied to the characterization of velocities developed from a single type of measurement. When data from multiple types of measurement were used to characterize velocities, the combined median was computed as the geometric mean of the medians for each type of measurement. This is equivalent to computing an equal-weighted average of the mean log velocity for each measurement type, and is consistent with the lognormal assumption used above. The combined 16th percentile, mean, and 84th percentile were computed by taking the geometric means of the 16th percentiles, means, and 84th percentiles of the individual data sets. As a result, the combined 16th percentile, mean, and 84th percentiles are only approximations. They are shown on the figures presented in this report to indicate the general level of variability in the data, but are not used to develop design ground motions.

Figures 6.2-97 and 6.2-98 show the calculated mean, median, and 16th and 84th percentile velocity profiles for the WHB Area. Microsoft Excel 2000 was used to compute these profiles (see Appendix I). Because the vertical component of displacement across the Exile Hill fault splay reaches about 300 ft, data from the different sides of the fault were also considered separately. Mean, median, and 16th and 84th percentile velocity profiles on the upthrown (southwest) and downthrown (northeast) sides of the fault were computed and compared. Boreholes on the downthrown side were RF#14, 17, 19, 22, and 29 (Figure 6.2-92). Borehole RF#14 was classified as being on the downthrown side of the Exile Hill fault based on the surface projection of the fault trace. Comparison of the median profiles across the fault indicates differences in velocities are consistent with the existence of a fault between the two sets of velocity profiles. At a depth of about 230 ft, the V_S increases significantly on the upthrown side. This increase corresponds to the sharp velocity contrasts observed in boreholes RF#13 to #16, all located on the upthrown side. Design ground motions described in this report are for the portion of the WHB Area *southwest* of the Exile Hill fault splay. Ground motions northeast of the Exile Hill fault splay are also evaluated and compared to the design ground motions in Section 6.3.5.

Downhole Surveys on the Repository Block

V_S and V_P surveys were performed in 8 boreholes along or near the crest of Yucca Mountain to supplement the SASW data (Section 6.2.3.2.4, Figure 6.2-108) (BSC 2002a [DIRS 157829], Section 6.4.3). These downhole velocity surveys were performed in the few open holes in the upper block on Yucca Mountain.

The surveyed holes, known as neutron-logging holes, were shallow, generally less than 100 ft deep. Table 6.2-21 lists the 8 holes that were surveyed and their locations are shown on Figure 6.2-108.

Table 6.2-21. Boreholes Used for Downhole Surveys on the Repository Block

Borehole Number	Elevation Above MSL (ft)	Depth of Survey (ft)
UZ-N27	4857	179
UZ-N33	4329	71
UZ-N46	4501	95
UZ-N64	4789	54
UZ-N66	4358	48

Borehole Number	Elevation Above MSL (ft)	Depth of Survey (ft)
UZ-N71	4925	48
UZ-N75	4799	28
UZ-N94	4926	25

Source: BSC 2002a [DIRS 157829], Table 25

The V_S profiles are shown on Figure 6.2-99 illustrating the large variability in V_S. Note that there are considerable differences in elevation of the ground surface at these boreholes (maximum of 597 ft). This variability is reflected in the mean, median, and 16th and 84^{th} percentile profiles (Figure 6.2-100). The wide range in the values of V_S and the apparent lack of correlation of velocities between holes demonstrate the heterogeneous nature of the velocities of the volcanic deposits that comprise the Yucca Mountain site. V_P data are not tabulated because of questionable results due to interference from casing waves.

6.2.3.2.3 Suspension Velocity Surveys

Suspension seismic P-S logging at boreholes RF#13 through #26, #28, and #29 in the WHB Area was conducted using an OYO Model 170 P-S suspension logging system (BSC 2002a [DIRS 157829], Section 6.2.6). To conduct the survey, the boreholes were filled with water and the suspension tool was lowered to the bottom of the casing by a winch and armored cable containing the data leads. Logging was conducted from lower elevations to higher ones, with velocity measurements being made at 0.5-meter (1.64-foot) intervals (occasional variations occurred). Table 6.2-22 lists the depth range of data collected in the boreholes.

Based on an assessment of data quality, some data collected at shallow depths (generally to 25-foot depth, but as deep as 77 feet in borehole RF#25) were rejected as unreliable as discussed in BSC (2002a [DIRS 157829], Section 6.2.6). Rejected data are not included in the data associated with DTN MO0204SEPBSWHB.001 [DIRS 158088] and thus are not part of the input data considered in developing velocity profiles.

The results of suspension seismic surveys are usually presented as plots of interval velocities versus depth. Such profiles show extremely variable velocities representing small-scale heterogeneity that has negligible effect on seismic waves in the frequencies of engineering relevance. Thus the profiles were smoothed "by eye" and the smoothed V_S and V_P profiles are shown on Figures 6.2-101 and 6.2-102. The mean, median, and 16th and 84th percentile V_S and V_P profiles are shown on Figures 6.2-103 and 6.2-104. Microsoft Excel 2000 was used to compute these profiles (see Appendix I).

Table 6.2-22. Depth Extent of Suspension Logging

Borehole No. and Casing Condition	Depth of Logging	Depth of Data Determined to be Unreliable
RF#13	343.0 ft	Not determined
RF#14 Cased	543.3 ft	surface to 44.30 ft bgs
RF#15 Cased	316.9 ft	surface to 19.69 ft bgs
RF#16 Cased	446.4 ft	surface to 22.97 ft bgs
RF#17 Cased	648.3 ft	surface to 47.60 ft bgs

Borehole No. and Casing Condition	Depth of Logging	Depth of Data Determined to be Unreliable
RF#18 Cased	484.3 ft	surface to 27.90 ft bgs
RF#19 Cased	638.5 ft	surface to 27.90 ft bgs
RF#20 Cased	151.2 ft	surface to 14.80 ft bgs
RF#21 Cased	184.0 ft	surface to 13.12 ft bgs
RF#22 Uncased	393.7 ft	not applicable
RF#23 Cased	151.2 ft	Data OK
RF#24 Cased	262.1 ft	surface to 23.00 ft bgs
RF#25 Cased	151.2 ft	surface to 77.10 ft bgs
RF#26 Cased	256.2 ft	surface to 13.12 ft bgs
RF#28 Cased	93.8 ft	surface to 22.97 ft bgs
RF#29 Cased	402.2 ft	surface to 19.69 ft bgs

Source: BSC 2002a [DIRS 157829], Table 11; CRWMS M&O (1999 [DIRS 109209], Section 4.4 and Appendix O)

6.2.3.2.4 SASW Surveys

SASW surveys were performed in the WHB Area, primarily in the upper block of the Repository Block, and in the ESF main drift.

SASW Surveys in the WHB Area

SASW surveys were performed in the WHB Area in the summers 2000 and 2001 (BSC 2002a [DIRS 157829], Section 6.2.7). The objective of these investigations was to estimate the V_S structure to a depth of approximately 150 ft at closely-spaced intervals on and near the proposed footprint of the WHB Area. A total of 35 V_S profiles were developed from 40 SASW surveys.

The SASW methodology is a non-destructive and non-intrusive seismic method. It utilizes the dispersive nature of Rayleigh-type surface waves propagating through a layered material to estimate the V_S profile of the material (Stokoe et al. 1994 [DIRS 157265]). In this context, dispersion arises when surface-wave velocity varies with wavelength or frequency. Dispersion in surface-wave velocity arises from changing stiffness properties of the soil and rock layers with depth. Spectral analysis is used to separate the waves by frequency (wavelength) to determine the experimental ("field") dispersion curve for the site. An analytical approach is then used to theoretically match the field dispersion curve with a 1D layered system of varying layer stiffnesses and thicknesses (Joh 1996 [DIRS 157248]). The 1D V_S profile that generates a dispersion curve that matches the field dispersion curve provides an estimate of the profile along that survey line (Stokoe et al. 2004 [DIRS 170521]).

A total of 40 SASW surveys were evaluated in the area of the WHB Area. Their locations are shown on Figure 6.2-105. At least one line was laid out in the vicinity of every borehole to allow comparison of the SASW results with the downhole velocity measurements. The majority of the surveys were laid out approximately along strike of the bedding at the WHB Area to minimize possible 2D and 3D variations in the velocity structure.

The V_S profiles are shown on Figure 6.2-106. Five of the surveys were combined with other adjacent surveys (SASW-8a+8; SASW-9a+9; SASW-10+37, SASW-32+35, and SASW-34+36) resulting in 35 experimental dispersion curves. A total of 35 V_S profiles were thus generated within the WHB Area. A total of 20 profiles extend to depths of 150 ft or greater. V_S profiles to depths of 300 feet or greater were generated along five of the surveys (SASW-3, 24, 26, 31, 32+35, and 34+36). The mean, median, and 16th and 84th percentile V_S profiles from the SASW are shown on Figure 6.2-107. Microsoft Excel 2000 was used to compute these profiles (see Appendix I).

SASW Surveys in the Vicinity of the Repository Block

SASW surveys were performed in the vicinity of the Repository Block, generally in the upper block of the emplacement area (BSC 2002a [DIRS 157829], Section 6.4.2). The goal of these measurements was to determine the V_S structure to depths of approximately 500 to 700 ft at several locations. A total of 7 deep SASW surveys were carried out along the crest and these are designated with a "C" (e.g., C-1) to signify "crest" surveys (Figure 6.2-108). Additional SASW measurements were made at 26 locations along the crest of Yucca Mountain as well as downslope of the crest to the east (Figure 6.2-108). Twelve of these surveys were performed to attempt to obtain V_S profiles to depths of 150 to 200 ft. These SASW tests are designated with an "S" to represent relatively shallow profiling depths (S1 to S12)[3]. Eleven surveys were performed in an effort to obtain profiles to depths of 400 ft or greater, where spatial access was not limited; however, this was not achieved. These surveys are designated with the letter "D" (D-1 to D-11) to represent relatively deep profiling depths. In addition to the C, S, and the D surveys, 3 sets of SASW measurements were performed on the surface of exposed rock at the crest. These surveys are designated with the letter "R" for rock and are referred to as R-1, R-2, and R-3 herein. Thus a total of 33 SASW surveys were performed on Yucca Mountain in the vicinity of the Repository Block. The lengths of the lines are approximately equal to the maximum receiver spacing along the survey.

Of the 33 SASW surveys performed on Yucca Mountain, 22 were on or near the crest of Yucca Mountain (Figure 6.2-108). C-2, C-6, D-6, and D-11 resulted in dispersion curves that indicated significant lateral variability. Thus at these sites, multiple V_S profiles were estimated to reflect the variability over the distance of the survey. A total of 38 profiles are shown in composite on Figure 6.2-109 (R surveys not shown). The median, mean, and 16th and 84th percentile profiles are shown on Figure 6.2-110. Microsoft Excel 2000 was used to compute these profiles (see Appendix I).

Examination of the individual V_S profiles suggests that unlike the typical increase in velocity with depth observed in most geologic settings, many of the profiles indicate low-velocity zones beneath higher velocity rock, which are often observed in volcanic terrane (Wong et al. 1995 [DIRS 105550], pages 6-15 to 6-20). The limited shallow downhole V_S data are consistent with the presence of these zones (Figure 6.2-109).

[3] Note that in Technical Data Management System, for DTN MO0203SEPSASWD.000 [DIRS 158084], surveys herein labeled "C" are labeled "SASW-CYM." For DTN MO0110SASWVDYM.000 [DIRS 158076], surveys herein labeled "S" are labeled "CYM-S."

SASW Surveys in the ESF Main Drift

A total of five SASW surveys were performed along the north-south main drift in the ESF (Figure 6.2-111) (BSC 2002a [DIRS 157829], Section 6.3.2). The purpose of these measurements was to provide information on the V_S structure in the emplacement area. SASW data were only obtained to depths of about 700 ft from surveys atop Yucca Mountain and thus V_S information was lacking at depths of 700 to 1000 ft immediately above the emplacement area. To help constrain the deeper portion of the V_S model, surveys were performed in the ESF.

Five locations along the main drift of the exploratory tunnel wall (rib) were surveyed using the SASW method. All surveys were performed on the west rib at a height of about 4 to 5 ft above the tunnel invert. The sites were selected to represent a range in materials exposed along the main drift. T-1 and T-3 had highly fractured tuff at the surface. In addition, at T-1, the rock sounded "hollow" at many places along the rib. T-2, T-4, and T-5 exhibited much less fracturing, with T-2 showing only a few fractures over the maximum receiver spacing of 32 ft.

Figure 6.2-112 shows the V_S profiles obtained in the ESF surveys and Figure 6.2-113 shows the mean, median, 16th and 84th percentile profiles for T-2 to T-5. Microsoft Excel 2000 was used to compute these profiles (see Appendix I). The SASW results in the tunnel demonstrate that the intact rock with few fractures exhibit V_S values in the range of 6,000 to 7,000 ft/sec. When the rock is fractured, these values fall into the general range of 3,000 to 4,000 ft/sec. Based on the limited number of surveys, there is no reason to believe that the velocities of the softest (highly fractured rock) nor the stiffest (unfractured) rock were measured.

6.2.3.2.5 Vertical Seismic Profiling Surveys

Prior to the 2000-2001 geotechnical field program, VSP surveys were conducted in six boreholes in the vicinity of Yucca Mountain (Majer et al. 1996a [DIRS 106330]; Majer et al. 1996b [DIRS 104685], Section IV; Balch and Erdemir 1996 [DIRS 105351]) (Figure 6.2-90). The goal of the VSP surveys in WT-2, NRG-6, and UZ#16 primarily was to provide constraints for reflection surveys; measurements in G-2, G-4, and SD-12, however, were designed to provide estimates of shallow velocities for use in ground motion estimation (Majer et al. 1996a [DIRS 106330]; Majer et al. 1996b [DIRS 104685], Section IV). The VSP field measurements were processed to obtain interval V_P and V_S (Majer et al. 1996a [DIRS 106330]; Majer et al. 1996b [DIRS 104685], Section IV).

P-wave data for the four VSP surveys and S-wave data from two of the surveys are judged to be of sufficient quality to yield an engineering model interpretation (Wong and Silva 2003 [DIRS 163201], pages 24-32). Data from SD-12 and G-4 were considered to be of insufficient quality to analyze because of the emergent character of the onsets of the P- and S-waves. For the boreholes where good or marginal V_S profiles were interpreted, Poisson's ratio (ν) was computed and found to be about 0.3 (Wong and Silva 2003 [DIRS 163201], page 23). This value is reasonable for the materials encountered at this site. The good correlation of computed ν to measured V_S profiles was used to infer V_S profiles for boreholes with inadequate or unreliable S-wave data. Table 6.2-23 summarizes the borehole data.

Table 6.2-23. Summary of VSP Borehole Data Used to Derive Velocity Profiles

Borehole	Survey Depth (ft)	Comments	Interpretation
UZ-16	1610	3-component geophones cemented at 15-ft intervals; Source offsets of 80, 377 and 679 ft.	Independent V_P and V_S profiles
NRG-6	1080	Measurement intervals of 20 ft. Vibratory source offsets of 80, 377 and 659 ft.	V_P profile; V_S profile unreliable; V_S profile derived assuming Poisson's ratio
WT-2	2010	Measurement interval of 30 ft. Vibratory source offsets of 80 and 1000 ft.	V_P profile; V_S profile questionable; V_S profile derived assuming Poisson's ratio
G-2	2600	Hammer source for depths < 200 ft. Vibratory source for depths > 200 ft	Independent V_P and V_S profiles

Source: Wong and Silva 2003 [DIRS 163201], page 24

The interpreted P-wave profiles are shown on Figure 6.2-114. They are based on good quality data and although they exhibit considerable variability, they become more consistent with increasing depth. The directly measured V_S profiles and those profiles calculated from the V_P profiles based on ν are illustrated on Figure 6.2-115. There is considerable variability in these profiles. Microsoft Excel 2000 was used to compute these profiles (see Appendix I).

6.2.3.3 Repository Block Profiles

Based on the velocity information previously described, base case V_S and V_P profiles required for input into the site-response model were developed for the Repository Block. The following subsections describe their development.

6.2.3.3.1 Repository Block Tuff V_S

To accommodate the epistemic uncertainty in tuff V_S data, two base case profiles are developed for use as input to the site response model. As described below, one profile is based on results of the SASW and downhole seismic surveys on and near the Repository Block. The second profile is based on results of the VSP surveys obtained in boreholes at the edge of or slightly outside of the Repository Block. The two data sets have little spatial overlap and indicate significantly different results. Whereas the geology of the area suggests that velocities should show some lateral continuity, there is currently no technical basis to prefer one profile over the other and, thus, they are both included in the site-response modeling to accommodate the current uncertainty.

Available data for development of tuff V_S profiles for the Repository Block consist of V_S results from SASW surveys (Section 6.2.3.2.4; DTNs MO0203SEPSASWD.000 [DIRS 158084], MO0110SASWVDYM.000 [DIRS 158076], and MO0206SASWROCK.000 [DIRS 159081]), downhole surveys (Section 6.2.3.2.3; DTN MO0202DVDWHBSC.002 [DIRS 158078]), and VSP surveys (Section 6.2.3.2.5, DTN LB0306VSP95DAT.001 [DIRS 164559]). All data from the SASW and downhole surveys were used in the analysis except for SASW survey D-12,

which is located on Exile Hill west of the WHB Area. For the VSP surveys, as discussed in Section 6.2.3.2.5, only data from boreholes G-2, WT-2, NRG-6, and UZ-16 were used. Although more removed from the repository outline than the other boreholes, data from G-2 are included in the analysis to provide spatial coverage to the north of the repository outline where other data are lacking (Figure 6.2-108).

For the base case #1 (also referred to as BC) profile using the SASW and downhole data, the analysis approach was to determine the median velocity profile for the combined dataset and then develop a smoothed profile "by eye." This approach provides a profile to a depth of 700 ft. Microsoft Excel 2000 was used to develop this profile (see Appendix I).

Because of the lack of data from a depth of 700 ft to the depth of the emplacement level at about 1000 ft, a linear interpolation was made in V_S from 3800 ft/sec at a depth of 700 ft to 6000 ft/sec at 1100 ft where SASW measurements were made in the ESF (Figure 6.2-116). The sensitivity of the ground motion calculations to how this "connection" was made (e.g., straight line extrapolation, layered gradient, single step over) was investigated and the result was that the character of the "connection" was not significant (Wong and Silva, 2003 [DIRS 163201], page 25).

For the second base case velocity profile, smooth V_S and V_P profiles were derived from the VSP interpretations (Wong and Silva 2003 [DIRS 163201], p. 24-32). These smooth profiles (Figures 6.2-114 and 6.2-115) are judged to be plausible average profiles based on the limited data. Shallow portions of the average profile were judged to be very uncertain. Due to the absence of velocity data in the northern portion of the Repository Block (Figure 6.2-108), the V_S profile derived from the VSP results was increased by about 600 ft/sec, approximately one standard error in the VSP measurements (Figure 6.2-116). By increasing the whole profile by this amount, the gradient of the VSP V_S profile is maintained. The mean plus one sigma V_S profile agrees well with the SASW measurements in the ESF (Figure 6.2-116) and was adopted as base case profile #2 (also referred to as upper-range [UR] profile). Microsoft Excel 2000 was used to develop this profile (see Appendix I). Both base case profiles are used in the ground motion calculations for the Repository Block.

Base case V_S profiles for the tuff were submitted to the TDMS and have DTN MO0206SASWVSP1.001 [DIRS 163777]. Details of the analysis are documented in Scientific Notebook SN-M&O-SCI-037-V1 (Wong and Silva 2003 [DIRS 163201], pages 18-55, Supplemental Records 5 and 6).

OCRWM Project Condition Report 2674 documents that an incorrect V_S value at the depths of 600 to 700 ft for repository block base case profile #1 was used in carrying out the analysis/modeling. Sensitivity studies were carried out to evaluate the impact of the use of incorrect data and show that the ground motion output generally differ by less than 10% with a maximum difference of 12%. The sensitivity studies are documented in Wong and Silva (2004d [DIRS 172075], pages 15 and 18). Differences in the ground motion output are negligible when compared to the variability and uncertainty incorporated into the overall analysis and modeling. Thus, the results obtained using the incorrect input are considered valid and are used in this study.

6.2.3.3.2 Repository Block Tuff V_P

V_P profiles for Repository Block tuff were calculated from the V_S profiles (Section 6.2.3.3.1) and Poisson's ratio. Poisson's ratio was determined using data from Repository Block boreholes in which P-wave and S-wave quality was sufficient (DTN LB0306VSP95DAT.001 [DIRS 164559]; boreholes UZ-16, G-2, NRG-6, and WT-2). This ratio decreased slightly from 0.33 to 0.30 from the surface to 250 ft depth (Figure 6.2-117). At depths deeper than 250 ft, ν remains fairly constant at 0.30. To calculate base case #1 and #2 V_P profiles from the respective V_S profiles, ν was taken to decrease linearly from 0.33 (V_P/V_S = 1.99) at the surface to 0.30 (V_P/V_S = 1.87) at a depth of 250 ft and to maintain a constant value of 0.30 at depths below 250 ft (Figure 6.2-118). For the ground motion calculations, all four profiles, V_P and V_S, were discretized for input into the site response model calculations.

Base case V_P profiles for the tuff were submitted to the TDMS and have DTN MO0206SASWVSP1.001 [DIRS 163777]. Details of the analysis are documented in Scientific Notebook SN-M&O-SCI-037-V1 (Wong and Silva 2003 [DIRS 163201], pages 18-55, SR 5 and 6).

6.2.3.4 Surface Facilities Area Profiles

Velocity profiles for the Surface Facilities Area are based on downhole, suspension, and SASW results from the surveys carried out in that area. Data included in the analysis are restricted to those obtained southwest of the Exile Hill splay fault. In Section 6.3.5, ground motions for the area northeast of Exile Hill fault splay are compared with ground motions in the Surface Facilities Area in a sensitivity analysis. Velocity profiles are developed for this new area.

For the Surface Facilities Area, epistemic uncertainty is less than for the Repository Block. More data are available and the area to be represented by the profiles is smaller. Thus, a single base case profile is developed for each of the two materials that are present: tuff and alluvium.

6.2.3.4.1 Surface Facilities Area Tuff V_S

A base case V_S tuff profile was calculated based on the SASW, downhole, and suspension surveys performed in the WHB Area (Sections 6.2.3.2.2 to 6.2.3.2.4) (DTNs MO0110SASWWHBS.000 [DIRS 157969], MO0110SASWVDYM.000 [DIRS 158076], MO0111DVDWHBSC.001 [DIRS 157296], MO0204SEISDWHB.001 [DIRS 158086], and MO0204SEPBSWHB.001 [DIRS 158088]). Data from SASW surveys 3, 15, 16, 19, 30, 34, and 36, and boreholes RF#14, 17, 19, 22, and 29 were not used because they were obtained to the northeast of the Exile Hill splay fault. Of the SASW survey data with DTN MO0110SASWVDYM.000 [DIRS 158076], only survey D-12 is used; the other surveys associated with this DTN were acquired on the Repository Block. For the individual SASW, the downhole and suspension V_S profiles, only data for the tuff were considered. The shallow V_S data for alluvium were separated out by estimating the depth of alluvium for each profile based on the borehole logs (DTN GS030783114233.001 [DIRS 164561]). The suspension data were used only below a depth of 100 ft because some of the shallower data were deemed unreliable (Wong and Silva 2003 [DIRS 163201], page 18; Section 6.2.3.2.3).

The base case profile was computed by calculating a geometric mean of the median SASW, downhole, and suspension profiles. The profile was then smoothed "by eye" (Figure 6.2-119) and digitized into discrete layers for input into the site response model. Details of the analysis are documented in Scientific Notebook SN-M&O-SCI-037-V1 (Wong and Silva 2003 [DIRS 163201], pages 18-55, Supplemental Records 18 and 21). Microsoft Excel 2000 was used to develop this profile (see Appendix I). The profile was submitted to the TDMS and has DTN MO0209VELPRWHB.000 [DIRS 163798].

6.2.3.4.2 Surface Facilities Area Tuff V_P

Similar to the Surface Facilities Area base case V_S profile, the base case V_P profile was computed from the downhole and suspension data (Figure 6.2-120). The base case profile is the geometric mean of the two median profiles. As for the V_S profile, it is only appropriate for the area southwest of the Exile Hill fault splay. The base case V_P profile was smoothed and discretized for input into the site response model. Details of the analysis are documented in Scientific Notebook SN-M&O-SCI-037-V1 (Wong and Silva 2003 [DIRS 163201], pages 18-55, SR 18 and 21). Microsoft Excel 2000 was used to develop this profile (see Appendix I). The profile was submitted to the TDMS and has DTN MO0209VELPRWHB.000 [DIRS 163798].

6.2.3.4.3 Surface Facilities Area Alluvium V_S

The base case V_S profile for the alluvium was developed by calculating a geometric mean of the median downhole and SASW profiles southwest of the Exile Hill fault splay. The suspension data were not used because of the unreliability of some of the shallower data (Section 6.2.3.2.3). The base case profile does not include velocities from the fill (tunnel muck), which was excluded from the SASW and downhole data by estimating its depth from the borehole logs. As for all profiles, the base case V_S profiles were smoothed and discretized (Figure 6.2-121). Details of the analysis are documented in Scientific Notebook SN-M&O-SCI-037-V1 (Wong and Silva 2003 [DIRS 163201], pages 18-55, SR 18 and 21). Microsoft Excel 2000 was used to develop this profile (see Appendix I). The profile was submitted to the TDMS and has DTN MO0209VELPRWHB.000 [DIRS 163798].

6.2.3.4.4 Surface Facilities Area Alluvium V_P

The only available V_P data for the alluvium were the downhole data. SASW does not yield a direct measurement of V_P (Poisson's ratio has to be assumed) and the suspension data were not considered reliable. To maintain consistency with the alluvium V_S base case model, which was based on both downhole and SASW data, the base case V_P profile was calculated by multiplying the discretized base case V_S profile by smoothed depth-varying V_P/V_S ratios for the alluvium from the downhole data south of the fault. The resulting base case V_P profile is shown on Figure 6.2-122. Details of the analysis are documented in Scientific Notebook SN-M&O-SCI-037-V1 (Wong and Silva 2003 [DIRS 163201], pages 18-55, SR 18 and 21). Microsoft Excel 2000 was used to develop this profile (see Appendix I). The profile was submitted to the TDMS and has DTN MO0209VELPRWHB.000 [DIRS 163798].

6.2.3.5 Treatment of Variability of Velocity Profiles

Treatment of uncertainties and randomness in velocity profiles for the Repository Block and the Surface Facilities Area has two components. First, epistemic uncertainty in velocity is handled through the development of multiple base case profiles, as appropriate. For the Repository Block, two tuff velocity base case profiles were developed (Sections 6.2.3.3.1 and 6.2.3.3.2). One base case model is indicated from an analysis of SASW and downhole velocity survey data, whereas the second base case model is indicated from an analysis of VSP surveys. The difference in the results for the two sets of data is unexpected, but no technical basis has yet been determined for preferring one data set to the other. This epistemic uncertainty in base case velocity profile is propagated through the site-response ground motion model by running the model for each base case and enveloping the results. For the Surface Facilities Area, the data supported development of single V_S and V_P profiles for tuff and alluvium (Sections 6.2.3.4.1 through 6.2.3.4.4) with two different profile thicknesses.

In the second component, randomness in velocity is accommodated by using the base case V_S profiles, along with information on the observed randomness in velocity at the site, to synthesize a suite of 60 random velocity profiles that have similar overall statistics as the observed data. This is accomplished using the software program RANPAR V2.0 (Software Tracking Number 10486-2.0-00) (Pacific Engineering and Analysis 2002i [DIRS 163315]). Corresponding random V_P profiles are determined using the random V_S profiles and the Poisson's ratio as a function of depth associated with the base case velocity profile being used. The randomization process involves velocity, layer thickness, and the depth of the profile. For velocity and layer thickness, results of a probabilistic representation of velocity profiles at the site (MO0208VCPRBWHB.000 [DIRS 163801], see Section 6.2.3.6) are implemented in RANPAR V2.0.

For repository depth, a uniform distribution varying from 700 to 1500 ft is used. As documented in scientific notebook SN-M&O-SCI-037-V3 (Wong and Silva 2004b [DIRS 170444], page 70), this distribution is based on an analysis of overburden thickness that subtracted the waste emplacement area elevation (BSC 2004d [DIRS 164519]) from the topography (MO0012MWDGFM02.002 [DIRS 153777]) using EarthVision 5.1 (Dynamic Graphics 1998 [DIRS 167994]). This range also reflects uncertainty in the depth at which Point A conditions (i.e., S-wave velocity of about 1900 m/sec are obtained. For the Surface Facilities Area the overall depth of the profile is varied from 400 to 600 ft to reflect uncertainty in the depth of Point A conditions. A uniform distribution is again used (Wong and Silva 2004a [DIRS 170443], page 38).

For the Surface Facilities Area, the variation in the thickness of alluvium (35 ft to 110 ft) above competent rock material (i.e., tuff) is accommodated through consideration of two base case profiles. These two base case profiles are developed from the Surface Facilities Area alluvium and tuff profiles (Section 6.2.3.4). In addition, an additional base case is developed for a site with shallow alluvium. For each base case velocity profile, 60 model runs are performed, one for each random profile, and the resulting amplification factors are averaged (Section 6.3.1.1.2). As described in Section 6.2.4.5, this same approach is used to accommodate randomness in dynamic material properties.

6.2.3.6 Probabilistic Representation of Velocity Profiles

This section presents the development and application of a probabilistic representation of velocity profiles in the Repository Block and at the Surface Facilities Area. This representation considers both the variability among profiles in each area and the variability in velocity with depth within a given profile. As discussed above, this probabilistic representation was used for the generation of 60 random synthetic velocity profiles, which in turn were used as inputs for the site response model. These synthetic profiles are statistically similar to the observed profiles.

The same probabilistic representation of velocity profiles has been utilized in the development of the EPRI Ground Motion Guidelines (EPRI 1993b [DIRS 103320], Appendix 6.A), in studies for the Savannah River Site (Lee et al. 1997 [DIRS 110451]), and in NUREG/CR-6728 (McGuire et al. 2001 [DIRS 157510]) and CR-6769 (McGuire et al. 2002 [DIRS 163799], Section 2.3.1). The development of the probabilistic representation is documented in scientific notebook SN-M&O-SCI-036-V1 (Wong and Toro 2003 [DIRS 163848]).

6.2.3.6.1 Overview of Formulation

The probabilistic representation of velocity profiles consists of three elements, as illustrated on Figure 6.2-123. The first element consists of a probabilistic description of velocity layer thicknesses for the ensemble of profiles. The second element is the median velocity profile. Although each profile consists of discrete constant-velocity layers, the median profile is smooth as if the layer boundaries are randomly located. The third element is a probabilistic description of the deviations of the velocity at the mid-point of each layer from the median and its correlation with the velocity in the layer above.

6.2.3.6.2 Formulation for Layer Thickness

Previous stochastic investigations of soil profiles indicate that layers tend to be thinner near the surface and thicker at depth (EPRI 1993b [DIRS 103320], Appendix 6.A; Lee et al. 1997 [DIRS 110451], Appendix A; Silva et al. 1996 [DIRS 110474], Appendix C). A simple probabilistic formulation developed in these studies to characterize the layering is a Poisson process with depth-dependent rate (i.e., a non-homogeneous Poisson process; see Parzen 1962 [DIRS 110462]). In this formulation, the mean layer thickness is depth-dependent, but the thickness of layer *i* is probabilistically independent of the thickness of layer *i-1*. In a Poisson process with constant rate, the layer thickness follows an exponential distribution, which has a memory-less property. Because this formulation utilizes a depth-dependent rate, the distribution of layer thickness is no longer exponential but the memory-less property still applies.

Following the above references, this study adopts a modified power-law to characterize the depth-dependent rate of layer boundaries, namely,

$$\begin{aligned} \lambda(h) &= 0 && \text{for } 0 < h \geq h_c \\ c_3\left[h + c_1\right]^{-c_2} && \text{for } h > h_c \end{aligned} \qquad \text{(Eq. 34)}$$

in which λ is the rate of layer boundaries (per meter), h denotes depth in meters, and h_c is a minimum depth (which may be set to zero) chosen by the user. The Poisson process is chosen

because it is the simplest possible stochastic representation for the location of discrete events. The power-law functional form is chosen for the variation of λ because this functional form is often used to represent the variation of V_S and other dynamic soil properties with depth and because its three parameters provide sufficient flexibility to fit most quantities that vary monotonically with depth.

Coefficients c_1 through c_3 in the above equation are estimated from interpreted velocity-profile data, using the method of maximum likelihood (Benjamin and Cornell 1970 [DIRS 110221]). The values used in the analysis are presented in Section 6.2.3.6.11. The ln-likelihood function for this process is given by the expression:

$$\ln L = \sum_{k \atop \text{(all profiles)}} \left[-\int_0^{H_k} \lambda(h)\,dh + \sum_{i=1 \atop \text{(all layer boundaries in profile)}}^{n_k} \ln\left(\lambda(h_{ik})\right) \right] \qquad \text{(Eq. 35)}$$

in which H_k is the maximum depth in profile k and h_{ik} is the depth of the *i-th* layer boundary in profile k. The statistical uncertainty in the estimated parameters is calculated from the Hessian matrix of the ln-likelihood function (i.e., the matrix of second derivatives of the likelihood function with respect to the coefficients). These calculations are implemented in the LAYERING Version 1.0 software (STN: 10648-1.0-00) (Risk Engineering, Inc. 2002c [DIRS 163307]).

Another useful result from these calculations is the normalized layer thickness, which is obtained from the observed thickness and from the expression for λ (Parzen 1962 [DIRS 110462]). The normalized layer thickness for layer i (between depths h_i and h_{i+1}), is computed as:

$$\begin{aligned} \tau_i &= \int_{h_i}^{h_{i+1}} \lambda(h)\,dh \\ &\approx (h_{i+1} - h_i)\,\lambda\left(\frac{h_{i+1} + h_i}{2}\right) \\ &\approx \frac{h_{i+1} - h_i}{\overline{T}\left(\frac{h_{i+1} + h_i}{2}\right)} \end{aligned} \qquad \text{(Eq. 36)}$$

in which $\overline{T}(h)$ represents the mean layer thickness at depth h.

For a non-homogeneous Poisson process, the normalized layer thickness should follow an exponential distribution with unit mean. In practice, values of the normalized thickness tend to exhibit a lognormal-like shape, where the mode does not occur at zero. This study adopts a lognormal distribution for the normalized thickness. The mean of this distribution is unity (by definition, because it is a normalized quantity). The coefficient of variation (which in this case is identical to the standard deviation) is computed from the normalized thickness data.

Adoption of a lognormal distribution for the normalized thickness does not conform exactly to the use of a nonhomogeneous Poisson process. The approach followed here is analogous to the common practice of using least-squares regression for data that have non-Gaussian residuals. Although this approach is not optimal, it generally leads to acceptable results (Kailath 1981 [DIRS 164981]).

6.2.3.6.3 Formulation for Velocity

As shown on Figure 6.2-123, the velocity representation operates on the velocities at the layer midpoints. These velocities can be regarded, for a given profile, as a sequence of velocity values (i.e., V_1, V_2, V_3, ... V_n). The probabilistic description of velocity defines the probability distribution of $\ln[V_i]$, and its correlation with the ln-velocities in adjacent layers. More precisely, the representation operates with the normalized quantity

$$Z_{i,j} = \frac{\ln(V_{i,j}) - \ln[V_{\text{median}}(h_{i,j})]}{\sigma_{\ln(V)}} \qquad \text{(Eq. 37)}$$

in which the standard deviation $\sigma_{\ln(V)}$ is treated as a function of depth. As a result of the normalization in Eq. 37, Z_i has a mean of zero and a standard deviation of unity.

The median velocity is assumed to be an arbitrary (i.e., non-parametric) smooth function of depth. It is represented by means of a table of approximately 60 (depth, ln-velocity) pairs. Smoothness is enforced by means of a penalty function. The depth-dependent standard deviation is represented by the value of sigma at several depth control points. These control points are chosen after performing exploratory statistical analyses of the data.

Normal probability plots in Lee et al. (1997 [DIRS 110451], Appendix A) and Silva et al. (1996 [DIRS 110474], Appendix C) indicate that the distribution of Z_i is well approximated by a normal distribution (or, equivalently, that V_i is well approximated by a log-normal distribution).

This study characterizes the lognormal distribution of velocities and the correlation among layers by means of a first-order auto-regressive representation, so that the conditional distribution of Z in layer i (given the values of Z in layers 1, 2, ... i-1) is normal with mean and standard deviation given by

$$\begin{aligned} &\text{mean}(Z_i \mid Z_{i-1}, Z_{i-2}, Z_{i-3}, \ldots) = \text{mean}(Z_i \mid Z_{i-1}) = \rho Z_{i-1} \\ &\sigma(Z_i \mid Z_{i-1}, Z_{i-2}, Z_{i-3}, \ldots) = \sigma(Z_i \mid Z_{i-1}) = \sqrt{1-\rho^2} \end{aligned} \qquad \text{(Eq. 38)}$$

The resulting distribution of the Z_i values is as follows:

$$\begin{aligned} f_Z(z_{1,j}) &= \frac{1}{\sqrt{2\pi}} \exp\left[-\frac{1}{2} {z_{1,j}}^2 \right] \\ f_{Z_i|Z_{i-1}}(z_{i,j} \mid z_{i-1,j}) &= \frac{1}{\sqrt{2\pi(1-\rho^2)}} \exp\left[-\frac{1}{2} \left(\frac{z_{i,j} - \rho z_{i-1,j}}{\sqrt{1-\rho^2}} \right)^2 \right] \end{aligned} \qquad \text{(Eq. 39)}$$

The correlation coefficient ρ is taken to depend on depth and on the distance between the midpoints of layers *i*-1 and *i*. Inter-layer correlation tends to be higher at greater depths and between thin layers. The expression used for ρ is as follows:

$$\rho(h,t) = (1-\rho_d(h))\rho_t(t) + \rho_d(h) \quad \text{(Eq. 40)}$$

in which ρ_d represents depth-dependent correlation (higher at greater depths) and ρ_t is the thickness-dependent correlation (higher for thin layers, which tend to occur at shallow depths). The depth-dependent correlation coefficient, ρ_d, is of the form

$$\rho_d(h) = \begin{cases} \rho_{200}\left[\dfrac{h+h_0}{200+h_0}\right]^b & for \quad h \le 200\ m \\ \rho_{200} & for \quad h > 200\ m \end{cases} \quad \text{(Eq. 41)}$$

and the thickness-dependent correlation coefficient, ρ_t, is of the form

$$\rho_t(t) = \rho_0 \exp\left[-\left(\frac{t}{\Delta}\right)^{\alpha}\right] \quad \text{(Eq. 42)}$$

in which h is the average of the midpoint depths of layers i and i-1 and t is the difference between these midpoint depths. Quantities ρ_{200}, h_0, b, ρ_0, and Δ are parameters determined from the data (see Section 6.2.3.6.11). These parameters, together with the median velocity and the depth-dependent standard deviation are estimated from the profile data using the method of maximum likelihood. The likelihood function is constructed as the product of the density functions in Eq. 39. The statistical uncertainty in the estimated parameters is calculated from the Hessian matrix of the ln-likelihood function.

Adopting a log-normal distribution of V_S, the median velocity is equal to the mean log-velocity. In this section, this quantity is referred to as the logarithmic mean velocity or as the mean velocity. These calculations are implemented in the VEL_STAT Version 1.0 software (STN: 10648-1.0-00) (Risk Engineering, Inc. 2002f [DIRS 163324]).

6.2.3.6.4 Input Data and Exploratory Statistical Analysis for the Repository Block

The following V_S data were used in the probabilistic analysis of the Repository Block:

- 8 downhole profiles, with typical depths of 30 m (100 ft) (DTN MO0202DVDWHBSC.002 [DIRS 158078]).
- 12 profiles obtained from shallow SASW surveys performed in the year 2001, with typical depths of 50 m (165 ft) (DTN MO0110SASWVDYM.000 [DIRS 158076]).

- 5 profiles obtained from deep SASW surveys performed in the year 2000, with typical depths of 220 m (720 ft) (DTN MO0203SEPSASWD.000 [DIRS 158084]). Data from surveys SASW-CYM-2 and SASW-CYM-6 were excluded because they did not yield unique solutions.

- 9 profiles obtained from deep SASW surveys performed in the year 2001, with typical depths of 150 m (490 ft) (DTN MO0110SASWVDYM.000 [DIRS 158076]). Data from surveys SASW-D-6 and SASW-D-11 were excluded because they did not yield unique solutions. Survey D-12, which is also included in DTN MO0110SASWVDYM.000 [DIRS 158076], was not included because it was located within the Surface Facilities Area, not on the Repository Block.

The spatial coverage provided by these profiles is shown on Figure 6.2-108.

Comparisons among profiles in close proximity and having some depth overlap indicates that the profiles obtained using different approaches are generally consistent (BSC 2002a [DIRS 157829], Section 6.7.2). Thus, it is justified to merge the data into one data set.

The top-left panel of Figure 6.2-124 shows the logarithmic mean $\pm$ σ values of the V_S as a function of depth, which were computed using all the data described above. The values on Figure 6.2-124 indicate the number of profiles available at that depth. The top-right panel shows the logarithmic σ and its associated statistical uncertainty. Figure 6.2-124 shows that the standard deviation is higher near the surface and it is roughly constant at greater depths.

Examination of the individual profiles show a number of velocity-residual reversals (i.e., velocity significantly greater than the median for one layer and a velocity significantly lower than the median for an adjacent layer). This is an indication of low values of ρ.

6.2.3.6.5 Analysis of Velocities for the Repository Block

The parameters of the probabilistic velocity formulation described in Section 6.2.3.6.3 were calculated for the entire data set and for the various subsets. These analyses produced consistent results. The bottom two panels on Figure 6.2-124 show some of the results obtained using the entire dataset, using a formulation that allows for higher σ near the surface. The bottom-left panel shows the logarithmic mean $\pm$ σ range and the mean $\pm$ its statistical uncertainty range. These values are consistent with the summary statistics on the top panels of Figure 6.2-124.

The parameters that control the correlation coefficient $\rho(h,t)$ for the Repository Block are discussed in Section 6.2.3.6.10.

6.2.3.6.6 Analysis of Layer Thickness for the Repository Block

Calculation of the layer-thickness parameters defined in Section 6.2.3.6.2 were performed for the downhole data, the deep and shallow SASW data, and all Repository Block data. The bottom panel on Figure 6.2-125 shows the results for the rate λ as a function of depth h (recall that λ may be interpreted as the reciprocal of the mean layer thickness). Comparisons among these results are difficult because the various data sets cover different depth ranges and different data

types. It is worth noting, however, that the deep SASW data indicate thicker layers than other approaches for depths greater than approximately 6 m. This result is consistent with the deep SASW data having thicker layers because they represent averages of properties over larger volumes. Despite these moderate differences, the results obtained using all data are adopted for the Repository Block.

The top panel of Figure 6.2-125 shows further details on the results obtained for all data, comparing the observed cumulative number of layer boundaries as a function of depth to the number of layer boundaries predicted by the probabilistic formulation (which depends on $\lambda(h)$ and on the number of profiles that extend to depth h). This comparison indicates a good fit between the observations and the probabilistic formulation.

Analysis of the calculated values of the normalized layer thickness (Eq. 36) indicates that these values are well represented by a lognormal distribution with a coefficient of variation of 0.79.

6.2.3.6.7 Input Data and Exploratory Statistical Analysis for the Surface Facilities Area

The following V_S data were used in the probabilistic analysis of the Surface Facilities Area (Sections 6.2.3.2.2 and 6.2.3.2.4):

- 13 downhole profiles, with depths ranging from 50 to 150 m (165 to 490 ft) (DTN MO0111DVDWHBSC.001 [DIRS 157296]). Four profiles (profiles number 17, 19, 22, and 29) were excluded because they are located northeast of the Exile Hill splay fault.

- 28 profiles obtained from SASW surveys, with depths ranging from 30 to 150 m (100 to 490 ft) (DTNs MO0110SASWWHBS.000 [DIRS 157969] and MO0110SASWVDYM.000 [DIRS 158076]). Six profiles (profiles number 3, 15, 16, 19, 30, and 34-36) were excluded because they are located northeast of the Exile Hill splay fault. For DTN MO0110SASWVDYM.000 [DIRS 158076], only survey D-12 is used; the other surveys are on the Repository Block.

All suspension logger data (DTN MO0204SEPBSWHB.001 [DIRS 158088]) were excluded because they sample the same boreholes as downhole data and yield similar velocities. Therefore, they do not provide additional information.

The alluvium and tuff portions of these profiles were separated for analysis, and the artificial-fill portion was removed. Some analyses were also performed with the merged (alluvium and tuff) data.

Figure 6.2-126 shows summary statistics (i.e., logarithmic mean $\pm$ σ, logarithmic σ and its statistical uncertainty) as a function of depth for the Surface Facilities Area alluvium and tuff data. The alluvium data on logarithmic σ versus depth shows a pattern similar to that shown by the Repository Block data, with higher values near the surface and roughly constant values further down. If one ignores the top 5 to 10 m (15 to 30 ft) of the tuff data, where there are few profiles, the logarithmic σ is roughly constant. The bulge at 80 m (260 ft) is not statistically

significant, as indicated by the statistical-uncertainty range. Microsoft Excel 2000 was used in the analyses of layer thickness (see Appendix I).

6.2.3.6.8 Analysis of Velocities for the Surface Facilities Area

Calculations for the alluvium data were performed using a formulation that allows higher σ near the surface. This formulation was chosen instead of a formulation with constant σ based on the pattern observed on the upper-left panel of Figure 6.2-124. Calculations for the tuff data were performed using a formulation with constant σ and one that allows for depth-dependent σ. The former was selected based on arguments of statistical significance. Results for both are shown on Figure 6.2-127, in the form of the logarithmic mean $\pm$ σ range, and the mean plus and minus its statistical uncertainty range for each set. The parameters that control the correlation coefficient $\rho(h,t)$ for the Surface Facilities Area are discussed in Section 6.2.3.6.10 below.

6.2.3.6.9 Analysis of Layer Thickness for the Surface Facilities Area

An analysis of the layer-thickness parameters was performed for the entire Surface Facilities Area data set (without separating alluvium from tuff). The results from these calculations were later modified after examination of the simulation results, because the simulated profiles exhibited two or more velocity contrasts in the 50 to 150 m depth range unlike the real profiles, which exhibited only one large velocity contrast in this depth range. To resolve this difference, it was necessary to reduce $\lambda(h)$ by approximately 30% in this depth range. The resulting $\lambda(h)$ versus depth is nearly identical to that obtained for the Repository Block in Section 6.2.3.6.6. For the sake of simplicity, the parameters for the Repository Block are used at both locations. Analysis of the calculated values of the normalized layer thickness indicates that these values are well represented by a lognormal distribution with a coefficient of variation of 0.62. Microsoft Excel 2000 was used in the analyses of layer thickness (see Appendix I).

6.2.3.6.10 Correlation Parameters for the Repository Block and the Surface Facilities Area

As a result of the small sample size, the calculations described in Sections 6.2.3.6.5 to 6.2.3.6.8 did not produce well-constrained estimates of parameters ρ_{200}, h_0, b, ρ_0, and Δ in Eq. 40 through 42 (i.e., the parameters that control the correlation coefficient $\rho(h,t)$) for the Repository Block or the Surface Facilities Area. Final estimates of these parameters were obtained by examining the values obtained at each location (and their respective subsets), and by examining the effects of these parameters on simulated profiles. Another consideration utilized in developing these parameters is that profile roughness (associated with low values of ρ) yields slightly lower ground-motion amplification factors, because they produce more wave scattering. Thus, over-estimation of ρ may result in conservative high-frequency ground motion. The resulting values of $\rho_d(h)$ and $\rho_t(t)$ for the Repository Block and the Surface Facilities Area are shown on Figure 6.2-128. Because $\rho_t(t)$ is a function of thickness and not of depth, it is plotted as a function of the average layer thickness $\bar{t}(h) = \lambda(h)^{-1}$ for each depth.

6.2.3.6.11 Parameter Values

Tables 6.2-24 and 6.2-25 show the parameters of the probabilistic representation for V_S and for layer thickness, for both the Repository Block and the Surface Facilities Area. The top seven entries in these tables indicate the values of the logarithmic σ at various control depths. Subsequent entries indicate the values of the parameters that control the correlation coefficient ρ and the rate of layer boundaries

The analysis of velocities also estimates median velocity profiles for both locations, but these values are not used in the development of amplification factors. These median velocity profiles, however, are compared to the base case profile to assure an unbiased statistical sampling of velocity profiles is used in the analysis. The base case V_S profiles obtained in Sections 6.2.3.3 and 6.2.3.4, which are similar to these median velocities, are used for the analysis.

OCRWM Project Condition Report 2823 documents that the incorrect probabilistic representation for both Repository Block and Surface Facilities Area base case velocity profiles was used in carrying out the analysis/modeling. A preliminary version of the Repository Block probabilistic representation was used instead of the final Repository Block and Surface Facilities Area representations. Sensitivity studies were carried out to evaluate the impact of the use of incorrect data and show that the ground motion output differs by less than 15%. The sensitivity studies are documented in Wong and Silva (2004d [DIRS 172075], page 14). Differences in the ground motion output are negligible when compared to the variability and uncertainty incorporated into the overall analysis and modeling. Thus, the results obtained using the incorrect input are considered to be valid and used in this study.

Table 6.2-24. Parameters of the Probabilistic Representation of Velocity Profiles for the Repository Block

Quantity	Value	Units
σ (0 m)	0.364	None
σ (10 m)	0.364	None
σ (60 m)	0.198	None
σ (100 m)	0.198	None
σ (101 m)	0.198	None
σ (102 m)	0.198	None
σ (366 m)	0.198	None
ρ_0	0.8	None
Δ	6	m
ρ_{200}	0.6	None
h_0	0.01	m
b	0.3	None
c_1	1.051	m
c_2	0.9601	None

Quantity	Value	Units
c_3	1.0999	m^{c2-1}
h_c	0.001	m
COV(τ)	0.79	None

Source: DTN: MO0208VCPRBWHB.000 [DIRS 163801]

NOTE: To convert meters for feet, multiply by 3.281

Table 6.2-25. Parameters of the Probabilistic Representation of Velocity Profiles for the Waste Handling Buildings Site Characterization Area

Quantity	Value	Units
σ (0 m)	0.331	None
σ (5 m)	0.331	None
σ (10 m)	0.181	None
σ (10.01 m)	0.181	None
σ (10.02 m)	0.181	None
σ (10.02 m)	0.181	none
σ (366 m)	0.181	none
ρ_0	0.95	none
Δ	6	m^{c2-1}
ρ_{200}	0.6	none
h_0	0.01	m
b	0.15	none
c_1	1.051	m
c_2	0.9601	none
c_3	1.0999	m^{c2-1}
h_c	0.001	m
COV(τ)	0.62	None

Source: DTN: MO0208VCPRBWHB.000 [DIRS 163801]

NOTE: To convert meters for feet, multiply by 3.281

6.2.3.6.12 Randomized Profiles

Examples of the randomized profiles, in this case, for the V_S base case #1 profile for the Repository Block and the V_S base case (30 ft of alluvium) profile for the Surface Facilities Area are shown on Figures 6.2-129 and 6.2-130, respectively.

6.2.3.7 Densities

In addition to seismic velocities, densities are required for input into the site response analysis. A uniform density was assumed for the tuff, alluvium, and fill. For the tuff, a mean dry bulk density of 2.26 ± 0.06 g/cm^3 (141 ± 4 pcf) has been reported for the middle-nonlithophysal unit of the Topopah Springs Tuff based on qualified data only (SNL01A05059301.002 [DIRS 150042], SNL01A05059301.005 [DIRS 109002], SNL02030193001.004 [DIRS 108415], SNL02030193001.012 [DIRS 108416], SNL02030193001.019 [DIRS 108431], SNL02030193001.021 [DIRS 108433]). If non-qualified and to be verified data (MO0204RIB00130.000 [DIRS 159744]) are also considered along with the qualified data to corroborate the result, a density of 2.25 ± 0.07 g/cm^3 (140 ± 4 pcf) is obtained. Corresponding values for the lower-lithophysal zone of the Topopah Springs Tuff are 2.25 ± 0.05 g/cm^3 (141 ± 3 pcf) (SNL01A05058301.002 [DIRS 150042], SNL02030193001.004 [DIRS 108415], SNL02030193001.019 [DIRS 108431], SNL02030193001.020 [DIRS 108432], SNL02030193001.021 [DIRS 108433]) and 2.23 ± 0.08 g/cm^3 (139 ± 5 pcf) (MO0204RIB00130.000 [DIRS 159744]), respectively. These values do not account for a 20% additional lithophysal porosity and so a density of 2.2 g/cm^3 (137 pcf) was adopted for the tuff. Values measured in 2000 from gamma-gamma density measurements in two of the geotechnical boreholes (MO0204SEPGAMDM.000 [DIRS 158125]; BSC 2002a [DIRS 157829], Table 12) yield average values of 2.32 ± 0.05 g/cm^3 (145 ± 3 pcf) and 2.17 ± 0.10 g/cm^3 (135 ± 6 pcf) for the middle nonlithophysal and lower lithophysal zones respectively, which are consistent with a value of 2.2 g/cm^3 (137 pcf).

Similarly, gamma-gamma measurements yield a mean density of 1.85 ± 0.12 g/cm^3 (115 ± 7 pcf) for the alluvium (RF#16, RF#18, RF#20, RF#21, RF#22, RF#24, RF#28) (MO0204SEPGAMDM.000 [DIRS 158125]; BSC 2002a [DIRS 157829], Table 12). A value of 1.80 g/cm^3 (112 pcf) was adopted for input into the site response analysis.

6.2.4 Characterization of Nonlinear Dynamic Material Properties

The development of nonlinear dynamic properties for input into the site response analyses is presented in this section. As discussed in Section 6.1, in equivalent-linear site response analyses there is a need for shear modulus reduction and damping curves. A single relationship relates shear stress to shear strain in horizontal layers, as vertical motions are decoupled and run linearly. EPRI (1993b [DIRS 103320], Appendix 6.B) provides a thorough summary of the incorporation of nonlinear dynamic properties. Shear modulus reduction and damping curves are used directly in equivalent-linear analyses in which the modulus reduction factor and the damping ratio are simply "looked up" as a function of the peak shear strain over the duration of excitation for the layer in question. Since the peak strains are not known at the outset of the analysis, initial values are assumed and the analysis iterates until "strain-compatible" values are found (EPRI 1993b [DIRS 103320], Appendix 7, p. 7.A-4). Thus shear modulus reduction and damping curves are required for each horizontal layer represented in the site profile. Curves were developed for tuff (Section 6.2.4.2) and alluvium (Section 6.2.4.3). Nonlinear dynamic properties were developed by a team of experts in ground motion analyses and geotechnical engineering: Drs. Kenneth Stokoe, II, Walter Silva and Patricia Thomas with peer review by Drs. Carl Costantino and Robert Pyke. As described in SN-M&O-SCI-037-V1 (Wong and Silva 2003 [DIRS 163201], pages 99-134) and SN-M&O-SCI-037-V3 (Wong and Silva 2004b [DIRS

170444], pages 77-86), the curves are the result of the available laboratory test data, current research on similar materials, and expert judgment.

6.2.4.1 Inputs for Development of Nonlinear Dynamic Material Property Curves

Development of shear modulus reduction and material damping curves is based in part on dynamic laboratory testing of tuff and alluvium taken from boreholes at the WHB Area and the North Portal area of the ESF. Resonant column and torsional shear testing of specimens are described in BSC (2002a [DIRS 157829], Sections 6.2.10, 6.3.3, and 6.5.3). Two series of tests were performed. In 1999, dynamic laboratory testing was performed on 6 intact tuff specimens and 4 reconstituted alluvium specimens from RF#13. In 2000, dynamic laboratory testing was performed on 18 intact tuff specimens from RF#14, RF#15, RF#16, and RF#17, five intact tuff specimens from the North Portal area, and one reconstituted alluvial specimen from RF#17. Table 6.2-26 lists the tuff and alluvium specimens tested in 1999 and 2000.

Table 6.2-26. Input Data for Development of Nonlinear Dynamic Material Properties Curves

Specimen ID	Borehole No. or Collection Location	Specimen Depth* (ft)	Lithostratigraphic Unit	DTN
Tuff Samples				
UTA-11-E	RF#13	138.3	Tpki	MO9905LABDYNRS.000 [DIRS 103792]
UTA-11-B	RF#13	141.5	Tpki	MO9905LABDYNRS.000 [DIRS 103792]
UTA-11-F	RF#13	142.0	Tpki	MO9905LABDYNRS.000 [DIRS 103792]
UTA-11-I	RF#13	254.6	Tpcpmn	MO9905LABDYNRS.000 [DIRS 103792]
UTA-11-G	RF#13	255.5	Tpcpmn	MO9905LABDYNRS.000 [DIRS 103792]
UTA-11-H	RF#13	257.3	Tpcpmn	MO9905LABDYNRS.000 [DIRS 103792]
UTA-23-C	RF#14	361.0	Tpcpul	MO0203DHRSSWHB.001 [DIRS 158082]
UTA-23-D	RF#14	397.0	Tpcpmn	MO0203DHRSSWHB.001 [DIRS 158082]
UTA-23-G	RF#15	192.5	Tpcpul	MO0203DHRSSWHB.001 [DIRS 158082]
UTA-23-T	RF#15	192.5	Tpcpul	MO0203DHRSSWHB.001 [DIRS 158082]
UTA-23-H	RF#15	322.0	Tpcpln	MO0203DHRSSWHB.001 [DIRS 158082]
UTA-23-J	RF#17	575.6	Tpcpul	MO0203DHRSSWHB.001 [DIRS 158082]
UTA-20-B	RF#16	189.5	Tpcrn	MO0203DHRSSWHB.001 [DIRS 158082]
UTA-20-C	RF#16	235.5	Tpcpul	MO0203DHRSSWHB.001 [DIRS 158082]
UTA-23-B	RF#14	241.5	Tpcrn	MO0203DHRSSWHB.001 [DIRS 158082]
UTA-23-R	RF#14	241.5	Tpcrn	MO0203DHRSSWHB.001 [DIRS 158082]
UTA-23-E	RF#15	27.3	Tpcrn	MO0203DHRSSWHB.001 [DIRS 158082]
UTA-23-F	RF#15	88.7	Tpcpul	MO0203DHRSSWHB.001 [DIRS 158082]
UTA-23-S	RF#15	88.7	Tpcpul	MO0203DHRSSWHB.001 [DIRS 158082]
UTA-20-A	RF#16	126.8	Tpki	MO0203DHRSSWHB.001 [DIRS 158082]

Specimen ID	Borehole No. or Collection Location	Specimen Depth* (ft)	Lithostratigraphic Unit	DTN
UTA-23-Q	RF#16	126.8	Tpki	MO0203DHRSSWHB.001 [DIRS 158082]
UTA-20-D	RF#16	80.5	Tpki	MO0203DHRSSWHB.001 [DIRS 158082]
UTA-23-A	RF#14	104.5	Tpki	MO0203DHRSSWHB.001 [DIRS 158082]
UTA-23-I	RF#17	400.2	Tpcrn	MO0203DHRSSWHB.001 [DIRS 158082]
UTA-20-F	ESF	4.5	Tpki	MO0203DHRSSWHB.001 [DIRS 158082]
UTA-20-G	ESF	6.5	Tpki	MO0203DHRSSWHB.001 [DIRS 158082]
UTA-20-I	ESF	Not measured	Tpcrv	MO0203DHRSSWHB.001 [DIRS 158082]
UTA-20-J	ESF	Not measured	Tmbt1	MO0203DHRSSWHB.001 [DIRS 158082]
UTA-20-L	ESF	Not measured	Tpki	MO0203DHRSSWHB.001 [DIRS 158082]
Alluvium Samples				
UTA-11-C	RF#13	57.3	Qal	MO9905LABDYNRS.000 [DIRS 103792]
UTA-11-A	RF#13	57.5	Qal	MO9905LABDYNRS.000 [DIRS 103792]
UTA-11-J	RF#13	66.9	Qal	MO9905LABDYNRS.000 [DIRS 103792]
UTA-11-D	RF#13	67.0	Qal	MO9905LABDYNRS.000 [DIRS 103792]
UTA-23-X	RF#17	59.0	Qal	MO0203DHRSSWHB.001 [DIRS 158082]

NOTE: *Depth is measured from the top of the boreholes. For samples from the ESF, depth is horizontal distance from the tunnel wall.

Corroborative Data–Laboratory dynamic testing was conducted in 1998 on 10 intact tuff specimens recovered from three boreholes (SD-9, SD-12, and NRG-7/7a) on Yucca Mountain (Stokoe et al. 1998). These data do not form direct input to the development of nonlinear dynamic material properties curves, but rather are corroborative information. These dynamic test results are the only ones available for specimens within the Repository Block and are used only to corroborate the applicability to the Repository Block of curves developed for tuff based on specimen test results from the WHB Area. Table 6.2-27 lists the specimens tested in 1998.

Table 6.2-27. Corroborative Data for Development of Nonlinear Dynamic Material Properties Curves for Tuff

Specimen ID	Borehole No.	Specimen Depth (ft)	Material Type
UTA-2-A	USW NRG-7/7A	43	Welded Tuff
UTA-2-B	USW SD-12	92	Welded Tuff
UTA-2-C	USW NRG-7/7A	86	Unwelded Tuff
UTA-2-D	USW NRG-7/7A	94	Unwelded Tuff
UTA-2-E	USW NRG-7/7A	136	Unwelded Tuff
UTA-2-F	USW SD-9	79	Unwelded Tuff
UTA-2-H	USW SD-9	79	Unwelded Tuff

Specimen ID	Borehole No.	Specimen Depth (ft)	Material Type
UTA-2-K	USW NRG-7/7A	78	Unwelded Tuff
UTA-2-L	USW SD-12	135	Welded Tuff
UTA-2-M	USW NRG-7/7A	44	Welded Tuff

Source: Stokoe et al. 1998 [DIRS 107635], Table 1

Other Information–EPRI (1993b [DIRS 103320], Section 7.A.5) developed a simple hyperbolic model of nonlinear shear stress-shear strain behavior for use in equivalent-linear site response analyses. A simple model of soil behavior under simple shear loading conditions can be constructed by assuming that the shape of the shear stress-shear strain relationship can be represented by a hyperbola which has an initial slope equal to G_{max}, the shear modulus at small strains, and is asymptotic to τ_{max}, the shear strength (EPRI 1993b [DIRS 103320], Appendix 7, p. 7.A-17). The ratio of τ_{max} to G_{max}, defined as the reference strain, γ_r, is useful both in expressing the stress-strain relationship in mathematical form and as a measure of the relative values of τ_{max} and G_{max}. Soils with larger values of γ_r have greater shear strengths relative to their small strain modulus and show more elastic stress-strain behavior than soils with smaller values of γ_r. Thus gravelly soils have low reference strain values and more plastic clays have high values (EPRI 1993b [DIRS 103320], Appendix 7, p. 7.A-17). The hyperbolic shape used in the EPRI (1993b [DIRS 103320]) generalized curves provides a good fit to laboratory data on the variation of the secant, or equivalent-linear shear modulus with shear strain up to cyclic shear strains of 0.1 to 1.0 percent (EPRI 1993b [DIRS 103320], Appendix 7, p. 7.A-28).

The work presented in EPRI (1993b [DIRS 103320], Section 7.A.5) forms part of the basis for the development of the shear modulus reduction and damping curves. As discussed in Sections 6.2.4.2 and 6.2.4.3, the EPRI (1993b [DIRS 103320], Section 7.A.5) work is used to guide the extrapolation of the curves beyond the range of available data.

6.2.4.2 Tuff Normalized Shear Modulus Reduction and Material Damping Curves

Evaluation of input data for tuff specimens and of other relevant information leads to the development of two sets of curves for normalized shear modulus reduction and hysteretic damping as a function of shearing strain. Use of two sets of curves is required to represent the uncertainty in characterizing these dynamic material properties. Both sets of curves serve as the basis for input to the equivalent-linear site-response model. Thus, model output reflects the uncertainties in dynamic material properties at Yucca Mountain. Laboratory dynamic testing data available to serve as direct input to an analysis of dynamic material properties for tuff are associated with DTNs MO9905LABDYNRS.000 [DIRS 103792] and MO0203DHRSSWHB.001 [DIRS 158082].

Tuff samples tested cover a range of lithostratigraphic units and rock characteristics. Samples from units Tpki, Tpcrn, Tpcpul, Tpcpmn, Tpcpln, Tmbt1, and Tpcrv were tested. The distribution of these materials in the WHB Area is presented in BSC (2002a [DIRS 157829], Section 6.6). The only tuff material in the WHB Area that was not dynamically tested in the laboratory was Tpbt5. As shown on Figure 6.2-94, the repository host horizon consists of the lower units of the Topopah Spring Tuff. Dynamic laboratory test data are not available for the Topopah Spring Tuff nor some of the overlying bedded tuff units. Units for which dynamic

laboratory test data are available are noted on Figure 6.2-94. As shown on Figure 6.2-131, a correlation between tuff unit and dynamic properties is not supported by the available data. This is consistent with the lack of strong evidence of correlation between tuff units and V_S.

Testing results are unavailable for some lithostratigraphic units contained in the site response model, including those of the Topopah Spring Tuff and overlying bedded tuffs. However, the lack of correlation between dynamic properties and lithostratigraphic unit, and the similarity between the units of the Tiva Canyon Tuff and the Topopah Spring Tuff, provide justification for using the available data to develop dynamic material property curves applicable to all tuff units in the site response model.

Laboratory dynamic test results also were divided into two groups, welded and nonwelded, to determine if the degree of welding significantly influenced the dynamic behavior of the tuff. Laboratory test results for welded and nonwelded tuff specimens are shown on Figures 6.2-132 and 6.2-133. These data indicate no consistent difference in modulus reduction and material damping relationships between welded and nonwelded tuff units.

Dynamic testing results for tuff samples were also examined with respect to dry unit weight (γ_{dry}). A plot of dry unit weight (γ_{dry}) versus low-strain V_S (Figure 6.2-134), indicates a trend of increasing low-strain V_S with increasing γ_{dry} for the tuff specimens. As a result, three groups were identified on the basis of dry unit weight: Group 1 specimens have 147 pcf > γ_{dry} > 133 pcf; Group 2 specimens have 132 pcf > γ_{dry} > 117 pcf; and Group 3 specimens have 94 pcf > γ_{dry} > 78 pcf. Dynamic testing results from these three groups are shown on Figures 6.2-135 and 6.2-136. The trends in G/G_{max} and damping in these three groups do not warrant developing separate curves for each group.

Based on the available data, correlations between shear modulus reduction and damping properties and lithostratigraphic unit, degree of welding, or dry unit weight are not supported. Therefore, these dynamic properties were developed for all tuff units as a whole.

Although laboratory test results provide information on the dynamic properties of tuff samples at Yucca Mountain, uncertainties exist with respect to how well the test results represent *in situ* conditions. The relatively small intact specimens do not contain the fractures, voids, and planes of weaknesses that are present in the field. In fact, to facilitate testing, samples are preferentially selected from unfractured, competent materials. As a result, laboratory G/G_{max} curves tend to be more linear than field behavior and hysteretic damping values tend to be lower than field behavior. This bias is shown on Figure 6.2-137 by comparing the values of V_S measured in the field and in the laboratory. In every case, the laboratory value exceeds any value of V_S measured seismically in the field at the specimen depth. In addition, smaller laboratory specimens (~/inch diameter) cored from larger laboratory specimens (~2 inch diameter) generally exhibit slightly higher values of V_S as shown on Figure 6.2-138. Hence, sample disturbance and/or specimen size seem to have a small but measurable effect on the intact specimens. On the other hand, samples are subject to disturbance associated with their collection and, thus, may exhibit more nonlinear behavior than *in situ* unfractured rock. Both of these potential effects must be accommodated in developing dynamic material property curves.

To accommodate the resulting uncertainty in appropriate mean shear modulus reduction and hysteretic damping curves to be used for the tuff, two sets of mean normalized shear modulus reduction and damping curves are developed. One set of curves represents the case in which *in situ* conditions consist of unfractured rock. The second set is developed to represent *in situ* conditions that reflect fracturing and heterogeneity, the effects of which are not captured in laboratory testing. No accommodation has been made for the potential effects of confining pressure (depth) on the curves. The effects of confining pressure on shear modulus reduction and hysteretic damping curves is expected to be small, particularly for the upper mean tuff curves. Additionally, for depths below about 100 ft, the material is quite stiff, with V_S at and above 3,000 ft/sec, likely resulting in significantly less confining pressure dependence than in the top 100 ft.

For the first case, referred to as the "upper mean tuff (UMT) curves," the normalized shear modulus reduction curve is developed by visually fitting a generic, cohesionless soil curve (EPRI 1993b [DIRS 103320], Appendix 7.A-5) (for shape) through the most linear tuff data (Figure 6.2-139). The EPRI (1993b [DIRS 103320]) shape is fit to the most linear data rather than through an average of the data because of the possibility that the samples exhibit disturbance effects and to account for the possibility of unfractured tuff units, which were not tested, behaving more linearly. For shearing strains above about 0.1 percent, the EPRI (1993b [DIRS 103320]) shape forms the entire basis for the curve, as data are unavailable for these higher shearing strain levels. For the material damping curve, the corresponding EPRI (1993b [DIRS 103320]) damping curve was used. However, the curve is constrained to have a small-strain material damping value of 0.5 percent for consistency with the site attenuation (kappa) (0.0186 sec) used in the PSHA. Damping curves reach a maximum of 15 percent in accordance with guidance from NUREG-0800, Section 3.7.2 (NRC 1989b [DIRS 165111]).

For the second case, termed the "lower mean tuff (LMT) curves," the normalized shear modulus reduction curve is developed by first visually fitting the generic, cohesionless soil curve (EPRI 1993b [DIRS 103320]) through the middle of the laboratory testing data. Next, the reference strain for the EPRI (1993b [DIRS 103320]) curve is adjusted downward by a factor of 4 based on the ratio of G_{max} in the field and laboratory (determined from V_S) to account for *in situ* fracturing and heterogeneity. As for the UMT curve, the shape of the EPRI (1993b [DIRS 103320]) generic curve provides the primary basis for the normalized shear modulus reduction curve at shearing strains greater than 0.1 percent. The resulting curve corresponds to the EPRI (1993b [DIRS 103320]) 21-50 ft curve for cohesionless soil. For material damping, the corresponding curve from EPRI (1993b [DIRS 103320]) is used. As was the case for the UMT curves, a small-strain material damping of 0.5 percent was used to constrain the curves at small strains.

Data used as direct input in developing the nonlinear dynamic material property curves come from the WHB Area and the ESF. Data from the Repository Block were unavailable for use as direct input. However, data from the Repository Block are available to corroborate the curves developed. The available Repository Block data from boreholes SD-9, SD-12, and NRG-7/7a (Stokoe et al. 1998 [DIRS 107635]) fit within the range of the data from the WHB Area, as shown on Figure 6.2-140. Thus, application of the dynamic material property curves to the entire Yucca Mountain site is justified.

The developed tuff curves for normalized shear modulus reduction and material damping, as a function of shearing strain, are associated with DTN MO0403SDIAWHBC.003 [DIRS 170434].

6.2.4.3 Alluvium Normalized Shear Modulus Reduction and Material Damping Curves

Evaluation of input data for alluvium specimens and of other relevant information leads to the development of two sets of curves for normalized shear modulus reduction and hysteretic damping as a function of shearing strain. Use of two sets of curves is required to represent the uncertainty in characterizing these dynamic material properties. Both sets of curves serve as the basis for input to the equivalent linear site-response model. Thus, model output reflects the uncertainties in dynamic material properties at Yucca Mountain.

Laboratory dynamic and static testing data available to serve as direct input to an analysis of dynamic material properties for alluvium are associated with DTNs MO9905LABDYNRS.000 [DIRS 103792], MO0203DHRSSWHB.001 [DIRS 158082], and GS020483114233.004 [DIRS 158242].

Laboratory dynamic tests were performed on five reconstituted alluvium specimens recovered from boreholes in the WHB Area. Alluvial materials in the WHB Area consist of interbedded caliche-cemented and non-cemented, poorly sorted gravel with some fines, cobbles and boulders. The depth to groundwater is approximately 1270 ft, and the water content in the alluvium is estimated at less than 5 percent. The nature of the alluvium (highly-cemented to poorly-cemented) and the presence of cobbles and bounders did not allow for intact samples of the alluvium to be taken from the boreholes or test pits, although several methods were attempted. Consequently, these disturbed samples were reconstituted in the laboratory to create test specimens. Sample reconstitution, including destruction of cementation present in the field, is likely to have a significant effect on the measured dynamic properties in the laboratory. Figure 6.2-141 shows the measured laboratory specimen V_S compared to field measurements of the alluvium.

The comparison shows that contrary to the intact tuff specimens where the laboratory values of V_S were greater than the field values, the reconstituted alluvial specimen is not as “good” as the in situ material and hence likely exhibits more nonlinearity and more damping than the in situ material.

In addition to the breaking of cementation bonds, the reconstituted specimens have a different grain size distribution and coefficient of uniformity than the alluvium in the field due to specimen retrieval techniques and scalping. Gradation curves from bag samples taken from 4 test pits are shown on Figure 6.2-142. Note that these samples consisted of material from 20-inch sand cone density tests and do not contain boulders. Limitations on the test specimen sizes due to testing equipment constraints required that the alluvium be scalped on the ½-inch sieve. The removal of the larger particles reduces the average particle size and decreases the coefficient of uniformity of the test specimen relative to the field.

Six testing related factors were considered when developing the G/G_{max} curves for alluvium based on the laboratory test specimens:

1. Destruction of cementation
2. Decrease in coefficient of uniformity
3. Variation of confining pressure in the field
4. Variation of density in the field
5. Increase in mean particle size
6. The test boundary conditions

The largest influences on the normalized shear modulus curve are due to the cementation destroyed during sampling and the change in gradation. Cementation in the field, which is not preserved in the test specimens, can cause the field behavior to be more nonlinear than exhibited by the test specimens. This situation exists if high strains cause the *in situ* cementation to break. Research on naturally cemented sands indicates that this effect can be large (Stokoe and Valle 2003 [DIRS 164689]). Figure 6.2-143 illustrates the difference in nonlinear behavior between a naturally cemented sand and the same sand with the cementation removed. However, if cementation is strong enough to be maintained during seismic loading, the field behavior can be more linear than the reconstituted test specimens. Research on sand artificially cemented with varying amounts of cement indicates that with the addition of some initial cementation, the specimen behaves in a more nonlinear manner. However, at some level of increased cementation, the specimen becomes more linear as cementation is strong enough to be maintained during shear loading (Figure 6.2-144). Degree of cementation of the alluvium across the site is unknown. However, data from the literature on cemented sands also shows that cement content as low as 0.5% can cause a factor of about 2.5 increase in the low-strain shear-wave velocity (Figure 6.2-145). The laboratory measured low-strain shear-wave velocity of the reconstituted alluvium was 925 ft/sec, while the field measurements from downhole, suspension, and SASW averaged 2300 ft/sec (Figure 6.2-141), resulting in a field to laboratory ratio of approximately 2.5. These data suggest that the field to laboratory ratio of 2.5 in low-strain shear-wave velocity may be due to the loss of a low level of cementation (< 2%) in the reconstituted laboratory samples. At this low level of cementation implied, the normalized shear modulus curve is more nonlinear than the uncemented sand (Figure 6.2-144). The normalized shear modulus curves in the artificially cemented sands did not become more linear (relative to the uncemented sand) again until the cement content reached 8%, at which time the ratio of low-strain shear-wave velocities was more than 7 (much higher than the ratio observed for site data). See Figure 6.2-145.

Factor (2), the larger coefficient of uniformity in the field, will cause the field behavior to be more nonlinear than the test specimens. Figure 6.2-146 illustrate the effect of variation of C_u on normalized shear modulus and material damping ratio for dense granular materials. In general, the normalized shear modulus curve becomes more nonlinear and the material damping ratio increases (at a given shearing strain) as C_u increases. This same trend holds for very loose to loose and loose to medium dense granular materials (Menq 2003 [DIRS 164681], page 252). The variations of confining pressure and density in the field (alluvium thickness varies from 0 to 110 ft across the site), factors (3) and (4), are considered to play a less significant role on the dynamic material properties, relative to the other factors (Van Hoff 1993 [DIRS 163890], page). Increase in mean particle size of the field relative to the test specimen, factor (5), will cause the shear modulus to increase, but has little impact on the shape (i.e., the normalized curve).

Ratios of laboratory to *in-situ* shear moduli, a factor of about 0.25 (Figure 6.2-141) suggest *in-situ* nonlinearity should be significantly less than that shown by laboratory test results (Figure 6.2-147). However, due to the scalping and loss of cementation, unambiguous adjustment of the reference strain associated with the laboratory test results was not possible. The development of two sets of mean shear modulus reduction and hysteretic damping curves, based primarily on anticipated effects of cementation loss and scalping on test results is considered to adequately accommodate uncertainty in the properties of the alluvium. This uncertainty (range in mean properties) is large, as it is intended to acknowledge the lack of experience of the geotechnical community in the response of these generally stiff, dry, and cemented soils, particularly at high loading levels.

Hence, two mean alluvium normalized shear modulus and material damping curves were developed (Figure 6.2-147). One curve, termed the lower mean alluvium (LMA) G/G_{max} curve (upper hysteretic damping curve), represents the case in which cementation in the field breaks under ground motion producing strains. The curve is developed taking into account the difference between reconstituted, scalped specimens and the field conditions. A generic, cohesionless soil EPRI (1993b [DIRS 103320], Appendix 7) curve was visually fit through the middle of the data, then adjusted downward (more nonlinear) to represent the cementation breaking during shearing. The correction factor implied in the literature is large (Figure 6.2-143) and implies a curve more nonlinear than used to date for sands or gravels. Therefore, the middle of the gravel range (EPRI 1993b [DIRS 103320], Figure 7.A-3) was used for the lower mean. In contrast to the curves for tuff, significant nonlinear behavior is evident for shearing strains reached during testing. Thus, for alluvium there is less reliance on the shape of the generic cohensionless soil curve (EPRI 1993b [DIRS 103320], Appendix 7) in defining site-specific normalized shear modulus reduction curve at high strains.

A second curve, termed the upper mean alluvium (UMA) G/G_{max} curve was developed as an envelope of the data above 0.01% strain and a general fit to the data at small strains (< 0.01%). It reflects the uncertainty due to lack of intact specimens as well as to acknowledge the lack of experience with this type of material in the geotechnical literature. The corresponding hysteretic damping was taken as a curve visually fit through the most linear data. This set of curves generally correspond to the EPRI (1993b [DIRS 103320], Figure 7.A-18) 250-500 ft cohesionless soil curves and are considered to adequately reflect potential cementation effects and state of knowledge.

The developed alluvium curves for normalized shear modulus reduction and material damping, as a function of shearing strain, are associated with DTN MO0403SDIAWHBC.003 [DIRS 170434].

6.2.4.4 Treatment of Uncertainties and Randomness of Dynamic Material Properties

Uncertainty in the variation of normalized shear modulus and damping as a function of shearing strain is represented through the use of multiple base case curves. For tuff and alluvium, two curves are provided to represent the epistemic uncertainty in dynamic material properties. The curves, which are intended to represent *in situ* conditions, are based on dynamic testing of site samples, generic modeling, and engineering judgment. The curves extend beyond the range of available data at shear strains higher than 0.1%. This limitation may not be significant in terms

of its eventual impact on TSPA because of the PGV bounding study (BSC 2004c [DIRS 170137], Section 6.4.3) where the failure shear strains ranged from about 0.1 to 0.25%.

To accommodate randomness in strain-dependent shear modulus and damping, the curves are independently randomized about the base case values (Figure 6.3-1b). The random curves are generated by sampling a transformed normal distribution (lognormal), computing the change in normalized shear modulus reduction or percent damping at $3x10^{-2}$ percent shear strain, and applying this factor at all strains. The random perturbation factor is reduced or tapered near the ends of the strain range to preserve the general shape of the mean curves (EPRI 1993b [DIRS 103320], Appendix 7). Following NUREG-0800, Section 3.7.1 (NRC 1989a [DIRS 165110]) the maximum damping ratio allowed is 15 percent. The bounds are taken as plus and minus 2 sigma, in which sigma(ln)=0.3. The bounds are developed on log axes as symmetric about the base case. The distribution is empirical, based on examining series of laboratory dynamic test results on materials comprising the same geologic unit. The variability is taken to reflect within unit randomness.

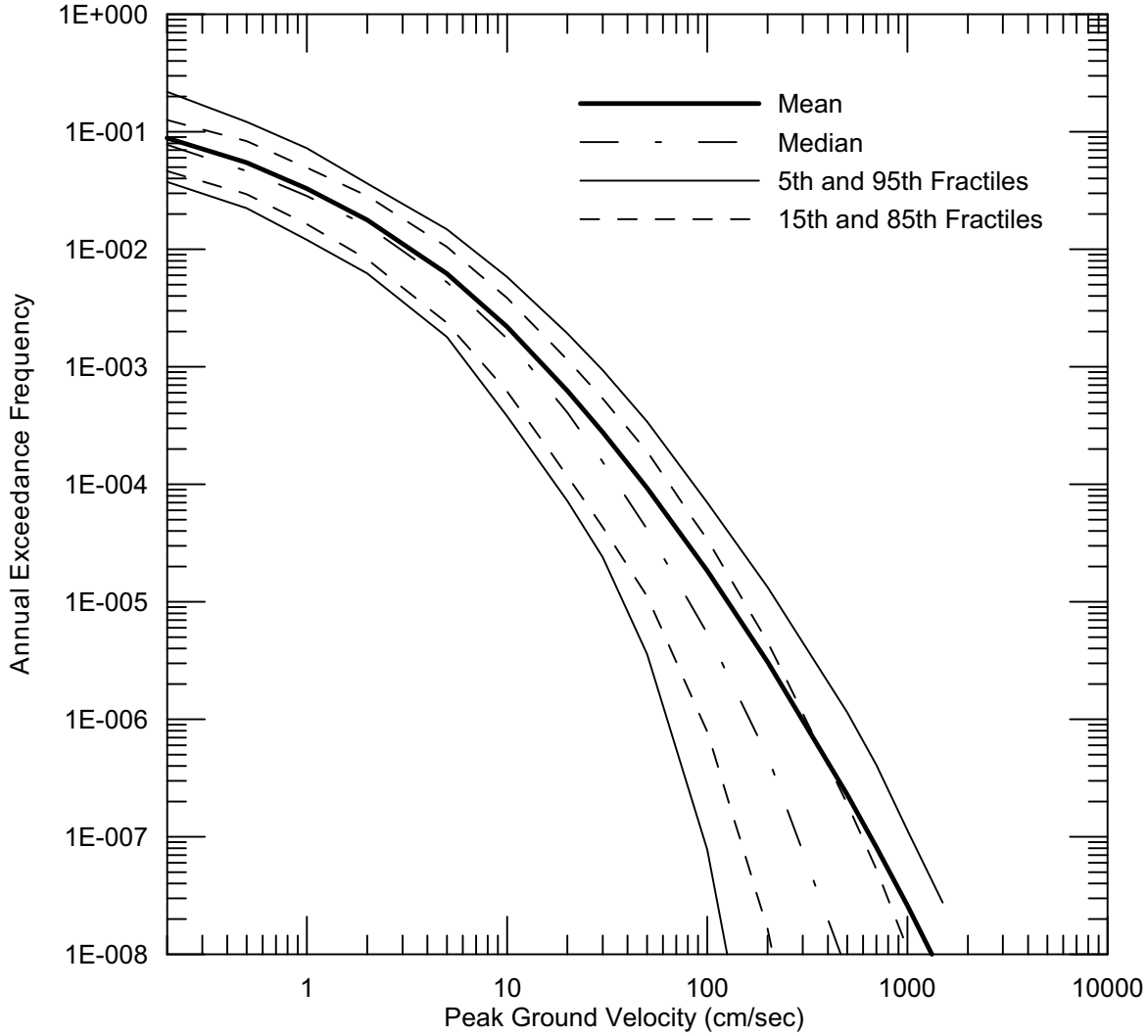

DTN: MO03061E9PSHA1.000 [DIRS 163721]

Figure 6.2-1. Hazard Curve at Point A for Peak Horizontal Ground Acceleration

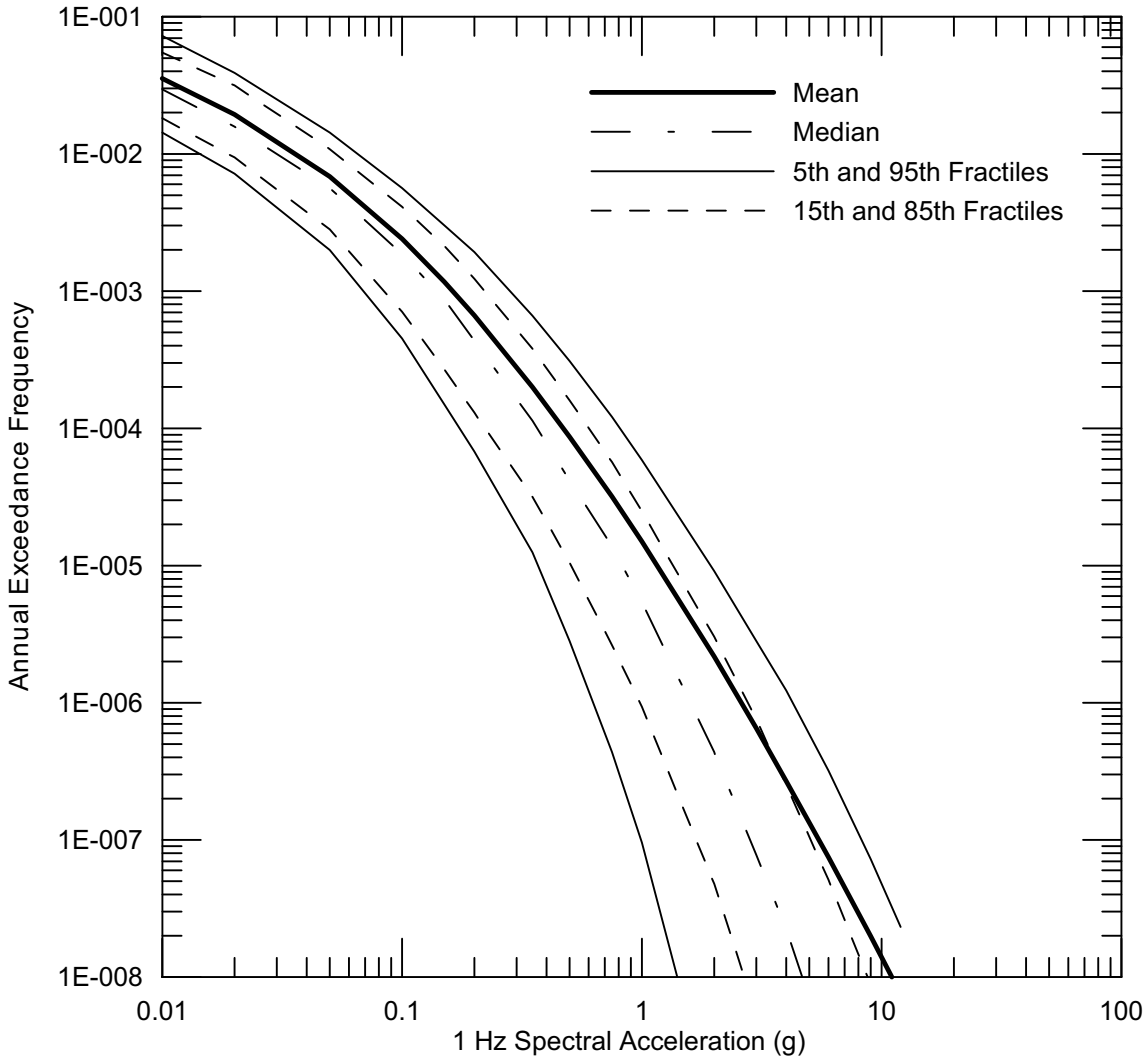

DTN: MO03061E9PSHA1.000 [DIRS 163721]

Figure 6.2-2. Hazard Curve at Point A for 10 Hz Horizontal Spectral Acceleration

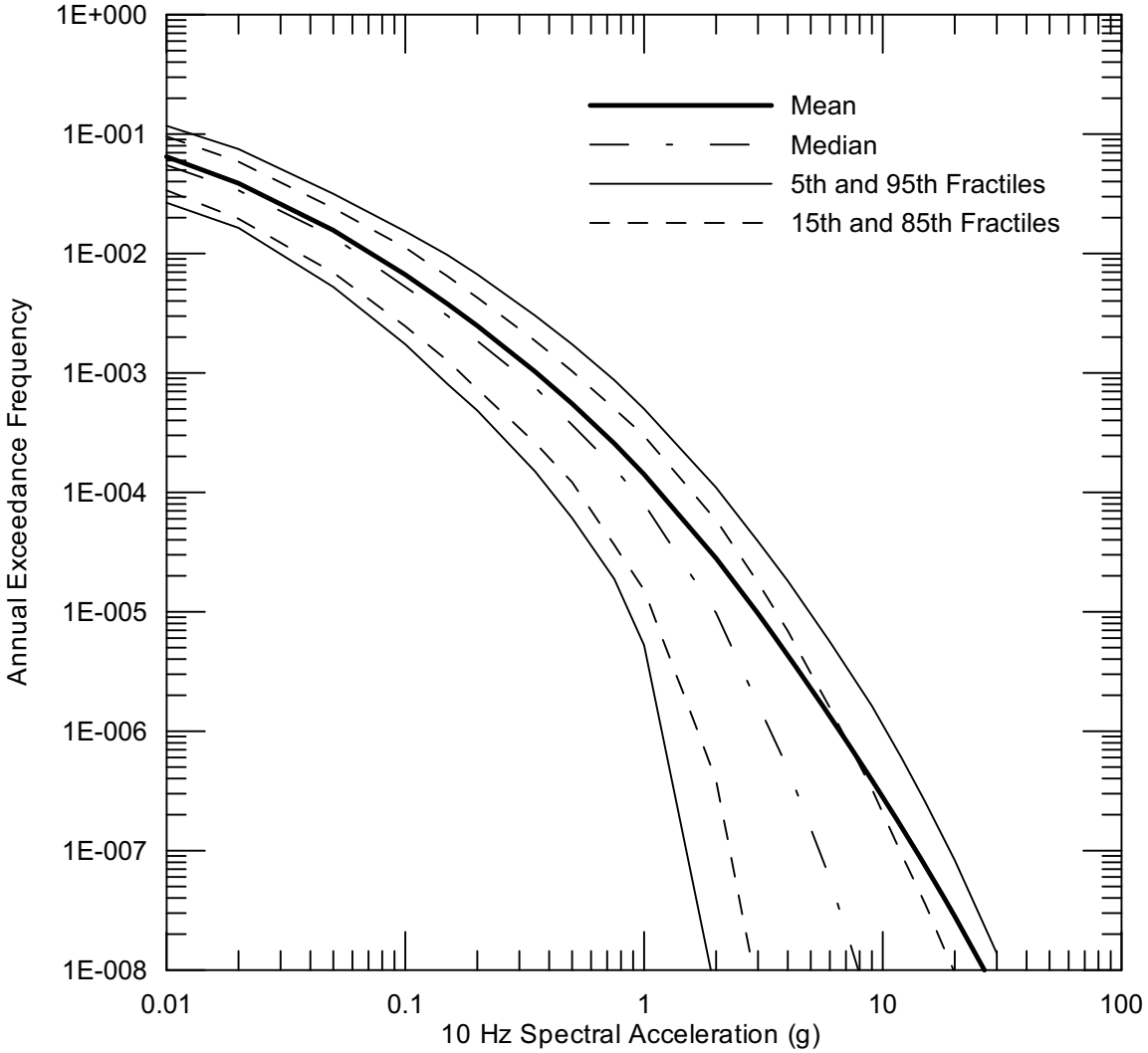

DTN: MO03061E9PSHA1.000 [DIRS 163721]

Figure 6.2-3. Hazard Curve at Point A for 1 Hz Horizontal Spectral Acceleration

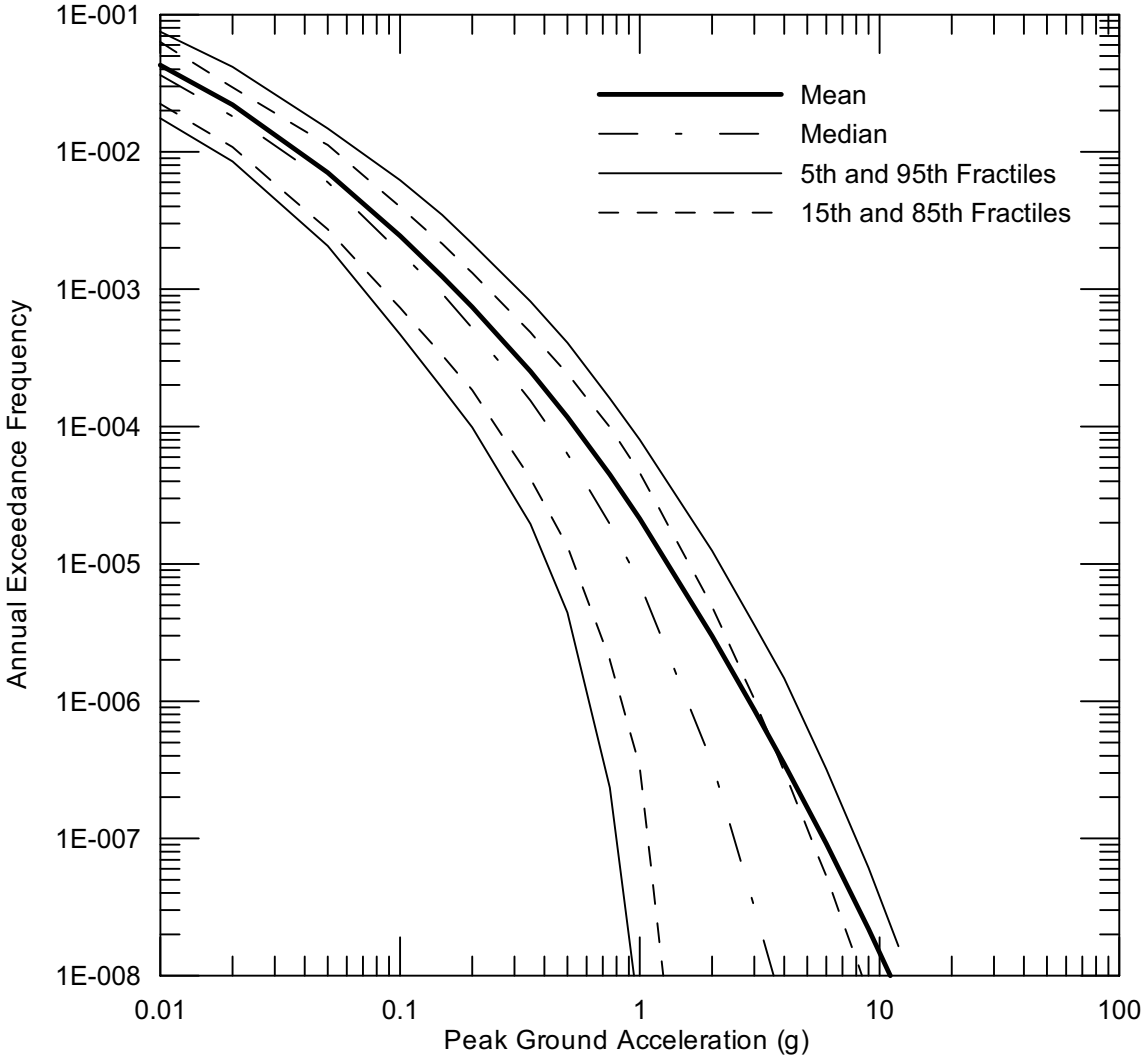

DTN: MO03061E9PSHA1.000 [DIRS 163721]

Figure 6.2-4. Hazard Curve at Point A for Peak Horizontal Ground Velocity

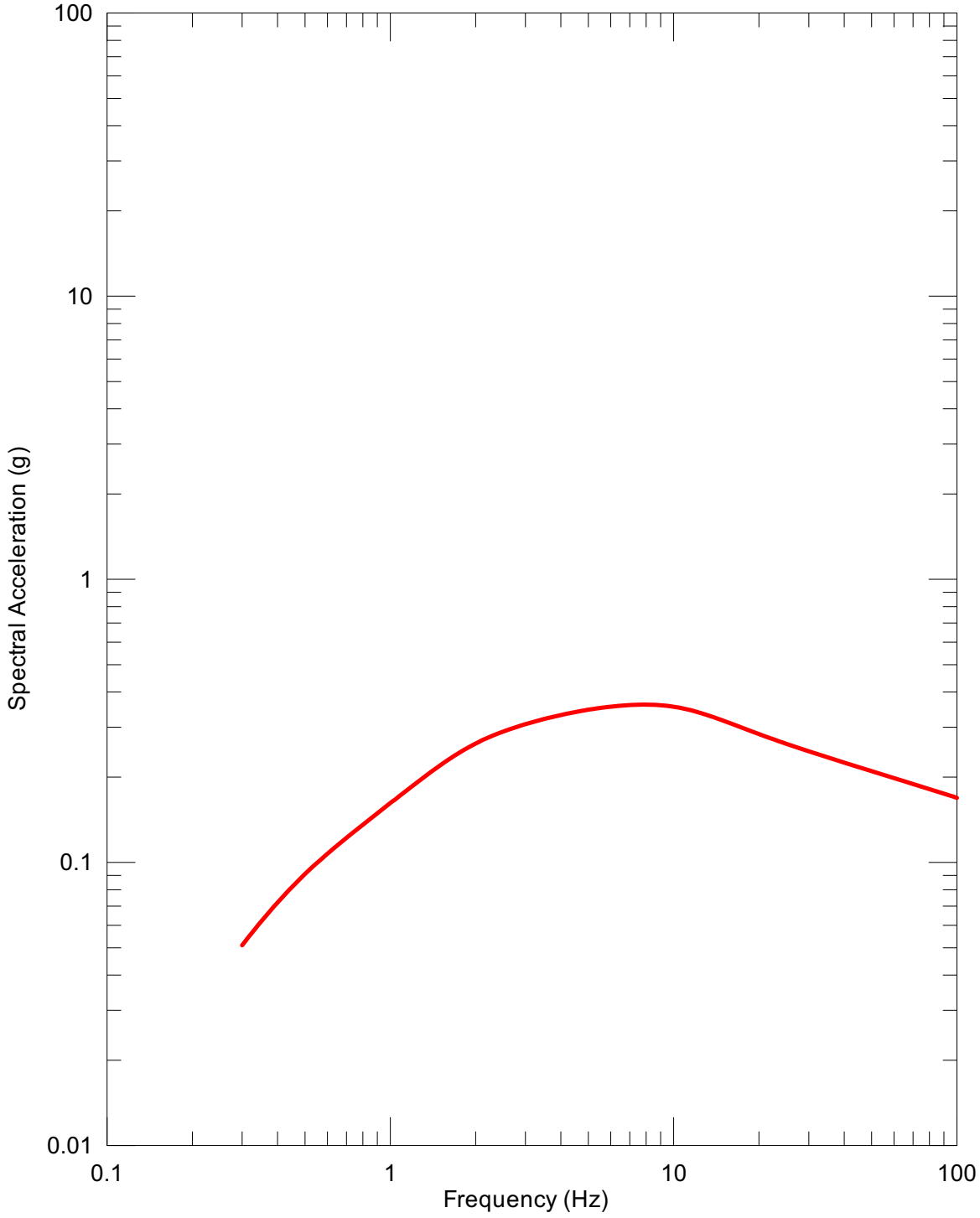

DTN: MO0401MWDRPSHA.000 [DIRS 166962]

Figure 6.2-5. Horizontal UHS at Point A, 10^{-3} Annual Exceedance Frequency

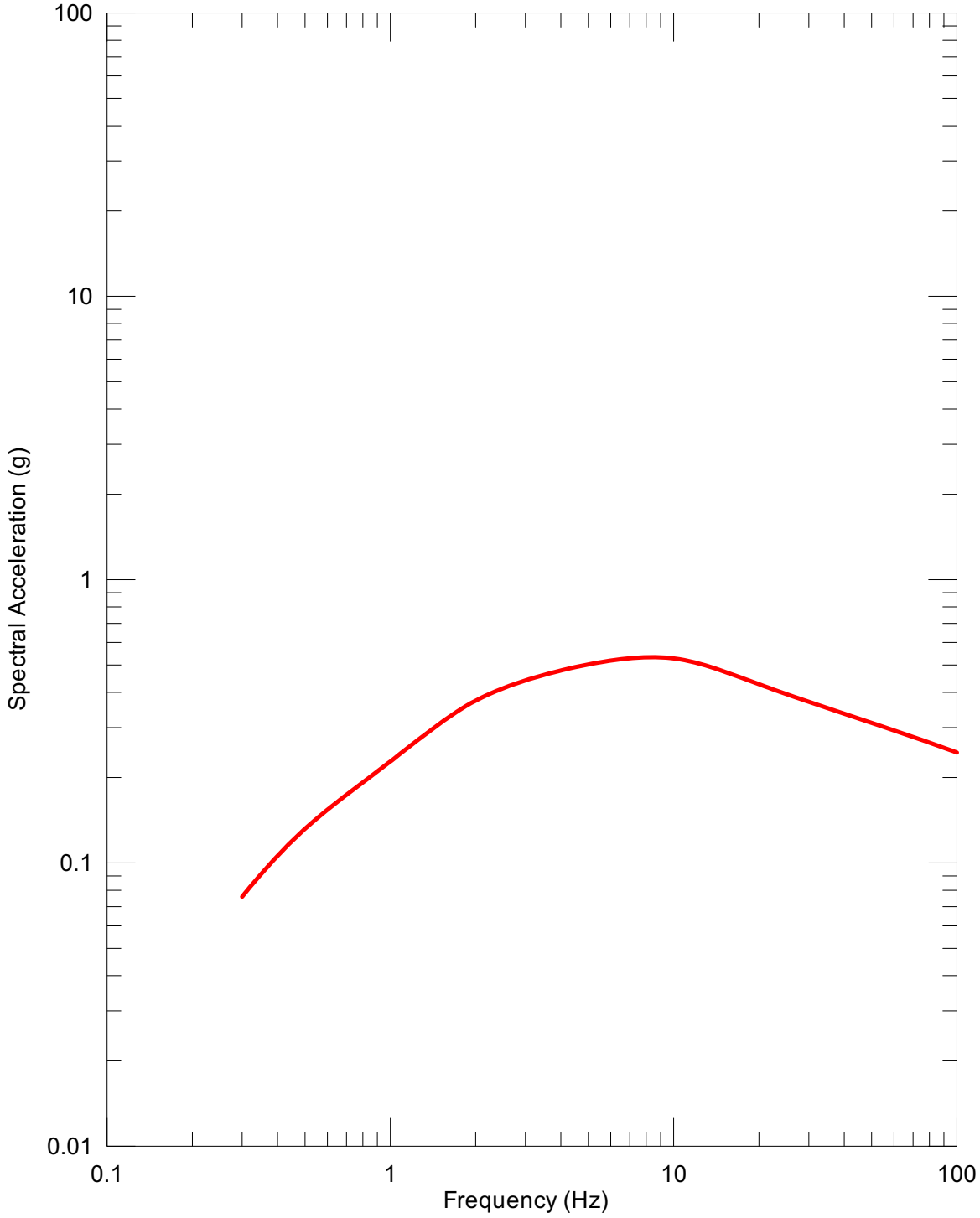

DTN: MO0208UNHZ5X10.000 [DIRS 163722]

Figure 6.2-6. Horizontal UHS at Point A, 5×10^{-4} Annual Exceedance Frequency

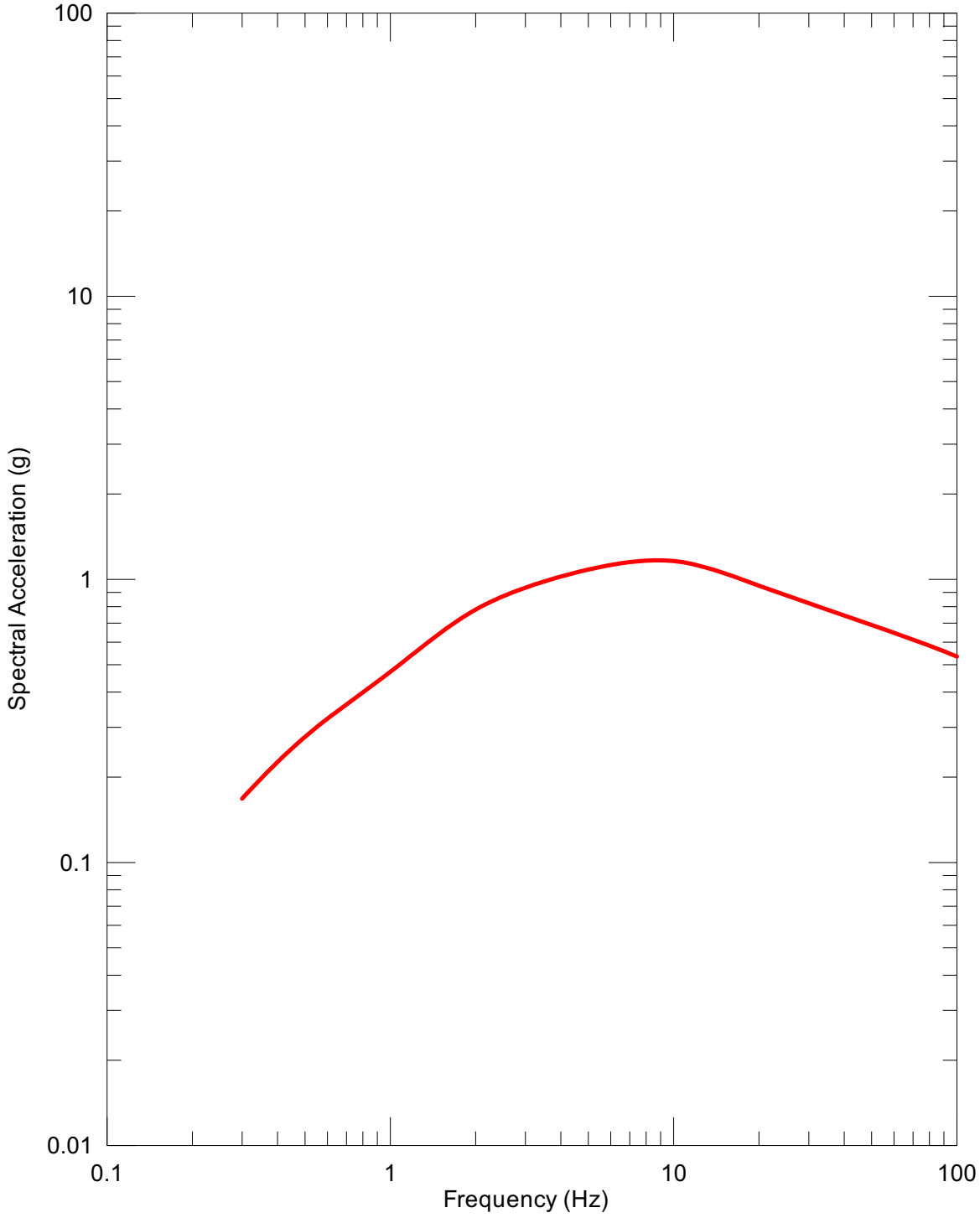

DTN: MO0401MWDRPSHA.000 [DIRS 166962]

Figure 6.2-7. Horizontal UHS at Point A, 10^{-4} Annual Exceedance Frequency

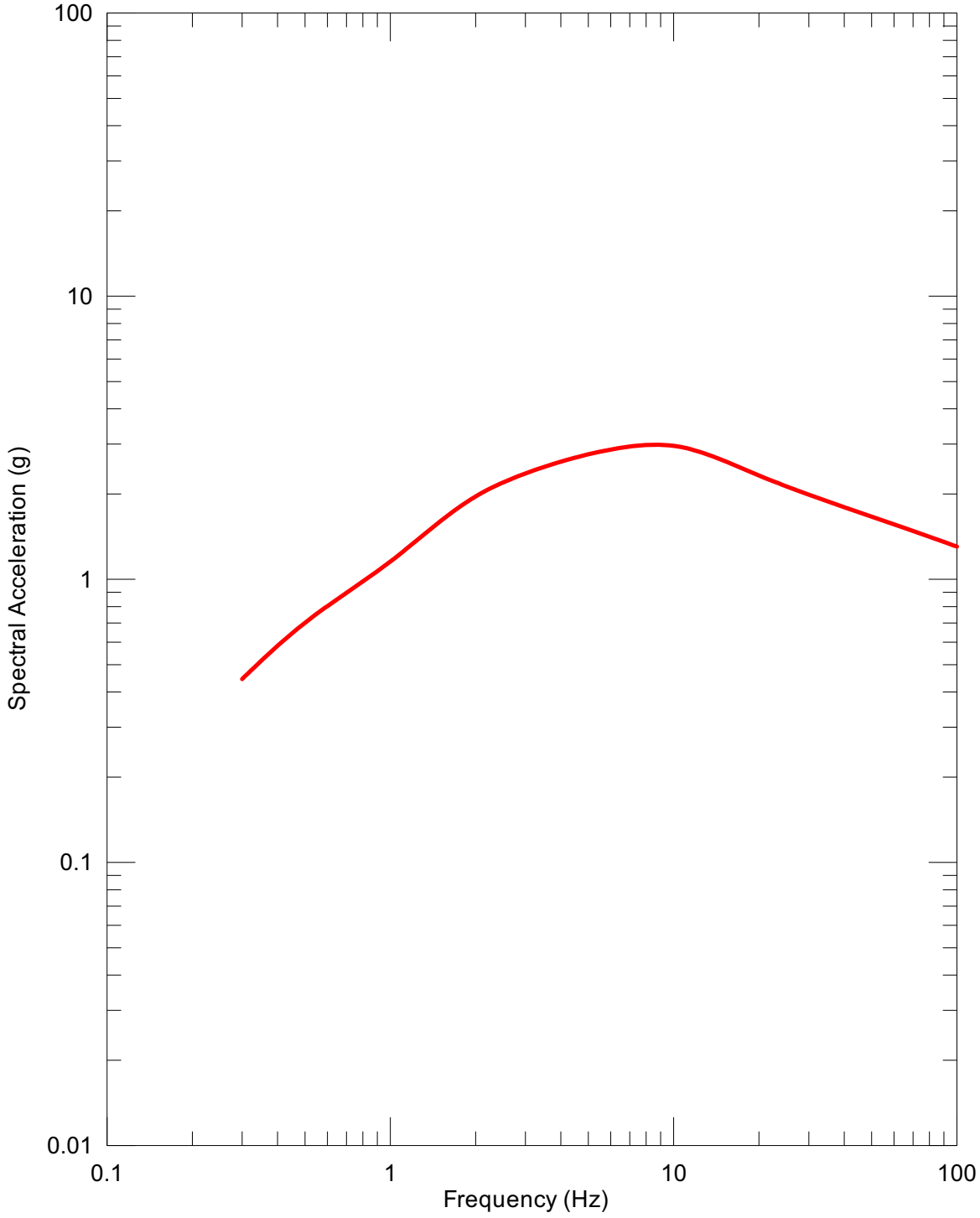

DTN: MO0308UNHAZ105.000 [DIRS 170425]

Figure 6.2-8. Horizontal UHS at Point A, 10^{-5} Annual Exceedance Frequency

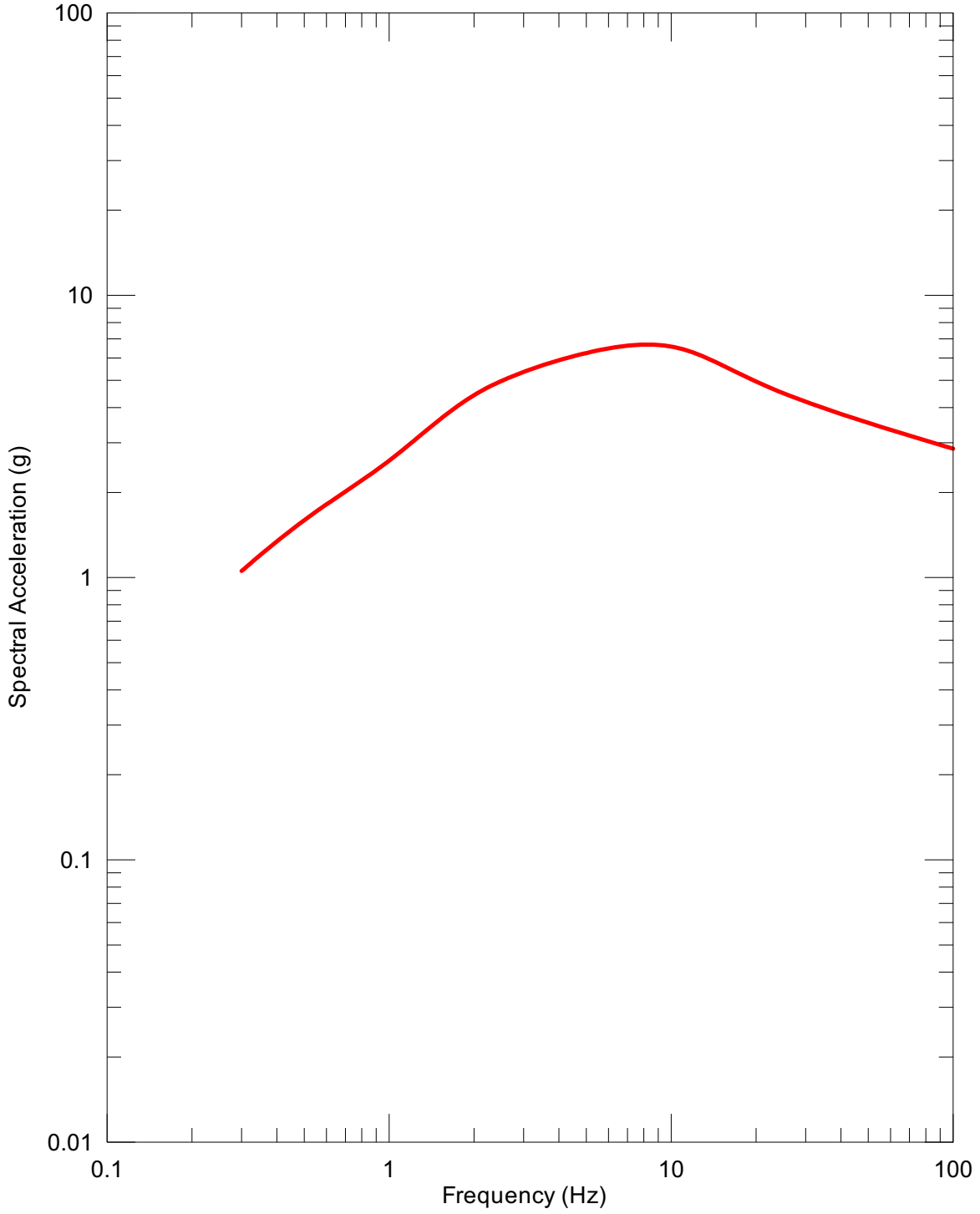

DTN: MO0206UNHAZ106.001 [DIRS 163723]

Figure 6.2-9. Horizontal UHS at Point A, 10^{-6} Annual Exceedance Frequency

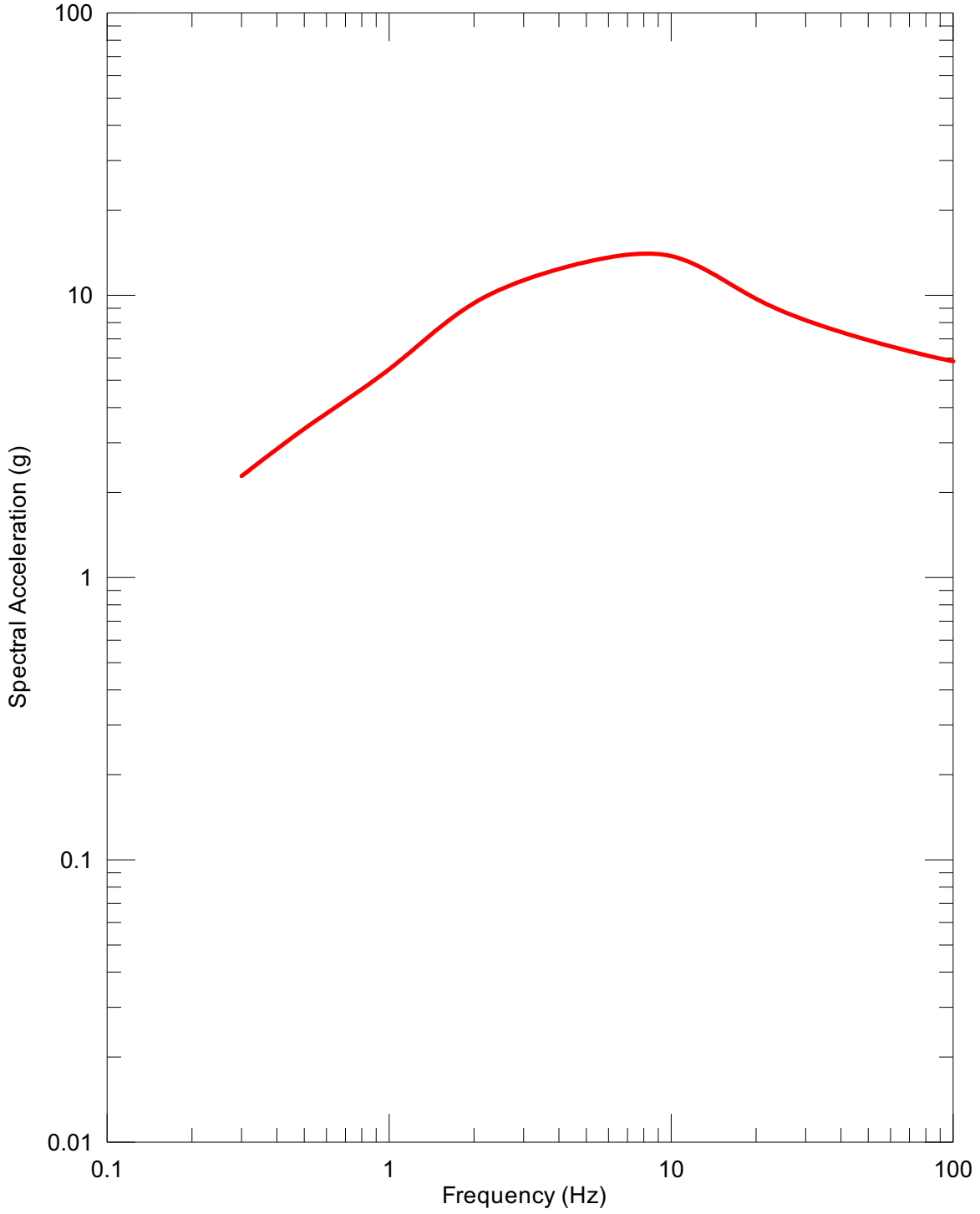

DTN: MO0209UNHAZ107.000 [DIRS 163724]

Figure 6.2-10. Horizontal UHS at Point A, 10^{-7} Annual Exceedance Frequency

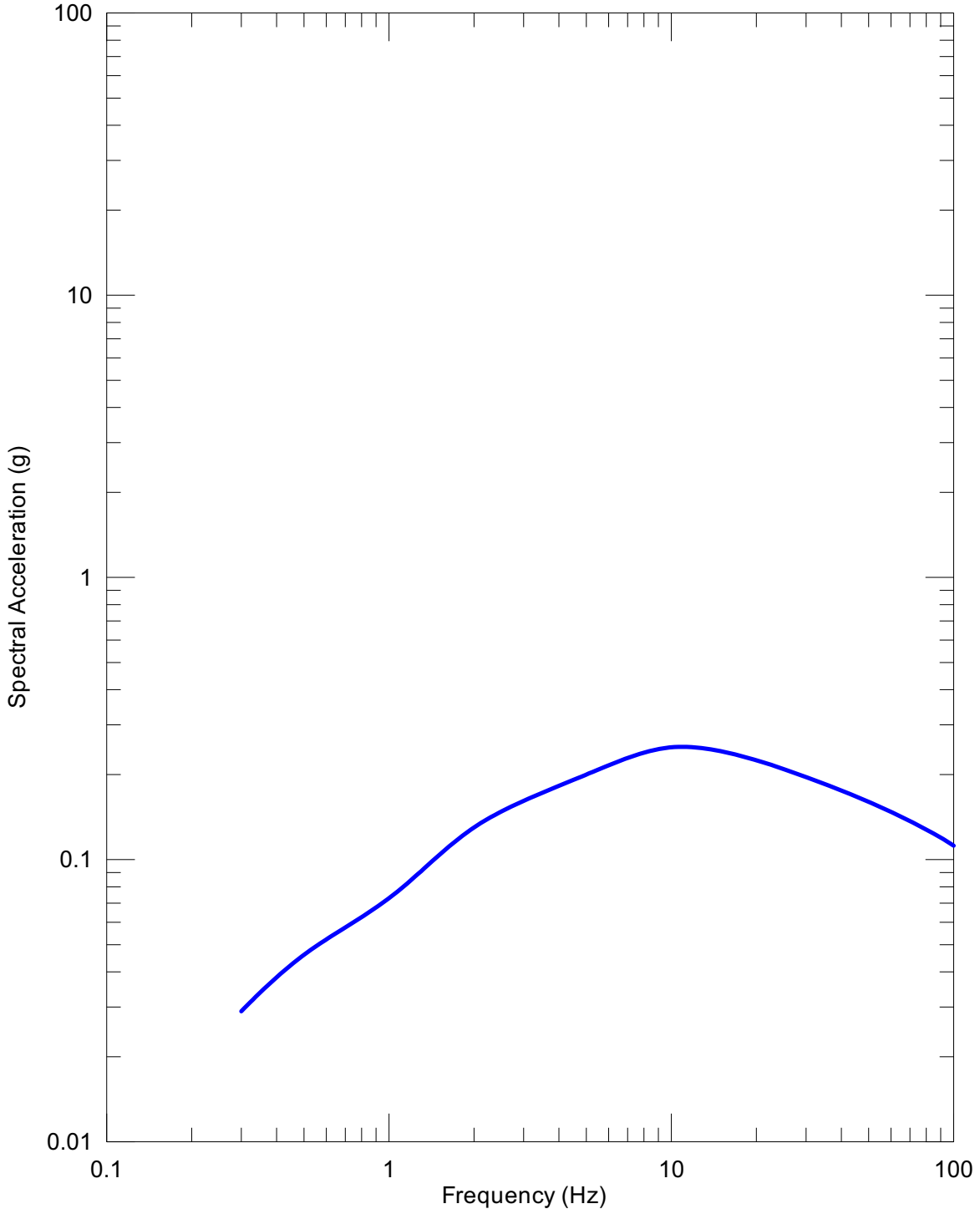

DTN: MO0401MWDRPSHA.000 [DIRS 166962]

Figure 6.2-11. Vertical UHS at Point A, 10^{-3} Annual Exceedance Frequency

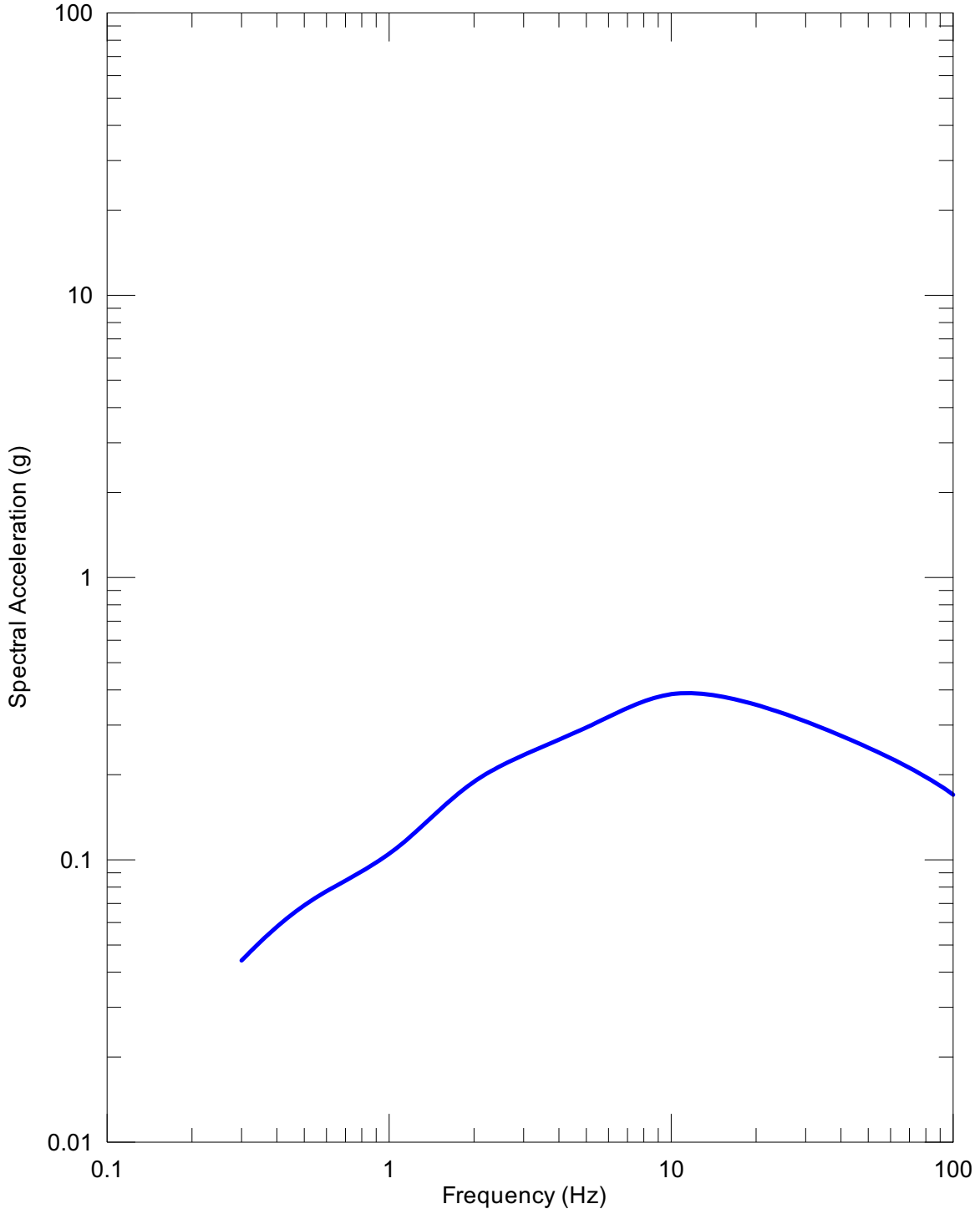

DTN: MO0208UNHZ5X10.000 [DIRS 163722]

Figure 6.2-12. Vertical UHS at Point A, 5×10^{-4} Annual Exceedance Frequency

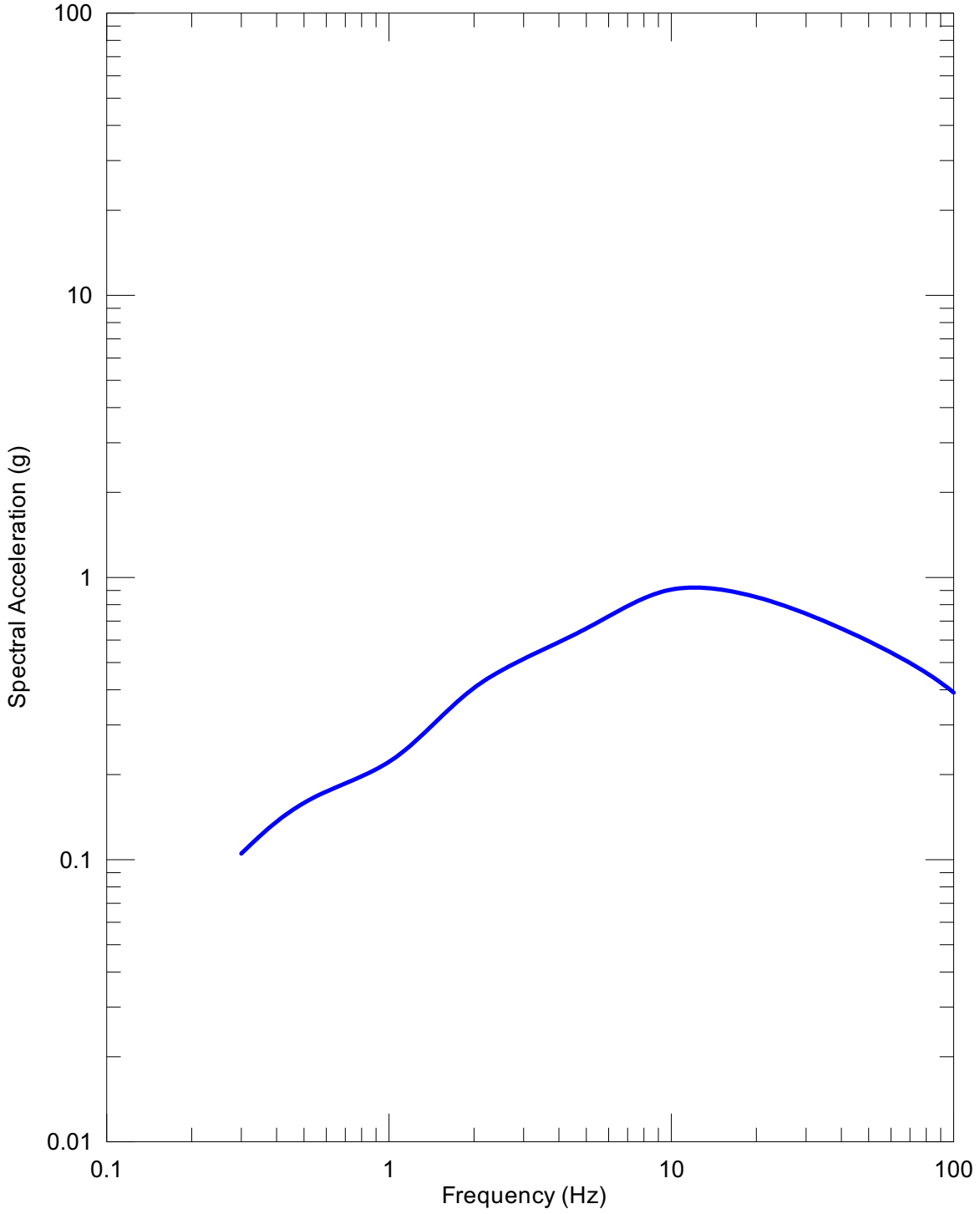

DTN: MO0401MWDRPSHA.000 [DIRS 166962]

Figure 6.2-13. Vertical UHS at Point A, 10^{-4} Annual Exceedance Frequency

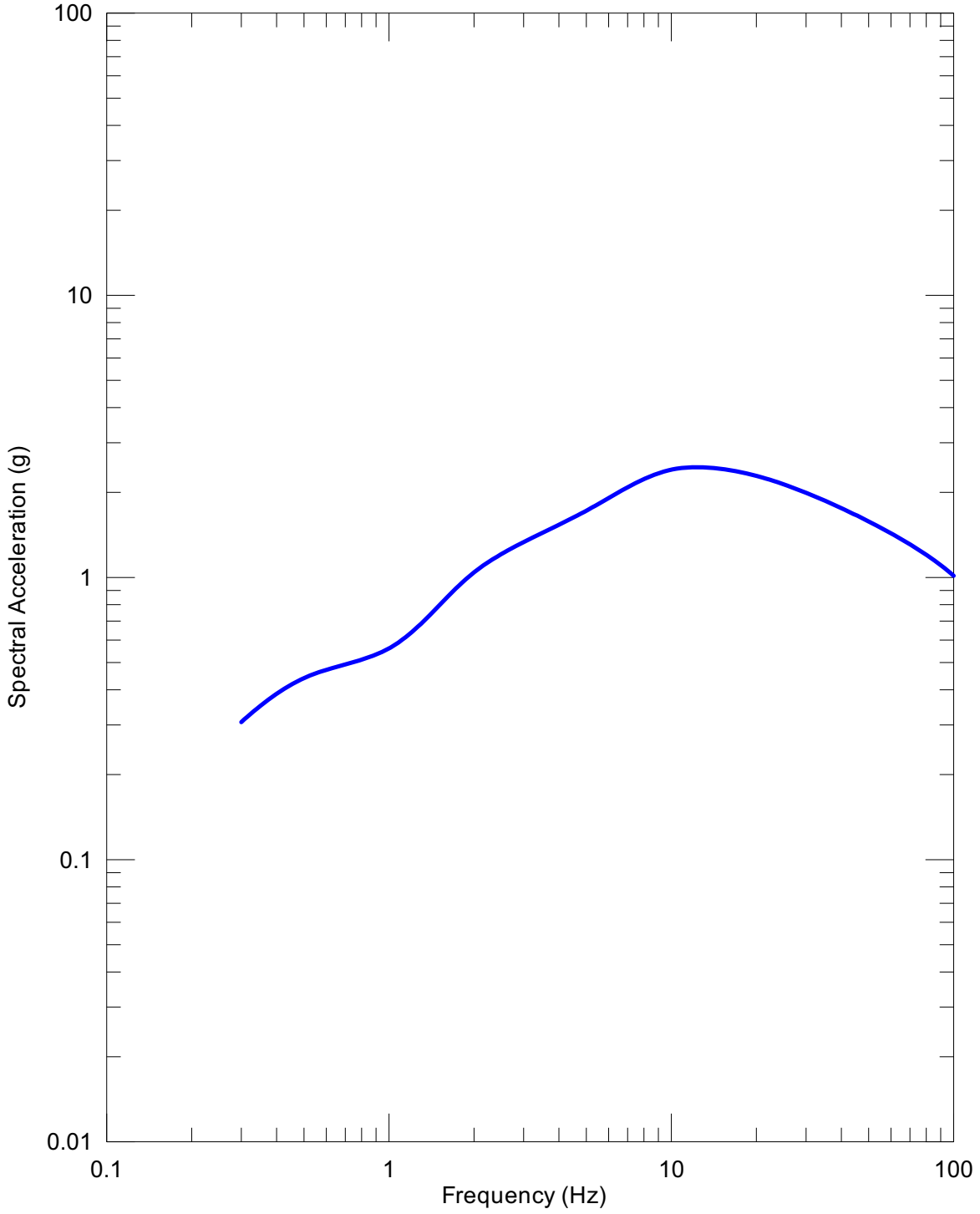

DTN: MO0308UNHAZ105.000 [DIRS 170425]

Figure 6.2-14. Vertical UHS at Point A, 10^{-5} Annual Exceedance Frequency

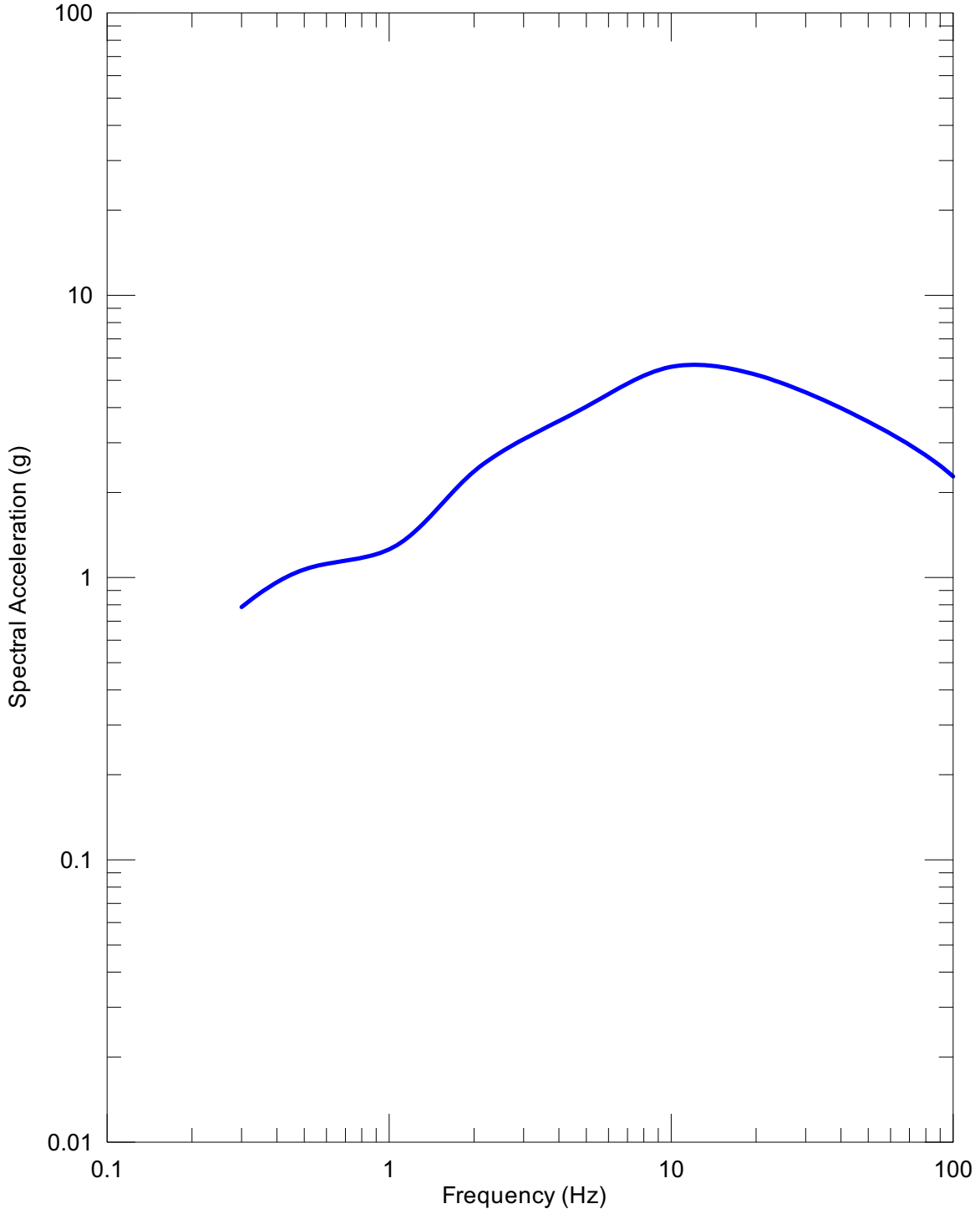

DTN: MO0206UNHAZ106.001 [DIRS 163723]

Figure 6.2-15. Vertical UHS at Point A, 10^{-6} Annual Exceedance Frequency

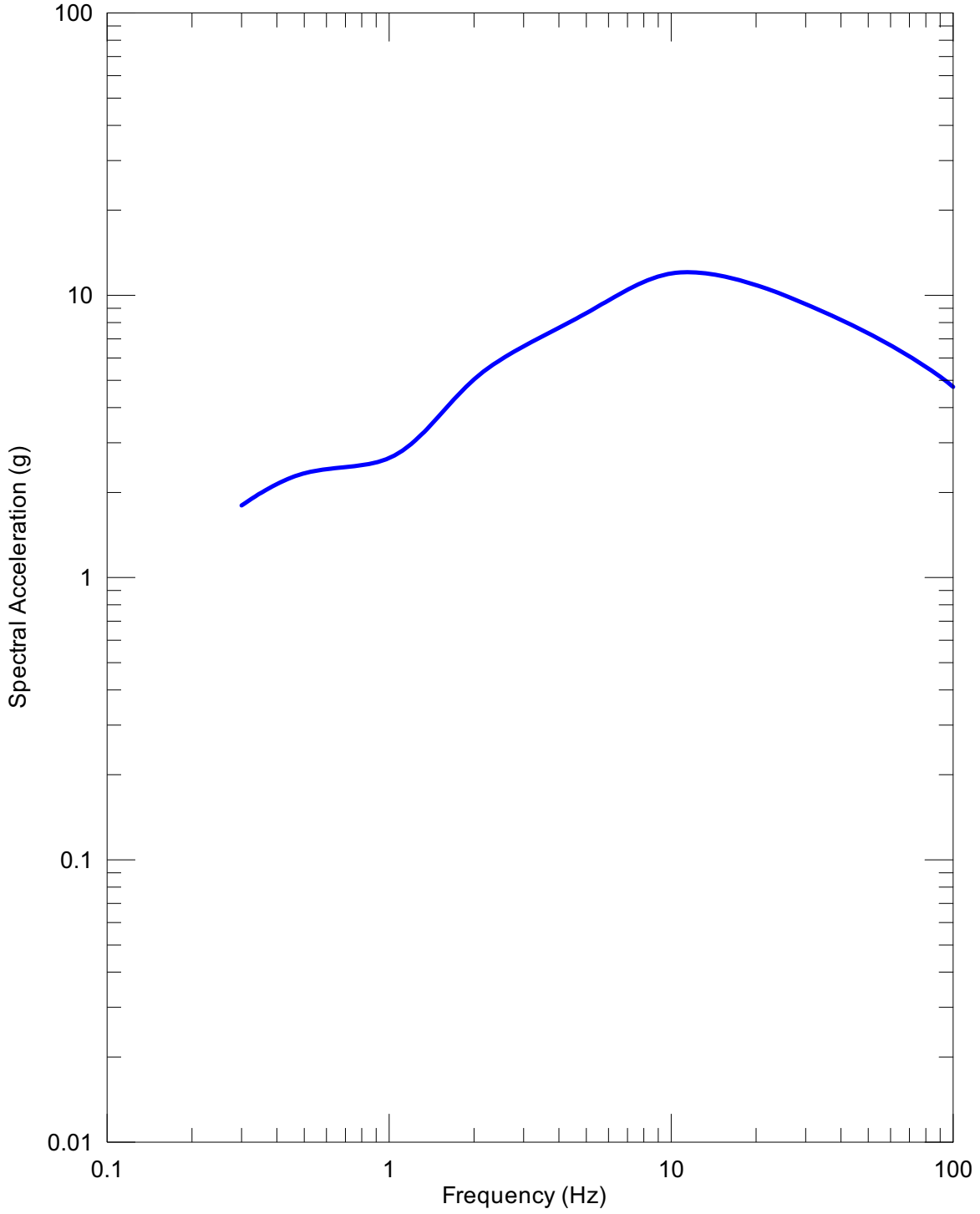

DTN: MO0209UNHAZ107.000 [DIRS 163724]

Figure 6.2-16. Vertical UHS at Point A, 10^{-7} Annual Exceedance Frequency

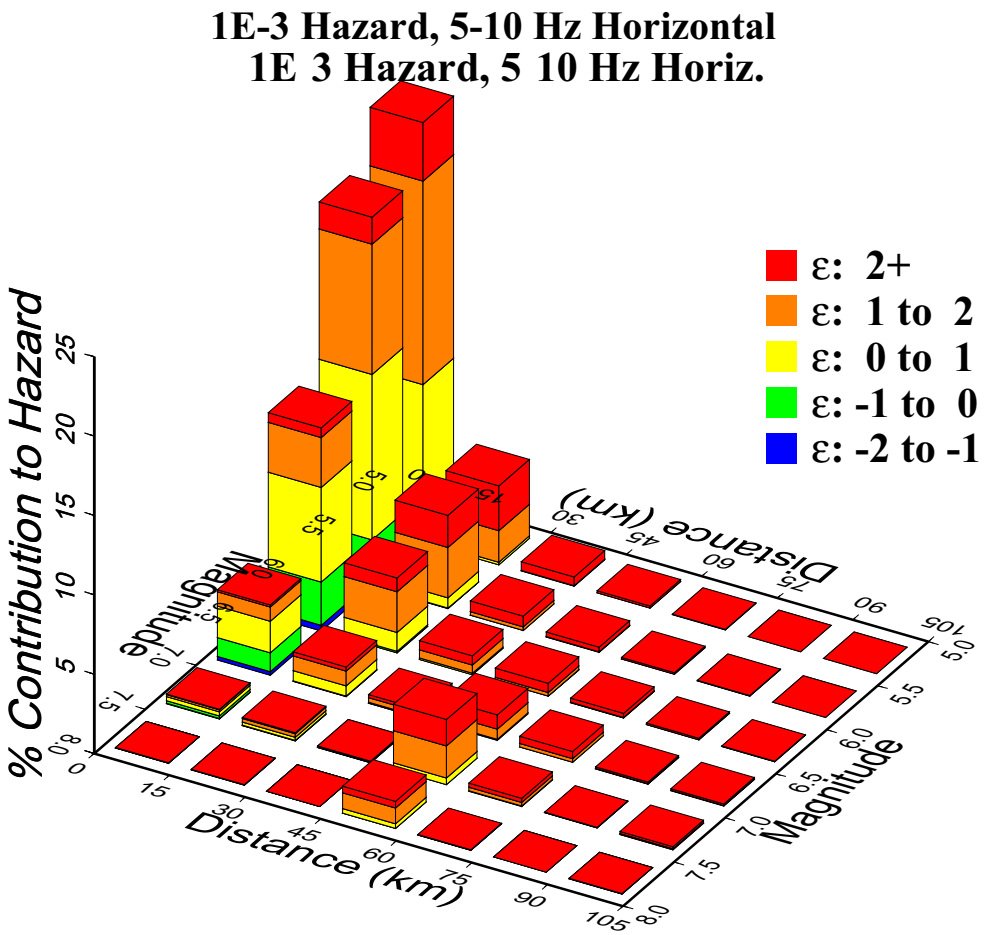

Source: Toro (2003 [DIRS 163720], SR-184, page 7)

Figure 6.2-17. Contribution to Mean Hazard by Magnitude, Distance, and Epsilon (ε) for the 5-10 Hz Horizontal Ground Motions, 10^{-3} Annual Exceedance Frequency

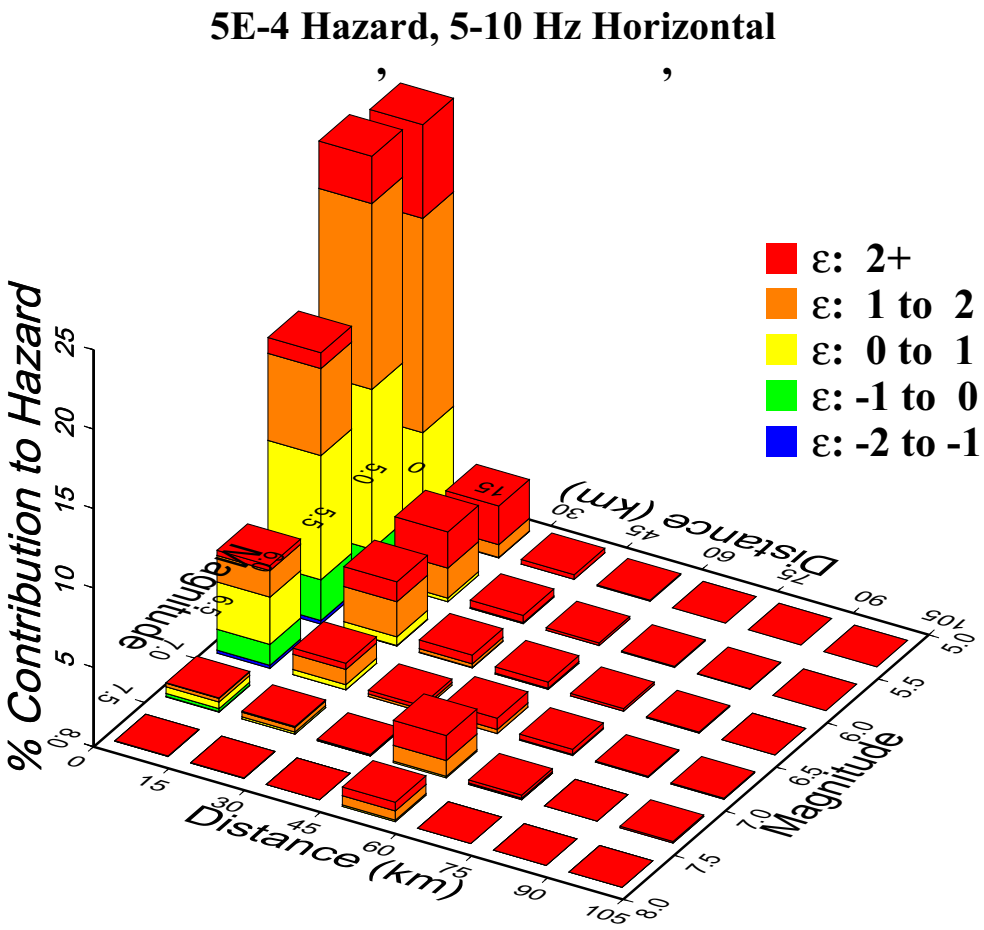

Source: Toro (2003 [DIRS 163720], SR-104, page 1)

Figure 6.2-18. Contribution to Mean Hazard by Magnitude, Distance, and Epsilon (ε) for the 5-10 Hz Horizontal Ground Motions, $5x10^{-4}$ Annual Exceedance Frequency

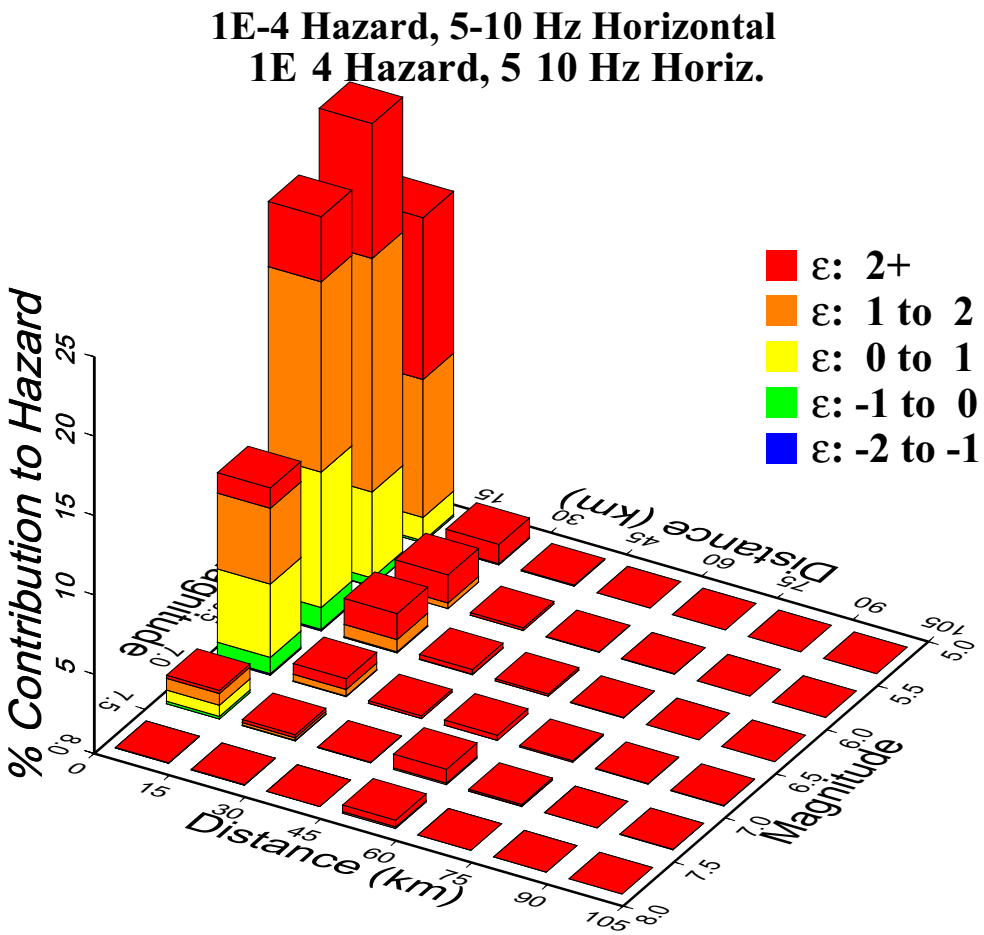

Source: Toro (2003 [DIRS 163720, SR-168, page 5)

Figure 6.2-19. Contribution to Mean Hazard by Magnitude, Distance, and Epsilon (ε) for the 5-10 Hz Horizontal Ground Motions, 10^{-4} Annual Exceedance Frequency

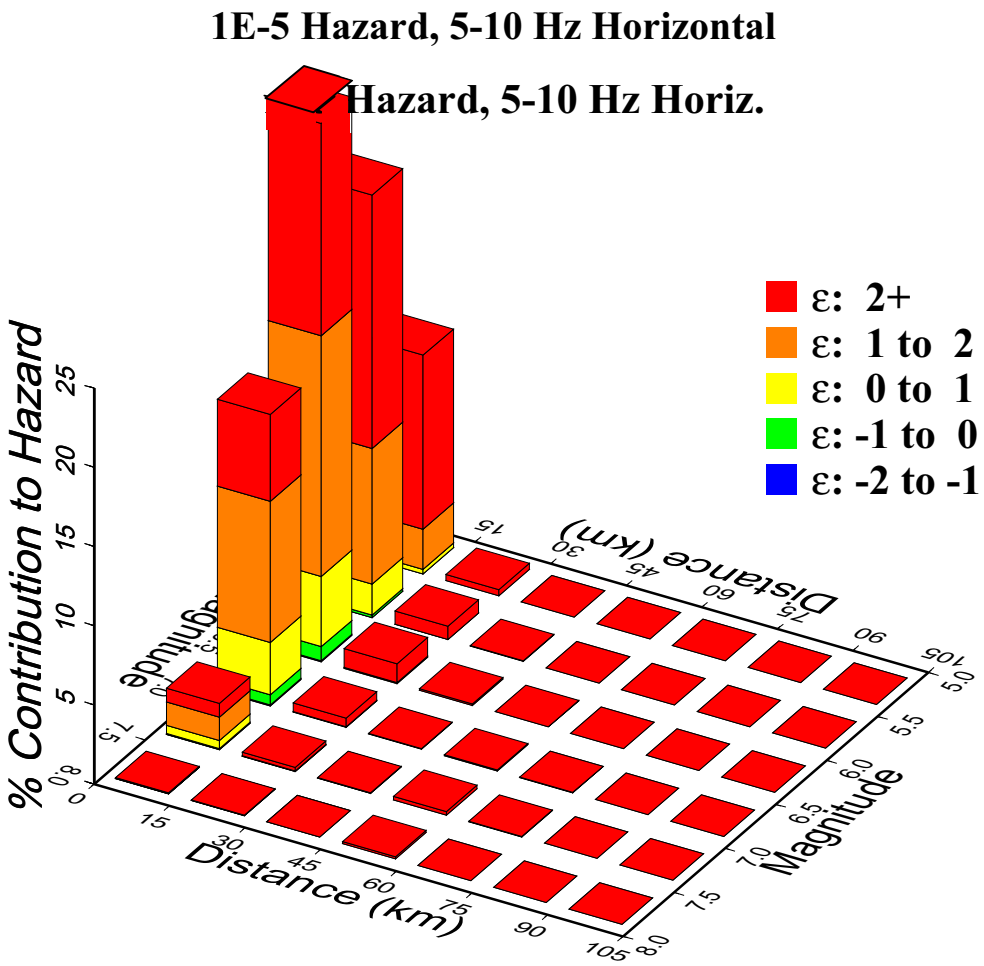

Source: Toro (2004 [DIRS 172034], SR-33, page 2)

Figure 6.2-20. Contribution to Mean Hazard by Magnitude, Distance, and Epsilon (ε) for the 5-10 Hz Horizontal Ground Motions, 10^{-5} Annual Exceedance Frequency

1E-6 Hazard, 5-10 Hz Horizontal

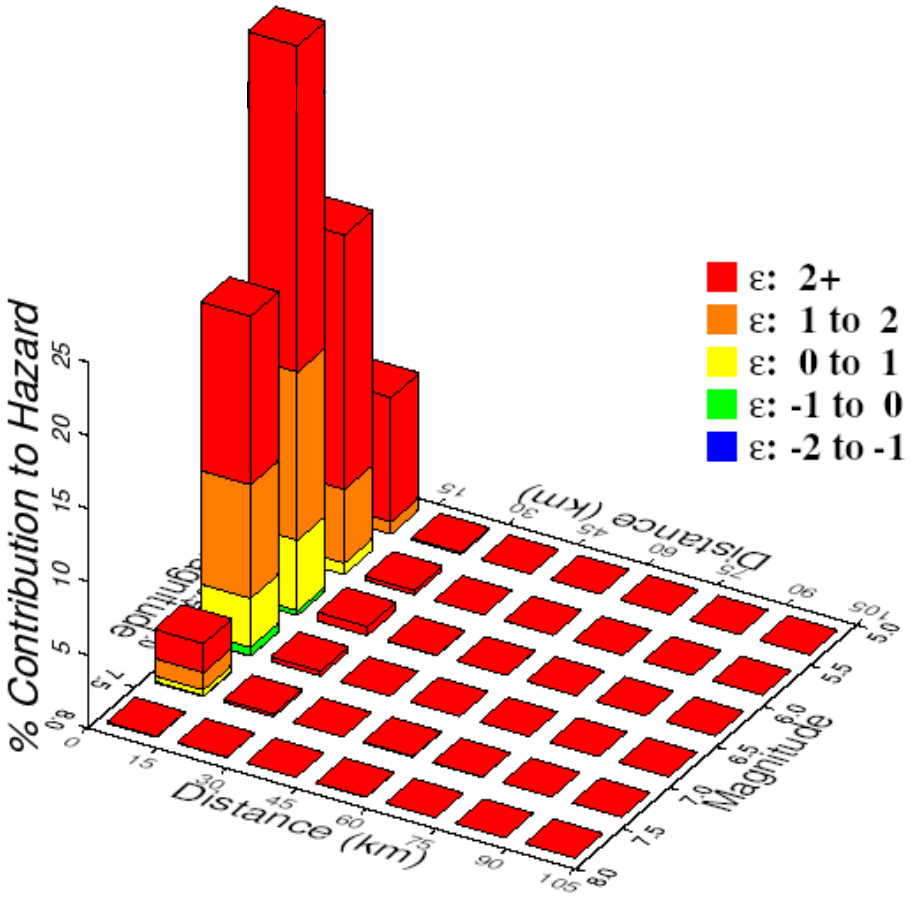

Source: Toro (2003 [DIRS 163720], SR-67, page 1)

Figure 6.2-21. Contribution to Mean Hazard by Magnitude, Distance, and Epsilon (ε) for the 5-10 Hz Horizontal Ground Motions, 10^{-6} Annual Exceedance Frequency

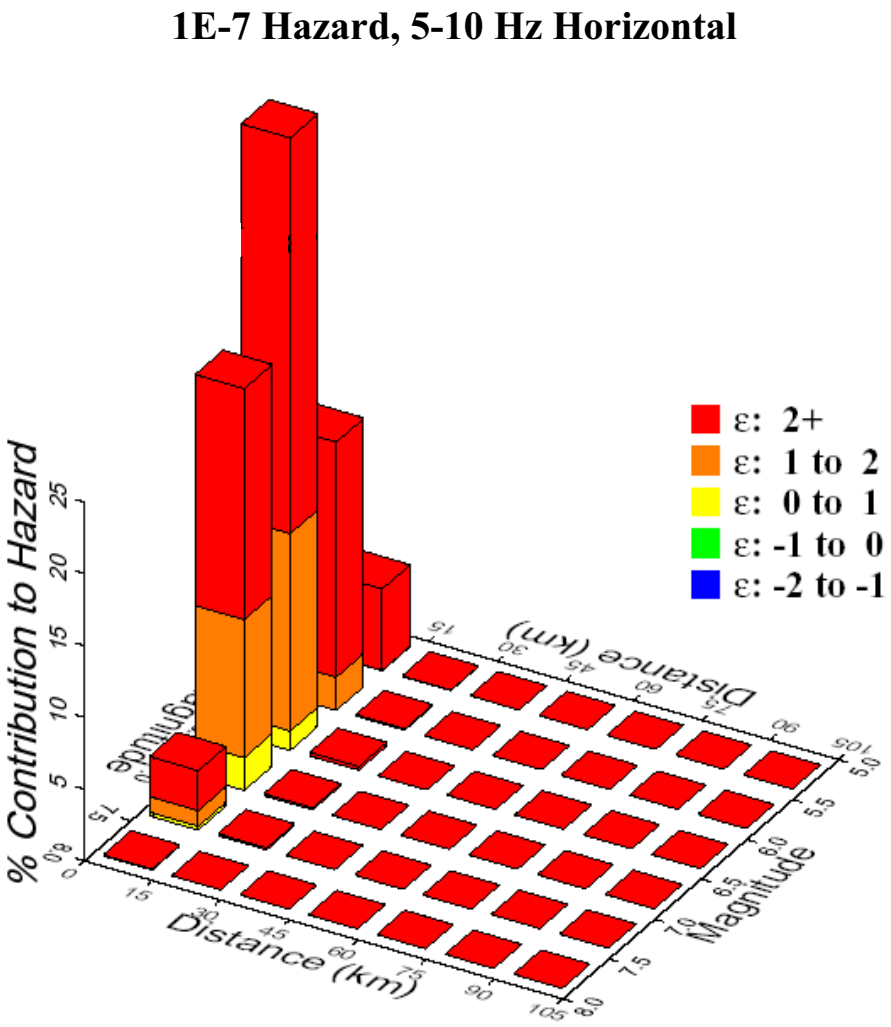

Source: Toro (2003 [DIRS 163720], SR-138, page 6)

Figure 6.2-22. Contribution to Mean Hazard by Magnitude, Distance, and Epsilon (ε) for the 5-10 Hz Horizontal Ground Motions, 10^{-7} Annual Exceedance Frequency

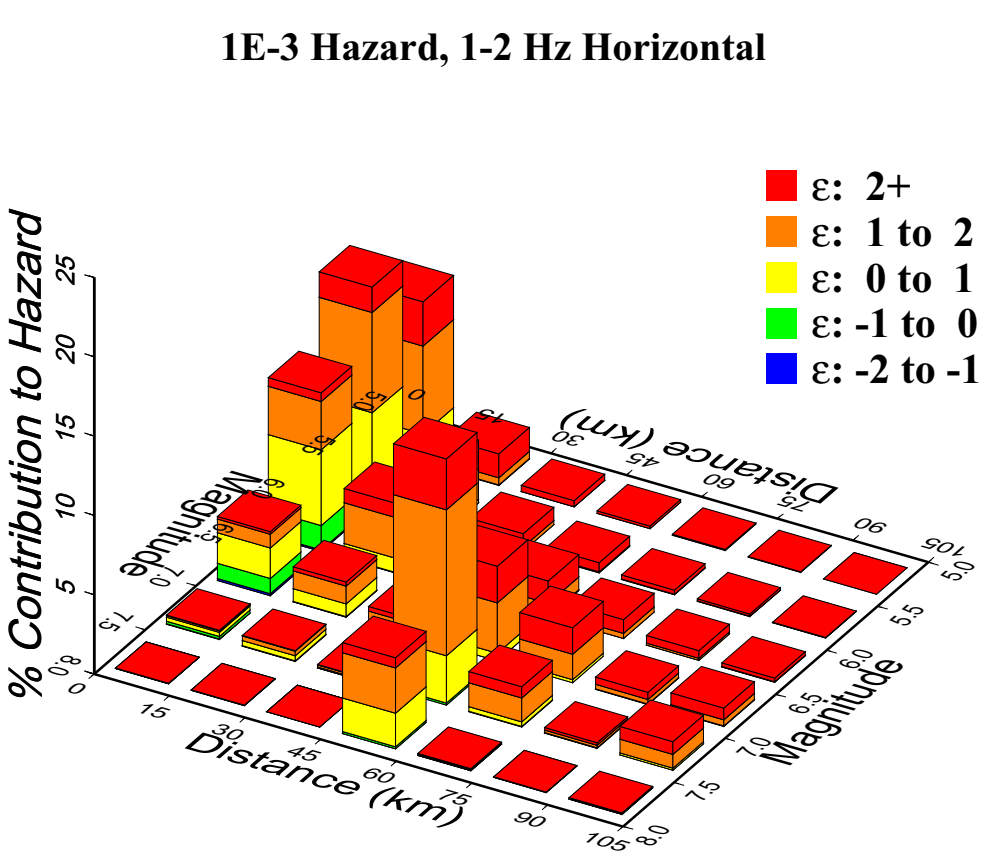

Source: Toro (2003 [DIRS 163720], SR-184, page 1)

Figure 6.2-23. Contribution to Mean Hazard by Magnitude, Distance, and Epsilon (ε) for the 1-2 Hz Horizontal Ground Motions, 10^{-3} Annual Exceedance Frequency

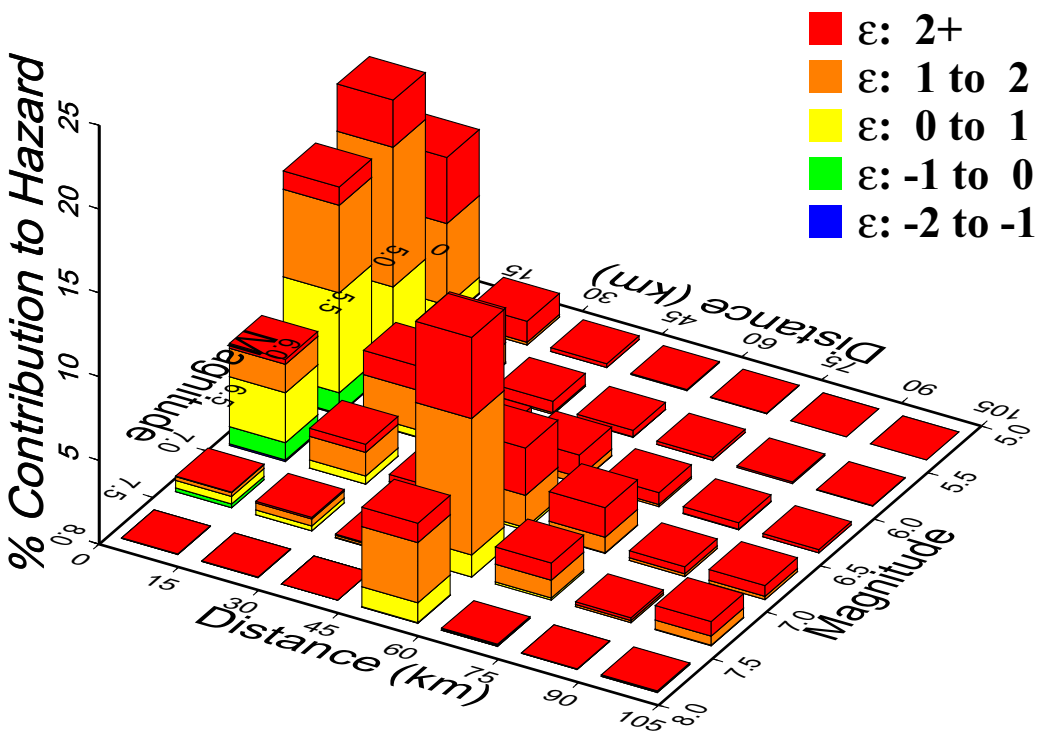

Source: Toro (2003 [DIRS 163720], SR-104, page 2)

Figure 6.2-24. Contribution to Mean Hazard by Magnitude, Distance, and Epsilon (ε) for the 1-2 Hz Horizontal Ground Motions, $5x10^{-4}$ Annual Exceedance Frequency

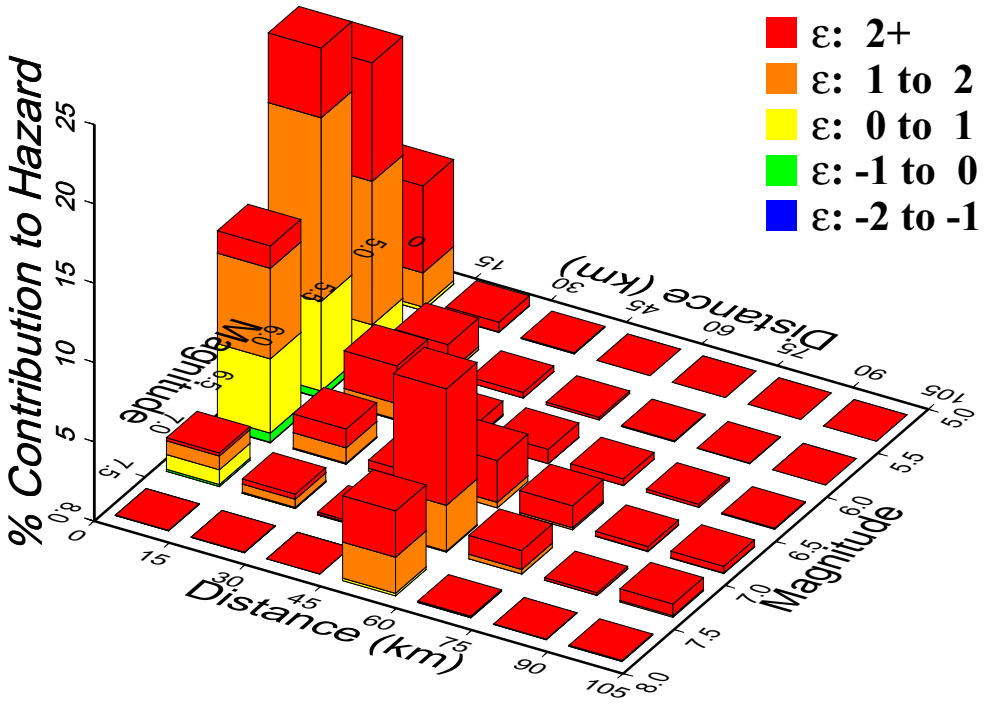

Source: Toro (2003 [DIRS 163720], SR-168, page 1)

Figure 6.2-25. Contribution to Mean Hazard by Magnitude, Distance, and Epsilon (ε) for the 1-2 Hz Horizontal Ground Motions, 10^{-4} Annual Exceedance Frequency

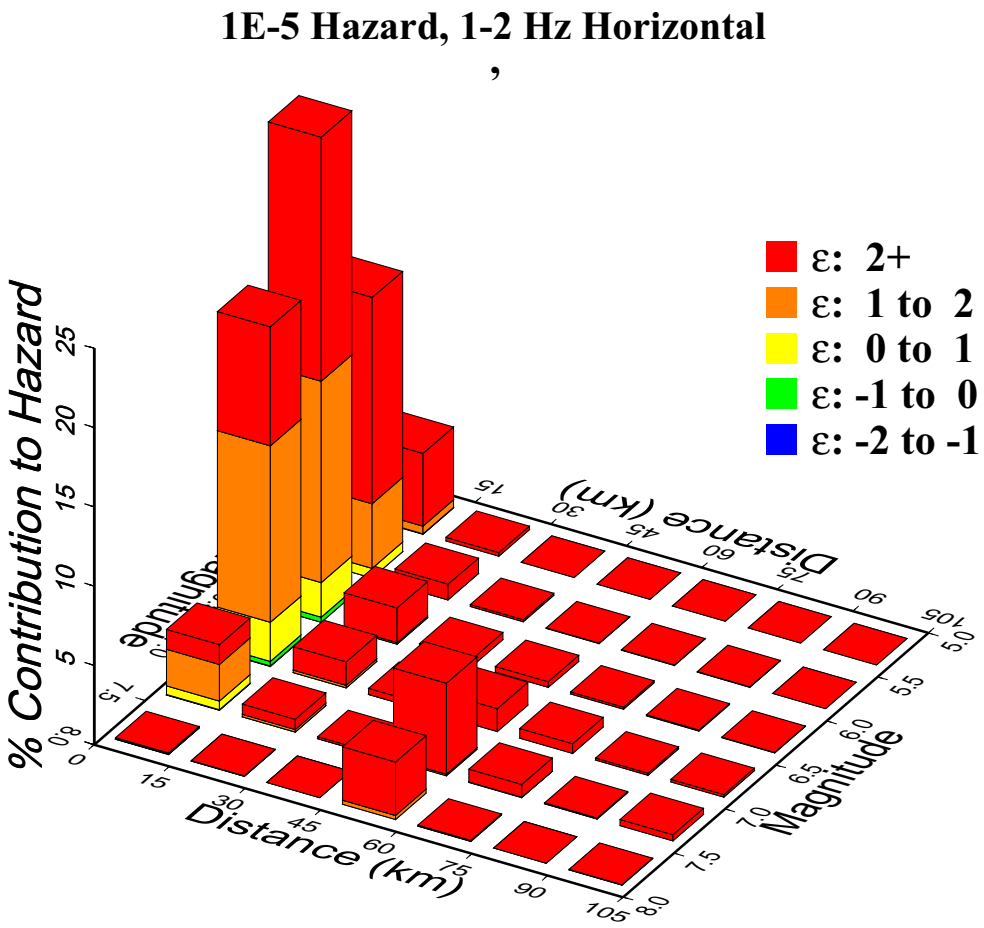

Source: Toro (2004 [DIRS 172034], SR-33, page 4)

Figure 6.2-26. Contribution to Mean Hazard by Magnitude, Distance, and Epsilon (ε) for the 1-2 Hz Horizontal Ground Motions, 10^{-5} Annual Exceedance Frequency

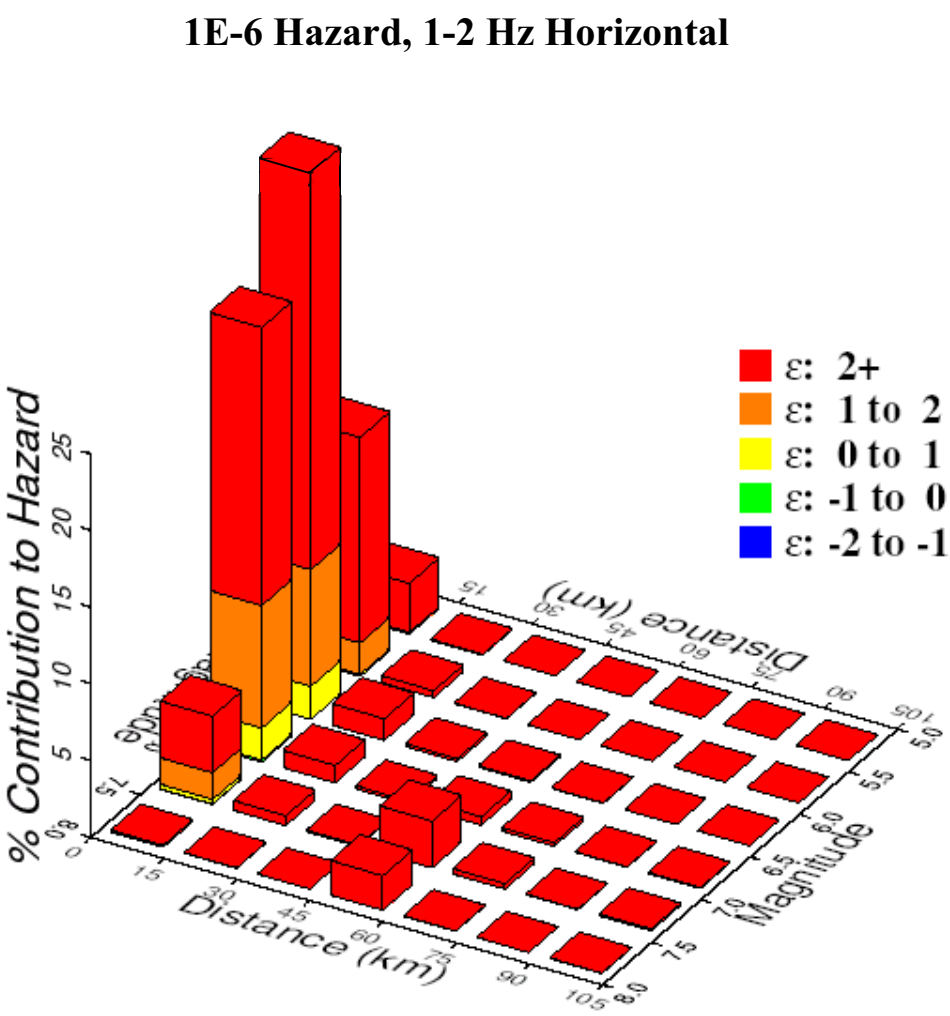

Source: Toro (2003 [DIRS 163720], SR-65, page 1)

Figure 6.2-27. Contribution to Mean Hazard by Magnitude, Distance, and Epsilon (ε) for the 1-2 Hz Horizontal Ground Motions, 10^{-6} Annual Exceedance Frequency

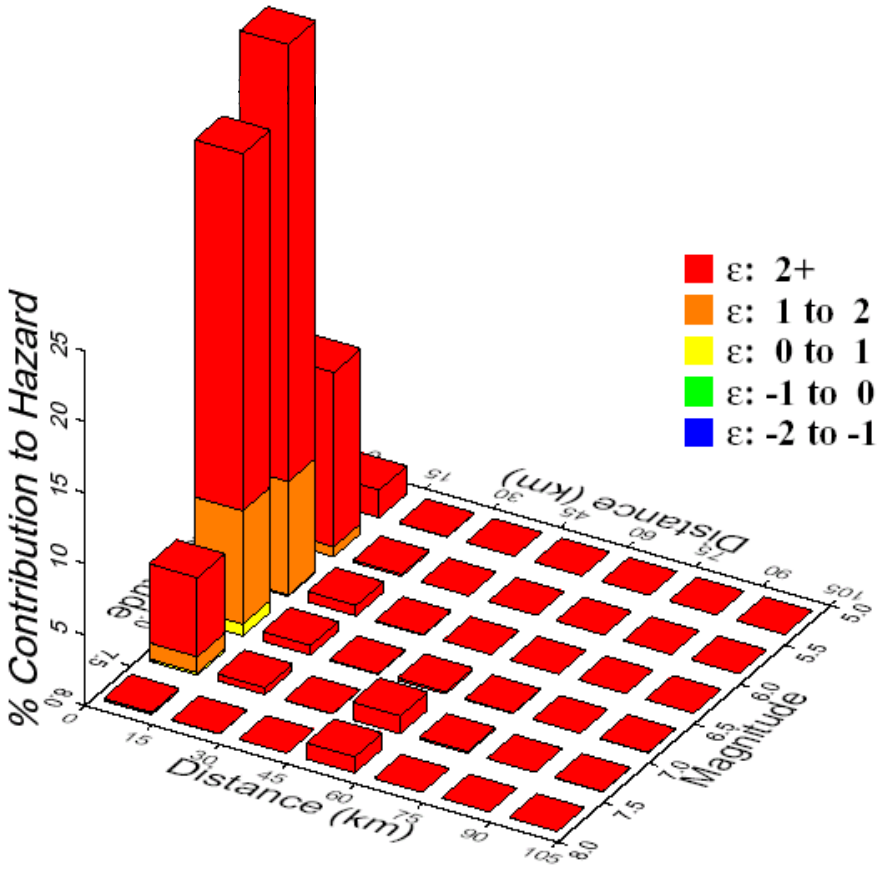

Source: Toro (2003 [DIRS 163720], SR-138 page 4)

Figure 6.2-28. Contribution to Mean Hazard by Magnitude, Distance, and Epsilon (ε) for the 1-2 Hz Horizontal Ground Motions, 10^{-7} Annual Exceedance Frequency

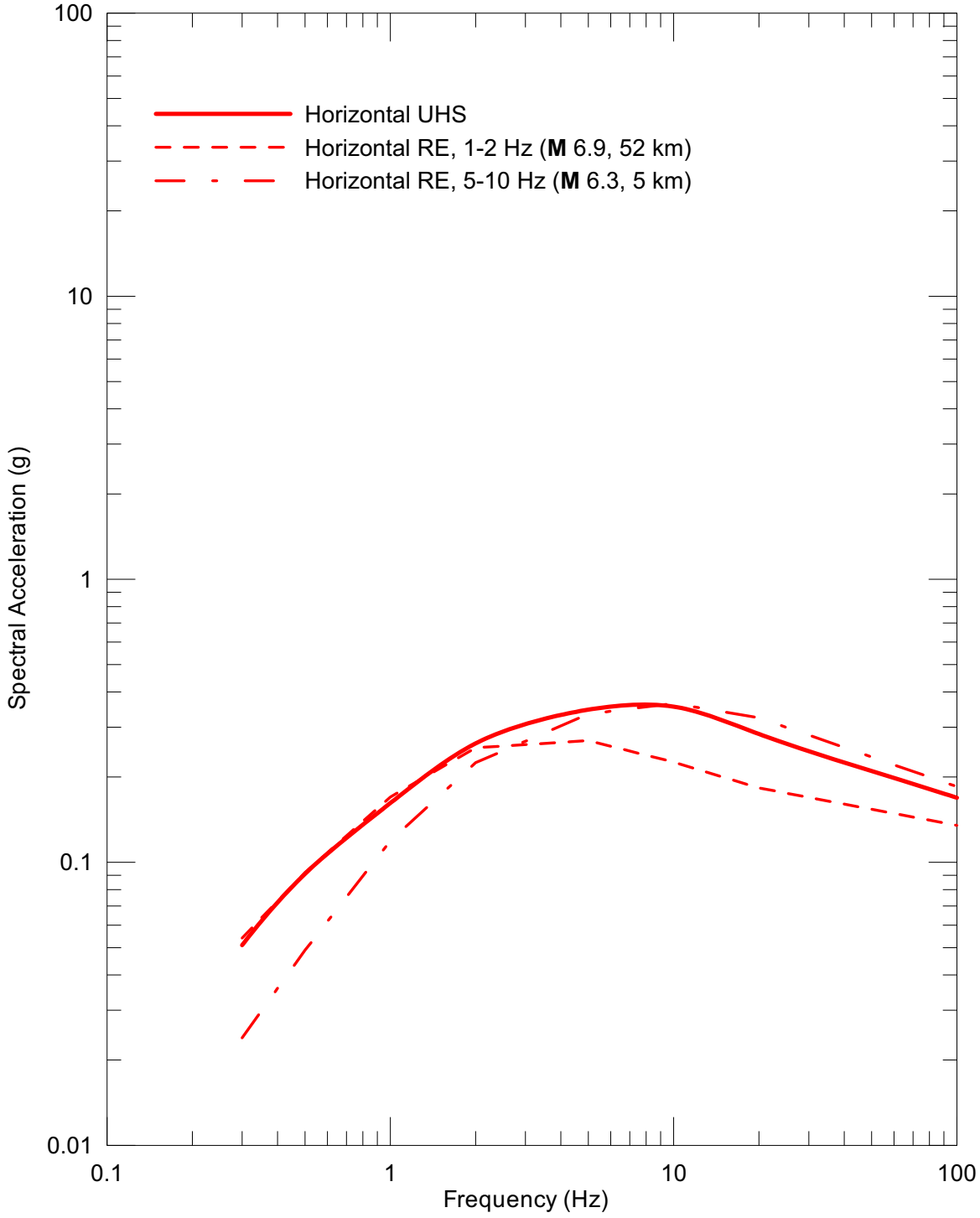

DTNs: MO0211REDES103.000 [DIRS 170424] (REs),
MO0401MWDRPSHA.000 [DIRS 166962] (UHS)

Figure 6.2-29. Point A UHS and RE Spectra at an Annual Exceedance Frequency of 10^{-3}, Horizontal Component

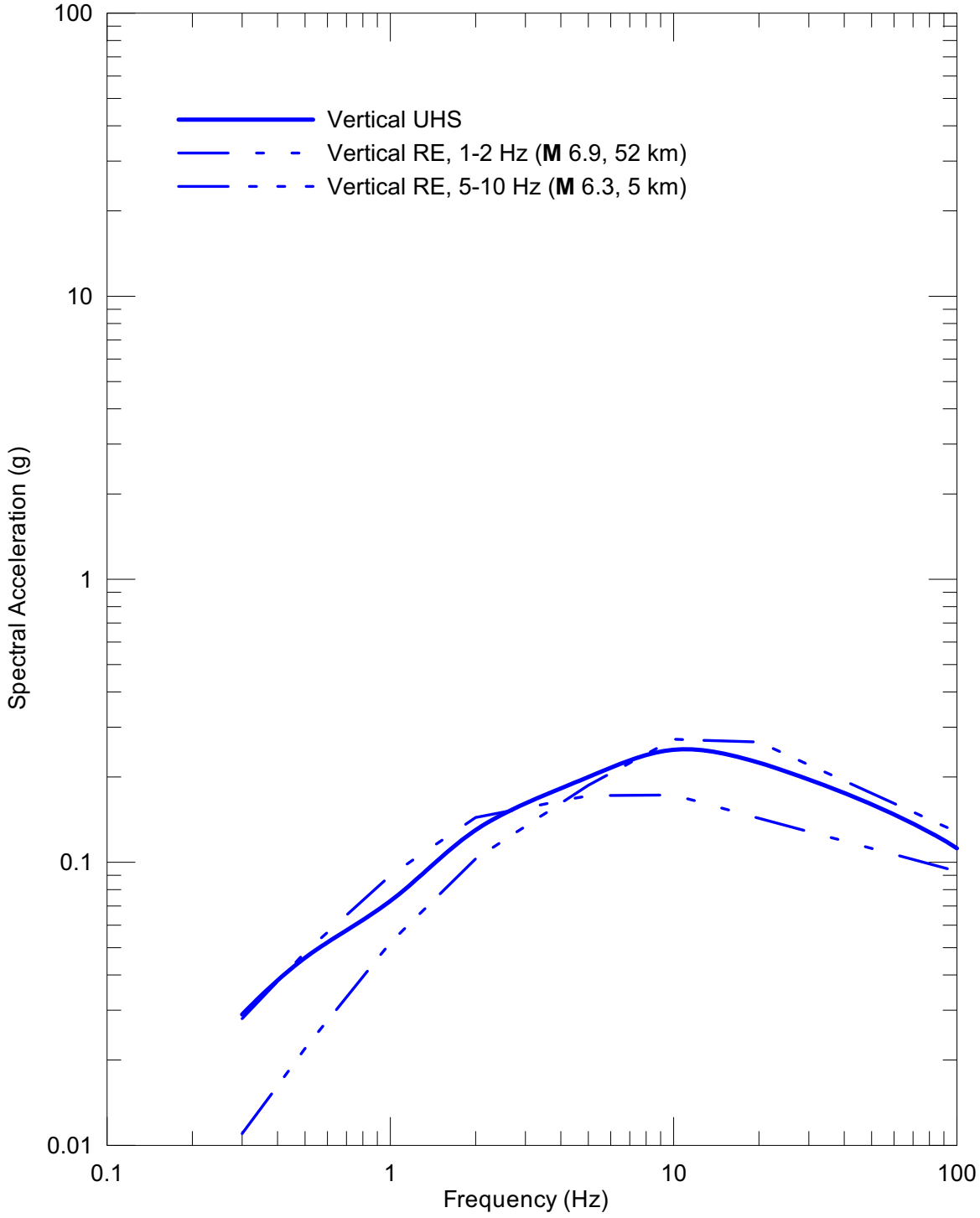

DTNs: MO0211REDES103.000 [DIRS 170424] (REs),
MO0401MWDRPSHA.000 [DIRS 166962] (UHS)

Figure 6.2-30. Point A UHS and RE Spectra at an Annual Exceedance Frequency of 10^{-3}, Vertical Component

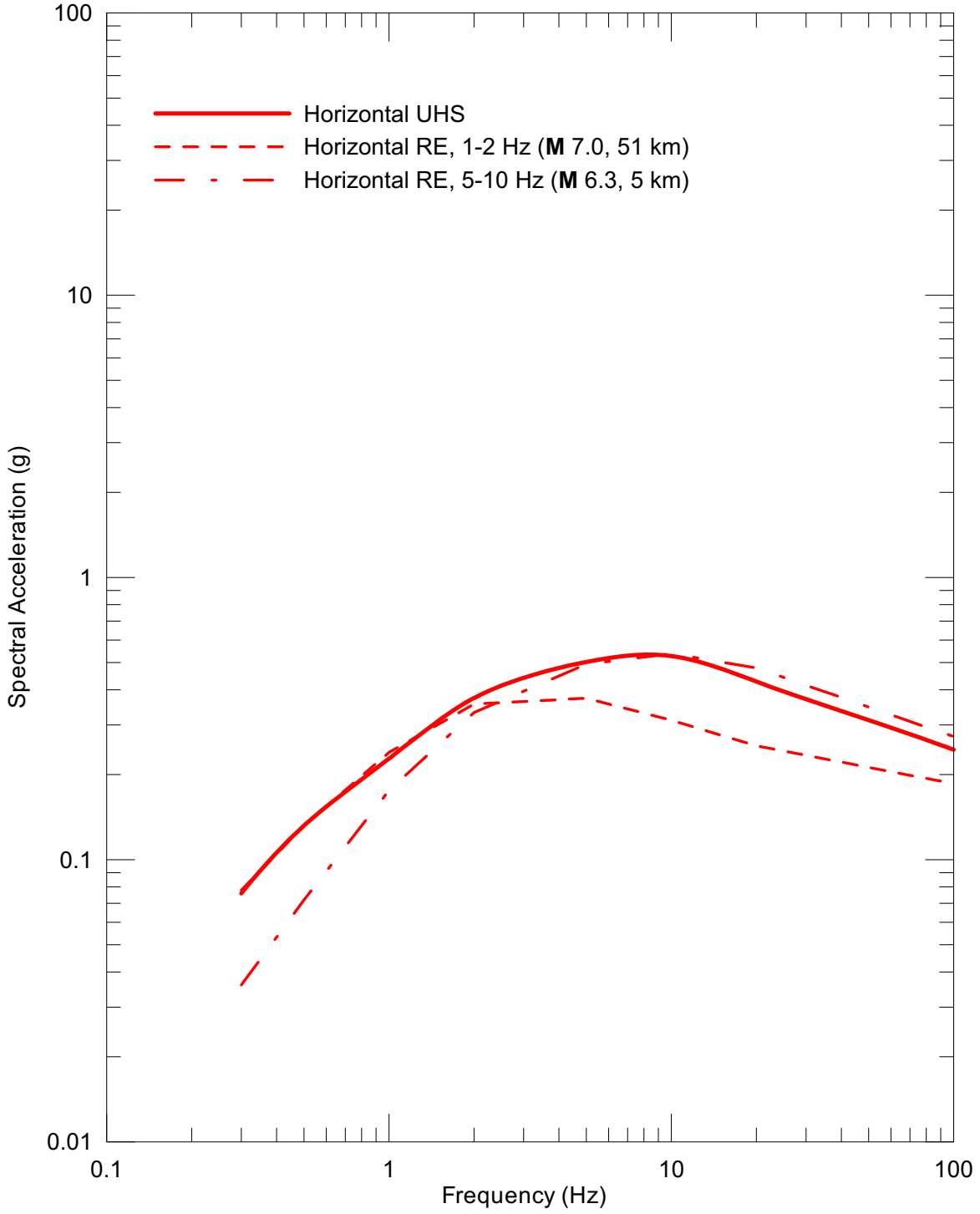

DTN: MO0208UNHZ5X10.000 [DIRS 163722]

Figure 6.2-31. Point A UHS and RE Spectra at an Annual Exceedance Frequency of 5×10^{-4}, Horizontal Component

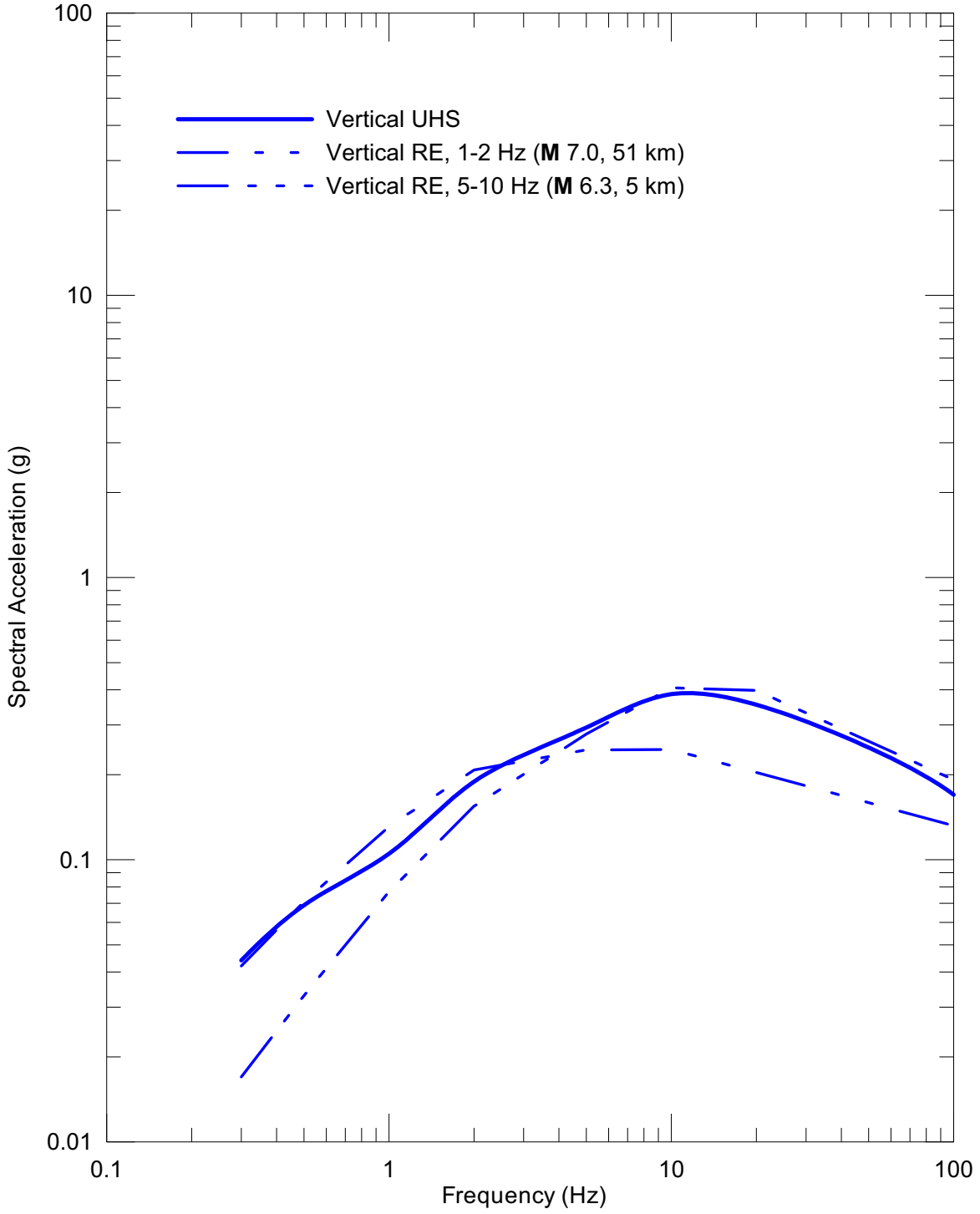

DTN: MO0208UNHZ5X10.000 [DIRS 163722]

Figure 6.2-32. Point A UHS and RE Spectra at an Annual Exceedance Frequency of 5×10^{-4}, Vertical Component

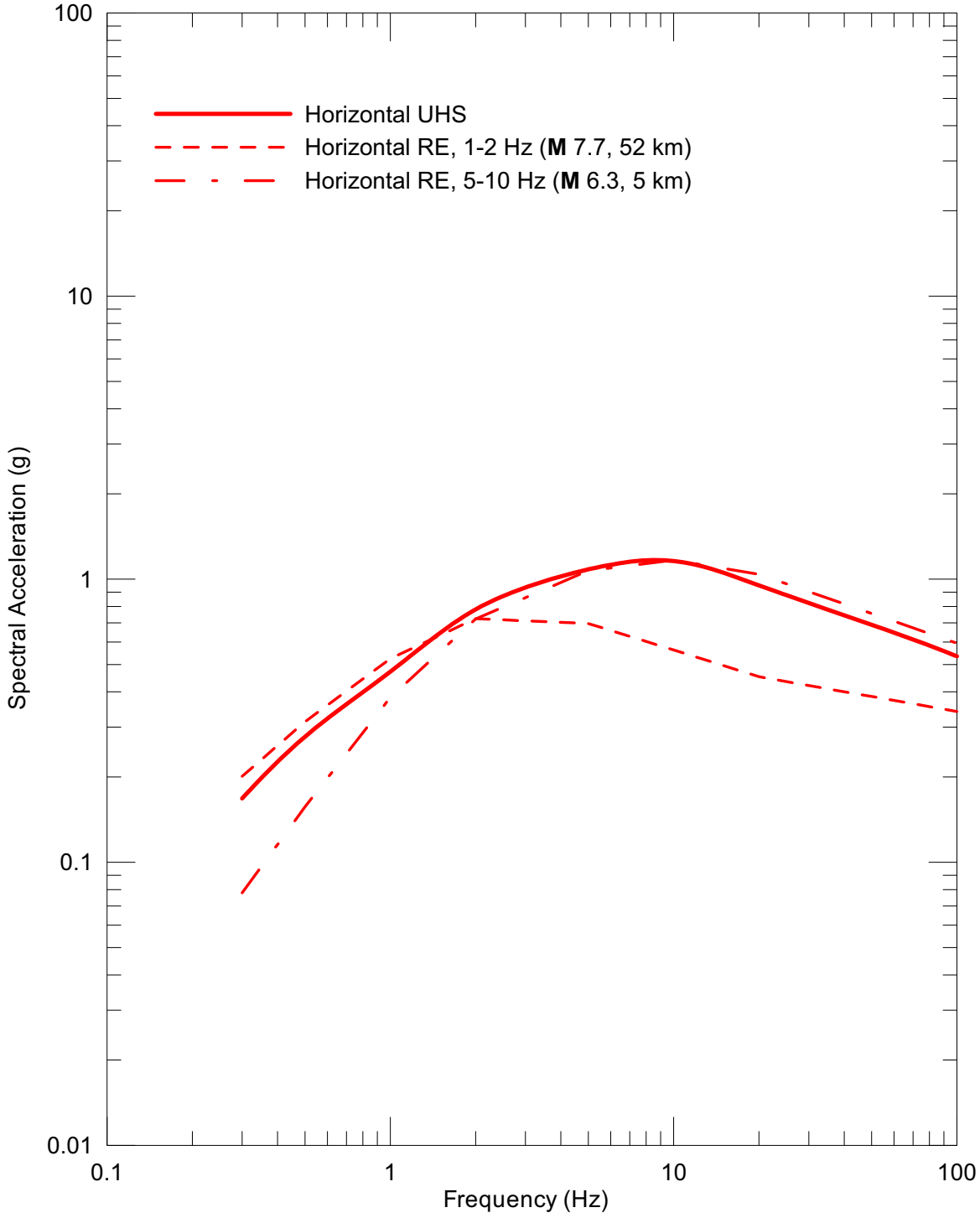

DTNs: MO0211DERES104.000 [DIRS 170423] (REs), MO0401MWDRPSHA.000 [DIRS 166962] (UHS)

Figure 6.2-33. Point A UHS and RE Spectra at an Annual Exceedance Frequency of 10^{-4}, Horizontal Component

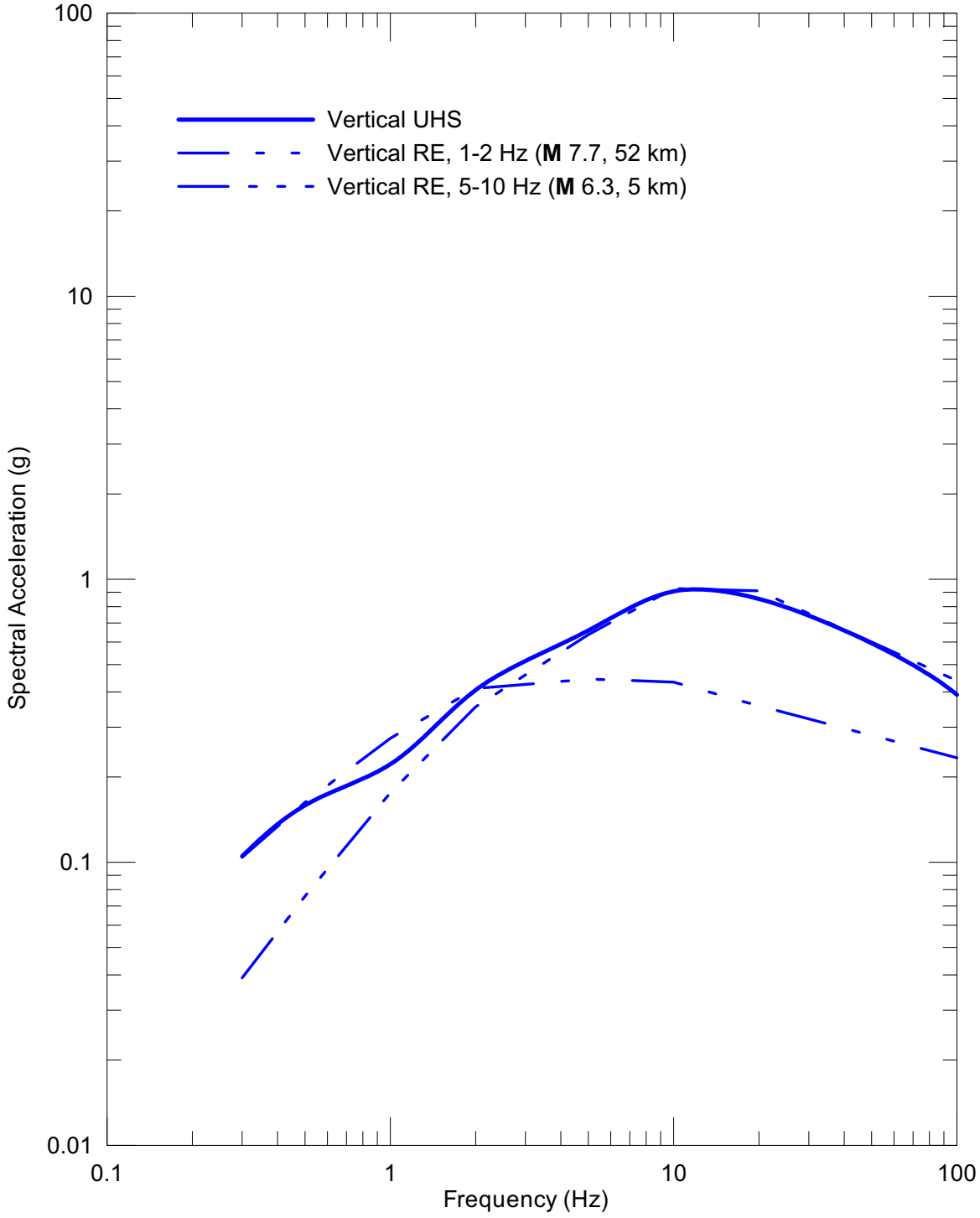

DTNs: MO0211DERES104.000 [DIRS 170423] (REs), MO0401MWDRPSHA.000 [DIRS 166962] (UHS)

Figure 6.2-34. Point A UHS and RE Spectra at an Annual Exceedance Frequency of 10^{-4}, Vertical Component

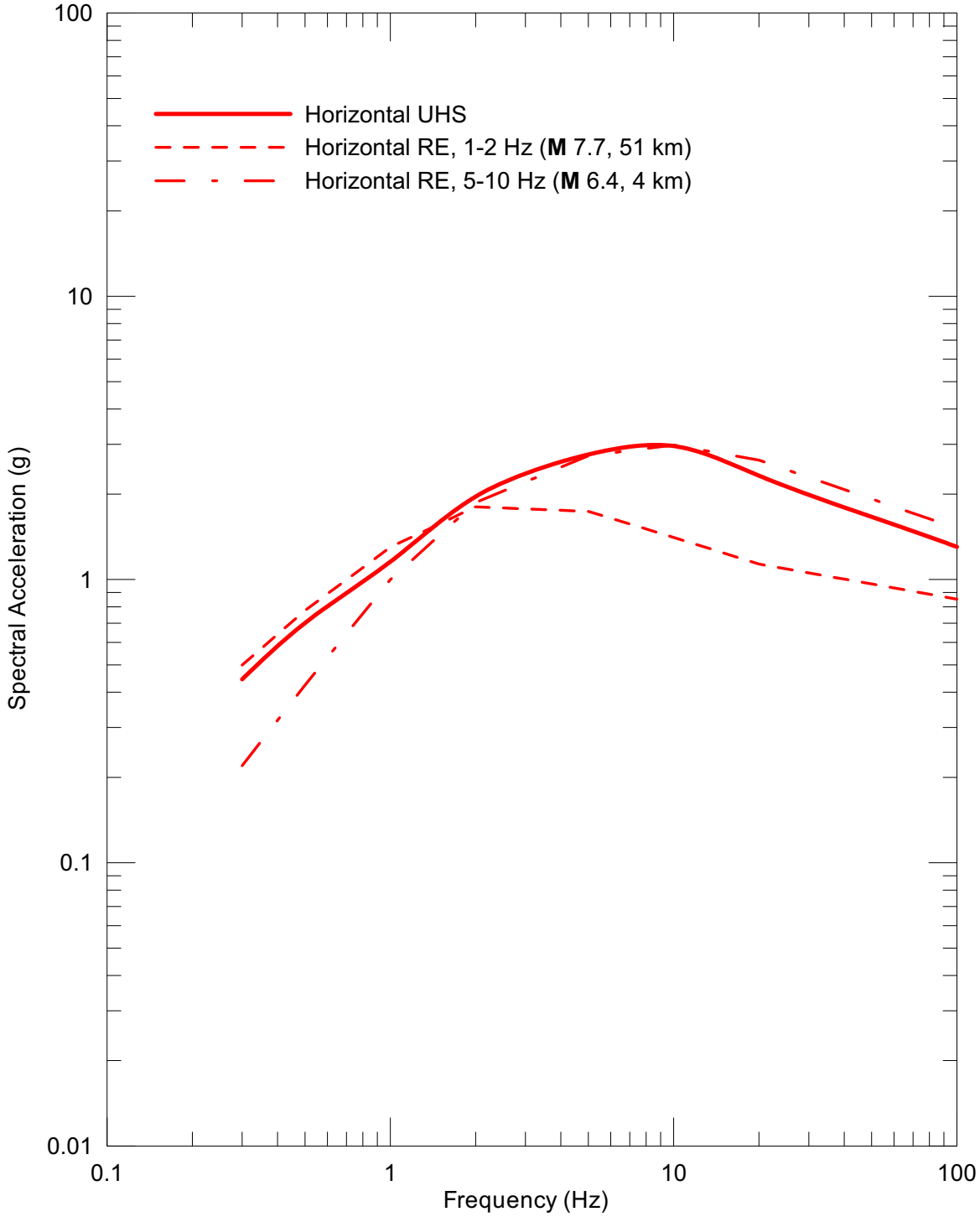

DTN: MO0308UNHAZ105.000 [DIRS 170425]

Figure 6.2-35. Point A UHS and RE Spectra at an Annual Exceedance Frequency of 10^{-5}, Horizontal Component

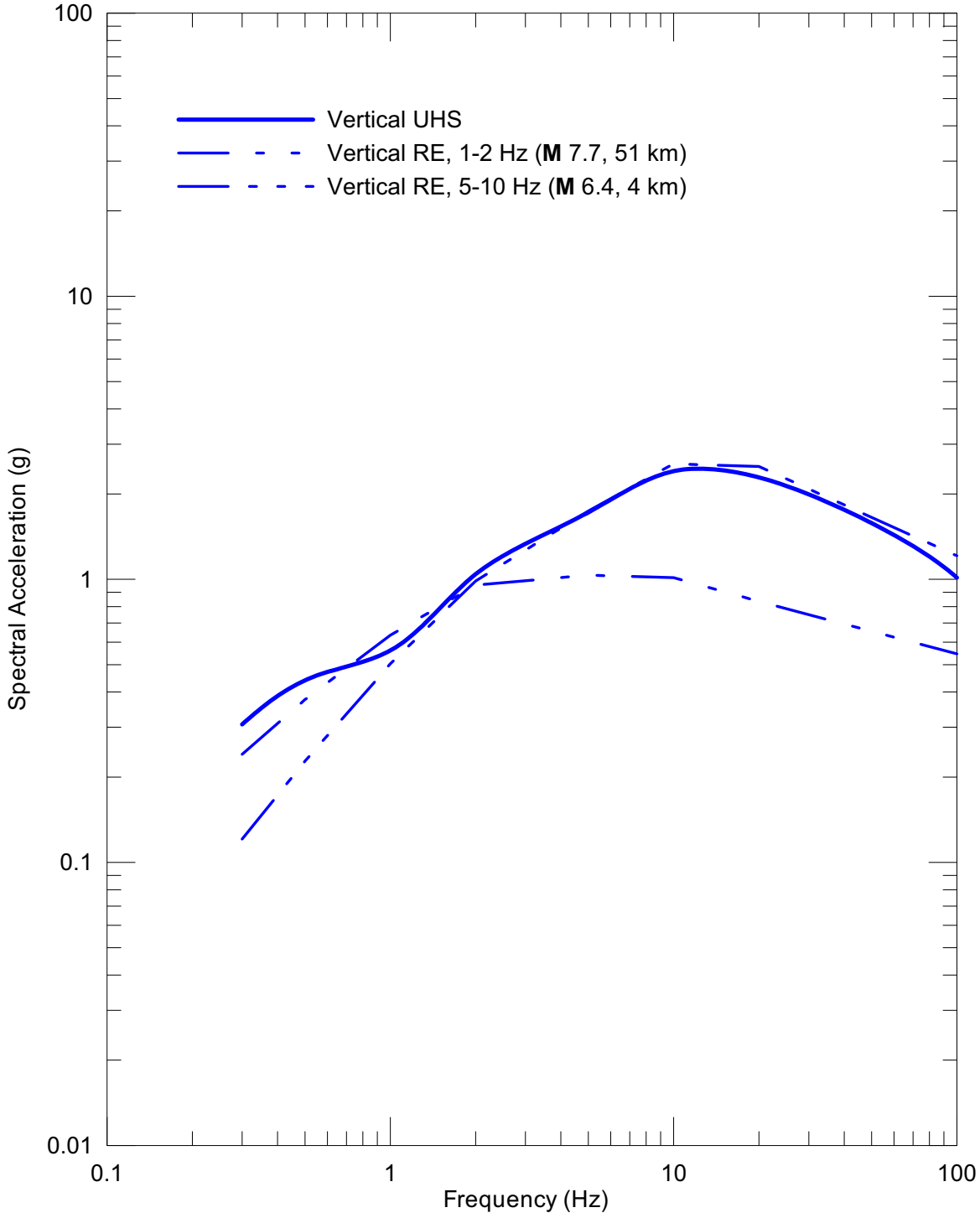

DTN: MO0308UNHAZ105.000 [DIRS 170425]

Figure 6.2-36. Point A UHS and RE Spectra at an Annual Exceedance Frequency of 10^{-5}, Vertical Component

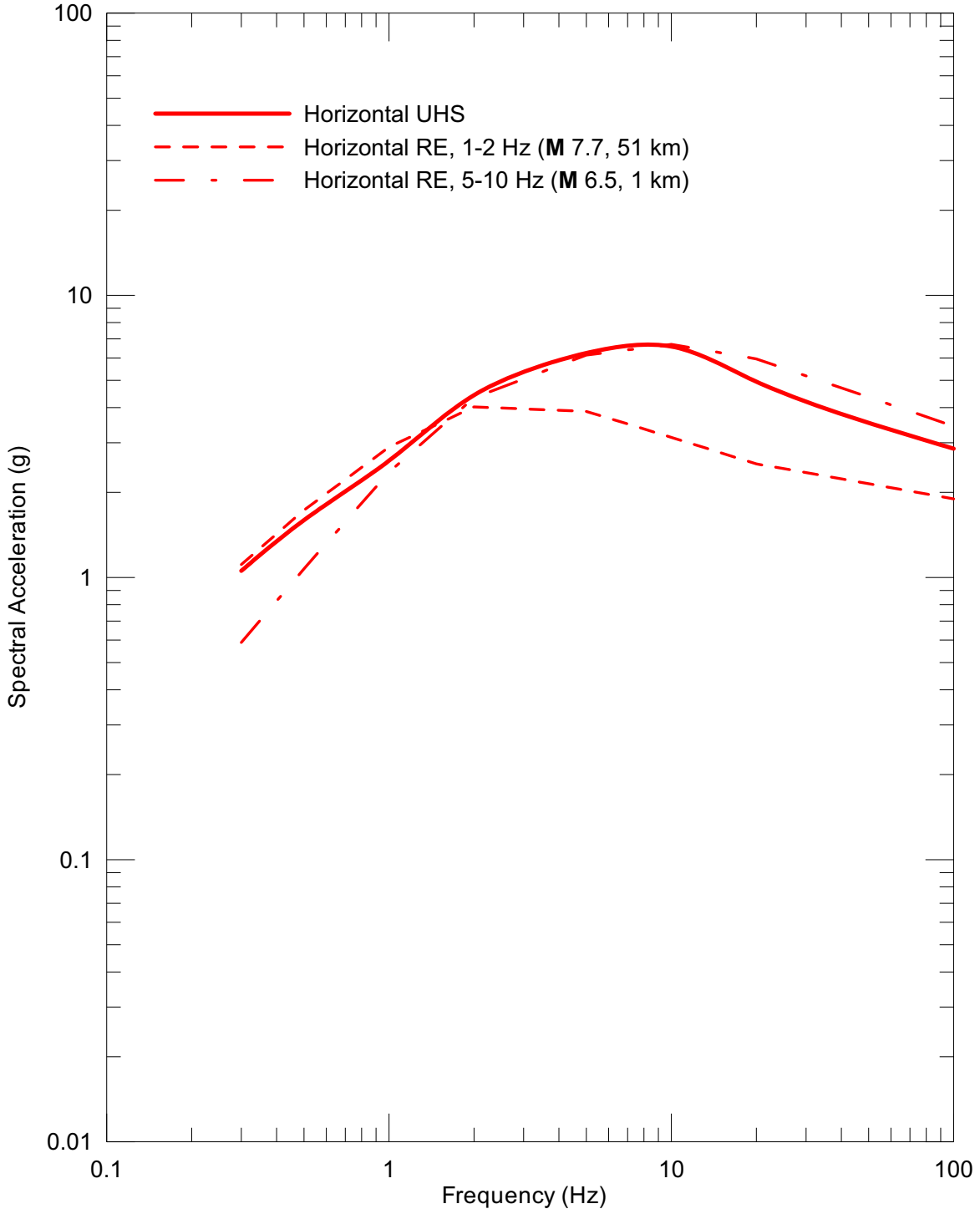

DTN: MO0206UNHAZ106.001 [DIRS 163723]

Figure 6.2-37. Point A UHS and RE Spectra at an Annual Exceedance Frequency of 10^{-6}, Horizontal Component

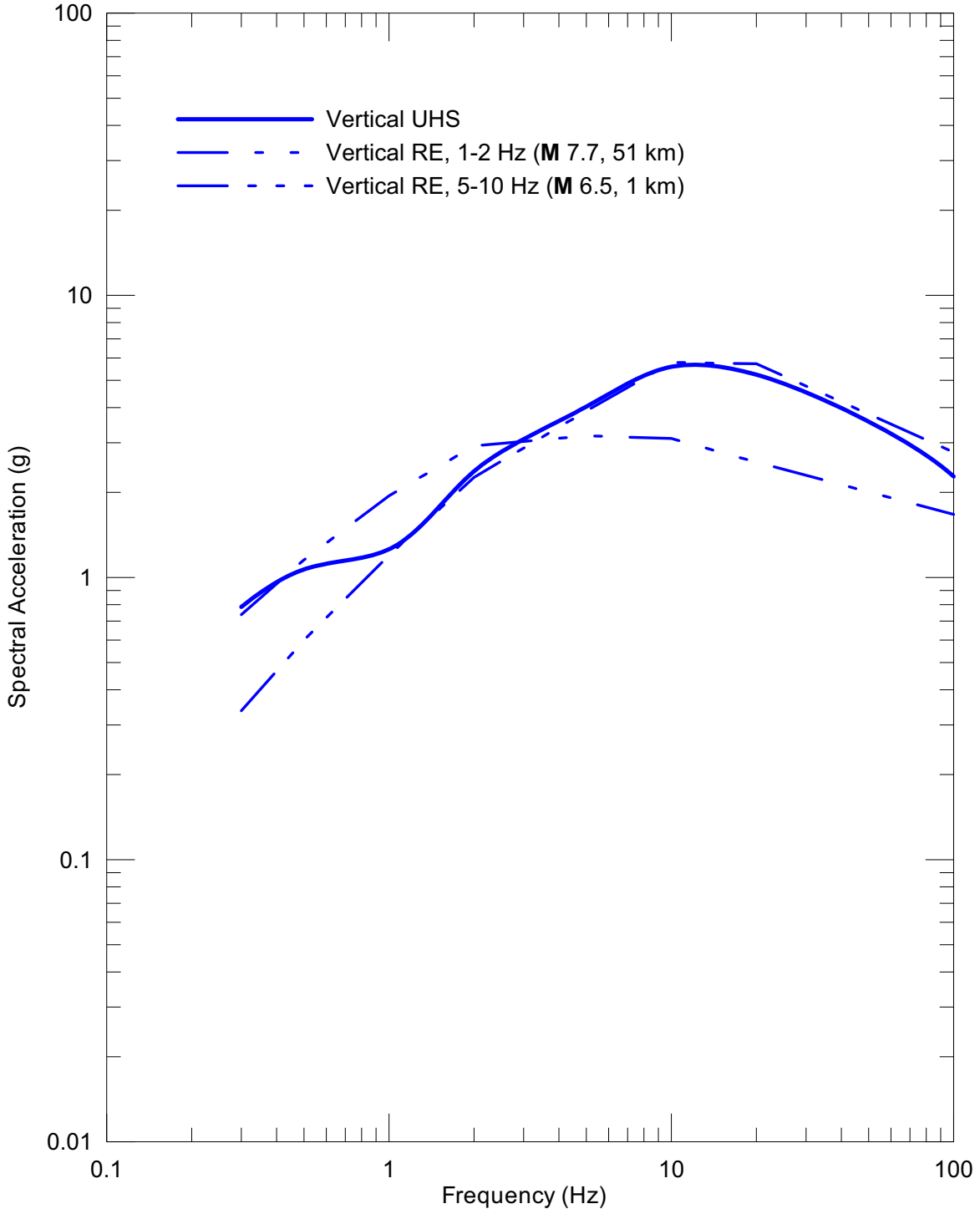

DTN: MO0206UNHAZ106.001 [DIRS 163723]

Figure 6.2-38. Point A UHS and RE Spectra at an Annual Exceedance Frequency of 10^{-6}, Vertical Component

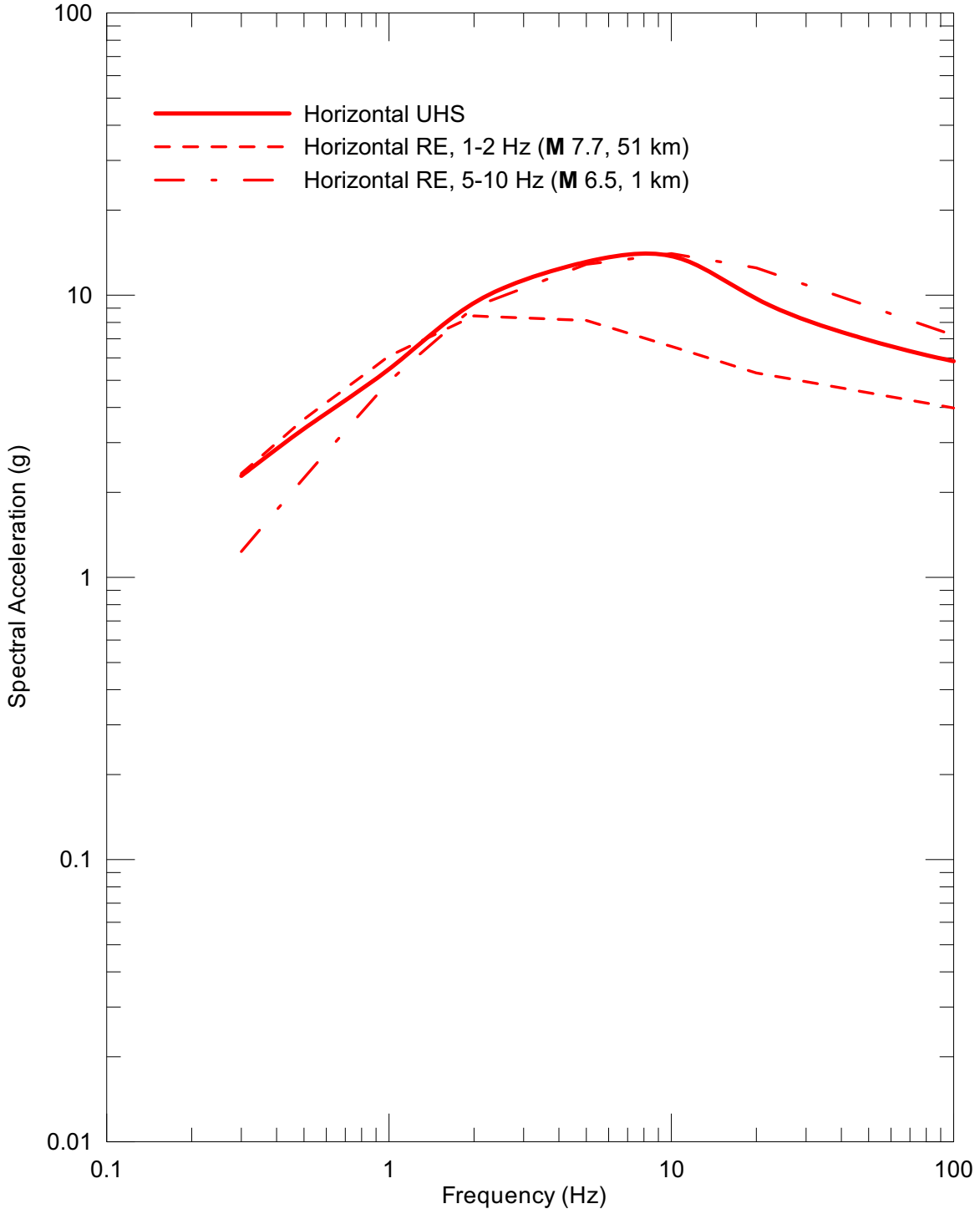

DTN: MO0209UNHAZ107.000 [DIRS 163724]

Figure 6.2-39. Point A UHS and RE Spectra at an Annual Exceedance Frequency of 10^{-7}, Horizontal Component

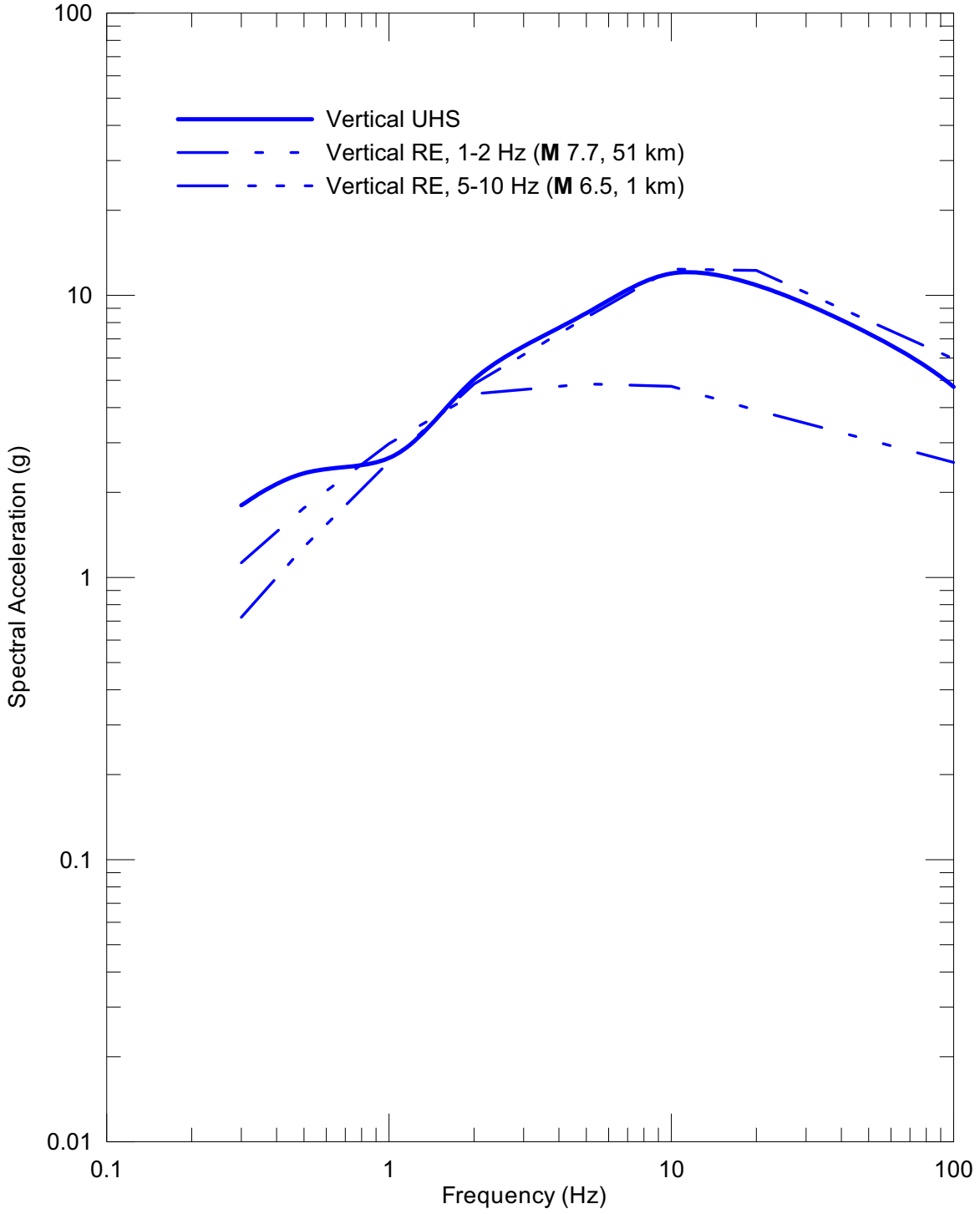

DTN: MO0209UNHAZ107.000 [DIRS 163724]

Figure 6.2-40. Point A UHS and RE Spectra at an Annual Exceedance Frequency of 10^{-7}, Vertical Component

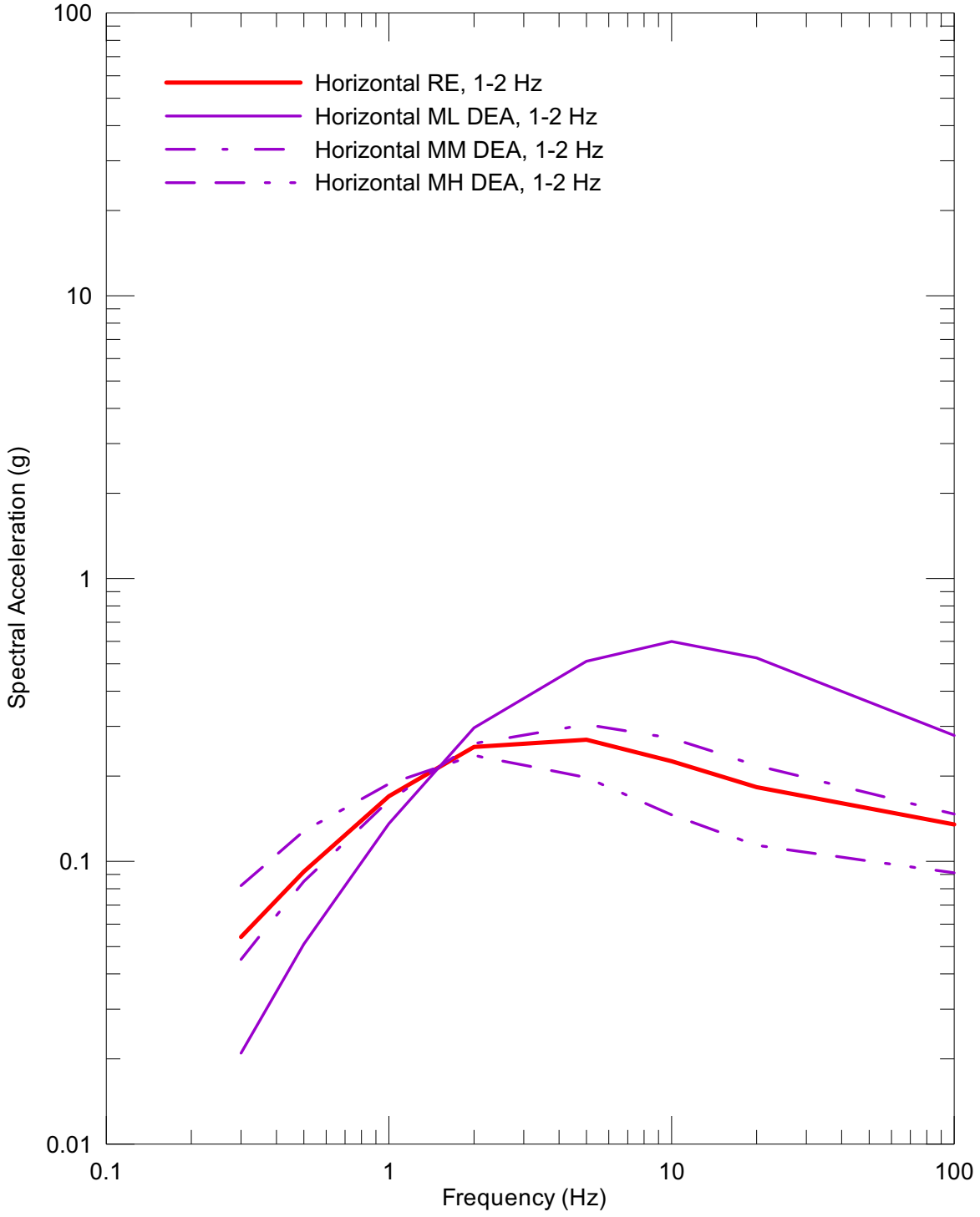

DTN: MO0211REDES103.000 [DIRS 170424]

Figure 6.2-41. Point A RE and DEA Spectra at an Annual Exceedance Frequency of 10^{-3} and 1-2 Hz, Horizontal Component

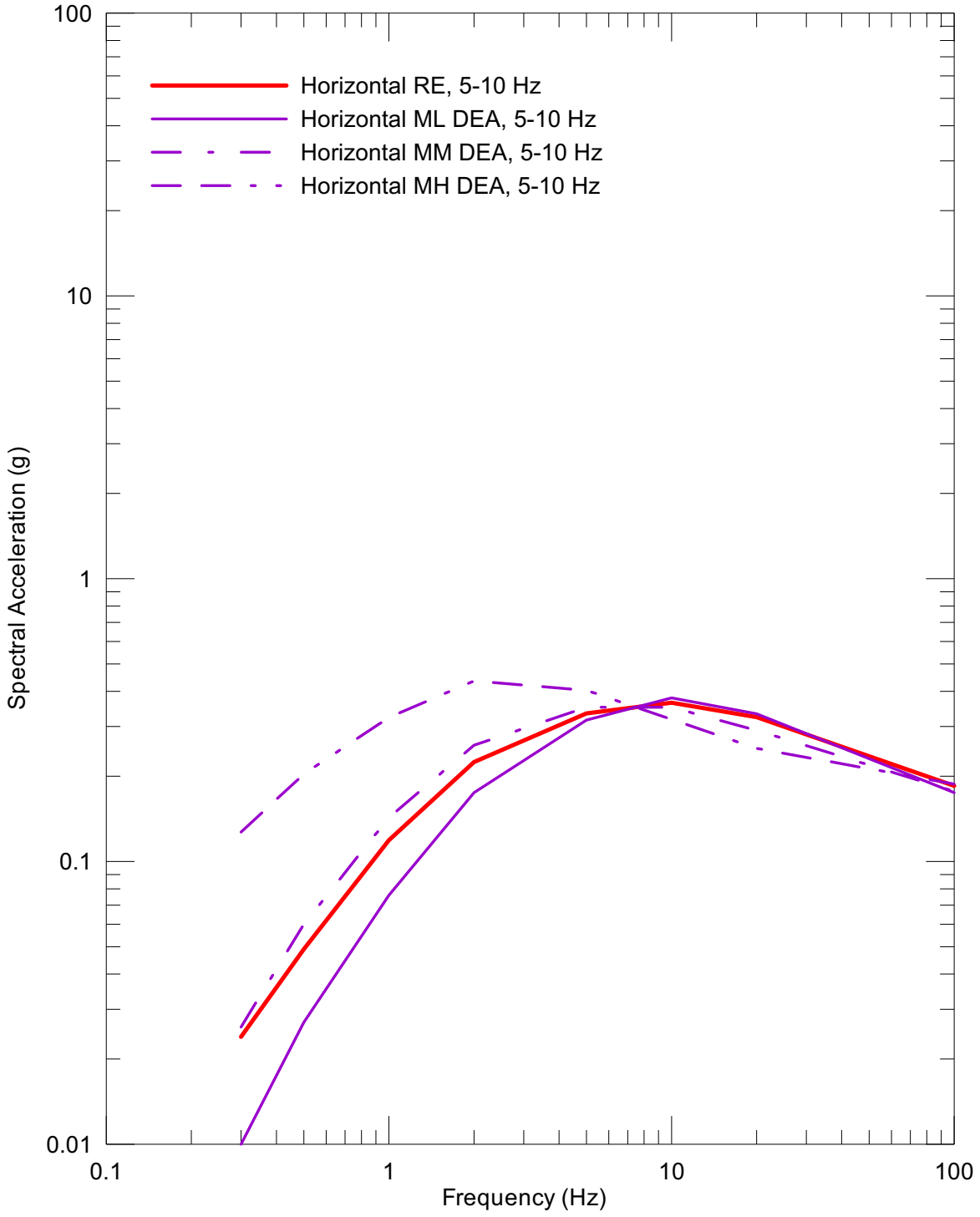

DTN: MO0211REDES103.000 [DIRS 170424]

Figure 6.2-42. Point A RE and DEA Spectra at an Annual Exceedance Frequency of 10^{-3} and 5-10 Hz, Horizontal Component

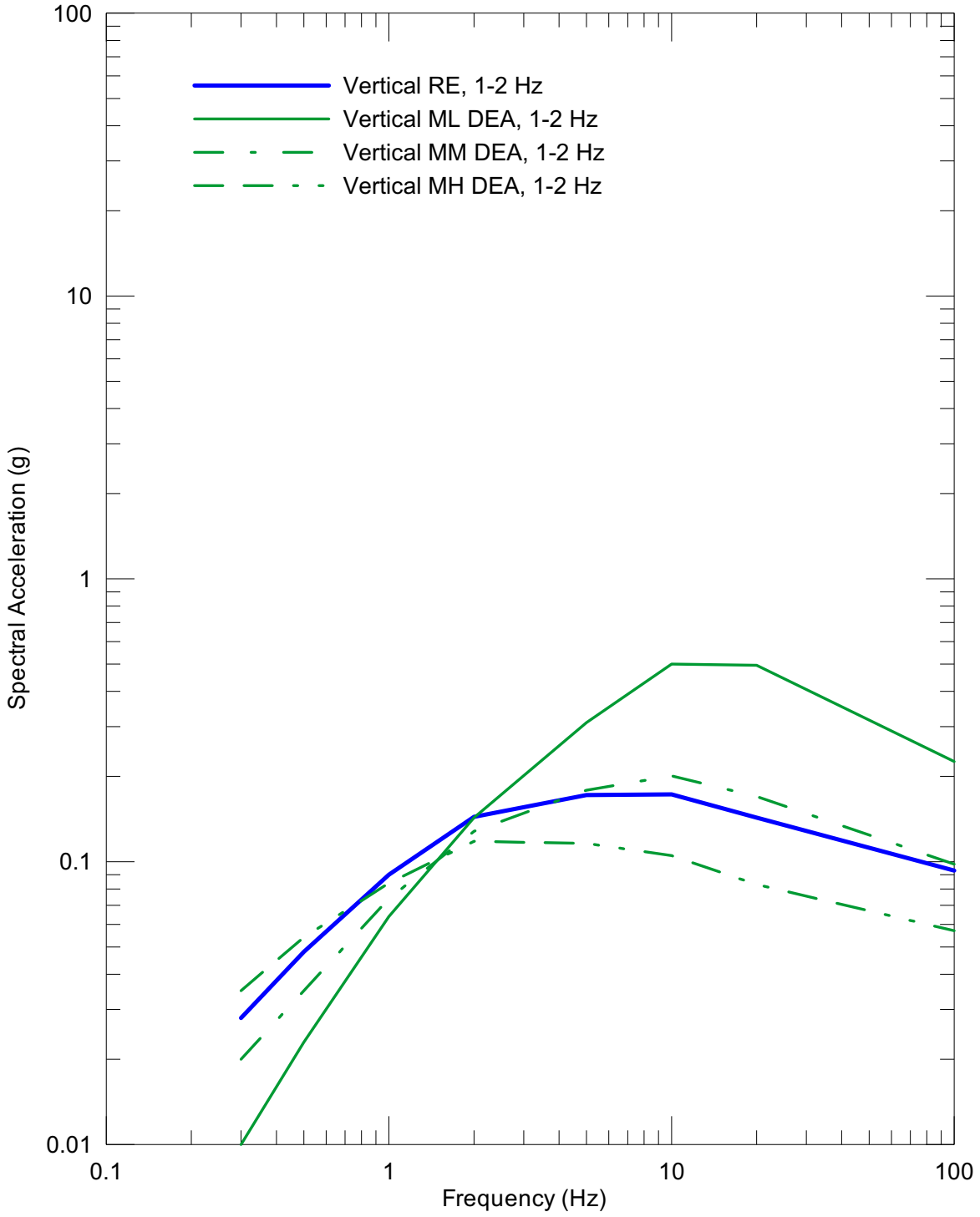

DTN: MO0211REDES103.000 [DIRS 170424]

Figure 6.2-43. Point A RE and DEA Spectra at an Annual Exceedance Frequency of 10^{-3} and 1-2 Hz, Vertical Component

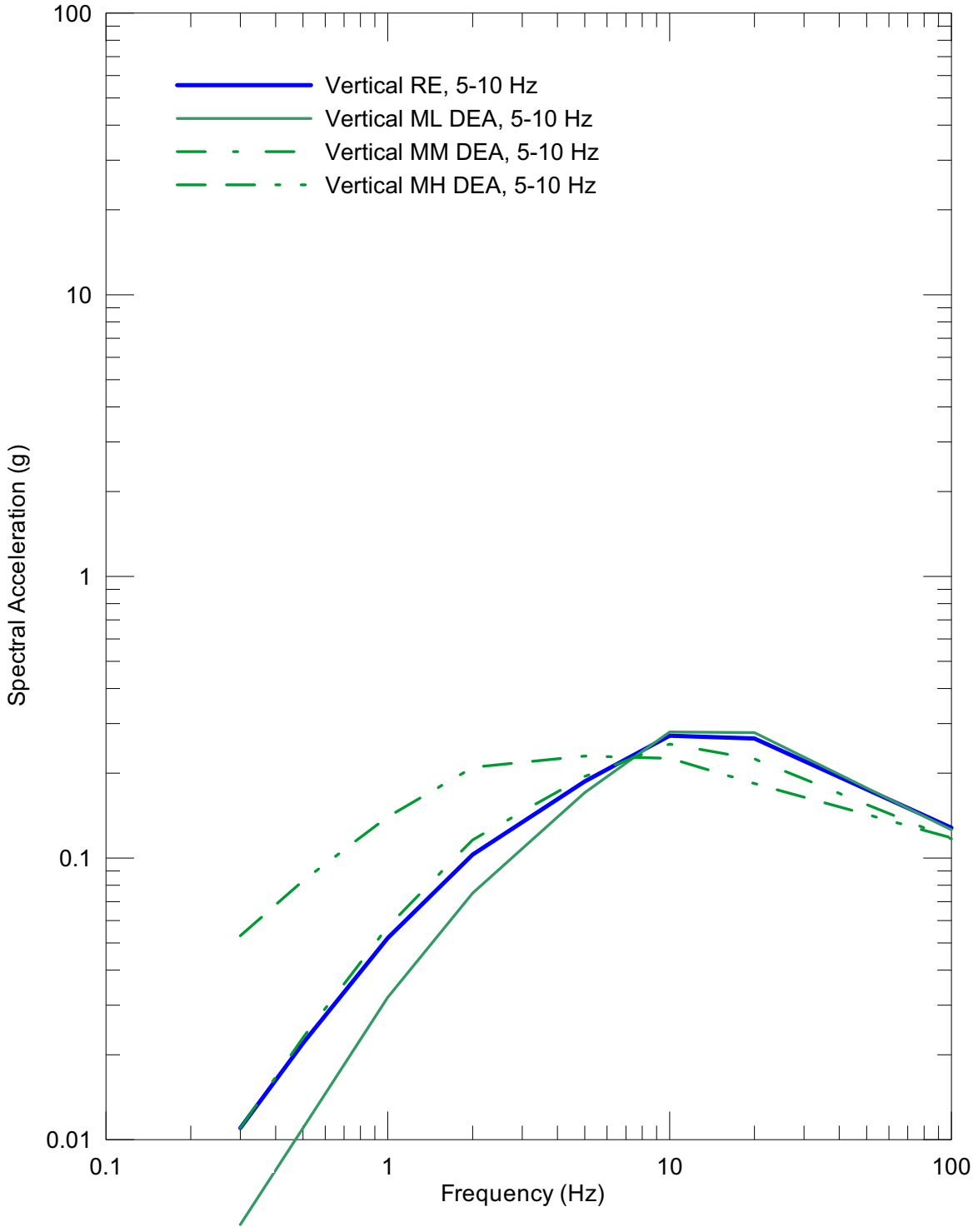

DTN: MO0211REDES103.000 [DIRS 170424]

Figure 6.2-44. Point A RE and DEA Spectra at an Annual Exceedance Frequency of 10^{-3} and 5-10 Hz, Vertical Component

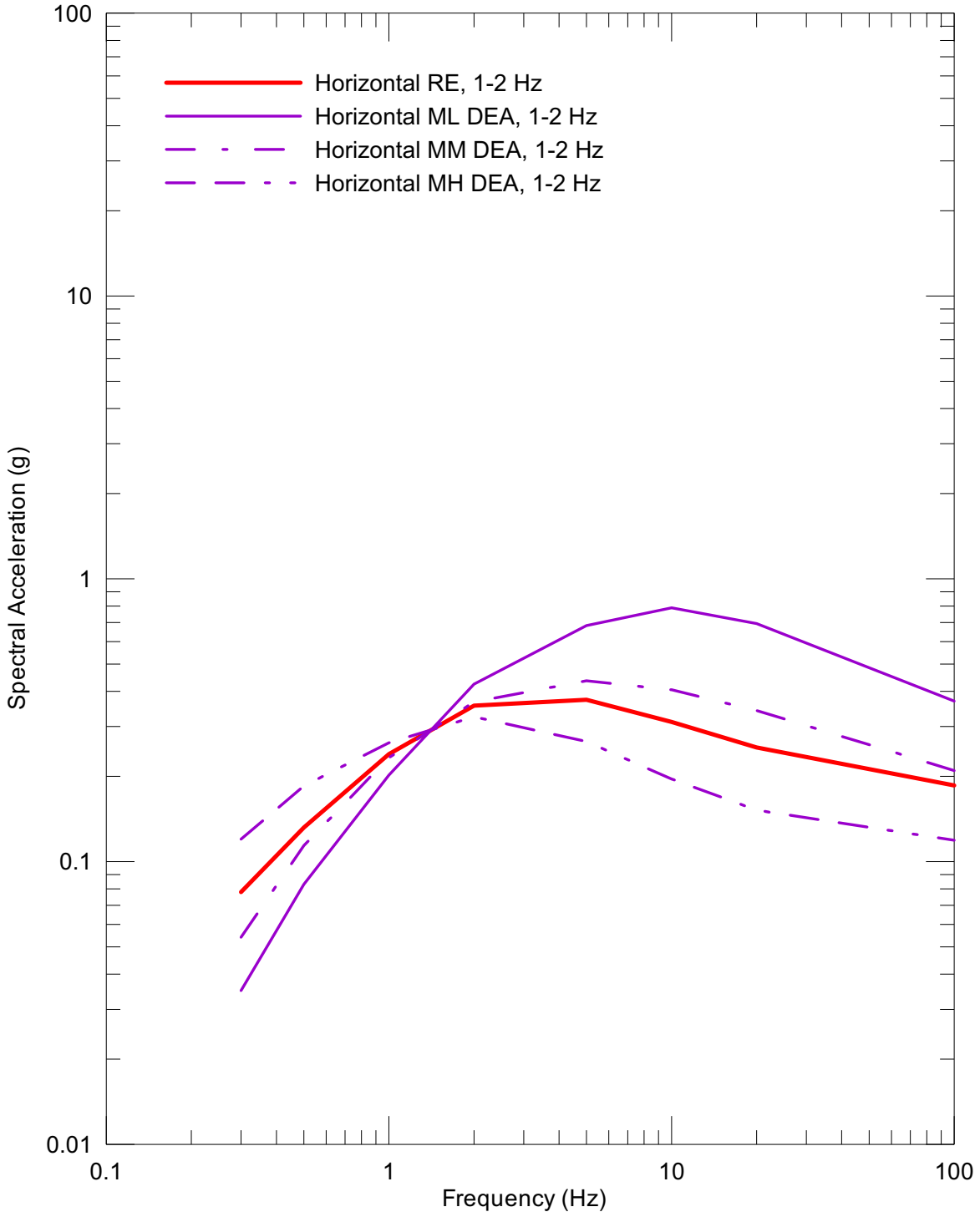

DTN: MO0208UNHZ5X10.000 [DIRS 163722]

Figure 6.2-45. Point A RE and DEA Spectra at an Annual Exceedance Frequency of 5×10^{-4} and 1-2 Hz, Horizontal Component

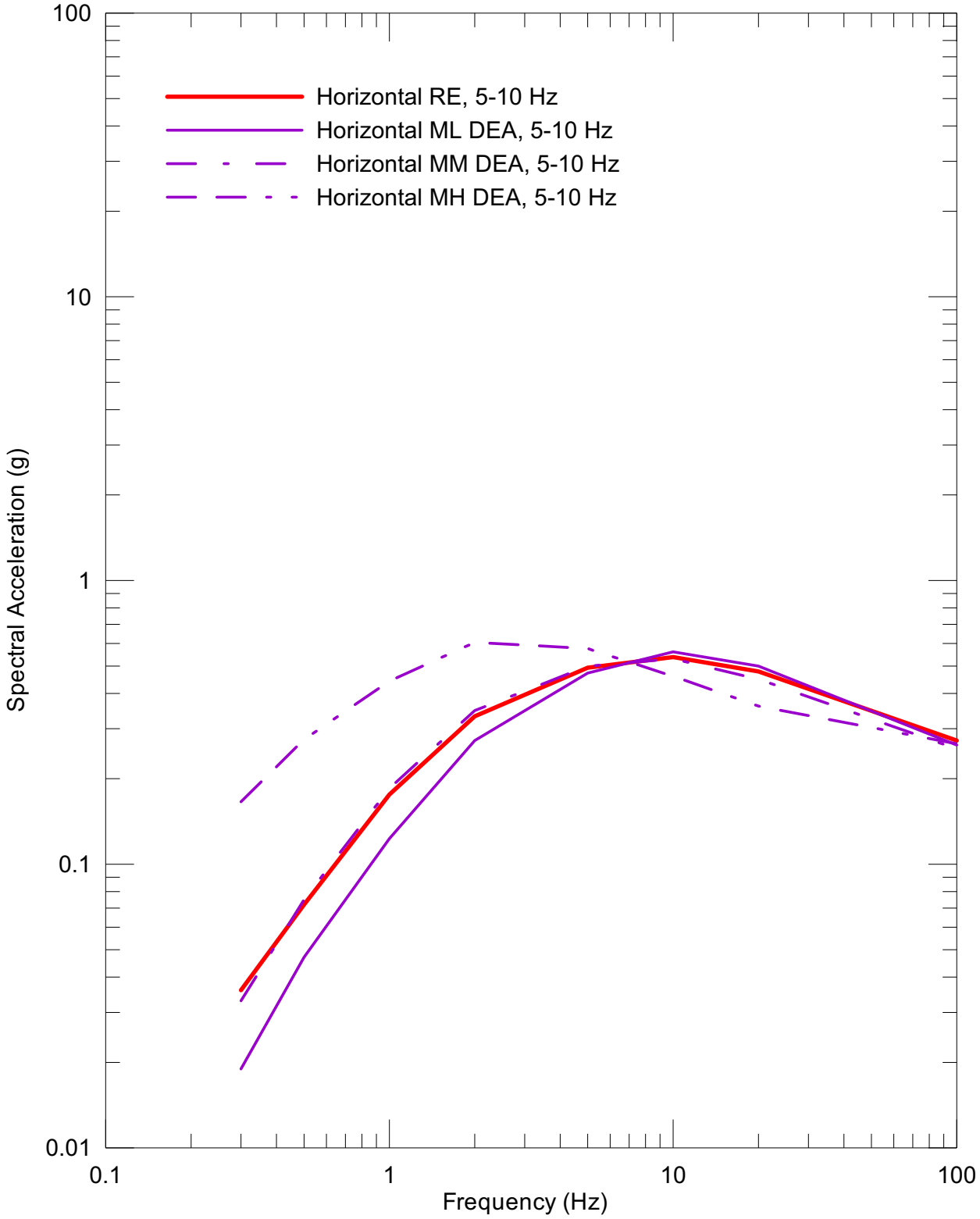

DTN: MO0208UNHZ5X10.000 [DIRS 163722]

Figure 6.2-46. Point A RE and DEA Spectra at an Annual Exceedance Frequency of 5×10^{-4} and 5-10 Hz, Horizontal Component

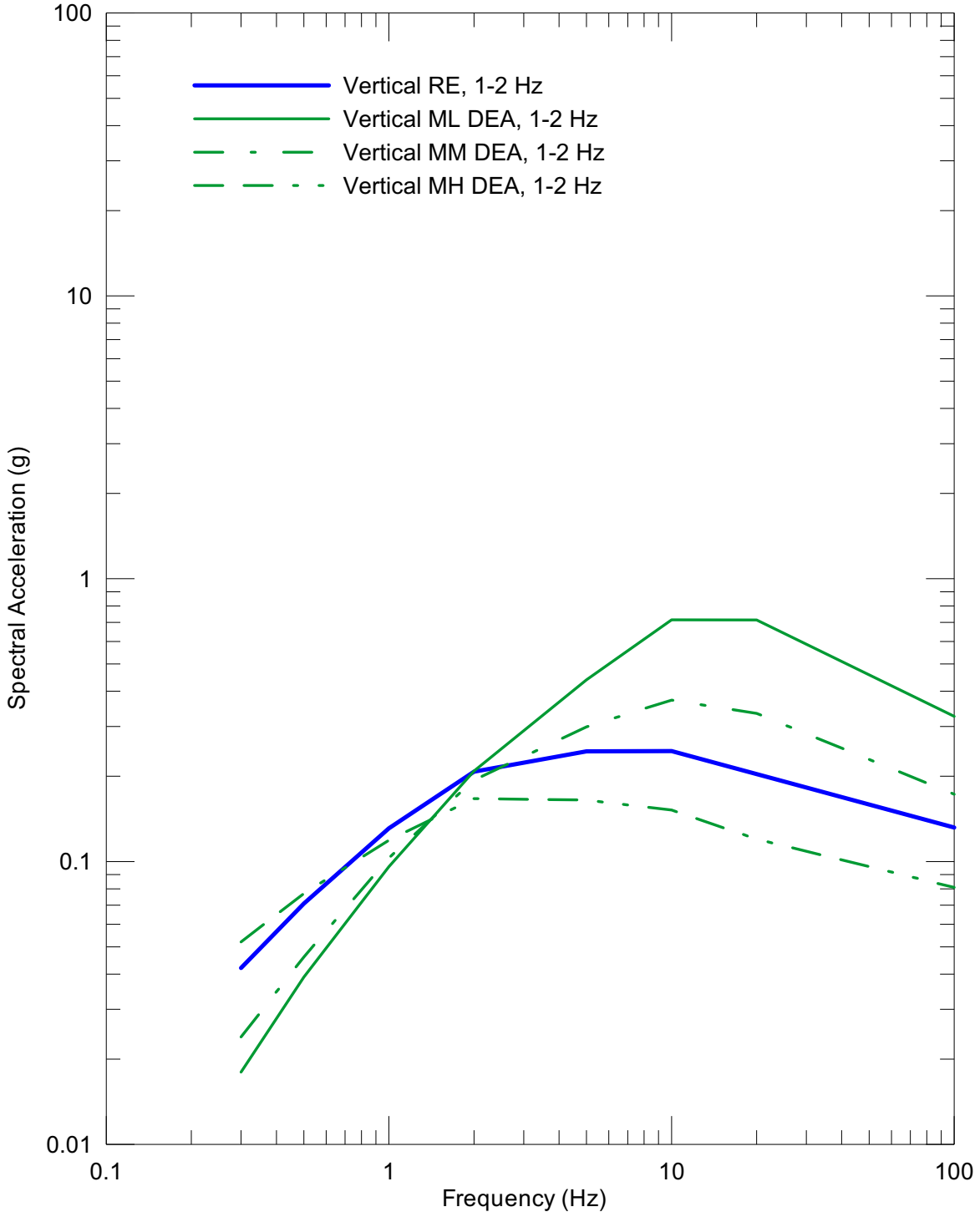

DTN: MO0208UNHZ5X10.000 [DIRS 163722]

Figure 6.2-47. Point A RE and DEA Spectra at an Annual Exceedance Frequency of 5×10^{-4} and 1-2 Hz, Vertical Component

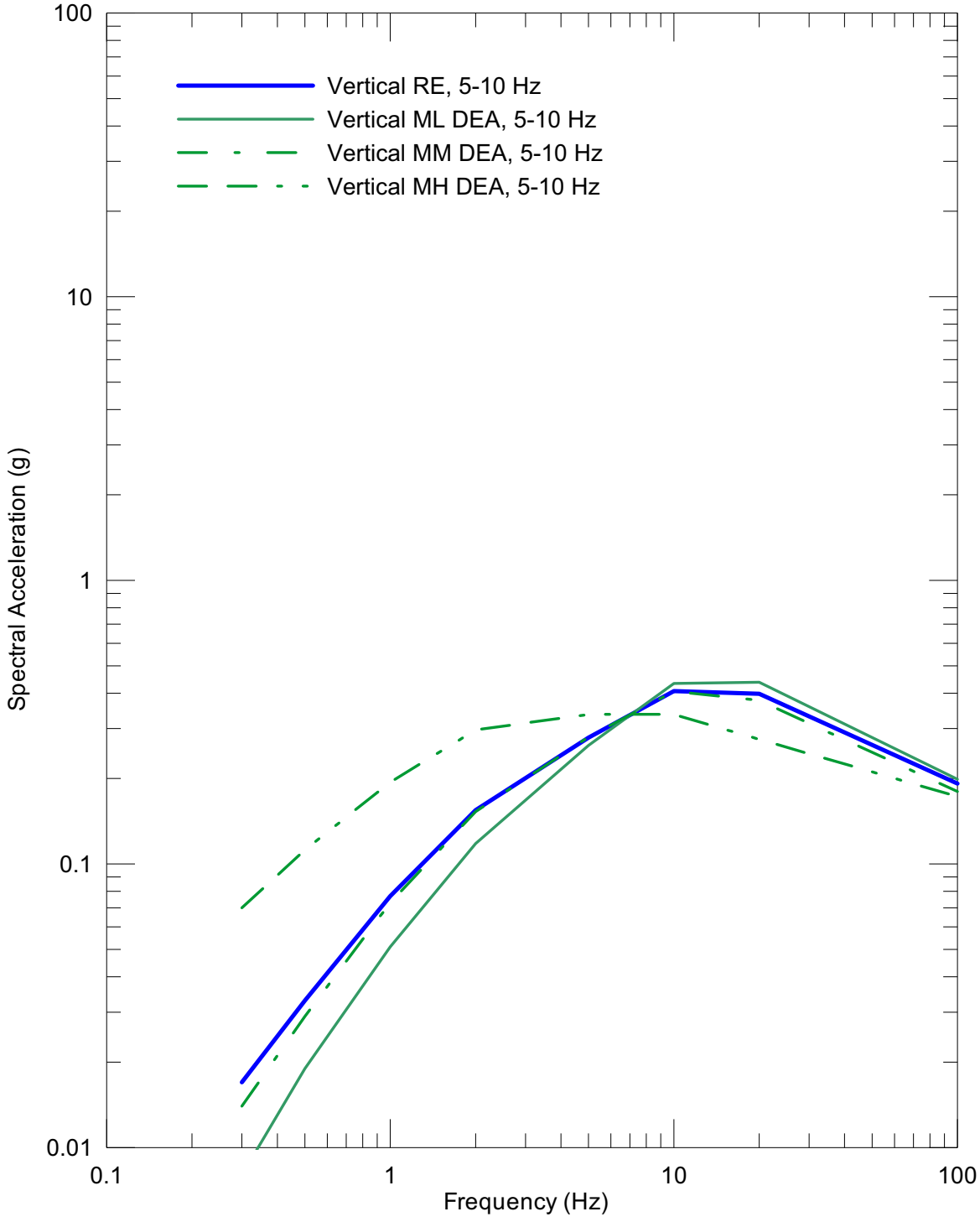

DTN: MO0208UNHZ5X10.000 [DIRS 163722]

Figure 6.2-48. Point A RE and DEA Spectra at an Annual Exceedance Frequency of 5×10^{-4} and 5-10 Hz, Vertical Component

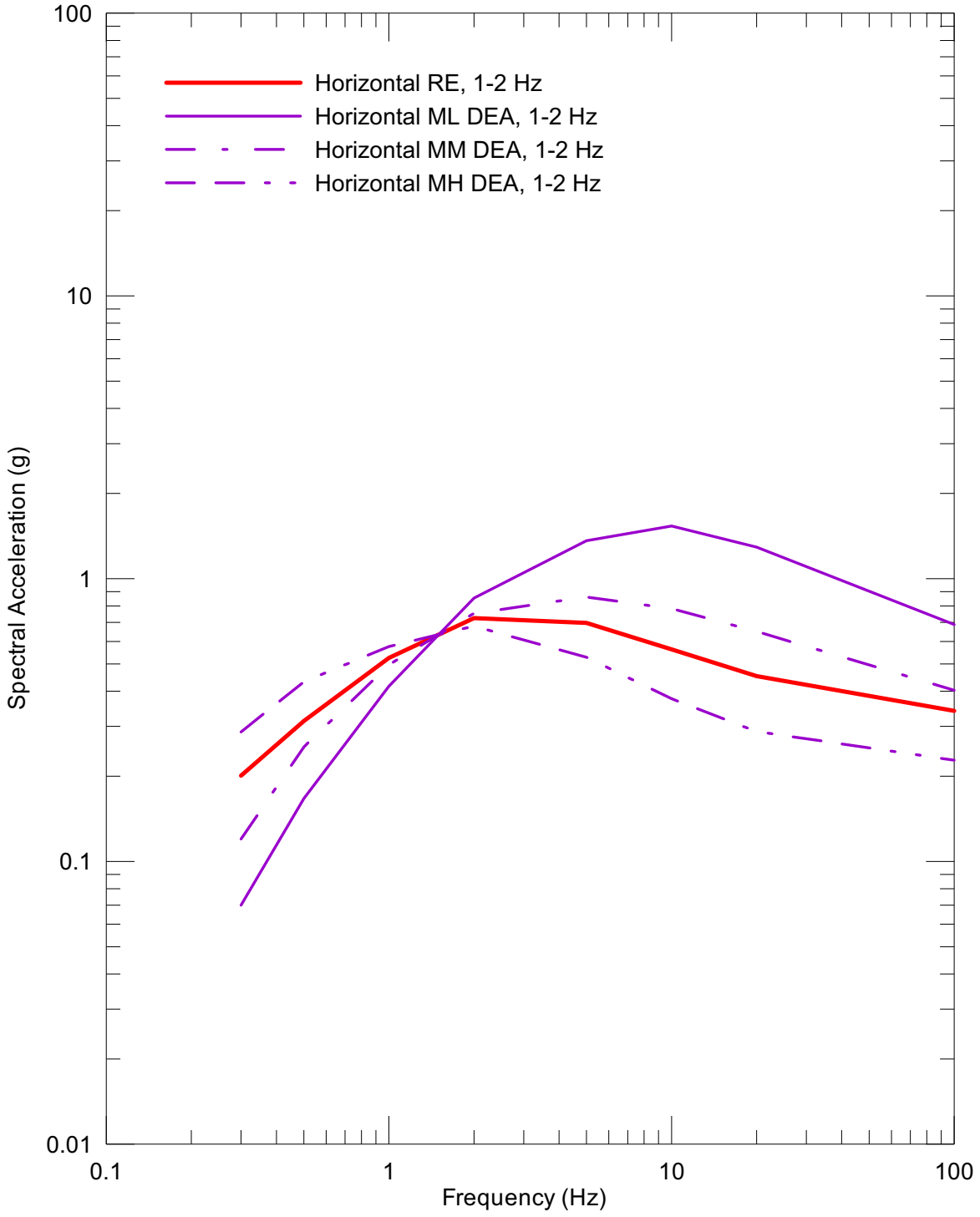

DTN: MO0211DERES104.000 [DIRS 170423]

Figure 6.2-49. Point A RE and DEA Spectra at an Annual Exceedance Frequency of 10^{-4} and 1-2 Hz, Horizontal Component

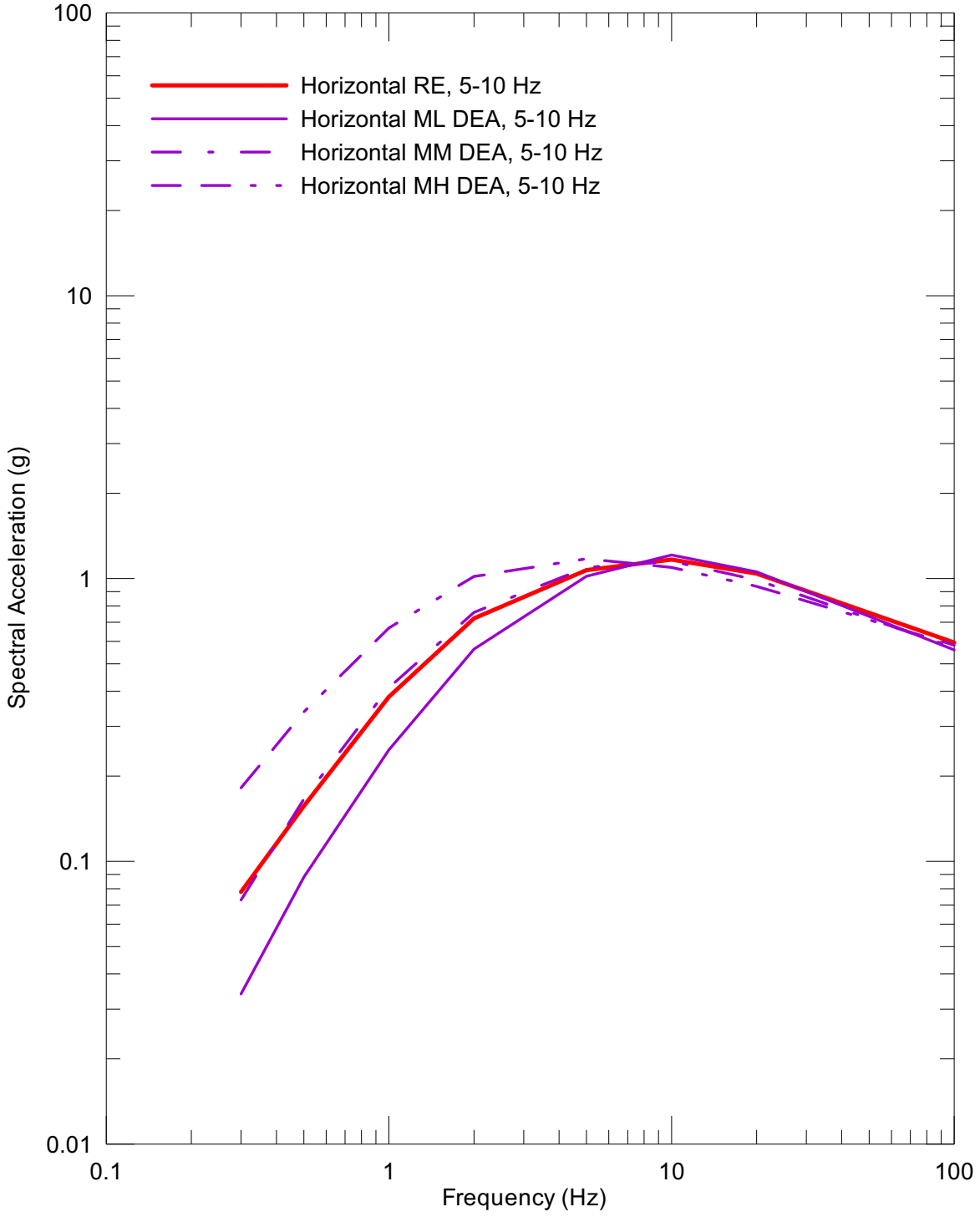

DTN: MO0211DERES104.000 [DIRS 170423]

Figure 6.2-50. Point A RE and DEA Spectra at an Annual Exceedance Frequency of 10^{-4} and 5-10 Hz, Horizontal Component

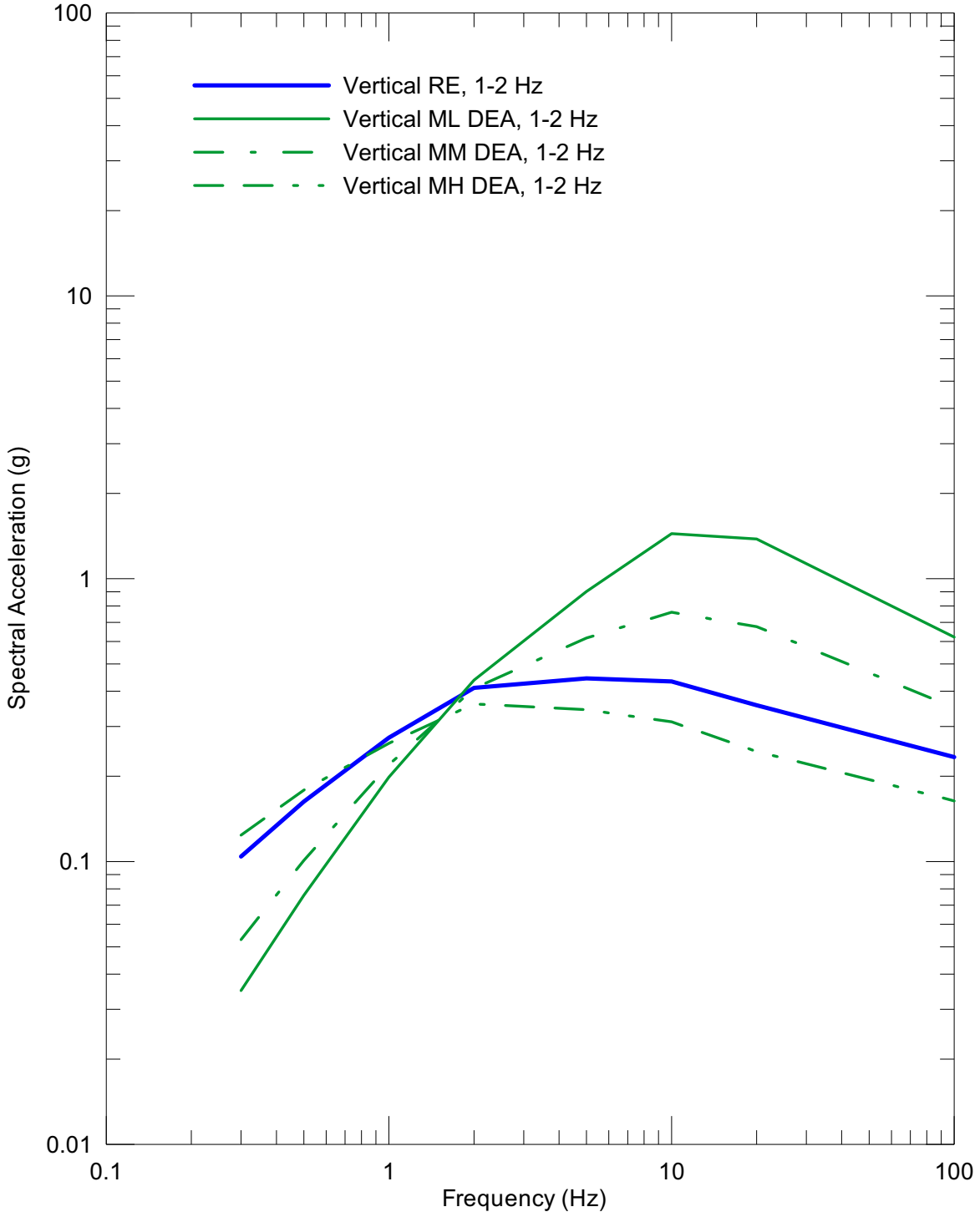

DTN: MO0211DERES104.000 [DIRS 170423]

Figure 6.2-51. Point A RE and DEA Spectra at an Annual Exceedance Frequency of 10^{-4} and 1-2 Hz, Vertical Component

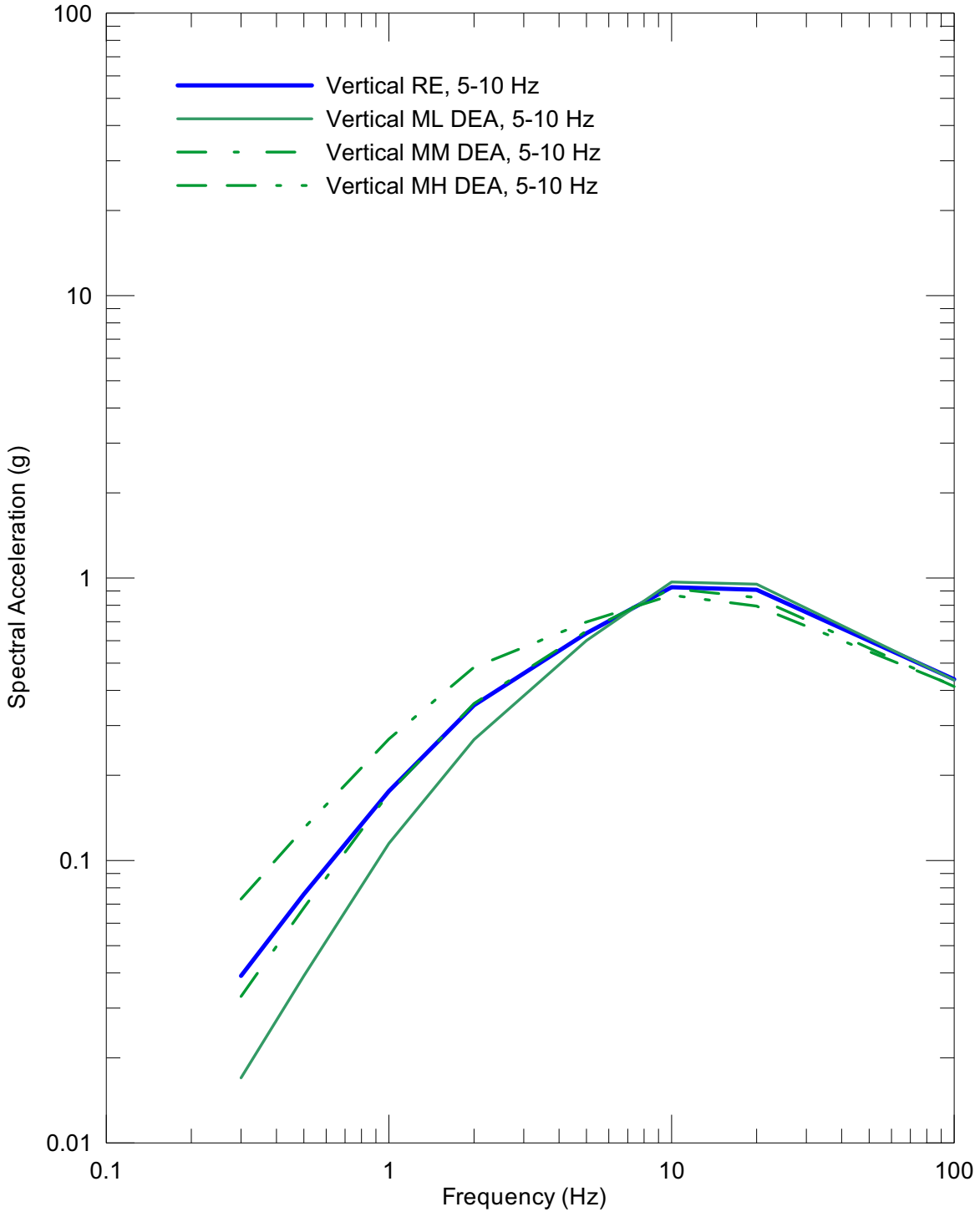

DTN: MO0211DERES104.000 [DIRS 170423]

Figure 6.2-52. Point A RE and DEA Spectra at an Annual Exceedance Frequency of 10^{-4} and 5-10 Hz, Vertical Component

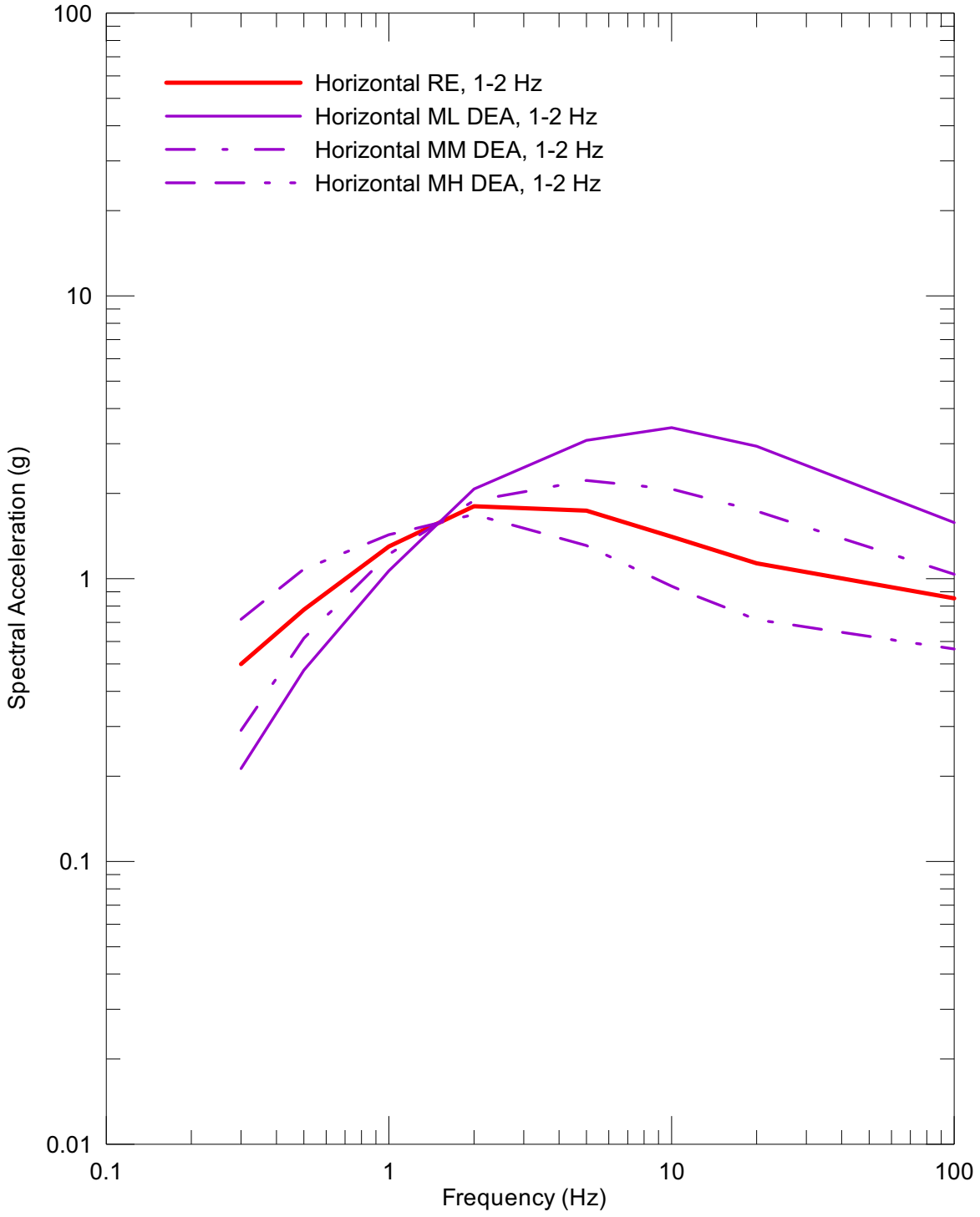

DTN: MO0308UNHAZ105.000 [DIRS 170425]

Figure 6.2-53. Point A RE and DEA Spectra at an Annual Exceedance Frequency of 10^{-5} and 1-2 Hz, Horizontal Component

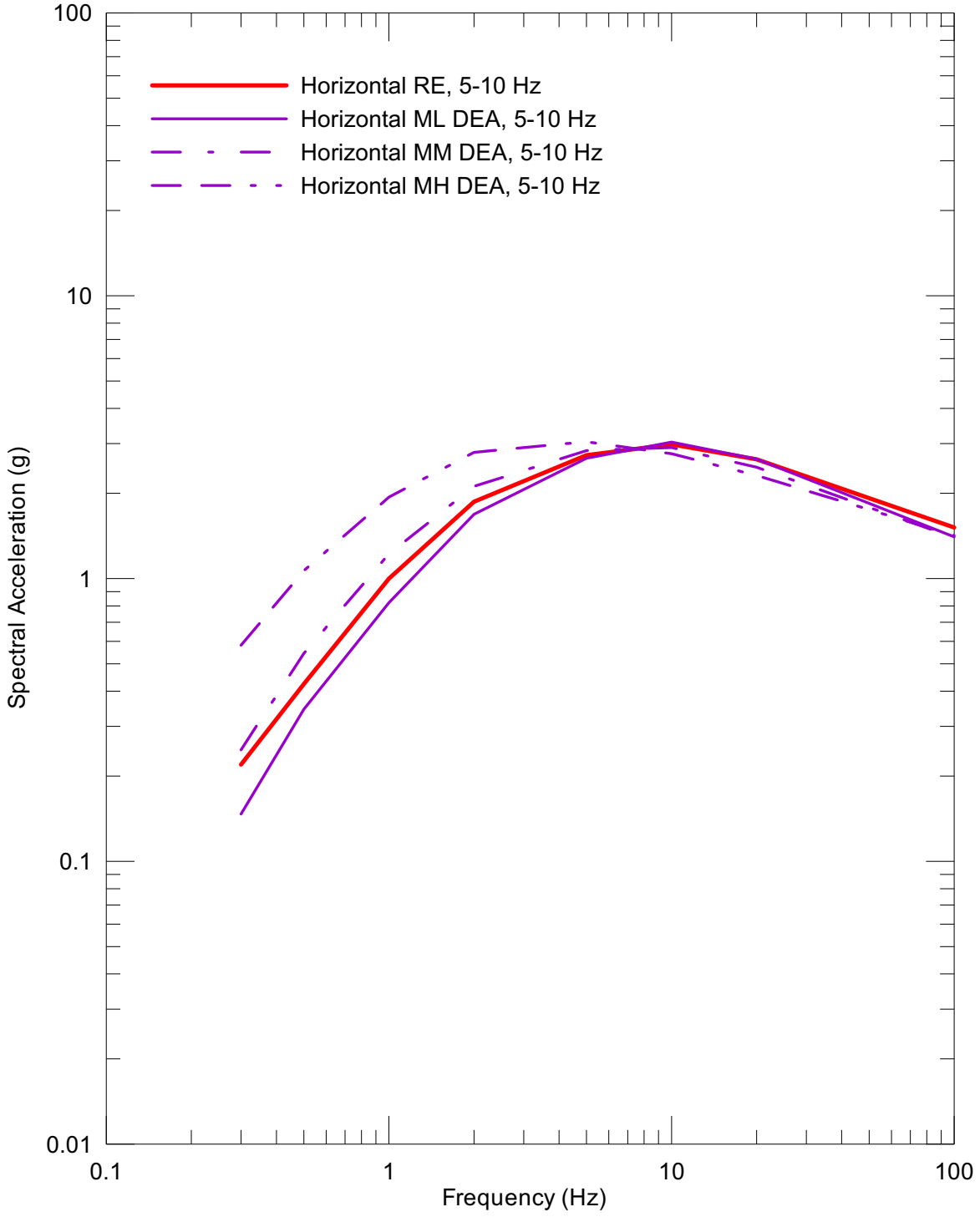

DTN: MO0308UNHAZ105.000 [DIRS 170425]

Figure 6.2-54. Point A RE and DEA Spectra at an Annual Exceedance Frequency of 10^{-5} and 5-10 Hz, Horizontal Component

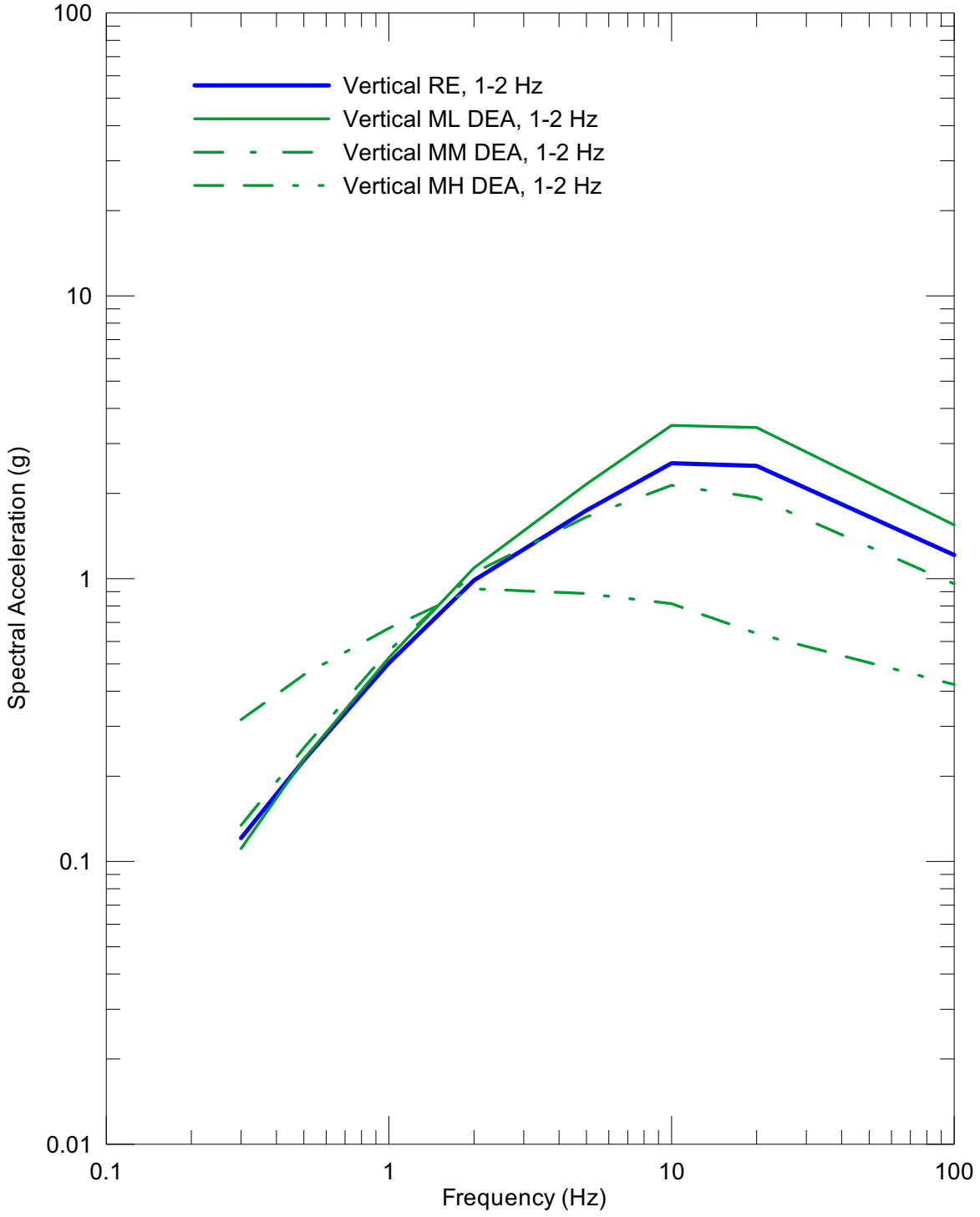

DTN: MO0308UNHAZ105.000 [DIRS 170425]

Figure 6.2-55. Point A RE and DEA Spectra at an Annual Exceedance Frequency of 10^{-5} and 1-2 Hz, Vertical Component

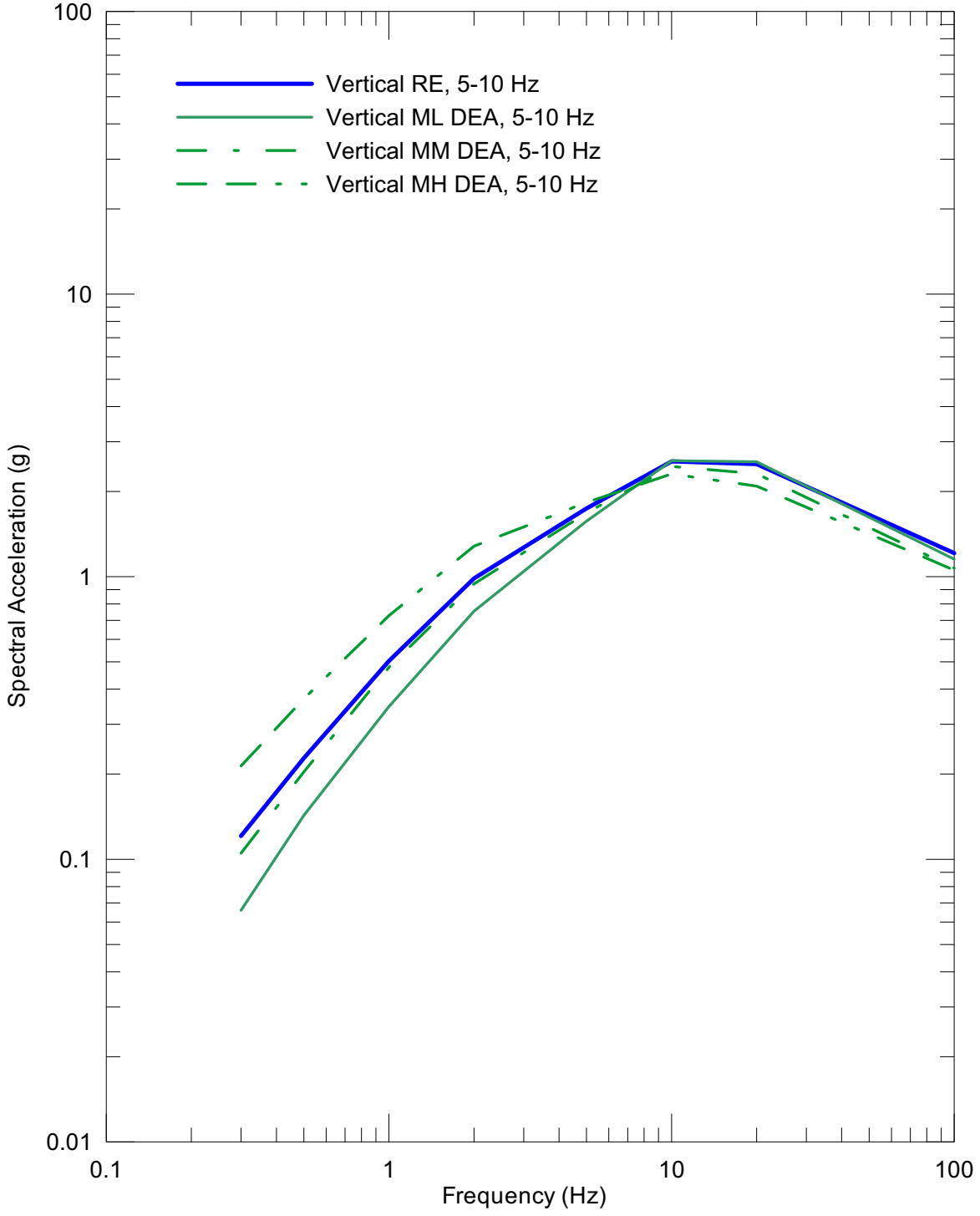

DTN: MO0308UNHAZ105.000 [DIRS 170425]

Figure 6.2-56. Point A RE and DEA Spectra at an Annual Exceedance Frequency of 10^{-5} and 5-10 Hz, Vertical Component

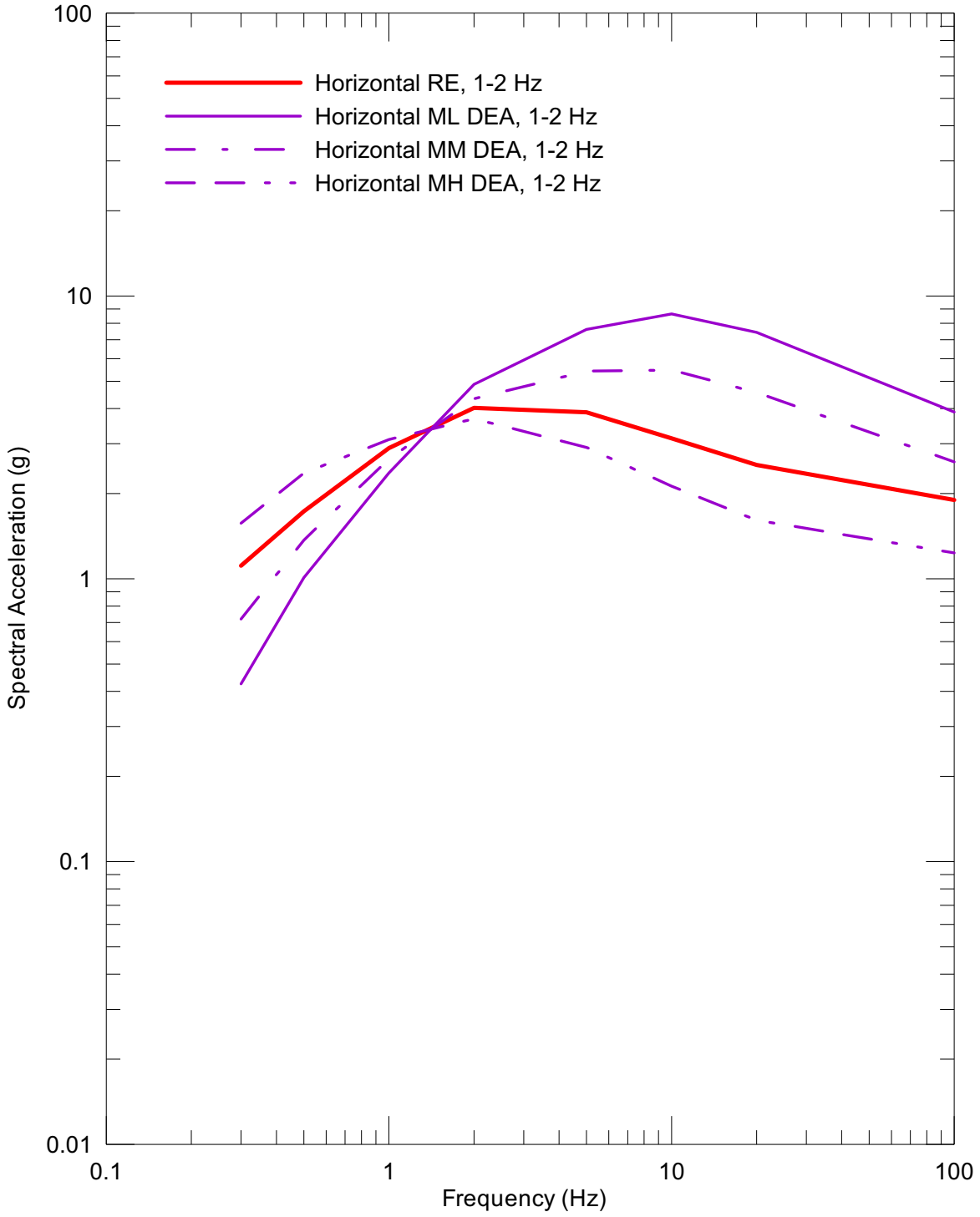

DTN: MO0206UNHAZ106.001 [DIRS 163723]

Figure 6.2-57. Point A RE and DEA Spectra at an Annual Exceedance Frequency of 10^{-6} and 1-2 Hz, Horizontal Component

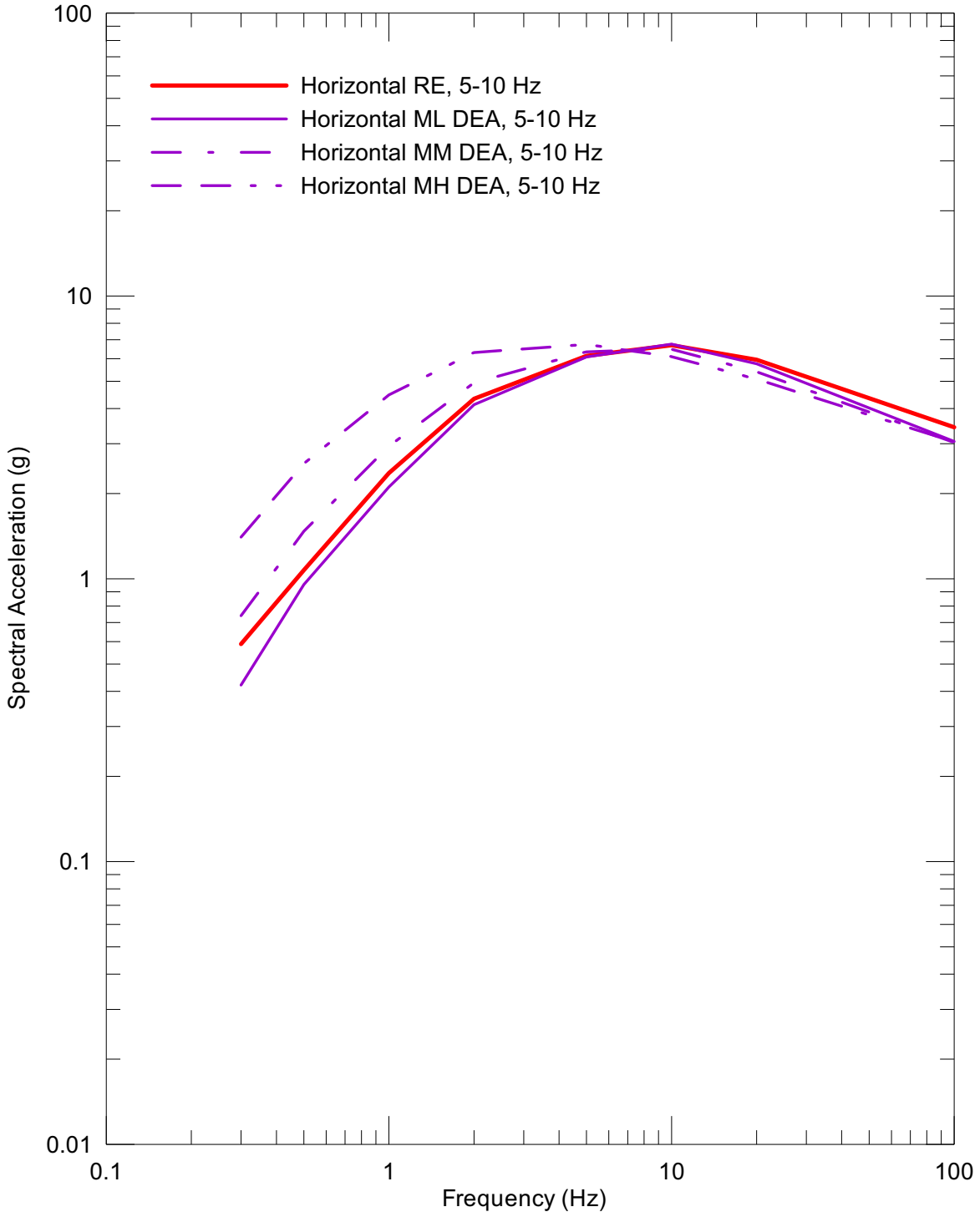

DTN: MO0206UNHAZ106.001 [DIRS 163723]

Figure 6.2-58. Point A RE and DEA Spectra at an Annual Exceedance Frequency of 10^{-6} and 5-10 Hz, Horizontal Component

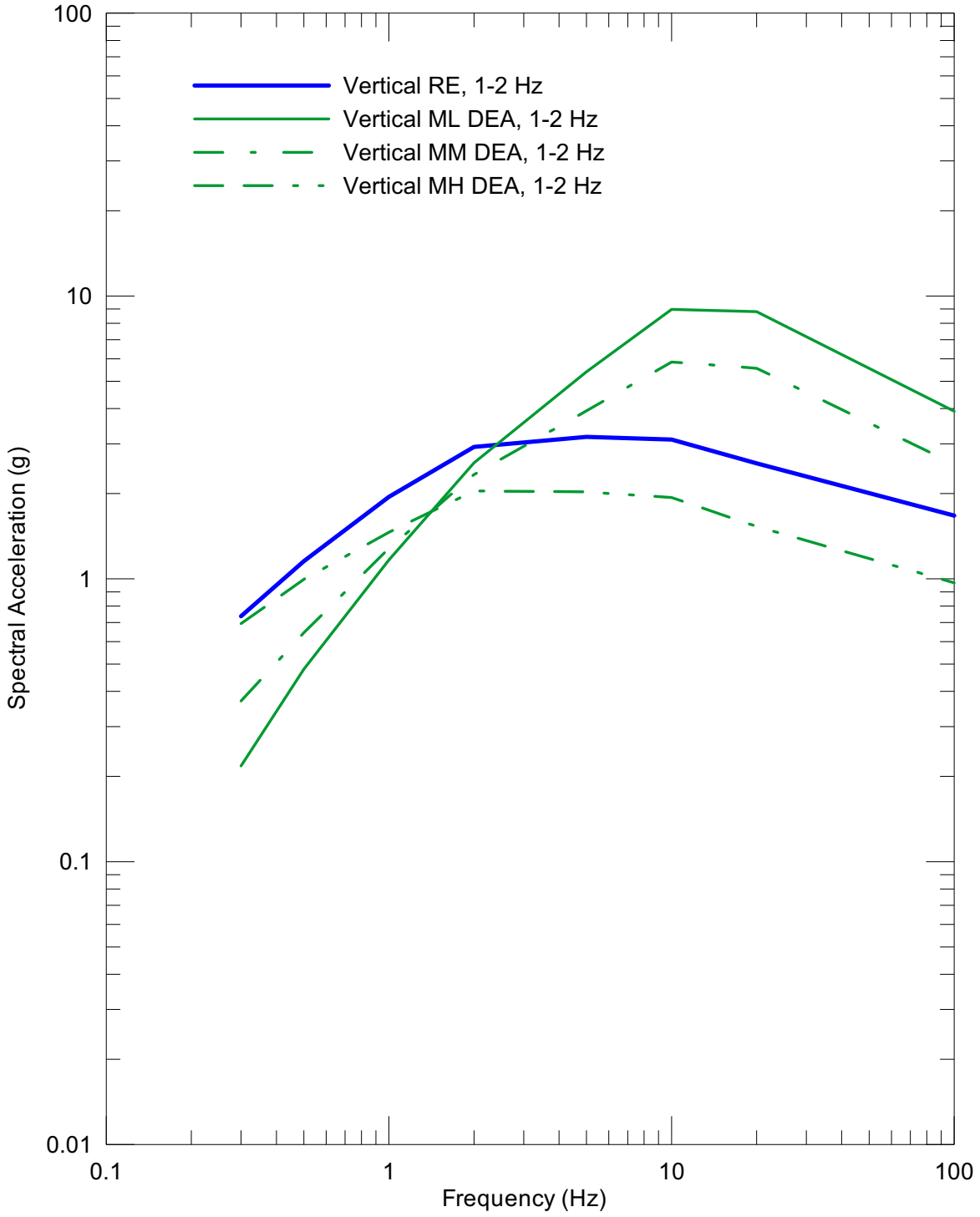

DTN: MO0206UNHAZ106.001 [DIRS 163723]

Figure 6.2-59. Point A RE and DEA Spectra at an Annual Exceedance Frequency of 10^{-6} and 1-2 Hz, Vertical Component

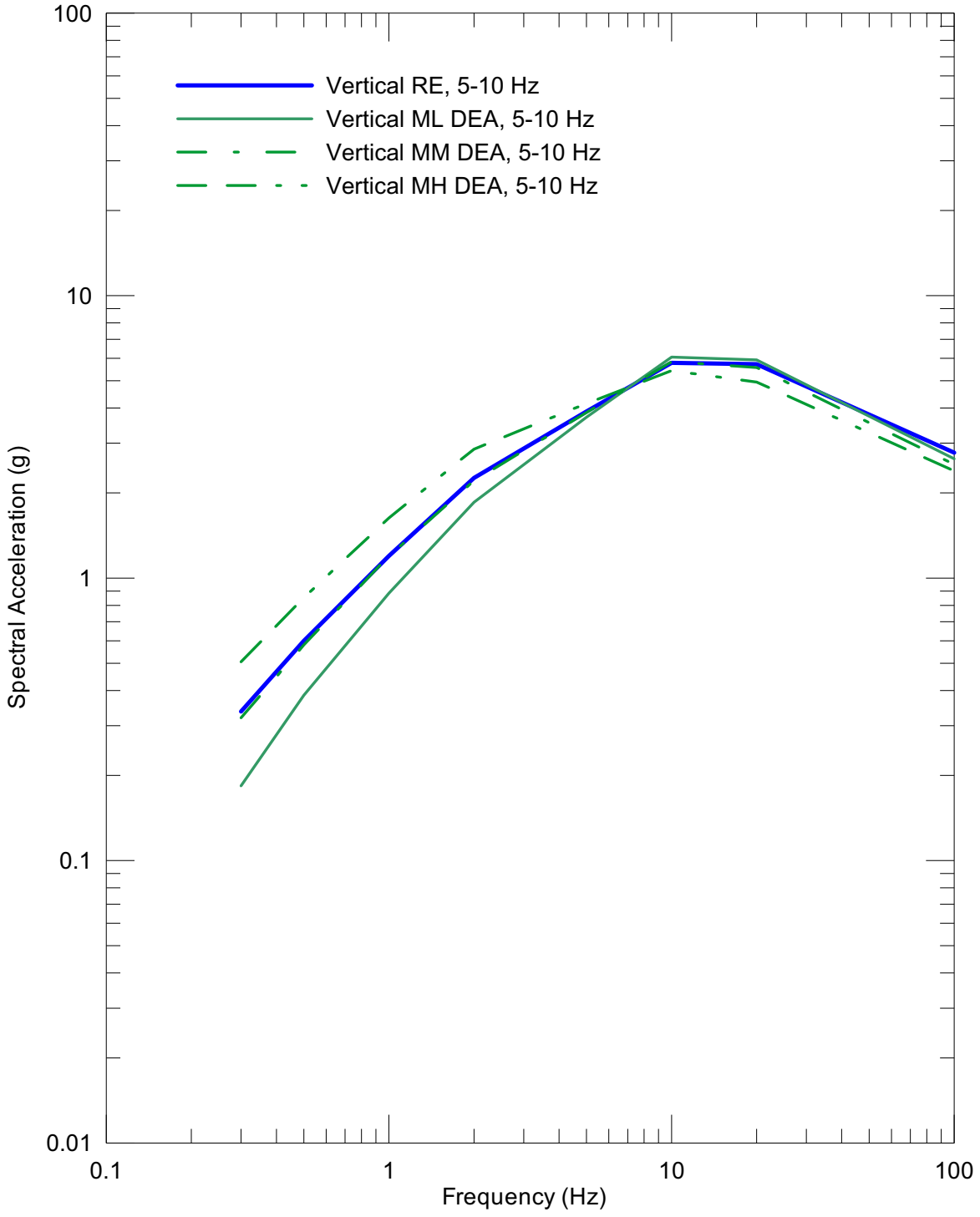

DTN: MO0206UNHAZ106.001 [DIRS 163723]

Figure 6.2-60. Point A RE and DEA Spectra at an Annual Exceedance Frequency of 10^{-6} and 5-10 Hz, Vertical Component

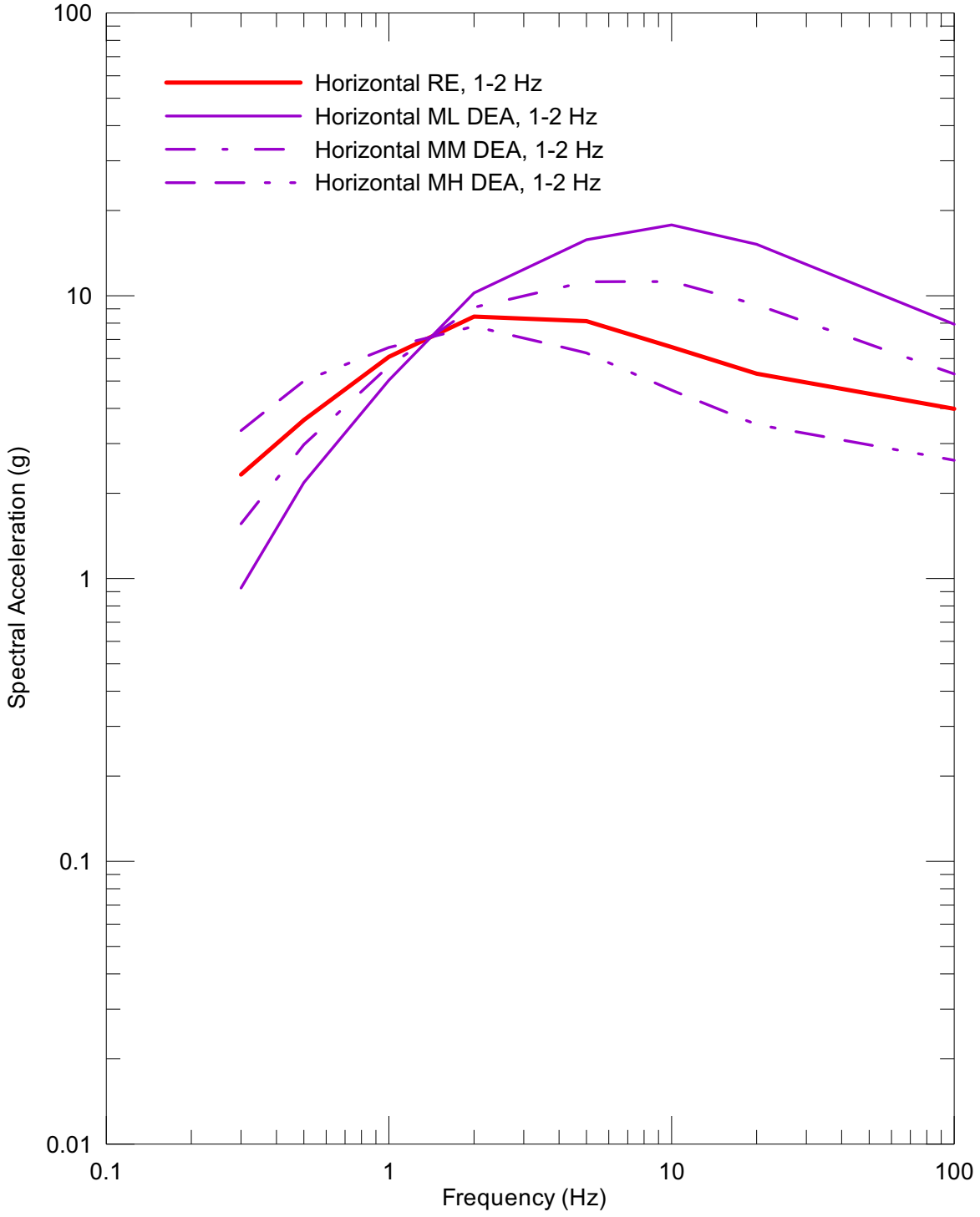

DTN: MO0209UNHAZ107.000 [DIRS 163724]

Figure 6.2-61. Point A RE and DEA Spectra at an Annual Exceedance Frequency of 10^{-7} and 1-2 Hz, Horizontal Component

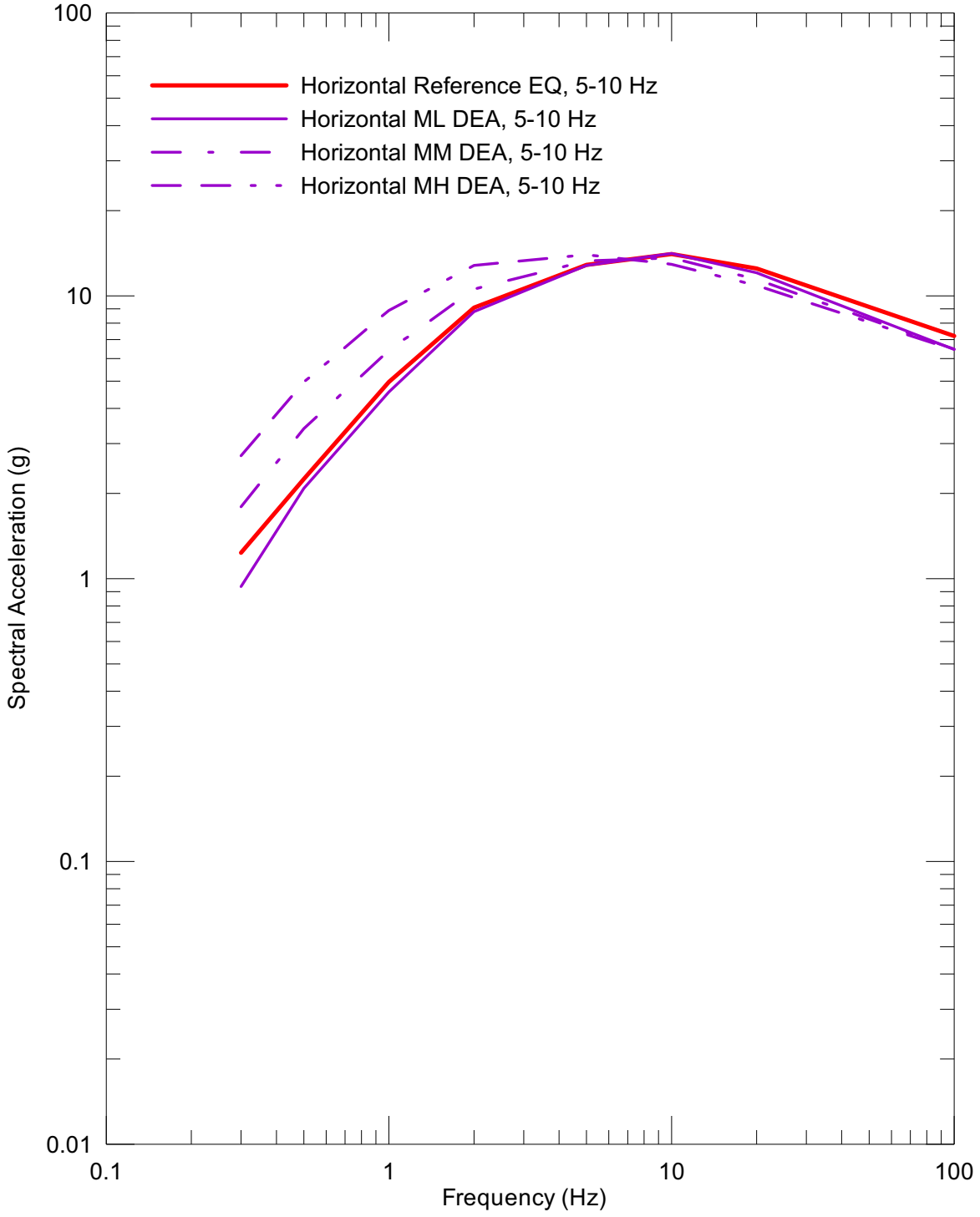

DTN: MO0209UNHAZ107.000 [DIRS 163724]

Figure 6.2-62. Point A RE and DEA Spectra at an Annual Exceedance Frequency of 10^{-7} and 5-10 Hz, Horizontal Component

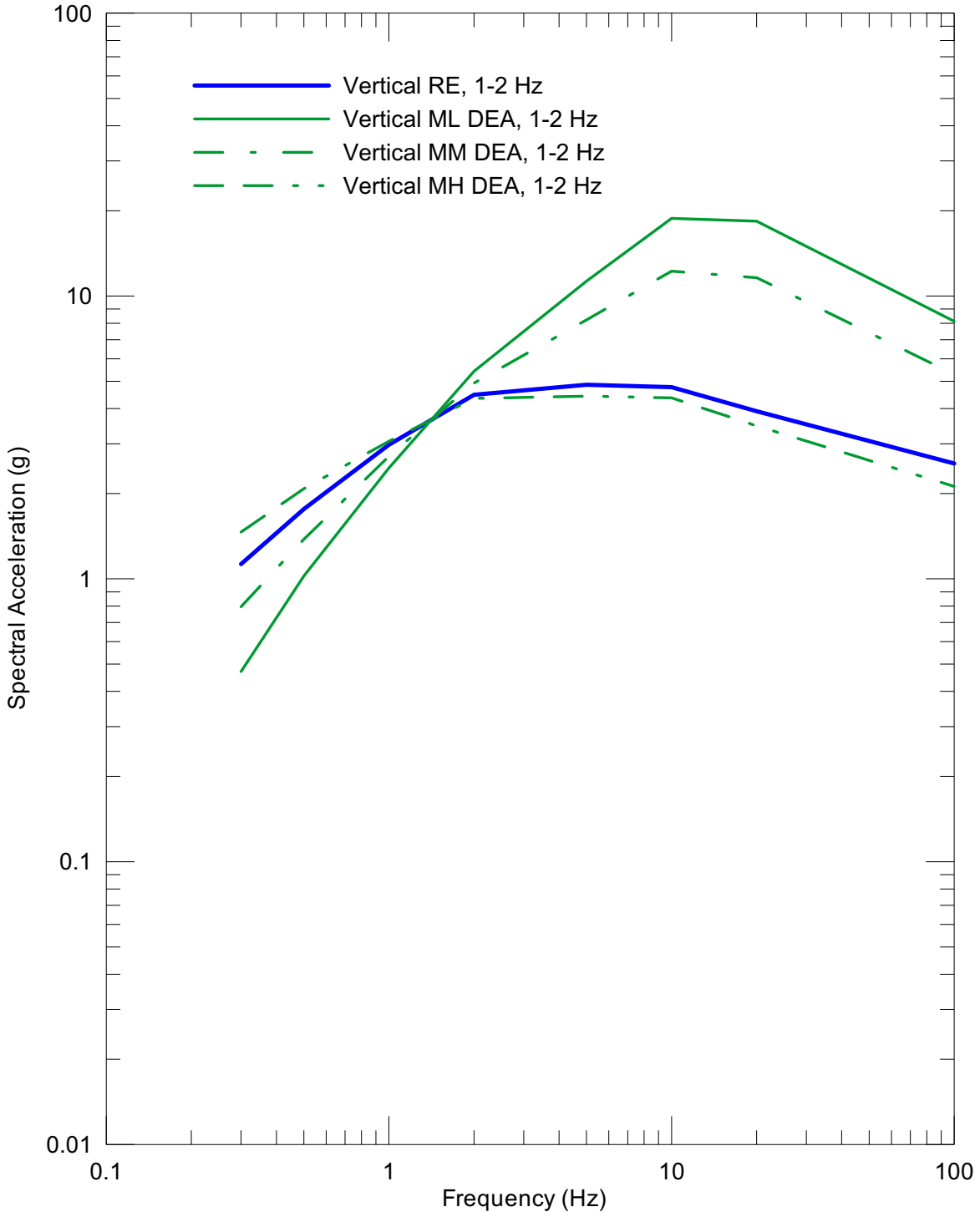

DTN: MO0209UNHAZ107.000 [DIRS 163724]

Figure 6.2-63. Point A RE and DEA Spectra at an Annual Exceedance Frequency of 10^{-7} and 1-2 Hz, Vertical Component

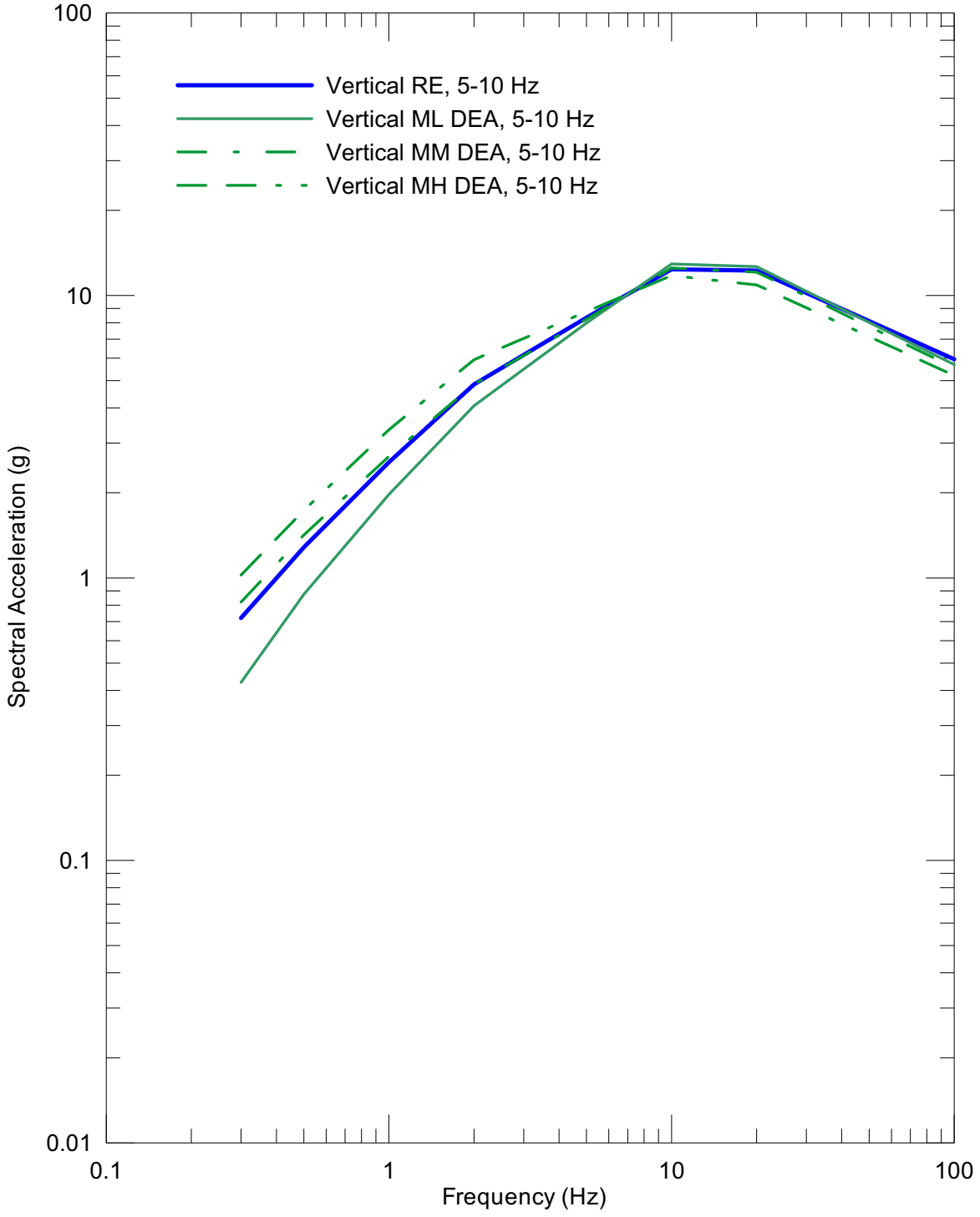

DTN: MO0209UNHAZ107.000 [DIRS 163724]

Figure 6.2-64. Point A RE and DEA Spectra at an Annual Exceedance Frequency of 10^{-7} and 5-10 Hz, Vertical Component

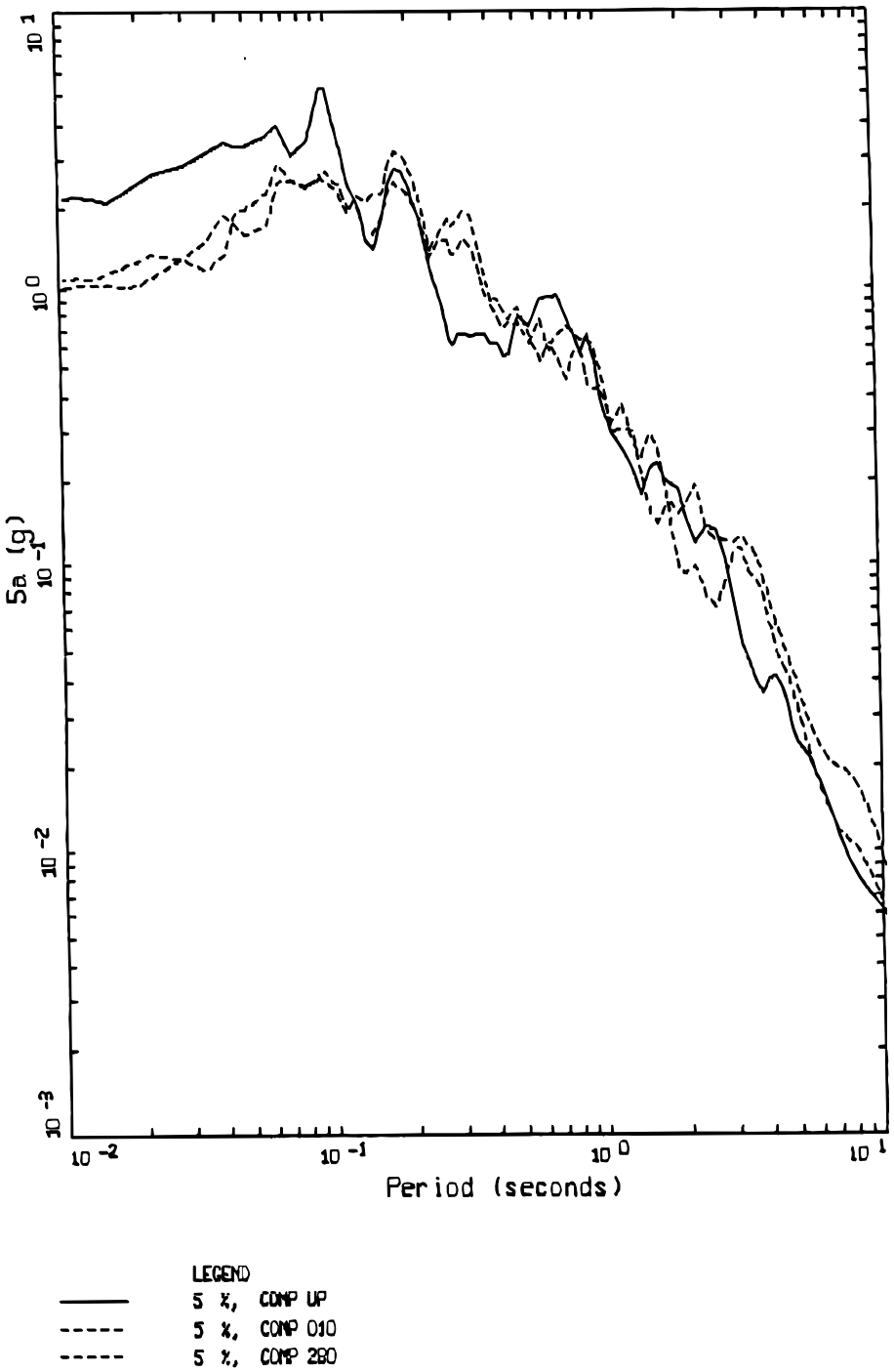

Source: Wong and Silva (2004a [DIRS 170443], SR 9, page 25)

Figure 6.2-65. Comparison of Vertical- and Horizontal-Component 5%-Damped Response Spectra for Site S1 Recording of the 1985 **M** 6.8 Nahanni Earthquake

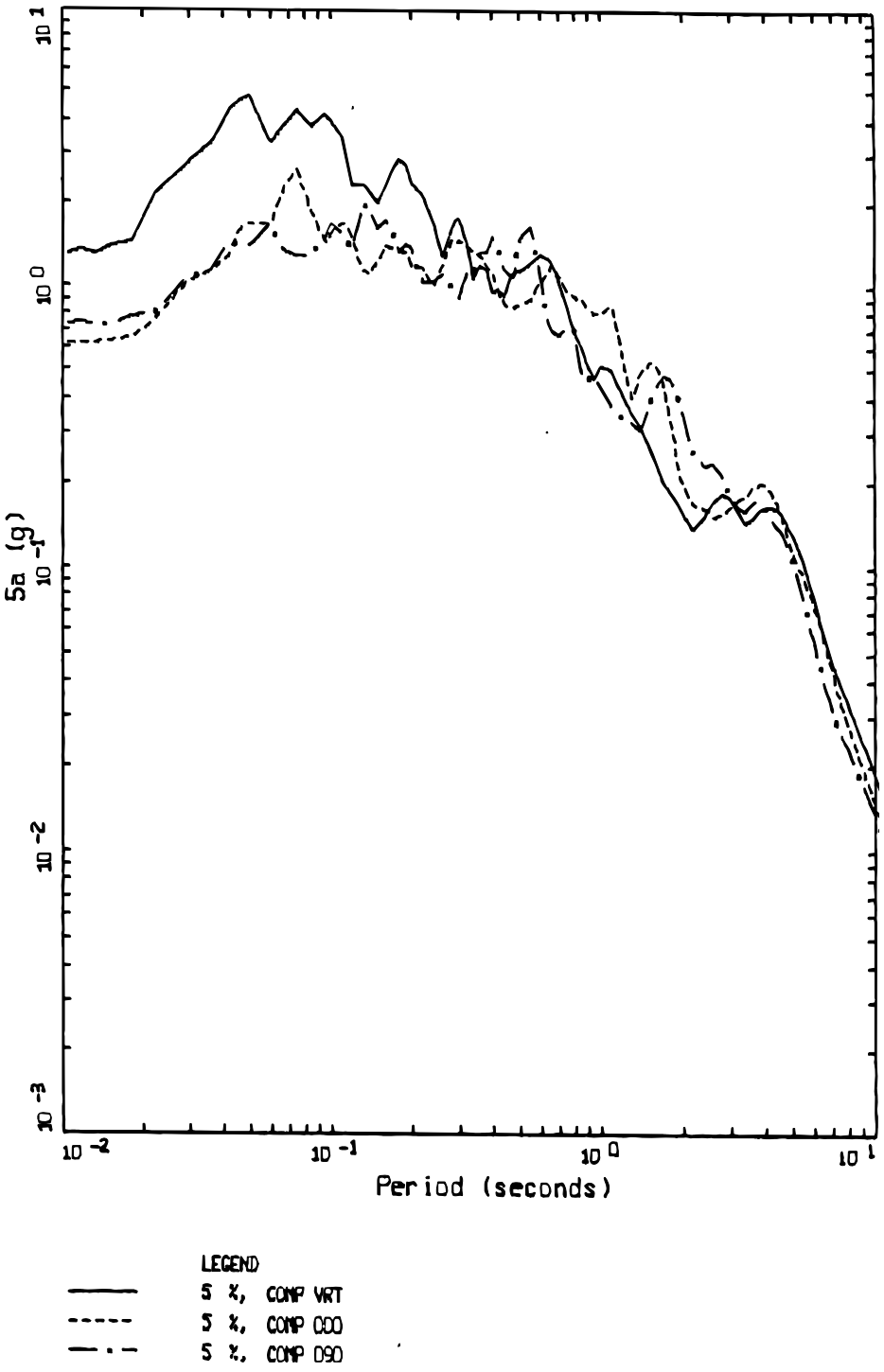

Source: Wong and Silva (2004a [DIRS 170443], SR 9, page 29)

Figure 6.2-66. Comparison of Vertical- and Horizontal-Component 5%-Damped Response Spectra for the Karakyr Recording of the 1976 **M** 6.8 Gazli Earthquake

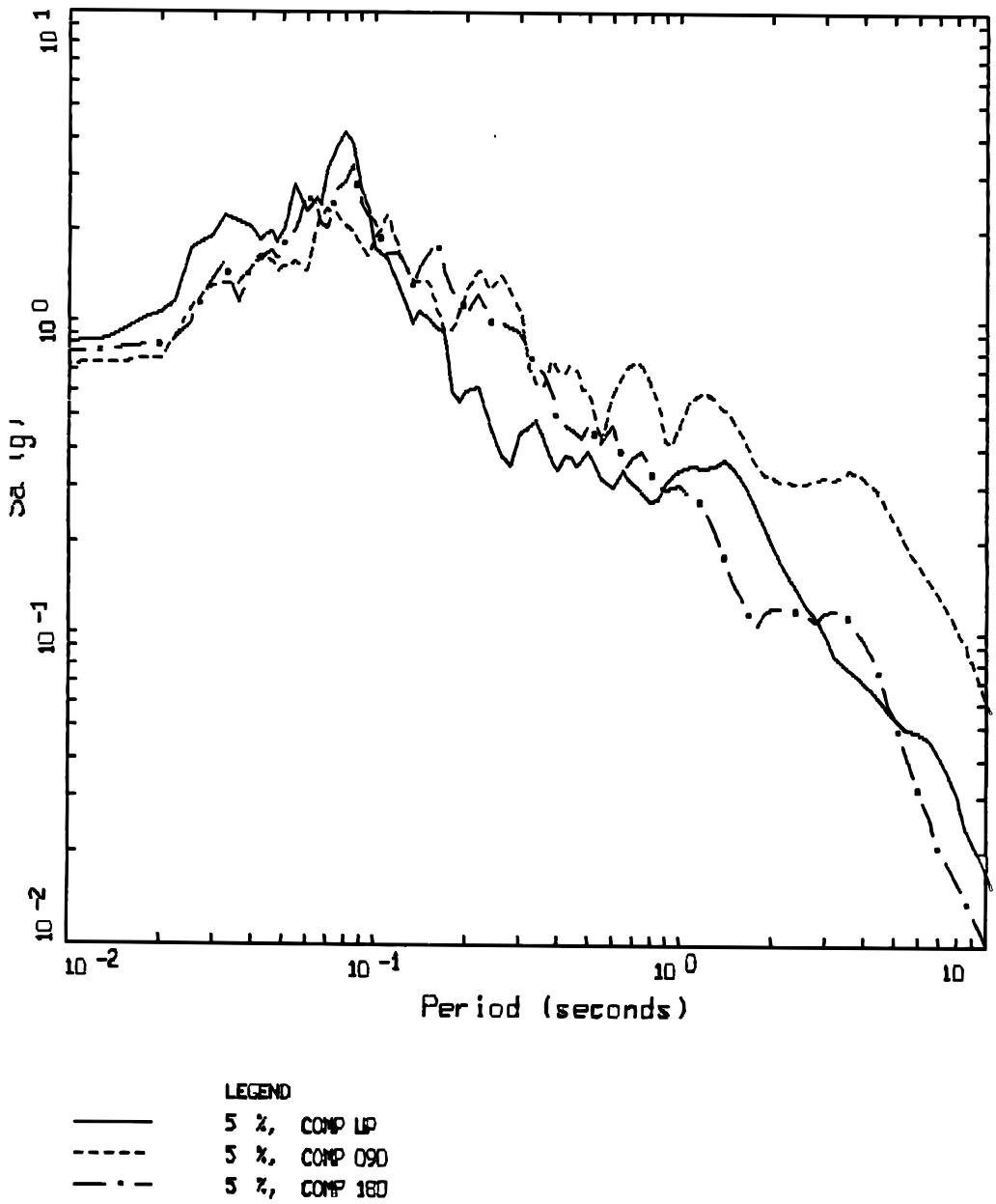

Source: Wong and Silva (2004a [DIRS 170443], SR 9, page 37)

Figure 6.2-67. Comparison of Vertical- and Horizontal-Component 5%-Damped Response Spectra for the Lucerne Recording of the 1992 **M** 7.3 Landers Earthquake

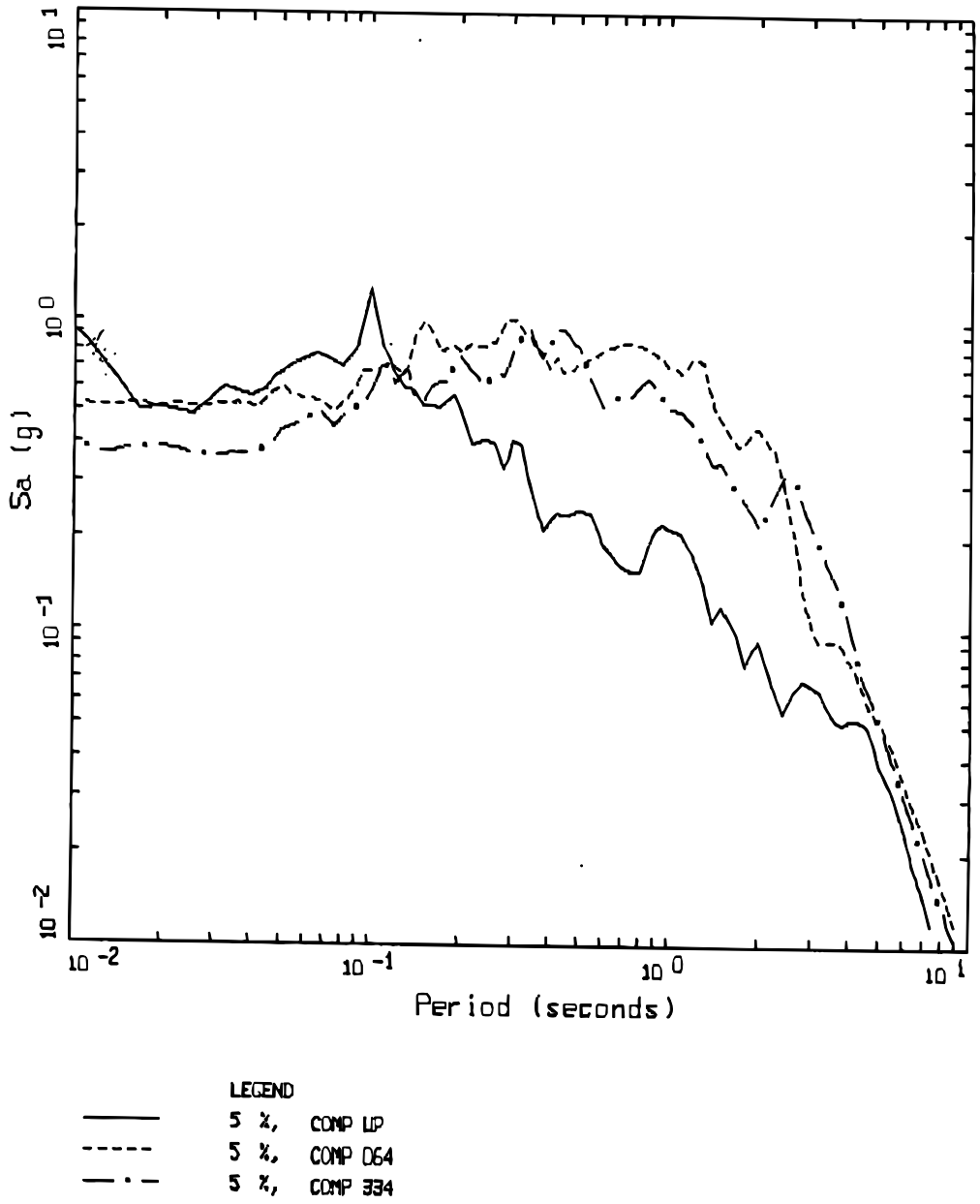

Source: Wong and Silva (2004a [DIRS 170443], SR 9, page 33)

Figure 6.2-68. Comparison of Vertical- and Horizontal-Component 5%-Damped Response Spectra for the Los Angeles Dam Recording of the 1994 **M** 6.7 Northridge Earthquake

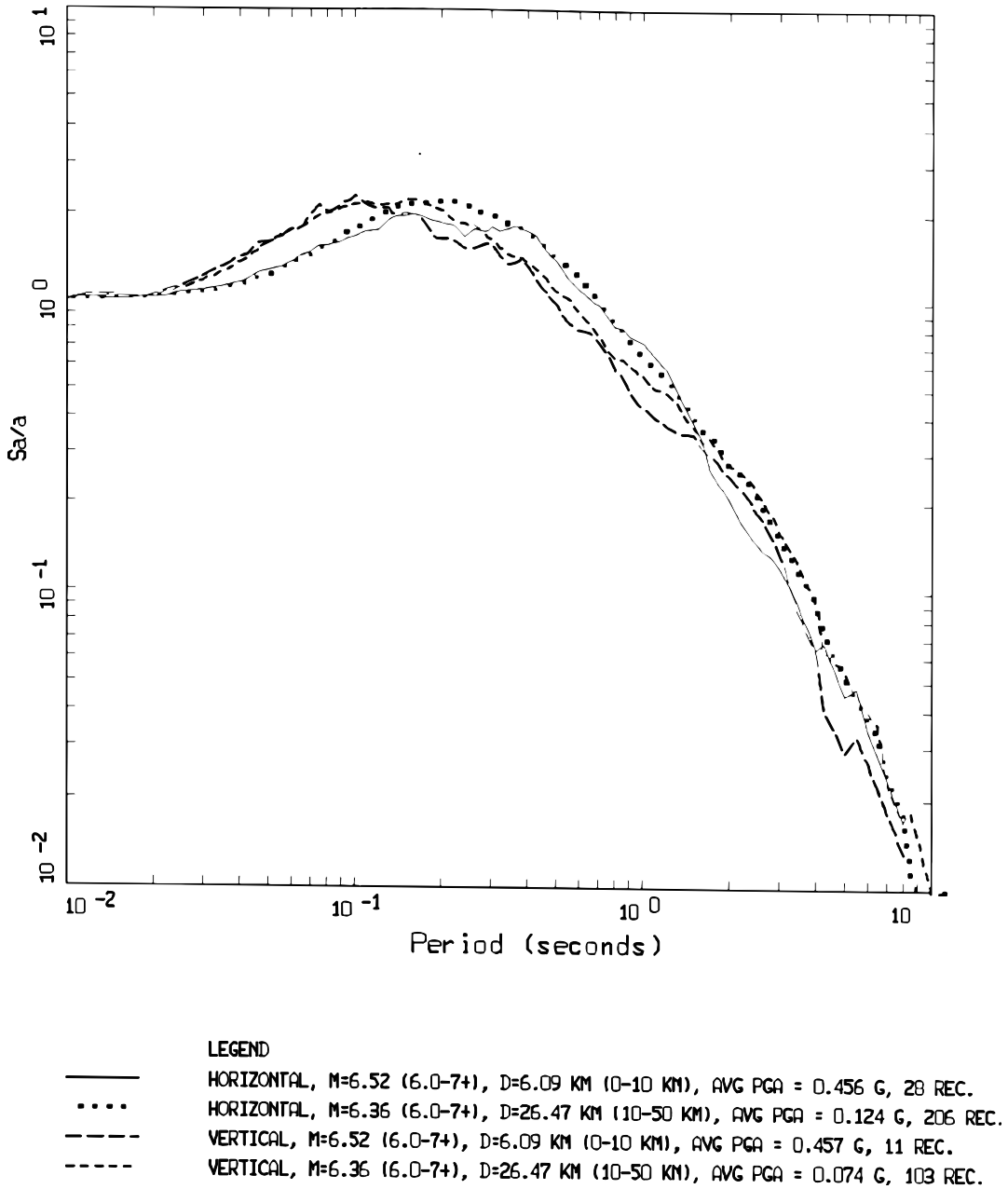

Source: Silva (1997 [DIRS 163747, Figure 21)

Figure 6.2-69. Median Response Spectral Shapes (5%-Damped) Computed from WUS Data Recorded at Rock Sites in the Range of **M** 6 to **M** 7+

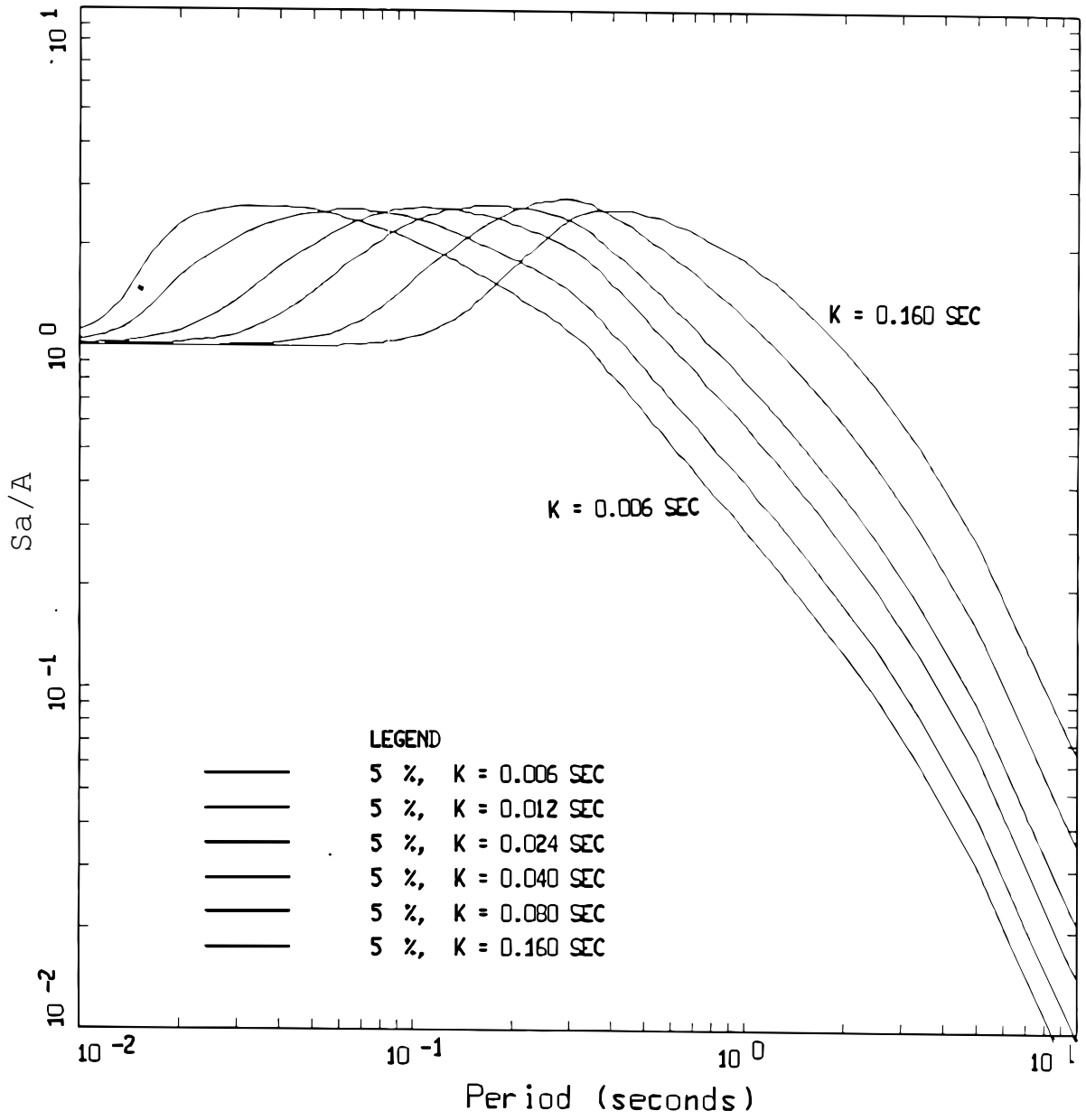

Source: Silva (1997 [DIRS 163747], Figure 20)

NOTE: As kappa increases, the peak shifts to longer periods and remains essentially constant in amplitude.

Figure 6.2-70. Effects of Kappa on 5%-Damped Response Spectral Shapes Computed for a **M** 6.5 Earthquake at 10 km (6 mi.) Using WUS Parameters

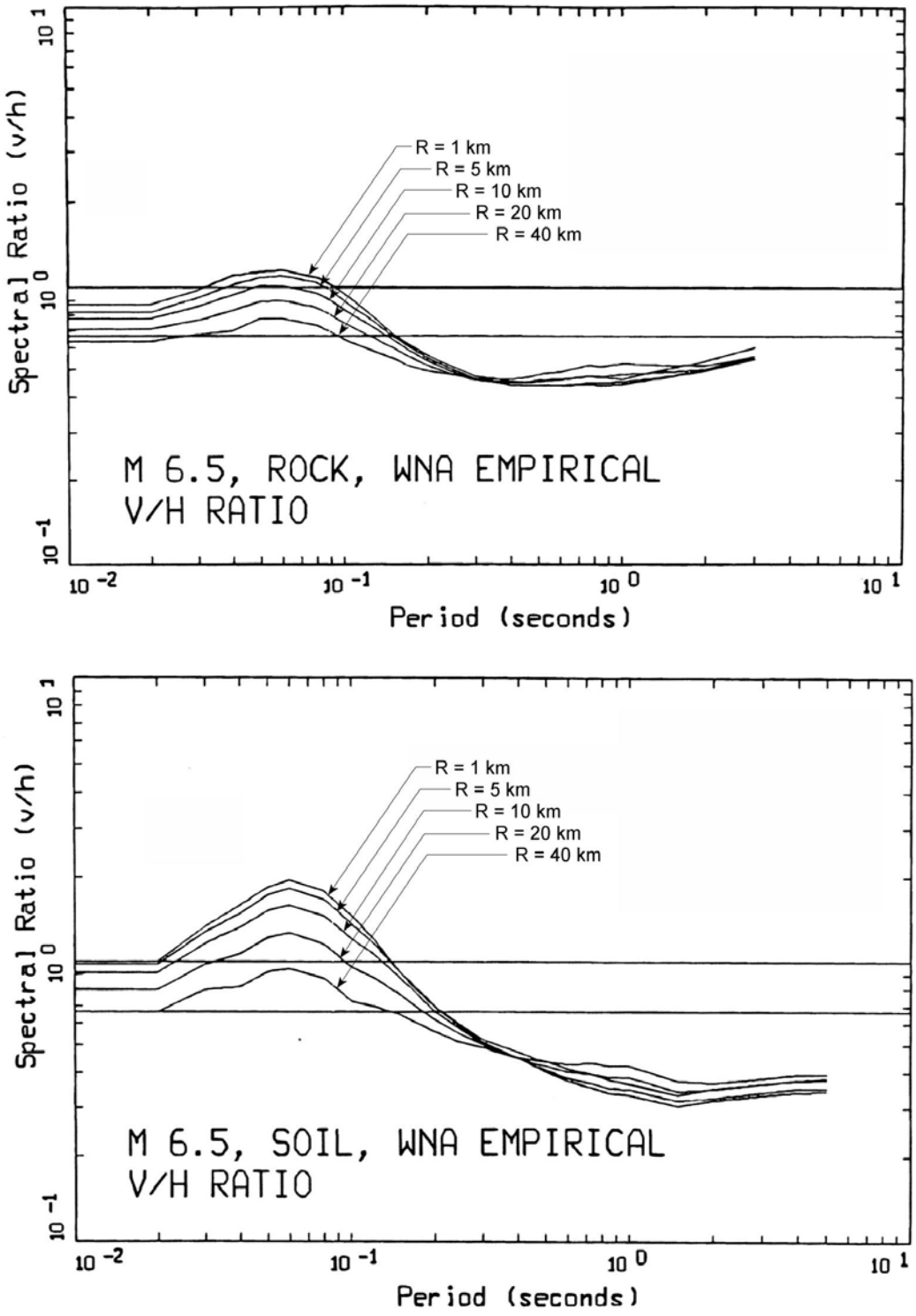

Source: Silva (1997 [DIRS 163747], Figure 26)

NOTE: Line at 0.66 indicates the constant ratio of 2/3.

Figure 6.2-71. Distance (Fault) Dependency of WUS Empirical Response Spectral Ratios (V/H) for **M** 6.5 at Rock and Soil Sites

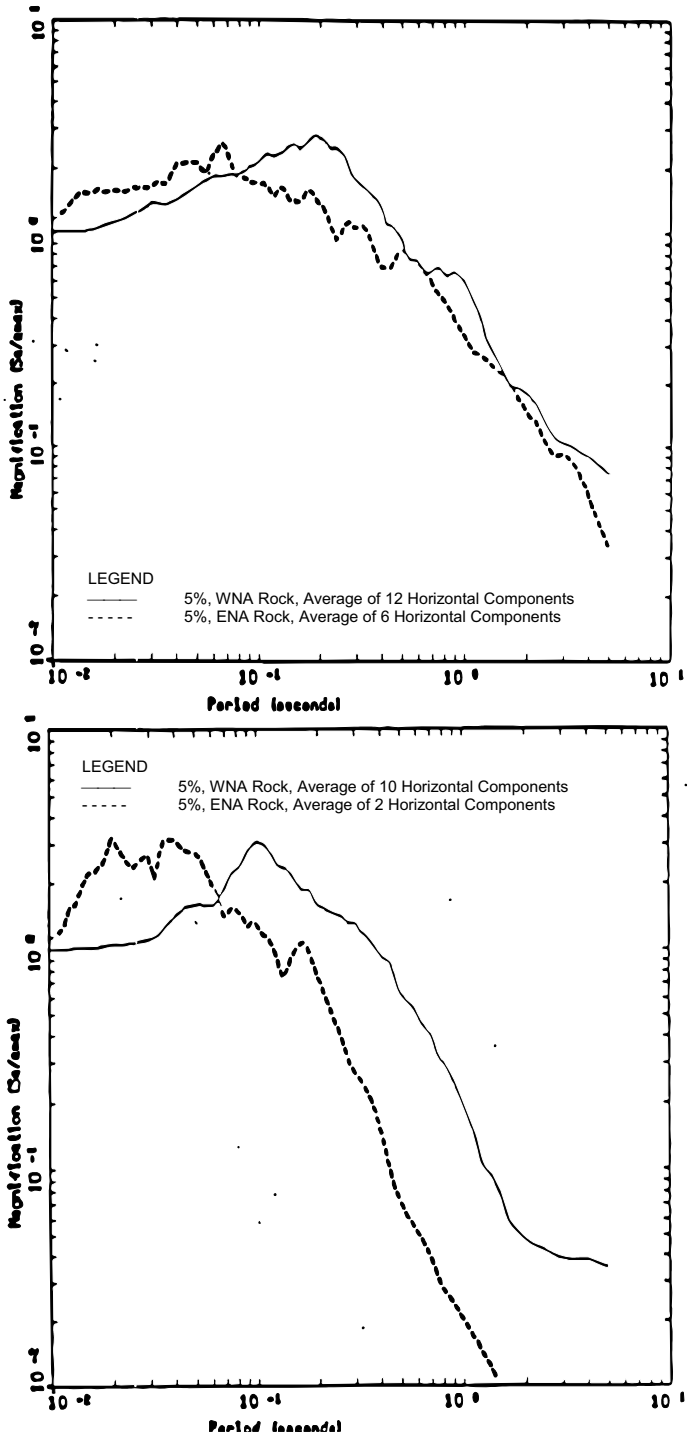

Source: Silva (1997 [DIRS 163747], Figure 24)

NOTE: In each figure, the solid line corresponds to motions recorded in WNA, dashed line to motions recorded in ENA.

Figure 6.2-72. Average 5%-Damped Response Spectral Shapes (Sa/a) Computed from Motions Recorded on Rock Sites at Close Distances to **M** 6.4 (top) and **M** 4.0 Earthquakes (bottom)

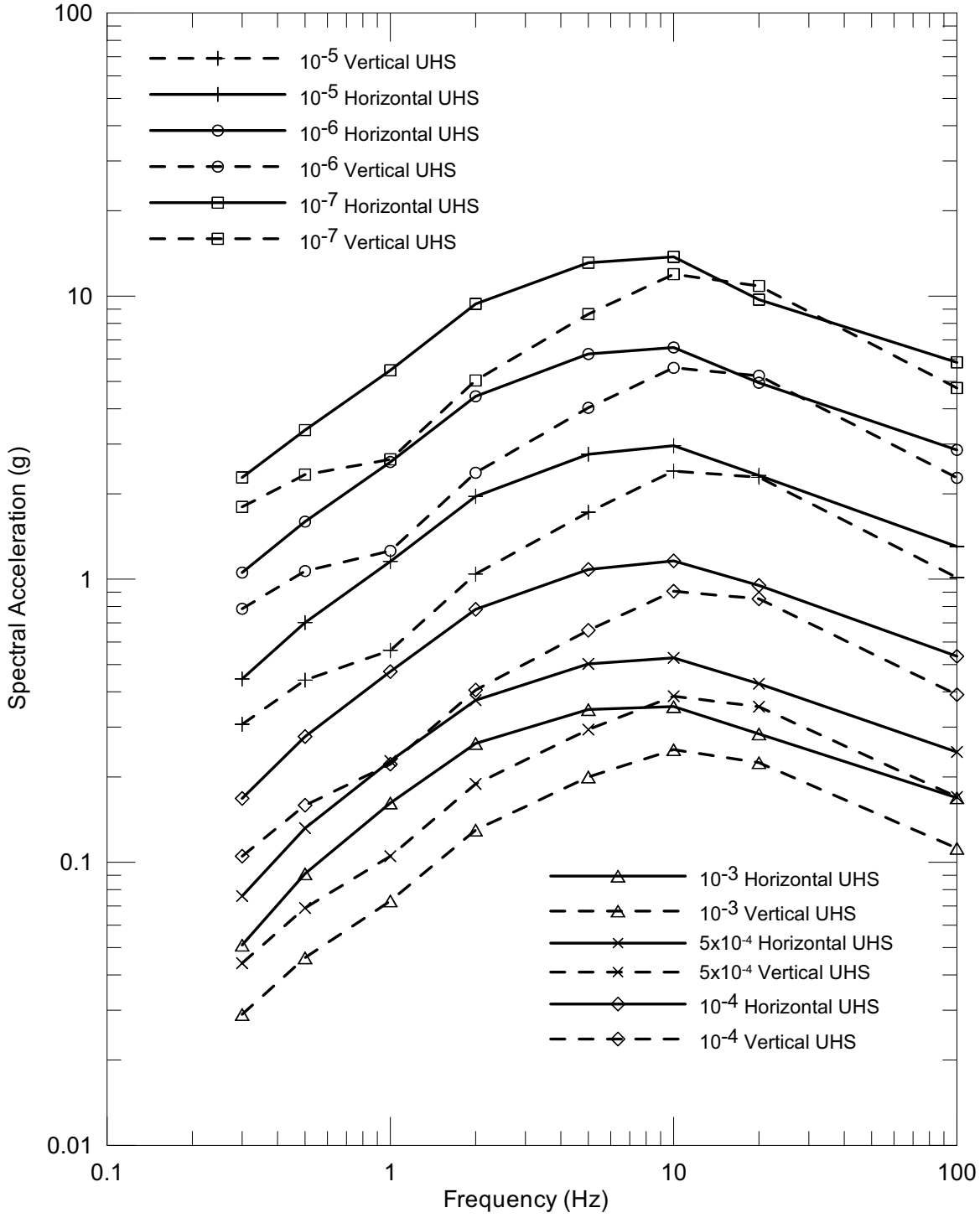

DTN: MO0401MWDRPSHA.000 [DIRS 166962], ,
MO0208UNHZ5X10.000 [DIRS 163722], MO0308UNHAZ105.000 [DIRS 170425],
MO0206UNHAZ106.001 [DIRS 163723], MO0209UNHAZ107.000 [DIRS 163724]

Figure 6.2-73. Mean Point A Vertical and Horizontal 5%-Damped Response Spectra for Annual Frequencies of Exceedance of 10^{-3}, $5x10^{-4}$, 10^{-4}, 10^{-5}, 10^{-6}, and 10^{-7}

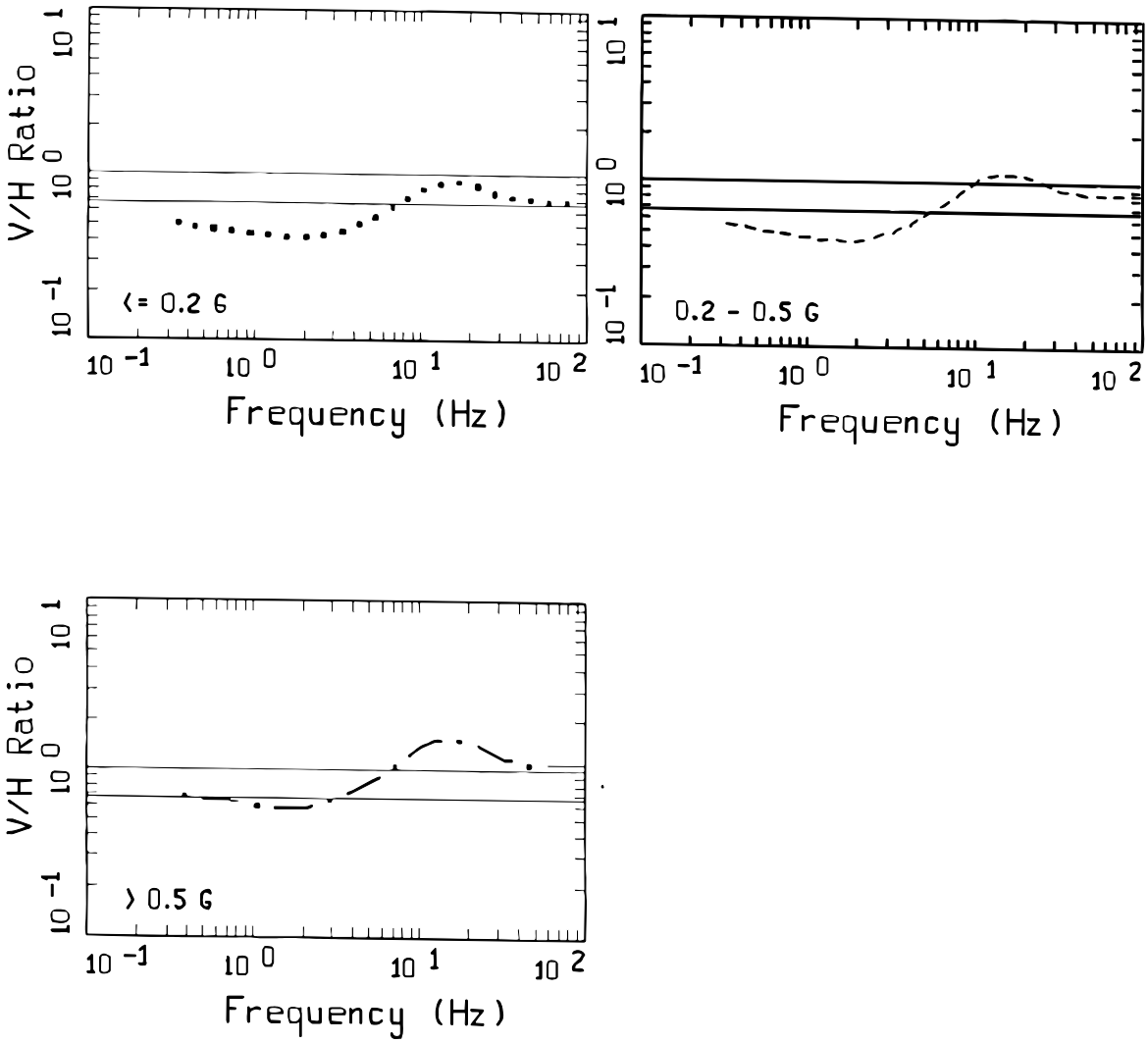

Source: McGuire et al. (2001 [DIRS 157510], Table 4-4, Figure 4-36)

Figure 6.2-74. V/H Spectral Ratios for Loading Levels of < 0.2g, 0.2-0.5g and > 0.5g for Western U.S. Rock (Soft Rock Conditions)

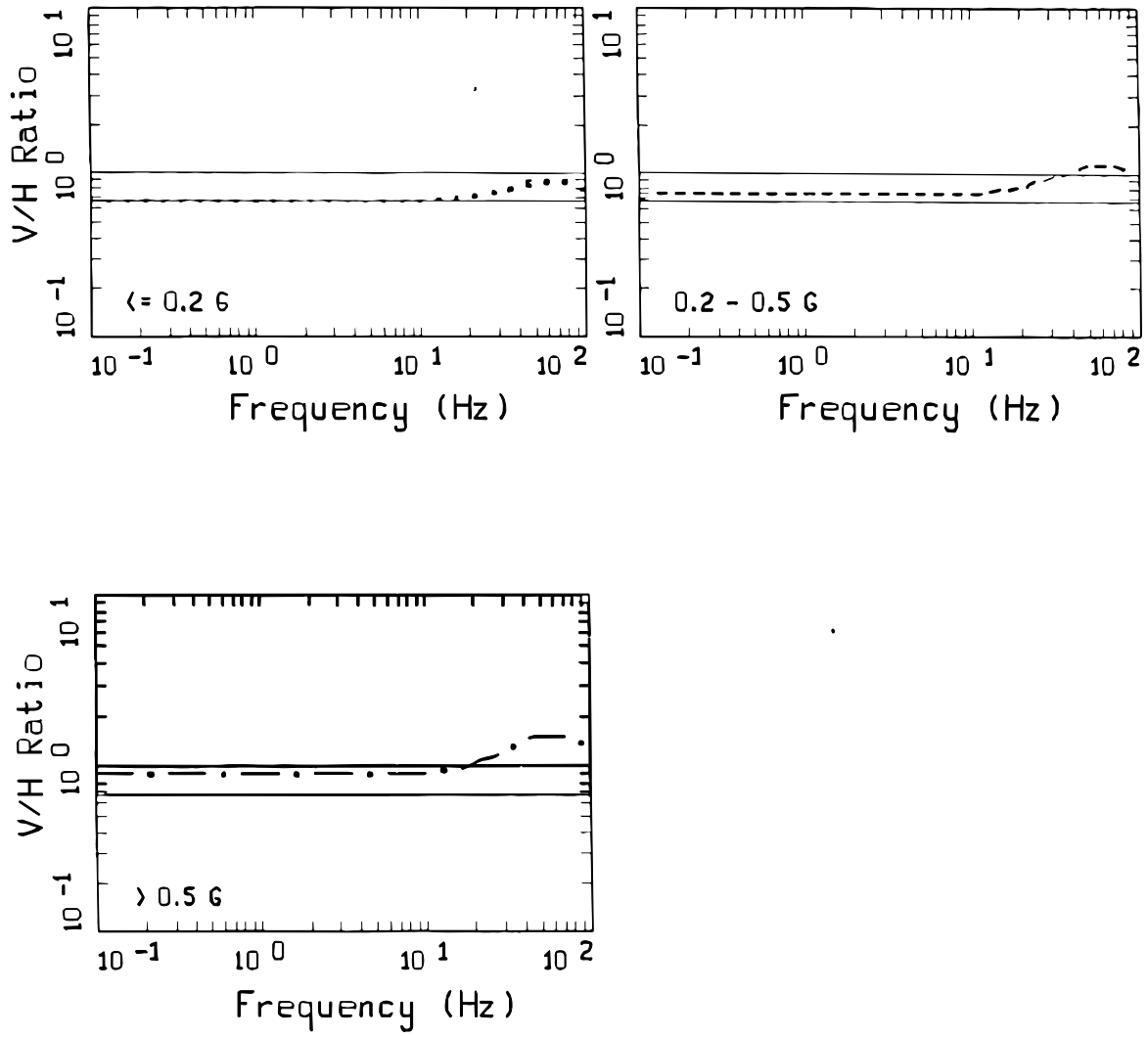

Source: McGuire et al. (2001 [DIRS 157510], Table 4-5, Figure 4-39)

Figure 6.2-75. V/H Spectral Ratios for Loading Levels of < 0.2g, 0.2-0.5g and > 0.5g for Central and Eastern U.S. Rock (Hard-Rock Conditions)

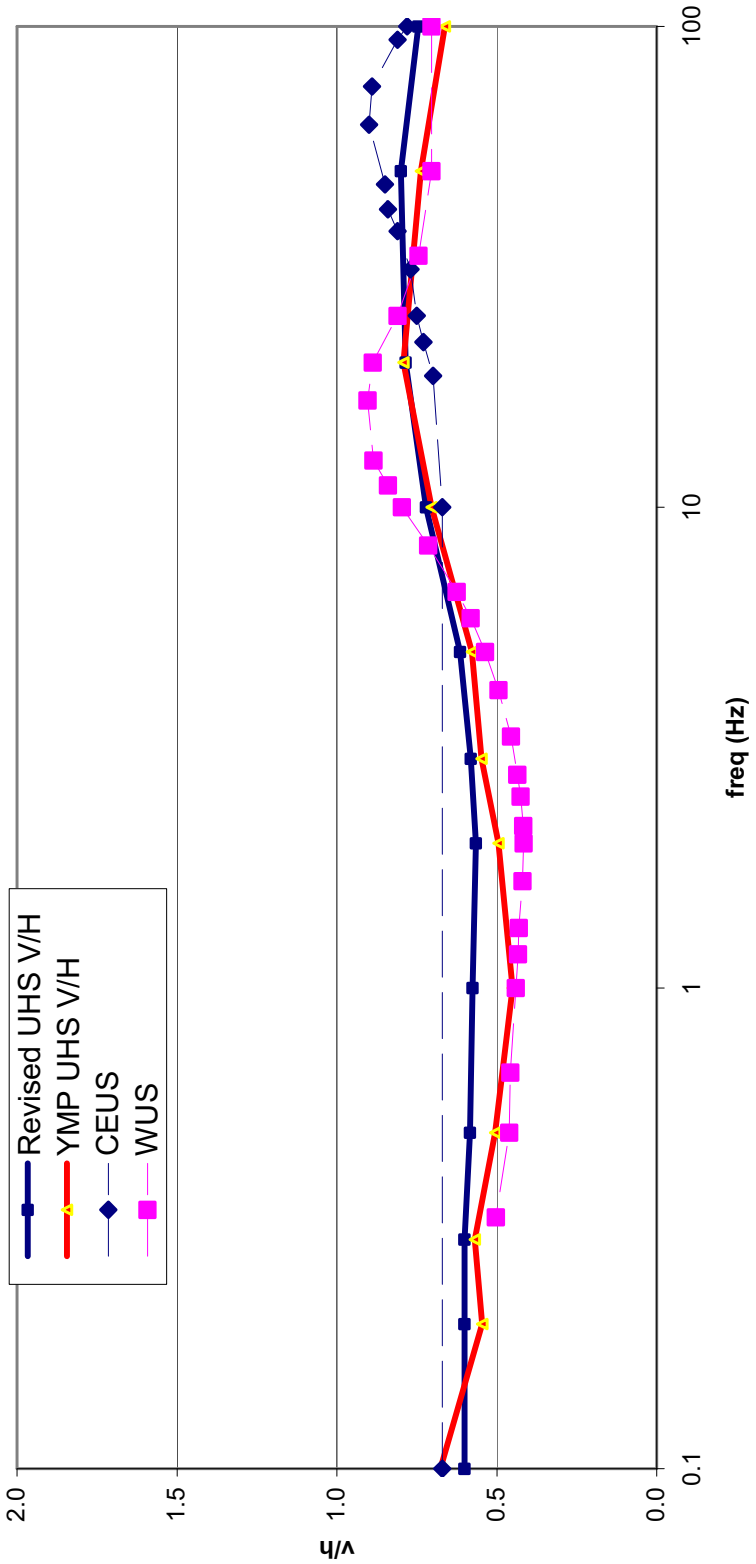

Source: Appendix I, Filename: \10-3\vertic3.xls(p-ceus(3))

Figure 6.2-76. Comparison of 10^{-3} UHS V/H with Revised UHS V/H and with CEUS and WUS V/H Recommendations from NUREG/CR-6728 (McGuire et al. 2001 [DIRS 157510], Tables 4-4 and 4-5, Figures 4-36 and 4-39)

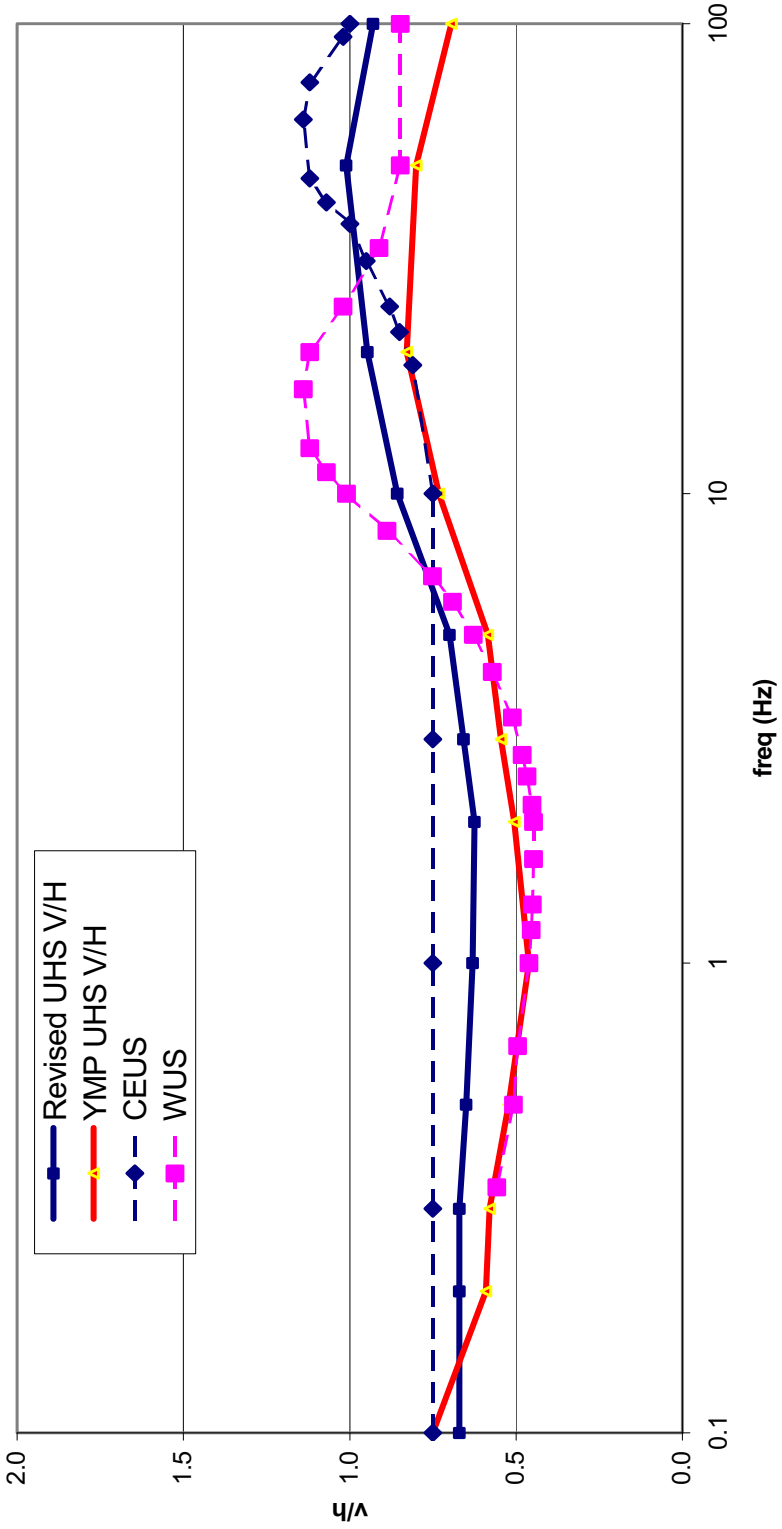

Source: Appendix I, Filename: \5e-4\VERT5-4.xls(p-ceus(3))

Figure 6.2-77. Comparison of 5×10^{-4} UHS V/H with Revised UHS V/H and with CEUS and WUS V/H Recommendations from NUREG/CR-6728 (McGuire et al. 2001 [DIRS 157510], Tables 4-4 and 4-5, Figures 4-36 and 4-39)

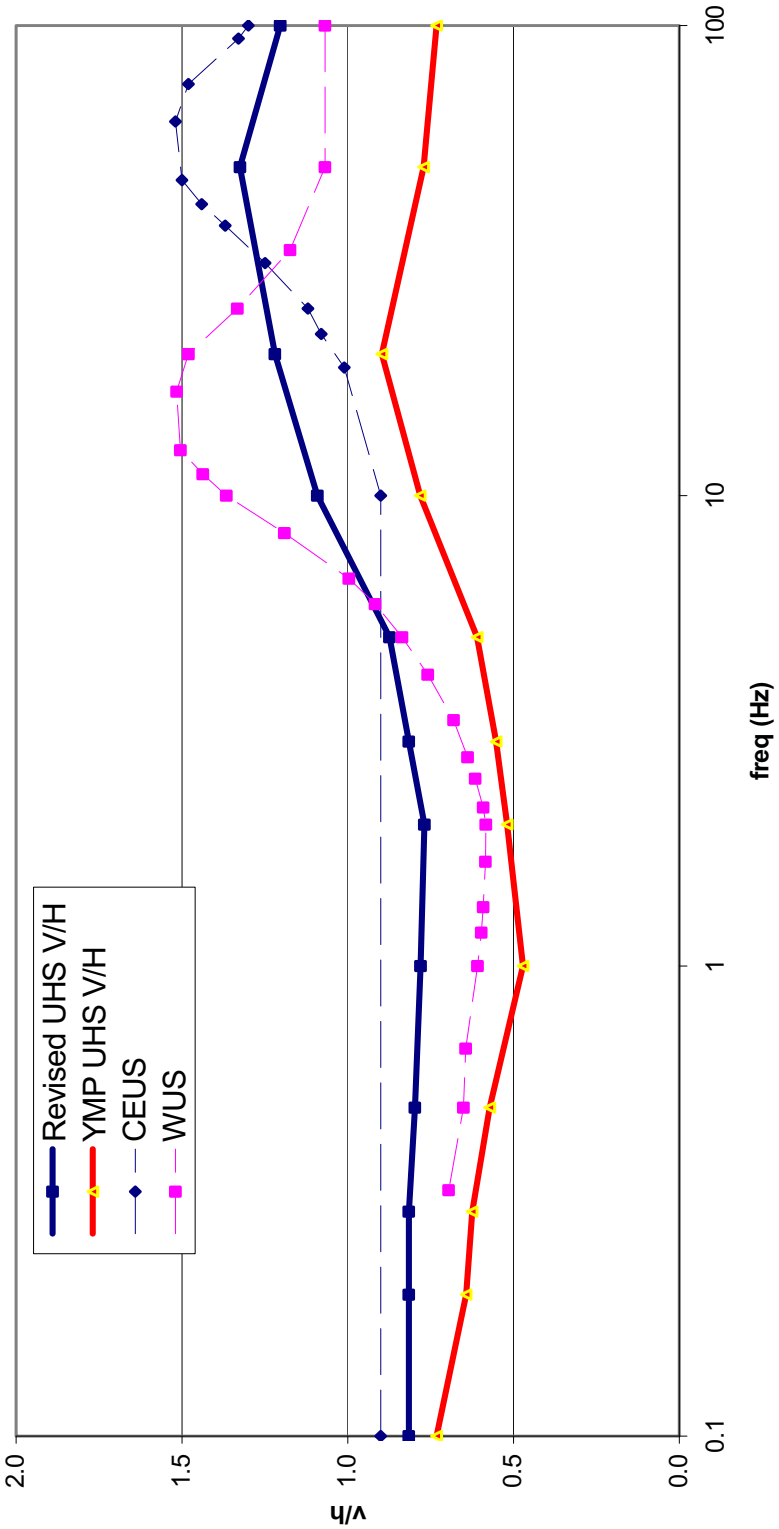

Source: Appendix I, Filename: \10-4\VERTIC4.xls(p-ceus(3))

Figure 6.2-78. Comparison of 10^{-4} UHS V/H with Revised UHS V/H and with CEUS and WUS V/H Recommendations from NUREG/CR-6728 (McGuire et al. 2001 [DIRS 157510], Tables 4-4 and 4-5, Figures 4-36 and 4-39)

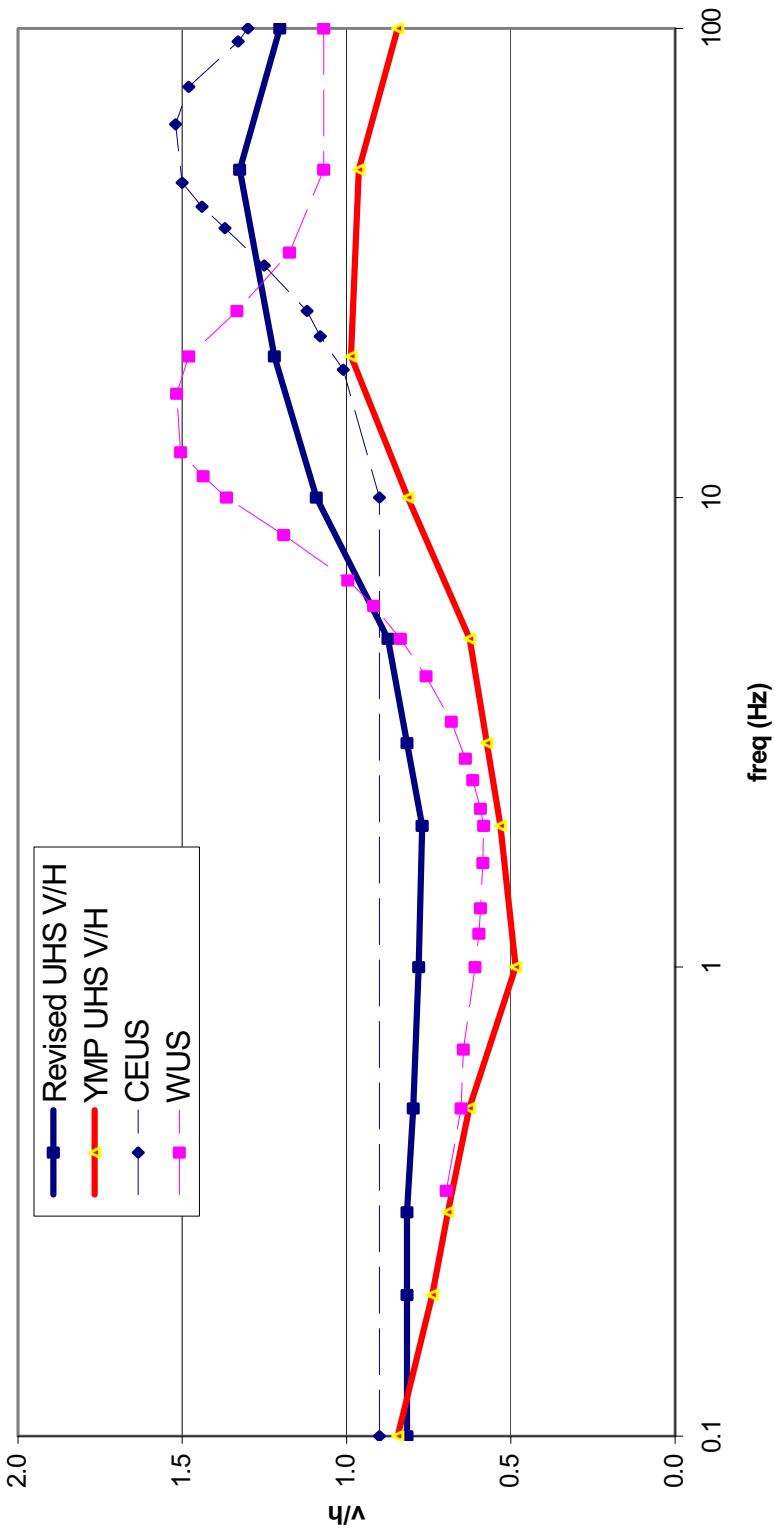

Source: Appendix I, Filename: \10-5\VERTIC5.xls(p-ceus(3))

Figure 6.2-79. Comparison of 10^{-5} UHS V/H with Revised UHS V/H and with CEUS and WUS V/H Recommendations from NUREG/CR-6728 (McGuire et al. 2001 [DIRS 157510], Tables 4-4 and 4-5, Figures 4-36 and 4-39)

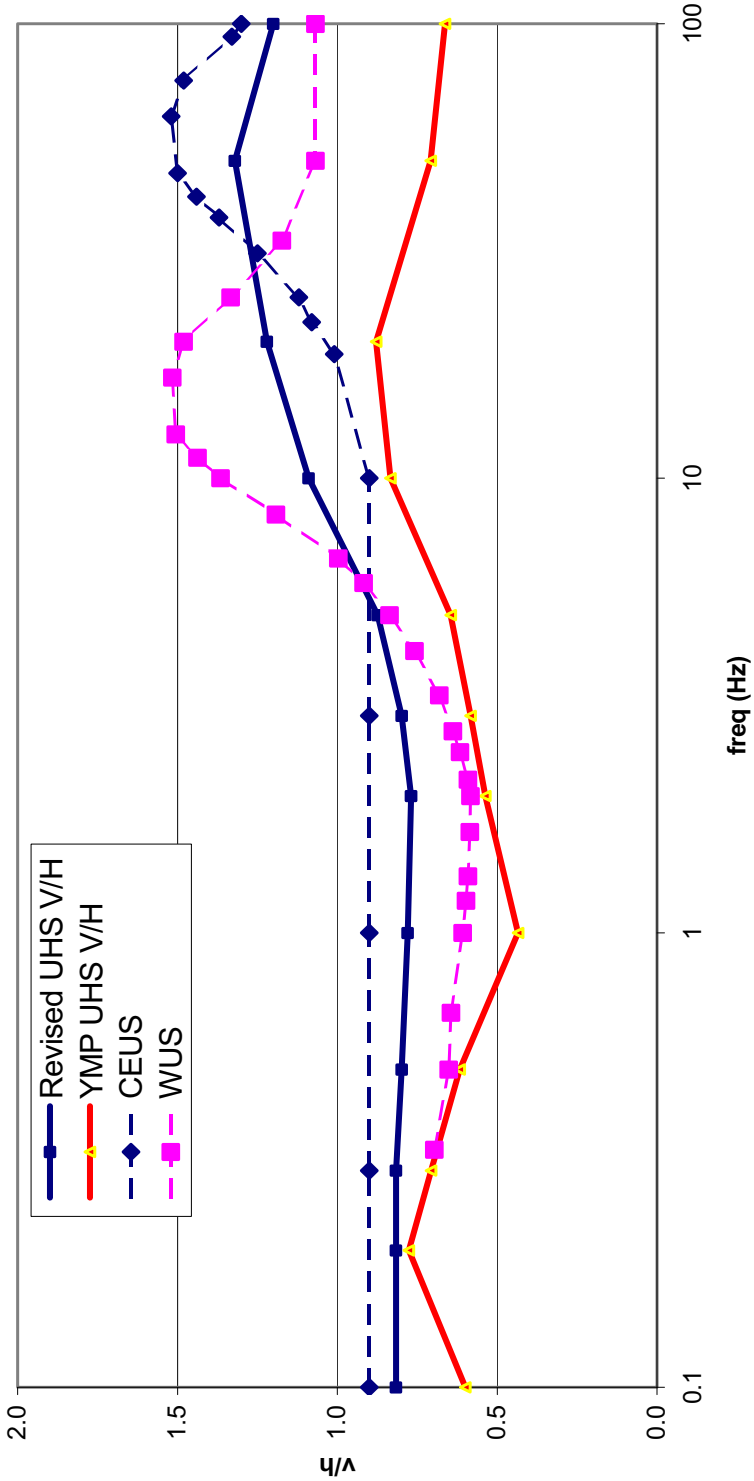

Source: Appendix I, Filename: \10-6\VERTICA1.xls(p-ceus(3))rev

Figure 6.2-80. Comparison of 10^{-6} UHS V/H with Revised UHS V/H and with CEUS and WUS V/H Recommendations NUREG/CR-6728 (McGuire et al. 2001 [DIRS 157510], Tables 4-4 and 4-5, Figures 4-36 and 4-39)

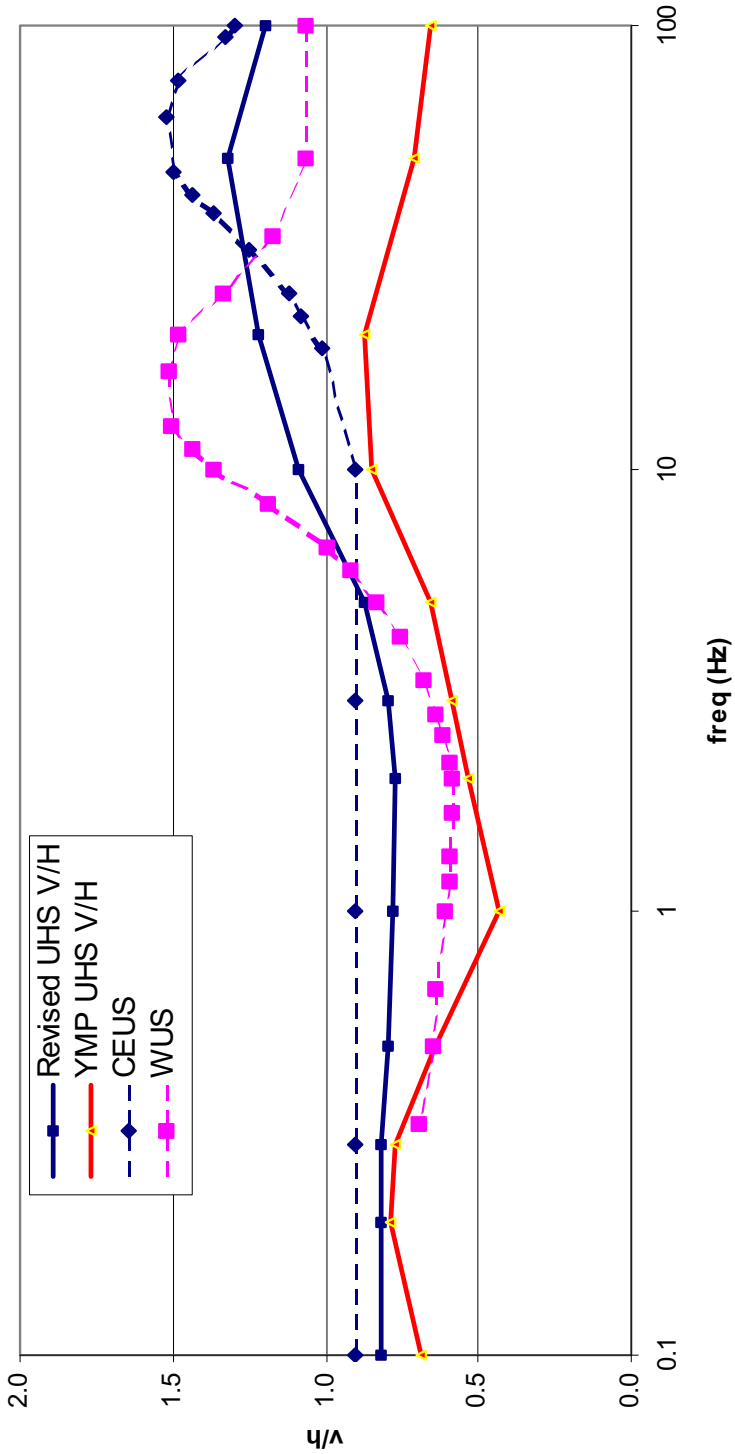

Source: Appendix I, Filename: \10-7\VERTICA1.xls(p-ceus(3)rev)

Figure 6.2-81. Comparison of 10^{-7} UHS V/H with Revised UHS V/H and with CEUS and WUS V/H Recommendations NUREG/CR-6728 (McGuire et al. 2001 [DIRS 157510], Tables 4-4 and 4-5, Figures 4-36 and 4-39)

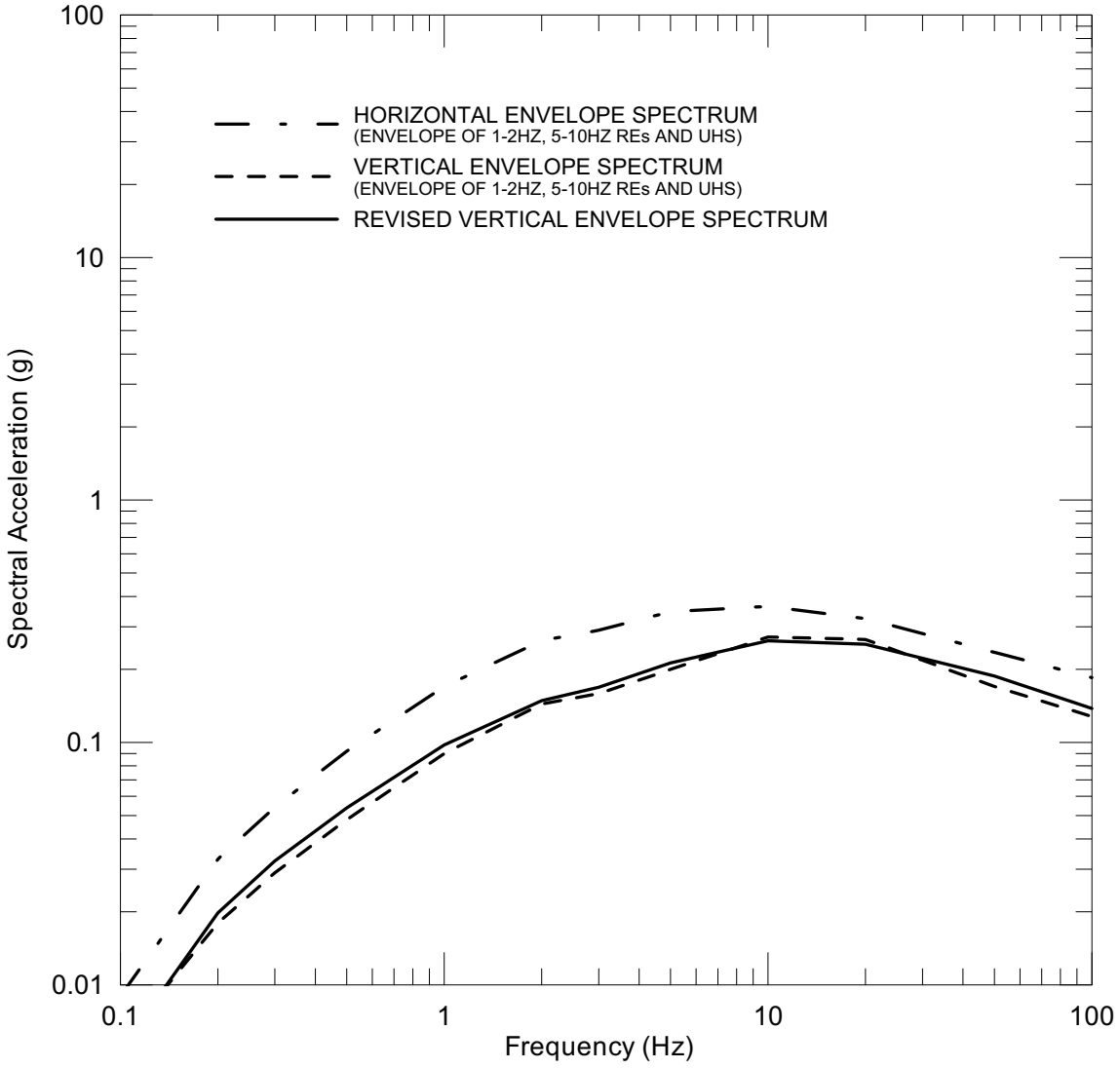

Source: Appendix I, Filename: \10-3\vertic3.xls(p-targetuhs1)

Figure 6.2-82. Comparison of Revised Point A Vertical Envelope Spectrum to the Point A Horizontal Envelope and Original Vertical Envelope Spectra for an Annual Exceedance Frequency of 10^{-3}

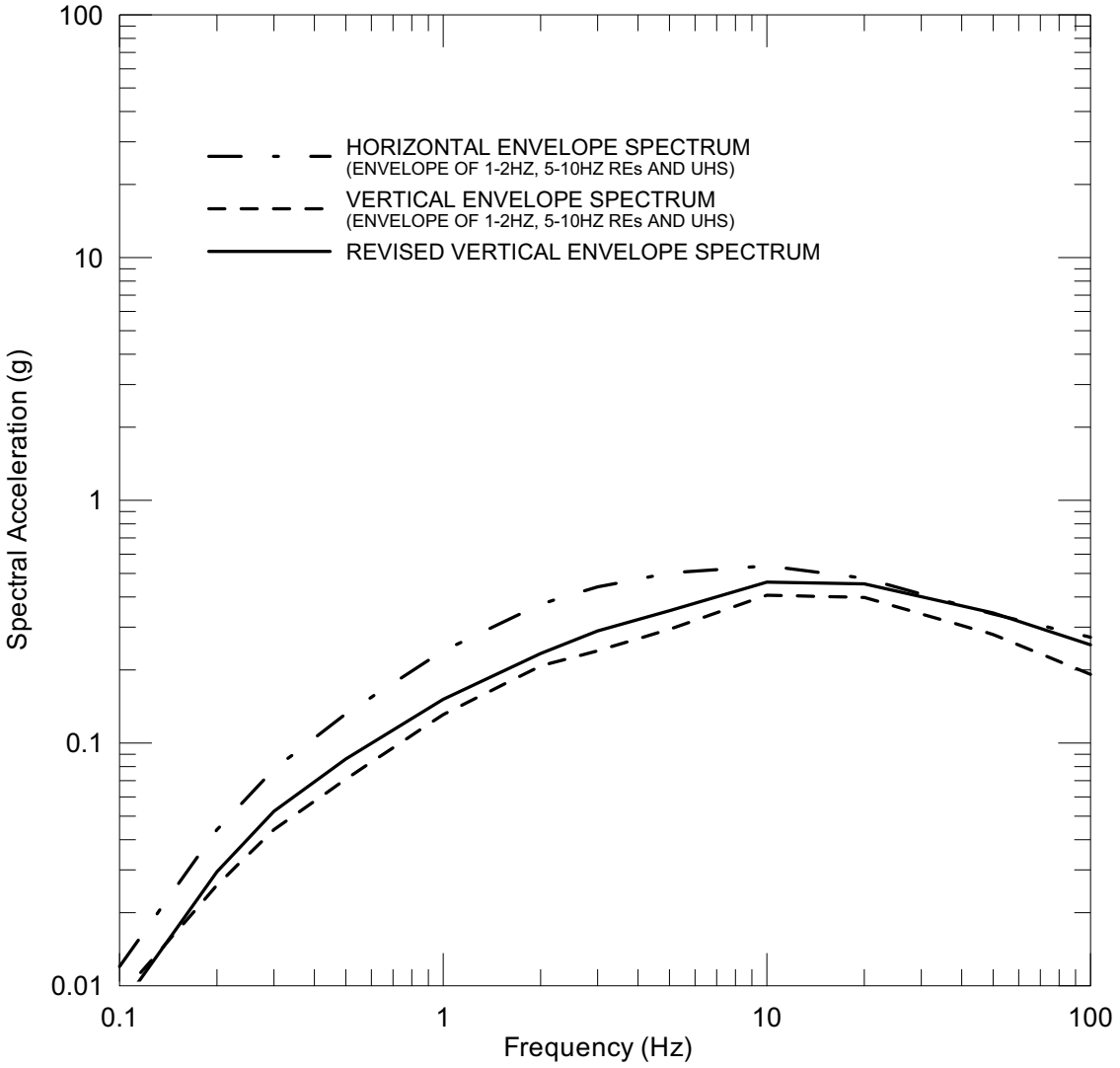

Source: Appendix I, Filename: \53-4\vert5-4.xls(p-targetuhs)

Figure 6.2-83. Comparison of Revised Point A Vertical Envelope Spectrum to the Point A Horizontal Envelope and Original Vertical Envelope Spectra for an Annual Exceedance Frequency of 5×10^{-4}

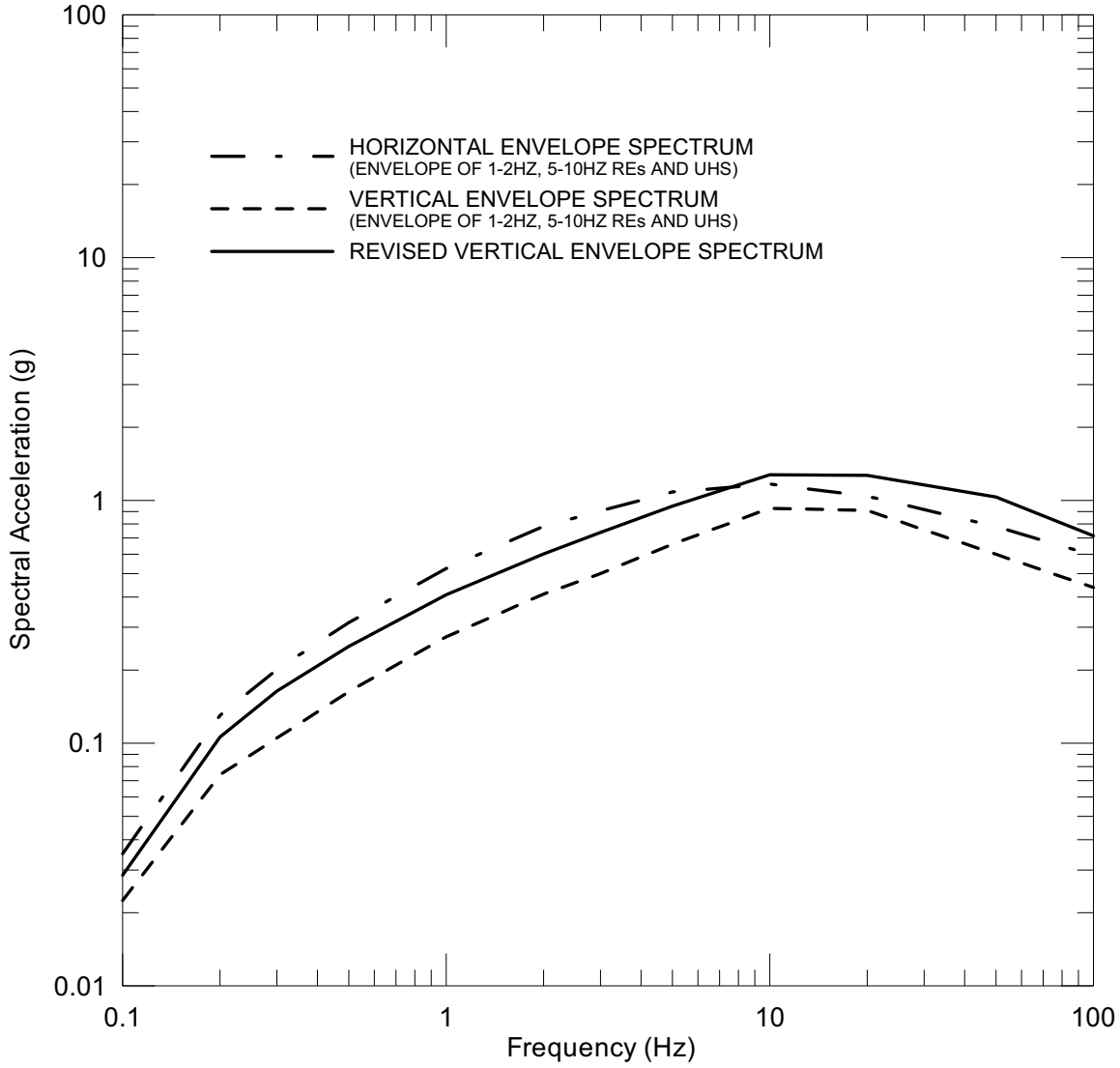

Source: Appendix I, Filename: \10-4\vertic4.xls(p-targetuhs)

Figure 6.2-84. Comparison of Revised Point A Vertical Envelope Spectrum to the Point A Horizontal Envelope and Original Vertical Envelope Spectra for an Annual Exceedance Frequency of 10^{-4}

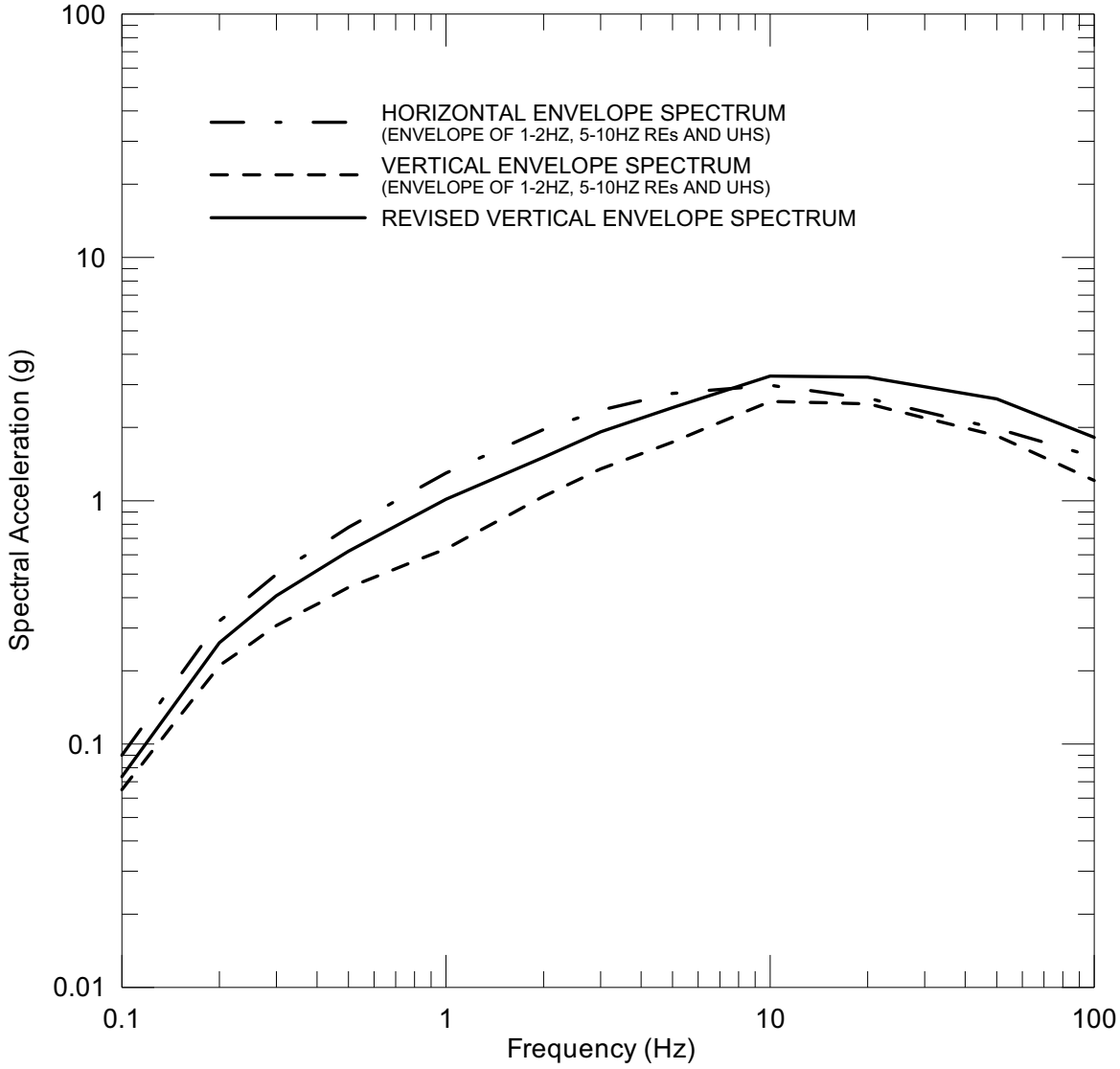

Source: Appendix I, Filename: \10-5\vertic5.xls(p-targetuhs)

Figure 6.2-85. Comparison of Revised Point A Vertical Envelope Spectrum to the Point A Horizontal Envelope and Original Vertical Envelope Spectra for an Annual Exceedance Frequency of 10^{-5}

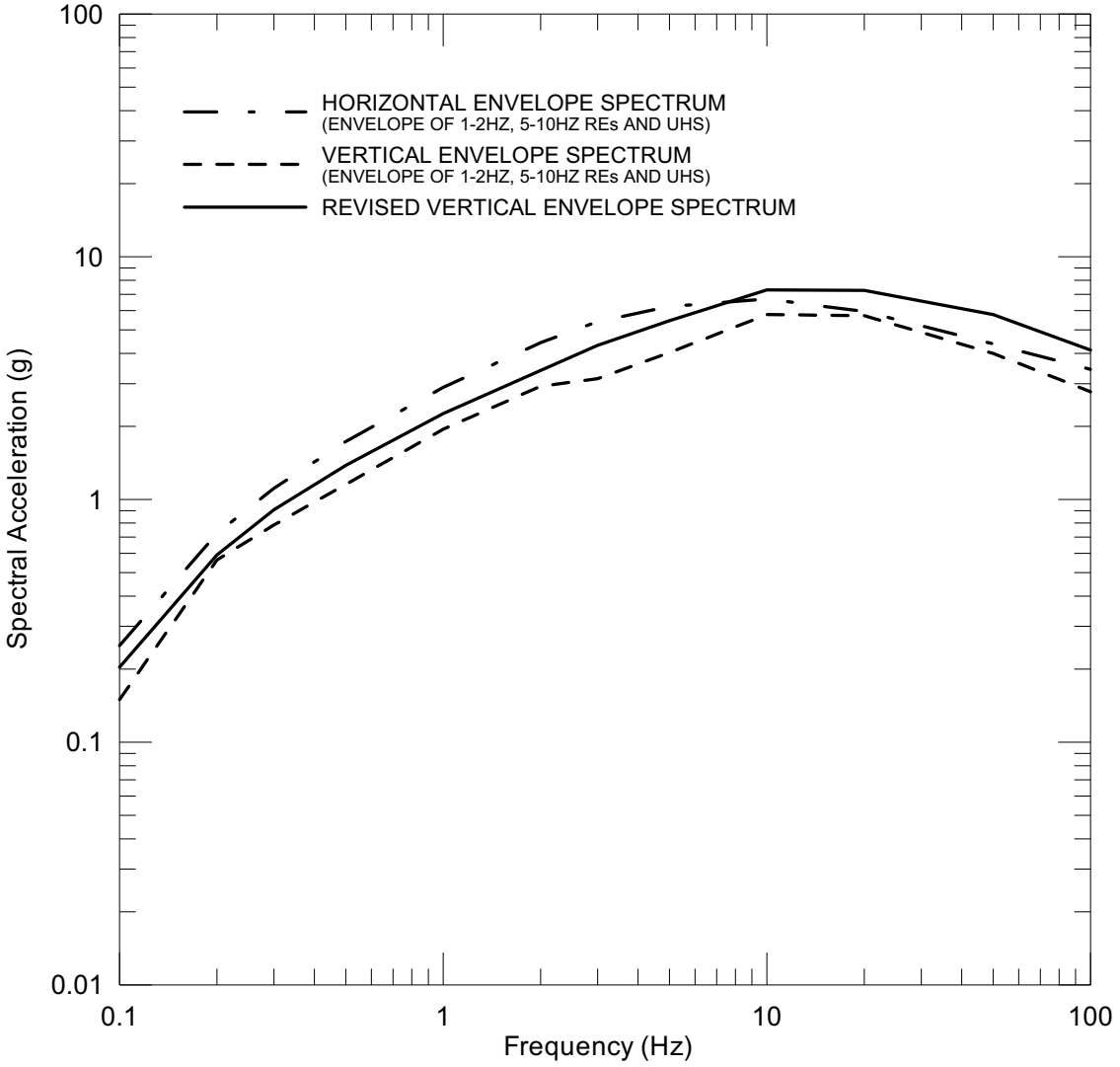

Source: Appendix I, Filename: \10-6\vertica1.xls(p-targetuhs1)

Figure 6.2-86. Comparison of Revised Point A Vertical Envelope Spectrum to the Point A Horizontal Envelope and Original Vertical Envelope Spectra for an Annual Exceedance Frequency of 10^{-6}

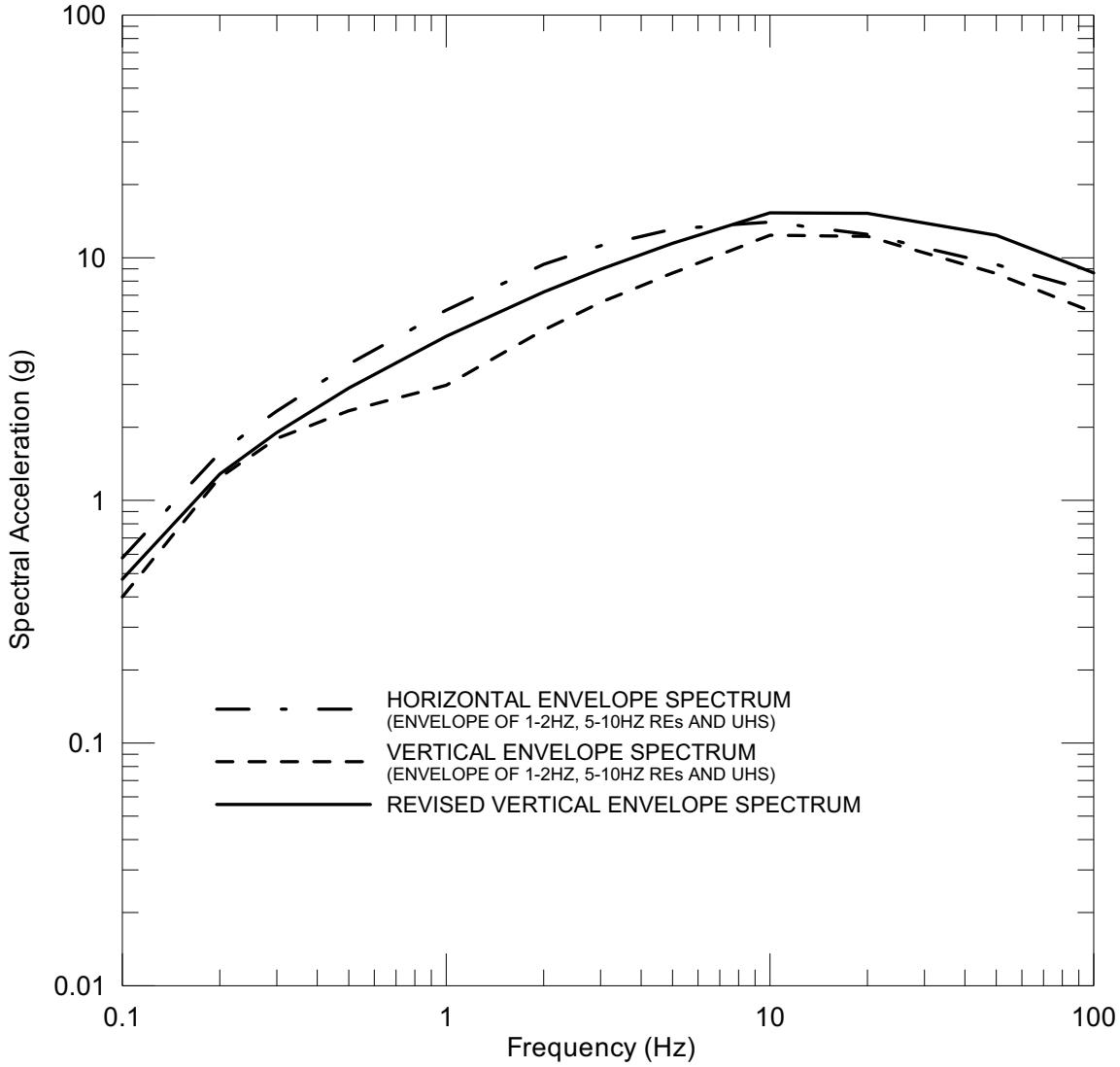

Source: Appendix I, Filename: \10-7\vertica1.xls(p-targetuhs1)

Figure 6.2-87. Comparison of Revised Point A Vertical Envelope Spectrum to the Point A Horizontal Envelope and Original Vertical Envelope Spectra for an Annual Exceedance Frequency of 10^{-7}

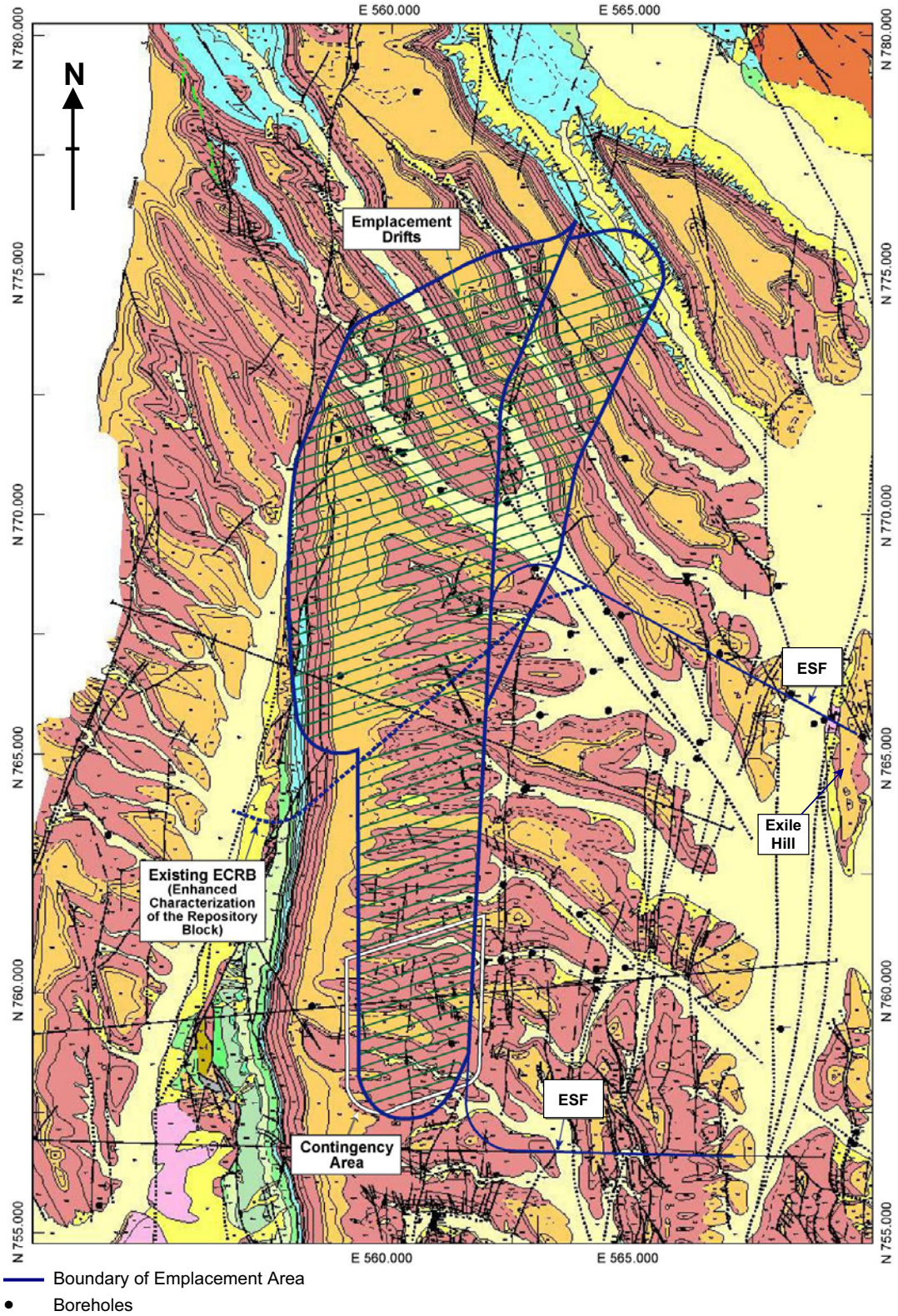

Source: BSC 2002b [DIRS 157756], Figures 4-5 and 5-4

NOTES: 1) The Waste Handling Buildings (WHB) area, depicted in Figure 6.2-89, is located just to the east of Exile Hill.
2) Not to scale.

Figure 6.2-88. Map of Subsurface Emplacement Area Layout

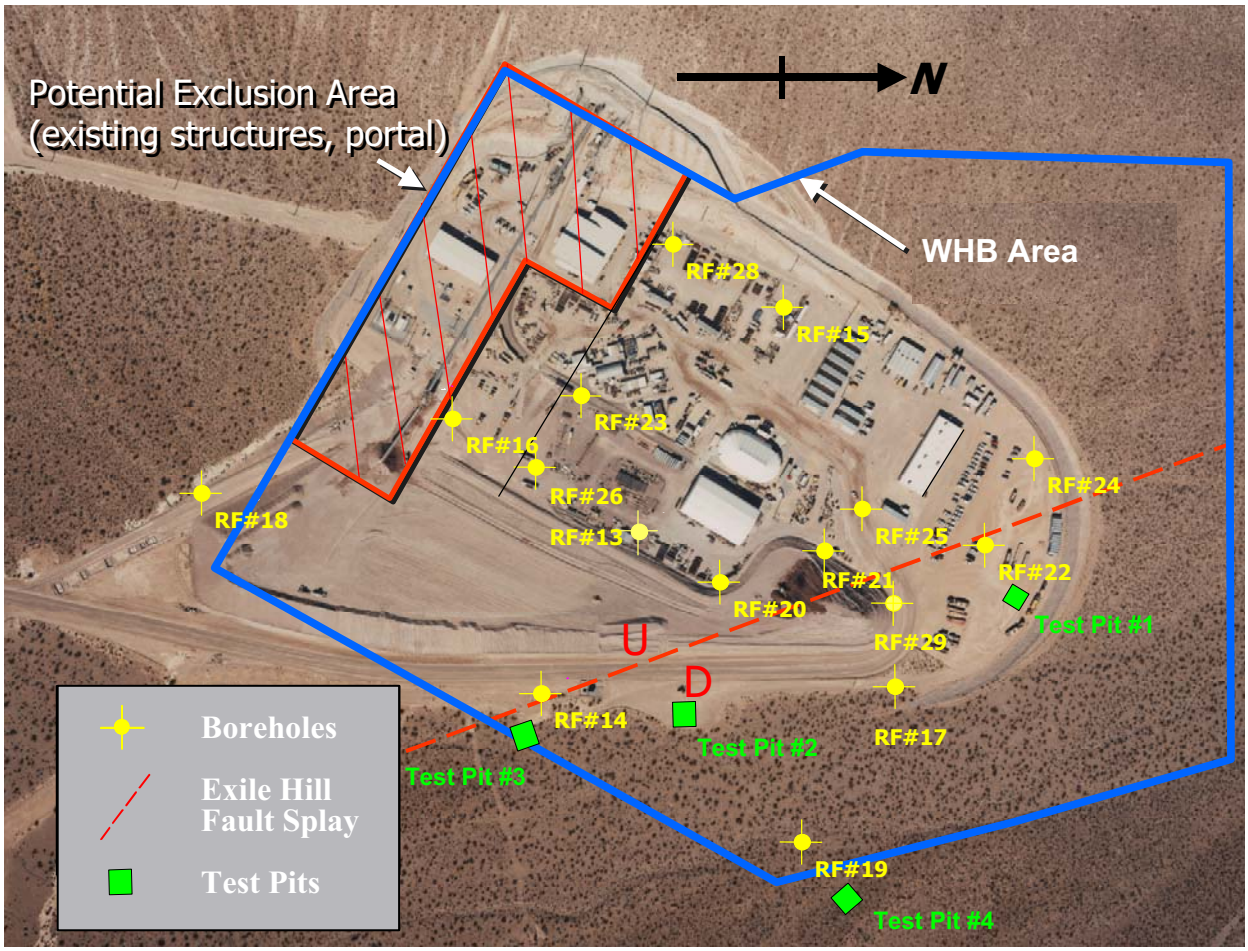

NOT TO SCALE

Source: BSC 2002a [DIRS 157829], Figures 2 and 3, YMP Photograph #BN8811_50

NOTE: "U" and "D" signify the upthrown and downthrown sides, respectively, of the Exile Hill fault splay.

Figure 6.2-89. WHB Area and Locations of Boreholes and Test Pits

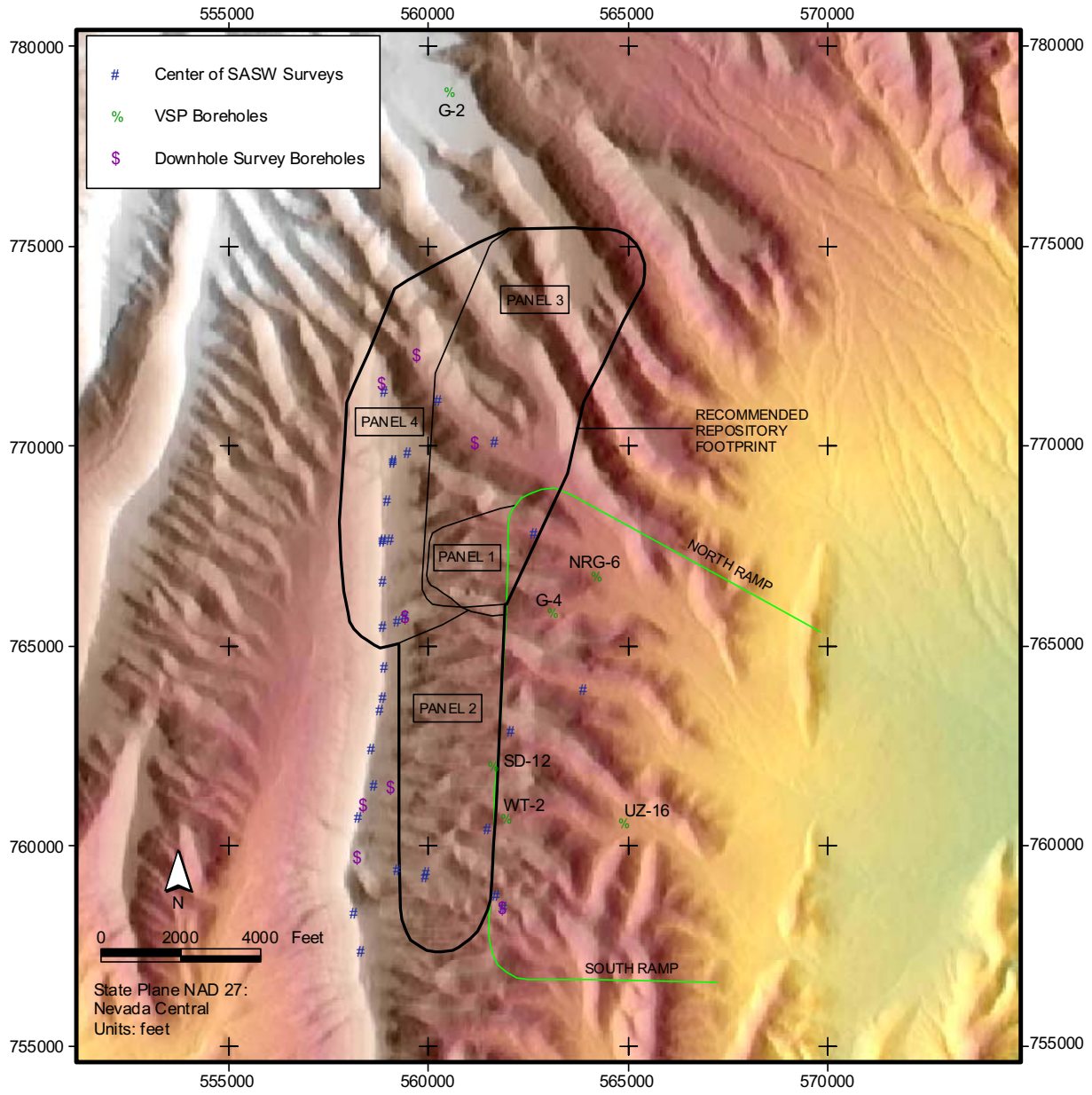

Source: Wong and Silva 2003 [DIRS 163201], Figure 1

Figure 6.2-90. Repository Panel Layout for the Emplacement Area and Locations of SASW, Downhole Velocity, and VSP Surveys on or Near the Repository Block

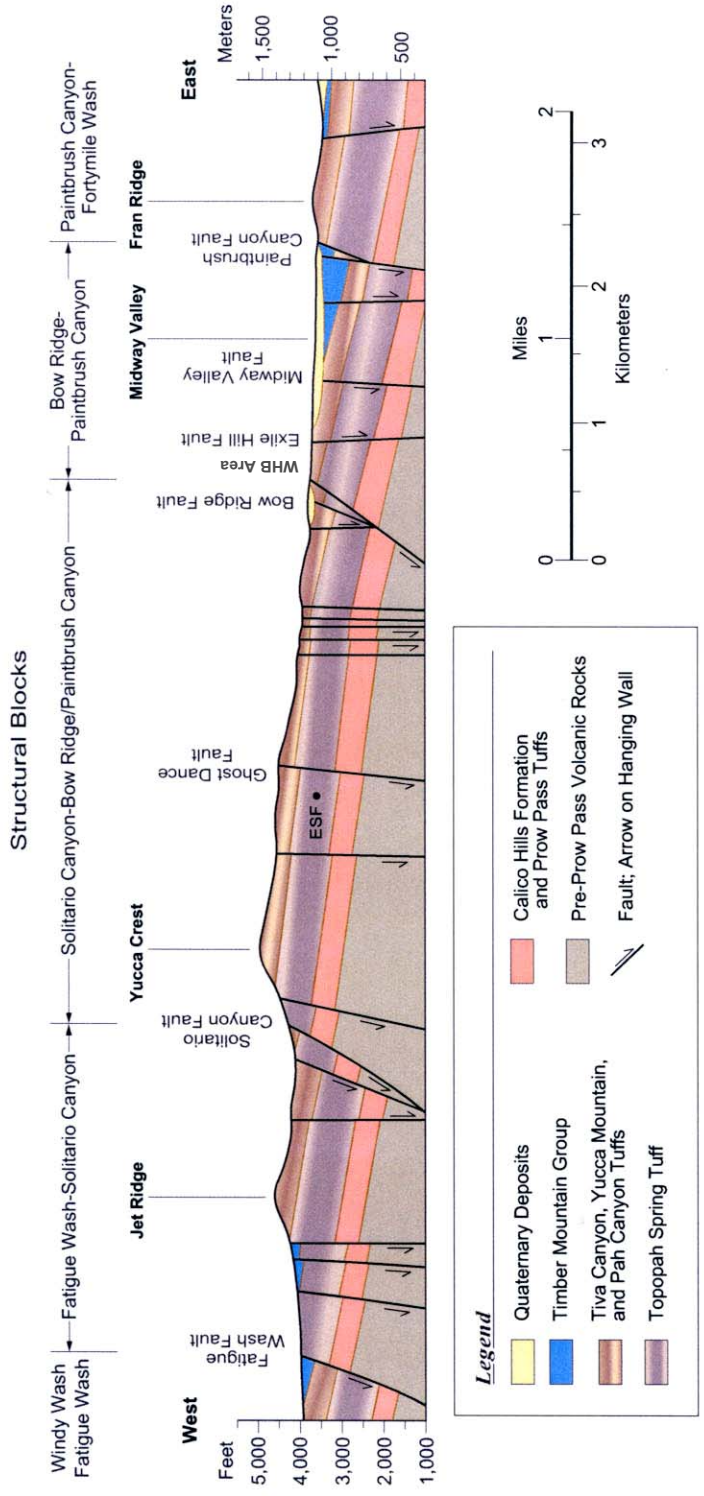

DTN: GS990908314224.010 [DIRS 152631]

Figure 6.2-91. Northeast-Southwest Schematic Cross Section thro ugh Yucca Mountain along the Enhanced Characterization of the Repository Block Cross-Drift

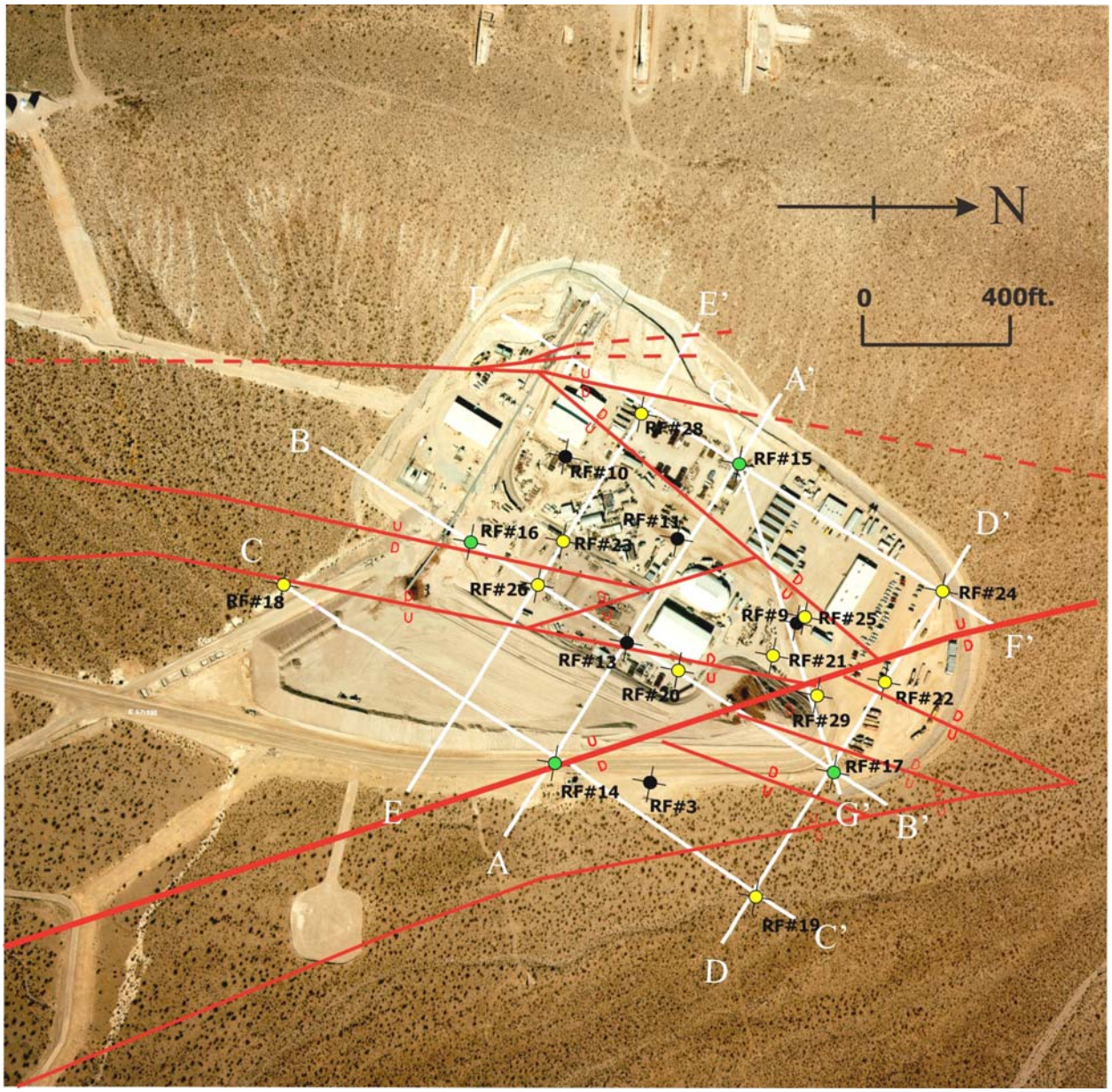

Source: BSC 2002a [DIRS 157829], Figure 224

NOTE: Boreholes in black are pre-existing holes, boreholes in yellow are mud rotary, and boreholes in green are core holes.

Figure 6.2-92. Locations of Cross Sections and Interpreted Faults through the WHB Area

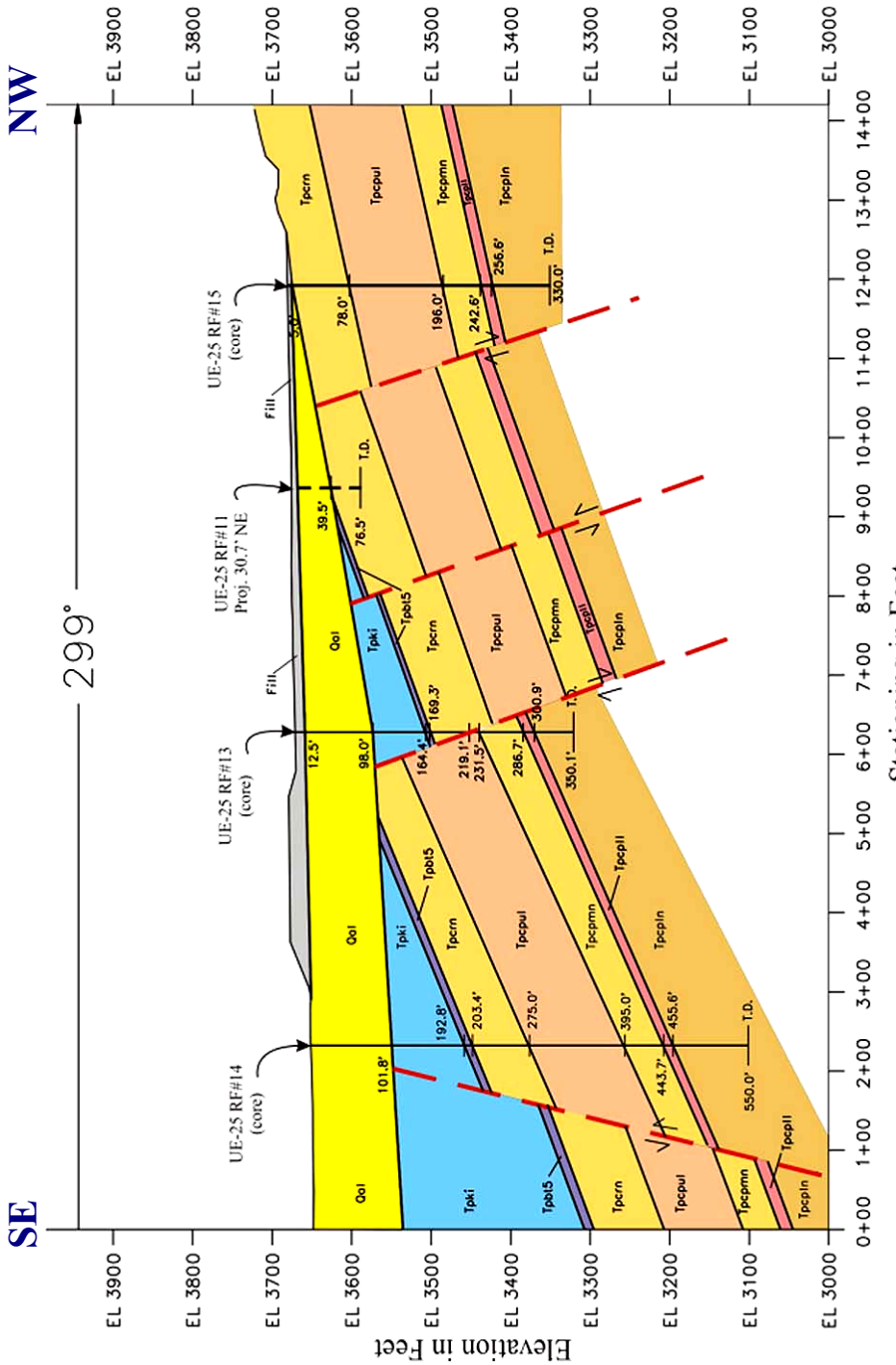

Source: BSC 2002a [DIRS 157829], Figure 225

Figure 6.2-93. WHB Area Geologic Cross Section A-A', Looking South

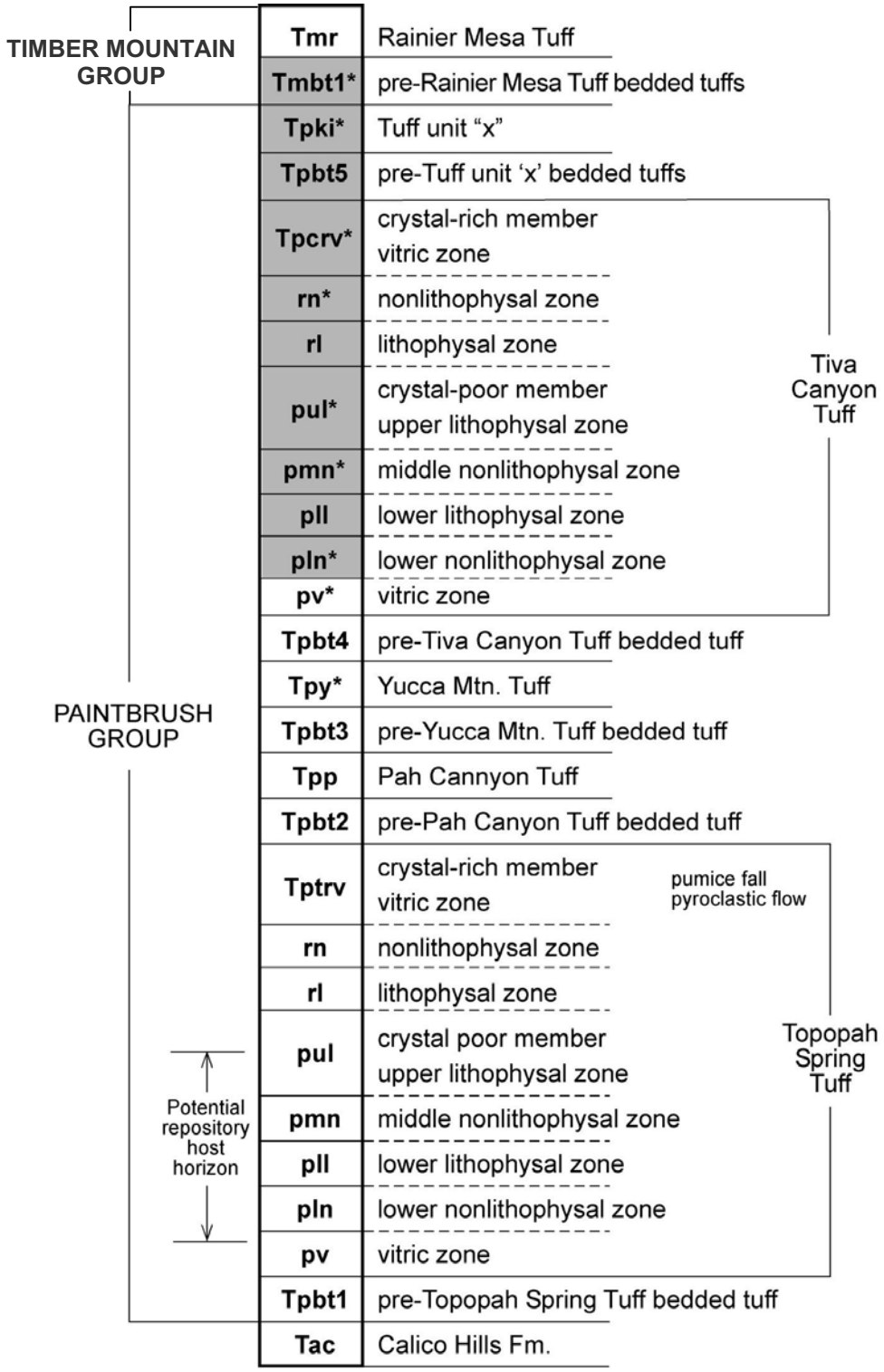

Source: BSC 2002a [DIRS 157829], Figure 233

NOTES: 1. Gray-shaded areas indicate the units that were evaluated in BSC 2002a [DIRS 157829].
2. Dynamic laboratory tests available for units marked with *.

Figure 6.2-94. Generalized Lithostratigraphic Column of the Paintbrush Group

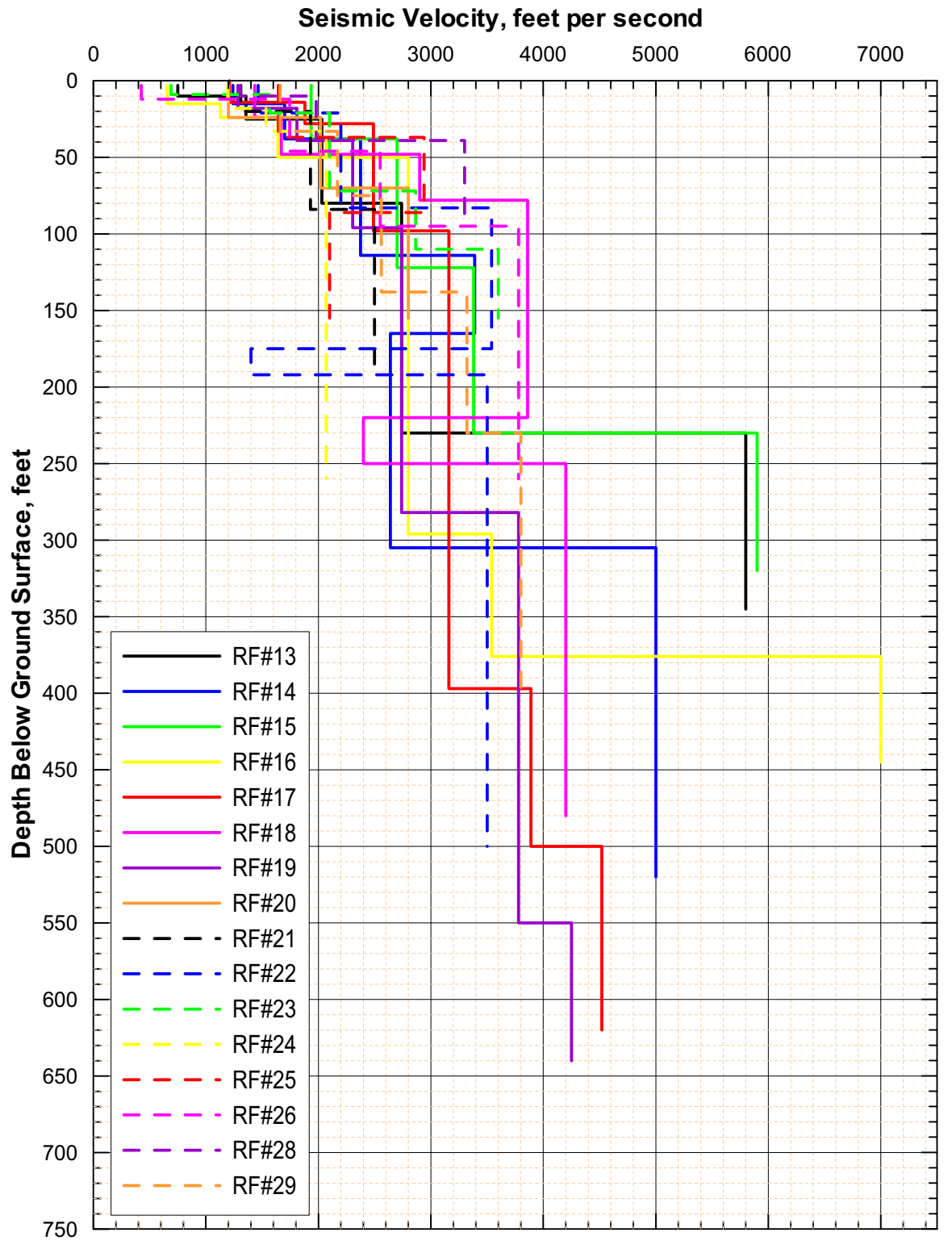

DTN: MO0111DVDWHBSC.001 [DIRS 157296]

Source: BSC 2002a [DIRS 157829], Figure 20

Figure 6.2-95. Downhole V_S Profiles in the WHB Area from the 2000-2001 Surveys

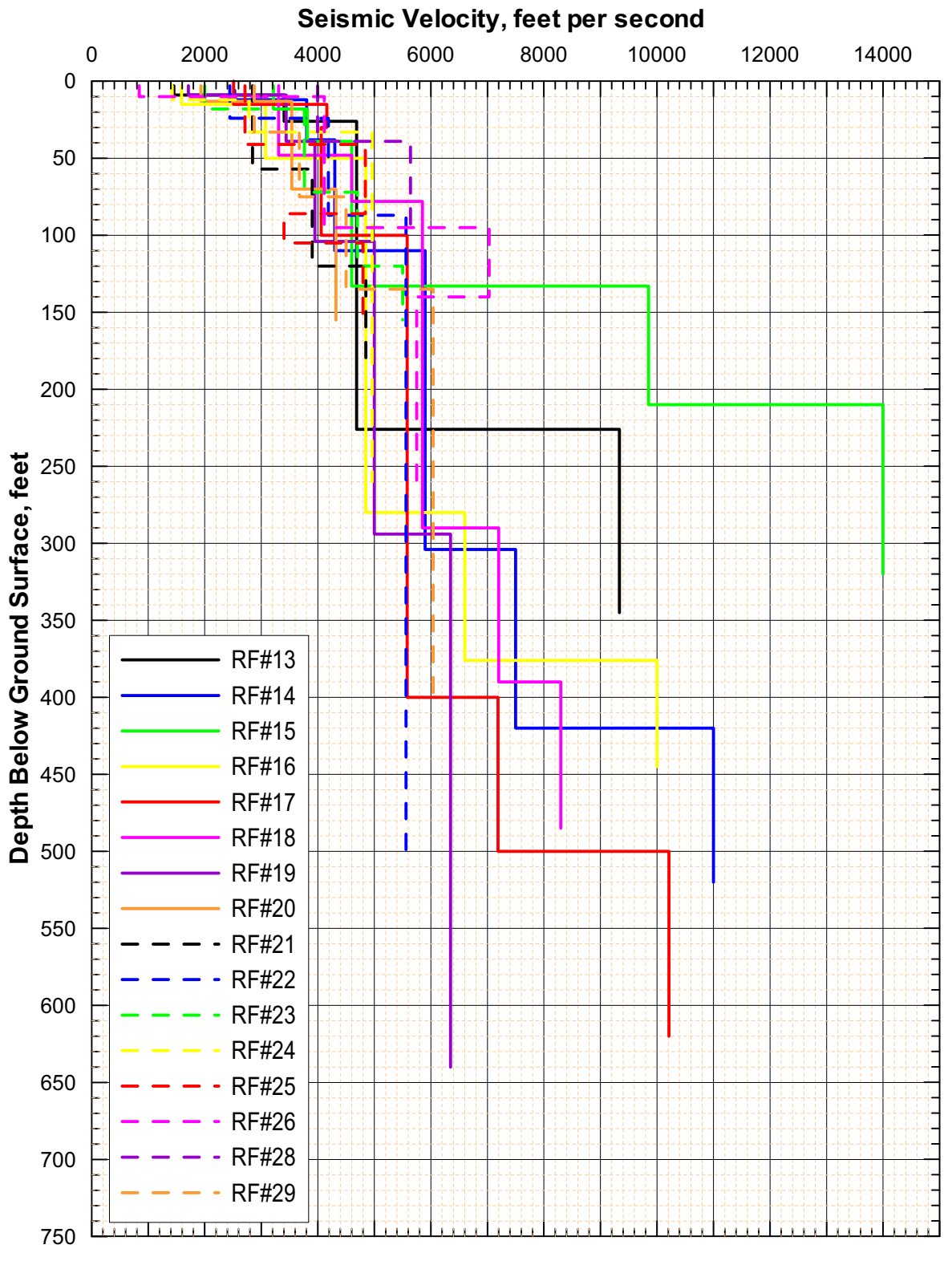

DTN: MO0111DVDWHBSC.001 [DIRS 157296]

Source: BSC 2002a [DIRS 157829], Figure 21

Figure 6.2-96. Downhole V_P Profiles in the WHB Area from the 2000-2001 Surveys

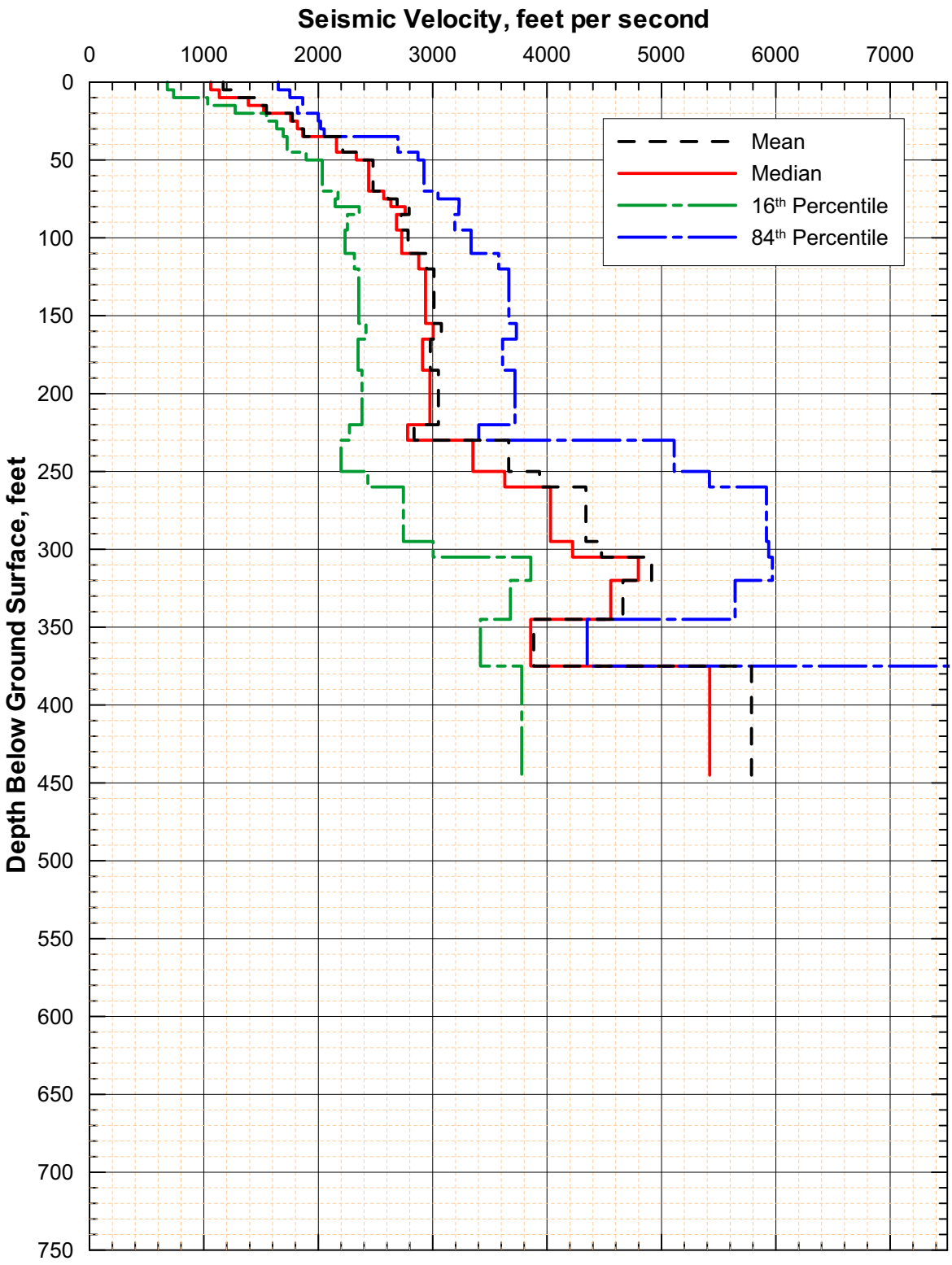

Source: BSC 2002a [DIRS 157289], Figure 25; Appendix I (Filename: velocity\statistics\downhole_whb_s_stats_up_log.xls)

Figure 6.2-97. Mean, Median, and 16th and 84th Percentile Downhole V_S Profiles in the WHB Area

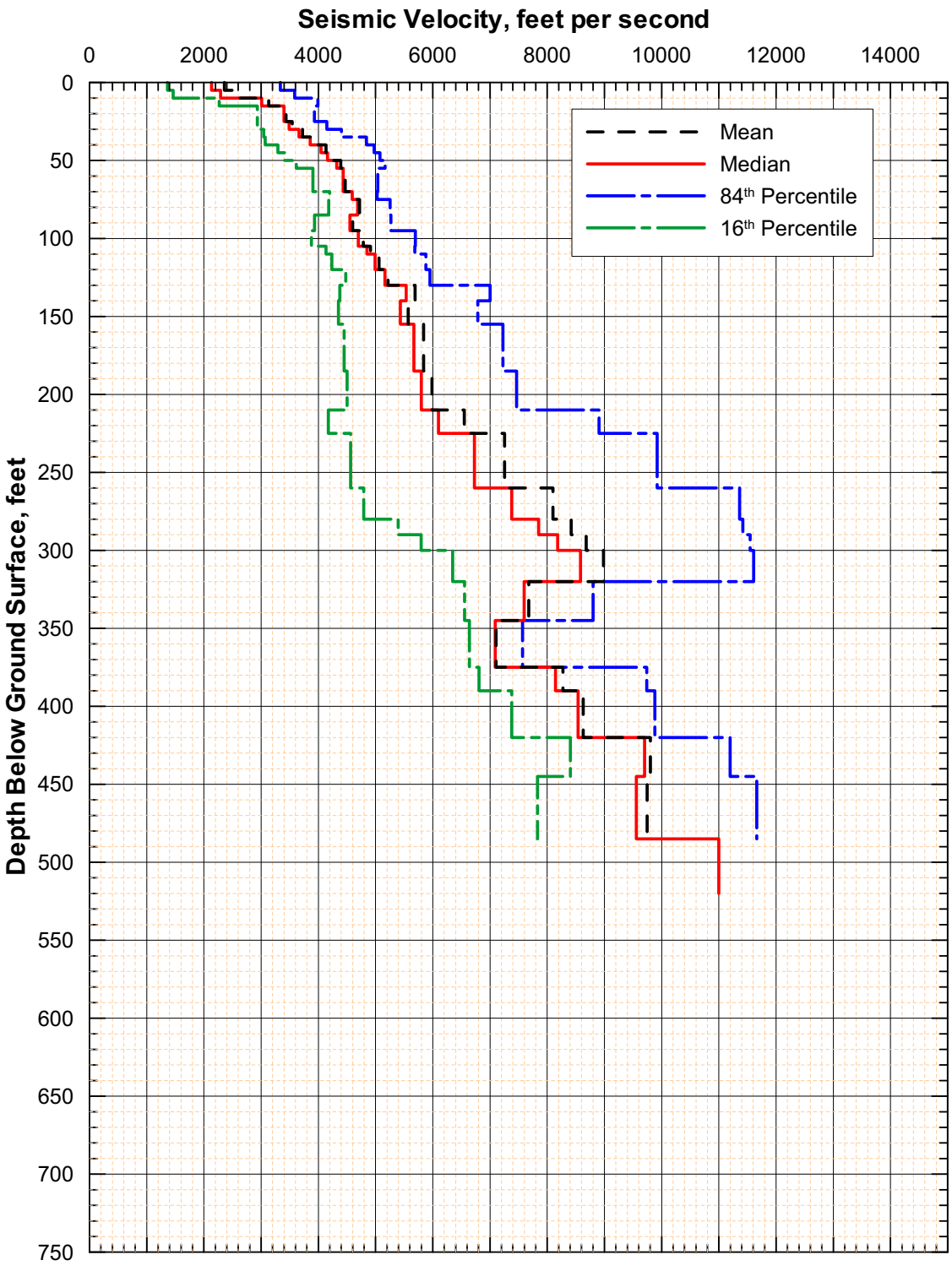

Source: Wong and Silva 2004b [DIRS 170444], SR-1, page 2; Appendix I (Filename: velocity\statistics\downhole_whb_p_stats_up_log.xls)

Figure 6.2-98. Mean, Median, and 16th and 84th Percentile Downhole V_P Profiles in the WHB Area

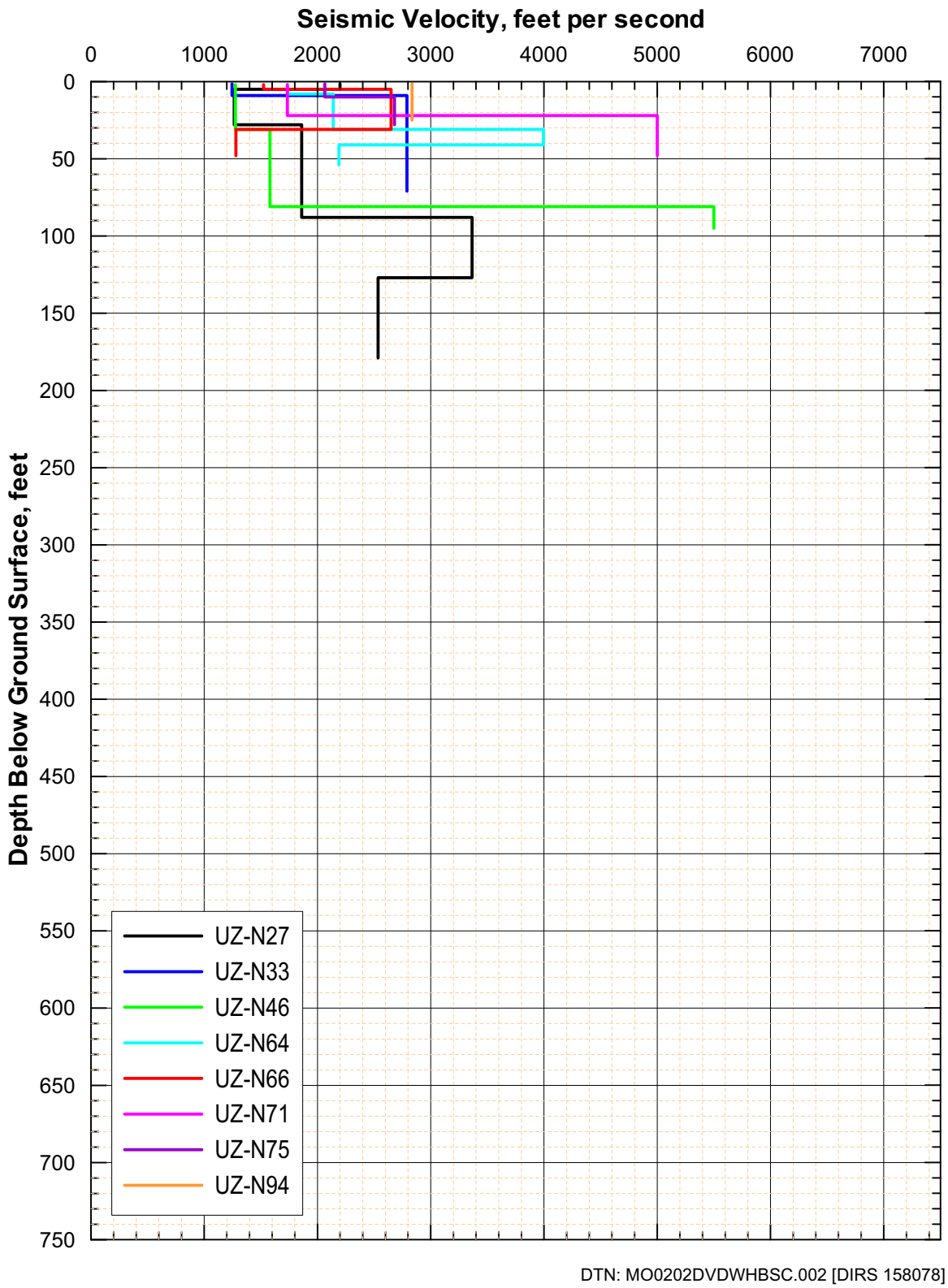

DTN: MO0202DVDWHBSC.002 [DIRS 158078]

Source: BSC 2002a [DIRS 157829], Figure 211

Figure 6.2-99. Downhole V_S Profiles on or Near the Repository Block

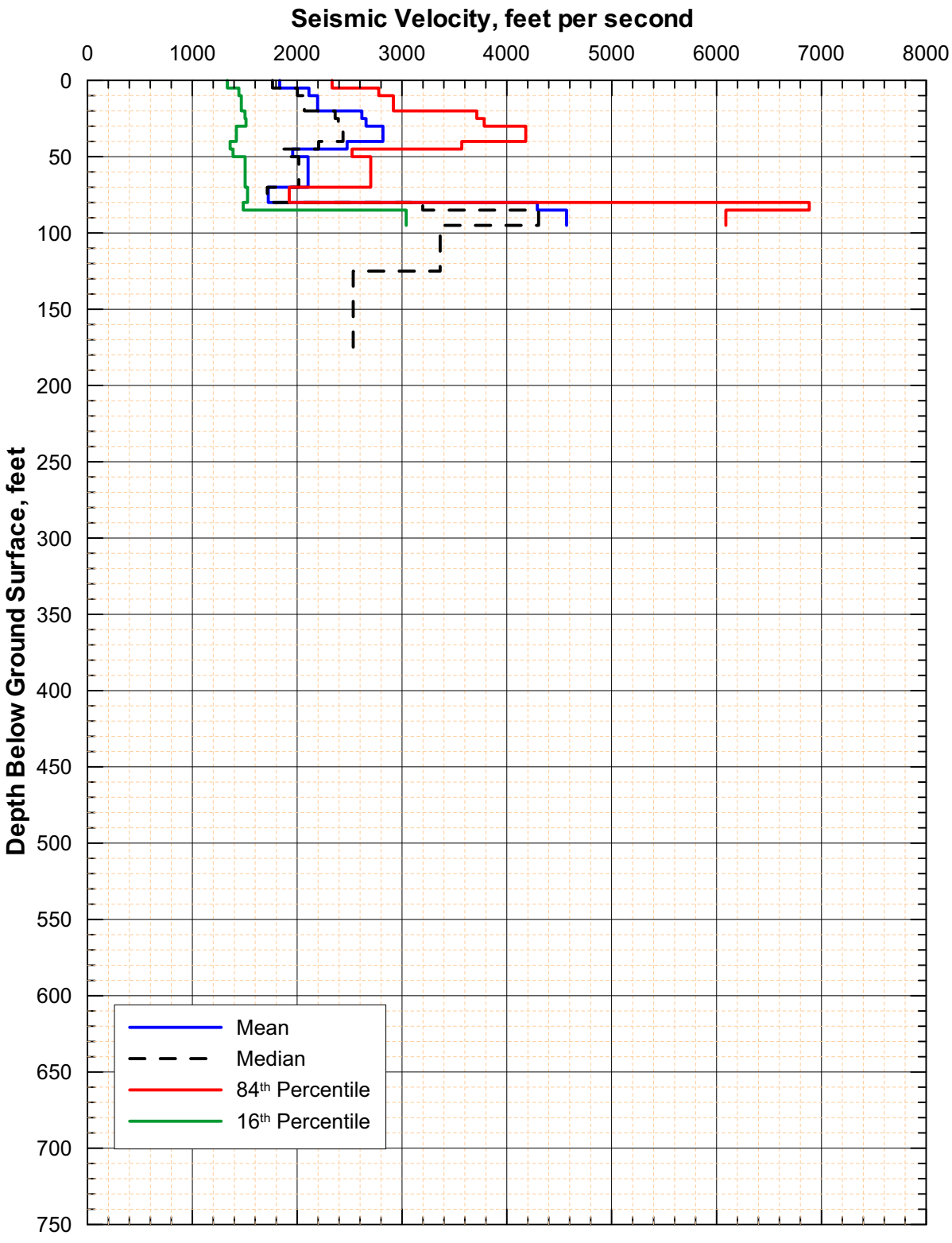

Source: BSC 2002a [DIRS 157829], Figure 212; Appendix I (Filename: downhole_crest_s_stats_log,xls)

Figure 6.2-100. Mean, Median, and 16th and 84 Percentile Downhole V_S Profiles on or Near the Repository Block

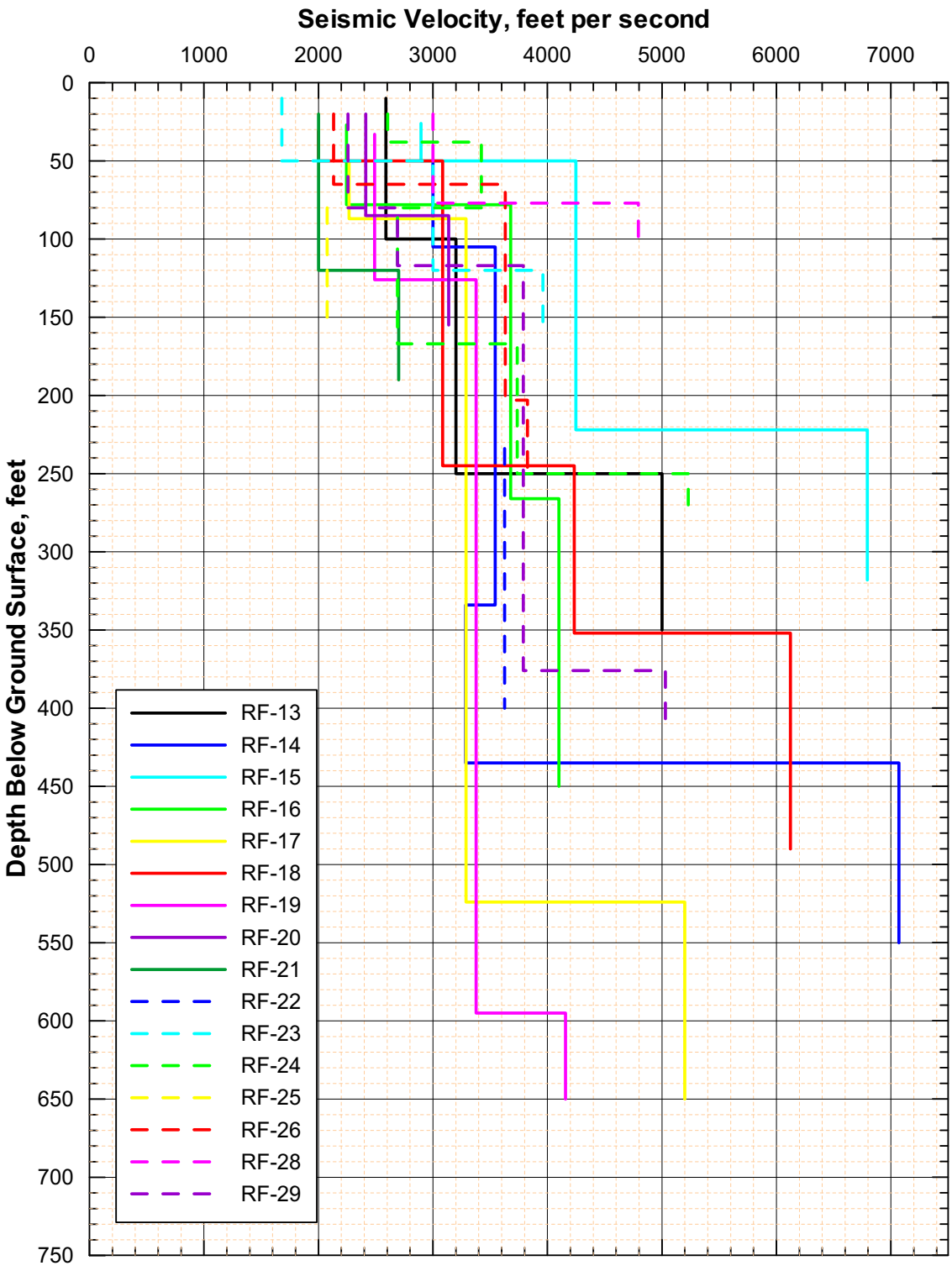

Source: Wong and Silva 2004b [DIRS 170444], SR-1, page 18

Figure 6.2-101. Smoothed V_S Suspension Profiles in the WHB Area

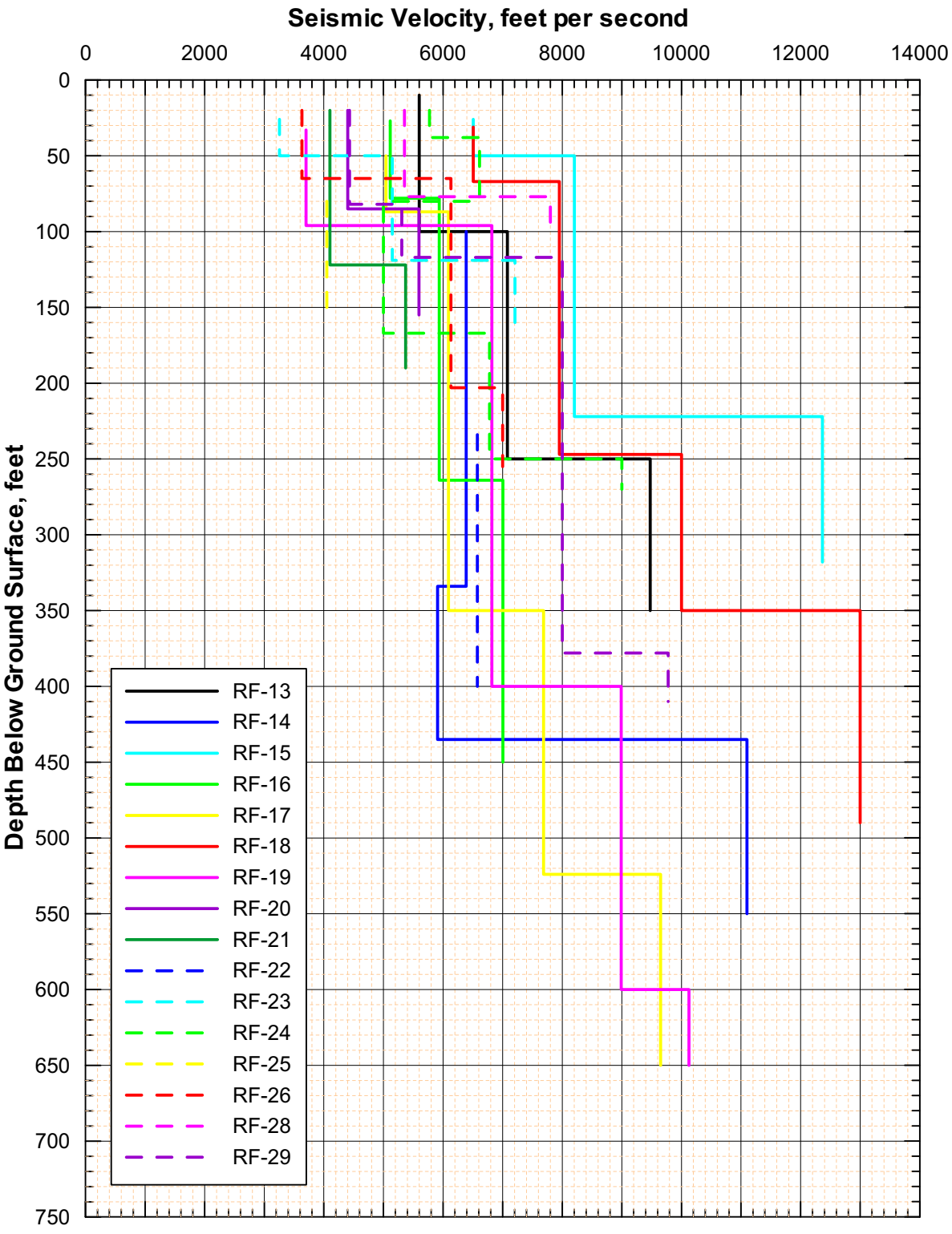

Source: Wong and Silva 2004b [DIRS 170444], SR-1, page 19

Figure 6.2-102. Smoothed V_P Suspension Profiles in the WHB Area

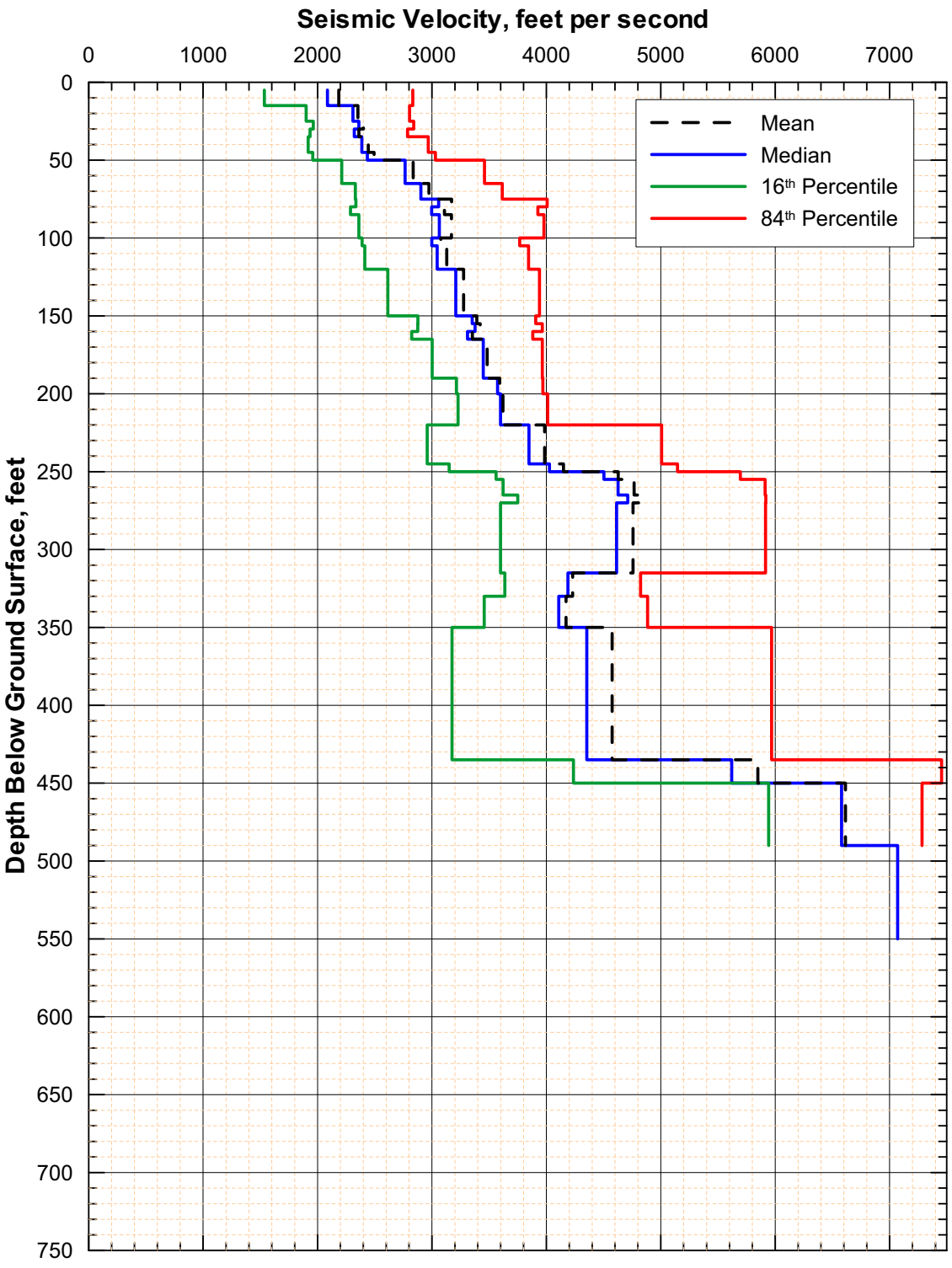

Source: Wong and Silva 2004b [DIRS 170444], SR-1, page 25; Appendix I (Filename: suspension_whb_s_stats_log_up.xls)

Figure 6.2-103. Mean, Median, and 16th and 84 Percentile V_S Suspension Profiles in the WHB Area

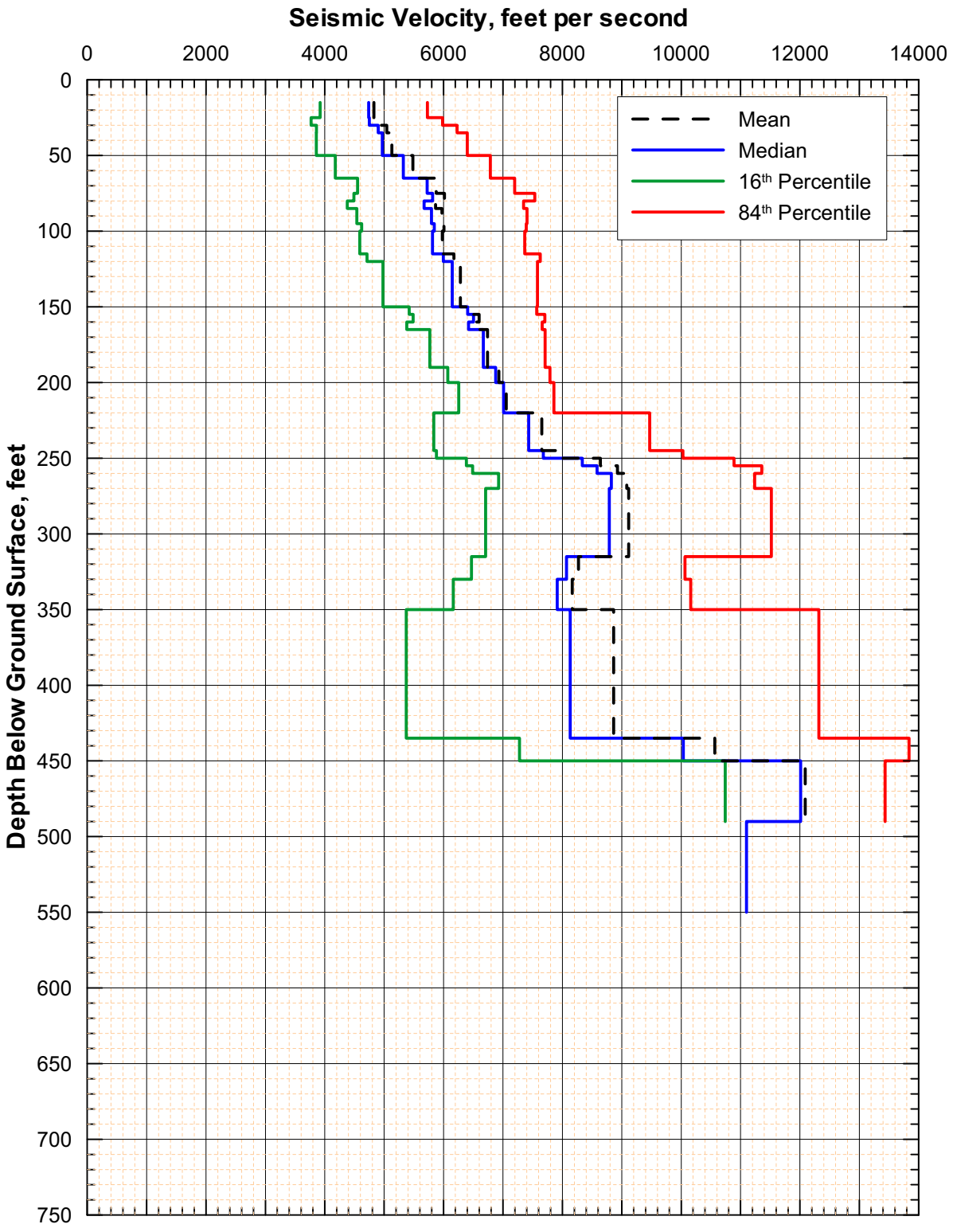

Source: Wong and Silva 2004b [DIRS 170444], SR-1, page 41; Appendix I (Filename: suspension_whb_p_stats_log_up.xls)

Figure 6.2-104. Mean, Median, and 16th and 84 Percentile V_P Suspension Profiles in the WHB Area

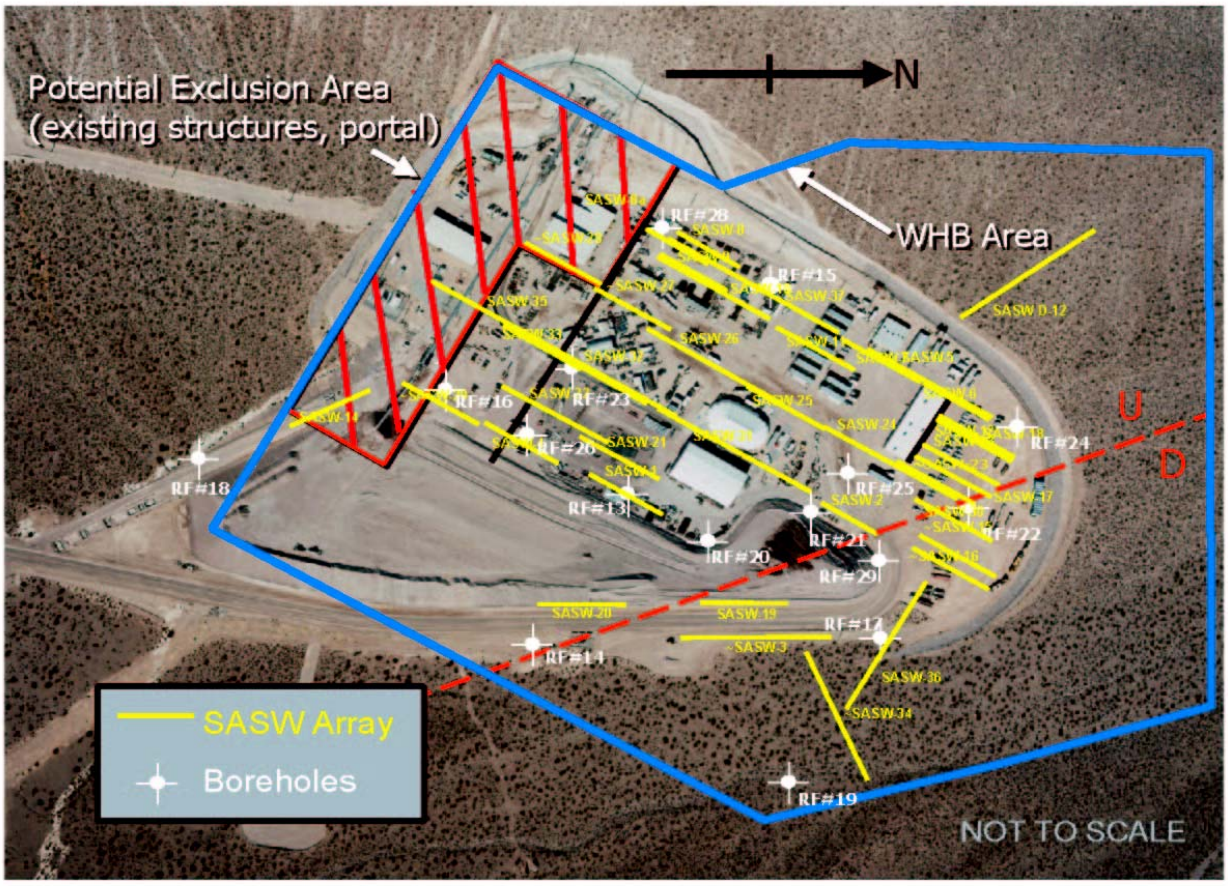

Source: BSC 2002a [DIRS 157829], Figure 43

NOTE: The dashed line is the Exile Hill fault splay.

Figure 6.2-105. Locations of SASW Surveys in the WHB Area

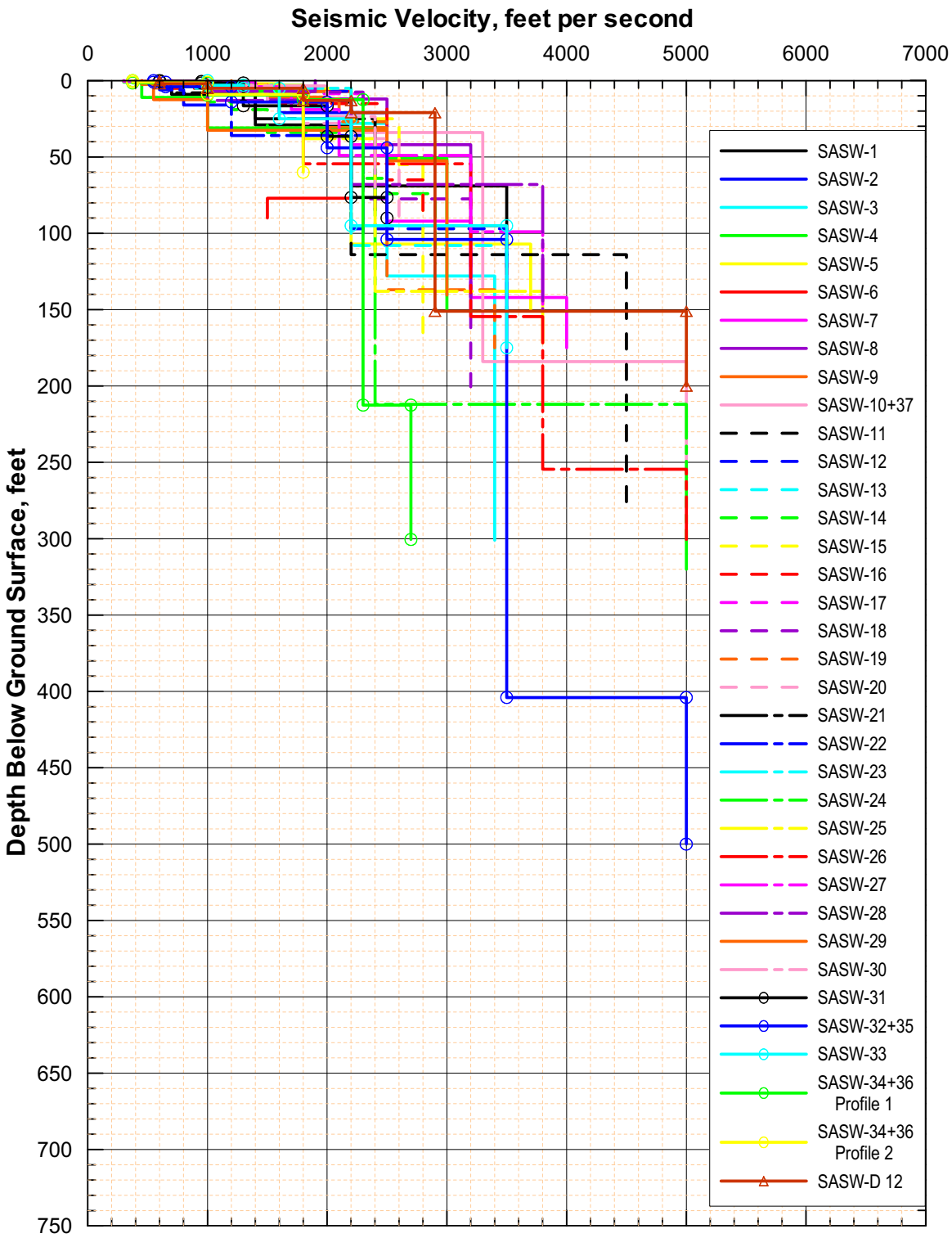

DTN: MO0110SASWWHBS.000 [DIRS 157969]

Source: BSC 2002a [DIRS 157829], Figure 89

Figure 6.2-106. SASW V_S Profiles in the WHB Area

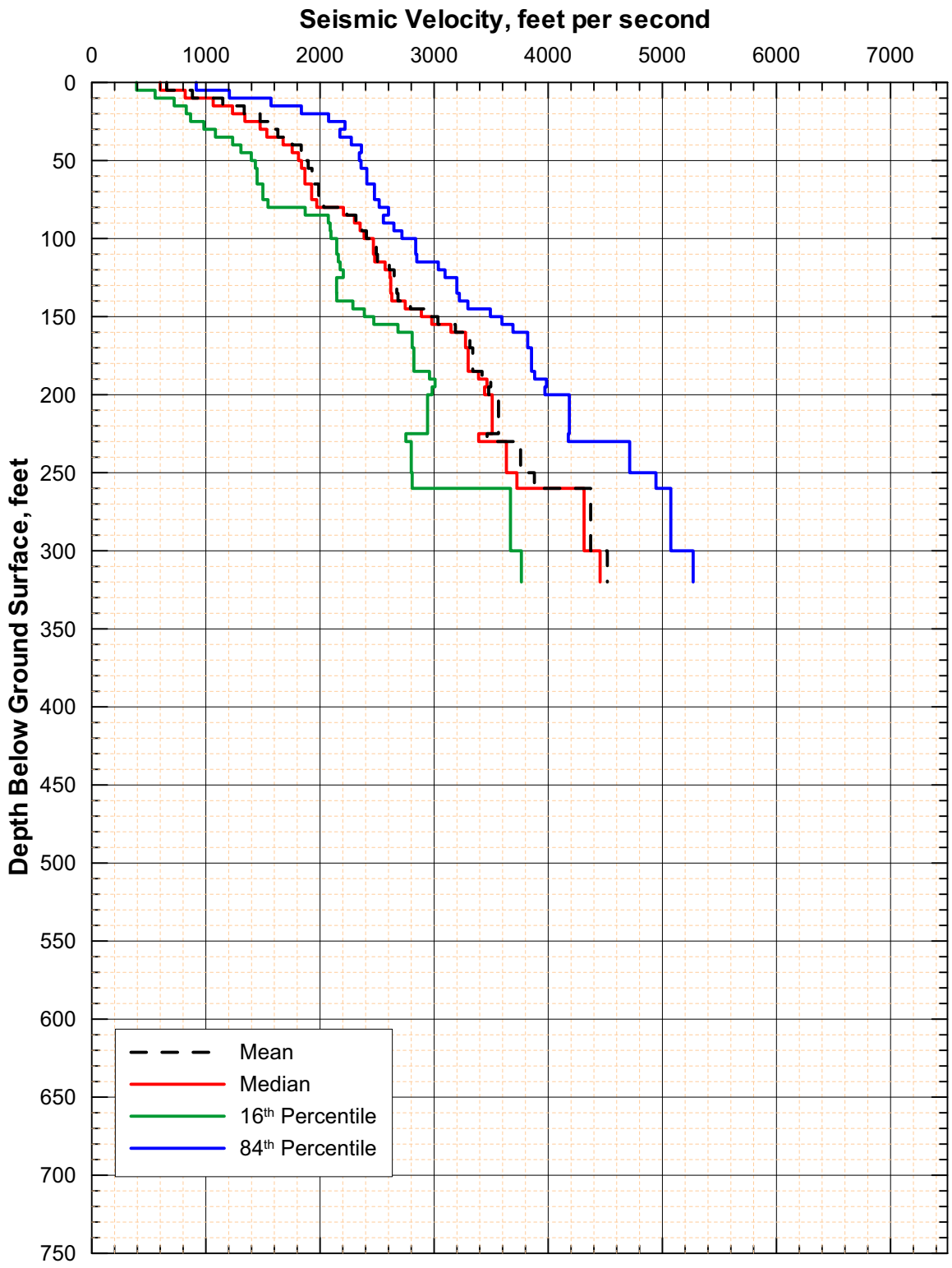

Source: BSC 2002a [DIRS 157829], Figure 97 (Filename: sasw_whb_s_stats_up_log.xls)

Figure 6.2-107. Mean, Median, and 16th and 84th Percentile SASW V_S Profiles in the WHB Area

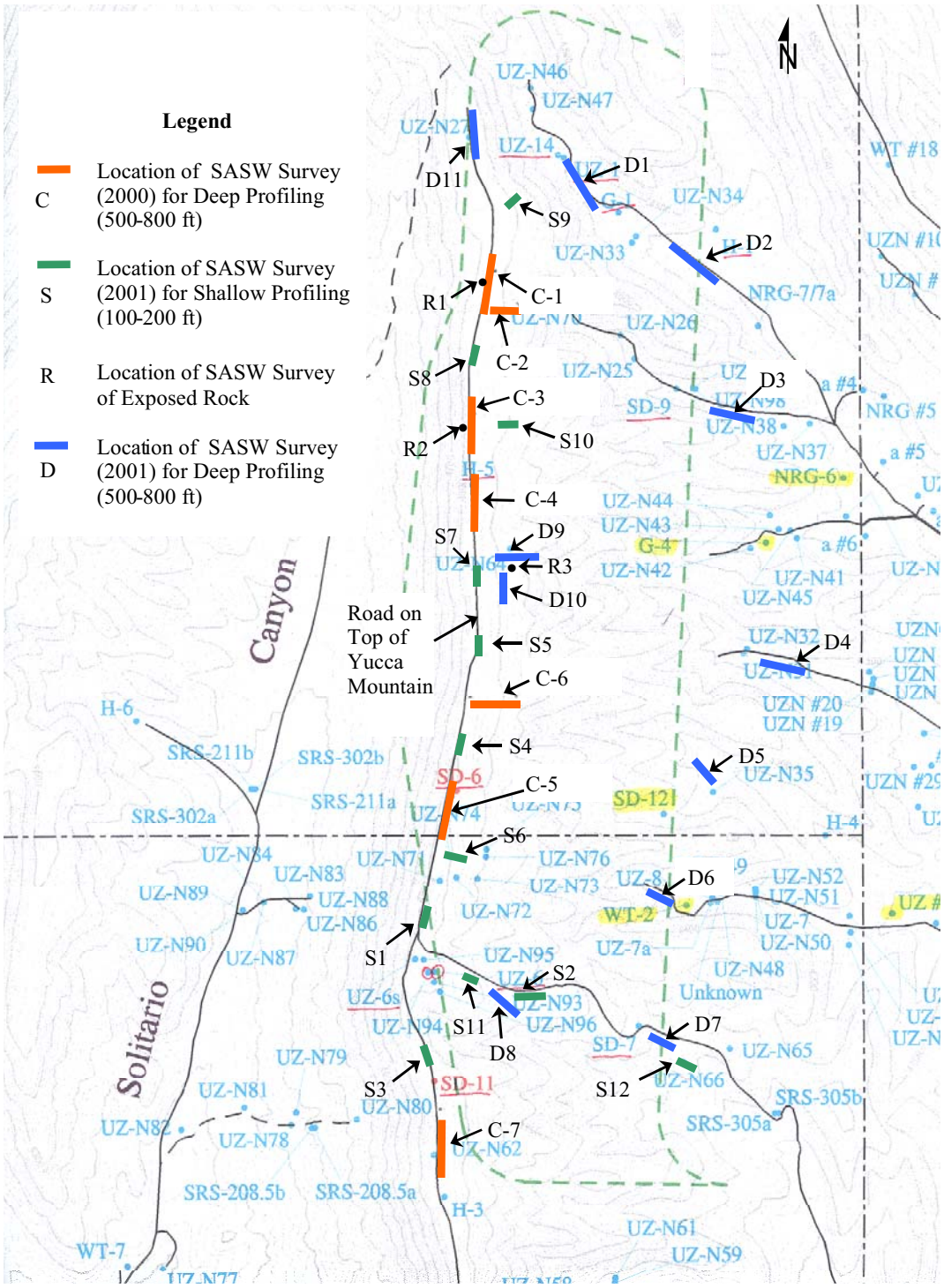

Source: BSC 2002a [DIRS 157829], Figure 157

NOTE: Dashed green line shows the emplacement area proposed as of July 2000. Boreholes used for VSP are highlighted in yellow.

Figure 6.2-108. Locations of SASW Surveys on or Near the Repository Block

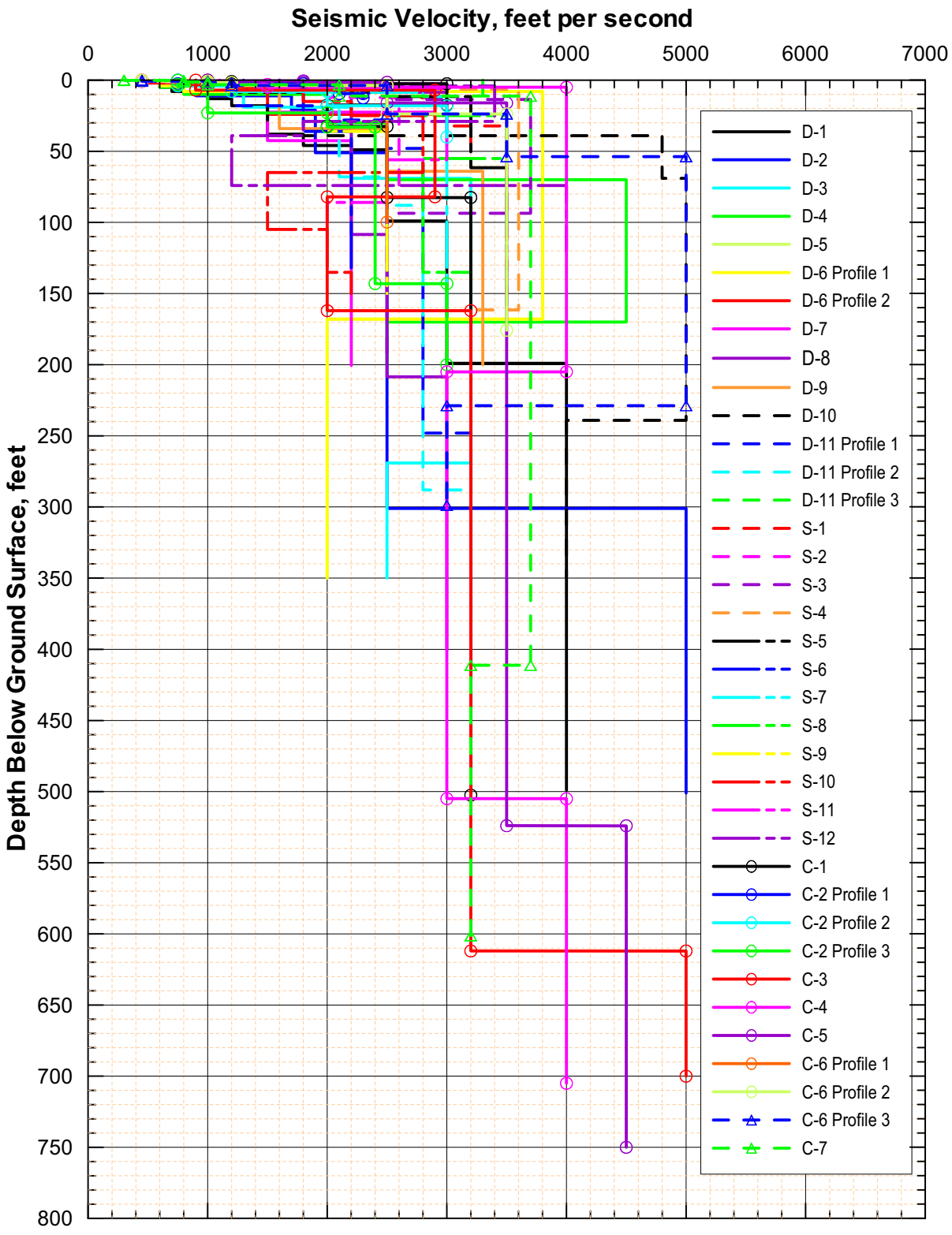

DTN: MO0203SEPSASWD.000 [DIRS 158084], MO0110SASWVDYM.000 [DIRS 158076], MO0206SASROCK.000 [DIRS 159081]

Source: BSC 2002a [DIRS 157829], Figure 192

Figure 6.2-109. SASW V_S Profiles on or Near the Repository Block

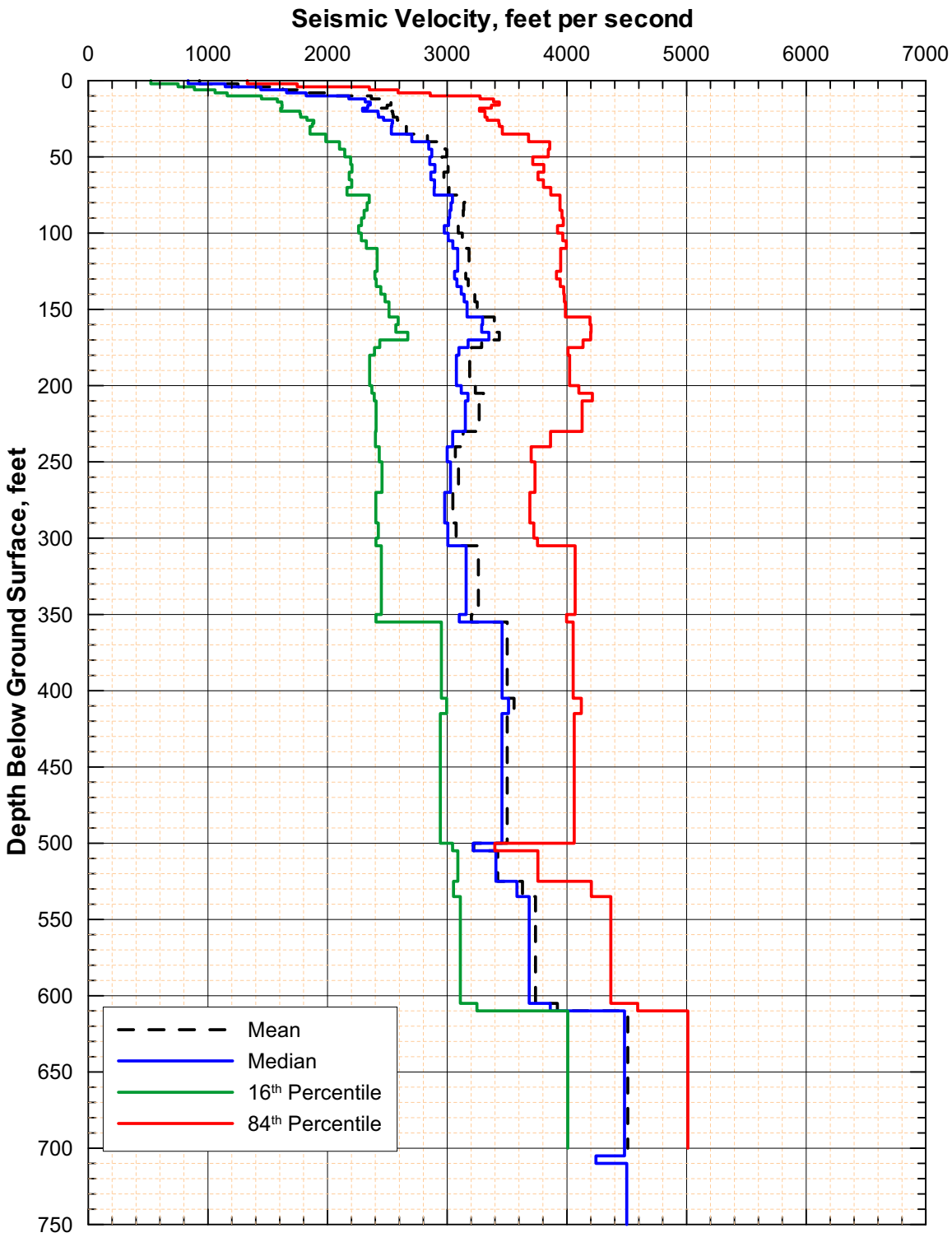

Source: Appendix I (\velocity\statistics\sasw_crest_s_stats_log5.xls)

Figure 6.2-110. Mean, Median, and 16th and 84th Percentile SASW V_S Profiles on or Near the Repository Block

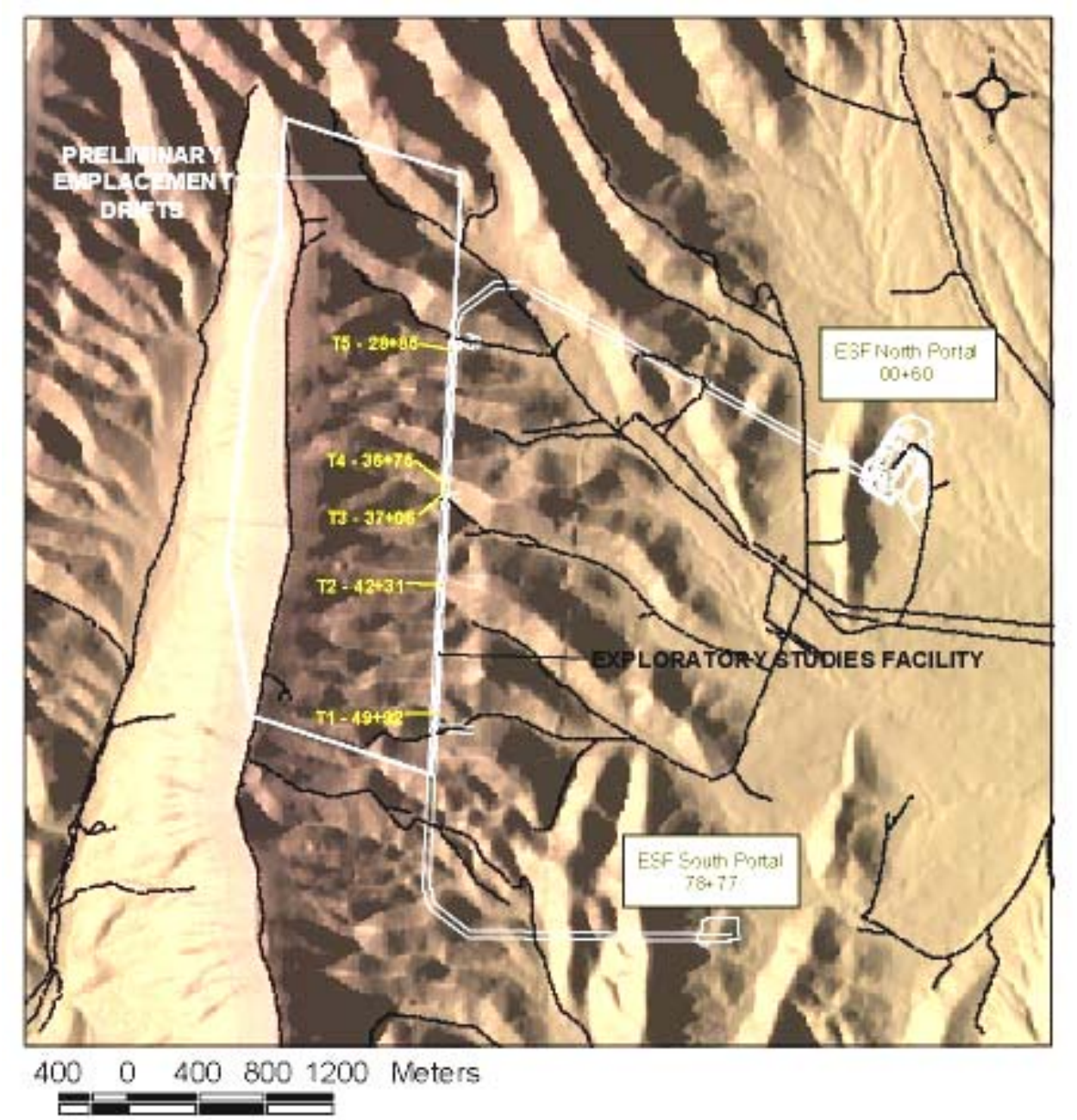

Source: BSC 2002a [DIRS 157829], Figure 144

NOTE: To convert meters to feet, multiply by 3.281

Figure 6.2-111. Locations of SASW Surveys in the ESF Main Drift

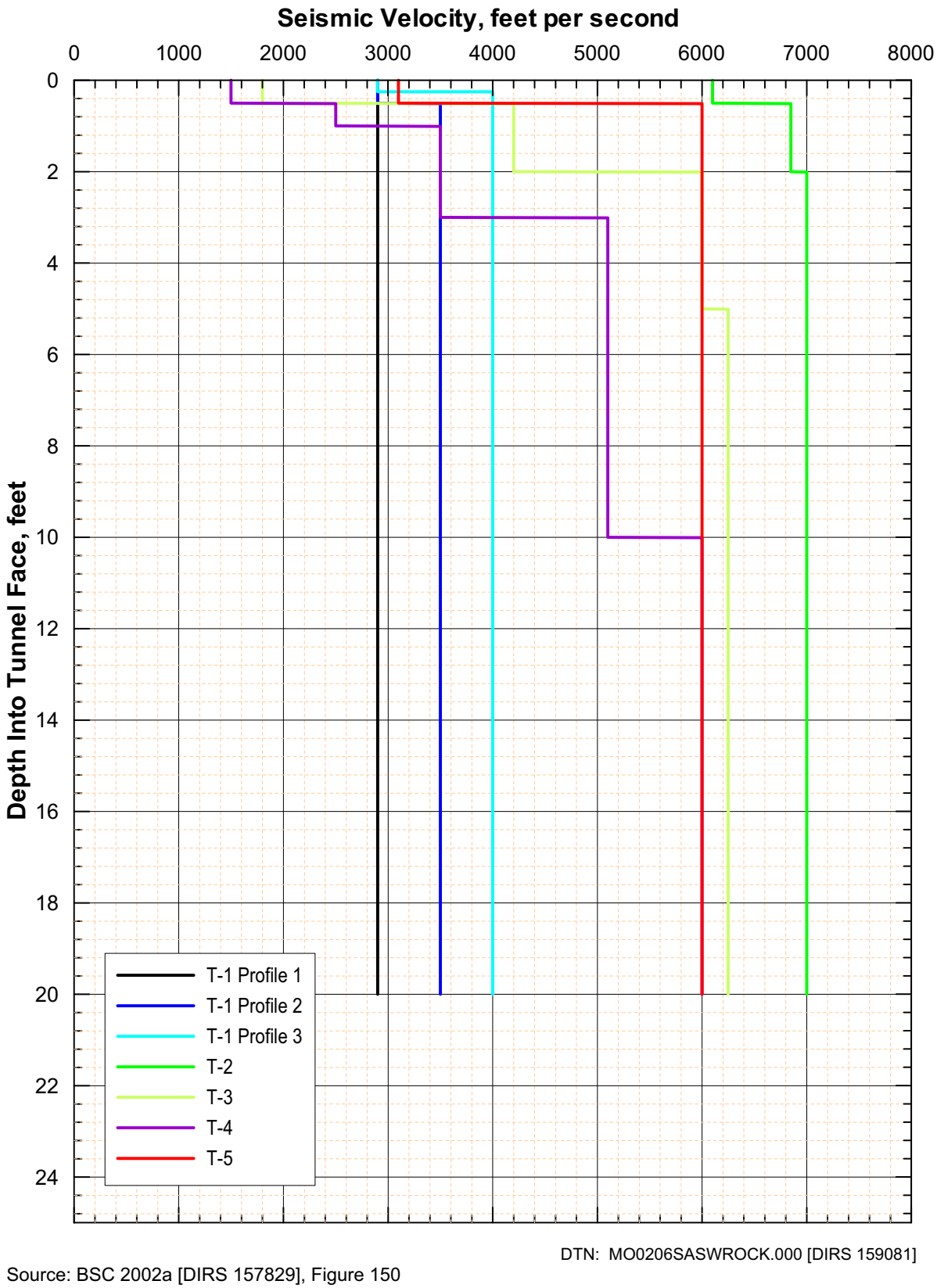

DTN: MO0206SASWROCK.000 [DIRS 159081]

Source: BSC 2002a [DIRS 157829], Figure 150

Figure 6.2-112. SASW V_S Profiles in the ESF Main Drift

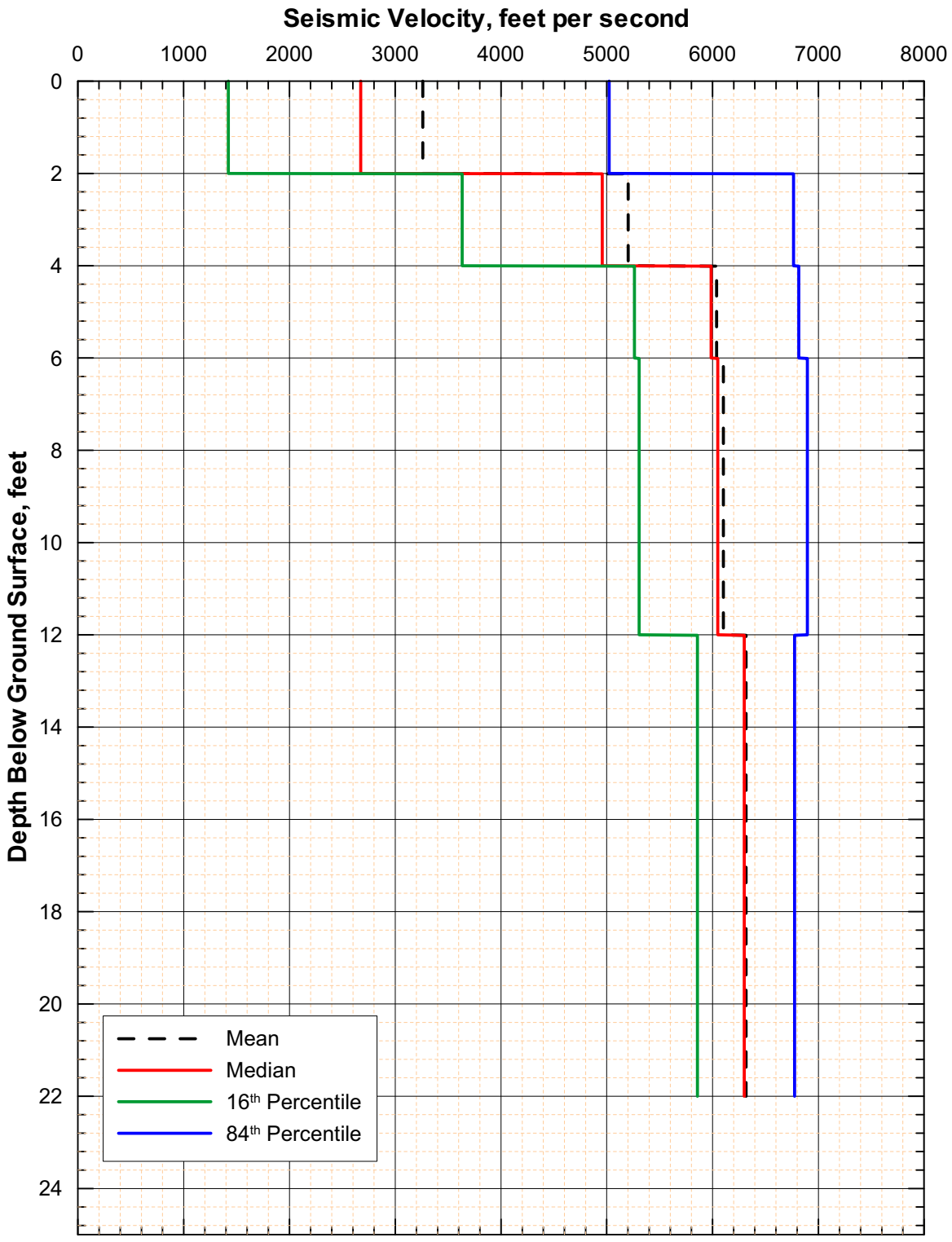

Source: BSC 2002a [DIRS 157829], Figure 151; Appendix I (Filename: \velocity\statistics\sasw_tunnel_s_stats_log.xls)

Figure 6.2-113. Mean, Median, and 16th and 84th Percentile SASW V_S Profiles in the ESF Main Drift

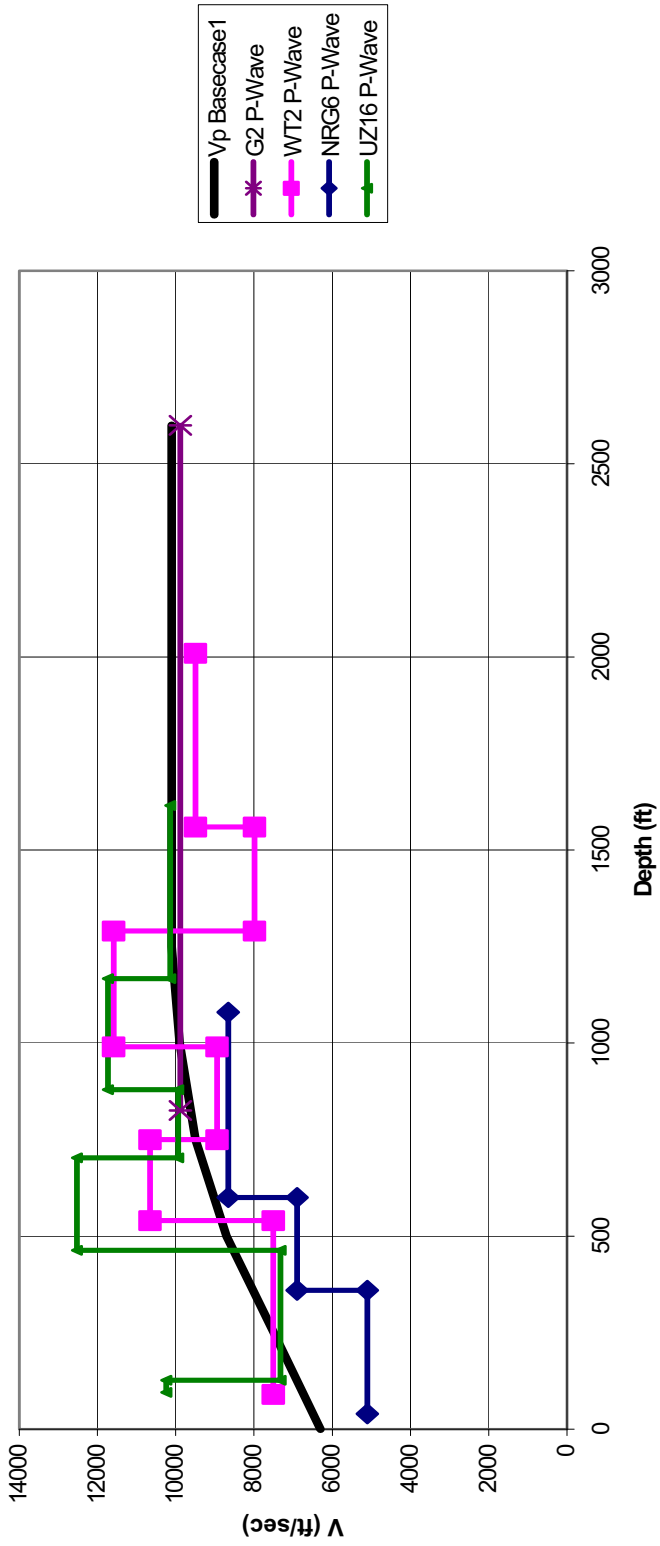

Source: Wong and Silva 2003 [DIRS 163201], p. 31; Appendix I (Filename: velocity\travel_vsp.xls)

NOTE: Corrected for source offset.

Figure 6.2-114. Comparison of VSP V_P Profiles

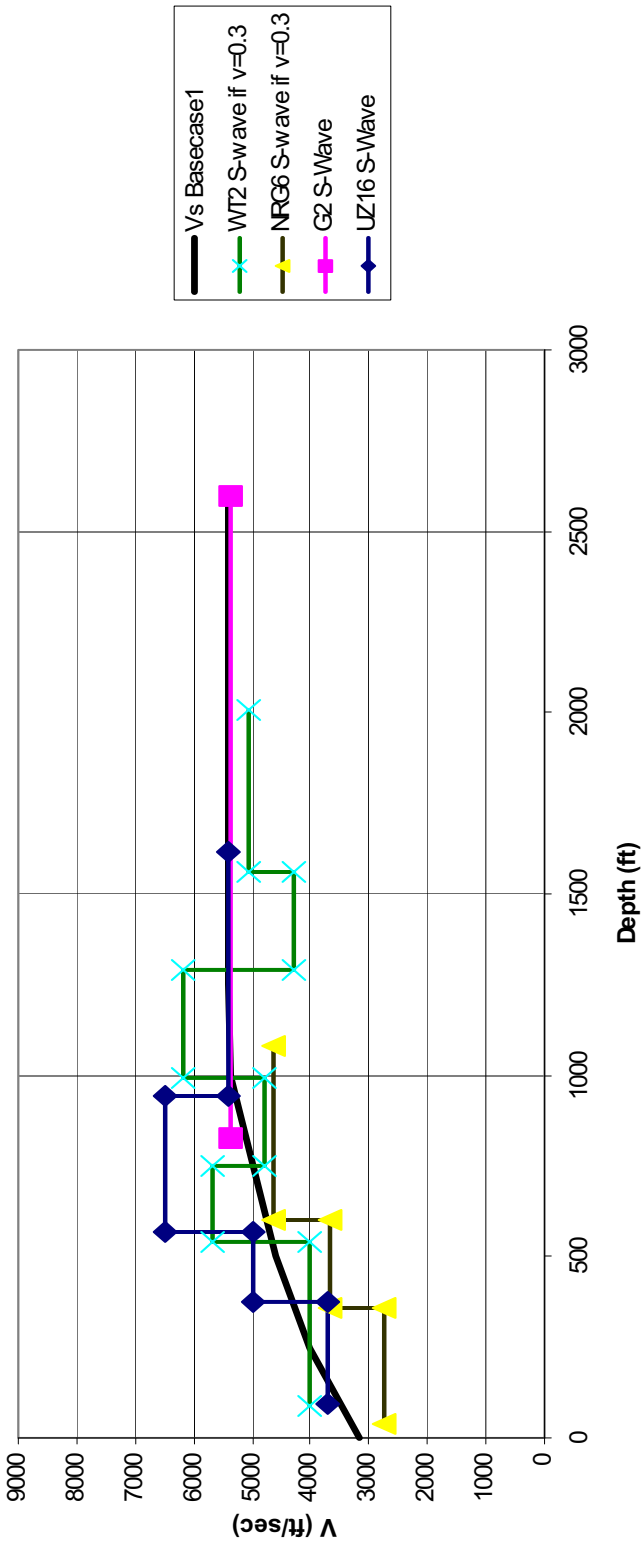

Source: Wong and Silva 2003 [DIRS 163201], p. 32; Appendix I (velocity\travel_vsp.xls)

NOTE: Corrected for source offset.

Figure 6.2-115. Comparison of VSP V_S Profiles

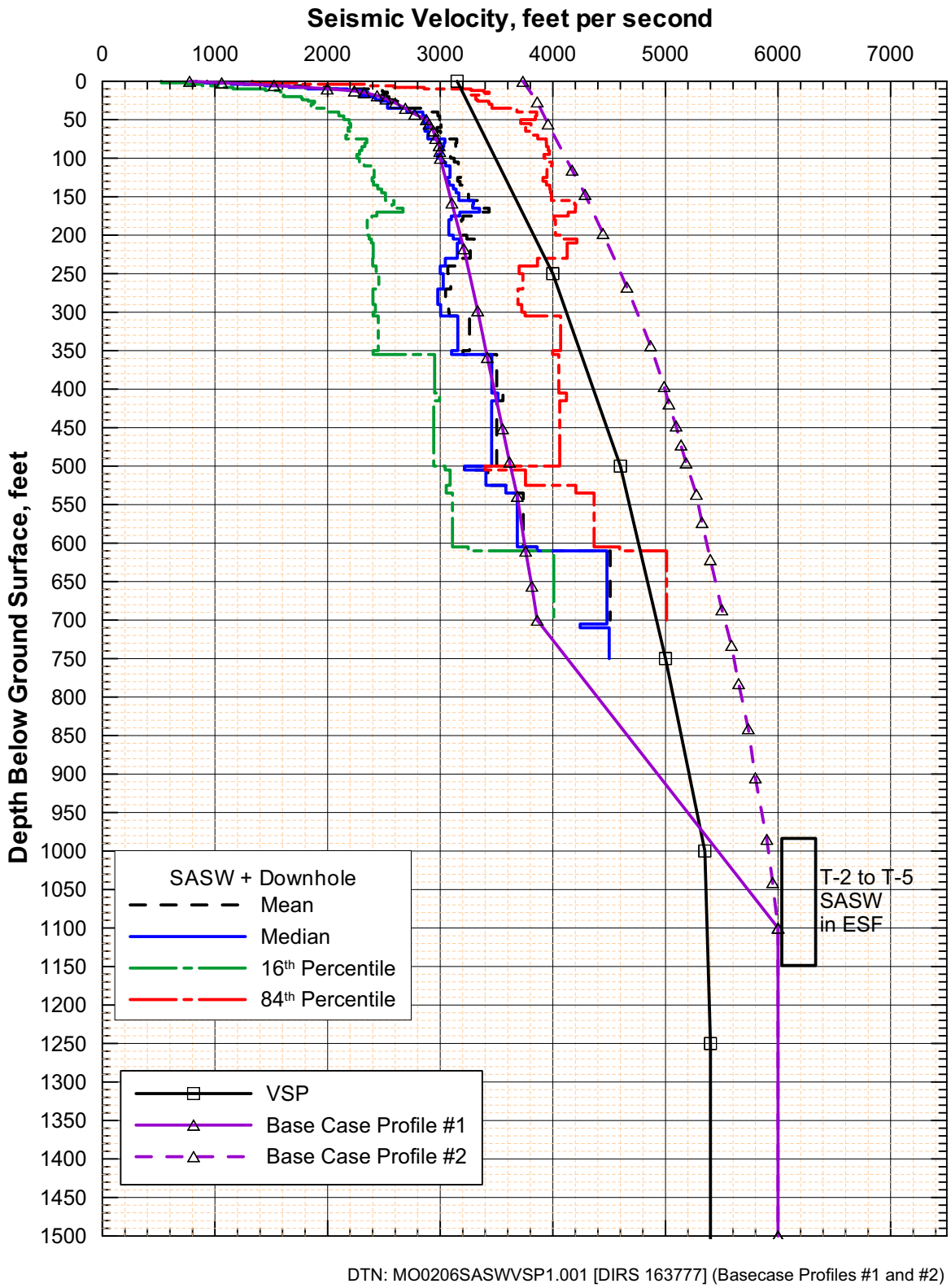

DTN: MO0206SASWVSP1.001 [DIRS 163777] (Basecase Profiles #1 and #2)

Source: Wong and Silva 2003 [DIRS 163201], p. 20

Figure 6.2-116. Base Case V_S Profiles for Repository Block

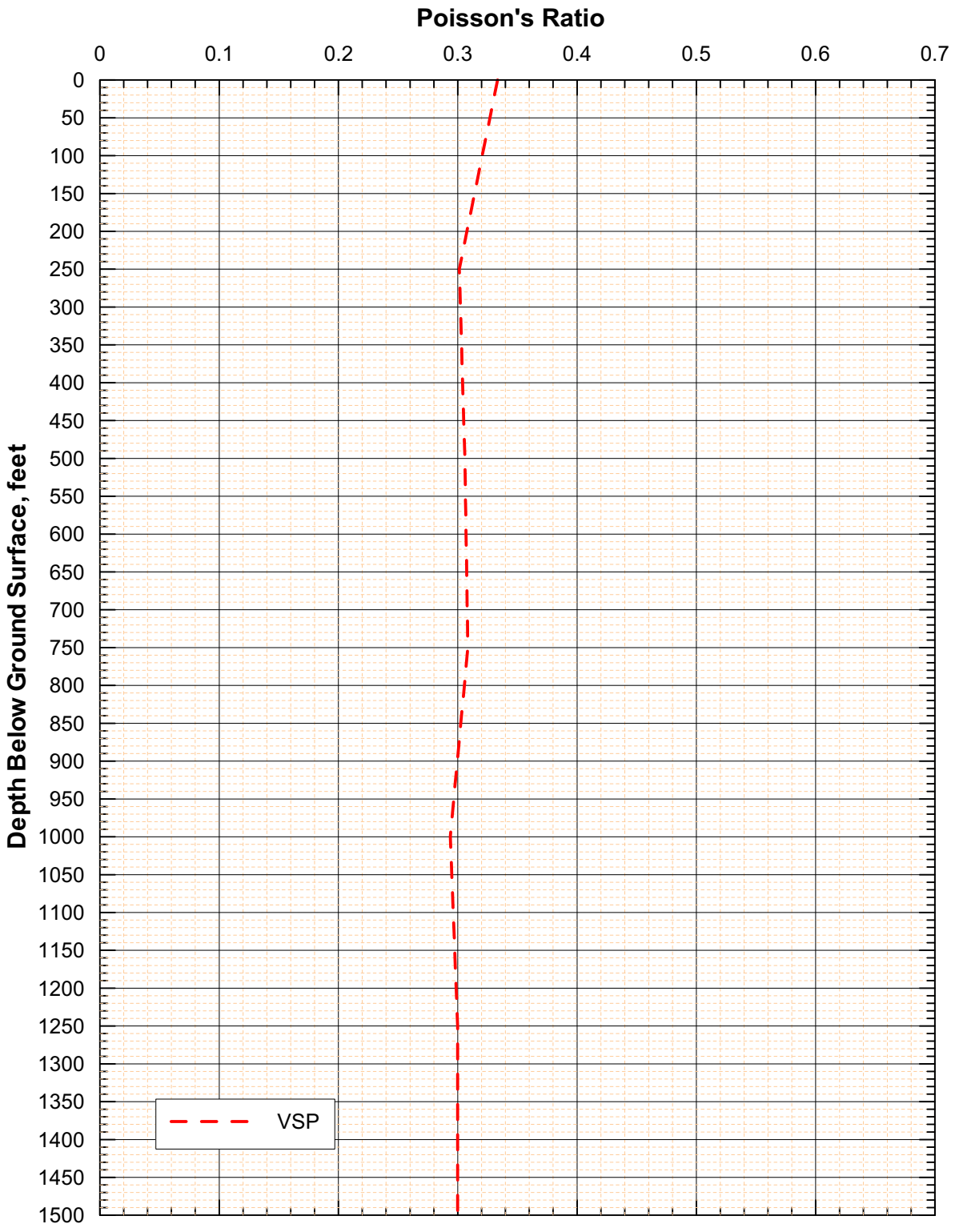

Source: Wong and Silva 2003 [DIRS 163201], p. 23

Figure 6.2-117. Computed Poisson's Ratios for the Repository Block from the VSP Surveys

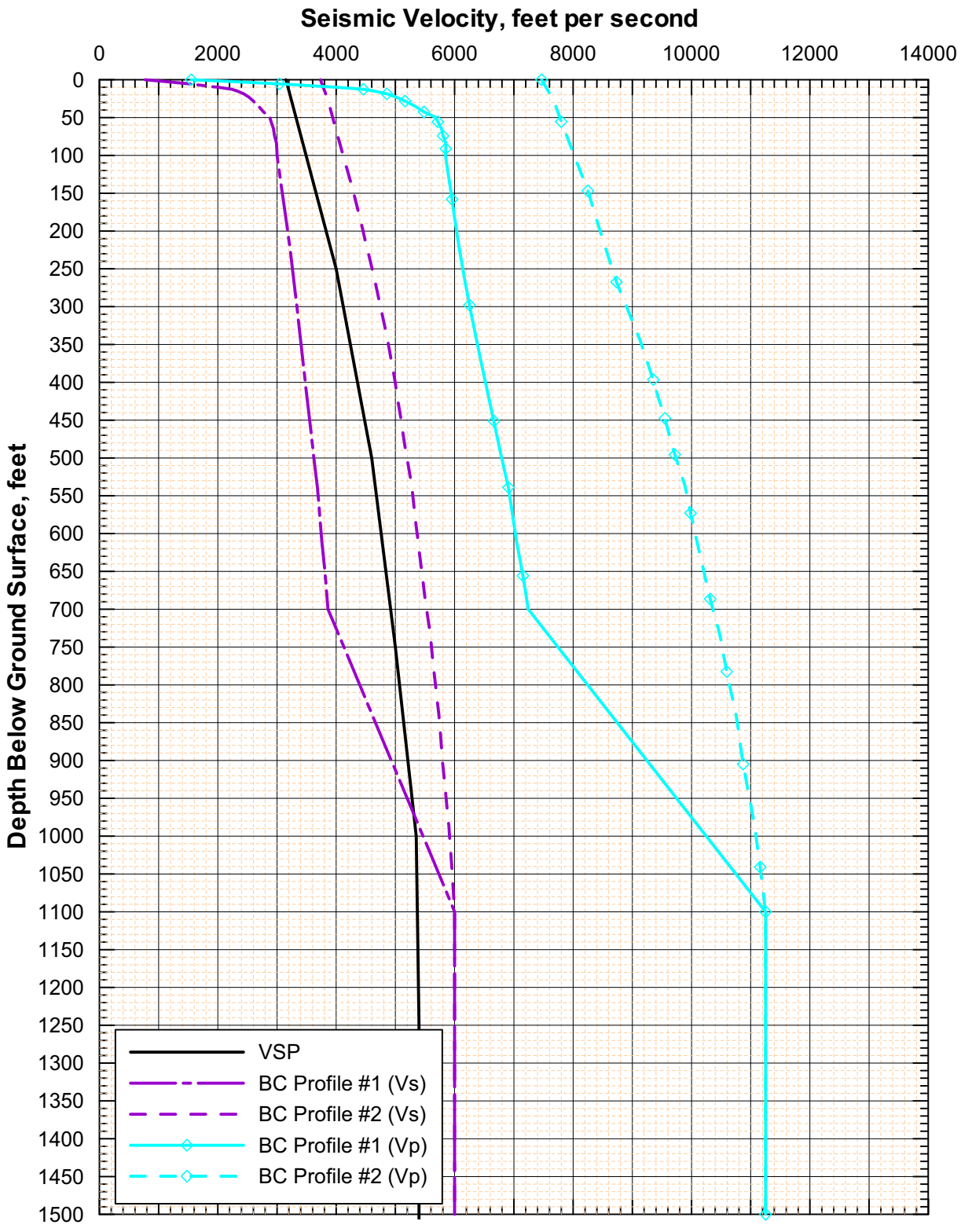

DTN: MO0206SASWVSP1.001 [DIRS 163777] (Basecase Profiles #1 and #2)

Source: Wong and Silva 2003 [DIRS 163201], p. 22

Figure 6.2-118. Base Case V_S and V_P Profiles for the Repository Block

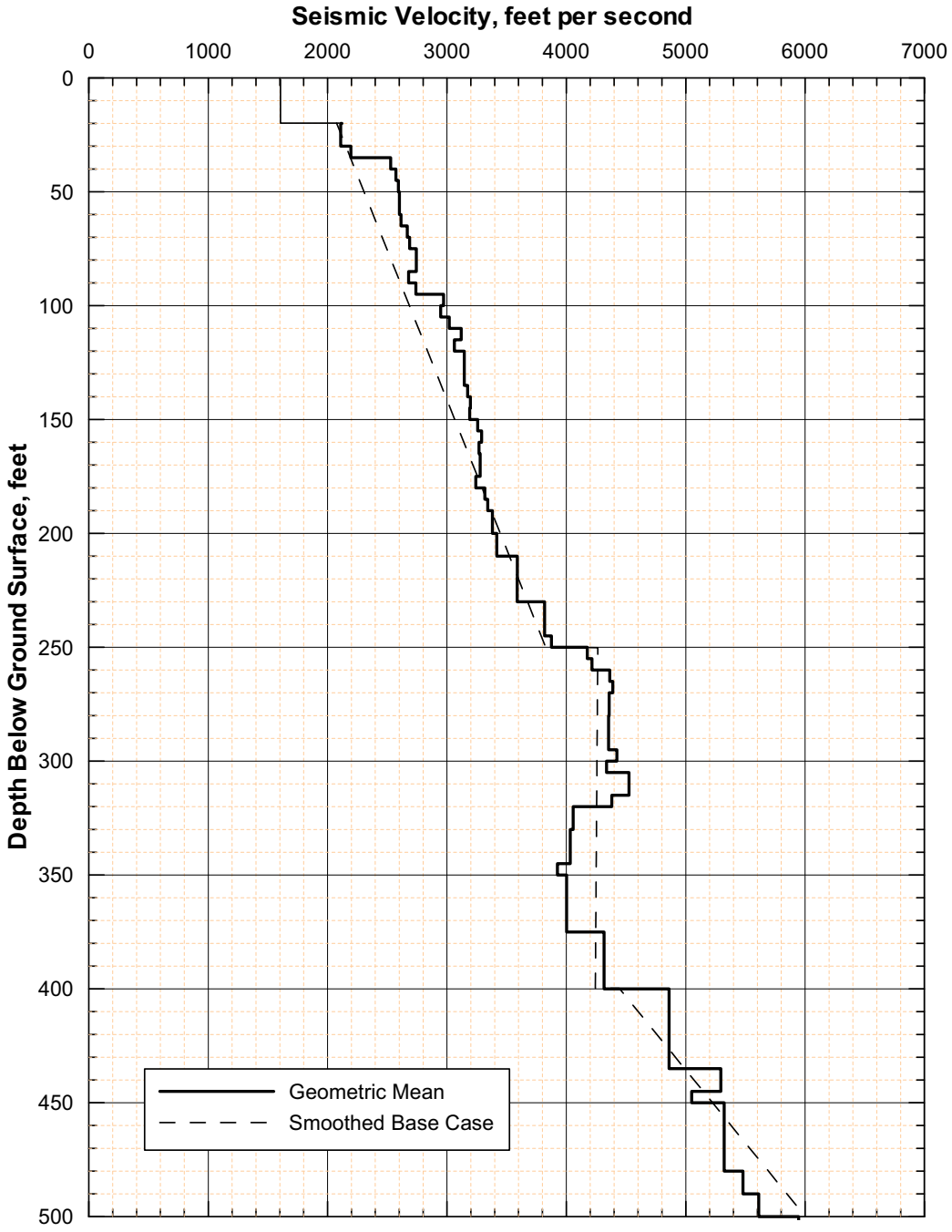

Source: Wong and Silva 2003 [DIRS 163201], p. 91, Figure 30

Figure 6.2-119. Base Case V_S Profile for Tuff in the Surface Facilities Area

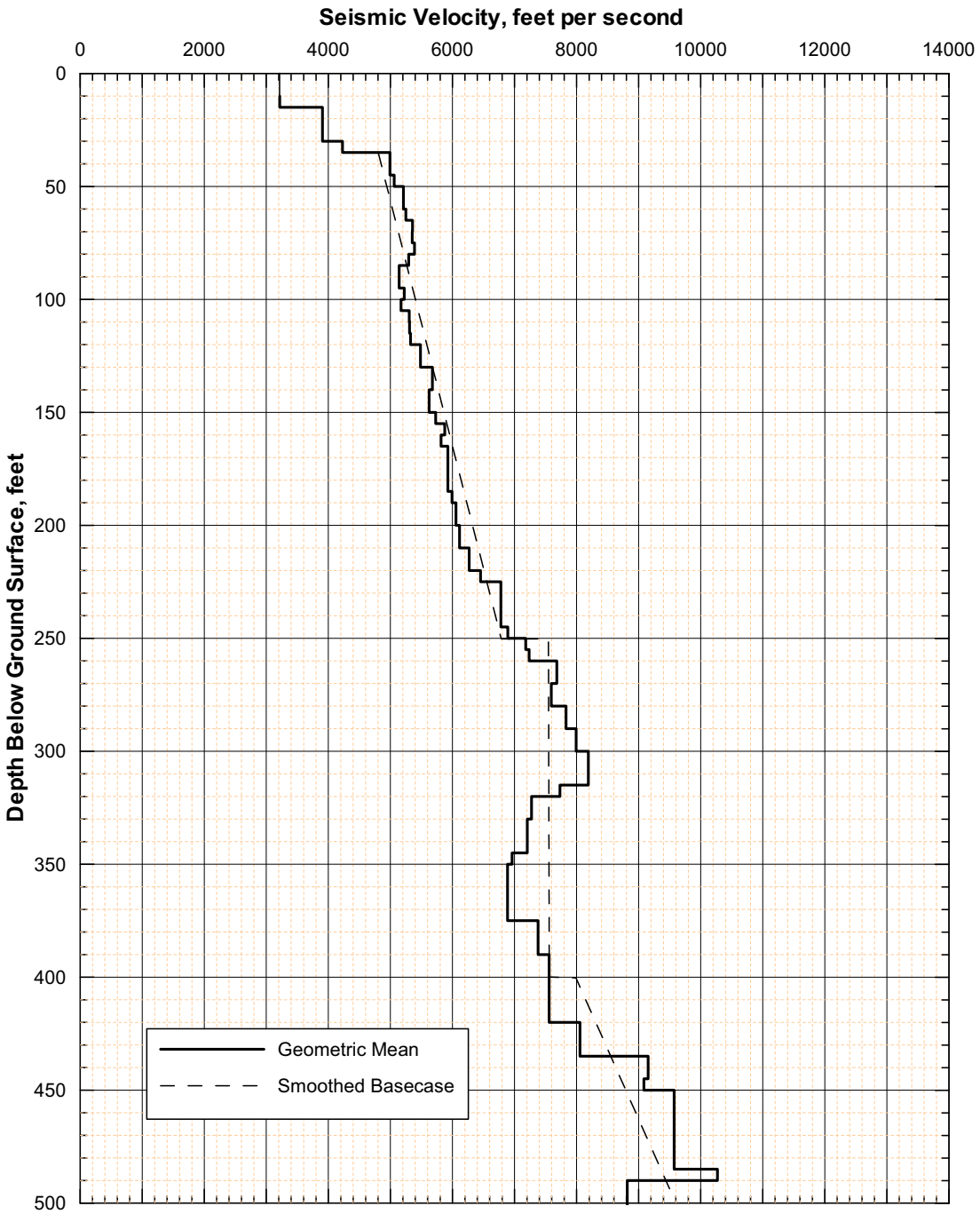

Source: Wong and Silva 2003 [DIRS 163201], p. 93, Figure 32

Figure 6.2-120. Base Case V_P Profile for Tuff in the Surface Facilities Area

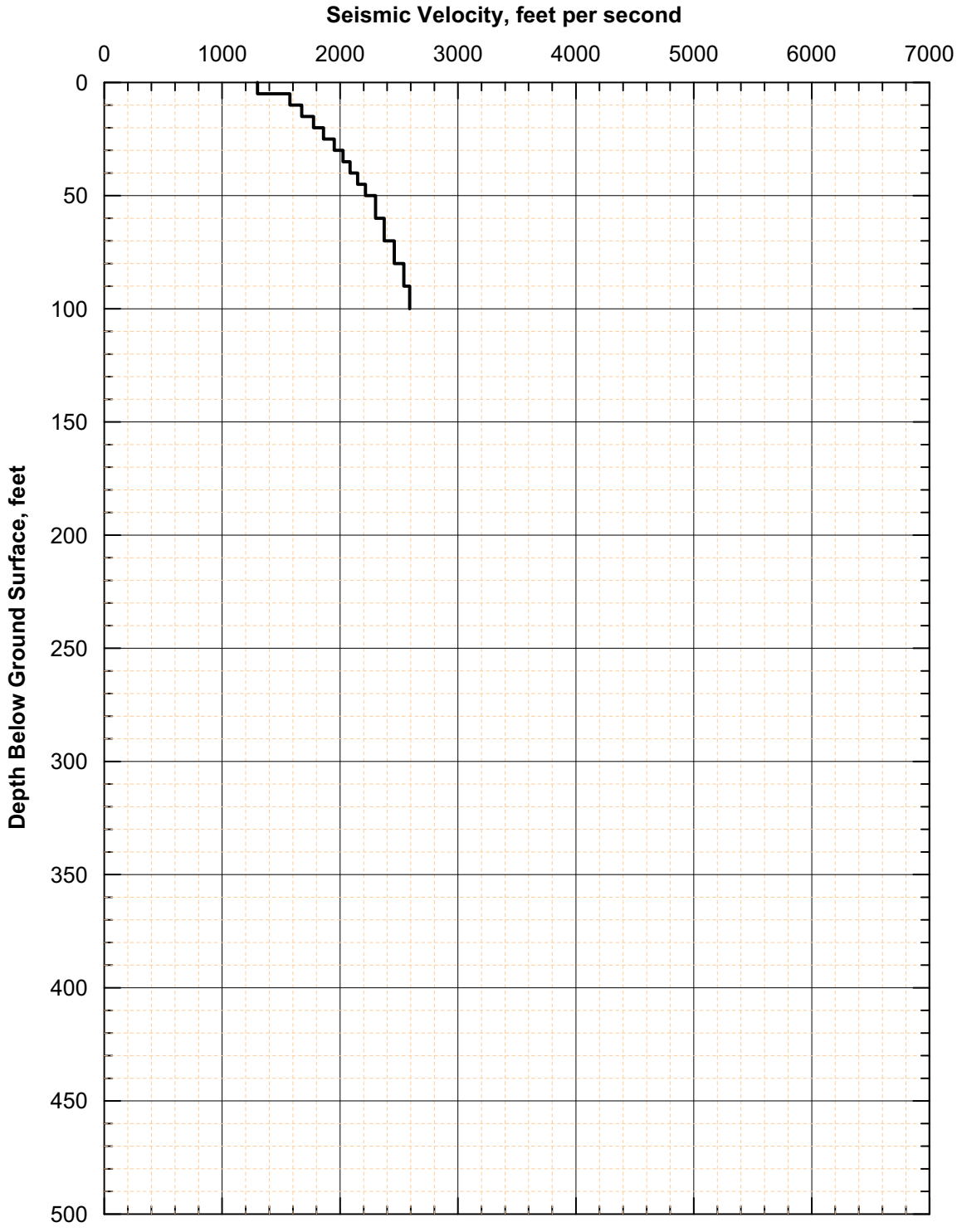

Source: Wong and Silva 2003 [DIRS 163201], p. 88, Figure 27

Figure 6.2-121. Base Case V_S Profile for Alluvium in the Surface Facilities Area

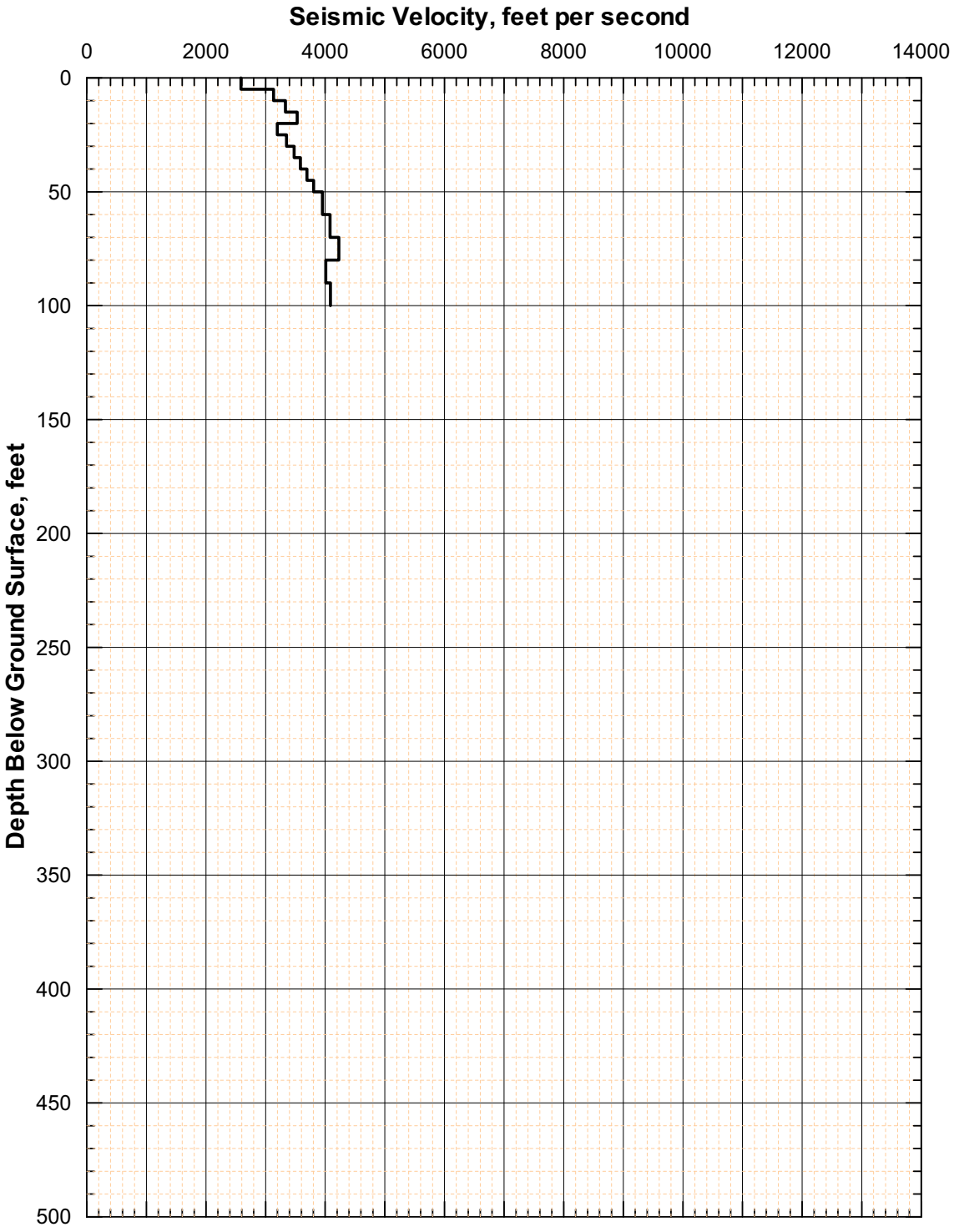

Source: Wong and Silva 2003 [DIRS 163201], p. 90, Figure 29

Figure 6.2-122. Base Case V_P Profile for Alluvium in the Surface Facilities Area

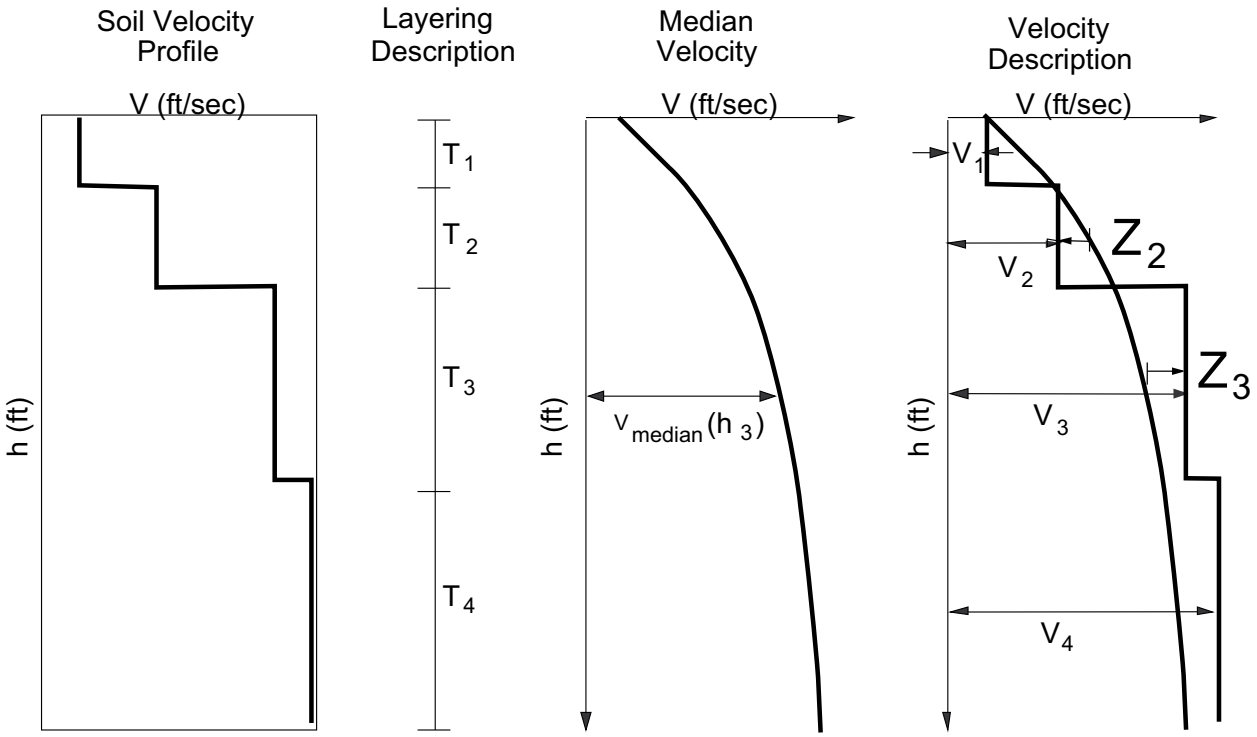

Source: Silva et al. 1996 [DIRS 110474], Appendix C, Figure 14

Figure 6.2-123. Formulation of Probabilistic Representation of Velocity Models

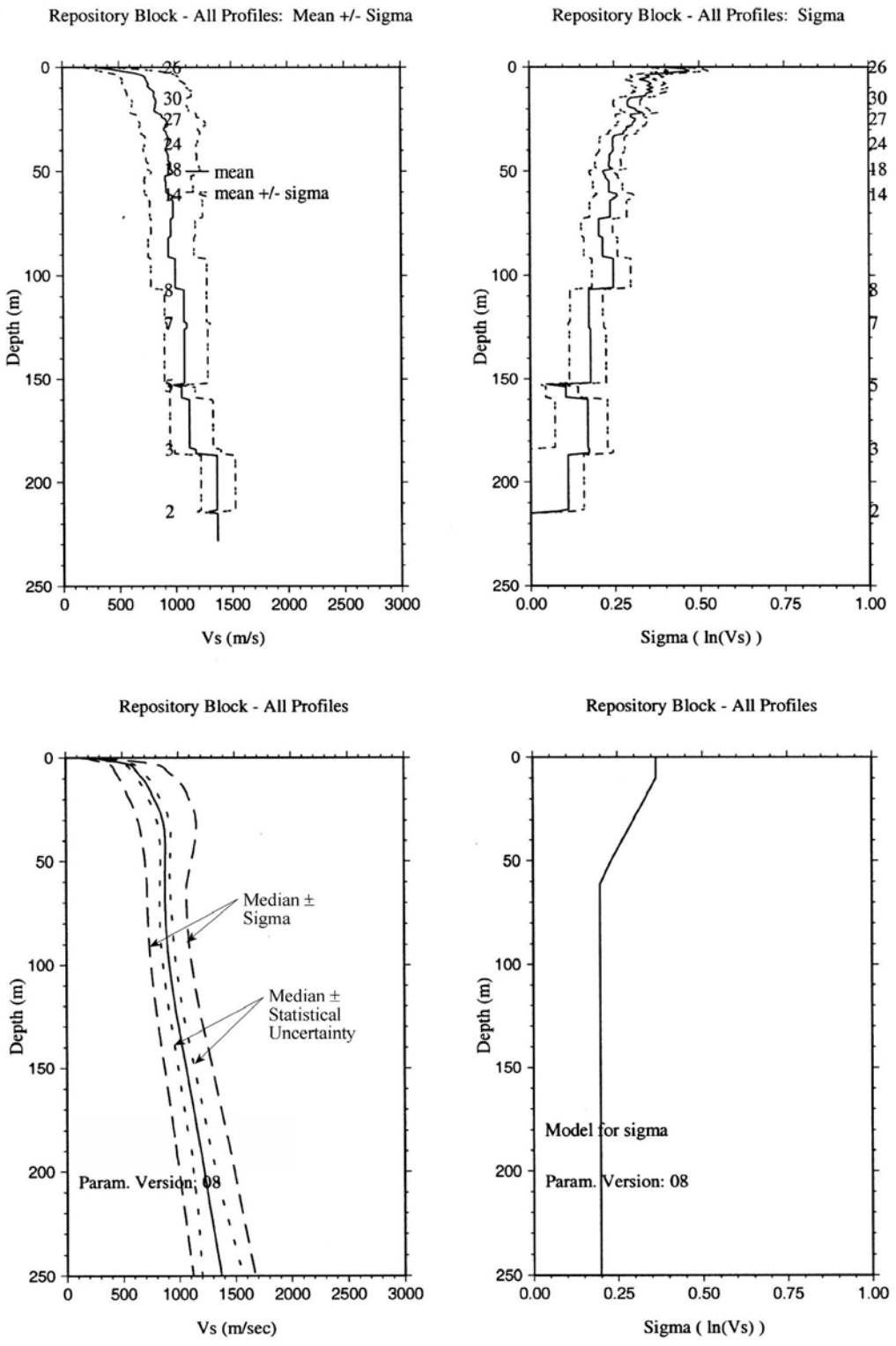

Source: Wong and Toro 2003 [DIRS 163848], Supplemental Records 35 and 40

NOTE: Values on right side of profiles indicate number of profiles used in statistics as a function of depth.

Figure 6.2-124. Summary Statistics and Probabilistic Representation of Repository Block V_S Profiles

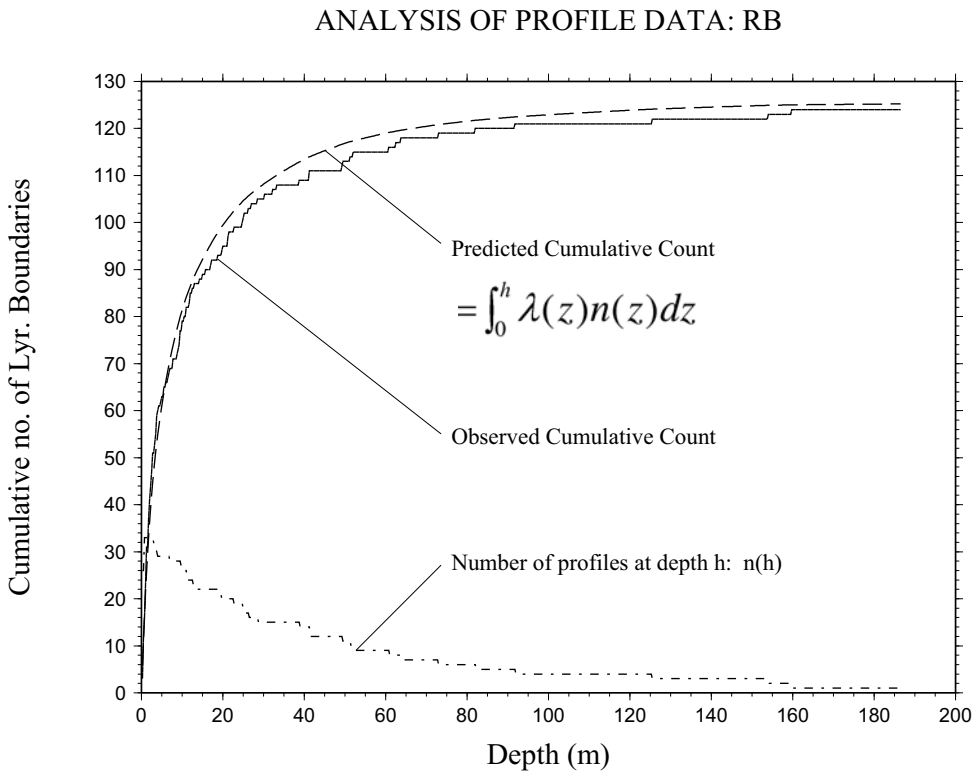

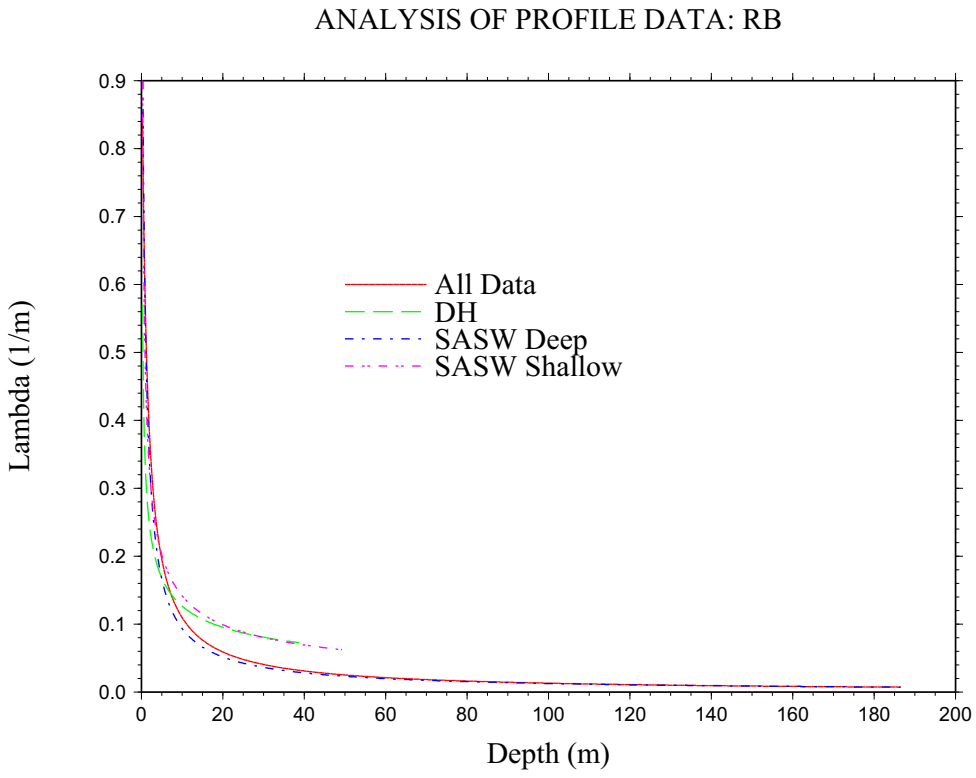

Source: Wong and Toro 2003 [DIRS 163848], Supplemental Record 54, pages 15 and 17

Figure 6.2-125. Analysis of Repository Block Layer Thickness Data

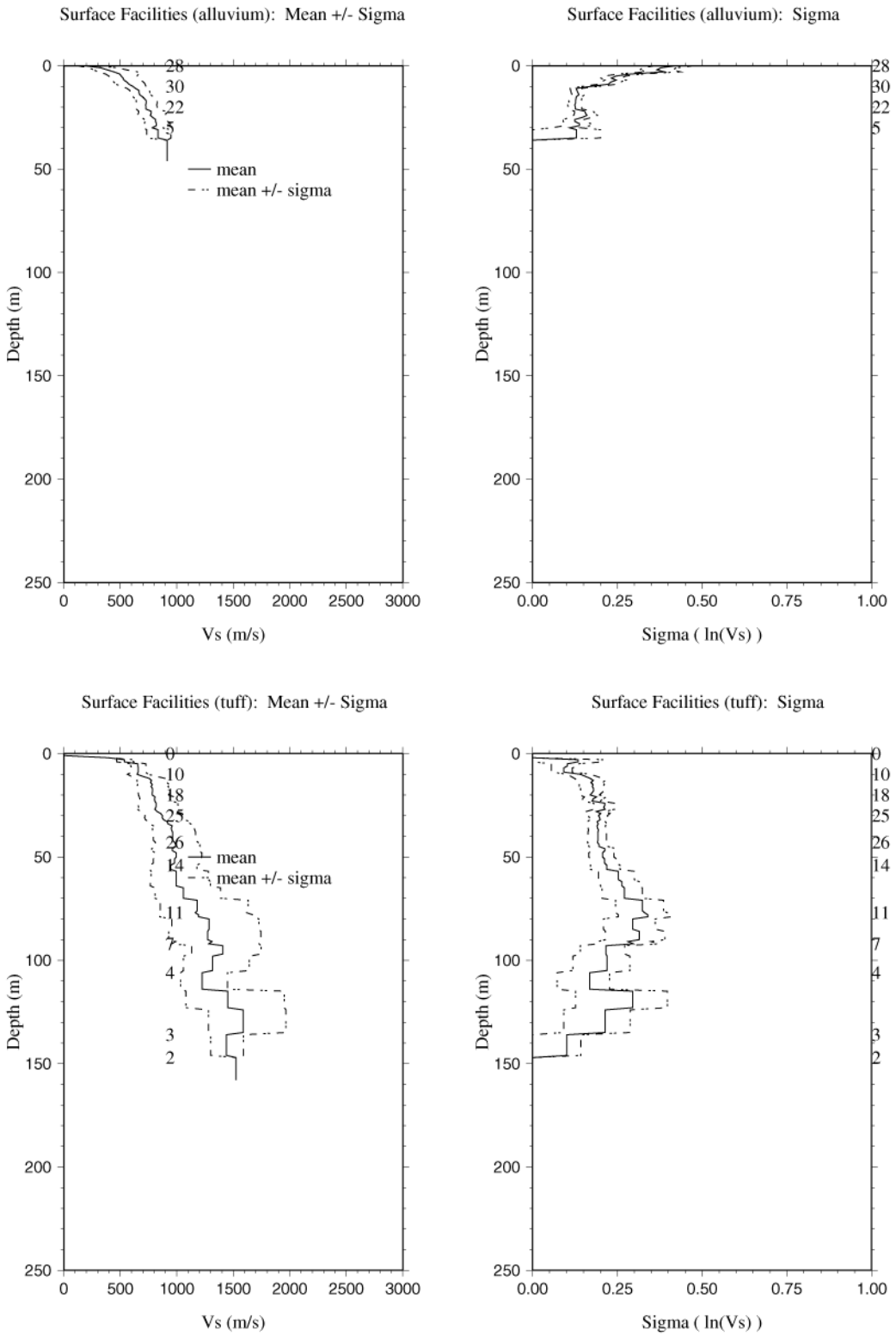

Source: Wong and Toro 2003 [DIRS 163848], Supplemental Record 47, pages 16, 17, 29, 30

NOTE: Values on right side of profiles indicate number of profiles used in statistics as a function of depth.

Figure 6.2-126. Summary Statistics of Surface Facilities V_S Profiles in Alluvium and Tuff

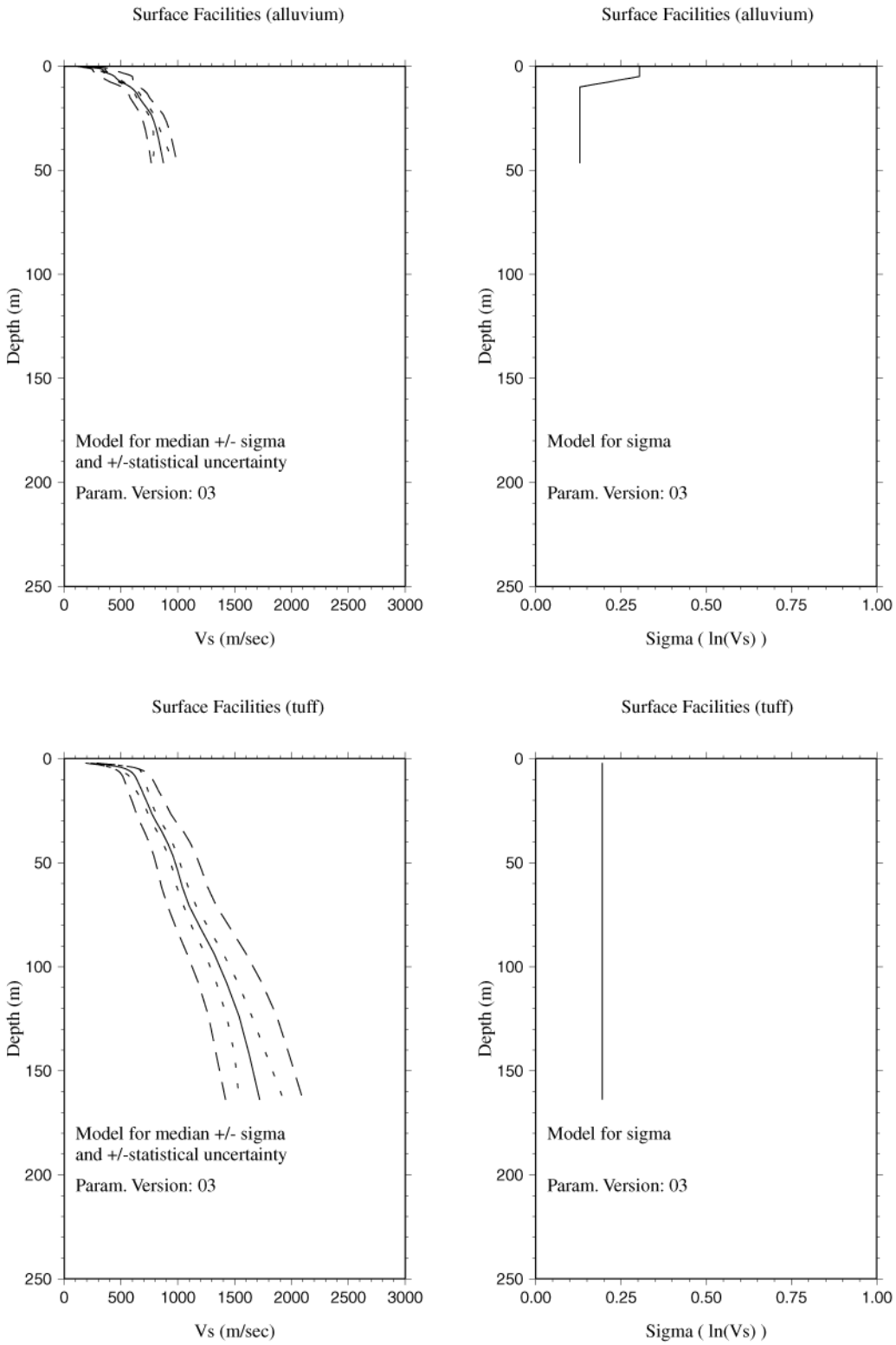

Source: Wong and Toro 2003 [DIRS 163848], Supplemental Record 48, pages 3 and 4; and Supplemental Record 49, pages 3 and 4

Figure 6.2-127. Probabilistic Representation of Surface Facilities V_S Profiles in Alluvium and Tuff

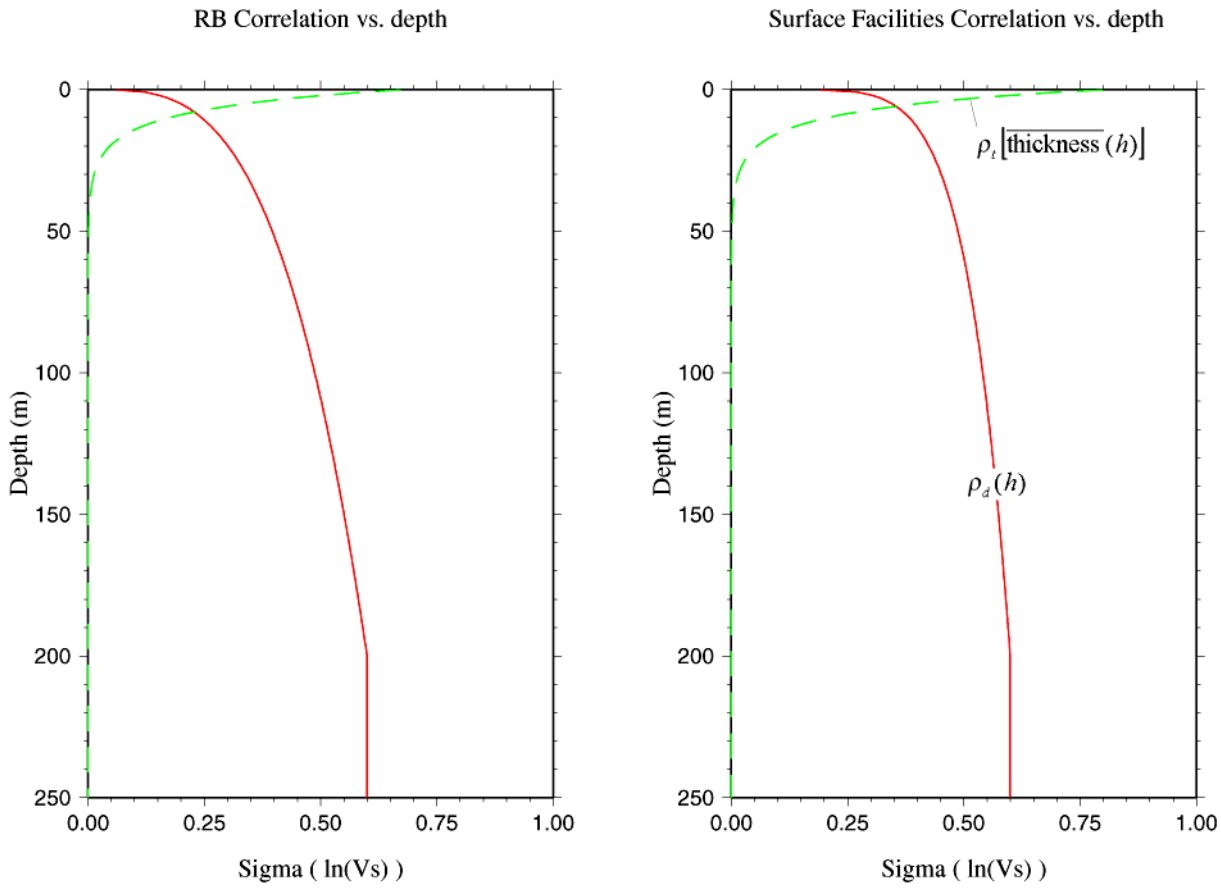

Source: Wong and Toro 2003 [DIRS 163848], Supplemental Records 71 and 72

Figure 6.2-128. Correlation Coefficients Versus Depth for Repository Block and Surface Facilities Area

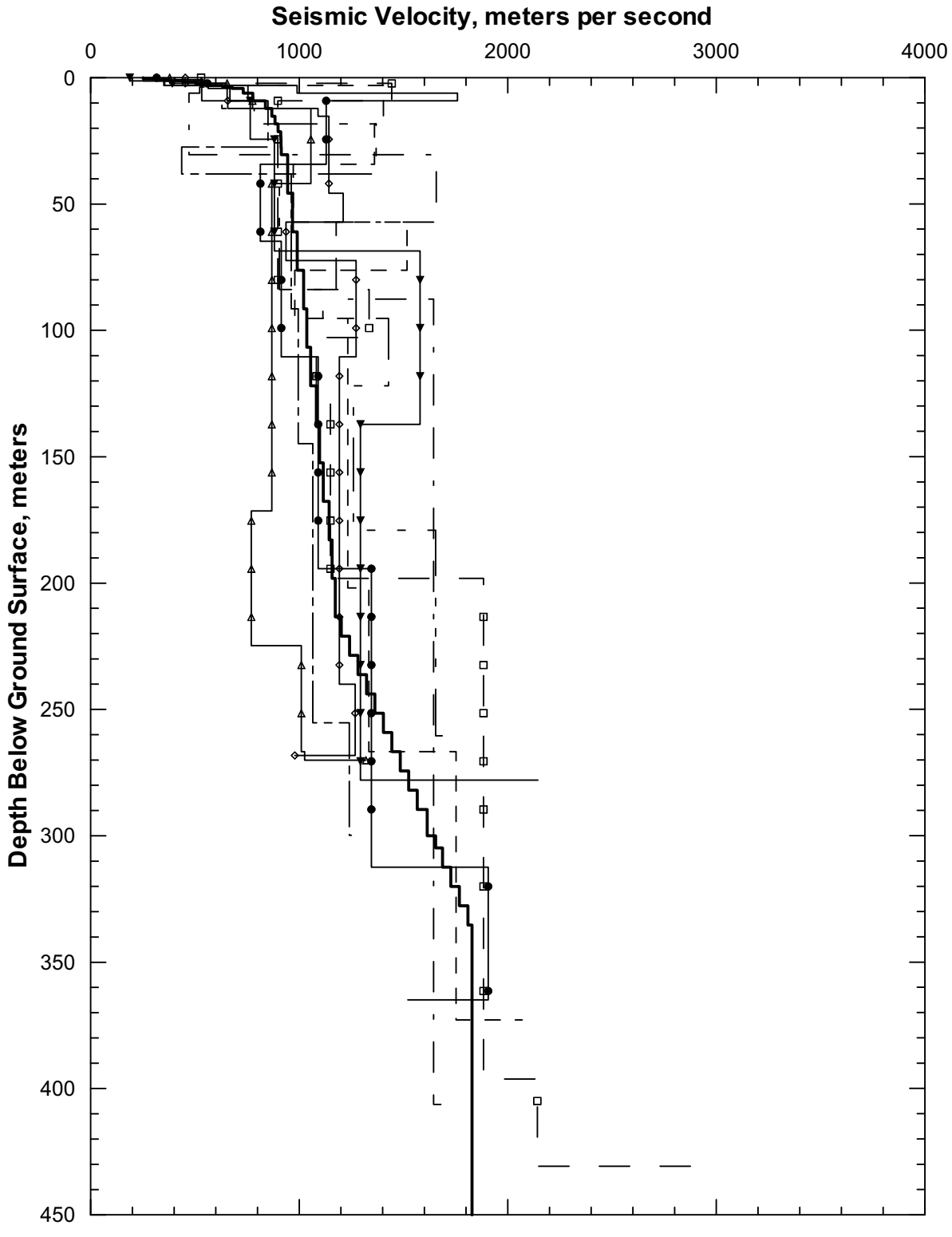

DTN: MO0206SASWVSP1.001 [DIRS 163777] (Basecase #1)

Source: Wong and Silva 2004a [DIRS 170443], page 72, Supplemental Record 81, page 2

NOTE: The 9 randomized V_S profiles shown are a subset of the 60 generated for Repository Block Basecase #1

Figure 6.2-129. Randomized V_S Profiles Generated from Repository Block Base Case #1

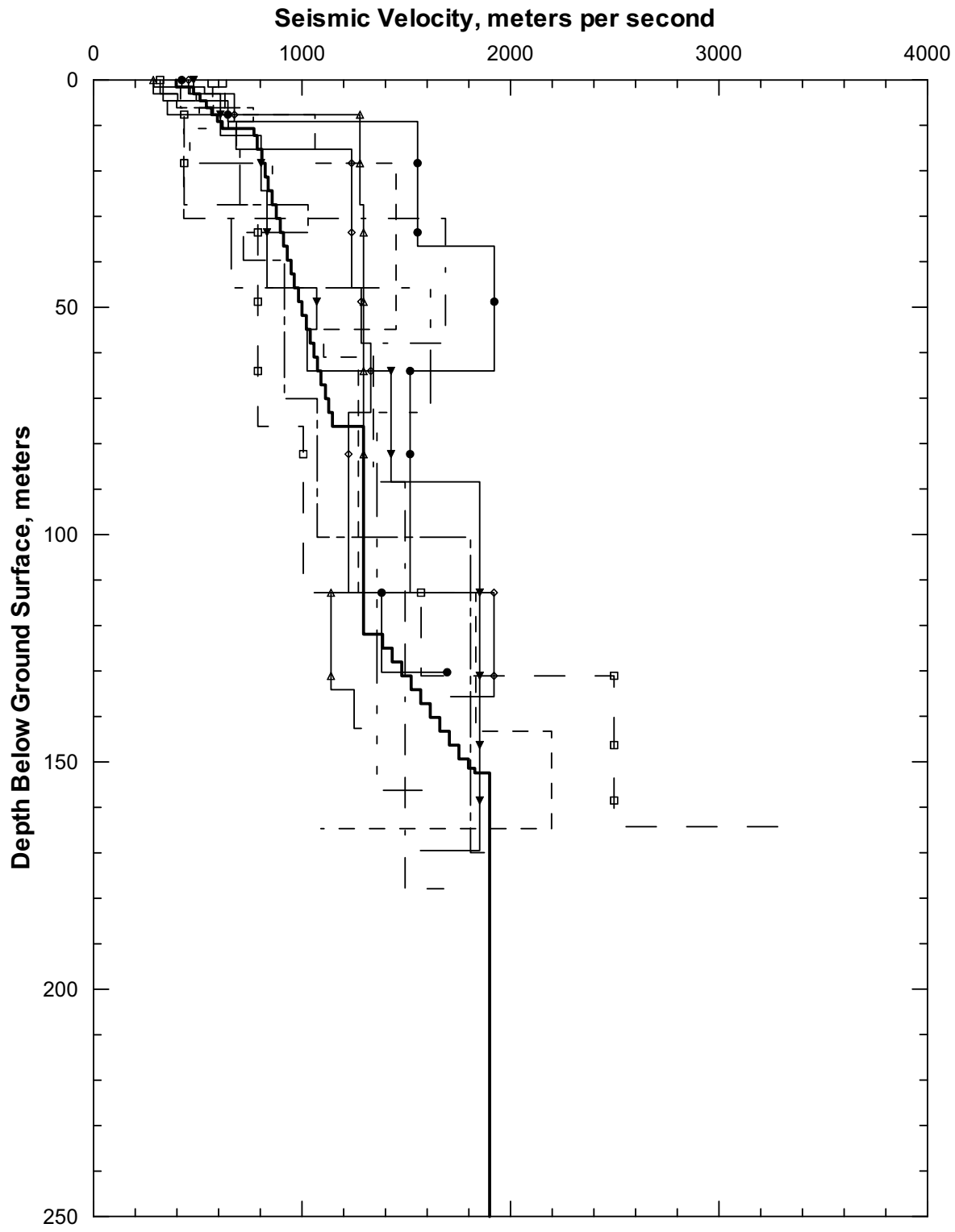

Source: Wong and Silva 2004d [DIRS 172075], page 34

NOTE: The 9 randomized V_S profiles shown are a subset of the 60 generated for the Surface Facilities Area

Figure 6.2-130. Randomized V_S Profiles at the Surface Facilities Area

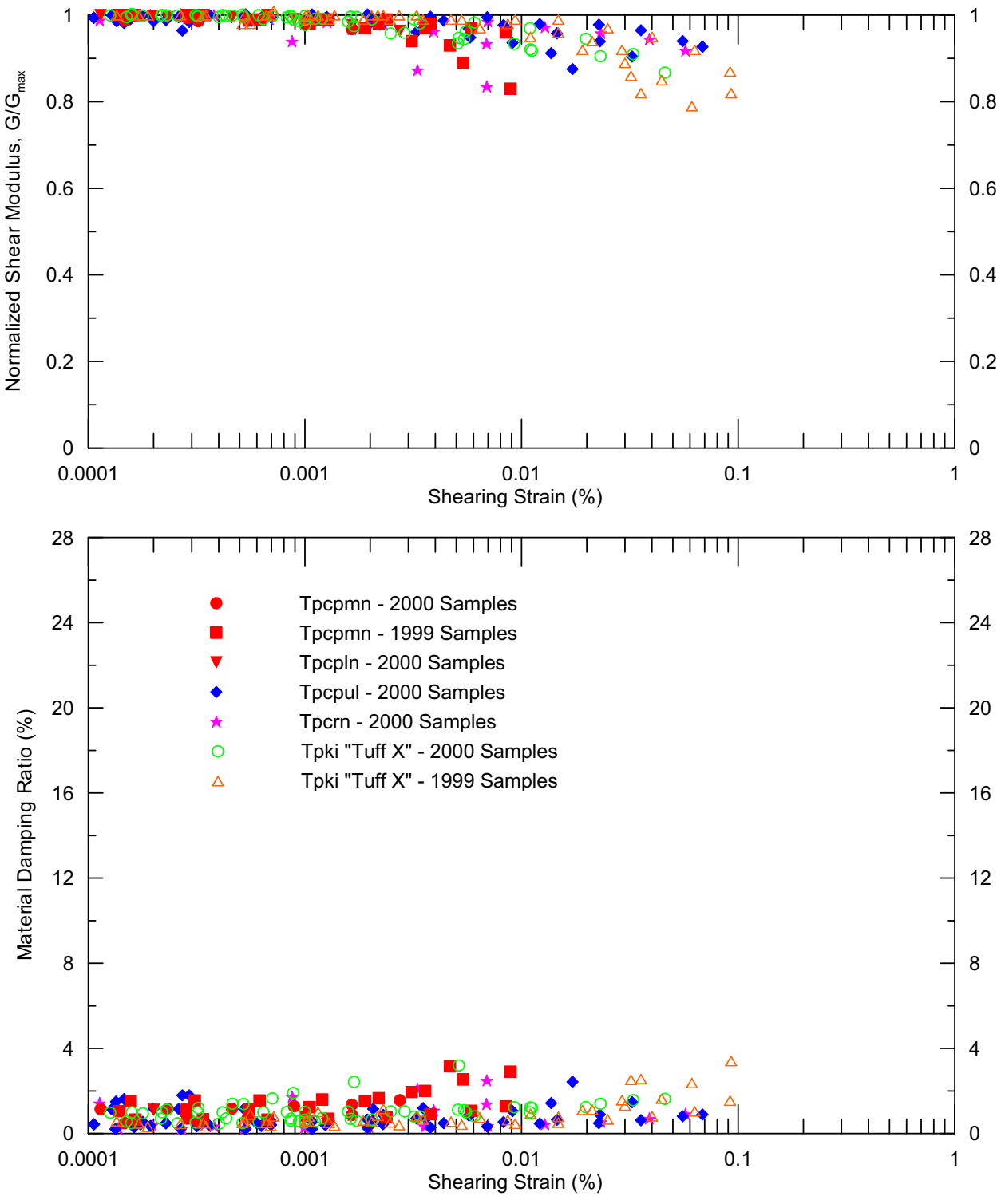

DTN: MO0203DHRSSWHB.001 [DIRS 158082], MO9905LABDYNRS.000 [DIRS 103792]

Figure 6.2-131. Laboratory Test Results on Tuff Specimens Grouped by Stratigraphic Unit

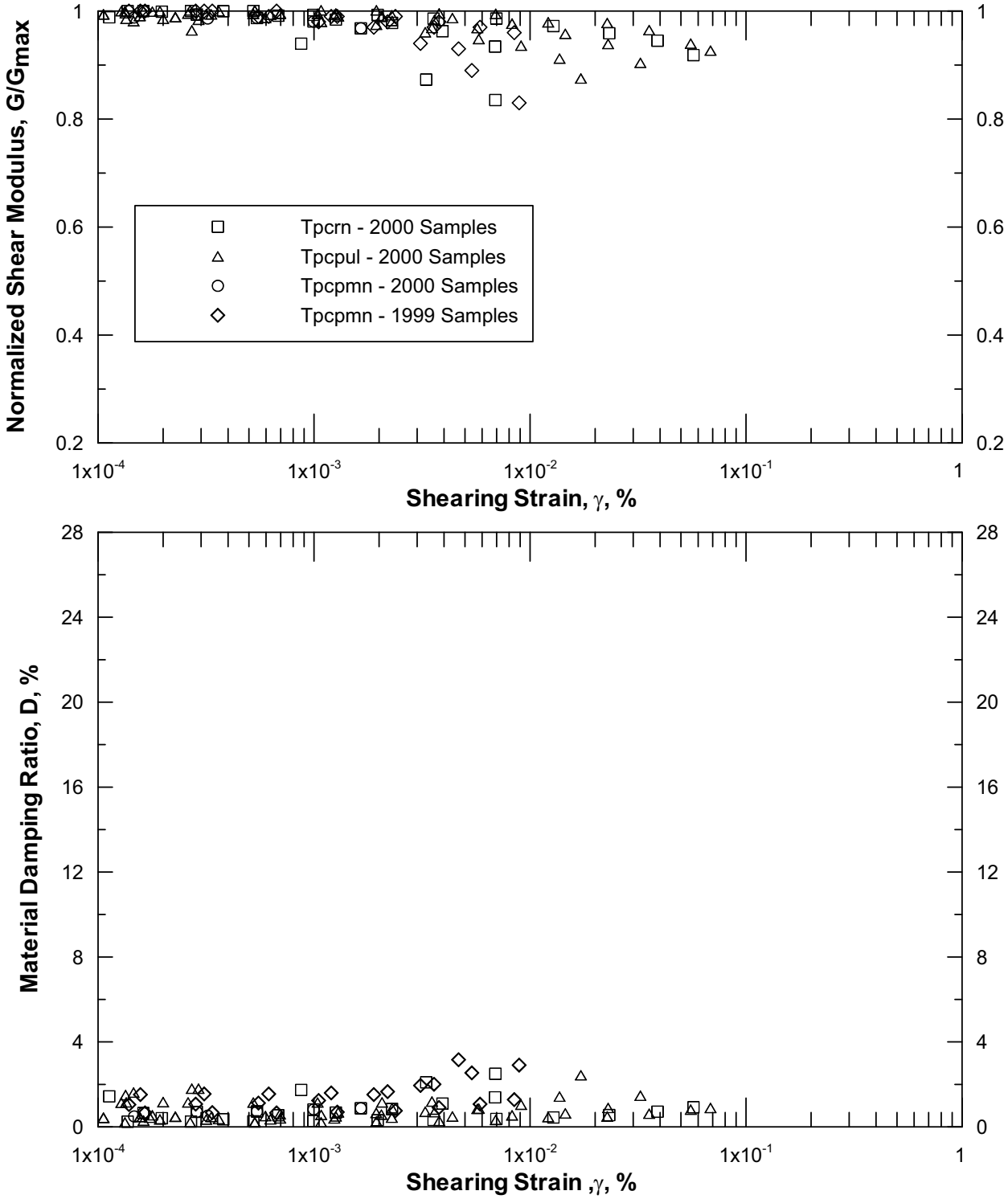

DTN: MO0203DHRSSWHB.001 [DIRS 158082], MO9905LABDYNRS.000 [DIRS 103792]

Figure 6.2-132. Laboratory Test Results on Welded Tuff Specimens

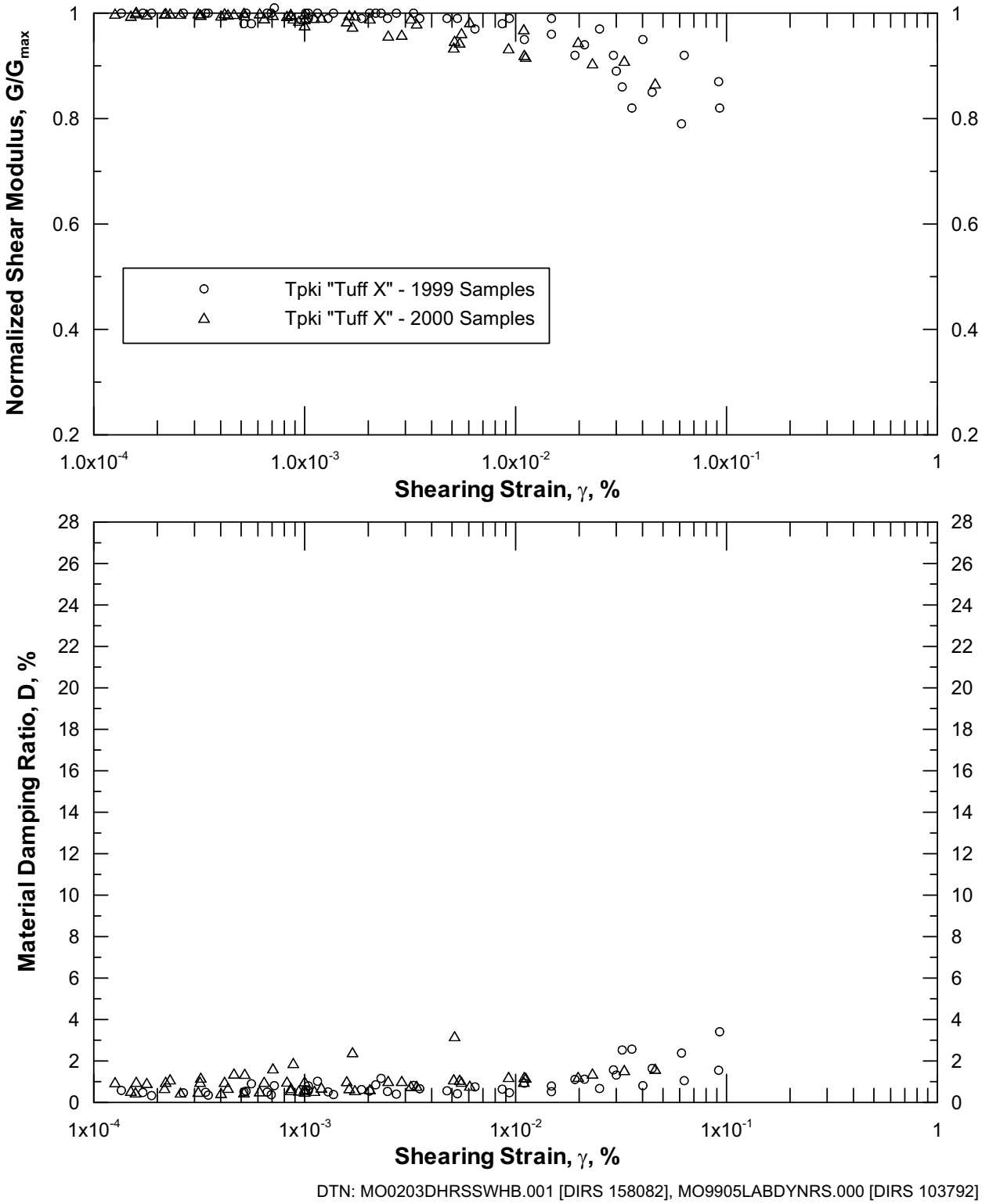

DTN: MO0203DHRSSWHB.001 [DIRS 158082], MO9905LABDYNRS.000 [DIRS 103792]

Figure 6.2-133. Laboratory Test Results on Nonwelded Tuff Specimens

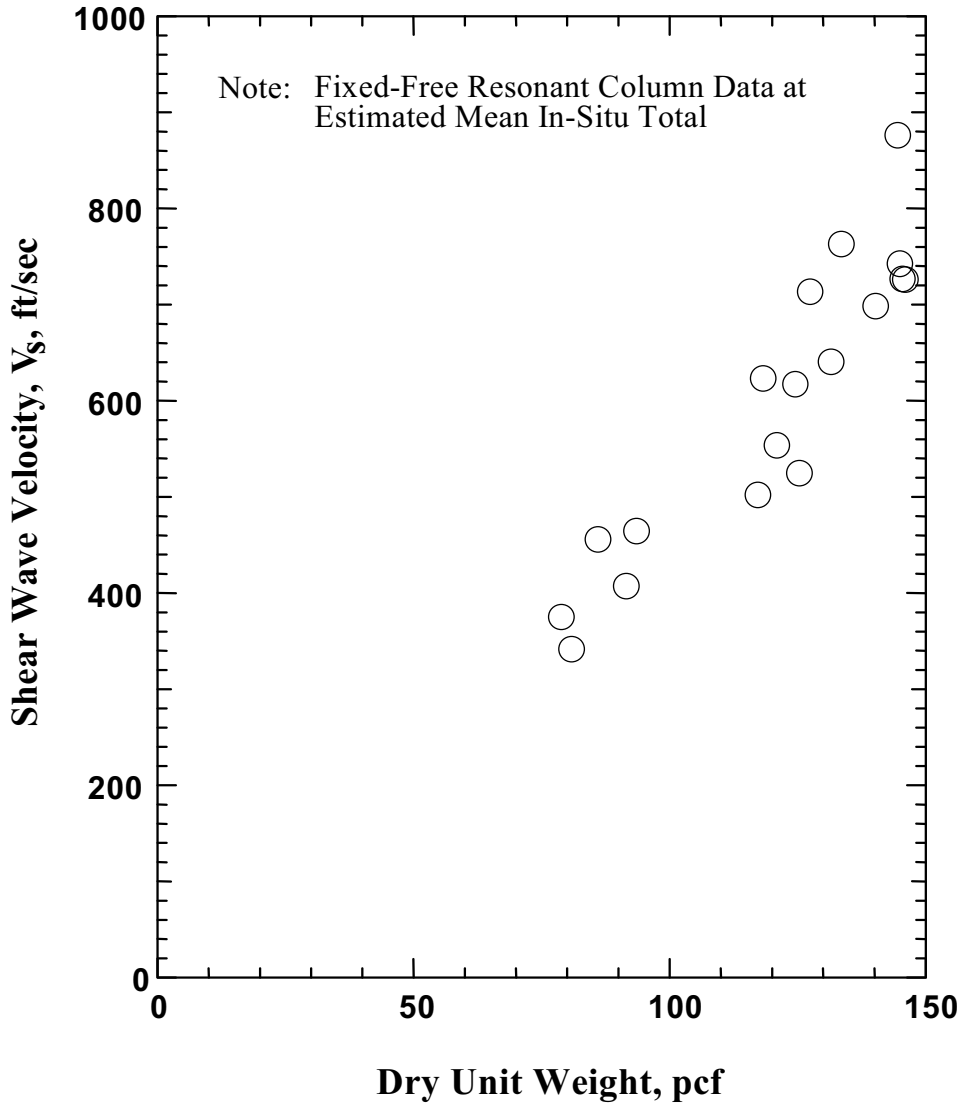

DTN: MO0203DHRSSWHB.001 [DIRS 158082]

Figure 6.2-134. Variation of V_S Measured in the Laboratory at In-Situ Mean Total Stress with Dry Unit Weight of Intact Tuff Specimens

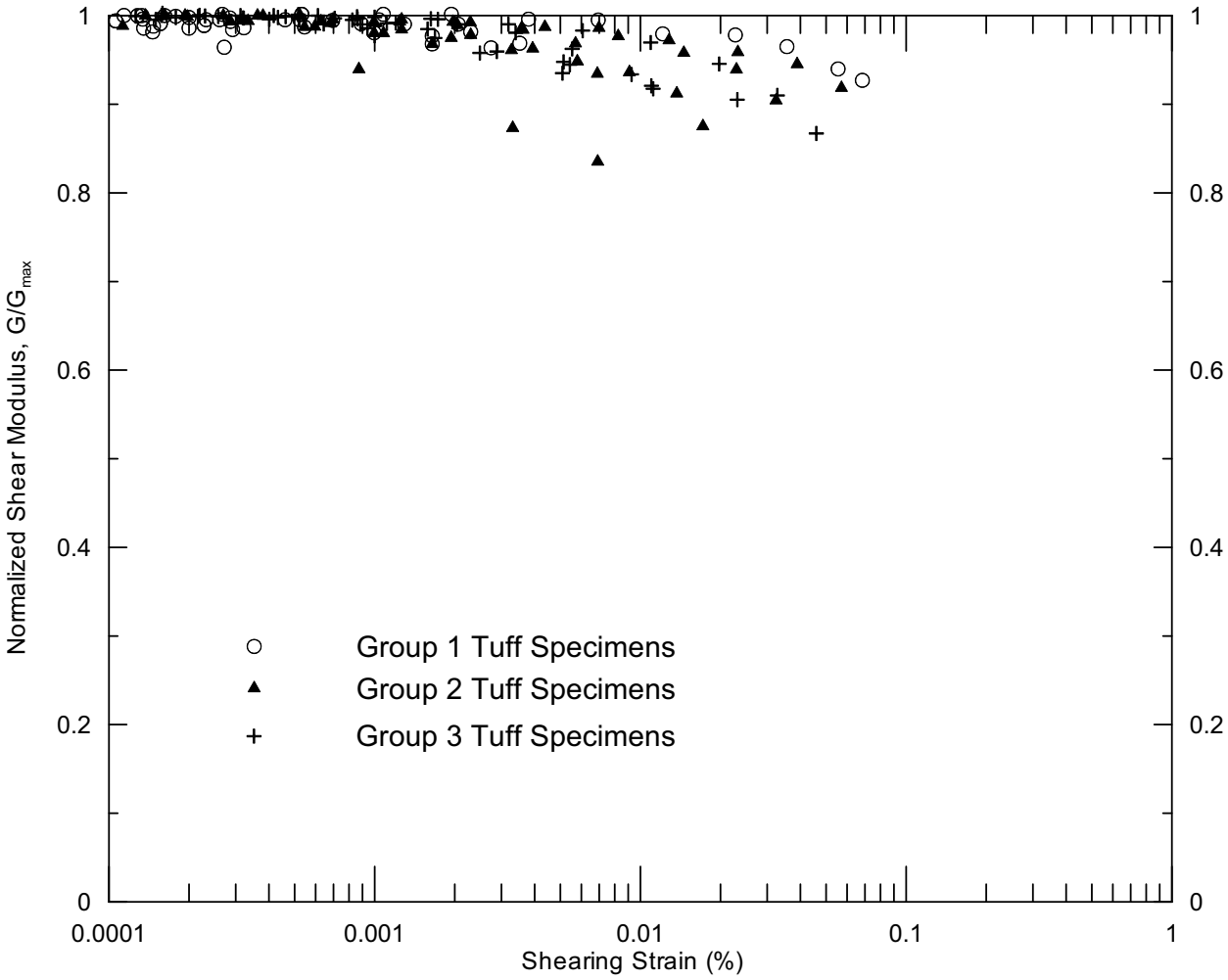

DTN: MO0203DHRSSWHB.001 [DIRS 158082]

Figure 6.2-135. Variation in Normalized Shear Modulus with Shearing Strain of Intact Tuff Specimens for Groups Based on Dry Unit Weight

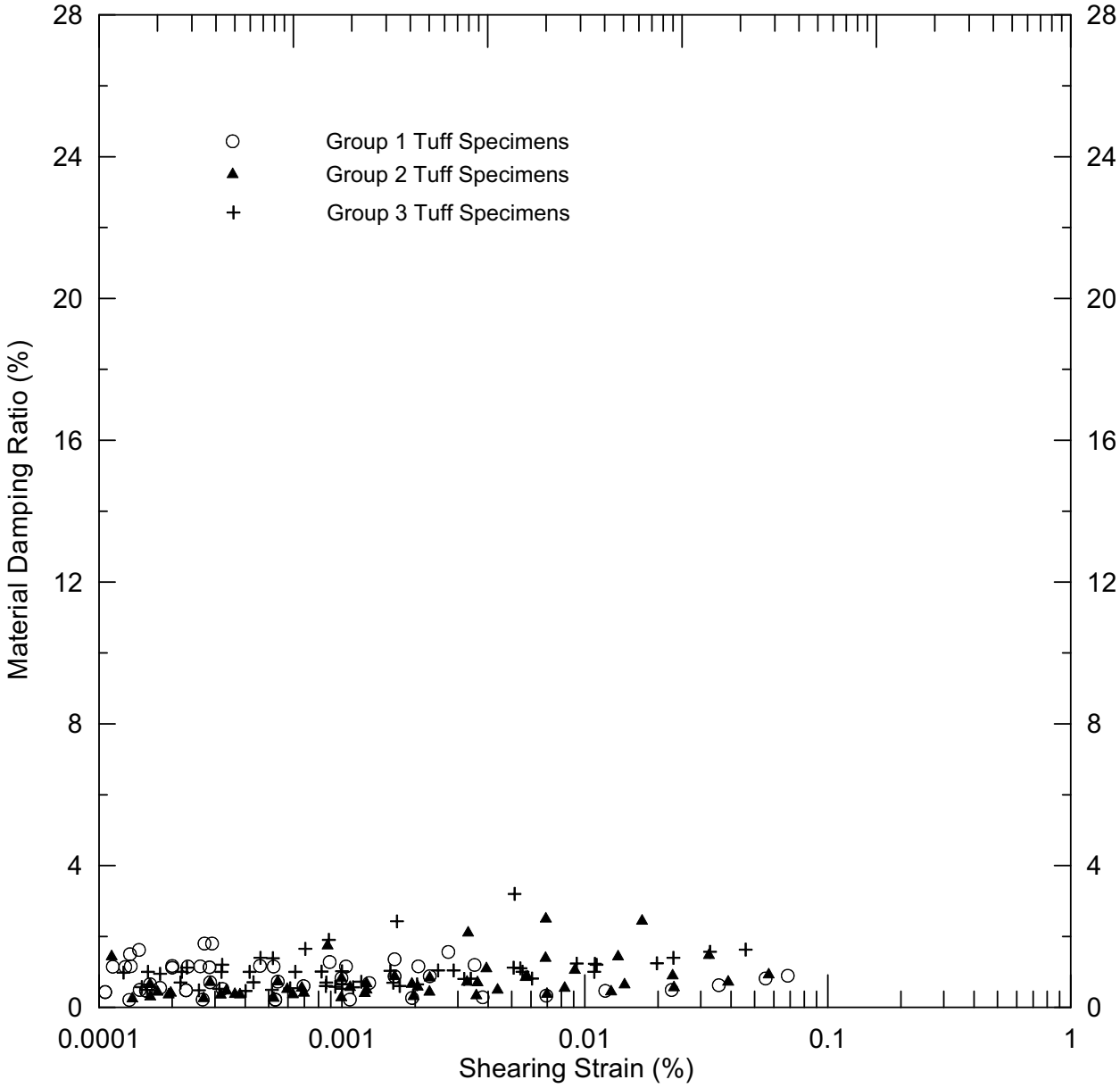

DTN: MO0203DHRSSWHB.001 [DIRS 158082]

Figure 6.2-136. Variation in Material Damping Ratio with Shearing Strain of Intact Tuff Specimens for Groups Based on Dry Unit Weight

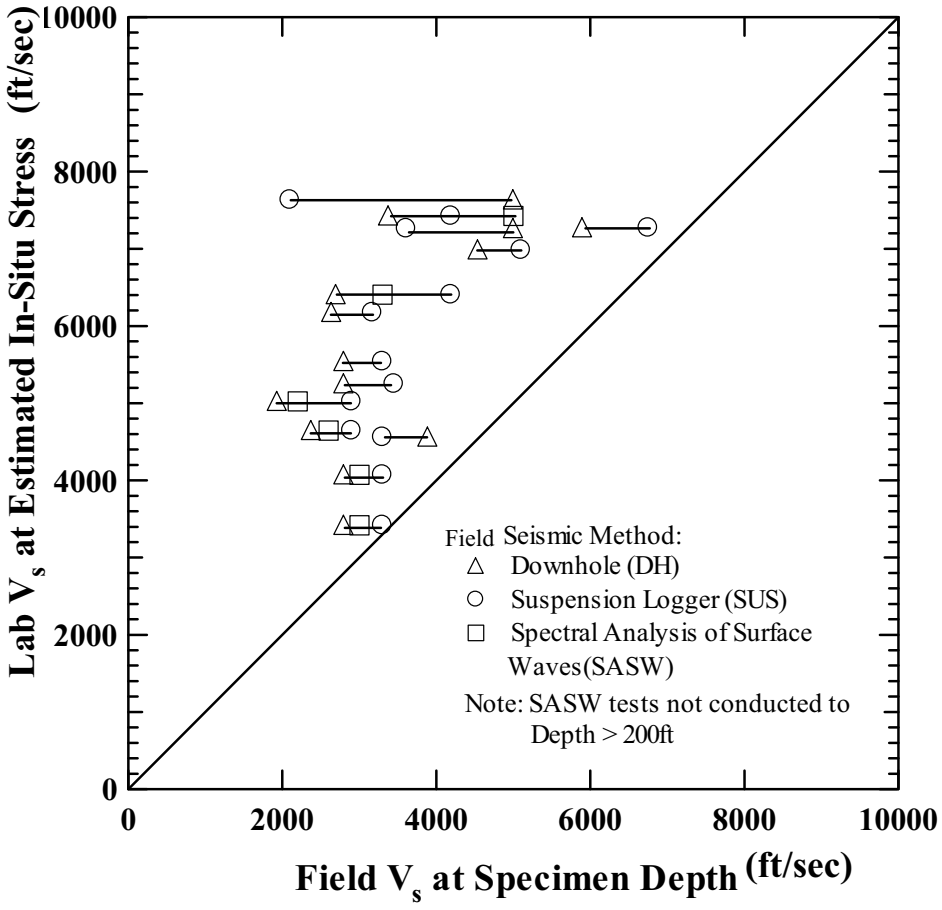

Source: Wong and Silva 2003 [DIRS 163201], page 117

Figure 6.2-137. Comparison of V_S Measured in the Laboratory and in the Field with Three Different Seismic Methods: Tuff Materials in the Surface Facilities Area

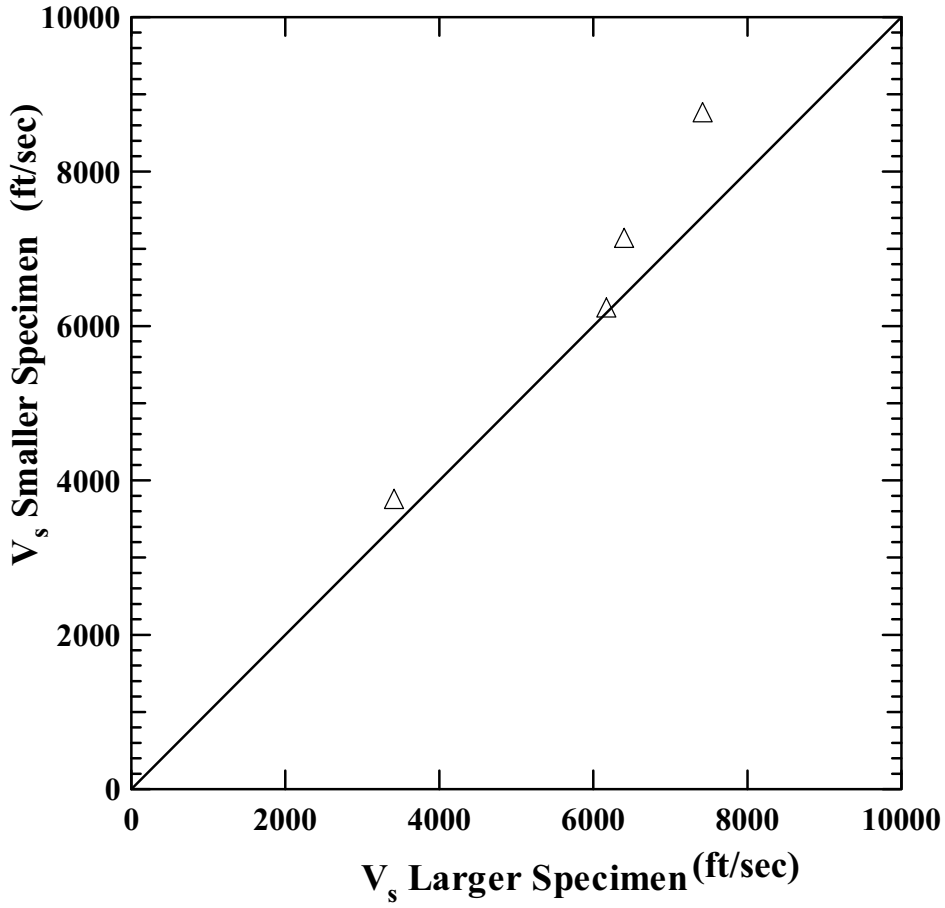

Source: Wong and Silva 2003 [DIRS 163201], page 118

Figure 6.2-138. Comparison of V_S Measured in the Laboratory: Large and Small Tuff Specimens

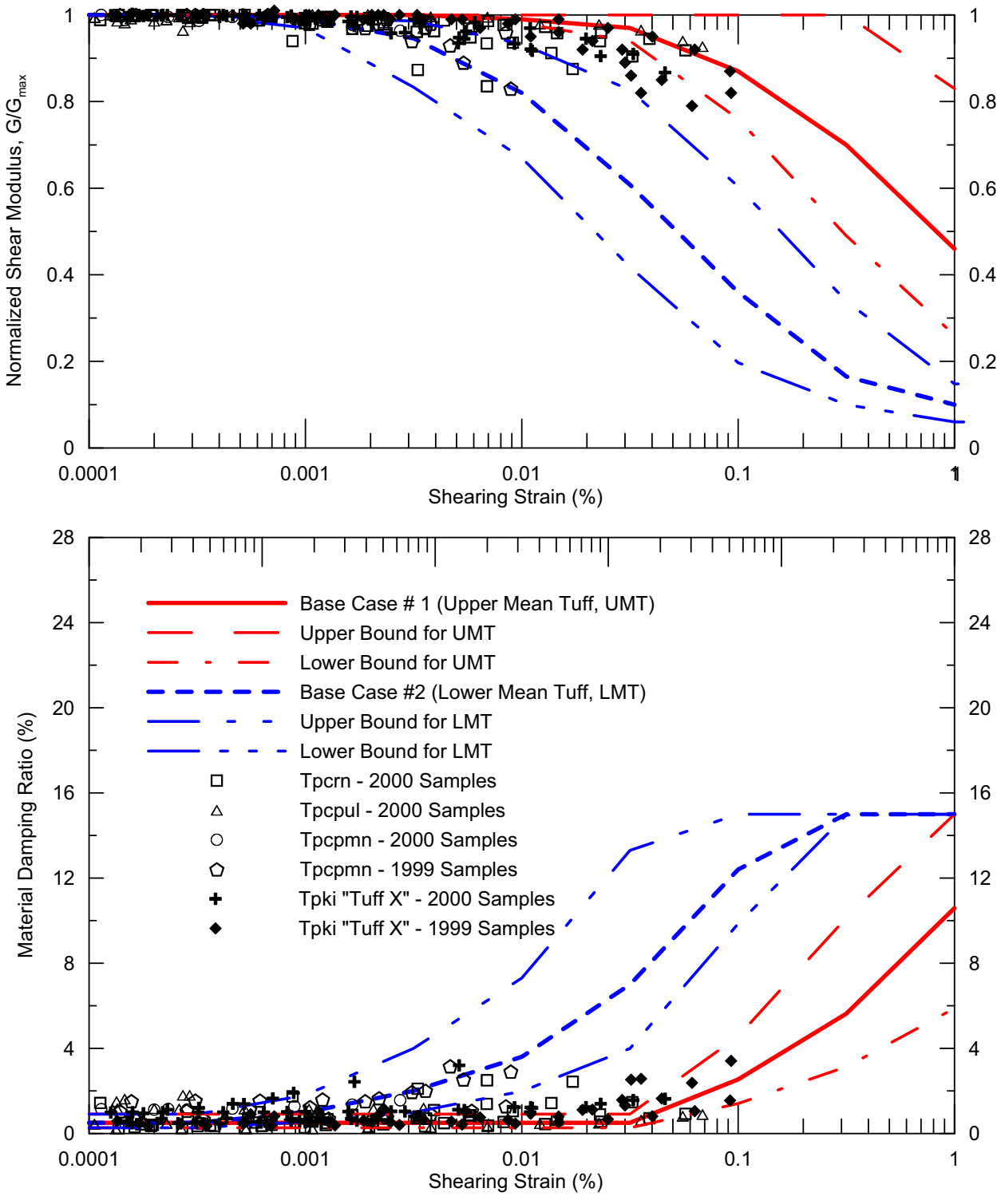

DTN: MO0403SDIAWHBC.003 [DIRS 170434] (CURVES), MO0203DHRSSWHB.001 [DIRS 158082] (DATA), MO9905LABDYNRS.000 [DIRS 103792] (DATA)

Figure 6.2-139. Mean Normalized Shear Modulus and Material Damping Curves for Tuff

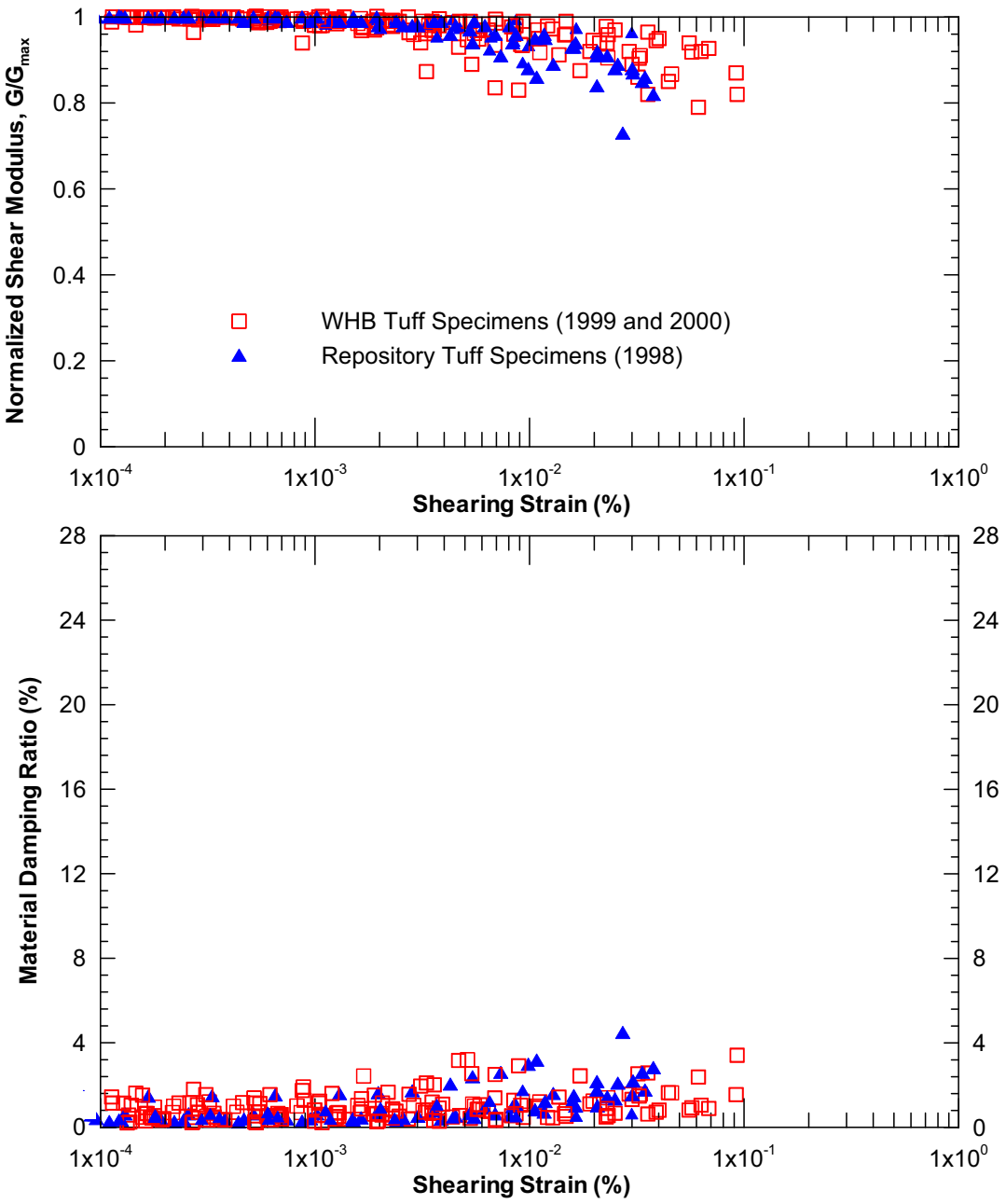

Source: Wong and Silva 2003 [DIRS 163201], page 119

Figure 6.2-140. Laboratory Test Results on Tuff Specimens from WHB Area and Repository Block

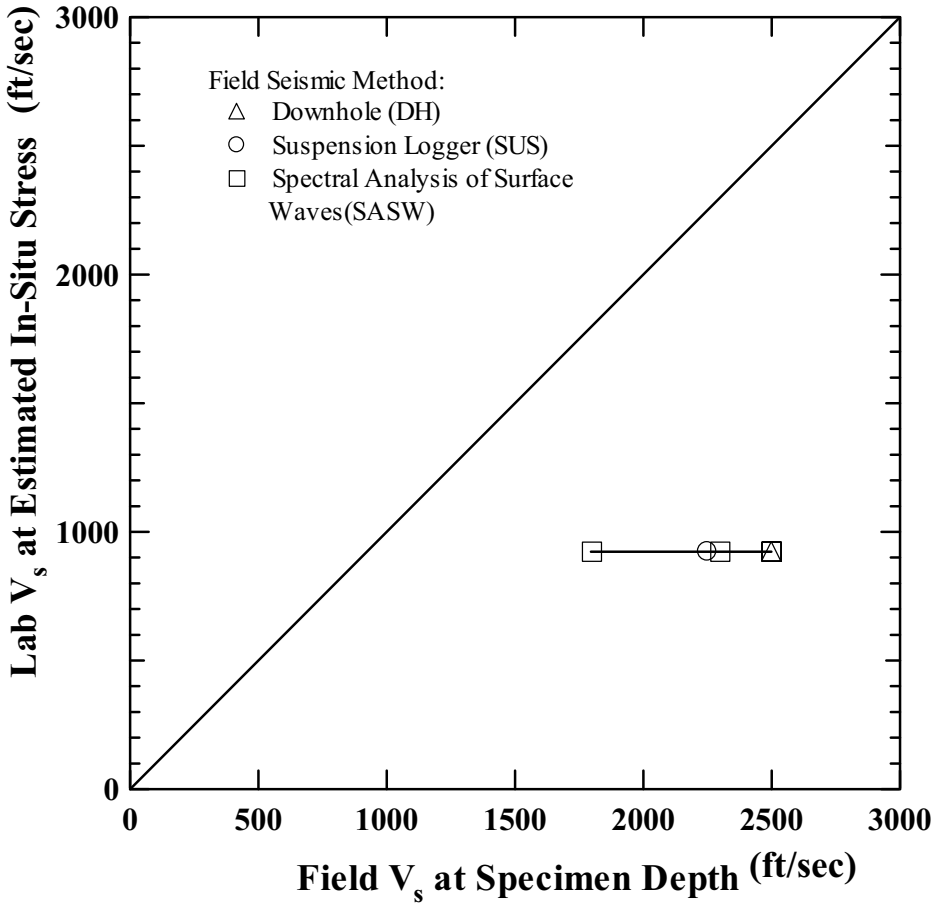

Source: Wong and Silva 2003 [DIRS 163201], page 131

Figure 6.2-141. Comparison of V_S Measured in the Laboratory and V_S Measured in the Field with Three Different Seismic Methods: Reconstituted Alluvium Specimen from a Depth of 59 ft in Borehole UE-25 RF#17

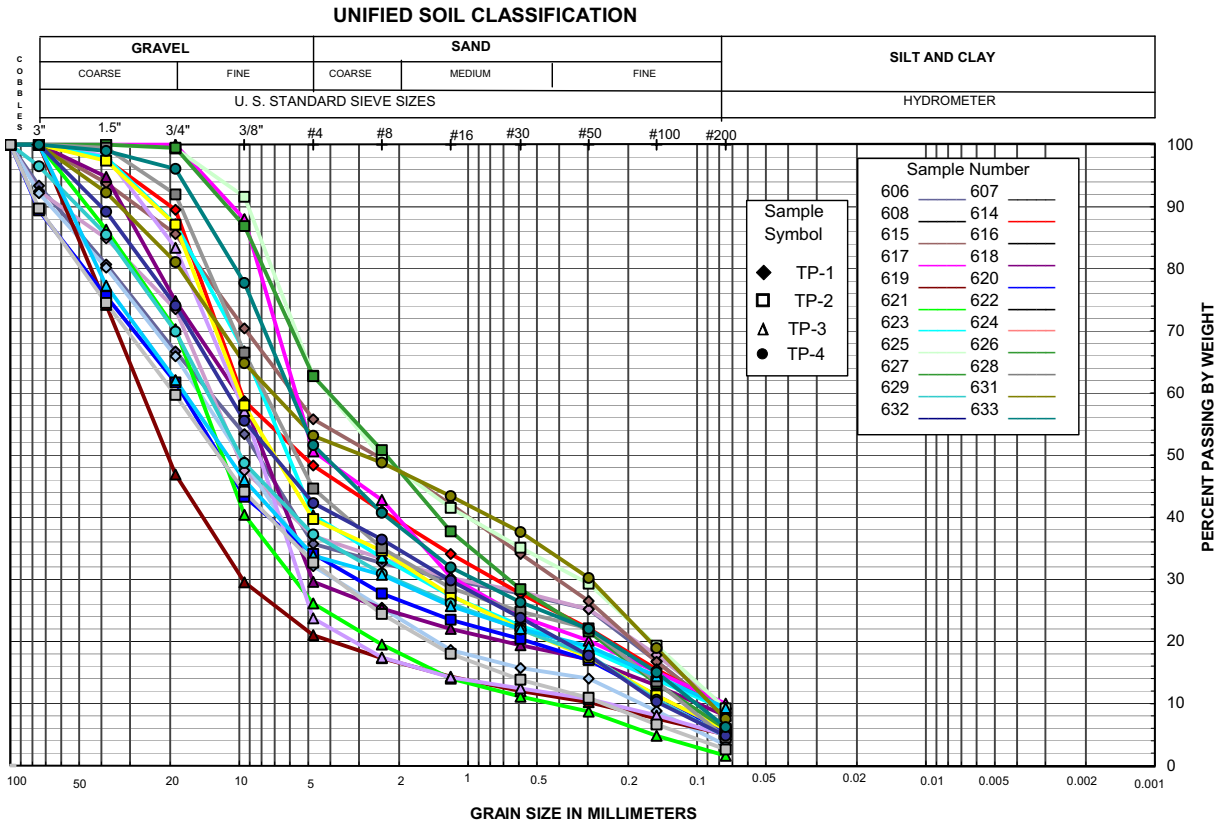

DTN: GS020783114233.005 [DIRS 159542]

Figure 6.2-142. Gradation Curves from WHB Test Pit Bag Samples

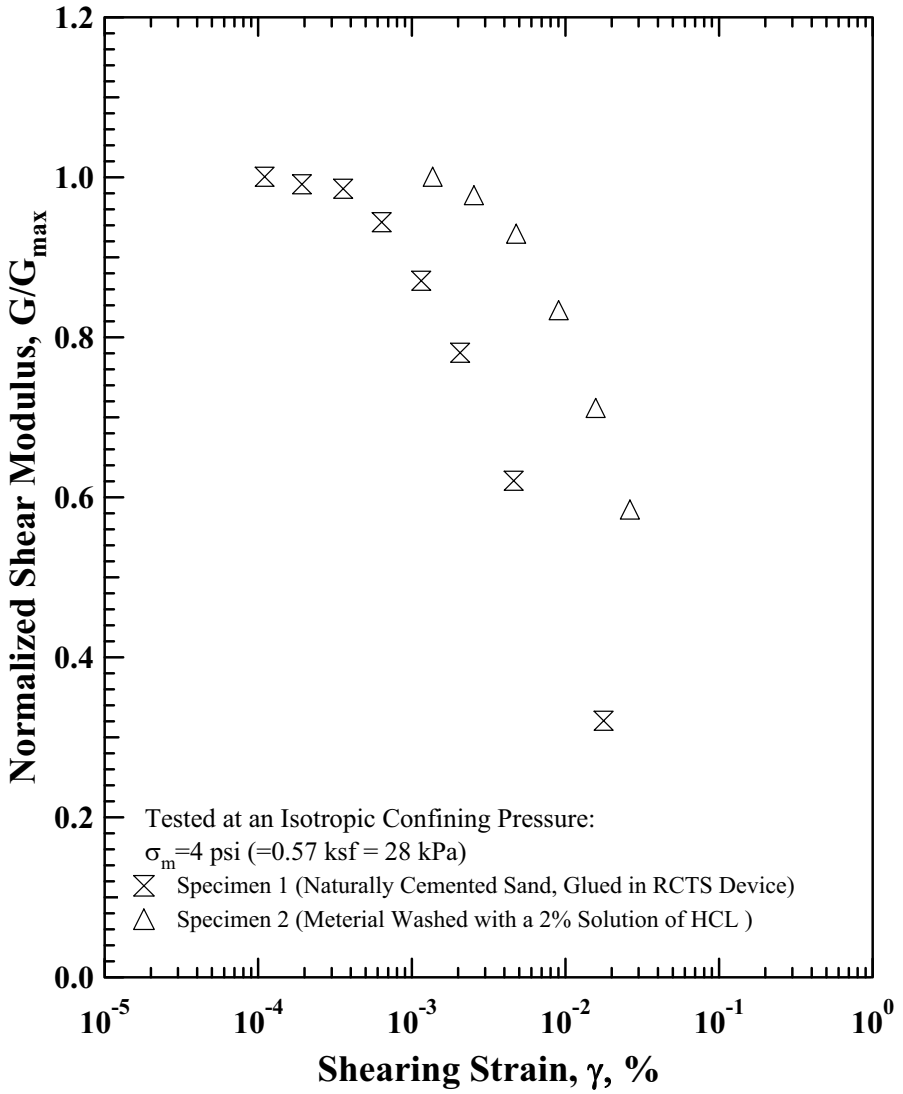

Source: Stokoe and Valle 2003 [DIRS 164689], Figure 10

Figure 6.2-143. Comparison of the Normalized Shear Modulus with Shearing Strain for Naturally Cemented Sand with and without Cementation Removed

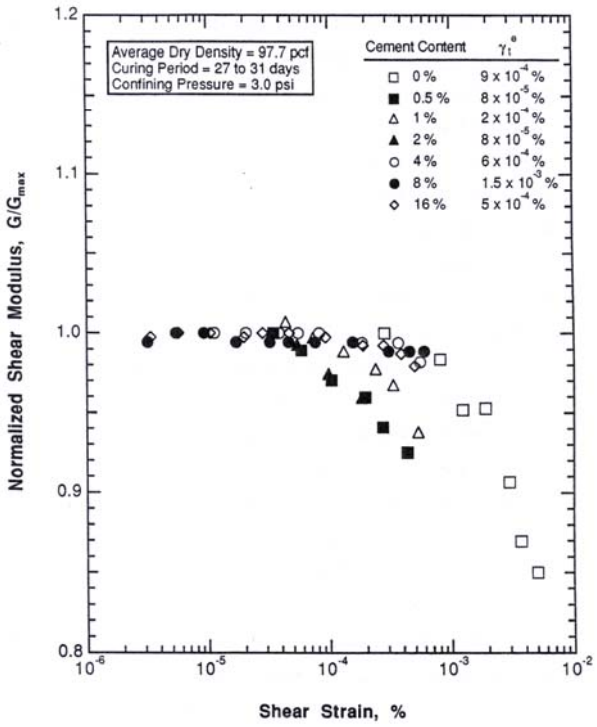

(a) Dense Sand

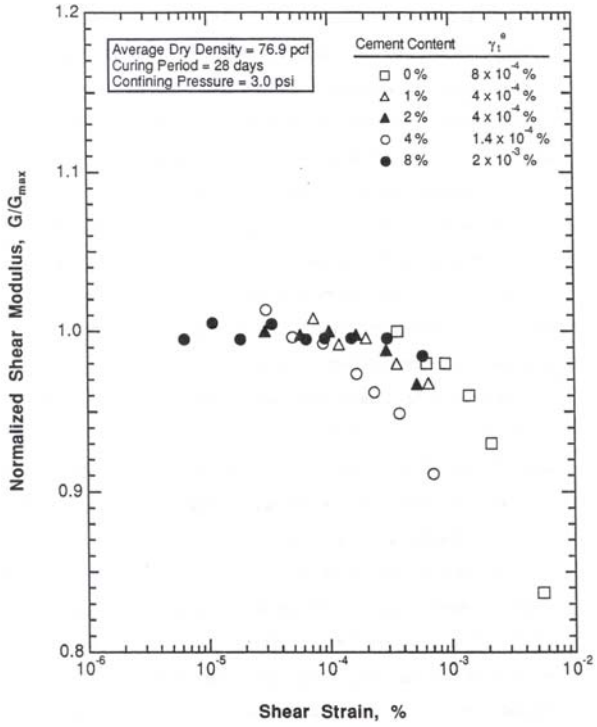

(b) Loose Sand

Source: Van Hoff 1993 [DIRS 163890], Figures 7.16 and 7.17

Figure 6.2-144. Normalized Shear Modulus with Shearing Strain for Artificially Cemented Sands

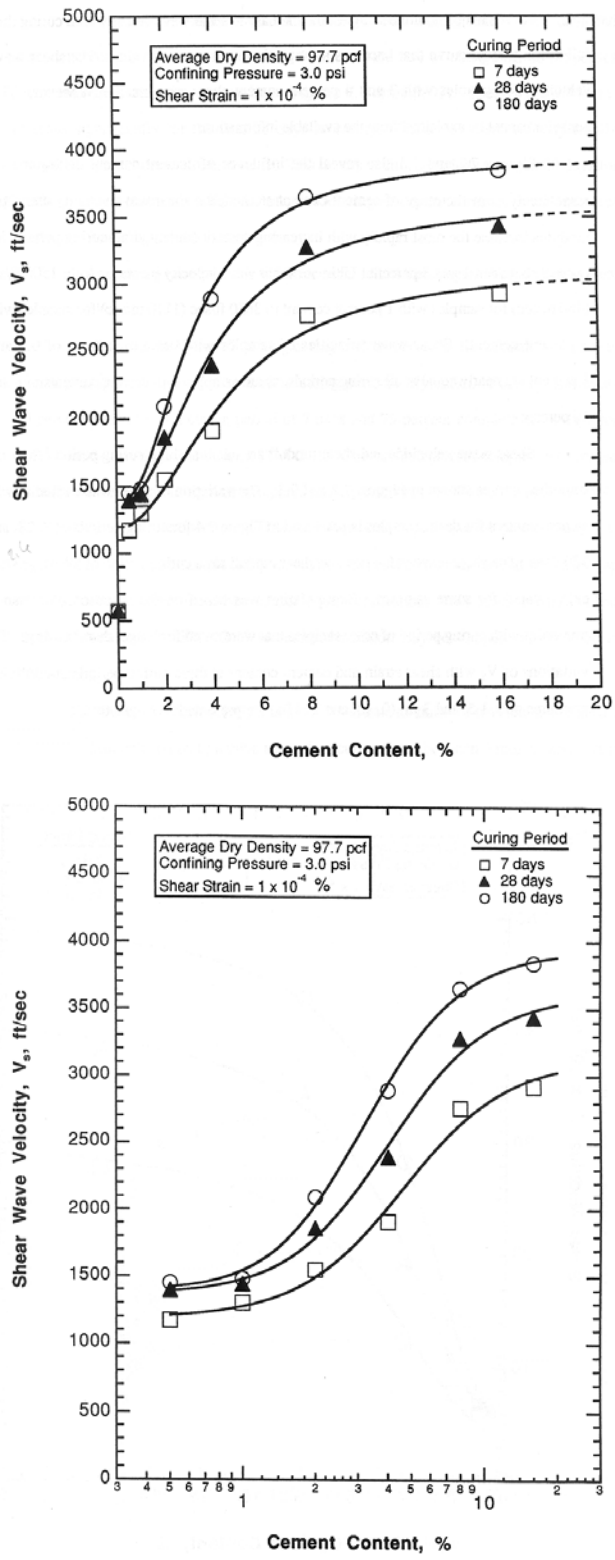

Source: Van Hoff 1993 [DIRS 163890], Figures 7.4 and 7.5

Figure 6.2-145. Low Strain Shear Wave Velocity Versus Cement Content for Artificially Cemented Sands

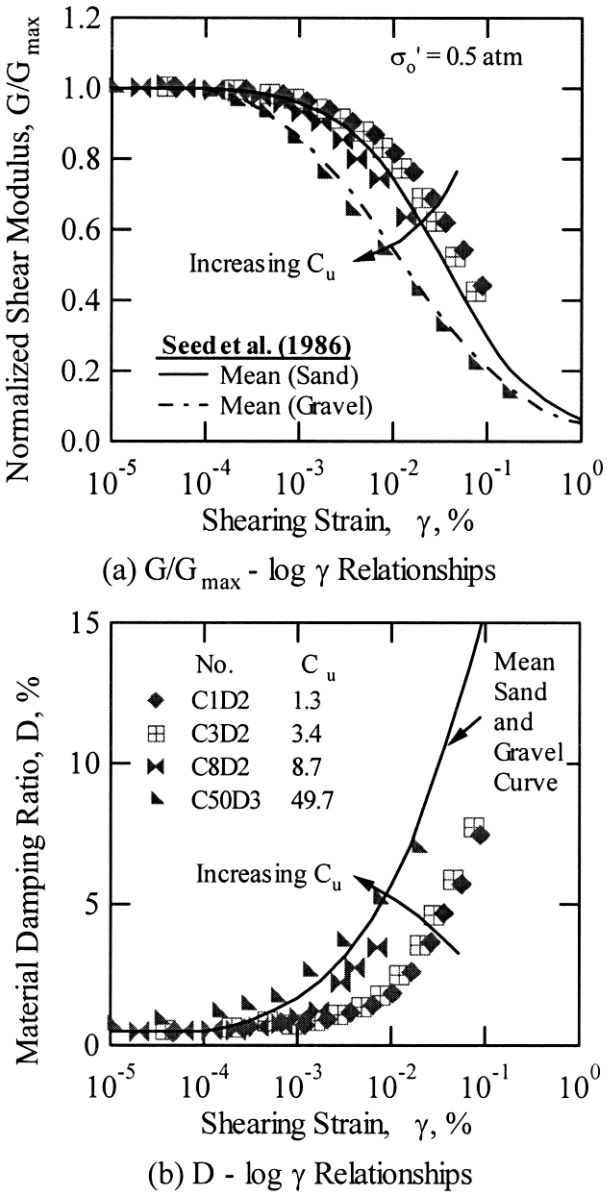

Source: Menq 2003 [DIRS 164681], page 252

Figure 6.2-146. Effect of Uniformity Coefficient, C_u, on Nonlinear Shear Modulus and Material Damping Curves of Dense to Very Dense Specimens

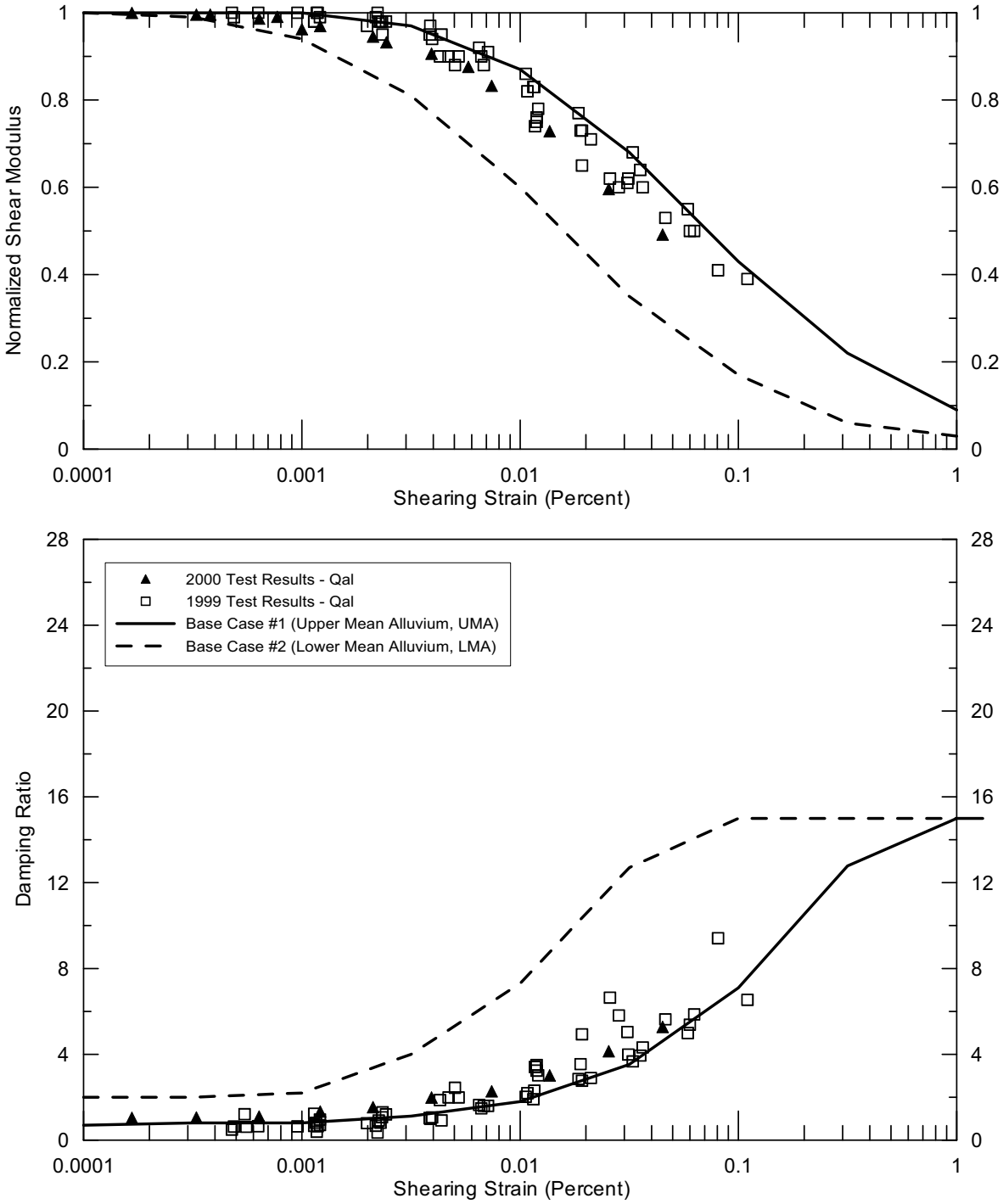

DTN: MO0403SDIAWHBC.003 [DIRS 170434] (CURVES), MO0203DHRSSWHB.001 [DIRS 158082] (DATA), MO9905LABDYNRS.000 [DIRS 103792] (DATA)

Figure 6.2-147. Mean Normalized Shear Modulus and Material Damping Curves for Alluvium

6.3 MODELING, ANALYSES, AND RESULTS

The overall approach, methodology, modeling, and analyses performed to develop ground motion inputs for preclosure design and postclosure performance assessment are described in the following subsections. Results are presented for annual exceedance frequencies of 10^{-3}, $5x10^{-4}$, 10^{-4}, 10^{-5}, 10^{-6}, and 10^{-7}.

Ground motion inputs are based on mean estimates of the seismic hazard as determined by the PSHA for Yucca Mountain (CRWMS M&O 1998a [DIRS 103731]). As such, they do not represent worst-case ground motions, but rather reflect the distribution of the seismic hazard results. Mean-based ground motions are appropriate for use within a risk-informed framework such as defined by 10 CFR 63 [DIRS 156605].

While mean-based ground motions do not represent the worst-case ground motions for Yucca Mountain, ground motions with mean annual exceedance frequencies of less than about 10^{-6} are equivalent to the 80^{th} to 90^{th} or higher percentile of the distribution of the seismic hazard results. Assessment of ground motion uncertainty and incorporation of ground motion randomness in the PSHA without bounds results in ground motion, for mean annual exceedance frequencies less than about 10^{-6}, that may not be credible at Yucca Mountain. As stated in Section 1.3, this issue is being addressed by placing a bound on peak horizontal velocity (BSC 2004c [DIRS 170137]). The bound on peak horizontal velocity documented in BSC 2004c [DIRS 170137] is not incorporated in the postclosure ground motions developed in this report. However, a bound on PGV is incorporated into the sampling process for TSPA.

6.3.1 Development of Response Spectra and Peak Ground Velocities

In this section, the methodology used to develop response spectra and peak ground velocities (PGVs) based on reference rock outcrop motions is presented. For preclosure design, response spectra are developed for two locations shown on Figure 1-1: (1) the emplacement level, ranging from 213 to 457 m (700 to 1500 ft) below the ground surface (Point B) and (2) the proposed location of the surface facilities in Midway Valley (Points D and E). Strain-compatible soil properties are also developed for Point D. For postclosure, response spectra and peak ground velocities are developed for Point B. As described in Section 6.2.2, the outcrop motions developed from the PSHA are referenced at Point A. The development of time histories from the spectra and peak ground velocities for these sites is discussed in Section 6.3.3.

6.3.1.1 Site Response Methodology

The goal of the site response methodology for Yucca Mountain is to develop seismic inputs that are consistent with the seismic hazard results from the PSHA. The PSHA determined seismic hazard for a reference rock outcrop (Point A), not the locations for which seismic inputs are needed (i.e., Points B, D, and E). Developing site-specific seismic inputs that are consistent with the seismic hazard determined for Point A is not trivial because the site response can vary depending on the magnitude and distance of earthquakes contributing to the hazard. In addition, variability in the site material properties needs to be appropriately incorporated.

McGuire et al. (2001 [DIRS 157510], Section 6) discuss approaches for developing hazard-consistent spectra taking into account site response. McGuire et al. (2001 [DIRS 157510],

Table 6-1) identify four basic approaches for determining the UHS at a soil site. The approaches range from a probabilistic seismic hazard analysis using ground motion attenuation relations for the specific site (or location) of interest (Approach 4) to scaling the rock UHS on the basis of a site response analysis using a broadband input motion (Approach 1). Conceptually, Approach 4 is the ideal approach and other approaches are approximations to it. Approach 4 was not used in this study because the results of the PSHA were for the hypothetical site condition at Point A.

In this analysis, Approach 2B is adopted (McGuire et al. 2001 [DIRS 157510], Table 6-1) because comparisons detailed in McGuire et al. (2001 [DIRS 157510], Section 6) indicate that this approach is adequately conservative at annual exceedance frequencies down to 10^{-4} with respect to Approach 4. Thus for preclosure ground motions, the use of Approach 2B is appropriate. McGuire et al. (2001 [DIRS 157510]) did not address at-depth (emplacement level) motions. The unconservative bias inherent in the approximate methods at annual exceedance frequencies below 10^{-4} is at high frequency and is due mainly to site nonlinearity being more dominant in the approximate methods than in the full hazard integration (McGuire et al. 2001 [DIRS 157510]). Waste emplacement level ground motions, even at hazard levels as low as 10^{-7}, reflect very little nonlinearity, being dominated by upgoing wavefields defined by the Point A UHS. Because at-depth motions are dominated by upgoing wavefields, much as are surface outcrop motions, and nonlinearity is not a controlling mechanism at high frequency, Approach 2B is considered to appropriately maintain the Point A hazard levels for waste emplacement level ground motions.

Approach 2B scales the reference rock (Point A) UHS to a site UHS for Points B, D, and E based on site response analyses that take into account variability in site material properties and magnitude deaggregation. Magnitude deaggregation is taken into account to reflect differences in nonlinear site response that are related to magnitude (e.g., response spectral shape).

These analyses include the following steps for each site:

- Development of appropriate control motions (Section 6.2.2).
- Development of base case site properties (small-strain velocity profiles and nonlinear dynamic properties) (Sections 6.2.3 and 6.2.4).
- Randomization of base case site dynamic material properties to produce a suite of velocity profiles as well as G/G_{max} and hysteretic damping curves that incorporate site randomness (Sections 6.2.3.6 and 6.2.4.5).
- Computation of mean transfer functions for each set of base case site properties using the equivalent-linear site response model (Section 6.3.1.1.2).
- Combination of mean transfer functions from all control motions and base case site properties (Section 6.3.1.1.2).
- Computation of response spectra and peak ground velocity (Sections 6.3.1.2 to 6.3.1.4).

- Development of design and performance assessment ground motions (Section 6.3.1.2 to 6.3.1.4).

Software used to develop response spectra and peak ground velocities consists of:

- RANPAR V2.0 (Software Tracking Number 10486-2.0-00) (Pacific Engineering and Analysis 2002i [DIRS 163315])
- RASCALS V5.4 (Software Tracking Number 10389-5.4-00) (Pacific Engineering and Analysis 2002l [DIRS 163317])
- RASCALP V2.01 (Software Tracking Number 10388-2.01-00) (Pacific Engineering and Analysis 2002j [DIRS 163367])
- NORM V1.01 (Software Tracking Number 10386-1.01-00) (Pacific Engineering and Analysis 2002g [DIRS 163313])
- SMRATIO V1.0 (Software Tracking Number 10917-1.0-00) (Pacific Engineering and Analysis 2002n [DIRS 163320])
- REPLOT V1.0 (Software Tracking Number 10949-1.0-00) (Pacific Engineering and Analysis 2003b [DIRS 163318])
- SPMEAN V1.0 (Software Tracking Number 10918-1.0-00) (Pacific Engineering and Analysis 2002o [DIRS 163322])
- INTERPOL V1.0 (Software Tracking Number 10944-1.0-00) (Pacific Engineering and Analysis 2002d [DIRS 163305])

These steps are repeated for each annual exceedance frequency level. These ground motions are used as the basis to develop time histories, as described in Section 6.3.2.

6.3.1.1.1 Control Motions

As described in Section 6.2.2.5, control motions forming input to the site-response model are developed for DEAs. The DEAs are used to account for any magnitude dependence in the nonlinear response of the site and represent the REs controlling response at structural frequencies of 1-2 Hz and 5-10 Hz (Figure 6.3-1a). INTERPOL and RASCALS are used to compute the Fourier amplitude spectra for each DEA response spectra.

The use of REs (and associated DEAs) rather than a broadband control motion, such as the UHS, avoids potential problems in determining the site response. Broadband at-depth outcrop control motions reflect contributions from earthquakes of varying magnitudes and distances. Thus, when the dynamic material properties and the level of control motions result in significant nonlinear response, use of broadband spectra can induce higher strains than any single earthquake scaled to the same peak acceleration level and result in ground motions that are unconservative at high (> 1-2 Hz) frequency. Accordingly, specific earthquakes have been identified, as described in Section 6.2.2.4, by deaggregating the hazard at each target hazard

level (annual frequencies of exceedance of 10^{-3}, $5x10^{-4}$, and 10^{-4} for preclosure and 10^{-5}, 10^{-6} and 10^{-7} for postclosure). For a given hazard level, the earthquakes correspond to the most likely earthquake magnitude and distance controlling ground motion with structural frequencies in the 1-2 Hz range and in the 5-10 Hz range. Thus, considering both horizontal and vertical motion, a total of four response spectra are identified at the reference rock outcrop (Point A) and are called the REs (Section 6.2.2.4).

While the REs represent the most-likely magnitude and distance controlling the UHS at the given frequency interval, a range of magnitudes contributes to the UHS in each interval (Section 6.2.2.4). To account for possible magnitude-dependence on the site response nonlinearity, the DEAs were developed, as described in Section 6.2.2.5. For each RE, a set of three DEAs, which represents the range of magnitudes contributing to the hazard in that frequency interval, is used as control motions.

6.3.1.1.2 Spectral Amplification Functions

Evaluation of site-response using the equivalent-linear site response model is based on convolution of appropriate DEA control motions through randomized velocity profiles combined with randomized G/G_{max} and hysteretic damping curves. The randomized profiles and curves are generated from base case velocity and nonlinear dynamic properties. The convolutions yield transfer functions or SAFs for 5%-damped response spectra and peak particle velocity.

For the computation of spectra for a site with uncertain properties and exhibiting a degree of lateral variability, a best-estimate (mean) base case velocity profile (or profiles) is developed and used to simulate a number of V_S and V_P profiles (EPRI 1993a [DIRS 103319], Section 6.3.4). Additionally, strain-dependent shear modulus and hysteretic damping are also randomized about best-estimate base cases. A large number of simulations can be required to achieve stable statistics on the response. The simulations attempt to capture the variability in the soil or rock parameters and layer thickness. To achieve statistical stability, 60 randomizations were produced using RANPAR and the velocity correlation models for each base case velocity profile and each base case nonlinear dynamic property curve (Figure 6.3-1b), as discussed in Sections 6.2.3.6 and 6.2.4.5.

For each of the three DEAs (MM, ML, and MH), ground motions at each location are computed using the site response model (RASCALS and RANPAR) for each set of 60 velocity profiles and dynamic property curves (Figure 6.3-1c). RASCALS is used for horizontal DEA spectra using normally incident and inclined SH-waves. RASCALP is used for horizontal component DEA spectra using inclined SV-waves and vertical component DEA spectra using inclined SV-waves normally incident and inclined P-waves. For each control motion (horizontal and vertical, 1-2 Hz and 5-10 Hz ML, MM, and MH), NORM is used to compute the mean of the 60 response spectra (from 60 randomized profiles). The mean response spectrum from the 60 convolutions is divided by the DEA spectrum using SMRATIO to produce a mean SAF for each DEA (Figure 6.3-1d). The mean SAFs for each DEA are averaged using NORM and the weights in Tables 6.2-8 and 6.2-9. The weighted average of the three mean SAFs, which reflects the distribution of earthquake magnitudes contributing to the UHS, produces a magnitude-weighted mean SAF for each combination of structural frequency range (1-2 Hz or 5-10 Hz), base case velocity profile, and base case dynamic property curves. These magnitude-weighted mean SAFs include the

effects of the inherent aleatory variability (randomness) of the site properties about each base case and any possible effects of magnitude of the control motions. Epistemic variability (uncertainty) is captured in consideration of alternate base case (mean) profiles and properties.

The 1-2 Hz and 5-10 Hz magnitude-weighted mean SAFs are enveloped using SPMEAN to produce a single transfer function for each base case velocity profile and set of nonlinear dynamic material properties. For horizontal motions, this transfer function is applied to the smooth envelope of the 1-2 Hz RE, 5-10 Hz RE, and UHS (Point A) using XYMULT to produce mean response spectra at Point B, D, or E for each combination of base case properties (Figure 6.3-1e). For vertical motions, the transfer function is applied using XYMULT to the revised vertical envelope of the 1-2 Hz RE, 5-10 Hz RE, and UHS at Point A (see Section 6.2.2.6.3). Application of the horizontal transfer function to the smooth envelope of the 1-2 Hz, RE 5-10 Hz RE and UHS, rather than the horizontal UHS, results in lower frequency of exceedance levels (than the Point A UHS), especially at high frequencies. As shown on Figure 6.2-29, the 5-10 Hz RE at 10^{-3} annual exceedance frequency exceeds the UHS by a maximum of 9.5 percent at 100 Hz. For $5x10^{-4}$, 10^{-4}, 10^{-5}, 10^{-6}, and 10^{-7} annual exceedance frequencies, the differences at 100 Hz are 11.4, 11.2, 16.1, 20.2, and 23.5 percent, respectively (Figures 6.2-31 through 6.2-41). The exceedance of the UHS at high frequencies is a result of scaling the REs to the UHS such that the envelope of the REs is no less than 95 percent of the UHS at any frequency.

This entire process, from propagation of the DEAs to calculation of the response spectra for each set of base case profiles and properties, is completed for each type of wave propagator (Figure 6.3-1e). For horizontal-component analyses, incident vertical and inclined SH-wave (HSHH) and incident inclined SV-wave (HSVH) propagation are used. For vertical-component analyses, incident vertical and inclined P-wave (VPV) and incident inclined SV-wave (VSVV) propagation are used. In these analyses, the calculations of the vertical-component ground motions use linear site response analyses (EPRI 1993a [DIRS 103320], Section 6.6.2.1; Silva 1997 [DIRS 163747], page 10). The use of linear analysis for vertical motions is supported by observations of recorded ground motions (EPRI 1993a [DIRS 103319]; Silva 1997 [DIRS 163747]). Linear response, even at high loading levels, has been observed at both rock and soil sites associated with recorded vertical peak accelerations up to about 1 g, although the majority of sites are at 0.5 g and less. Nonlinearity in horizontal motions at frequencies above about 1 to 2 Hz becomes detectable at about 0.3 g, for typical firm soil sites, and is quantifiable down to 0.05 g at soft soil sites (e.g., Lotung, Taiwan). The lack of clearly observed nonlinearity in vertical motions is likely at most recording sites due to the presence of water. At high frequencies (above 1 to 2 Hz), vertical ground motions tend to be dominated by compression waves and nonlinearity may be suppressed by the incompressibility of pore fluids (Silva 1997 [DIRS 163747]). At Yucca Mountain, even at emplacement level depths, apart from localized perched water, the site is unsaturated. At high loading levels, with vertical peak accelerations exceeding about 0.5 g, strains may be large enough to induce nonlinearity in compression waves with an accompanying increase in material damping and a decrease in high frequency motions. Ideally, modulus reduction and damping curves are used for constrained moduli, but laboratory dynamic test devices for constrained moduli and under confining pressure simply do not exist. In consequence, the conservative assumption of linear behavior makes it likely that high level vertical motions are conservative at high frequencies, due to the assumption of linear analyses, along with some conservatism in the Point A V/H ratio and the application of that V/H ratio to the envelop of the Point A reference earthquake response spectra and UHS.

The set of mean response spectra derived using each combination of base case velocity profiles and base case nonlinear dynamic properties reflect the epistemic uncertainty in the site properties. A target spectrum is drawn based on this set of response spectra using judgment to provide a smooth spectrum suitable for design purposes. The target spectrum envelopes most of the individual response spectra peaks except where narrow peaks in a small frequency range in the spectra for a particular combination of properties and wavetype exist (Figure 6.3-1e). The enveloping over site epistemic variability reflects a conservative approximation to averaging over probability level, the exact way to accommodate epistemic variability in a hazard analysis. The process, from control motion to final spectrum, is illustrated on Figure 6.3-1 (a to e) for Point B at $5x10^{-4}$ annual exceedance frequency. The site response methodology flow chart on Figure 6.3-2 also illustrates the process of developing site-specific ground motion inputs for design and performance assessment.

6.3.1.1.3 Peak Ground Velocity

Peak ground velocity (PGV) was computed for postclosure levels of ground motion. The computation of PGV follows the methodology described above for response spectra. PGV is calculated for each convolution of DEA control motion through the sets of 60 profiles for each combination of base case site properties. Mean PGVs are calculated for each set of 60 convolutions. For each set of base case site properties, mean PGVs for the three DEA control motions are combined using the weights in Tables 6.2-8 and 6.2-9. The largest resulting PGV is taken as the value used in performance assessment. Note that the PGVs calculated using this approach do not incorporate the results of the PGV bounding analysis discussed in Section 1.3.

6.3.1.2 Preclosure Emplacement Level Design Ground Motions

This section describes use of the equivalent-linear site response model to develop seismic inputs with annual exceedance frequencies of 10^{-3}, $5x10^{-4}$, and 10^{-4} for the waste emplacement level (Point B). These inputs are used for preclosure design of underground facilities, as appropriate. At each level of exceedance frequency, site response modeling results in horizontal and vertical 5%-damped seismic design response spectra and expected peak ground accelerations. Peak ground motions, strains, and curvatures as a function of depth for the top of Yucca Mountain to the emplacement level are also provided at 10^{-3}, $5x10^{-4}$, and 10^{-4} annual exceedance frequencies and are presented in Section 6.3.4.

6.3.1.2.1 10^{-3} Annual Exceedance Frequency Ground Motions

Inputs to the site response model to develop seismic inputs with 10^{-3} annual exceedance frequency are summarized in Table 6.3-1.

Details of the modeling and analysis are documented in Scientific Notebook SN-M&O-SCI-037-V2 (Wong and Silva 2004a [DIRS 170443], pages 61, 62, 64, and 123, and supplemental records 64, 72, and 111).

Table 6.3-1. Model Inputs for Development of Seismic Inputs with an Annual Exceedance Frequency of 10^{-3} for Point B

Model Input	Source
Twelve 10^{-3} deaggregation earthquake response spectra (three each for the 1-2 Hz and 5-10 Hz 10^{-3} reference earthquakes; horizontal and vertical components)	Section 6.2.2.5; deaggregation earthquakes have DTN MO0211REDES103.000 [DIRS 170424]. Weights for combining results for each deaggregation earthquake are provided in Tables 6.2-8 and 6.2-9.
Incidence angles for the deaggregation earthquakes	Section 6.2.2.5.1; Table 6.2-11
60 randomized velocity profiles for each of the two Repository Block base case profiles	Section 6.2.3.5; base case velocity profiles have DTN MO0206SASWVSP1.001 [DIRS 163777]
60 randomized sets of shear modulus reduction and damping curves for each of the two tuff base case curves	Section 6.2.4.4; base case curves have DTN MO0403SDIAWHBC.003 [DIRS 170434]
Tuff density	Section 6.2.3.7

For the development of the emplacement level (Point B) motions, magnitude-weighted mean SAFs are determined using the site response model and the inputs summarized in Table 6.3-1. The mean SAFs for each of the three DEAs associated with 1-2 Hz and 5-10 Hz structural frequency range are averaged using the weights from Tables 6.2-8 and 6.2-9. For horizontal motions, each of the resulting magnitude-weighted mean SAFs is then applied to the reference rock outcrop control motion (the envelope of the 1-2 Hz, 5-10 Hz REs, and UHS) to produce site-response RE spectra for the two base case velocity profiles and the two base case dynamic property curves (four combinations). The smooth envelope of these spectra is taken as the Point B seismic design response spectrum (Point B). For vertical motions, the magnitude-weighted mean SAFs (envelope of 1-2 Hz and 5-10 Hz SAFs) are applied to the revised vertical RE envelope spectrum (see Section 6.2.2.6.3) and the smooth envelope is taken as the corresponding vertical seismic design response spectrum.

Representative Point B horizontal-component mean SAFs for the 1-2 Hz and 5-10 Hz DEAs, using base case #1 velocity profile and lower mean tuff (LMT) nonlinear dynamic properties are shown on Figure 6.3-3 for an annual exceedance frequency of 10^{-3}. Note that the magnitude dependence for the tuff response (horizontal) is small for this target level. The prominent dip (spectral hole) near 0.9 Hz is due to the cancellation of upgoing and downgoing wavefields, broadened by the velocity and depth randomizations. One magnitude-weighted mean SAF is generated for each set of DEAs driven through each base case profile using each type of wave propagation. Representative Point B magnitude-weighted mean SAFs (horizontal component) for all base case site properties are shown on Figure 6.3-4 for the 1-2 Hz and 5-10 Hz DEAs for the inclined horizontally-polarized shear wave case. For frequencies greater than 1.3 Hz, the upper mean tuff properties give the largest site amplification values, with little difference between the two base case velocity profiles. Representative Point B magnitude-weighted mean SAFs (vertical component) for both base case velocity profiles are shown on Figure 6.3-5 for the 1-2 Hz and 5-10 Hz DEAs for the inclined vertically-polarized shear wave case. Note that there is no dependence on nonlinear dynamic material properties, as vertical analyses are linear. For frequencies greater than approximately 3 Hz the upper range profile gives the largest spectral amplification values. The effect of magnitude on the vertical site response is small because the

site response analysis is performed using linear material properties for all annual exceedance frequencies.

Point B horizontal-component spectra at an annual exceedance frequency of 10^{-3} estimated for each wave type and base case set of dynamic material properties are shown on Figure 6.3-6. Also shown on Figure 6.3-6 is the seismic design response spectrum, which is the smooth envelope (over site epistemic uncertainty) of the RE spectra as modified by the transfer functions corresponding to all base case dynamic material properties and all wave types. Note that only the BC and UR results are plotted for the inclined vertically-polarized shear wave case using the UMT curves because these vertical motions are modeled as being linear (see Section 6.2.2.6.1) and hence the results using the LMT curves would be identical. General features noted in these spectra are (1) for frequencies greater than 2-Hz, there is little difference between the two velocity profiles and (2) the upper mean tuff properties control over much of the frequency range. The broadened spectral hole from about 0.6 Hz to about 2 Hz has been smoothed over in the design motions because it results from simplifications in the model representation of the site (a plane-layered system with a flat (featureless) surface topography). Figure 6.3-7 shows the emplacement level vertical-component spectra and seismic design response spectrum at an annual exceedance frequency of 10^{-3}. Note again that for the vertical motion, which is modeled as linear motion, the results from the LMT and UMT curves are identical and hence only one set of curves is plotted on Figure 6.3-7. The spectrum is controlled by the velocity base case profile #2 at most frequencies. The preclosure emplacement level seismic design response spectra at 10^{-3} annual exceedance frequency are provided in Table 6.3-2. These results have been submitted to TDMS and have DTN MO0405SDSTPNTB.001 [DIRS 169851].

Table 6.3-2. Preclosure Point B Seismic Design Response Spectra (5%-Damped) in g's at 10^{-3} Annual Exceedance Frequency

Frequency (Hz)	Horizontal Motion	Vertical Motion
0.3	0.0480	0.0374
0.5	0.0777	0.0591
0.7	0.1014	0.0741
1.0	0.1330	0.0934
2.0	0.2007	0.1443
5.0	0.2541	0.2187
7.0	0.2615	0.2314
10.0	0.2553	0.2387
20.0	0.2249	0.2220
30.0	0.1984	0.1949
50.0	0.1676	0.1624
100.0	0.1316	0.1226

Source: DTN: MO0405SDSTPNTB.001 [DIRS 169851]

6.3.1.2.2 $5x10^{-4}$ Annual Exceedance Frequency Ground Motions

The process for development of emplacement level (Point B) motions with $5x10^{-4}$ annual exceedance frequency is identical to that outlined in Section 6.3.1.2.1 for 10^{-3} motions. Inputs to the site response for this case are summarized in Table 6.3-3.

Table 6.3-3. Model Inputs for Development of Seismic Inputs with an Annual Exceedance Frequency of $5x10^{-4}$ for Point B

Model Input	Source
Twelve $5x10^{-4}$ deaggregation earthquake response spectra (three each for the 1-2 Hz and 5-10 Hz $5x10^{-4}$ reference earthquakes; horizontal and vertical components)	Section 6.2.2.5; deaggregation earthquakes have DTN MO0208UNHZ5X10.000 [DIRS 163722]. Weights for combining results for each deaggregation earthquake are provided in Tables 6.2-8 and 6.2-9.
Incidence angles for the deaggregation earthquakes	Section 6.2.2.5.1; Table 6.2-12
60 randomized velocity profiles for each of the two Repository Block base case profiles	Section 6.2.3.5; base case velocity profiles have DTN MO0206SASWVSP1.001 [DIRS 163777]
60 randomized sets of shear modulus reduction and damping curves for each of the two tuff base case curves	Section 6.2.4.4; base case curves have DTN MO0403SDIAWHBC.003 [DIRS 170434]
Tuff density	Section 6.2.3.7

Software programs used to model this case are identical to those listed in Section 6.3.1.1. Details of the modeling and analysis are documented in Scientific Notebook SN-M&O-SCI-037-V2 (Wong and Silva 2004a [DIRS 170443], pages 31-38, 52, 59, 61, and supplemental records 12, 13, 14, 18, 21, 24, 25, 58, 61, 62).

Representative Point B horizontal-component mean SAFs for the 1-2 Hz and 5-10 Hz DEAs, using base case #1 velocity profile and lower mean tuff (LMT) nonlinear dynamic properties are shown on Figure 6.3-8 for an annual exceedance frequency of $5x10^{-4}$. Note that the magnitude dependence for the tuff response (horizontal) is small for this target level. Representative Point B magnitude-weighted mean SAFs (horizontal component) for all base case site properties are shown on Figure 6.3-9 for the 1-2 Hz and 5-10 Hz DEAs for the inclined horizontally-polarized shear wave case. For frequencies greater than 2 Hz, the upper mean tuff properties give the largest site amplification values, with little difference between the two base case velocity profiles. Representative Point B magnitude-weighted mean SAFs (vertical component) for both base case velocity profiles are shown on Figure 6.3-10 for the 1-2 Hz and 5-10 Hz DEAs for the inclined vertically-polarized shear wave case. For frequencies greater than approximately 3 Hz the base case velocity profile #2 gives the largest spectral amplification values.

Point B horizontal-component spectra at an annual exceedance frequency of $5x10^{-4}$ estimated for each wave type and base case set of dynamic material properties are shown on Figure 6.3-11. Also shown on Figure 6.3-11 is the seismic design response spectrum, which is the smooth envelope (over site epistemic uncertainty) of the RE spectra modified by the transfer functions corresponding to all base case dynamic material properties and all wave types. General features noted in these spectra are (1) for frequencies greater than 2-Hz, there is little difference between the two velocity profiles and (2) the upper mean tuff properties control over much of the

frequency range. The broadened spectral hole from about 0.3 Hz to about 2 Hz has been smoothed over in the design motions because it results from simplifications in the model representation of the site (a plane-layered system with a flat (featureless) surface topography). Figure 6.3-12 shows the emplacement level vertical-component spectra and seismic design response spectrum at an annual exceedance frequency of $5x10^{-4}$. The spectrum is controlled by base case velocity profile #2 at most frequencies. The preclosure emplacement level seismic design response spectra at $5x10^{-4}$ annual exceedance frequency are provided in Table 6.3-4. These results have been submitted to TDMS and have DTN MO0407SDARS104.001 [DIRS 170683].

Table 6.3-4. Preclosure Point B Seismic Design Response Spectra (5%-Damped) in g's at $5x10^{-4}$ Annual Exceedance Frequency

Frequency (Hz)	Horizontal Motion	Vertical Motion
0.3	0.0703	0.0583
0.5	0.1164	0.0976
0.7	0.1478	0.1270
1.0	0.1880	0.1641
2.0	0.2749	0.2646
5.0	0.3567	0.3903
7.0	0.3773	0.4126
10.0	0.3789	0.4208
20.0	0.3299	0.4071
30.0	0.2855	0.3607
50.0	0.2406	0.3019
100.0	0.1911	0.2324

Source: DTN: MO0407SDARS104.001 [DIRS 170683]

6.3.1.2.3 10^{-4} Annual Exceedance Frequency Ground Motions

The process for development of emplacement level (Point B) motions with 10^{-4} annual exceedance frequency is identical to that outlined in Section 6.3.1.2.1 for 10^{-3} motions. Inputs to the site response model for this case are summarized in Table 6.3-5.

Table 6.3-5. Model Inputs for Development of Seismic Inputs with an Annual Exceedance Frequency of 10^{-4} for Point B

Model Input	Source
Twelve 10^{-4} deaggregation earthquake response spectra (three each for the 1-2 Hz and 5-10 Hz 10^{-4} reference earthquakes; horizontal and vertical components)	Section 6.2.2.5; deaggregation earthquakes have DTN MO0211DERES104.000 [DIRS 170423]. Weights for combining results for each deaggregation earthquake are provided in Tables 6.2-8 and 6.2-9.
Incidence angles for the deaggregation earthquakes	Section 6.2.2.5.1; Table 6.2-13
60 randomized velocity profiles for each of the two Repository Block base case profiles	Section 6.2.3.5; base case velocity profiles have DTN MO0206SASWVSP1.001 [DIRS 163777]

Model Input	Source
60 randomized sets of shear modulus reduction and damping curves for each of the two tuff base case curves	Section 6.2.4.4; base case curves have DTN MO0403SDIAWHBC.003 [DIRS 170434]
Tuff density	Section 6.2.3.7
Horizontal peak ground velocity at Point A	DTN MO0404PGVAPSHA.000 [DIRS 170436]
Revised vertical peak ground velocity at Point A	Section 6.2.2.6.3

Software programs used to model this case are identical to those listed in Section 6.3.1.1 with the addition of Microsoft Excel 2000, which was used to compute the PGVs discussed below (see Appendix I). Details of the modeling and analysis are documented in Scientific Notebook SN-M&O-SCI-037-V2 (Wong and Silva 2004a [DIRS 170443], pages 61, 64, 71-73 and supplemental records 40-42, 44, 64, 70, 77, and 82).

Representative Point B horizontal-component mean SAFs for the 1-2 Hz and 5-10 Hz DEAs, using base case #1 velocity profile and lower mean tuff (LMT) nonlinear dynamic properties are shown on Figure 6.3-13 for an annual exceedance frequency of 10^{-4}. Note that the magnitude dependence for the tuff response (horizontal) is small for this target level. Representative Point B magnitude-weighted mean SAFs (horizontal component) for all base case site properties are shown on Figure 6.3-14 for the 1-2 Hz and 5-10 Hz DEAs for the inclined horizontally-polarized shear wave case. For frequencies greater than 2 Hz, the upper mean tuff properties give the largest site amplification values, with little difference between the two base case velocity profiles. Representative Point B magnitude-weighted mean SAFs (vertical component) for both base case velocity profiles are shown on Figure 6.3-15 for the 1-2 Hz and 5-10 Hz DEAs for the inclined vertically-polarized shear wave case. For frequencies greater than approximately 3 Hz base case velocity profile #2 gives the largest spectral amplification values.

Point B horizontal-component spectra at an annual exceedance frequency of 10^{-4} developed for each wave type and base case set of dynamic material properties are shown on Figure 6.3-16. Also shown on Figure 6.3-16 is the seismic design response spectrum, which is the smooth envelope (over site epistemic uncertainty) of the RE spectra modified by the transfer functions corresponding to all base case dynamic material properties and all wave types. General features noted in these spectra are (1) for frequencies greater than 2-Hz, there is little difference between the two velocity profiles and (2) the upper mean tuff properties control over much of the frequency range. The broadened spectral hole from about 0.3 Hz to about 2 Hz has been smoothed over in the design motions because it results from simplifications in the model representation of the site (a plane-layered system with a flat (featureless) surface topography). Figure 6.3-17 shows the emplacement level vertical-component spectra and seismic design response spectrum at an annual exceedance frequency of 10^{-4}. The spectrum is controlled by base case velocity profile #2 at most frequencies. The preclosure emplacement level seismic design response spectra at 10^{-4} annual exceedance frequency are provided in Table 6.3-6. These results have been submitted to TDMS and have DTN MO0306SDSAVDTH.000 [DIRS 164033].

In addition to response spectra, PGVs were also computed (Table 6.3-6). The horizontal PGV at Point A is 48.34 cm/sec (DTN: MO0404PGVAPSHA.000 [DIRS 170436]). The vertical PGV at Point A was revised to 46.56 cm/sec based on V/H ratios (see Section 6.2.2.6.3 and Table

6.2-17). Microsoft Excel 2000 was used to compute the mean PGV transfer functions for all control motions, base case velocity profiles and dynamic property curves, and wavetypes. The maximum PGVs (horizontal and vertical) resulting from applying the mean transfer functions to the Point A PGVs is taken as the Point B PGVs (see Appendix I). Point B PGVs at 10^{-4} annual exceedance frequency have been submitted to TDMS and have DTN MO0404PGVRL104.000 [DIRS 170437].

Table 6.3-6. Preclosure Point B Seismic Design Response Spectra (5%-Damped) in g's and Peak Ground Velocities in cm/sec at 10^{-4} Annual Exceedance Frequency

Frequency (Hz)	Horizontal Motion	Vertical Motion
0.3054	0.1805 g	0.1836 g
0.5094	0.2785 g	0.2786 g
0.7055	0.3426 g	0.3439 g
1.0000	0.4197 g	0.4277 g
2.0092	0.6139 g	0.6565 g
5.0941	0.8211 g	0.9691 g
7.0548	0.8552 g	1.0343 g
10.0000	0.8355 g	1.0886 g
20.0923	0.7284 g	1.0818 g
30.5386	0.6442 g	0.9832 g
50.9414	0.5518 g	0.8387 g
100.000	0.4257 g	0.6193g
PGV	40.19 cm/sec	48.07 cm/sec

Source: DTN: MO0306SDSAVDTH.000 [DIRS 164033], MO0404PGVRL104.000 [DIRS 170437]

NOTE: This table provides a subset of the data points in DTN: MO0306SDSAVDTH.000 [DIRS 164033].

6.3.1.3 Preclosure Surface Facilities Area Design Ground Motions

The site response methodology for the Surface Facilities Area is designed to produce ground motions for use in soil-structure interaction (SSI) analyses. This methodology follows the guidance contained in NUREG/CR-6728 (McGuire et al. 2001 [DIRS 157510]). This guidance differs in some aspects from NUREG-0800, *Standard Review Plan for the Review of Safety Analysis Reports for Nuclear Power Plants (SRP)* (NRC 1989b [DIRS 165111]). As described in McGuire et al. (2001 [DIRS 157510]) (NUREG/CR-6728), the guidance should be followed to perform an SSI analysis that is consistent with a probabilistically-defined seismic hazard.

NUREG-0800, Section 3.7.2 (NRC 1989b [DIRS 165111]) describes procedures and criteria that are acceptable to the NRC for SSI analyses of structures, systems and components (SSCs) important to safety. Topics addressed include:

- Criteria for development of "enveloping" time histories for free-field ground motions needed for SSI analyses

- Generation of best-estimate, upper- and lower-bound soil columns which are consistent with site information as well as the defined surface ground motion, and properly account for the variability and uncertainty in definition of geotechnical properties and geometry of the site as well as potential SSI analysis model uncertainties

- Performance of deconvolution studies to ensure that the ground motions at the facility foundation level in the free-field satisfy the "60 percent rule;" that is, do not fall below 60 percent of the defined surface target spectrum

- Characteristics of the analysis procedures used to conduct the complex SSI analyses

- Performance of enveloping and peak broadening procedures for definition of in-structure seismic design response spectra.

Many of the recommendations in NUREG-0800, Section 3.7.2 (NRC 1989b [DIRS 165111]) are still appropriate and provide conservatisms that are intended to cover the uncertainties in the analyses. Some of the recommendations, however, are inconsistent with the current probabilistic approaches used in defining free-field target seismic design response spectra.

Recommendations in NUREG-0800, Section 3.7.2 (NRC 1989b [DIRS 165111]) that are still appropriate include (a) the development of best-estimate, upper- and lower-bound soil columns, (b) the use of enveloping and spectral broadening approaches for developing in-structure spectra, (c) the use of the 60 percent minimum rule for free-field motions at foundation levels, and (d) criteria for SSI analyses. These recommendations are intended to ensure that resulting member seismic loads and in-structure response spectra are conservatively estimated and consistent with respect to the free-field design motions.

Although some recommendations in NUREG-0800, Section 3.7.2 (NRC 1989b [DIRS 165111]) are still pertinent, other aspects of the guidance are inconsistent with probabilistically determined ground motions. In deterministic analyses, the upper/lower-bound soil columns were generated from the best-estimate approximation by multiplying and dividing the best estimate shear modulus by a factor of 2. This is equivalent to using a coefficient of variation (COV) in the assumed shear modulus properties of 1.0. As indicated in NUREG-0800, Section 3.7.2 (NRC 1989b [DIRS 165111]), this large value of COV is recommended for use where the site is not particularly well characterized. This factor can be reduced depending on the confidence in the site descriptions developed by the site investigation program. As recommended in ASCE 4-86 (1986 [DIRS 148636]), however, no matter how well characterized the site, the COV should not fall below 0.5 since it is intended to accommodate analysis uncertainties as well as variability and uncertainty in site geotechnical properties.

In the probabilistic framework currently used to develop surface design ground motions, a relatively large number of seismic convolutions of bedrock outcrop ground motions is performed using low-strain shear modulus and damping properties that are randomly selected to represent the variability of the site geotechnical properties. Full equivalent-linear (or iterated) calculations are then performed leading to a range of soil columns, each with its own set of iterated soil properties, and corresponding surface spectra. The best-estimate surface spectrum and corresponding soil column is then determined from the mean of these calculations. The

properties of the upper and lower bound columns corresponding to this mean column are selected at the ± 1-sigma level from the range of iterated soil columns. This process is being implemented for the Surface Facilities Area. In keeping with the range of COV mentioned above, the range in properties used for the upper/lower bound soil columns should fall within the range of COV of 0.5 to 1.0, which is intended to accommodate both profile uncertainty and variability as well as model uncertainties.

In performing SSI analyses using motions derived following these approaches, no additional site deconvolutions with strain iteration are required since the developed surface spectra already are consistent with the strain iterated soil columns. This process avoids potential complications associated with deconvolving a broad-band spectrum (EPRI 1988 [DIRS 107489]). However, consistent with NUREG-0800, Section 3.7.2 (NRC 1989b [DIRS 165111]) recommendations, it is still appropriate to check the 60 percent rule to ensure that the envelope spectra at the foundation level do not fall below 60 percent of the mean surface spectrum. If small exceedances occur, which are not anticipated, the design surface spectra will be modified to satisfy this requirement. The result of this process then will be three defined soil columns, a best-estimate, an upper-bound and a lower-bound column. The range in dynamic material properties defined by the ± 1 sigma columns then reflects the range in properties used in developing the soil design motions. This envelope spectrum can be used with the three soil columns, if desired, to perform SSI analyses.

The site response methodology for the Surface Facilities Area soil surface spectra (Points D and E) follows much the same general approach as the emplacement level methodology described in Section 6.3.1.1. The use of the site response model to develop seismic inputs with annual exceedance frequencies of 10^{-3}, $5x10^{-4}$, and 10^{-4} for the Surface Facilities Area is described in Sections 6.3.1.3.1 through 6.3.1.3.3.

6.3.1.3.1 10^{-3} Annual Exceedance Frequency Ground Motions

Inputs to the model for this case are summarized in Table 6.3-7.

Table 6.3-7. Model Inputs for Development of Seismic Inputs with an Annual Exceedance Frequency of 10^{-3} for Points D/E

Model Input	Source
Twelve 10^{-3} deaggregation earthquake response spectra (three each for the 1-2 Hz and 5-10 Hz 10^{-3} reference earthquakes; horizontal and vertical components)	Section 6.2.2.5; deaggregation earthquakes have DTN MO0211REDES103.000 [DIRS 170424]. Weights for combining results for each deaggregation earthquake are provided in Tables 6.2-8 and 6.2-9.
Incidence angles for the deaggregation earthquakes	Section 6.2.2.5.1; Table 6.2-11
60 randomized velocity profiles for each of three cases: 35 ft profile (35 ft of alluvium over tuff), 110 ft profile (110 ft of alluvium over tuff), and shallow alluvium (15 ft of alluvium over tuff).	Section 6.2.3.5. Base case velocity profiles for tuff and alluvium have DTN MO0209VELPRWHB.000. [DIRS 163798]
60 randomized sets of shear modulus reduction and damping curves for each of the two tuff and alluvium base case curves (four combinations). Each combination is run for each of the three modeling cases.	Section 6.2.4.4; base case curves have DTN MO0403SDIAWHBC.003 [DIRS 170434].
Tuff and alluvium density	Section 6.2.3.7

Software programs used to model this case are identical to those listed in 6.3.1.1 with the addition of Microsoft Excel 2000, which was used to compute the response spectra at additional damping levels (See Appendix I) and the substitution of RANPAR V2.1 (Software Tracking Number 10486-2.1-00) (Pacific Engineering and Analysis 2003d [DIRS 170442]).

Details of the modeling and analysis are documented in Scientific Notebook SN-M&O-SCI-037-V2 (Wong and Silva 2004a [DIRS 170443], pages 72, 76-78, 89, and 90, and supplemental records 50, 64, 67, 68, 80, 81, 102, 107, and 108).

As discussed in Section 6.2.3.4, a single base case velocity profile was developed based on the results of the site investigation program. This base case profile was developed for the natural alluvium and underlying tuff. However, the depth of alluvium in the Surface Facilities Area thickens from near zero at the base of Exile Hill to greater than 110 ft at the eastern boundary. Depending on the foundation design and layout of the Surface Facilities Area structures, the thickness of alluvium could vary significantly. Ground motion inputs are developed to provide a set of motions applicable to the entire Surface Facilities Area. To accommodate the effect of varying thicknesses of alluvium, ground motion analyses were performed for two profiles: (1) 35 ft of alluvium over tuff and (2) 110 ft of alluvium over tuff (Point D). For the first case, the alluvium profile was used to a depth of 35 ft and the tuff profile for depths deeper than 35 ft. The second case was treated similarly. The resulting two profiles are referred to as the 35 foot and 110 foot profiles reflecting the total thickness of alluvium over rock. In addition, one case is run for a shallow alluvium site (15 ft) (Point E). Uncertainty in the V_P and V_S and nonlinear dynamic material properties was incorporated through randomization about the best-estimate base case profiles and curves, as discussed in Sections 6.2.3.5 and 6.2.4.5. For Point E (shallow soil site) an average of the UMA and LMA dynamic properties was used.

Similar to the analyses for the Point B ground motions, the DEAs are used as control motions to develop mean SAFs that include potential magnitude dependency in the horizontal-component site response. At-depth motions, strains and curvatures are not required at the proposed location of the Surface Facilities Area. Representative mean SAFs and the magnitude-weighted SAF for the Point D 110 foot profile using the 1-2 Hz and 5-10 Hz DEAs (horizontal component) at an annual exceedance frequency of 10^{-3} are shown on Figures 6.3-18 and 6.3-19. Magnitude dependency of site response for the upper mean tuff and upper mean alluvium [UMT-UMA] case is small, about 12% near 1-2 Hz and approximately 10% above 80 Hz. Magnitude dependency of site response is more significant for the lower mean tuff and upper mean alluvium [LMT-UMA] case, about 11% near 1-2 Hz and about 20% near 30 Hz.

Representative magnitude-weighted mean SAFs for Point D (35 foot profile) at 10^{-3} annual exceedance frequency using the 1-2 Hz and 5-10 Hz horizontal-component DEAs are shown on Figure 6.3-20 for the horizontally-polarized shear wave case. For frequencies greater than approximately 5 Hz, the UMT-UMA properties give the largest spectral amplification. Between approximately 1.3 Hz and 5 Hz, the UMT-LMA properties control. The LMT-LMA properties control for frequencies less than approximately 1.3 Hz. Figure 6.3-21 shows representative magnitude-weighted mean SAFs for Point D (110 foot profile) at 10^{-3} annual exceedance frequency using the 1-2 Hz and 5-10 Hz horizontal component DEAs for the horizontally-polarized shear wave case. Site response (horizontal component) at Point D (110 foot profile) is controlled by the UMT-UMA properties for frequencies greater than approximately 2.3 Hz.

Point E (15 feet of alluvium) representative magnitude-weighted mean SAFs are shown on Figure 6.3-22 for the 1-2 Hz and 5-10 Hz horizontal-component DEAs for the vertically-polarized shear wave case. Site response (horizontal component) for Point E is controlled by the UMT properties for frequencies greater than approximately 2 Hz and the LMT properties below 2 Hz. (A single set of alluvial curves was used, i.e., the average of the UMA and LMA.)

The magnitude-weighted mean SAFs for 1-2 Hz and 5-10 Hz DEAs are enveloped and applied to the envelope of the reference earthquake spectra and UHS for the reference rock outcrop (Point A). The resulting spectra for each set of base case nonlinear dynamic material properties and vertically incident waves are shown on Figure 6.3-23 for the horizontal component at an annual exceedance frequency of 10^{-3}. Spectra for Point D (35 foot profile), Point D (110 foot profile) and Point E (shallow alluvium) are all shown on this figure. A single envelope, the seismic design response spectrum, was drawn to provide one set of ground motions applicable to all locations within the Surface Facilities Area. The corresponding vertical-component site-response spectra and seismic design response spectrum are shown on Figure 6.3-24. The preclosure Point D/E seismic design response spectra (5%-damped) at 10^{-3} annual exceedance frequency are provided in Table 6.3-8. These results have been submitted to the TDMS and have DTN MO0410SDSDE103.002 [DIRS 172236].

Table 6.3-8. Preclosure Point D/E Seismic Design Response Spectra (5%-Damped) in g's at 10^{-3} Annual Exceedance Frequency

Frequency (Hz)	Horizontal Motion (g)	Vertical Motion (g)
0.333	0.0650	0.0427
0.500	0.1037	0.0644
0.667	0.1451	0.0841
1.000	0.2506	0.1243
2.000	0.5470	0.2271
5.000	0.7763	0.4650
6.667	0.8072	0.5439
10.000	0.8180	0.5867
20.000	0.7446	0.5471
33.333	0.6005	0.4742
50.000	0.4745	0.3935
100.000	0.3709	0.2868

Source: DTN: MO0410SDSDE103.002 [DIRS 172236]

NOTE: Preclosure Point D/E Seismic Design Response Spectra at 10^{-3} Annual Exceedance Frequency are also provided at 0.5, 1.0, 2.0, 3.0, 7.0, 10,0, 15.0, and 20.0% damping levels in DTN MO0410SDSDE103.002 [DIRS 172236]. Seismic design response spectra in DTN are provided in Period(s). Frequency (Hz) = 1/Period(s).

Response spectra for Point D/E at 10^{-3} annual exceedance frequency were also computed at damping values of 0.5, 1,0, 2.0, 3.0, 7.0, 10.0, 15.0, and 20.0%. These spectra were computed using the 5%-damped spectra and the approach documented in Wong and Silva (2004d [DIRS 172075], pages 36-44).

Response spectra reflect the peak time domain amplitude (response) of a suite of damped oscillators to a force typically defined by an acceleration time history. Because the suite of oscillators has constant damping (e.g., 5%), the range of frequencies sensed by each oscillator varies with oscillator frequency, being very narrow for low frequency (e.g., 1 Hz) oscillators and quite broad for high frequency (e.g., 10 Hz) oscillators. Ratios of response spectra for different damping values depend strongly on the spectral composition (spectral shape) of the acceleration time history. As a result, spectral scaling relations developed for WUS soft rock site conditions and corresponding spectra are inappropriate for scaling CEUS hard rock spectra. Since Yucca Mountain reflects intermediate site conditions and spectral shape, between WUS and CEUS, shape-specific damping scaling relations are required to preserve the hazard level of the 5%-damped design spectra scaled to higher or lower damping values Wong and Silva 2004d [DIRS 172075], pages 36-44).

In order to determine the shape-specific damping scaling factors for Yucca Mountain, the following relationships adopted from Idriss (1993 [DIRS 105524]) were assumed:

$$\text{Spectral Ratio (Freq, Damping (D))} = a1 - b1 \ln(D) \text{ for } D <= 5\% \quad \text{Eq. (43)}$$

$$= a2 - b2 \ln(D) \text{ for } D > 5\% \quad \text{Eq. (44)}$$

Spectra at different damping values were generated using the computer program SPCTLR v. 1.0 (Software Tracking Number 10947-1.0-00) (Pacific Engineering and Analysis 2003c [DIRS 163321]). The spectrally-matched seismic design time histories for Point D/E at 10^{-3}, $5x10^{-4}$, and 10^{-4} annual exceedance frequencies were input into the program. The ratio of spectral values at dampings other than 5% to the spectral values at 5% damping were computed and substituted into the above equations for different values of damping and frequency. A best-fit line through a set of data points provided the values for a1, b1 for damping values less than 5% and a2, b2 for damping values more than 5%. Based on these coefficients, the computed damping factors were used to generate the damped spectra (Wong and Silva 2004d [DIRS 172075], pages 36-44).

6.3.1.3.2 $5x10^{-4}$ Annual Exceedance Frequency Ground Motions

Inputs to the model for this case are summarized in Table 6.3-9.

Table 6.3-9. Model Inputs for Development of Seismic Inputs with an Annual Exceedance Frequency of $5x10^{-4}$ for Points D/E

Model Input	Source
Twelve $5x10^{-4}$ deaggregation earthquake response spectra (three each for the 1-2 Hz and 5-10 Hz $5x10^{-4}$ reference earthquakes; horizontal and vertical components)	Section 6.2.2.5; deaggregation earthquakes have DTN MO0208UNHZ5X10.000 [DIRS 163722]. Weights for combining results for each deaggregation earthquake are provided in Tables 6.2-8 and 6.3-9.
Incidence angles for the deaggregation earthquakes	Section 6.2.2.5.1; Table 6.2-12

Model Input	Source
60 randomized velocity profiles for each of three cases: 35 ft profile (35 ft of alluvium over tuff), 110 ft profile (110 ft of alluvium over tuff), and shallow alluvium (15 ft of alluvium over tuff).	Section 6.2.3.5. Base case velocity profiles for tuff and alluvium have DTN MO0209VELPRWHB.000 [DIRS 163798].
60 randomized sets of shear modulus reduction and damping curves for each of the two tuff and alluvium base case curves (four combinations). Each combination is run for each of the three modeling cases.	Section 6.2.4.4; base case curves have DTN MO0403SDIAWHBC.003 [DIRS 170434]
Tuff and alluvium density	Section 6.2.3.7

Software programs used to model this case are identical to those listed in Section 6.3.1. 1 with the addition of Microsoft Excel 2000, which was used to compute response spectra at additional damping levels (see Appendix I) and the substitution of RANPAR V2.1 (Software Tracking Number 10486-2.1-00) (Pacific Engineering and Analysis 2003d [DIRS 170442]). Details of the modeling and analysis are documented in Scientific Notebook SN-M&O-SCI-037-V2 (Wong and Silva 2004a [DIRS 170443], pages 72, 73, 76-78, 80, 89, 90, and 103, and supplemental records 40-42, 50, 64, 70, 79-81, 88, 99, 101, and 103).

The process for development of Surface Facilities Area (Points D and E) with $5x10^{-4}$ annual exceedance frequency is identical to that outlined in Section 6.3.1.3.1 for 10^{-3} motions. Representative mean SAFs and the magnitude-weighted SAF for the Point D 110 foot profile using the 1-2 Hz and 5-10 Hz DEAs (horizontal component) at an annual exceedance frequency of $5x10^{-4}$ are shown on Figures 6.3-25 and 6.3-26. Magnitude dependency of site response for the upper mean tuff and upper mean alluvium [UMT-UMA] case is small, about 13.5% near 1-2 Hz and about 10% above 80 Hz. Magnitude dependency of site response is more significant for the lower mean tuff and upper mean alluvium [LMT-UMA] case, about 12% near 1-2 Hz and approximately 20% near 30 Hz.

Representative magnitude-weighted mean SAFs for Point D (35 foot profile) at $5x10^{-4}$ annual exceedance frequency using the 1-2 Hz and 5-10 Hz horizontal-component DEAs are shown on Figure 6.3-27 for the horizontally-polarized shear wave case. For frequencies greater than approximately 6 Hz, the UMT-UMA properties give the largest spectral amplification. Between approximately 1.3 Hz and 6 Hz, the UMT-LMA properties control. The LMT-LMA properties control for frequencies less than approximately 1.3 Hz. Figure 6.3-28 shows representative magnitude-weighted mean SAFs for Point D (110 foot profile) at $5x10^{-4}$ annual exceedance frequency using the 1-2 Hz and 5-10 Hz horizontal component DEAs for the horizontally-polarized shear wave case. Site response (horizontal component) at Point D (110 foot profile) is controlled by the UMT-UMA properties for frequencies greater than approximately 2 Hz. Point E (15 feet of alluvium) representative magnitude-weighted mean SAFs are shown on Figure 6.3-29 for the 1-2 Hz and 5-10 Hz horizontal-component DEAs. Site response (horizontal component) for Point E is controlled by the UMT properties for frequencies greater than approximately 2 Hz and the LMT properties below 2 Hz. (A single set of alluvial curves was used.)

The magnitude-weighted mean SAFs for 1-2 Hz and 5-10 Hz DEAs are enveloped and applied to the envelope of the reference earthquake spectra and UHS for the reference rock outcrop (Point A). The resulting spectra for each set of base case nonlinear dynamic material properties and

vertically incident waves are shown on Figure 6.3-30 for the horizontal component at an annual exceedance frequency of $5x10^{-4}$. Spectra for Point D (35 foot profile), Point D (110 foot profile) and Point E (shallow alluvium) are all shown on this figure. A single envelope, the seismic design response spectrum, was drawn to provide one set of ground motions applicable to all locations within the Surface Facilities Area. The corresponding vertical-component site-response spectra and seismic design response spectrum are shown on Figure 6.3-31. The preclosure Point D/E seismic seismic design response spectra at $5x10^{-4}$ annual exceedance frequency are provided in Table 6.3-10. These results have been submitted to the TDMS and have DTN MO0410SDSTMHIS.005 [DIRS 172237].

Table 6.3-10. Preclosure Point D/E Seismic Design Response Spectra (5%-Damped) in g's at $5x10^{-4}$ Annual Exceedance Frequency

Frequency (Hz)	Horizontal Motion (g)	Vertical Motion (g)
0.333	0.0957	0.0684
0.500	0.1664	0.1084
0.667	0.2387	0.1376
1.000	0.3918	0.1980
2.000	0.8281	0.3689
5.000	1.1787	0.7841
6.667	1.2257	0.9379
10.000	1.2512	1.0166
20.000	1.0917	0.9850
33.333	0.8767	0.8377
50.000	0.7287	0.7126
100.000	0.5802	0.5188

Source: DTN: MO0410SDSTMHIS.005 [DIRS 172237]

NOTE: Preclosure Point D/E Seismic Design Response Spectra at $5x10^{-4}$ annual exceedance frequency are also provided at 0.5, 1.0, 2.0, 3.0, 7.0, 10.0, 15.0, and 20.0% damping levels in DTN MO0410SDSTMHIS.005 [DIRS 172237]. This table provides a subset of the data points in DTN: MO0410SDSTMHIS.005 [DIRS 172237].

Response spectra for Point D/E at $5x10^{-4}$ annual exceedance frequency were also computed at damping values of 0.5, 1,0, 2.0, 3.0, 7.0, 10.0, 15.0, and 20.0%. These spectra were computed using the approach described in Section 6.3.1.3.1. Microsoft Excel 2000 was used for this analysis (see Appendix I).

6.3.1.3.3 10^{-4} Annual Exceedance Frequency Ground Motions

Inputs to the model for this case are summarized in Table 6.3-11.

Table 6.3-11. Model Inputs for Development of Seismic Inputs with an Annual Exceedance Frequency of 10^{-4} for Points D/E

Model Input	Source
Twelve 10^{-4} deaggregation earthquake response spectra (three each for the 1-2 Hz and 5-10 Hz 10^{-4} reference earthquakes; horizontal and vertical components)	Section 6.2.2.5; deaggregation earthquakes have DTN MO0211DERES104.000 [DIRS 170423]. Weights for combining results for each deaggregation earthquake are provided in Tables 6.2-8 and 6.2-9.
Incidence angles for the deaggregation earthquakes	Section 6.2.2.5.1; Table 6.2-13
60 randomized velocity profiles for each of three cases: 35 ft profile (35 ft of alluvium over tuff), 110 ft profile (110 ft of alluvium over tuff), and shallow alluvium (15 ft of alluvium over tuff).	Section 6.2.3.5. Base case velocity profiles for tuff and alluvium have DTN MO0209VELPRWHB.000 [DIRS 163798].
60 randomized sets of shear modulus reduction and damping curves for each of the two tuff and alluvium base case curves (four combinations). Each combination is run for each of the three modeling cases.	Section 6.2.4.4; base case curves have DTN MO0403SDIAWHBC.003 [DIRS 170434].
Tuff and alluvium density	Section 6.2.3.7

Software programs used to model this case are identical to those listed in Section 6.3.1.1 with the addition of Microsoft Excel 2000, which was used to compute response spectra at additional damping levels (see Appendix I) and the substitution of RANPAR V2.1 (Software Tracking Number 10486-2.1-00) (Pacific Engineering and Analysis 2003d [DIRS 170442]). Details of the modeling and analysis are documented in Scientific Notebook SN-M&O-SCI-037-V2 (Wong and Silva 2004a [DIRS 170443], pages 73, 80, 89, 122, and 123, and supplemental records 80 and 101).

The process for development of Surface Facilities Area (Points D and E) ground motions with 10^{-4} annual exceedance frequency is identical to that outlined in Section 6.3.1.3.1 for 10^{-3} motions. Representative mean SAFs and the magnitude-weighted SAF for the Point D 110 foot profile using the 1-2 Hz and 5-10 Hz DEAs (horizontal component) at an annual exceedance frequency of 10^{-4} are shown on Figures 6.3-32 and 6.3-33. Magnitude dependency of site response is significant for the lower mean tuff [LMT] and upper mean alluvium [UMA] nonlinear dynamic material properties, about 36 percent near 30 Hz. For the upper mean tuff and upper mean alluvium [UMT-UMA] material properties, magnitude dependency of site response is less significant, about 17% at 1-2 Hz and about 13% near 30 Hz.

Representative magnitude-weighted mean SAFs for Point D (35 foot profile) at 10^{-4} annual exceedance frequency using the 1-2 Hz and 5-10 Hz horizontal-component DEAs are shown on Figure 6.3-34 for the horizontally-polarized shear wave case. For frequencies greater than approximately 4 Hz, the UMT-UMA properties give the largest spectral amplification. Between approximately 1.3 Hz and 4 Hz, the UMT-LMA properties control. The LMT-LMA properties control for frequencies less than approximately 1.3 Hz. Figure 6.3-35 shows representative magnitude-weighted mean SAFs for Point D (110 foot profile) at 10^{-4} annual exceedance frequency using the 1-2 Hz and 5-10 Hz horizontal component DEAs for the horizontally-polarized shear wave case. Site response (horizontal component) at Point D (110 foot profile) is controlled by the UMT-UMA properties for frequencies greater than approximately 1.5 Hz. Below 1.5 Hz, the LMT-LMA properties control the site response (Figure 6.3-35). Point E (15

feet of alluvium) representative magnitude-weighted mean SAFs are shown on Figure 6.3-36 for the 1-2 Hz and 5-10 Hz horizontal-component DEAs. Site response (horizontal component) for Point E is controlled by the UMT properties for frequencies greater than approximately 2 Hz and the LMT properties below 2 Hz.

The magnitude-weighted mean SAFs for 1-2 Hz and 5-10 Hz DEAs are enveloped and applied to the envelope of the reference earthquake spectra and UHS for the reference rock outcrop (Point A). The resulting spectra for each set of base case nonlinear dynamic material properties and vertically incident waves are shown on Figure 6.3-37 for the horizontal component at an annual exceedance frequency of 10^{-4}. Spectra for Point D (35 foot profile), Point D (110 foot profile) and Point E (shallow alluvium) are all shown on this figure for just the vertically inclined SH wave case. The corresponding spectra from the inclined SH and SV cases were used in the analysis but are not plotted in the figure for the sake of clarity. A single envelope, the seismic design response spectrum, was drawn to provide one set of ground motions applicable to all locations within the Surface Facilities Area. The corresponding vertical-component site-response spectra and seismic design response spectrum are shown on Figure 6.3-38. The preclosure Point D/E seismic design response spectra at 10^{-4} annual exceedance frequency are provided in Table 6.3-12. These results have been submitted to the TDMS and have DTN MO0410WHBDF104.002 [DIRS 172238].

Table 6.3-12. Preclosure Point D/E Seismic Desig n Response Spectra (5%-Damped) in g's at 10^{-4} Annual Exceedance Frequency

Frequency (Hz)	Horizontal Motion (g)	Vertical Motion (g)
0.333	0.2626	0.2124
0.500	0.4546	0.3123
0.667	0.6451	0.3913
1.000	1.0704	0.5317
2.000	1.9418	0.9335
5.000	2.4759	2.0608
6.667	2.5105	2.3917
10.000	2.5548	2.8744
20.000	2.2778	2.7453
33.333	1.8153	2.3872
50.000	1.4953	2.0792
100.000	1.1926	1.4932

Source: DTN: MO0410WHBDF104.002 [DIRS 172238]

Note: Preclosure Point D/E Seismic Design Response Spectra at 10^{-4} annual exceedance frequency are also provided at 0.5, 1.0, 2.0, 3.0, 7.0, 10.0, 15.0, and 20.0% damping levels in DTN MO0410WHBDF104.002 [DIRS 172238]. This table provides a subset of the data points in DTN: MO0410WHBDF104.002 [DIRS 172238]. Values in DTN are provided for Period(s). Frequency (Hz) = 1/Period(s).

Response spectra for Point D/E at 10^{-4} annual exceedance frequency were also computed at damping values of 0.5, 1,0, 2.0, 3.0, 7.0, 10.0, 15.0, and 20.0%. These spectra were computed using the approach described in Section 6.3.1.3.1. Microsoft Excel 2000 was used for this analysis (see Appendix I).

6.3.1.4 Postclosure Emplacement Level Performance Assessment Ground Motions

The site response methodology used to develop ground motions for Point B for analyses supporting postclosure performance assessments is the same as discussed in Section 6.3.1.2 for developing preclosure response spectra. Peak ground velocities are also computed. The use of 5%-damped response spectra and peak ground velocities in developing time histories is discussed in Section 6.3.2. These analyses were performed for three annual exceedance frequency levels, 10^{-5}, 10^{-6}, and 10^{-7}.

The approach employed to develop postclosure emplacement level motions supporting TSPA-LA uses expected levels of peak particle velocity as the key ground motion parameters associated with damage to underground structures (McGarr 1984 [DIRS 163996], Dowding and Rozen 1978 [DIRS 160065]).

6.3.1.4.1 10^{-5} Annual Exceedance Frequency Ground Motions

This section describes use of the equivalent-linear site response model to develop response spectra and peak particle velocities with an annual exceedance frequency of 10^{-5} for Point B. Inputs to the model for this case are summarized in Table 6.3-13.

Table 6.3-13. Model Inputs for Development of Seismic Inputs with an Annual Exceedance Frequency of 10^{-5} for Point B

Model Input	Source
Twelve 10^{-5} deaggregation earthquake response spectra (three each for the 1-2 Hz and 5-10 Hz 10^{-5} reference earthquakes; horizontal and vertical components)	Section 6.2.2.5; deaggregation earthquakes have DTN MO0308UNHAZ105.000 [DIRS 170425]. Weights for combining results for each deaggregation earthquake are provided in Tables 6.2-8 and 6.2-9.
Incidence angles for the deaggregation earthquakes	Section 6.2.2.5.1; Table 6.2-14
60 randomized velocity profiles for each of the two Repository Block base case profiles	Section 6.2.3.5; base case velocity profiles have DTN MO0206SASWVSP1.001 [DIRS 163777]
60 randomized sets of shear modulus reduction and damping curves for each of the two tuff base case curves	Section 6.2.4.4; base case curves have DTN MO0403SDIAWHBC.003 [DIRS 170434]
Tuff density	Section 6.2.3.7
Horizontal peak ground velocity at Point A	Section 6.2.2.2, peak ground velocities at Point A with an annual exceedance frequency of 10^{-5} have DTN MO0309PGVDEAGG.000 [DIRS 170426]
Revised vertical peak ground velocity at Point A	Section 6.2.2.6.3

Software programs used to model this case are identical to those listed in Section 6.3.1.1 with the substitutions of RASCALP V2.02 (Software Tracking Number 10388-2.02-00) (Pacific Engineering and Analysis 2004k [DIRS 163316]) and RANPAR V2.1 (Software Tracking

Number 10486-2.1-00) (Pacific Engineering and Analysis 2003d [DIRS 170442]) and addition of Microsoft Excel 2000 (Appendix I) . Details of the modeling and analysis are documented in Scientific Notebook SN-M&O-SCI-037-V2 (Wong and Silva 2004a [DIRS 170443], pages 79-81, 89, and supplemental records 86, 89, 90, 92, 94, 100).

Representative emplacement level mean horizontal-component SAFs for the 1-2 Hz and 5-10 Hz DEAs, velocity profile base case #1 and lower mean tuff (LMT) nonlinear dynamic properties are shown on Figure 6.3-39 for an annual exceedance frequency of 10^{-5}. Note that the magnitude dependence for the tuff response (horizontal) is small. Representative Point B magnitude-weighted mean SAFs (horizontal component) for all base case site properties are shown on Figure 6.3-40 for the 1-2 Hz and 5-10 Hz DEAs for the horizontally-polarized shear wave case. For frequencies greater than approximately 1.3 Hz, the upper mean tuff (UMT) properties give the largest site amplification values, with little difference between the two base case velocity profiles. Representative Point B magnitude-weighted mean SAFs (vertical component) for both base case velocity profiles are shown on Figure 6.3-41 for the 1-2 Hz and 5-10 Hz DEAs for the vertically-polarized shear wave case. For frequencies greater than approximately 3 Hz, base case velocity profile #2 gives the largest spectral amplification values.

Point B horizontal-component spectra at an annual exceedance frequency of 10^{-5} are shown on Figure 6.3-42. General features noted in these spectra are (1) for frequencies greater than 2 Hz, there is little difference between the two velocity profiles and (2) the upper mean tuff curve controls at most frequencies. Figure 6.3-43 shows the Point B vertical-component site-response spectra at an annual exceedance frequency of 10^{-5}. Also shown on Figures 6.3-42 and 6.3-43 are the smooth envelopes of the spectra used as target spectra in spectral-conditioning time histories (see Section 6.3.2.3.3). Response spectra for 10^{-5} annual exceedance frequency have been submitted to TDMS and have DTN MO0312SEPRSRLB.019 [DIRS 170427].

In addition to response spectra, PGVs were also computed. The horizontal PGV value at Point A is 126.57 cm/sec (DTN: MO0309PGVDEAGG.000 [DIRS 170426]). The vertical Point A PGV was revised to 116.4 cm/sec based on V/H ratios (see Section 6.2.2.6.3 and Table 6.2-17). PGVs and response at Point B at 10^{-5} annual exceedance frequency are given in Table 6.3-14. Microsoft Excel 2000 was used to compute the mean PGV transfer functions for all control motions, base case velocity profiles and dynamic property curves, and wavetypes. The maximum PGVs (horizontal and vertical) resulting from applying the mean transfer functions to the Point A PGVs is taken as the Point B PGVs (see Appendix I). PGVs have been submitted to the TDMS and have DTN MO0401SEPPGVRL.022 [DIRS 169099].

Table 6.3-14. Postclosure Point B Envelope Spectra and PGVs at 10^{-5} Annual Exceedance Frequency

Frequency (Hz)	Horizontal Motion (g)	Vertical Motion (g)
0.300	0.4758	0.4391
0.500	0.7060	0.6935
0.700	0.8717	0.8643
1.000	1.0715	1.1000
2.000	1.5512	1.7232
5.000	2.0017	2.5169

Frequency (Hz)	Horizontal Motion (g)	Vertical Motion (g)
7.000	2.0848	2.7157
10.000	2.0757	2.8940
20.000	1.8127	2.8054
30.000	1.6203	2.5590
50.000	1.3994	2.2007
100.000	1.0753	1.5977
PGV	105 cm/sec	137 cm/sec

DTNs: MO0401SEPPGVRL.022 [DIRS 169099], MO0312SEPRSRLB.019 [DIRS 170427]

6.3.1.4.2 10^{-6} Annual Exceedance Frequency Ground Motions

This section describes use of the equivalent-linear site response model to develop response spectra and peak particle velocities seismic inputs with an annual exceedance frequency of 10^{-6} for Point B. Inputs to the model for this case are summarized in Table 6.3-15.

Table 6.3-15. Model Inputs for Development of Seismic Inputs with an Annual Exceedance Frequency of 10^{-6} for Point B

Model Input	Source
Twelve 10^{-6} deaggregation earthquake response spectra (three each for the 1-2 Hz and 5-10 Hz 10^{-6} reference earthquakes; horizontal and vertical components)	Section 6.2.2.5; deaggregation earthquakes have DTN MO0206UNHAZ106.001 [DIRS 163723]. Weights for combining results for each deaggregation earthquake are provided in Tables 6.2-8 and 6.2-9.
Incidence angles for the deaggregation earthquakes	Section 6.2.2.5.1; Table 6.2-15
60 randomized velocity profiles for each of the two Repository Block base case profiles	Section 6.2.3.5; base case velocity profiles have DTN MO0206SASWVSP1.001 [DIRS 163777]
60 randomized sets of shear modulus reduction and damping curves for each of the two tuff base case curves	Section 6.2.4.4; base case curves have DTN MO0403SDIAWHBC.003 [DIRS 170434]
Tuff density	Section 6.2.3.7
Horizontal peak ground velocity at Point A	Section 6.2.2.2, peak ground velocities at Point A with an annual exceedance frequency of 10^{-6} have DTN MO0208PGVDEAG6.001 [DIRS 164203]
Revised vertical peak ground velocity at Point A	Section 6.2.2.6.3

Software programs used to model this case are identical to those listed in Section 6.3.1.1 with the substitution of RASCALP V2.02 (Software Tracking Number 10388-2.02-00) (Pacific Engineering and Analysis 2002k [DIRS 163316]) and Microsoft Excel 2000 (Appendix I). Details of the modeling and analysis are documented in Scientific Notebook SN-M&O-SCI-037-V2 (Wong and Silva 2004a [DIRS 170443], pages 14-22, 25-33, 42, 46, 51, 54, 56, 58, 59, and supplemental records 7, 9, 10, 11, 33, 39, 54, 60, 62).

Representative emplacement level horizontal-component SAFs for the 1-2 Hz and 5-10 Hz DEAs, velocity profile base case #1 and lower mean tuff (LMT) nonlinear dynamic properties are shown on Figure 6.3-44 for an annual exceedance frequency of 10^{-6}. Note that the magnitude

dependence for the tuff response (horizontal) is small. Representative Point B magnitude-weighted mean SAFs (horizontal component) for all base case site properties are shown on Figure 6.3-45 for the 1-2 Hz and 5-10 Hz DEAs for the horizontally-polarized shear wave case. For frequencies greater than approximately 0.7 Hz, the lower mean tuff (LMT) properties give the largest site amplification values, with little difference between the two base case velocity profiles. Representative Point B magnitude-weighted mean SAFs (vertical component) for both base case velocity profiles are shown on Figure 6.3-46 for the 1-2 Hz and 5-10 Hz DEAs for the vertically-polarized shear wave case. For frequencies greater than approximately 2.5 Hz, the base case velocity profile #2 gives the largest spectral amplification values.

Point B horizontal-component spectra at an annual exceedance frequency of 10^{-6} are shown on Figure 6.3-47. General features noted in these spectra are (1) for frequencies greater than 2 Hz, there is little difference between the two velocity profiles and (2) the lower mean tuff curve controls at most frequencies. Figure 6.3-48 shows the Point B vertical-component site-response spectra at an annual exceedance frequency of 10^{-6}. Also shown on Figures 6.3-47 and 6.3-48 are the smooth envelopes of the spectra that are used as target spectra in spectral conditioning time histories (see Section 6.3.2.3). Response spectra for 10^{-6} annual exceedance frequency have been submitted to TDMS and have DTN: MO04065DSRSPTB.000 [DIRS 170506].

In addition to response spectra, PGVs were also computed. The horizontal and vertical PGV values at Point A were 301 and 156 cm/sec (DTN: MO0208PGVDEAG6.001 [DIRS 164203]). The vertical Point A PGV was revised to 224 cm/sec based on V/H ratios (see Section 6.2.2.6.3 and Table 6.2-17). PGVs at Point B at 10^{-6} annual exceedance frequency are given in Table 6.3-16. Microsoft Excel 2000 was used to compute the mean PGV transfer functions for all control motions, base case velocity profiles and dynamic property curves, and wavetypes. The maximum PGVs (horizontal and vertical) resulting from applying the mean transfer functions to the Point A PGVs is taken as the Point B PGVs (see Appendix I). These results have been submitted to the TDMS and have DTN MO0303DPGVB106.002 [DIRS 162712].

Table 6.3-16. Postclosure Point B Envelope Spectra and PGVs at 10^{-6} Annual Exceedance Frequency

Frequency (Hz)	Horizontal Motion (g)	Vertical Motion (g)
0.3	0.9995	0.9455
0.4	1.2311	1.2646
0.5	1.4189	1.4957
0.7	1.7767	1.8702
1.0	2.2450	2.3778
2.0	3.3299	3.6167
5.0	4.5319	5.4942
7.0	4.7252	5.8948
10.0	4.8154	6.2904
20.0	4.3155	6.1105
30.0	3.8960	5.4765

Frequency (Hz)	Horizontal Motion (g)	Vertical Motion (g)
50.0	3.2575	4.6645
100.0	2.4625	3.4351
PGV	244 cm/sec	236 cm/sec

DTN: MO0303DPGVB106.002 [DIRS 162712], MO04065DSRSPTB.000 [DIRS 170506]

6.3.1.4.3 10^{-7} Annual Exceedance Frequency Ground Motions

This section describes use of the equivalent-linear site response model to develop response spectra and peak particle velocities seismic inputs with an annual exceedance frequency of 10^{-7} for Point B. Inputs to the model for this case are summarized in Table 6.3-17.

Table 6.3-17. Model Inputs for Development of Seismic Inputs with an Annual Exceedance Frequency of 10^{-7} for Point B

Model Input	Source
Twelve 10^{-7} deaggregation earthquake response spectra (three each for the 1-2 Hz and 5-10 Hz 10^{-7} reference earthquakes; horizontal and vertical components)	Section 6.2.2.5; deaggregation earthquakes have DTN MO0209UNHAZ107.000 [DIRS 163724]. Weights for combining results for each deaggregation earthquake are provided in Tables 6.2-8 and 6.2-9.
Incidence angles for the deaggregation earthquakes	Section 6.2.2.5.1; Table 6.2-16
60 randomized velocity profiles for each of the two Repository Block base case profiles	Section 6.2.3.5; base case velocity profiles have DTN MO0206SASWVSP1.001 [DIRS 163777]
60 randomized sets of shear modulus reduction and damping curves for each of the two tuff base case curves	Section 6.2.4.4; base case curves have DTN MO0403SDIAWHBC.003 [DIRS 170434]
Tuff density	Section 6.2.3.7
Horizontal peak ground velocity at Point A	Section 6.2.2.2, peak ground velocities at Point A with an annual exceedance frequency of 10^{-7} have DTN MO0210PGVD1E07.000 [DIRS 164205]
Revised vertical peak ground velocity at Point A	Section 6.2.2.6.3

Software programs used to model this case are identical to those listed in Section 6.3.1.1 with the substitution of RASCALP V2.02, Software Tracking Number 10388-2.02-00 (Pacific Engineering and Analysis 2002k [DIRS 163316]) and Microsoft Excel 2000 (Appendix I). Details of the modeling and analysis are documented in Scientific Notebook SN-M&O-SCI-037-V2 (Wong and Silva 2004a [DIRS 170443], pages 42 through 46, 51, 52, 59, 61, and supplemental records 34, 35, 36, 37, 38, 57, 59, 62).

Representative Point B horizontal component mean SAFs for the 1-2 Hz and 5-10 Hz DEAs, velocity profile base case #1 and lower mean tuff (LMT) nonlinear dynamic properties are shown on Figure 6.3-49 for an annual exceedance frequency of 10^{-7}. As with all other ground motion levels at Point B, magnitude dependence for the tuff response (horizontal) is small. Representative Point B magnitude-weighted mean SAFs (horizontal component) for all base case site properties and vertically incident waves are shown on Figure 6.3-50 for the 1-2 Hz and 5-10 Hz DEA for the horizontally-polarized shear wave case. As with the response at the 10^{-6} ground motion level, there are noticeable differences between the UMT and LMT nonlinear dynamic

properties responses, with the LMT properties cases controlling at all frequencies greater than approximately 0.5 Hz. Given the same nonlinear dynamic properties, the transfer functions for both velocity base case profiles are very similar. Representative Point B magnitude-weighted mean SAFs (vertical component) for both base case velocity profiles are shown on Figure 6.3-51 for the 1-2 Hz and 5-10 Hz DEAs for the vertically-polarized shear wave case. For frequencies greater than approximately 3 Hz the base case velocity profile #2 gives the largest spectral amplification values.

Point B horizontal-component site-response spectra at an annual exceedance frequency of 10^{-7} are shown on Figure 6.3-52. Also shown is the smooth envelope of the site-response spectra, which is provided in Table 6.3-18.This spectrum was calculated for possible future use in spectrally matching time histories (Section 6.3.2.3.2). General features noted in these spectra are (1) for frequencies greater than 0.6 Hz, there is little difference between the two velocity profiles and (2) the lower mean tuff nonlinear dynamic properties base case controls at most frequencies. Figure 6.3-53 shows the Point B vertical-component envelope spectrum and the site-response spectra at an annual exceedance frequency of 10^{-7}. The base case velocity profile #2 controls at most frequencies.

Table 6.3-18. Postclosure Point B Envelope Spectra and PGVs at 10^{-7} Annual Exceedance Frequency

Frequency (Hz)	Horizontal Motion (g)	Vertical Motion (g)
0.3	2.0414	2.0164
0.5	3.0073	3.2359
0.7	3.6953	4.0917
1.0	4.7876	5.1263
2.0	7.3451	8.4299
5.0	10.4000	13.1835
7.0	10.7963	14.1456
10.0	10.9262	14.8189
20.0	9.7758	14.2894
30.0	8.7920	12.9984
50.0	7.4349	11.1321
100.0	5.5310	8.4140
PGV	535 cm/sec	625 cm/sec

Source: Wong and Silva 2004a [DIRS 170443], Supplemental Record 69
DTN: MO0210PGVPB107.000 [DIRS 162713]

In addition to response spectra, PGVs were also computed. The Point A horizontal and vertical PGVs were 655 and 340 cm/sec (revised to 572 cm/sec based on V/H ratios), respectively (Table 6.2-17). PGVs at Point B are presented in Table 6.3-18. Microsoft Excel 2000 was used to compute the Point B PGVs (see Appendix I). These results were submitted to the TDMS and have DTN MO0210PGVPB107.000 [DIRS 162713].

6.3.1.5 Comparison of Seismic Design Response Spectra

Figures 6.3-54 through 6.3-59 compare the Point A spectra with the Point B and the Point D/E seismic design response spectra for annual exceedance frequencies of 10^{-3}, $5x10^{-4}$, 10^{-4}, 10^{-5}, 10^{-6}, and 10^{-7}. As might be expected based on empirical evidence, the response spectrum at D/E is consistently the higher of the three spectra as it reflects the effect of the near-surface velocity gradient and the amplification of the shallow low velocity alluvium typically observed in earthquakes worldwide. The Point B response spectra are lower than the Point A UHS. At-depth motions are generally lower than outcrop motions due to the presence of downgoing waves and the absence of the free-surface effect, which is a factor of two for vertically propagating waves. For the vertical motions, the Point B spectra are lower than the Point A spectra at higher frequencies (> 5-8 Hz) similar to the horizontal motions (Figures 6.3-54 to 6.3-59). At lower frequencies the Point A and Point B spectra are similar.

6.3.2 Development of Time Histories

In this section, the approaches used to develop time histories are presented along with the resulting time histories for inputs to preclosure and postclosure analyses. Sets of time histories were developed for Point B at 10^{-3}, $5x10^{-4}$, 10^{-4}, 10^{-5}, 10^{-6}, and 10^{-7} annual exceedance frequencies and for Point D/E at 10^{-3}, $5x10^{-4}$, and 10^{-4} annual exceedance frequencies. The approach used to develop each set of time histories is a function of the use of the time histories in design or performance assessment analyses. Time histories for inputs to preclosure analyses at the emplacement level (Point B) and the Surface Facilities Area (Point D/E) are presented in Sections 6.3.2.1 and 6.3.2.2, respectively. Time histories for input to postclosure analyses at the emplacement level (Point B) are presented in Section 6.3.2.3. For all time histories, strong ground motion recordings from past earthquakes are used as the basis for the matching or scaling process to provide realistic time histories with characteristics of observed ground motion. The initial strong ground motion recordings are chosen from the NUREG/CR-6728 (McGuire et al. 2001 [DIRS 157510], Appendix B) analysis time history database (Table 6.3-19). Specific recordings were chosen based on the deaggregated hazard at Yucca Mountain, as described in Sections 6.3.1.2 through 6.3.1.4. H1 and H2 components were taken as defined in the NUREG/CR-6728 (McGuire et al. 2001 [DIRS 157510], Appendix B) time history database.

6.3.2.1 Preclosure Emplacement Level Seismic Design

Time histories are presented for inputs to preclosure analysis for the emplacement level (Point B) at 10^{-3}, $5x10^{-4}$ and 10^{-4} annual exceedance frequencies. All of these time histories were developed by spectrally matching an input time history to a target response spectrum. The target response spectra are the seismic design response spectra for the emplacement level (Point B) presented in Section 6.3.1.2.

Table 6.3-19. Summary of Input Strong Ground Motion Recordings

	Earthquake	Date	Magnitude (M)	Station	Distance (km	PGA (g)			PGV (cm/sec)			Used as Input Time Histories for:
						H1	H2	V	H1	H2	V	
1	Coalinga, CA	7/22/83	5.8	Oil City	10.0	0.387	0.370	0.210	13.8	12.4	4.6	Postclosure time histories for the emplacement level (Point B). See Section 6.3.2.3.1
2	Whitter Narrows, CA	10/1/87	6.0	Garvey Res. – Control Building	12.1	0.384	0.457	0.362	15.8	19.0	9.9	Postclosure time histories for the emplacement level (Point B). See Section 6.3.2.3.1
3	Helena, Montana	10/31/35	6.2	Carroll Coll.	8.0	0.15	0.173	0.102	5.8	16.5	7.3	Postclosure time histories for the emplacement level (Point B). See Section 6.3.2.3.1
4	Parkfield, CA	6/28/66	6.1	Cholame #8	9.2	0.246	0.273	0.116	10.2	11.3	4.3	Postclosure time histories for the emplacement level (Point B). See Section 6.3.2.3.1
5	Parkfield, CA	6/28/66	6.1	Temblor	9.9	0.357	0.272	0.136	21.5	15.0	4.4	Postclosure time histories for the emplacement level (Point B). See Section 6.3.2.3.1
6	San Fernando, CA	2/9/71	6.6	Pacoima Dam	2.8	1.226	1.16	0.699	112.5	54.3	56.5	Postclosure time histories for the emplacement level (Point B). See Section 6.3.2.3.1
7	Gazli, USSR	5/17/76	6.8	Karakyr	3.0	0.608	0.718	1.264	65.4	71.6	54.2	Postclosure time histories for the emplacement level (Point B). See Section 6.3.2.3.1
8	Morgan Hill, CA	4/24/84	6.2	Coyote Lake Dam	0.1	0.711	1.298	0.388	51.6	80.8	15.6	Postclosure time histories for the emplacement level (Point B). See Section 6.3.2.3.1

	Earthquake	Date	Magnitude (M)	Station	Distance (km	PGA (g)			PGV (cm/sec)			Used as Input Time Histories for:
						H1	H2	V	H1	H2	V	
9	Morgan Hill, CA	4/24/84	6.2	Gilroy Arr #6	11.8	0.222	0.292	0.405	11.4	36.7	14.1	Postclosure time histories for the emplacement level (Point B). See Section 6.3.2.3.1
10	Whitter Narrows, CA	10/1/87	6.0	San Gabriel – E Grand Ave	9.0	0.304	0.199	0.227	23.0	11.0	5.5	Postclosure time histories for the emplacement level (Point B). See Section 6.3.2.3.1
11	Loma Prieta, CA	10/18/89	6.9	Corralitos	5.1	0.644	0.479	0.455	55.2	45.2	17.7	Postclosure time histories for the emplacement level (Point B). See Section 6.3.2.3.1
12	Northridge, CA	1/17/94	6.7	Pacoima Kag Canyon	8.2	0.301	0.433	0.169	31.4	51.5	15.1	Postclosure time histories for the emplacement level (Point B). See Section 6.3.2.3.1
13	Loma Prieta, CA	10/18/89	6.9	Gilroy Arr #6	19.9	0.126	0.17	0.101	12.8	14.2	9.5	Postclosure time histories for the emplacement level (Point B). See Section 6.3.2.3.1
14	Landers, CA	6/28/92	7.3	Lucerne	1.1	0.721	0.785	0.818	97.6	31.9	45.9	Postclosure time histories for the emplacement level (Point B). See Section 6.3.2.3.1
15	Chi-Chi, Taiwan	9/20/99	7.6	TCU025	54.3	0.058	0.075	0.034	10.5	19.0	13.8	Postclosure time histories for the emplacement level (Point B). See Section 6.3.2.3.1
16	Kobe, Japan	1/16/95	6.9	Kobe Univ.	0.2	0.29	0.31	0.38	54.8	34.2	20.2	Postclosure time histories for the emplacement level (Point B). See Section 6.3.2.3.1
17	Koaceli, Turkey	8/17/99	7.4	Izmit	7.7	0.152	0.22	0.149	22.6	29.8	11.9	Postclosure time histories for the emplacement level (Point B). See Section 6.3.2.3.1

	Earthquake	Date	Magnitude (M)	Station	Distance (km	PGA (g)			PGV (cm/sec)			Used as Input Time Histories for:
						H1	H2	V	H1	H2	V	
18	Northridge, CA	1/17/94	6.7	Duarte-Mel Canyon Rd.	51.6	0.079	0.028	0.046	3.4	2.4	2.2	Preclosure time histories for the emplacement level (Point B) at 10^{-3} and $5x10^{-4}$ annual exceedance frequencies. See Sections 6.3.2.1.1 and 6.3.2.1.2.
19	Northridge, CA	1/17/94	6.7	Wrightwood-Jackson Flat	68.4	0.056	0.037	0.034	10.0	7.0	5.8	Preclosure time histories for the Surface Facilities Area (Point D/E) at 10^{-3} and $5x10^{-4}$ annual exceedance frequencies. See Sections 6.3.2.2.1 and 6.3.2.2.2.
20	Northridge, CA	1/17/94	6.7	Rancho Cucamonga-Deer Canyon	80.0	0.071	0.051	0.025	4.2	5.9	2.2	Preclosure time histories for the Surface Facilities Area (Point D/E) at 10^{-3} and $5x10^{-4}$ annual exceedance frequencies. See Sections 6.3.2.2.1 and 6.3.2.2.2.
21	Whittier Narrows, CA	10/1/87	6.0	Calabasos-N. Las Virg. (see Note)	53.3	0.119	0.075	0.086	2.8	1.5	2.7	Preclosure time histories for the Surface Facilities Area (Point D/E) at 10^{-3} and $5x10^{-4}$ annual exceedance frequencies. See Sections 6.3.2.2.1 and 6.3.2.2.2.
22	Whittier Narrows, CA	10/1/87	6.0	Pasadena Blvd. – CIT Calif Blvd.	15.5	0.177	0.271	0.171	8.1	15.4	7.0	Preclosure time histories for the Surface Facilities Area (Point D/E) at 10^{-3} and $5x10^{-4}$ annual exceedance frequencies. See Sections 6.3.2.2.1 and 6.3.2.2.2.
23	Chi-Chi, Taiwan	9/20/99	7.6	Tap 036	95.6	0.039	0.03	0.017	6.1	7.6	6.9	Preclosure time histories for the Surface Facilities Area (Point D/E) at 10^{-3} and $5x10^{-4}$ annual exceedance frequencies. See Sections 6.3.2.2.1 and 6.3.2.2.2.

	Earthquake	Date	Magnitude (M)	Station	Distance (km	PGA (g)			PGV (cm/sec)			Used as Input Time Histories for:
						H1	H2	V	H1	H2	V	
24	Koaceli, Turkey	8/17/99	7.4	Iznik	29.7	0.103	0.136	0.083	16.5	28.8	7.7	Preclosure time histories for the Surface Facilities Area (Point D/E) at 10^{-4} annual exceedance frequencies. See Section 6.3.2.2.3.
25	Chi-Chi, Taiwan	9/20/99	7.6	TCU015	47.3	0.114	0.119	0.068	29.5	49.8	17.2	Preclosure time histories for the emplacement level (Point B) at 10^{-4} annual exceedance frequencies. See Section 6.3.2.1.3.

Source: McGuire et al. (2001 [DIRS 157510], Appendix B, Tables B-1 and B-2)

NOTES: To convert kilometers to miles, multiply by 0.621. To convert cm/sec to in./sec, multiply by 0.394.
Record #21 has been modified for CEUS conditions (McGuire et al. 2001 [DIRS 157510], Appendix B). This set of records was used in place of the original records (Wong and Silva 2004d [DIRS 172075], page 46).

Time histories that are individually spectrally matched to a target response spectrum (Figure 6.3-60) are appropriate for use in cases in which a single three-component set of time histories will be used in an analysis. Alternatively, when multiple sets of time histories will be used in an analysis, they can be spectrally matched individually or such that the mean response spectra for the suite of records match the target spectra, but individual records do not. Seismic inputs described in this report that are based on spectral matching generally were developed following the recommendations in NUREG/CR-6728 (McGuire et al. 2001 [DIRS 157510], Section 5). These recommendations suggest modifications to the guidance for nuclear power plants (NUREG-0800, Section 3.7.1 [NRC 1989a [DIRS 165110]]). NUREG-0800, Section 3.7.1 (NRC 1989a [DIRS 165110]) incorporates specific guidance to consider the minimum Power Spectral Density (PSD) of ground motion records input to building, component and soil models. This guidance was to prevent the development of time histories with response spectra that envelop the seismic design response spectra across a given frequency range, even though the PSD (or equivalently the Fourier amplitude spectrum) of the input ground motion could possess low levels (gaps) within the same frequency range. For this case, the computed system response may be underpredicted if, for example, the soil-structure interaction (SSI) frequencies fall within those gaps. Because of the ambiguities in the definition of a PSD as well as the effort involved in developing a minimum PSD requirement for an arbitrary target response spectrum, the recommended revised criteria in NUREG/CR-6728 (McGuire et al. 2001 [DIRS 157510], Section 5) eliminate the need for a separate PSD check but require a minimum and maximum matching criteria for the target 5%-damped response spectrum. The intent of the more stringent matching guidance is to ensure that the developed ground motion does not possess any significant gaps in frequency content. These revised criteria satisfy the general intent of the guidance in NUREG-0800, Section 3.7.1 (NRC 1989a [DIRS 165110]), which is currently defined in detail only for the spectral shape embodied by the Regulatory Guide 1.60 (1973 [DIRS 151402]) spectrum.

The recommended guidelines on spectral matching contained in NUREG/CR-6728 (McGuire et al. 2001 [DIRS 157510], Section 5) are outlined below:

- The artificial accelerogram should achieve approximately a mean-based fit to the target spectrum. The average ratio of the spectral acceleration calculated from the accelerogram to the target, calculated frequency by frequency, is only slightly greater than one to insure there are no significant gaps and the result is not biased high with respect to the target.

- Records should have a sufficiently small frequency increment and sufficiently high maximum frequency (or alternatively time increment and maximum duration). The total duration of the record can be increased by zero packing to satisfy these frequency requirements. It is recommended that records have a maximum frequency increment of 0.05 Hz with a Nyquist frequency of at least 50 Hz or a time increment of at most 0.01 sec for a total duration of 20 sec.

- Spectral accelerations at 5 percent damping should be computed at a minimum of 100 points per frequency decade, uniformly spaced over the log frequency scale from 0.1 Hz to 50 Hz or the Nyquist frequency. The computed 5%-damped response spectrum of the accelerogram (if one artificial motion is used for analysis) or the average

of all accelerograms (if a suite of motions is used for analysis) should not fall more than 10 percent below the target spectrum at any one frequency point. No more than 9 adjacent spectral points may be allowed to fall below the target spectrum at any frequency. This corresponds to a moving frequency window of ± 10 percent centered on the frequency.

- The computed 5%-damped response spectrum of the artificial ground motion (if one motion is used for analysis) or the average of the 5%-damped response spectra (if a suite of motions is used for analysis) should not exceed the target spectrum by more than 30 percent in the frequency range between 0.2 Hz and 25 Hz.

- Artificial motions should have durations, and ratios PGV/PGA and PGA*PGD/PGV^2 that are generally consistent with appropriate WUS or CEUS magnitude and distance bin median values.

- The upper limit for the zero-lag cross-correlation coefficient between any two design ground motions (acceleration time histories) be 0.3.

These criteria ensure that no gaps in the PSD or Fourier amplitude spectrum will occur over a significant frequency range.

The recommendations outlined above for spectrally-matched artificial time histories were followed in analyses documented in this report, with the following exceptions. For the waste emplacement level (Point B), it is inappropriate to check the durations, PGV/PGA, and PGA*PGD/PGV^2 for consistency with the bin median values from NUREG/CR 6728 (McGuire et al. 2001 [DIRS 157510], Appendix C) because the Point B motions are at-depth motions not free-surface motions. Also, for Point D/E preclosure motions, it is inappropriate to compare time domain characteristics (i.e., PGV/PGA and PGA*PGD/PGV^2) with the WUS median bin values because Point D/E motions are an envelope of hard rock and shallow soil, whereas the bin median values in NUREG/CR-6728 (McGuire et al. 2001 [DIRS 157510], Appendix C) are for WUS soft rock and deep soil.

In this report, spectrally matched sets of three-component time histories are described for annual exceedance frequencies of 10^{-3}, $5x10^{-4}$, 10^{-4} for the emplacement level (Point B) (Sections 6.3.2.1.1 through 6.3.2.1.3). The approach outlined above is also used to develop the spectrally matched sets of time histories for the surface Facilities Area (Point D/E) presented in Section 6.3.2.2. Representative spectral matching for the emplacement level at $5x10^{-4}$ annual exceedance frequency is illustrated on Figure 6.3-60.

6.3.2.1.1 10^{-3} Annual Exceedance Frequency Motions

For preclosure design at Point B at 10^{-3} annual exceedance frequency, a set of three-component time histories was developed by spectrally matching to the Point B seismic design response spectrum following the guidelines outlined above in Section 6.3.2.1. Inputs to this analysis for these motions are summarized in Table 6.3-20.

Table 6.3-20. Analysis Inputs for Development of Seismic Design Time Histories with an Annual Exceedance Frequency of 10^{-3} for Point B

Analysis Input	Source
Strong Ground Motion Recording of 1994 Northridge Earthquake, Duarte-Mel Canyon Station	Section 6.3.2, Table 6.3-9, Number 18; NUREG-CR-6728 (McGuire et al. 2001 [DIRS 157510], Appendix B)
Seismic Design Response Spectra at Point B with an Annual Exceedance Frequency of 10^{-3}	Section 6.3.1.2.1, Table 6.3-2; seismic design response spectra have DTN MO0405SDSTPNTB.001 [DIRS 169851]

Software used in the analysis for this case consists of:

- INTERPOL V. 1.0 (Software Tracking Number 10944-1.0-00) (Pacific Engineering and Analysis 2002d [DIRS 163305])
- RASCALS V. 5.4 (Software Tracking Number 10389-5.4-00) (Pacific Engineering and Analysis 2002l [DIRS 163317])
- BASE4 V. 4.0 (Software Tracking Number 10940-4.0-00) (Pacific Engineering and Analysis 2002a [DIRS 163293])
- MAXMIN V. 1.0 (Software Tracking Number 10945-1.0-00) (Pacific Engineering and Analysis 2002f [DIRS 163309])
- SPCTLR V. 1.0 (Software Tracking Number 10947-1.0-00) (Pacific Engineering and Analysis 2003c [DIRS 163321])
- SMRATIO V. 1.0 (Software Tracking Number 10917-1.0-00) (Pacific Engineering and Analysis 2003n [DIRS 163320])
- CORBB V. 1.0 (Software Tracking Number 10941-1.0-00) (Pacific Engineering and Analysis 2002b [DIRS 163295])
- DUR V. 1.0 (Software Tracking Number 10942-1.0-00) (Pacific Engineering and Analysis 2003a [DIRS 163303])

INTERPOL is used to interpolate the Emplacement Level (Point B) seismic design response spectra to several hundred frequencies required for spectral matching. RASCALS is used to spectrally match the input strong ground motion recording to the emplacement level design spectra. The resulting spectrally-matched acceleration time history is baseline corrected using BASE4. Output from BASE4 are baseline corrected acceleration, velocity, and displacement time histories. MAXMIN is used to calculate the PGA and PGV of the time histories. SPCTLR is used to calculate the 5% response spectra of the time histories. The ratio between the time histories' response spectra and the target spectra are computed using SMRATIO. Cross-correlation statistics between time history components are computed using CORBB. Arias intensity versus duration is computed using DUR. This process is followed for two horizontal components and one vertical component. The analysis is described in scientific notebook SN-

M&O-SCI-037-V2 (Wong and Silva 2004a [DIRS 170443], pages 123, 126-128, and supplemental records 67, 119, and 120).

The input strong ground motion was the 1994 Northridge earthquake, Duarte-Mel Canyon Rd. Station recording (Number 18 in Table 6.3-19). This record (**M** 6.7, R 51.6 km (32.1 mi.), rock site) was selected from the M: 6.5, D: 50 – 100 km (31 – 62 mi.) bin of the NUREG/CR-6728 (McGuire et al. 2001 [DIRS 157510], Appendix B) analysis time history database. As shown on Figures 6.2-17 and 6.2-23, the deaggregation of the hazard at 10^{-3} annual exceedance frequency shows that the hazard is dominated by a **M** 6.9 event at 52 km (32 mi.) at the 1-2 Hz frequency range and a **M** 6.3 event at 5 km (3 mi.) at the 5-10 Hz frequency range. Following NUREG/CR-6728 (McGuire et al. 2001 [DIRS 157510], Section 5), when matching to UHS (one spectrum instead of the two deaggregated reference events), it is recommended that the strong ground motion duration be the longer duration associated with the low-frequency event. The matching criteria presented in NUREG/CR-6728 (McGuire et al. 2001 [DIRS 157510]) were followed for time history spectral matching.

The response spectra for the 10^{-3} Point B time histories compared to the target spectrum are shown on Figures 6.3-61 through 6.3-63. The matches at frequencies above 40 Hz are low but match at peak acceleration (100 Hz). Because the match is not important between 33 and 100 Hz due to these frequencies being of no engineering relevance, very little effort is made to improve the match at those frequencies. Corresponding plots of the ratio between the time histories' response spectra and the target spectra also shown on these figures. The acceleration, velocity, and displacement time histories are presented in Appendix II, Figures II-1 through II-3. These results have been submitted to TDMS and have DTN MO0405SDSTPNTB.001 [DIRS 169851].

6.3.2.1.2 $5x10^{-4}$ Annual Exceedance Frequency Motions

For preclosure design at Point B at $5x10^{-4}$ annual exceedance frequency, a set of three-component time histories were developed by spectrally matching to the Point B seismic design response spectrum following the guidelines outlined above in Section 6.3.2.1. Inputs to this analysis for these motions are summarized in Table 6.3-21.

Table 6.3-21. Analysis Inputs for Development of Seismic Design Time Histories with an Annual Exceedance Frequency of $5x10^{-4}$ for Point B

Analysis Input	Source
Strong Ground Motion Recording of 1994 Northridge Earthquake, Duarte-Mel Canyon Station	Section 6.3.2, Table 6.3-19, Number 18; NUREG-CR-6728 (McGuire et al. 2001 [DIRS 157510], Appendix B)
Seismic Design Response Spectra at Point B with an Annual Exceedance Frequency of $5x10^{-4}$	Section 6.3.1.2.2, Table 6.3-4; seismic design response spectra have DTN MO0407SDARS104.001 [DIRS 170683]

Software used in the analysis for this case are identical to those listed in Section 6.3.2.1.1 for 10^{-3} annual exceedance frequency motions.

The analysis is described in scientific notebook SN-M&O-SCI-037-V2 (Wong and Silva 2004a [DIRS 170443], pages 38, 57-59 and supplemental record 58).

The input strong ground motion was the 1994 Northridge earthquake, Duarte-Mel Canyon Rd. Station recording (Number 18 in Table 6.3-19). This record (**M** 6.7, R 51.6 km (32.1 mi.), rock site) was selected from the M: 6.5, D: 50 – 100 km (31 – 62 mi.) bin of the NUREG/CR-6728 (McGuire et al. 2001 [DIRS 157510]) analysis time history database. As shown in Figures 6.2-18 and 6.2-24, the deaggregation of the hazard at $5x10^{-4}$ annual exceedance frequency shows that the hazard is dominated by a **M** 7.0 event at 51 km (32 mi.) at the 1-2 Hz frequency range and a **M** 6.3 event at 5 km (3 mi.) at the 5-10 Hz frequency range. Following NUREG/CR-6728 (McGuire et al. 2001 [DIRS 157510], Section 5), when matching to UHS (one spectrum instead of the two deaggregated reference events), it is recommended that the strong ground motion duration be the longer duration associated with the low-frequency event.

The response spectra for the $5x10^{-4}$ Point B time histories compared to the target spectrum are shown on Figures 6.3-64 through 6.3-66. The matches are low at frequencies above 40 Hz for the reasons given previously. Corresponding plots of the ratio between the time histories' response spectra and the target spectra are also shown on these figures. The acceleration, velocity, and displacement time histories are presented in Appendix II, Figures II-4 through II-6. These results have been submitted to TDMS and have DTN MO0407TMHIS104.003 [DIRS 170599].

6.3.2.1.3 10^{-4} Annual Exceedance Frequency Motions

For preclosure design at Point B at 10^{-4} annual exceedance frequency, a set of three-component time histories were developed by spectrally matching to the Point B seismic design response spectrum following the guidelines outlined above in Section 6.3.2.1. Inputs to this analysis for these motions are summarized in Table 6.3-22.

Table 6.3-22. Analysis Inputs for Development of Seismic Design Time Histories with an Annual Exceedance Frequency of 10^{-4} for Point B

Analysis Input	Source
Strong Ground Motion Recording of 1999 Chi-Chi, Taiwan Earthquake, TUC Station	Section 6.3.2, Table 6.3-19, Number 25; NUREG-CR-6728 (McGuire et al. 2001 [DIRS 157510], Appendix B)
Seismic Design Response Spectra at Point B with an Annual Exceedance Frequency of 10^{-4}	Section 6.3.1.2.3, Table 6.3-6; seismic design response spectra have DTN MO0306SDSAVDTH.000 [DIRS 164033]

Software used in the analysis for this case are identical to those listed in Section 6.3.2.2.1 for 10^{-3} annual exceedance frequency motions.

The analysis is described in scientific notebook SN-M&O-SCI-037-V2 (Wong and Silva 2004a [DIRS 170443], pages 71-73 and supplemental records 78 and 82).

The input strong ground motion was the 1999 Chi-Chi, Taiwan earthquake, TCU015 Station recording (Number 25 in Table 6.3-19). This record (**M** 7.6, R 47.3 km (29.6 mi.), rock site) was selected from the M: 7.5, D: 10 – 50 km (6-31 mi.) bin of the NUREG/CR-6728 (McGuire et al. 2001 [DIRS 157510]) analysis time history database. As shown in Figures 6.2-19 and 6.2-25, the deaggregation of the hazard at 10^{-4} annual exceedance frequency shows that the hazard is dominated by a **M** 7.7 event at 52 km (32 mi.) at the 1-2 Hz frequency range and a **M** 6.3 event

at 5 km (3 mi.) at the 5-10 Hz frequency range. Following NUREG/CR-6728 (McGuire et al. 2001 [DIRS 157510], Section 5), when matching to UHS (one spectrum instead of the two deaggregated reference events), it is recommended that the strong ground motion duration be the longer duration associated with the low-frequency event.

The response spectra for the 10^{-4} Point B time histories compared to the target spectrum are shown on Figures 6.3-67 through 6.3-69. A small underprediction above 50 Hz is noted on the Point B horizontal-1 time history (Figure 6.3-67). Corresponding plots of the ratio between the time histories' response spectra and the target spectra are also shown on these figures. The acceleration, velocity, and displacement time histories are presented in Appendix II, Figures II-7 through II-9. These results have been submitted to TDMS and have DTN MO0306SDSAVDTH.000 [DIRS 164033].

6.3.2.2 Surface Facilities Seismic Design

For preclosure design of the Surface Facilities Area, a single set of three-component, spectrally matched time histories is developed at each annual exceedance frequency of interest using the approach outlined in 6.3.2.1 for preclosure time histories for the emplacement level. At 10^{-3} and $5x10^{-4}$ annual exceedance frequencies, an additional four sets of spectrally-matched time histories are provided for additional design analyses. As described in Section 6.3.1.3, the spectra for Point D and E were enveloped to provide a single seismic design response spectrum at Point D/E. In addition, strain-compatible soil properties were developed for use with the time histories in SSI analyses of surface facilities. The motions and strain-compatible soil properties developed at 10^{-3}, $5x10^{-4}$, and 10^{-4} annual exceedance frequencies are presented in Sections 6.3.2.2.1 through 6.3.2.2.3.

Design of the surface facilities will include SSI analyses. The approaches for performing SSI analyses should be consistent with the probabilistic approaches to the development of free-field design ground spectra discussed in NUREG/CR-6728 (McGuire et al. 2001 [DIRS 157510], Section 6.4). The process includes developing 5%-damped surface spectra (Point D/E seismic design response spectrum) defined as the mean of spectra generated from Point A convolved with a suite of soil columns generated to capture variability in site properties and geometry. The median soil column developed from these calculations should be used to define the best-estimate soil column associated with this spectrum. Upper- and lower-bound soil columns, generated from the results of these calculations, are the ± 1-sigma (16th and 84th percentile) iterated soil columns assuming a normal or lognormal distribution. These columns are to be used to define the range of site properties that need to be considered in the SSI analyses and will satisfy the minimum range of COV of 0.5. Artificial time histories were generated by spectrally matching the Point D/E seismic design response spectra (5% damped level) generally following the recommendations in NUREG/CR-6728 (McGuire et al. 2001 [DIRS 157510], Section 5.4). The time histories are associated with the iterated soil properties in the three soil columns. Therefore no further deconvolution with iteration of soil properties needs to be performed for the SSI analyses since this would double-count nonlinear soil strain effects.

6.3.2.2.1 10^{-3} Annual Exceedance Frequency Motions

Inputs to the analysis for the Point D/E 10-3 annual exceedance proability motions are summarized in Table 6.3-23.

Table 6.3-23. Analysis Inputs for Development of Seismic Design Time Histories with an Annual Exceedance Frequency of 10^{-3} for Points D and E

Analysis Input	Source
Strong Ground Motion Recording of 1994 Northridge Earthquake, Wrightwood-Jackson Flat Station	Section 6.3.2, Table 6.3-19, Number 19; NUREG-CR-6728 (McGuire et al. 2001 [DIRS 157510], Appendix B)
Strong Ground Motion Recording of 1994 Northridge Earthquake, Rancho Cucamonga-Deer Canyon Station	Section 6.3.2, Table 6.3-19, Number 20; NUREG-CR-6728 (McGuire et al. 2001 [DIRS 157510], Appendix B)
Strong Ground Motion Recording of 1987 Whittier Narrows Earthquake, Calabasas-N. Las Virgus Station	Section 6.3.2, Table 6.3-19, Number 21; NUREG-CR-6728 (McGuire et al. 2001 [DIRS 157510], Appendix B)
Strong Ground Motion Recording of 1987 Whittier Narrows Earthquake, Pasadena Blvd. Station	Section 6.3.2, Table 6.3-19, Number 22; NUREG-CR-6728 (McGuire et al. 2001 [DIRS 157510], Appendix B)
Strong Ground Motion Recording of 1999 Chi-Chi, Taiwan Earthquake, TAP036 Station	Section 6.3.2, Table 6.3-19, Number 23; NUREG-CR-6728 (McGuire et al. 2001 [DIRS 157510], Appendix B)
Seismic Design Response Spectra at Points D/E with an Annual Exceedance Frequency of 10^{-3}	Section 6.3.1.3, Table 6.3-8; seismic design response spectra have DTN MO0410SDSDE103.002 [DIRS 172236]

Software used in the development of time histories for this case is the same as used for the Point B preclosure seismic design described in Section 6.3.2. In addition, PARINP V. 1.1 (Software Tracking Number 10387-1.0-00) (Pacific Engineering and Analysis 2002h [DIRS 163314]) and LOGNORM V. 1.01 (Software Tracking Number 10384-1.01-00) (Pacific Engineering and Analysis 2004 [DIRS 170313]) are used to compute strain compatible soil properties. The analysis is documented in scientific notebook SN-M&O-SCI-037-V2 (Wong and Silva 2004a [DIRS 170443], pages 89-103, 127, and 128 and supplemental records 102, 107, and 108).

For generation of set 1 of spectrally-matched time histories, the input strong ground motion was the 1994 Northridge earthquake, Wrightwood-Jackson Flat Station recording (Number 19 in Table 6.3-19). As discussed in Section 6.3.2.1.1, this record was chosen based on the deaggregated hazard at 10^{-3} annual exceedance frequency. The response spectra for the 10^{-3} Point D/E time histories set 1 compared to the target spectrum are shown on Figures 6.3-70 through 6.3-72. A small underprediction is again observed at frequencies above 40 to 70 Hz. Corresponding plots of the ratio between the time histories and the target are also shown on these figures. The zero-lag, cross-correlation values between the acceleration time histories are 0.007, 0.065, and 0.021 for H1-H2, H1-V, and H2-V components, respectively. These are well below the recommended 0.3 maximum in NUREG/CR-6728 (McGuire et al. 2001 [DIRS 157510], page 5-5). The durations for the 5-75 percent build up of Arias Intensity are 16.12, 17.09, and 15.85 seconds for the H1, H2, and V components, respectively. The acceleration, velocity and displacement time histories are presented in Appendix II, Figures II-10 through II-12. These results have been submitted to TDMS and have DTN MO0410SDSDE103.002 [DIRS 172236].

An additional 4 sets of spectrally-matched time histories were developed for the surface facilities at 10^{-3} annual exceedance frequency. Input strong ground motions (listed in Table 6.3-23) were

chosen based on the range of magnitude and distances of earthquakes in the deaggregated hazard at 10^{-3} annual exceedance frequency. These additional sets of spectrally-matched time histories are provided for design analyses which may require multiple time histories. All are spectrally-matched to the Point D/E seismic design response spectra at 10^{-3} annual exceedance frequency, but retain the characteristics of the original recorded strong ground motions generated from earthquakes with a range of magnitudes and distances. The response spectra for the 10^{-3} Point D/E time histories (sets 2 through 5) compared to the target spectrum are shown on Figures 6.3-73 through 6.3-84. The zero-lag cross correlation values between the acceleration time histories are 0.002, 0.007, and 0.011 for set 2; 0.146, 0.038, and 0.059 for set 3; 0.035, 0.010, and 0.138 for set 4; and 0.016, 0.058, and 0.232 for set 5 (Wong and Silva 2004a [DIRS 170443], supplemental record 108). The acceleration, velocity and displacement time histories are presented in Appendix II, Figures II-13 through II-24. These results have been submitted to TDMS and have DTN MO0410SDSDE103.002 [DIRS 172236].

Associated strain-compatible soil columns were generated for the two base case velocity profiles. That is, for the 35 foot and 110 foot soil columns the results of the four sets of nonlinear dynamic material property base cases (UMT-UMA, UMT-LMA, LMT-UMA, and LMT-LMA) were averaged. The development of strain-compatible soil properties is documented in scientific notebook SN-M&O-SCI-037-V2 (Wong and Silva 2004a [DIRS 170443], pages 124-125 and supplemental records 108 and 116). Strain-compatible soil properties generated include V_S and damping, and V_P and damping. For each of these properties, the median and ± 1-sigma (16th and 84th percentile) iterated values are presented. The ± 1-sigma iterated values exceed the recommendation of a minimum COV of 0.5. Figures 6.3-85 through 6.3-88 show the strain-compatible properties for the 35 ft soil column. Figures 6.3-89 through 6.3-92 show the strain-compatible properties for the 110 ft soil column. These results have been submitted to the TDMS and have DTN MO0404SPCDAMPD.001 [DIRS 169344].

6.3.2.2.2 $5x10^{-4}$ Annual Exceedance Frequency Motions

Inputs to the analysis for the Point D/E $5x10^{-4}$ annual exceedance frequency motions are summarized in Table 6.3-24.

Table 6.3-24. Analysis Inputs for Development of Seismic Design Time Histories with an Annual Exceedance Frequency of $5x10^{-4}$ for Points D and E

Analysis Input	Source
Strong Ground Motion Recording of 1994 Northridge Earthquake, Wrightwood-Jackson Flat Station	Section 6.3.2, Table 6.3-19, Number 19; NUREG-CR-6728 (McGuire et al. 2001 [DIRS 157510], Appendix B)
Strong Ground Motion Recording of 1994 Northridge Earthquake, Rancho Cucamonga-Deer Canyon Station	Section 6.3.2, Table 6.3-19, Number 20; NUREG-CR-6728 (McGuire et al. 2001 [DIRS 157510], Appendix B)
Strong Ground Motion Recording of 1987 Whittier Narrows Earthquake, Calabasas-N. Las Virgus Station	Section 6.3.2, Table 6.3-19, Number 21; NUREG-CR-6728 (McGuire et al. 2001 [DIRS 157510], Appendix B)
Strong Ground Motion Recording of 1987 Whittier Narrows Earthquake, Pasadena Blvd. Station	Section 6.3.2, Table 6.3-19, Number 22; NUREG-CR-6728 (McGuire et al. 2001 [DIRS 157510], Appendix B)

Analysis Input	Source
Strong Ground Motion Recording of 1999 Chi-Chi, Taiwan Earthquake, TAP036 Station	Section 6.3.2, Table 6.3-19, Number 23; NUREG-CR-6728 (McGuire et al. 2001 [DIRS 157510], Appendix B)
Seismic Design Response Spectra at Points D/E with an Annual Exceedance Frequency of $5x10^{-4}$	Section 6.3.1.3.2, Table 6.3-10; seismic design response spectra have DTN MO0410SDSTHMIS.005 [DIRS 172237]

Software used in the analysis for this case is the same as used for the 10^{-3} Point D/E preclosure seismic design described in Section 6.3.2.2.1. The analysis is documented in scientific notebook SN-M&O-SCI-037-V2 (Wong and Silva 2004a [DIRS 170443], page 103 and supplemental record 106).

For generation of set 1 of spectrally-matched time histories, the input strong ground motion was the 1994 Northridge earthquake, Wrightwood-Jackson Flat Station recording (Number 19 in Table 6.3-19). As discussed in Section 6.3.2.1.2, this record was chosen based on the deaggregated hazard at $5x10^{-4}$ annual exceedance frequency. The response spectra for the $5x10^{-4}$ Point D/E time history set 1 compared to the target spectrum are shown on Figures 6.3-93 through 6.3-95. Corresponding plots of the ratio between the time histories and the target are also shown on these figures. The zero-lag, cross-correlation values between the acceleration time histories are 0.007, 0.070, and 0.021 for H1-H2, H1-V, and H2-V components, respectively. These are well below the recommended 0.3 maximum in NUREG/CR-6728 (McGuire et al. 2001 [DIRS 157510], page 5-5). The durations for the 5-75 percent build up of Arias Intensity are 16.04, 16.75, and 15.38 seconds for the H1, H2, and V components, respectively. The acceleration, velocity and displacement time histories are presented in Appendix II, Figures II-25 through II-27. These results have been submitted to TDMS and have DTN MO0410SDSTHMIS.005 [DIRS 172237].

An additional 4 sets of spectrally-matched time histories were developed for the surface facilities at $5x10^{-4}$ annual exceedance frequency. Input strong ground motions (listed in Table 6.3-24) were chosen based on the range of magnitudes and distances of earthquakes in the deaggregated hazard at $5x10^{-4}$ annual exceedance frequency. The response spectra for the $5x10^{-4}$ Point D/E time histories (sets 2 through 5) compared to the target spectrum are shown on Figures 6.3-96 through 6.3-107. Corresponding plots of the ratio between the time histories and the target are also shown on these figures. The zero-lag, cross correlation values between the acceleration time histories are 0.006, 0.009, and 0.006 for set 2; 0.143, 0.039, and 0.060 for set 3; 0.001, 0.00008, and 0.161 for set 4; and 0.025, 0.052, and 0.227 for set 5 (Wong and Silva 2004a [DIRS 170443], supplemental record 97). The acceleration, velocity and displacement time histories are presented in Appendix II, Figures II-28 through II-39. These results have been submitted to the TDMS and have DTN MO0410SDSTHMIS.005 [DIRS 172237].

Associated strain-compatible soil columns were generated for the two base case velocity profiles. That is, for the 35 foot and 110 foot soil columns the results of the four sets of nonlinear dynamic material property base cases (UMT-UMA, UMT-LMA, LMT-UMA, and LMT-LMA) were averaged. The development of strain-compatible soil properties is documented in scientific notebook SN-M&O-SCI-037-V2 (Wong and Silva 2004a [DIRS 170443], pages 124-126 and supplemental records 97 and 116). Strain-compatible soil properties generated include V_S and

damping, and V_P and damping. For each of these properties, the median and ± 1-sigma (16th and 84th percentile) iterated values are presented. The ± 1-sigma iterated values exceed the recommendation of a minimum COV of 0.5. Figures 6.3-108 through 6.3-111 show the strain-compatible properties for the 35 ft soil column. Figures 6.3-112 through 6.3-115 show the strain-compatible properties for the 110 ft soil column. These results have been submitted to the TDMS and have DTN MO0403SPWHB5E4.005 [DIRS 168376].

6.3.2.2.3 10^{-4} Annual Exceedance Frequency Motions

Inputs to the analysis for the Point D/E 10^{-4} annual exceedance frequency motions are summarized in Table 6.3-25.

Table 6.3-25. Analysis Inputs for Development of Seismic Design Time Histories with an Annual Exceedance Frequency of 10^{-4} for Points D and E

Analysis Input	Source
Strong Ground Motion Recording of 1999 Koaceli, Turkey Earthquake, Iznik Station	Section 6.3.2, Table 6.3-19, Number 24; NUREG-CR-6728 (McGuire et al. 2001 [DIRS 157510], Appendix B)
Seismic Design Response Spectra at Points D/E with an Annual Exceedance Frequency of 10^{-4}	Section 6.3.1.3.3, Table 6.3-12; seismic design response spectra have DTN MO0410WHBDF104.002 [DIRS 172238]

Software used in the analysis for this case is the same as used for the 10^{-3} Point D/E preclosure seismic design as described in Section 6.3.2.2.1. The analysis is documented in scientific notebook SN-M&O-SCI-037-V2 (Wong and Silva 2004a [DIRS 170443], page 89 and supplemental record 101).

For generation of set 1 of spectrally-matched time histories, the input strong ground motion was the 1999 Koaceli, Turkey earthquake, Iznik Station recording (Number 24 in Table 6.3-19). As discussed in Section 6.3.2.1.3, this record was chosen based on the deaggregated hazard at 10^{-4} annual exceedance frequency. The response spectra for the 10^{-4} Point D/E time histories compared to the target spectrum are shown on Figures 6.3-116 through 6.3-118. Corresponding plots of the ratio between the time histories and the target are also shown on these figures. The zero-lag, cross-correlation values between the acceleration time histories are 0.054, 0.046, and 0.060 for H1-H2, H1-V, and H2-V components, respectively. These are well below the recommended 0.3 maximum in NUREG/CR-6728 (McGuire et al. 2001 [DIRS 157510], page 5-5). The durations for the 5-75 percent build up of Arias Intensity are 15.59, 14.66, and 9.76 seconds for the H1, H2, and V components, respectively. The acceleration, velocity and displacement time histories are presented in Appendix II, Figures II-40 through II-42. These results have been submitted to TDMS and have DTN MO0410WHBDF104.002 [DIRS 172238].

Associated strain-compatible soil columns were generated for the two base case velocity profiles. That is, for the 35 foot and 110 foot soil columns and the results of the four sets of nonlinear dynamic material property base cases (UMT-UMA, UMT-LMA, LMT-UMA, and LMT-LMA) were averaged. The development of strain-compatible soil properties is documented in scientific notebook SN-M&O-SCI-037-V2 (Wong and Silva 2004a [DIRS 170443], pages 124-125 and supplemental records 103 and 116). Strain-compatible soil properties generated include V_S and

damping, and V_P and damping. For each of these properties, the median and ± 1-sigma (16th and 84th percentile) iterated values are presented. The ± 1-sigma iterated values exceed the recommendation of a minimum COV of 0.5 (ASCE 4-86 1986 [DIRS 148636]). Figures 6.3-119 through 6.3-122 show the strain-compatible properties for the 35 ft soil column. Figures 6.3-123 through 6.3-126 show the strain-compatible properties for the 110 ft soil column. These results have been submitted to the TDMS and have DTN MO0403SCSPSFAD.001 [DIRS 169342].

6.3.2.3 Postclosure Emplacement Level Performance Assessment

This section presents the sets of time histories developed for postclosure performance assessments at Point B at 10^{-5}, 10^{-6}, and 10^{-7} annual exceedance frequencies.

For postclosure analyses, key goals are to determine seismic consequences for the engineered barrier system (e.g., rockfall, damage to the waste package) and to evaluate the variability in those consequences resulting from the range of earthquakes contributing to the hazard at a given annual frequency of exceedance. Thus, rather than matching a single three-component set of time histories to target spectra, multiple sets of time histories are scaled according to some measure of the site-specific ground motion. Because damage to underground structures has been correlated with peak ground velocity (McGarr 1984 [DIRS 163996], pages 204-207), this ground motion measure is selected as the scaling parameter. To include appropriate variability in the seismic inputs for postclosure analyses, 17 sets of three-component time histories are developed for each annual frequency of exceedance considered. Strong motion records selected from the NUREG/CR-6728 database (McGuire et al. 2001 [DIRS 157510], Appendix B) to serve as the basis for these time histories are chosen to represent the range of magnitudes and distances indicated by deaggregation of the PGV hazard (Section 6.2.2.4). This ensures a reasonable and defensible distribution of spectral shapes and time history durations. PGV scaling is also generally carried out in a manner that preserves the observed inter-component variability of the strong motion records serving as the basis for the scaled time histories. For one case, each component was scaled to the Point B PGV independently without maintaining inter-component variability.

Selection of 17 three-component sets of strong motion records to represent the PGV deaggregation for a given annual frequency of exceedance ensures that appropriate variability related to magnitude and distance is incorporated in the seismic inputs. The mean response spectrum for the inputs reflects characteristics of the region in which the events occurred and were recorded (e.g., California). Alternatively, the records can be spectrally conditioned prior to scaling such that their mean response spectrum is more characteristic of the Yucca Mountain site. Spectral conditioning can be carried out with respect to the Point A or Point B target spectrum. At the present time, the influence of general spectral shape on structural response is not well defined for systems and structures of the Yucca Mountain Repository. An example of time history scaling to PGV spectrally conditioned to the target is shown on Figure 6.3-127.

The time histories developed for postclosure performance assessment are presented in the following sections in the order in which they were developed. At 10^{-6} and 10^{-7} annual exceedance frequencies, alternate sets of time histories are presented. These sets of time histories vary in the approach to PGV scaling and or spectral conditioning of the input strong ground

motion recordings and are presented in Sections 6.3.2.3.1 and 6.3.2.3.2. The single set of time histories for 10-5 annual exceedance frequency are presented in Section 6.3.2.3.3

6.3.2.3.1 $1x10^{-6}$ Annual Exceedance Frequency Motions

Scaled Time Histories

For postclosure performance assessments at 10^{-6} annual exceedance frequency, 17 sets of three-component time histories were developed by scaling recorded motions to the expected Point B PGVs. Inputs to this analysis for these motions are summarized in Table 6.3-26.

Table 6.3-26. Analysis Inputs for Development of PGV-Scaled Time Histories with an Annual Exceedance Frequency of 10^{-6} for Point B

Analysis Input	Source
17 strong ground motion earthquake recordings	Section 6.3.2, Table 6.3-19 Numbers 1-17; NUREG-CR-6728 (McGuire et al. 2001 [DIRS 157510], Appendix B)
Seismic peak ground velocity results for an annual exceedance frequency of 10^{-6} at Point B	Section 6.3.1.4.2, Table 6.3-16; peak ground velocity results at 10^{-6} have DTN MO0303DPGVB106.002[1] [DIRS 162712]
Seismic magnitude and distance deaggregation of PGV at Point A	Point A PGV deaggregation results have DTN MO0208PGVDEAG6.001 [DIRS 164203]

NOTE: [1]Vertical component time histories were scaled to a preliminary vertical Point B PGV (DTN MO0301DPGVB106.001 [DIRS 165935]). An impact review for the scaled time histories indicated no significant impact due to the change in vertical Point B PGV of at most 2.6 percent (BSC 2003a [DIRS 165937]).

Software used in the analysis for this case consists of:

- MAXMIN V. 1.0 (Software Tracking Number 10945-1.0-00) (Pacific Engineering and Analysis 2002f [DIRS 163309])
- SCALE1 V. 1.0 (Software Tracking Number 10946-1.0-00) (Pacific Engineering and Analysis 2002m [DIRS 163319])
- INTEG1 V. 1.0 (Software Tracking Number 10943-1.0-00) (Pacific Engineering and Analysis 2002c [DIRS 163304])
- SPCTLR V. 1.0 (Software Tracking Number 10947-1.0-00) (Pacific Engineering and Analysis 2003c [DIRS 163321])
- DUR V. 1.0 (Software Tracking Number 10942-1.0-00) (Pacific Engineering and Analysis 2003a [DIRS 163303])

MAXMIN is used to determine the PGV of each of the input strong ground motion earthquake recordings. Scale factors for each time history are calculated based on these PGVs and the target PGVs (Point B horizontal and vertical PGV). SCALE1 applies the scale factors to the input strong ground motion acceleration time histories. The output is a scaled acceleration time history. INTEG1 is used to generate the corresponding scaled velocity and displacement time

histories. MAXMIN is used to verify that the PGV of the scaled time history matches the target PGV. The 5%-damped response spectra of the resulting time histories are computed using SPCTLR. Arias intensity versus duration for each time history are also computed using DUR. The analysis is documented in scientific notebook SN-M&O-SCI-037-V2 (Wong and Silva 2004a [DIRS 170443], page 31-32, 48, 55-56, 124, 126 and supplemental records 39, 52, 54, 55, 60, 114 and 117).

A suite of 15 sets was developed as input ground motions, the number recommended by NUREG/CR-6728 (McGuire et al. 2001 [DIRS 157510], page 3-3) when using a suite of time histories. An additional two sets were provided as alternative time histories. All horizontal component time histories were scaled to a PGV of 244 cm/sec, and all vertical component time histories were scaled to a PGV of 230 cm/sec. Note that following the development of these time histories, the Point B PGV vertical component was revised to 236 cm/sec (Table 6.3-16). Therefore, there is at most a 2.6% difference in the PGV of the vertical components time histories and the Point B vertical PGV.

The input strong ground motion recordings selected are Numbers 1 through 17 in Table 6.3-19. These recordings were selected based on obtaining a magnitude distribution reflective of the horizontal component PGV deaggregation at 10^{-6} annual exceedance frequency. The Point A magnitude and distance seismic hazard deaggregations, in the form of probability densities, for the 10^{-6} annual exceedance frequency horizontal-component PGV were used as input (DTN: MO0208PGVDEAG6.001 [DIRS 164203]). The magnitude probability densities were provided in a range from **M** 5.0 to 8.1 in increments of 0.1 magnitude units. Each of the probability densities was converted to a percent total of the hazard. The fraction of hazard in each magnitude bin was normalized so that the bins summed to a value of 15, the desired number of time histories. Because of the small size of the magnitude bins and the small number of desired earthquakes, only fractional numbers of earthquakes are computed for each bin. For this reason, bin size was increased to ½ magnitude unit, and the numbers of earthquake in each bin were rounded to integer numbers. Table 6.3-27 provides the results of this approach.

Table 6.3-27. Earthquake Counts by Magnitude Bin at 10^{-6} Annual Exceedance Frequency

Magnitude Range	Earthquake Count
5 – 5.5	0
5.5 – 6	2
6 – 6.5	6
6.5 – 7	5
7 – 7.5	2
7.5 – 8	0
8+	0

DTN: MO0301TMHIS106.001 [DIRS 161868]

Source: Wong and Silva (2004a [DIRS 170443], Supplemental Record 10, page 4)

Earthquake distance probability densities were provided in distance ranges of 0 to 100 km in 2.5 km bins. Similarly, each of these probability densities was converted to a percent of the total hazard. These total hazard bins were also normalized to a value of 15. The bin size in this case was increased to 10 km, and the numbers of earthquakes in each bin were rounded to integers. Table 6.3-28 gives the results of this approach.

Table 6.3-28. Earthquake Counts by Distance Bin at 10^{-6} Annual Exceedance Frequency

Distance Range (km)	Earthquake Count
0 - 10	13
10 – 20	1
20 – 30	0
30 – 40	0
40 – 50	0
50 – 60	1
60 - 70	0
70 – 80	0
80 – 90	0
90+	0

DTN: MO0301TMHIS106.001 [DIRS 161868]

Source: Wong and Silva 2004a [DIRS 170443], Supplemental Record 10, page 5

NOTE: To convert kilometers to miles, multiple by 0.621

Based on the magnitude and distance deaggregation provided, the single earthquakes at distance ranges of 10-20 and 50-60 km fall into bins **M** 6.5-7 and 7-7.5 respectively. Three-component recordings from 15 earthquakes (and two alternates) were chosen from the NUREG/CR-6728 (McGuire et al. 2001 [DIRS 157510], Appendix B) strong ground motion database to match the results in Tables 6.3-27 and 6.3-28.

To examine the range in 5%-damped response spectra of the motions conditioned on PGVs, Figure 6.3-128 shows individual horizontal component spectra while Figure 6.3-129 shows the median and $\pm 1\sigma$ spectra for all 17 sets of time histories. The range in motions is consistent with the variability in existing empirical attenuation relations, with a σ_{ln} of about 0.45 (at PGA) (Abrahamson and Shedlock 1997 [DIRS 164486], Figure 11).

Figure 6.3-130 and 6.3-131 show corresponding plots for the vertical component. In this case an outlier exists (Chi-Chi, Taiwan recording) which increases the σ_{ln} to the value of about 0.7 (at PGA). The Chi-Chi record is anomalous with respect to the western U.S. empirical attenuation relations used by the PSHA ground motion experts in their estimation of the Yucca Mountain ground motions (CRWMS M&O, 1998a [DIRS 103731], Table 5-3). It is recommended that the Chi-Chi record not be used and thus two additional sets of time histories were also selected based on the deaggregation information discussed previously. The TCU025 record of the Chi-Chi earthquake is the only record in the dataset that represents a large earthquake (**M** 7.6) at a distance of about 50 km (Table 6.3-19). Although the deaggregation at long-period ground motions indicate a contribution from large distant events (e.g., Figure 6.2-25), the contribution at

an annual exceedance frequency of 10^{-5} for PGV is less than 15% and is less than 4% at an annual exceedance frequency of 10^{-7} (Toro 2004 [DIRS 172034], pages 88-89).

The acceleration, velocity, and displacement scaled time histories at 10^{-6} annual exceedance frequency are presented in Appendix II, Figures II-43 through II-93. These results have been submitted to TDMS and have DTN MO0301TMHIS106.001 [DIRS 161868].

Spectrally Conditioned Scaled Time Histories

An alternate suite of 17 sets of time histories was developed for Point B corresponding to 10^{-6} annual exceedance frequency. The development of these time histories differs from the scaled time histories discussed above in three aspects: (1) Point A site-specific spectral shapes were incorporated by spectral conditioning prior to scaling to PGV, (2) the correlation between the two horizontal components and the vertical component of the original strong ground motion records is maintained, and (3) the vertical PGV increased slightly (from 230 to 236 cm/sec). The change in the vertical PGV was a result of a change in the nonlinear dynamic properties of the tuff following the development of the scaled time histories. Inputs to this analysis for these motions are summarized in Table 6.3-29.

Table 6.3-29. Analysis Inputs for Development of Spe ctrally Conditioned Time Histories with an Annual Exceedance Frequency of 10^{-6} for Point B

Analysis Input	Source
17 strong ground motion earthquake recordings	Section 6.3.2, Table 6.3-19 Numbers 1-17; NUREG-CR-6728 (McGuire et al. 2001 [DIRS 157510], Appendix B)
Seismic peak ground velocity results for an annual exceedance frequency of 10^{-6} at Point B	Section 6.3.1.4.2, Table 6.3-16; peak ground velocity results at 10^{-6} have DTN MO0303DPGVB106.002 [DIRS 162712]
Seismic magnitude and distance deaggregation of PGV at Point A at 10^{-6} annual exceedance frequency	Point A PGV deaggregation results have DTN MO0208PGVDEAG6.001 [DIRS 164203]
UHS at Point A at 10^{-6} annual exceedance frequency	Section 6.2.2.3, UHS have DTN MO0206UNHAZ106.001 [DIRS 163723]
Generic western U.S. rock velocity profile	Silva et al. (1996 [DIRS 110474], Figure 3.8)

Spectral shape was incorporated into this alternate suite of time histories to make the records more representative of the Yucca Mountain site conditions. The input strong ground motion records are predominantly WUS recordings. As discussed in Section 6.2.2.6, spectra from the WUS generally peak at frequencies lower than those expected at Yucca Mountain. To incorporate the possible effects of spectral shape on performance assessment, the records were conditioned such that the mean of the response spectra was consistent with those at Point A. First, a transfer function was developed based on the ratio of Point A spectra and WUS soft rock spectra for horizontal and vertical components (Wong and Silva 2004d [DIRS 172075], page 32). The transfer function is the ratio of median Point A response spectrum to median generic WUS response spectrum. Both spectra were derived using a **M** 6.5 control motion at a distance of 5 km. This control motion was chosen to be consistent with the deaggregation of the hazard at postclosure annual exceedance frequency levels. Generic WUS site conditions were modeled using 30 randomizations about the generic rock velocity profile from Silva et al. (1996 [DIRS 110474], Figure 3.8) and generic rock dynamic properties from EPRI (1993b [DIRS 103320]).

Point A crustal properties are presented in Section 6.2.2. Transfer functions were developed for both horizontal and vertical component motions. The transfer functions were applied to the horizontal and vertical component response spectra of each of the 17 strong ground motion recordings. For each time history, the resulting response spectrum was then used as the target for a "weak" spectral match (i.e., one iteration of RVT spectral matching). The resulting time history, baseline corrected, is used as input to the scaling to peak ground velocity.

Scaling to PGV was done so as to maintain the correlation between the two horizontal components and the vertical components inherent in the original recording. For each set of time histories, the horizontal-1 component was scaled to the expected Point B mean PGV calculated in Section 6.3.1.4.2. As discussed in Section 6.2.2, the PSHA was calculated for the random component of the horizontals, not the geometric mean. For consistency, horizontal-1 was chosen as the random component to scale to the mean PGV. Horizontal-2 was scaled such that the variability between components of the original recording is maintained. Thus, horizontal-2 component time histories have PGVs that vary above and below the Point B PGV. The scaling factors were determined as follows:

$$H_{1A} = H_1 * PGV(H_B)/PGV(H_1) \quad \text{(Eq. 45)}$$

where H_{1A} = horizontal component 1 time history
H_1 = horizontal component 1 input time history (spectrally conditioned)
$PGV(H_B)$ = 244 cm/sec
PGV (H_1) = PGV from horizontal component 1 input time history

$$H_{2A} = H_2 * PGV(H_B)/PGV(H_1) \quad \text{(Eq. 45)}$$

where H_{2A} = horizontal component 2 time history
H_2 = horizontal component 2 input time history (spectrally conditioned)

$$V_A = V * PGV(V_B)/PGV(V) * (PGV(V)/PGV(H1))/(E*(PGV(V)/PGV(H1))) \quad \text{(Eq. 47)}$$

where V_A = vertical component time history
V = vertical component input time history (spectrally conditioned)
$PGV(V_B)$ = 236 cm/sec
PGV (V) = PGV from vertical component input time history
$PGV(H_1)$ = PGV from horizontal component 1 input time history
E*(PGV(V)/PGV(H1)) = mean value of ln(PGV(V)/PGV(H_1))

Software used in the analysis for this case consists of:

- RASCALS V5.4 (Software Tracking Number 10389-5.4-00) (Pacific Engineering and Analysis 2002l [DIRS 163317])
- SMRATIO V. 1.0 (Software Tracking Number 10917-1.0-00) (Pacific Engineering and Analysis 2002n [DIRS 163320])
- XYMULT V. 1.0 (Software Tracking Number 10919-1.0-00) (Pacific Engineering and Analysis 2002q [DIRS 163326])

- BASE4 V. 4.0 (Software Tracking Number 10940-4.0-00) (Pacific Engineering and Analysis 2002a [DIRS 163293])
- MAXMIN V. 1.0 (Software Tracking Number 10945-1.0-00) (Pacific Engineering and Analysis 2002f [DIRS 163309])
- SCALE1 V. 1.0 (Software Tracking Number 10946-1.0-00) (Pacific Engineering and Analysis 2002m [DIRS 163319])
- INTEG1 V. 1.0 (Software Tracking Number 10943-1.0-00) (Pacific Engineering and Analysis 2002c [DIRS 163304])
- SPCTLR V. 1.0 (Software Tracking Number 10947-1.0-00) (Pacific Engineering and Analysis 2003c [DIRS 163321])
- DUR V. 1.0 (Software Tracking Number 10942-1.0-00) (Pacific Engineering and Analysis 2003a [DIRS 163303])
- Microsoft Excel 2000 (Appendix I)

RASCALS is used to generate a median Point A response spectrum and median generic WUS response spectrum using a **M** 6.5 control motion at a distance of 5 km. The ratio of these two spectra is computed using SMRAT. This transfer function is applied to the response spectra of each of the 17 input strong ground motion recordings using XYMULT. For each input time history, the resulting spectra (horizontal and vertical) are used as targets for one iteration of spectral matching the input strong ground motion recording using RASCALS. Output from this weak match are new spectrally conditioned time histories, which are baseline corrected using BASE4. The PGVs for these spectrally conditioned time histories are computed using MAXMIN. Scale factors for PGV scaling are computed using EXCEL 2000, Eq. 45 through 47, and the Point B horizontal and vertical PGVs (see Appendix I). SCALE1 applies the scale factors to the spectrally conditioned acceleration time histories. The output is a scaled acceleration time history. INTEG1 is used to generate the corresponding velocity and displacement time histories. MAXMIN is used to verify that the PGVs of the time histories match the targets. The 5%-damped response spectra of the resulting time histories are computed using SPCTLR. Arias intensity versus duration for each time history are also computed using DUR.

The analysis is documented in scientific notebook SN-M&O-SCI-037-V2 (Wong and Silva 2004a [DIRS 170443], pages 48, 55-56, 124, 126 and supplemental records 39, 52, 54-55, 60, 114 and 117).

Figure 6.3-132 shows the individual horizontal-component 5%-damped response spectra for the 17 time history sets while Figure 6.3-133 shows the median and $\pm 1\sigma$ spectra. Similar plots for the vertical component time histories are shown on Figures 6.3-134 and 6.3-135. The individual acceleration, velocity, and displacement spectrally conditioned time histories at 10^{-6} annual exceedance frequency are presented in Appendix II, Figures II-94 through II-144. These results have been submitted to TDMS and have DTN MO0403AVDSC106.001 [DIRS 168891].

The similarities and differences between the scaled time histories and the spectrally conditioned and scaled time histories for 10^{-6} annual exceedance frequency are summarized as follows:

- In terms of PGV, the median values are not significantly different. However, the variability (sigma) of the PGV values in the two suites is different. Thus while the scaled time histories were all scaled to PGVs of 244 cm/sec (horizontal sets H1 and H2) and 230 cm/sec (vertical), the spectrally-conditioned time histories contain a large spread in the PGVs for the vertical and H2 component time histories, consistent with the observed variability of the original strong motion records. All H1 time histories were scaled to 244 cm/sec PGV as was done previously. For the H2 time histories, the minimum and maximum PGVs are 78 and 817 cm/sec, respectively, with a median PGV of 236 cm/sec. For the vertical time histories, the minimum and maximum PGVs are 85 and 637 cm/sec, respectively, with a median PGV of 234 cm/sec.

- In terms of PGA, the median value for the H1 time histories for the spectrally-conditioned scaled time histories (3.33 g) is larger by 17 percent than the scaled time histories (2.85 g). For H2, the median PGA differs by only 3 percent. For the vertical time histories, the median PGA for the spectrally conditioned scaled time histories (3.61 g) is 18 percent lower than the scaled time histories (4.41 g). There are some significant differences in the range of PGAs when looking at individual records.

- Comparing the 5 to 75 percent cumulative Arias intensity durations in the time histories, the spectrally-conditioned scaled time histories have slightly longer median durations for the H1 and vertical components. The median duration for the H2 spectrally-conditioned scaled time histories is slightly shorter than the scaled time histories. There is little difference between the two cases for the median 5 to 75 percent Arias intensity for the horizontal scaled time histories. However, for the vertical component median 5 to 75 percent Arias intensity of the spectrally conditioned time histories (48.42 m/sec) is 50 percent lower than the scaled time histories (103.44 m/sec).

In summary, differences between the two suites of 10-6 time histories, in terms of median values of PGA, PGV, Arias intensity content and 5 to 75 percent of Arias intensity duration range from about 3 to 50 percent. Results of any analyses using these time histories should be quantified in terms of distributions just as the time histories represent a distribution of potential ground motions that could occur for a selected mean annual exceedance frequency (given their inherent variability). The impact of the differences in average spectral shape is unknown and will likely depend on the type of structural analysis performed using the time histories as inputs.

6.3.2.3.2 $1x10^{-7}$ Annual Exceedance Frequency Motions

Spectrally Conditioned to Point A Time Histories

For postclosure performance assessments at 10^{-7} annual exceedance frequency, 17 sets of three-component time histories were developed by spectrally conditioning input time histories to Point A and scaling the resulting motions to the expected Point B PGV. Inputs to this analysis for these motions are summarized in Table 6.3-30.

Table 6.3-30. Analysis Inputs for Development of Spectrally Conditioned Time Histories with an Annual Exceedance Frequency of 10^{-7} for Point B

Analysis Input	Source
17 strong ground motion earthquake recordings	Section 6.3.2, Table 6.3-19 Numbers 1-17; NUREG-CR-6728 (McGuire et al. 2001 [DIRS 157510], Appendix B)
Seismic peak ground velocity results for an annual exceedance frequency of 10^{-7} for Point B	Section 6.3.1.4.3, Table 6.3-18; peak ground velocity results at 10^{-7} have DTN MO0210PGVPB107.000 [DIRS 162713]
Seismic magnitude and distance deaggregation of PGV at Point A at 10^{-7} annual exceedance frequency	Point A PGV deaggregation results have DTN MO0210PGVD1E07.000 [DIRS 164205]
Generic western U.S. rock velocity profile	Silva et al. (1996 [DIRS 110474], Figure 3.8)

The software used in this analysis is the same that was used for the spectrally conditioned 10^{-6} annual exceedance frequency scaled time histories (Section 6.3.2.3.1). Microsoft Excel 2000 was used to compute the scale factors for scaling to PGV (see Appendix I). The analysis is documented in scientific notebook SN-M&O-SCI-037-V2 (Wong and Silva 2004a [DIRS 170443], pages 48, 50, 53-54, 60, 62, 66, 125-126 and supplemental records 38, 51, 59, 69, 115, and 117).

The input strong ground motion recordings are Numbers 1 through 17 in Table 6.3-19, chosen based on the deaggregation of the PGV hazard. Note that these input strong ground motion recordings are identical to those used for the 10^{-6} time histories. The development method for this suite of time histories is identical to the spectrally-conditioned scaled time histories at 10^{-6} annual exceedance frequency described above. The expected peak ground velocities for Point B at 10^{-7} annual exceedance frequency used in the scaling are 535 and 625 cm/sec (211 and 246 in./sec) for the horizontal and vertical components, respectively (Table 6.3-18).

Figure 6.3-136 shows individual horizontal-component 5%-damped response spectra of the 17 sets of time histories while Figure 6.3-137 shows the median and $\pm 1\sigma$ spectra. Similar plots for the vertical-component time histories are shown on Figures 6.3-138 and 6.3-139. The individual acceleration, velocity, and displacement spectrally-conditioned scaled time histories at 10^{-7} annual exceedance frequency are presented in Appendix II, Figures II-145 through II-195. These results have been submitted to TDMS and have DTN MO0403AVTMH107.003 [DIRS 168892].

Spectrally Conditioned to Point B Scaled Time Histories

Alternate suites of time histories for Point B at 10^{-7} annual exceedance frequency were developed by spectrally conditioning to the expected Point B spectral shape and scaling to the expected Point B PGVs. These input time histories are Numbers 1 through 17 in Table 6.3-19. The analysis is documented in scientific notebook SN-M&O-SCI-037-V2 (Wong and Silva 2004a [DIRS 170443], pages 50, 62, 66 and supplemental records 38, 51, 59, 69). Microsoft Excel 2000 was used to compute the PGV scaling factors (see Appendix I).

A transfer function was developed based on the ratio of Point B spectra and WUS soft rock spectra for horizontal and vertical components Wong and Silva 2004d [DIRS 172075], page 33). The transfer function was applied to the response spectra of each of the 17 strong ground motion recordings. For each time history, the resulting response spectrum was then used as the target for

a "weak" spectral match. A "weak" match of the original strong motion records to the target spectra created 17 sets of time histories "conditioned" to Point B, but maintaining realistic frequency-to-frequency, record-to-record, and component-to-component variability. The resulting time history, baseline corrected, is used as input to the scaling to PGV. This approach is similar to the development of the spectrally conditioned to Point A 10^{-6} time histories, except that the expected Point B target spectra are used instead of the Point A spectra. The time histories were scaled to PGV maintaining the variability between the horizontal and vertical components, as described in 6.3.2.3.1 for the spectrally conditioned 10^{-6} time histories.

Figure 6.3-140 shows individual horizontal-component 5%-damped response spectra while Figure 6.3-141 shows the median and ± 1σ spectra. Similar plots for the vertical component time histories are shown on Figures 6.3-142 and 6.3-143. The individual acceleration, velocity, and displacement spectrally conditioned to Point B scaled time histories at 10^{-7} annual exceedance frequency are presented in Appendix II, Figures II-196 through II-246 (MO0301TMHSB107.000 [DIRS 164207]).

6.3.2.3.3 1x10^{-5} Annual Exceedance Frequency Motions

For postclosure performance assessments at 10^{-5} annual exceedance frequency, 17 sets of three-component time histories were developed by spectrally conditioning input time histories to Point B and scaling the resulting motions to the expected Point B PGV. Inputs to this analysis for these motions are summarized in Table 6.3-31.

Table 6.3-31. Analysis Inputs for Development of Spectrally Conditioned Time Histories with an Annual Exceedance Frequency of 10^{-5} for Point B

Analysis Input	Source
17 strong ground motion earthquake recordings	Section 6.3.2, Table 6.3-19 Numbers 1-17; NUREG-CR-6728 (McGuire et al. 2001 [DIRS 157510], Appendix B)
Seismic peak ground velocity results for an annual exceedance frequency of 10^{-5} at Point B	Section 6.3.1.4.1, Table 6.3-14; peak ground velocity results at 10^{-5} have DTN MO0401SEPPGVRL.022 [DIRS 169099]
Seismic magnitude and distance deaggregation of PGV at Point A at 10^{-5} annual exceedance frequency	Point A PGV deaggregation results have DTN MO0208PGVDEAG6.001 [DIRS 164203]
Response spectra for Point A at 10^{-5} annual exceedance frequency	Section 6.3.1.4.1, response spectra have DTN MO0312SEPRSRLB.019 [DIRS 170427]
Generic western U.S. rock velocity profile	Silva et al. (1996 [DIRS 110474], Figure 3.8)

Software used in the analysis for this case is the same used for the spectrally conditioned 10^{-6} annual exceedance frequency time histories (Section 6.3.2.1.3). Microsoft Excel 2000 was used to compute the scale factors for PGV scaling (see Appendix I). The analysis is documented in scientific notebook SN-M&O-SCI-037-V2 (Wong and Silva 2004a [DIRS 170443], pages 79-82, 89, 101, 103 and supplemental records 86, 89, 90, 92, 94, 100, and 104-106).

The input strong ground motion recordings are Numbers 1 through 17 in Table 6.3-19, chosen based on the deaggregation of the PGV hazard. Note that these input strong ground motion recordings are identical to those used for the 10^{-6} and 10^{-7} time histories. The development

method for this suite of time histories is identical to the spectrally-conditioned to Point B time histories at 10^{-7} annual exceedance frequency described above. The expected peak ground velocities for Point B at 10^{-5} annual exceedance frequency used in the scaling are 105 and 137 cm/sec (41 and 54 in./sec) for the horizontal and vertical components, respectively (Table 6.3-14).

Figure 6.3-144 shows individual horizontal component 5%-damped response spectra of the 17 sets of time histories while Figure 6.3-145 shows the median and ± 1σ spectra. Similar plots for the vertical component time histories are shown on Figures 6.3-146 and 6.3-147. The individual acceleration, velocity, and displacement spectrally conditioned time histories at 10^{-5} annual exceedance frequency are presented in Appendix II, Figures II-247 through II-297. These results have been submitted to TDMS and have DTN MO0402AVDTM105.001 [DIRS 168890].

6.3.3 Limitations and Uncertainties of Results

Four limitations apply to the results of this modeling activity:

- McGuire et al. (2001 [DIRS 157510]) did not address at-depth (emplacement level) motions. For surface motions, the unconservative bias inherent in the approximate methods at annual exceedance frequencies below 10^{-4} is at high frequency and is due mainly to site nonlinearity being more dominant in the approximate methods than in the full hazard integration (McGuire et al. 2001 [DIRS 157510]). Waste emplacement level motions, even at hazard levels as low as 10^{-7}, reflect very little nonlinearity, being dominated by upgoing wavefields defined by the Point A UHS. Since at-depth motions are dominated by upgoing wavefields, much as are surface outcrop motions, and nonlinearity is not a controlling mechanism at high frequency, Approach 2B is considered to appropriately maintain the Point A hazard levels for waste emplacement level ground motions.

- At very low annual frequencies of exceedance, the interpretations of the PSHA ground motion experts result in ground motion levels that may not be realizable at Yucca Mountain. These motions, particularly for annual frequencies of exceedance less than about 10^{-6} likely reflect source processes (e.g., dynamic stress drop) that are physically non-realizable. Additionally, large strains associated with such motions would have left a distinct signature of deformation within the 12 million-year-old lithophysal units of the Topopah Spring Tuff (BSC 2004c DIRS[170137], Section 6.6). Thus the very low annual frequency of exceedance ground motions in the mean, and certainly the narrow band spectral exceedances due to maintaining frequency-to-frequency variability as well as between component randomness are larger than source processes likely permit and are larger than the site has likely experienced. These results are used in postclosure analyses to show the sensitivity of seismic consequences to such high levels of ground motion. In the abstraction of seismic consequences (BSC 2004m [DIRS 169183], Section 6.9.1.1), an upper bound to PGV (BSC 2004c [DIRS 170137], Section 6.6) is incorporated to restrict consequences to those resulting from ground motions that are credible for Yucca Mountain.

- Design response spectra and time histories developed for the Surface Facilities Area (Points D and E) are strictly applicable in that portion of the WHB Area that lies southwest of the Exile Hill splay fault. This limitation results from the exclusion of velocity data for boreholes and SASW survey lines located to the north of that fault in developing velocity profiles. Applicability of the developed ground motions to the area northeast of the Exile Hill splay fault is addressed in Section 6.3.5.

- Design response spectra and time histories developed for the Surface Facilities Area (Points D/E) envelope results for three cases: 15 ft, 35 ft, and 110 ft of alluvium overlying tuff. These results are judged to be appropriate for sites with the depth of alluvium ranging from 0 to 120 ft. For sites, if any, at which the depth of alluvium is greater than 120 ft, the applicability of the developed seismic inputs should be evaluated.

Epistemic uncertainty and aleatory variability in the preclosure and postclosure ground motions developed in Section 6.3 have been formally accommodated in the PSHA for the Point A control motions through the corresponding UHS, REs, and DEAs. Propagation of the motions from Point A to other locations through site response analyses have followed an approach developed to maintain the Point A hazard level (McGuire et al. 2001 [DIRS 157510], Approach 2B) as well as accommodate variability in dynamic material properties throughout the site. In this process, both parametric uncertainty (uncertainty in mean or base case values) as well model uncertainty have been addressed. Uncertainty in best-estimate parameter values was accommodated through multiple base case values with resulting mean motions enveloped (Sections 6.2.3.5 and 6.2.4.5). Model uncertainty has been addressed through validations with recorded motions (Section 7) and is included in the aleatory variability in the Point A attenuation relations and resulting Point A UHS's. While model uncertainty was not directly incorporated in developing Points B, D, and E ground motion, it is implicitly included through the site response analysis process used to maintain the Point A hazard levels (McGuire et al. 2001 [DIRS 157510]).

6.3.4 At-Depth Motions, Strains, and Curvatures

This section describes the determination of vibratory motions, dynamic strains, and dynamic curvatures as a function of depth in the tuff between the emplacement level (Point B) and the top of Yucca Mountain. These results may be used for the seismic design of inclined and vertical shafts, ventilation shafts, and associated SSCs. These preclosure seismic design values are determined throughout the tuff based on the control motions corresponding to 10^{-3}, $5x10^{-4}$, and 10^{-4} annual exceedance frequencies as described in Section 6.2.2.

6.3.4.1 Analyses Procedures

The procedure used to compute the variations of motions, strains, and curvatures with depth employs RVT to estimate peak time domain values. The use of RVT permits response analyses to be done without the use of time histories. This approach results in peak estimates from a single run that represent an average over a number of analyses using different time histories, all of which have response spectra matched to the target spectrum. Peak values for acceleration and particle velocity are computed at layer interfaces (since displacements and stresses are continuous at boundaries) while strains and curvatures are estimated at layer midpoints.

To compute the motions, strains, and curvatures with depth, transfer functions are not used since this approach would necessitate developing these parameters for the control motions (DEAs) and would result in hundreds of transfer functions. The approach implemented here is to simply compute mean motions, strains, and curvatures for the DEAs. For vertical control motions (which are linear analyses), the envelope of the REs and UHS is used as the control motions. A mismatch will then occur at emplacement level (Point B) because the PGAs calculated directly from the DEAs do not match those of the corresponding seismic design response spectra, which were developed using transfer functions. This difference in peak acceleration values is a consequence of different computational approaches in the two types of analyses. Peak accelerations and velocities are adjusted at the surface and repository level to match the seismic design PGA and PGV, computed in Section 6.3.1.

The following software was used in the analysis for at-depth motions, strains and curvatures at 10^{-3}, $5x10^{-4}$ and 10^{-4} annual exceedance frequencies:

- RANPAR V.2.0 (Software Tracking Number 10486-2.0-00) (Pacific Engineering and Analysis 2002i [DIRS 163315])
- RASCALS V.5.4 (Software Tracking Number 10389-5.4-00) (Pacific Engineering and Analysis 2002l [DIRS 163317])
- RASCALP V.2.02 (Software Tracking Number 10388-2.02-00) (Pacific Engineering and Analysis 2002k [DIRS 163316])
- PARINP V.1.01 (Software Tracking Number 10387-1.1-00) (Pacific Engineering and Analysis 2002h [DIRS 163314])
- NORM V.1.01 (Software Tracking Number 10386-1.01-00) (Pacific Engineering and Analysis 2002g [DIRS 163313])
- Microsoft EXCEL 2000 (Appendix I, Table I-1)

As discussed in Section 6.3.1, site-response modeling of Yucca Mountain is carried out using sets of randomized velocity profiles and nonlinear dynamic properties for each of the 6 control motions (1-2 Hz and 5-10 Hz, ML, MM, and MH DEAs). For each base case velocity curve and base case set of nonlinear dynamic property curves, RANPAR is used to develop 60 randomized profiles. The three control motions (ML, MM, and MH DEAs) are convolved with the set of 60 profiles, resulting in 180 site-response analysis runs for each base case velocity profile and set of nonlinear dynamic property curves. These convolutions are performed using RASCALS for HSHH wavetypes and RASCALP for HSVH, VPV, and VSVV wavetypes. This analysis is done for both the three 1-2 Hz DEAs and the three 5-10 Hz DEAs. The output from RASCALS and RASCALP includes peak ground acceleration, peak ground velocity, strains, and curvatures as a function of depth from the top of Yucca Mountain to the repository level. PARINP is used to extract the at-depth results from the output files. Each set of 180 at-depth profiles (three control motions combined with 60 randomized site property profiles) are averaged using NORM. This is a weighted average using the weights corresponding to the three DEAs discussed in Section 6.2.2 (i.e., the weight for the ML DEA is divided by 60 and assigned to the 60 at-depth

profiles computed using the ML DEA as a control motion). NORM is used on each set of 180 at-depth profiles, resulting in weighted-mean at-depth results for 1-2 Hz and 5-10 Hz control motions, the two velocity base case profiles for Yucca Mountain, the two base case tuff nonlinear dynamic property curves, and each wavetype. The envelope of these at-depth profiles is taken as the design at-depth profile for peak ground velocity, strains and curvatures. For vertical control motions, the envelope of the REs is used as the control motions instead of the DEAs. This approach was used because the revision to the vertical ground motions for Point A (discussed in Section 6.2.2.6) was done for the envelope of the horizontal RE and UHS only, not to the vertical DEAs. Details of these analyses are documented in SN-M&O-SCI-037-V4 (Wong and Silva 2004d [DIRS 172075], page 16).

For peak ground accelerations versus depth, the envelope profile is compared to the surface and emplacement level (Point B) PGAs computed using the transfer function approach described in Section 6.3.1. Surface PGAs are computed as part of the analysis for emplacement level PGAs, but are not reported or submitted to TDMS as they are not presently required for design analyses. Calculation of surface PGAs using the transfer function approach are documented in scientific notebook SN-M&O-SCI-037-V4 (Wong and Silva 2004d [DIRS 172075], page 14 and 16). At-depth PGAs are scaled to match the PGAs at the surface and at the emplacement level. Scale factors for intermediate depths are computed by linear interpolation of the scale factors at the surface and at the emplacement level. Microsoft EXCEL is used to compute these scaled at-depth PGAs. (See Appendix I for At-Depth PGA Adjustment.xls.) Because the PGA scaling factors were, in general, near unity, the at-depth PGVs and strains and curvatures were not scaled.

6.3.4.1.1 Three-Dimensional Strain Fields

Because the control motions are specified through design response spectra rather than as a specific earthquake through magnitude and distance, an analytical or empirical ground motion model incorporating the source is not required. To compute motions at depth, all that is required is an adequate representation of wave propagation that is consistent with the magnitude and distance of the controlling earthquake(s).

The wave propagation analyses used to estimate at-depth motions in terms of peak accelerations, peak particle velocities, strains, and curvatures (bending strains) assumes plane P-, SV-, and SH-waves. Effects due to wavefront curvature such as head waves and near-source effects are expected to be small in view of the uncertainties in crustal structure and site profile as well as source properties such as mechanism, slip distribution, and nucleation point.

Strain Tensor

The general three-dimensional strain tensor results from inclined P-, SV-, and SH-waves (Lay and Wallace 1995 [DIRS 171473]) as depicted on Figure 6.3-148. As illustrated on the figure, the xy-plane corresponds to the ground surface and the z-axis is vertical with ‘up’ positive. For cases 1 and 2 below, it is assumed, without loss of generality, that the incident plane wavefield is within the xz-plane with incident angle α. Particle motion is in the xz-plane for P- and SV-waves and in the xy-plane for SH-waves. Inclined P-SV wavefields result in the following nonzero, three-dimensional strain components;

$$\gamma_{xz}, \varepsilon_{xx}, \varepsilon_{zz}$$

in which $\varepsilon_{xx} = \partial u_x/\partial x$, $\varepsilon_{xz} = \frac{1}{2} \left| (\partial u_x/\partial z + \partial u_z/\partial x) \right|$ etc., $\gamma_{xz} = 2\varepsilon_{xz}$ etc., and ε_{yy}, γ_{xy} and γ_{yz} are identically zero. Inclined SH wavefields result in the following non-zero, three-dimensional strain components

$$\gamma_{xy}, \gamma_{yz};$$

ε_{xx}, ε_{yy}, ε_{zz}, and γ_{xz} are identically zero.

The general strain tensor becomes:

$$\begin{matrix} \varepsilon_{xx} & \frac{\gamma_{xy}}{2} & \frac{\gamma_{xz}}{2} \\ \frac{\gamma_{xy}}{2} & 0 & \frac{\gamma_{yz}}{2} \\ \frac{\gamma_{xz}}{2} & \frac{\gamma_{yz}}{2} & \varepsilon_{zz} \end{matrix} \qquad \text{(Eq. 48)}$$

The principal strains ε_1, ε_2, and ε_3 are given by the roots of the determinant equation:

$$\begin{vmatrix} \varepsilon_{xx} - \varepsilon & \frac{\gamma_{xy}}{2} & \frac{\gamma_{xz}}{2} \\ \frac{\gamma_{xy}}{2} & -\varepsilon & \frac{\gamma_{yz}}{2} \\ \frac{\gamma_{xz}}{2} & \frac{\gamma_{yz}}{2} & \varepsilon_{zz} - \varepsilon \end{vmatrix} = 0 \qquad \text{(Eq. 49)}$$

which results in the cubic equation in ε

$$\varepsilon^3 - \varepsilon^2 [\varepsilon_{zz} + \varepsilon_{xx}] + \varepsilon [\varepsilon_{xx}\varepsilon_{zz} - \frac{1}{4}(\gamma_{xy}^2 + \gamma_{yz}^2 + \gamma_{xz}^2)] + \frac{1}{4}[\gamma_{xy}^2 \varepsilon_{zz} + \gamma_{yz}^2 \varepsilon_{xx} - \gamma_{xy}\gamma_{yz}\gamma_{xz}] = 0 \qquad \text{(Eq. 50)}$$

In this general case ε (ε_1, ε_2, ε_3) has three values corresponding to the maximum, minimum, and intermediate normal strains. The maximum shear strain γ is the difference between the maximum and minimum normal strains (here taken as ε_1, ε_2):

$$\gamma = \frac{(\varepsilon_1 - \varepsilon_2)}{2} \qquad \text{(Eq. 51)}$$

This shear strain, as a function of time, represents the shear strain that induces nonlinear soil response to shear motion within a three-dimensional profile. For normally incident S-waves this

reduces to the usual normal shear strain acting on the xy plane. In general three-dimensional theory, however, the plane upon which the maximum shear strain acts may not be horizontal and its orientation varies in time with the principal directions.

Case 1: Incident Inclined P-SV Wavefields

In this case the motion is confined to the xz-plane (Figure 6.3-148) and the nonzero strain elements are

$$\gamma_{xz}, \varepsilon_{xx}, \varepsilon_{zz}$$

and Eq. (50) reduces to

$$\varepsilon^2 - \varepsilon\theta + \varepsilon_{xx}\,\varepsilon_{zz} - \frac{\gamma_{xz}^2}{4} = 0 \qquad \text{(Eq. 52)}$$

in which $\theta = \varepsilon_{xx} + \varepsilon_{yy} + \varepsilon_{zz} = \varepsilon_{xx} + \varepsilon_{zz}$ = cubical (plane) dilation or volume change. Solving for ε

$$\begin{aligned} 2\varepsilon &= \theta \pm \sqrt{\theta^2 - 4\,\varepsilon_{xx}\,\varepsilon_{zz} + \gamma_{zz}^2} \\ &= \theta \pm \sqrt{(\varepsilon_{xx} - \varepsilon_{zz})^2 + \gamma_{xz}^2} \end{aligned} \qquad \text{(Eq. 53)}$$

then

$$\varepsilon_1 = \theta + \sqrt{(\varepsilon_{xx} - \varepsilon_{zz})^2 + \gamma_{xz}^2}$$
$$\varepsilon_2 = \theta - \sqrt{(\varepsilon_{xx} - \varepsilon_{zz})^2 + \gamma_{xz}^2}$$

and

$$\gamma = \sqrt{(\varepsilon_{xx} - \varepsilon_{zz})^2 + \gamma_{xz}^2} \qquad \text{(Eq. 54)}$$

Case 2: Incident Inclined SH Wavefields

In this case the motion is confined to the xy plane and the nonzero strain elements are:

$$\gamma_{yx}, \gamma_{yz}$$

and Eq. (50) reduces to

$$\varepsilon^2 = \frac{1}{4}[\gamma^2_{yx} + \gamma^2_{yz}]$$

$$2\varepsilon = \pm\sqrt{\gamma_{yx}^2 + \gamma_{yz}^2}$$

$$2\varepsilon_1 = \sqrt{\gamma_{yx}^2 + \gamma_{yz}^2}$$

$$2\varepsilon_2 = -\sqrt{\gamma_{yx}^2 + \gamma_{yz}^2}$$

and the maximum shear strain is given by

$$\gamma = \sqrt{\gamma_{yx}^2 + \gamma_{yz}^2} \qquad \text{(Eq. 55)}$$

As with the incident inclined P-SV wavefield, the angle of incidence must be known with inclined SH motion.

Case 3: Normally Incident S-Wavefields (SH)

The nonzero strain fields are

$$\gamma_{xz}, \gamma_{yz}$$

then Eq. (50) reduces to

$$\varepsilon^2 = \frac{1}{4}[\gamma_{yz}^2 + \gamma_{xz}^2]$$

$$2\varepsilon = \pm\sqrt{\gamma_{yz}^2 + \gamma_{xz}^2}$$

and

$$\gamma = \sqrt{\gamma_{yz}^2 + \gamma_{xz}^2} \qquad \text{(Eq. 56)}$$

The maximum shear strain is then the vector sum of the two normal shear strains and is independent of azimuth. If the azimuth changes during the time window, it has no effect on the maximum shear strain γ. This consideration is important for sites close to extended ruptures.

Case 4: Normally Incident P-Wavefields

The only nonzero strain element is the axial strain ε_{zz}.

6.3.4.2 Control Motions for At-Depth Motions, Strains, and Curvatures

Horizontal and vertical component DEA spectra, computed in Section 6.2.2, are used as control motions for computing at-depth motions, strains, and curvatures. Appropriate body wave incidence angles are estimated using source distance and depth of the DEAs, as discussed in Section 6.2.2.5.1. Ray-tracing methods were used, together with the best-estimate profile, to determine P- and S-wave incidence angles at the repository interface (Section 6.2.2.5.1).

For SV-waves, the 1-2 Hz DEAs distances and depths are beyond the critical angles. As a result, for a pure point source in a plane-layered structure, little SV energy will propagate into the repository interface layer. However, since the source location and crustal structure have uncertainties, and SV-wave energy would be expected to be observed at the site reflecting these uncertainties, subcritical incidence angles are assumed for the SV-wave analyses.

For analysis of SH-waves, both normal and inclined incidences are considered. Normal incidence is important to consider since shear strains are a maximum for this case.

Motions, strains, and curvatures are produced for each base case velocity profile, base case dynamic property curves (upper mean tuff and lower mean tuff), and type of wave propagator. The seismic design peak motions, strains, and curvatures are developed based on all of these cases. The seismic design peak acceleration with depth curve is drawn to match the peak acceleration calculated based on transfer functions at the emplacement level.

6.3.4.3 Analyses for At-Depth Motions, Strains, and Curvatures

6.3.4.3.1 Peak Acceleration Versus Depth

Mean peak accelerations as a function of depth for annual exceedance frequencies of 10^{-3}, $5x10^{-4}$, and 10^{-4} are shown on Figures 6.3-149 through 6.3-151. The seismic design motions with depth presented here have been adjusted to match the 100-Hz response spectral acceleration of the seismic design response spectra at the emplacement level (Point B). The increase in PGA near the surface is due to the low velocity material in the upper 10 to 20 feet of the repository block.

6.3.4.3.2 Peak Particle Velocity Versus Depth

Seismic design peak particle velocities are shown on Figures 6.3-152 through 6.3-154 for annual exceedance frequencies of 10^{-3}, $5x10^{-4}$, and 10^{-4}, respectively. An increase in PGV is seen near the surface, similar to the PGAs.

6.3.4.3.3 Bending Strains (Curvatures)

Curvatures, or bending strains, are confined to the xz-plane for P- and SV-waves and to the yz plane for SH-waves. Seismic design curvatures are shown on Figures 6.3-155 through 6.3-157 for annual exceedance frequencies of 10^{-3}, $5x10^{-4}$, and 10^{-4}, respectively. Horizontal component curvatures are computed using inclined and vertically incident SH- and inclined SV-waves. Vertical component curvatures are computed using inclined SV- and P-waves. Mean curvatures tend to decrease with depth in the tuff, especially in the top 25 m. The curvatures from inclined SV-waves are nonphysical because the small SV-motions on the vertical component combined with the vertical spectra produce nonphysical curvatures. The small curvature values are expected as the wavefield is dominated by P-waves and associated vertical motions with small horizontal motion.

6.3.4.3.4 Coupled P-SV Strain Fields

Axial Strains ε_{xx}

Seismic design strains ε_{xx} are shown on Figures 6.3-158 through 6.3-160 for annual exceedance frequencies of 10^{-3}, $5x10^{-4}$, and 10^{-4}, respectively. Inclined SV-waves are used to propagate horizontal component motions, while inclined SV- and P-waves are used to propagate vertical motions to excite ε_{xx} strains. Mean strains indicate a very slight decrease with depth in the tuff. The largest strains ε_{xx} are vertical component inclined P-waves because the strains from the SV-wave are nonphysical. The ε_{xx} strains are zero for normal incidence (vertically propagating P-wave).

Axial Strains ε_{zz}

Seismic design axial strains ε_{zz} are shown on Figures 6.3-161 through 6.3-163 for annual exceedance frequencies of 10^{-3}, $5x10^{-4}$, and 10^{-4}, respectively. Inclined SV-waves are used to propagate horizontal motions, while inclined SV- and vertical and inclined P-waves are used to propagate vertical motions to excite axial strains, ε_{zz}.

Shear Strains γ_{xz}

Seismic design shear strains γ_{xz} are shown on Figures 6.3-164 through 6.3-166 for annual exceedance frequencies of 10^{-3}, $5x10^{-4}$, and 10^{-4}, respectively. Inclined SV-waves are used to propagate horizontal component motions and inclined P-waves are used to propagate vertical component motions to excite shear strains γ_{xz}. The γ_{xz} strains are zero for normal incidence P-wave.

6.3.4.3.5 SH Strain Field

Shear Strains γ_{yz}

Seismic design shear strains γ_{yz} are shown on Figures 6.3-167 through 6.3-169 for annual exceedance frequencies of 10^{-3}, $5x10^{-4}$, and 10^{-4}, respectively. Vertical and inclined SH-waves are used to propagate horizontal component motions to excite shear strains γ_{yz}.

Shear Strains γ_{yx}

Seismic design shear strains γ_{yz} are shown on Figures 6.3-170 through 6.3-172 for annual exceedance frequencies of 10^{-3}, $5x10^{-4}$, and 10^{-4}, respectively. Inclined SH-waves (this strain field is identically zero for vertically propagating shear waves) are used to compute shear strains γ_{yx}. Mean shear strains γ_{yz} decrease very slightly with depth in the tuff.

6.3.5 Comparison of Ground Motions Across the Exile Hill Fault Splay

The seismic design ground motions for Point D/E described above have been calculated for the Surface Facilities Area southwest of the Exile Hill splay fault. In the site characterization program performed in 2000 and 2001, the focus of the geotechnical program was on the WHB

area southwest of the fault (BSC 2002a [DIRS 157829], Section 6.2.3). Recent developments in the placement and design of the surface facilities now require that facilities be located northeast of the fault. This location is designated as Point F. To evaluate on a preliminary basis the possible differences between ground motions on the northeast and southwest sides of the Exile Hill splay fault, ground motions for an annual exceedance frequency of $5x10^{-4}$ at Point F have been calculated.

Base case velocity models for Point F were developed based on the V_S data described in BSC (2002a [DIRS 157829]). The following data were used:

- Downhole – RF#19, 22, and 29 (DTN MO0111DVDWHBSC.001 [DIRS 157296])
- Suspension – RF#17, 19, 22, and 29 (DTN MO0204SEPBSWHB.001 [DIRS 158088])
- SASW – 3, 15, 16, 19, 24, 30, and 36 (DTN MO0110SASWWHBS.000 [DIRS 157969]).

Data for RF#14 were not used because it was uncertain on which side of the Exile Hill splay fault the borehole was located. Similar to the approach taken for the Point D/E velocity profiles south of the fault (Section 6.2.3.4), V_S and V_P profiles were developed for both alluvium and tuff (Wong and Silva 2004b [DIRS 170444], pages 109-115). Microsoft Excel 2000 was used to compute geometric mean velocity profiles for Point F (see Appendix I).

The Point F V_S tuff profile is the geometric mean computed from the median profiles from the SASW, suspension, and downhole data. The three datasets reach depths of 275 ft, 650 ft, and 450 ft, respectively. The shallow V_S data for the alluvium were separated out of the data as described in Section 6.2.3.4.1. The Point F V_S profile extends to a depth of only 650 ft or the limit of the velocity data (Figure 6.3-173). However, the profile needs to reach a V_S of 6000 ft/sec, the Point A V_S for the seismic design calculations. The Point D/E V_S profile shows a velocity gradient that begins with a V_S of 4000 ft/sec at a depth of about 350 ft reaching 7000 ft/sec V_S at a depth of 520 ft (Figure 6.3-174). Thus the Point D/E V_S profile from depths of 400 to 550 ft was attached to the bottom of the Point F profile (Figure 6.3-175). This extrapolation of the Point F V_S profile is geologically reasonable because the strata below Point F are downdropped about 200 to 300 ft relative to Point D/E due to the displacement across the Exile Hill splay fault. For example, the top of Tpcpul is at an elevation of 3380 ft below Point D/E and 3150 ft below Point F (Figure 227 in BSC 2002a [DIRS 157829]). Thus the profile from Point D/E at 400 ft depth, which is in Tpcpul, was attached to the Point F profile at 650 ft depth, which also is in Tpcpul (Figure 6.3-175).

The Point F V_S profile for the alluvium was calculated based on the geometric mean of the SASW and downhole median profiles (Figure 6.3-176). The suspension data were not used because it was considered unreliable above a depth of 100 ft (Wong and Silva 2003 [DIRS 163201], page 18). Figure 6.3-176 also shows a plot of the Point D/E alluvium V_S profile. The comparison shows similar profiles on either side of the fault, which is not unexpected because the alluvium should be relatively uniform across the site and the Exile Hill splay fault does not displace the alluvium.

Figure 6.3-177 shows the smoothed base case V_S profile alluvium and tuff profiles. As for the D/E profiles, smoothing was done "by eye" (Section 6.2.3.4). The alluvium thicknesses were modeled similar to Point D/E: 35 ft and 110 ft.

Figure 6.3-178 shows the median V_P profiles for the tuff from the downhole and suspension velocity measurements. The profiles are significantly different and thus both profiles were used in the calculations. No extrapolation of the V_P suspension data profile was required since it reached a value of 10,000 ft/sec. The V_P downhole data profile used in the calculations was extrapolated to a V_P of 10,000 ft/sec (Wong and Silva 2004b [DIRS 170444], page 89). The V_P alluvium profile was adopted from only the downhole data since the shallow suspension data was not considered reliable (Figure 6.3-179). The smoothed base case V_P profile for both alluvium and tuff is shown on Figure 6.3-180. The development of the Point F base case velocity profiles is documented in Scientific Notebook SN-M&O-SCI-037-V3 (Wong and Silva 2004b [DIRS 170444], pages 109-115 and supplemental record 3).

The shear modulus reduction and damping curves for the alluvium and tuff used in the Point D/E ground motions were used for Point F. Inputs to the site response model are summarized in Table 6.3-32.

Table 6.3-32. Model Inputs for Development of Seismic Inputs with an Annual Exceedance Frequency of $5x10^{-4}$ for Point F

Model Input	Source
Twelve $5x10^{-4}$ deaggregation earthquake response spectra (three each for the 1-2 Hz and 5-10 Hz $5x10^{-4}$ reference earthquakes; horizontal and vertical components)	Section 6.2.2.5; deaggregation earthquakes have DTN MO0208UNHZ5X10.000 [DIRS 163722]. Weights for combining results for each deaggregation earthquake are provided in Table 6.2-6.
Incidence angles for the deaggregation earthquakes	Section 6.2.2.5.1; Table 6.2-12
Downhole velocity measurements in RF#19, 22, and 29	DTN MO0111DVDWHBSC.001 [DIRS 157296] (subset of data in DTN)
Suspension velocity measurements in RF#17, 19, 22, and 29	DTN MO0204SEPBSWHB.001 [DIRS 158088] (subset of data in DTN)
SASW velocity measurements for Surveys 3, 15, 16, 19, 24, 30, and 36	DTN MO0110SASWWHBS.000 [DIRS 157969] (subset of data in DTN)
60 randomized sets of shear modulus reduction and damping curves for each of the two tuff and alluvium base case curves (four combinations). Each combination is run for each of the three modeling cases.	Section 6.2.4.5; base case curves have DTN MO0403SDIAWHBC.003 [DIRS 170434]
Tuff and alluvium density	Section 6.2.3.7

Software programs used to model this case are identical to those listed in Section 6.3.1.1 with the substitution of RANPAR V2.1 (Software Tracking Number 10486-2.1-00) (Pacific Engineering and Analysis 2003d [DIRS 170442]). Details of the modeling and analysis are documented in Scientific Notebook SN-M&O-SCI-037-V2 (Wong and Silva 2004a [DIRS 170443], pages 129-130 and 138-139, and supplemental records 125 and 128). Microsoft Excel 2000 was used to compute the ratio of Point F to Point D/E response spectra (see Appendix I).

Calculations similar to Point D/E (Section 6.3.1.3.2) were performed for Point F except only one wave type, HSHH was considered since it was the controlling wave type and the preliminary Point F ground motions are only being computed for comparison. Magnitude-weighted mean SAFs for 1-2 Hz and 5-10 Hz DEA were computed and applied to the envelope of the reference earthquake spectra and UHS for Point A. The final spectrum is an envelope of each set of base case nonlinear dynamic material properties. The horizontal and vertical response spectra for Point F at $5x10^{-4}$ have been submitted to TDMS and have DTN MO0410SDSEHFSF.002 [DIRS 172218]. Figure 6.3-181 shows a comparison of the preliminary Point F horizontal spectrum with the Point D/E seismic design response spectrum. The latter exceeds the Point F horizontal spectrum at nearly all frequencies. The ratio of the two spectra are shown on Figure 6.3-182 where it indicates that the maximum spectral ratio of Point F/Point D/E is slightly above 1.0 at 1 Hz.

The vertical spectra comparison is shown on Figure 6.3-183 and the ratio is shown on Figure 6.3-184. The Point F vertical spectrum exceeds the Point D/E vertical spectrum over a broad range of frequencies but by less than 15% (Figure 6.3-184). Planned SSCs at the Surface Facilities Area at Yucca Mountain have natural frequencies in the range of 8 to 9 Hz (Section 8). The small exceedance of less than 5% at Point F at these frequencies should have negligible impact on the design of the surface facilities.

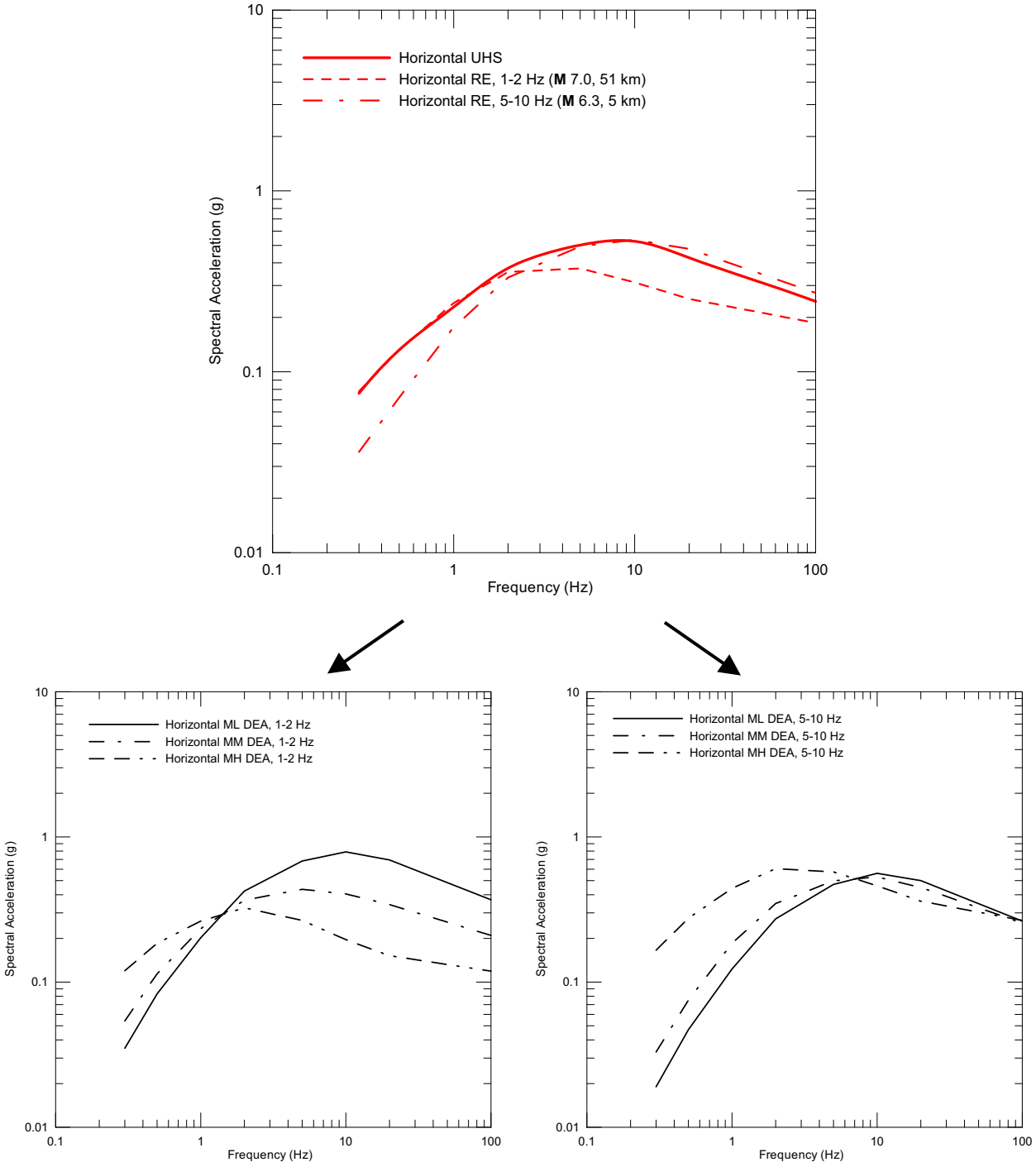

Note: This figure illustrates the development of the horizontal reference earthquake (RE) and deggregation earthquake (DEA) spectra from the UHS horizontal spectra at 5×10^{-4} annual exceedance frequency (See Section 6.2.2.4 and 6.2.2.5). DEA spectra are used as control motions for site-response modeling. (For information only.)

Figure 6.3-1a. Site Response Methodology: Point A Control Motions

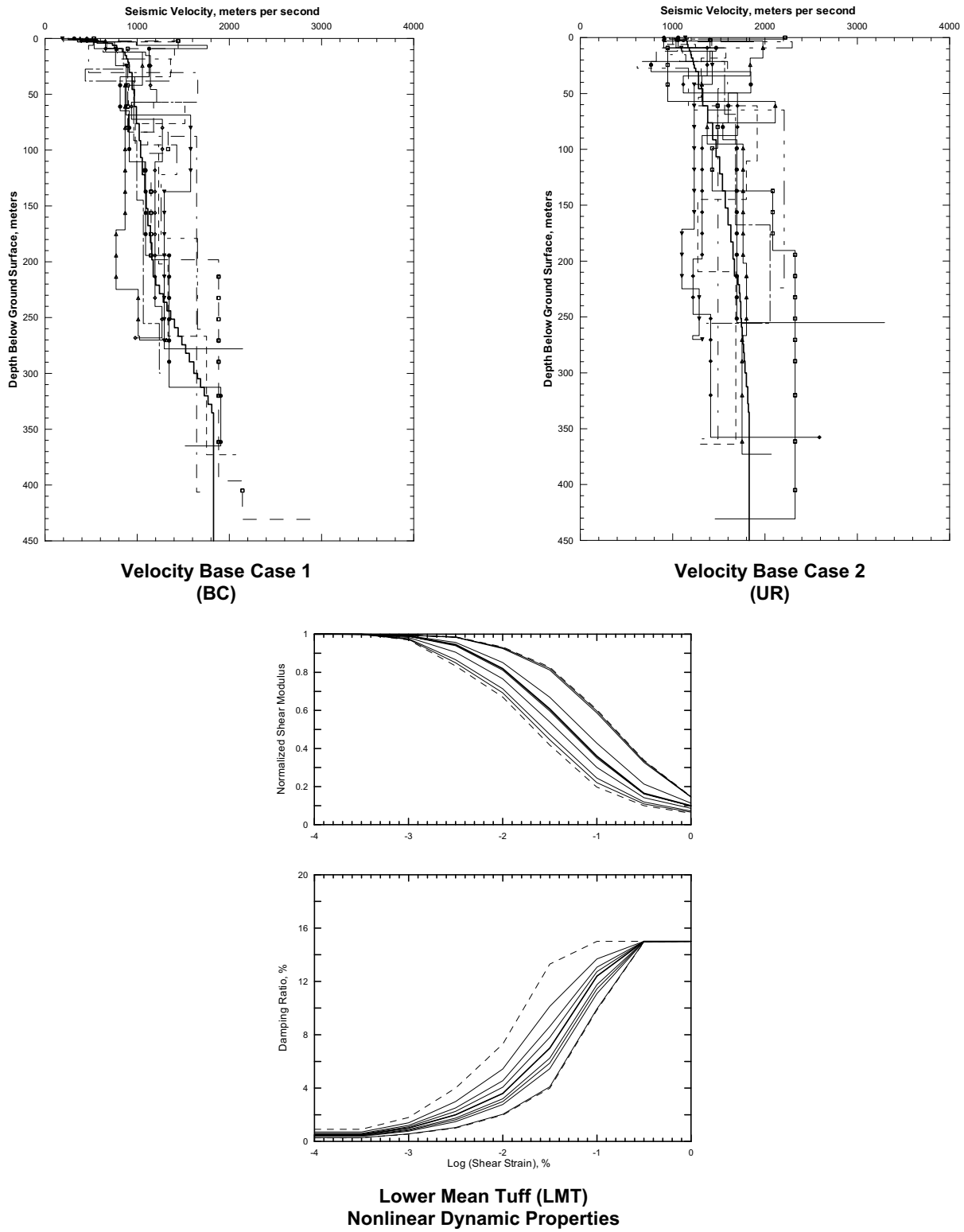

Figure 6.3-1b. Site Response Methodology: Examples of Repository Block V_S Profile and Nonlinear Dynamic Material Properties Randomizations (For information only.)

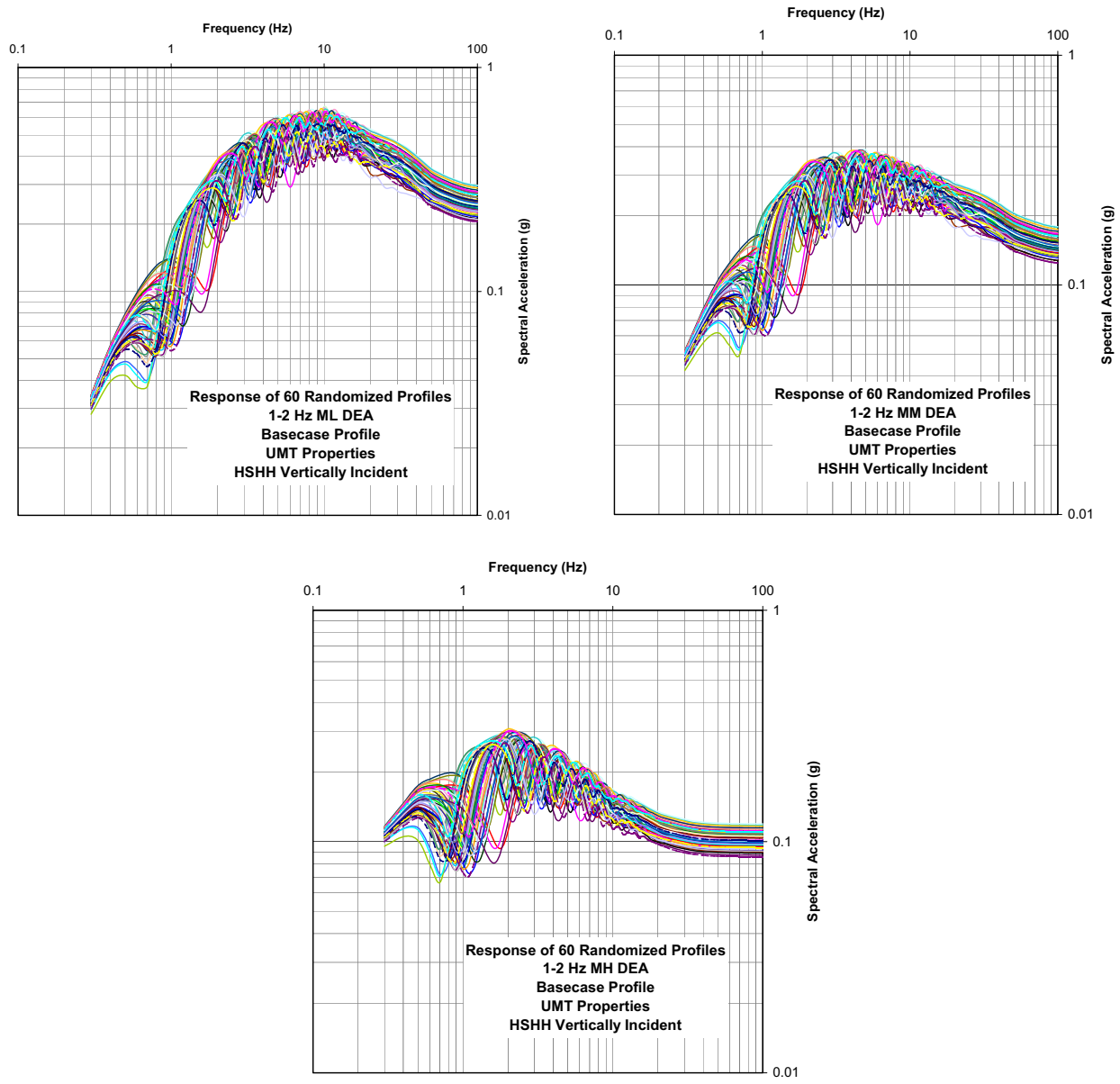

NOTE: Convolution modeling is performed using the six horizontal DEA control motions (1-2 Hz and 5-10 Hz; ML, MM, and MH) for sets of 60 randomized velocity profiles and nonlinear dynamic curves. These analyses are repeated for each combination of basecase properties (i.e., two basecase velocity profiles and two basecase nonlinear dynamic curves). This figure illustrates the response of the randomized profiles for velocity base case BC profile and UMT properties to the 1-2 Hz horizontal DEAs.

Figure 6.3-1c. Site Response Methodology: Response of Simulated Profiles to DEA Control Motion (For information only.)

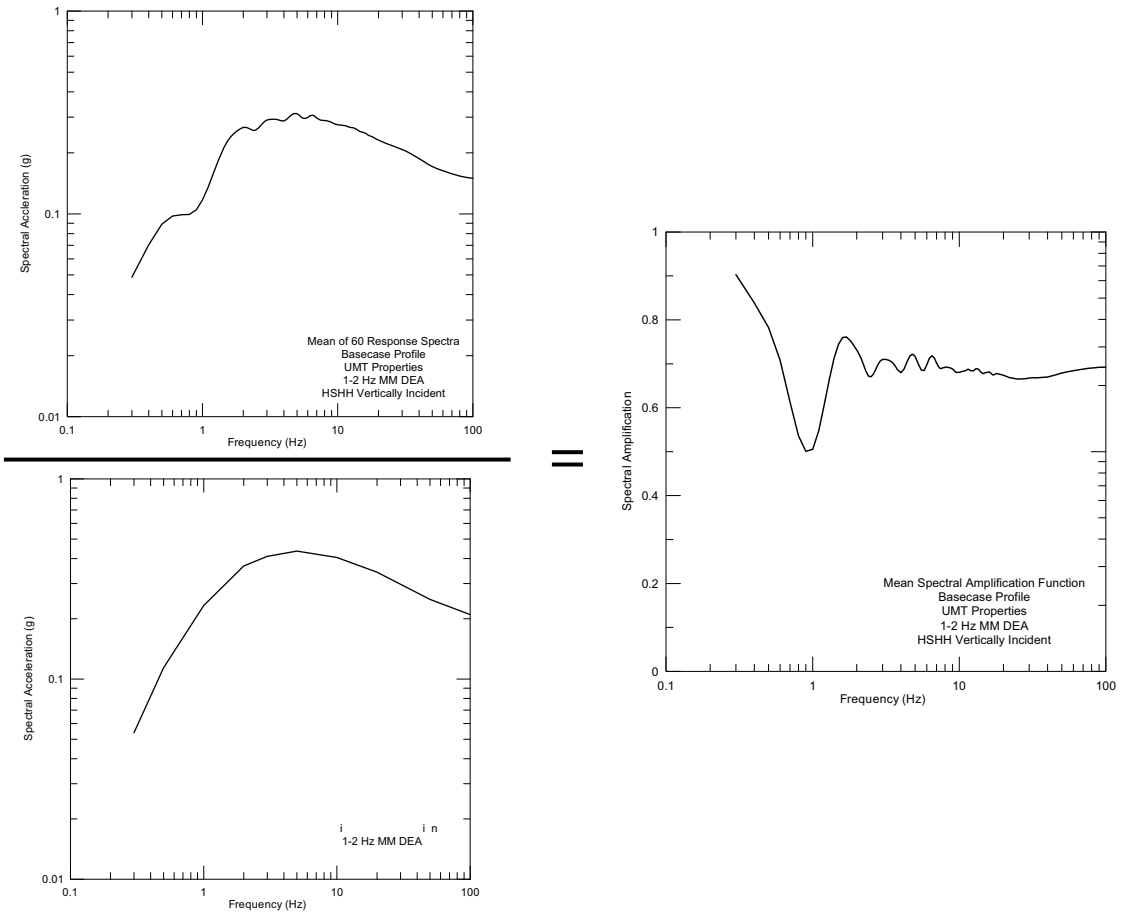

NOTE: Spectral Amplification Functions (SAFs) are computed for all convolutions.

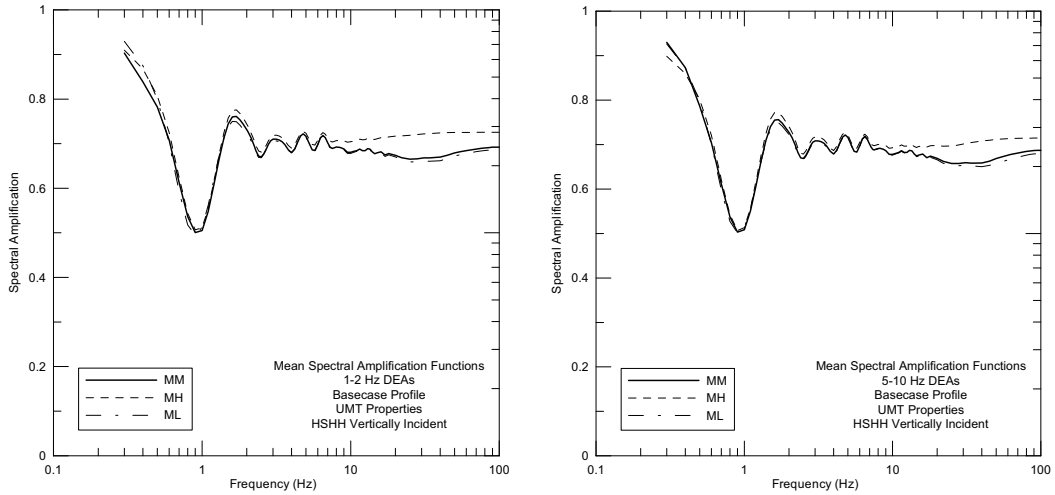

NOTE: Mean SAFs are computed for each set of 60 res ponses. Magnitude dependency is reflected in the differences between SAFs for ML, MM, and MH control motions.

Figure 6.3-1d. Site Response Methodology: Computation of Mean SAFs (For information only.)

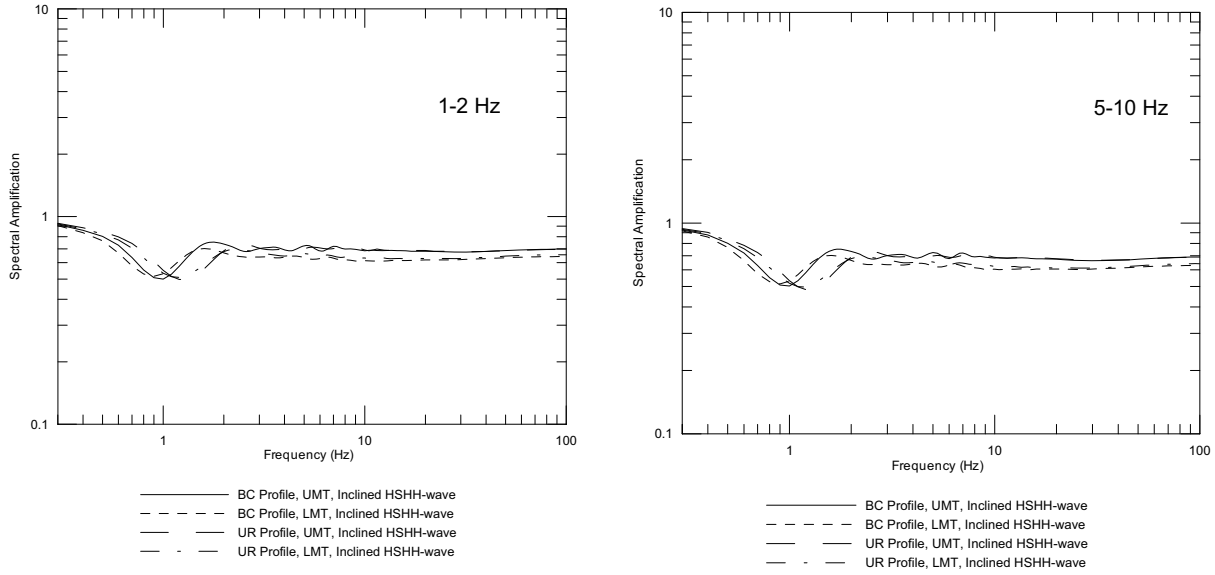

NOTE: Envelope the 1-2 Hz and 5-10 Hz magnitude- weighted mean SAFs for each set of base case site properties and control motion wavetype. Apply resulting SAFs to envelope of 1-2 Hz and 5-10 Hz REs to obtain site-specific response spectra for Point B.

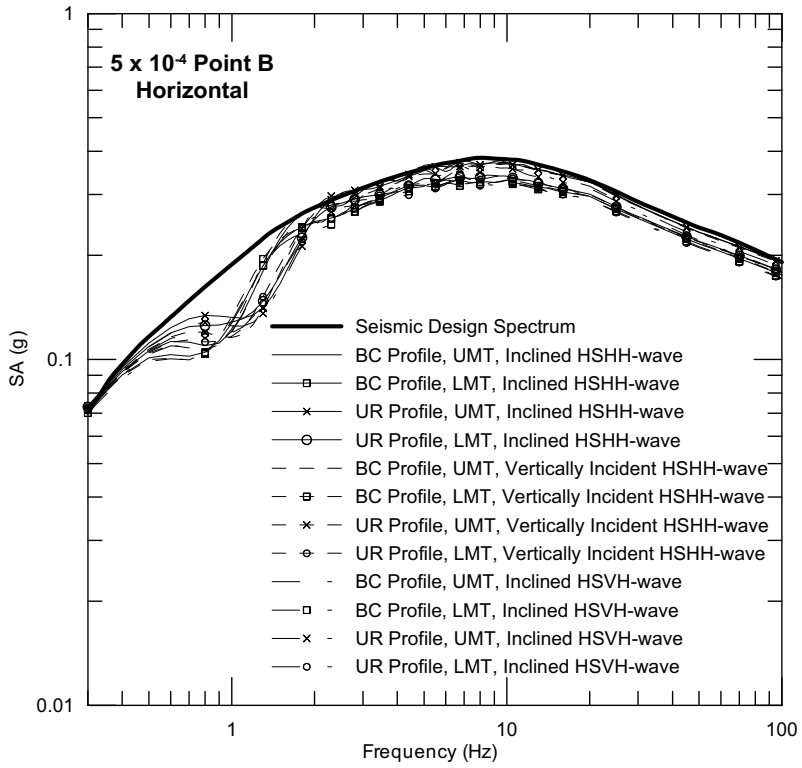

NOTE: Envelope site-specific spectra for all site properties and control motion wavetypes to obtain the seismic design response spectrum.

Figure 6.3-1e. Site Response Methodology: Magnitude-Weighted Mean SAFs, Site-Specific Spectra, and Seismic Design Response Spectrum (Envelope) at an Annual Exceedance Frequency of 5×10^{-4}, Horizontal Component (For information only.)

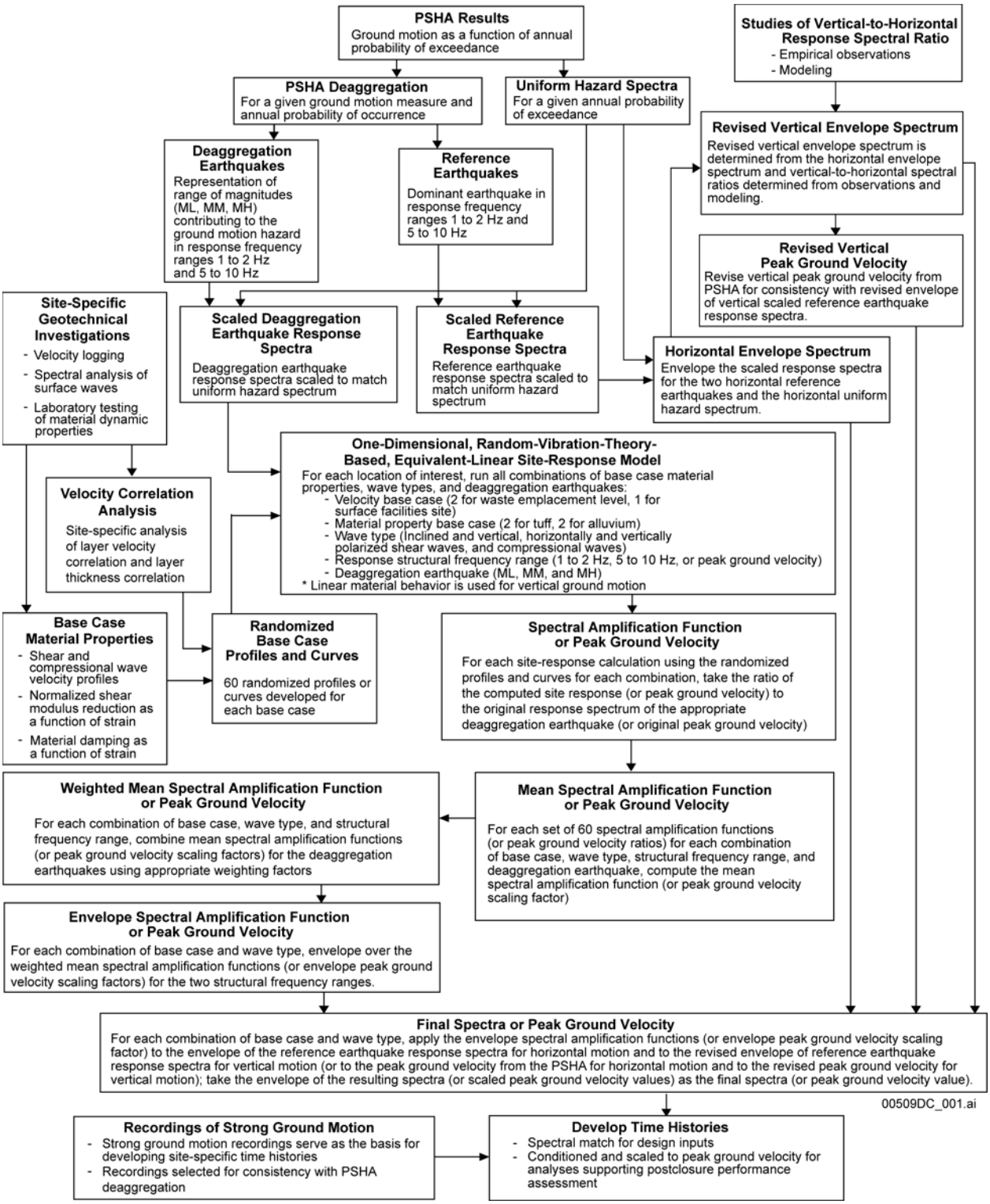

Figure 6.3-2. Site Response Methodology Flow Chart

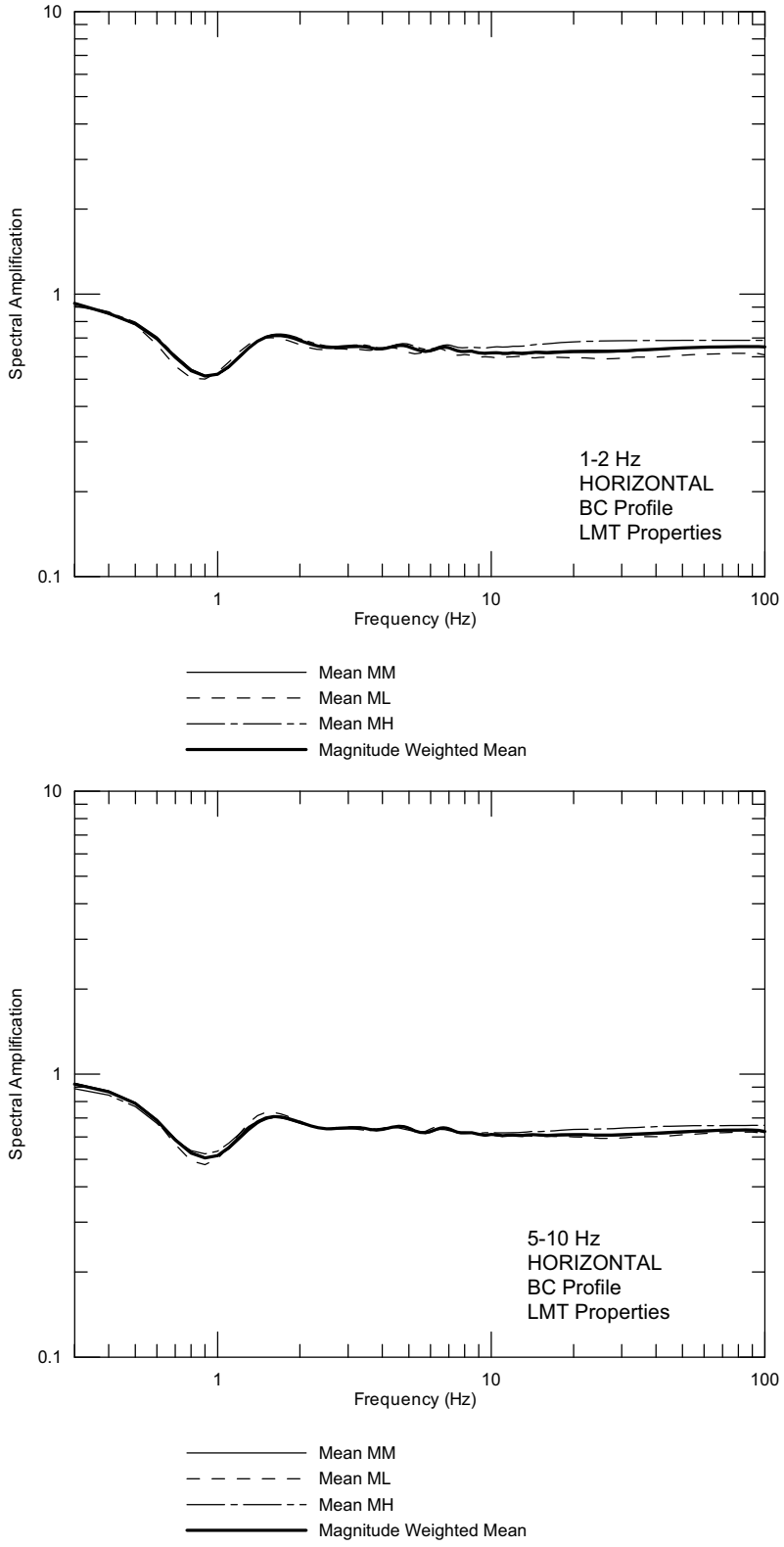

Source: Wong and Silva 2004a [DIRS 170443], Supplemental Record 111

Figure 6.3-3. Representative Point B Mean SAFs at an Annual Exceedance Frequency of 10^{-3}

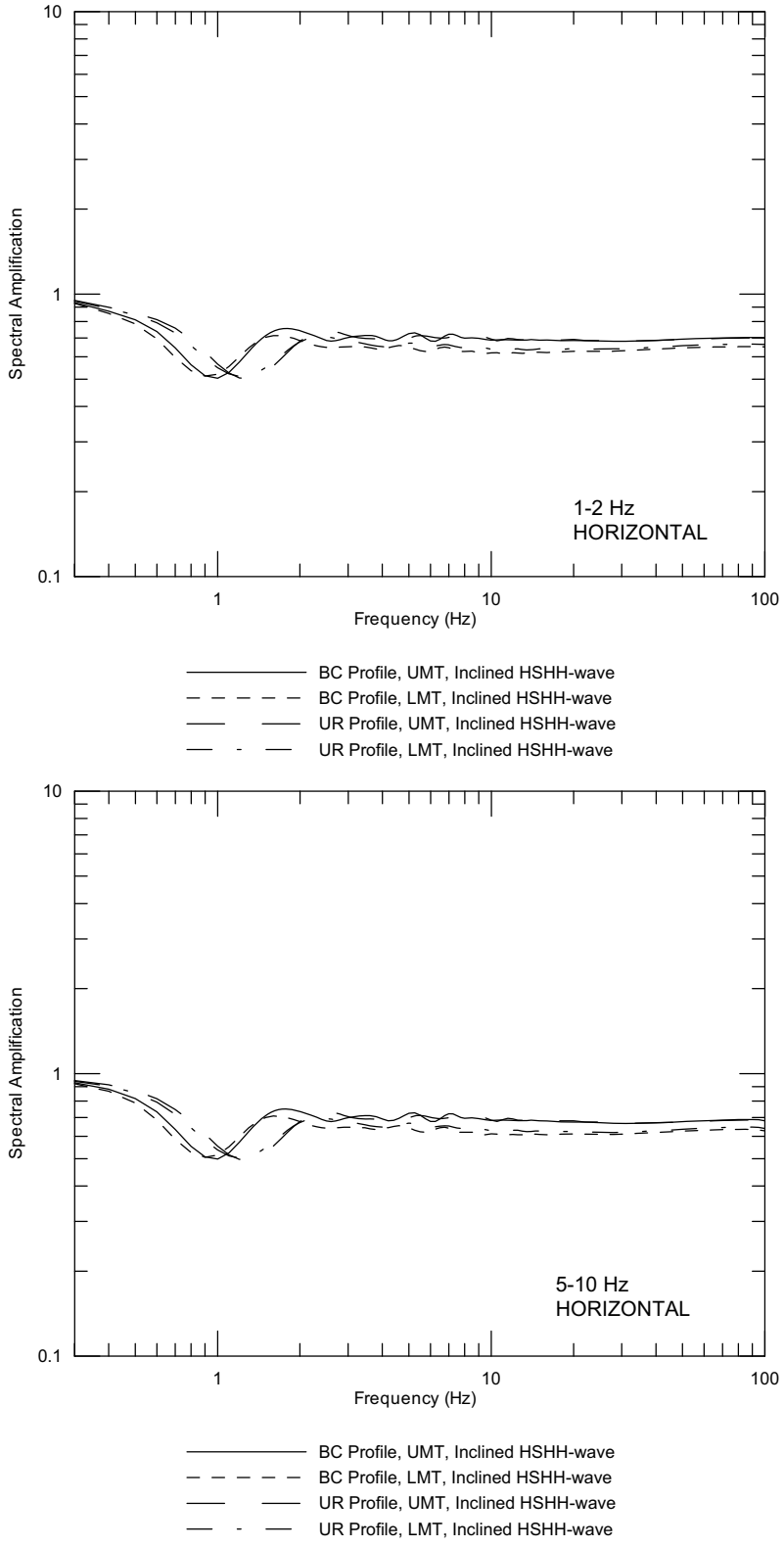

Source: Wong and Silva 2004a [DIRS 170443], Supplemental Record 111

Figure 6.3-4. Point B Horizontal Magnitude-Weighted Mean SAF at an Annual Exceedance Frequency of 10^{-3}

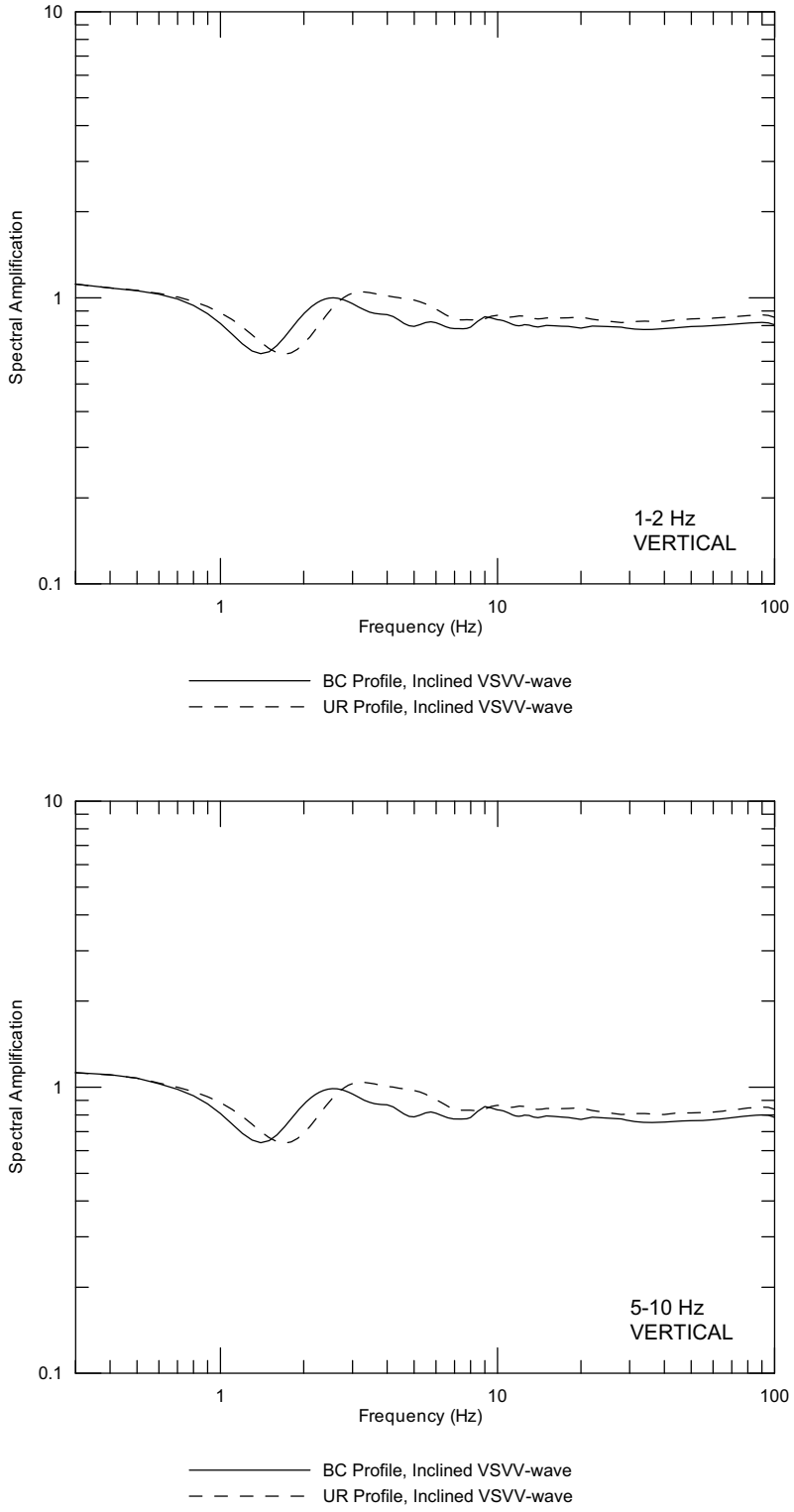

Source: Wong and Silva 2004a [DIRS 170443], Supplemental Record 111

Figure 6.3-5. Point B Vertical Magnitude-Weighted Mean SAF at an Annual Exceedance Frequency of 10^{-3}

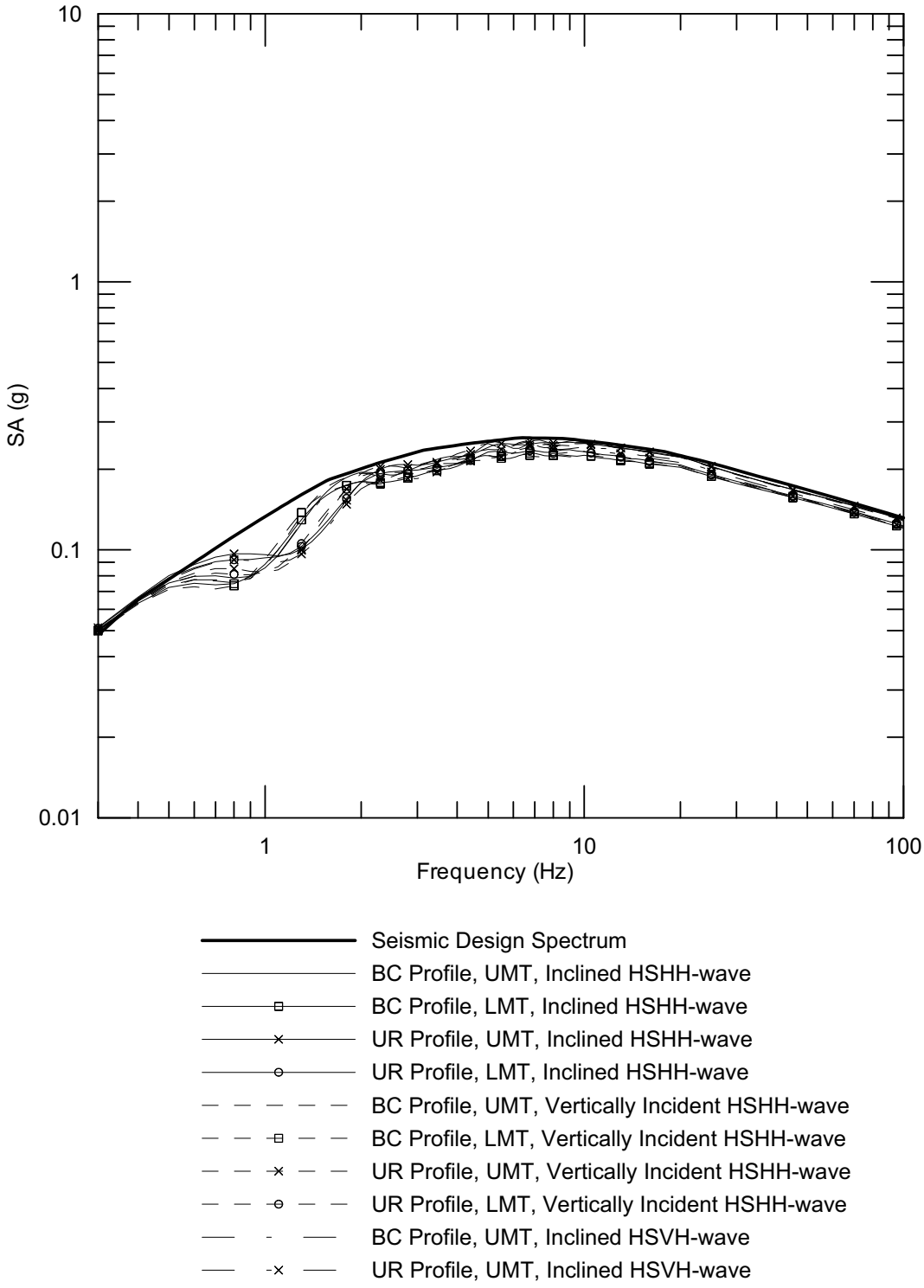

DTN: MO0405SDSTPNTB.001 [DIRS 169851]

Source: Wong and Silva 2004a [DIRS 170443], Supplemental Record 111

Figure 6.3-6. Point B Horizontal Site-Specific Spectra and Seismic Design Response Spectrum (5%-Damped) at an Annual Exceedance Frequency of 10^{-3}

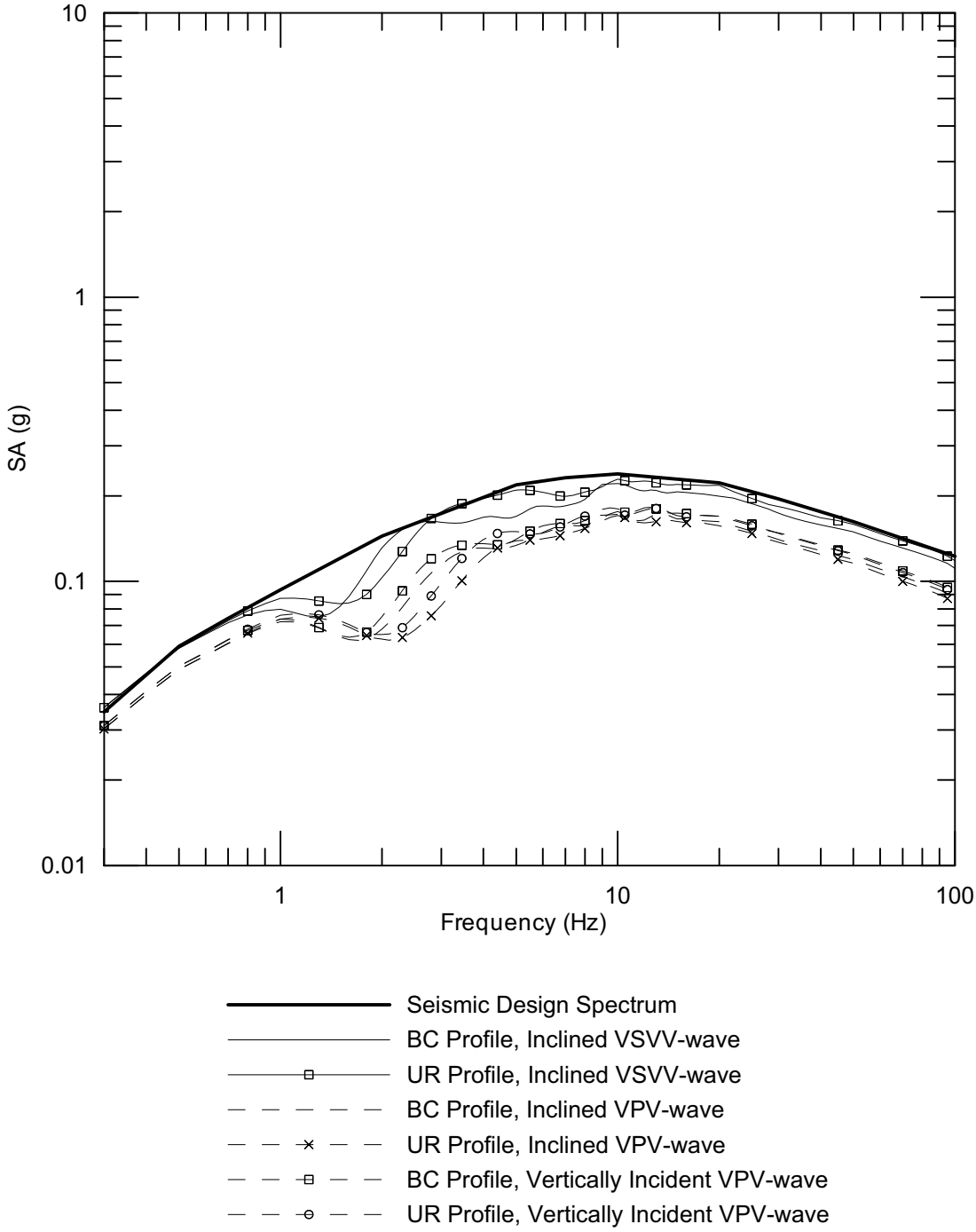

DTN: MO0405SDSTPNTB.001 [DIRS 169851]

Source: Wong and Silva 2004a [DIRS 170443], Supplemental Record 111

Figure 6.3-7. Point B Vertical Site-Specific Spectra and Seismic Design Response Spectrum (5%-Damped) at an Annual Exceedance Frequency of 10^{-3}

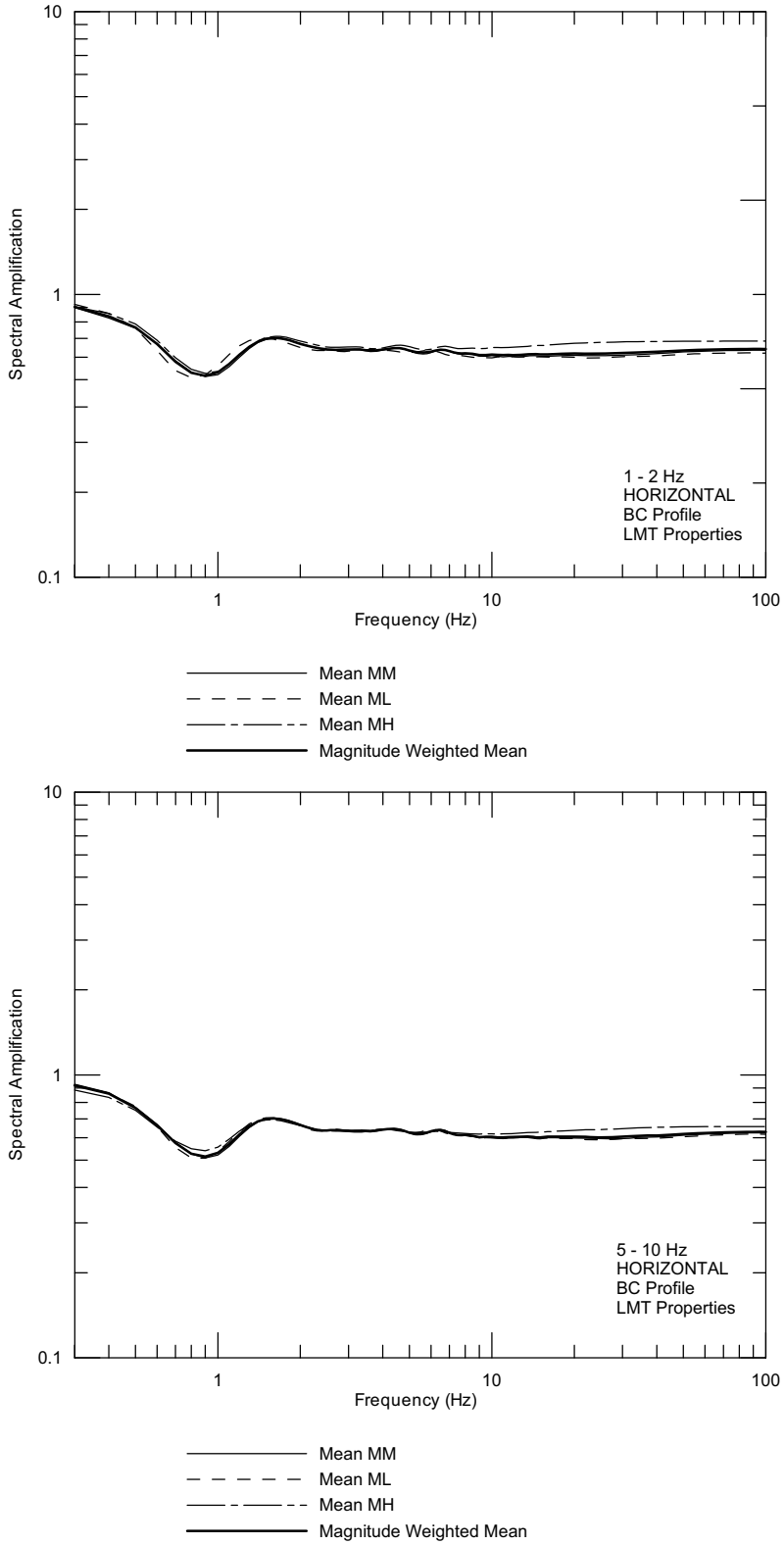

Source: Wong and Silva 2004a [DIRS 170443], Supplemental Record 61

Figure 6.3-8. Representative Point B Mean SAFs at an Annual Exceedance Frequency of 5×10^{-4}

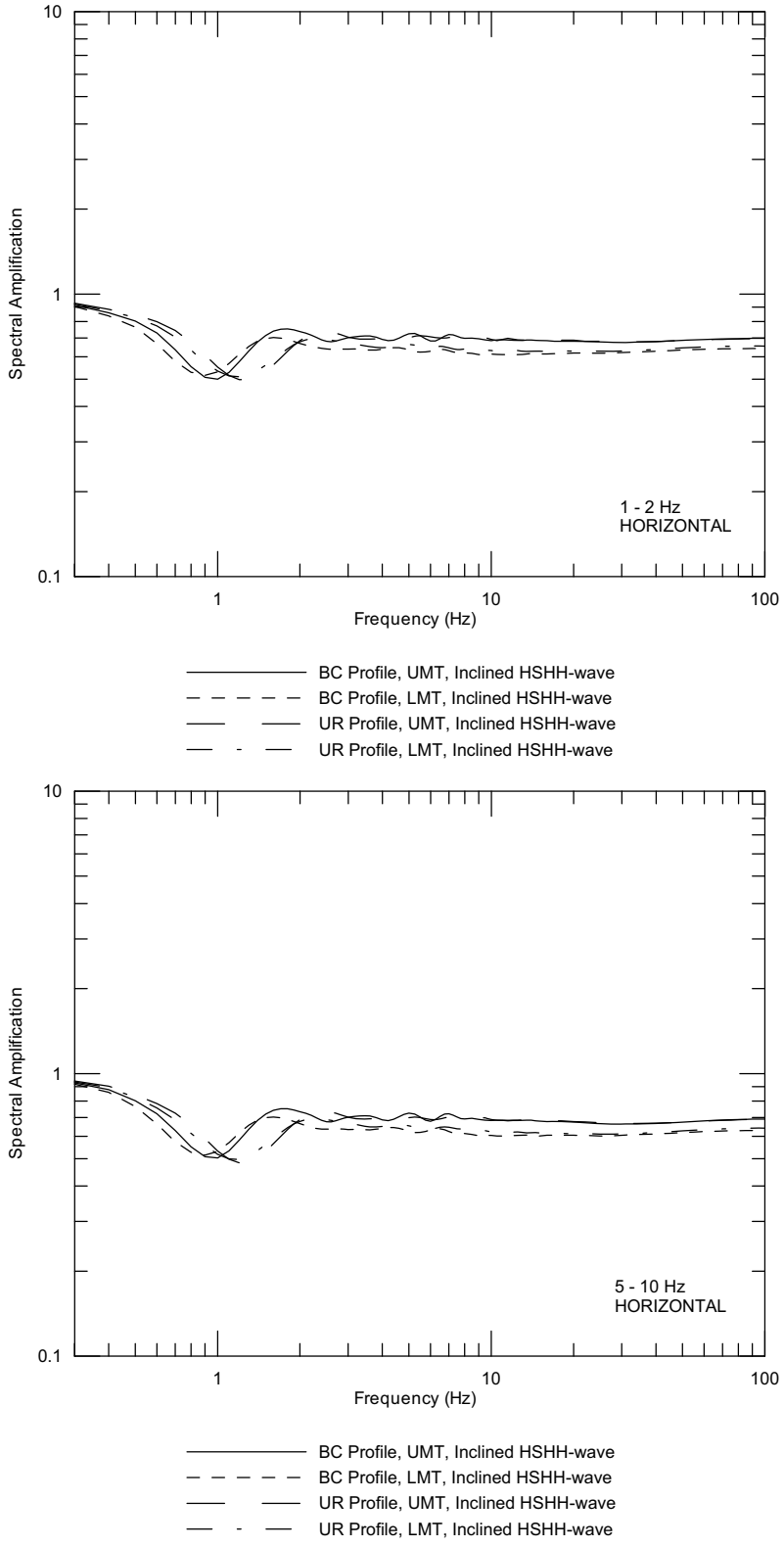

Source: Wong and Silva 2004a [DIRS 170443], Supplemental Record 61

Figure 6.3-9. Point B Horizontal Magnitude-Weighted Mean SAF at an Annual Exceedance Frequency of 5×10^{-4}

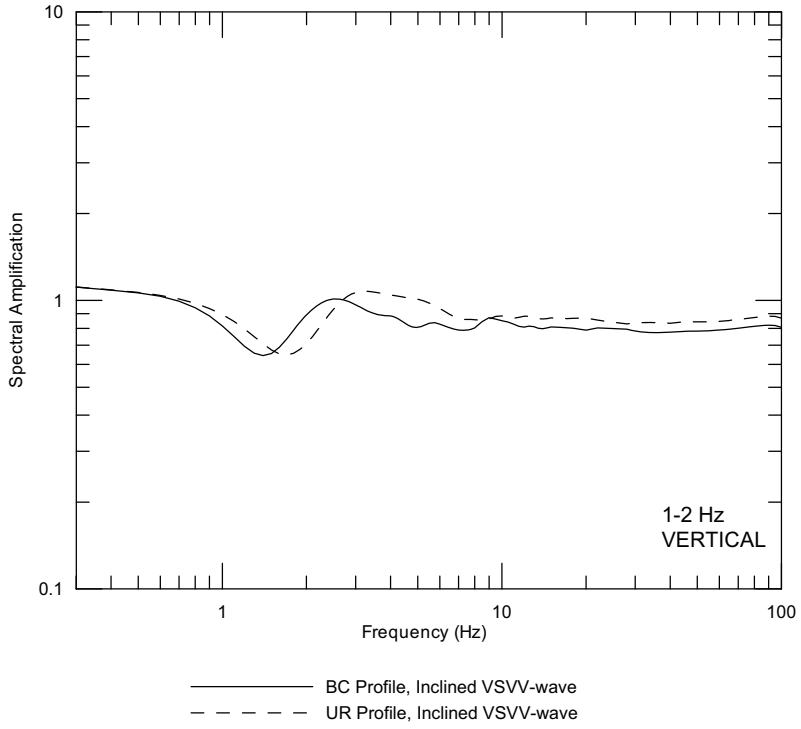

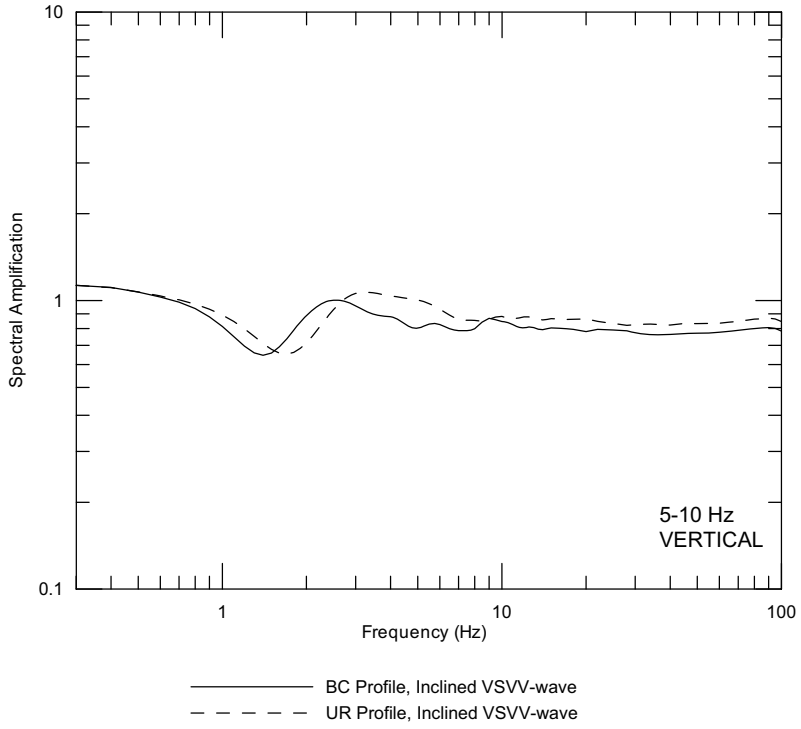

Source: Wong and Silva 2004a [DIRS 170443], Supplemental Record 61

Figure 6.3-10. Point B Vertical Magnitude-Weighted Mean SAF at an Annual Exceedance Frequency of 5×10^{-4}

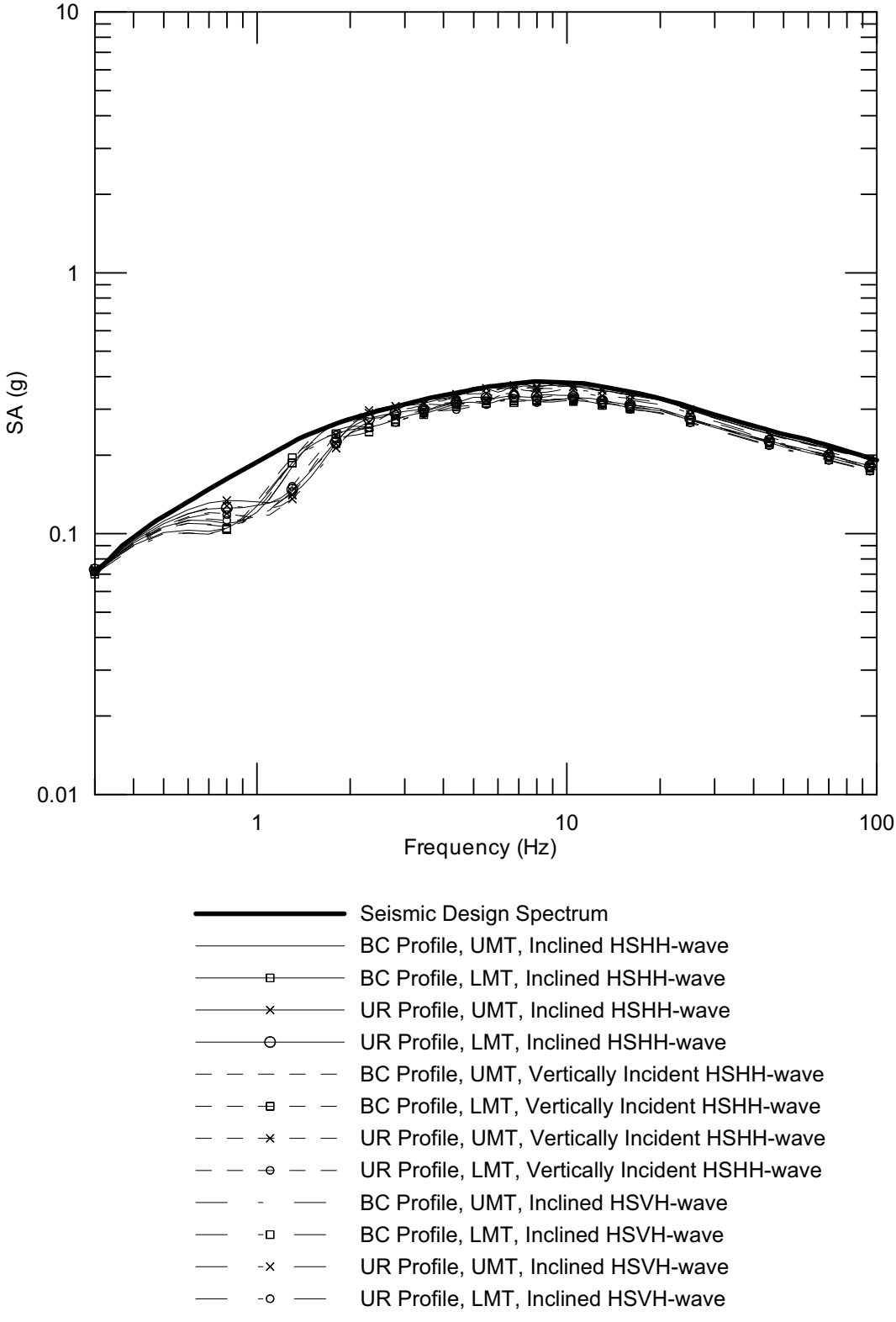

DTN: MO0407SDARS104.001 [DIRS 170683]

Source: Wong and Silva 2004a [DIRS 170443], Supplemental Record 61

Figure 6.3-11. Point B Horizontal Site-Specific Spectra and Seismic Design Response Spectrum (5%-Damped) at an Annual Exceedance Frequency of 5×10^{-4}

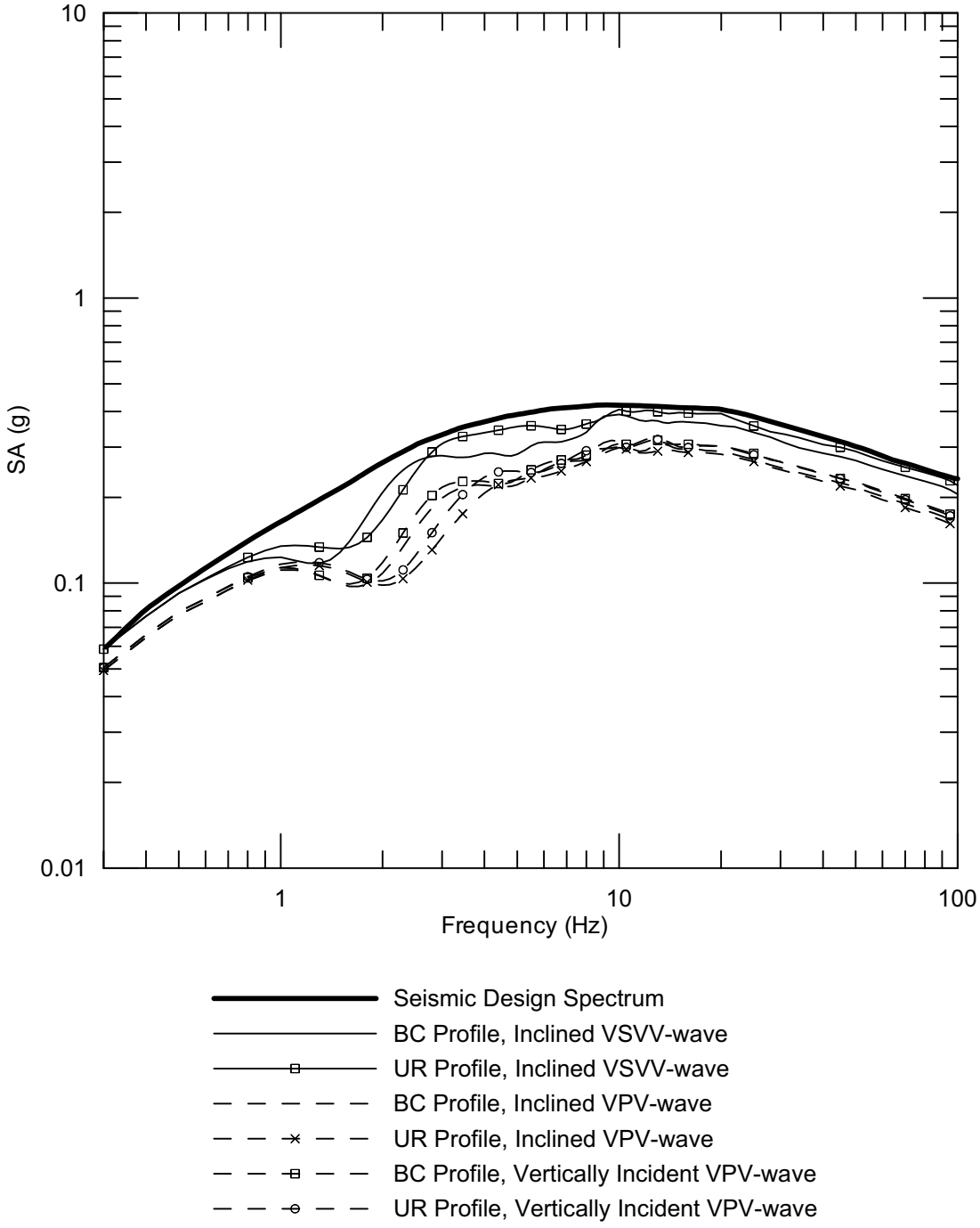

DTN: MO0407SDARS104.001 [DIRS 170683]

Source: Wong and Silva 2004a [DIRS 170443], Supplemental Record 61

Figure 6.3-12. Point B Vertical Site-Specific Spectra and Seismic Design Response Spectrum (5%-Damped) at an Annual Exceedance Frequency of 5×10^{-4}

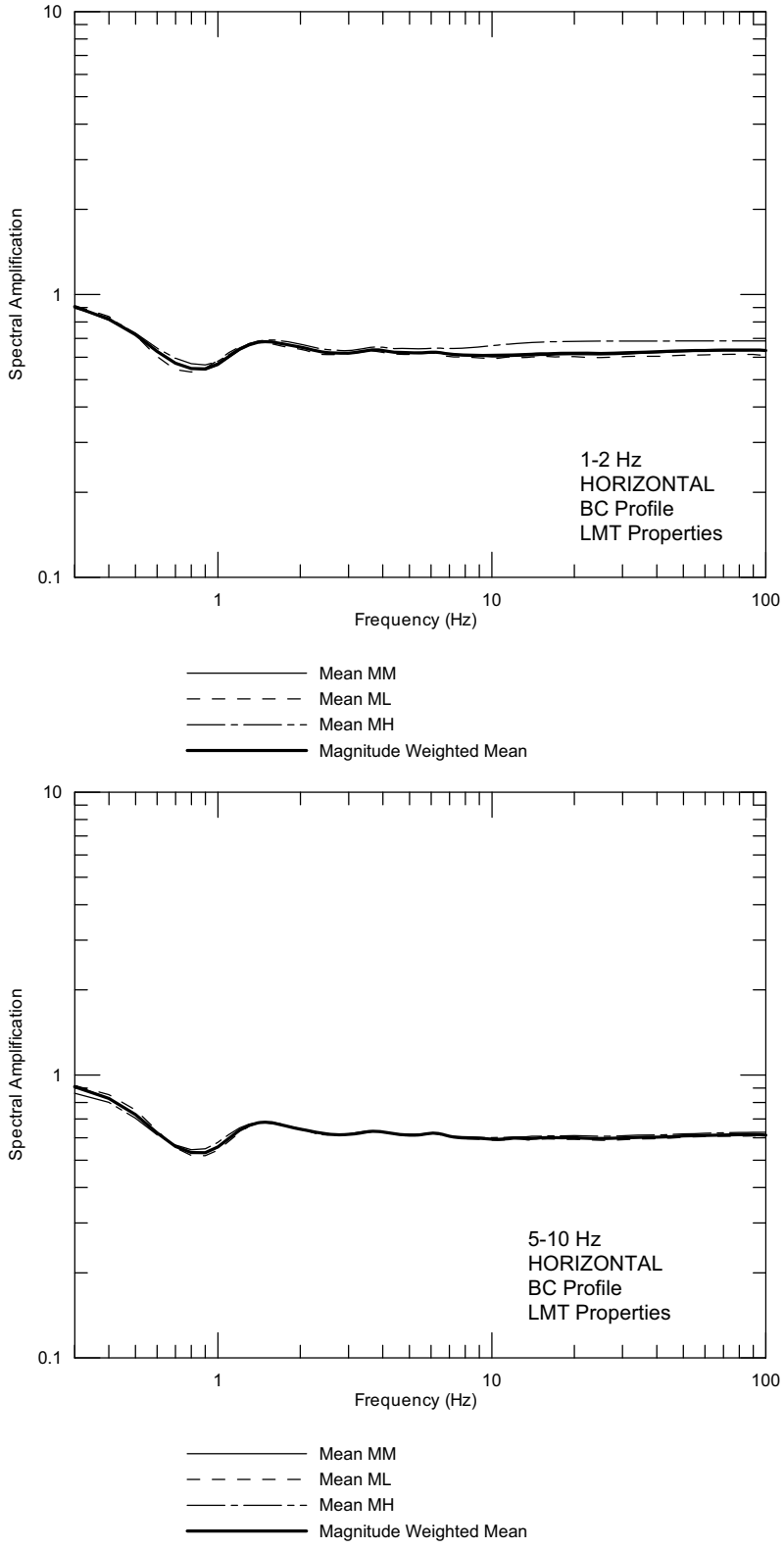

Source: Wong and Silva 2004a [DIRS 170443], Supplemental Record 82

Figure 6.3-13. Representative Point B Mean SAFs at an Annual Exceedance Frequency of 10^{-4}

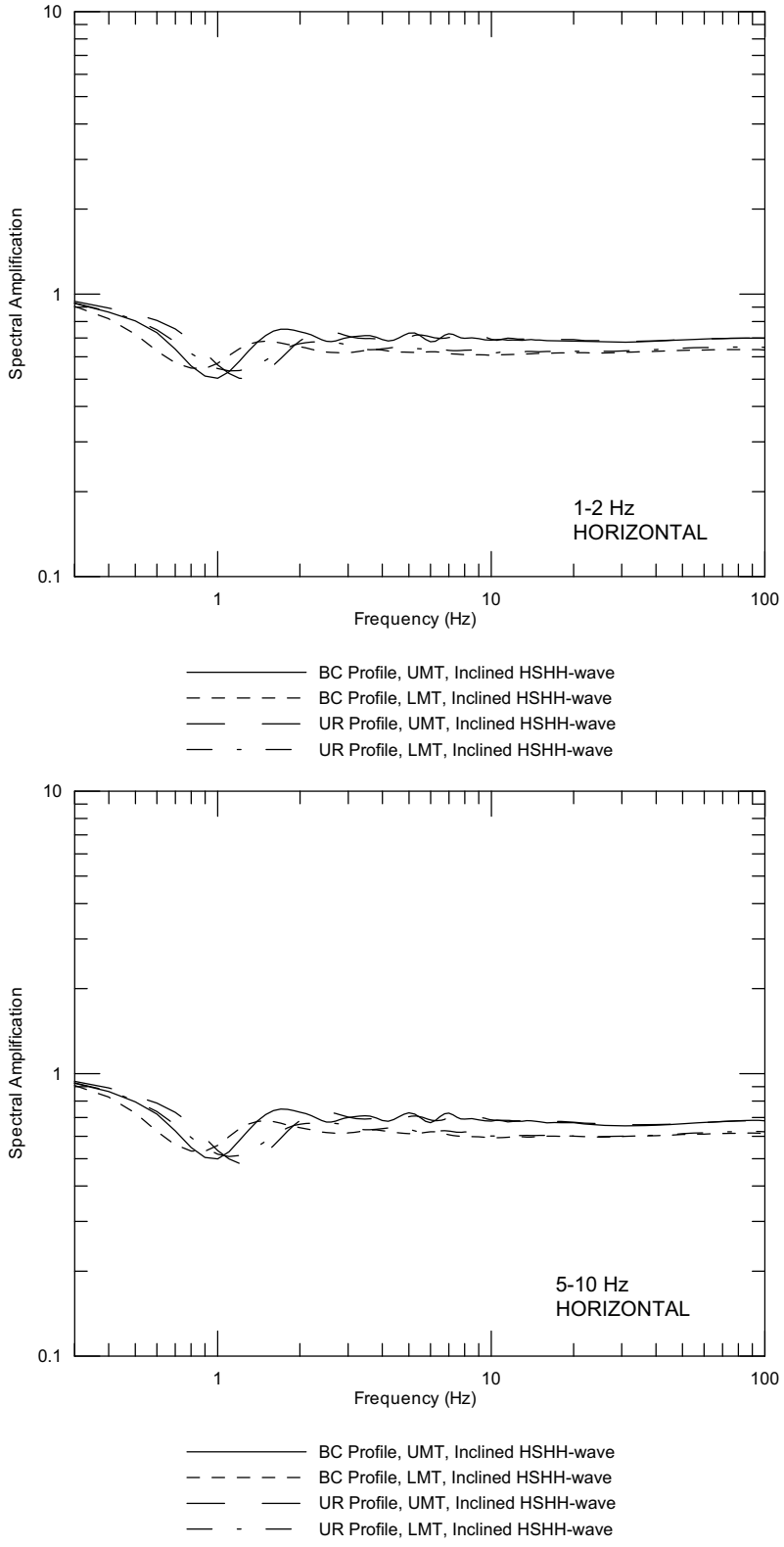

Source: Wong and Silva 2004a [DIRS 170443], Supplemental Record 82

Figure 6.3-14. Point B Horizontal Magnitude-Weighted Mean SAF at an Annual Exceedance Frequency of 10^{-4}

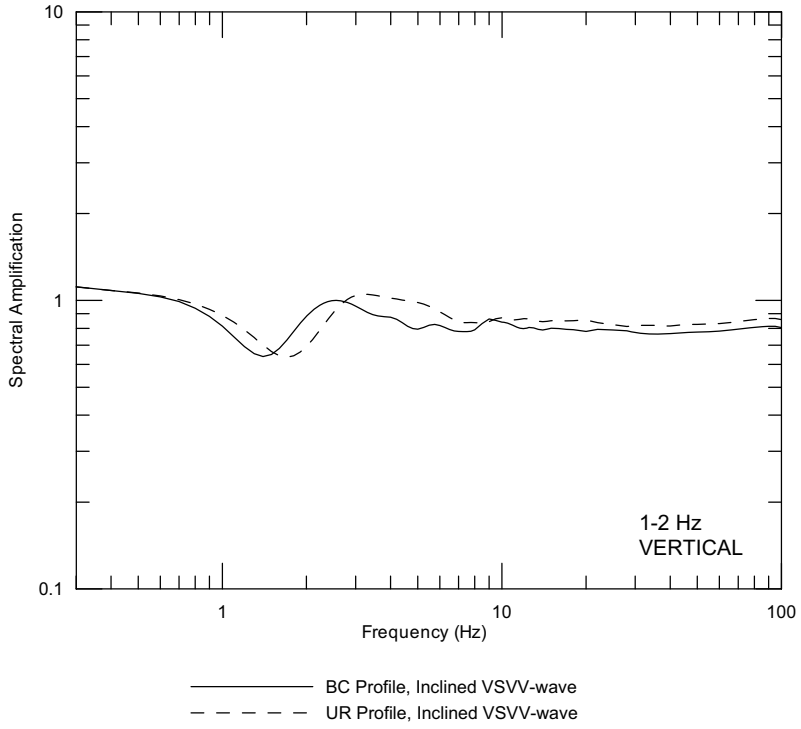

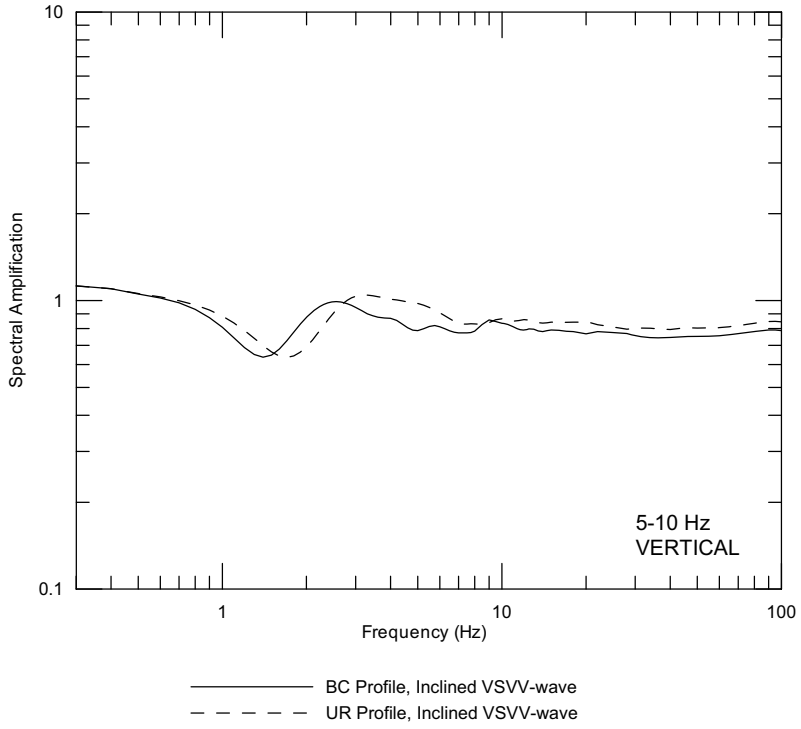

Source: Wong and Silva 2004a [DIRS 170443], Supplemental Record 82

Figure 6.3-15. Point B Vertical Magnitude-Weighted Mean SAF at an Annual Exceedance Frequency of 10^{-4}

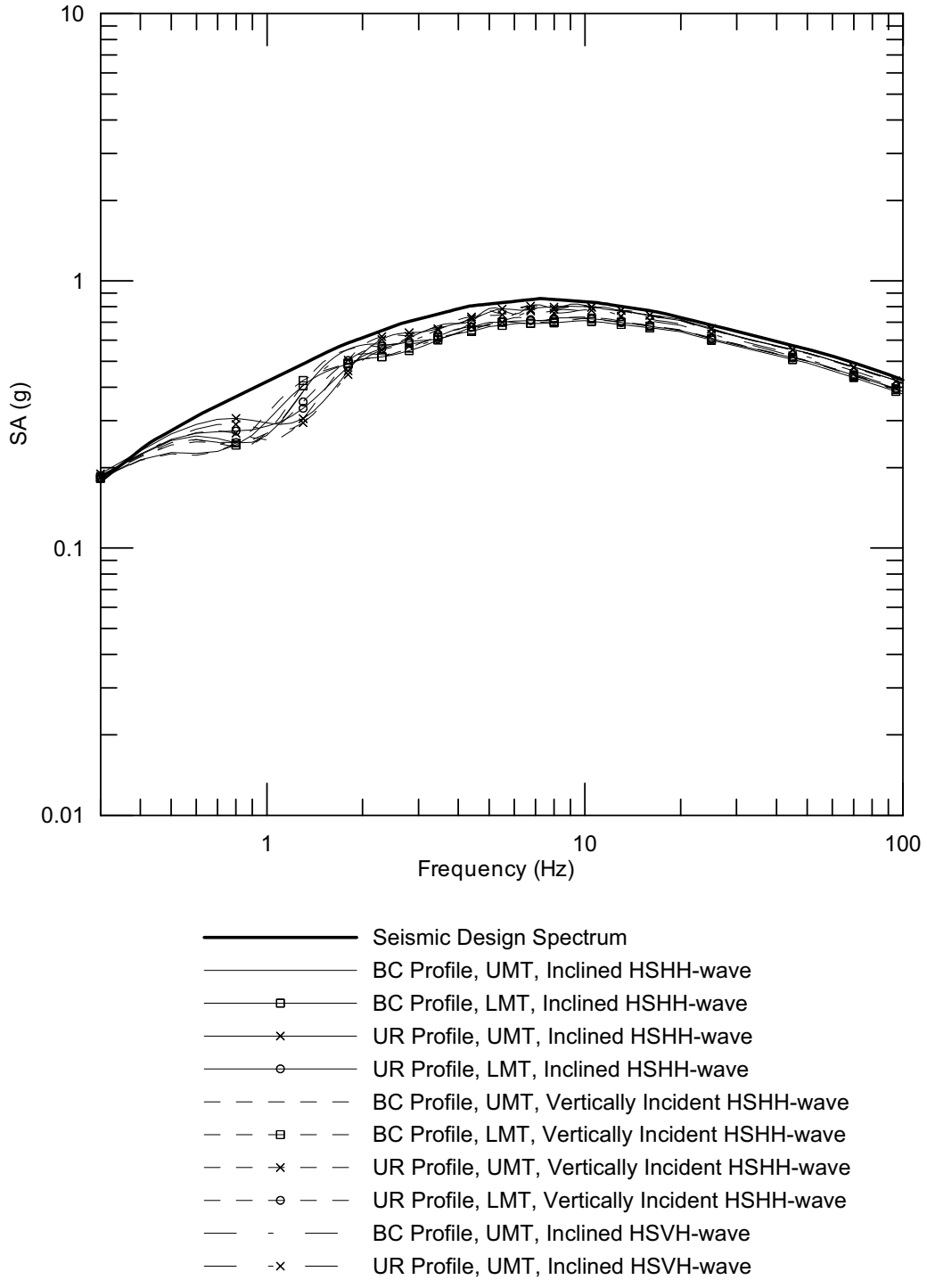

DTN: MO0306SDSAVDTH.000 [DIRS 164033]

Source: Wong and Silva 2004a [DIRS 170443], Supplemental Record 82

Figure 6.3-16. Point B Horizontal Site-Specific Spectra and Seismic Design Response Spectrum (5%-Damped) at an Annual Exceedance Frequency of 10^{-4}

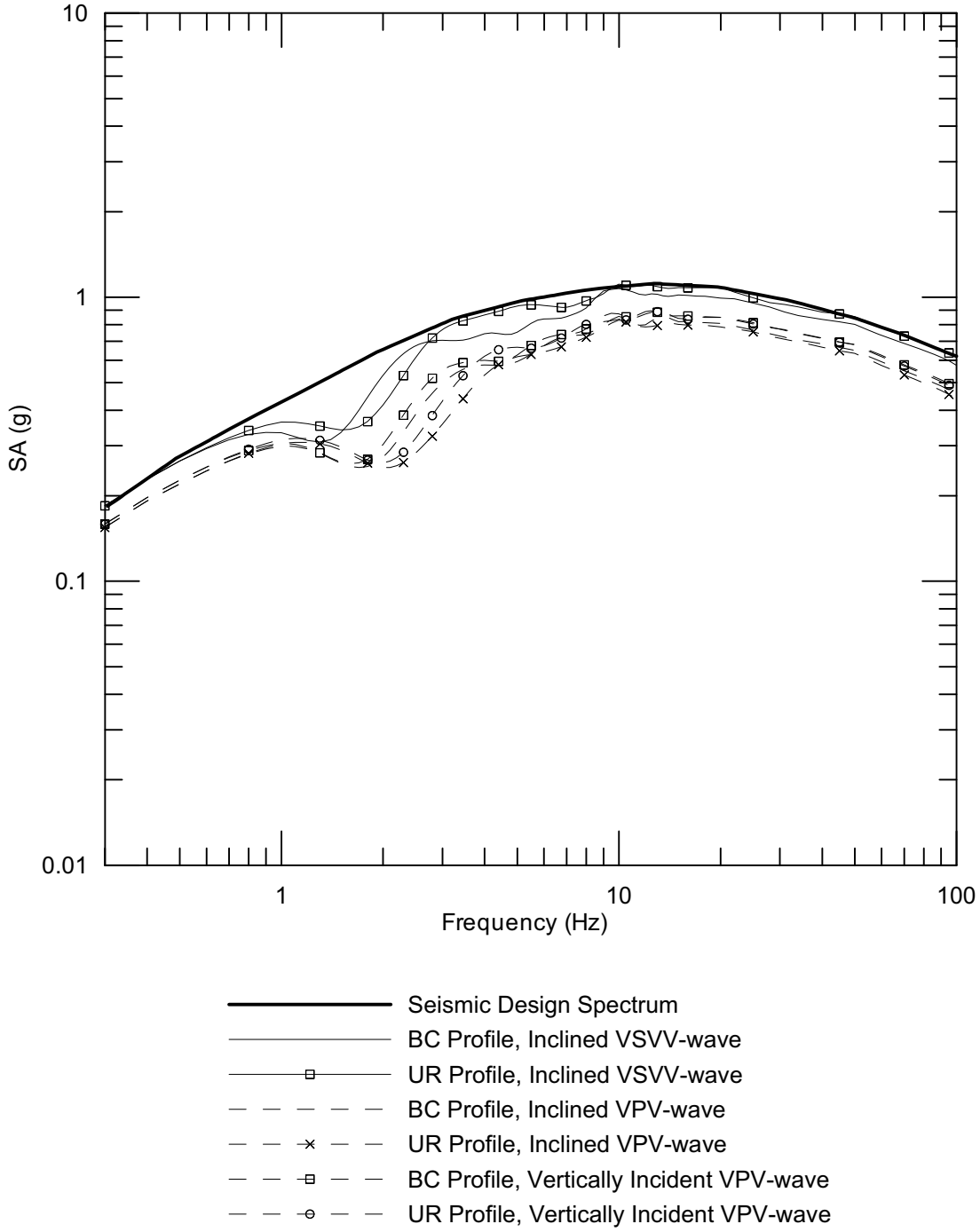

DTN: MO0306SDSAVDTH.000 [DIRS 164033]

Source: Wong and Silva 2004a [DIRS 170443], Supplemental Record 82

Figure 6.3-17. Point B Vertical Site-Specific Spectra and Seismic Design Response Spectrum (5%-Damped) at an Annual Exceedance Frequency of 10^{-4}

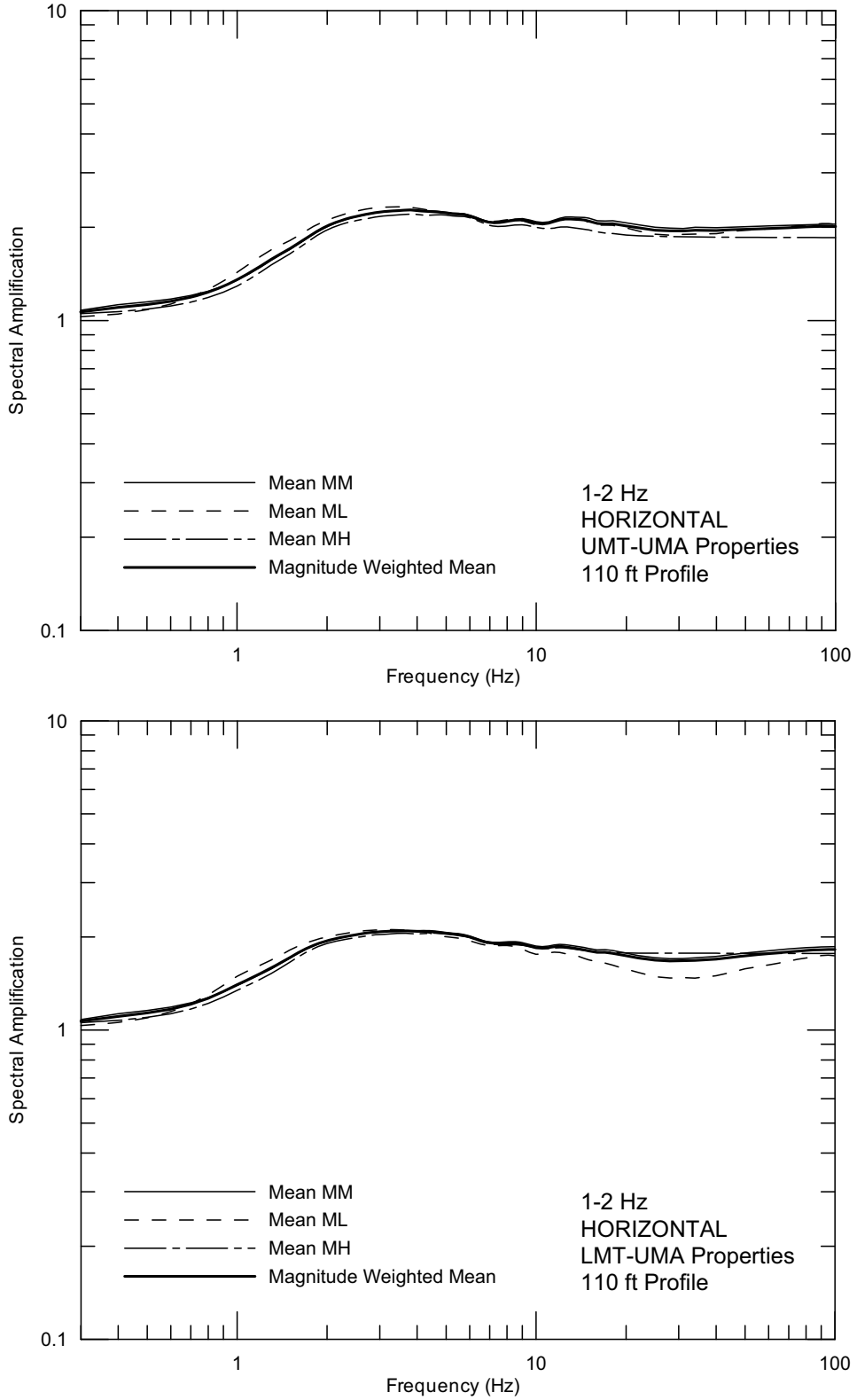

Source: Wong and Silva 2004a [DIRS 170443], Supplemental Record 108

Figure 6.3-18. Representative Point D 1-2 Hz Mean SAFs at an Annual Exceedance Frequency of 10^{-3}, Upper Mean Alluvium Curve, 110 ft Alluvium

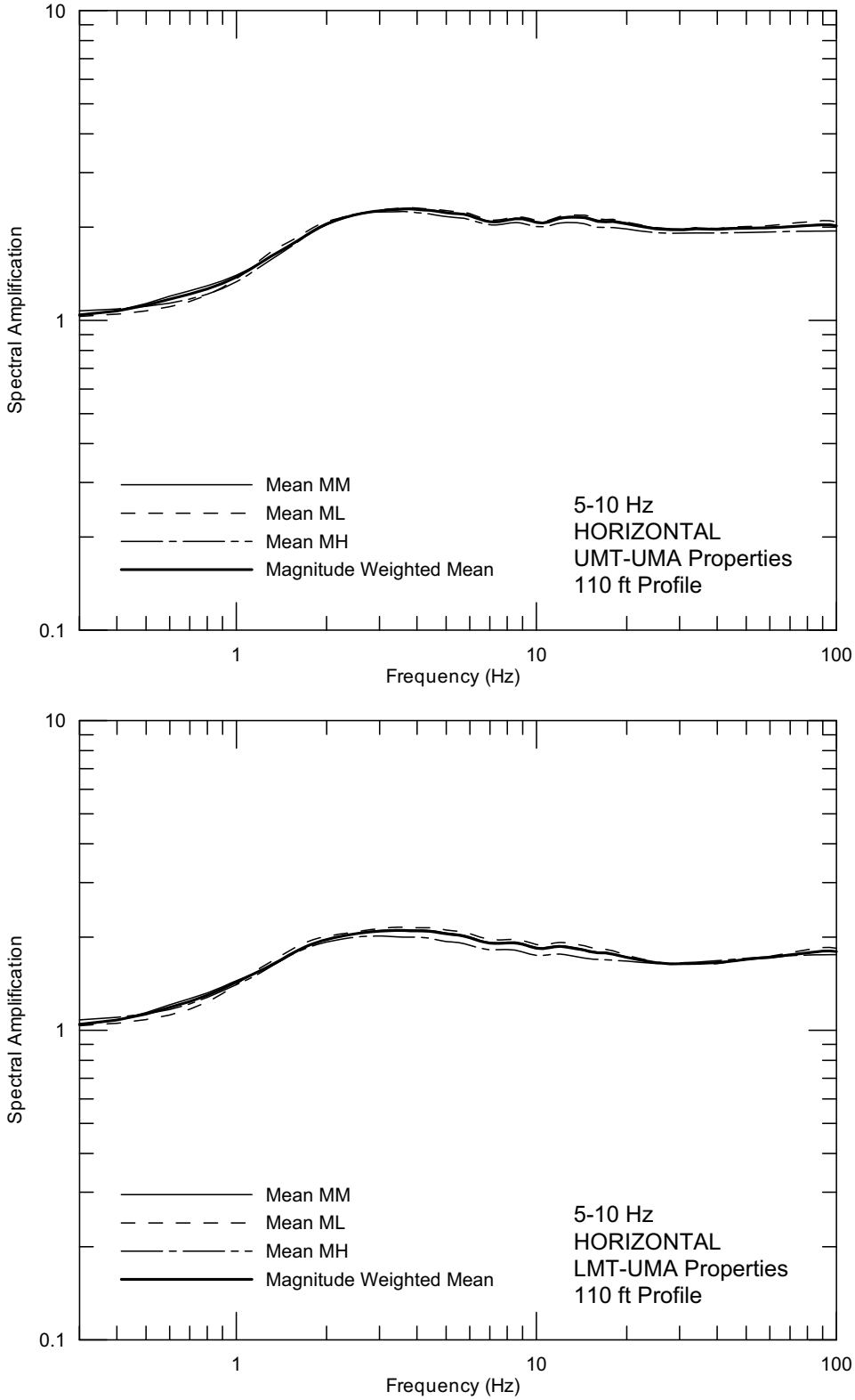

Source: Wong and Silva 2004a [DIRS 170443], Supplemental Record 108

Figure 6.3-19. Representative Point D 5-10 Hz Mean SAFs at an Annual Exceedance Frequency of 10^{-3}, Upper Mean Alluvium Curve, 110 ft Alluvium

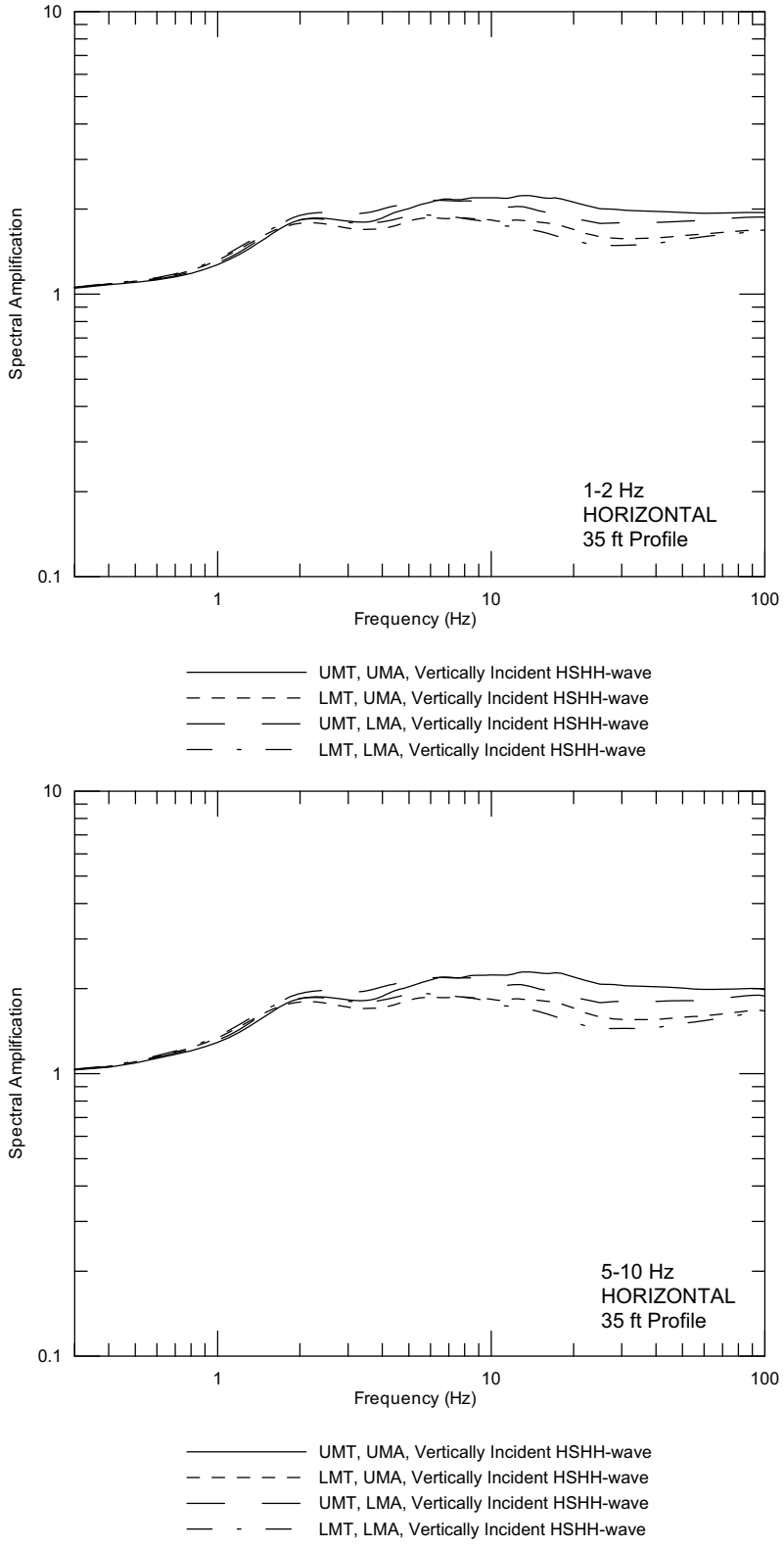

Source: Wong and Silva 2004a [DIRS 170443], Supplemental Record 108

Figure 6.3-20. Representative Point D (35 ft of alluvium) Magnitude-Weighted Mean SAFs at an Annual Exceedance Frequency of 10^{-3}

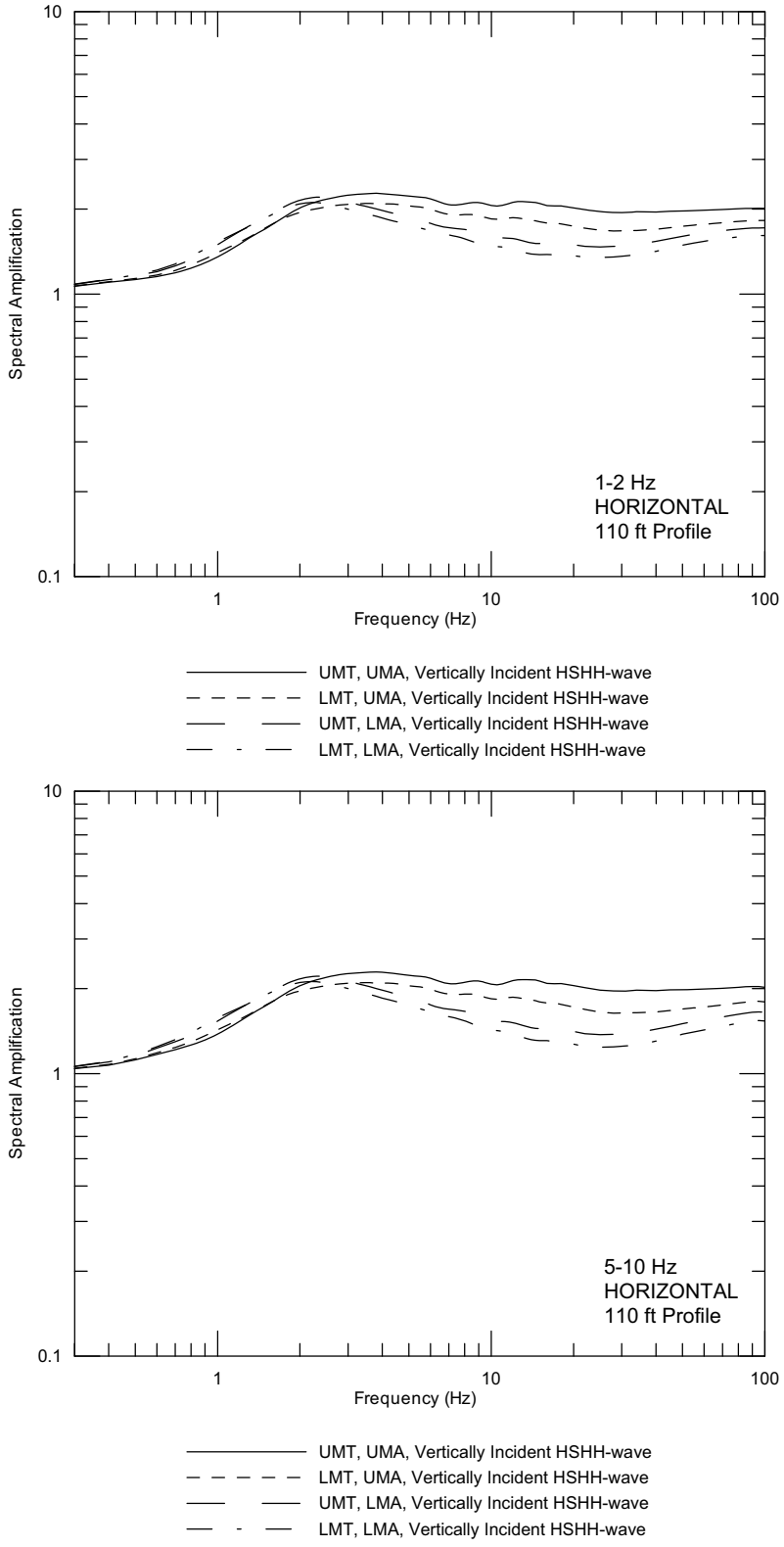

Source: Wong and Silva 2004a [DIRS 170443], Supplemental Record 108

Figure 6.3-21. Representative Point D (110 ft of alluvium) Magnitude-Weighted Mean SAFs at an Annual Exceedance Frequency of 10^{-3}

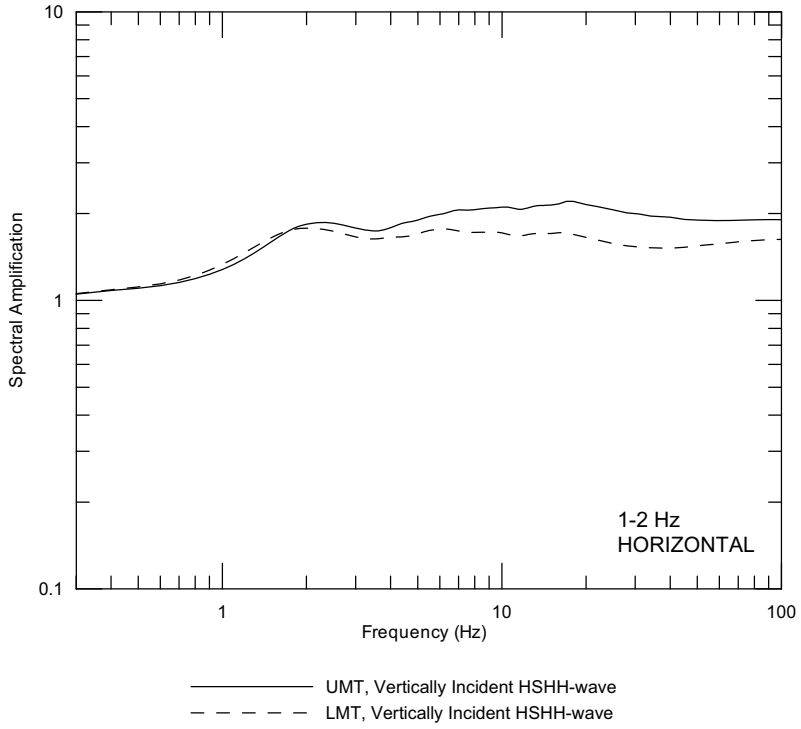

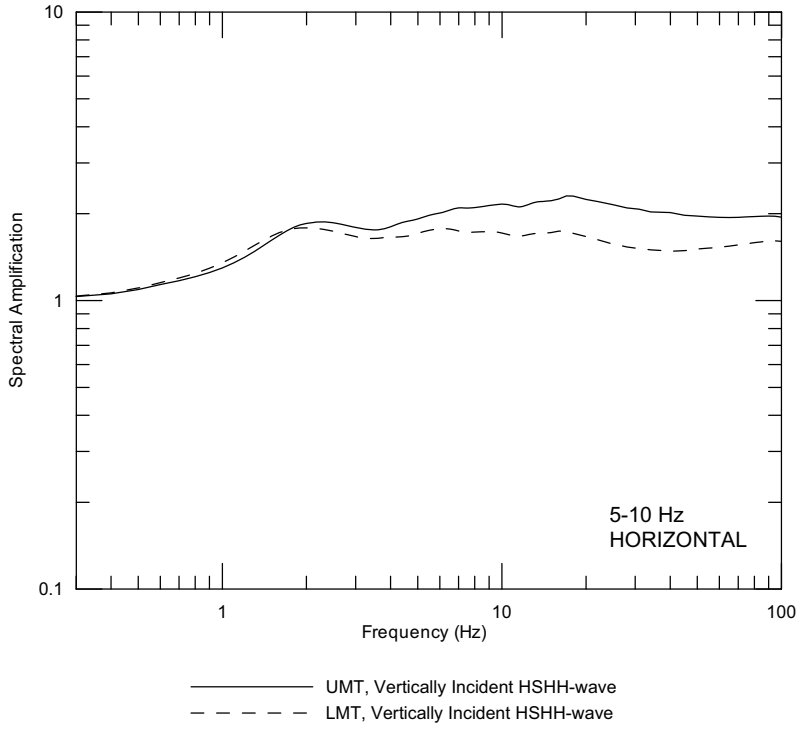

Source: Wong and Silva 2004a [DIRS 170443], Supplemental Record 108

Figure 6.3-22. Representative Point E Magnitude-Weighted Mean SAFs at an Annual Exceedance Frequency of 10^{-3}

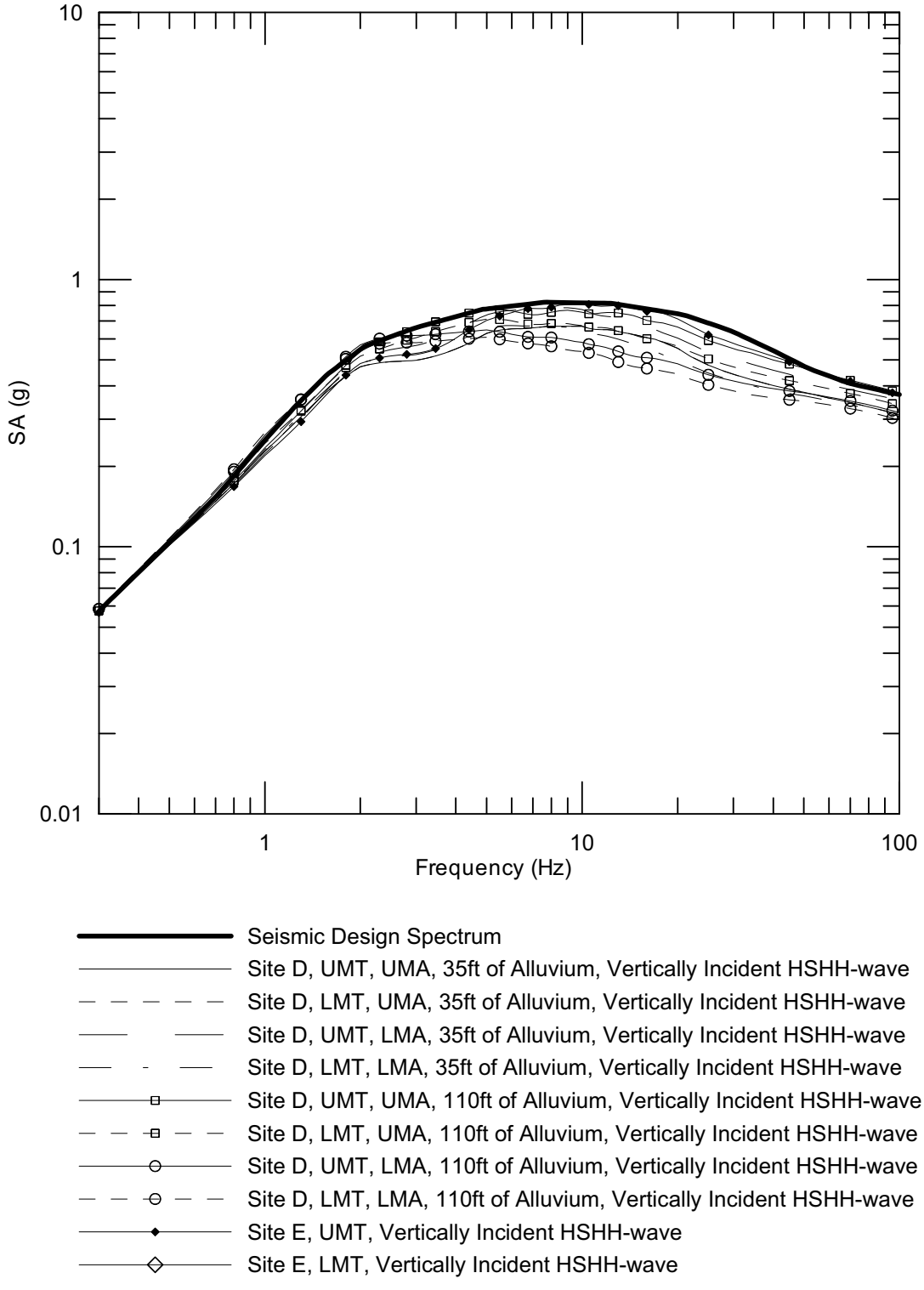

DTN: MO0410SDSDE103.002 [DIRS 172236]

Source: Wong and Silva 2004a [DIRS 170443], Supplemental Record 108

Figure 6.3-23. Point D/E Horizontal Site-Specific Spectra and Seismic Design Response Spectrum (5%-Damped) at an Annual Exceedance Frequency of 10^{-3}

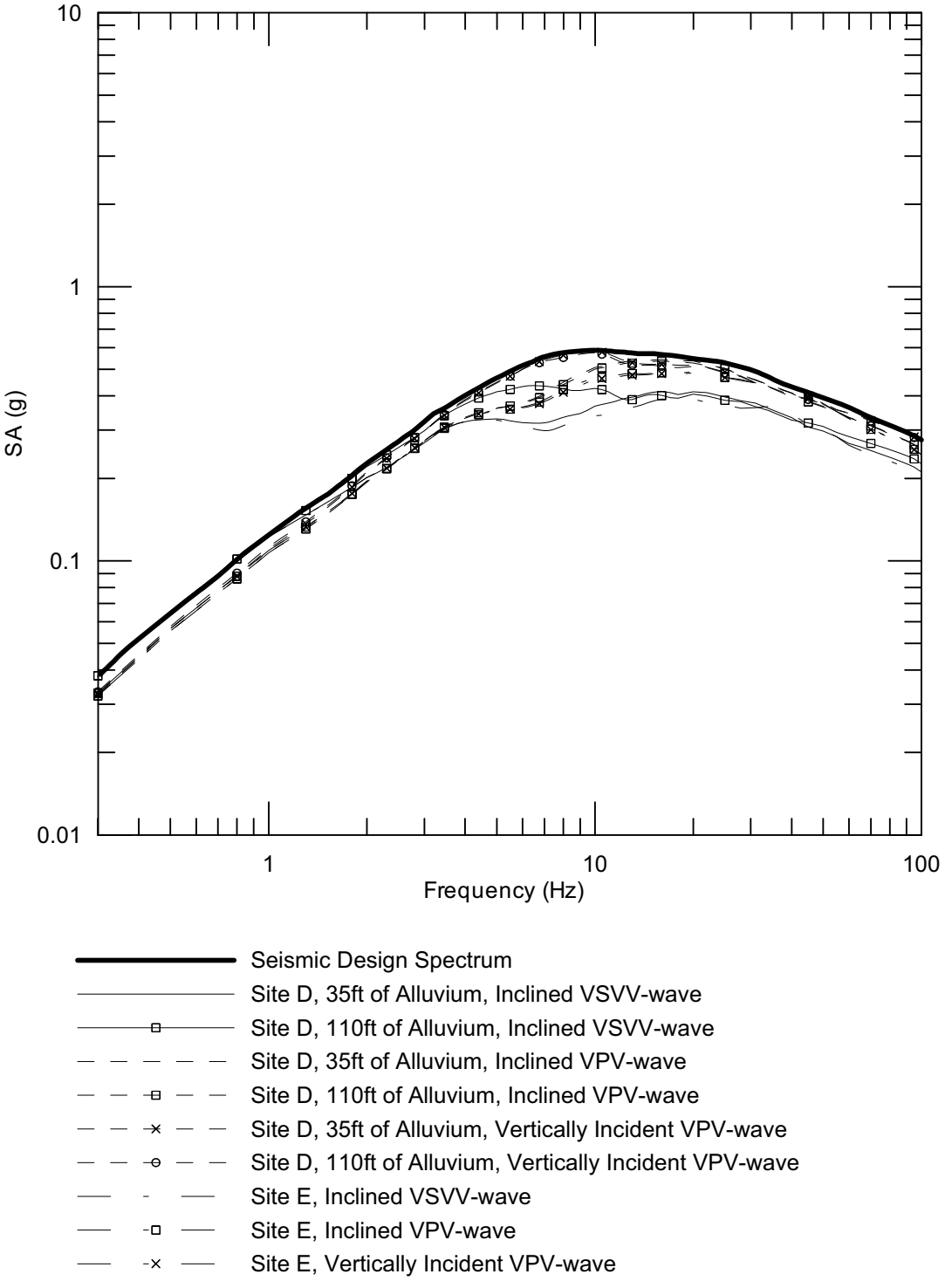

DTN: MO0410SDSDE103.002 [DIRS 172236]

Source: Wong and Silva 2004a [DIRS 170443], Supplemental Record 108

Figure 6.3-24. Point D/E Vertical Site-Specific Spectra and Seismic Design Response Spectrum (5%-Damped) at an Annual Exceedance Frequency of 10^{-3}

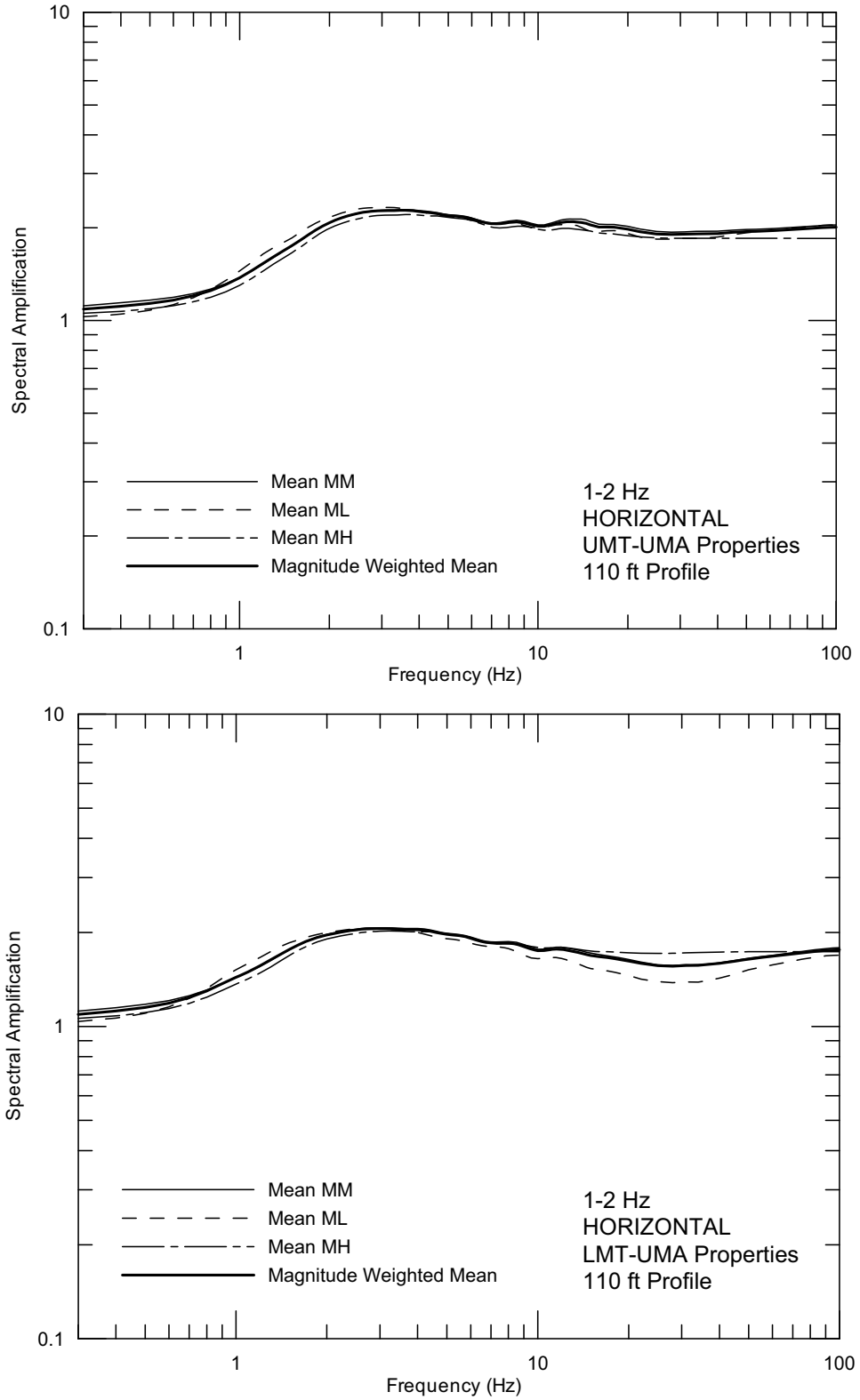

Source: Wong and Silva 2004a [DIRS 170443], Supplemental Record 97

Figure 6.3-25. Representative Point D 1-2 Hz Mean SAFs at an Annual Exceedance Frequency of 5×10^{-4}, Upper Mean Alluvium Curve, 110 ft Alluvium

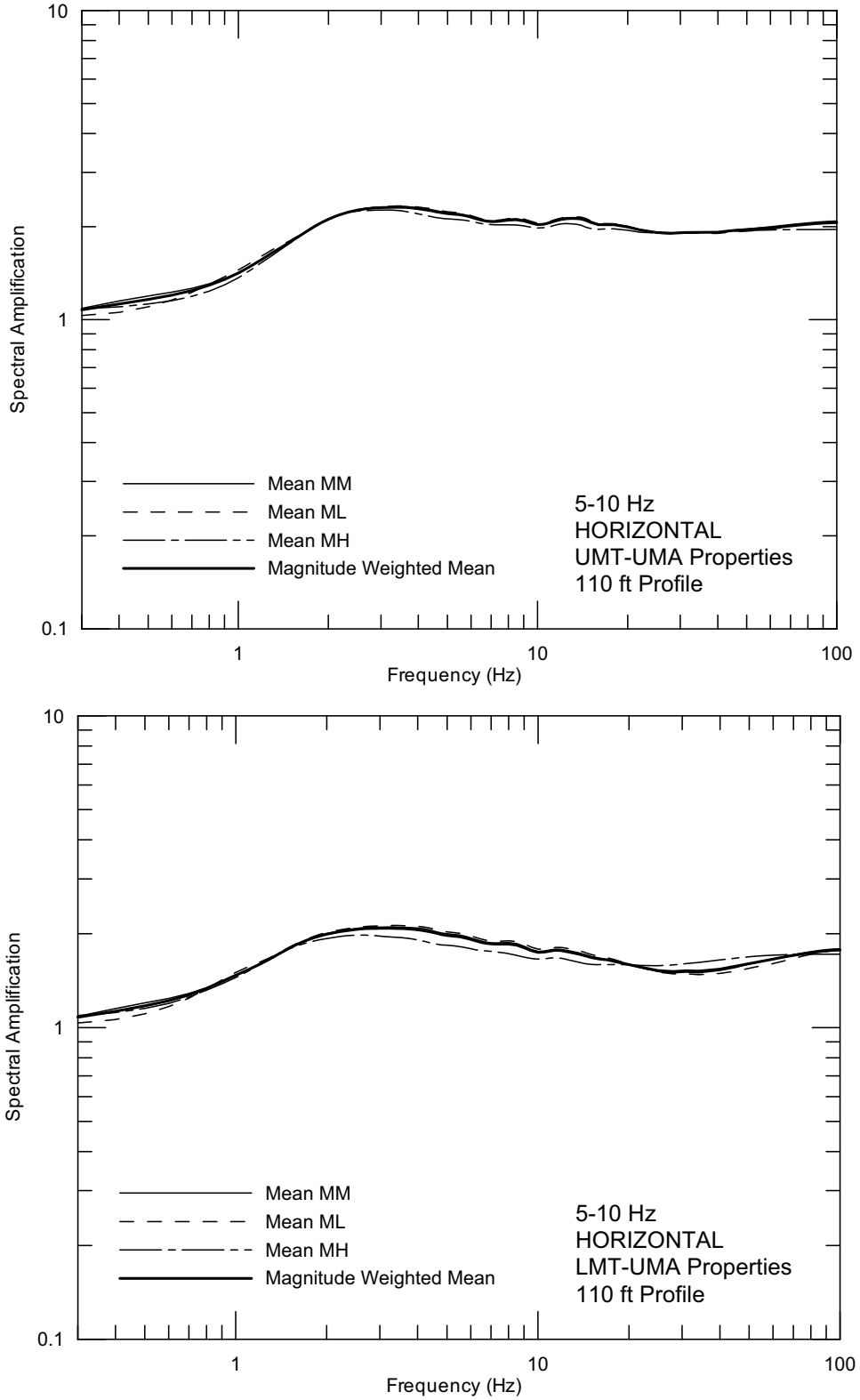

Source: Wong and Silva 2004a [DIRS 170443], Supplemental Record 97

Figure 6.3-26. Representative Point D 5-10 Hz Mean SAFs at an Annual Exceedance Frequency of 5×10^{-4}, Upper Mean Alluvium Curve, 110 ft Alluvium

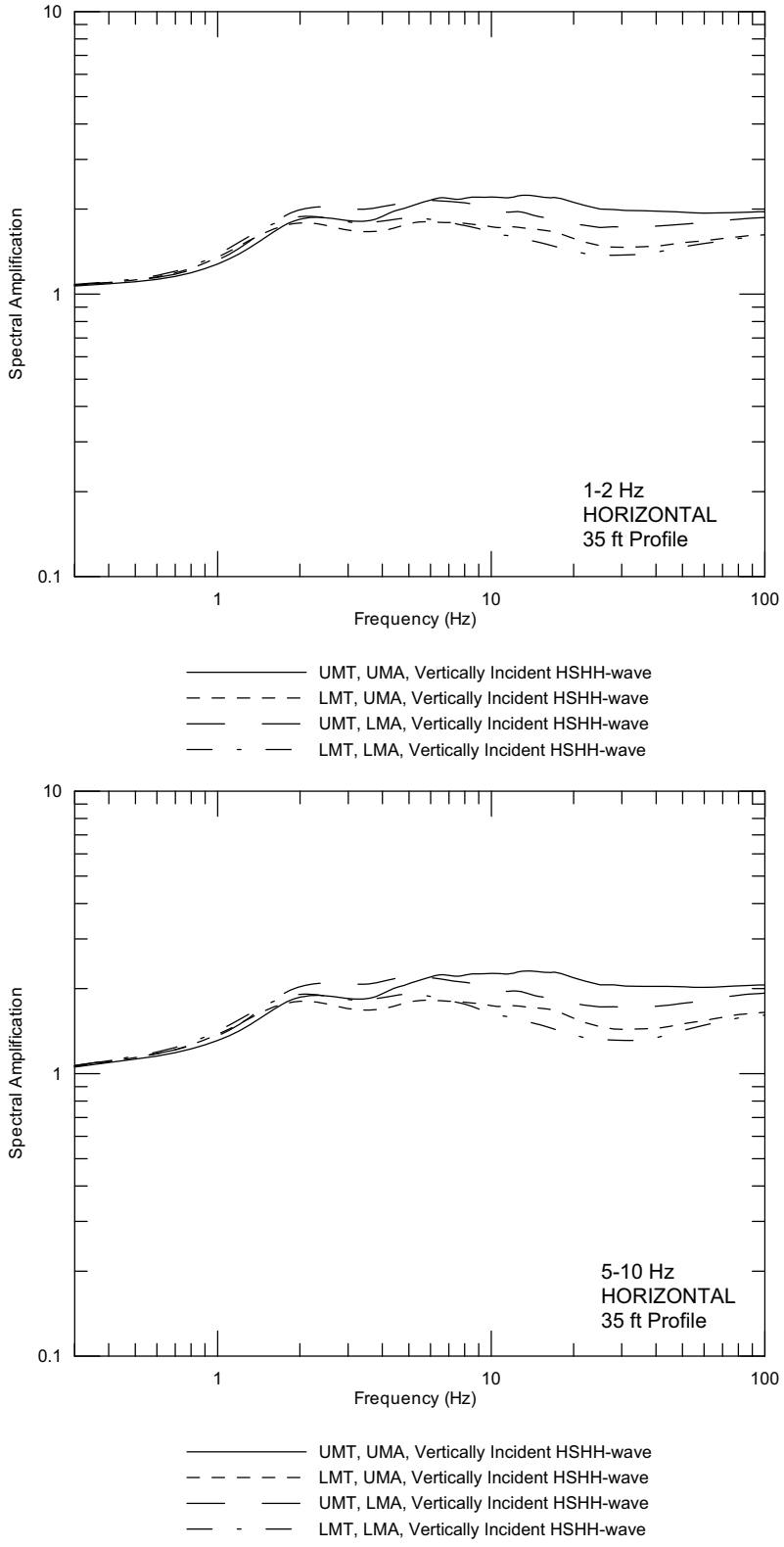

Source: Wong and Silva 2004a [DIRS 170443], Supplemental Record 97

Figure 6.3-27. Representative Point D (35 ft of alluvium) Magnitude-Weighted Mean SAFs at an Annual Exceedance Frequency of 5×10^{-4}

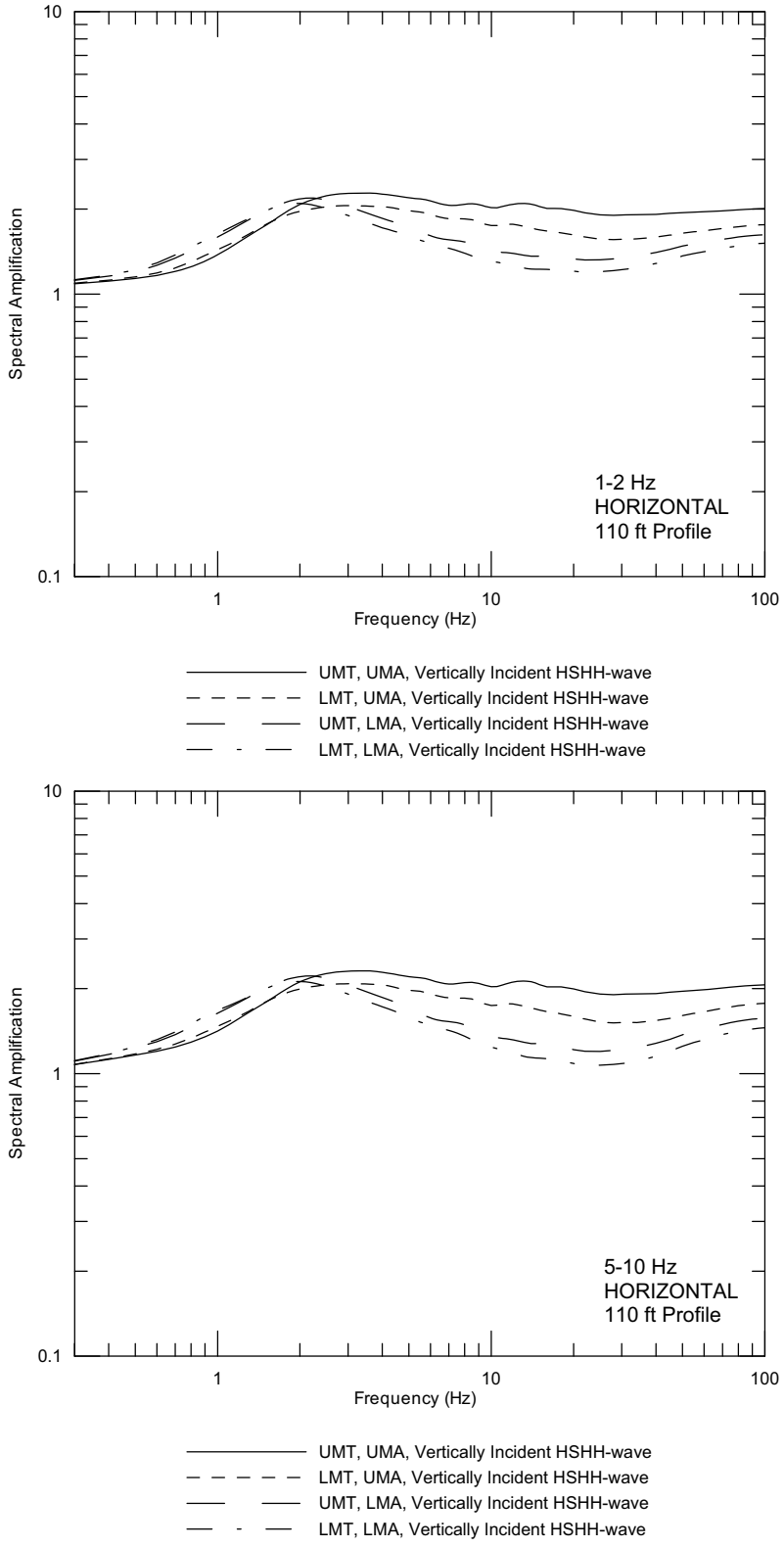

Source: Wong and Silva 2004a [DIRS 170443], Supplemental Record 97

Figure 6.3-28. Representative Point D (110 ft of alluvium) Magnitude-Weighted Mean SAFs at an Annual Exceedance Frequency of 5×10^{-4}

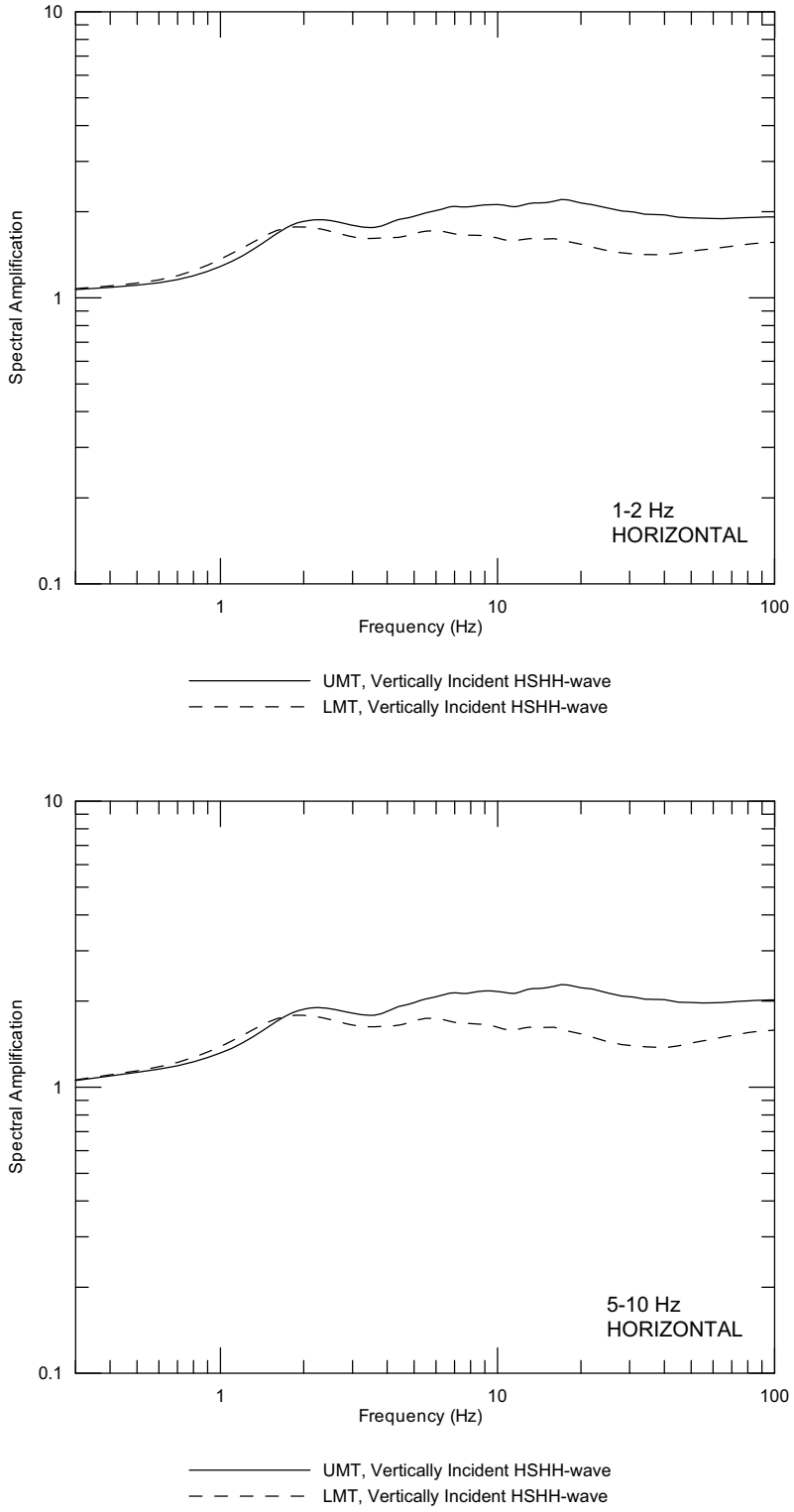

Source: Wong and Silva 2004a [DIRS 170443], Supplemental Record 97

Figure 6.3-29. Representative Point E Magnitude-Weighted Mean SAFs at an Annual Exceedance Frequency of 5×10^{-4}

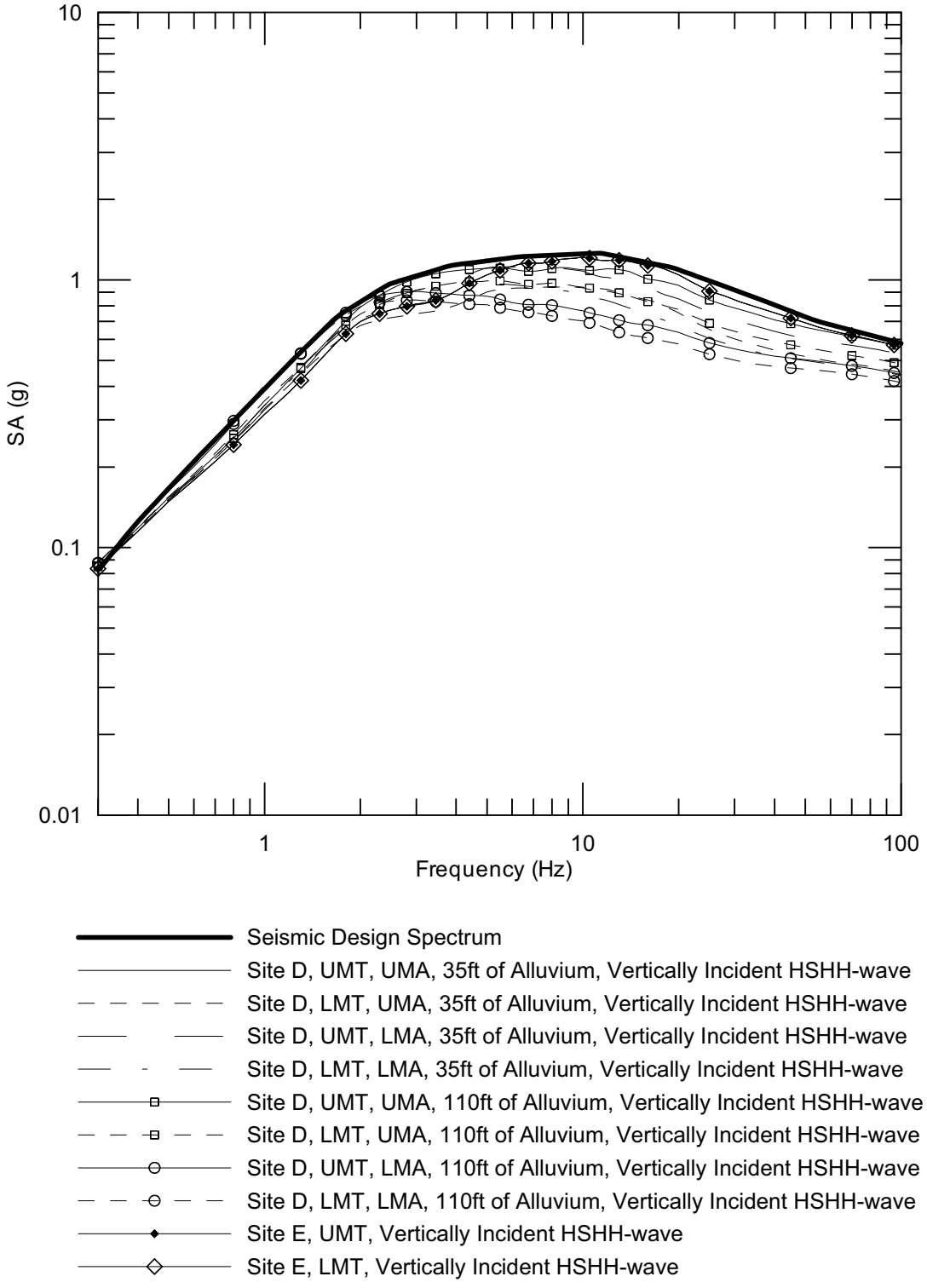

DTN: MO0410SDSTMHIS.005 [DIRS 172237]

Source: Wong and Silva 2004a [DIRS 170443], Supplemental Record 97

Figure 6.3-30. Point D/E Horizontal Site-Specific Spectra and Seismic Design Response Spectrum (5%-Damped) at an Annual Exceedance Frequency of 5×10^{-4}

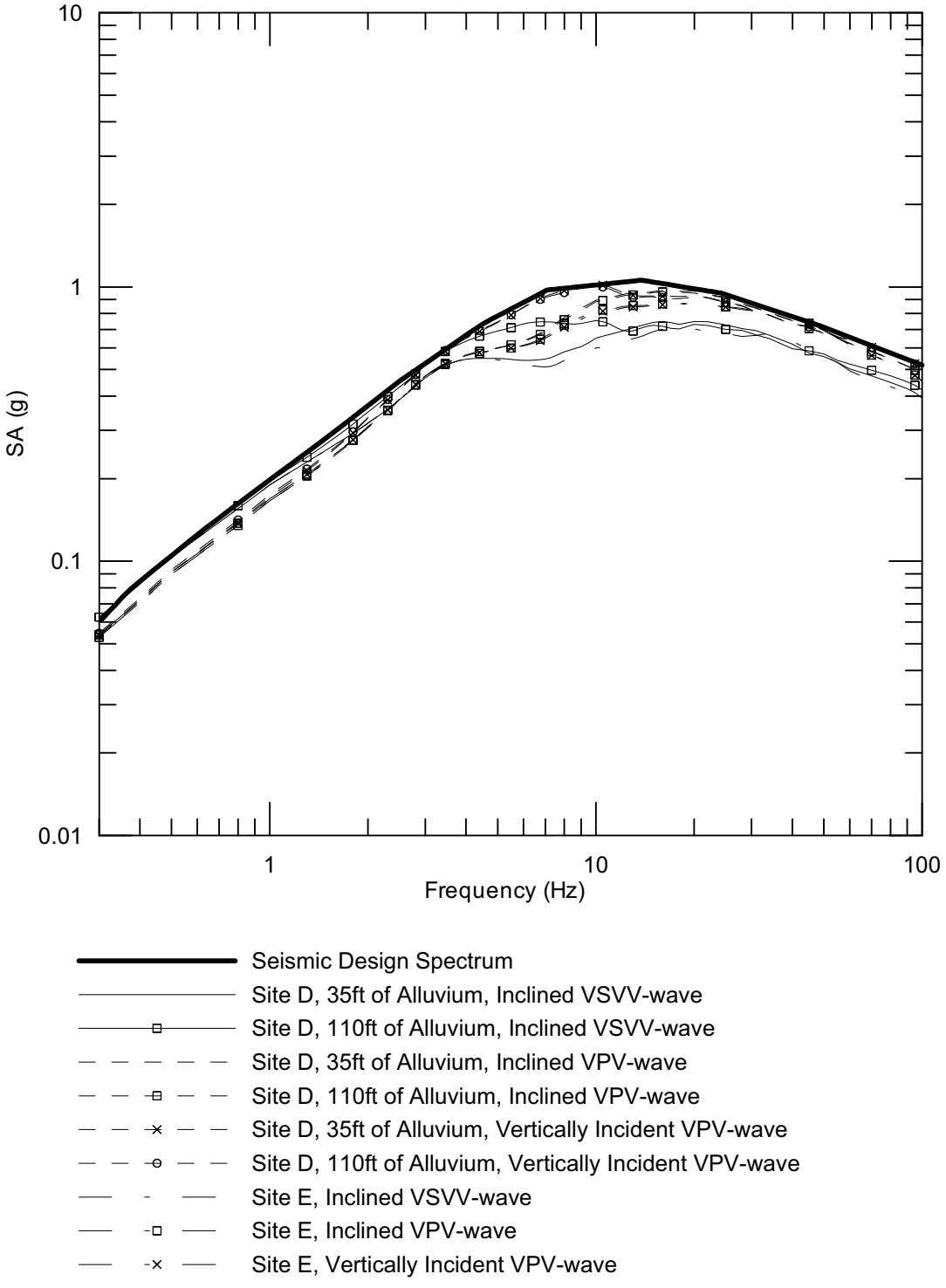

DTN: MO0410SDSTMHIS.005 [DIRS 172237]

Source: Wong and Silva 2004a [DIRS 170443], Supplemental Record 97

Figure 6.3-31. Point D/E Vertical Site-Specific Spectra and Seismic Design Response Spectrum (5%-Damped) at an Annual Exceedance Frequency of 5×10^{-4}

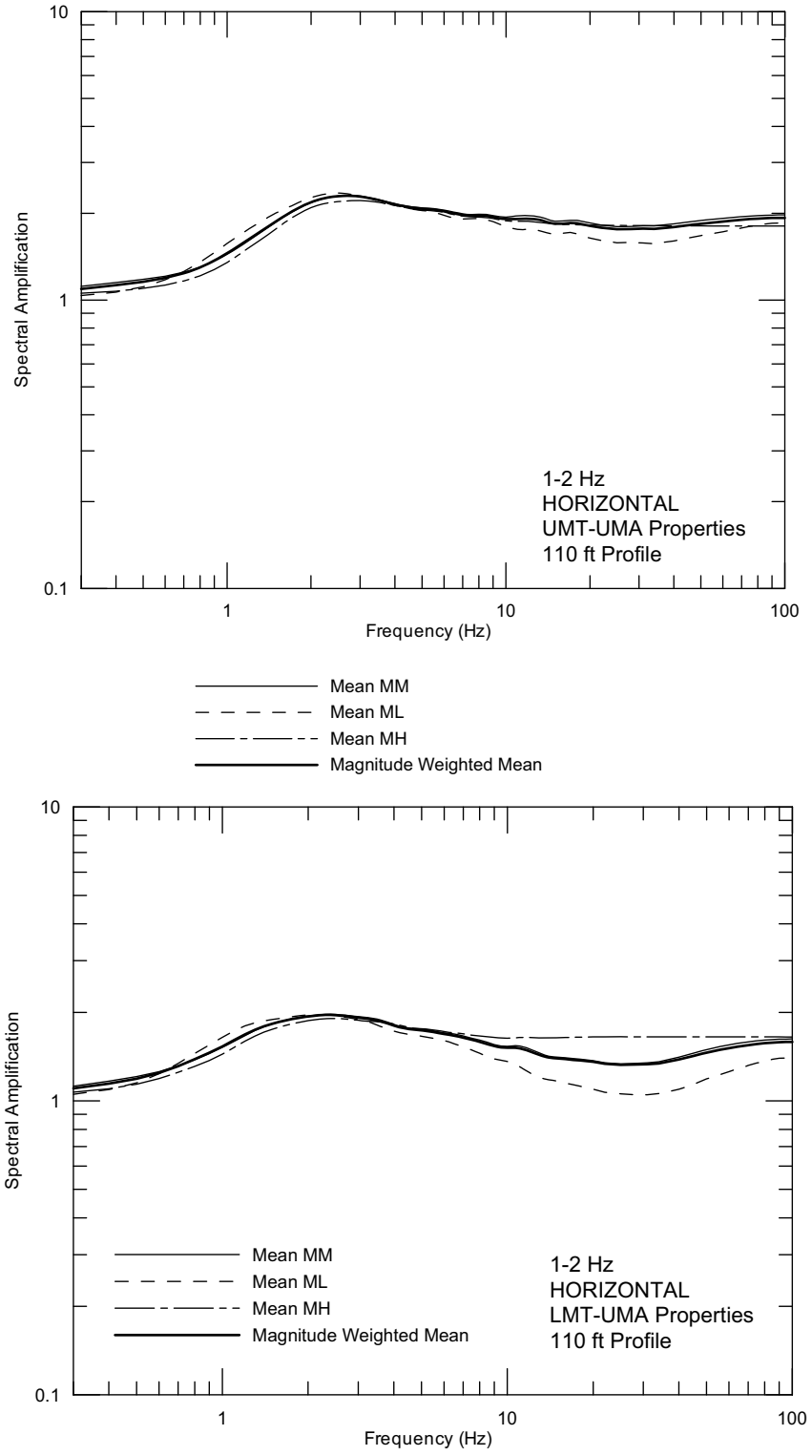

Source: Wong and Silva 2004a [DIRS 170443], Supplemental Record 103

Figure 6.3-32. Representative Point D 1-2 Hz Mean SAFs at an Annual Exceedance Frequency of 10^{-4}, Upper Mean Alluvium Curve, 110 ft Alluvium

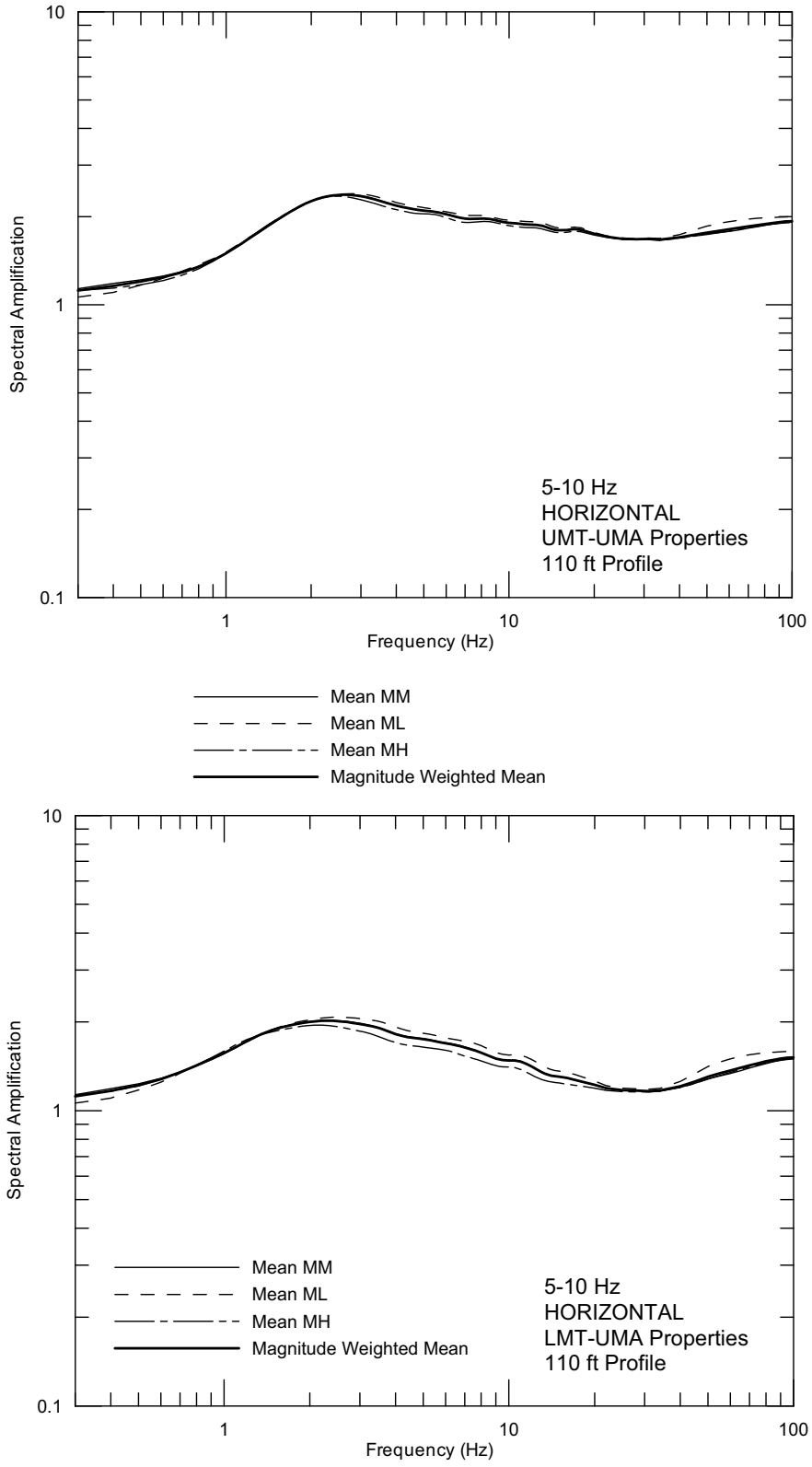

Source: Wong and Silva 2004a [DIRS 170443], Supplemental Record 103

Figure 6.3-33. Representative Point D 5-10 Hz Mean SAFs at an Annual Exceedance Frequency of 10^{-4}, Upper Mean Alluvium Curve, 110 ft Alluvium

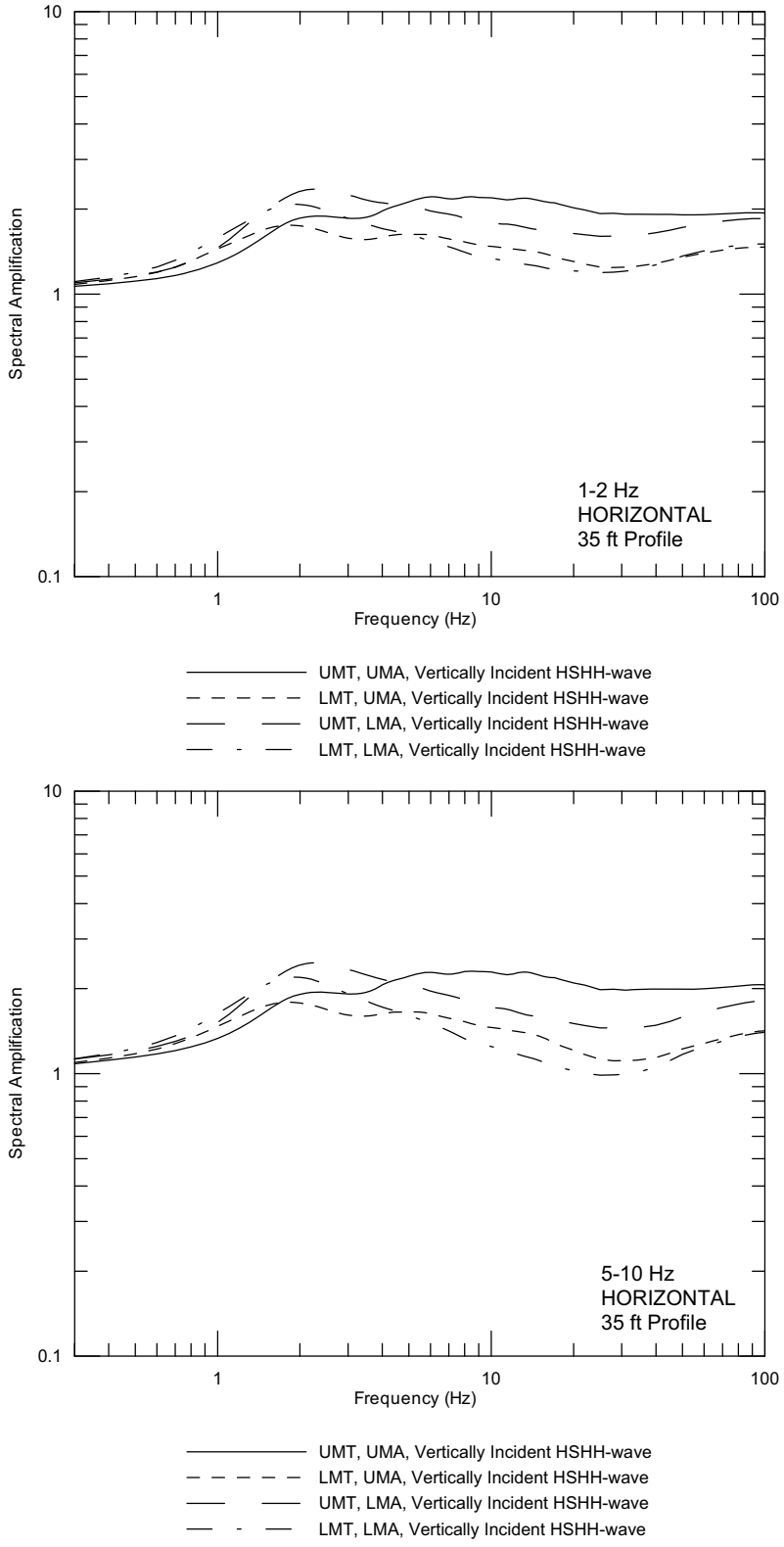

Source: Wong and Silva 2004a [DIRS 170443], Supplemental Record 103

Figure 6.3-34. Representative Point D (35 ft of alluvium) Magnitude-Weighted Mean SAFs at an Annual Exceedance Frequency of 10^{-4}

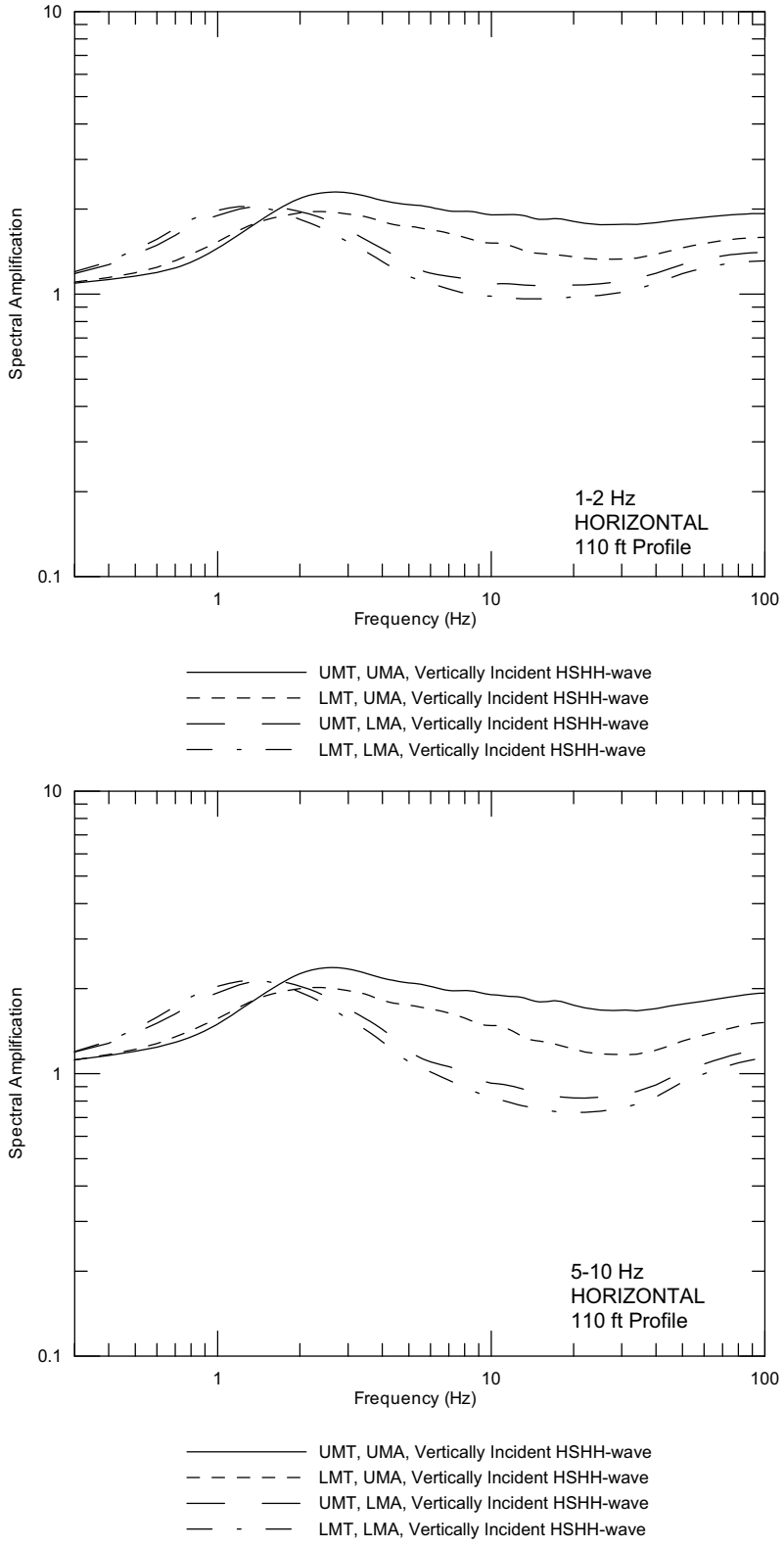

Source: Wong and Silva 2004a [DIRS 170443], Supplemental Record 103

Figure 6.3-35. Representative Point D (110 ft of alluvium) Magnitude-Weighted Mean SAFs at an Annual Exceedance Frequency of 10^{-4}

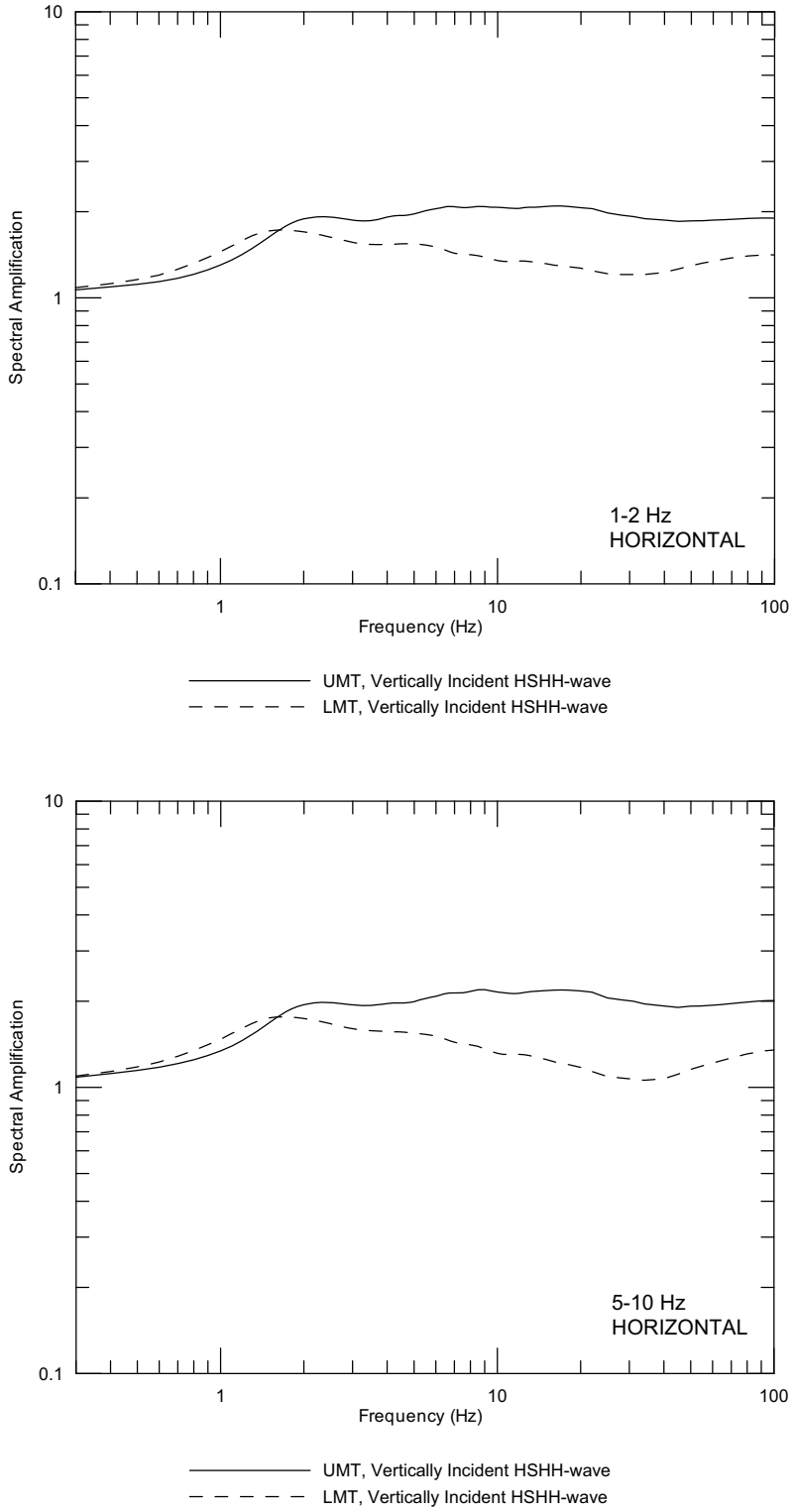

Source: Wong and Silva 2004a [DIRS 170443], Supplemental Record 103

Note: An average of the UMA and LMA curves was used for Point D.

Figure 6.3-36. Representative Point E Magnitude-Weighted Mean SAFs at an Annual Exceedance Frequency of 10^{-4}

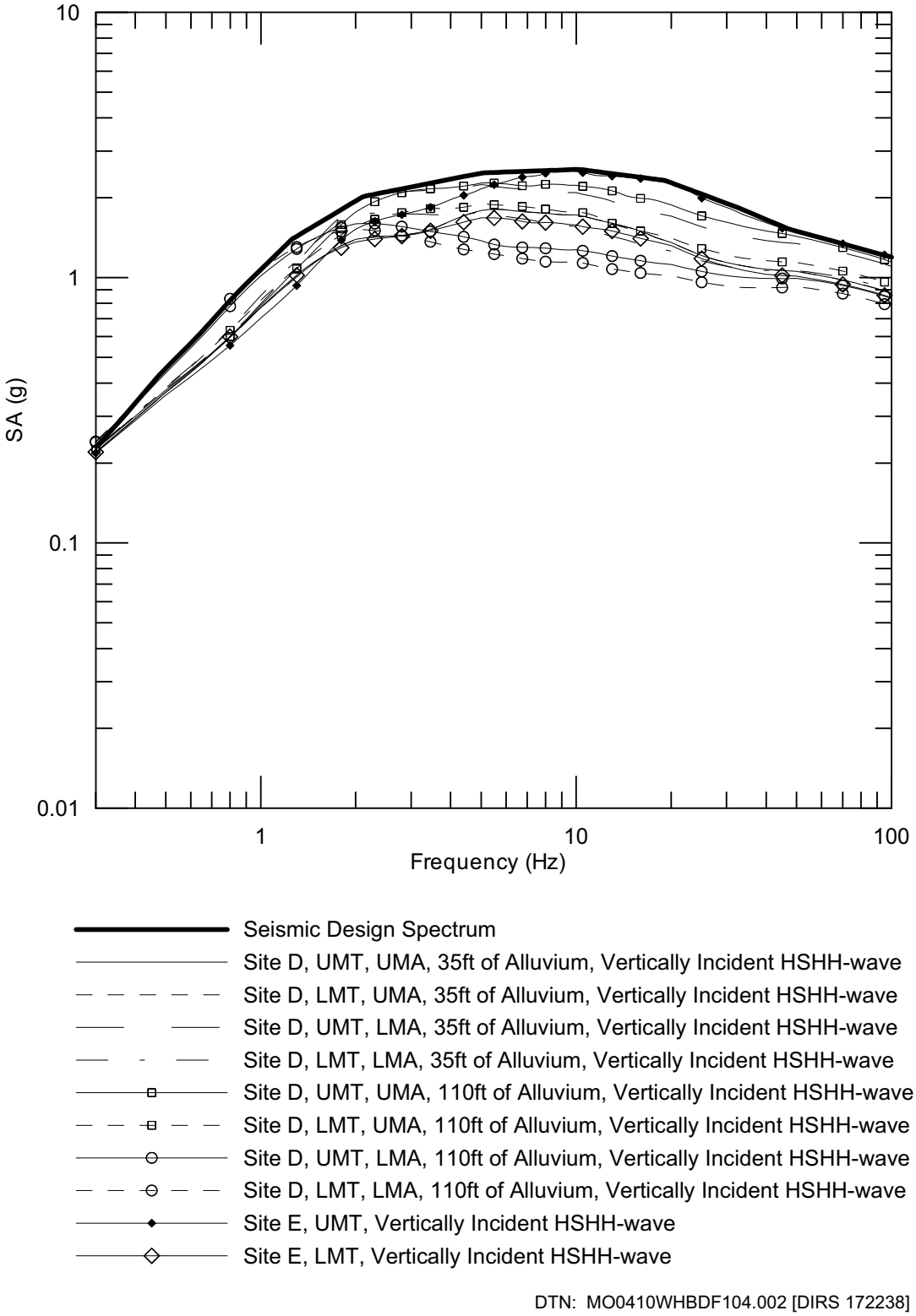

DTN: MO0410WHBDF104.002 [DIRS 172238]

Source: Wong and Silva 2004a [DIRS 170443], Supplemental Record 103

Figure 6.3-37. Point D/E Horizontal Site-Specific Spectra and Seismic Design Response Spectrum (5%-Damped) at an Annual Exceedance Frequency of 10^{-4}

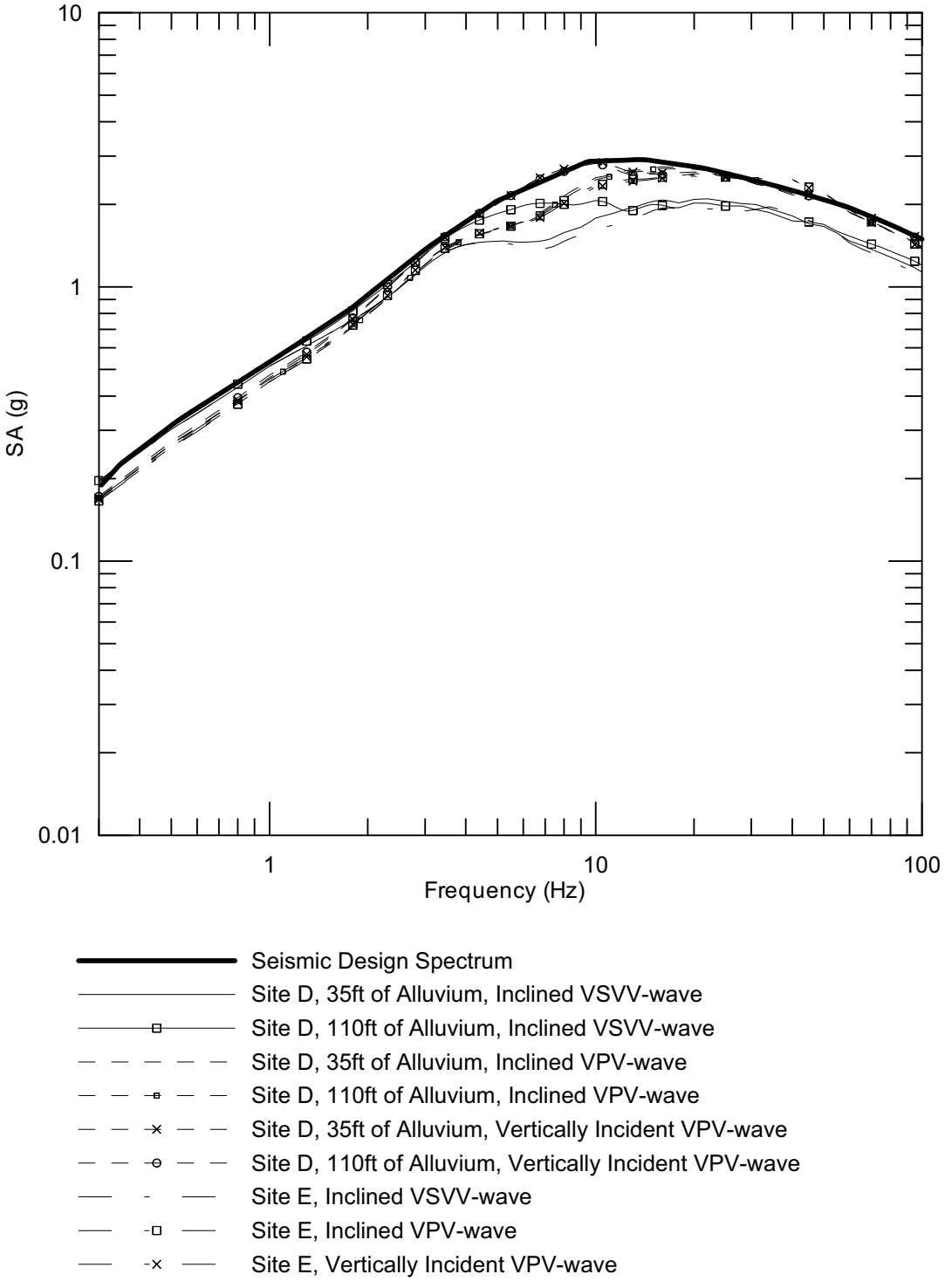

DTN: MO0410WHBDF104.002 [DIRS 172238]

Source: Wong and Silva 2004a [DIRS 170443], Supplemental Record 103

Figure 6.3-38. Point D/E Vertical Site-Specific Spectra and Seismic Design Response Spectrum (5%-Damped) at an Annual Exceedance Frequency of 10^{-4}

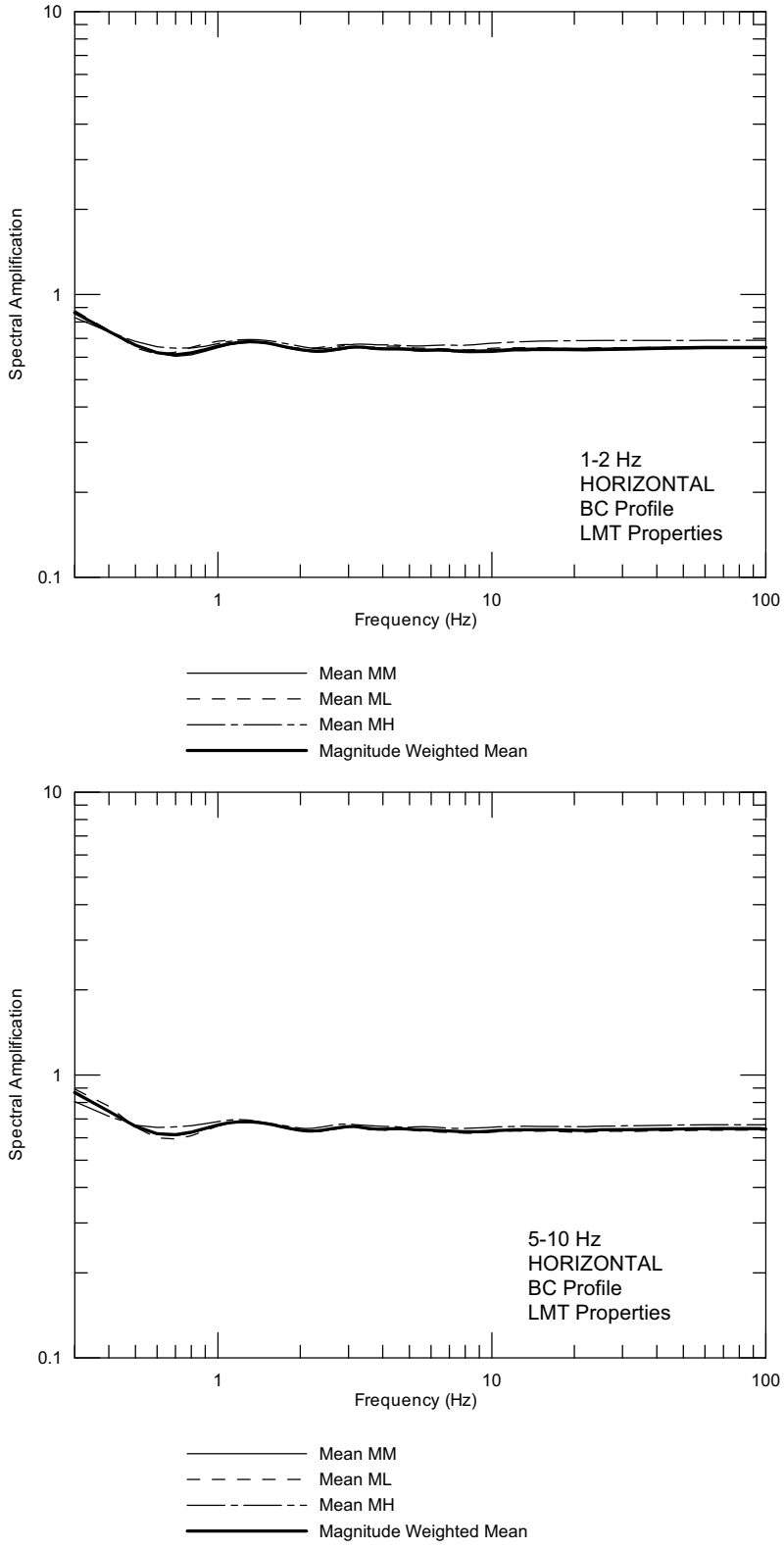

Source: Wong and Silva 2004a [DIRS 170443], Supplemental Record 105

Figure 6.3-39. Representative Point B Mean SAFs at an Annual Exceedance Frequency of 10^{-5}

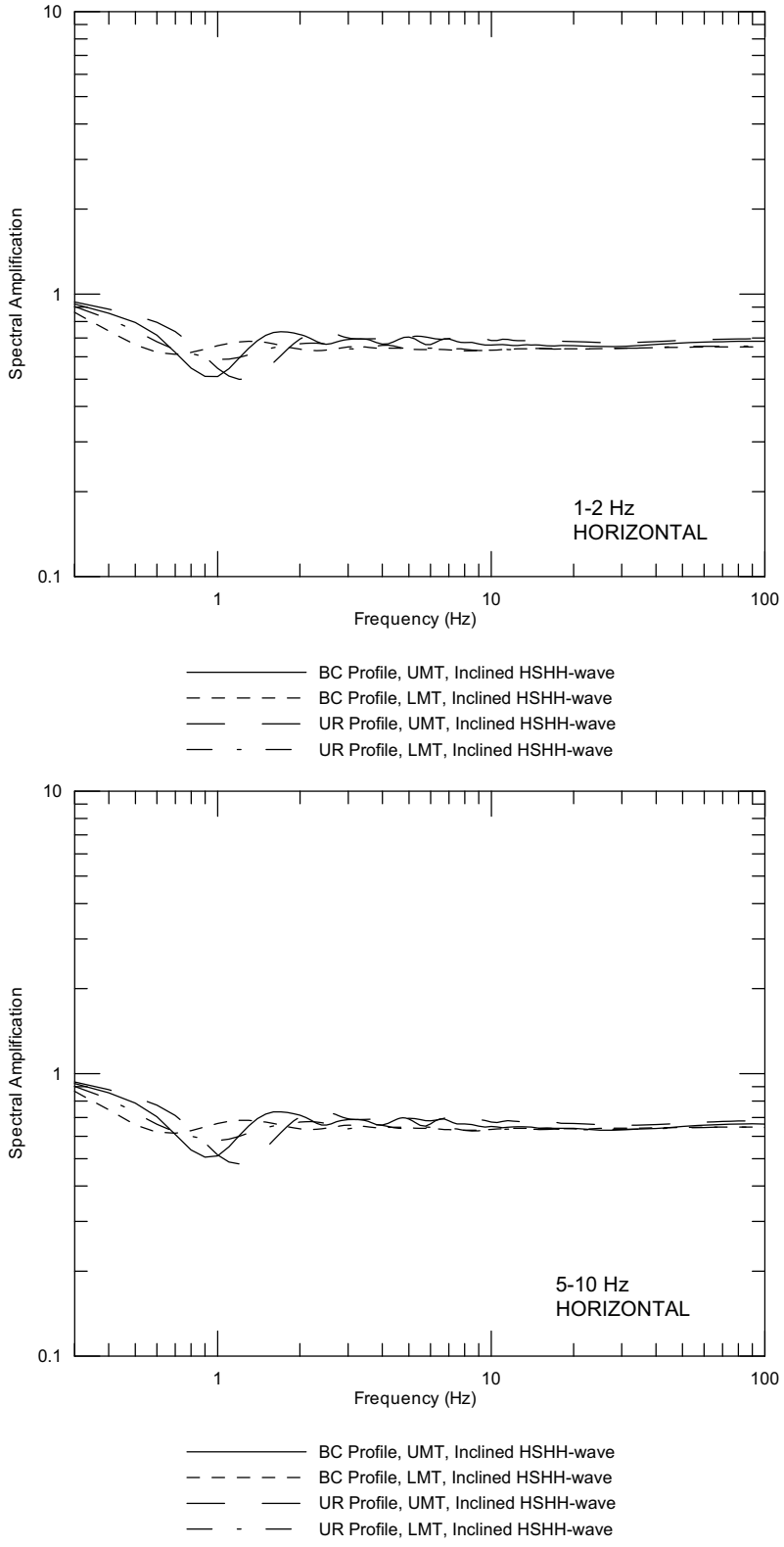

Source: Wong and Silva 2004a [DIRS 170443], Supplemental Record 105

Figure 6.3-40. Point B Horizontal Magnitude-Weighted Mean SAF at an Annual Exceedance Frequency of 10^{-5}

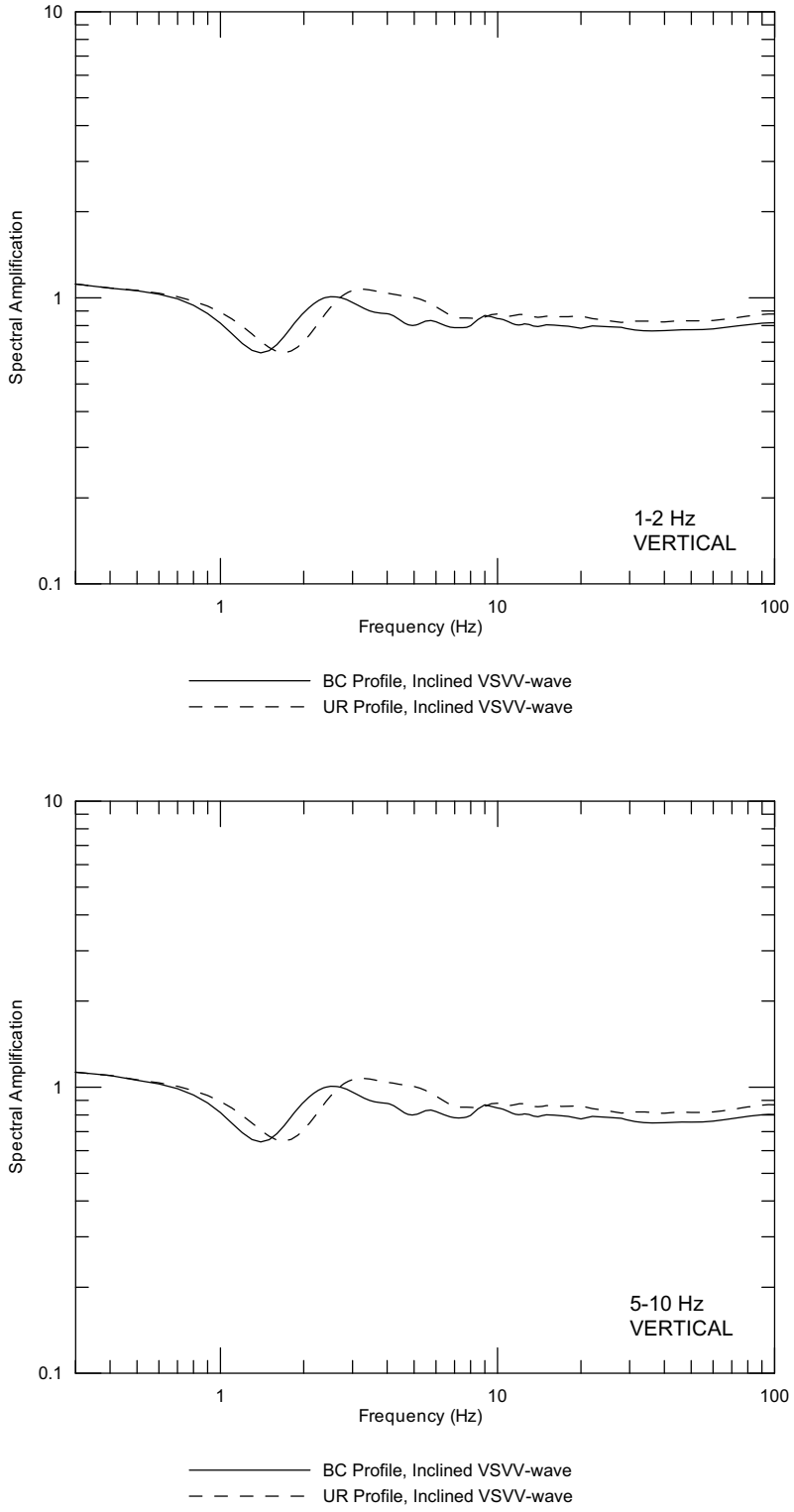

Source: Wong and Silva 2004a [DIRS 170443], Supplemental Record 105

Figure 6.3-41. Point B Vertical Magnitude-Weighted Mean SAF at an Annual Exceedance Frequency of 10^{-5}

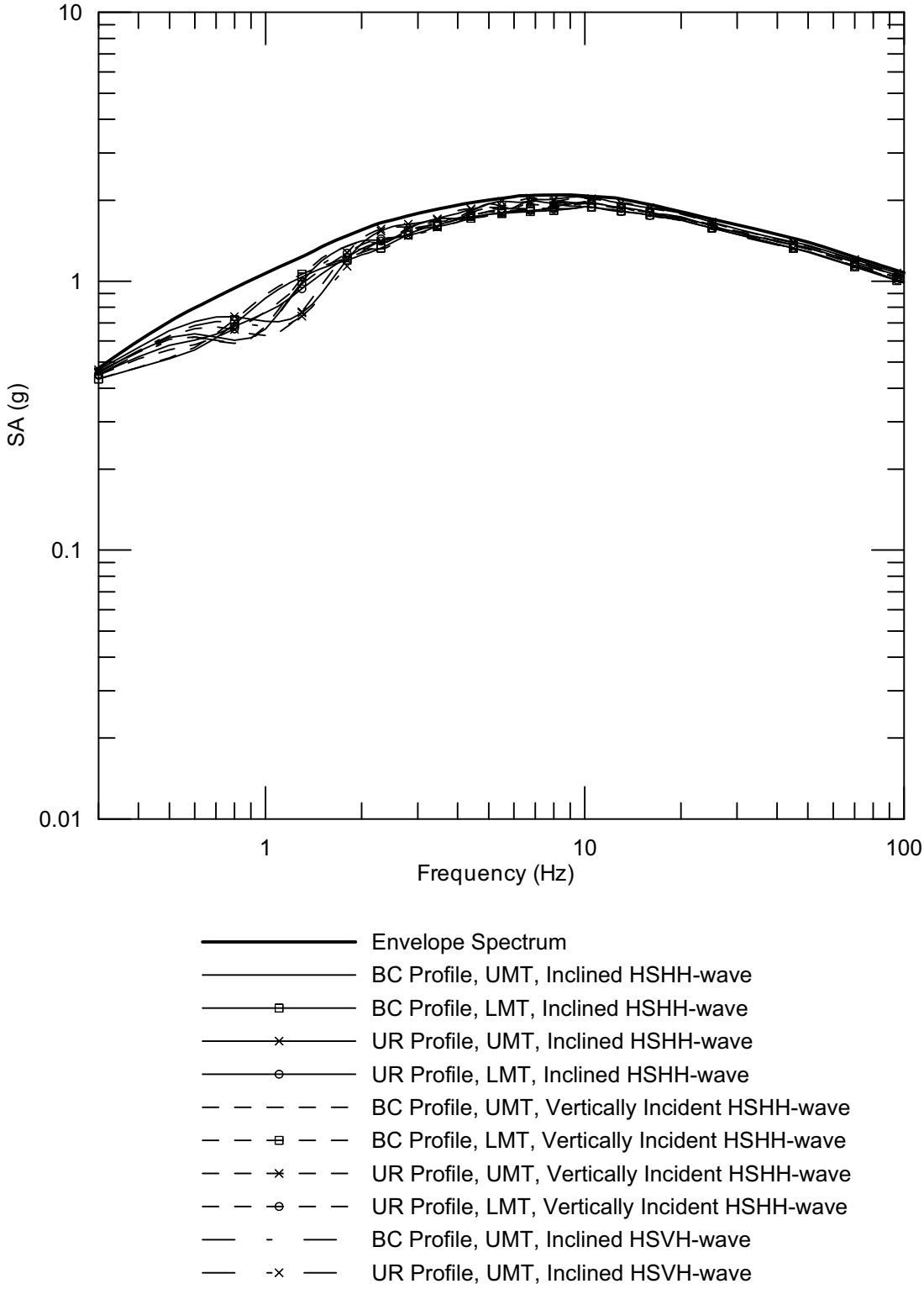

DTN: MO0312SEPRSRLB.019 [DIRS 170427]

Source: Wong and Silva 2004a [DIRS 170443], Supplemental Record 105

Figure 6.3-42. Point B Horizontal Site-Specific Spectra and Postclosure Envelope Spectrum at an Annual Exceedance Frequency of 10^{-5}

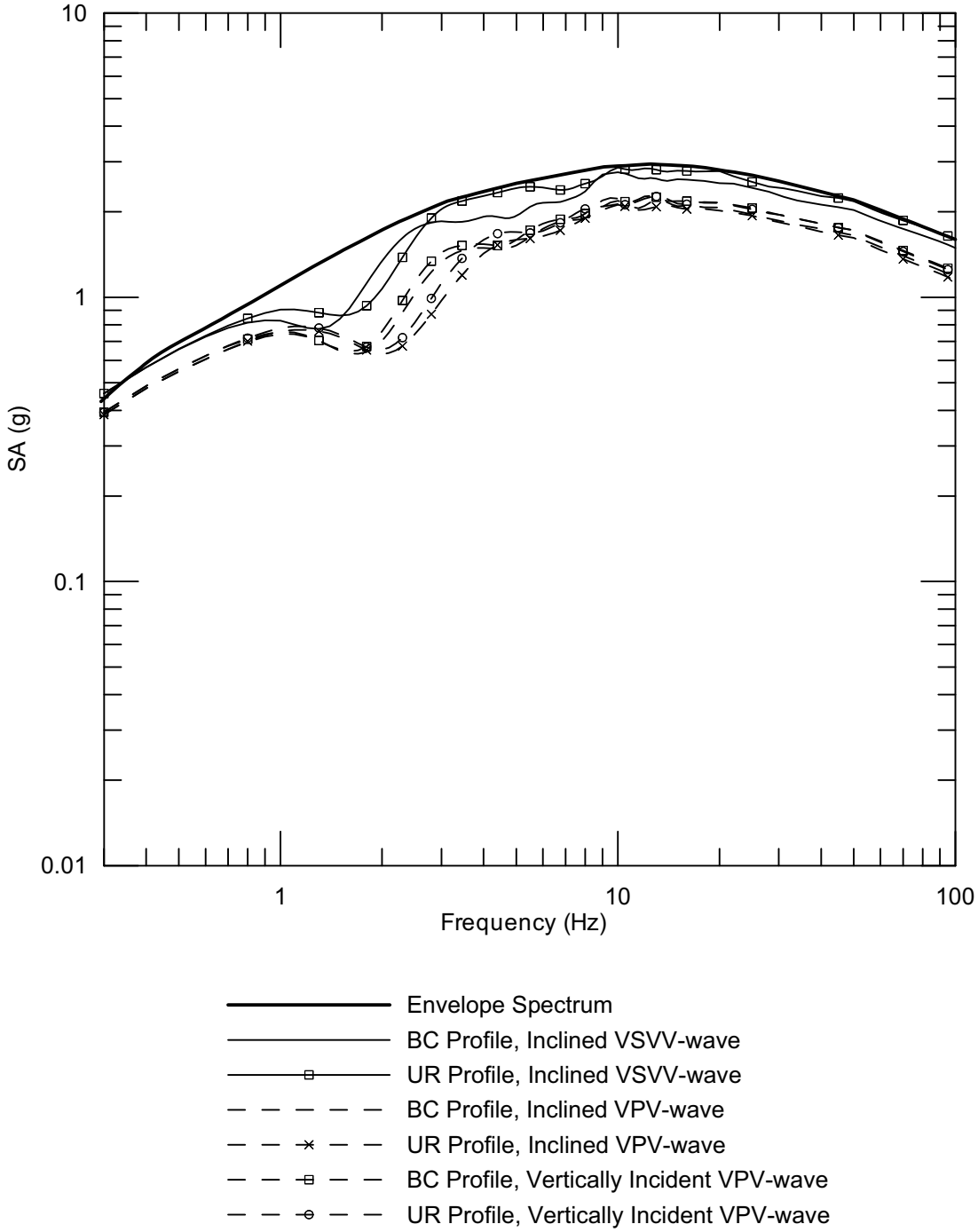

DTN: MO0312SEPRSRLB.019 [DIRS 170427]

Source: Wong and Silva 2004a [DIRS 170443], Supplemental Record 105

Figure 6.3-43. Point B Vertical Site-Specific Spectra and Postclosure Envelope Spectrum at an Annual Exceedance Frequency of 10^{-5}

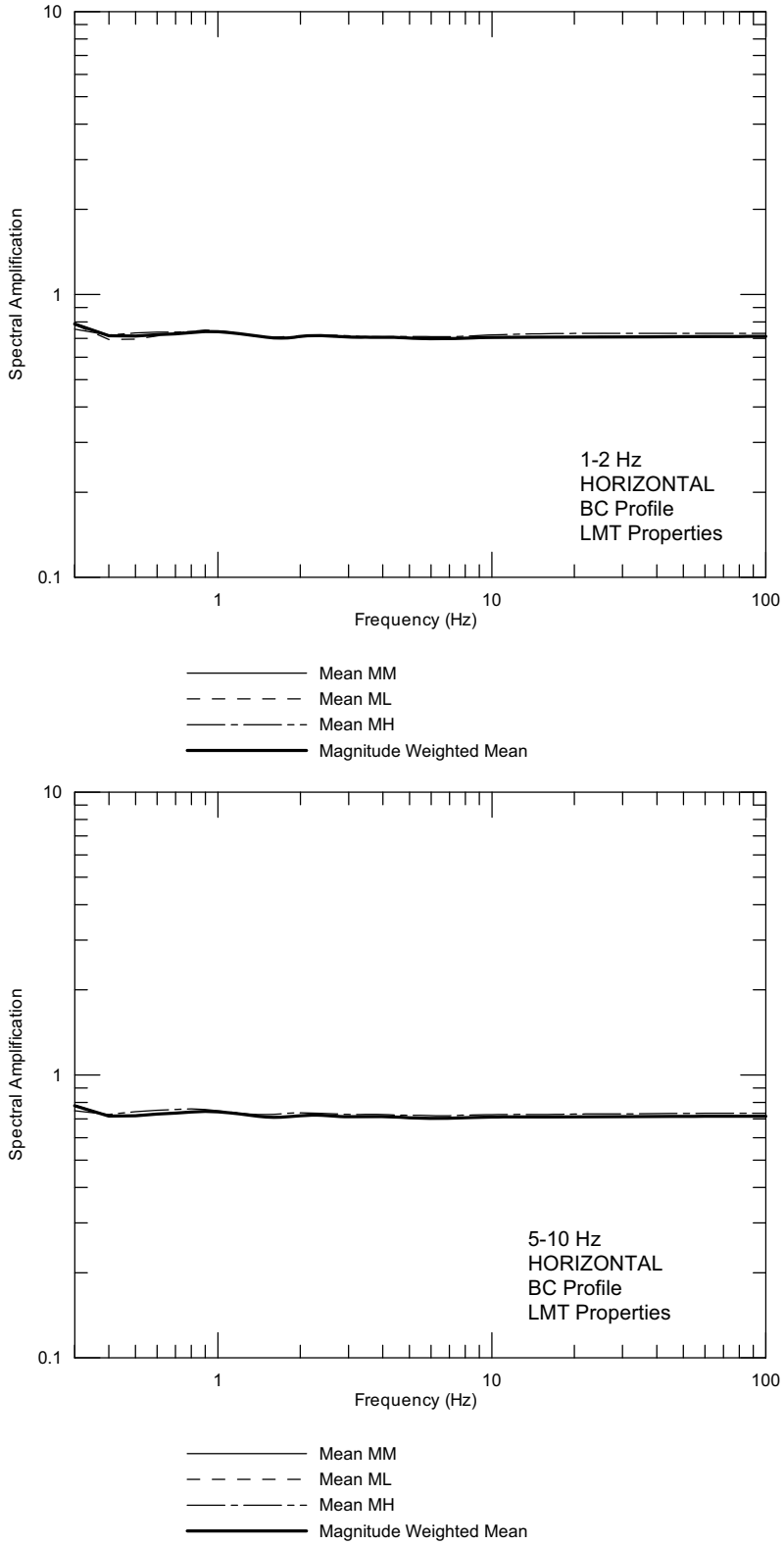

Source: Wong and Silva 2004a [DIRS 170443], Supplemental Record 60

Figure 6.3-44. Representative Point B Mean SAFs at an Annual Exceedance Frequency of 10^{-6}

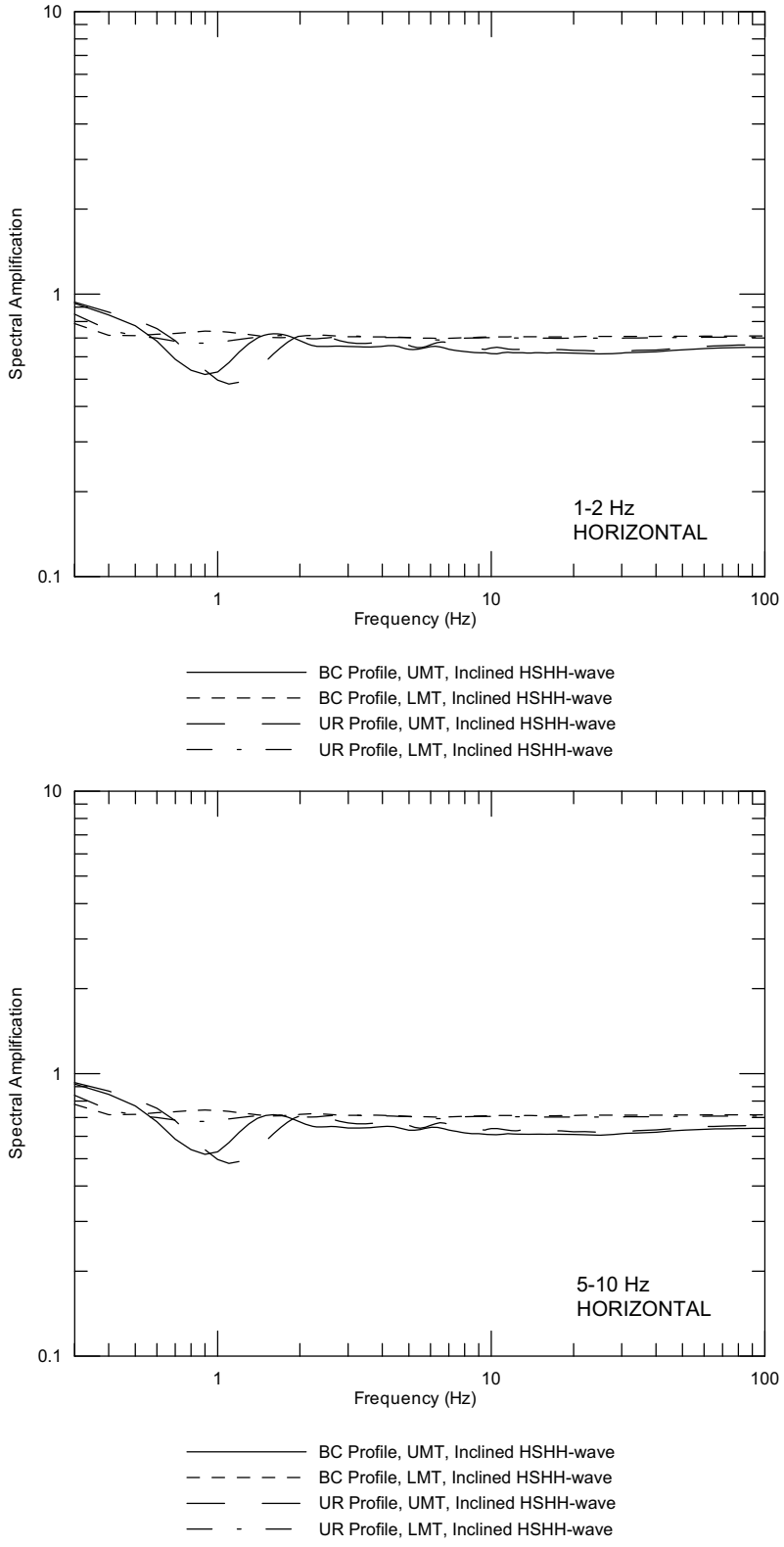

Source: Wong and Silva 2004a [DIRS 170443], Supplemental Record 60

Figure 6.3-45. Point B Horizontal Magnitude-Weighted Mean SAF at an Annual Exceedance Frequency of 10^{-6}

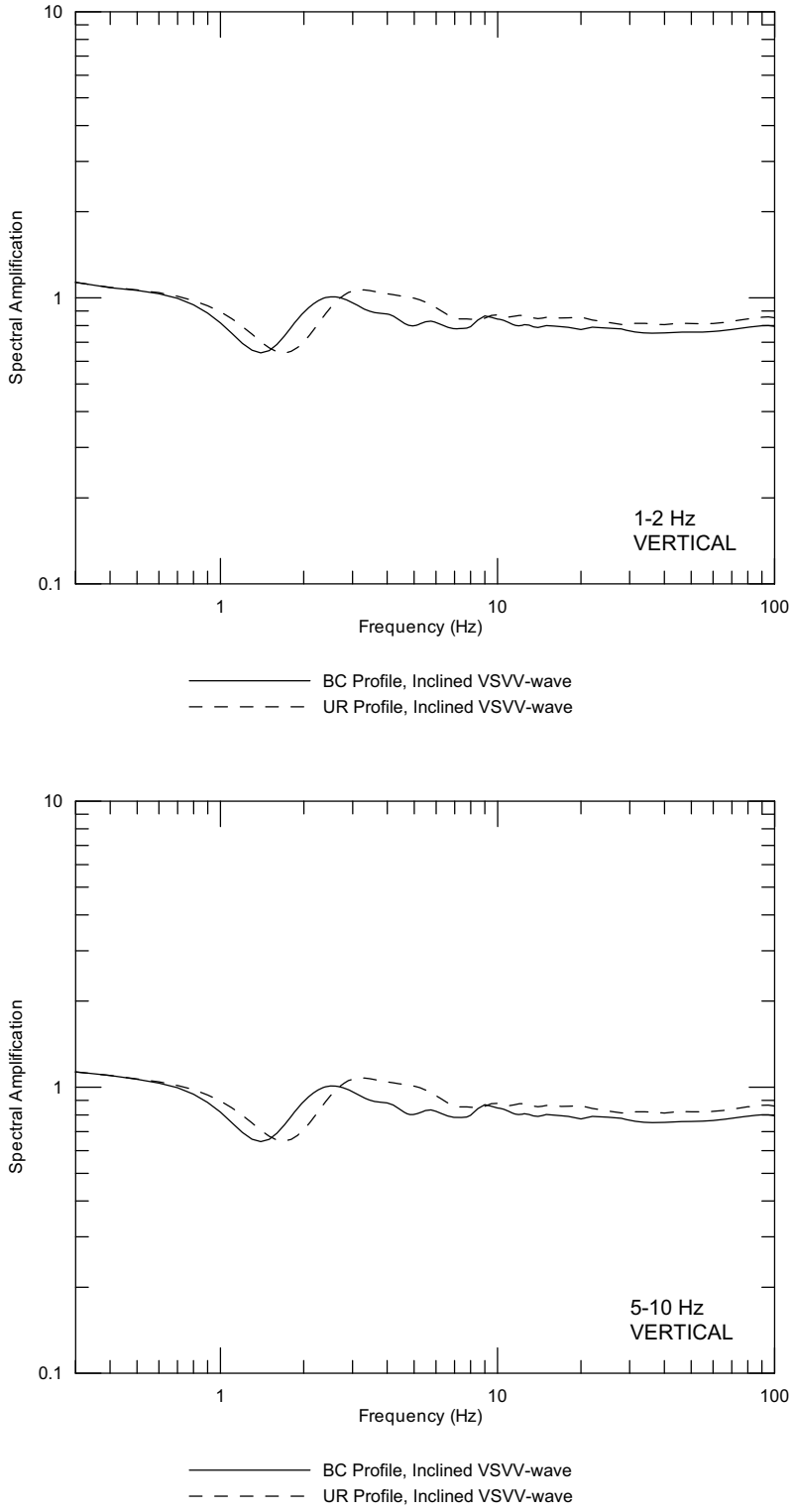

Source: Wong and Silva 2004a [DIRS 170443], Supplemental Record 60

Figure 6.3-46. Point B Vertical Magnitude-Weighted Mean SAF at an Annual Exceedance Frequency of 10^{-6}

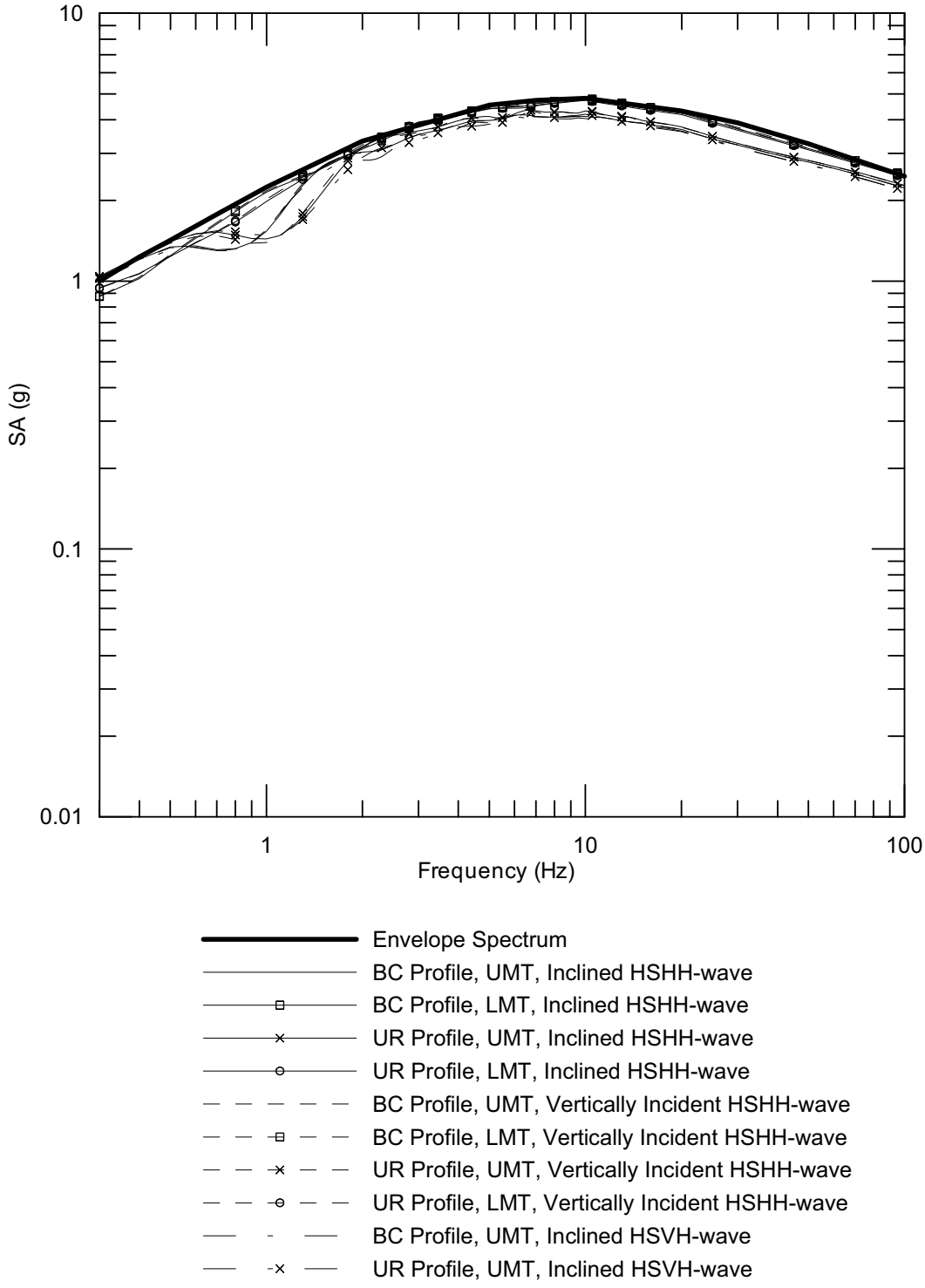

DTN: MO04065DSRSPTB.000 [DIRS 170506]

Source: Wong and Silva 2004a [DIRS 170443], Supplemental Record 60

Figure 6.3-47. Point B Horizontal Site-Specific Spectra and Postclosure Envelope Spectrum at an Annual Exceedance Frequency of 10^{-6}

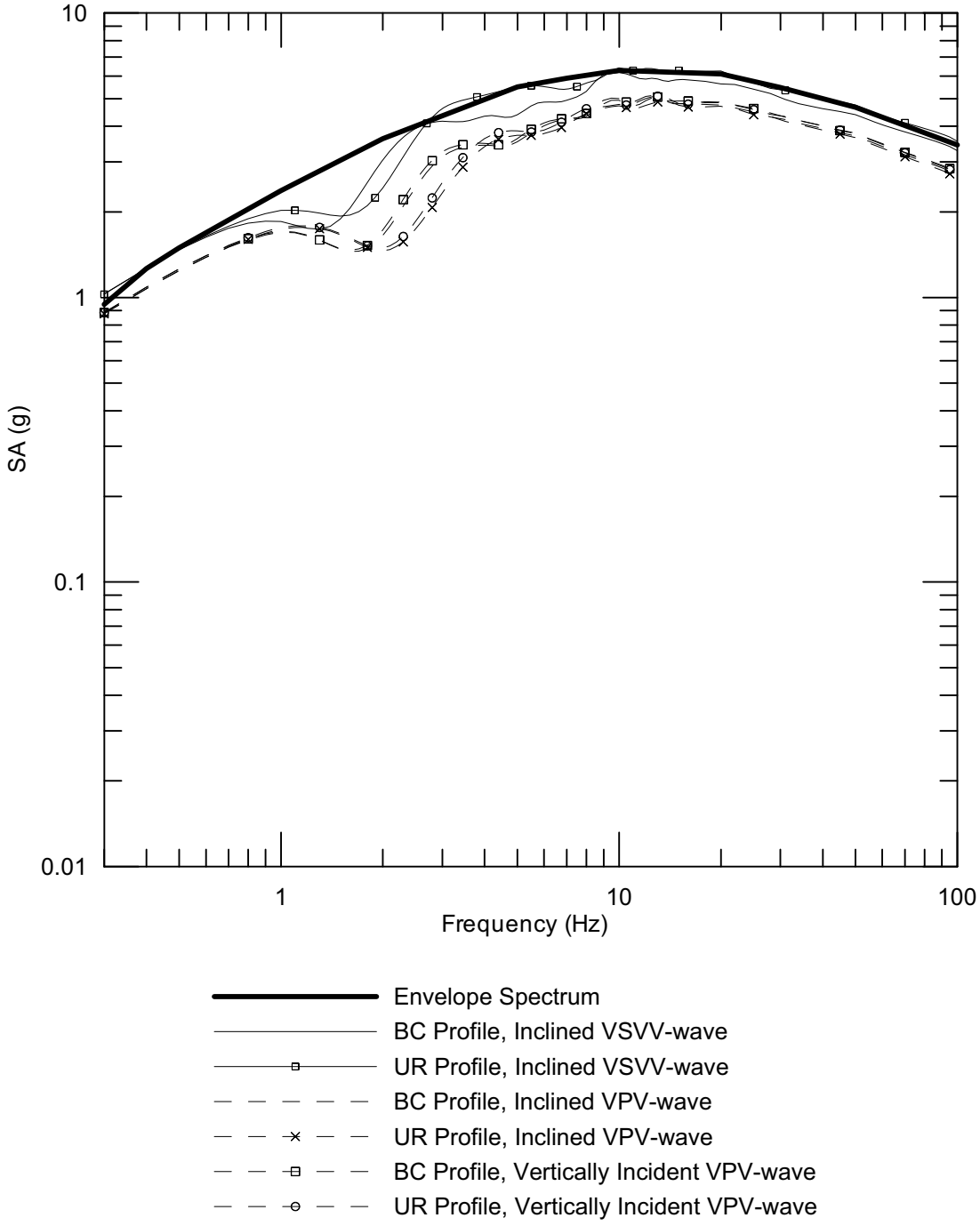

DTN: MO04065DSRSPTB.000 [DIRS 170506]

Source: Wong and Silva 2004a [DIRS 170443], Supplemental Record 60

Figure 6.3-48. Point B Vertical Site-Specific Spectra and Postclosure Envelope Spectrum at an Annual Exceedance Frequency of 10^{-6}

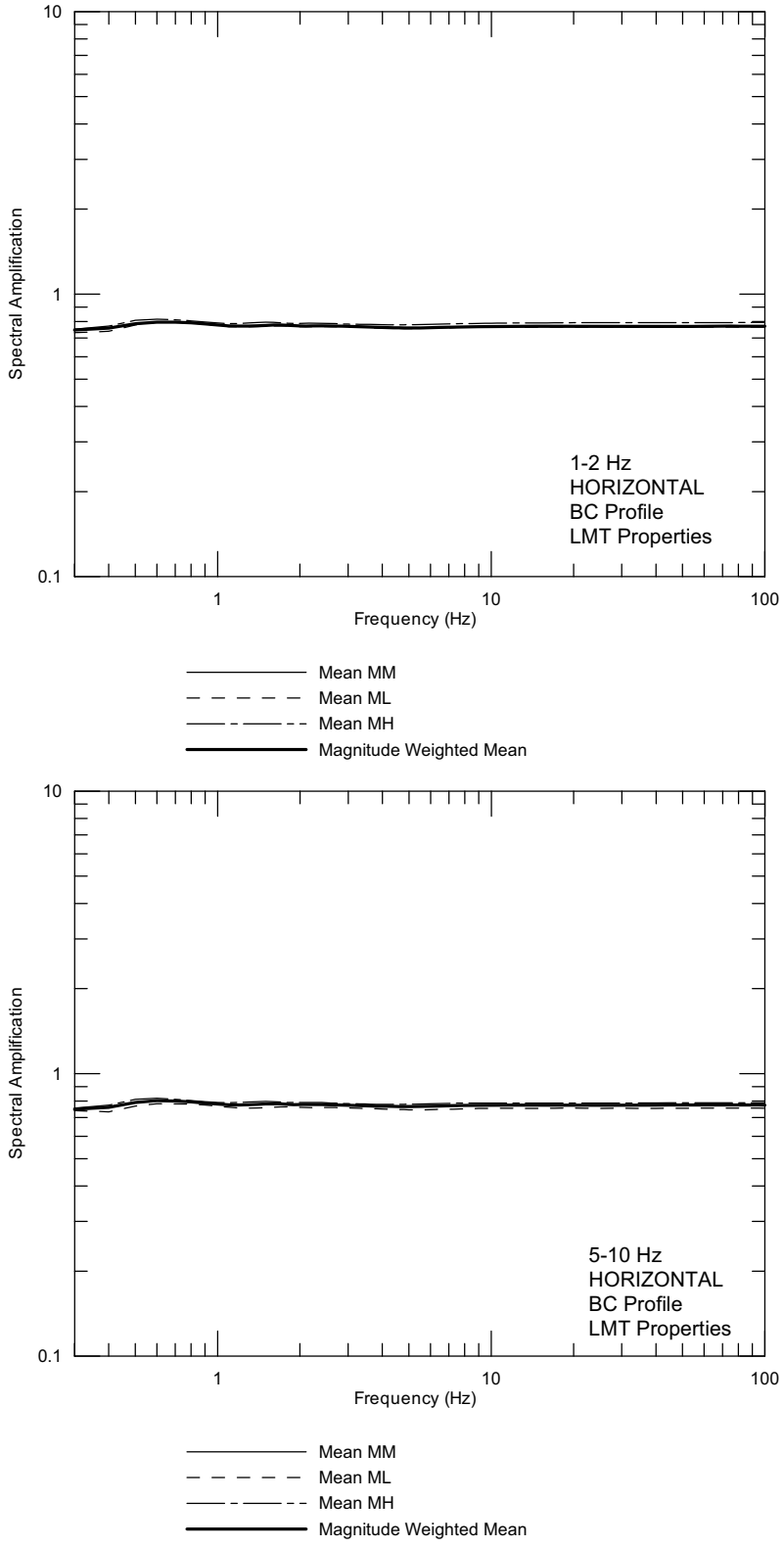

Source: Wong and Silva 2004a [DIRS 170443], Supplemental Record 69

Figure 6.3-49. Representative Point B Mean SAF s at an Annual Exceedance Frequency of 10^{-7}

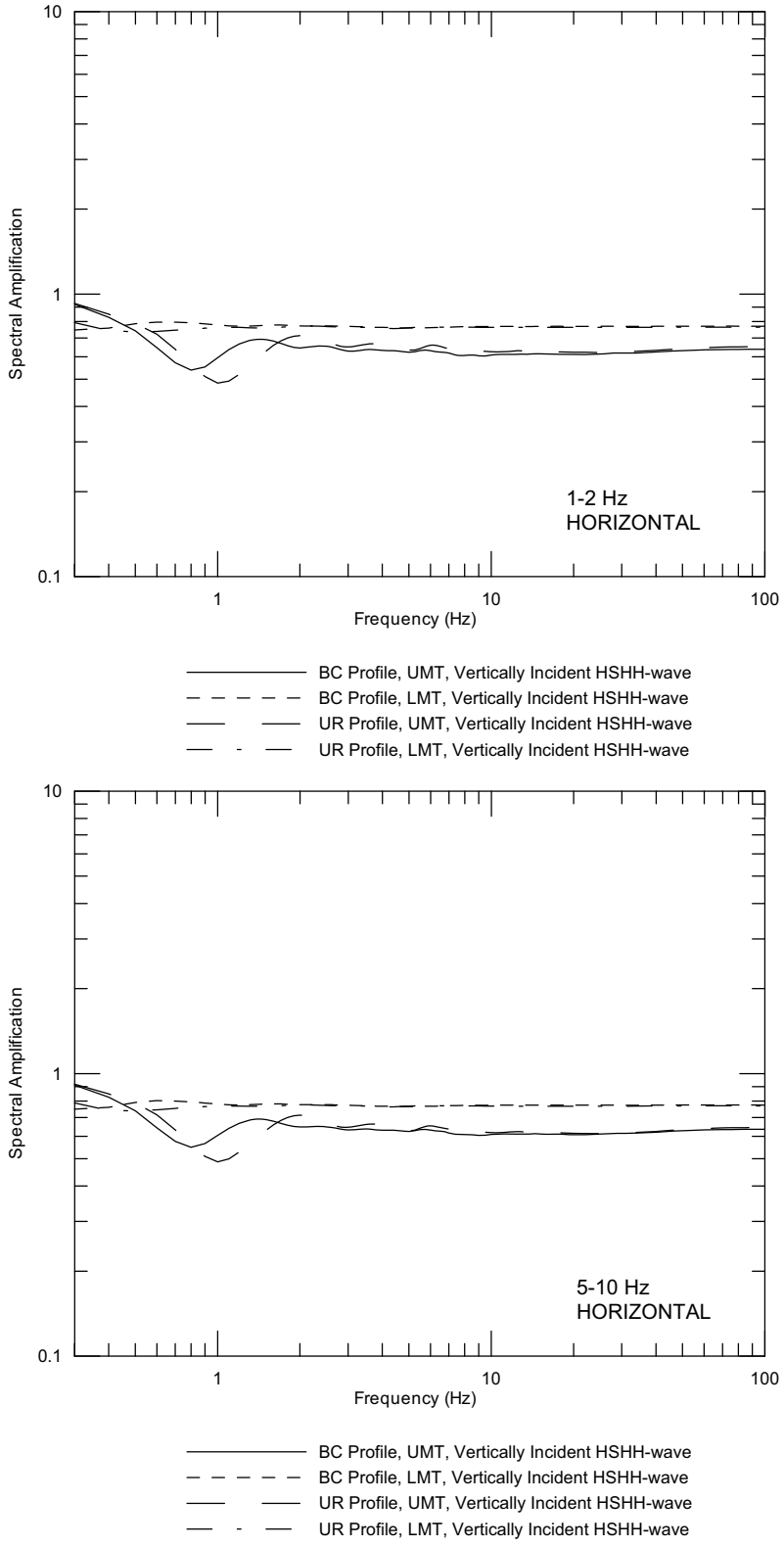

Source: Wong and Silva 2004a [DIRS 170443], Supplemental Record 69

Figure 6.3-50. Point B Horizontal Magnitude-Weighted Mean SAF at an Annual Exceedance Frequency of 10^{-7}

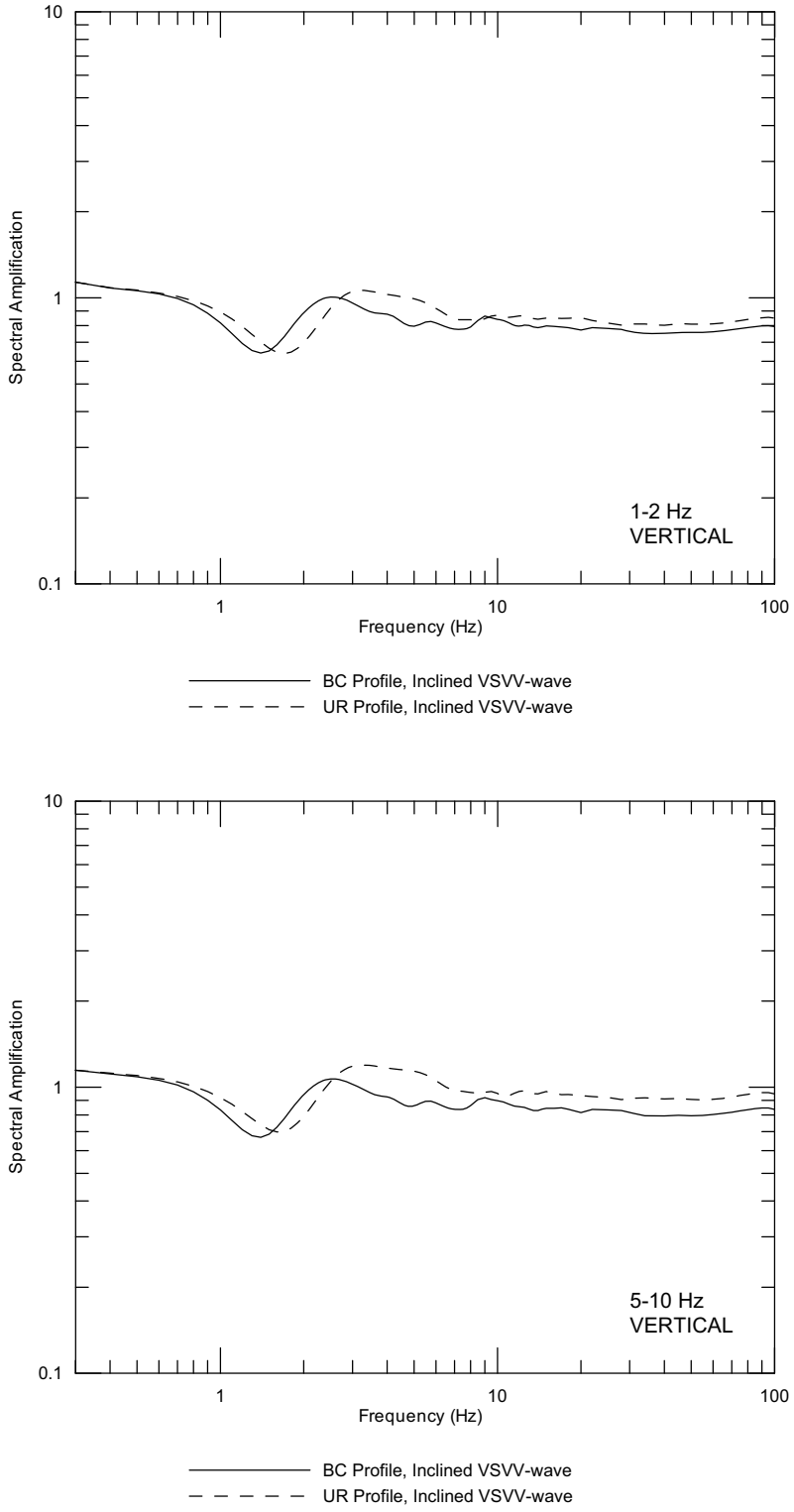

Source: Wong and Silva 2004a [DIRS 170443], Supplemental Record 69

Figure 6.3-51. Point B Vertical Magnitude-Weighted Mean SAF at an Annual Exceedance Frequency of 10^{-7}

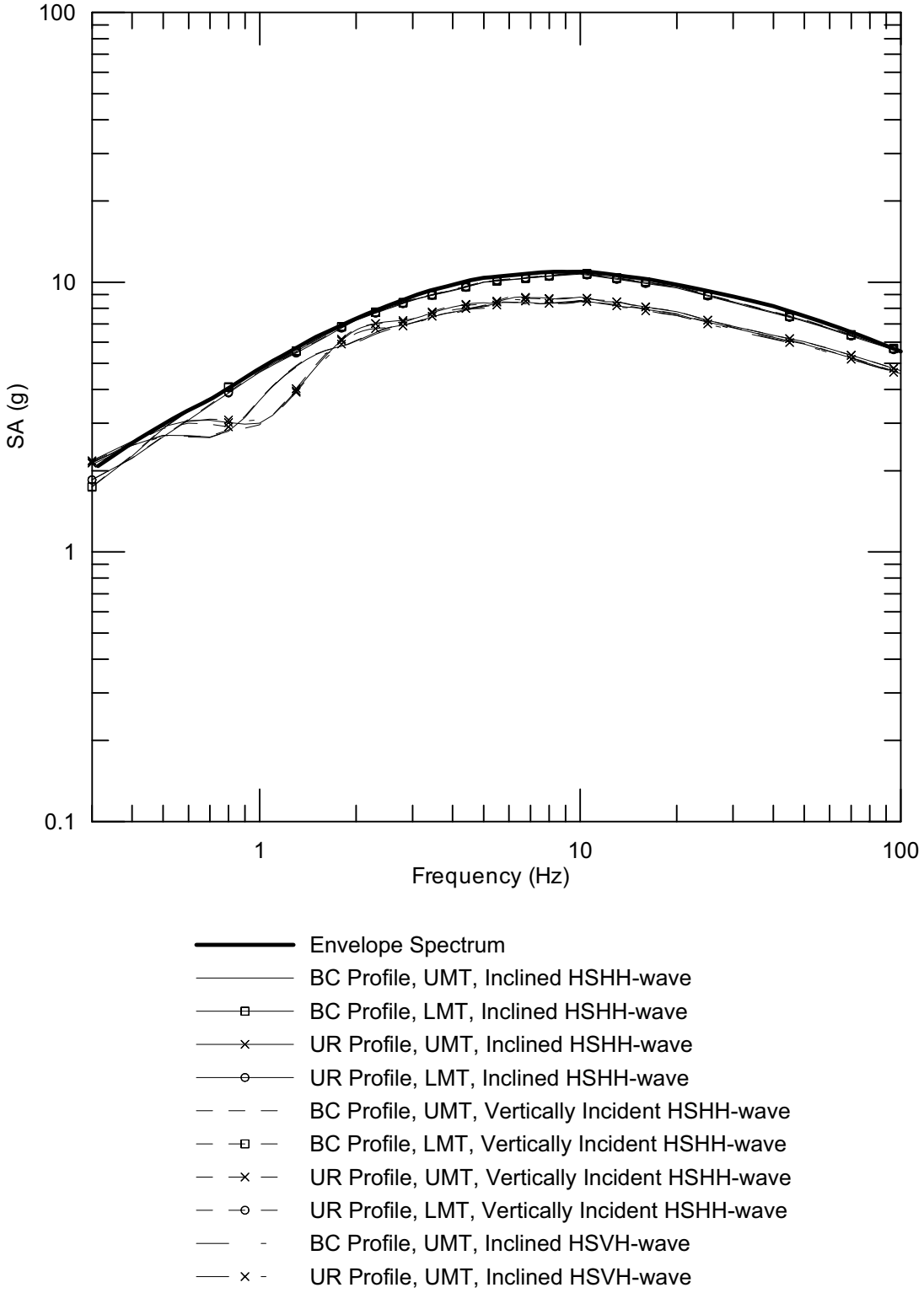

DTN: MO0403AVTMH107.003 [DIRS 168892]

Source: Wong and Silva 2004a [DIRS 170443], Supplemental Record 69

Figure 6.3-52. Point B Horizontal Site-Specific Spectra and Postclosure Envelope Spectrum at an Annual Exceedance Frequency of 10^{-7}

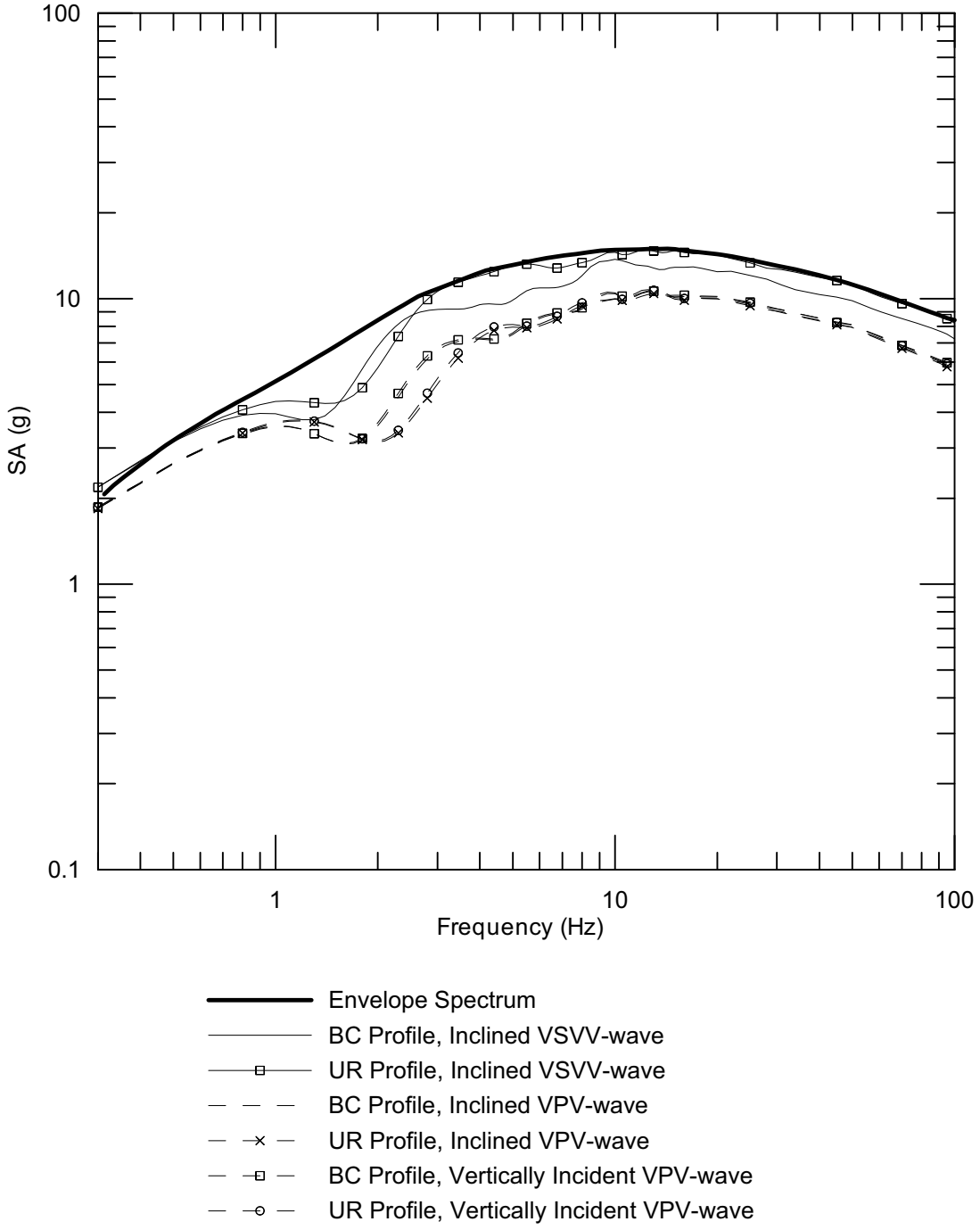

DTN: MO0403AVTMH107.003 [DIRS 168892]

Source: Wong and Silva 2004a [DIRS 170443], Supplemental Record 69

Figure 6.3-53. Point B Vertical Site-Specific Spectra and Postclosure Envelope Spectrum at an Annual Exceedance Frequency of 10^{-7}

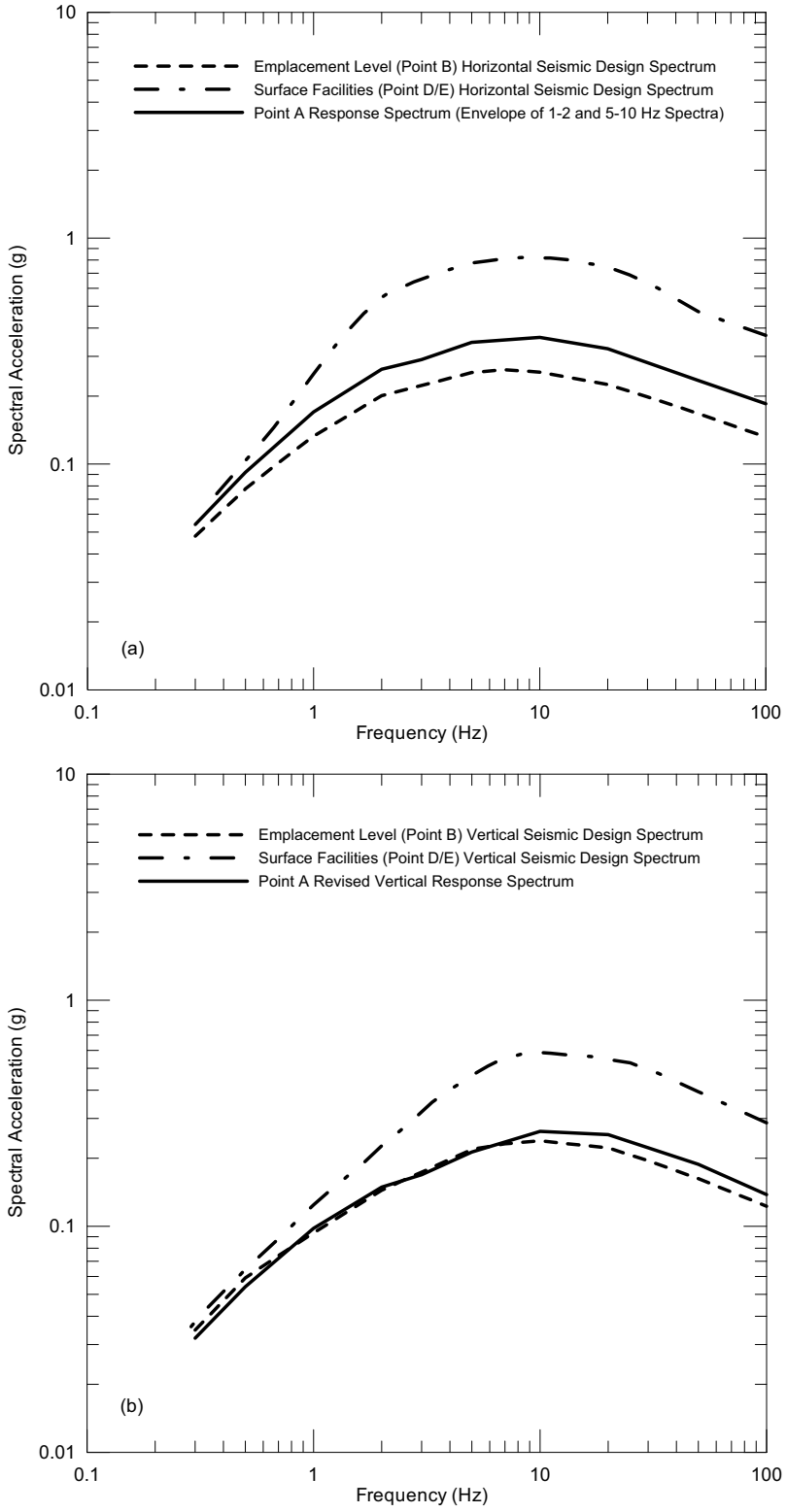

DTN: MO0401MWDRPSHA.000 [DIRS 166962] (Point A), MO0405SDSTPNTB.001 [DIRS 169851] (Point B), MO0410SDSDE103.002 [DIRS 172236] (Point D/E)

Figure 6.3-54. Response Spectra at Points A, B, and D/E for Annual Exceedance Frequency of 10^{-3}, (a) Horizontal Component, (b) Vertical Component

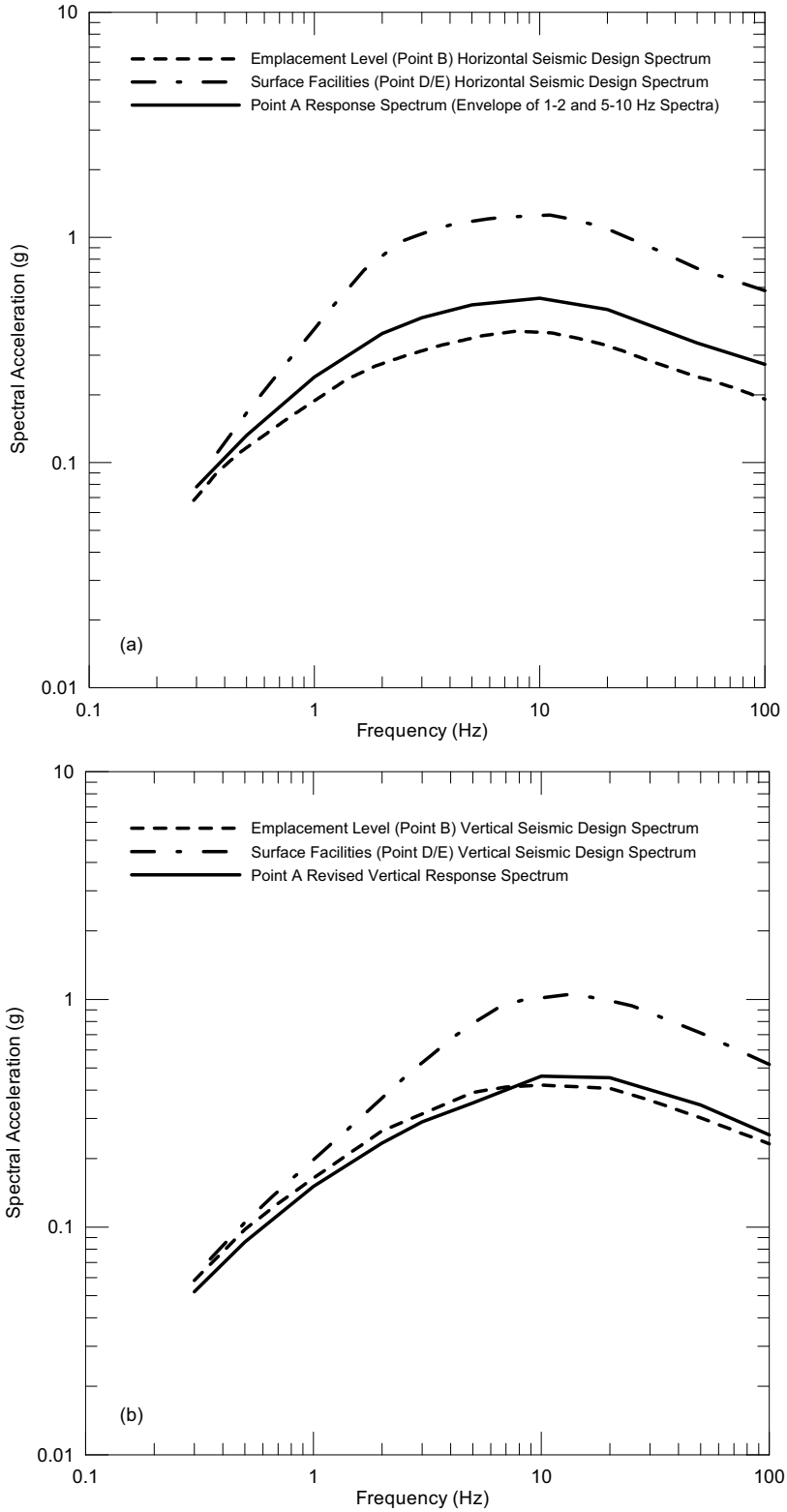

DTN: MO0208UNHZ5X10.000 [DIRS 163722] (Point A), MO0407SDARS104.001 [DIRS 170683] (Point B), MO0410SDSTMHIS.005 [DIRS 172237] (Point D/E)

Figure 6.3-55. Response Spectra at Points A, B, and D/E for Annual Exceedance Frequency of 5×10^{-4}, (a) Horizontal Component, (b) Vertical Component

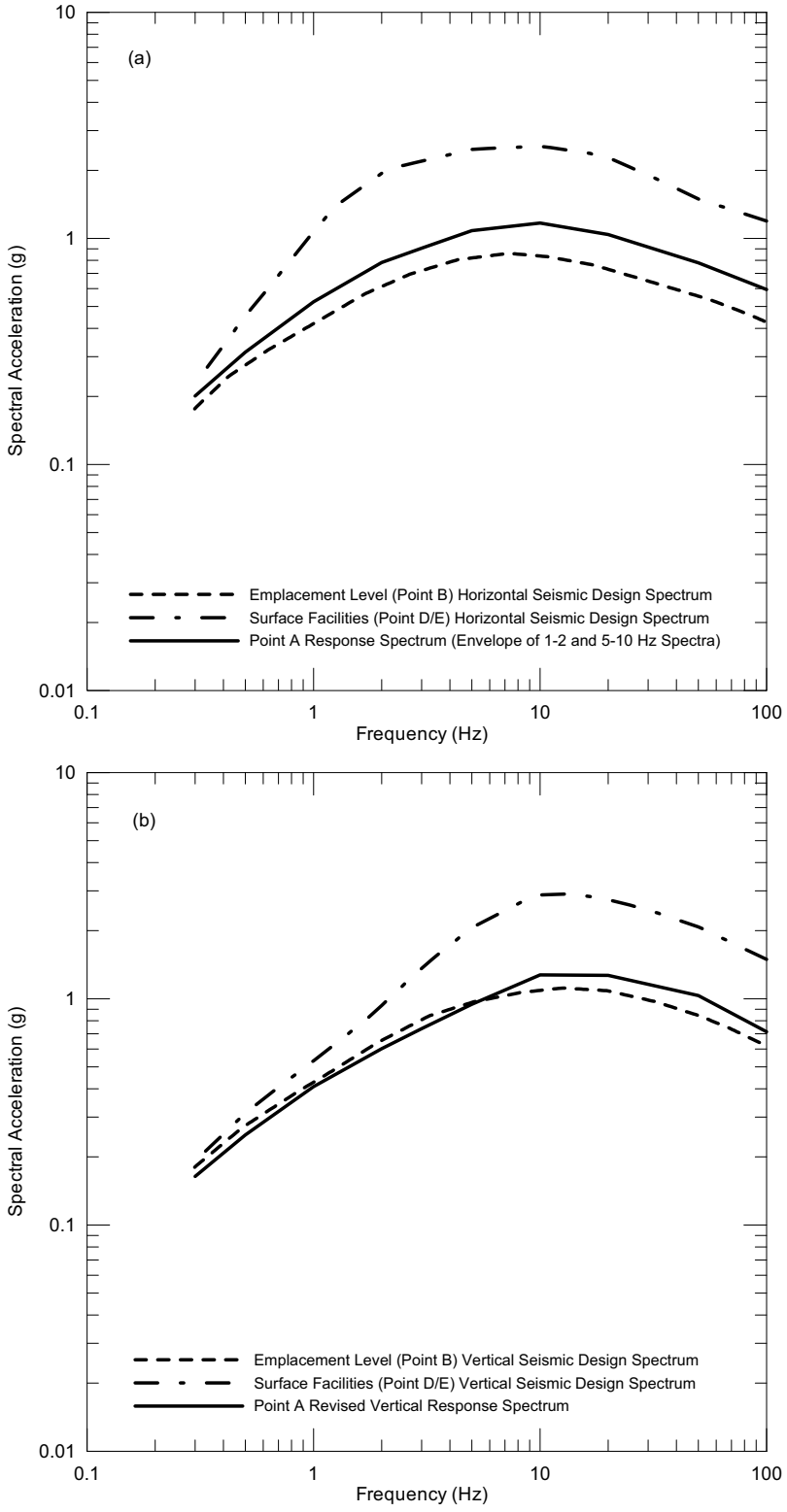

DTN: MO0401MWDRPSHA.000 [DIRS 166962] (Point A), MO0306SDSAVDTH.000 [DIRS 164033] (Point B), MO0410WHBDF104.002 [DIRS 172238] (Point D/E)

Figure 6.3-56. Response Spectra at Points A, B, and D/E for Annual Exceedance Frequency of 10^{-4}, (a) Horizontal Component, (b) Vertical Component

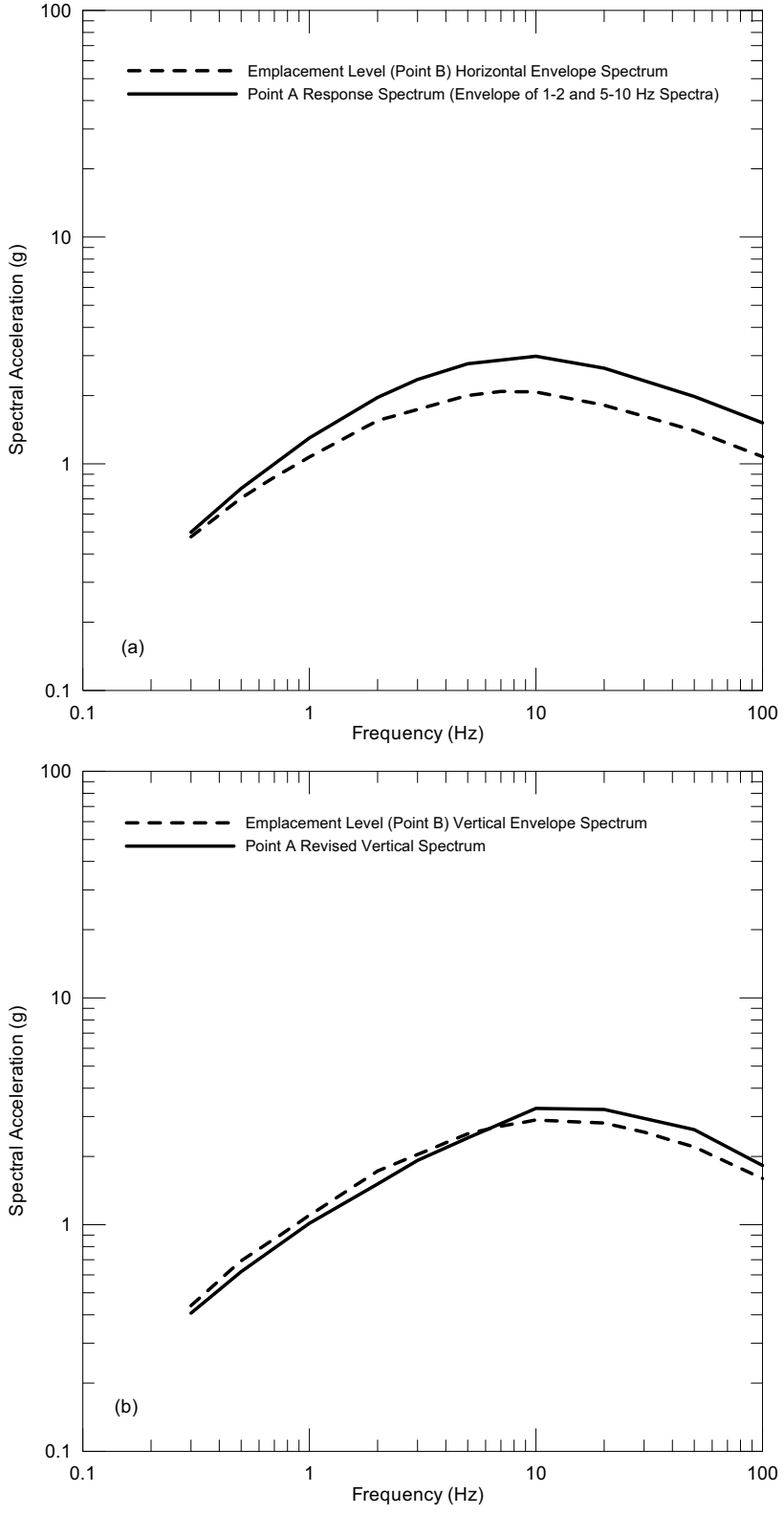

DTN: MO0308UNHAZ105.000 [DIRS 170425] (Point A), MO0312SEPRSRLB.019 [DIRS 170427] (Point B)

Figure 6.3-57. Response Spectra at Points A and B for Annual Exceedance Frequency of 10^{-5}, (a) Horizontal Component, (b) Vertical Component

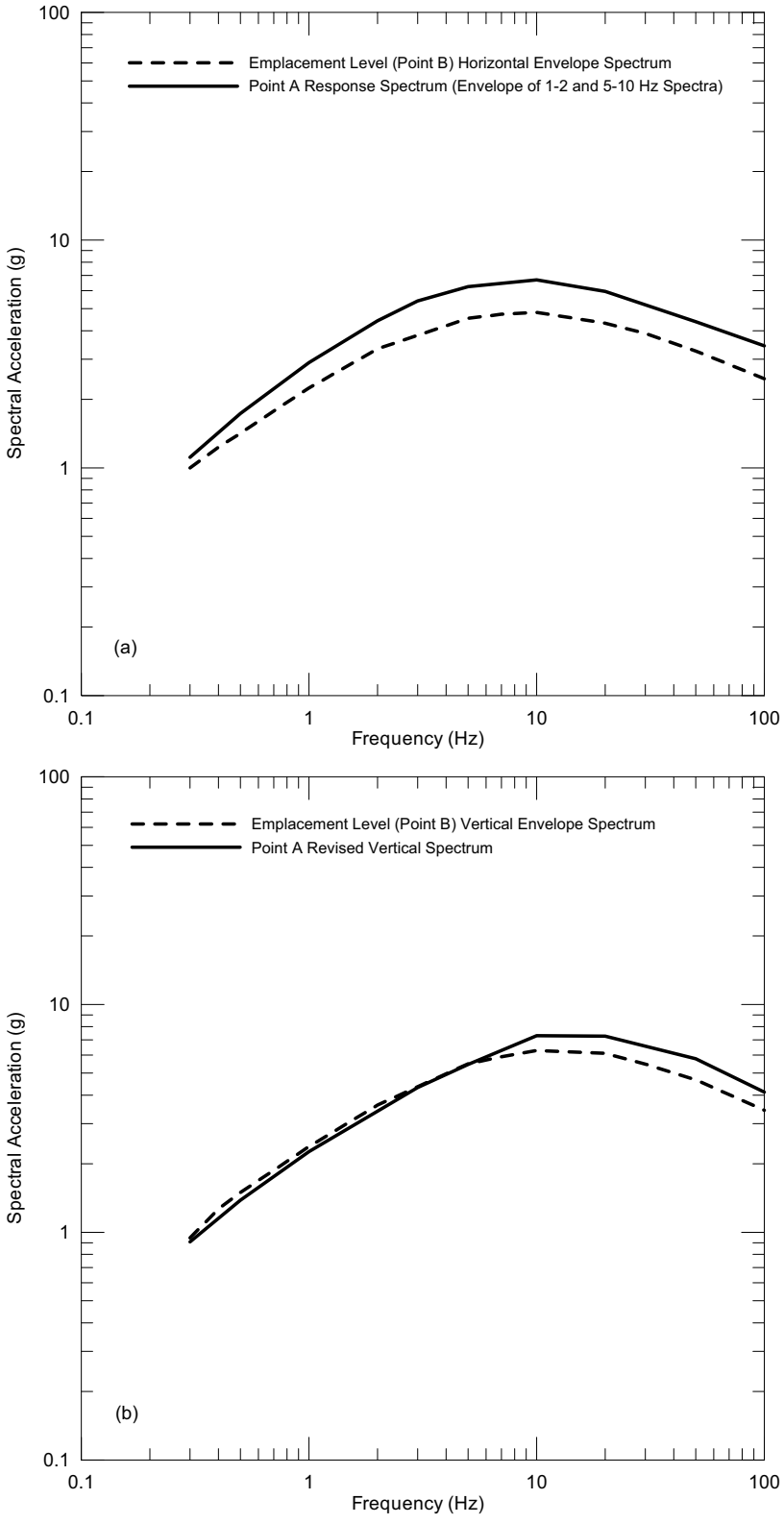

DTN: MO0206UNHAZ106.001 [DIRS 163723] (Point A), MO04065DSRSPTB.000 [DIRS 170506] (Point B)

Figure 6.3-58. Response Spectra at Points A and B for Annual Exceedance Frequency of 10^{-6}, (a) Horizontal Component, (b) Vertical Component

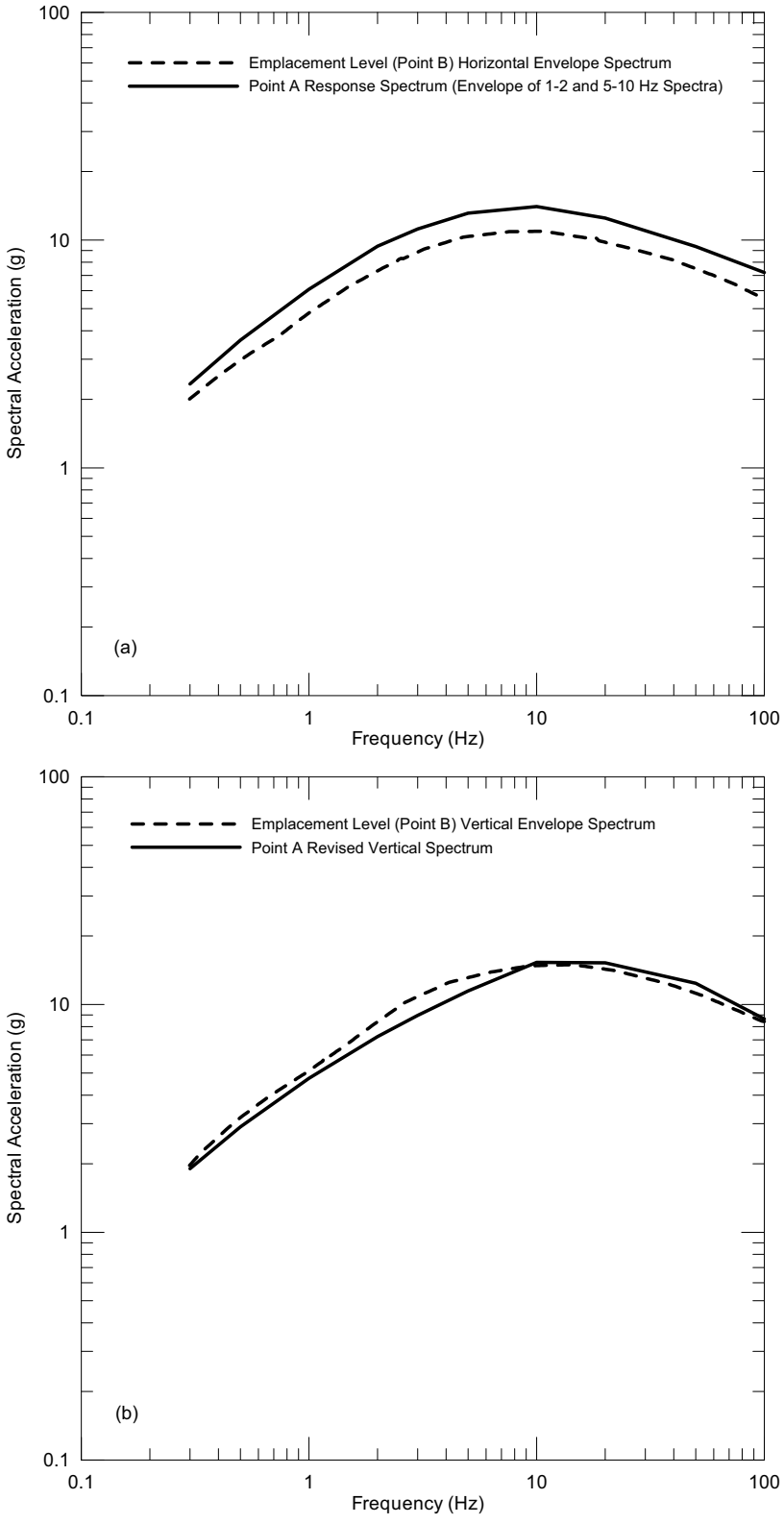

DTN: MO0209UNHAZ107.000 [DIRS 163724] (Point A), MO0403AVTMH107.003 [DIRS 168892] (Point B)

Figure 6.3-59. Response Spectra at Points A and B for Annual Exceedance Frequency of 10^{-7}, (a) Horizontal Component, (b) Vertical Component

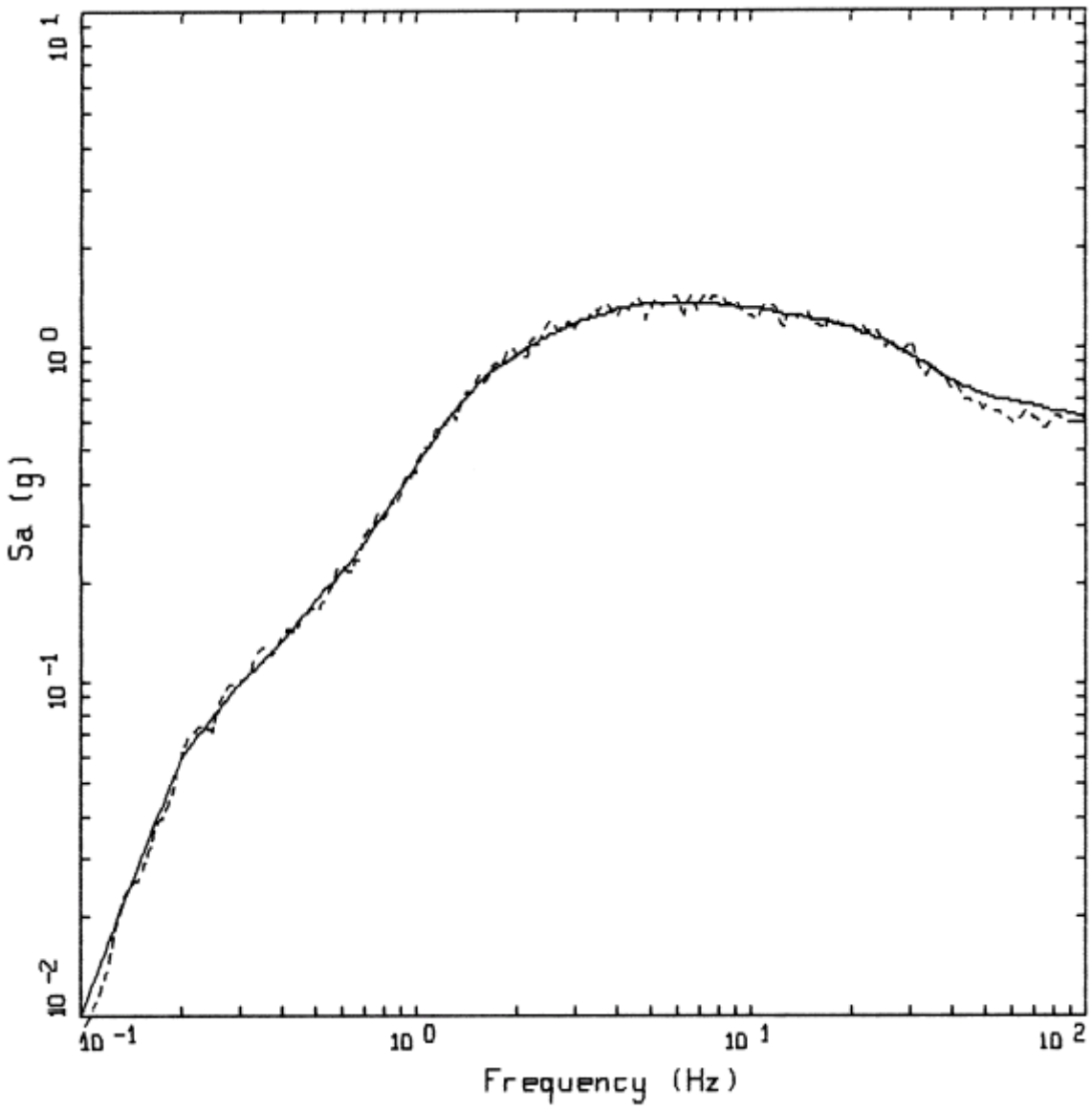

Figure 6.3-60. Example of Spectral Matching of Individual Time Histories

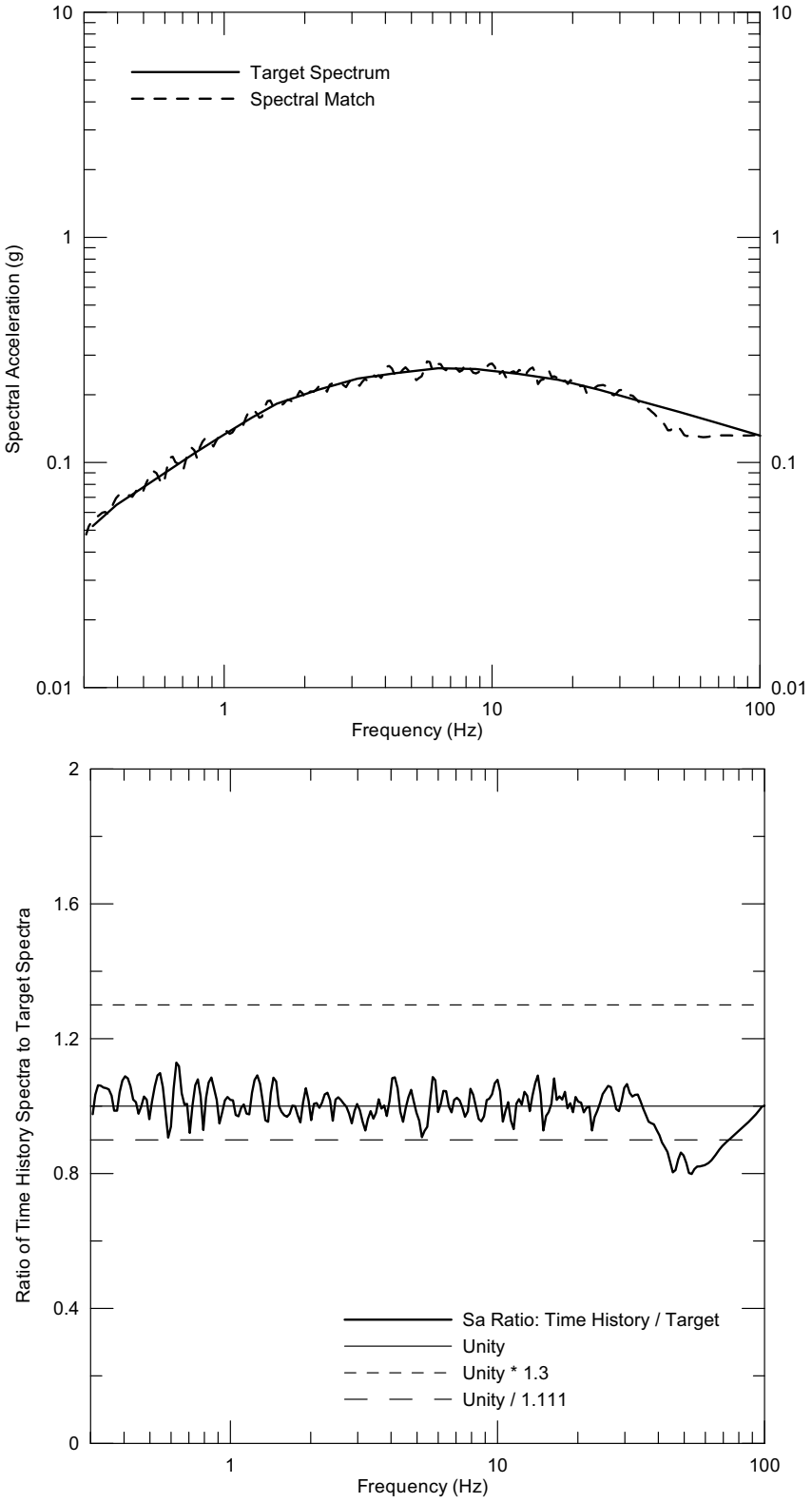

Source: Wong and Silva 2004a [DIRS 170443], Supplemental Record 110, Pages 6 & 8

Figure 6.3-61. Response Spectrum of Point B 10^{-3} Horizontal-1 Time History and Seismic Design Target Spectrum

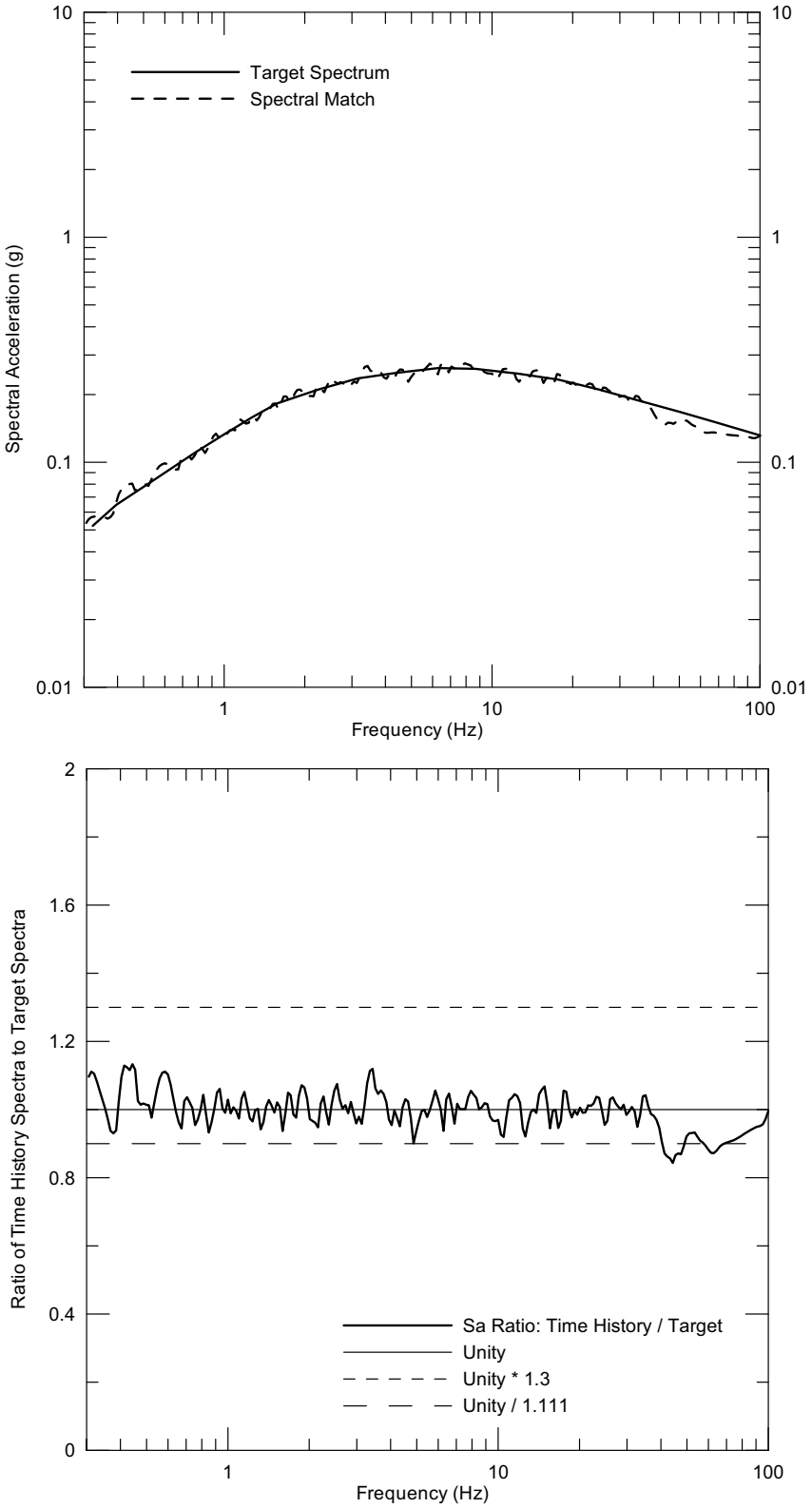

Source: Wong and Silva 2004a [DIRS 170443], Supplemental Record 110, Pages 10 & 12

Figure 6.3-62. Response Spectrum of Point B 10^{-3} Horizontal-2 Time History and Seismic Design Target Spectrum

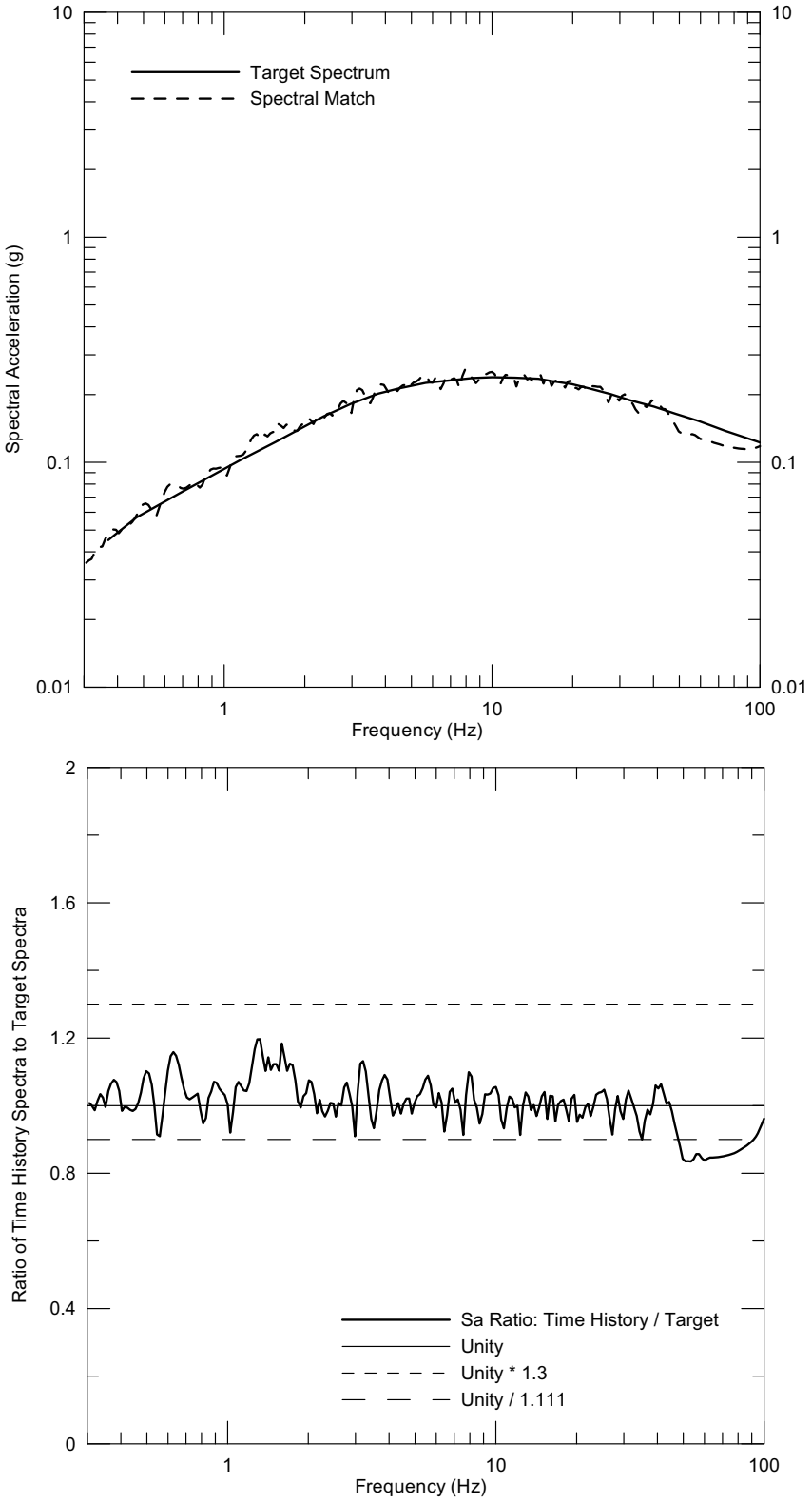

Source: Wong and Silva 2004a [DIRS 170443], Supplemental Record 120, Pages 20 & 22

Figure 6.3-63. Response Spectra of Point B 10^{-3} Vertical Time History and Seismic Design Target Spectrum

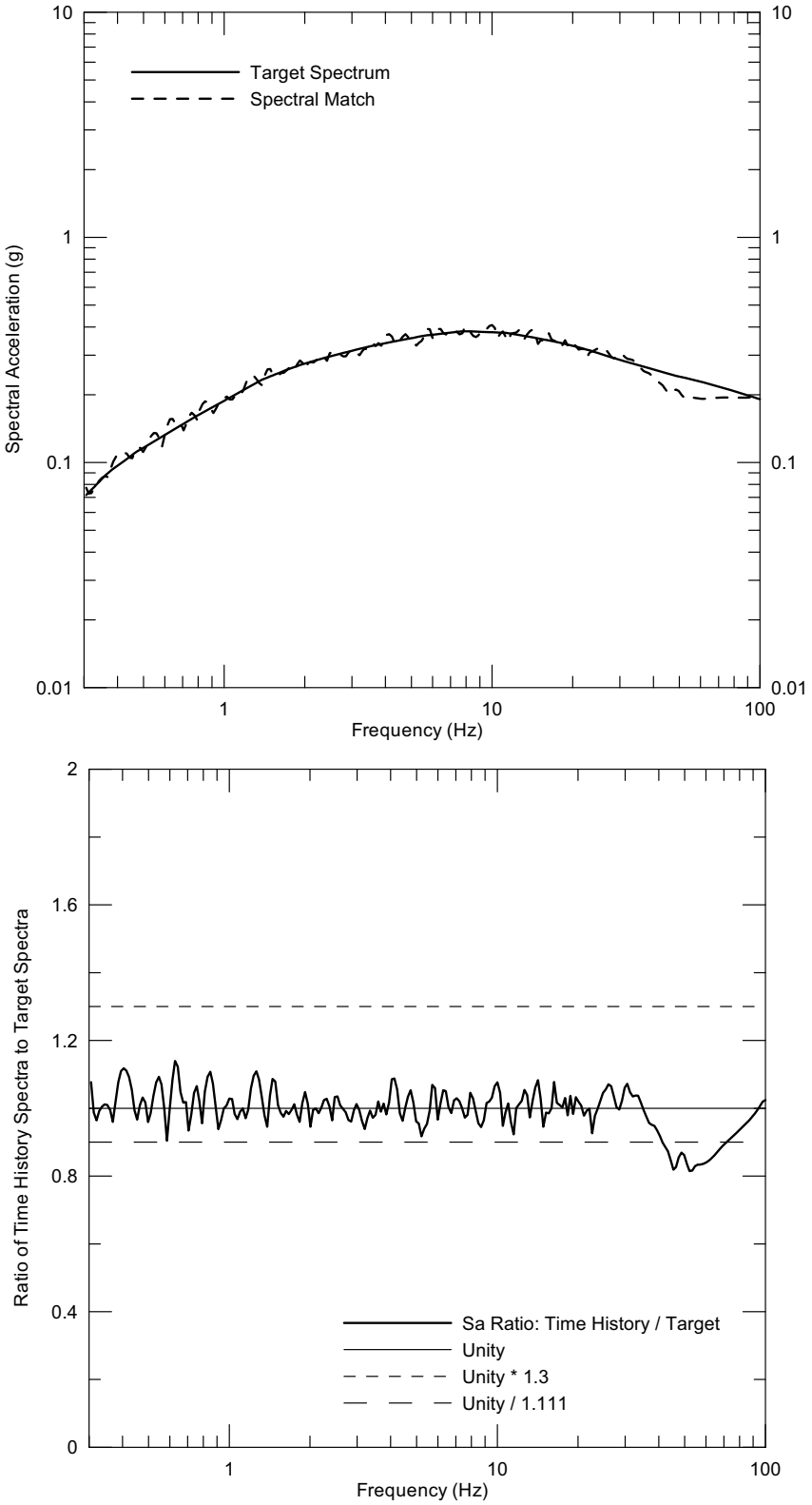

Source: Wong and Silva 2004a [DIRS 170443], SR-58, page 44 & 46

Figure 6.3-64. Response Spectrum of Point B 5x10 $^{-4}$ Horizontal-1 Time History and Seismic Design Target Spectrum

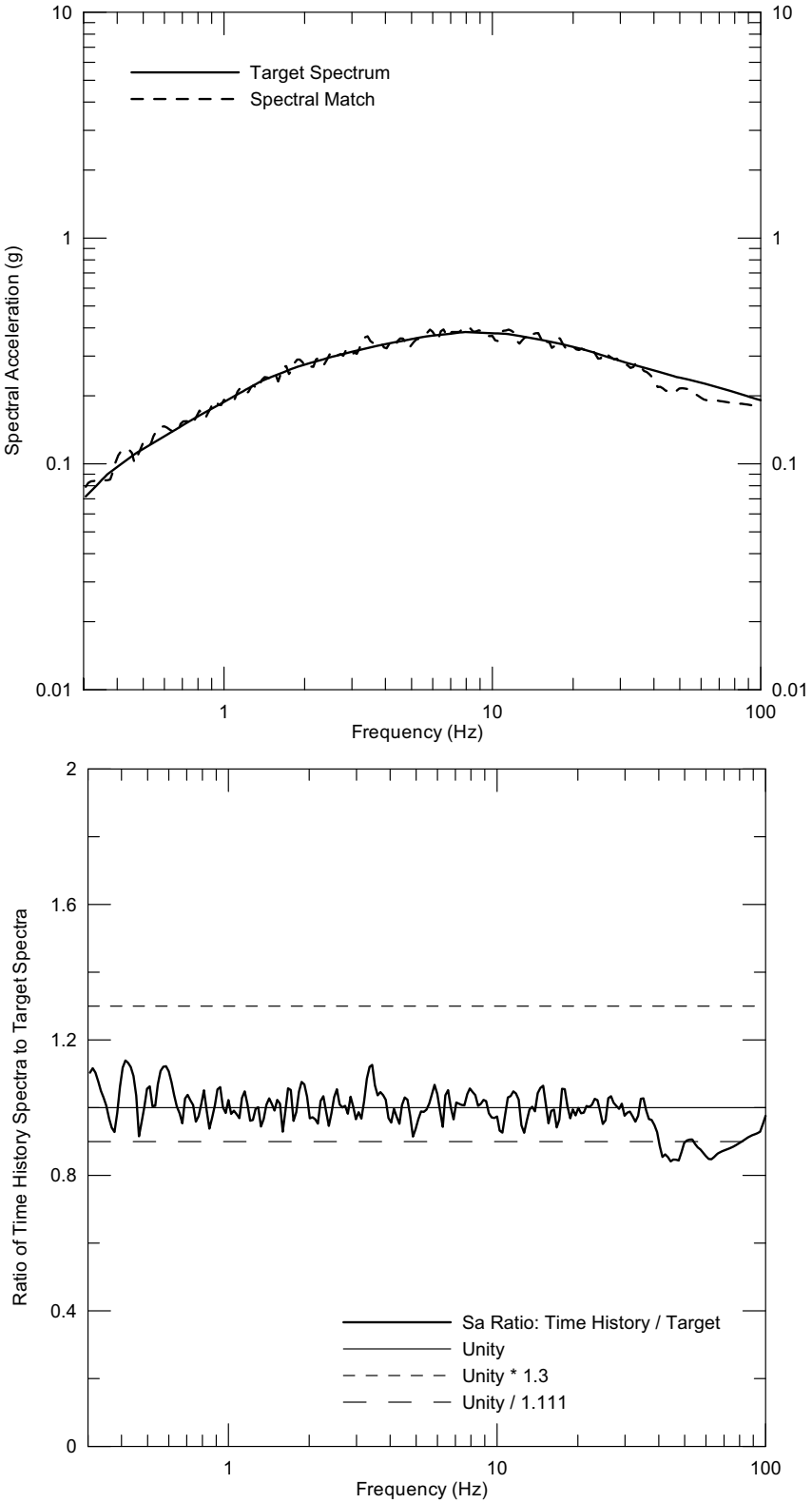

Source: Wong and Silva 2004a [DIRS 170443], SR-58, page 48 & 50

Figure 6.3-65. Response Spectrum of Point B 5x10 $^{-4}$ Horizontal-2 Time History and Seismic Design Target Spectrum

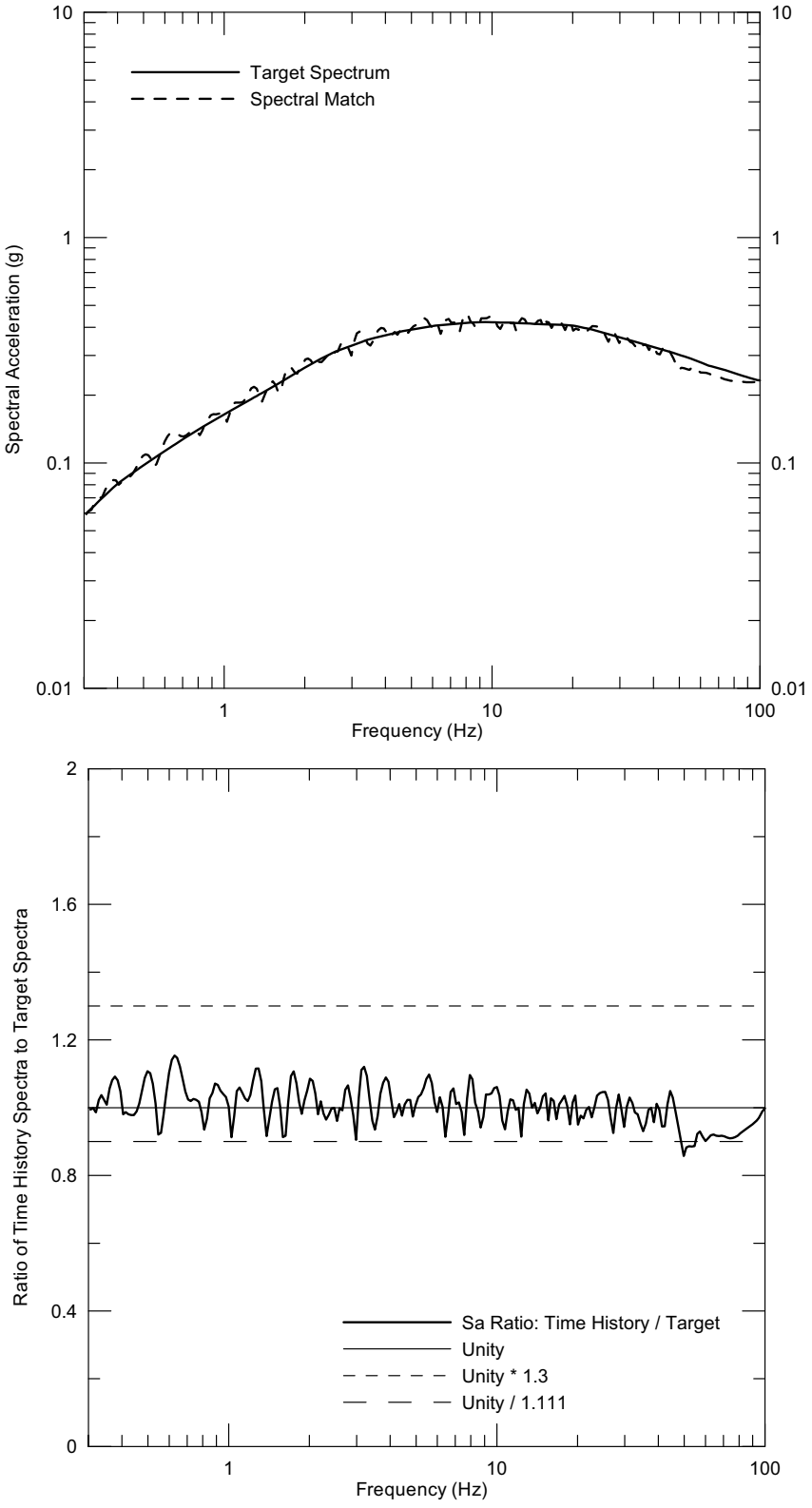

Source: Wong and Silva 2004a [DIRS 170443], SR-58, page 53 & 55

Figure 6.3-66. Response Spectra of Point B 5x10 $^{-4}$ Vertical Time History and Seismic Design Target Spectrum

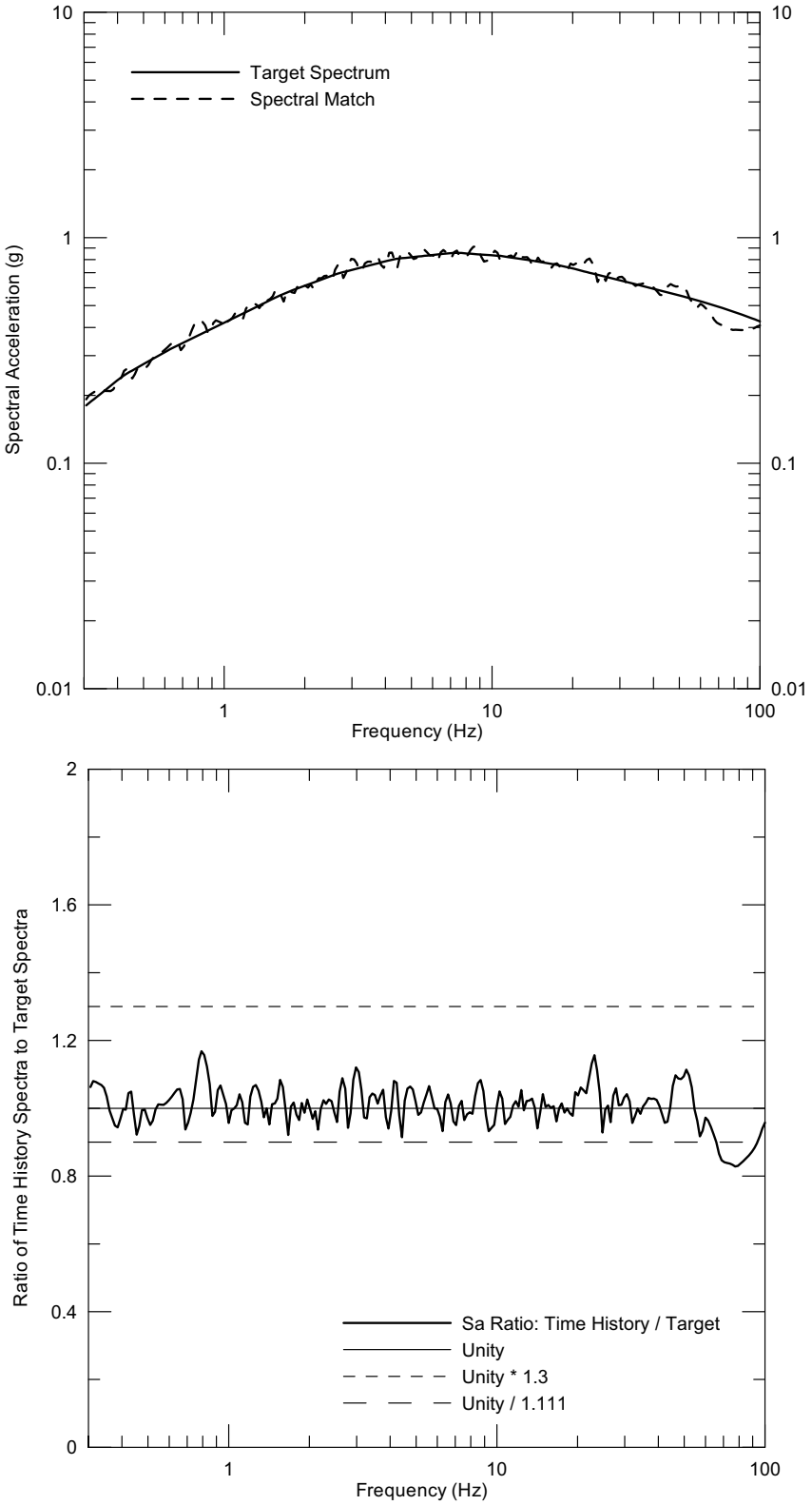

Source: Wong and Silva 2004a [DIRS 170443], Supplemental Record 78, Pages 4 & 6

Figure 6.3-67. Response Spectrum of Point B 10^{-4} Horizontal-1 Time History and Seismic Design Target Spectrum

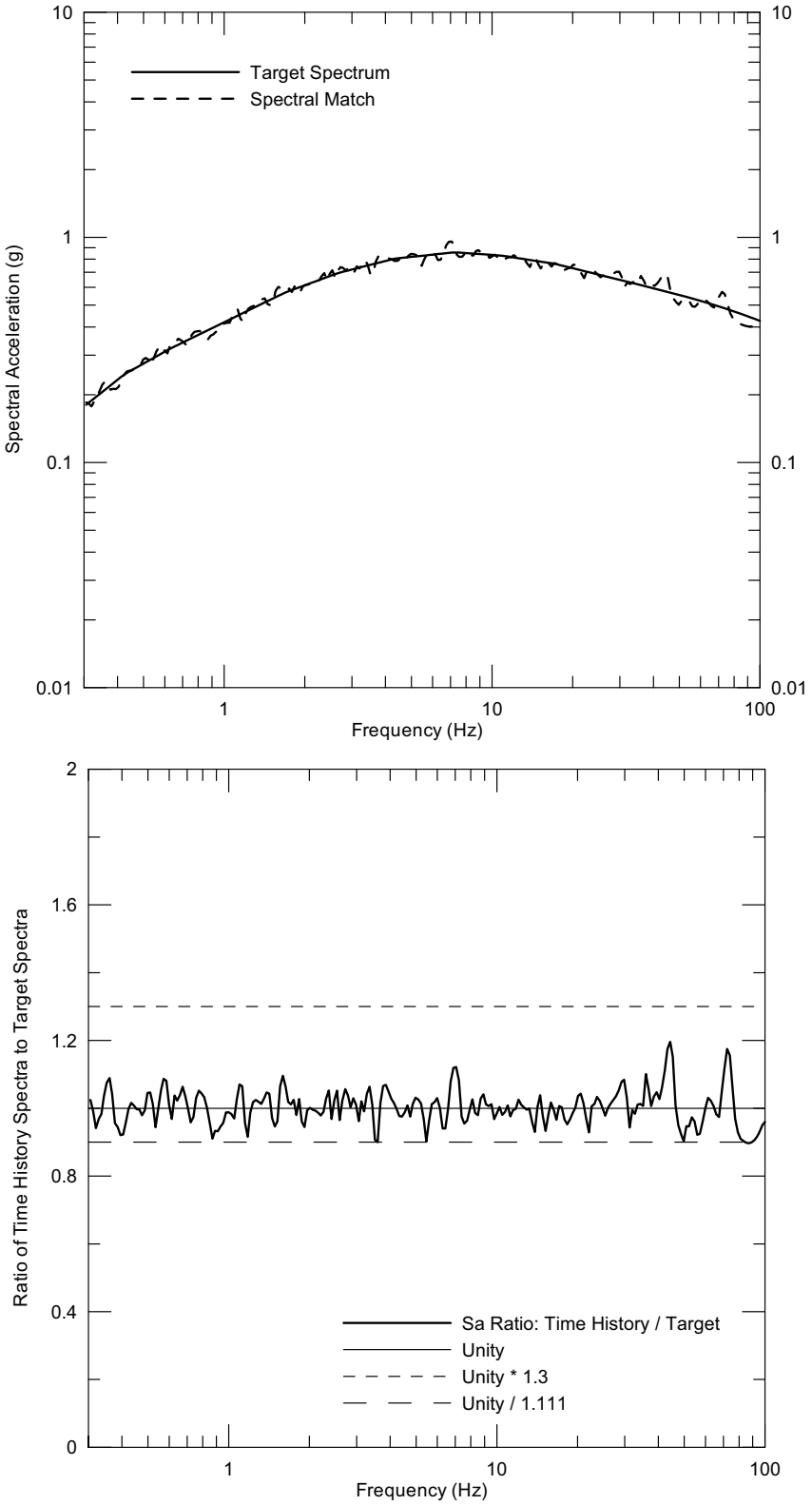

Source: Wong and Silva 2004a [DIRS 170443], Supplemental Record 78, Pages 7 & 9

Figure 6.3-68. Response Spectrum of Point B 10^{-4} Horizontal-2 Time History and Seismic Design Target Spectrum

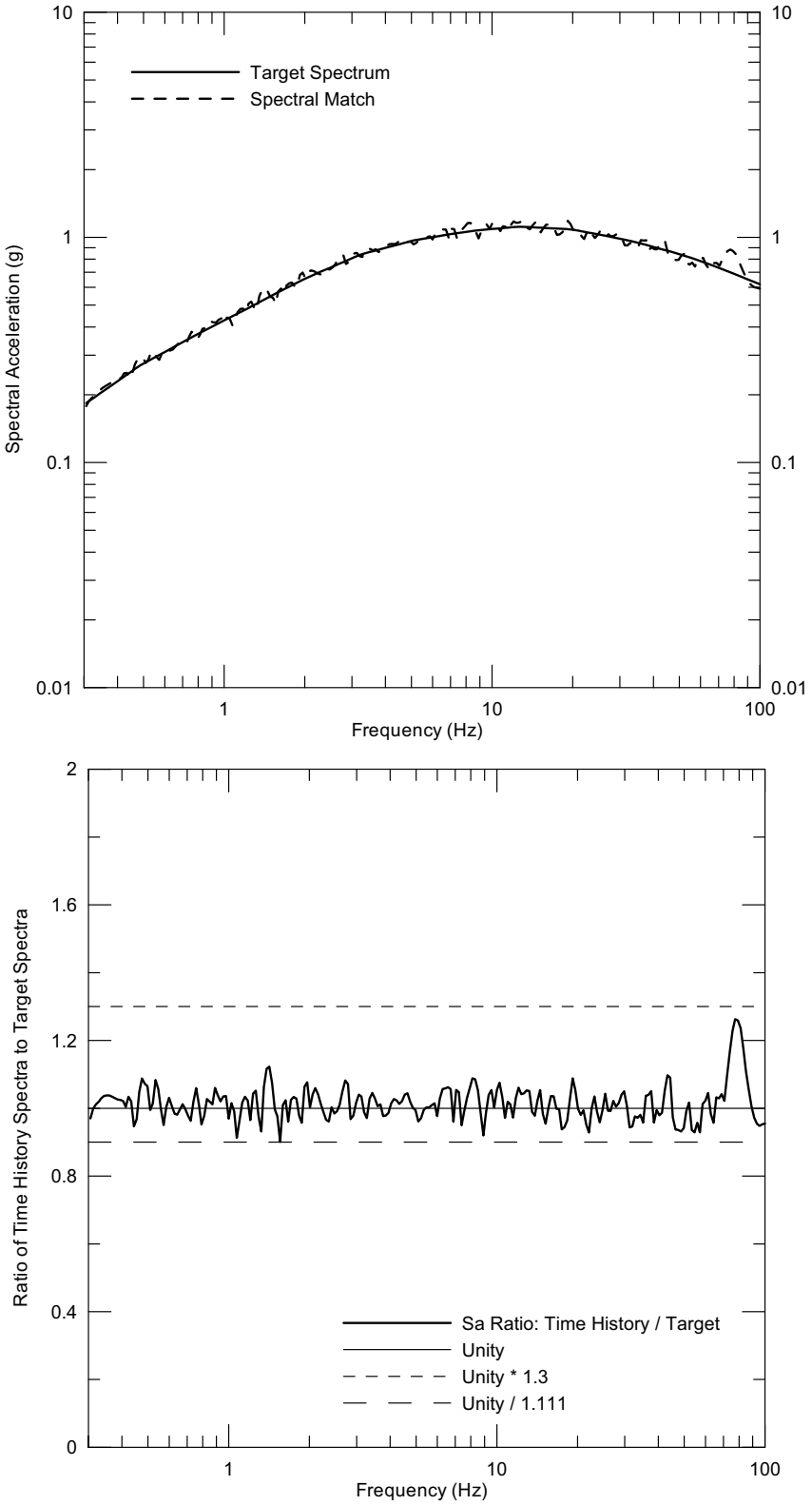

Source: Wong and Silva 2004a [DIRS 170443], Supplemental Record 78, Pages 12 & 14

Figure 6.3-69. Response Spectra of Point B 10^{-4} Vertical Time History and Seismic Design Target Spectrum

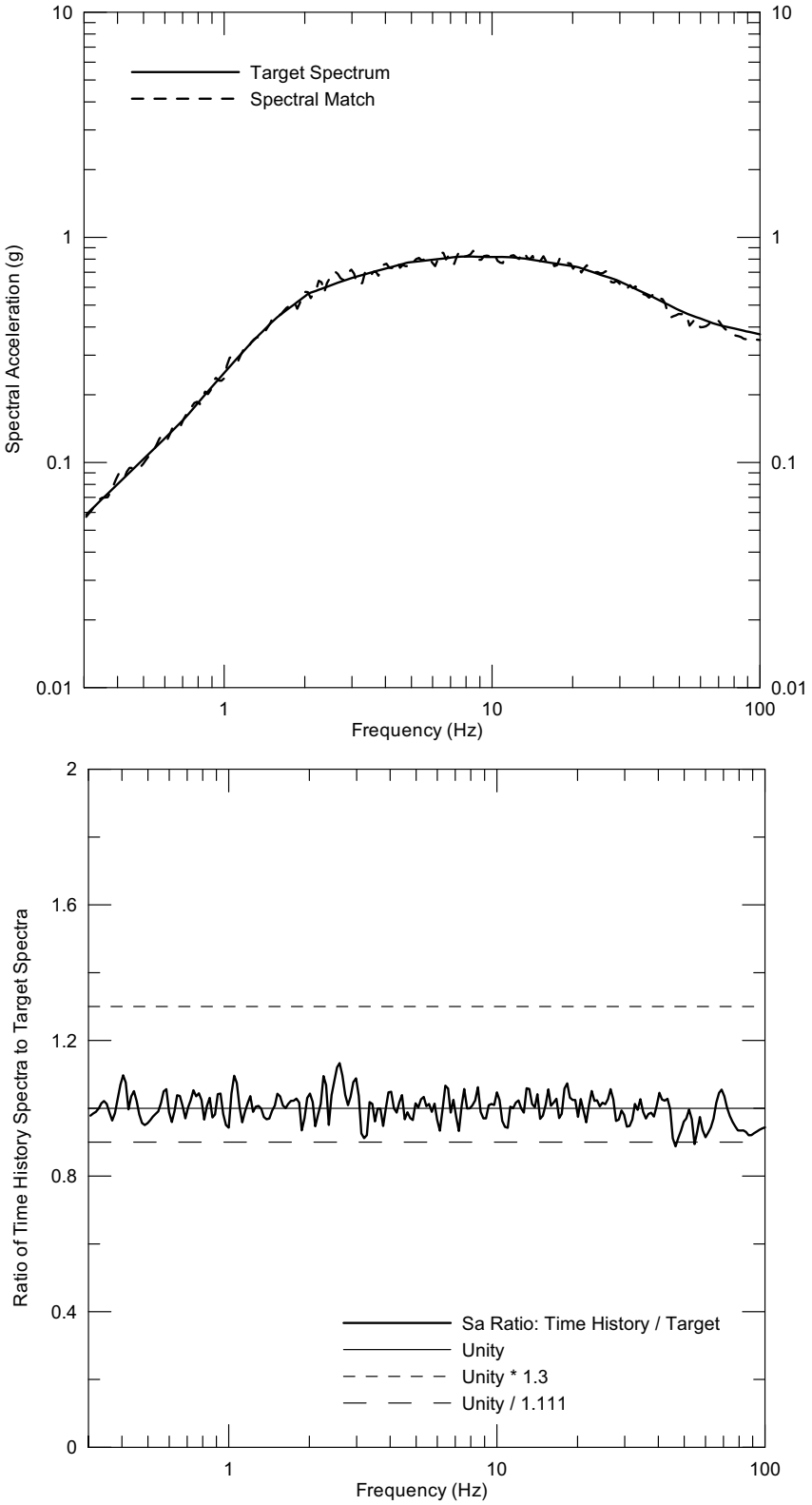

Source: Wong and Silva 2004a [DIRS 170443], Supplemental Record 107, Pages 6 & 7

Figure 6.3-70. Response Spectrum of Point D/E 10^{-3} Horizontal-1 Time History No. 1 and Seismic Design Target Spectrum

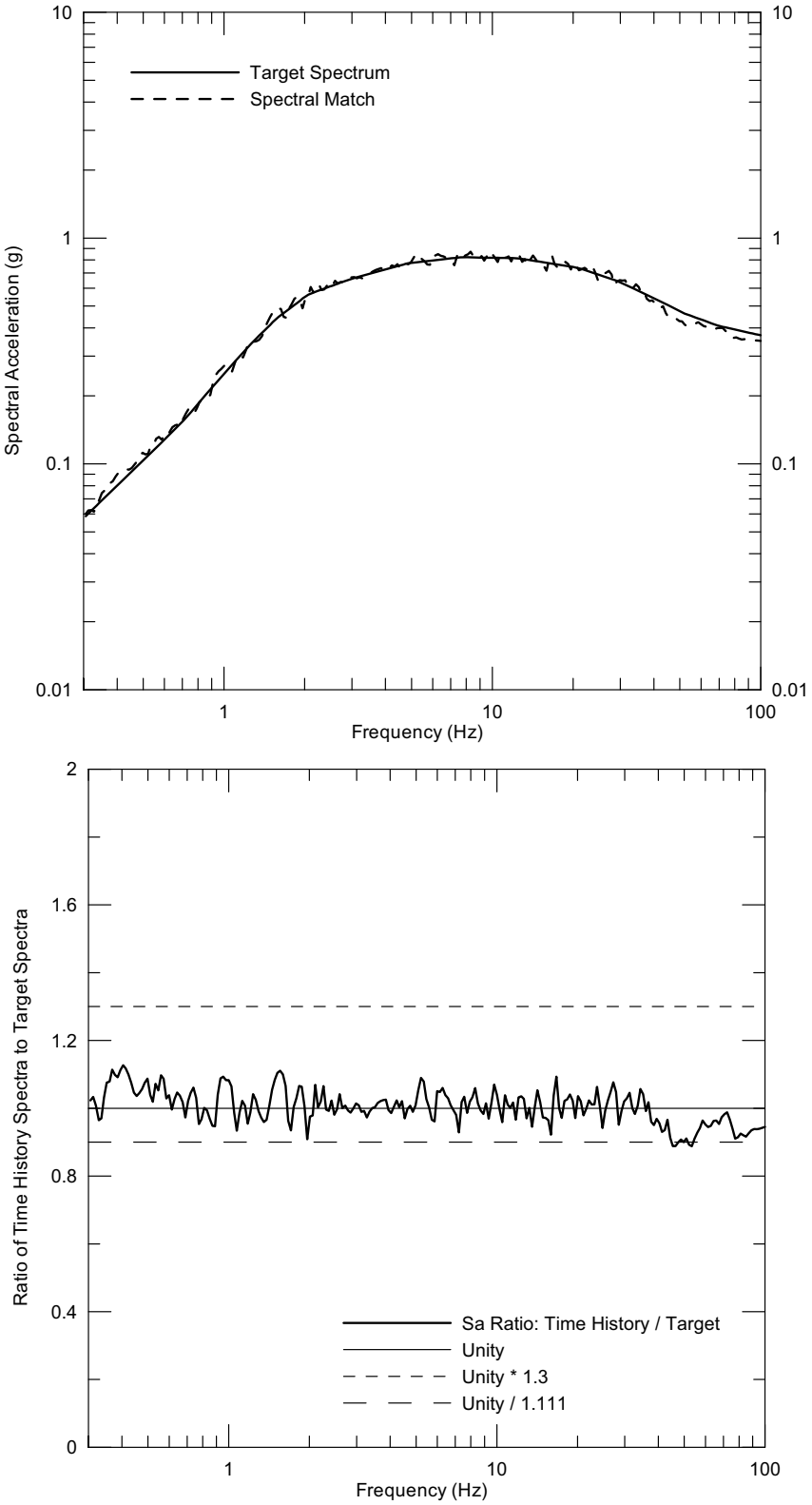

Source: Wong and Silva 2004a [DIRS 170443], Supplemental Record 107, Pages 10 & 11

Figure 6.3-71. Response Spectrum of Point D/E 10^{-3} Horizontal-2 Time History No. 1 and Seismic Design Target Spectrum

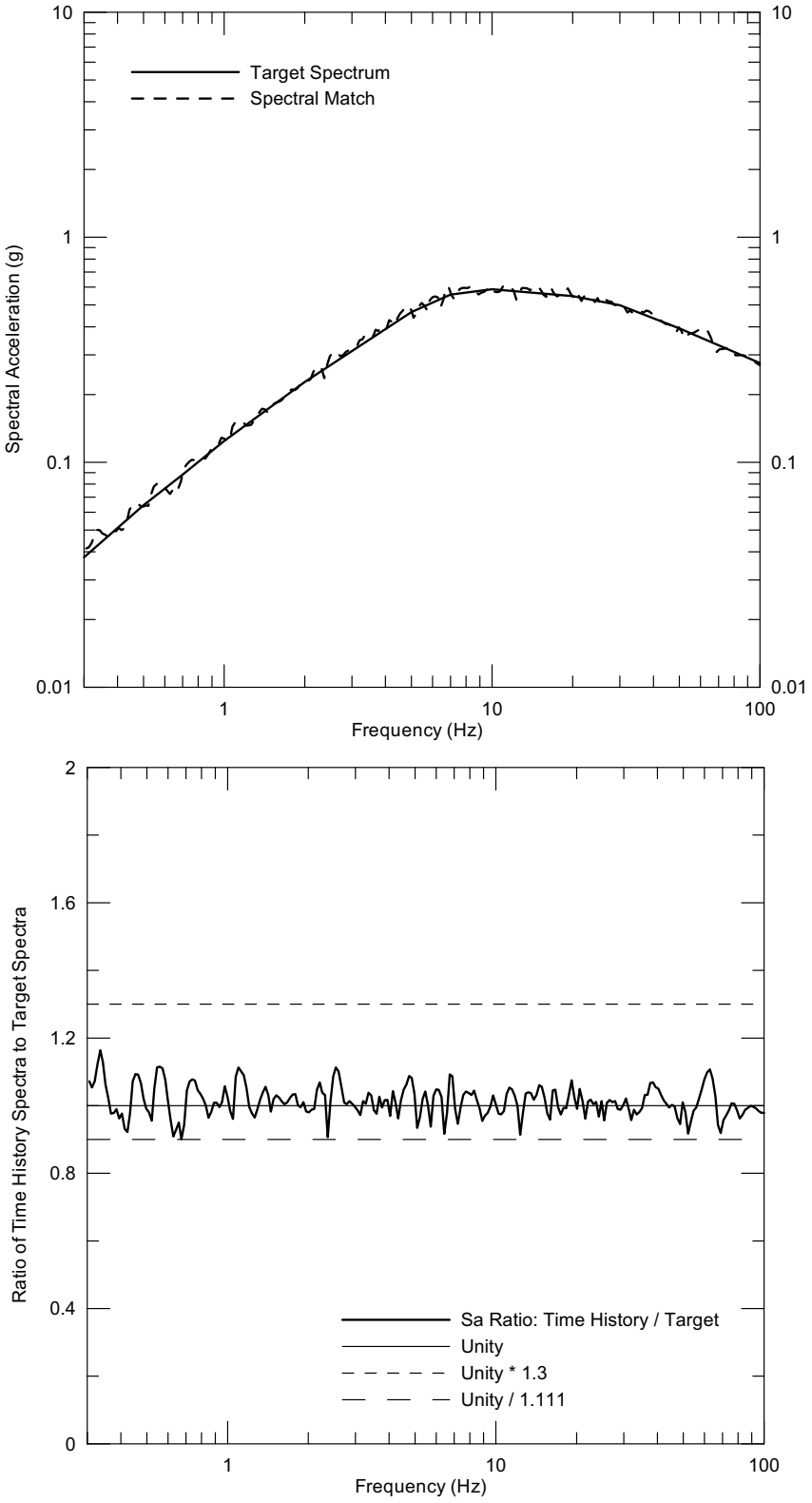

Source: Wong and Silva 2004a [DIRS 170443], Supplemental Record 120, Pages 46 & 47

Figure 6.3-72. Response Spectrum of Point D/E 10^{-3} Vertical Time History No. 1 and Seismic Design Target Spectrum

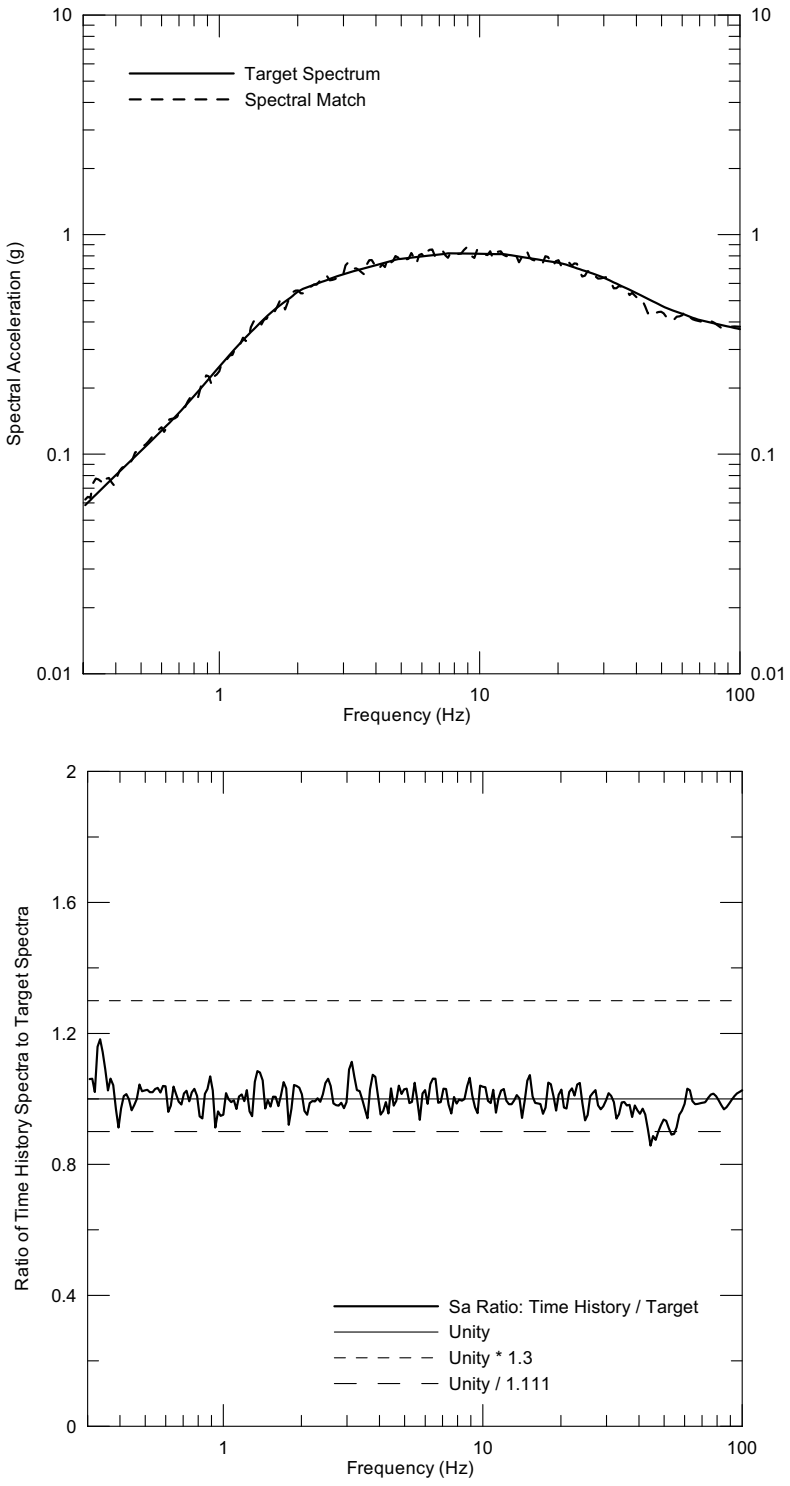

Source: Wong and Silva 2004a [DIRS 170443], Supplemental Record 107, Pages 18 & 20

Figure 6.3-73. Response Spectrum of Point D/E 10^{-3} Horizontal-1 Time History No. 2 and Seismic Design Target Spectrum

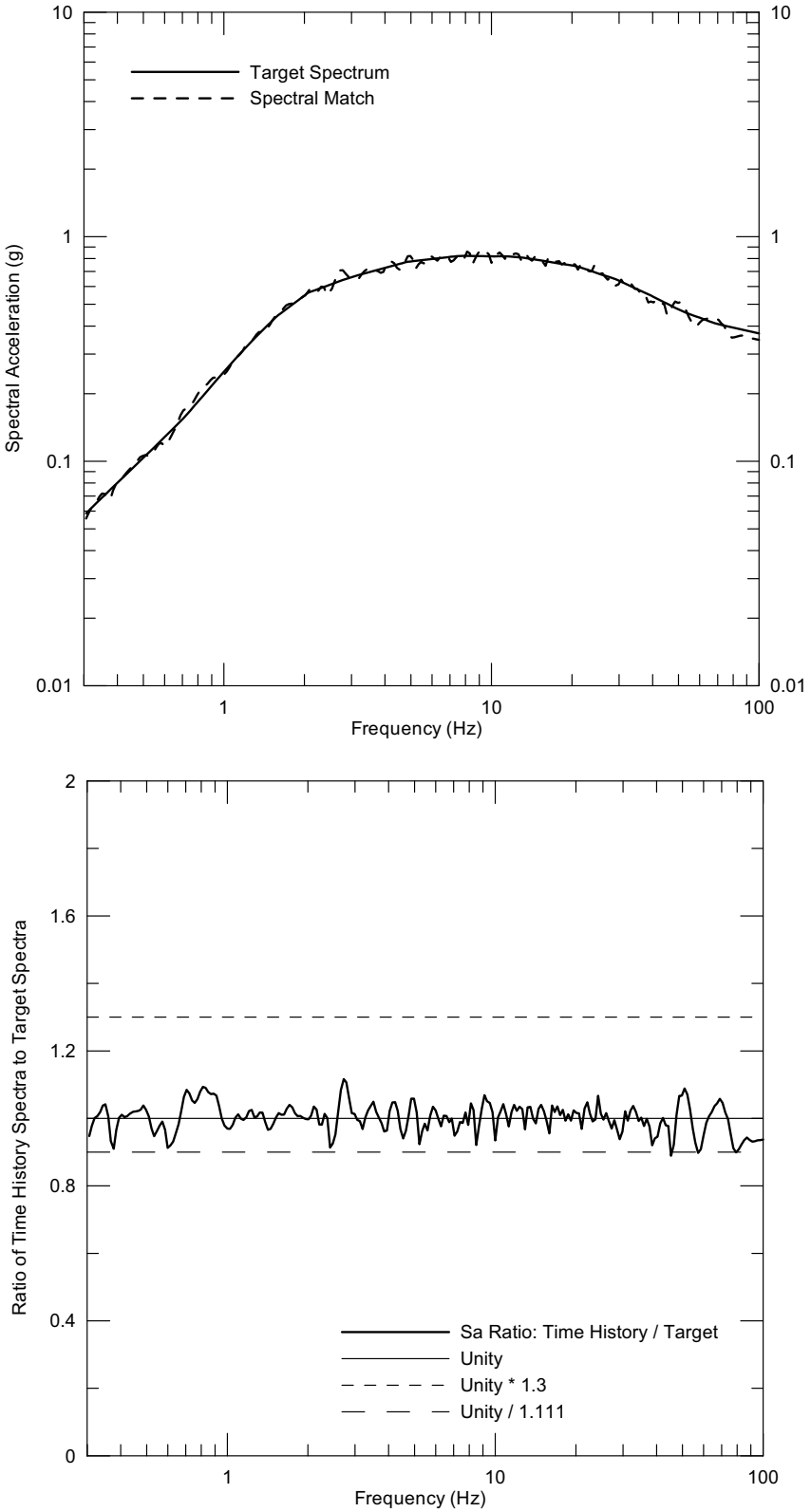

Source: Wong and Silva 2004a [DIRS 170443], Supplemental Record 107, Pages 22 & 24

Figure 6.3-74. Response Spectrum of Point D/E 10^{-3} Horizontal-2 Time History No. 2 and Seismic Design Target Spectrum

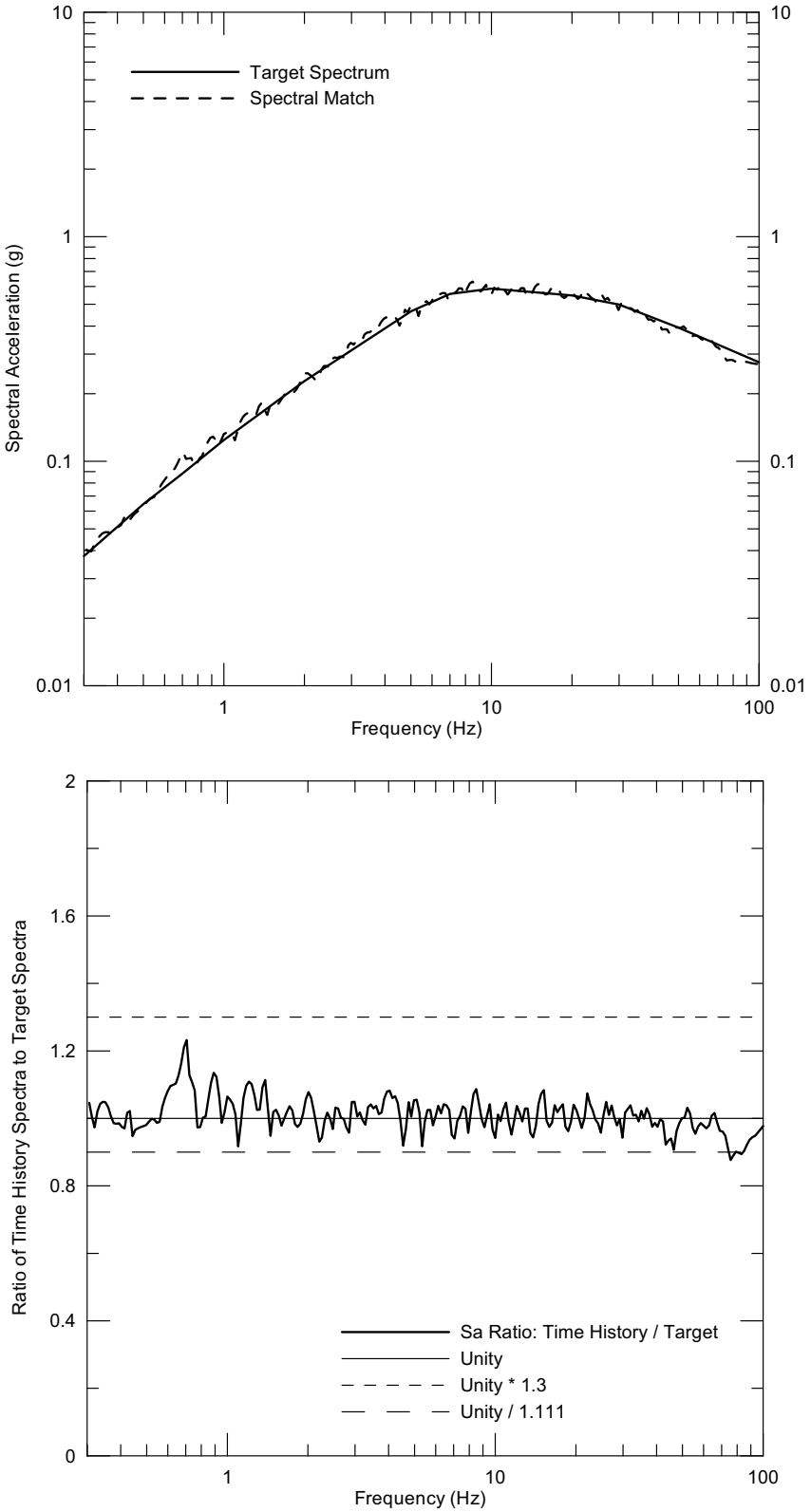

Source: Wong and Silva 2004a [DIRS 170443], Supplemental Record 120, Pages 50 & 52

Figure 6.3-75. Response Spectrum of Point D/E 10^{-3} Vertical Time History No. 2 and Seismic Design Target Spectrum

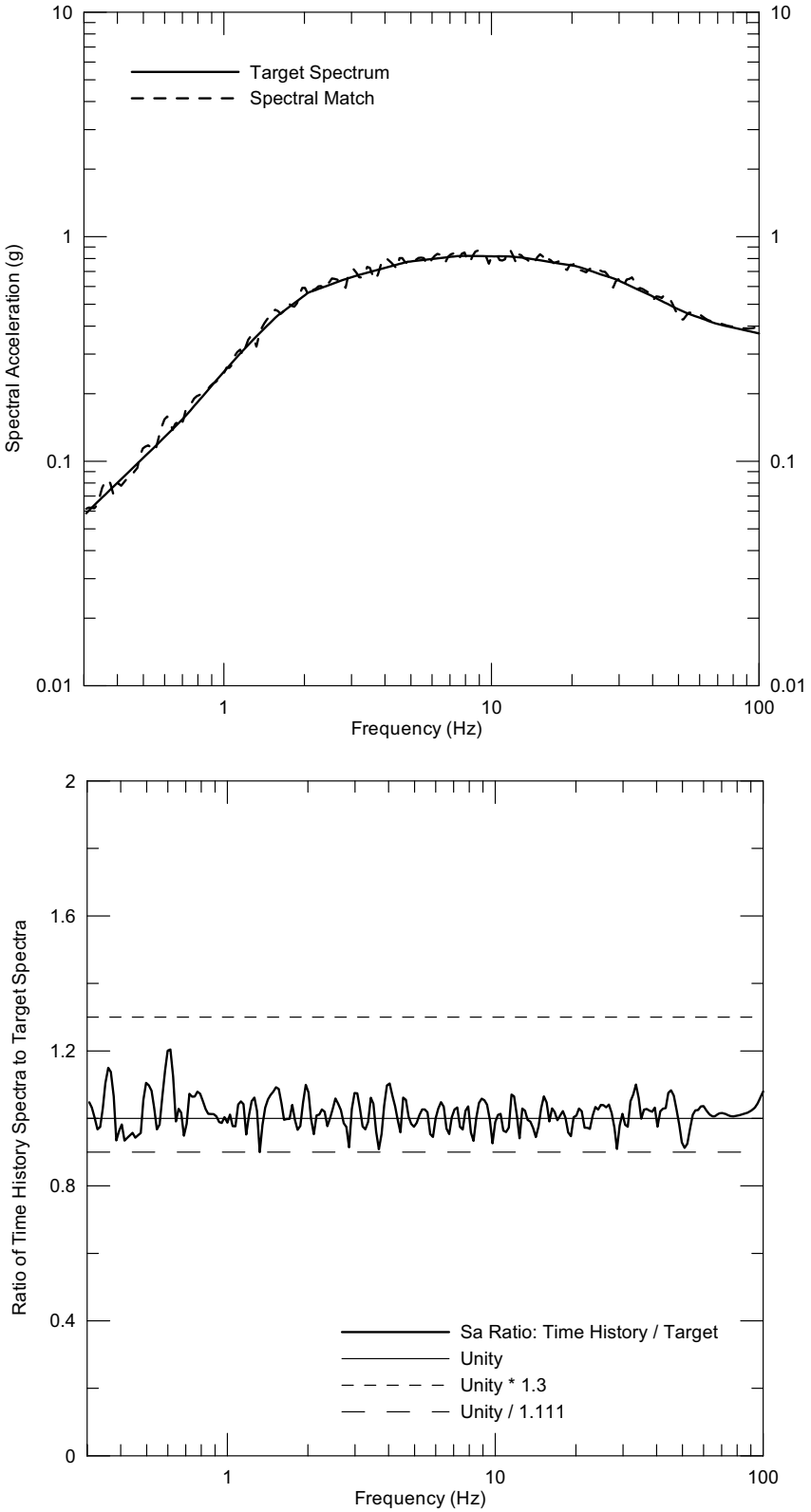

Source: Wong and Silva 2004a [DIRS 170443], Supplemental Record 107, Pages 30 & 32

Figure 6.3-76. Response Spectrum of Point D/E 10^{-3} Horizontal-1 Time History No. 3 and Seismic Design Target Spectrum

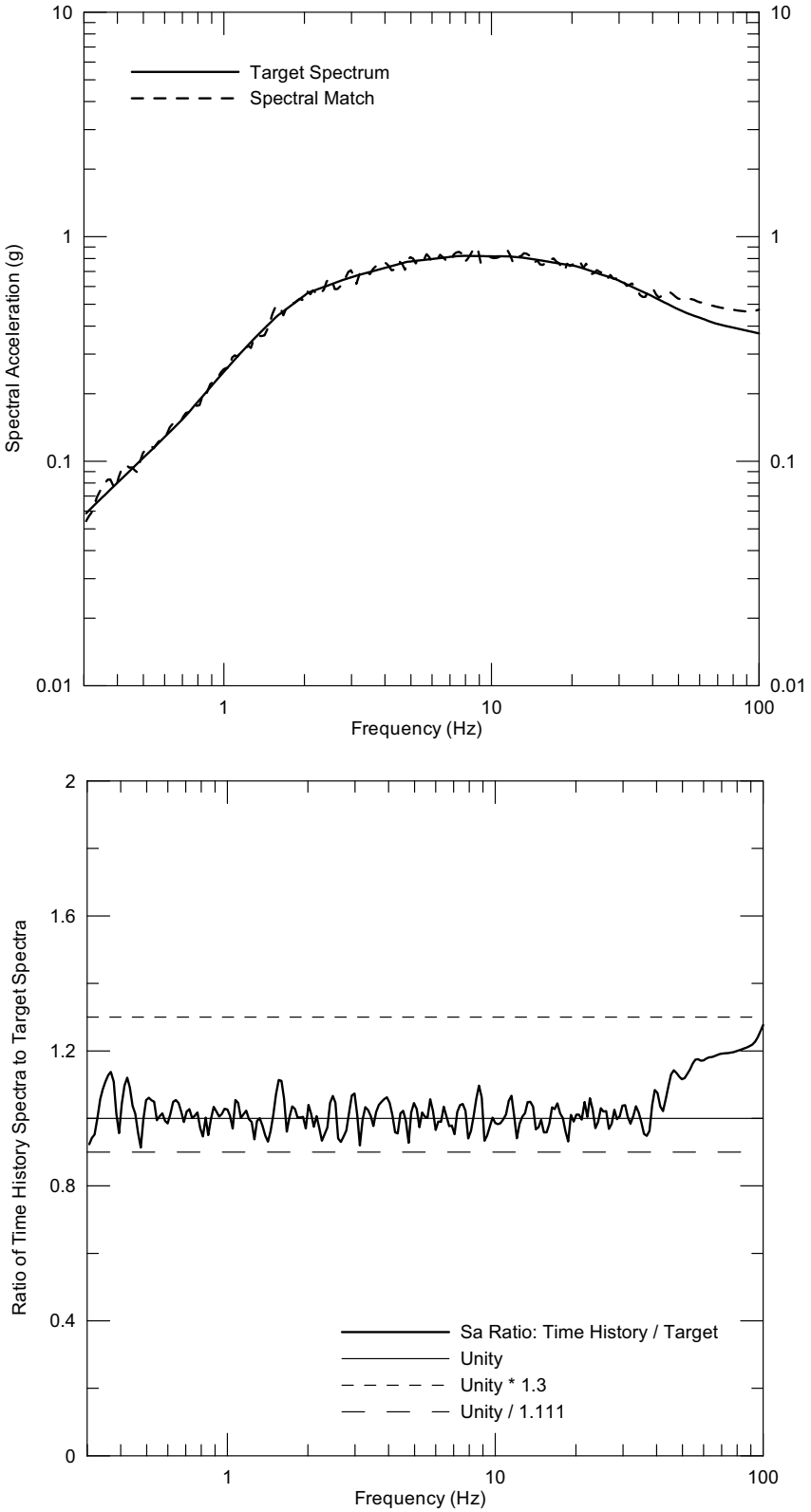

Source: Wong and Silva 2004a [DIRS 170443], Supplemental Record 107, Pages 34 & 36

Figure 6.3-77. Response Spectrum of Point D/E 10^{-3} Horizontal-2 Time History No. 3 and Seismic Design Target Spectrum

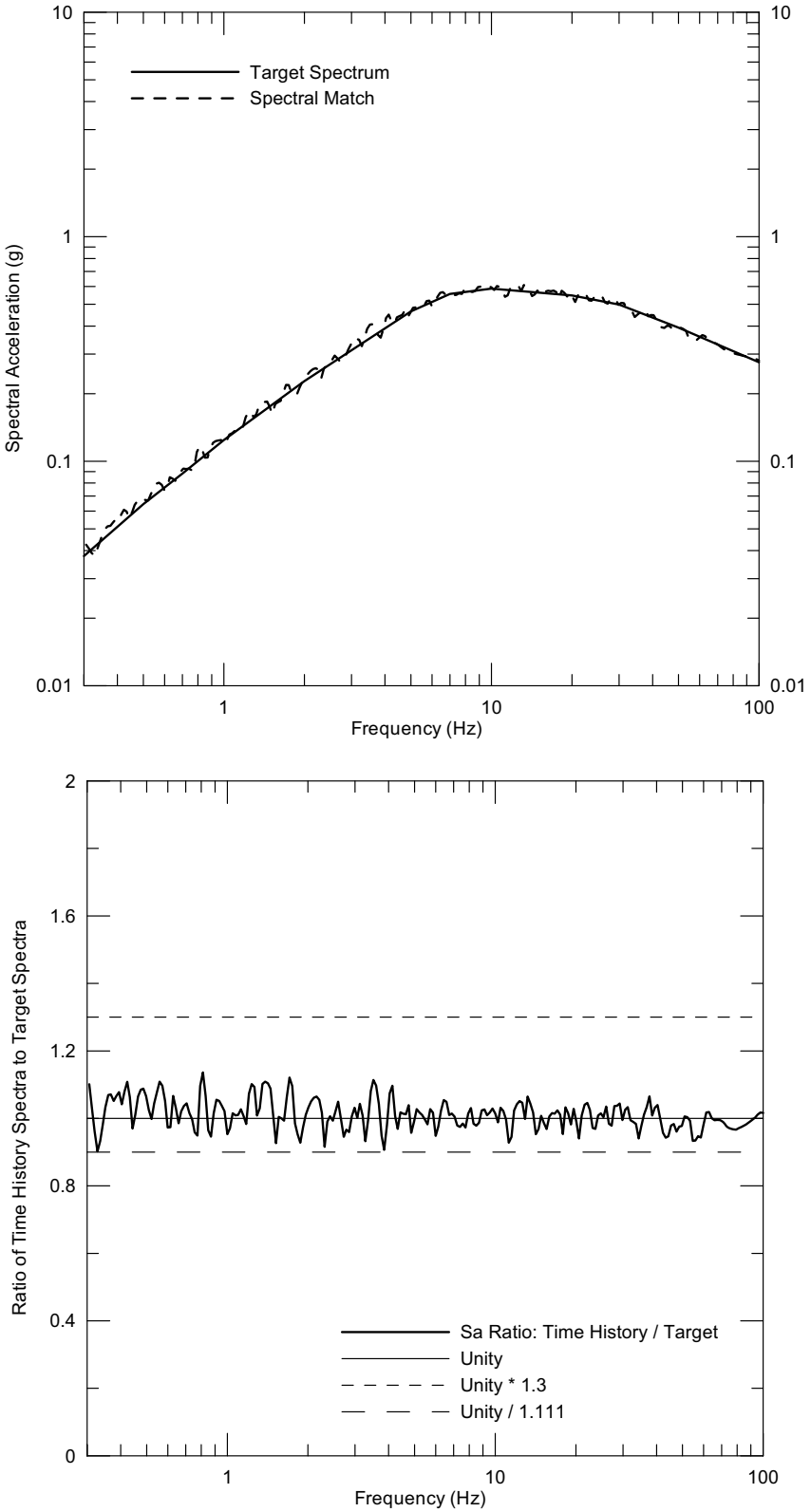

Source: Wong and Silva 2004a [DIRS 170443], Supplemental Record 120, Pages 54 & 55

Figure 6.3-78. Response Spectrum of Point D/E 10^{-3} Vertical Time History No. 3 and Seismic Design Target Spectrum

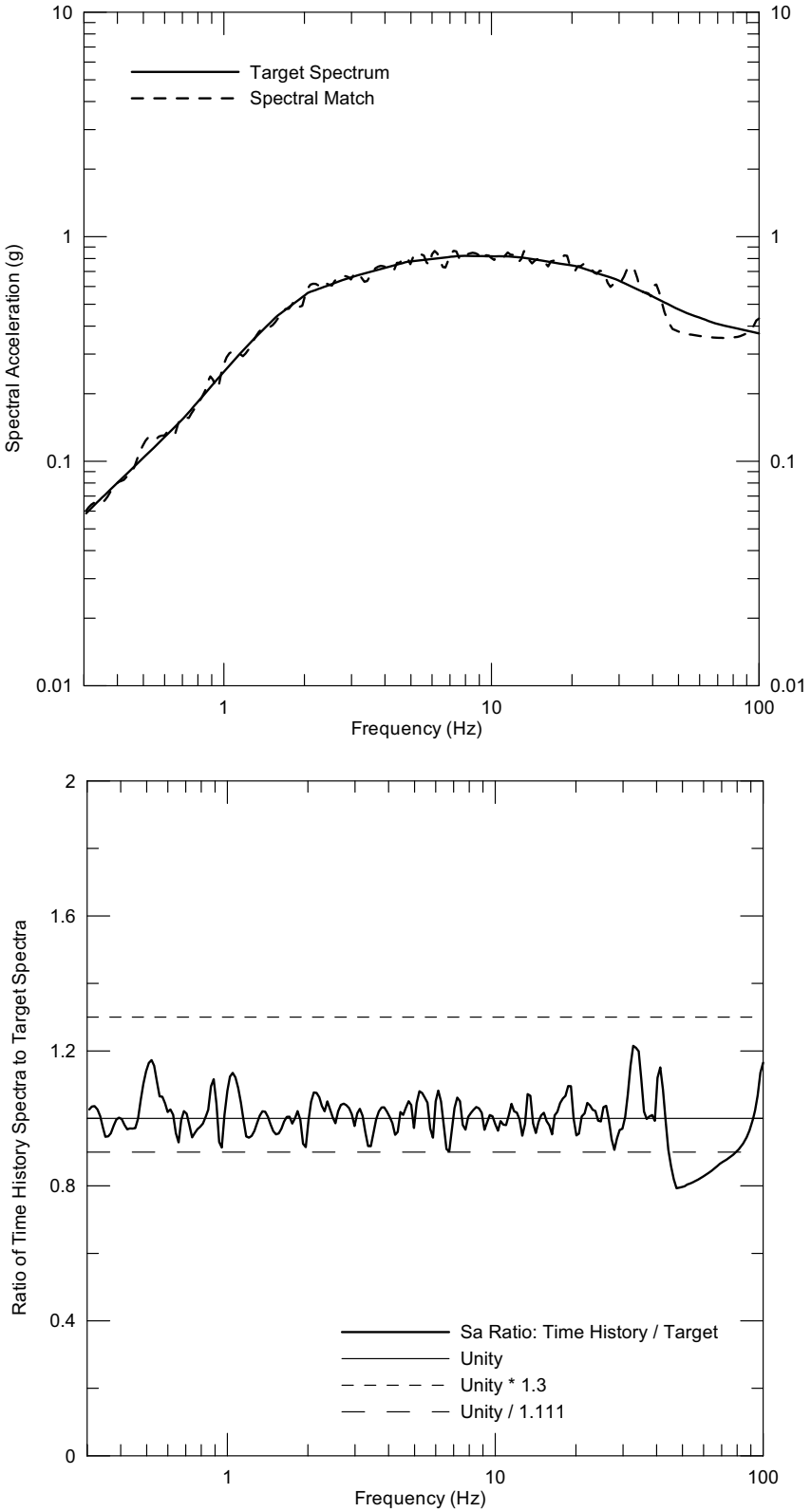

Source: Wong and Silva 2004a [DIRS 170443], Supplemental Record 107, Pages 42 & 44

Figure 6.3-79. Response Spectrum of Point D/E 10^{-3} Horizontal-1 Time History No. 4 and Seismic Design Target Spectrum

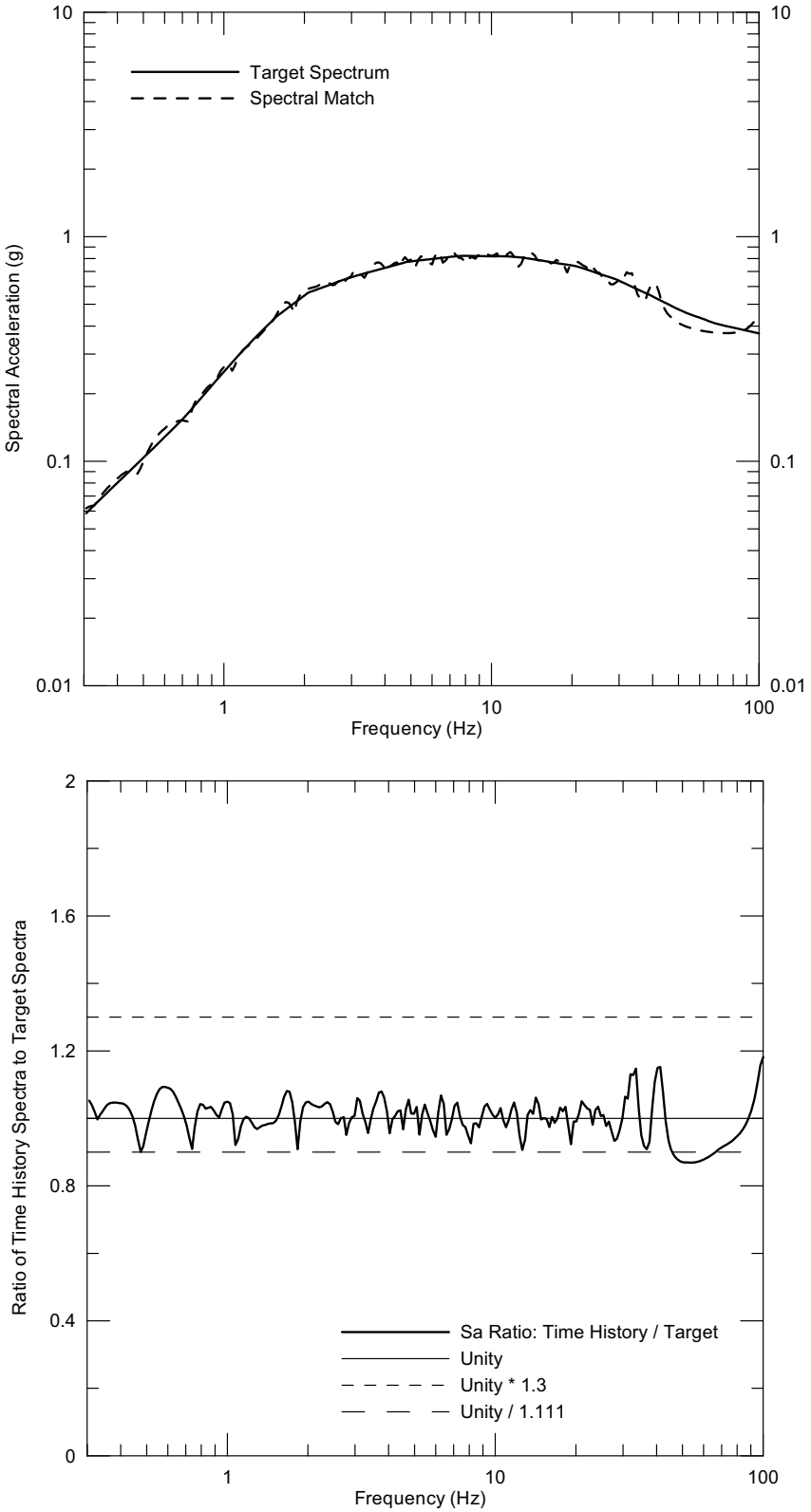

Source: Wong and Silva 2004a [DIRS 170443], Supplemental Record 107, Pages 46 & 48

Figure 6.3-80. Response Spectrum of Point D/E 10^{-3} Horizontal-2 Time History No. 4 and Seismic Design Target Spectrum

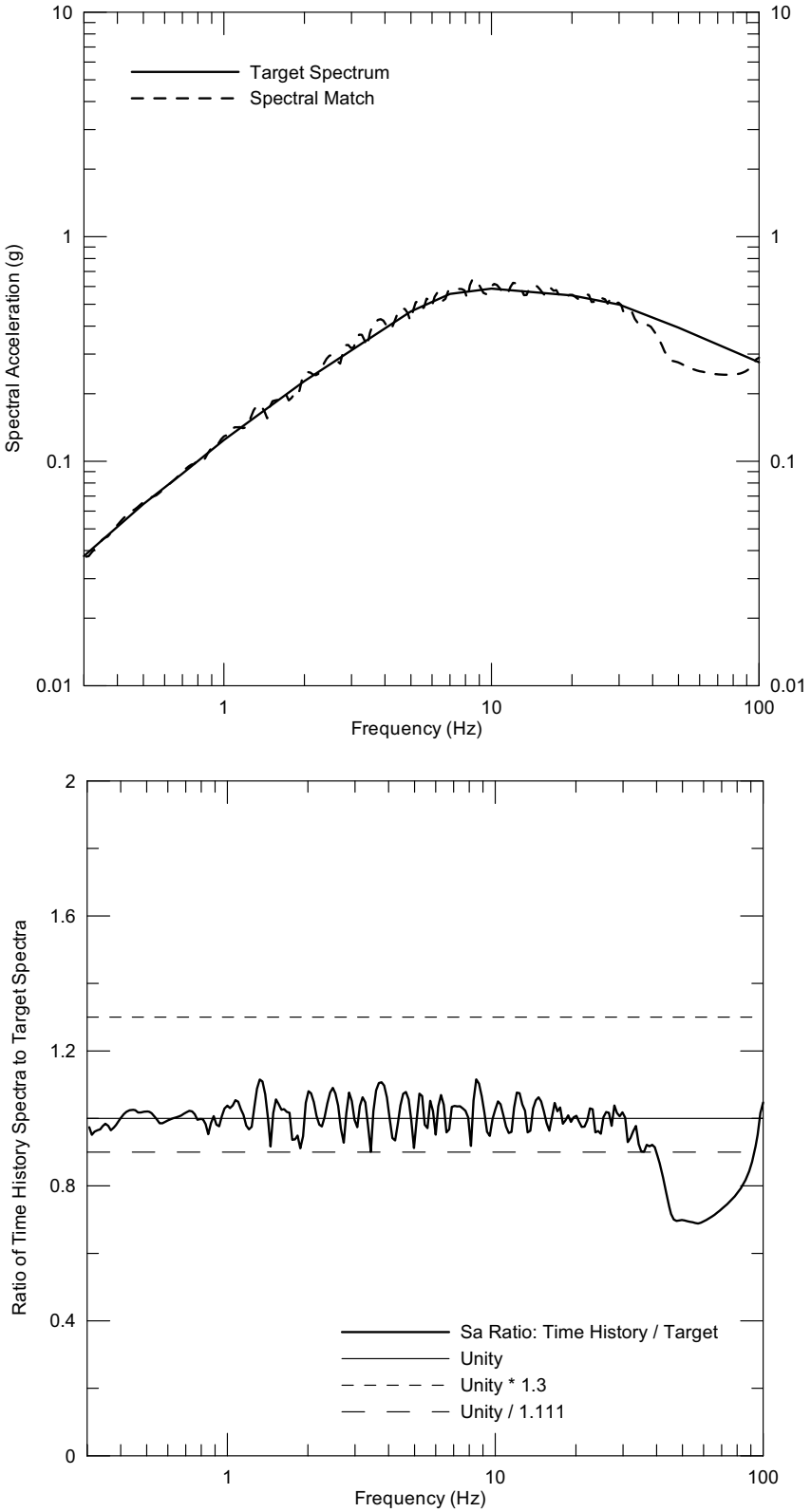

Source: Wong and Silva 2004a [DIRS 170443], Supplemental Record 120, Pages 58 & 60

Figure 6.3-81. Response Spectrum of Point D/E 10^{-3} Vertical Time History No. 4 and Seismic Design Target Spectrum

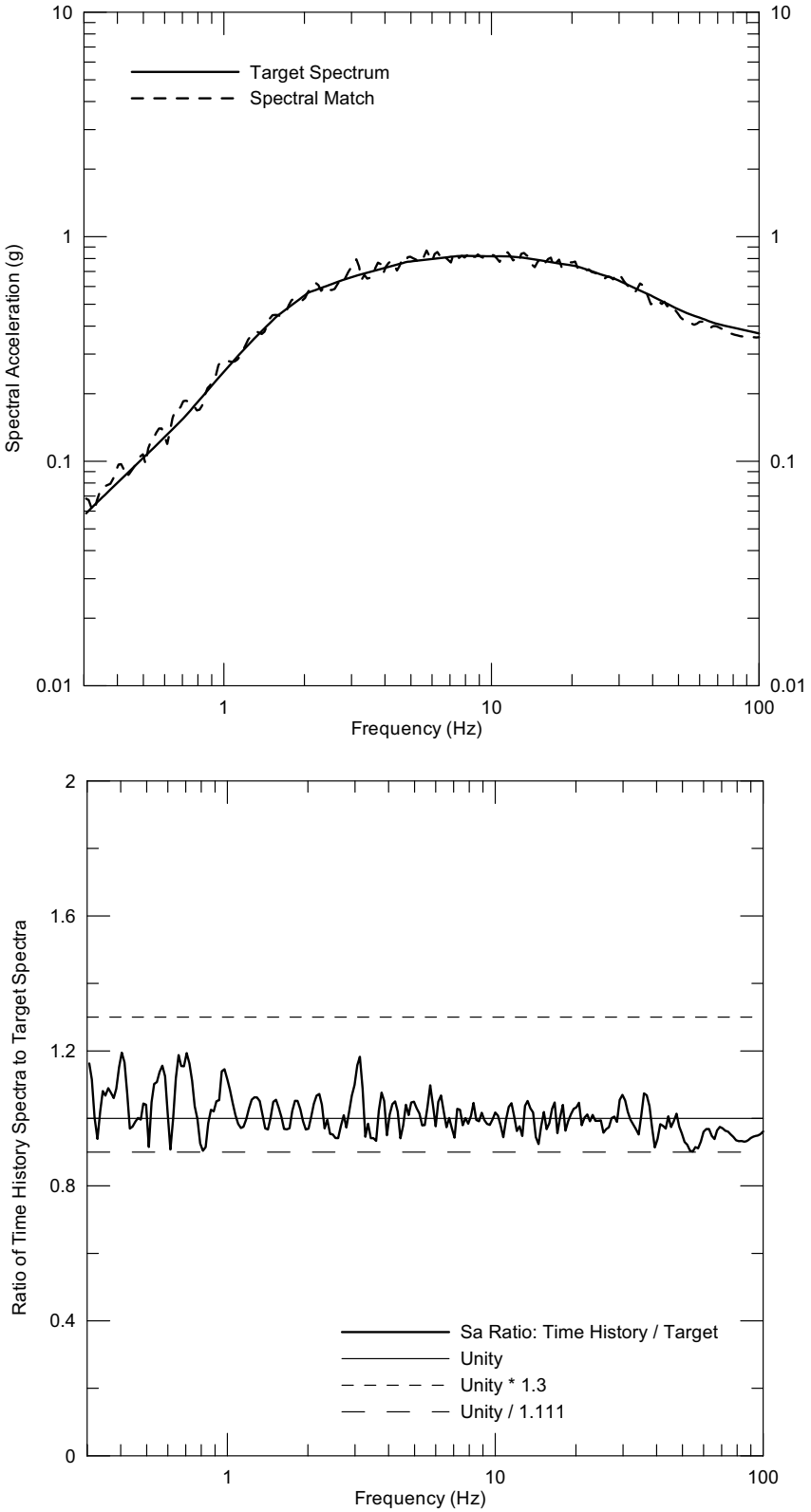

Source: Wong and Silva 2004a [DIRS 170443], Supplemental Record 107, Pages 54 & 56

Figure 6.3-82. Response Spectrum of Point D/E 10^{-3} Horizontal-1 Time History No. 5 and Seismic Design Target Spectrum

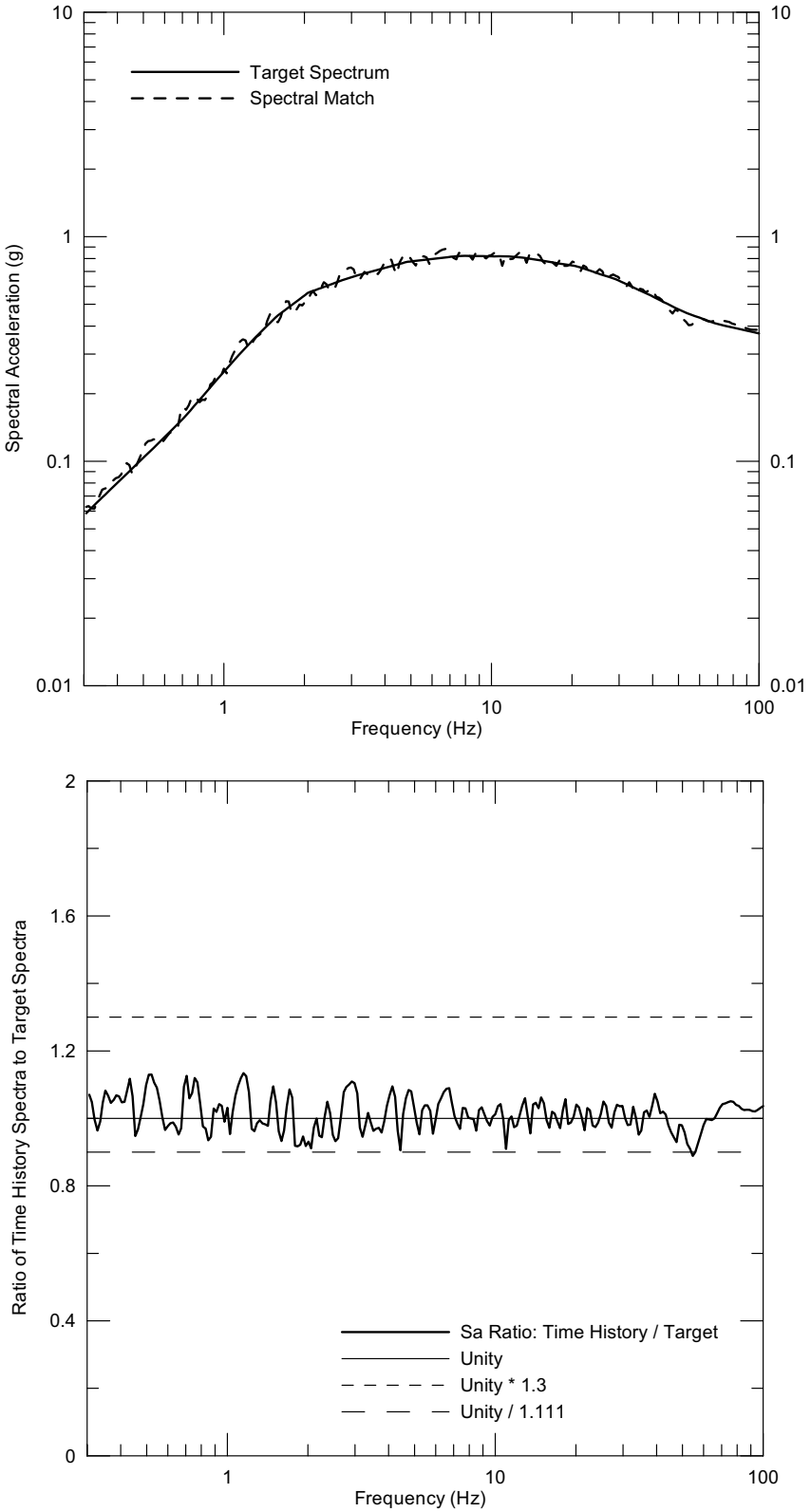

Source: Wong and Silva 2004a [DIRS 170443], Supplemental Record 107, Pages 58 & 60

Figure 6.3-83. Response Spectrum of Point D/E 10^{-3} Horizontal-2 Time History No. 5 and Seismic Design Target Spectrum

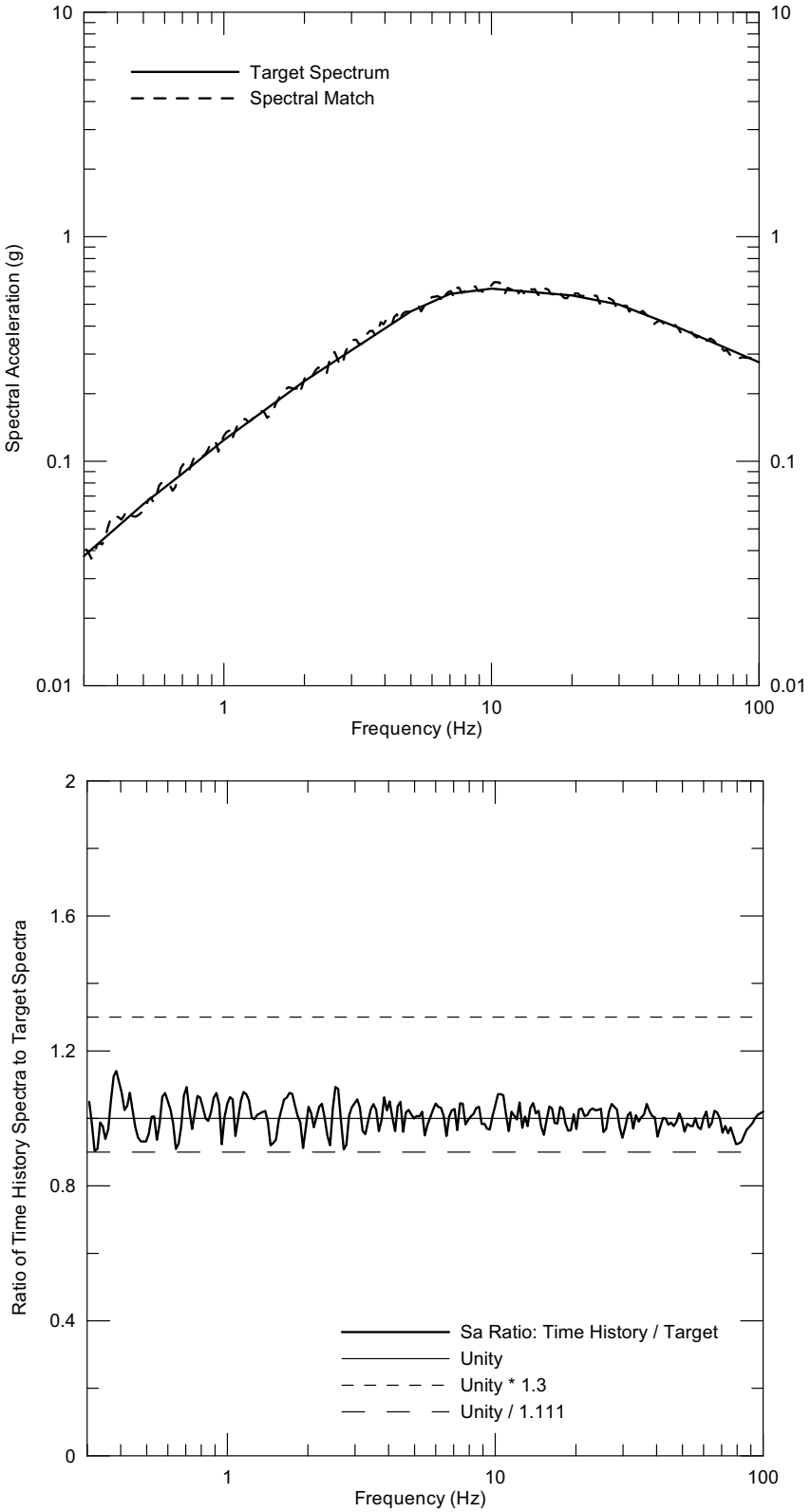

Source: Wong and Silva 2004a [DIRS 170443], Supplemental Record 120, Pages 62 & 63

Figure 6.3-84. Response Spectrum of Point D/E 10^{-3} Vertical Time History No. 5 and Seismic Design Target Spectrum

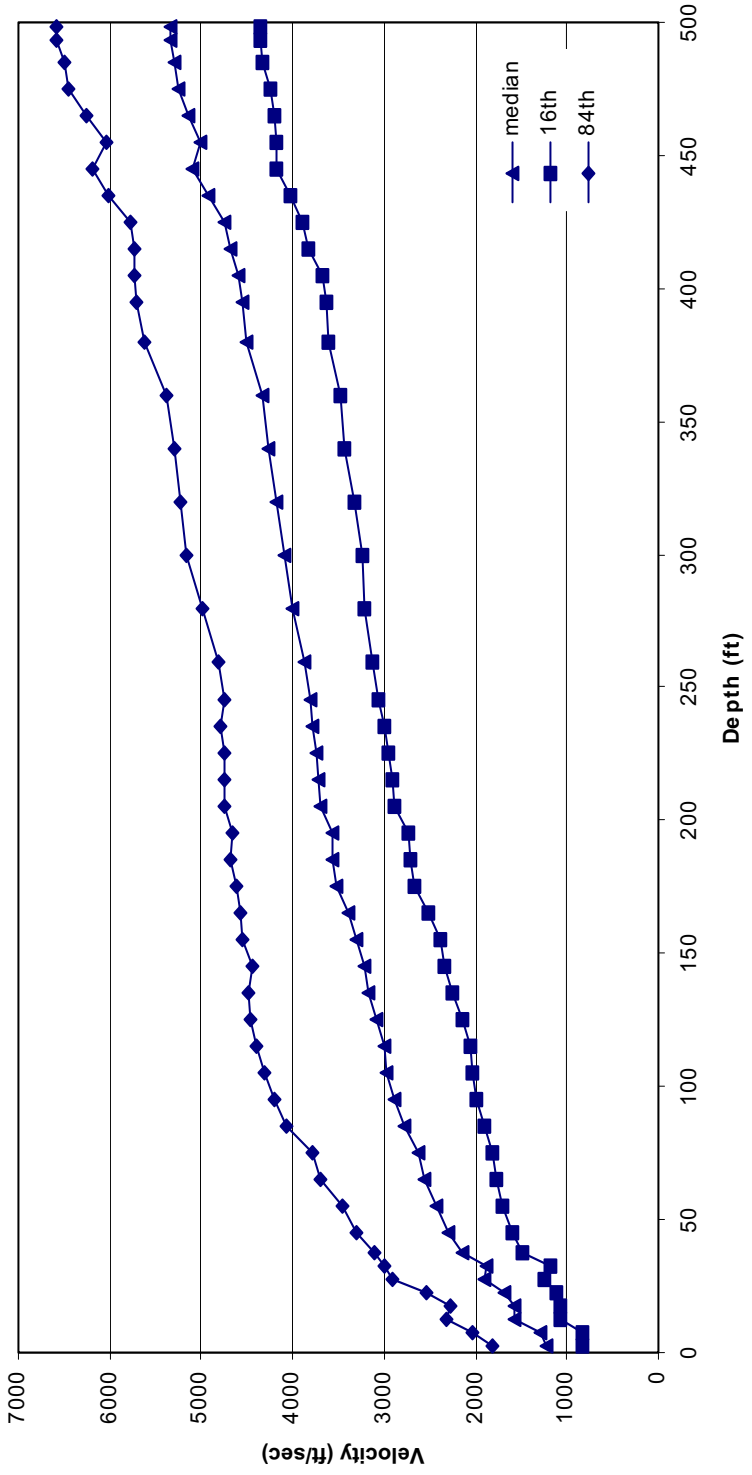

DTN: MO0404SPCDAMPD.001 [DIRS 169344]

Figure 6.3-85. Point D 10^{-3} Strain-Compatible Soil Properties: V_S, 35 ft Profile (35 ft Alluvium)

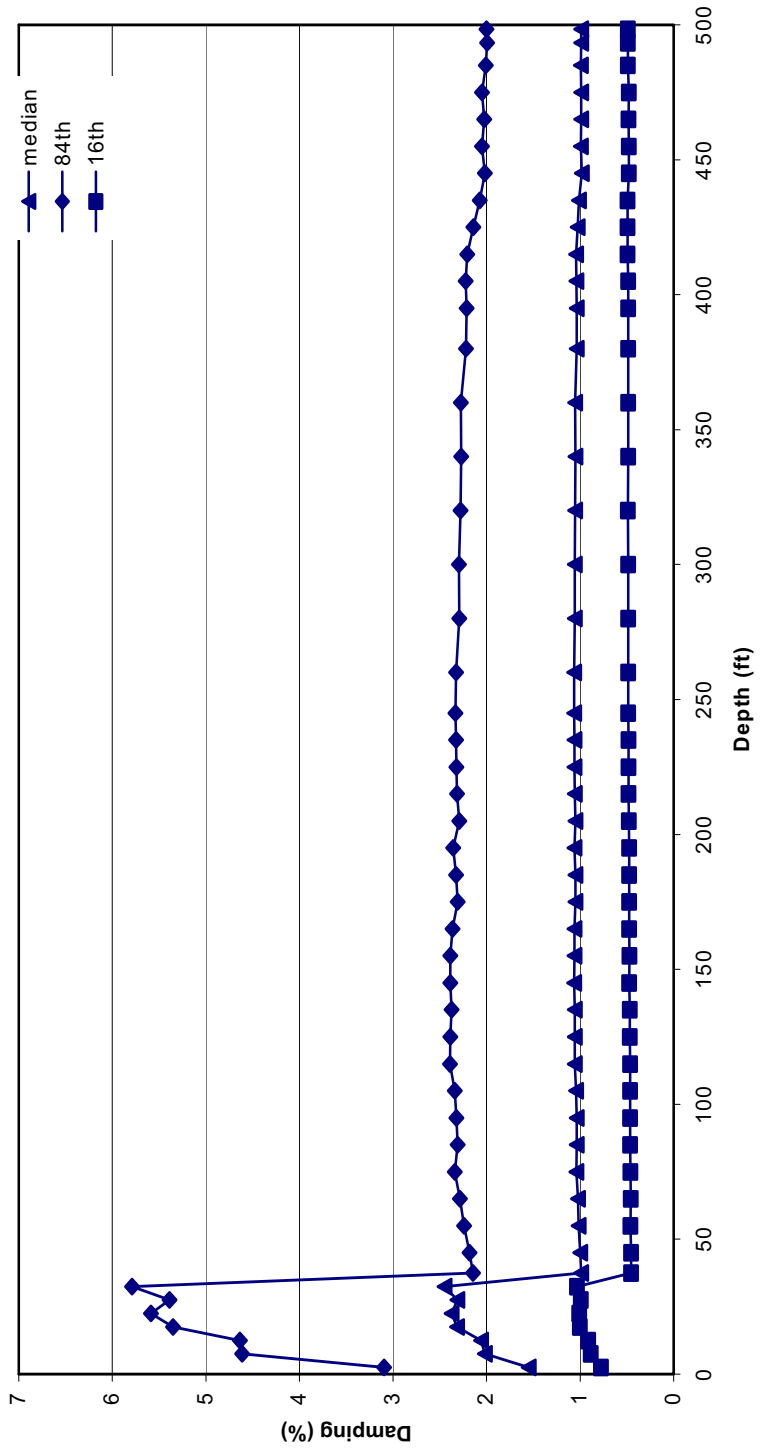

DTN: MO0404SPCDAMPD.001 [DIRS 169344]

Figure 6.3-86. Point D 10^{-3} Strain-Compatible Soil Properties: S-Wave Damping, 35 ft Profile (35 ft Alluvium)

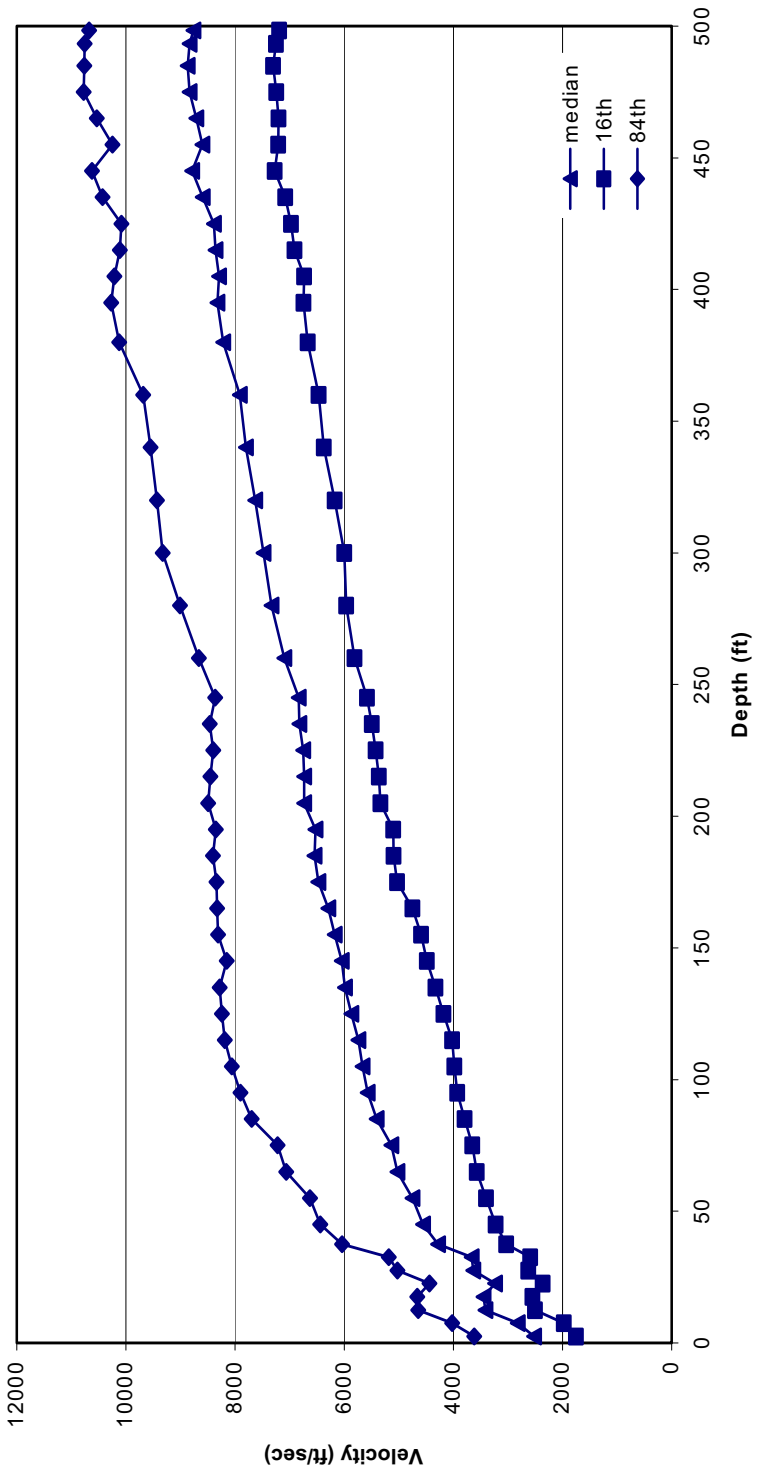

DTN: MO0404SPCDAMPD.001 [DIRS 169344]

Figure 6.3-87. Point D 10^{-3} Strain-Compatible Soil Properties: V_P, 35 ft Profile (35 ft Alluvium)

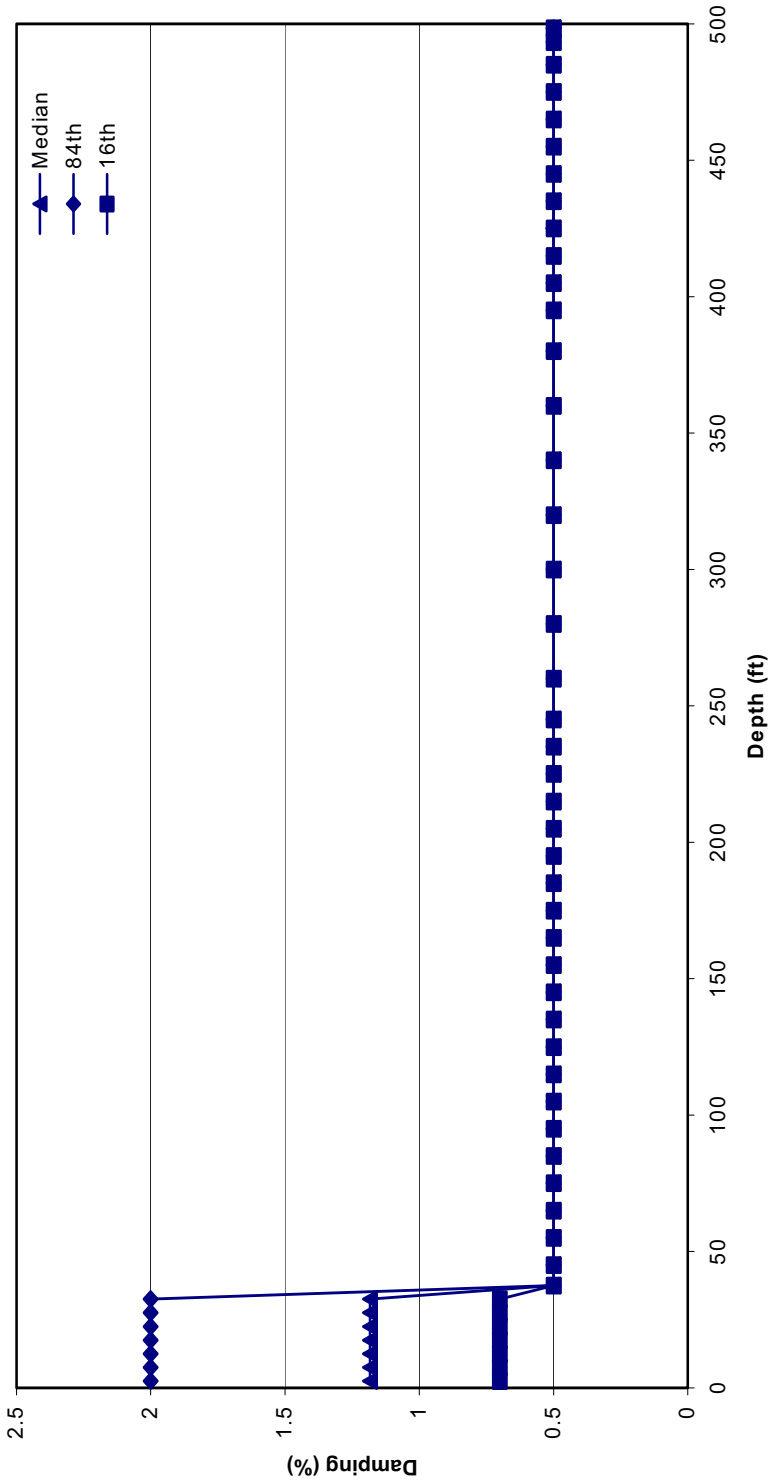

Figure 6.3-88. Point D 10^{-3} Strain-Compatible Soil Properties: P-Wave Damping, 35 ft Profile (35 ft Alluvium)

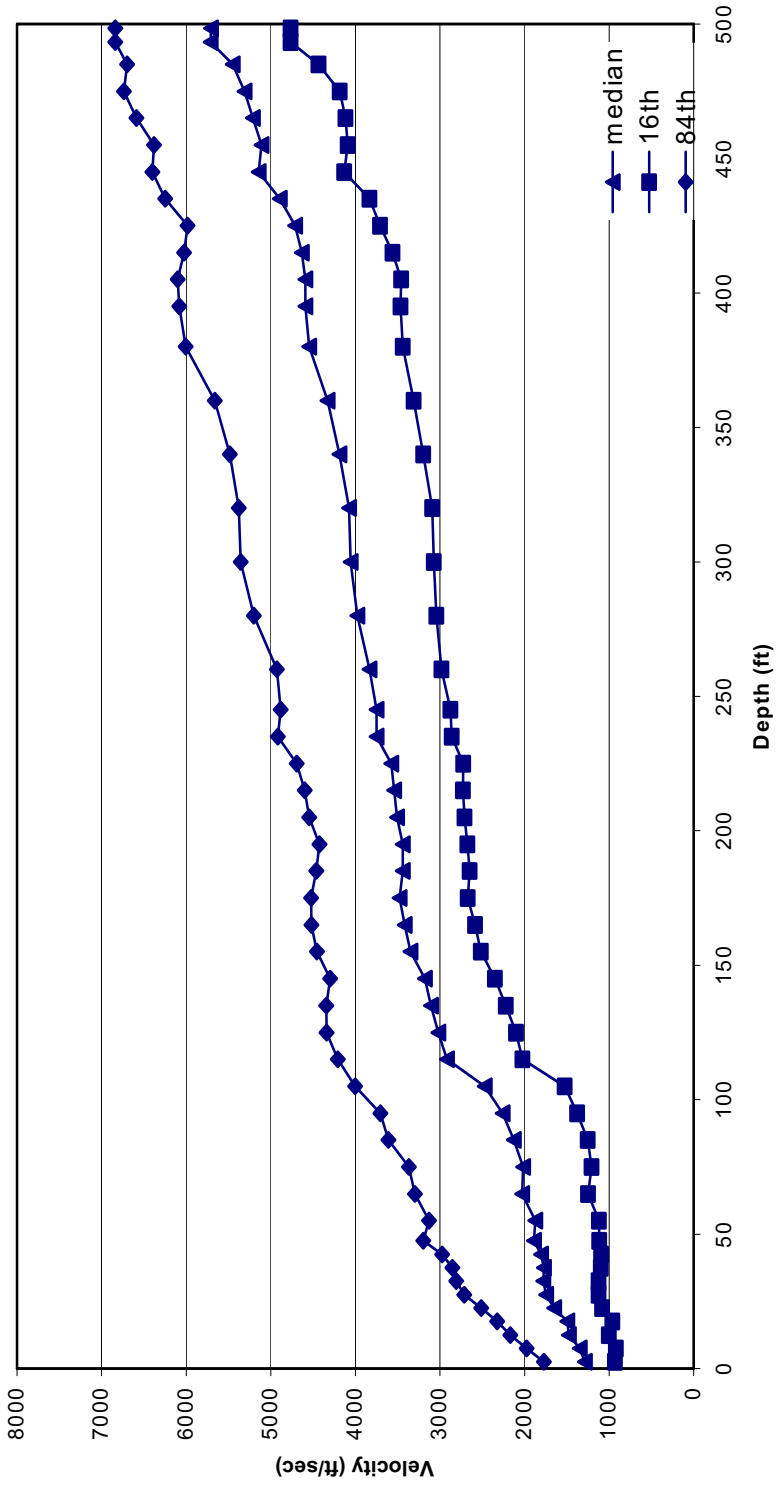

DTN: MO0404SPCDAMPD.001 [DIRS 169344]

Figure 6.3-89. Point D 10^{-3} Strain-Compatible Soil Properties: V_S, 110 ft Profile (110 ft Alluvium)

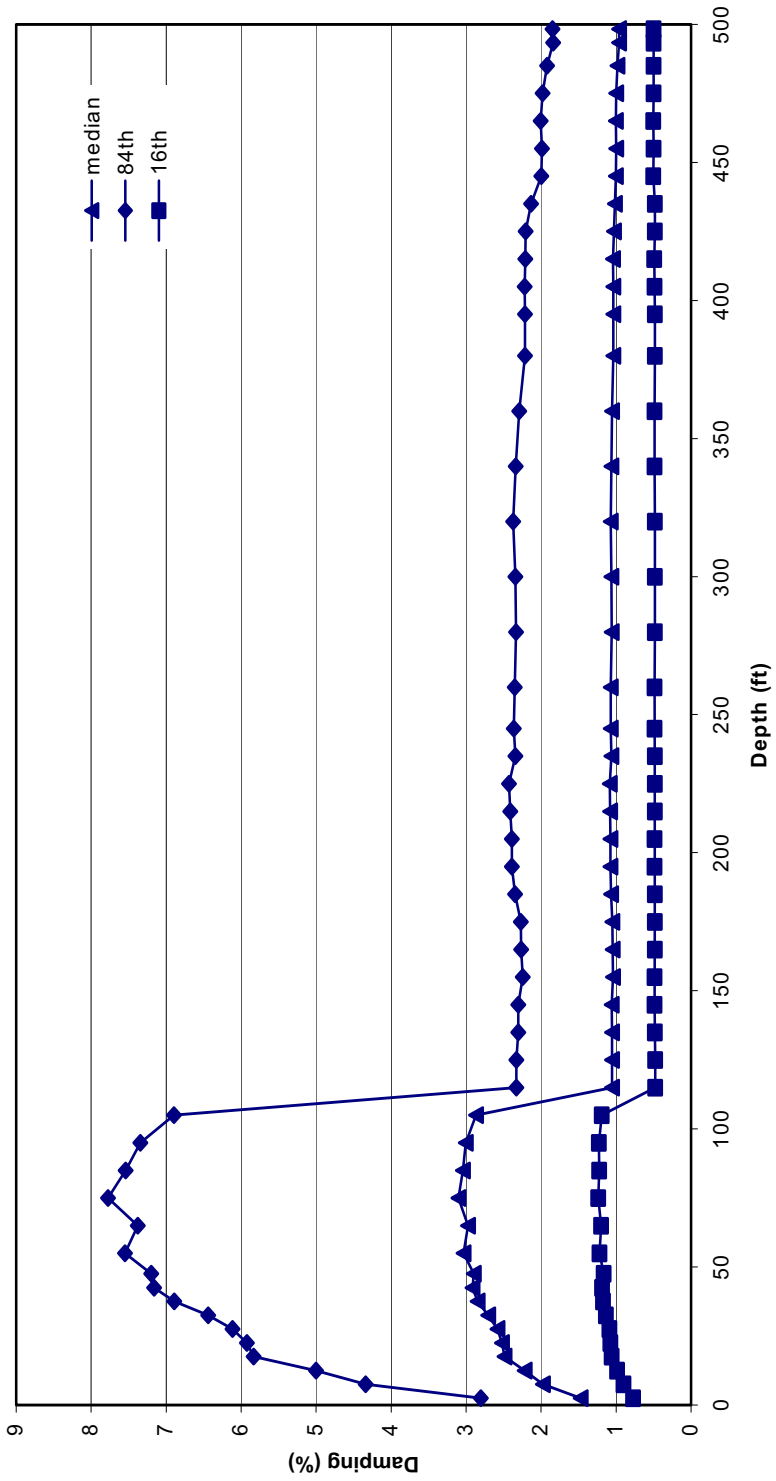

DTN: MO0404SPCDAMPD.001 [DIRS 169344]

Figure 6.3-90. Point D 10^{-3} Strain-Compatible Soil Properties: S-Wave Damping, 110 ft Profile (110 ft Alluvium)

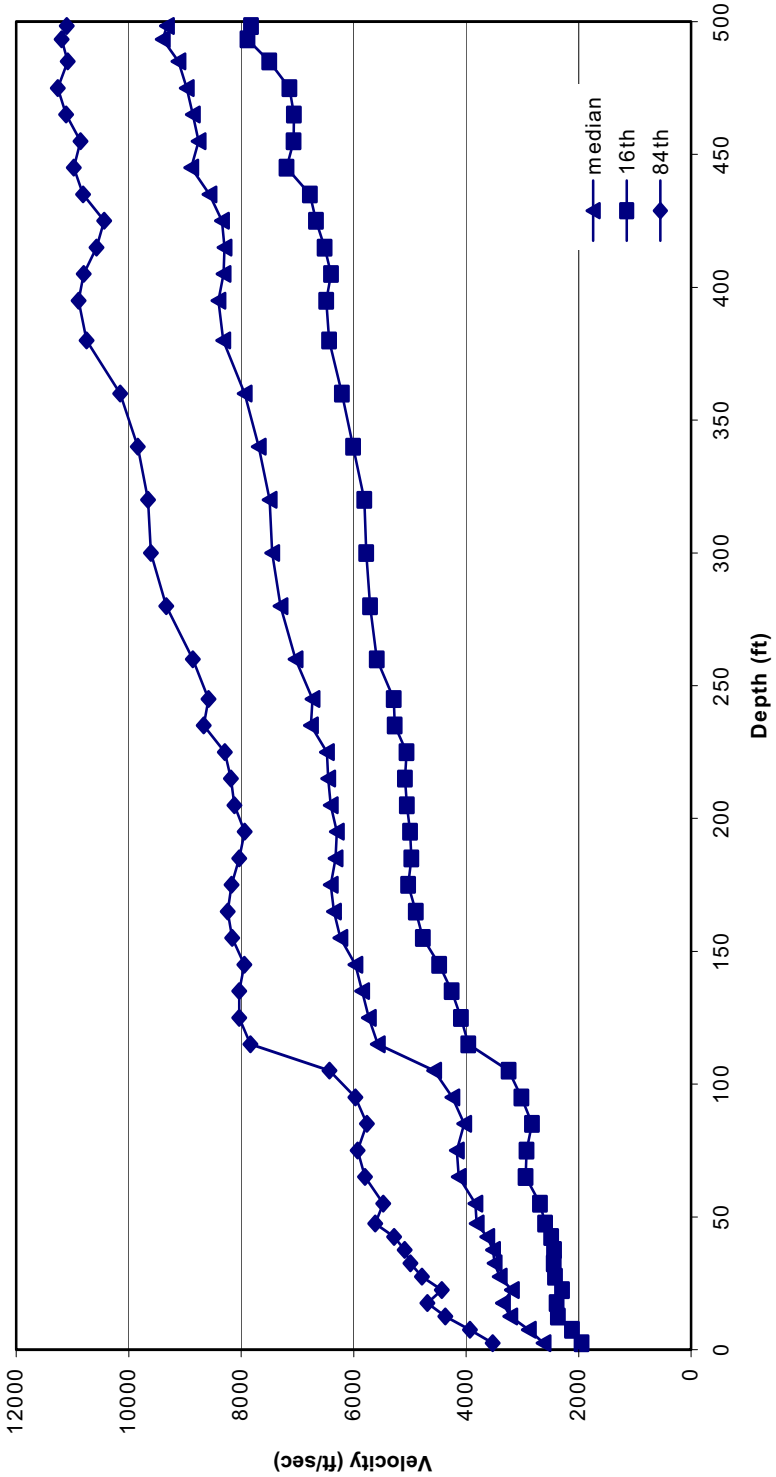

DTN: MO0404SPCDAMPD.001 [DIRS 169344]

Figure 6.3-91. Point D 10^{-3} Strain-Compatible Soil Properties: V_P, 110 ft Profile (110 ft Alluvium)

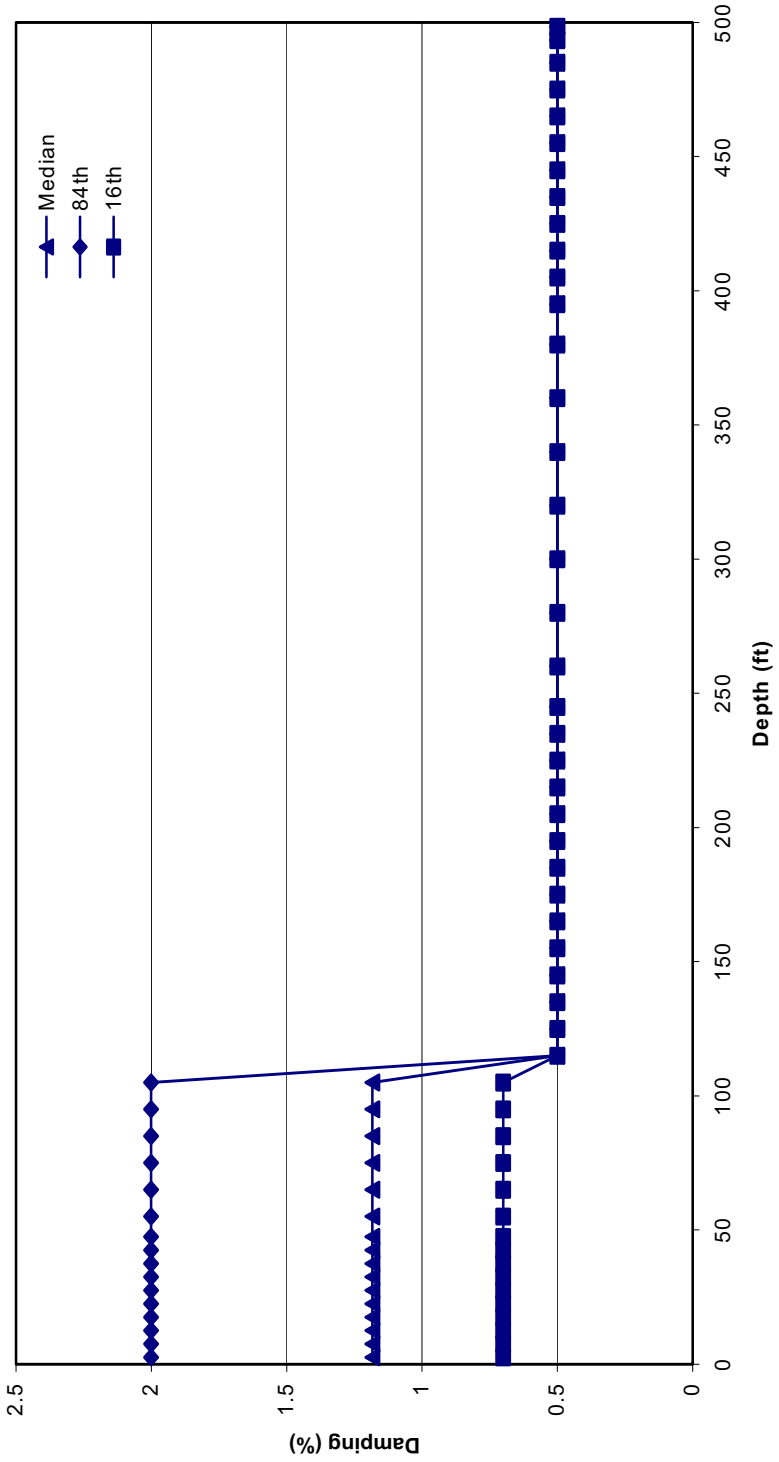

DTN: MO0404SPCDAMPD.001 [DIRS 169344]

Figure 6.3-92. Point D 10^{-3} Strain-Compatible Soil Properties: P-Wave Damping, 110 ft Profile (110 ft Alluvium)

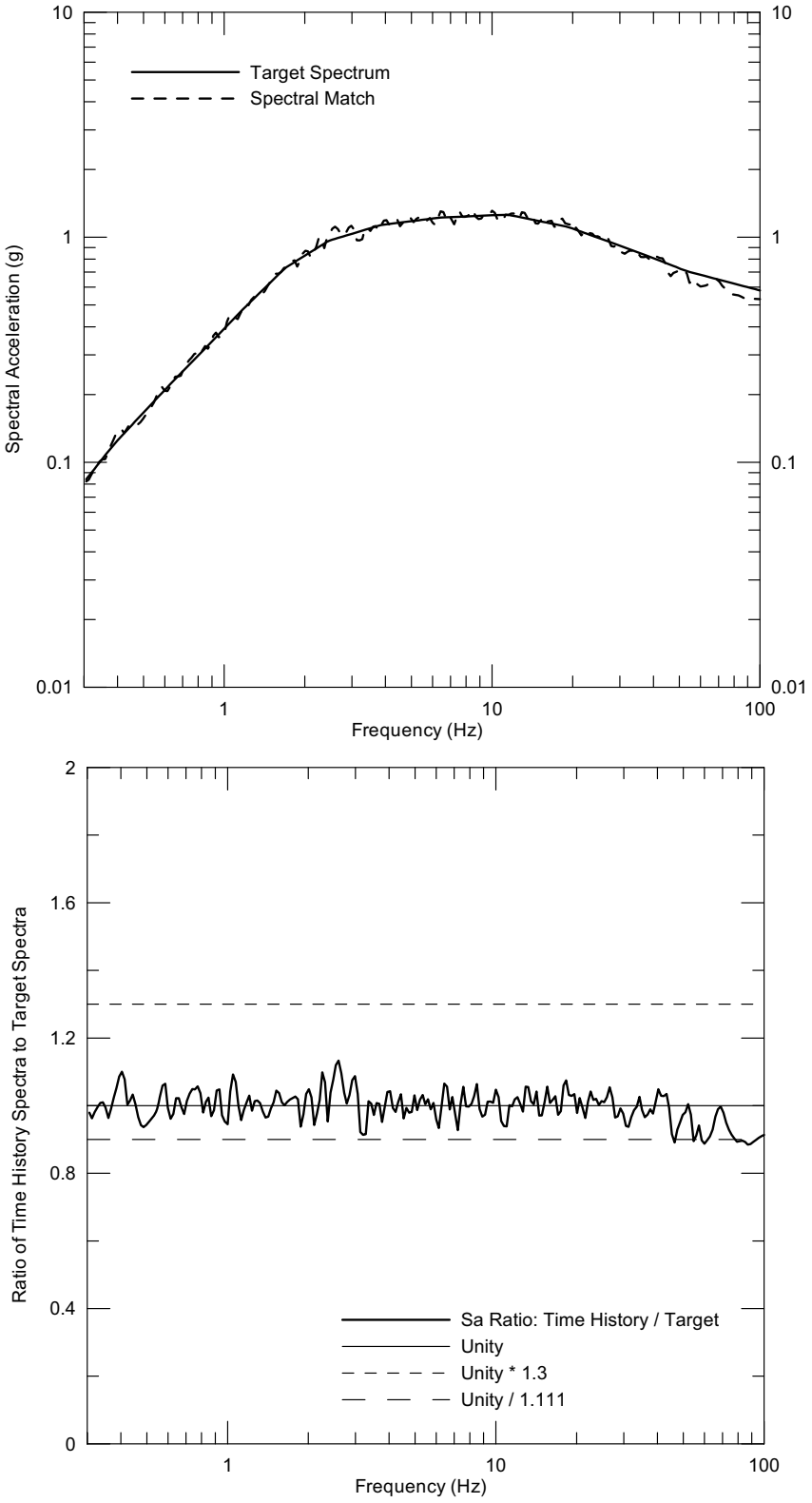

Source: Wong and Silva 2004a [DIRS 170443], Supplemental Record 87, pages 8 & 9

Figure 6.3-93. Response Spectrum of Point D/E 5x10 $^{-4}$ Horizontal-1 Time History No. 1 and Seismic Design Target Spectrum

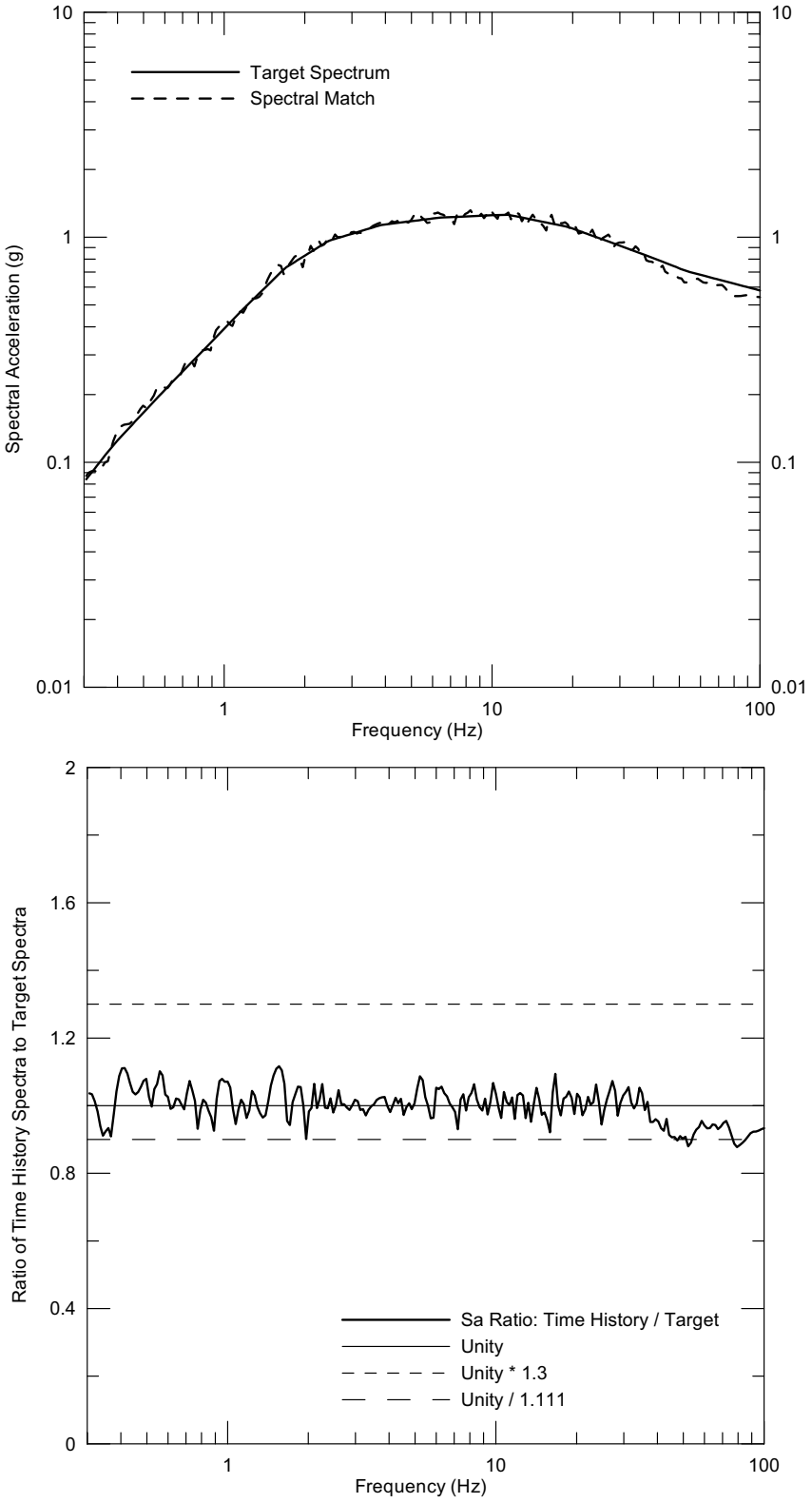

Source: Wong and Silva 2004a [DIRS 170443], Supplemental Record 87, pages 12 & 13

Figure 6.3-94. Response Spectrum of Point D/E 5x10 $^{-4}$ Horizontal-2 Time History No. 1 and Seismic Design Target Spectrum

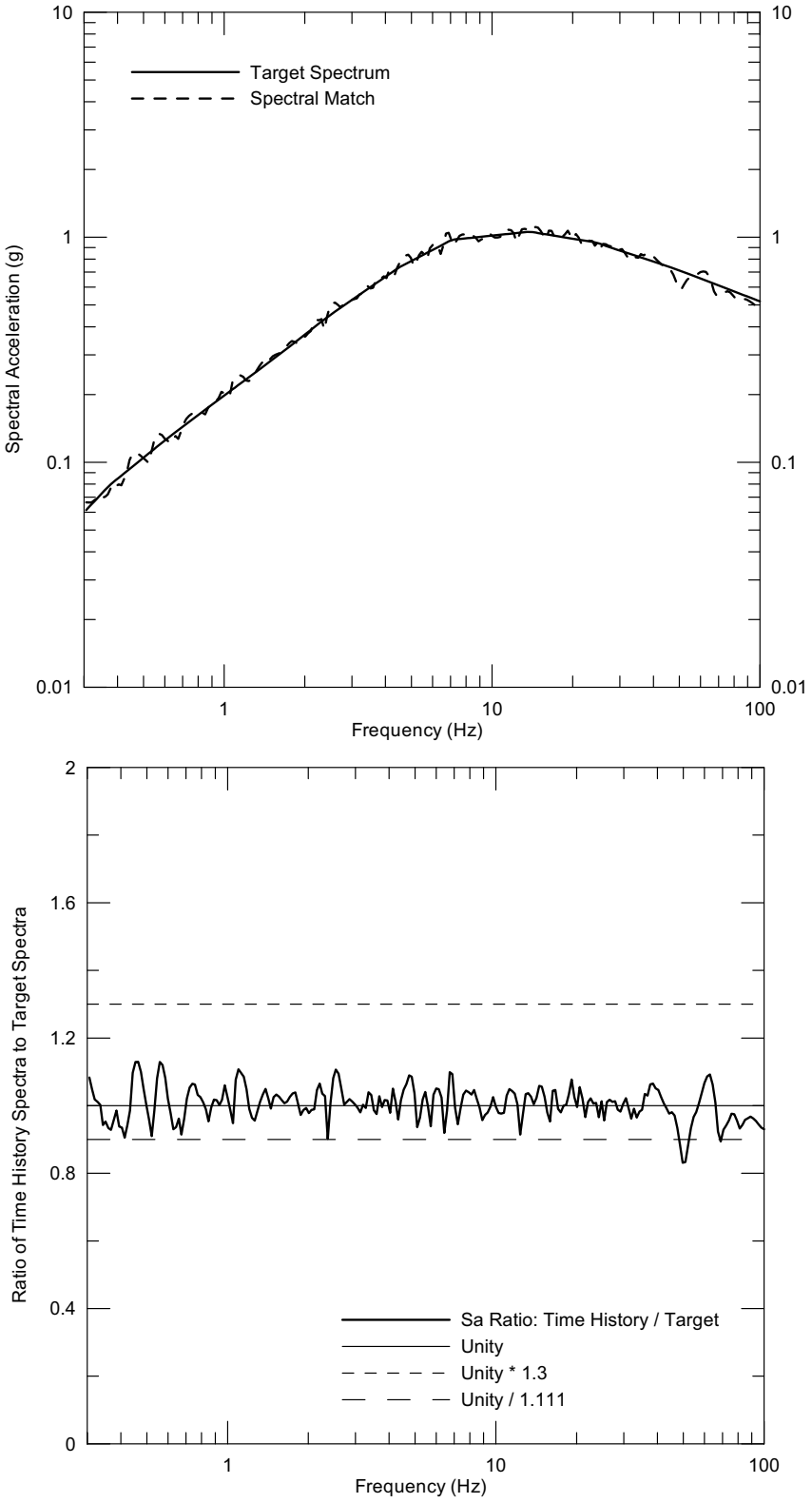

Source: Wong and Silva 2004a [DIRS 170443], Supplemental Record 87, pages 16 & 17

Figure 6.3-95. Response Spectrum of Point D/E 5x10 $^{-4}$ Vertical Time History No. 1 and Seismic Design Target Spectrum

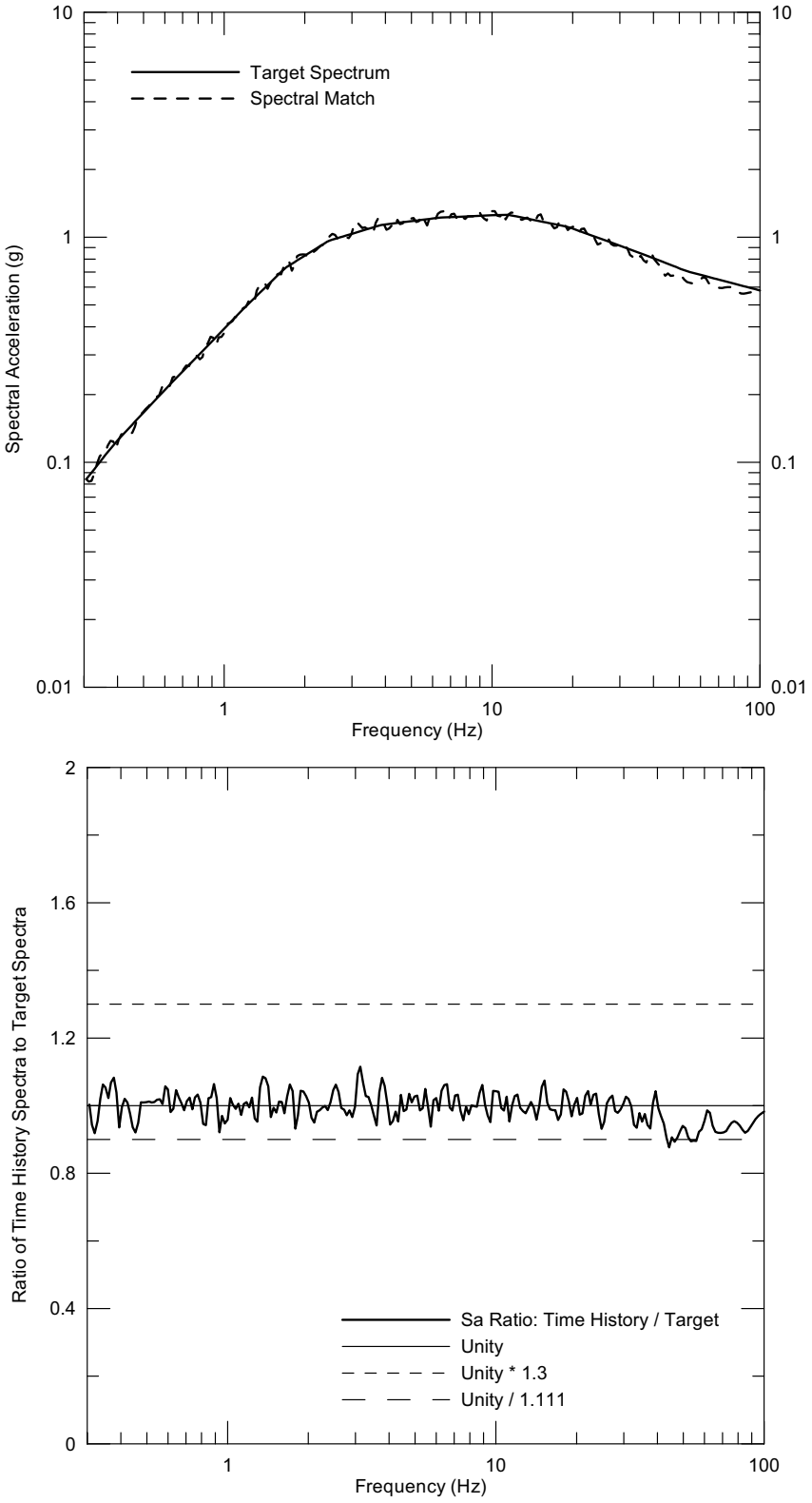

Source: Wong and Silva 2004a [DIRS 170443], Supplemental Record 87, pages 20 & 21

Figure 6.3-96. Response Spectrum of Point D/E 5×10^{-4} Horizontal-1 Time History No. 2 and Seismic Design Target Spectrum

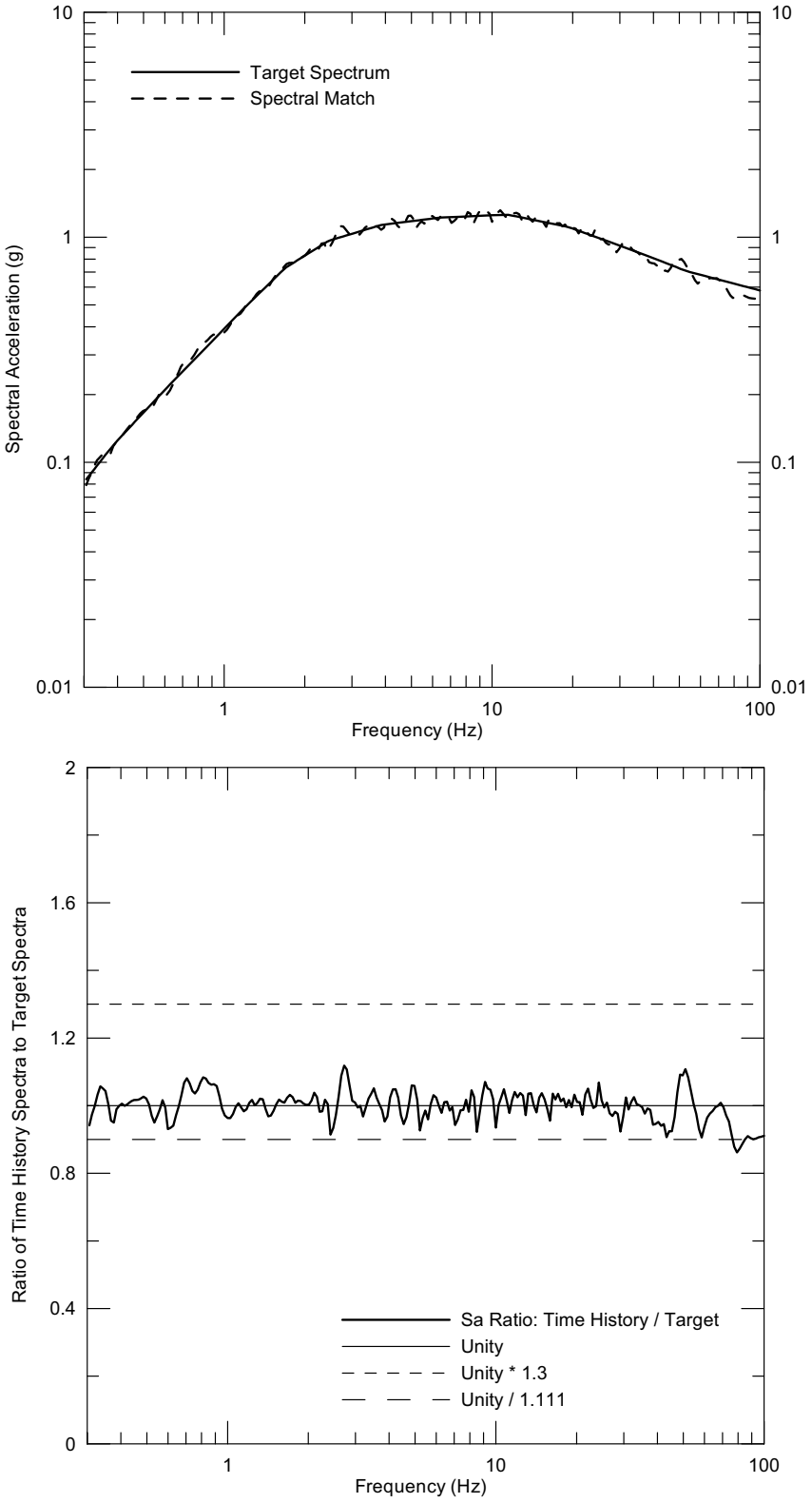

Source: Wong and Silva 2004a [DIRS 170443], Supplemental Record 87, pages 24 & 25

Figure 6.3-97. Response Spectrum of Point D/E 5x10^{-4} Horizontal-2 Time History No. 2 and Seismic Design Target Spectrum

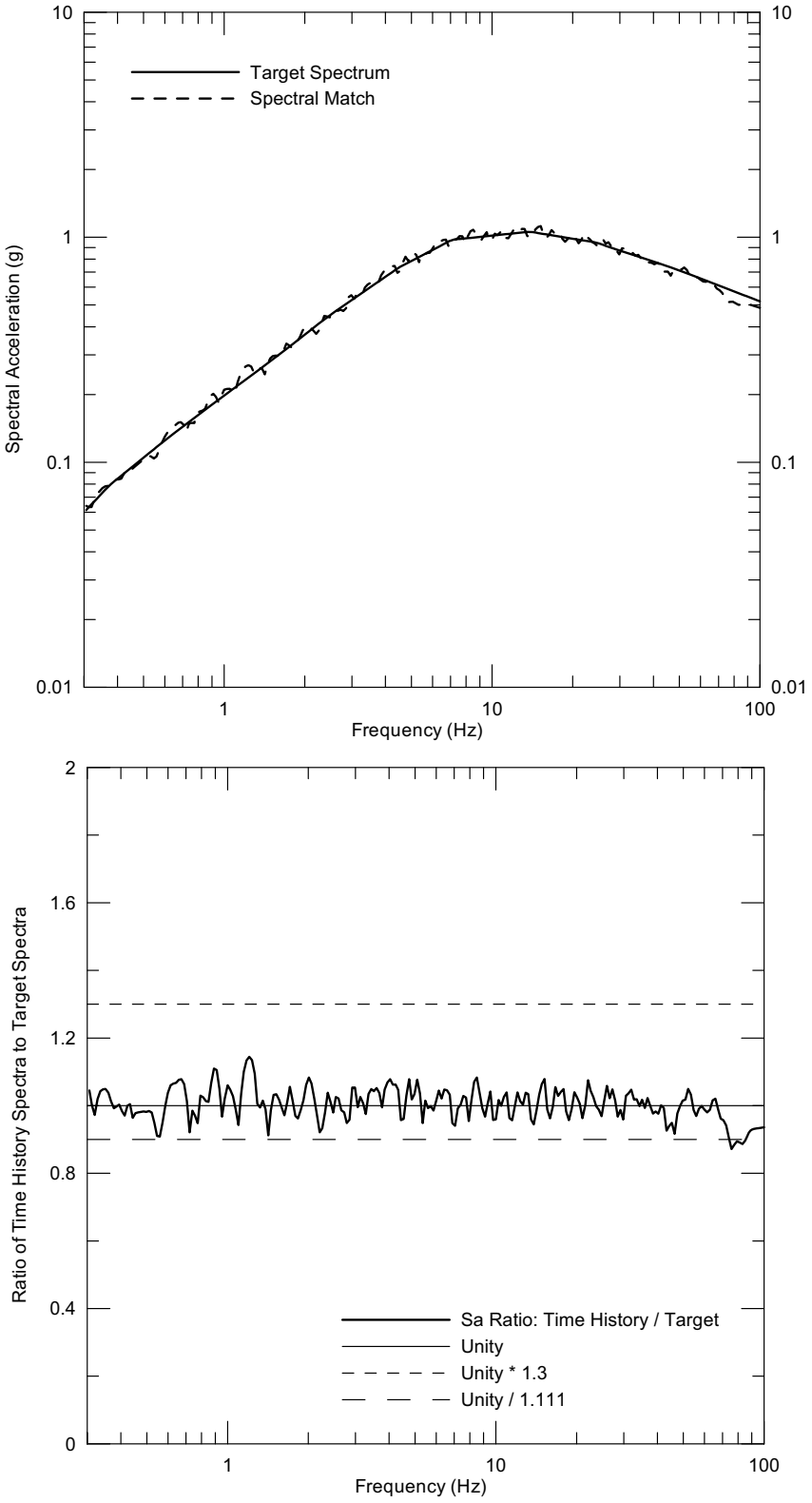

Source: Wong and Silva 2004a [DIRS 170443], Supplemental Record 87, pages 28 & 29

Figure 6.3-98. Response Spectrum of Point D/E 5×10^{-4} Vertical Time History No. 2 and Seismic Design Target Spectrum

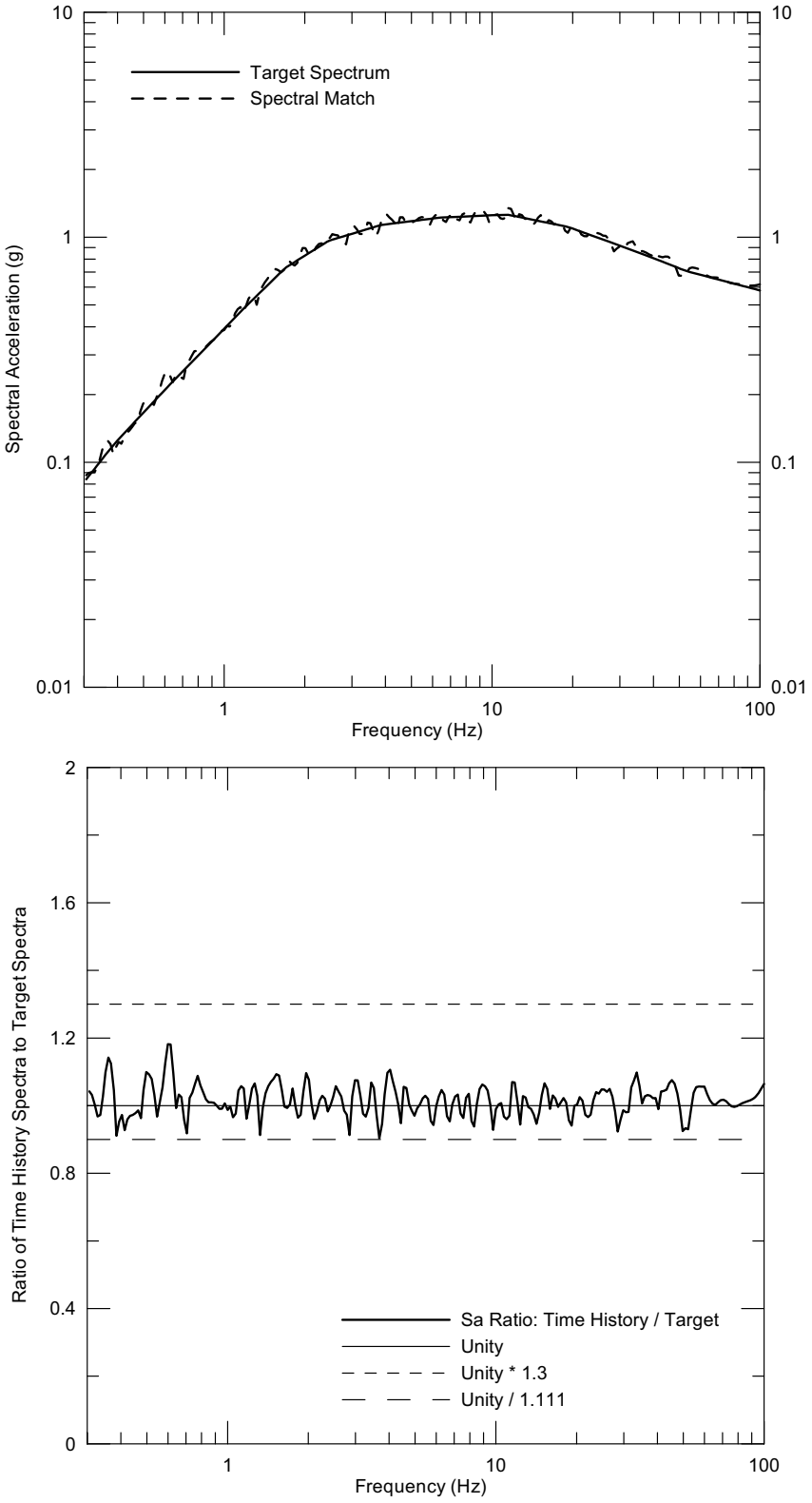

Source: Wong and Silva 2004a [DIRS 170443], Supplemental Record 87, pages 32 & 33

Figure 6.3-99. Response Spectrum of Point D/E 5×10^{-4} Horizontal-1 Time History No. 3 and Seismic Design Target Spectrum

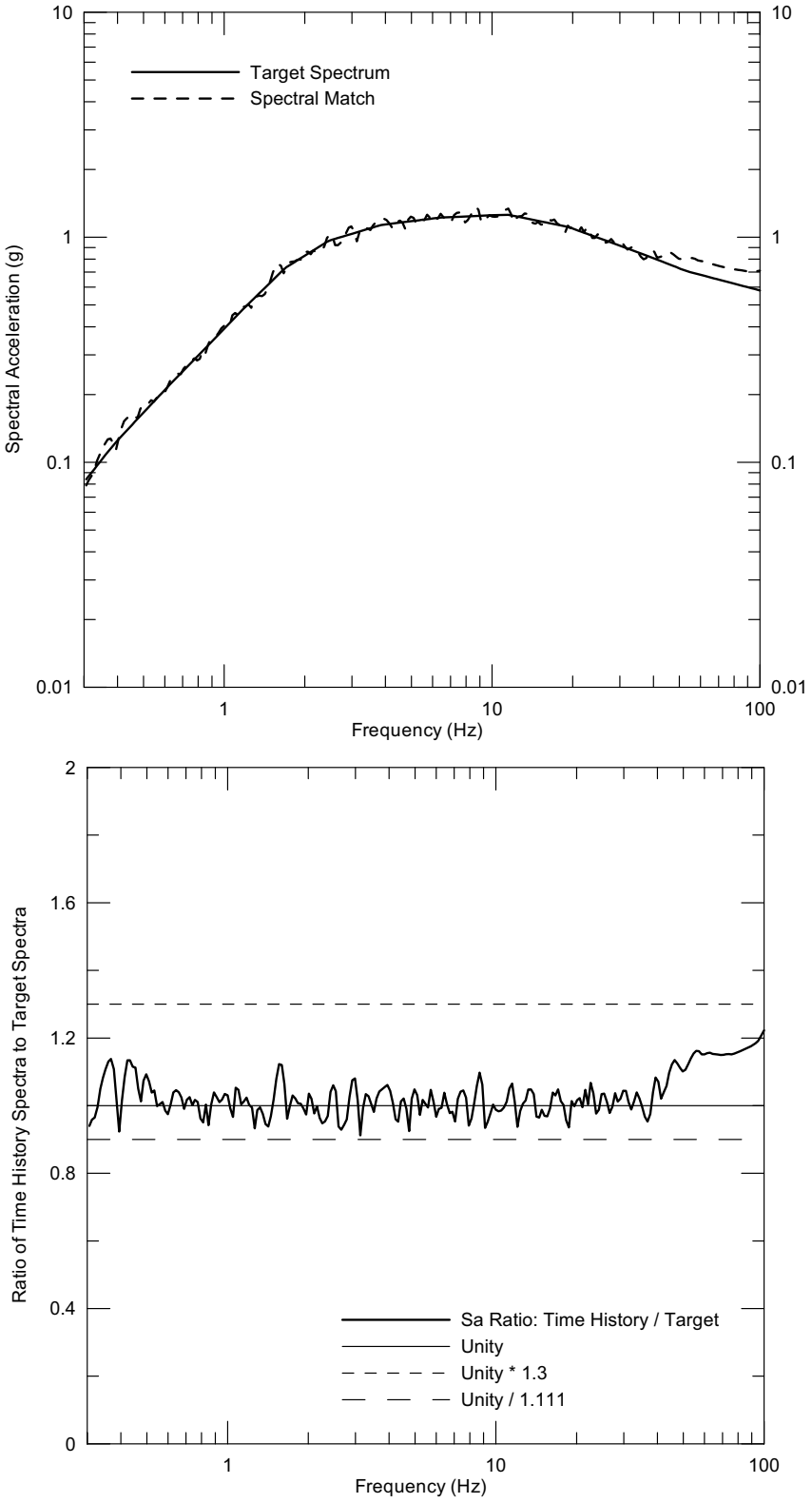

Source: Wong and Silva 2004a [DIRS 170443], Supplemental Record 87, pages 36 & 37

Figure 6.3-100. Response Spectrum of Point D/E 5x10^{-4} Horizontal-2 Time History No. 3 and Seismic Design Target Spectrum

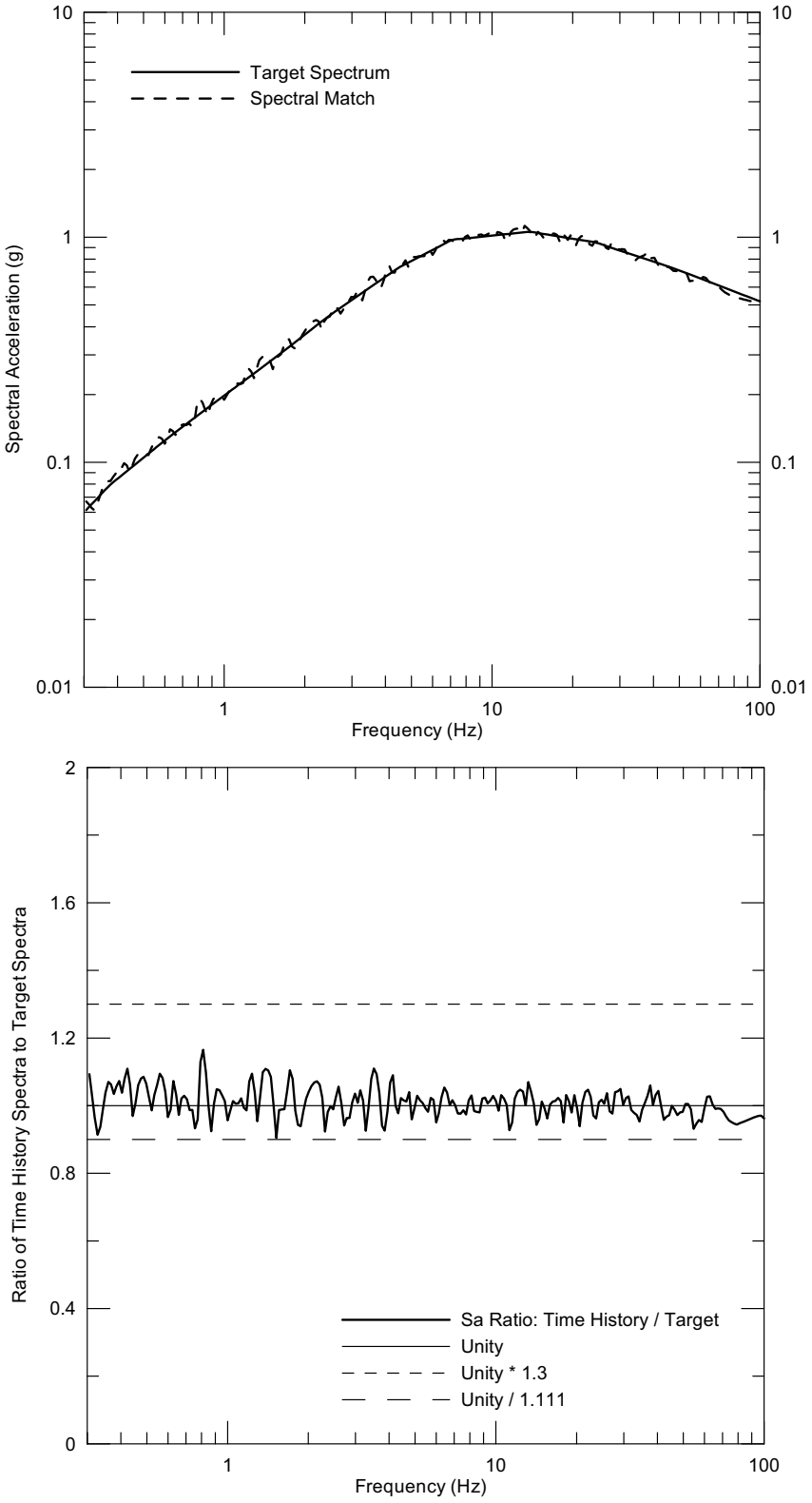

Source: Wong and Silva 2004a [DIRS 170443], Supplemental Record 87, pages 40 & 41

Figure 6.3-101. Response Spectrum of Point D/E 5×10^{-4} Vertical Time History No. 3 and Seismic Design Target Spectrum

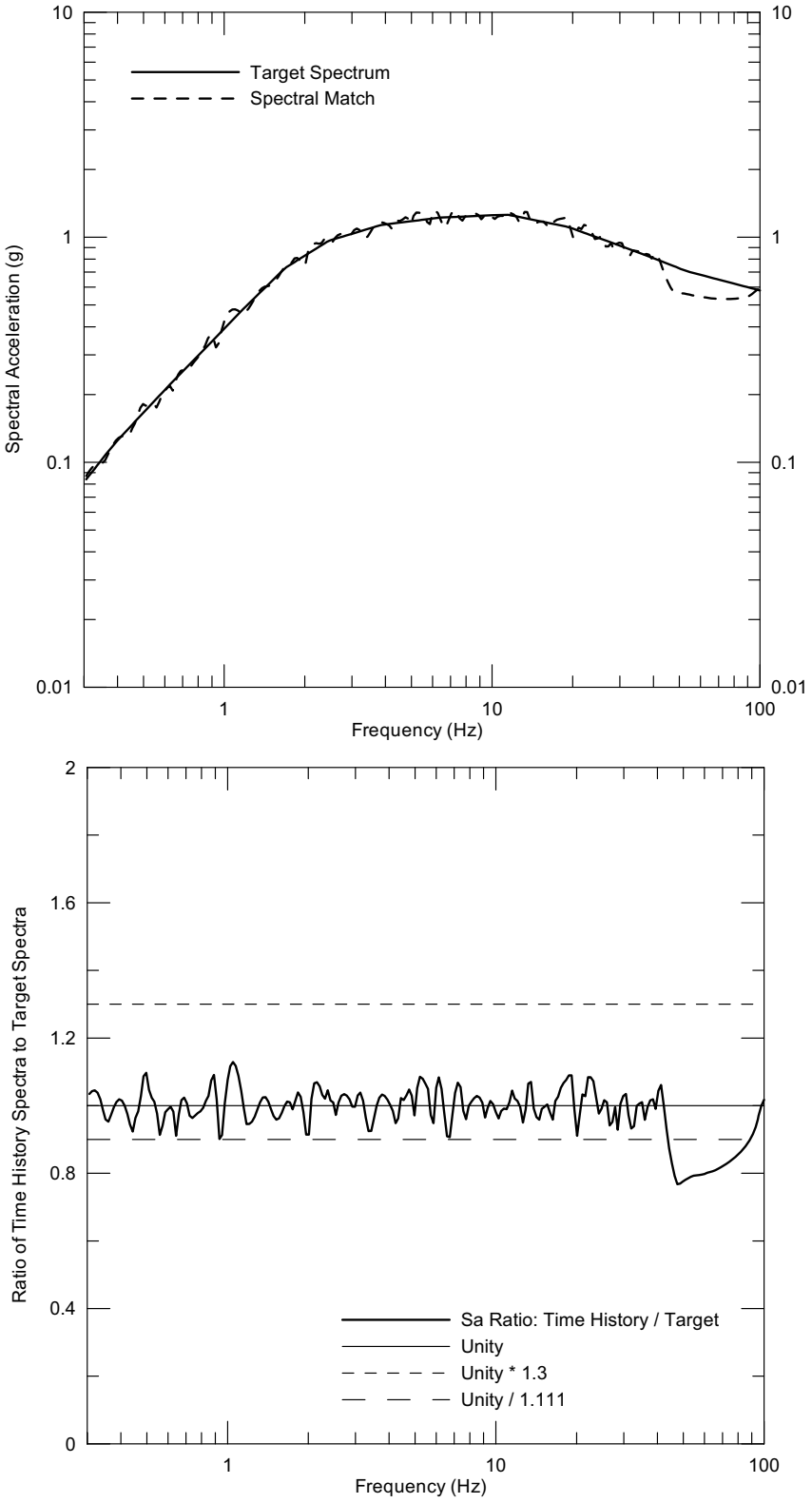

Source: Wong and Silva 2004a [DIRS 170443], Supplemental Record 87, pages 44 & 45

Figure 6.3-102. Response Spectrum of Point D/E 5×10^{-4} Horizontal-1 Time History No. 4 and Seismic Design Target Spectrum

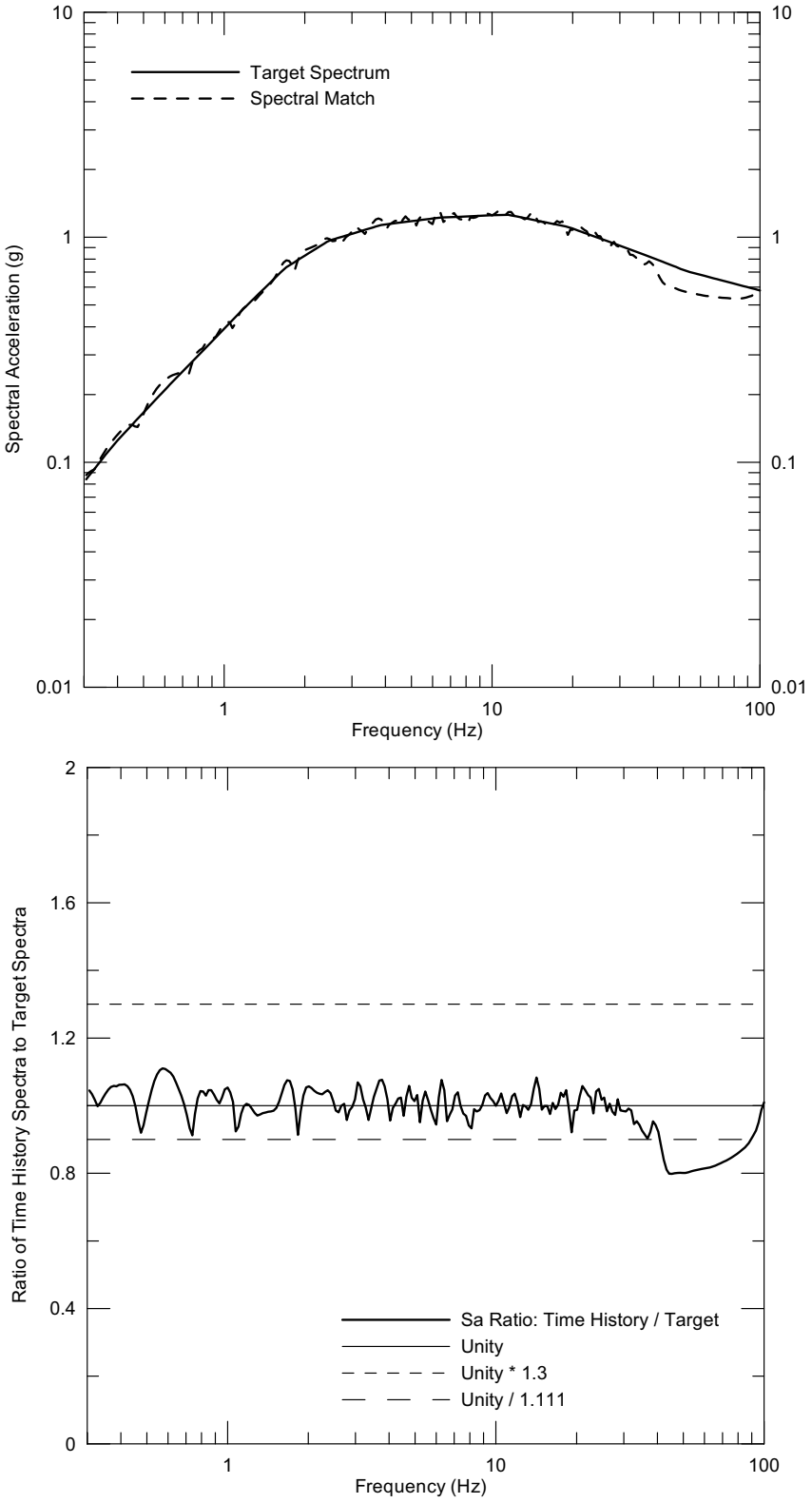

Source: Wong and Silva 2004a [DIRS 170443], Supplemental Record 87, pages 48 & 49

Figure 6.3-103. Response Spectrum of Point D/E 5x10^{-4} Horizontal-2 Time History No. 4 and Seismic Design Target Spectrum

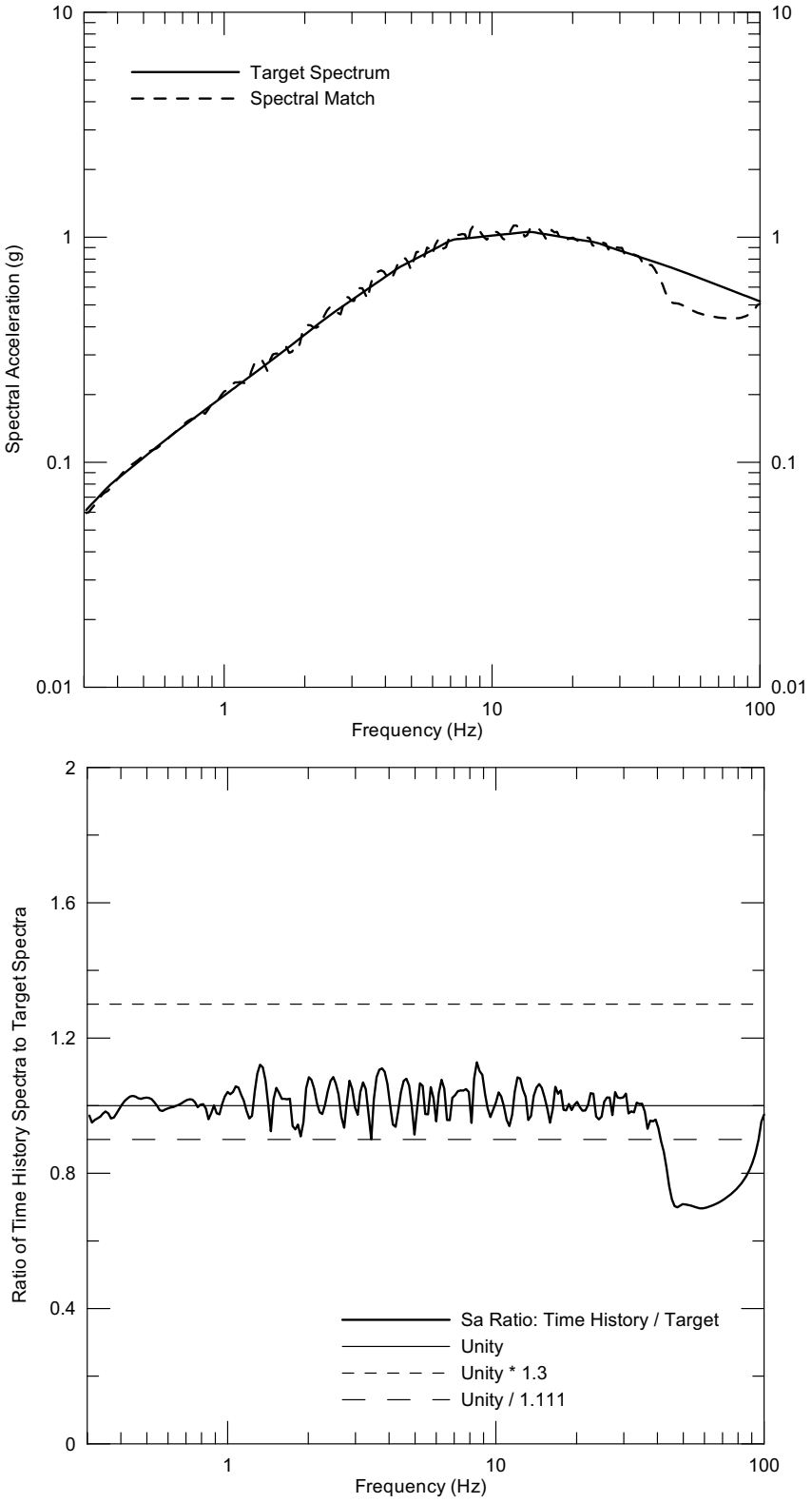

Source: Wong and Silva 2004a [DIRS 170443], Supplemental Record 87, pages 52 & 53

Figure 6.3-104. Response Spectrum of Point D/E $5x10^{-4}$ Vertical Time History No. 4 and Seismic Design Target Spectrum

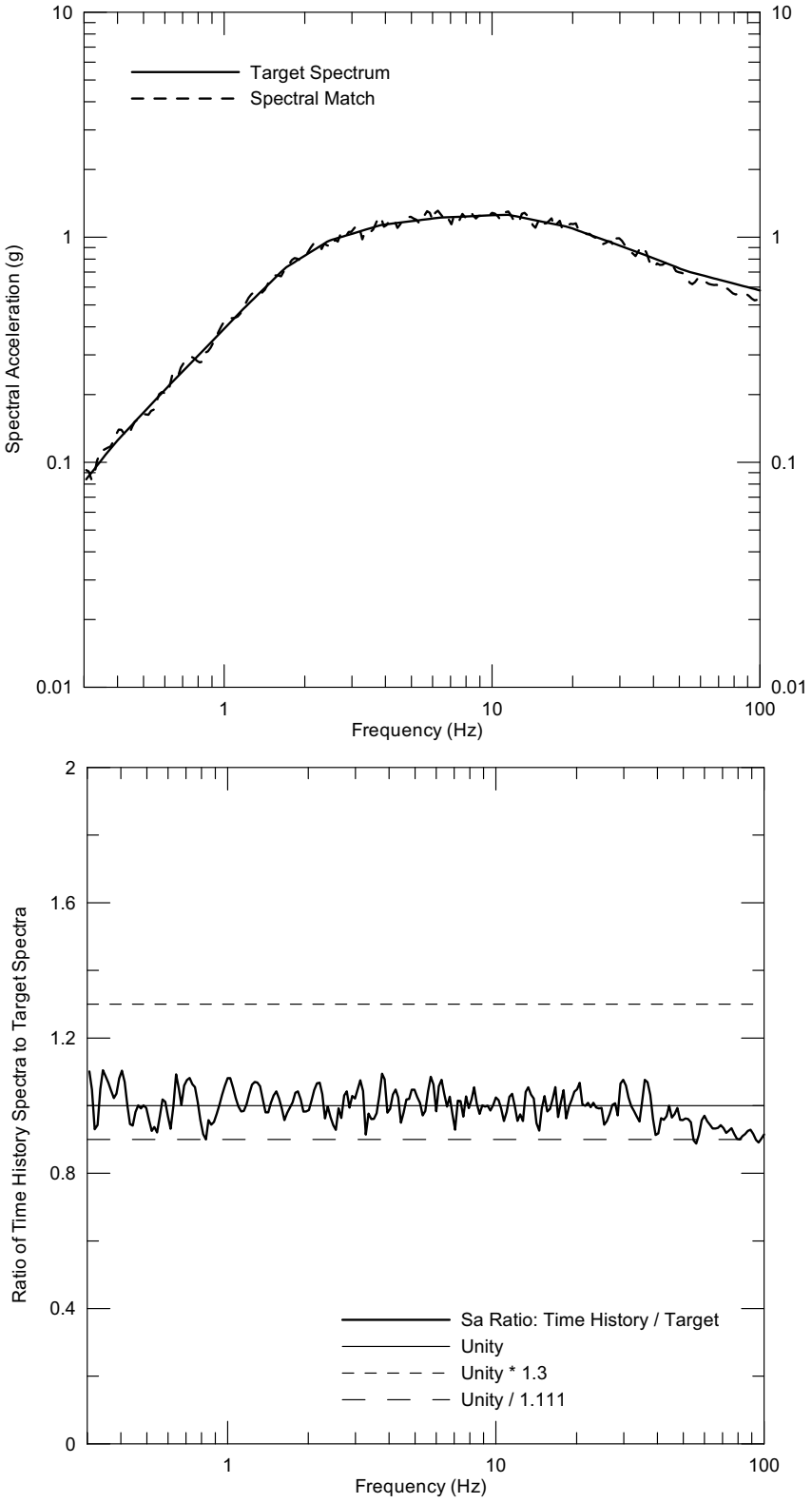

Source: Wong and Silva 2004a [DIRS 170443], Supplemental Record 87, pages 56 & 57

Figure 6.3-105. Response Spectrum of Point D/E 5x10^{-4} Horizontal-1 Time History No. 5 and Seismic Design Target Spectrum

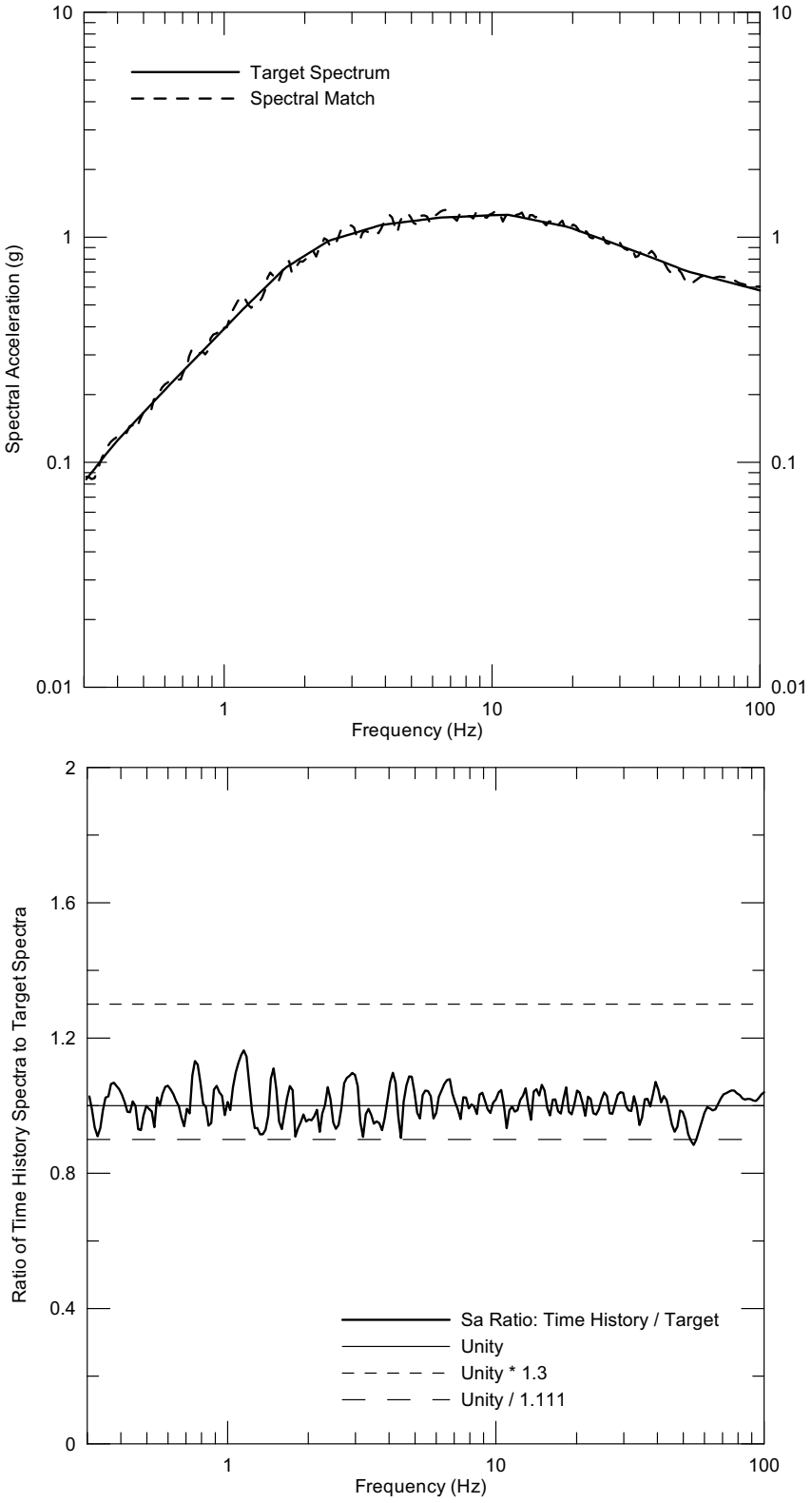

Source: Wong and Silva 2004a [DIRS 170443], Supplemental Record 87, pages 60 & 61

Figure 6.3-106. Response Spectrum of Point D/E 5x10^{-4} Horizontal-2 Time History No. 5 and Seismic Design Target Spectrum

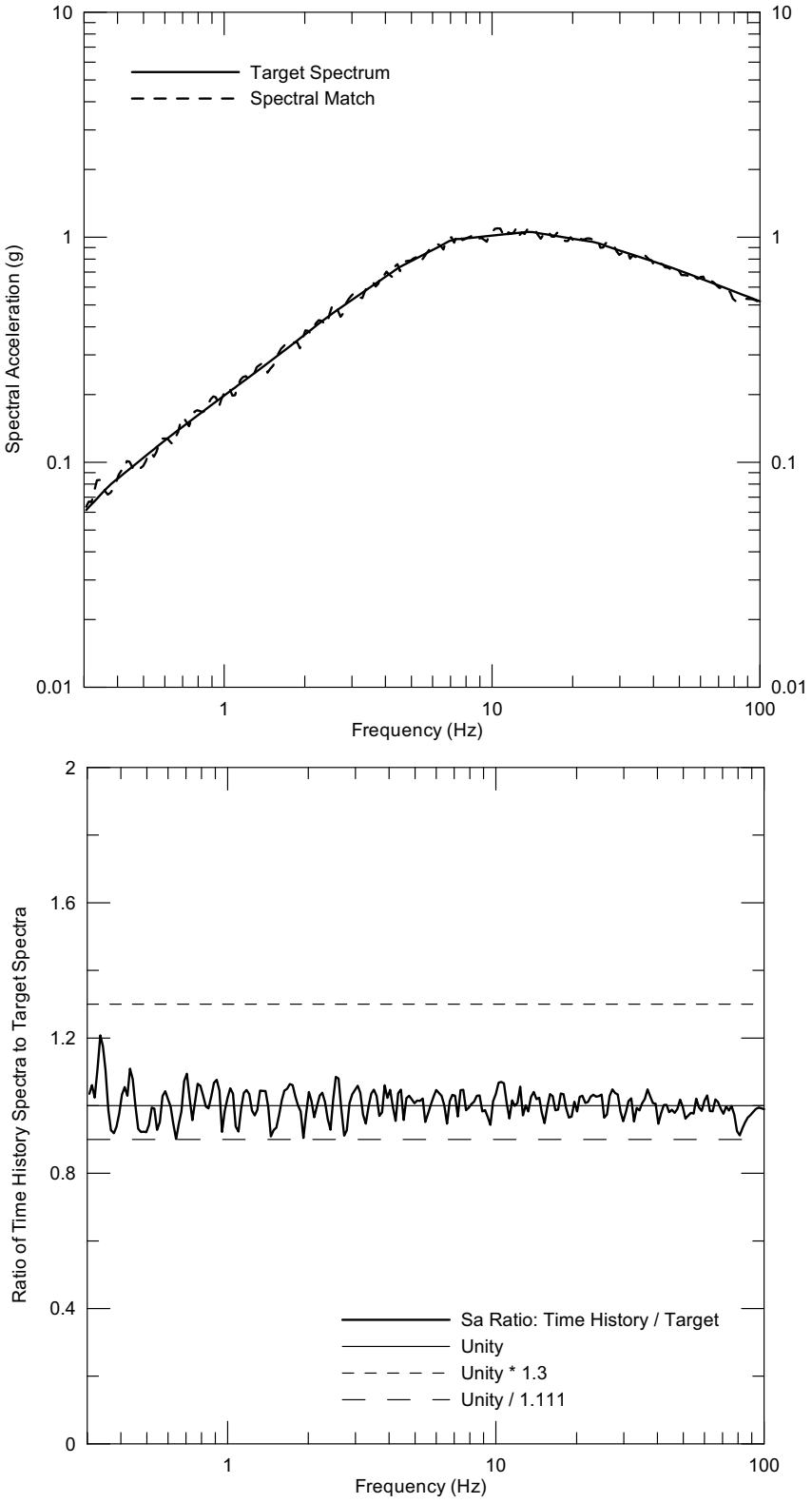

Source: Wong and Silva 2004a [DIRS 170443], Supplemental Record 87, pages 64 &: 65

Figure 6.3-107. Response Spectrum of Point D/E 5x10-4 Vertical Time History No. 5 and Seismic Design Target Spectrum

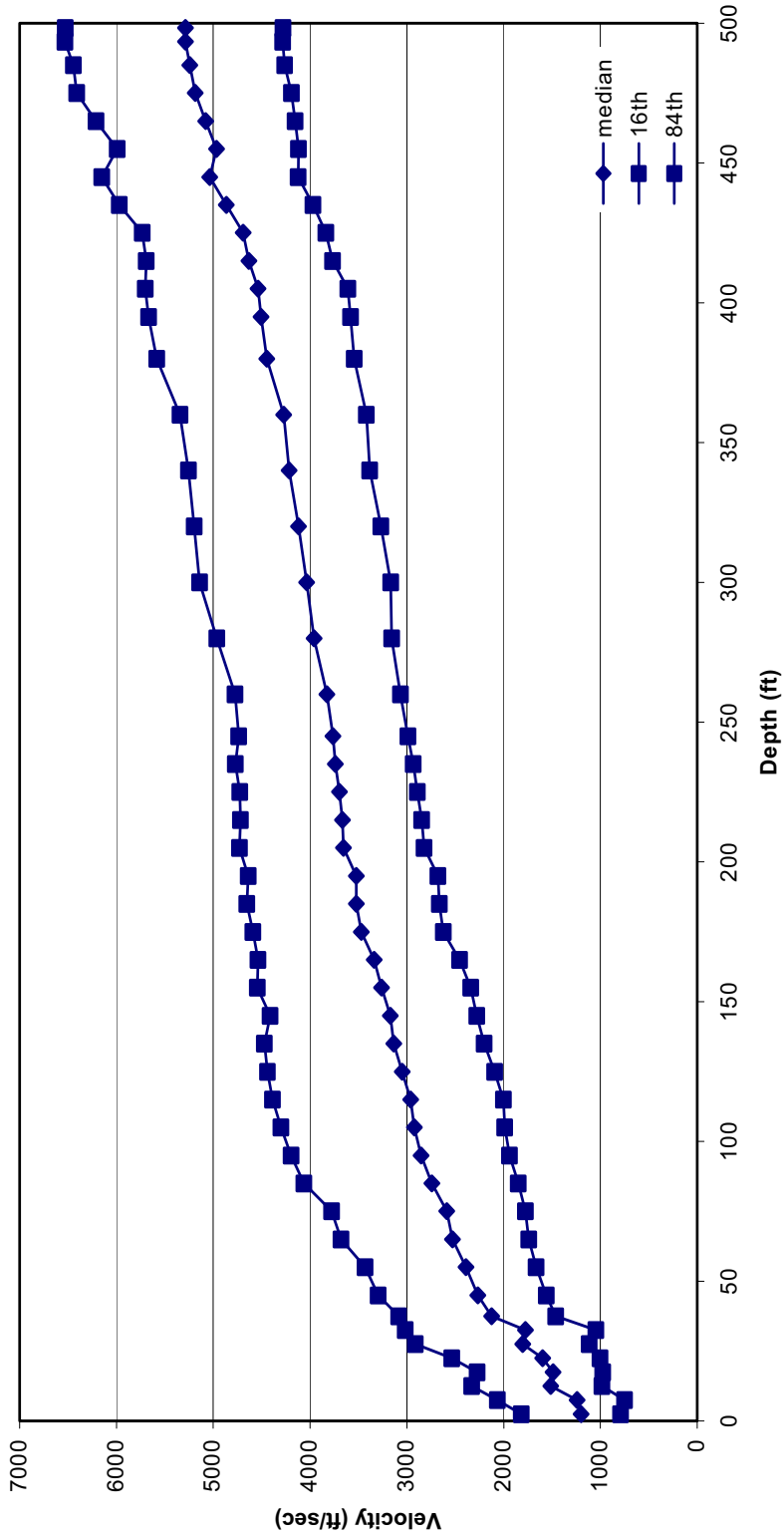

DTN: MO0403SPWHB5E4.005 [DIRS 168376]

Figure 6.3-108. Point D 5×10^{-4} Strain-Compatible Soil Properties: V_S, 35 ft Profile (35 ft Alluvium)

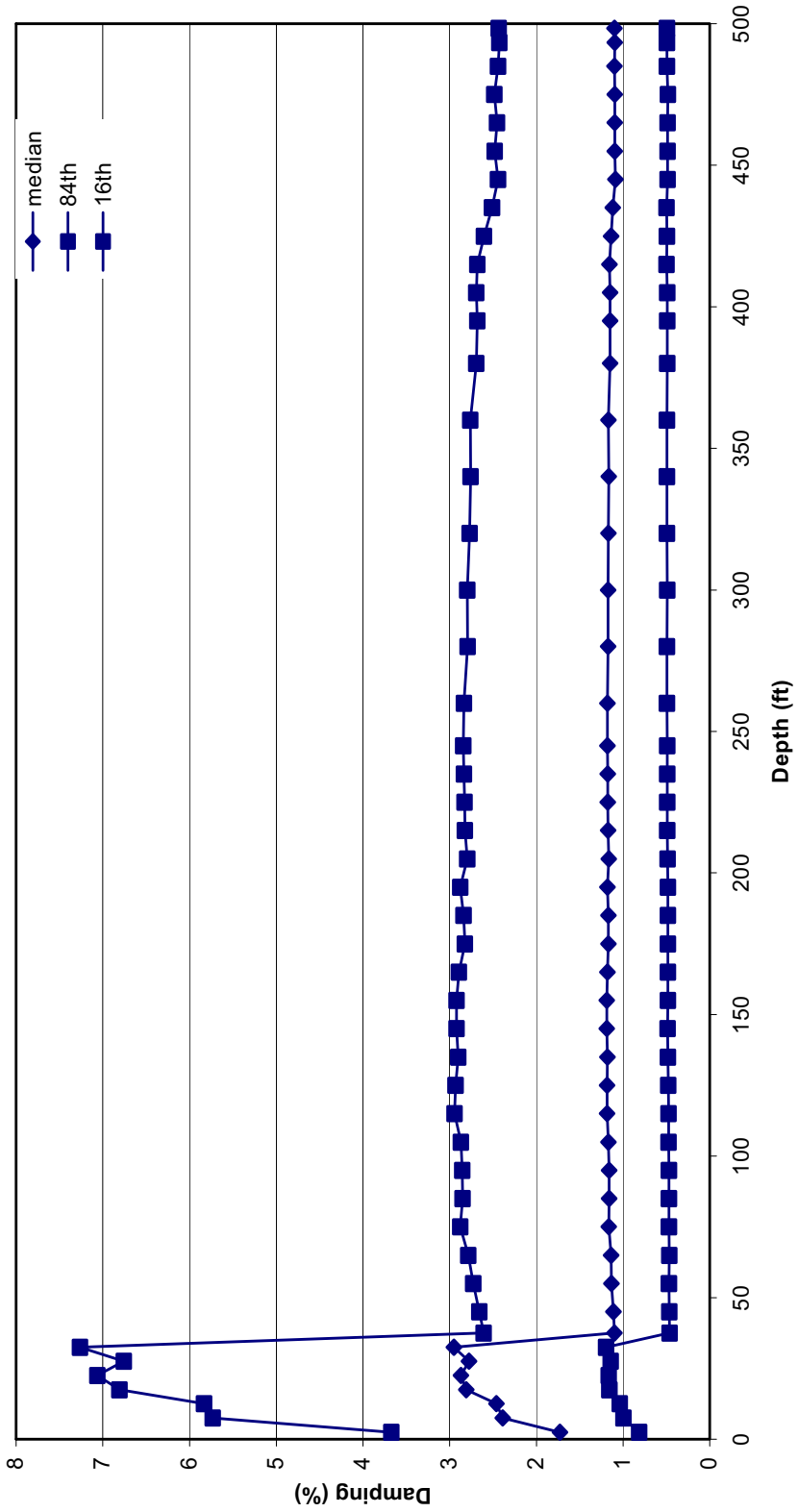

DTN: MO0403SPWHB5E4.005 [DIRS 168376]

Figure 6.3-109. Point D $5x10^{-4}$ Strain-Compatible Soil Properties: S-Wave Damping, 35 ft Profile (35 ft Alluvium)

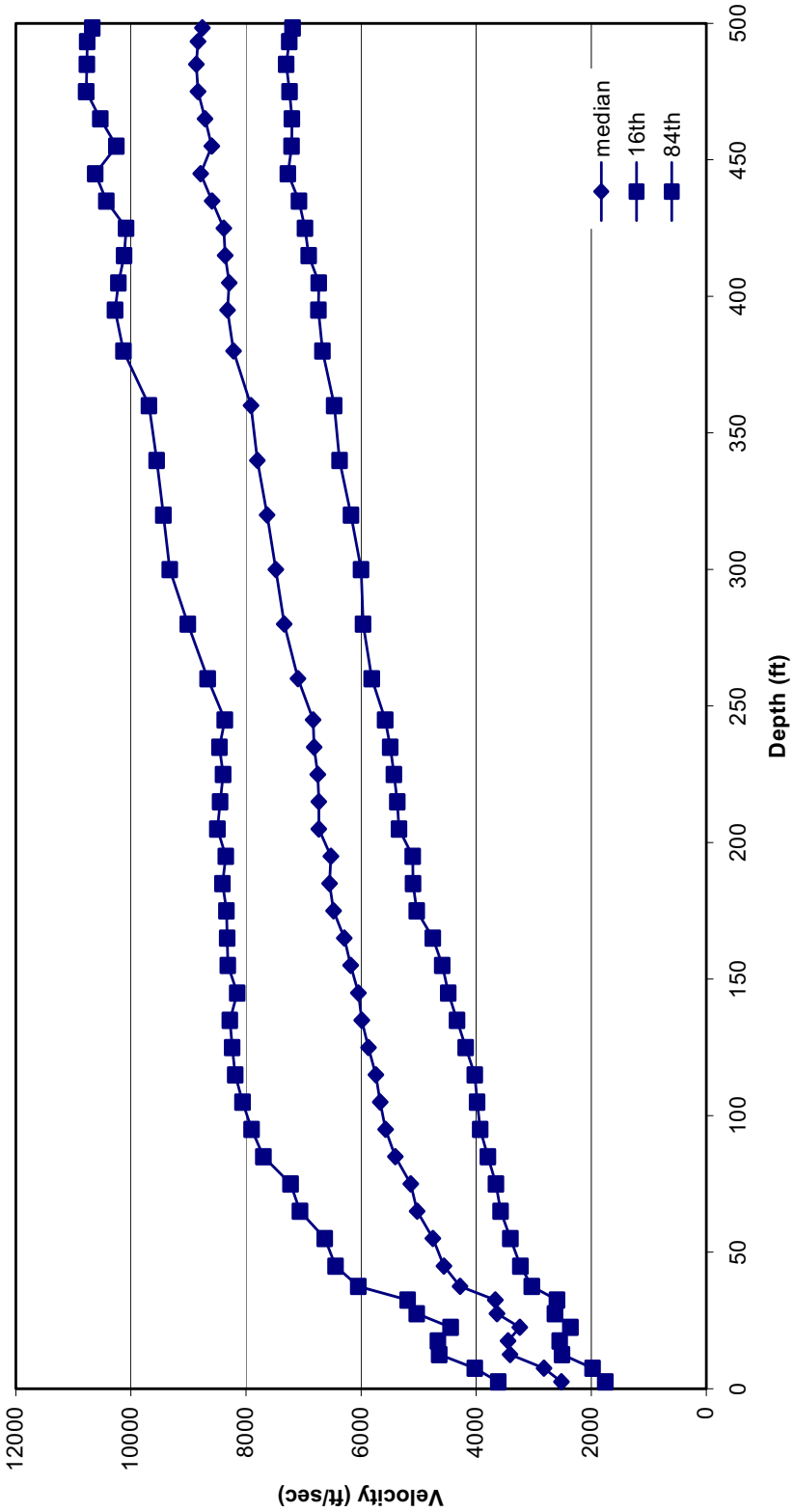

DTN: MO0403SPWHB5E4.005 [DIRS 168376]

Figure 6.3-110. $5x10^{-4}$ Point D Strain-Compatible Soil Properties: V_P, 35 ft Profile (35 ft Alluvium)

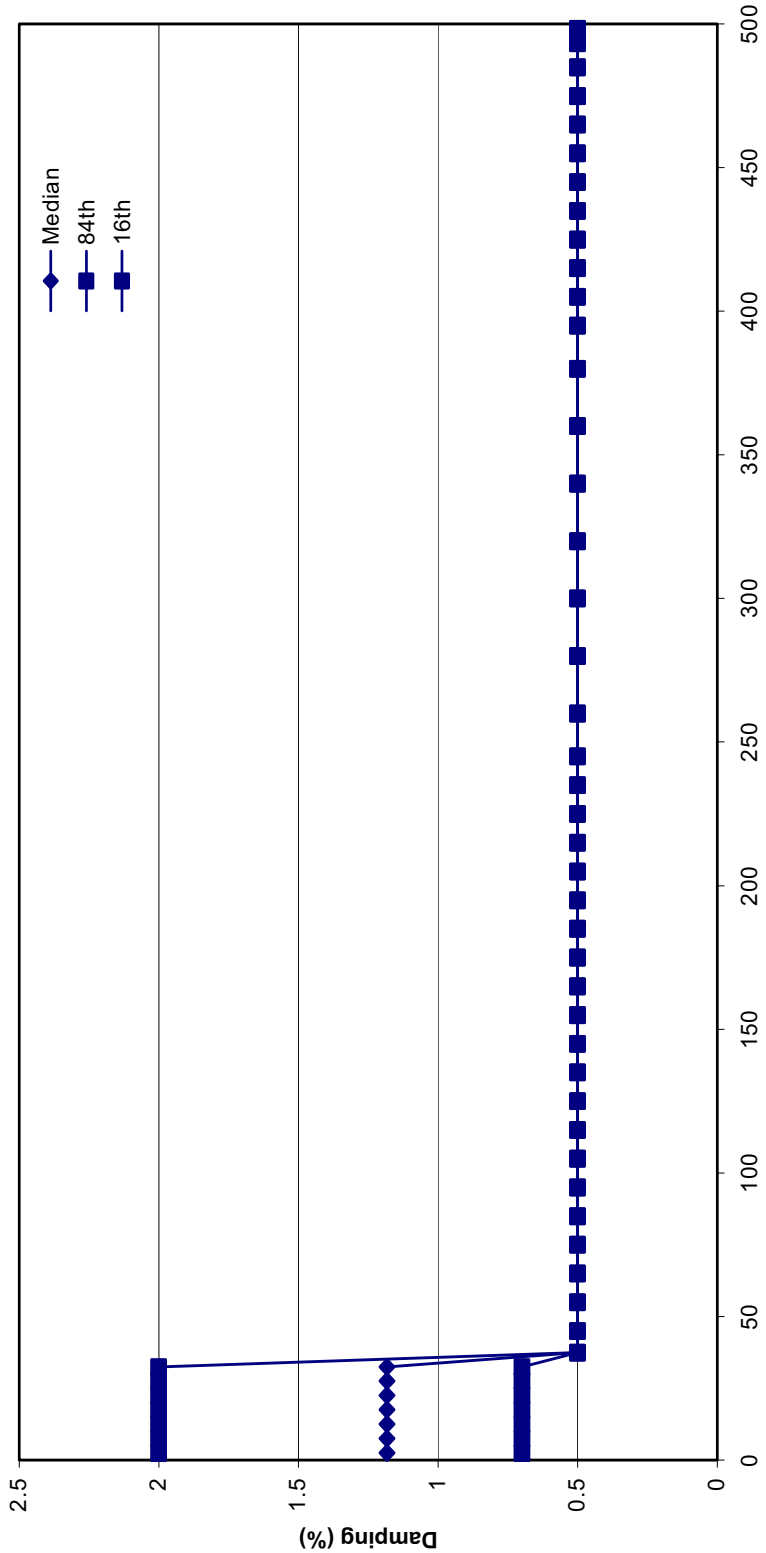

DTN: MO0403SPWHB5E4.005 [DIRS 168376]

Figure 6.3-111. Point D $5x10^{-4}$ Strain-Compatible Soil Properties: P-Wave Damping, 35 ft Profile (35 ft Alluvium)

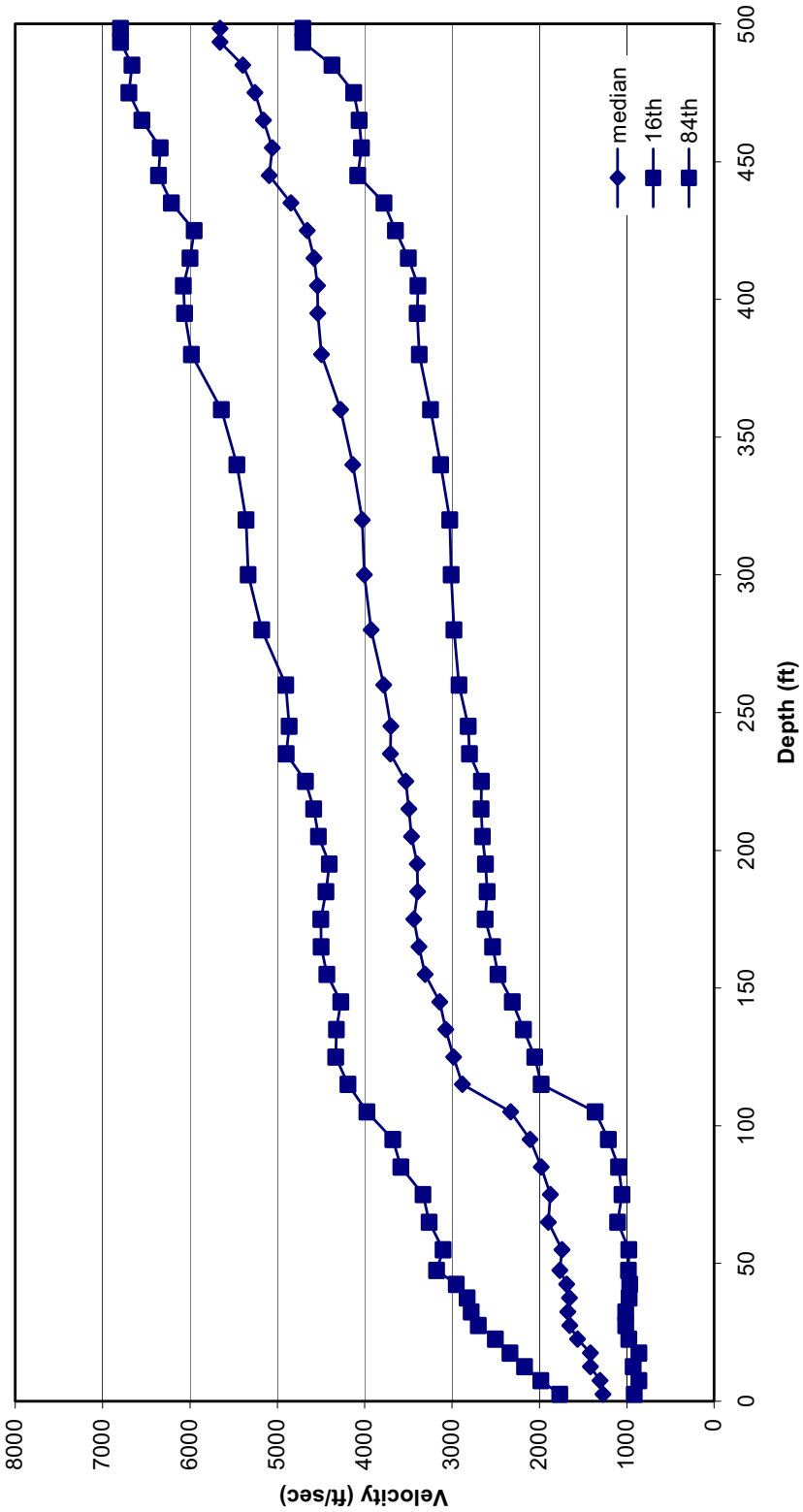

DTN: MO0403SPWHB5E4.005 [DIRS 168376]

Figure 6.3-112. Point D 5×10^{-4} Strain-Compatible Soil Properties: V_S, 110 ft Profile (110 ft Alluvium)

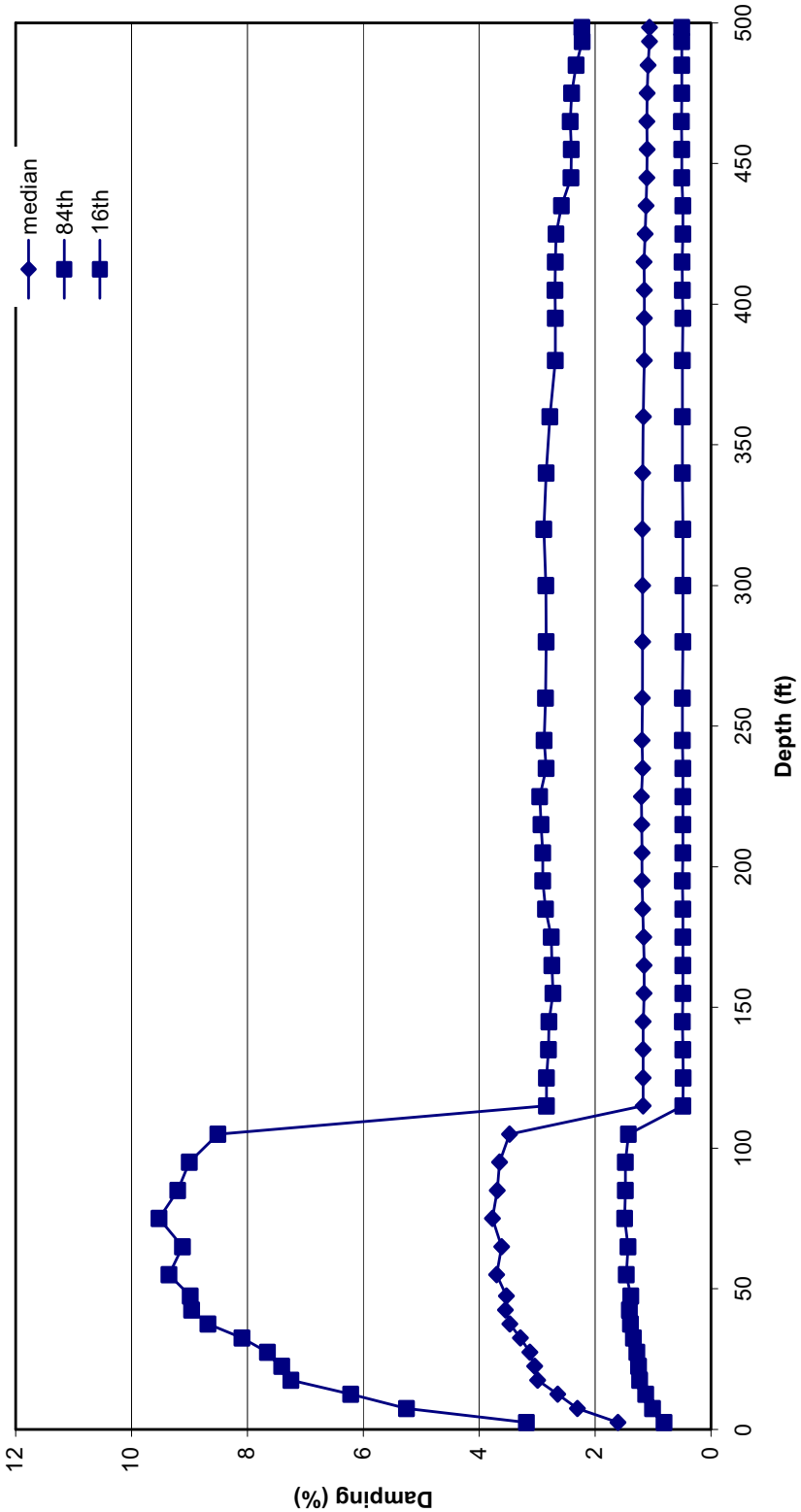

DTN: MO0403SPWHB5E4.005 [DIRS 168376]

Figure 6.3-113. Point D 5×10^{-4} Strain-Compatible Soil Properties: S-Wave Damping, 110 ft Profile (110 ft Alluvium)

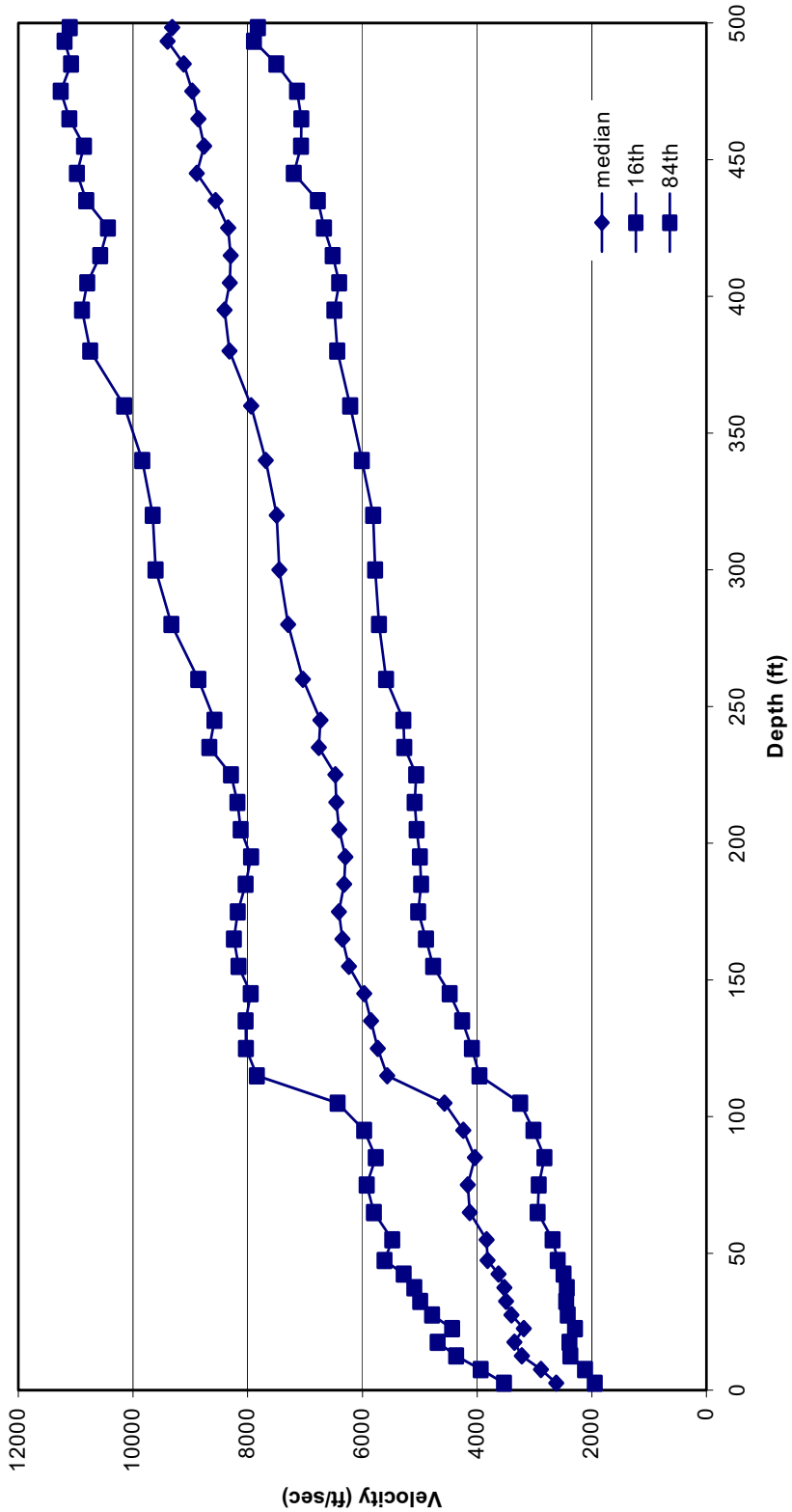

DTN: MO0403SPWHB5E4.005 [DIRS 168376]

Figure 6.3-114. Point D 5×10^{-4} Strain-Compatible Soil Properties: V_P, 110 ft Profile (110 ft Alluvium)

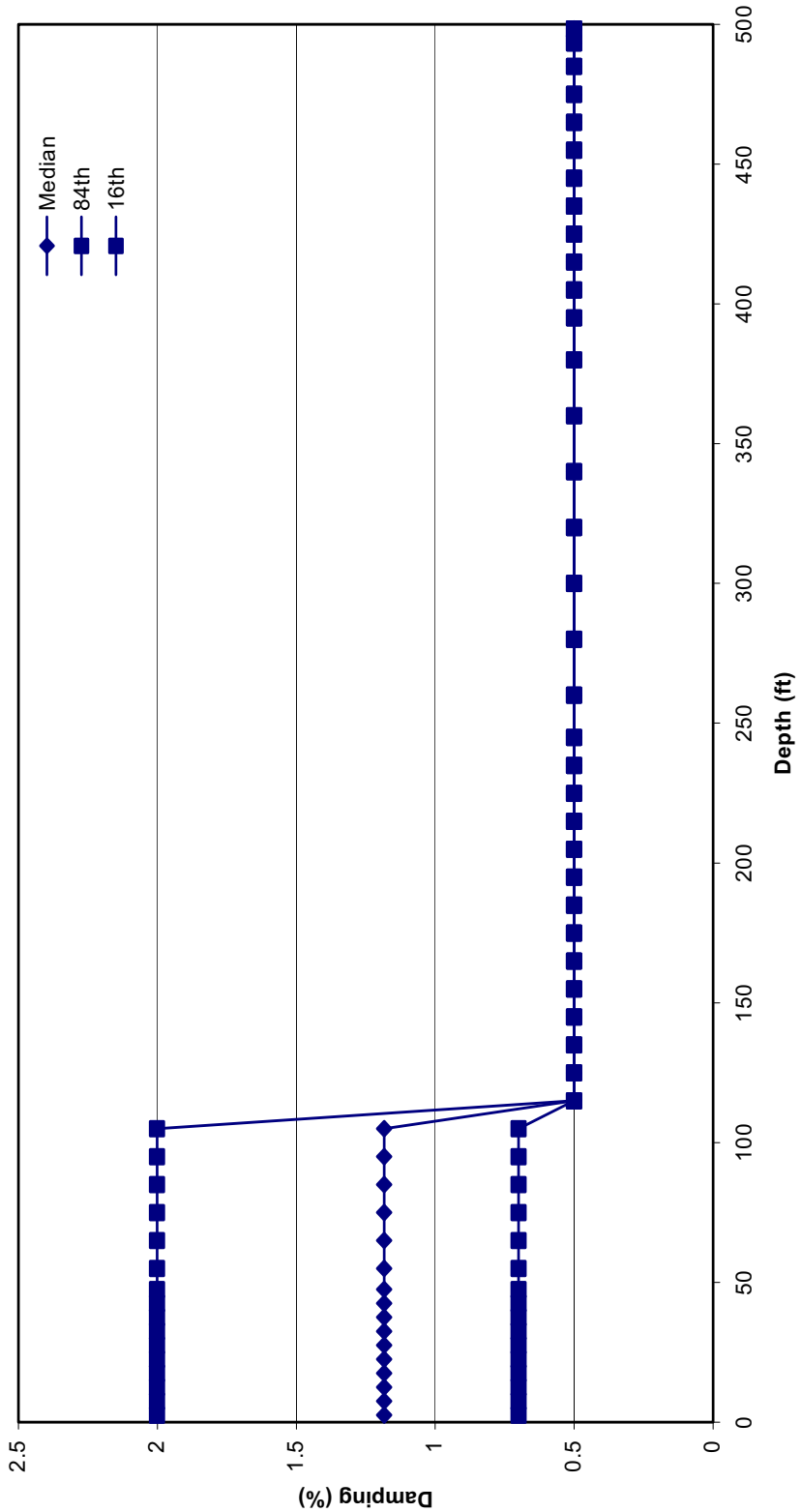

DTN: MO0403SPWHB5E4.005 [DIRS 168376]

Figure 6.3-115. Point D $5x10^{-4}$ Strain-Compatible Soil Properties: P-Wave Damping, 110 ft Profile (110 ft Alluvium)

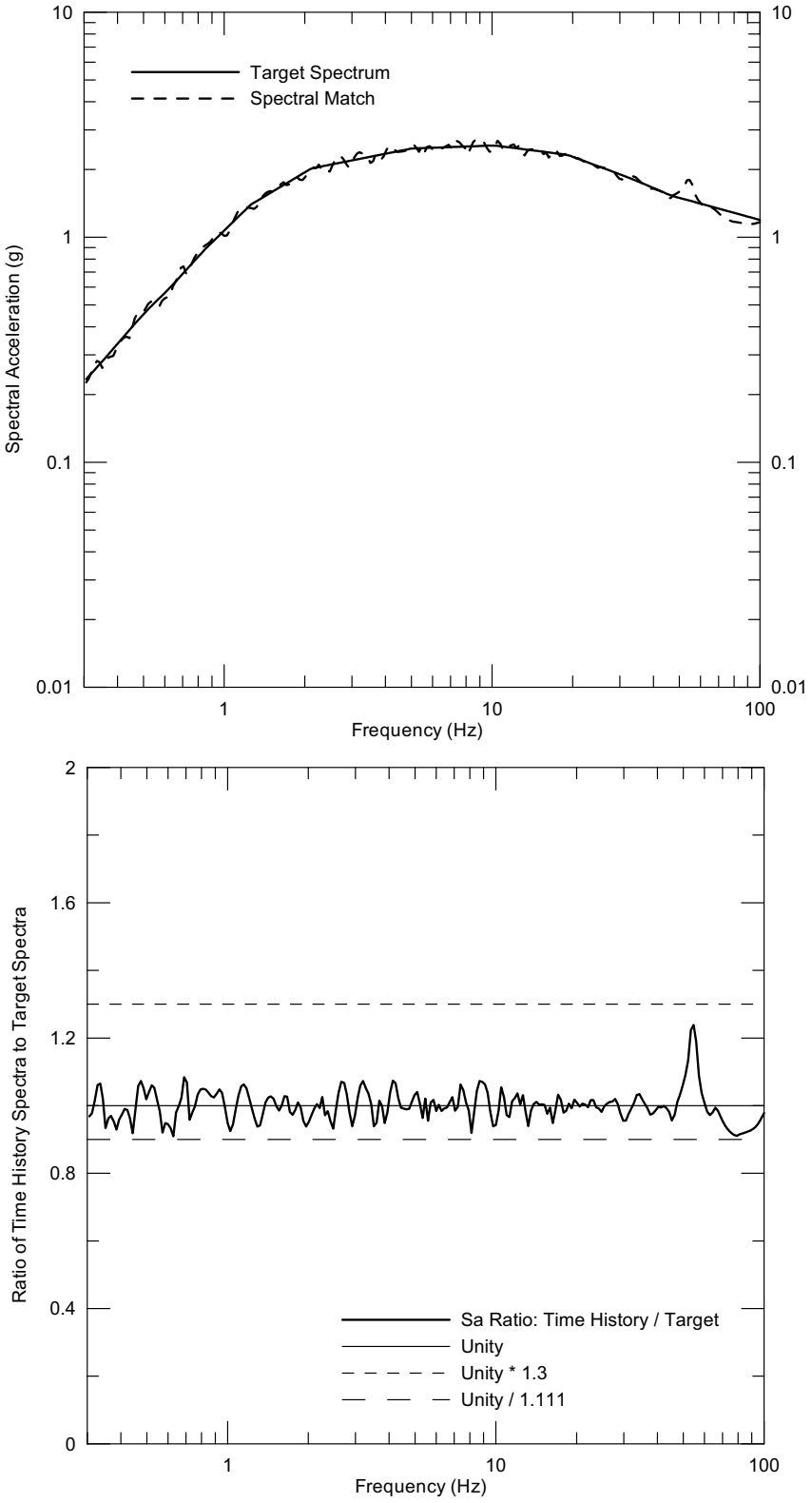

Source: Wong and Silva 2004a [DIRS 170443], Supplemental Record 101, pages 6 & 8

Figure 6.3-116. Response Spectrum of Point D/E 10^{-4} Horizontal-1 Time History and Seismic Design Target Spectrum

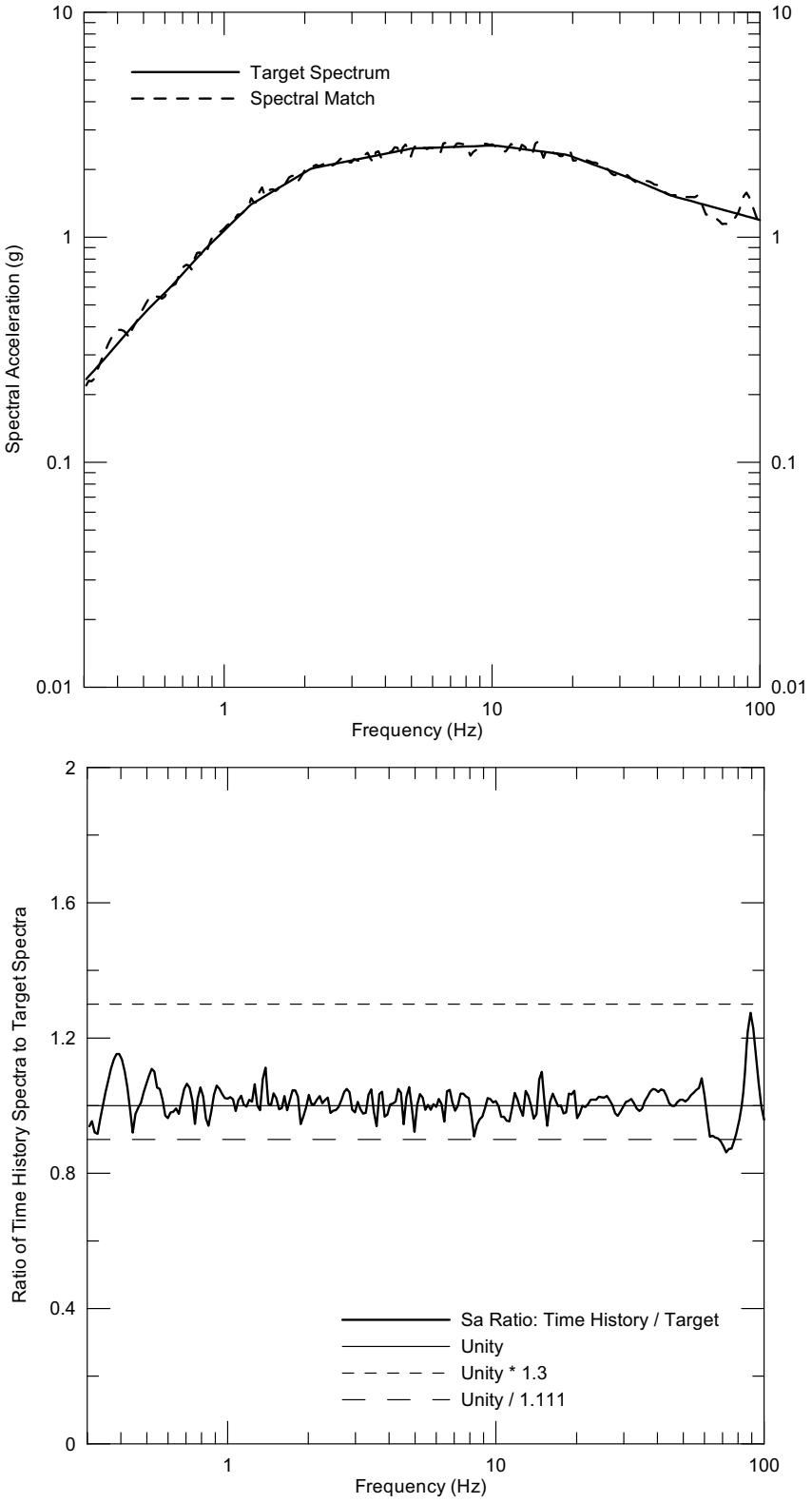

Source: Wong and Silva 2004a [DIRS 170443], Supplemental Record 101, pages 10 & 12

Figure 6.3-117. Response Spectrum of Point D/E 10^{-4} Horizontal-2 Time History and Seismic Design Target Spectrum

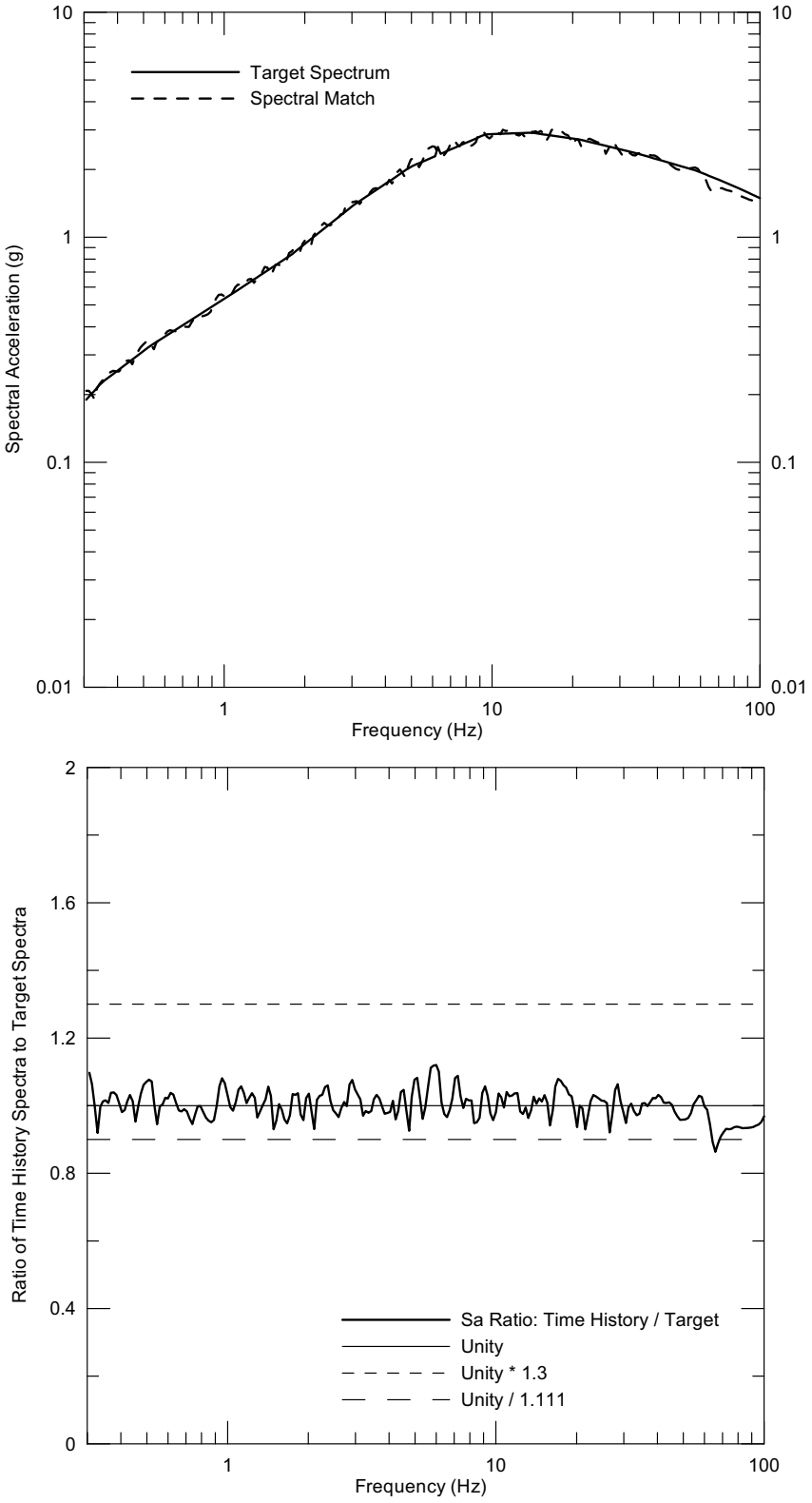

Source: Wong and Silva 2004a [DIRS 170443], Supplemental Record 101, pages 14 & 16

Figure 6.3-118. Response Spectrum of Point D/E 10^{-4} Vertical Time History and Seismic Design Target Spectrum

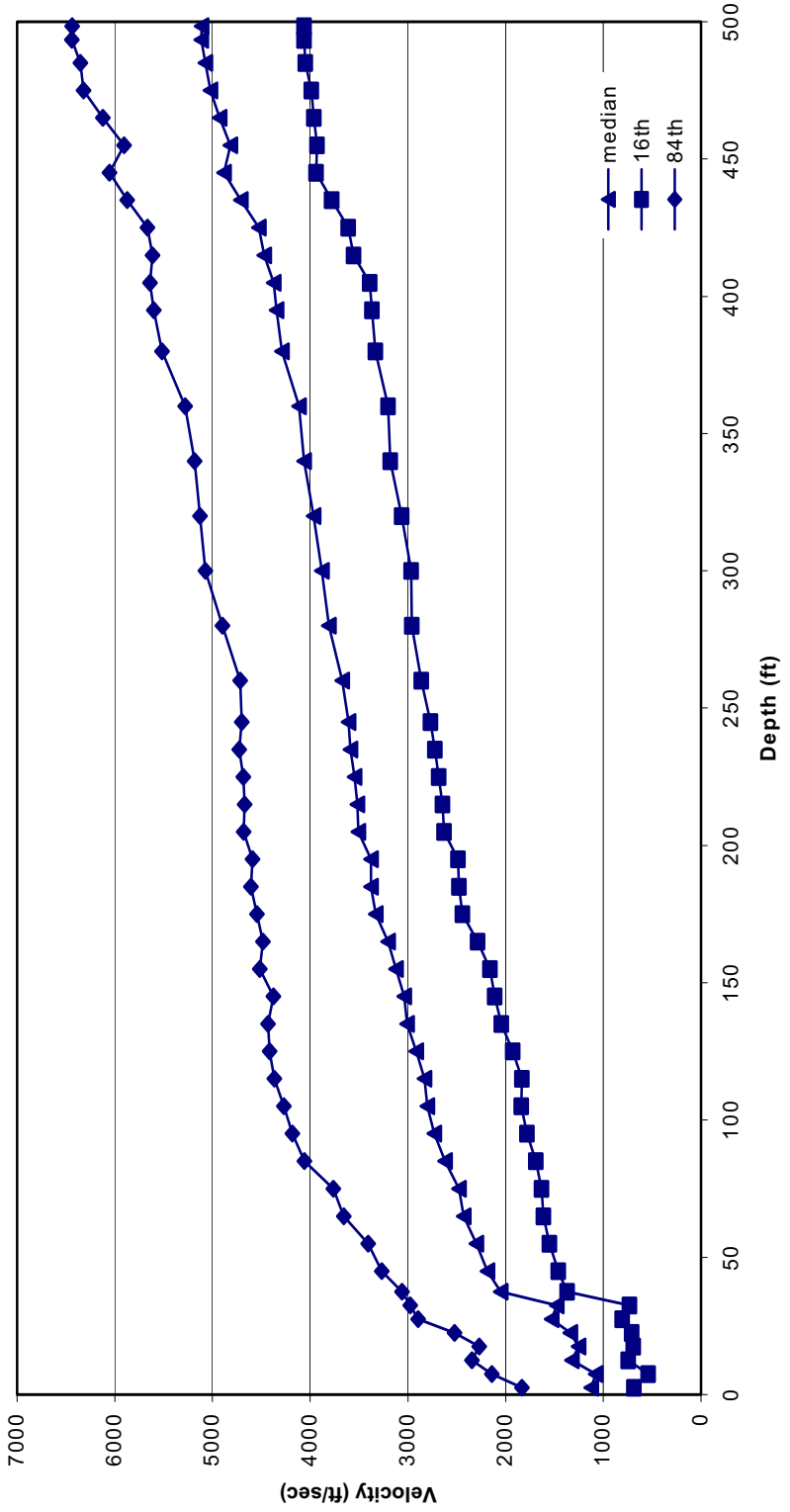

DTN: MO0403SCSPSFAD.001 [DIRS 169342]

Source: Wong and Silva 2004a [DIRS 170443], Supplemental Record 113, pages 9-11

Figure 6.3-119. Point D 10^{-4} Strain-Compatible Soil Properties: V_S, 35 ft Profile (35 ft Alluvium)

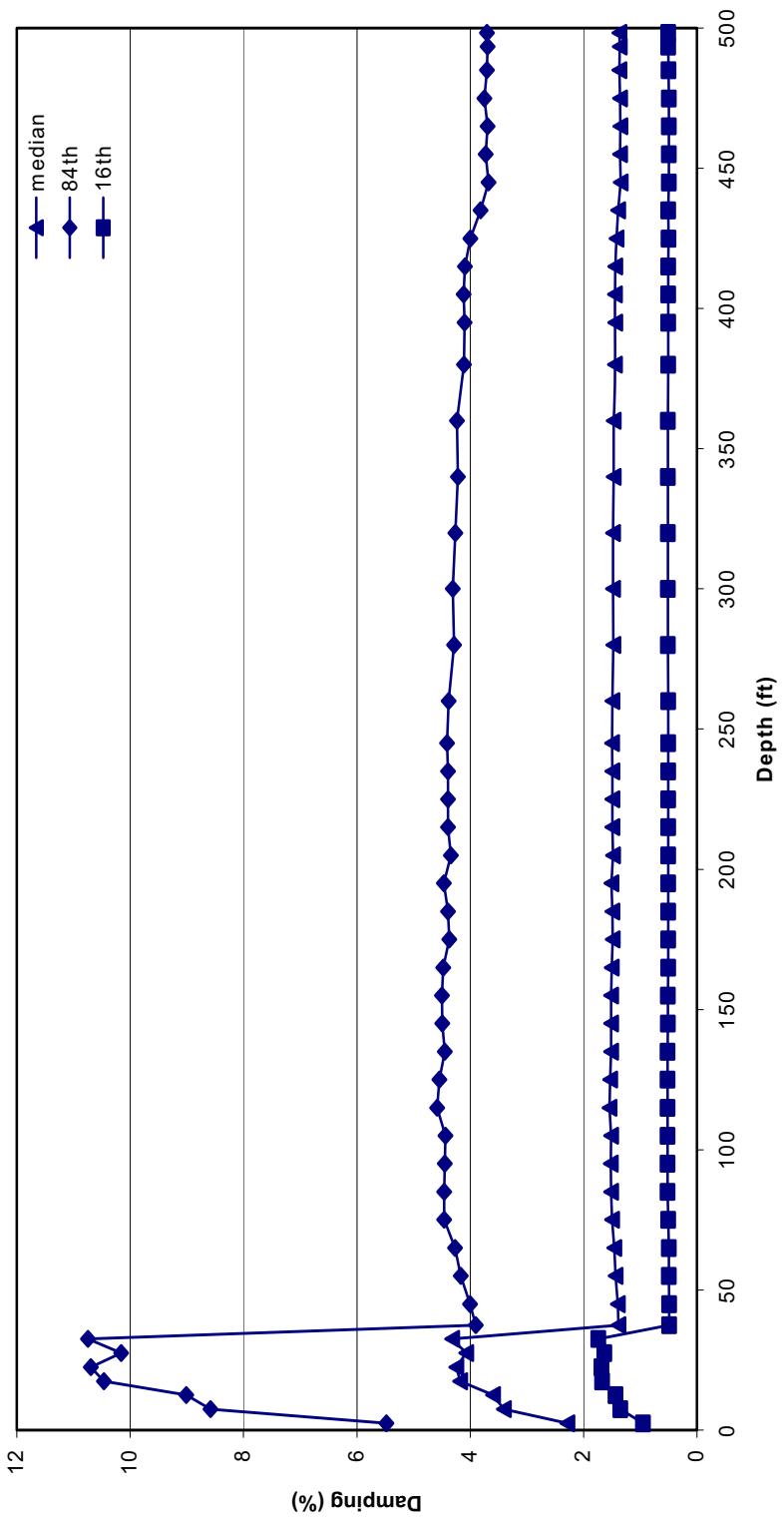

DTN: MO0403SCSPSFAD.001 [DIRS 169342]

Figure 6.3-120. Point D 10^{-4} Strain-Compatible Soil Properties: S-Wave Damping, 35 ft Profile (35 ft Alluvium)

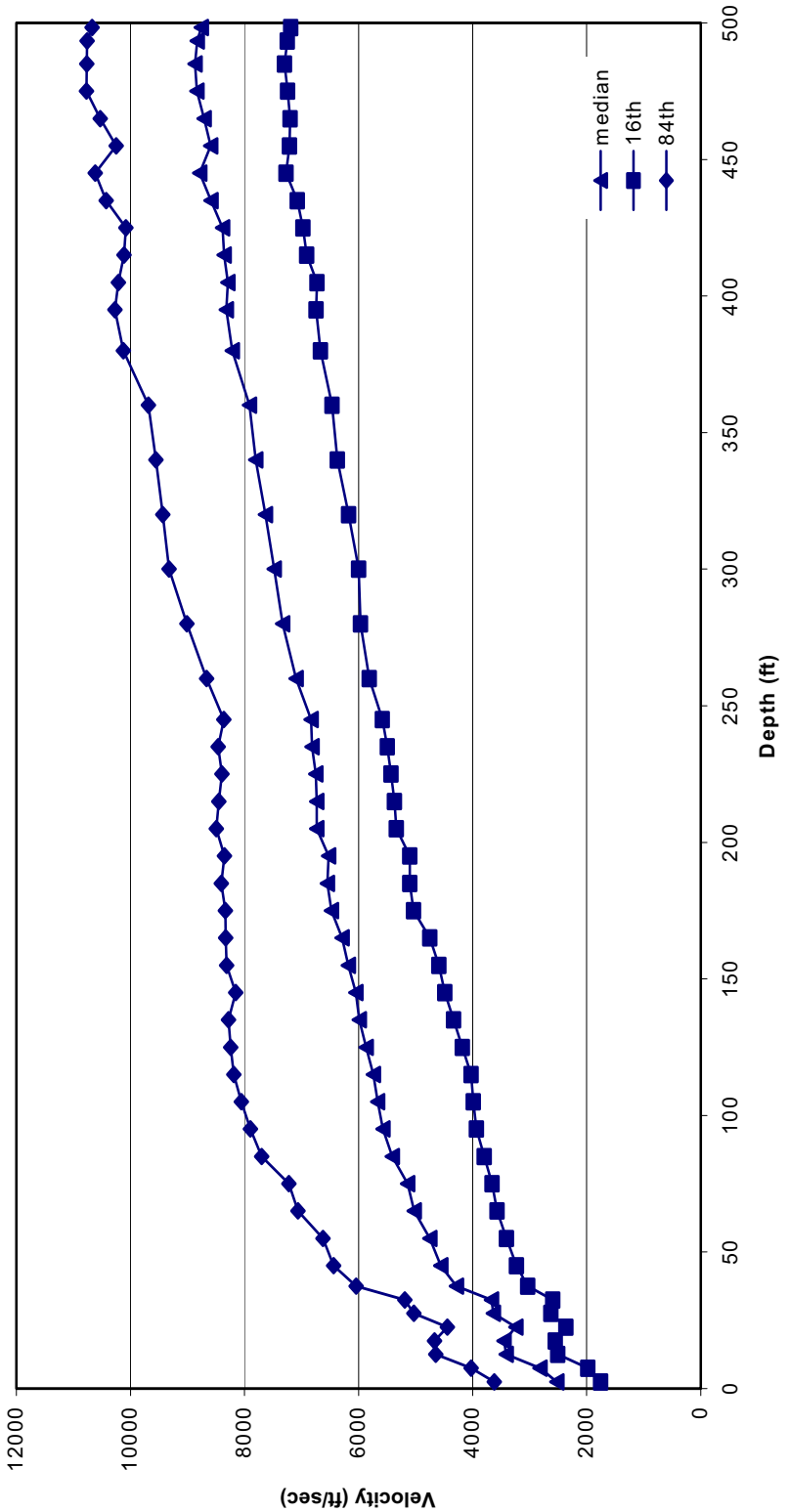

DTN: MO0403SCSPSFAD.001 [DIRS 169342]

Figure 6.3-121. Point D 10^{-4} Strain-Compatible Soil Properties: V_P, 35 ft Profile (35 ft Alluvium)

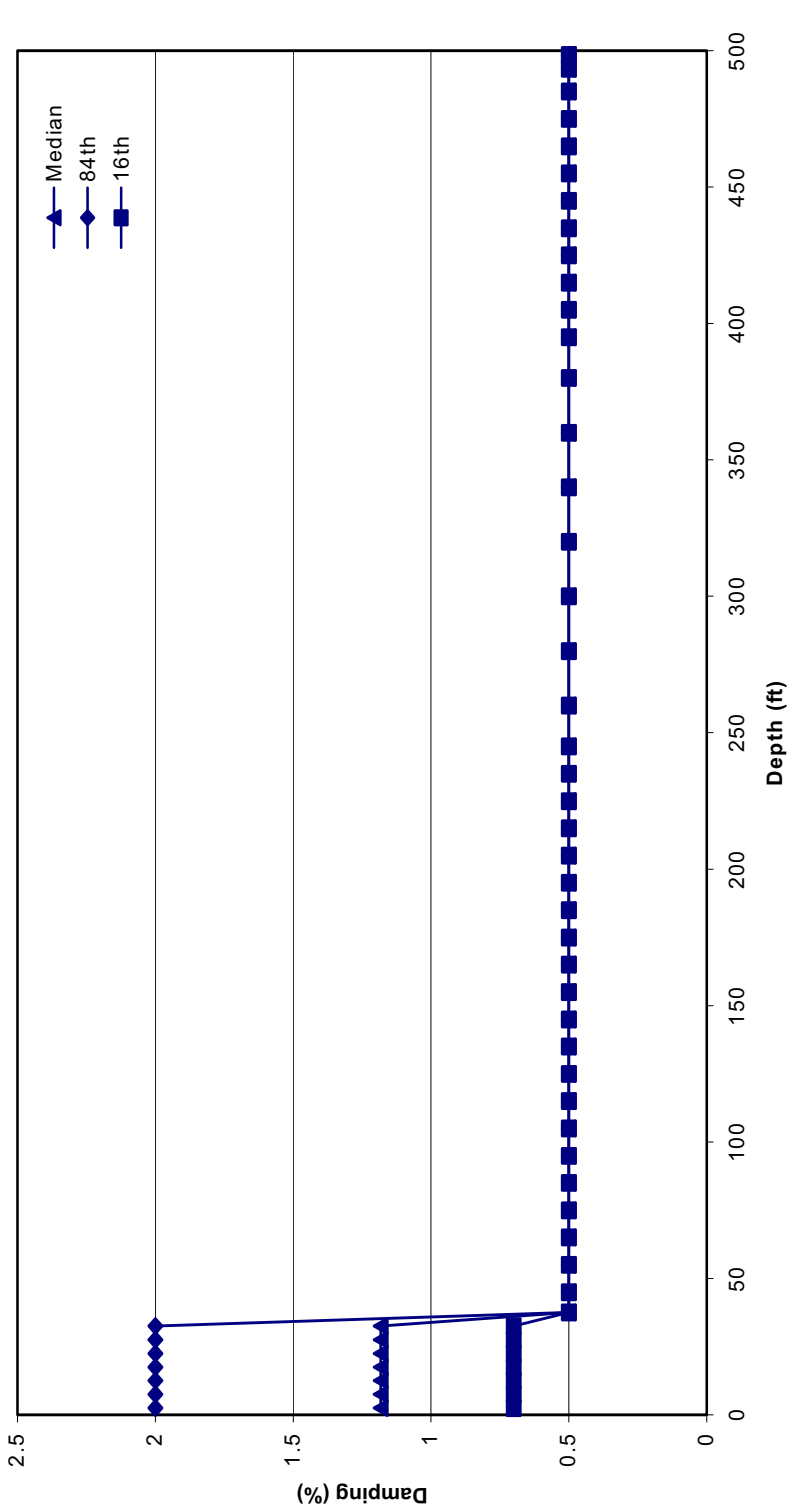

DTN: MO0403SCSPSFAD.001 [DIRS 169342]

Figure 6.3-122. Point D 10^{-4} Strain-Compatible Soil Properties: P-Wave Damping, 35 ft Profile (35 ft Alluvium)

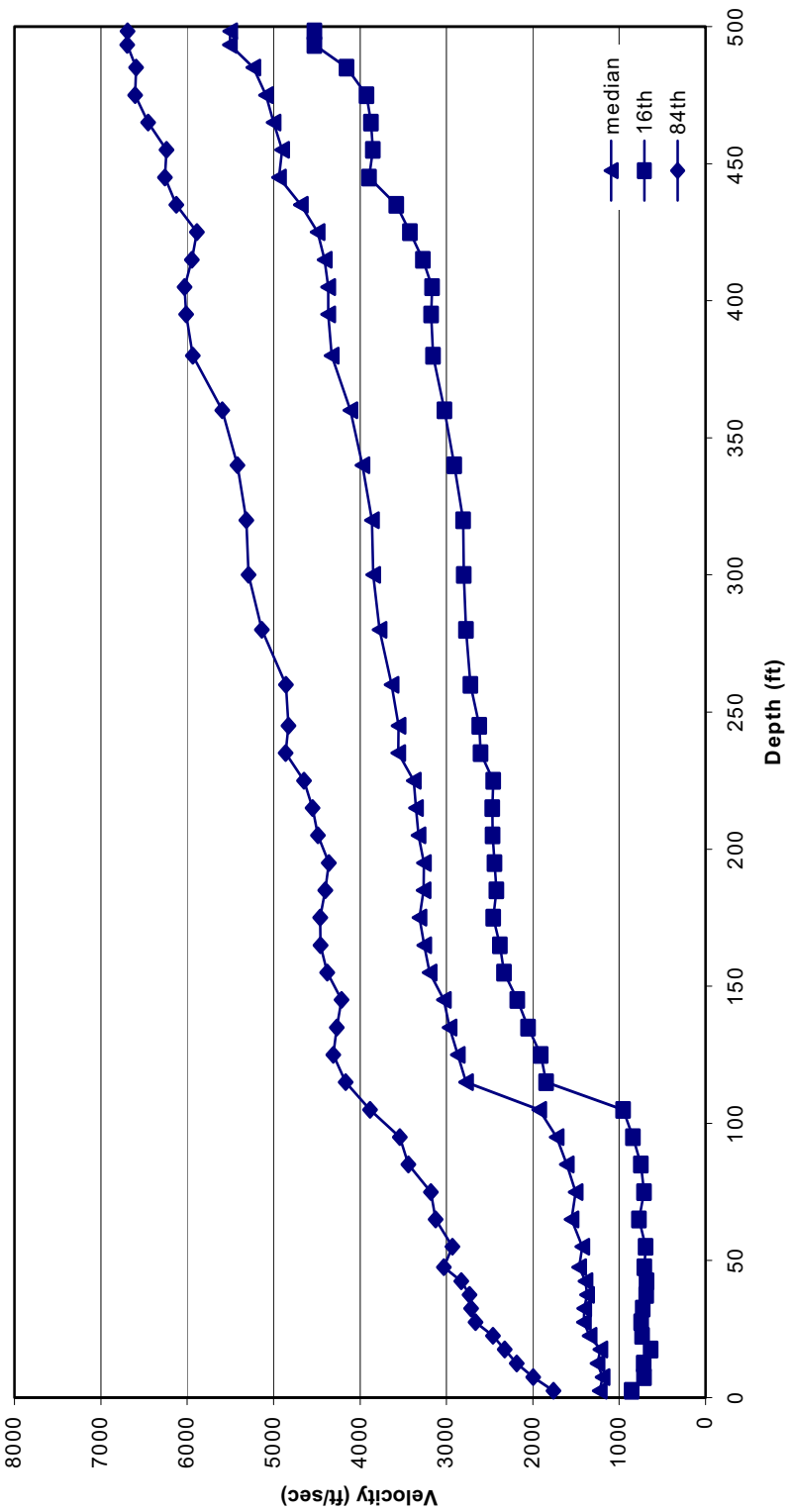

DTN: MO0403SCSPSFAD.001 [DIRS 169342]

Figure 6.3-123. Point D 10^{-4} Strain-Compatible Soil Properties: V_S, 110 ft Profile (110 ft Alluvium)

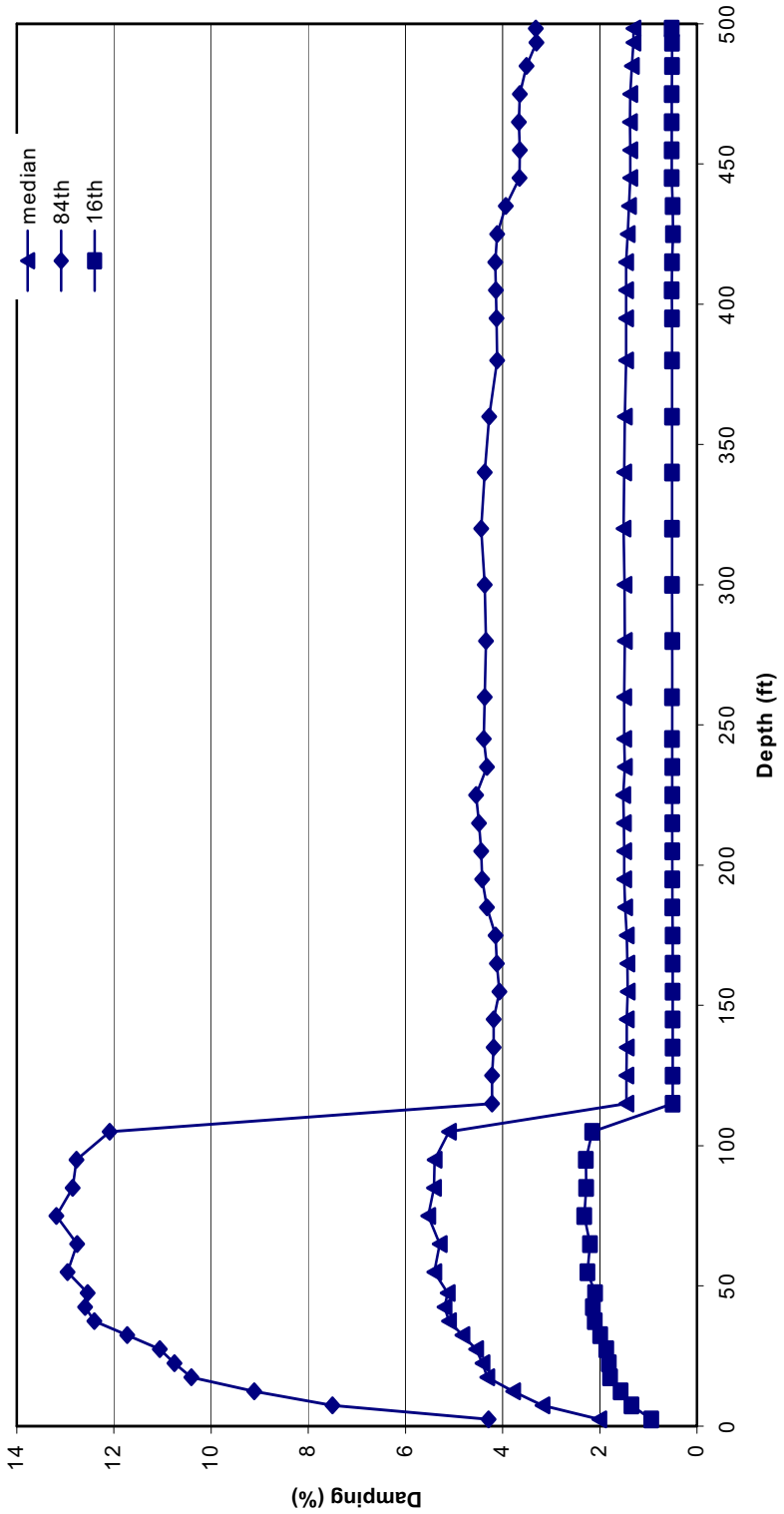

DTN: MO0403SCSPSFAD.001 [DIRS 169342]

Figure 6.3-124. Point D 10^{-4} Strain-Compatible Soil Properties: S-Wave Damping, 110 ft Profile (110 ft Alluvium)

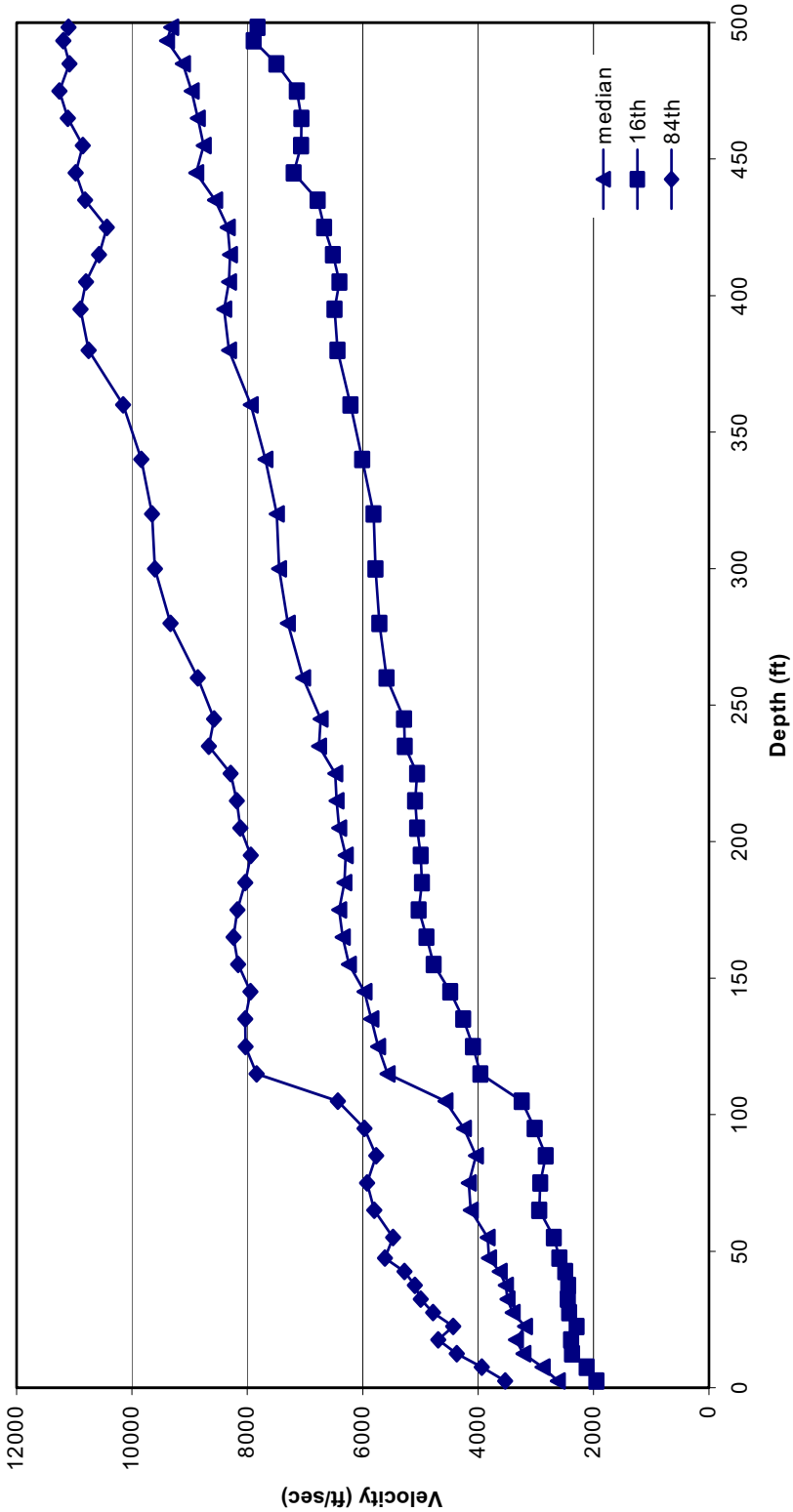

DTN: MO0403SCSPSFAD.001 [DIRS 169342]

Figure 6.3-125. Point D 10^{-4} Strain-Compatible Soil Properties: V_P, 110 ft Profile (110 ft Alluvium)

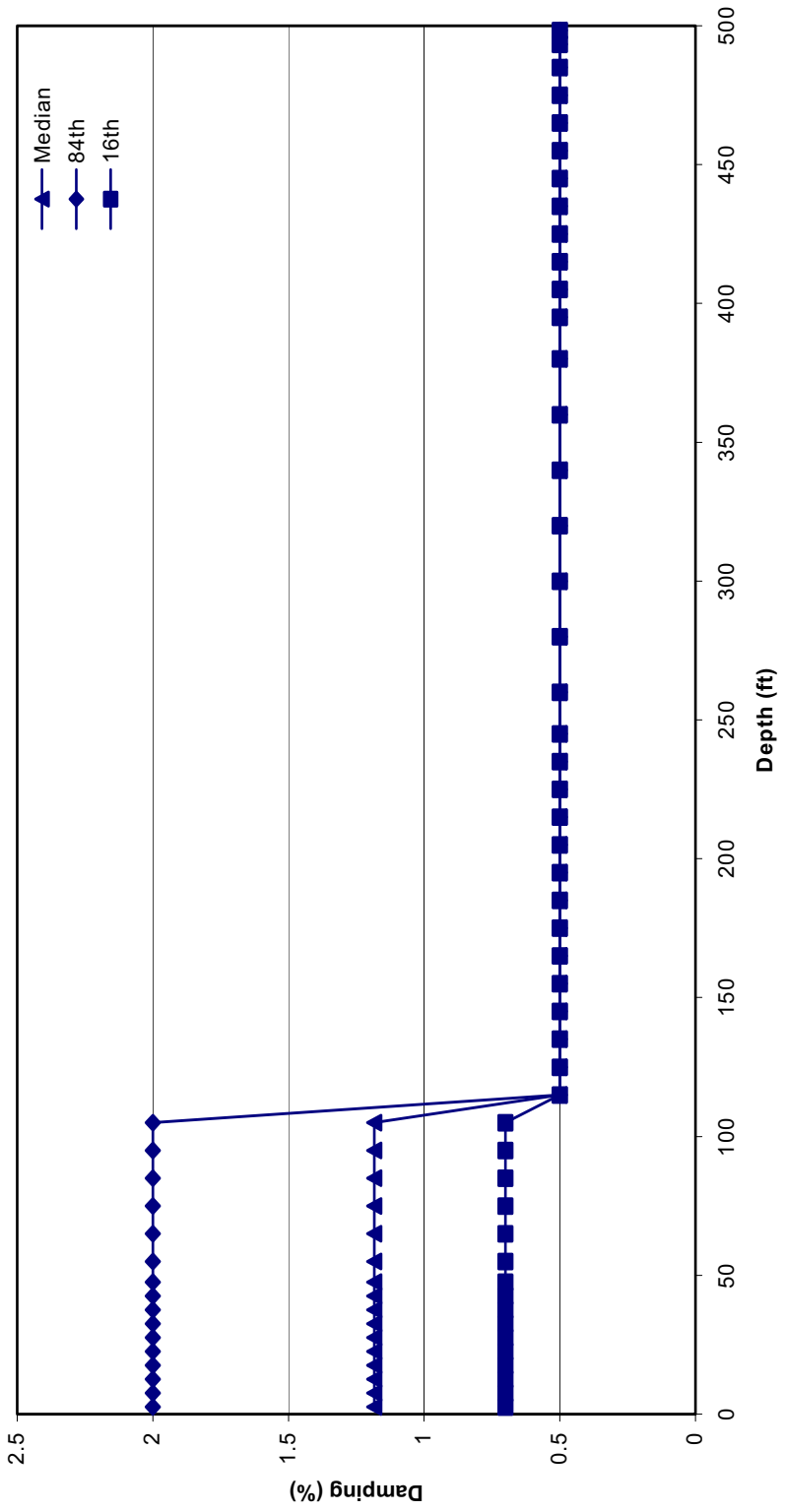

DTN: MO0403SCSPSFAD.001 [DIRS 169342]

Figure 6.3-126. Point D 10^{-4} Strain-Compatible Soil Properties: P-Wave Damping, 110 ft Profile (110 ft Alluvium)

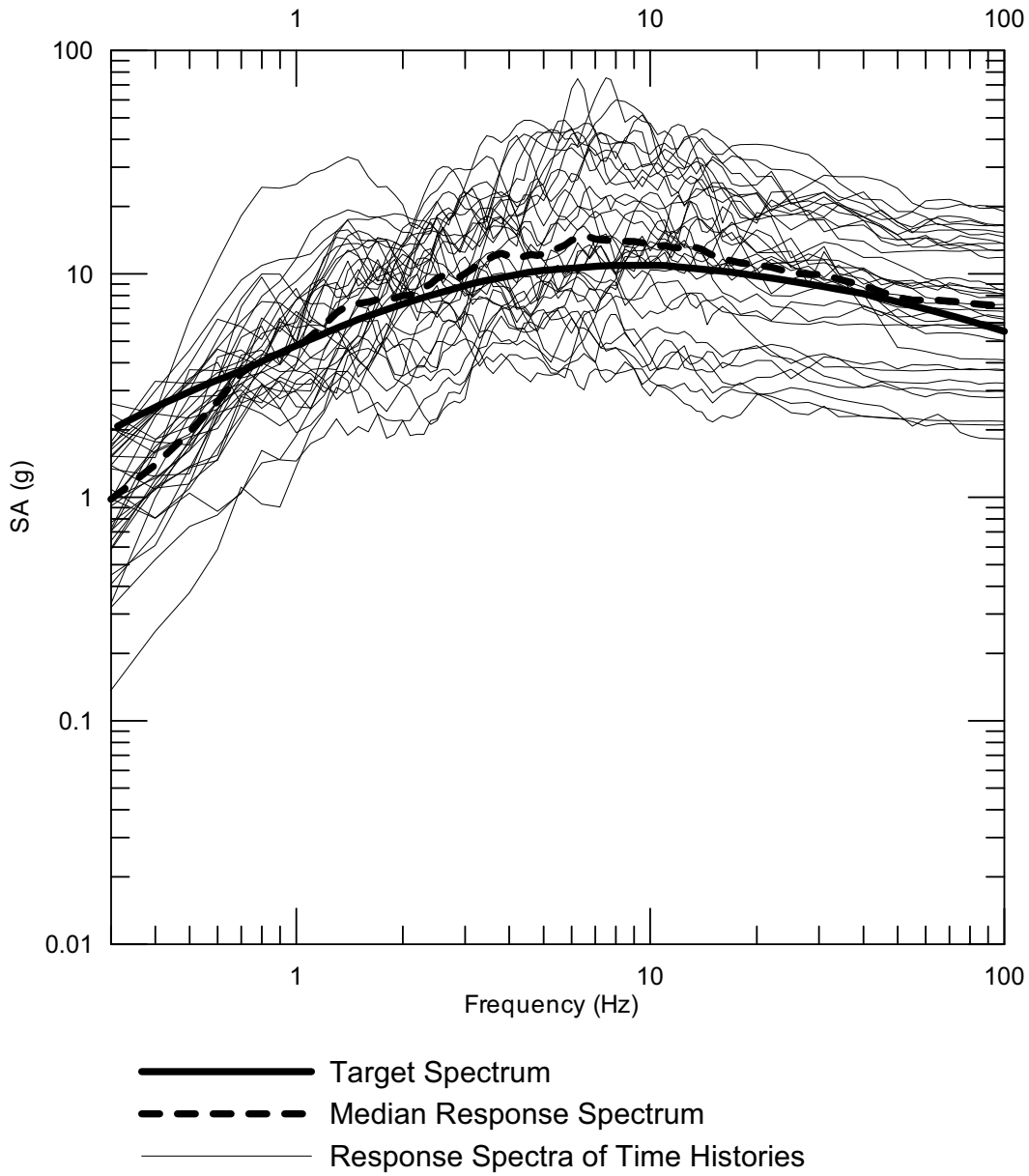

Figure 6.3-127. Example of a Suite of Spectrally Conditioned, PGV-Scaled Time Histories (For information only)

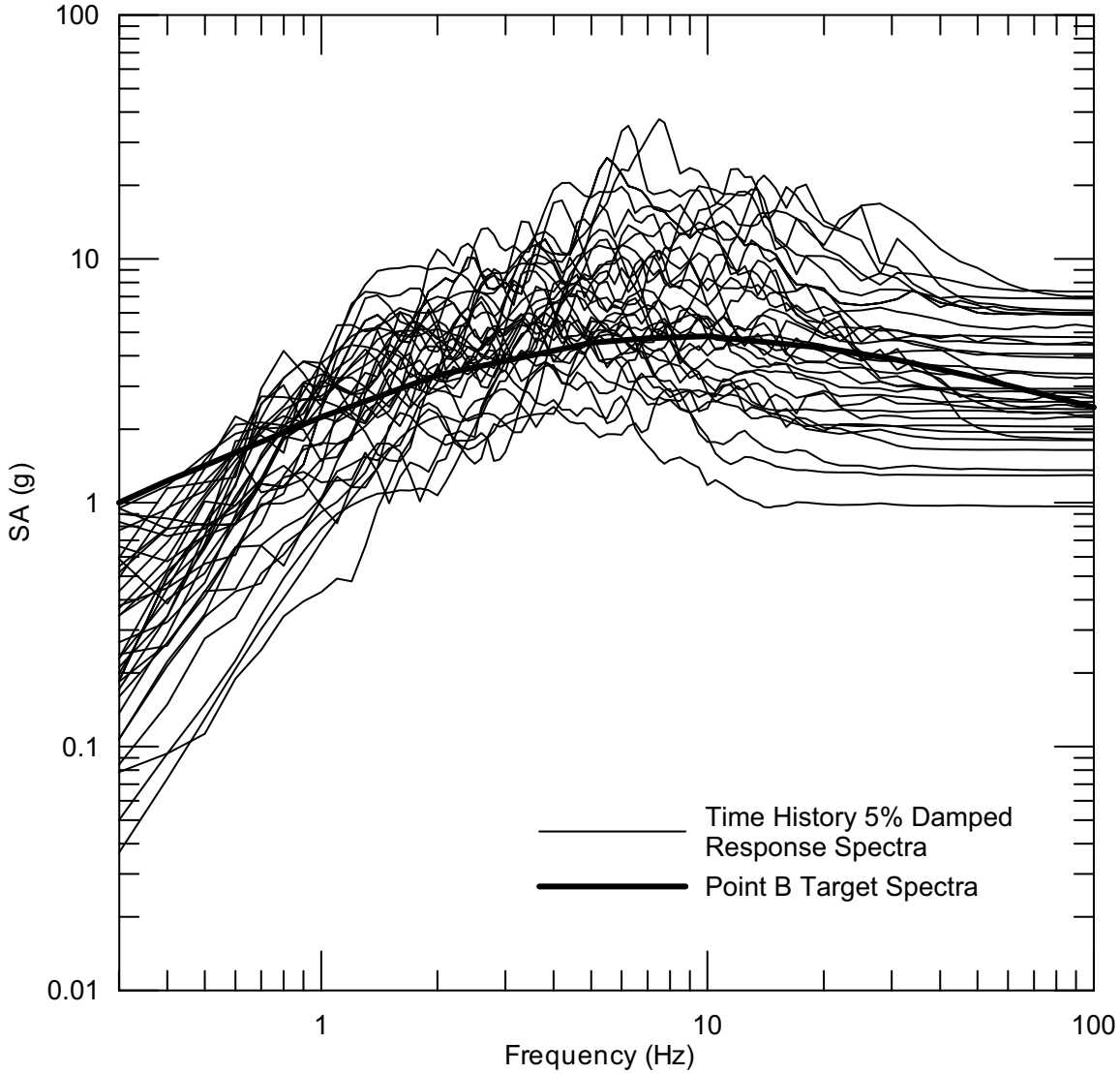

DTNS: MO0301TMHIS106.001 [DIRS 161868], MO04065DSRSPTB.000 [DIRS 170506]

Figure 6.3-128. Response Spectra of Point B 10^{-6} Horizontal Time Histories (PGV Scaled)

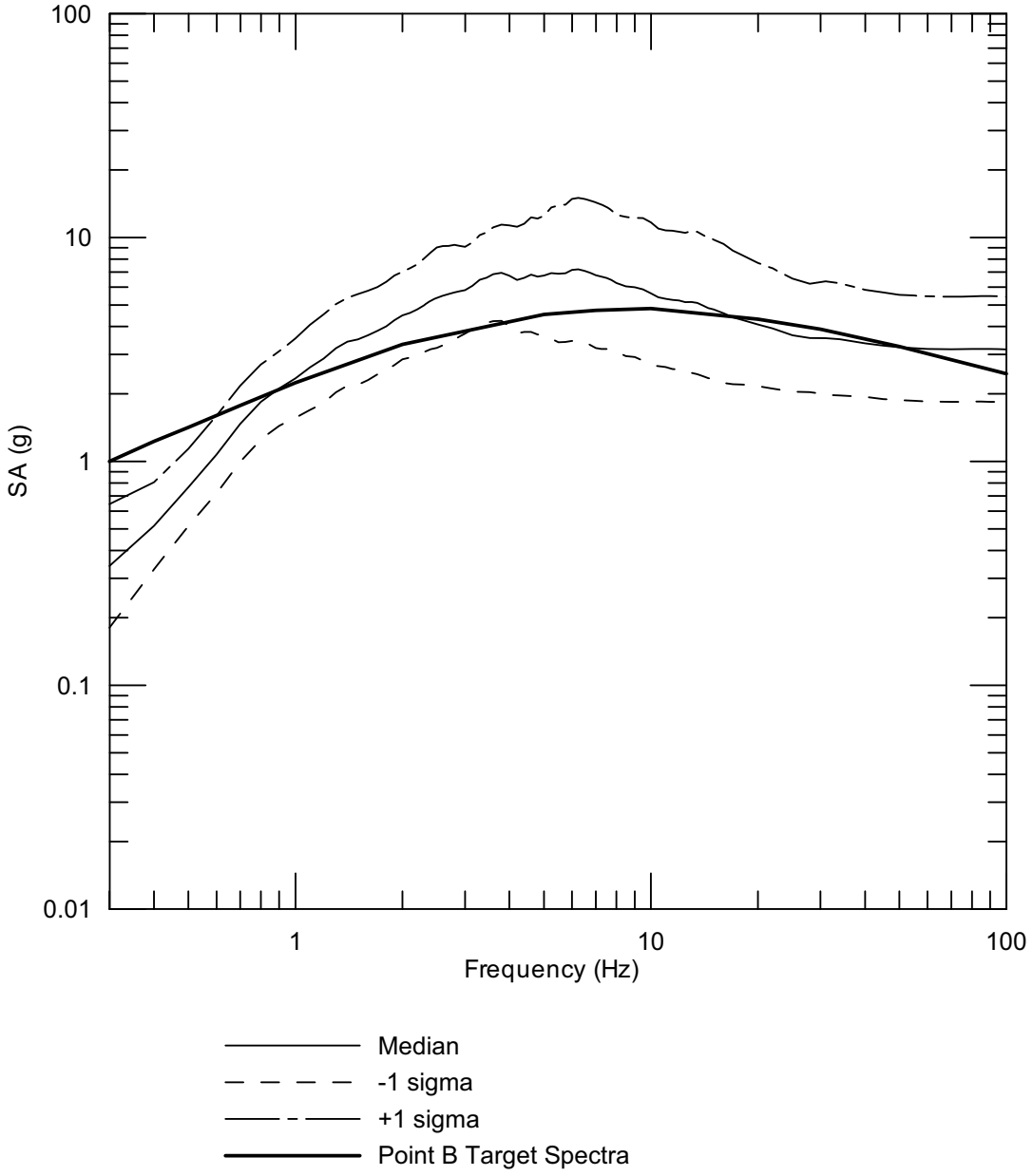

DTN: MO04065DSRSPTB.000 [DIRS 170506]

Source: Wong and Silva 2004a [DIRS 170443], Supplemental Record 60

Figure 6.3-129. Median and $\pm$ 1 σ Response Spectra of Point B 10^{-6} Horizontal Time Histories (PGV Scaled)

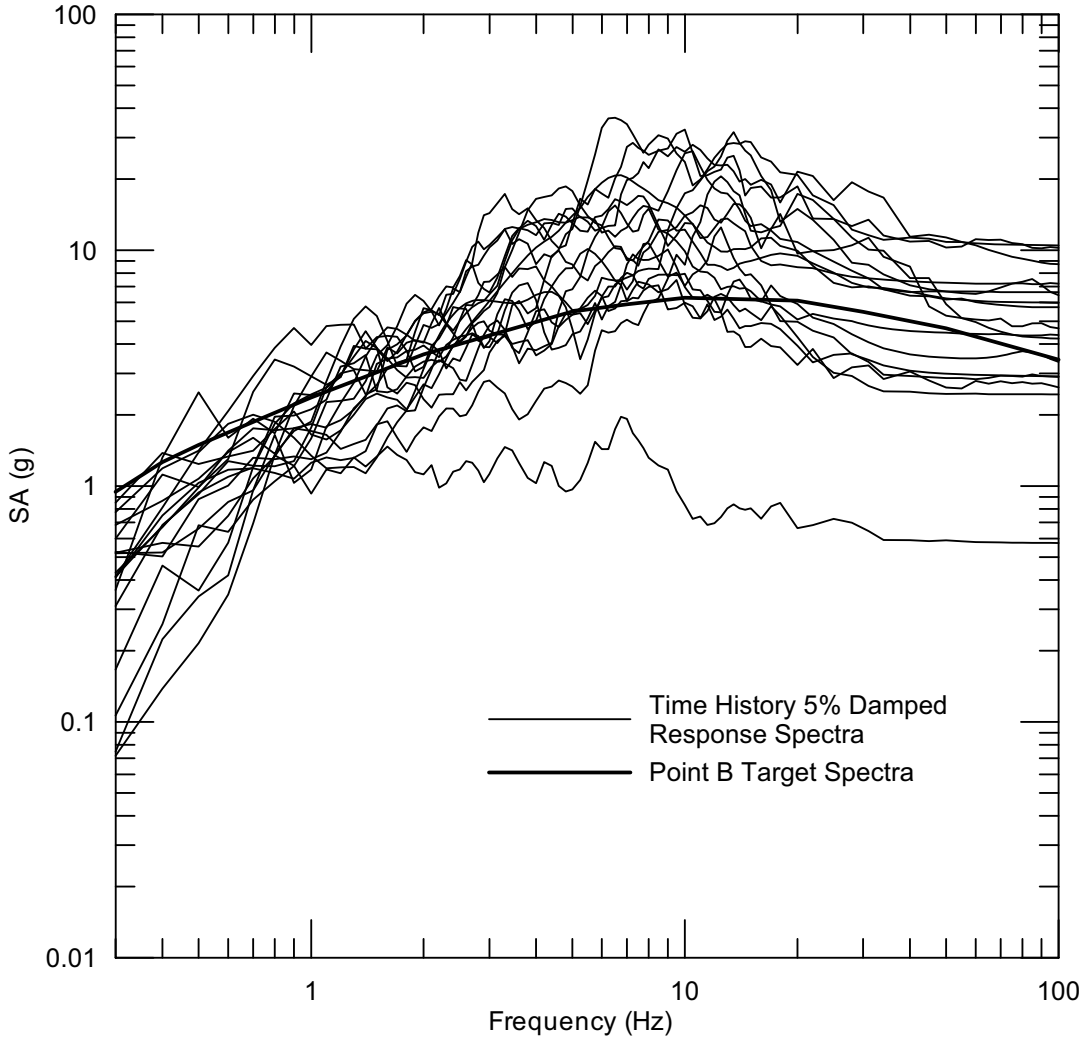

DTNS: MO0301TMHIS106.001 [DIRS 161868], MO04065DSRSPTB.000 [DIRS 170506]

Figure 6.3-130. Response Spectra of Point B 10^{-6} Vertical Time Histories (PGV Scaled)

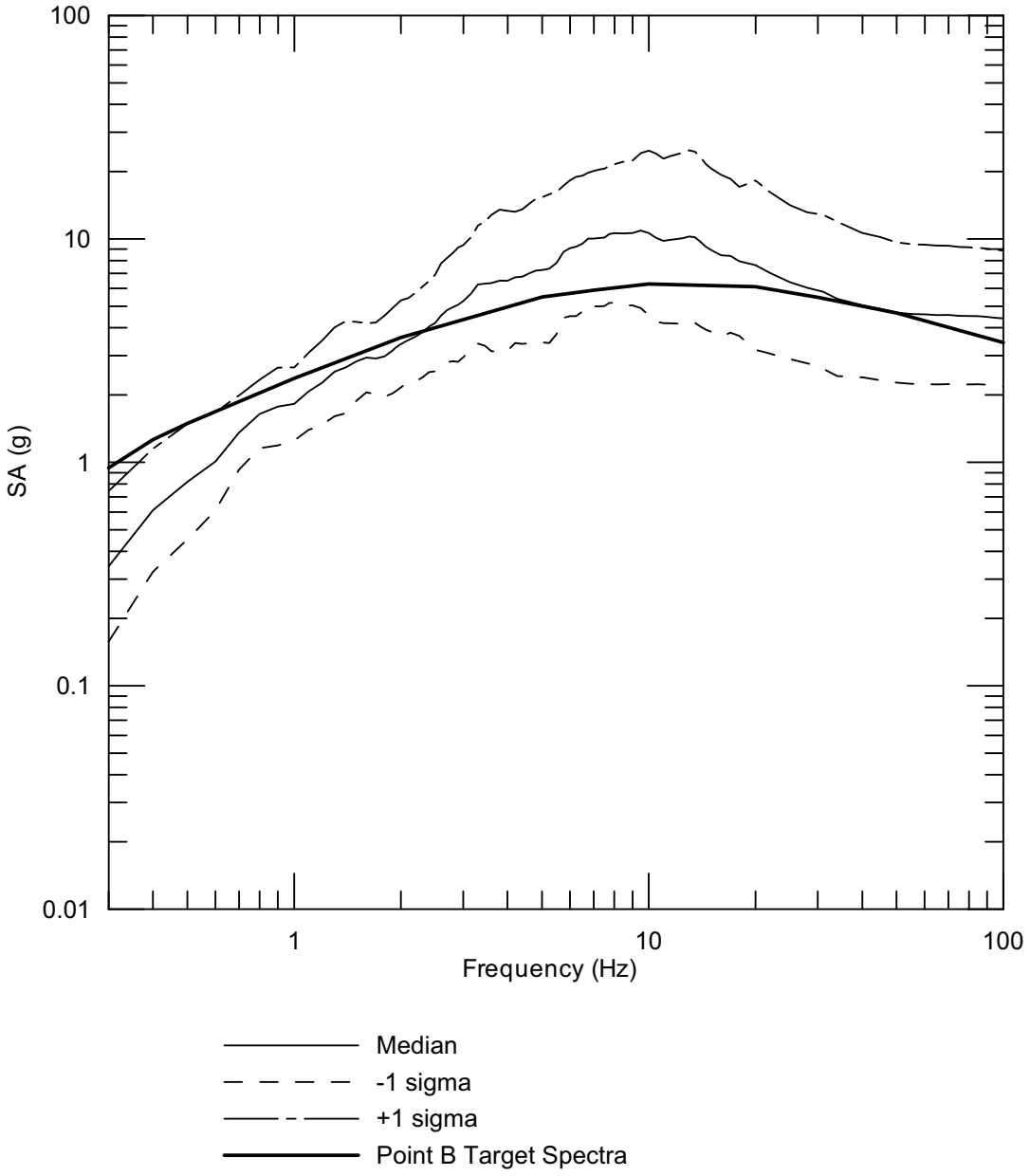

DTN: MO04065DSRSPTB.000 [DIRS 170506]

Source: Wong and Silva 2004a [DIRS 170443], Supplemental Record 60

Figure 6.3-131. Median and $\pm$ 1 σ Response Spectra of Point B 10^{-6} Vertical Time Histories (PGV Scaled)

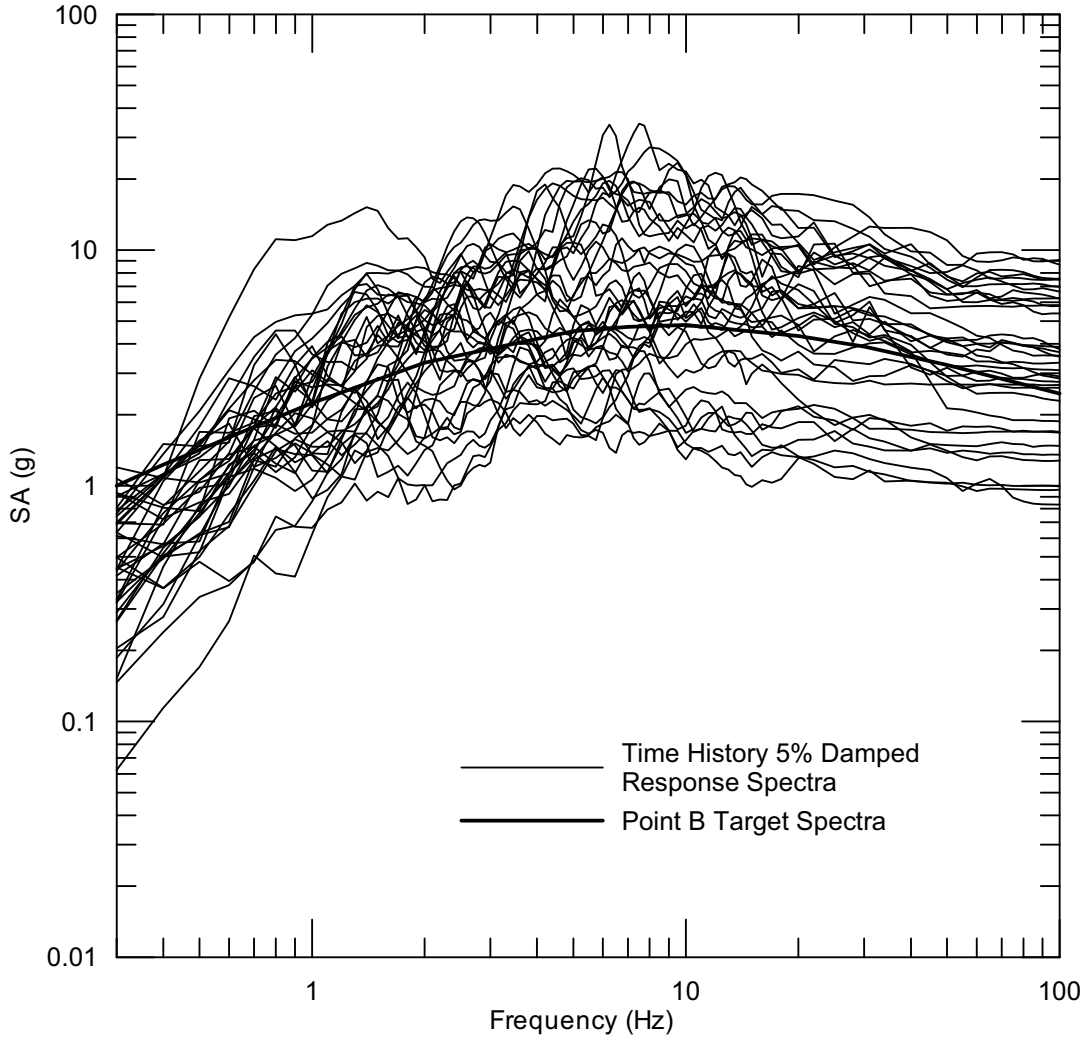

DTNS: MO0403AVDSC106.001 [DIRS 168891], MO04065DSRSPTB.000 [DIRS 170506]

Figure 6.3-132. Response Spectra of Point B 10^{-6} Spectrally Conditioned to Point A Horizontal Time Histories

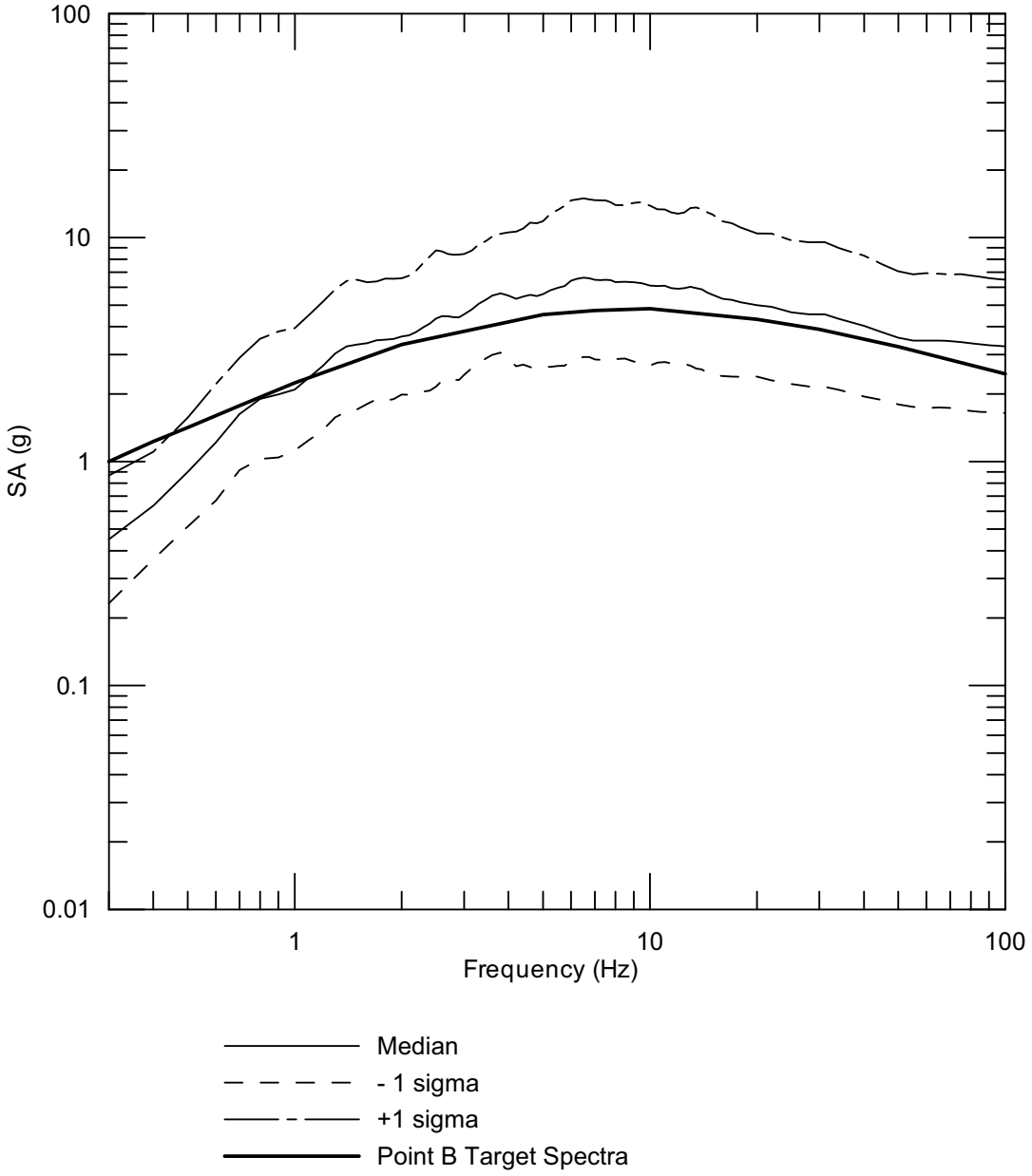

DTN: MO04065DSRSPTB.000 [DIRS 170506]

Source: Wong and Silva 2004a [DIRS 170443], SR 60

Figure 6.3-133. Median and $\pm$ 1 σ Response Spectra of Point B 10^{-6} Spectrally Conditioned to Point A Horizontal Time Histories

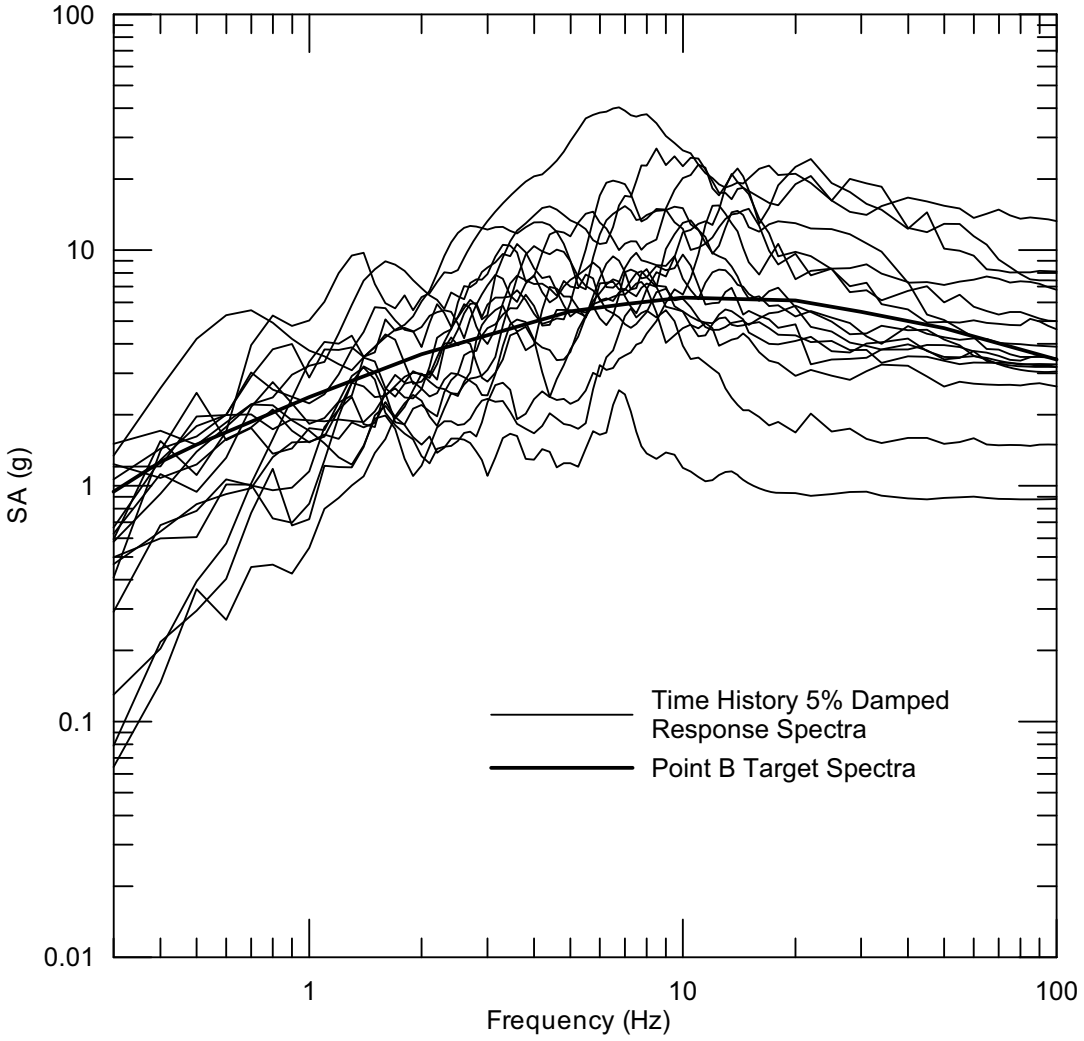

DTNS: MO0403AVDSC106.001 [DIRS 168891], MO04065DSRSPTB.000 [DIRS 170506]

Figure 6.3-134. Response Spectra of Point B 10^{-6} Spectrally Conditioned to Point A Vertical Time Histories

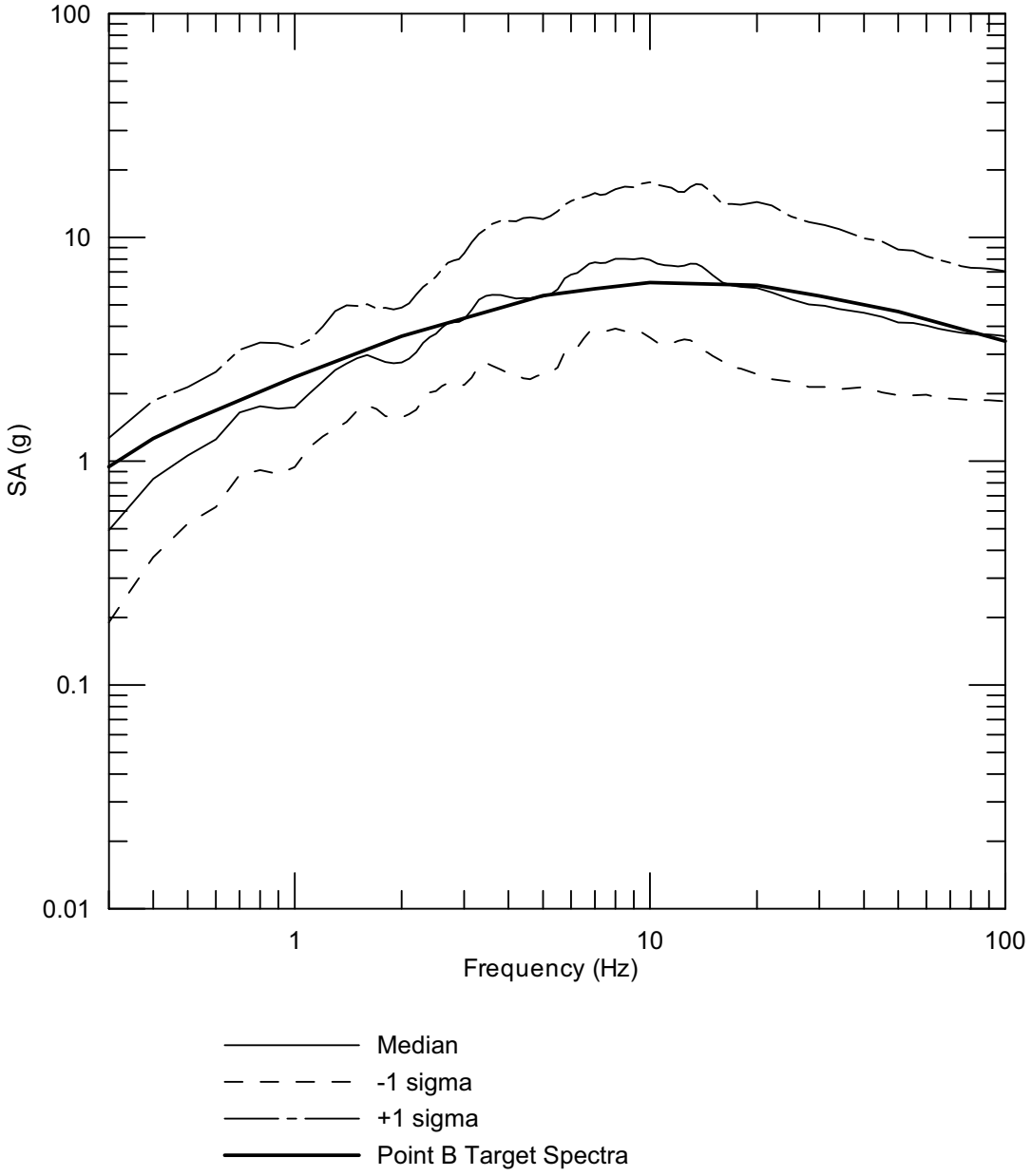

DTN: MO04065DSRSPTB.000 [DIRS 170506]

Source: Wong and Silva 2004a [DIRS 170443], Supplemental Record 60

Figure 6.3-135. Median and $\pm$ 1 σ Response Spectra of Point B 10^{-6} Spectrally Conditioned to Point A Vertical Time Histories

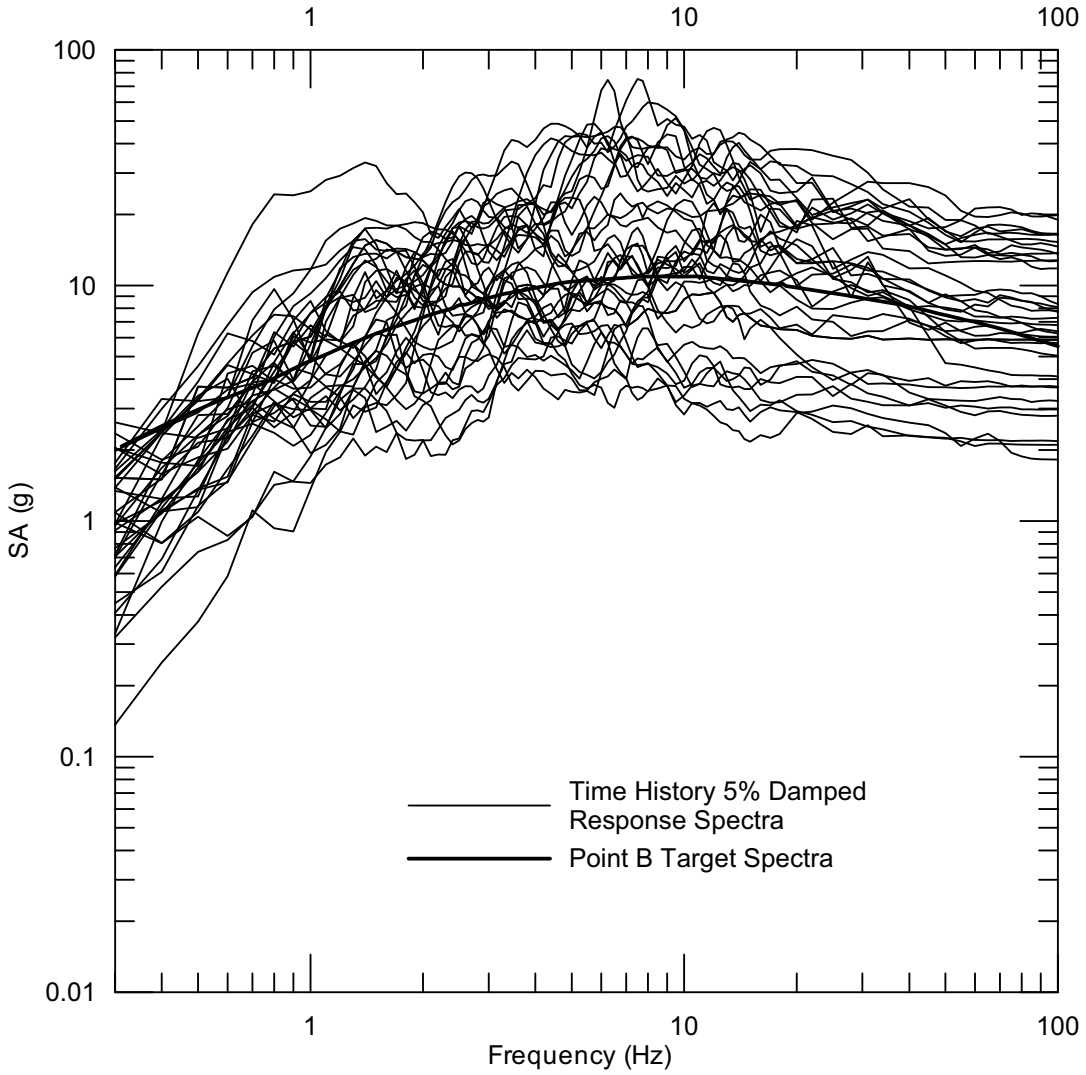

DTN: MO0403AVTMH107.003 [DIRS 168892]

Figure 6.3-136. Response Spectra of Point B 10^{-7} Horizontal Spectrally Conditioned to Point A Time Histories

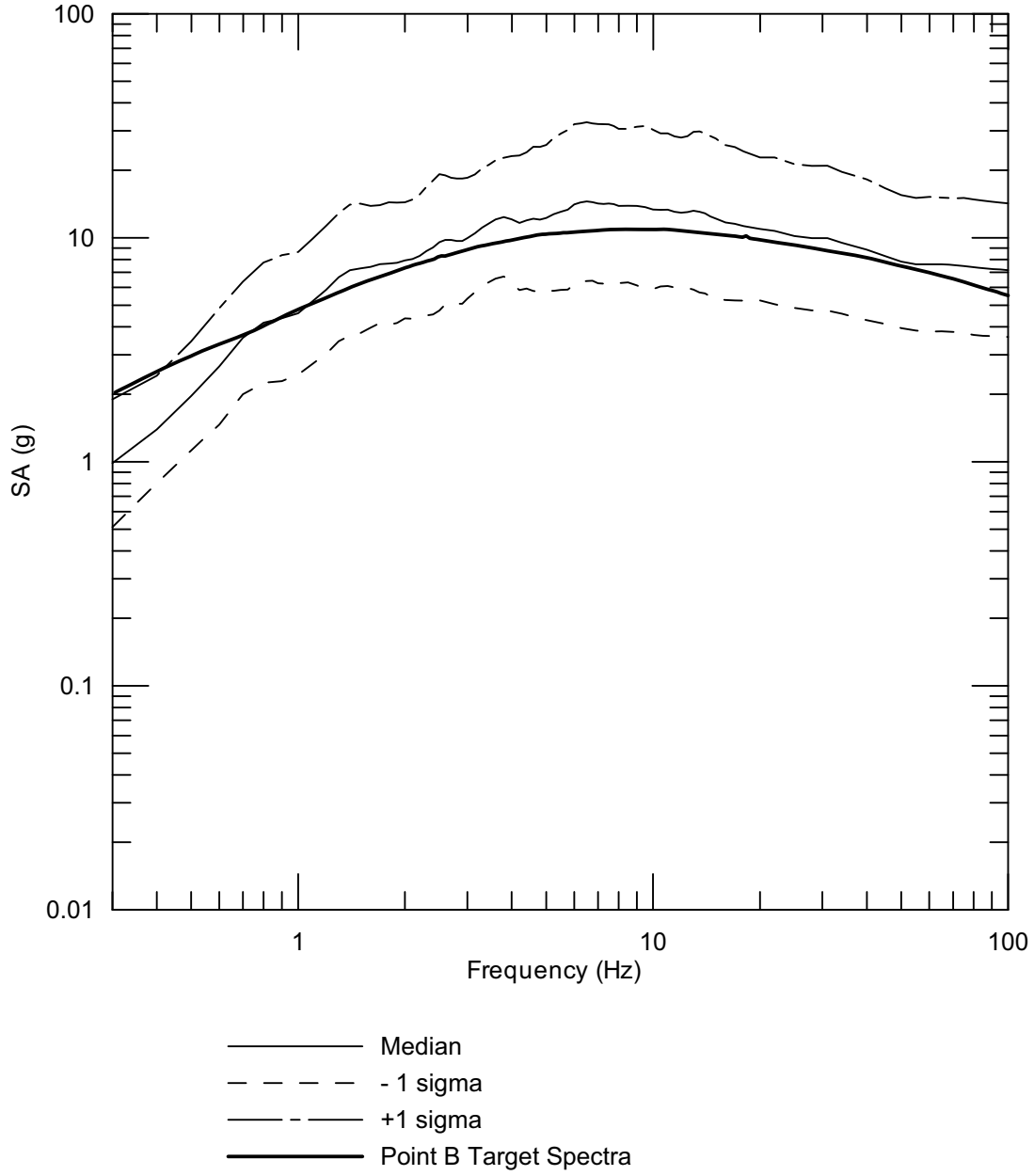

DTN: MO0403AVTMH107.003 [DIRS 168892]

Figure 6.3-137. Median and $\pm$ 1 σ Response Spectra of Point B 10^{-7} Spectrally Conditioned to Point A Horizontal Time Histories

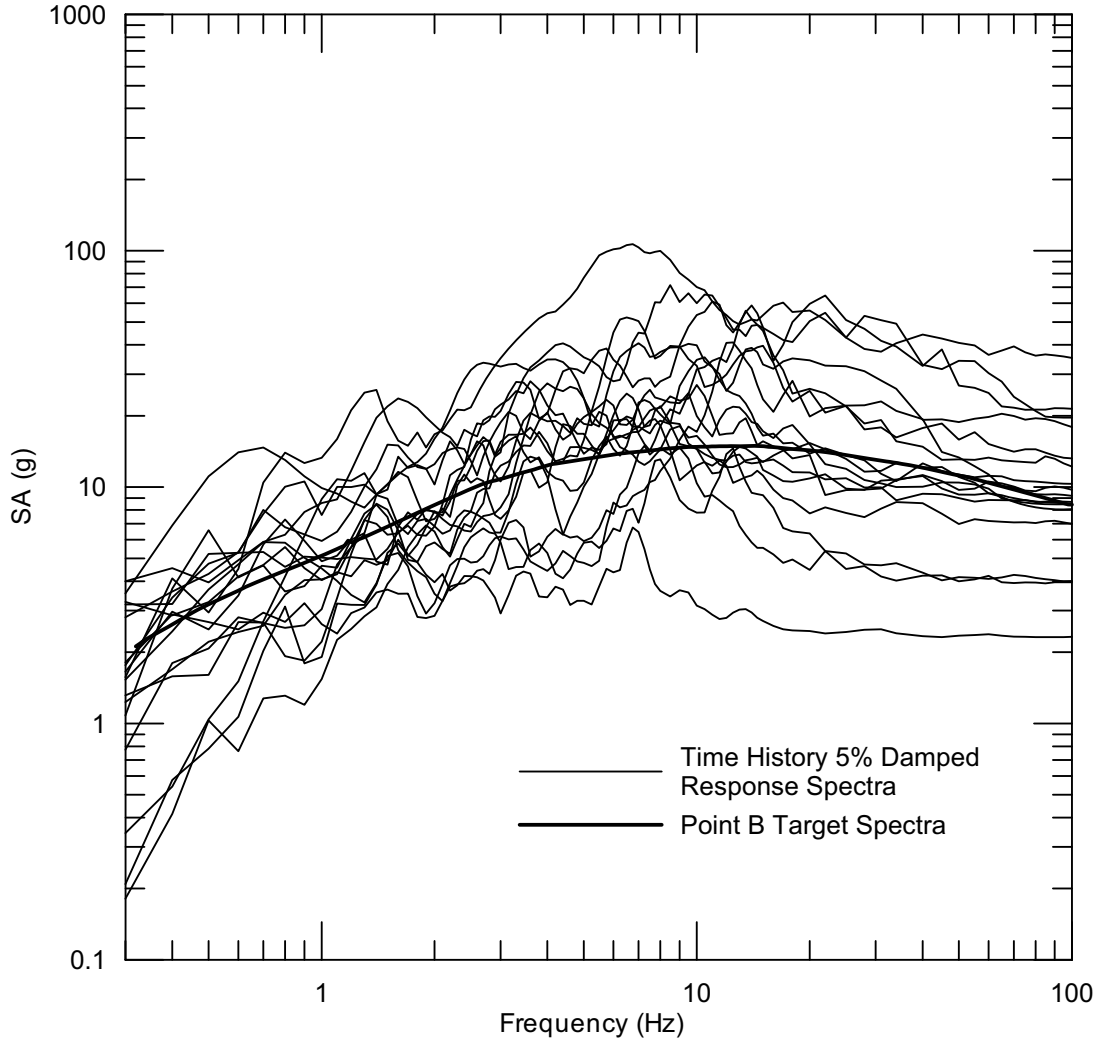

DTN: MO0403AVTMH107.003 [DIRS 168892]

Figure 6.3-138. Response Spectra of Point B 10^{-7} Vertical Spectrally Conditioned to Point A Time Histories

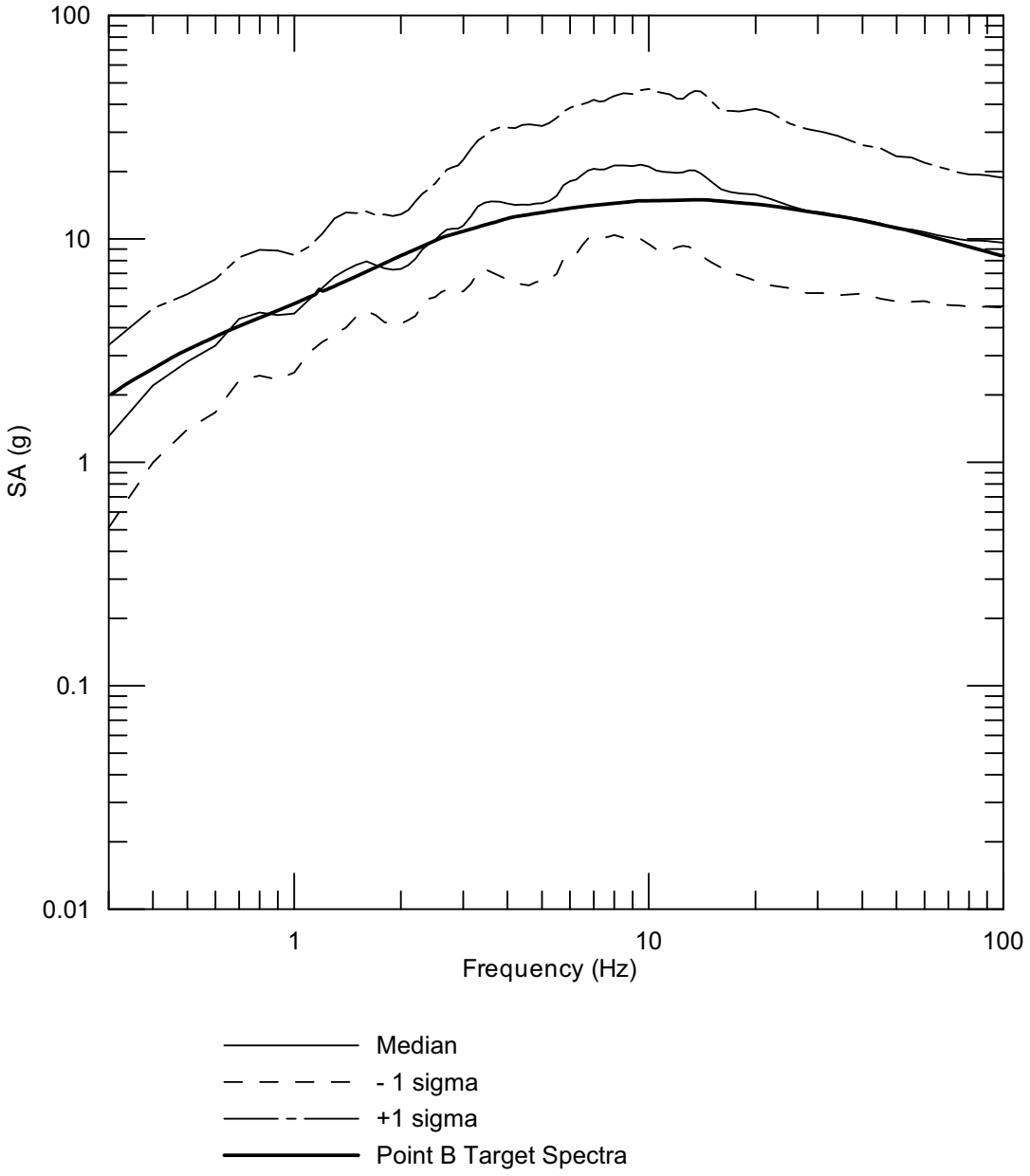

Source: Wong and Silva 2004a [DIRS 170443[, Supplemental Record 69

Figure 6.3-139. Median and $\pm$ 1 σ Response Spectra of Point B 10^{-7} Spectrally Conditioned to Point A Vertical Time Histories

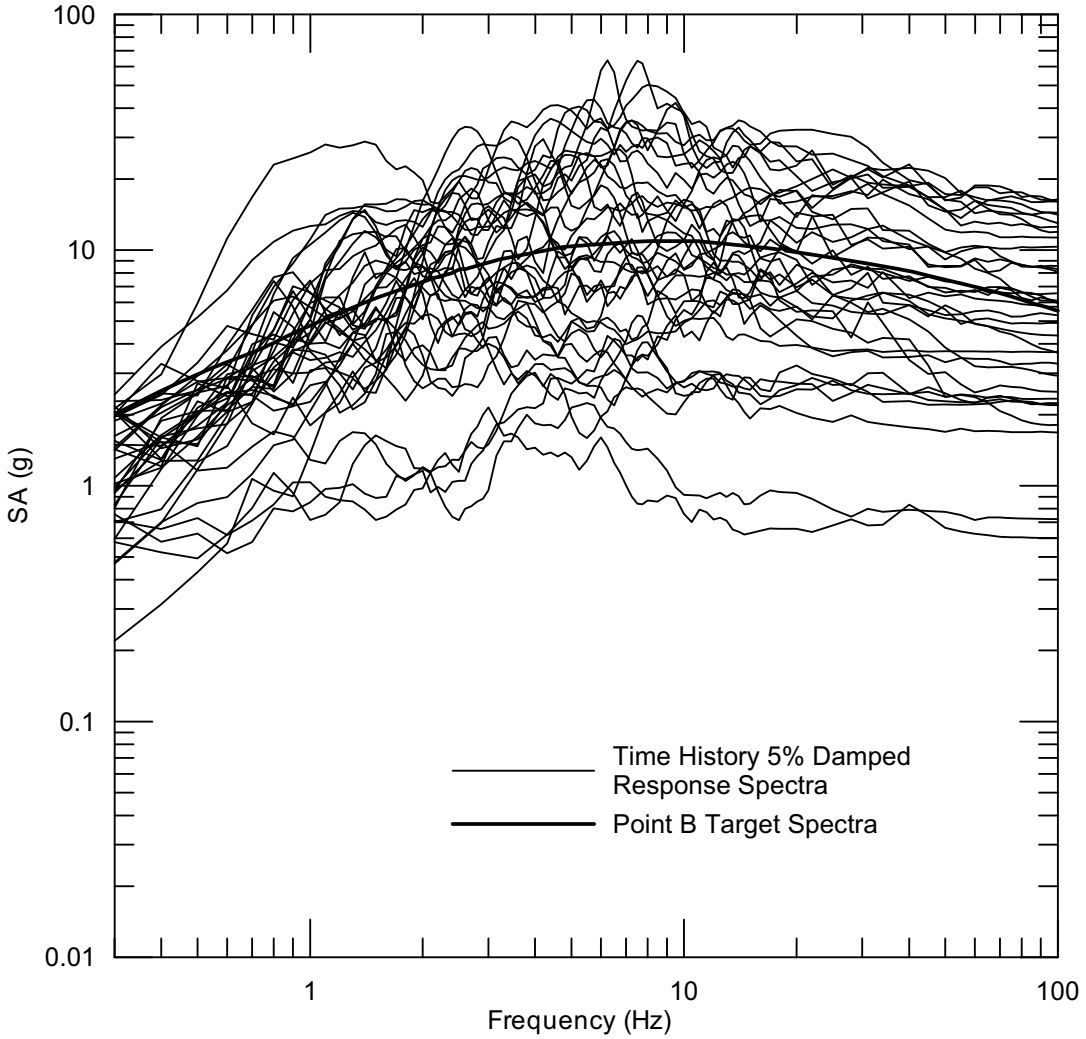

DTN: MO0301TMHSB107.000 [DIRS 164207]

Figure 6.3-140. Response Spectra of Point B 10^{-7} Horizontal Spectrally Conditioned to Point B Time Histories

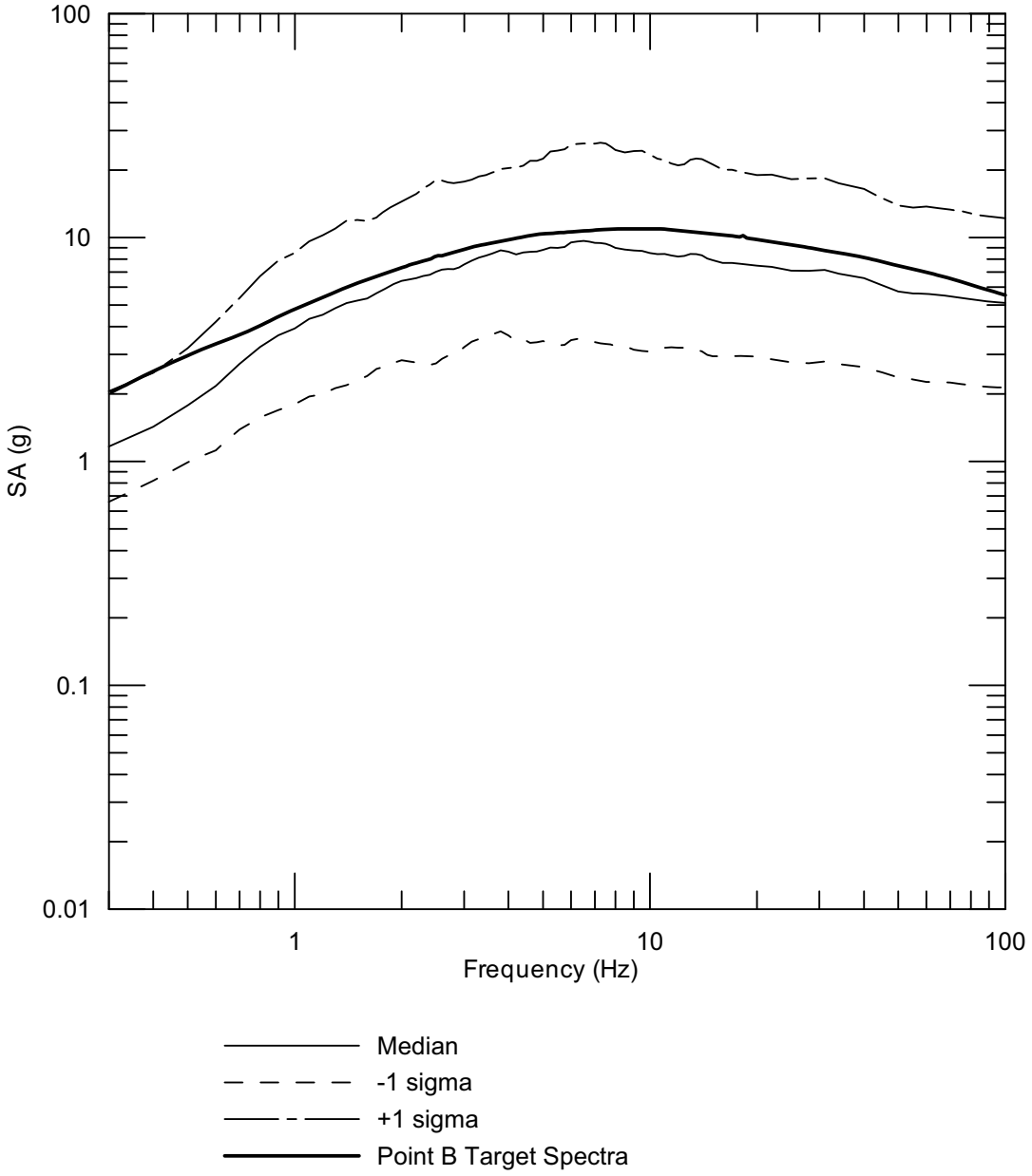

Source: Wong and Silva 2004a [DIRS 170443], Supplemental Record 69

Figure 6.3-141. Median and $\pm$ 1 σ Response Spectra of Point B 10^{-7} Spectrally Conditioned to Point B Horizontal Time Histories

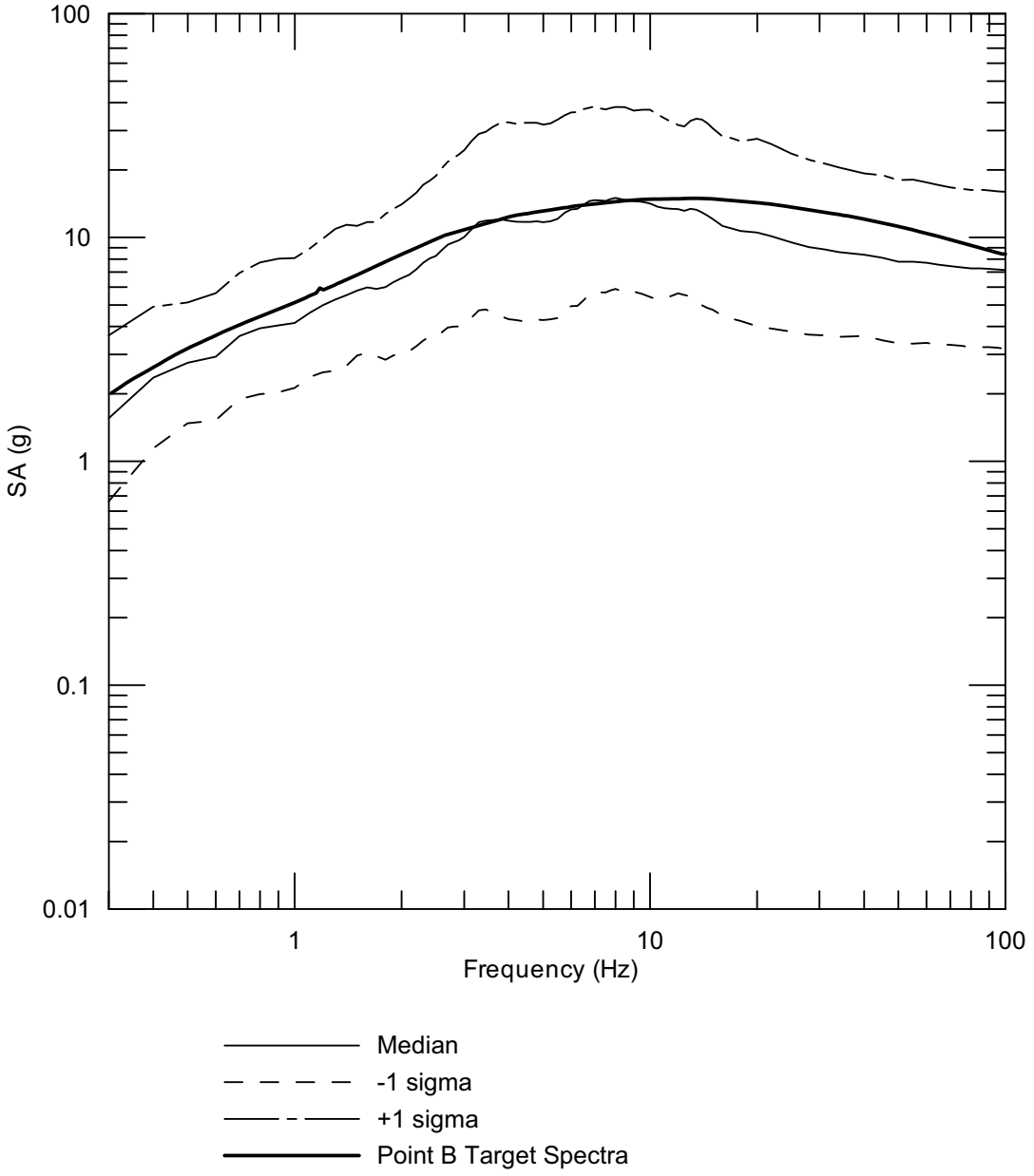

DTN: MO0301TMHSB107.000 [DIRS 164207]

Figure 6.3-142. Response Spectra of Point B 10^{-7} Vertical Spectrally Conditioned to Point B Time Histories

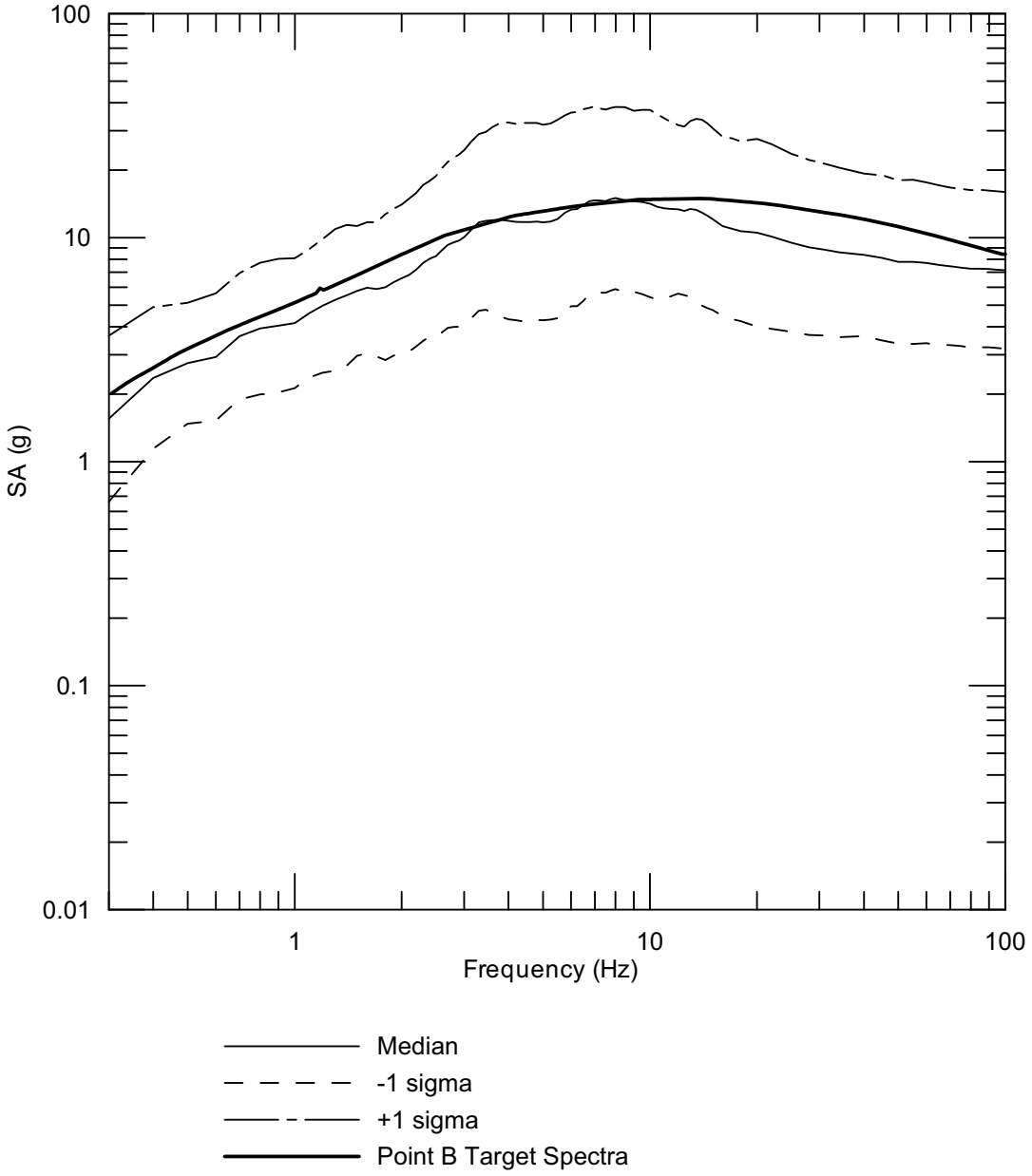

Source: Wong and Silva 2004a [DIRS 170443], Supplemental Record 69

Figure 6.3-143. Median and $\pm$ 1 σ Response Spectra of Point B 10^{-7} Spectrally Conditioned to Point B Vertical Time Histories

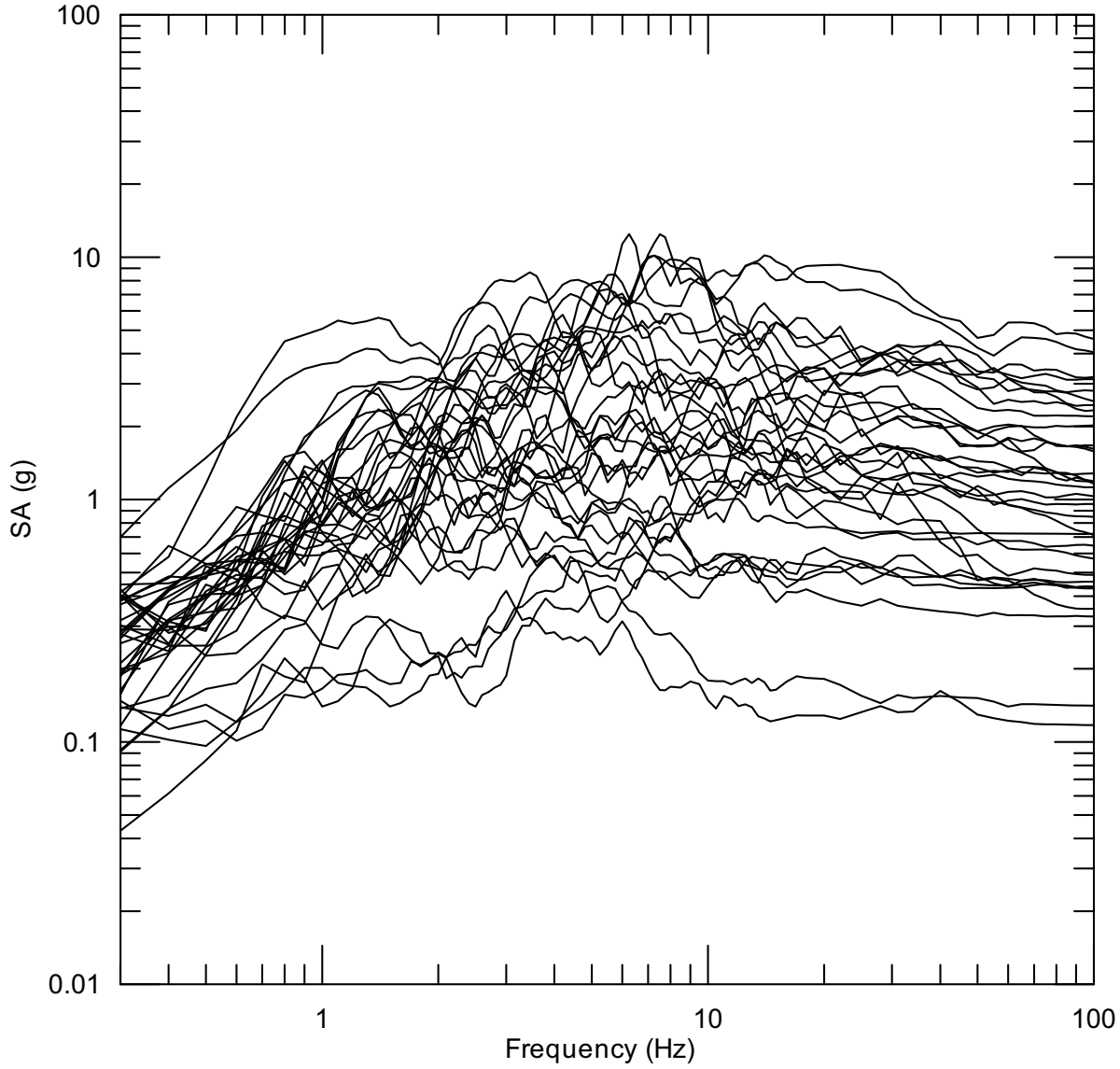

DTN: MO0402AVDTM105.001 [DIRS 168890]

Figure 6.3-144. Response Spectra of Point B 10^{-5} Spectrally Conditioned to Point B Horizontal Time Histories

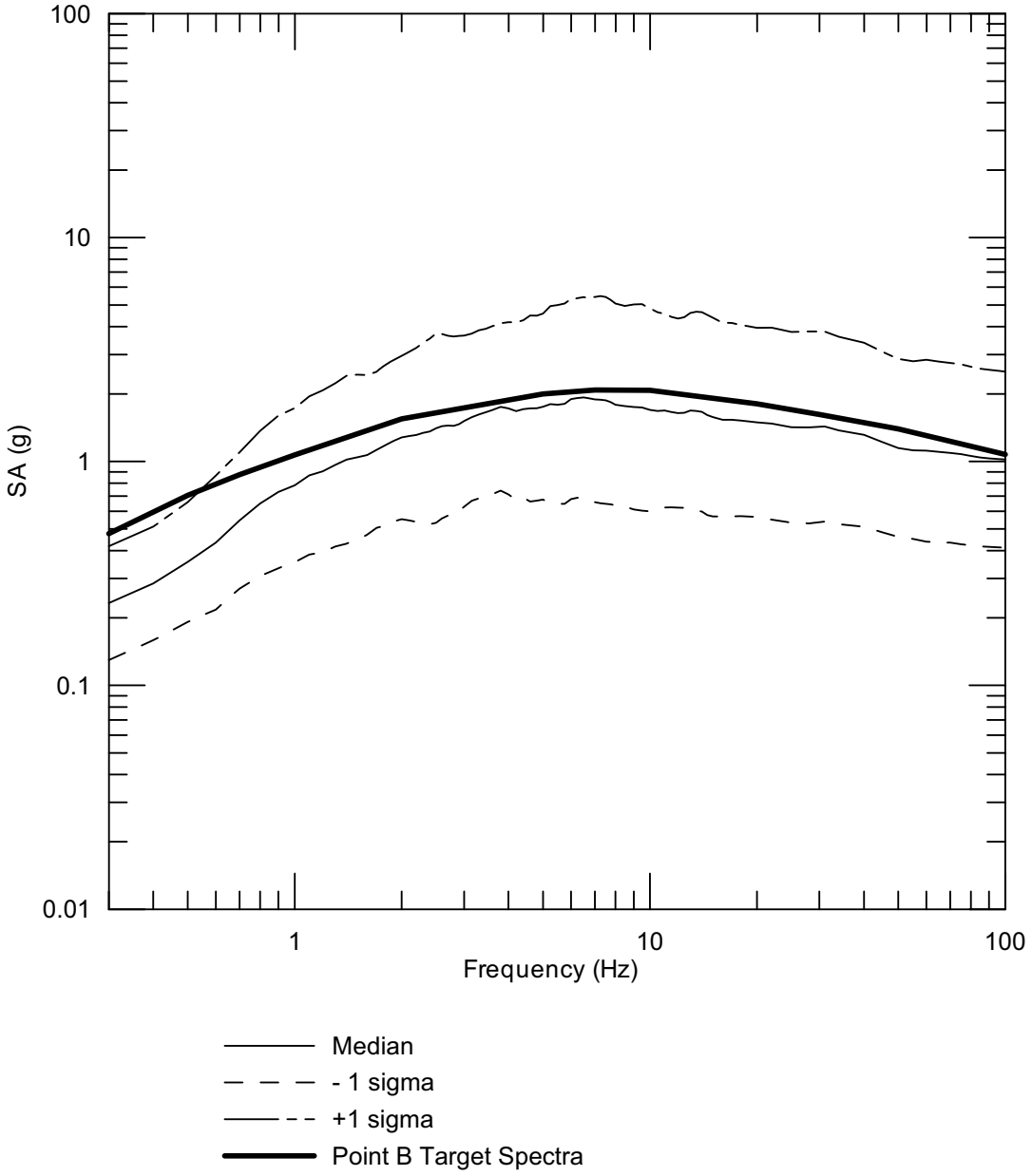

DTN: MO0402AVDTM105.001 [DIRS 168890]

Figure 6.3-145. Median and ± 1 σ Response Spectra of Point B 10^{-5} Spectrally Conditioned to Point B Horizontal Time Histories

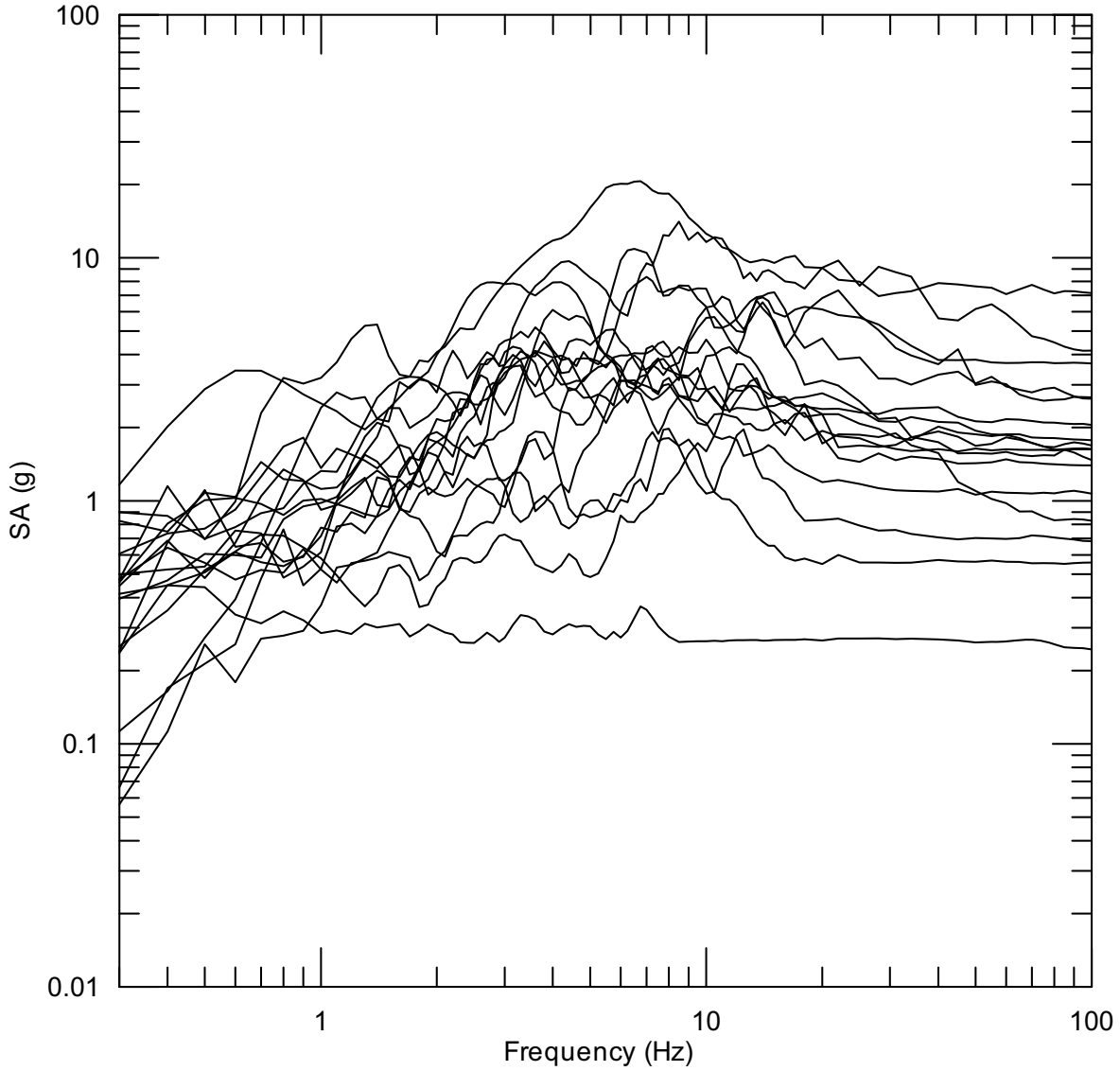

DTN: MO0402AVDTM105.001 [DIRS 168890]

Figure 6.3-146. Response Spectra of Point B 10^{-5} Spectrally Conditioned to Point B Vertical Time Histories

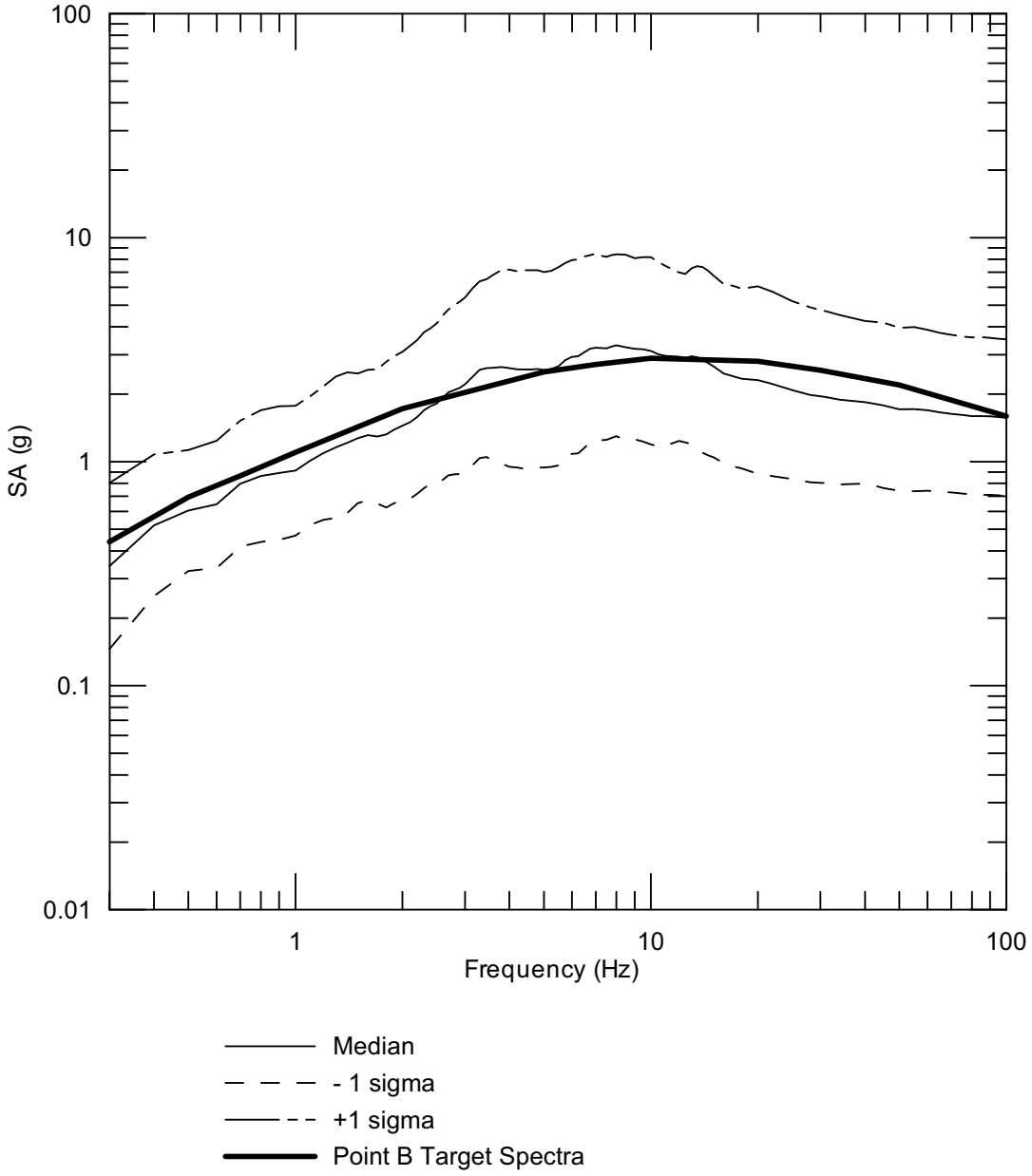

DTN: MO0402AVDTM105.001 [DIRS 168890]

Figure 6.3-147. Median and ± 1 σ Response Spectra of Point B 10^{-5} Spectrally Conditioned to Point B Vertical Time Histories

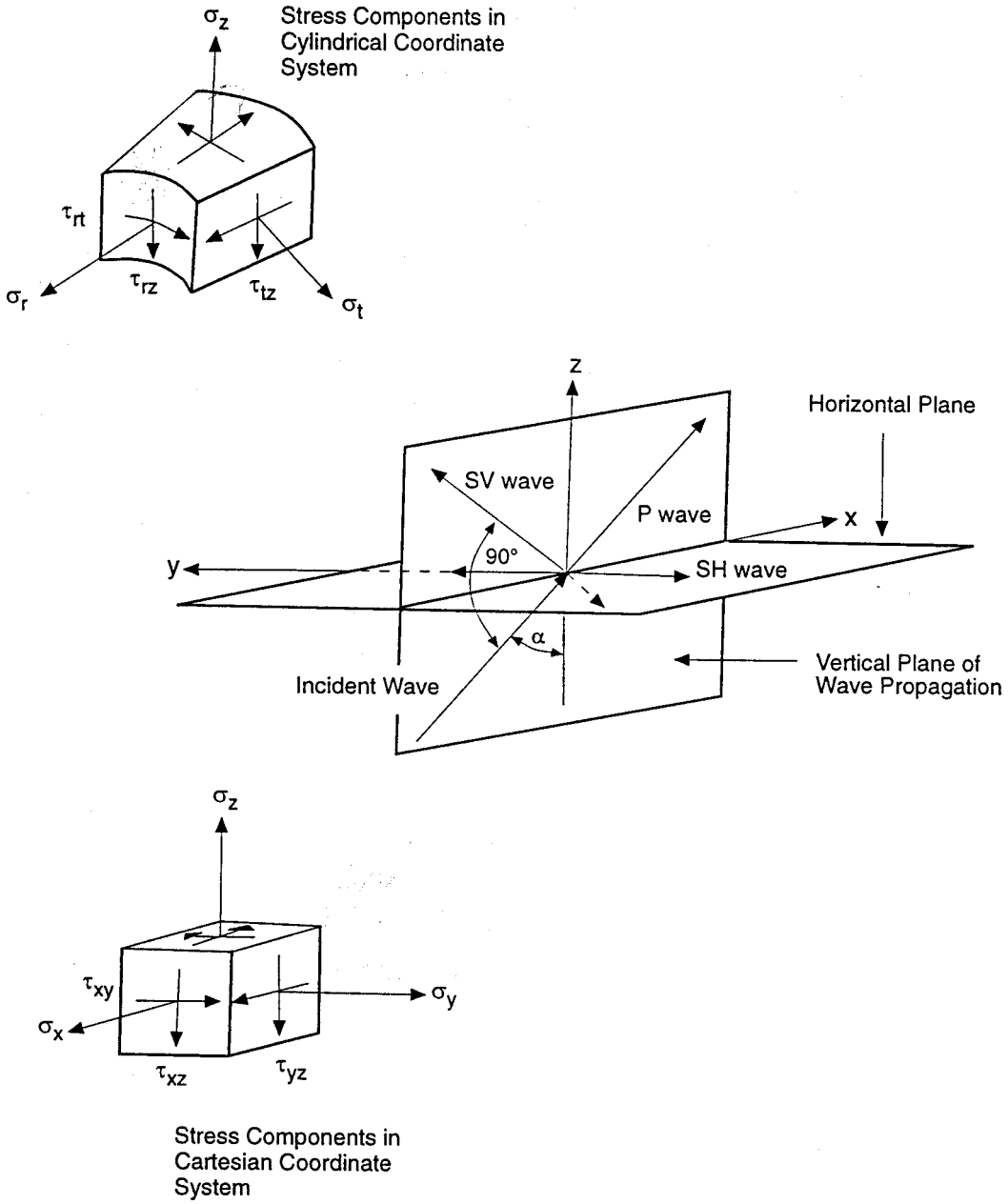

Source: Modified from Fowler 1990 [DIRS 171474]

Figure 6.3-148. Illustration of Inclined P-, SV-, and SH-Waves Demonstrating Wave Types and Angle of Incidence

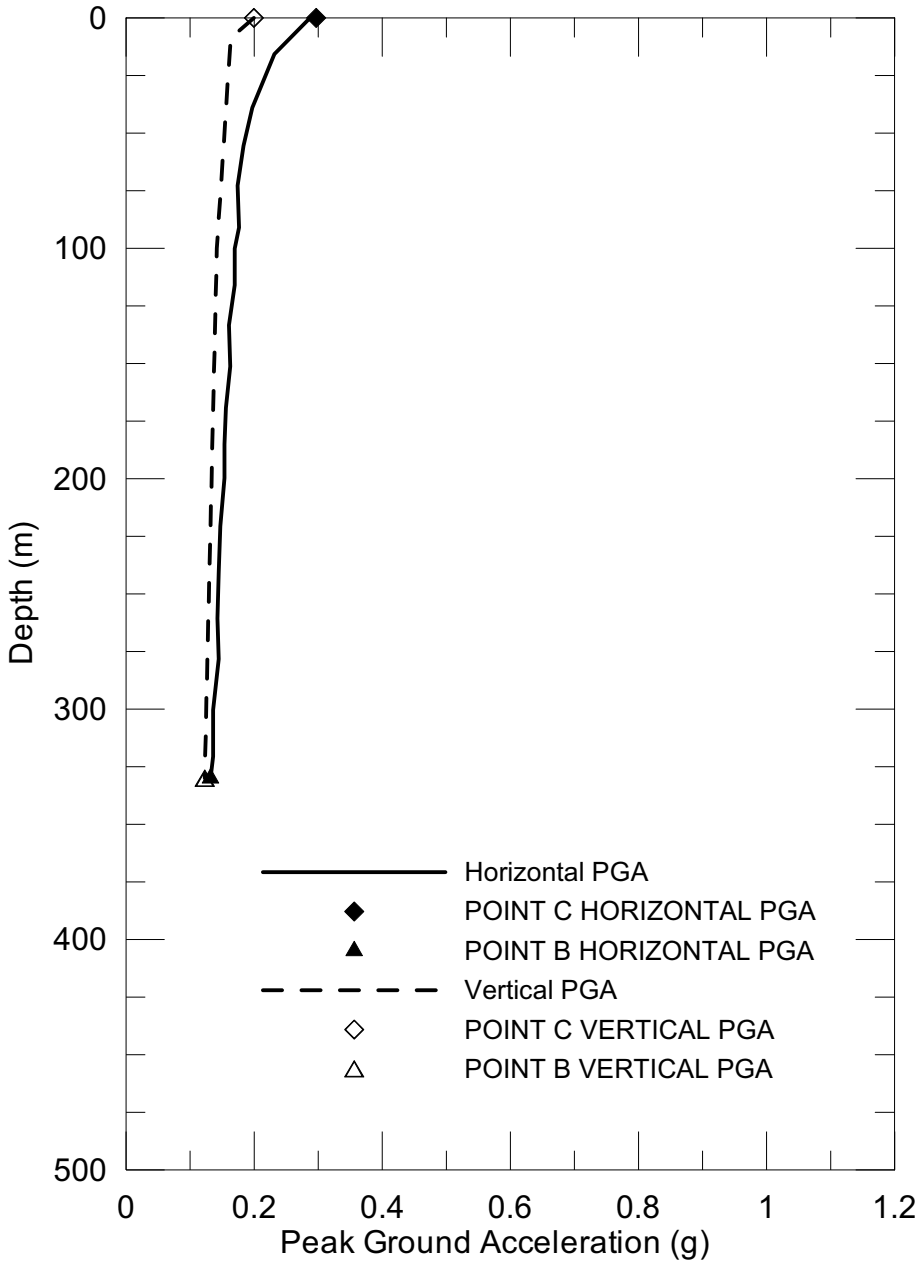

DTN: MO0408PGAPGVSC.001 [DIRS 171434]

Source: Appendix I, Filename: At-depth PGA Adjustment.xls

Figure 6.3-149. At-Depth Peak Ground Acceleration at an Annual Exceedance Frequency of 10^{-3}

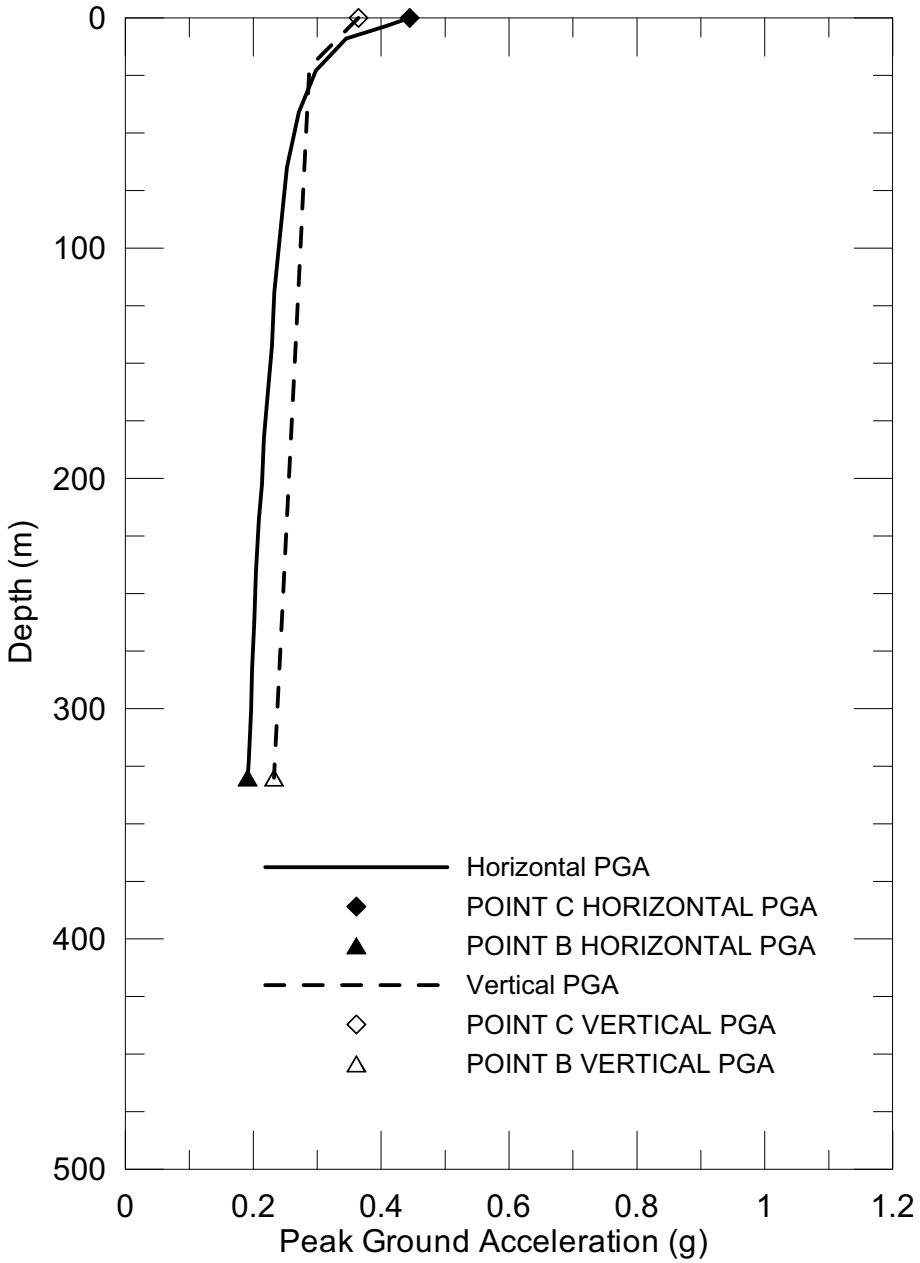

DTN: MO0408PGAPGVSC.001 [DIRS 171434]

Source: Appendix I, Filename: At-depth PGA Adjustment.xls

Figure 6.3-150. At-Depth Peak Ground Acceleration at an Annual Exceedance Frequency of 5×10^{-4}

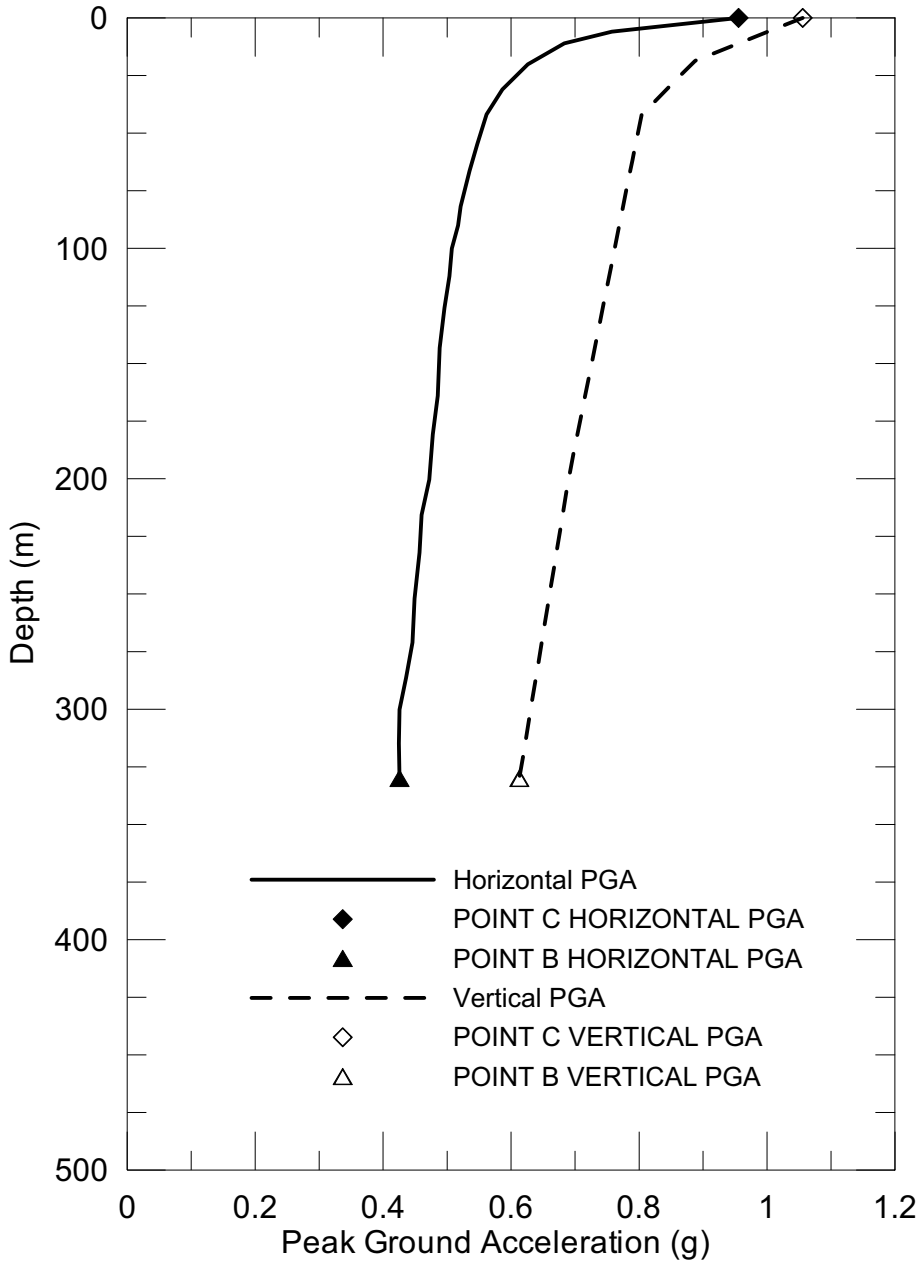

DTN: MO0408PGAPGVSC.001 [DIRS 171434]

Source: Appendix I, Filename: At-depth PGA Adjustment.xls

Figure 6.3-151. At-Depth Peak Ground Acceleration at an Annual Exceedance Frequency of 10^{-4}

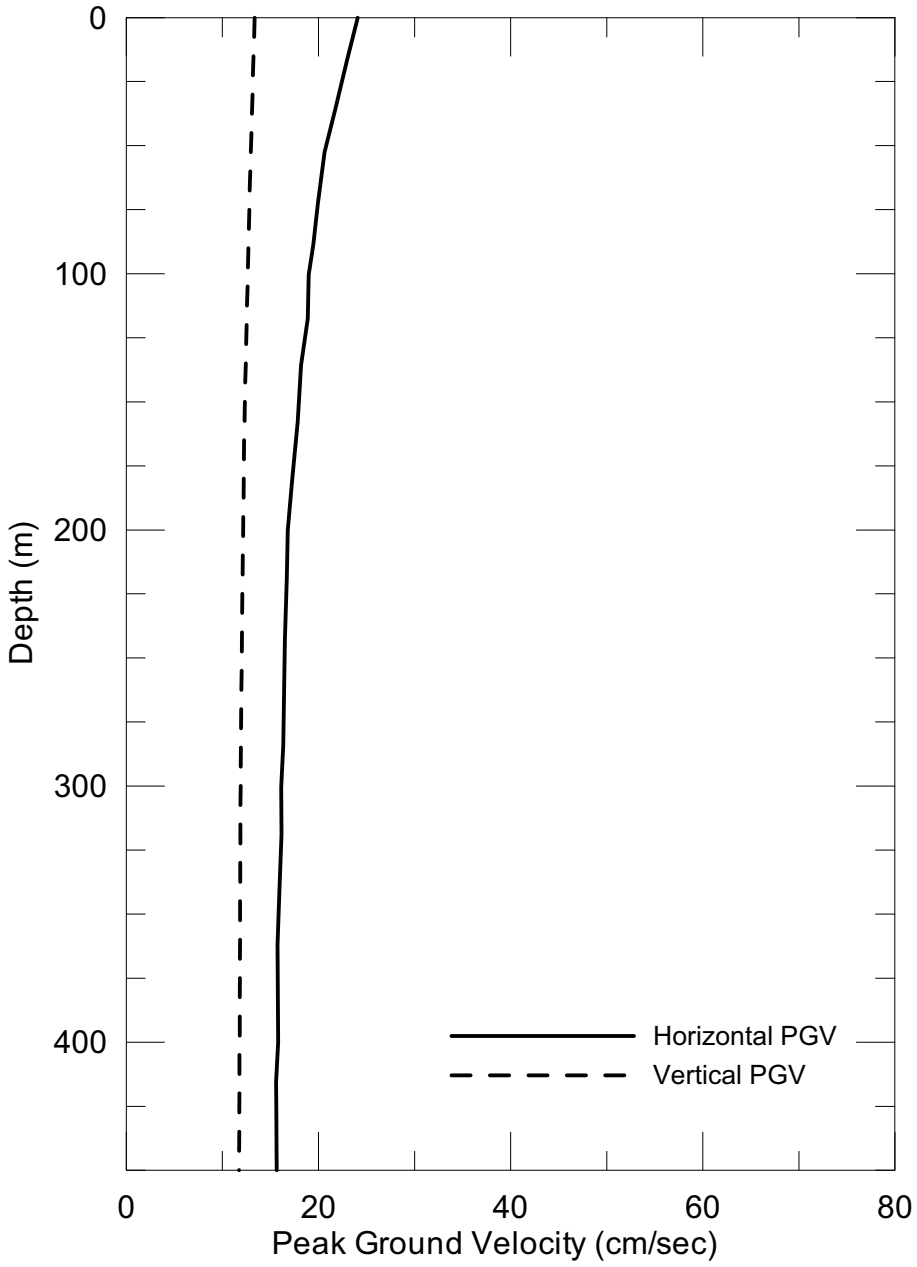

DTN: MO0408PGAPGVSC.001 [DIRS 171434]

Figure 6.3-152. At-Depth Peak Ground Velocity at an Annual Exceedance Frequency of 10^{-3}

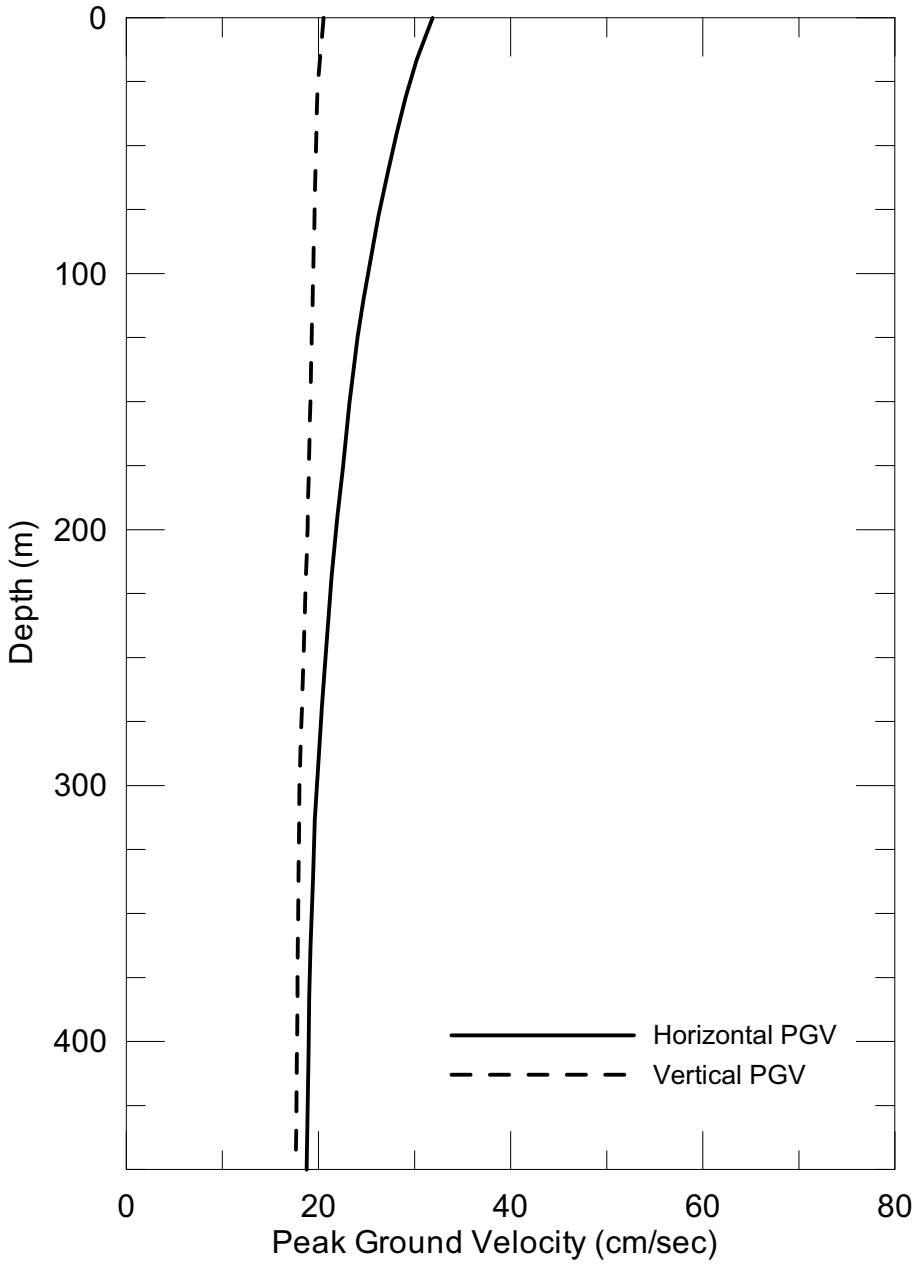

DTN: MO0408PGAPGVSC.001 [DIRS 171434]

Figure 6.3-153. At-Depth Peak Ground Velocity at an Annual Exceedance Frequency of 5×10^{-4}

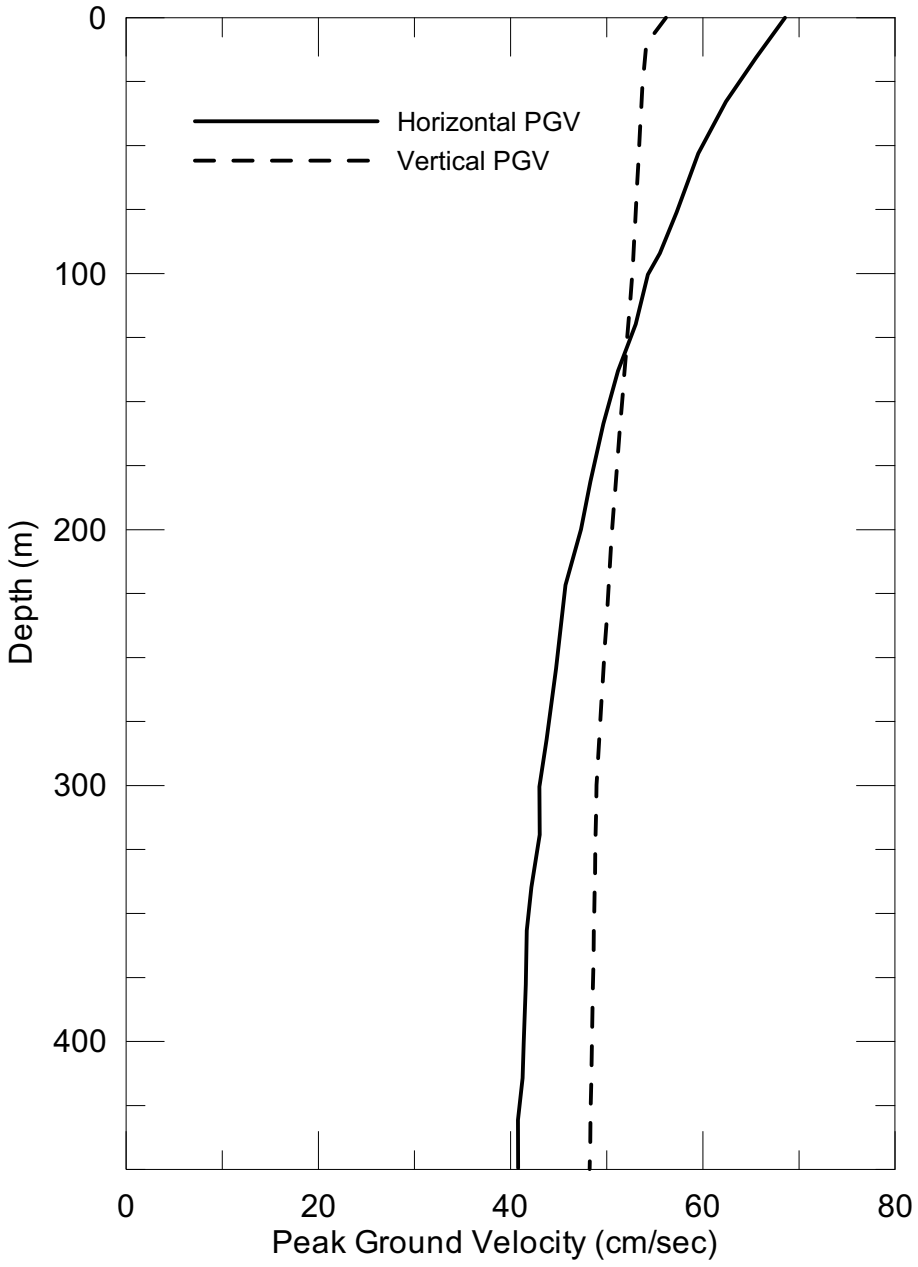

DTN: MO0408PGAPGVSC.001 [DIRS 171434]

Figure 6.3-154. At-Depth Peak Ground Velocity at an Annual Exceedance Frequency of 10^{-4}

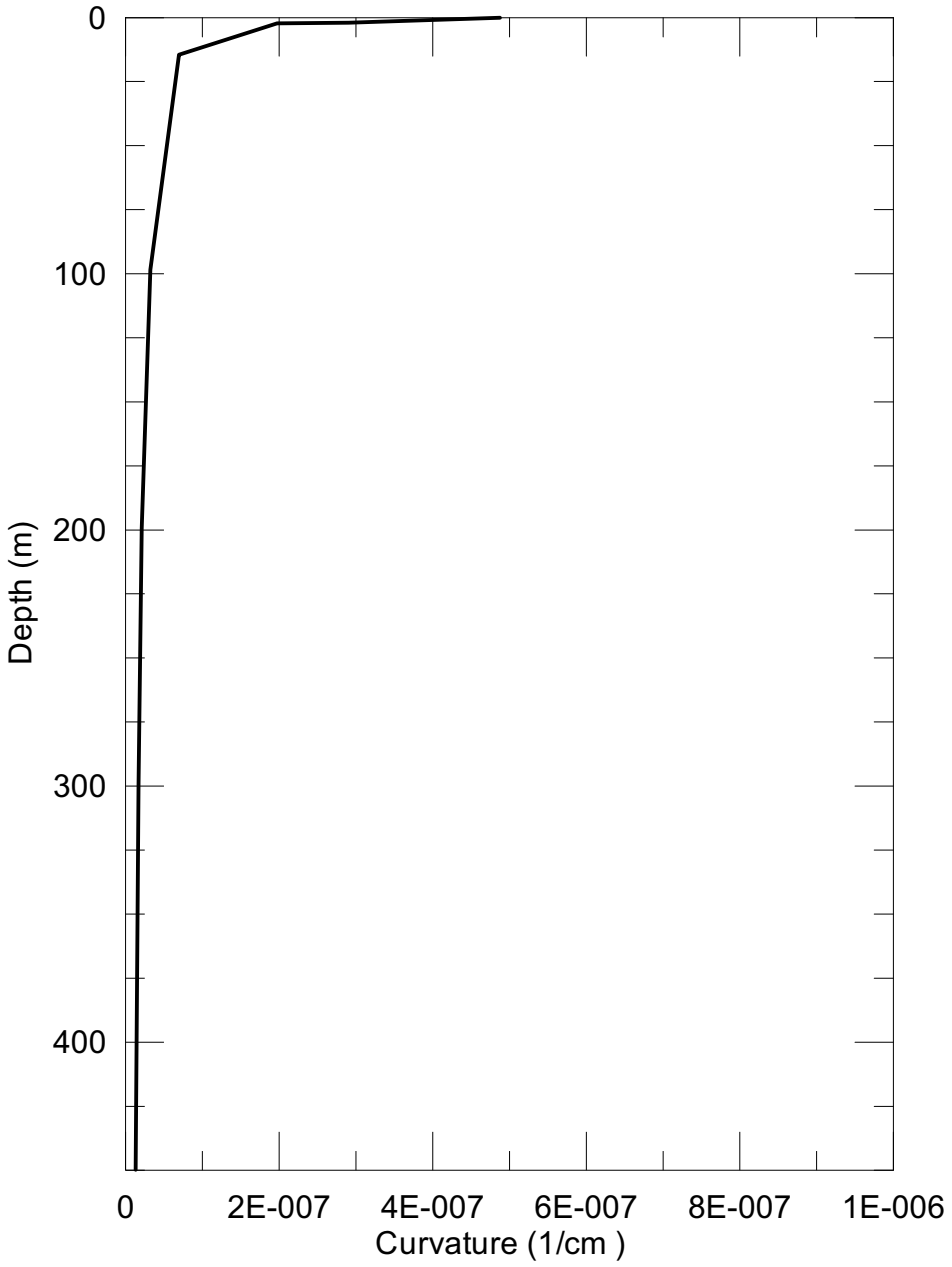

DTN: MO0408PGAPGVSC.001 [DIRS 171434]

Figure 6.3-155. At-Depth Curvatures at an Annual Exceedance Frequency of 10^{-3}

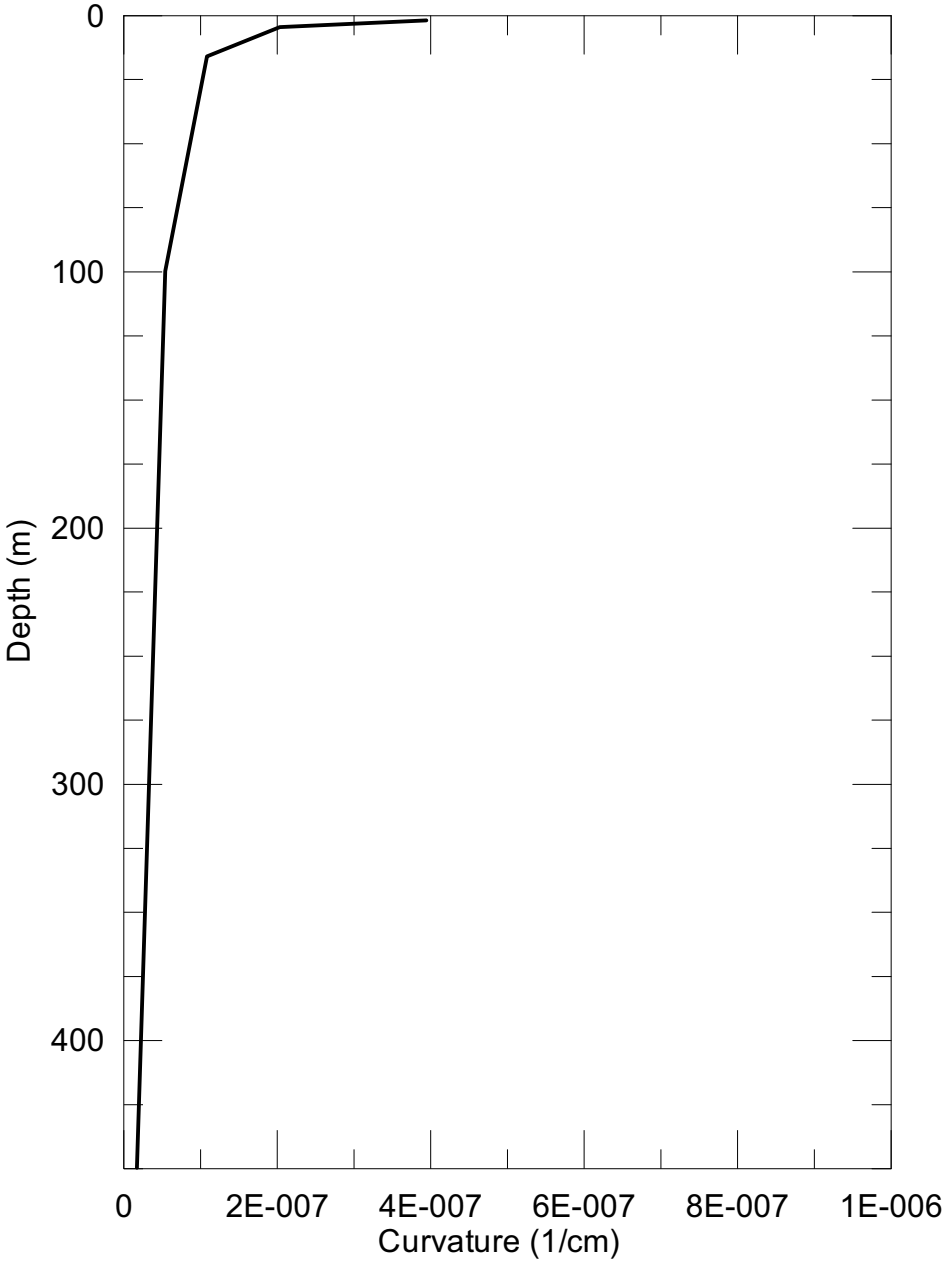

DTN: MO0408PGAPGVSC.001 [DIRS 171434]

Figure 6.3-156. At-Depth Curvatures at an Annual Exceedance Frequency of 5×10^{-4}

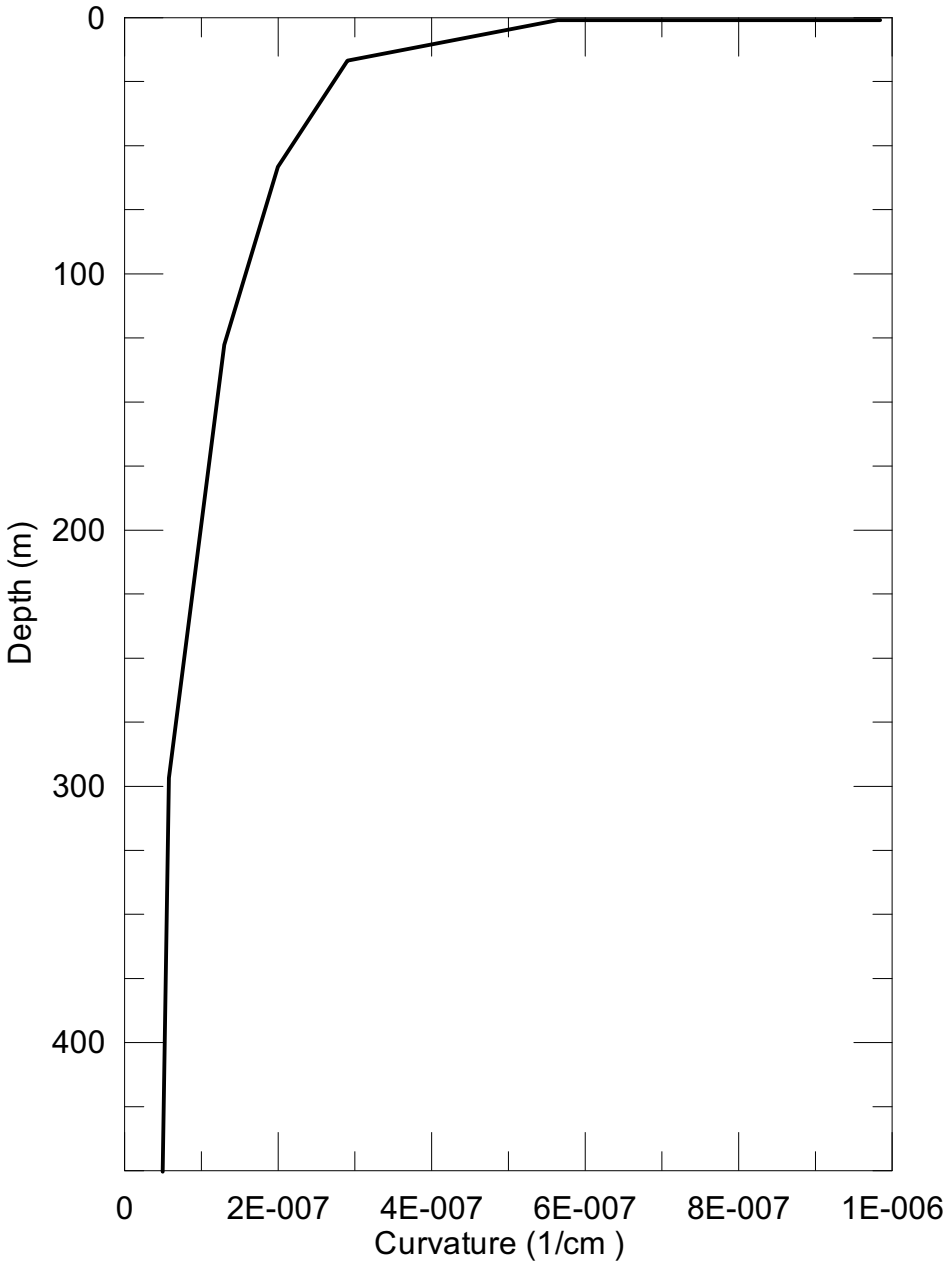

DTN: MO0408PGAPGVSC.001 [DIRS 171434]

Figure 6.3-157. At-Depth Curvatures at an Annual Exceedance Frequency of 10^{-4}

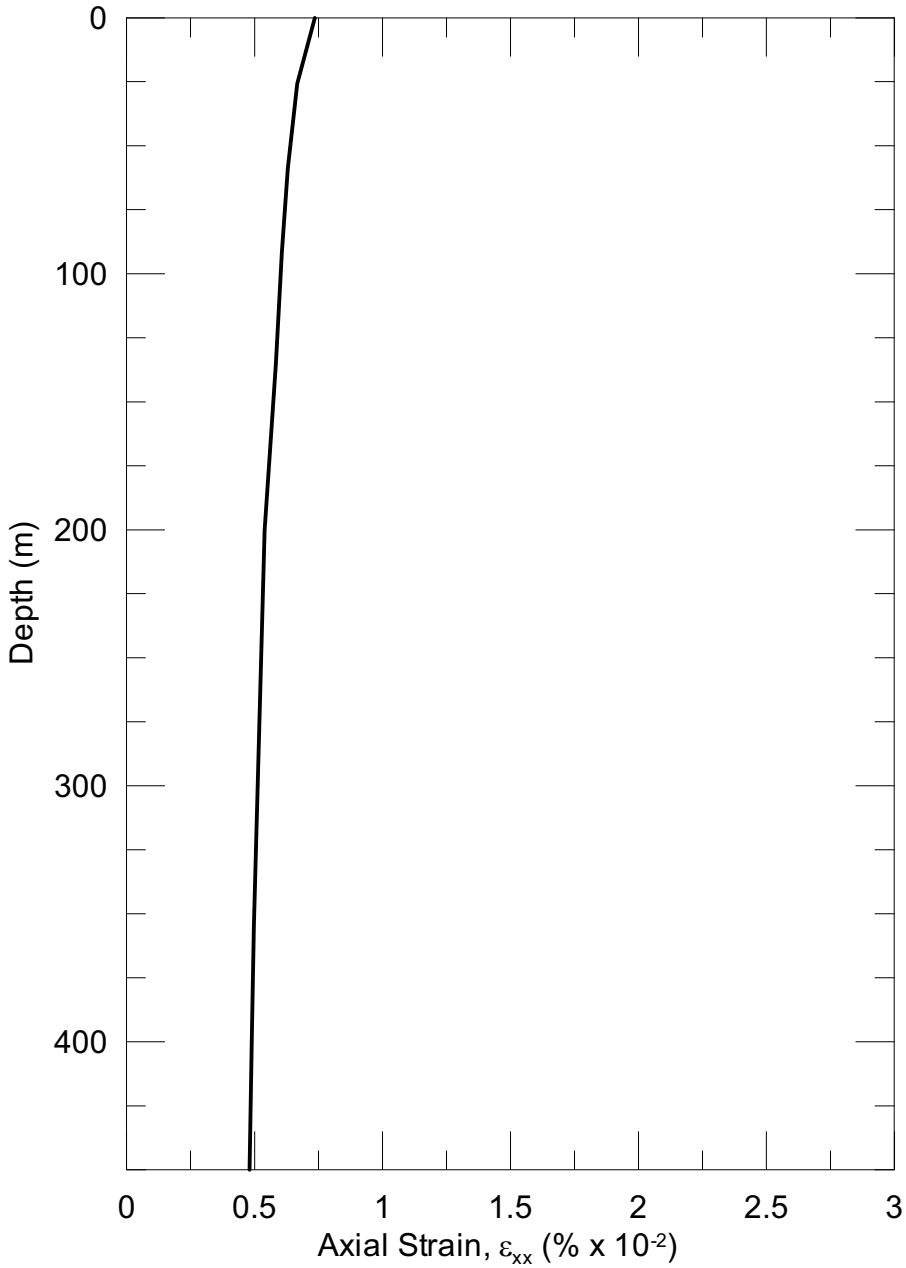

DTN: MO0408PGAPGVSC.001 [DIRS 171434]

Figure 6.3-158. At-Depth Axial Strains (ε_{xx}) at an Annual Exceedance Frequency of 10^{-3}

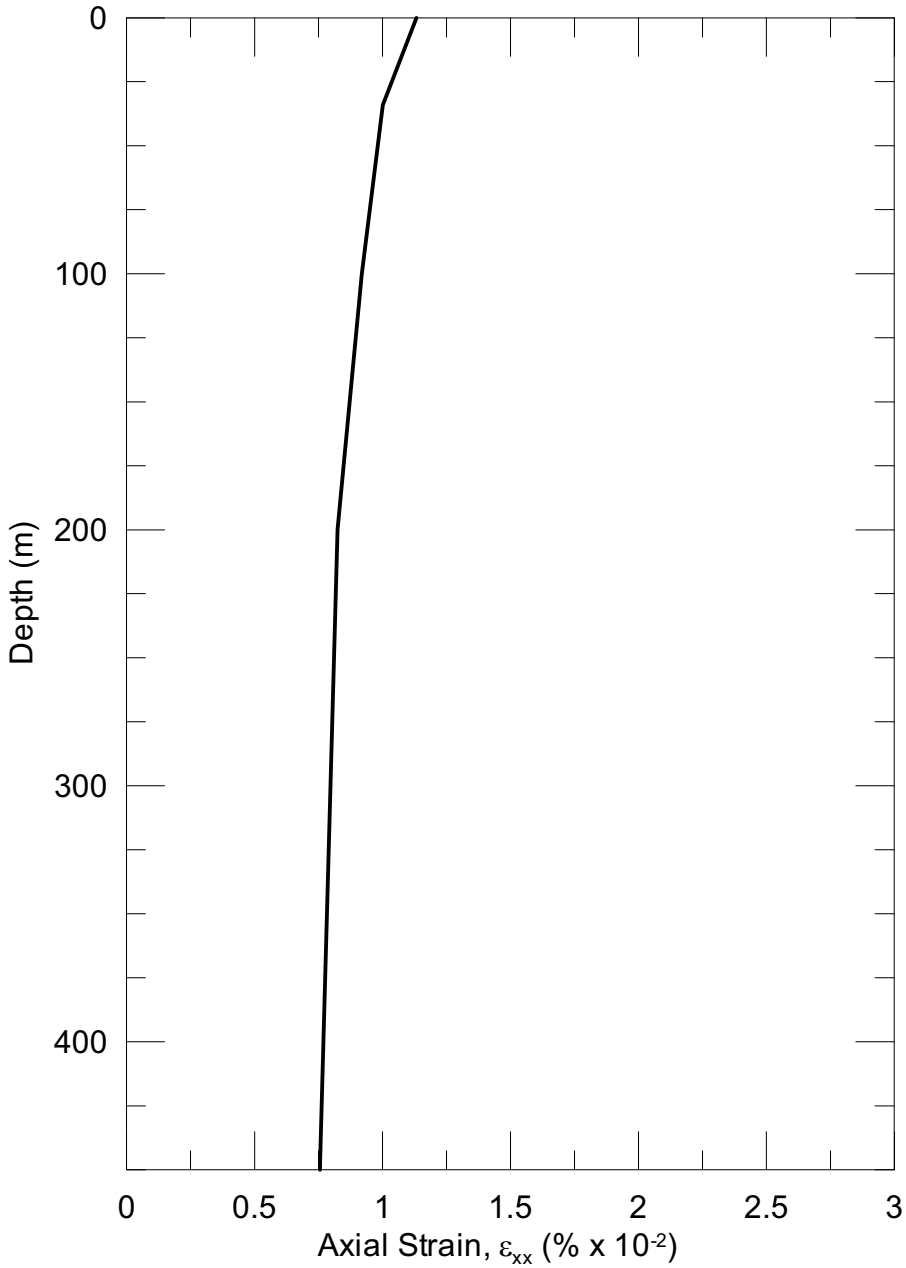

DTN: MO0408PGAPGVSC.001 [DIRS 171434]

Figure 6.3-159. At-Depth Axial Strains (ε_{xx}) at an Annual Exceedance Frequency of 5×10^{-4}

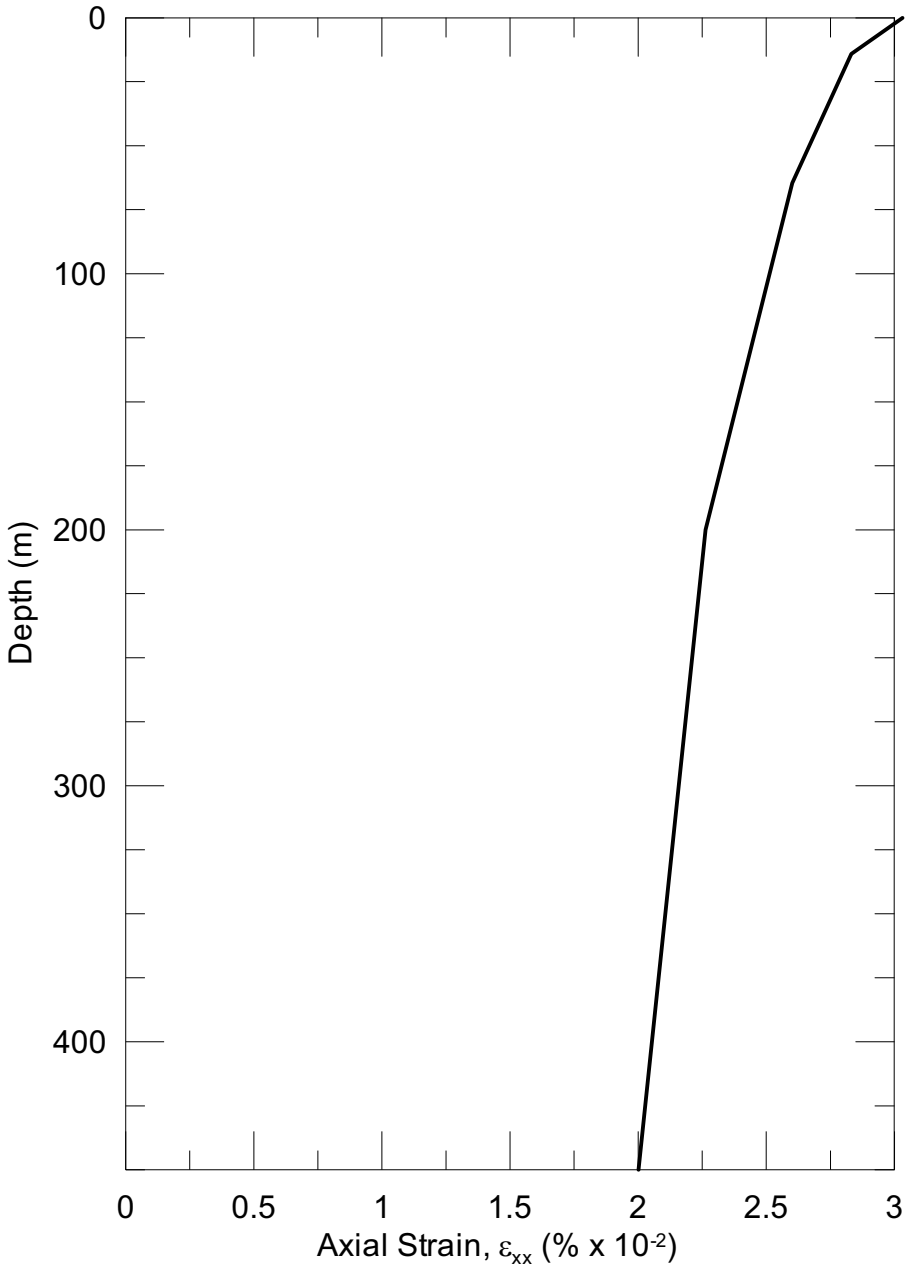

DTN: MO0408PGAPGVSC.001 [DIRS 171434]

Figure 6.3-160. At-Depth Axial Strains (ε_{xx}) at an Annual Exceedance Frequency of 10^{-4}

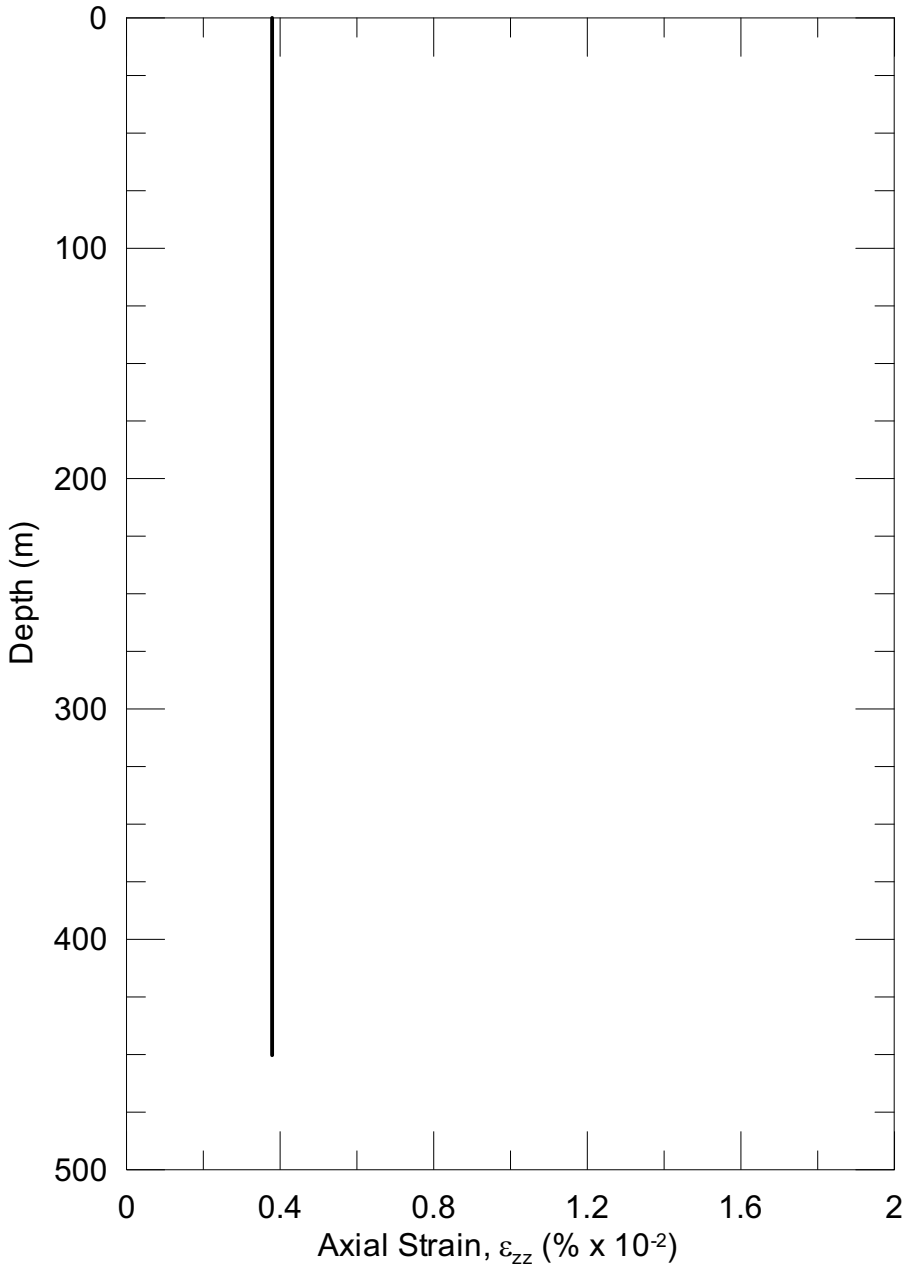

DTN: MO0408PGAPGVSC.001 [DIRS 171434]

Figure 6.3-161. At-Depth Axial Strains (ε_{zz}) at an Annual Exceedance Frequency of 10^{-3}

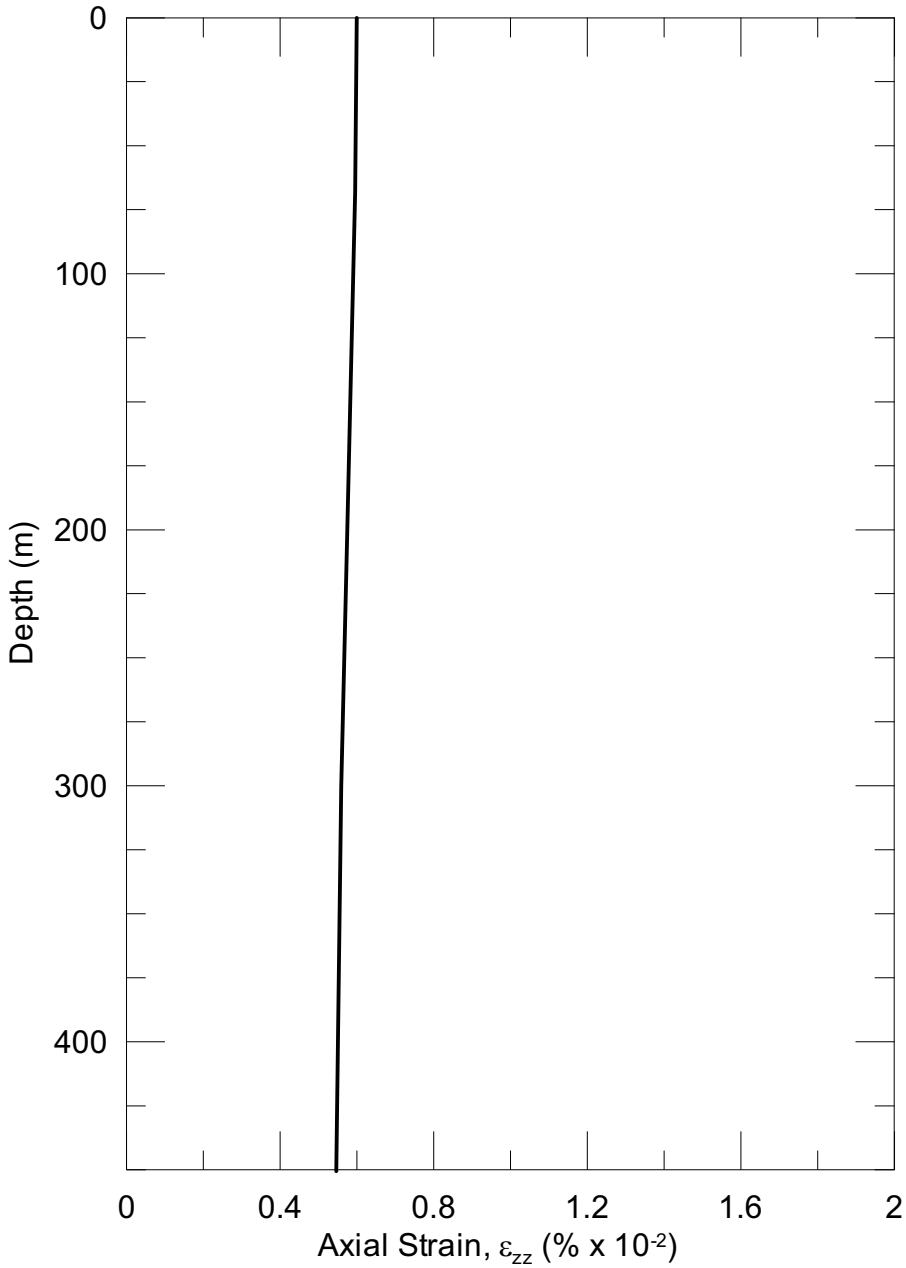

DTN: MO0408PGAPGVSC.001 [DIRS 171434]

Figure 6.3-162. At-Depth Axial Strains (ε_{zz}) at an Annual Exceedance Frequency of 5×10^{-4}

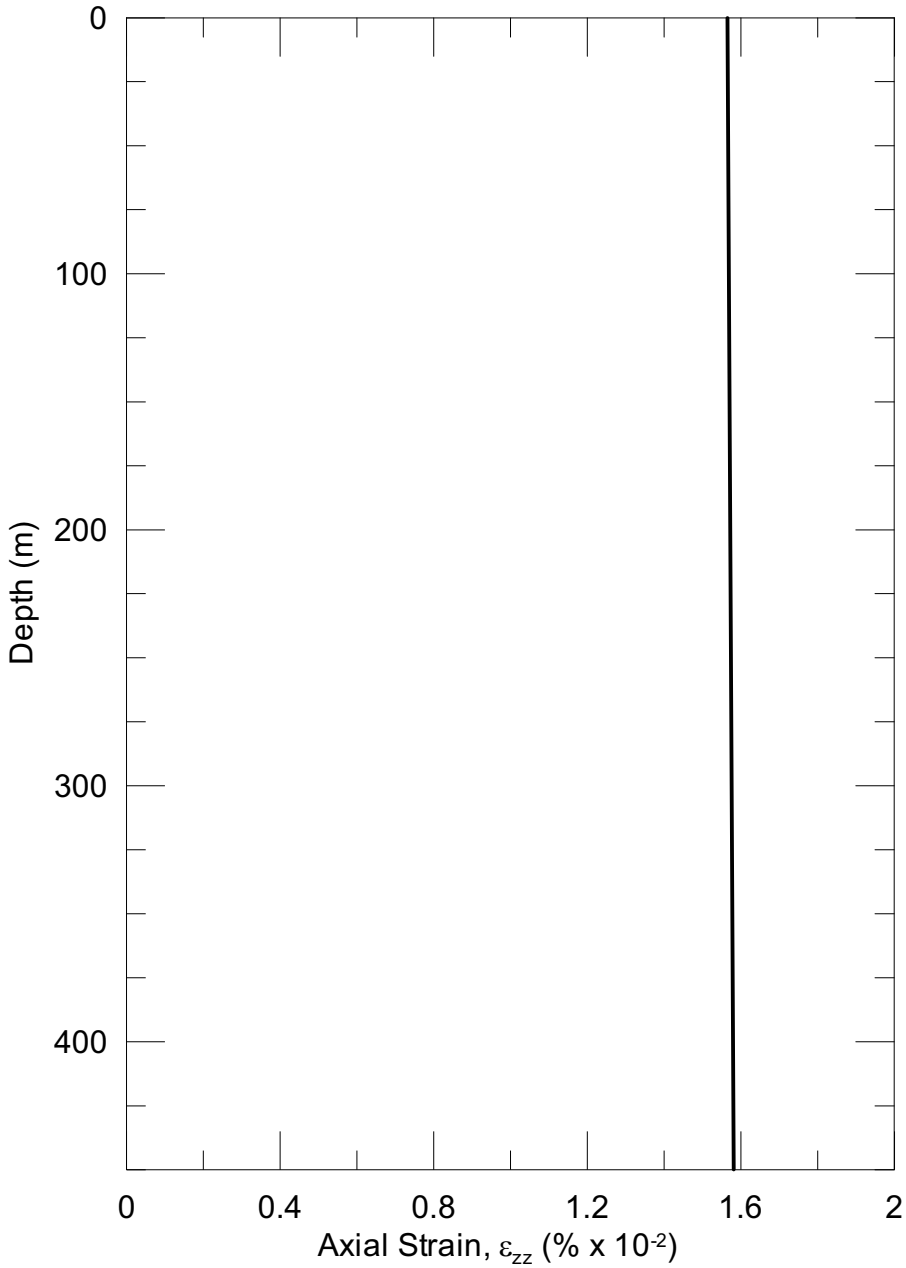

DTN: MO0408PGAPGVSC.001 [DIRS 171434]

Figure 6.3-163. At-Depth Axial Strains (ε_{zz}) at an Annual Exceedance Frequency of 10^{-4}

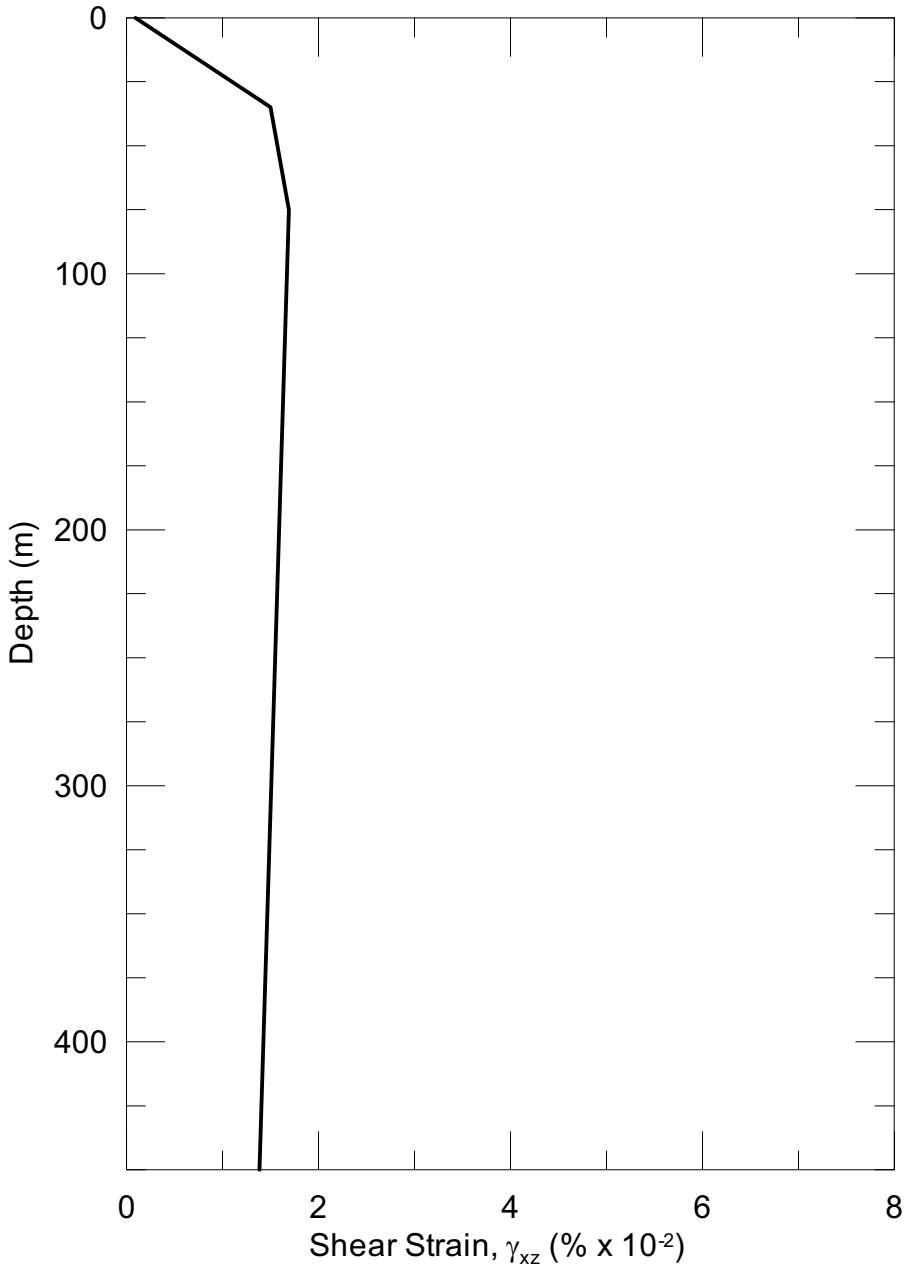

DTN: MO0408PGAPGVSC.001 [DIRS 171434]

Figure 6.3-164. At-Depth Shear Strains (γ_{xz}) at an Annual Exceedance Frequency of 10^{-3}

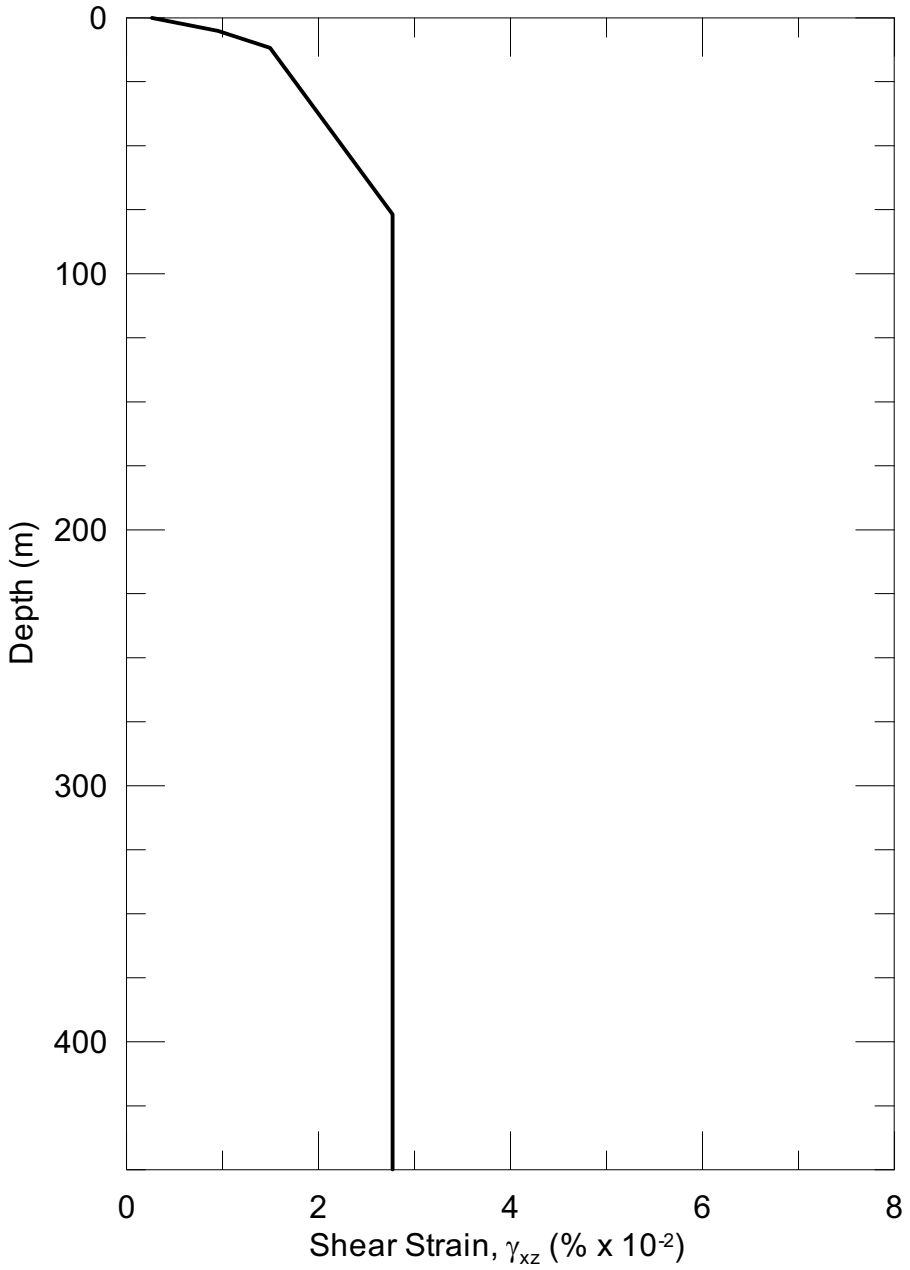

DTN: MO0408PGAPGVSC.001 [DIRS 171434]

Figure 6.3-165. At-Depth Shear Strains (γ_{xz}) at an Annual Exceedance Frequency of $5x10^{-4}$

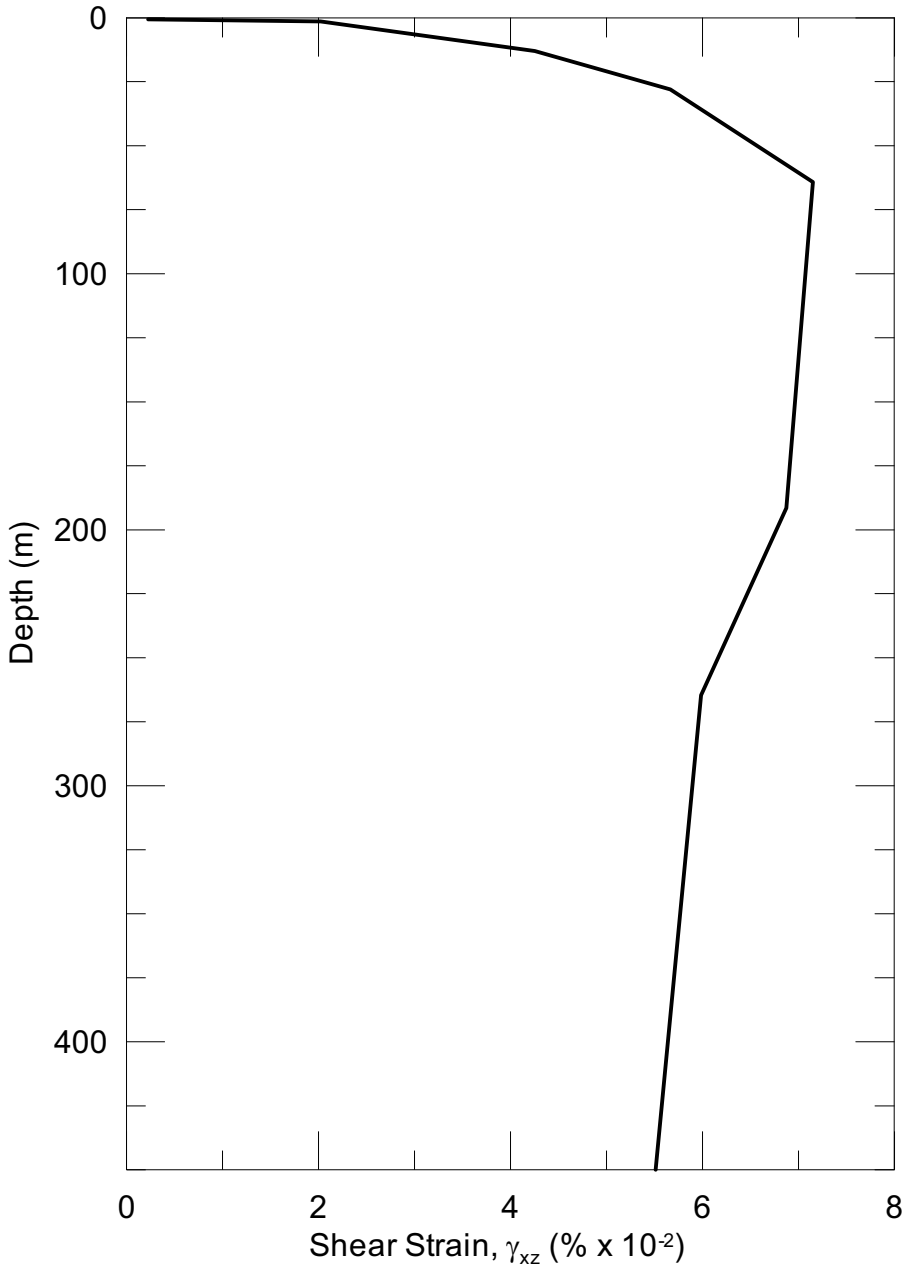

DTN: MO0408PGAPGVSC.001 [DIRS 171434]

Figure 6.3-166. At-Depth Shear Strains (γ_{xz}) at an Annual Exceedance Frequency of 10^{-4}

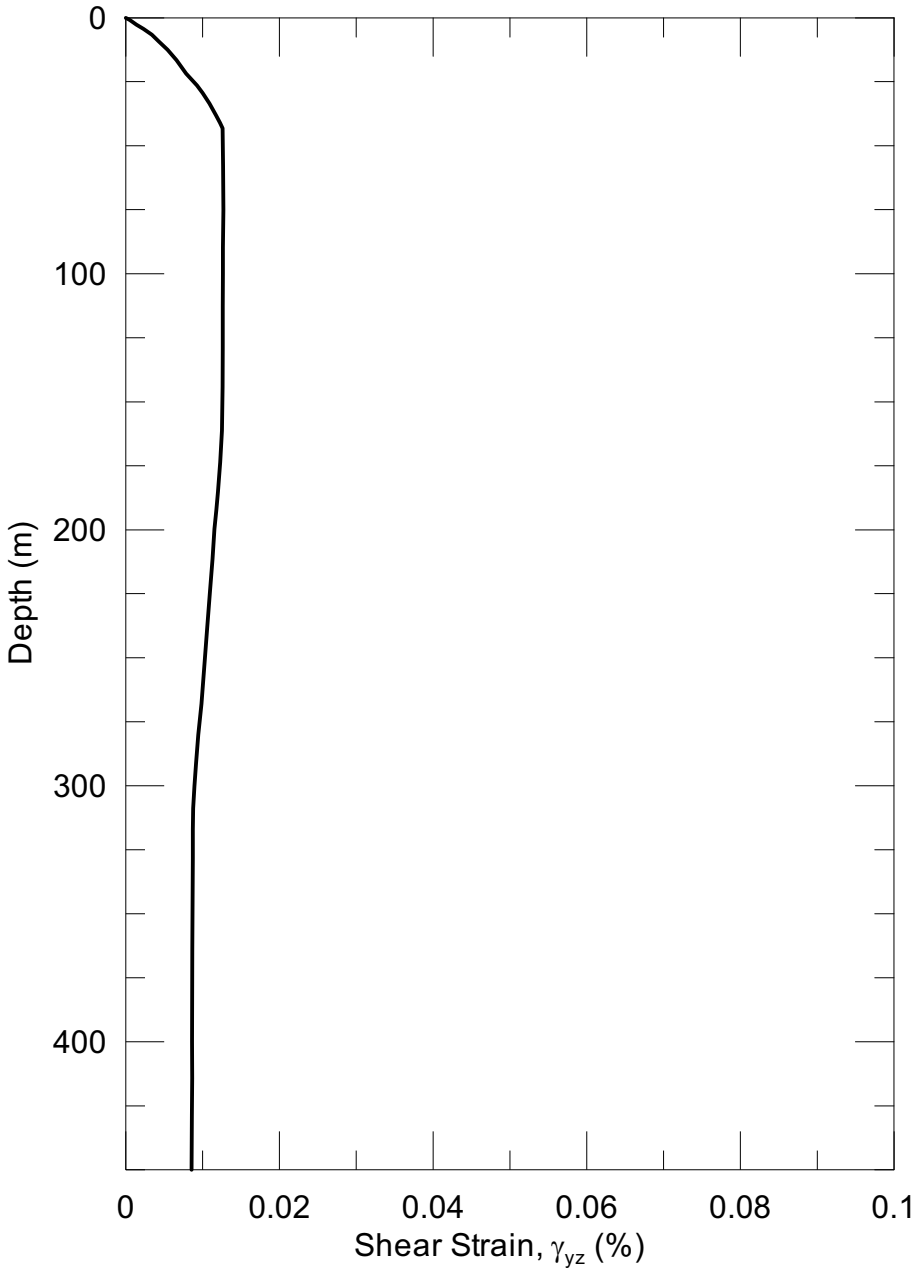

DTN: MO0408PGAPGVSC.001 [DIRS 171434]

Figure 6.3-167. At-Depth Shear Strains (γ_{yz}) at an Annual Exceedance Frequency of 10^{-3}

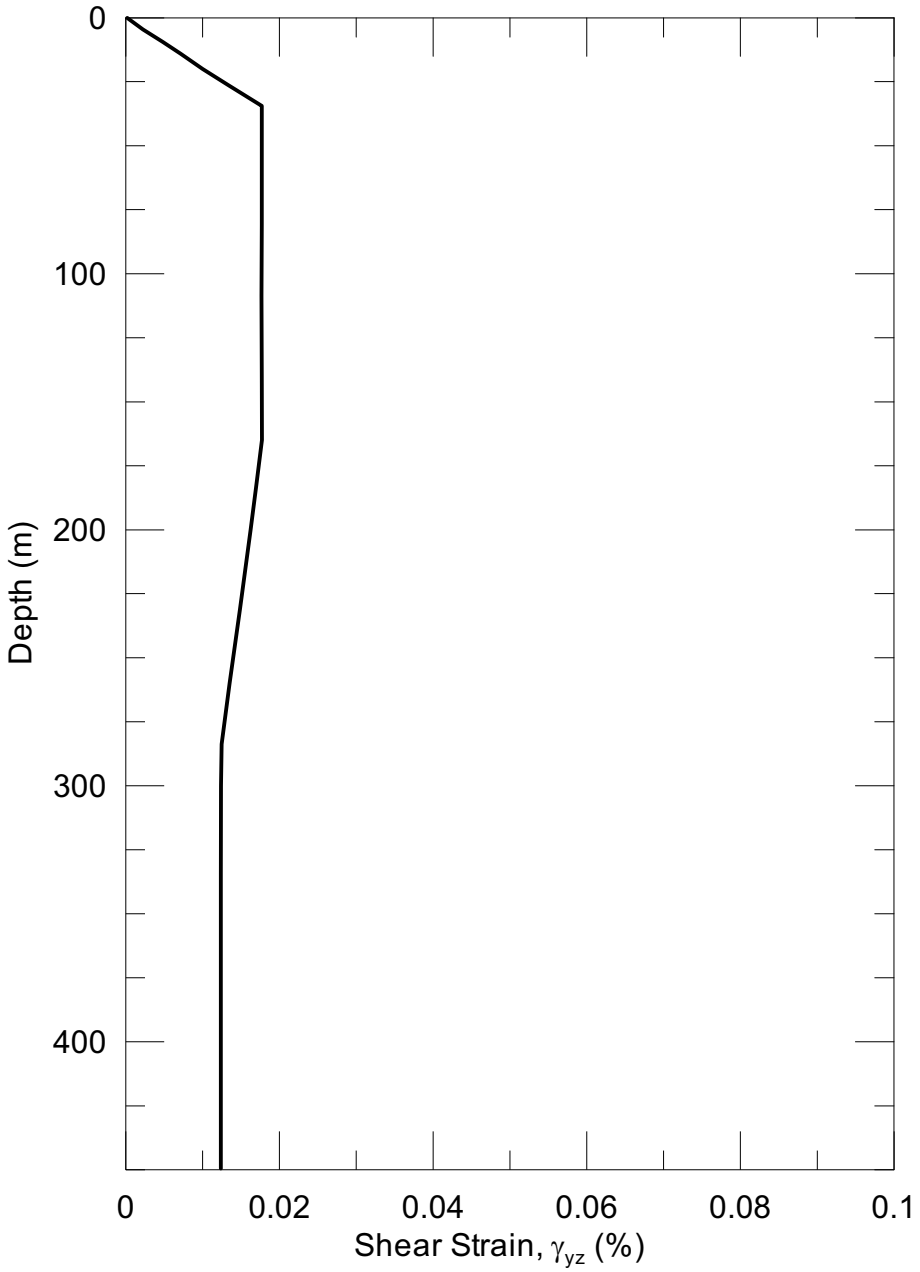

DTN: MO0408PGAPGVSC.001 [DIRS 171434]

Figure 6.3-168. At-Depth Shear Strains (γ_{yz}) at an Annual Exceedance Frequency of 5×10^{-4}

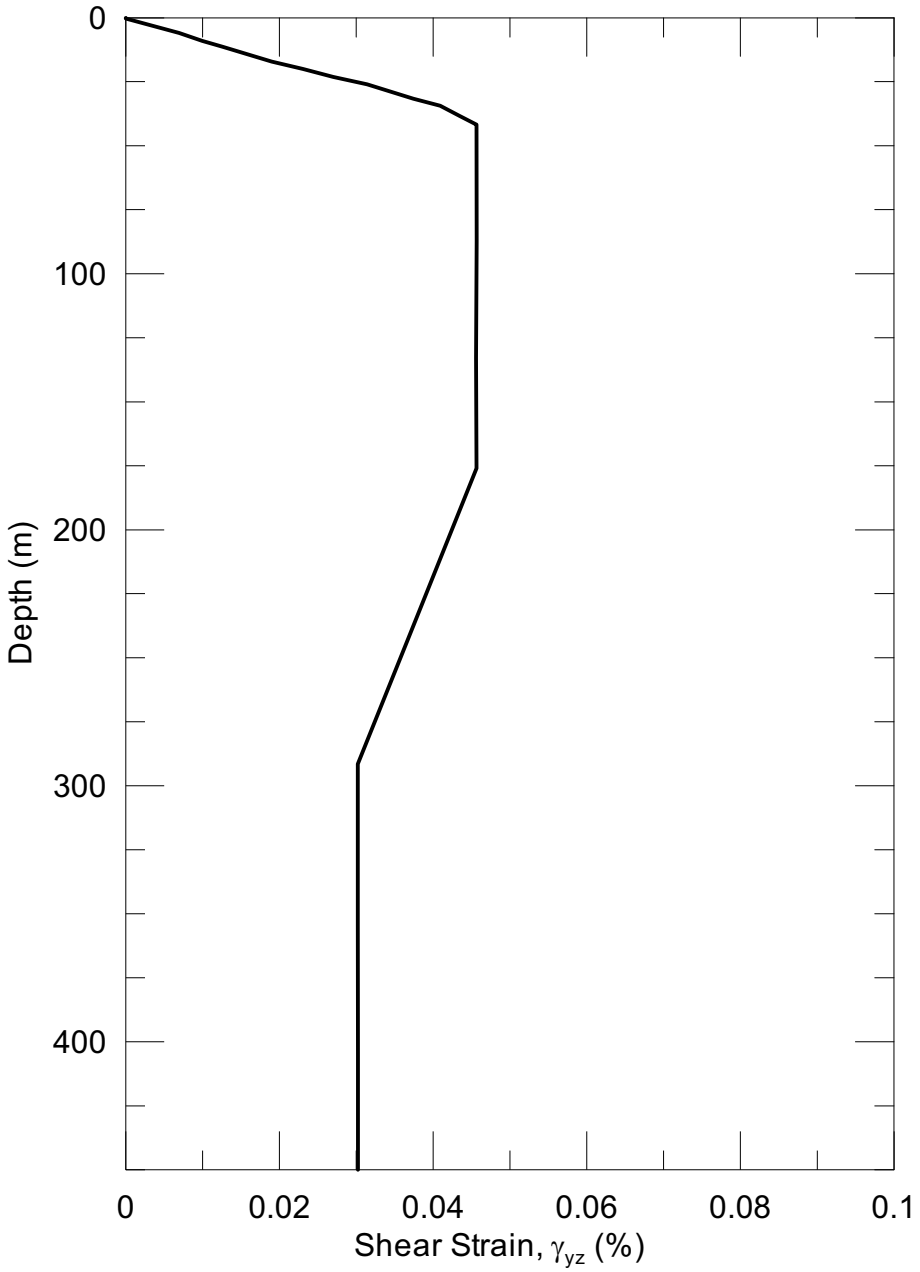

DTN: MO0408PGAPGVSC.001 [DIRS 171434]

Figure 6.3-169. At-Depth Shear Strains (γ_{yz}) at an Annual Exceedance Frequency of 10^{-4}

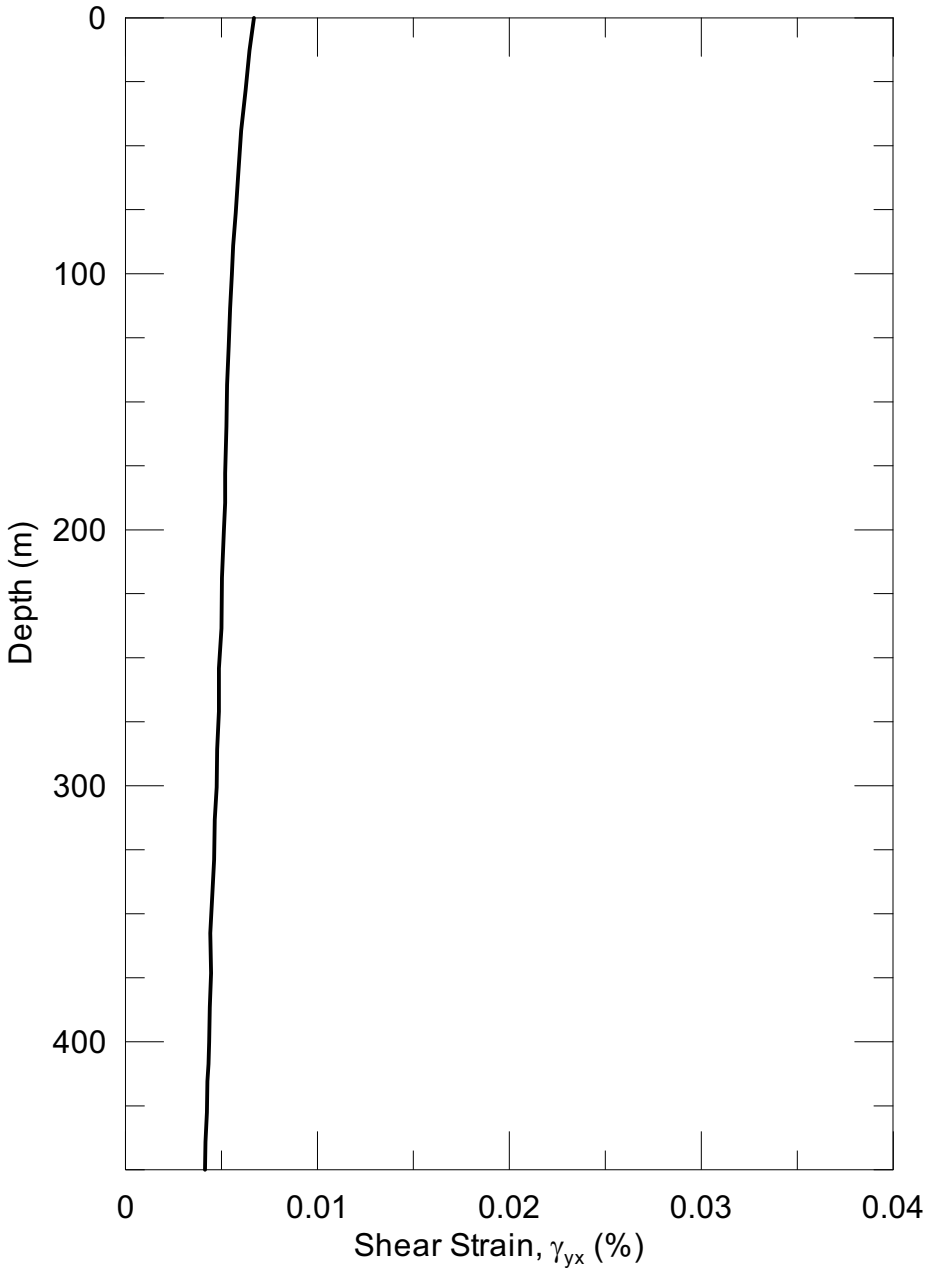

DTN: MO0408PGAPGVSC.001 [DIRS 171434]

Figure 6.3-170. At-Depth Shear Strains (γ_{yx}) at an Annual Exceedance Frequency of 10^{-3}

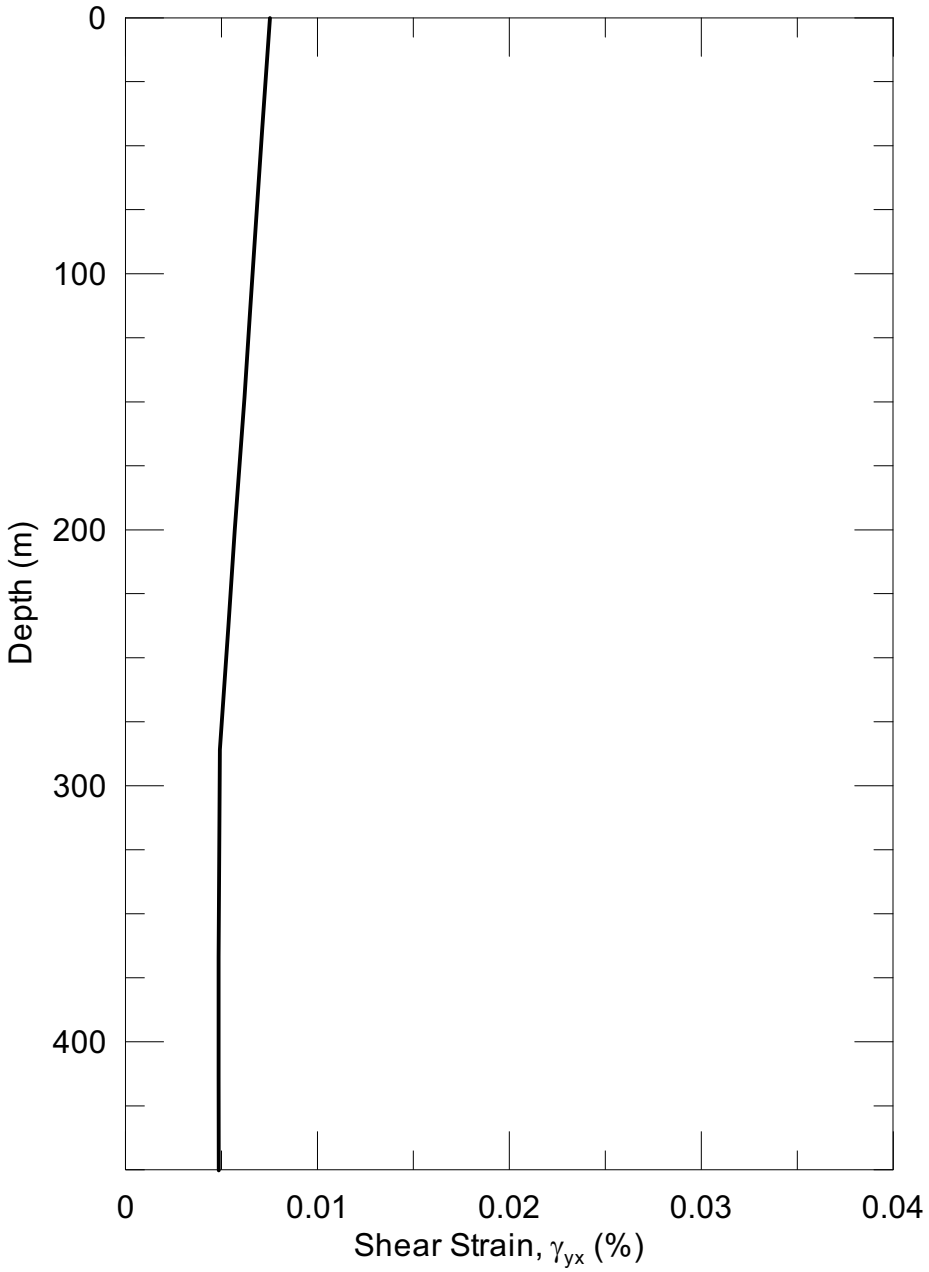

DTN: MO0408PGAPGVSC.001 [DIRS 171434]

Figure 6.3-171. At-Depth Shear Strains (γ_{yx}) at an Annual Exceedance Frequency of 5×10^{-4}

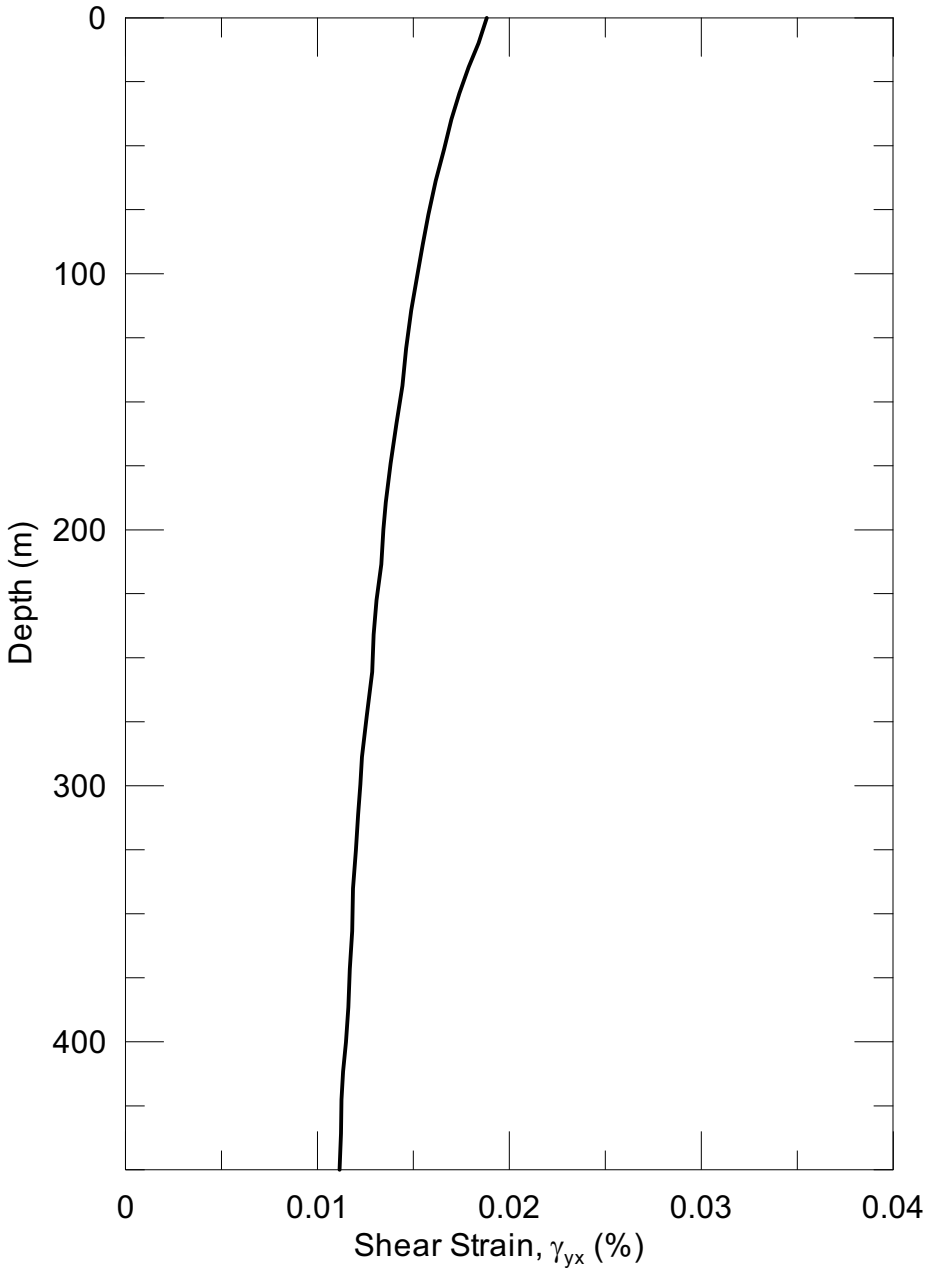

DTN: MO0408PGAPGVSC.001 [DIRS 171434]

Figure 6.3-172. At-Depth Shear Strains (γ_{yx}) at an Annual Exceedance Frequency of 10^{-4}

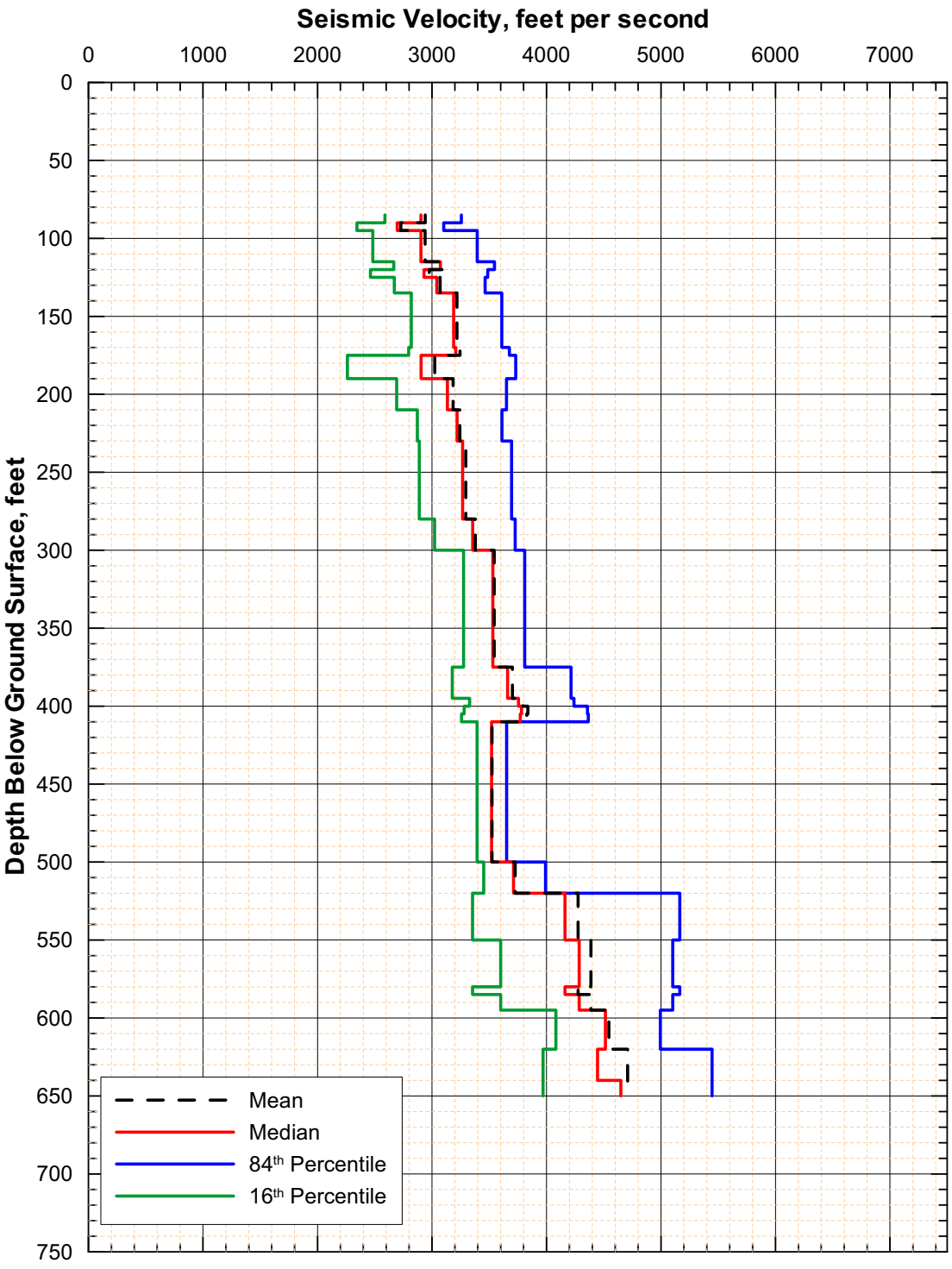

Source: Wong and Silva 2004b [DIRS 170444], page 112

Figure 6.3-173. Mean, Median, and 16th and 84th Percentile V_S Profiles to Tuff at Point F

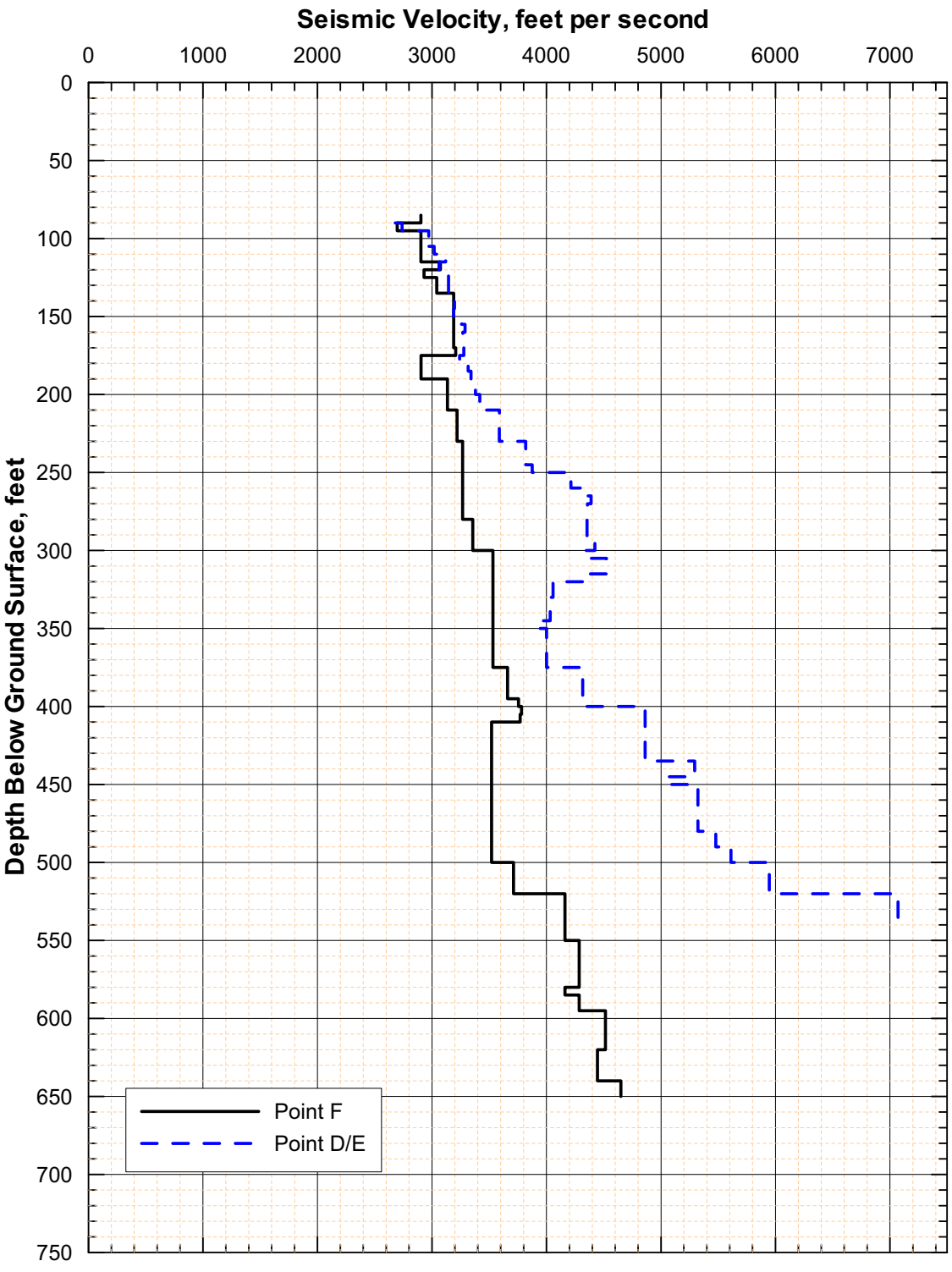

Source: Wong and Silva 2004b [DIRS 170444], page 113

Figure 6.3-174. Shallow V_S Profiles for Tuff at Points D/E and F

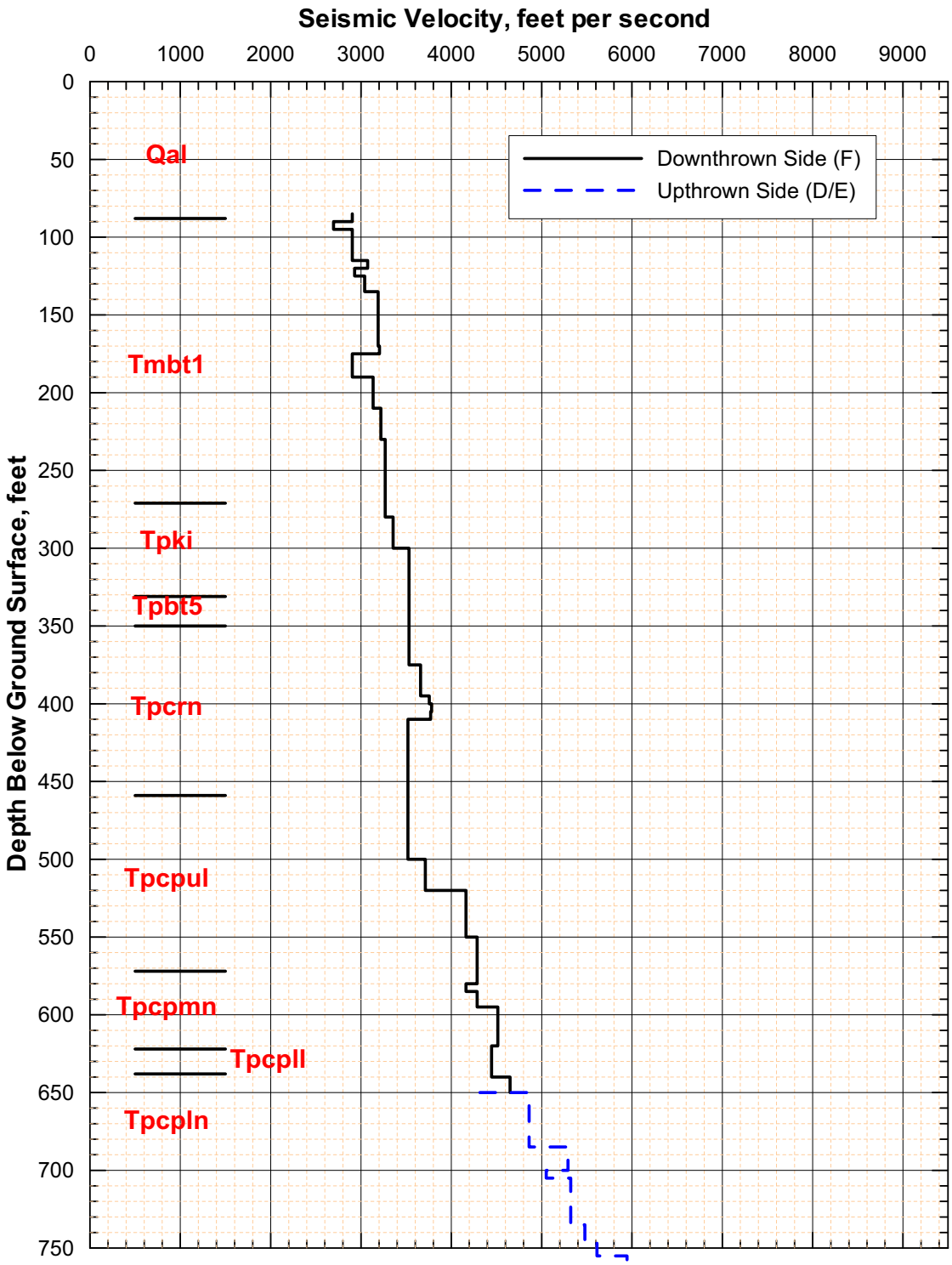

Source: Wong and Silva 2004b [DIRS 170444], page 114

Figure 6.3-175. Final V_S Profile for Tuff at Point F

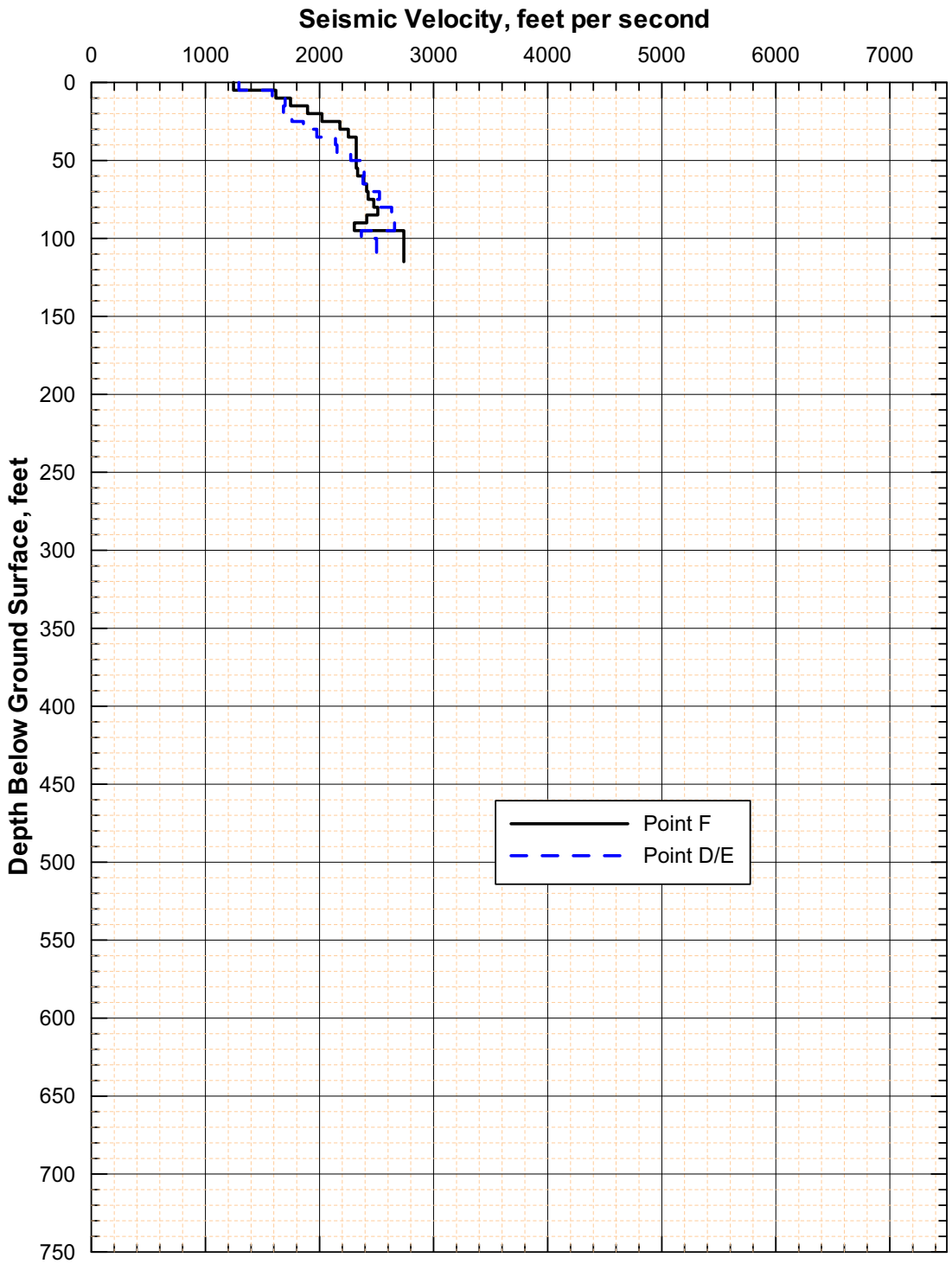

Source: Wong and Silva 2004b [DIRS 170444], page 102

Figure 6.3-176. Final V_S Profile for Alluvium at Points D/E and F

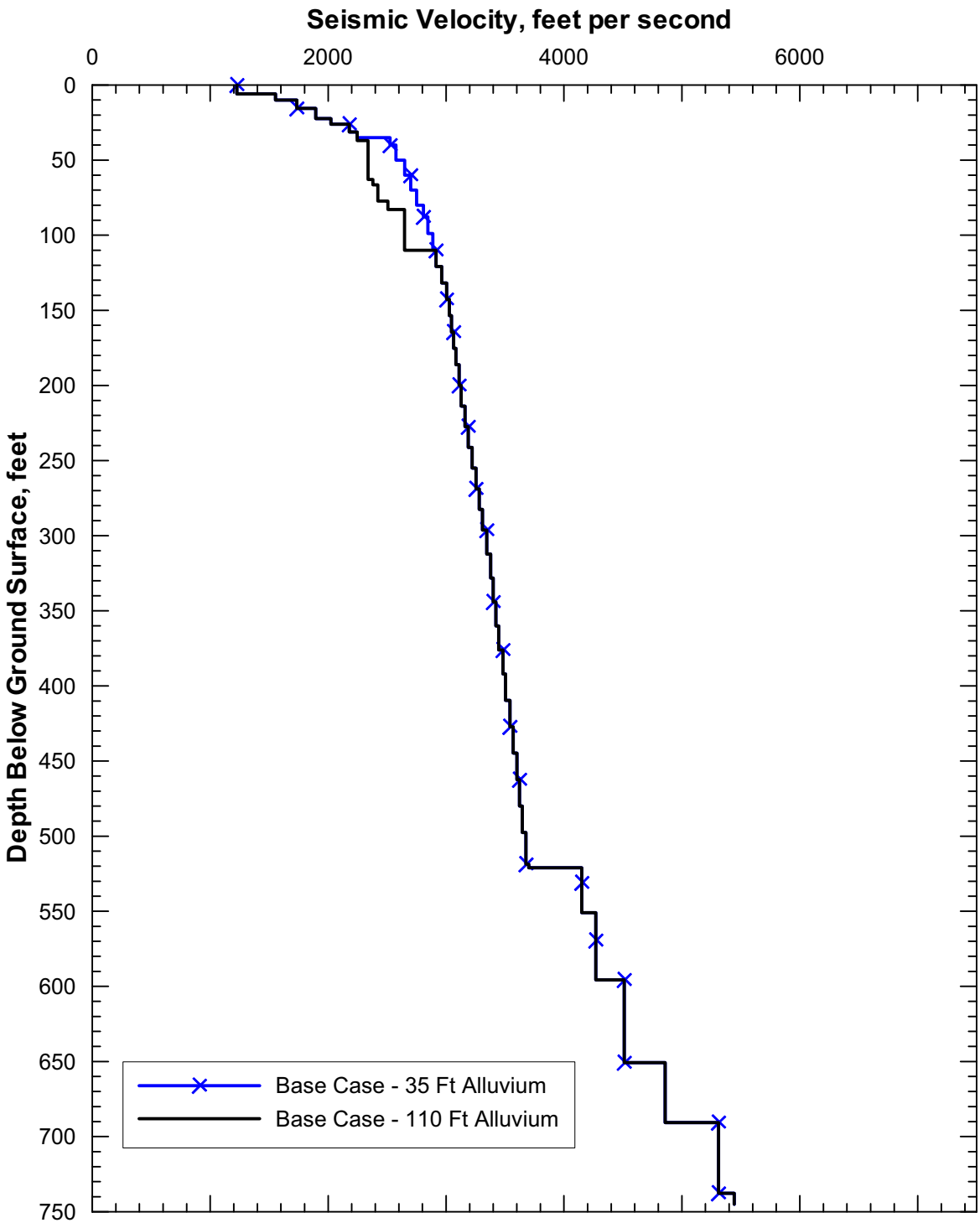

Source: Wong and Silva 2004b [DIRS 170444], page 115

Figure 6.3-177. Basecase V_S Profile for Alluvium and Tuff at Point F

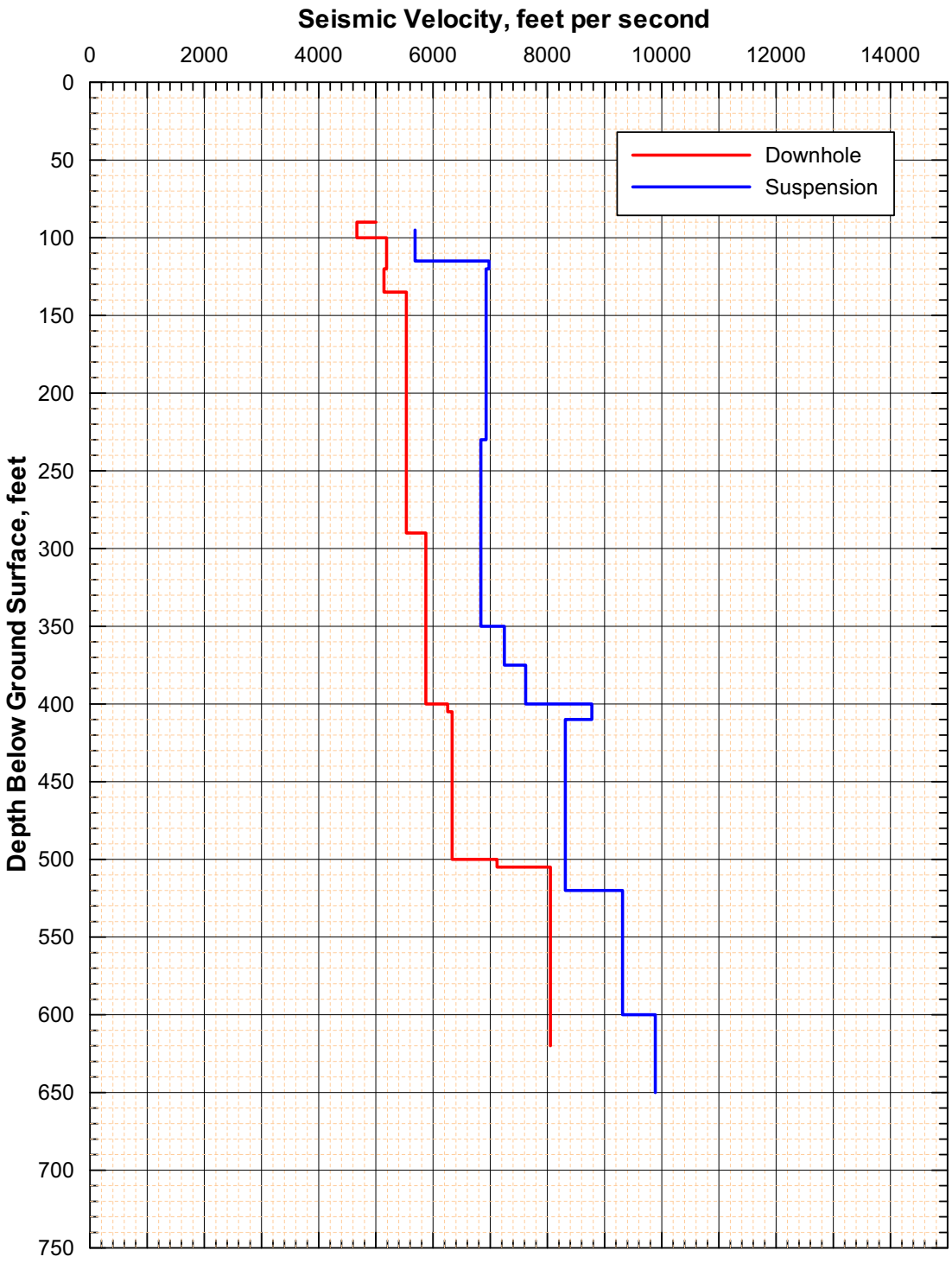

Source: Wong and Silva 2004b [DIRS 170444], page 105

Figure 6.3-178. Median V_P Profiles of the Tuff from the Downhole and Suspension Data at Point F

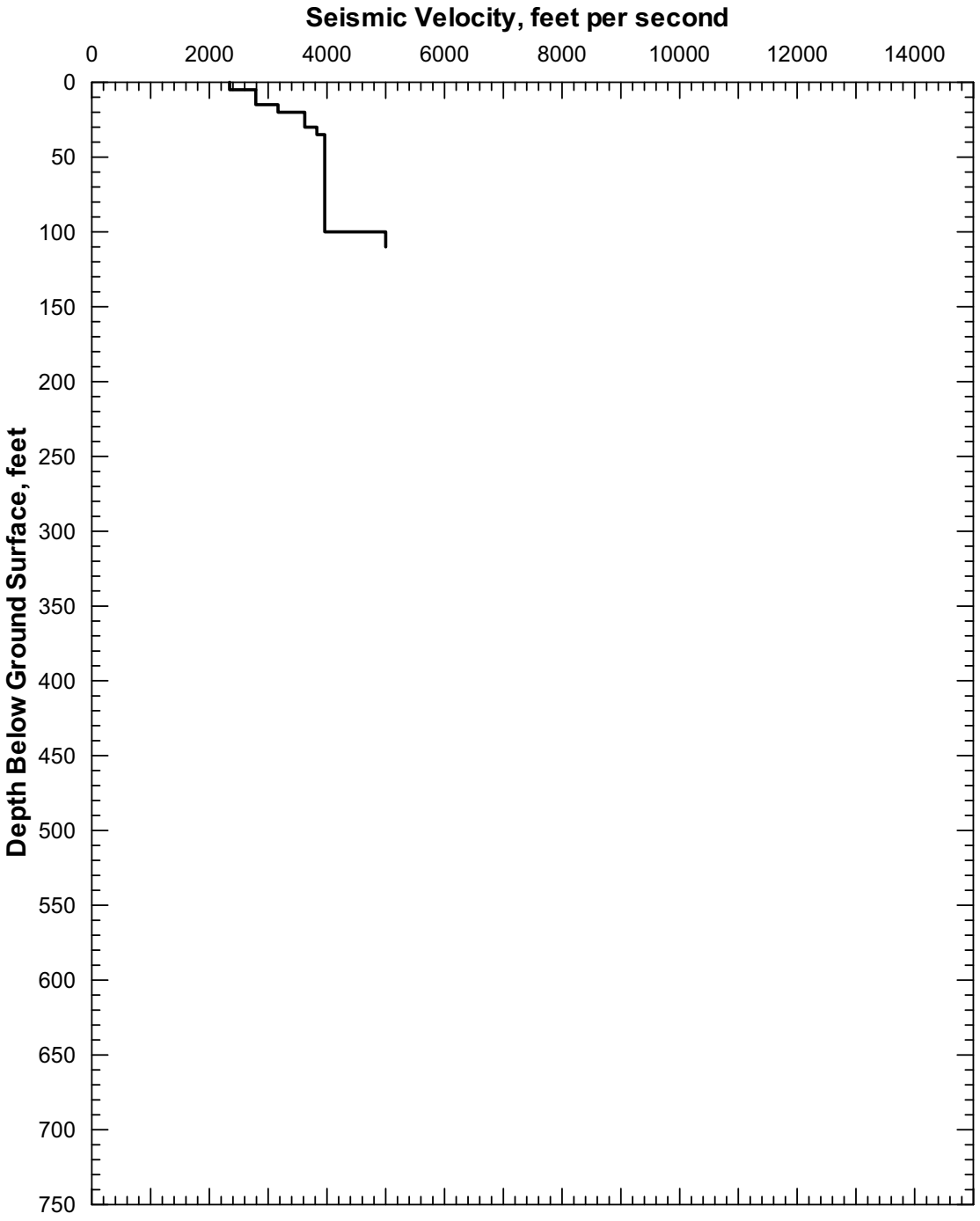

Source: Wong and Silva 2004b [DIRS 170444], page 108

Figure 6.3-179. Basecase V_P Profile for Alluvium at Point F

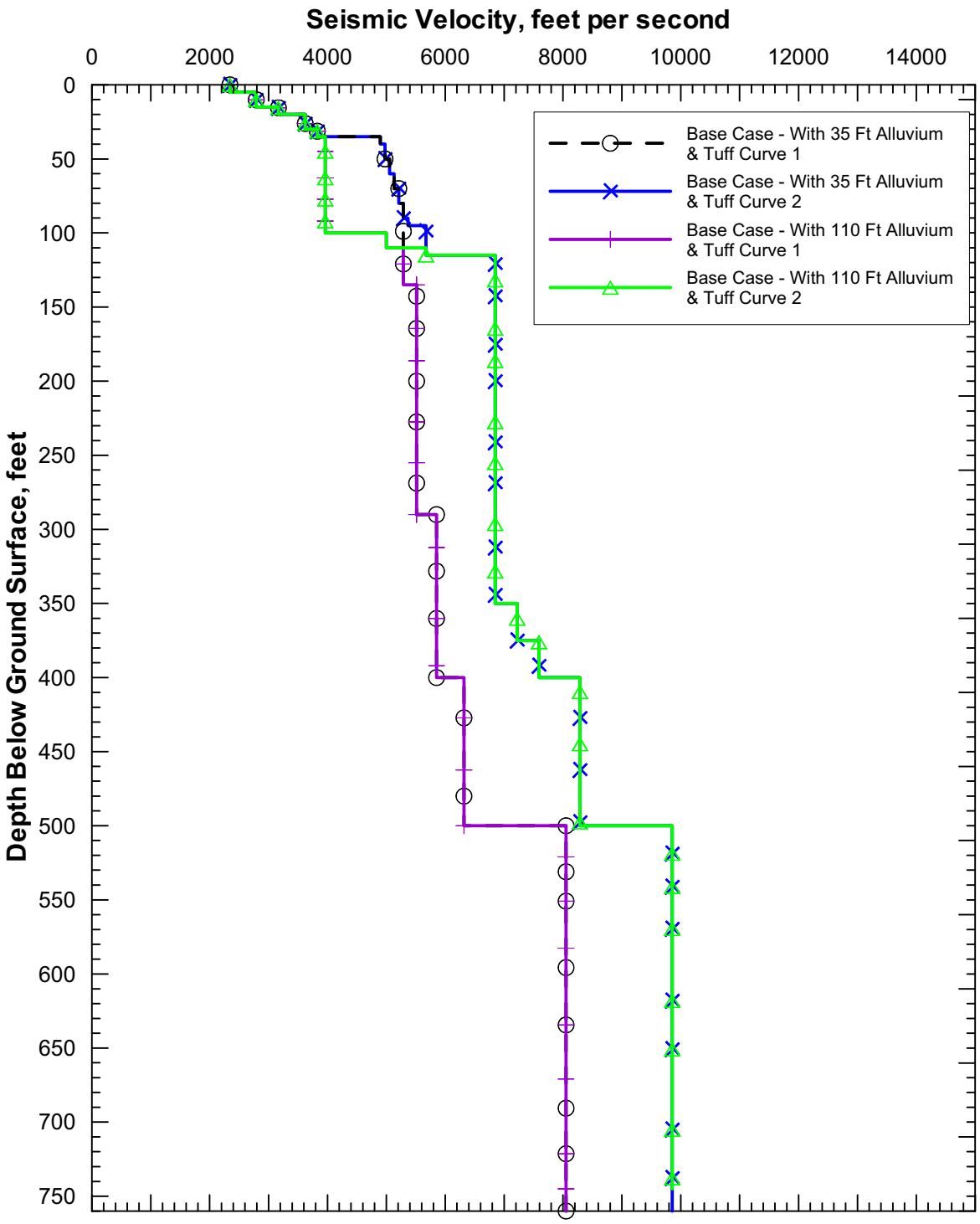

Source: Wong and Silva 2004a [DIRS 170443], SR 128, pages 3 and 4

Figure 6.3-180. Basecase V_P Profiles for Alluvium and Tuff at Point F

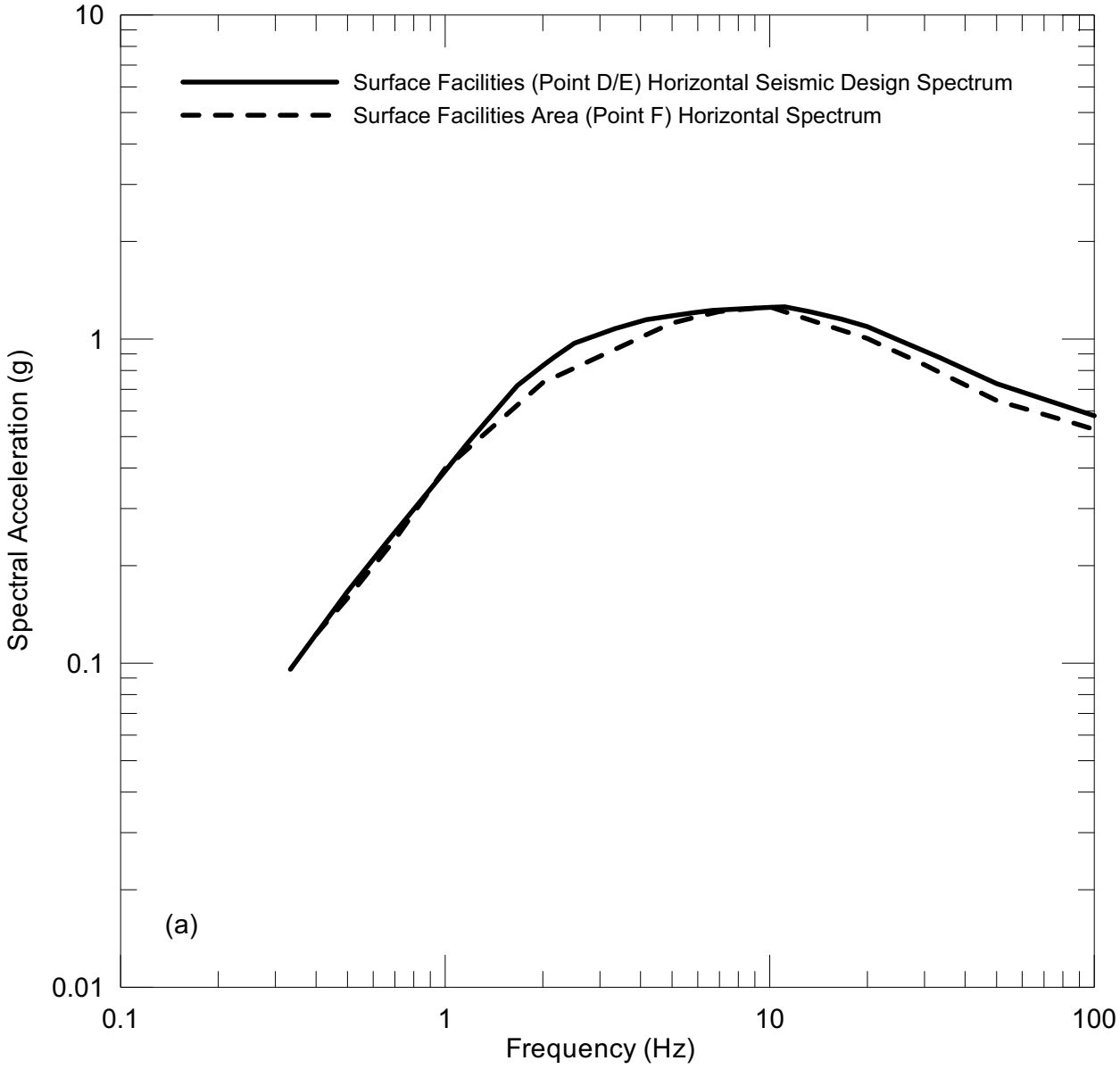

DTN: MO0410SDSEHFSF.002 [DIRS 172218], MO0410SDSTMHIS.005 [DIRS 172237]

Figure 6.3-181. Comparison of Points D/E and F Horizontal Response Spectra at 5×10^{-4}

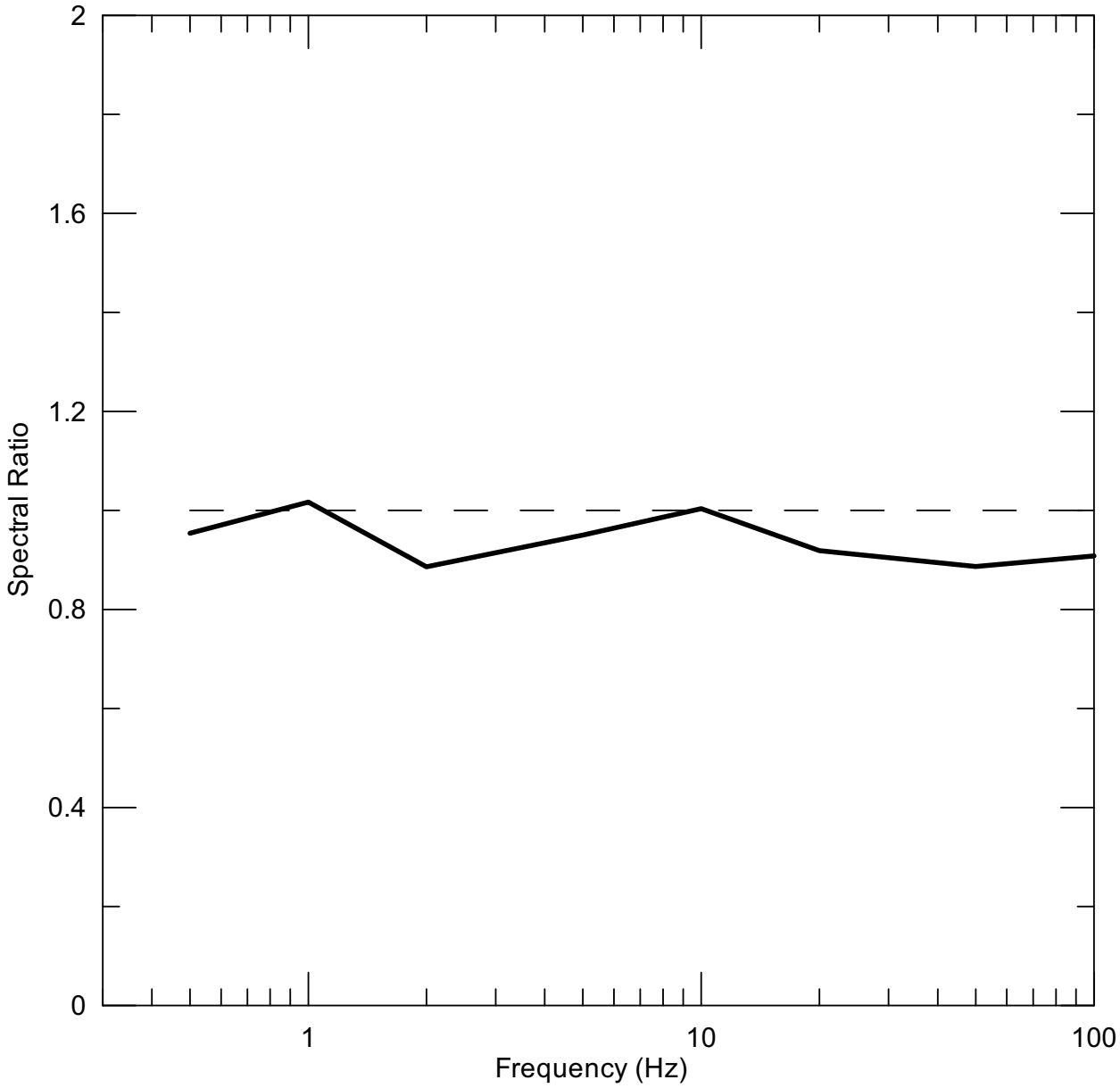

Source: Appendix I, Filename: Site F spectra comparison.xls

Figure 6.3-182. Ratio of Point F to Point D/E Horizontal Response Spectra at 5×10^{-4}

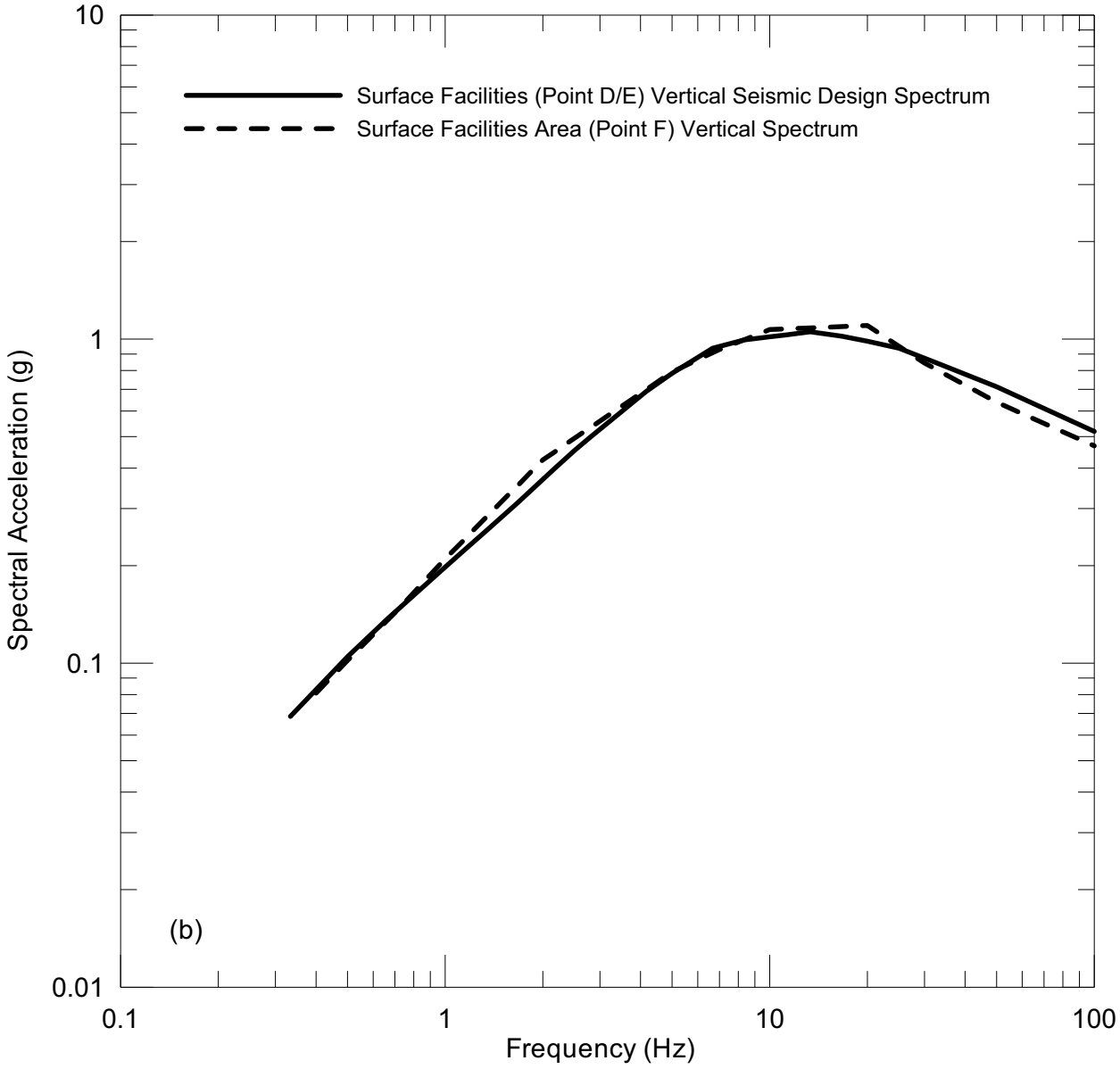

DTN: MO0410SDSEHFSF.002 [DIRS 172218], MO0410SDSTMHIS.005 [DIRS 172237]

Figure 6.3-183. Comparison of Points D/E and F Vertical Response Spectra at 5×10^{-4}

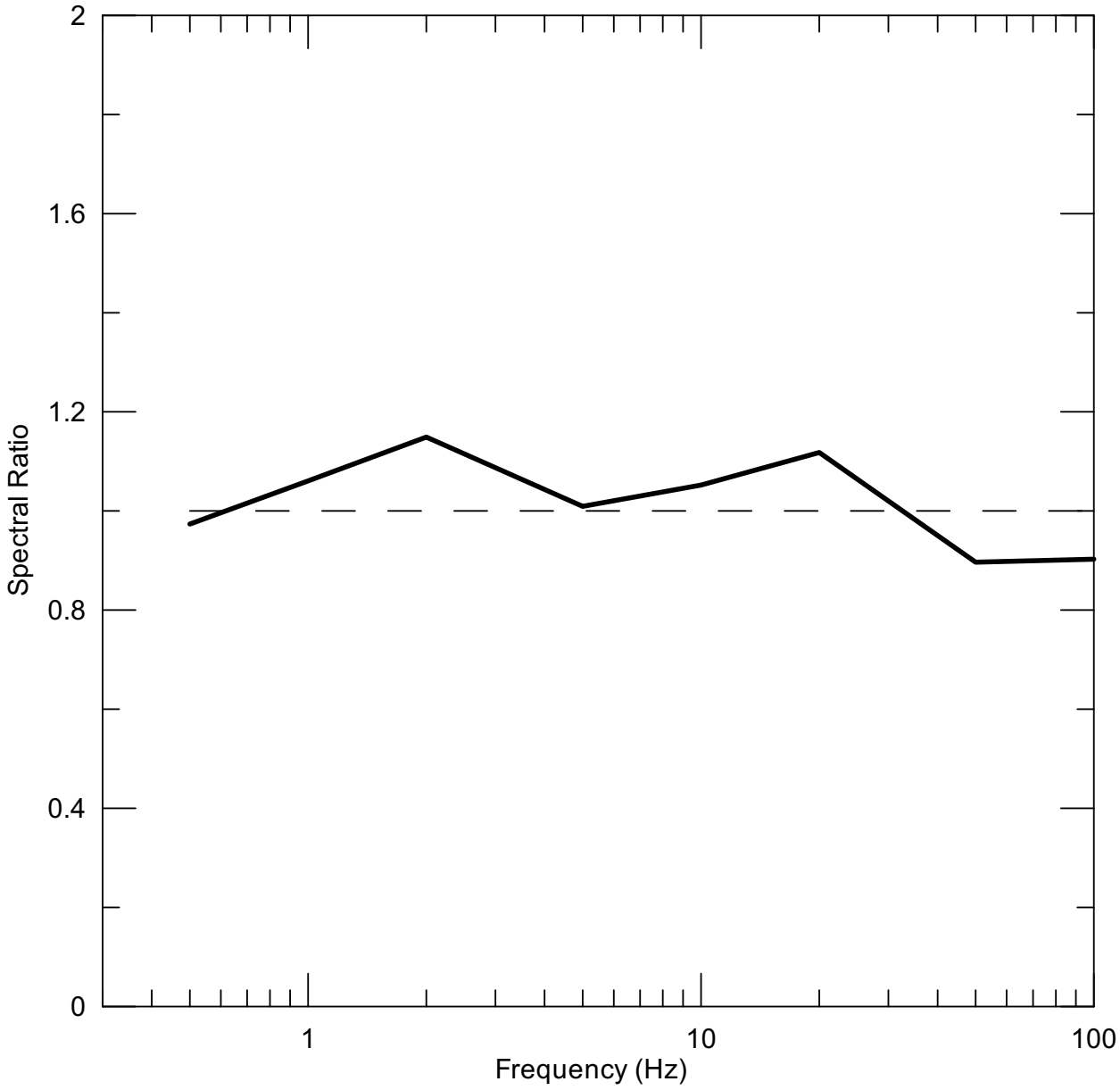

Source: Appendix I, Filename: Site F spectra comparison.xls

Figure 6.3-184. Ratio of Point F to Point D/E Vertical Response Spectra at 5×10^{-4}

6.4 FEATURES, EVENTS, AND PROCESSES INCLUDED IN THE SITE-RESPONSE MODEL

The development of a comprehensive list of features, events, and processes (FEPs) potentially relevant to postclosure performance of the planned Yucca Mountain repository is an ongoing, iterative process based on site-specific information, design, and regulations. Seismic ground motion related FEPs considered for TSPA are summarized in Table 6.4-1. The content of this report is relevant to these FEPs, which were extracted from the LA FEPs list (DTN: MO0407SEPFEPLA.000 [DIRS 170760]). Table 6.4-1 lists seismic ground motion related FEPs included in the seismic scenario class and identifies the section in this report providing information to address the FEP.

Table 6.4-1. Seismic Ground Motion Related FEPs Included in TSPA-LA

FEP No.	FEP Name	Report Section Providing Information to Address This FEP
1.2.03.02.0A	Seismic ground motion damages EBS components	6.3.1, 6.3.2
1.2.03.02.0D	Seismic-induced drift collapse damages alters in-drift thermohydrology	6.3.1, 6.3.2
1.2.03.03.0A	Seismicity associated with igneous activity	6.3.1, 6.3.2, 6.5

Source: BSC 2004e [DIRS 170017]. Information in columns 1 and 2 if from DTN: MO0407SEPFEPLA.000 [DIRS 170760]

The site-response ground motion model does not directly implement any of the included seismic ground motion related FEPs for TSPA-LA. Rather, for FEP 1.2.03.02.0A and 1.2.03.02.0D, the model results provide ground motion inputs for subsequent calculations and analyses (BSC 2004f [DIRS 167083]; BSC 2004g [DIRS 168385]; BSC 2004h [DIRS 166107]) that evaluate the effects of seismic ground motion on the engineered barrier system and the waste emplacement drifts during the postclosure period (BSC 2003b [DIRS 166296], Section 5.3.2, Figure F-10). The outputs of these subsequent calculations and analyses are then abstracted (BSC 2004m [DIRS 169183]) for incorporation into the seismic scenario of the TSPA-LA. This report also provides ground motion inputs for subsequent calculations and analyses that provide a basis for excluding FEPs 1.2.03.02.0B (seismic induced rockfall damages EBS components) and 1.2.03.02.0C (seismic induced drift collapse damages EBS components). The basis for exclusion is provided in BSC (2004m [169183], Section 6.9.2).

FEP 1.2.03.03.0A (Seismicity specifically associated with igneous activity) is also not explicitly incorporated into the site-specific ground motion model. However, it is implicitly incorporated because seismicity associated with igneous activity was considered in the PSHA (CRWMS M&O 1998a [DIRS 103731], Table 4-1; BSC 2004j [DIRS 168030], Table 5) that is used to develop inputs to the site-specific ground motion response model. As part of the seismic source characterization activity of the PSHA, the expert teams either considered seismicity associated with igneous activity within the context of areal source zones or explicitly identified volcanism related sources. Thus the seismic hazard computed for the Yucca Mountain site includes

contributions from seismicity related to igneous activity. Additional discussion is contained in BSC (2004e [DIRS 170017], Section 6.2.1.7).

Also with respect to FEP 1.2.03.03.0A, Section 6.5 of this report, describes ground motions from a maximum magnitude earthquake associated with basalt dike intrusion. Ground motions for the maximum magnitude event are treated deterministically, in contrast to the ground motions developed in the rest of this report on the basis of PSHA results.

6.5 GROUND MOTION FROM BASALT DIKE INTRUSIONS

In evaluating the potential for criticality events associated with an igneous intrusion at Yucca Mountain, it is necessary to assess the potential for drift collapse from intrusion-related earthquakes. Although seismicity related to igneous activity is included in the PSHA for Yucca Mountain, it is not addressed separately from other seismicity by all the PSHA seismic source characterization teams. That is, seismic inputs determined on the basis of the PSHA include hazard contributions from igneous intrusion-related events, but the specific ground motion related to the igneous intrusion-related earthquakes cannot be isolated. Thus, in this section, ground motion from deterministic scenario earthquakes is determined to address this need. The scenario earthquakes are selected based on the maximum magnitude of events potentially associated with igneous intrusions in the vicinity of Yucca Mountain. Results are presented in terms of acceleration response spectra.

The magnitude of earthquakes potentially associated with basalt dike intrusions near Yucca Mountain is addressed in *Characterize Eruptive Processes at Yucca Mountain, Nevada* (BSC 2004k [DIRS 169980], Section 6.3.1.3, Table 7-1; LA0407DK831811.001 [DIRS 170768]). In characterizing the maximum magnitude of dike-related earthquakes, a distribution was provided consisting of **M** 4.8, 5.8, and 6.2, weighted 0.18, 0.64, and 0.18, respectively. These magnitudes were based on dike lengths of 0.6, 4.0, and 10.1 km, which represent the 5th percentile, mean, and 95th percentile for dike length as assessed in the Probabilistic Volcanic Hazard Analysis for Yucca Mountain (BSC 2004l [DIRS 169989], Section 6.3.2). An empirical relation between tectonic rupture dimensions and earthquake magnitude (Wells and Coppersmith 1994 [DIRS 107201], Figure 9) was used. The estimated range of maximum magnitude for dike-related earthquakes is likely biased high because of the deformational processes associated with development of dike-related faults and fissures. Ruptures along dike-induced normal faults and fissures occur incrementally, as opposed to the sudden catastrophic release of strain along tectonic faults. The faults and fissures develop at shallow depths (less than 5 km) above the dike top limiting down-dip rupture widths (Smith et al. 1996 [DIRS 101020], p. 6,284), in contrast to typical tectonic faults that have rupture widths extending to midcrustal levels near the brittle-ductile transition.

In the PSHA, seismic source characterization expert teams considered igneous-related seismicity (BSC 2004j [DIRS 168030], Table 5). Two teams explicitly identified volcanic source zones. The RYA (Rogers, Yount, and Anderson) team assigned a maximum magnitude of **M** 5.5 to sites of existing basaltic cones. The SDO (Smith, dePolo, and O'Leary) team defined two volcanic source zones with maximum magnitudes of **M** 6.0 ± 0.2 (weighted 0.1), **M** 5.8 ± 0.4 (0.6), and **M** 5.5 ± 0.3 (0.3). The other source teams included igneous-related seismicity in their characterization of areal source zones. The maximum magnitudes assigned by the two source teams put greater weight on magnitudes from **M** 5.4 to 5.8. This range is consistent with the maximum magnitudes of **M** 4.8, **M** 5.8, and **M** 6.2 that are estimated for earthquakes associated with dike-intrusion at the Yucca Mountain Repository.

An analysis of the ground motion associated with the range of maximum magnitude earthquakes assessed for basalt dike intrusions in the Yucca Mountain vicinity is described in this section. Inputs consist of the distribution of maximum magnitudes from LA0407DK831811.001 [DIRS 170768], and the ground motion attenuation relations developed as part of the PSHA for Yucca

Mountain (BSC 2004j [DIRS 168030], Section 6.3.3.2; CRWMS M&O 1998a [DIRS 103731], Section 6, DTN MO0401MWDRPSHA.000 [DIRS 166962]). Calculations were carried out using the software program DESIGN_EVENTS V1.0 (STN 10362-1.0-00 [DIRS 163302]) and are documented in Toro (2004 [DIRS 172034], p. 71-73, Supplemental Records 62-64). Ground motions were calculated for distances of 0.5 and 1.0 km and for median ground motion and median plus 1 standard deviation ground motion.

Acceleration response spectra for the maximum igneous-related earthquakes are shown in Figures 6.5-1 through 6.5-4. Horizontal PGA ranges from about 0.14g for the **M** 4.8 earthquake to 0.39 g for the **M** 6.2 earthquake for the case using the attenuation relations for median ground motion. For the case using 84th percentile ground motions, the PGA ranges from 0.28 g to 0.70 g. The results are not sensitive to the choice of 0.5 km or 1.0 km for the distance. Results are summarized in Table 6.5-1 for the case in which distance equals 0.5 km. These response spectra represent ground motion at the PSHA reference rock outcrop (Point A). Based on site-response modeling presented in Section 6.3, these ground motions are slightly larger than the ground motions estimated for the waste emplacement level.

Table 6.5-1. Spectral Acceleration as a Function of Frequency for Basalt Dike-Related Earthquakes at a Distance of 0.5 km

Frequency (Hz)	Spectral Acceleration (g)					
	M 4.8		M 5.8		M 6.2	
	Median	84th Percentile	Median	84th Percentile	Median	84th Percentile
	Horizontal Ground Motion					
0.3	0.005	0.01	0.03	0.06	0.05	0.11
0.5	0.01	0.04	0.06	0.14	0.10	0.23
1	0.05	0.10	0.15	0.34	0.24	0.52
2	0.12	0.26	0.32	0.67	0.47	0.96
5	0.23	0.49	0.51	1.00	0.69	1.34
10	0.29	0.60	0.58	1.12	0.77	1.44
20	0.26	0.53	0.51	0.95	0.67	1.22
100	0.14	0.28	0.29	0.54	0.39	0.70
	Vertical Ground Motions					
0.3	0.003	0.01	0.02	0.04	0.04	0.08
0.5	0.01	0.02	0.04	0.08	0.06	0.13
1	0.02	0.04	0.08	0.16	0.12	0.25
2	0.05	0.11	0.15	0.31	0.24	0.47
5	0.12	0.25	0.29	0.57	0.41	0.80
10	0.20	0.42	0.44	0.88	0.61	1.19
20	0.20	0.41	0.43	0.84	0.58	1.13
100	0.09	0.19	0.21	0.40	0.28	0.54

Source: Toro 2004b [DIRS 170034], p. 73

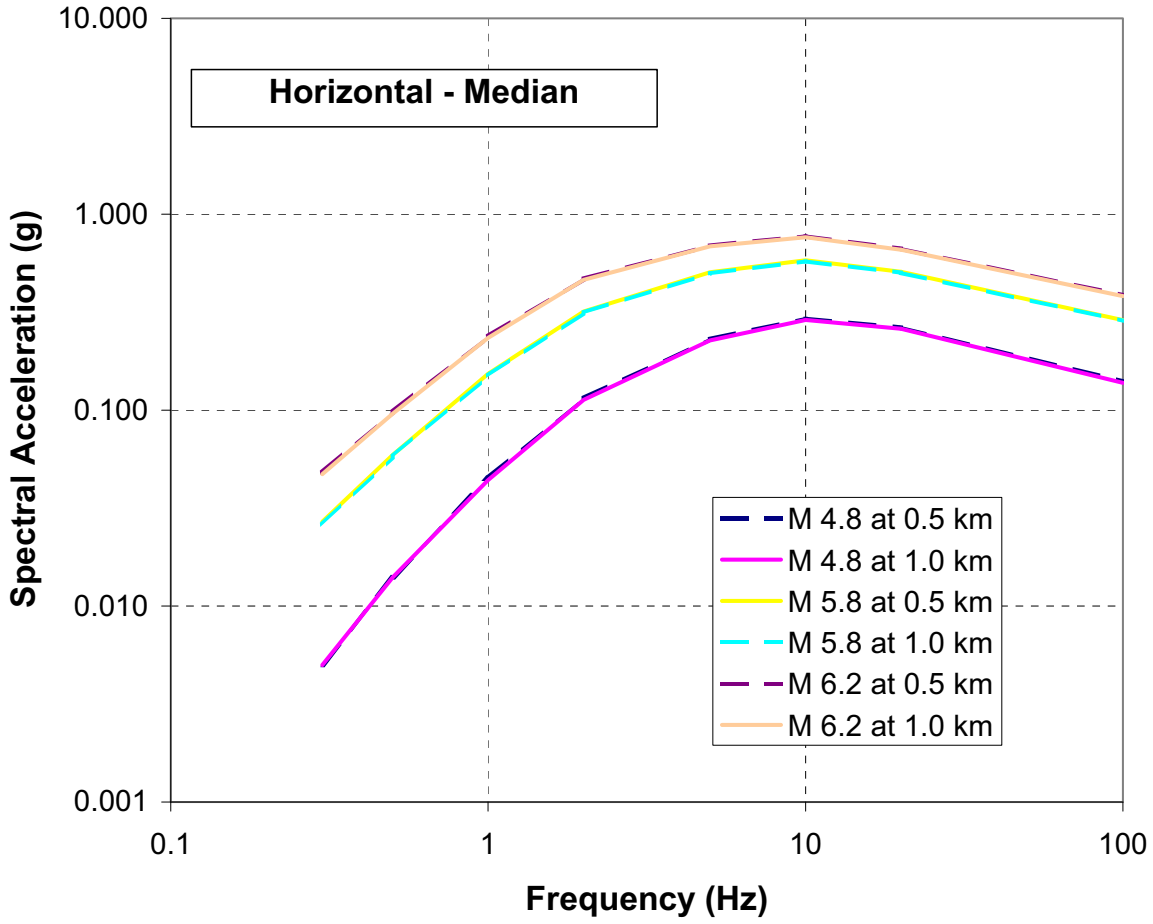

Source: Toro 2004 [DIRS 172034], Supplemental Record 64

Figure 6.5-1. Acceleration Response Spectra for Maximum Magnitude Basalt-dike-related Earthquakes: Horizontal Ground Motion, Median Attenuation Relation

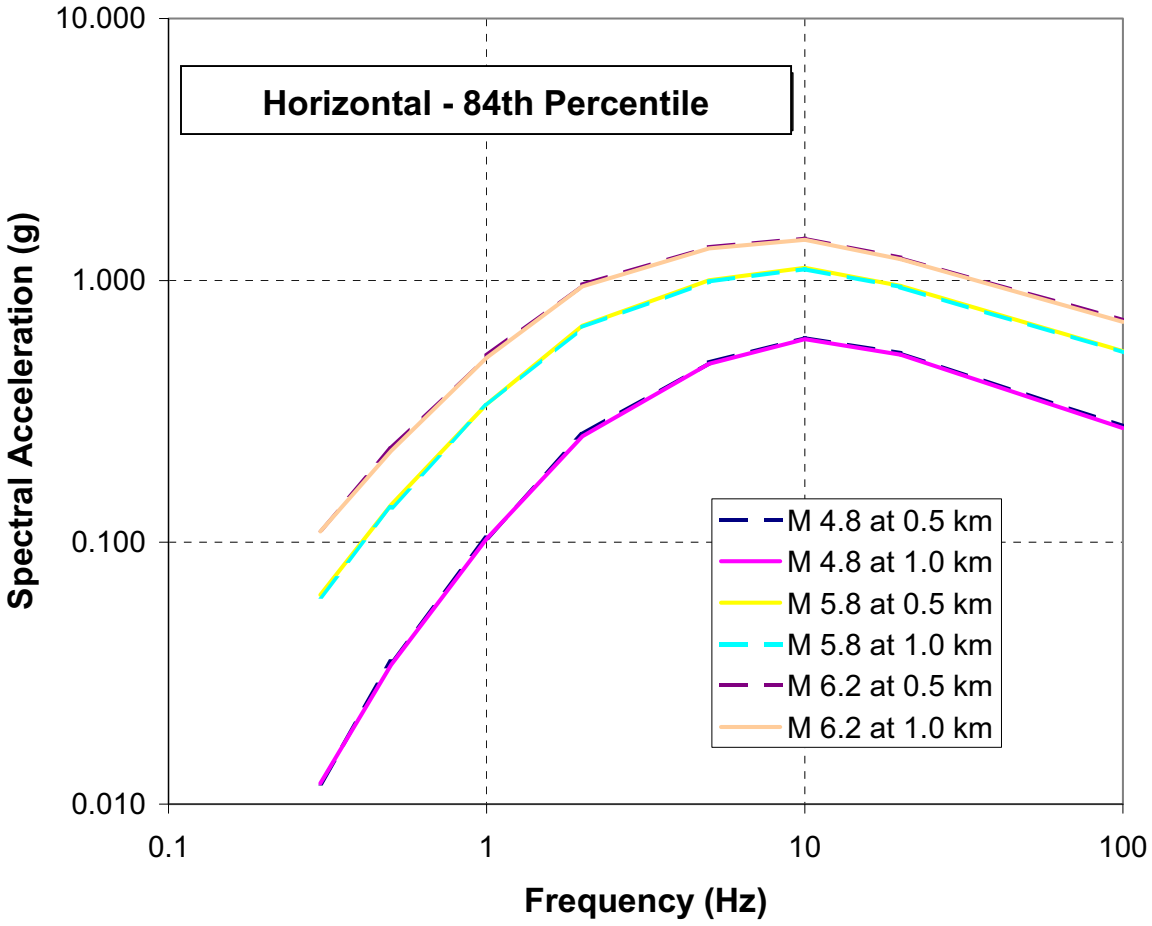

Source: Toro 2004 [DIRS 172034], Supplemental Record 64

Figure 6.5-2. Response Spectra for Maximum Magnitude Basalt-dike-related Earthquakes: Horizontal Ground Motion, 84th Percentile Attenuation Relation.

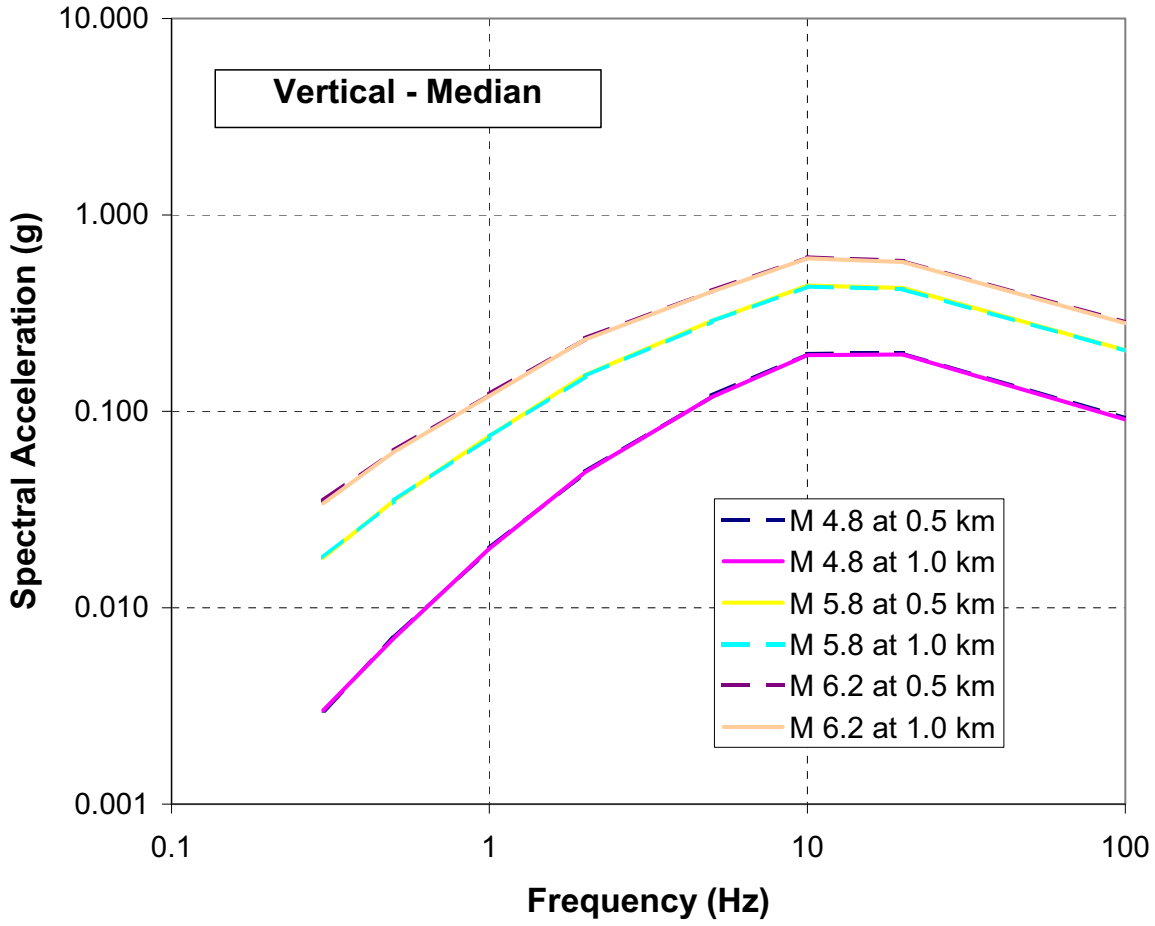

Source: Toro 2004 [DIRS 172034], Supplemental Record 64

Figure 6.5-3. Acceleration Response Spectra for Maximum Magnitude Basalt-dike-related Earthquakes: Vertical Ground Motion, Median Attenuation Relation.

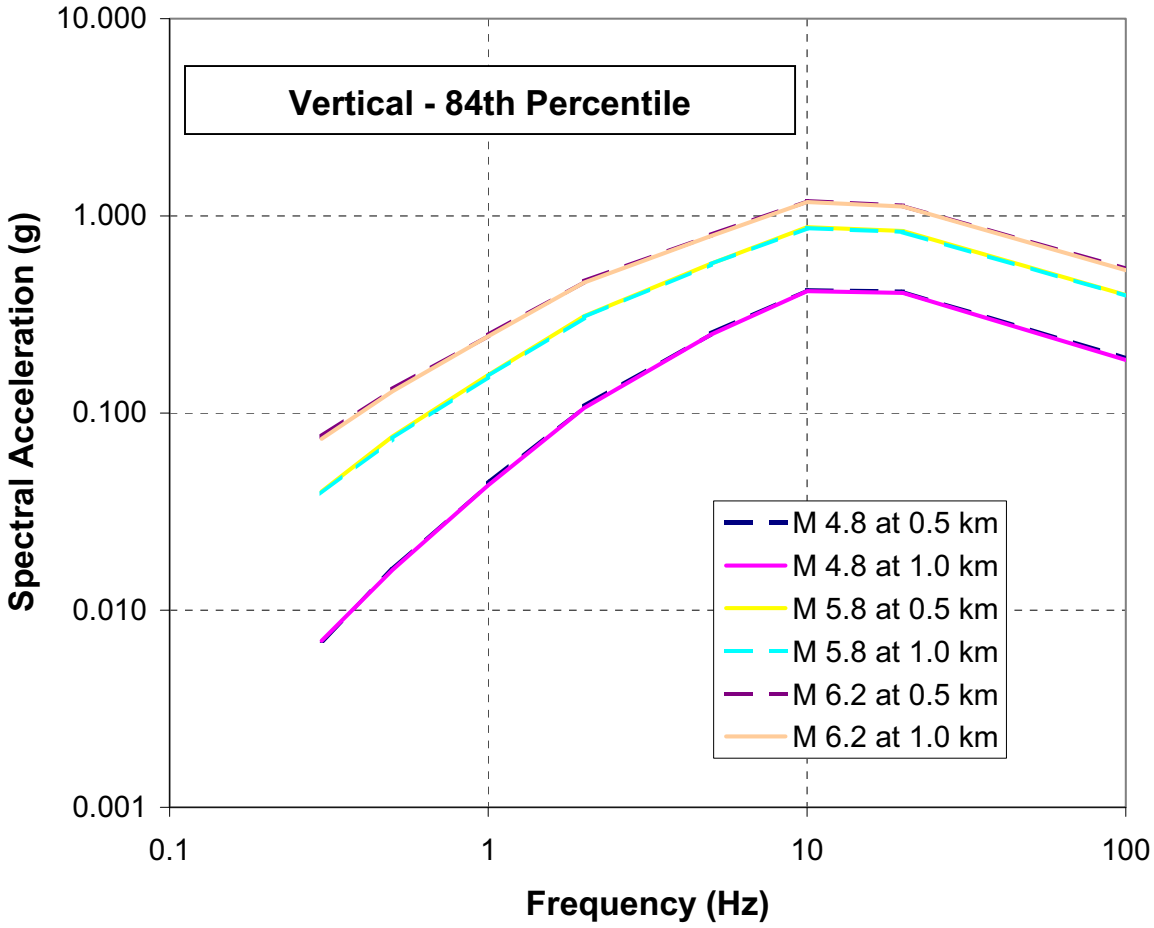

Source: Toro 2004 [DIRS 172034], Supplemental Record 64

Figure 6.5-4. Response Spectra for Maximum Magnitude Basalt-dike-related Earthquakes: Vertical Ground Motion, 84th Percentile Attenuation Relation.

7. MODEL VALIDATION

Model validation is the process used to establish confidence that a mathematical model and its underlying conceptual model adequately represent with sufficient accuracy the system, process, or phenomenon in question (AP-SIII.10Q, Section 3.14). AP-SIII.10Q, *Models*, identifies a number of methods for validating models that range from simple documentation to peer review. Model validation includes activities during model development to build confidence in the model and post-development model validation.

The TWP specifies that the RVT-based equivalent-linear site-response model requires a high level of confidence (Level III) and it identifies validation activities to provide that level (BSC 2004a [DIRS 171850], Section 2.1.4). The validation of the model was described in Rev 00 of this report (BSC 2003d [DIRS 166274]). This version, Rev 01 documents studies that increase the confidence in the model validation at high shear strains (Sections 7.2.5 and 7.3.5).

Confidence Building During Model Development to Establish Scientific Basis and Accuracy for Intended Use

The development of the model should be documented in accordance with the requirements of Section 5.3.2(b) of AP-SIII.10Q. The development of the site-response ground motion model was conducted according to these criteria , as follows:

1. *Selection of input parameters and/or input data, and a discussion of how the selection process builds confidence in the model. [AP-SIII.10 Q 5.3.2(b) (1) and AP-2.27Q Attachment 3 Level I (a)]*[1]

   Inputs to the site-response ground motion model consist of control motion response spectra (UHS), small strain velocities, densities, nonlinear dynamic material properties, and angles of incidence of the control motions. The inputs to the site-response ground motion model have been derived from the sources described in Section 4. Table 4-1 lists the Qualified data used in this report and their sources. Section 4.1.2 and Table 4-2 provides a discussion and justification for the appropriateness of additional data used in developing inputs for the model. Additional discussion of the model inputs can be found in Section 6.2. Thus, this requirement can be considered satisfied.

2. *Description of calibration activities, and/or initial boundary condition runs, and/or run convergences, simulation conditions set up to span the range of intended use and avoid inconsistent outputs, and a discussion of how the activity or activities build confidence in the model. Inclusion of a discussion of impacts of any non-convergence runs. [(AP-SIII.10Q 5.3.2(b)(2) and AP-2.27Q Attachment 3 Level I (e)].*

   Initial and boundary conditions for the site-response ground motion model can be found in Section 6.1.7. Section 6.3 provides detailed discussion of various model results (i.e., those of convergence runs). Simulation conditions span the range of intended use include 17 three-component sets of time histories for annual exceedance frequencies of

[1] Criteria listed here refer to Level I validation, but are also inclusive for Level II and Level III validation. Level III validation was carried out for the RVT-based equivalent-linear site-response model.

10^{-5}, 10^{-6}, and 10^{-7} in support of TSPA. Thus, this requirement can also be considered satisfied.

3. *Discussion of the impacts of uncertainties to the model results including how the model results represent the range of possible outcomes consistent with important uncertainties. [(AP-SIII.10 Q 5.3.2(b)(3) and AP-2.27Q Attachment 3 Level 1 (d) and (f)].*

   Discussion of model uncertainties and limitations is provided in Section 6.3.3. Uncertainties in the ground motions developed in Section 6.3 have been formally accommodated in the PSHA for the Point A control motions through the corresponding UHS, REs, and DEAs. Uncertainties associated with propagating the motions from Point A to other locations through site response analyses have followed an approach developed to maintain the Point A hazard level (McGuire et al. 2001 [DIRS 157510], Approach 2B) as well as accommodate variability in dynamic material properties throughout the site.

4. *Formulation of defensible assumptions and simplifications. [AP-2.27Q Attachment 3 Level I (b)].*

   Discussion of assumptions and simplifications are provided in Section 6.1.6.

5. *Consistency with physical principles, such as conservation of mass, energy, and momentum. [AP-2.27Q Attachment 3 Level I (c)]*

   Consistency with physical principles is demonstrated by the conceptual and mathematical formulation in Section 6.1.8.

Confidence Building after Model Development to Support the Scientific Bases of the Model

For the RVT equivalent-linear site-response model, the TWP (BSC 2004a [DIRS 171850], Section 2.1.4) identifies three methods to achieve the desired high level of confidence in the model validation (Level III):

1. Corroboration of model results with data acquired from the laboratory, field experiments, analog studies, or other relevant observations, not previously used to develop or calibrate the model.

2. Corroboration of results with alternative mathematical models.

3. Technical review by individuals independent of the development, checking, and interdisciplinary review of the model documentation.

This section describes the results of previous studies that provide the needed level of confidence in the validity of the RVT equivalent-linear site-response model. Sections 7.1 to 7.3 describe the results of various studies that implement methods 1 and 2. Some of these studies validate the full RVT equivalent-linear site-response modeling approach, while others address a component of it. Also, for some studies, validation pertaining to the site-response modeling approach forms a subset of the overall model validation work being cited. In these instances, the discussion in this

section focuses on the component of the work that deals with the RVT equivalent-linear site-response modeling approach. Section 7.4 discusses the applicability of the site-response model validation to Yucca Mountain. In addition, Section 7.5 describes the results of an independent technical review (method 3) that specifically addresses the site-response model for Yucca Mountain. Section 7.6 describes the conclusions.

7.1 VALIDATION STUDIES

The effects of a soil column upon strong ground motion have been well documented and studied analytically for many years. Wood (1908 [DIRS 163672], pages 220-245) and Reid (1910 [DIRS 163650], pages 49-56), using apparent intensity of shaking and distribution of damage from the 1906 San Francisco earthquake, gave evidence that the severity of shaking can be substantially affected by the local geology and soil conditions. More recently, Wiggins (1964 [DIRS 163671]), Idriss and Seed (1968 [DIRS 163520]), Seed and Idriss (1969 [DIRS 163655]), Borcherdt and Gibbs (1976 [DIRS 163177]), Joyner et al. (1976 [DIRS 163522]), Chin and Aki (1991 [DIRS 163451]), Darragh and Shakal (1991 [DIRS 163493]), Schneider et al. (1993 [DIRS 110467]), and Su et al. (1992 [DIRS 163182]) have shown that during small and large earthquakes, the surface soil motion can differ in significant and predictable ways from that on adjacent rock outcrops. Other investigators have utilized explosion data either independently or in conjunction with earthquake data to examine site response characteristics (Murphy et al. 1971 [DIRS 163608], Hays et al. 1979 [DIRS 163515], Rogers et al. 1984 [DIRS 163652]). Work using horizontal as well as vertical arrays of instruments have demonstrated the general consistency of the site response for seismic events of different size, distance, and azimuth (Tucker and King 1984 [DIRS 163181], Benites et al. 1985 [DIRS 163172], Hutchings and Wu 1990 [DIRS 163516], Chin and Aki 1991 [DIRS 163451], Borcherdt and Glassmoyer 1992 [DIRS 163342], Field et al. 1992 [DIRS 163505], Su et al. 1992 [DIRS 163182], Pitarka et al. 1994 [DIRS 163610], Satoh et al. 1995 [DIRS 163654], Elgamal et al. 1996 [DIRS 163503], Ganev et al. 1998 [DIRS 163508], Kokusho and Matsumoto 1997 [DIRS 164079], Dimitriu et al. 1998 [DIRS 163496], Silva et al. 1999 [DIRS 164081]). Results of these and other studies have demonstrated, in a general sense, the adequacy of assuming plane-wave propagation in modeling 1D site response.

In addition to the wave propagation approach used in site response analyses, dynamic material properties such as shear modulus and material damping control the amplitude and frequency content of computed motions. It is well known from laboratory testing that soils and soft rocks exhibit pronounced nonlinear behavior under large applied shear loading conditions. Shear modulus decreases with increasing strain with an accompanying increase in material damping (Seed and Idriss 1970 [DIRS 103324], Hardin and Drnevich 1972a [DIRS 157246], Seed et al. 1986 [DIRS 157263]). Accordingly, soil and soft rock site response calculations must accommodate these strain dependencies as nonlinear constitutive relations. In general, two approaches are used to model strain-dependent soil response: nonlinear and equivalent-linear. Since the early 1970's, reports of strong ground motion modeling in soils has been dominated by the application of the equivalent-linear approach.

In the following subsections, five validation studies based on validation methods (1) and (2) stated above, are described. These studies validate either the RVT equivalent-linear site-response modeling approach or its components:

1. Comparison of response spectra computed using time domain and RVT approaches. This validation is only of the RVT component of the site response model (Section 7.1.1)

2. Comparison of the predictions of recorded ground motions using the RVT equivalent-linear and four established equivalent-linear and nonlinear approaches (Section 7.1.2).

3. Validation of linear site response modeling to predict vertical ground motions (Section 7.1.3).

4. Comparison of predictions from a combined RVT point-source/RVT equivalent-linear site-response model with recorded earthquake data from 16 earthquakes recorded at more than 500 sites (Section 7.1.4). While the performance of the source and site-response components of the combined model are not evaluated separately, the general success of the combined model adds confidence that the site-response model is valid.

5. Comparison of the predictions of recorded ground motions using the equivalent-linear and nonlinear approaches is made for a site that experienced especially large shear-strains (Section 7.1.5).

In addition to the discussion of previous studies, an evaluation of the site-specific applicability of the site response model to Yucca Mountain is also provided. The acceptance criteria are presented in Section 7.2 and the results of each validation study are discussed in Section 7.3.

7.1.1 Comparison of Time Domain and RVT-Based Response Spectra

One aspect of the equivalent-linear site-response model is the use of RVT to determine peak time domain values of shear strain based on the shear strain power spectrum (Section 6.1.8.4). The work of Boore (1983 [DIRS 103317], 2003 [DIRS 163706]) demonstrates the validity of the RVT method to predict peak ground motion and response spectral values. In these studies, response spectral values derived from time domain simulations are compared to values obtained using RVT. Note that while these studies validate the RVT component of the site-response modeling approach, they do not address the equivalent-linear component.

7.1.2 Equivalent-Linear and Nonlinear Modeling Approaches for Site Response

The essence of ground motion modeling validation is the demonstration of the model's ability to predict recorded ground motions, particularly response spectra (EPRI 1993a [DIRS 103319], Section 3). Three fundamental issues in site response analyses are the adequacy of using vertically propagating S-wave and inclined P-SV plane waves to adequately characterize the ground motions at the ground surface, the determination of *in situ* dynamic soil properties, and the suitability of the approximate equivalent-linear method compared to fully nonlinear schemes.

EPRI (1993b [DIRS 103320], Appendix 6B) documents a systematic study to validate and compare 1D site-response methodologies. The RVT equivalent-linear site-response modeling approach, as implemented in a version of the software code RASCALS, was compared to nonlinear modeling approaches with respect to their ability to model recorded data. The validation study consisted of modeling ground motion response spectra for three soil sites, representing a range of soil conditions, that were reasonably well characterized geotechnically and for which control motions could be specified based on nearby rock site recordings or at-depth recordings from a vertical array. The study was structured to examine the predictive ability of the different modeling approaches. Iterative parameter adjustment to achieve improved fits to the data was minimized. For the nonlinear approaches, a single opportunity to revise input parameters was provided, such that any significant errors in assigning values could be corrected. No parameter adjustments were made for the RVT equivalent-linear approach.

Note that an accurate one-to-one comparison between the equivalent-linear site response program SHAKE and RASCALS is difficult to perform because RASCALS uses RVT to calculate response spectral acceleration, while SHAKE computes response spectra from an input time history. Section 7.3.5 contains a direct comparison of predictions of response spectra of the Port Island vertical array data of the 1995 Kobe earthquake.

7.1.3 Comparison of Vertical-Component Site Response Modeling Approach to Observed Data

As discussed in Section 6.1.11, vertical-component ground motions are computed using linear site-response analysis. The analysis is carried out for inclined P-SV waves using low-strain velocity profiles. Validation of this component of the overall modeling approach is addressed in EPRI (1993a [DIRS 103319], Sections 6.6.2.1 and 6.6.2.2) and in Silva (1997 [DIRS 163747]) through comparison with observed data. Both of these studies validate using a linear analysis for vertical component site response in the context of a combined RVT point-source/RVT site-response model. The EPRI (1993a [DIRS 103319], Sections 6.6.2.1 and 6.6.2.2) work compares model results to recordings at 24 sites from the 1989 Loma Prieta earthquake. The Silva (1997 [DIRS 163747]) work takes a complementary approach and compares modeled vertical-to-horizontal (V/H) response spectral ratios to those determined from empirical ground motion attenuation relations for the western U.S. Together these studies provide the needed level of confidence in the modeling approach for vertical-component site-response.

7.1.4 Comparison of Combined Source, Path and Site Response Modeling to Observed Data

Silva et al. (1996 [DIRS 110474], Section 5) document an extensive validation study that included use of the RVT equivalent-linear site-response model. In contrast to the EPRI (1993b [DIRS 103320], Appendix 6.B) study, which validated the RVT equivalent-linear site-response modeling approach for three well-characterized sites for which control motions could be taken from a nearby rock site or vertical array recordings, Silva et al. (1996 [DIRS 110474]) compares modeling results at hundreds of sites, using more generic site property information and control motions determined from a stochastic point-source or finite-source earthquake model. The RVT equivalent-linear site-response approach is used to model nonlinear effects at sites classified as either soft-rock or deep soil. Modeling results are compared to response spectra for recorded

ground motion data. The validation and comparisons are presented entirely in terms of 5%-damped pseudo-absolute response spectra. This representation of strong ground motion is the most appropriate, currently acceptable, and least ambiguous approach to defining seismic hazard through design ground motions.

7.1.5 Ground Motion Site Response Model Confirmation Studies for Port Island, Japan

A study similar to the one described in Section 7.1.2 was undertaken to compare the predictions of various approaches of 1-D site response analyses to recorded motions. The RVT equivalent-linear site response model was tested against observed data from the Kobe-Port Island strong motion recording site that experienced high shear strains (about 1%) in the upper 30 to 70 ft (9 to 21 m) of soil. In addition, another widely used equivalent-linear site response model, SHAKE (Schnabel et al. 1972 [DIRS 103323]) and two nonlinear models, TESS (Pyke [n.d.] [DIRS 163613]) and SUMDES (Li et al. 1992 [DIRS 163527]) were used in this study.

7.2 ACCEPTANCE CRITERIA

As described in the TWP (BSC 2004a [DIRS 171850], Section 2.1.4), the general criteria for acceptable model validation are that the validation demonstrates the model produces realistic ground motions for given inputs and reasonable agreement with observed ground motions. These criteria are necessarily qualitative in nature. Whether they are met requires the professional judgment of ground motion experts. Approval of this report signifies that these criteria have been met in the view of the report originators, the technical checker, a representative of the Chief Science Office (in Rev 00 of BSC 2003d, [DIRS 166274]) and independent technical reviewers who evaluated the adequacy of model validation, and the responsible manager.

7.2.1 Comparison of Time Domain and RVT Response Spectra

Although the use of random vibration theory to estimate peak time domain parameters has a long history in seismic related structural analyses (Clough and Penzien 1975 [DIRS 164683], pages 436-476), accuracy tolerances have not been documented. In evaluating the comparison of time domain and RVT generated response spectra, reasonable agreement is interpreted to be as accurate as typical estimates of strong ground motions used for engineering design. The preferred, and generally considered most accurate, approach to characterizing strong ground motions, is through empirical predictions using multiple empirical attenuation relations. The accuracy inherent in developing design ground motions (5%-damped spectral acceleration) may be assessed based on the variation in predicted median motions among typically-used empirical attenuation relations. For frequencies of interest (about 0.5 Hz to 50 Hz) and for magnitude and distance ranges of **M** 5.0 to 7.5 and 1 to 100 km (1 to 33 mi), respectively, variation in predicted median motions is about 50 percent for WUS crustal earthquakes (Abrahamson and Shedlock 1997 [DIRS 164486]). Thus, the variation in predicted motions about a mean is approximately ± 25 percent. This “variability” is interpreted as an estimate of expected accuracy in characterizing strong ground motions and is taken as a basis for judging reasonable agreement between time domain and RVT generated response spectra.

7.2.2 Comparison of Equivalent-Linear and Nonlinear Modeling Approaches with Site Response Data

Evaluations of reasonable agreement for the comparison between the RVT equivalent-linear and nonlinear modeling approaches focuses first on how the results of the different modeling approaches compare and second on how they match the observed data. The rationale behind this hierarchy is that, even if the material property or control motions used as model inputs are inaccurate, the different approaches should produce similar results, although they may all systematically differ from the observations.

7.2.3 Linear Vertical Component Response

In evaluating linear site response for vertical component motions, reasonable agreement (BSC 2004a [DIRS 171850], Section 2.1.4) is judged by comparing model results and observed data. Both response spectra and the variability and bias of the combined RVT point-source/linear site-response model are examined. In addition, modeled vertical-to-horizontal (V/H) response spectral ratios are compared to those derived from empirical ground motion attenuation relations.

7.2.4 Combined Source Path and Site Response Validation

Evaluation of reasonable agreement for the combined RVT point-source/RVT equivalent-linear site-response model is judged by comparing modeled and observed response spectra and assessing overall model bias and variability. These factors are examined for four earthquakes that produced nonlinear response at some sites. In addition, results of a linear analysis are considered for the 1992 Little Skull Mountain earthquake because of its proximity to Yucca Mountain. Overall model performance is also judged in terms of model bias and variability for the five individual earthquakes discussed in detail and for the complete data set of 16 earthquakes recorded at over 500 sites.

7.2.5 Ground Motion Site Response Model Confirmation Studies for Port Island, Japan

Evaluations of reasonable agreement for the comparison between equivalent-linear and nonlinear modeling approaches focus first on how the results of different modeling approaches compare and second on how they match the observed data.

7.3 VALIDATION RESULTS

The following subsections describe the results of the validation studies outlined in Section 7.1.

7.3.1 Validation of RVT-Derived Response Spectra

The ability of the RVT methodology to predict response spectra has been validated by Boore (1983 [DIRS 103317], 2003 [DIRS 163706]). Boore (1983 [DIRS 103317]) illustrated the RVT methodology by comparing mean peak motions from simulated time histories to RVT predictions. RVT peak motion is defined in terms of rms motion which, using Parseval's theorem, is expressed in terms of the integral of the squared amplitude spectrum. Boore (1983 [DIRS 103317]) defines the kth moment of the energy density spectrum as

$$m_k = \frac{1}{\pi}\int_0^\infty \omega^k \left|A(\omega)\right|^2 d\omega \qquad \text{(Eq. 57)}$$

in which $A(\omega)$ is the amplitude spectrum. $A(\omega)$ is derived from the source spectral shape and the seismic moment. Given the source distance, the amplitude spectrum is corrected for travel path and site factors:

$$A(\omega) = CM_0 S(\omega,\omega_c) e^{-\pi\kappa f} \frac{e^{-\omega R/2Q_\beta}}{R} \qquad \text{(Eq. 58)}$$

in which C is a constant that accounts for the radiation pattern, free-surface amplification, energy partition into one horizontal component and other factors including density and V_S at the source. M_0 is the seismic moment and $S(\omega,\omega_c)$ is the source spectral shape:

$$S(\omega,\omega_c) = \frac{\omega^2}{1+(\omega/\omega_c)^2} \qquad \text{(Eq. 59)}$$

in which the source corner frequency ($f_c = \omega_c/2\pi$) is given by:

$$f_c = \beta(\Delta\sigma / M_0)^{1/3} \qquad \text{(Eq. 60)}$$

and β is the crustal V_S and $\Delta\sigma$ is the source stress-drop. The near-site (zero epicentral distance) attenuation factor kappa (κ) is now used rather than the high-cut filter used by Boore (1983 [DIRS 103317]). The value of kappa is attributed to the attenuation in the shallow crust below the site (Hough and Anderson, 1988 [DIRS 104686]). R is the source distance and $Q_\beta(\omega)$ is the frequency-dependent crustal attenuation parameter.

A good approximation of the ratio of the peak motion to the rms motion is (Boore, 1983 [DIRS 103317]):

$$\frac{y\max}{yrms} = \left[2\ln(N)\right]^{1/2} + \frac{0.5772}{2\ln(N)^{1/2}} \qquad \text{(Eq. 61)}$$

in which

$$yrms = \sqrt{\frac{m_0}{T}} \qquad \text{(Eq. 62)}$$

and the period T is taken as the inverse of the corner frequency. N is the number of extrema in a time interval T and it is defined using the predominant frequency of motion:

$$N = 2\tilde{f}T \qquad \text{(Eq. 63)}$$

The predominant frequencies are defined by Boore (1983 [DIRS 103317]) as either the number of extrema (N):

$$\tilde{f} = \frac{1}{2\pi}\left(m_4 / m_2\right)^{1/2} \quad \text{(Eq. 64)}$$

or as the number of zero crossings (N):

$$\tilde{f} = \frac{1}{2\pi}\left(m_2 / m_0\right)^{1/2} \quad \text{(Eq. 65)}$$

Peak acceleration and velocity derived from the time domain simulations compared very well to RVT predicted peak motions for the magnitude range **M** 3 to 7. Comparisons of mean 5%-damped response spectra of time domain simulations (single-degree-of-freedom) and RVT predictions also were made and are illustrated in Figure 7-1. Ignoring the effects of oscillator duration or period (Boore 1983 [DIRS 103317]), Figure 7-1 illustrates generally good agreement except at low frequency for the **M** 7 earthquake and at intermediate frequencies for the **M** 4 event where the RVT predictions are sometimes significantly greater than the response spectra derived from the time domain simulations.

Boore (2003 [DIRS 163706]) has also examined the adequacy of the RVT response spectra predictions using more recent refinements in strong motion duration. Refinements are required when the oscillator period is longer than the ground motion duration. Figure 7-2 illustrates **M** 4 and **M** 7 simulations with their corresponding 10-second 5%-damped oscillator response. The figure clearly illustrates that the oscillator response for the **M** 7 earthquake exceeds the duration of the event. For an appropriate evaluation of RVT peak motions, the appropriate duration must be derived for the evaluation of rms motion and determination of zero crossings. Boore and Joyner (1984 [DIRS 163174]) and Liu and Pezeshk (1999 [DIRS 163995]) have made modifications to the duration by using one duration for evaluation of rms motions and another for evaluation of zero crossings. The results give good agreement as shown in Figures 7-3 and 7-4 and meet the acceptance criteria specified in Section 7.2.1. Figure 7-3 illustrates a comparison of response spectra derived using **M** 4 time domain simulations and RVT peak spectral values. Figure 7-4 illustrates a comparison of response spectra derived using **M** 7.0 time domain simulations and RVT peak spectral values.

7.3.2 Comparison of Equivalent-Linear and Nonlinear Modeling Approaches to Observed Data

This section describes the results of a validation study (EPRI 1993b [DIRS 103320], Appendix 6.B) that evaluates the appropriateness of 1D site response analysis and compares the RVT equivalent-linear modeling approach to fully nonlinear approaches. As described in Section 7.1.2, observed data from three sites were modeled. For each site, control motions and site geotechnical properties were relatively well known and provided consistent input in order to compare the modeling approaches. A summary of the sites, earthquakes, and recorded motions is presented in Table 7-1.

Table 7-1. Earthquakes, Sites, and Recorded Ground Motions

Earthquake	M	Site	Distance (km)	PGA (g)	
				NS	EW
1989 Loma Prieta	6.9	Gilroy #1	12	0.411	0.473
		Gilroy #2	14	0.367	0.322
		Yerba Buena Island	77	0.029	0.068
		Treasure Island	79	0.100	0.159
LSST Event 7 05/20/86	6.5	LSST-DB47 (154 ft depth)	64	0.099	0.081
		(Surface)		0.208	0.158
LSST Event 16 11/14/86	7.8	LSST-DB17 (56 ft depth)	79	0.086	0.074
		(Surface)		0.170	0.133
LSST Event 10 07/16/89	4.5	LSST-DB47 (154 ft depth)	6	0.020	0.013
		(Surface)		0.030	0.040

Source: Silva 2003 [DIRS 164688], Table 4

NOTE: To convert km to mi, multiply by 0.621

7.3.2.1 Reference Sites

Three sites were chosen to evaluate conventional 1D site response analysis (EPRI 1993b [DIRS 103320], Appendix 6.B, Section 6.B.2). Criteria for site selection were:

1. Proximity of the soil site to a nearby rock outcrop site (within 2-3 km [1-2 mi]) or to a vertical instrument array
2. Availability of recordings of both weak and strong motions
3. Accessibility of the site to drilling and testing for geotechnical characterization
4. Suitability of soil in terms of stiffness and particle size for obtaining undisturbed samples and performing dynamic soil tests
5. Representation of a broad range in soil conditions and type.

The three sites selected were Treasure Island, CA, with a nearby rock outcrop site at Yerba Buena Island; Gilroy #2, with Gilroy #1 (near Gilroy, CA) as the nearby rock outcrop site; and Lotung, Taiwan (Lotung Large-Scale Seismic Test [LSST]), with a vertical array of three-component accelerometers. For each site, geotechnical and geophysical characterization provided the basis to determine input parameters for the different modeling approaches (EPRI 1993b [DIRS 103320], Appendix 6.B, Section 6.B.2).

7.3.2.2 Modeling Approaches

The modeling approaches chosen for study in EPRI (1993b [DIRS 103320], Appendix 6.B) are the fully nonlinear formulations DESRA-2C, SUMDES, and TESS, and the equivalent-linear RASCALS.

7.3.2.2.1 DESRA-2C

Program DESRA-2C is an effective stress, 1D finite-element site response analysis code that does not couple the wave propagation and diffusion equations. The code contains three main options: 1) total stress analysis ignoring the effects of seismically-induced pore water pressures and strain hardening; 2) effective stress analysis with no redistribution of pore water pressure; and 3) effective stress analysis with redistribution and dissipation of pore water pressure. The DESRA-2C code implements a standard hyperbolic soil model using Masing's rules. Either a rigid or deformable base may be considered. Vertically propagating plane S-waves are considered. The code was implemented unmodified.

7.3.2.2.2 SUMDES

The SUMDES code (Li et al. 1992 [DIRS 163527]) is a 1D, finite-element vertical-wave propagation code that can optionally treat horizontal and vertical motions simultaneously using a 3D hypoplasticity model. The solution solves the fully coupled wave propagation and diffusion equations. The formulation is effective stress (optional total stress) and the code predicts three-directional motions as well as pore water pressure generation and dissipation. Either a rigid or compliant base may be used as well as a suite of five constitutive models. An elastoplastic model (1D) was used in the analyses. The code was implemented unmodified.

7.3.2.2.3 TESS

The computer program TESS (Pyke [n.d.] [DIRS 163613]) is a 1D, explicit finite-difference nonlinear site response analysis code that assumes vertically-propagating S-waves and treats the wave propagation and diffusion equations as uncoupled. Either a rigid or compliant base may be specified. Since the effective stress formulation is used, the code models excess pore pressure generation and dissipation. The soil model is hyperbolic (Hardin and Drnevich 1972b [DIRS 163511]), and the Cundall-Pyke hypothesis (Pyke 1979 [DIRS 163612]) is used for cyclic loading. The code was implemented unmodified.

7.3.2.2.4 RASCALS

The RASCALS code implements the RVT equivalent-linear site-response modeling approach. The version of RASCALS employed in the validation study is similar to the version qualified for use on the Yucca Mountain Project.

7.3.2.3 Validation Process

In implementing the modeling approaches, the authors of the codes, if available, assisted in selecting appropriate parameter values based on the geotechnical data obtained for each reference site. The information generally available was that contained in Tables 7-2, 7-3, and 7-4 in addition to velocity profiles and strain-dependent material properties described below. Standard Penetration Test (SPT) data at the Treasure Island and Lotung LSST reference sites were available. In addition, friction angles for the liquefiable sands at Treasure Island and at Lotung were estimated. While the geotechnical models may not have been as complete as some code authors desired, it was felt that the nature, number, and types of tests performed are those

typically available and represented an adequate basis for characterizing the dynamic response of the sites.

The process of conducting the comparative site response analysis involved parameter selection by the code authors, initial analyses at all three sites, and then a review of the comparisons of predicted and observed motions by each author of their code's results. At this stage, the authors of the nonlinear codes were permitted to revise their input parameters. No iterations of input parameters for RASCALS were required. This interaction provided an opportunity to correct any significant errors in assigning parameter values.

The intent was to perform, to the extent possible, a forward prediction at each site using measured material properties and implementing the analysis in a structured and consistent manner. The results provide a rational basis for evaluating how well the modeling approaches perform.

7.3.2.4 Results for Gilroy #2 Site

The Gilroy array in central California provides the data for the first validation exercise. Recordings of the 1989 Loma Prieta earthquake at the Gilroy #2 site provide the data to be modeled, and recordings from the Gilroy #1 site (a rock site 2 km [1 mi] away) provide the control motions (Table 7-2). The Gilroy strong motion accelerograph array begins with the rock site Gilroy #1 located just west of the western edge of the Santa Clara Valley. The remainder of the Gilroy array (2, 3, 4, 6, and 7) extends roughly eastward across the valley at 2 to 3 km (1 to 2 mi) intervals with Gilroy #7 founded on shallow soil on the eastern edge of the valley. The soil depth varies from zero at Gilroy #1 to about 600 ft at Gilroy #2 (2 km [1 mi] east) and to several thousand feet at Gilroy #3, 2-3 km (1-2 mi) east of Gilroy #2. The site at Gilroy #2 is located on the edge of a steeply-dipping bedrock interface, an area where two-dimensional basin effects are predicted to be most pronounced. Thus, validation results for this site are useful in assessing the performance of the RVT equivalent-linear site-response model for sites where 2D effects may occur.

Gilroy #2 Site Characterization–To characterize the Gilroy #2 site properties, a suite of geotechnical investigations was carried out. The investigations included a series of geophysical surveys and laboratory testing of borehole samples. Nine undisturbed samples were taken over the depth range of 10 to 420 ft. Properties of tested borehole samples are listed in Table 7-2. Based on geophysical surveys, velocity profiles were determined for V_S and V_P (Figure 7-5). The profiles represent an average of the *in situ* velocities measured at the site.

Based on laboratory testing of dynamic material properties, two sets of normalized shear modulus reduction and damping curves were developed (Figure 7-6). One set of curves is for the depth range of 0-130 ft and the other is for below 130 ft. The increased damping and lower shear modulus reduction at greater depths, which is counter to the effects of increasing confining pressure, are due to the presence of gravels below a depth of 130 ft (Table 7-2).

Table 7-2. Properties of Samples from Gilroy #2

Sample No.	Sample Depth ft (m)	Soil Description	Liquid Limit %	Plasticity Index %	Water Content %	Total Unit Weight pcf (g/cm^3)	Void Ratio e	Dry Unit Weight pcf (g/cc)	Specific Gravity Gs	Degree of Saturation %
G1	10 (3.0)	Dark Brown Clayey Silt with Sandy Material	29	7	26.1	117.1 (1.88)	0.78	93 (1.49)	2.70	86
G2	20 (6.1)	Dark Gray Silty Clay	43	23	30.0	118.8 (1.90)	0.84	91,96 (1.46,1.54)	2.70	96
G3	50 (15.2)	Silty Sand with Gravel	—	—	15.8	123.4 (1.98)	0.58	107 (1.71)	2.65	76
G4	85 (25.9)	Light Gray Stiff Clay with Horiz. Bedding	47	17	30.8	121.0 (1.94)	0.82	93,95 (1.49,1.52)	2.70	100
G5	120 (36.6)	Silty Sand	—	—	19.8	134.1 (2.15)	0.55	112,110 (1.79,1.76)	2.65	100
G6	210 (64.0)	Gravelly Sand	—	—	14.8	130.1 (2.08)	0.52	124 (1.99)	2.65	62
G7	420 (128.0)	Gravelly Clay	—	—	28.0	136.4 (2.19)	0.58	113 (1.81)	2.65	85
G8	348 (106.1)	Clayey Silt	35	13	23.7	127.7 (2.05)	0.60	103 (1.65)	2.70	100
G9	420 (128.0)	Gravelly Clay	—	—	14.0	136 (2.18)	0.41	120 (1.92)	2.70	92

Source: EPRI 1993b [DIRS 103320]; Appendix 6.B, Table 6.B-3

The profile is generally stiff, consisting of sands and clays near the surface and predominantly gravels from about 130 ft to near 400 ft. and possibly deeper. Weathered bedrock is reached at about 550 ft with a steep velocity increase to at least 800 ft (Figure 7-5).

Summary of Gilroy #2 Analyses–Response spectra results of the RVT equivalent-linear modeling approach show an acceptable match to the observed data over the entire frequency range (Figure 7-7), although there is an overprediction of the resonance near 3 Hz. Predicted PGA values are within 30 percent of those observed on the east-component and within 1 percent on the north-component. The differences between the data and the predictions are not unexpected in equivalent-linear analyses since the velocities are constant at the strain compatible values, while in nonlinear analyses they vary with time. As a result, resonance phenomena are less pronounced in nonlinear analyses at high strain levels and may, in fact, depend upon the character (duration) of the control motion. The average S-wave strain-iterated damping for the entire profile is about 7 percent, more than double the small-strain value of 3 percent obtained for a linear analysis (EPRI 1993b [DIRS 103320], Appendix 6.B, Section 6.B.4.1). Maximum iterated effective cyclic shear strains were about 0.1 percent.

In general, the nonlinear models also match the observed data reasonably well (Figure 7-8). For SUMDES and TESS, the log average response spectra of the horizontal components of the recorded motions agree well with the modeled motions over most of the frequency range.

DESRA shows a poorer fit with a general underprediction of the average observed spectrum. Comparison of results for the RVT equivalent-linear site-response model (RASCALS) to those for the nonlinear models shows a similar degree of agreement to the recorded data (Figure 7-8).

Effects of the dipping structure at the Gilroy #2 site do not seem to be significant even at very low frequencies. The generation of small amplitude surface waves by the dipping interface may be manifested in the increase in coda shown in the recorded motions relative to the modeled motions (Figure 7-7). The higher damping during the strong shaking may be severely damping these secondary scattered wavefields rendering their amplitudes much smaller than a linear 2D analysis with small-strain damping might suggest.

7.3.2.5 Results for Treasure Island Site

Recordings of the 1989 Loma Prieta earthquake at Treasure Island and Yerba Buena Island in San Francisco Bay provide the data for the second validation exercise (Table 7-3). Ground motions recorded at a rock site on Yerba Buena Island are used as the control motions to a site response model for the soil site at Treasure Island, about 2 km (1 mi) away.

Treasure Island Site Characterization–As for the Gilroy #2 site, a suite of geotechnical investigations was carried out to characterize the Treasure Island site, including geophysical surveys and laboratory testing of borehole samples. Properties of samples collected are listed in Table 7-3. The site consists of about 40 ft of sand (hydraulic fill) overlying Young Bay mud and then Old Bay clay with bedrock at a depth of about 300 ft. Groundwater is located approximately 4 ft below the surface.

Table 7-3. Properties of Samples From Treasure Island

Sample No.	Sample Depth ft (m)	Soil Description	Liquid Limit %	Plasticity Index %	Water Content %	Total Unit Weight pcf (g/cm^3)	Void Ratio e	Dry Unit Weight pcf (g/cc)	Specific Gravity Gs	Degree of Saturation %
T1	17.5 (5.3)	Medium Fine Sand	—	—	19.9	120 (1.92)	0.66	100 (1.60)	2.65	80
T2	30 (9.1)	Dark Gray Silty Sand	—	—	21.3	120 (1.92)	0.67	99 (1.59)	2.65	85
T3	60 (18.3)	Dark Greenish Soft Clay	51	26	50.2	108 (1.73)	1.34	72 (1.15)	2.70	100
T4	90 (27.4)	Dark Gray Soft Clay	42	19	41.9	113 (1.81)	1.10	80 (1.28)	2.70	100
T5	130 (39.6)	Dark Greenish Med.Stiff Clay with Shells	37	23	37.0	114 (1.83)	1.02	83 (1.33)	2.70	98
T6	170 (51.8)	Dark Greenish Gray Stiff Clay	34	19	20.7	128 (2.05)	0.58	106 (1.70)	2.70	96
T7	232 (70.7)	Dark Greenish Gray Clay w/Horiz. Beddings	48	30	33.3	115 (1.84)	0.95	87 (1.39)	2.70	95

Source: EPRI 1993b [DIRS 103320]; Appendix 6.B, Table 6.B-7

Based on the geophysical surveys, velocity profiles were determined for V_S and V_P (Figure 7-9). The profiles represent an average of the *in situ* velocities measured at the site.

Based on laboratory testing of dynamic material properties, two sets of normalized shear modulus reduction and damping curves were developed (Figure 7-10). One set of curves, for the 0 to 44 ft depth range, reflects the dynamic properties of the fill material. The second set of curves is for the deeper material, which is comprised largely of clays (Young Bay mud and Old Bay clay) with plasticity index (PI) values around 25 percent. The deeper materials exhibit less strain dependency on both the modulus reduction and damping reflecting dynamic properties typical of clays.

Since the hydraulic fill liquefied in places during the 1989 Loma Prieta earthquake, the generation and dissipation of excess pore pressure is an important consideration in nonlinear models of ground response at this site. To support this aspect of the nonlinear models, the permeability of the hydraulic fill material was estimated at 5×10^{-4} ft/sec. In addition, an average uncorrected SPT of 5 to 10 blows/ft, taken from other studies at Treasure Island (Power et al. 1998 [DIRS 164825]), was used for the fill material in assessing some of the input parameters for the nonlinear analyses.

Summary of Treasure Island Analyses–Modeled response spectra using the RVT equivalent-linear approach show a general underprediction at all frequencies (Figure 7-11). Maximum iterative cyclic effective strains were about 0.06 percent. This same result is also obtained for the nonlinear analyses (Figure 7-12). Results from the equivalent-linear and nonlinear analyses are comparable to a linear analysis that was also carried out (EPRI 1993b [DIRS 103320], Appendix 6.B, Section 6.B.4.2.1). These results indicate that nonlinear soil effects, in terms of surface response spectra, were not significant during the Loma Prieta earthquake at this site. Note however, that liquefaction was observed pervasively in the interior of the island where the strong motion instrument was located (Rollins et al. 1994 [DIRS 165592]).

The cause of the underprediction in modeling results of response spectra is unclear, but does not appear to be model dependent. One possibility is that the Yerba Buena recording is an inappropriate control motion for the Treasure Island site. Increasing the control motion uniformly would result in a direct (one-to-one) enhancement of low frequencies but, due to resulting increase in strain levels and accompanying higher damping, would show less of an effect at high frequencies. Alternatively, or in conjunction, an impedance contrast or steep velocity gradient at the base of the Treasure Island profile could cause such an effect. Until this issue is resolved, results of analyses with these recordings will have uncertainties regarding inferences on both site response analysis approaches and nonlinear soil models.

Other investigators have obtained different results at this site using similar methodologies with different material properties, modified control motions, and by varying sensitive parameters in the computer codes (EPRI 1993b [DIRS 103320], Appendix 6.B, Section 6.B.4.2.2) Rollins et al. (1994 [DIRS 165592]) also simulated the ground motions recorded at Treasure Island using SHAKE 90. They also were unable to match the recorded motions at periods of 1 sec and more, which they infer might be due to softening of the soil and the onset of liquefaction. This points out that better or worse comparisons may be obtained for earthquakes that have occurred. The

intent of the present analyses was to perform, to the extent possible, a forward prediction at each site using measured material properties and implementing the analysis approaches in a consistent manner. The results then provide a more rational basis for evaluating how well the prediction methodologies perform.

7.3.2.6 Results for Lotung Site

The LSST at Lotung, Taiwan includes an array of downhole accelerometers. Recordings from downhole instruments provide the control motions for site response modeling to match data recorded at the surface. Sensor packages are located at the surface and depths of 20 ft (6 m), 36 ft (11 m), 56 ft (17 m), and 154 ft (47m) (Anderson and Tang 1989 [DIRS 163169]). For the model validation exercise reported in EPRI (1993b [DIRS 103320], Appendix 6.B, Section 6.B.4.3), data from three earthquakes were analyzed (Table 7-1). Two of the events represent strong motion with surface peak acceleration values of 0.10 g to 0.20 g (LSST Events 7 and 16). The third earthquake (LSST Event 10), with an average surface peak acceleration value of about 0.04 g, was used for a small-strain analysis to assess the appropriateness of the base case (low strain) profile (velocity and damping) and the use of vertically-propagating S-waves in the modeling approach. Events 7 and 10 have recordings at all 5 levels and Event 16 recordings are available from the top 4 levels (surface, 20 ft, 36 ft, and 56 ft). Interestingly, even at these relatively low levels of motion associated with Event 16, the soil appears to have exhibited nonlinear behavior.

Model validation results presented here are for the strong motion analyses using LSST Events 7 and 16 as control motions. Analyses consist of propagating the motions recorded at the deepest sensor package to the surface. For LSST Event 7, the recordings at 154 ft were used while for LSST Event 16, the deepest recordings were at the 56 ft level. Results are presented for analyses from the deepest recording levels to the surface. Results of analyses from the deepest levels to subsurface levels are found in EPRI (1993b [DIRS 103320], Appendix 6.B, Section 6.B.4.3).

Lotung, Taiwan Site Characterization–Geotechnical investigations at the Lotung site included crosshole and uphole velocity surveys and borings to collect undisturbed samples for laboratory testing. The soil at the site extends to a depth of about 150 ft (47 m) and consists of silt, silty sand to clayey silt. Table 7-4 lists sample properties and depths. Groundwater is found at the ground surface.

Table 7-4. Properties of Samples From Lotung LSST

Sample No.	Depth ft (m)	Soil Description	Liquid Limit %	Plasticity Index %	Water Content %	Total Unit Weight pcf (g/cm^3)	Void Ratio e	Specific Gravity Gs	Degree of Saturation %
CH1 (TI)	18 (5.5)	Silt	—	—	31.0	112 (1.79)	0.93	2.65	88
CH2(T5)	34.5 (10.5)	Silt	—	—	32.5	118 (1.89)	0.85	2.65	100
CH1(T4)	59 (18.0)	Silty Fine Sand	—	—	33.3	109 (1.75)	1.02	2.65	87

Sample No.	Depth ft (m)	Soil Description	Liquid Limit %	Plasticity Index %	Water Content %	Total Unit Weight pcf (g/cm^3)	Void Ratio e	Specific Gravity Gs	Degree of Saturation %
CH2(T9)	93.5 (28.5)	Silty Sand	—	—	31.2	119 (1.91)	0.82	2.65	100
CH1(T8)	113 (34.5)	Clayey Silt	32	7	35.3	118 (1.89)	0.92	2.70	100
CH2(TI1)	133 (40.5)	Clayey Silt	33	8	31.1	117 (1.88)	0.89	2.70	95
CH1(TI0)	146 (44.5)	Silt	—	—	24.0	128 (2.05)	0.56	2.65	100

Source: EPRI 1993b [DIRS 103320]; Appendix 6.B, Table 6.B-11

Based on the velocity survey data, base case V_S and V_P profiles were determined (Figure 7-13). The profiles are fairly uniform below a depth of 25 ft. Shear modulus reduction and damping curves were based on the results of laboratory dynamic testing and the properties listed in Table 7-4 (Figure 7-14).

For the clayey silt samples, the PI is only about 7 to 8 percent, suggesting dynamic material properties closer to sands rather than highly plastic clays. The single set of curves for all depths is consistent with the general uniformity shown in both the V_S profile (Figure 7-13*)* and in material type.

Summary of Lotung Analyses–Results of the RASCALS analyses for LSST Events 7 and 16 indicate that the predicted spectra agree in overall shape and level with the empirical spectra data for both earthquakes (Figures 7-15 and 7-16). The resonances tend to be overpredicted, particularly for Event 7, but the agreement between the predicted and empirical spectrums is good. Similar results are obtained for recordings at other depth levels (EPRI 1993b [DIRS 103320], Appendix 6.B, Section 6.B.4.3). The vertically propagating S-wave model and laboratory derived material strain dependencies appear to provide an accurate representation of the response of this profile throughout the upper 154 ft.

Comparison of modeling results for the RVT equivalent-linear approach to those for the fully nonlinear approaches shows general agreement with the data and among the approaches (Figures 7-15 and 7-16). The laboratory derived dynamic material properties reflect the *in situ* strain dependencies well.

The individual component analyses (EPRI 1993b [DIRS 103320], Appendix 6.B, Figures 6.B-39 to 6.B-67) showed that some approaches performed better than others did for certain components, depths, and earthquakes but, on average, each approach produces acceptably good results. For Events 7 and 16, maximum iterated effective cyclic shear strains are about 0.06 and 0.04 percent, respectively.

In summary, the vertically-propagating S-wave component of the RVT equivalent-linear modeling approach adequately predicts the predominant motion at this site over the frequency range of 0.1 to over 30 Hz for the earthquakes studied (EPRI 1993b [DIRS 103320], Appendix

6.B). In addition, the equivalent-linear results are generally comparable to those of the nonlinear analyses with a tendency to overpredict the resonances, particularly the fundamental. These results are consistent with those for the Gilroy #2 and Treasure Island sites and together provide a strong validation of the RVT equivalent-linear approach to site response modeling.

7.3.3 Comparison of Vertical-Component Site Response Modeling Approach to Observed Data

For the vertical-component of ground motion, the site-response modeling approach uses a linear analysis rather than an equivalent-linear approximation to nonlinear behavior. Validation of this aspect of the overall modeling approach relies on two previous studies. EPRI (1993a [DIRS 103319], Section 6.6.2.2) validates a linear analysis for vertical-component site response as part of a study considering a combined RVT point-source/RVT site-response model. Recordings from the 1989 Loma Prieta earthquake at 24 sites are modeled. Silva (1997 [DIRS 163747]) also uses an RVT point-source/RVT site-response model. In this study, modeled vertical-to-horizontal (V/H) response spectral ratios are compared to empirical ratios.

EPRI (1993a [DIRS 103319], Section 6.6.2.2) examined the validity of the RVT point-source/site-response model for developing vertical-component ground motions. Vertical motions were computed for 24 sites (22 rock and 2 soil) that recorded the 1989 Loma Prieta **M** 6.9 earthquake at hypocentral distances ranging from 1 to 80 km (1 to 50 mi). In the computations, a linear site-response model was included for each site.

Site-specific kappa values for the RVT point-source component of the overall model were determined on the basis of template fits of response spectral shapes at the rock sites, using a Q(f) of 150 $f^{0.6}$ and a **M** 6.9. The average value of kappa at the rock sites (0.029 sec) was used for the soil site kappa value. A summary of sites, distances, and kappa values for all 24 sites is given in Table 7-5.

Table 7-5. Loma Prieta Modeling Summary for Vertical Motions

Name	Label	κ (sec)	R (km)
Corralitos	COR	0.028	12.0
Los Gatos	LGPC	0.012	12.4
Branciforte Dr.	BRAN	0.020	15.6
Gilroy 1	GL1	0.012	19.2
Gilroy 2*	GL2	0.029	20.0
Santa Cruz	UCS	0.020	20.0
UCSC - Seismic Lab	UCSC	0.020	23.3
Gilroy 6	GL6	0.025	26.8
SLAC	SLA	0.030	30.5
Redwood City – Cañada	RDC	0.060	39.9
SAGO South	SAS	0.050	40.8
APEEL 7	A07	0.050	45.6
APEEL 10	A10	0.050	45.6
Monterey City Hall	MON	0.030	45.6
Belmont - 2 story	BEL	0.040	47.5

Name	Label	κ (sec)	R (km)
APEEL 2E, CUSH	A2E	0.020	54.3
Sierra Point	SSP	0.020	66.1
SF Diamond Heights	SFD	0.020	74.0
Piedmont J.H.	PHS	0.025	75.0
SF Rincon	SFR	0.020	76.9
Yerba Buena Island	YBI	0.040	77.9
SF Pacific Heights	SFH	0.040	78.9
SF Telegraph Hill	SFT	0.020	78.9
Treasure Island*	TRI	0.029	79.9
SF Cliff House	SFC	0.040	80.9

Source: EPRI 1993a [DIRS 103319], Table 6-6

NOTES: * soil site
To convert km to mi, multiply by 0.621

For the RVT point-source model, a source depth of 12 km (7.5 mi), a stress drop of 200 bars, and the crustal velocity profile of Wald et al. (1991 [DIRS 164086]) were used. For sites with distances of about 20 km (12 mi), the incidence angle at the layer above the source is around 60 degrees; for more distant sites a greater angle of incidence results in a general underprediction of motions, which becomes progressively worse as distance increases. Rather than treat the wave propagation in a more rigorous manner, an upper-bound to the incidence angle was set at 60 degrees.

Comparison of model results to observed data indicates that the general shape, including level of spectra and frequency at the spectral peak, is captured reasonably well in the simulations (Figure 7-17). The vertical model fits are quite good for frequencies greater than about 6 to 7 Hz (Figure 7-18) and show about the same level of uncertainty as found for the horizontal component motions (EPRI 1993a [DIRS 103319], Section 3). Vertical-component bias for the RVT point-source/site-response model is positive at 0.2 Hz and negative from about 2 to 7 Hz (Figure 7-19). At all other frequencies the bias is near zero. The negative bias at about 4 Hz is a result of the resonance introduced in the crustal velocity profile (EPRI 1993a [DIRS 103319], Section 6.6.2.2).

While the EPRI (1993a [DIRS 103319], Section 6.6.2.2) results do not constitute an independent validation of linear analysis for vertical-component site response, the good agreement of the combined RVT point-source/site-response model to the observations contributes to providing the needed level of confidence in the overall site-response modeling approach for Yucca Mountain.

In a second study contributing to the needed confidence in the modeling approach for vertical-component motions, Silva (1997 [DIRS 163747]) compared modeled V/H response spectral ratios to empirically observed ratios for western U.S. earthquakes. The modeled ratios were developed using the RVT point-source model combined with an RVT equivalent-linear site-response model for horizontal motions and a linear site-response analysis for vertical motions. Generic shallow rock or soil velocity profiles were placed on top of a generic California crustal velocity profile (Silva 1997 [DIRS 163747], Figures 1, 2, and 31, respectively). For the equivalent-linear site-response model, generic curves for normalized shear

modulus reduction and material damping, for rock and soil sites, were taken from Silva et al. (1996 [DIRS 110474], Section 6.2.3). Inputs to the RVT point-source model, reflecting average western U.S. source characteristics, included a stress drop of 60 bars and a source depth of 8 km (5 mi).

Empirically-based ratios were determined for rock sites from the average of the attenuation relations of Sadigh et al. (1997 [DIRS 104531]) and Abrahamson and Silva (1997 [DIRS 104205]). For soil sites, only the Abrahamson and Silva (1997 [DIRS 104205]) was used because the Sadigh et al. (1997) work does not address vertical motions for soil conditions. Ratios were determined for **M** 6.5, the magnitude for which the empirical relations are best constrained.

In general, modeling results for rock and soil (Figures 7-20 and 7-21, respectively) capture the overall shapes and trends with distance of the empirical ratios, but show a stronger close-in distance effect. The rapid increase in the incidence angle at the top of the source layer with increasing epicentral distance controls this effect. Randomization of the crustal velocity profile to simulate crustal heterogeneity would reduce the near-source distance effect and increase agreement with the empirical ratios (Silva 1997 [DIRS 163747]).

As for the validation study in EPRI (1993a [DIRS 103319], Section 6.6.2.2), the results presented in Silva (1997 [DIRS 163747]) do not provide an independent validation of the use of a linear analysis for vertical component site response. However, this work further strengthens the case that this is a valid approach. While the EPRI (1993a [DIRS 103319], Section 6.6.2.2) study looked at recordings for a single earthquake, the Silva (1997 [DIRS 163747]) study compares model results to empirical attenuation relations that represent a large proportion of the western U.S. strong motion database. The two studies complement each other and together provide the necessary confidence that this aspect of the site response modeling approach for Yucca Mountain is valid.

7.3.4 Comparison of Combined Source, Path and Site Response Modeling to Observed Data

Silva et al. (1996 [DIRS 110474], Section 5) describe validation of a ground motion model that incorporates the RVT point-source modeling approach (e.g., EPRI 1993a [DIRS 103319], Section 3.2) and the equivalent-linear site-response modeling approach. Observed response spectra from 16 earthquakes recorded at over 500 sites (Table 7-6) are compared to modeling results.

Because site-specific information is unavailable for most of the recording sites, the sites were categorized in terms of two generic site conditions: soft-rock and deep-soil. Velocity profiles and curves for normalized shear modulus reduction and material damping were developed for the generic site conditions and generally used as input to the RVT equivalent-linear site-response model. For control motions, the RVT point-source model is used to generate hard-rock outcrop motions that serve as input to the site-response model. Silva et al. (1996 [DIRS 110474], Section 5) also consider a finite-source ground motion model to generate control motions, but that aspect of the work is not summarized here.

Inputs to the RVT point-source model including stress drop, frequency-dependent regional attenuation (Q[f]), and local site attenuation (kappa) were based on nonlinear least-squares inversion of observed Fourier amplitude spectra for each earthquake (Silva et al. 1996 [DIRS 110474], Section 4). For the input crustal velocity profile, an appropriate profile was determined from those reported in the literature.

Silva et al. (1996 [DIRS 110474], Section 5) evaluate the ability of the combined point-source and equivalent-linear site response models to predict the observed ground motions for the 16 earthquakes listed in Table 7-6. Model validity is evaluated in terms of the model variability and model bias. Model variability is defined as the standard error of the residuals of the log of the average response spectra. Residuals are defined as the difference of the logarithms of the observed average 5%-damped acceleration response spectra and the predicted response spectra. At each period, the residuals are squared and summed over the total number of sites. Dividing the resultant sum by the number of sites yields an estimate of the model variance. Model bias is the average offset between the observed and predicted response spectra.

To support the validation of the RVT equivalent-linear site-response model for use on the Yucca Mountain Project, validation results from Silva et al. (1996 [DIRS 110474], Section 5) are summarized for five of the earthquakes they studied: four events (1979 Imperial Valley, 1989 Loma Prieta, 1992 Landers, and 1994 Northridge) for which nonlinear site effects were observed and the 1992 Little Skull Mountain earthquake because of its proximity to Yucca Mountain. The first four of these events are similar in size to those that control probabilistic seismic hazard at Yucca Mountain (Section 6.2.2.5). While these validation results do not assess the performance of the RVT linear-equivalent site-response model by itself, validation of the combined RVT point-source/RVT equivalent-linear site-response modeling approaches adds confidence that the site-response component is providing valid results.

Table 7-6. Earthquakes Modeled

Earthquake	Date	M	Fault Distance Ranges(km)	Rock Sites	Soil Sites	Total Sites
San Fernando	1971	6.6	3 - 218	21	18	39
Tabas	1978	7.4	3 - 90	3	1	4
Coyote Lake	1979	5.7	3 - 30	3	7	10
Imperial Valley	1979	6.4	1 - 50	2	33	35
Imperial Valley(AS)	1979	5.3	12 - 52	0	16	16
Morgan Hill	1984	6.2	1 - 70	8	21	29
Nahanni	1985	6.8	6 - 16	3	0	3
North Palm Springs	1986	6.0	1 - 90	9	20	29
Whittier Narrows	1987	6.0	10 - 80	18	70	88
Superstition Hills(B)	1987	6.4* (6.7)	1 - 28	1	11	12
Saguenay	1988	5.8	47 - 460	22	0	22
Loma Prieta	1989	6.9	5 - 90	33	20	53
Little Skull Mtn.	1992	5.7 (4.4; 4.2**)	15 - 98	8	0	8
Landers	1992	7.2	1 - 177	5	52	57

Earthquake	Date	M	Fault Distance Ranges(km)	Rock Sites	Soil Sites	Total Sites
Cape Mendocino	1992	6.8	8 - 45	1	4	5
Northridge	1994	6.7	7 - 147	23	71	94
Totals				159	344	503

Source: Silva et al. 1996 [DIRS 110474], Table 5.2

NOTES: * Preferred value
** Aftershocks
To convert km to mi, multiply by 0.621

7.3.4.1 Crustal and Site Velocity Profiles Used for Validation Modeling

As discussed above, regional crustal and local site velocity profiles form part of the input to the RVT point-source model and the RVT equivalent-linear site-response model, respectively. Crustal velocity profiles are taken from the literature and cited below in the discussion of validation results for each earthquake. Development of site velocity profiles for the two generic site conditions is discussed in the following subsections.

7.3.4.1.1 Generic Site Velocity Profiles

Because reliable velocity profiles have not been determined for most strong motion recording sites, generic profiles must often be used in site response modeling. Silva et al. (1996 [DIRS 110474], Section 3.2) defined two site categories (soft-rock and deep-soil) and determined generic velocity profiles for each. Given the available data, use of such a broad classification scheme was considered an appropriate compromise between the goals of accurately modeling site response and of constraining modeling variability and bias.

Soft-Rock Site Category

Silva et al. (1996 [DIRS 110474], Section 3.1.1) define the soft-rock category to be a combination of Geomatrix categories A and B (rock and shallow/stiff soil, Table 7-7). They combine these categories based on an examination of median V_S profiles computed from measured profiles categorized as A and B (Figure 7-22a). The profile for category A shows low V_S values near the surface with a steep shallow gradient that, in view of their variabilities, is not unlike the profile for category B (shallow/stiff soil). Silva et al. (1996 [DIRS 110474], Section 3.1.1) argue that combining the two (Figure 7-23) is a reasonable representation of typical California soft-rock site conditions. The smoothed version represents the base case velocity profile for the soft-rock category used in the model validation exercises.

Table 7-7. Strong Motion Recording Site Classifications

Geomatrix Site Classification	
Geotechnical Subsurface Characteristics	
A	Rock. Instrument on rock (V_S > 600 m/sec (2000 ft/sec) or < 5 m (20 ft) of soil over rock).
B	Shallow (stiff) soil. Instrument on/in soil profile up to 20 m (70 ft) thick overlying rock.

Geomatrix Site Classification	
C	Deep narrow soil. Instrument on/in soil profile at least 20 m (70 ft) thick overlying rock, in a narrow canyon or valley no more than several km (102 mi) wide.
D	Deep broad soil. Instrument on/in a soil profile at least 20 m (70 ft) thick overlying rock, in a broad valley.
E	Soft deep soil. Instrument on/in deep soil profile with average V_S < 150 m/sec (490 ft/sec).

Source: Silva et al. 1996 [DIRS 110474], Table 3.1

Deep-Soil Site Category

For the deep soil category, Silva et al. (1996 [DIRS 110474], Section 3.1.2) combined the Geomatrix categories C and D. They noted that measured median V_S profiles for sites with these classifications (Figure 7-22b) are similar, considering their variabilities. They observed that profiles for Geomatrix category C (narrow valley deep soil) showed a slightly steeper gradient and stiffer conditions than those for category D, possibly due to depositional environment and perhaps shallower average depths. As with the combined rock/shallow soil (soft-rock) category, the profiles for the Geomatrix deep soils (C and D) were combined to produce a single deep-soil profile (Figure 7-24). The generic deep-soil profile may be characterized as cohesionless soils comprised of sands, gravels, and low PI clays. As with the soft-rock profile, the smoothed version represents the base case profile for the analyses.

7.3.4.2 Inversions to Determine Inputs for RVT Point-Source Model

To determine inputs for the RVT point-source model, Silva et al. (1996 [DIRS 110474], Section 4) carried out nonlinear least-squares inversions of Fourier amplitude spectra to determine stress drop, Q(f), and kappa values. In carrying out these inversions, data from earthquakes occurring in the same geologic province as defined by Wesnousky (1986 [DIRS 163926]) were grouped together. In these regional inversions, only events having recordings spanning a range in distance sufficient to constrain Q(f) and kappa (10 to beyond 50 km [6 to beyond 30 mi]) were used. For the remaining earthquakes, the region-specific Q(f) was fixed and inversions performed only for stress drop and kappa values.

The geologic provinces for which sufficient data were available are the North Coast, Mojave Desert, and Peninsular Ranges. The earthquakes (Table 7-6) and sites taken to be generally consistent with these provinces are: the Loma Prieta, Coyote Lake, and Morgan Hill for the North Coast; Landers and North Palm Springs for Mojave Desert; and the Whittier Narrows, Northridge, and San Fernando earthquakes for the Peninsular Ranges. Large source-to-site distances are required to obtain reasonably unique Q(f) models. This, however, results in some sites occurring across province boundaries (e.g., the Landers earthquake has sites in Los Angeles), which is undesirable. Silva et al. (1996 [DIRS 110474], Section 4) judged that a sufficient amount of the path lay within the desired province to have a dominant affect on the inversions.

7.3.4.2.1 Inversion Method

In the inversion scheme, Silva et al. (1996 [DIRS 110474], Section 4) obtain earthquake source, path and site parameters by using a nonlinear least-squares inversion of Fourier amplitude spectra. They selected the bandwidth for each amplitude spectrum computed from recordings based upon visual examination. In no cases did the bandwidth extend beyond the filter corner frequencies. The inversion scheme treats multiple earthquakes and sites simultaneously with the common crustal path damping parameter Q(f). The parameter covariance matrix is examined to determine which parameters may be resolved for each data set. Asymptotic standard errors are computed at the final iteration. The five parameters that may be determined include: kappa, Q_0 and η, **M**, and corner frequency (f_c). Q_0 and η define regional attenuation Q(f) through the relation $Q(f) = Q_0 f^{\eta}$ in which f is frequency. The inversion uses the Levenberg-Marquardt algorithm (Press et al. 1986 [DIRS 145343]). Crustal and soil profile amplification is accommodated in the inversion scheme by incorporating the appropriate mean transfer functions in the model spectra.

To reduce the non-uniqueness inherent in inversion schemes, Silva et al. (1996 [DIRS 110474], Section 4) employed a suite of starting models. The final set of parameters was selected based upon a visual inspection of the model fit to the Fourier amplitude spectrum, computed chi-square values, and the parameter covariance matrix.

The stress drop was calculated from the moment and corner frequency using the relation

$$f_C = \beta_0 \left(\frac{\Delta\sigma}{8.44 \cdot M_0} \right)^{1/3} \qquad \text{(Eq. 66)}$$

in which β_0 is V_S at the source. In the final inversions **M** was fixed at the values assigned in the strong motion catalogue.

The inversions were done on log amplitude spectra because strong ground motion data are generally treated to be log-normally distributed. The inversion bandwidth is magnitude dependent, extending to longer periods with increasing magnitude. The low frequency limit is site dependent as well and may be seen in the Fourier amplitude spectra. A high-frequency limit was set at 20 Hz (noise contamination permitting) to reduce the tendency toward high-frequency weighting when using linear frequencies (the density of points increases with frequency).

To constrain the inversions for Q(f), regional inversions were done using data from all the stations for each region but grouping them according to their site category: soft-rock or deep-soil. That is, multiple stations (at varying distances) were specified as belonging to a single site category and kappa values were determined for the two site categories rather than for each station site.

Based on the Q(f) relation determined from the regional inversions, the regional attenuation was kept constant and a second round of inversions were carried out for stress drop and individual station kappa values for the combined earthquakes in each province. In these inversions, **M** was also fixed at the values given in the strong motion catalogue (Silva et al. 1996 [DIRS 110474],

Appendix B). The resulting stress drops are summarized in Table 7-8 for the earthquakes summarized in Section 7.3.4.3.

Table 7-8. Silva et al. (1996 [DIRS 110474]) Inversion Results for Stress Drop

Earthquake	Magnitude (M)	Stress Drop (bars)
Imperial Valley (Q_0 = 264, η = 0.6)	6.4	23.2
Northridge (Q_0 = 264, η = 0.6)	6.7	62.9
Loma Prieta (Q_0 = 176, η = 0.6)	6.9	73.7
Landers (Q_0 = 371, η = 0.6)	7.19	40.7
Little Skull Mountain (Q_0 = 256, η = 0.47)	5.7	63.7

Source: Silva et al. (1996 [DIRS 110474], Tables 4.2, 4.3, 4.4, 5.22, and 5.34)

7.3.4.2.2 Inversion Results

The results indicate significant regional differences in Q(f) and kappa values between the North Coast and the two southern California provinces (i.e., the Peninsular Ranges and Mojave) (Silva et al. 1996 [DIRS 110474], Table 4.1). The North Coast appears to exhibit more deep crustal damping (lower Q[f]) as well as more shallow crustal and site damping (higher kappa values). The Mojave is least attenuating, particularly as reflected in soft-rock kappa values, and this is consistent with generally higher shallow crustal V_S values. Values of the parameter, η, for regional attenuation are quite distinct between northern and southern California, but there is significant coupling between Q_0 and η, probably resulting in highly non-unique results. As a result, Silva et al. (1996 [DIRS 110474], Section 4) fixed η at 0.6 and the resulting Q_0 values were considered the most reliable. The average Q_0 for the North Coast and Peninsular Ranges is about 200, close to the traditional value of 150 (Boore 1986 [DIRS 103318]).

For the Peninsular Range and North Coast provinces, soft-rock kappa values were determined to be 0.05 sec and 0.06 sec, respectively (Table 7-9). These values are in reasonable agreement with the 0.03 sec and 0.06 sec values obtained by Silva and Darragh (1995 [DIRS 105398]) in fitting response spectral shapes for data from limited number of sites for the San Fernando and Loma Prieta earthquakes, respectively. For the Mojave province, the kappa resulting from the regional inversion with η fixed at 0.6 is 0.03 sec for rock sites, the same value obtained from fits to response spectral shapes for rock site data from the Landers earthquake (Silva and Darragh 1995 [DIRS 105398]).

In the second round of inversions, the 1979 Imperial Valley earthquake (Silva et al. 1996 [DIRS 110474], Section 5.6) and the 1992 Little Skull Mountain earthquake (Silva et al. 1996 [DIRS 110474], Section 5.10) were analyzed. Q(f) and **M** were held constant at the values indicated in Table 7-8.

For the Imperial Valley earthquake, in addition to the mainshock, a **M** 5.3 aftershock was also included in the inversion. The crustal profile is taken from Liu and Helmberger (1985 [DIRS 163921]), but modified over the upper 98 m (320 ft) based on a smoothed version of a profile by Bycroft (1980 [DIRS 163497]). For rock sites, the generic soft-rock velocity profile replaces the upper 2.4 km (1.5 mi). Smooth mean transfer functions are used to incorporate appropriate amplification for the rock and soil sites. Inversion results indicated a stress drop of 23.2 bars.

Table 7-9. Regional Inversion Determinations of Crustal Q(f) and Average Kappa Values

Region	Number of Stations*	Q_o	η	κ(sec) Rock	κ(sec) Soil
Peninsular Range (Northridge, San Fernando, and Whittier Narrows)	221	264	0.60**	0.051	0.056
North Coast (Loma Prieta, Coyote Lake, and Morgan Hill)	92	176	0.60**	0.059	0.072
Mojave (Landers and North Palm Springs)	86	371	0.60**	0.030	0.056
Combined***	399	291	0.60**	0.051	0.060

Source: Silva et al. (1996 [DIRS 110474], Table 4.1)

NOTE: *number of sites for each inversion is 2 (rock and soil)
** Values held fixed
***V_S = 3.50 km/sec (9800 ft/sec), density = 2.7 g/cm^3 (170 pcf), crossover distance = 60 km (37 mi)
Starting values Q_o = 150, η = 0.60, κ = 0.040 sec

For the Little Skull Mountain earthquake, the two largest aftershocks were included in the inversion to help constrain kappa values at common sites. The crustal profile is based on a regional earthquake location model refined at the near surface by shallow geophysical data (Silva et al. 1996 [DIRS 110474], Section 5.10). A smooth transfer function is used to model the amplification from the source at 12 km to the surface. Inversion results indicated a stress drop of 63.7 bars and an average kappa value of 0.023 sec, a value significantly below the average WNA kappa value of 0.04 (Silva and Darragh 1995 [DIRS 105398]).

7.3.4.3 Earthquake-Specific Evaluations

As an illustration of the success of the combined RVT point-source and RVT equivalent-linear site-response modeling approaches, the modeling results from Silva et al. (1996 [DIRS 110474], Section 5) for five earthquakes are summarized in this section. The five earthquakes include four that were associated with nonlinear site response at some stations and the Little Skull Mountain earthquake because of its proximity to Yucca Mountain.

7.3.4.3.1 1979 Imperial Valley Earthquake

The analyses for the 1979 Imperial Valley earthquake include data from 33 soil and 2 rock sites, covering the distance range of about 1 to 50 km (1 to 30 mi) (Silva et al. 1996 [DIRS 110474], Section 5.6). The crustal and site velocity profile used for soil sites is from Liu and Helmberger (1985 [DIRS 163921]) (Table 7-10) with the top 98 m (320 ft) replaced by a smoothed version of the El Centro profile (Bycroft 1980 [DIRS 163497]). This shallow portion of the profile is based on downhole borehole measurements taken at the old El Centro strong motion site (near E09). For the 2 rock sites, the shallow generic soft-rock profile (see Section 7.3.4.1.1) replaces the top 2.4 km (1.5 mi) of the Imperial Valley profile where the V_S reaches 1.0 km/sec (3300 ft/sec). This velocity occurs at a depth of about 100 ft (34 m) in the generic soft-rock profile.

Table 7-10. Imperial Valley Velocity Profile

Thickness (m)	V_S (m/sec)	Density (g/cm^3)
1.524	121.92	1.52
1.129	137.16	1.52
1.129	137.16	1.52
1.829	152.40	1.52
1.890	152.40	1.52
2.286	176.79	1.52
2.286	176.79	1.52
2.286	198.12	1.52
2.286	198.12	1.52
2.286	220.98	1.52
2.286	220.98	1.52
2.591	236.22	1.52
2.591	236.22	1.52
2.412	259.08	1.52
2.413	259.08	1.52
2.412	271.28	1.52
2.413	271.28	1.52
2.615	288.75	1.52
2.615	288.75	1.52
2.615	303.48	1.52
2.615	303.48	1.52
2.615	313.89	1.52
2.615	313.89	1.52
2.857	327.30	1.52
2.858	327.30	1.52
2.857	338.27	1.52
2.858	338.27	1.52
2.857	349.25	1.52
2.858	349.25	1.52
3.048	363.88	1.52
3.048	363.88	1.52
3.048	373.73	1.52
3.048	373.73	1.52
3.048	386.73	1.52
3.048	386.73	1.52
3.230	395.73	1.52
3.230	395.73	1.52
3.230	400.00	1.52
3.230	400.00	1.52
4.765	400.00	1.52
5.250	400.00	1.52

Thickness (m)	V_S (m/sec)	Density (g/cm^3)
5.250	400.00	1.52
5.250	400.00	1.52
5.250	400.00	1.52
5.250	400.00	1.52
5.250	400.00	1.52
5.250	400.00	1.52
5.250	400.00	1.52
5.250	400.00	1.52
5.250	400.00	1.52
26.25	400.00	1.52
26.25	400.00	1.52
26.25	500.00	1.56
26.25	500.00	1.56
26.25	500.00	1.56
26.25	500.00	1.56
26.25	600.00	1.61
78.75	600.00	1.61
105.00	700.00	1.74
105.00	800.00	1.85
105.00	900.00	1.89
105.00	1000.00	1.94
105.00	1150.00	2.03
105.00	1300.00	2.15
339.00	1500.00	2.26
480.00	1640.00	2.36
160.00	1740.00	2.39
160.00	1910.00	2.44
160.00	2080.00	2.48
160.00	2150.00	2.50
640.00	2220.00	2.52
160.00	2300.00	2.55
160.00	2500.00	2.60
160.00	2710.00	2.63
2271.00	2750.00	2.65
5000.00	3400.00	2.75
10000.00	4100.00	2.80
0.00	4500.00	3.20

Source: Silva et al. (1996 [DIRS 110474], Table 5-20)

NOTE: To convert m to ft or m/sec to ft/sec, multiply by 3.281. To convert g/cm^3 to pcf, multiply by 62.4

Nonlinearity modeled by the equivalent-linear site-response model is permitted to a depth of 500 ft (132 m) in both the rock and soil profiles. For the soil sites, the V_S at 500 ft is only 1,312 ft/sec and, with this stiffness, considerable nonlinear response would be expected at even greater depths under the loading conditions (over 0.5 g at some soil sites) associated with the 1979 event. However, based on the validations, permitting nonlinearity to occur at greater depths, resulted in a general high frequency (≥ 3 Hz) positive bias or underprediction ranging from about 10 to 30 percent.

For the rock sites, Silva et al. (1996 [DIRS 110474], Section 5.6) used a set of generic soft-rock normalized shear modulus and hysteretic damping curves developed as part of their study (Silva et al. 1996 [DIRS 110474], Section 6.2.3). For the soil sites, analyses with the EPRI (1993a [DIRS 103319], Section 6.3.4) and generic deep-soil curves showed too much nonlinear response and, thus, a separate set of curves was also developed (Silva et al. 1996 [DIRS 110474], Section 5.3.2). Since the Imperial Valley soils generally consist of clays having classifications ranging from CL to CH and silty dense sands to at least 400 ft, it is not surprising that the curves for cohesionless soils appeared to be inappropriate. Source, path and site parameters are shown in Table 7-11.

Table 7-11. Imperial Valley Earthquake Source, Path, and Site Parameters Used in Model Validation

M 6.4
$\Delta\sigma$ bars = 23.2
Q_0 = 264, η = 0.60 (Peninsular Range)
Point Source Depth = 8 km (5 mi)
Crustal Model: Liu and Helmberger (1985 [DIRS 163921]) and Bycroft (1980 [DIRS 163497])
Rock Site Parameters
Nonlinear Zone: 500 ft
κ = 0.02 sec: material below nonlinear zone, V_S = 1,312 ft/sec
κ = 0.03 sec: total, small strain
Normalized Shear Modulus and Damping Curves: generic soft rock
Soil Site Parameters
Nonlinear Zone: 500 ft
κ = 0.02 sec: below nonlinear zone, V_S = 3,773 ft/sec
κ = 0.03 sec: total, small strain
Normalized Shear Modulus and Damping Curves: Imperial Valley

Source: Silva et al. 1996 [DIRS 110474], Table 5.21

Figure 7-25 shows the point-source/site-response model bias and variability plots computed over all 35 sites. The bias is low from about 0.2 Hz (the lower limit of the data) to 100 Hz. The variability also is low and is fairly uniform at about 0.5 over most of the frequency range (Figure 7-25). Considering just the 33 soil sites, the bias is less positive and the variability has dropped slightly indicating a general improvement (Figure 7-26). The 2 rock sites (CPR and SUP) are poorly fit with large underpredictions. Comparisons of the observed and predicted spectra are shown in Figure 7-27. For the soil sites, the predicted spectra provide a reasonably

good match to the recorded motions with the exception of site DTA, which also shows a large and broadband underprediction.

Sites EMO and E07 (Figure 7-27a) show a mismatch in the spectral peaks between the simulations and recorded motions indicating too little nonlinear response in the equivalent-linear analyses. These 2 sites appear to have undergone the greatest degree of nonlinear response and the derived normalized shear modulus and hysteretic damping curves are probably too linear for these sites. However, for the remaining sites, the computed motions appear to capture the shapes and overall levels of the recorded motions reasonably well. The spectral peaks for the other close-in sites (E06, AEP, AGR, and EOS) are near 0.2 sec in both the recorded and simulated motions (Figure 7-27a).

7.3.4.3.2 1989 Loma Prieta Earthquake

For the 1989 **M** 6.9 earthquake, Silva et al. (1996 [DIRS 110474], Section 5.3.1) modeled a total of 53 sites covering the fault distance range from about 5 to 90 km (3 to 56 mi). There were 33 rock and 20 oil sites. Most of the rock sites are located beyond about 30 km (20 mi) (20 sites) whereas most of the soil sites (17) are "close-in" or within about 30 km (20 mi) of the source.

The crustal velocity profile used by Silva et al. (1996 [DIRS 110474], Section 5.3.1) was modified from Wald et al. (1991 [DIRS 164086]). To model rock and soil sites, the generic soft-rock or deep-soil profile was placed on top of the regional crustal profile. The shallow generic soft-rock profile was truncated at velocities exceeding 1.0 km/sec (3300 ft/sec), the velocity of the top layer of the crustal profile (Table 7-12). Both the rock and soil sites were allowed to exhibit nonlinear response to depths of 500 ft. For the rock sites, the generic soft-rock normalized shear modulus and hysteretic material damping curves were used. For the soil sites, the EPRI (1993a [DIRS 103319], Section 6) cohesionless soil curves were used.

Table 7-12. Loma Prieta Crustal Profile

Thickness (km)	V_S (km/sec)	Density (g/cm^3)
0.1	1.00	2.00
0.4	1.95	2.30
0.5	2.48	2.35
2.0	2.77	2.35
2.0	3.10	2.35
2.0	3.31	2.45
2.0	3.55	2.58
4.0	3.61	2.62
5.0	3.62	2.63
7.0	3.85	2.77
	4.62	3.28

Source: Silva et al. 1996 [DIRS 110474], Table 5-7

NOTE: To convert km to mi, multiply by 0.621. To convert km/sec to ft/sec, multiply by 3281. To convert g/cm^3 to pcf, multiply by 62.4

Table 7-13. Loma Prieta Earthquake Source, Path, and Site Parameters Used in Model Validation

M 6.9
$\Delta\sigma$ bars = 73.7
Q_0 = 176, η = 0.60
Point-Source Depth = 12 km (7.3 mi)
Crustal Model: Modified from Wald et al. (1991 [DIRS 164086])
Rock Site Parameters
Nonlinear Zone: 500 ft
κ = 0.03 sec: rock below nonlinear zone, V_S = 3,281 ft/sec
κ = 0.04 sec: total, small strain
Normalized Shear Modulus and Damping Curves: generic soft rock
Soil Site Parameters
Nonlinear Zone: 500 ft
κ = 0.03 sec: below nonlinear zone, V_S = 3,281 ft/sec
κ = 0.04 sec: total, small strain
Normalized Shear Modulus and Damping Curves: EPRI

Source: Silva et al. 1996 [DIRS 110474], Table 5.8

The kappa value for the rock beneath the nonlinear zones at both rock and soil sites was taken as 0.03 sec (Table 7-13). This value was selected to give a total kappa (including nonlinear zone small strain damping) of about 0.04 sec, a value consistent with the empirical inversions at low levels of loading. The point-source depth is taken as 12 km (7.5 mi), the depth of the largest asperity in the Wald et al. (1991 [DIRS 164086]) slip model.

The model bias and variability estimates for the combined RVT point-source/RVT equivalent-linear site-response model, computed over all the 53 sites are shown in Figure 7-28. The bias is generally near zero (within the 90 percent confidence interval) between about 1 to 20 Hz and shows a slight underprediction at higher frequencies (equivalent to peak acceleration). The negative bias at low frequencies (< 1 Hz) is a manifestation of the general tendency for the point-source model component to overpredict over the low frequency range at large magnitudes. The model variability is about 0.5 above 2 Hz and rises significantly below 2 Hz, reflecting unmodeled low frequency site variations as the bias is near zero.

To compare site effects, Figures 7-29 and 7-30 show analogous plots for soil and rock sites, respectively. For the 20 soil sites, model bias is nearly constant for frequencies above about 1 Hz (Figure 7-29) and lower than for rock sites. For the rock sites, model bias shows a broad peak of about 0.3 (factor of about 1.4) at intermediate frequencies (about 1 to 5 Hz) and a general underprediction of about 0.2 (natural log) at very high frequencies. Silva et al. (1996 [DIRS 110474], Section 5.3.1) suggest that much of this positive bias may be due to just 5 sites with very high motions: PRS, CFH, BRK, CGB, and PTB. These are all rock sites at distances beyond about 70 km (40 mi). For these sites, comparison of response spectra for data (log average of 2 horizontal components) and model predictions shows recorded motions exceed the model predictions by a factor of over 3 at some periods (Figure 7-31). Recorded motions are very high at these sites, but other nearby rock sites, such as YBI, PHT, and TLH, reflect closer to

expected levels (about 0.05g) suggesting strong localized effects (Silva et al. 1996 [DIRS 110474], Section 5.3.1).

7.3.4.3.3 1992 Landers Earthquake

For the 1992 **M** 7.2 Landers earthquake, a total of 57 sites are modeled: 52 soil and 5 rock (Silva et al. 1996 [DIRS 110474], Section 5.4.1). The fault distance range is about 1 km (1 mi) to nearly 180 km (110 mi). The sites extend from the Mojave desert into the Los Angeles Basin to the west. The crustal profile is from Wald and Heaton (1994b [DIRS 164085]) and is listed in Table 7-14. To model rock and soil sites, the generic soft-rock or deep-soil profile was placed on top of the regional crustal profile. The shallow generic soft-rock profile was truncated at velocities exceeding 1.98 km/sec (6500 ft/sec), the velocity of the top layer of the Wald and Heaton (1994b [DIRS 164085]) Landers crust (Table 7-14).

Both the rock and soil sites were allowed to exhibit nonlinear response to depths of 500 ft. For the rock sites, the generic soft rock normalized shear modulus and hysteretic material damping curves were used. For the Mojave soil sites, the EPRI cohesionless soil curves were used as not enough soil sites are available having sufficiently high motions to discriminate between EPRI and the generic deep-soil curves. For the Peninsular Range soil sites, the generic deep-soil curves were used along with the Northridge crustal profile (Wald and Heaton 1994a [DIRS 164084]).

Table 7-14. Landers Crustal Profile

Thickness (km)	V_S (km/sec)	Density (g/cm^3)
1.5	1.98	2.30
2.5	3.15	2.60
22.0	3.52	2.70
6.0	3.83	2.87
	4.50	3.10

Source: Silva et al. 1996 [DIRS 110474], Tabl e 5-13; Wald and Heaton 1994b [DIRS 164085]

NOTE: To convert km to mi, multiply by 0.621. To convert km/sec to ft/sec, multiply by 3281. To convert g/cm^3 to pcf, multiply by 62.4

Table 7-15. Landers Earthquake Source, Path, and Site Parameters Used in Model Validation

M 7.2
$\Delta\sigma$ bars = 40.7
Q_0 = 371, η = 0.60
Point-Source Depth = 8 km (5 mi)
Crustal Model: Wald and Heaton (1994b [DIRS 164085]) Landers
Rock Site Parameters
Nonlinear Zone: 500 ft
κ = 0.02 sec: rock below nonlinear zone, V_S = 6,496 ft/sec
κ = 0.03 sec: total, small strain
Normalized Shear Modulus and Damping Curves: generic soft rock
Soil Site Parameters
Nonlinear Zone: 500 ft
κ = 0.02 sec: below nonlinear zone, V_S = 6,496 ft/sec

κ = 0.03 sec: total, small strain
Normalized Shear Modulus and Damping Curves: EPRI, Mojave soil; generic deep soil, Peninsular Range soil

Source: Silva et al. 1996 [DIRS 110474], Table 5.14

The kappa values for the hard-rock beneath the nonlinear zones (500 ft, Table 7-15) at both rock and Mojave soil sites is taken as 0.02 sec. This gives a total kappa value of 0.03 sec for Mojave rock and soil sites. For Peninsular Range soil sites, the hard-rock kappa value is 0.02 sec for a total small strain kappa of 0.03 sec**.** The point-source depth is taken as 8 km (5 mi), the depth of the largest asperity in the Wald and Heaton (1994b [DIRS 164085]) slip model.

For the RVT point-source/RVT equivalent-linear site-response model, the bias and variability plots are shown in Figure 7-32 for all the sites. Over most of the frequency range, the bias reflects a general underprediction, particularly at low frequency (around 1 Hz). The peaks and troughs are related to the profile resonances with a trough in bias reflecting a profile resonance peak. The variability is generally low, below 0.5, above 1 Hz and shows the typical increase at low frequency due to unmodeled site variations. In general, the RVT point-source/RVT equivalent-linear site-response model is capable of surprisingly accurate ground motion predictions for a **M** 7.2 extended rupture and for distances out to nearly 200 km (120 mi) (Silva et al. 1996 [DIRS 110474], Section 5.4.1).

Because there are only 5 rock sites out of 57 total sites, separate plots are not shown for rock site and soil sites analyses. To examine more closely the positive bias (underprediction) shown over all the sites (Figure 7-32), separate bias and variability estimates are shown for the Peninsular Range sites and Mojave sites alone (Figures 7-33 and 7-34, respectively). Results for the Peninsular Range sites (39 sites, beginning with site POM at about 120 km [75 mi]) show a much more positive bias, except around 3 to 20 Hz where the bias is considered low (Figure 7-33). The increase in bias estimates at very high frequency, above 20 Hz actually reflects peak ground acceleration and is controlled by much lower frequencies, in the range where the response spectral accelerations peak over these distances, 100 to 200 km (60 to 120 mi). The model bias then shows a large low frequency ($\leq$ 3 Hz) underprediction averaging about 0.5, a factor of about 1.6. This low frequency underprediction is apparent in the spectral plots (Figure 7-35), especially for the very distant sites beyond about 150 km (93 mi) (Figures 7-35d and 7-35e) and may be due to unmodeled development of basin waves.

For the Mojave Province sites, ranging in distance from about 1 to 100 km (1 to 60 mi), the bias estimates are near zero above 1 Hz and show the typical point-source overprediction below 1 Hz (Figure 7-34). The variability is low, about 0.5 above 0.5 Hz, suggesting that the model is performing quite well on average out to 100 km (60 mi) (Silva et al. 1996 [DIRS 110474], Section 5.4.1).

Comparison of predicted and observed response spectra (Figure 7-35) shows that the model simulations do very well within about 100 km (60 mi) and begin to seriously underpredict (at low frequency) beyond. Interestingly, site LUC, at a fault distance of about 2 km (1 mi) from an 80 km-long (50 mi-long) rupture is modeled very well by the simple point-source for periods as long as 10 sec (Figure 7-35a).

7.3.4.3.4 1992 Little Skull Mountain Earthquake

The 1992 **M** 5.7 Little Skull Mountain earthquake occurred about 20 km (10 mi) southeast of the Yucca Mountain site. The event was recorded at 8 sites (all rock) spanning the distance range of 13 to 98 km (8 to 61 mi). The crustal profile used in modeling is listed in Table 7-16 and consists of a shallow stiff tuff layer 40 m (130 ft) thick overlying much more competent materials. The shallow tuff, with V_S around 2,000 ft/sec, would be expected to exhibit some nonlinear response at high levels of loading (about 0.30 g). For the Little Skull Mountain earthquake, the highest peak acceleration is about 0.2 g, and, as a result, Silva et al. (1996 [DIRS 110474], Section 5.10) used linear analyses. Thus, while these results provide a 1D validation for an earthquake in the vicinity of Yucca Mountain, the validation does not exercise the equivalent-linear aspect of the site response model. The source parameters for modeling are listed in Table 7-17.

Table 7-16. Little Skull Mountain Crustal Profile

Thickness (km)	V_S (km/sec)	Density (g/cm^3)
0.04	0.6	1.70
0.04	1.2	2.00
0.14	1.5	2.30
0.60	2.1	2.40
0.78	1.9	2.40
1.50	2.9	2.40
2.20	3.4	2.50
10.70	3.5	2.75
16.00	3.8	2.90
	4.6	3.30

Source: Silva et al. 1996 [DIRS 110474], Table 5.32

NOTE: To convert km to mi, multiply by 0.621. To convert km/sec to ft/sec, multiply by 3281. To convert g/cm^3 to pcf, multiply by 62.4

Table 7-17. Little Skull Mountain Earthquake Source, Path, and Site Parameters Used in Model Validation

M 5.7
$\Delta\sigma$ bars = 63.7
Q_0 = 256, η = 0.47
Point Source Depth = 12 km (7.5 mi)
Crustal Model: Modified Regional
Rock Site Parameters
Nonlinear Zone: Rock, linear analysis (low levels of motion $\leq$ 0.20 g)
κ = site specific from inversion, V_S = 1,969 ft/sec
Soil Site Parameters
No soil sites

Source: Silva et al. 1996 [DIRS 110474], Table 5.33

Model bias and variability estimates were computed over all 8 sites (Figure 7-36). The 90 percent confidence interval is wide due to the small number of sites. The bias shows the typical low frequency point-source overprediction ranging from about -1 at 0.5 Hz (the lower limit of reliable analyses is about 0.2 Hz) and increasing to near zero around 5 Hz. The variability is low above 10 Hz and about 0.5 from about 2 to 10 Hz. Below 2 Hz, it is very high but the randomness (bias corrected variability) remains nearly uniform: most of the sites have a large misfit from 0.2 to 2 Hz that is constant in sign. This is easily seen in the response spectra plots (Figure 7-37). The model is doing generally well at short period (~ 0.5 sec), overpredicting at longer periods, and converging to the recorded motions at long periods (>1 sec) as the high-pass filter corners are approached.

7.3.4.3.5 1994 Northridge Earthquake

For the 1994 **M** 6.7 Northridge earthquake, Silva et al. (1996 [DIRS 110474], Section 5.2.1) modeled a total of 94 sites are modeled: 71 soil and 23 rock. The fault distance range is from about 7 km (4 mi) (sites over the rupture surface have zero horizontal distance) to nearly 150 km (93 mi). The sites extend from the San Fernando Valley into the Los Angeles Basin to the south and to the San Andreas fault to the north and east. The crustal profile is from Wald and Heaton (1994a [DIRS 164084]) and is listed in Table 7-18. To model rock and soil sites, the generic rock or soil profile is placed on top of the regional crustal profile. The shallow generic rock profile is truncated at velocities exceeding 1.0 km/sec (3300 ft/sec), the velocity of the top layer of the Wald and Heaton (1994a [DIRS 164084]) Northridge crustal profile. Both the rock and soil sites are allowed to exhibit nonlinear response to depths of 500 ft (Table 7-19). For the rock sites, the generic soft-rock normalized shear modulus and hysteretic material damping curves are used. The kappa values for the rock beneath the nonlinear zones at both rock and soil sites is taken as 0.03 sec (Table 7-19). This value was selected to give a total kappa (including nonlinear zone small strain damping) of about 0.04 sec.

The RVT point-source/RVT equivalent-linear site-response model bias computed over all 94 sites is generally near zero between about 1 to 20 Hz and shows a slight underprediction at higher frequencies (equivalent to peak acceleration) (Figure 7-38). The strong negative bias at low frequencies (< 1 Hz) is a manifestation of the general tendency for the point-source modeling approach to overpredict over the low frequency range at large magnitudes. The dip in the bias estimates starting at 10 Hz is where the 5%-damped pseudo-absolute response spectral acceleration is beginning to saturate to peak ground acceleration. The response spectra generally are decreasing with increasing frequency (Figure 7-39) and reach full saturation around 30 Hz where the bias estimates become constant with increasing frequency. Over this relatively constant portion, the bias plots reflect the behavior of peak ground acceleration, which is actually controlled by lower frequencies, in the 2 to 6 Hz range, where the spectral acceleration peaks.

Table 7-18. Northridge Crustal Profile

Thickness (km)	V_S (km/sec)	Density (g/cm^3)
0.5	1.0	2.1
1.5	2.0	2.3
2.5	3.2	2.5
23.0	3.6	2.6
5.0	3.9	2.9
	4.5	3.0

Source: Wald and Heaton 1994a [DIRS 164084]

NOTE: To convert km to mi, multiply by 0.621. To convert km/sec to ft/sec, multiply by 3281. To convert g/cm^3 to pcf, multiply by 62.4

Table 7-19. Northridge Earthquake Source, Path, and Site Parameters Used in Model Validation

M 6.7
$\Delta\sigma$ bars = 62.9
Q_0 = 264, η = 0.60
Point-Source Depth = 11 km (6.8 mi)
Crustal Model: Wald and Heaton (1994a [DIRS 164084])
Rock Site Parameters
Nonlinear Zone: 500 ft
κ = 0.03 sec: rock below nonlinear zone, V_S = 3,281 ft/sec
κ = 0.04 sec: total, small strain
Normalized Shear Modulus and Damping Curves: generic soft rock
Soil Site Parameters
Nonlinear Zone: 500 ft
κ = 0.03 sec: below nonlinear zone, V_S = 3,281 ft/sec
κ = 0.04 sec: total, small strain
Normalized Shear Modulus and Damping Curves: generic deep soil

Source: Silva et al. 1996 [DIRS 110474], Table 5.4

The model variability is about 0.5 about 1 Hz and rises significantly at below 1 Hz reflecting the stable point-source low-frequency overprediction (Figure 7-38). The bias corrected variability (randomness) is significantly lower over this frequency range due to the large statistically significant negative bias estimates. The randomness estimates provide a minimum estimate of model variability and represent the reduction in variability (total randomness) achievable with the model provided the ground motion estimates are corrected for the low frequency overprediction.

To compare rock and soil site effects, Figures 7-40 and 7-41 show analogous plots for soil and rock sites, respectively. Results for the 71 soil sites, are similar to those for the combined estimates due to the greater number of soil sites (71 soil verses 23 rock sites) (Figure 7-40). For the rock sites, a broad peak of about 0.4 (factor of about 1.5) at intermediate frequencies (about 2-3 Hz) and a general underprediction of about 0.25 (natural log) at high frequencies is observed (Figure 7-41). Approximately 25 percent of this positive bias is due to just two sites with very high motions: PUL (Pacoima Upper Left) (Figure 7-39a) and ORR (Castaic Old Ridge Route) (Figure 7-39c). Figure 7-39 shows the 5%-damped pseudo absolute response spectra, data (log

average of 2 horizontal components) and model predictions. The recorded motions exceed the model predictions by a factor of over 3 at some periods (less than about 2 sec). The recorded motions for the San Fernando earthquake are very high at these sites as well, suggesting strong site effects.

7.3.4.3.6 Combined Results

In addition to evaluating the model bias and variability for individual earthquakes, Silva et al. (1996 [DIRS 110474], Section 5.12) also determined bias and variability for the combined data set of 16 earthquakes. Over all the sites (Figure 7-42) the bias of the RVT point-source/RVT equivalent-linear site-response model is slightly positive for frequencies greater than about 10 Hz and is near zero from about 10 Hz to 1 Hz. Below 1 Hz, the negative bias indicates the model overpredicts the response spectra. The analyses are considered reliable down to about 0.3 Hz where the model shows about a 40 percent overprediction. Elimination of the overprediction when a RVT finite-source model is coupled with the RVT equivalent-linear site-response model (Silva et al. 1996 [DIRS 110474], Section 5.12) suggests that the low-frequency overprediction is a result of the RVT point-source component of the model, not the RVT equivalent-linear site-response component. This stable misfit may be interpreted as the presence of a second corner frequency due to source finiteness for WNA sources (Atkinson and Silva 1997 [DIRS 163171]).

For the combined data set, model variability is low, about 0.5 above about 3 to 4 Hz and increases with decreasing frequency to near 1 at 0.3 Hz (Figure 7-42). Above 1 Hz, there is little difference between the total variability and randomness (bias corrected variability), reflecting the near zero bias estimates. Below 1 Hz there is considerable randomness contributing to the total variability.

When only soil sites are considered (Figure 7-43), model bias and variability improve slightly at 1 Hz and above. This indicates that the rock sites (Figure 7-44) must reflect the converse showing larger bias and variability estimates than the results for all the sites. Soil sites are modeled more accurately than rock sites. This suggests that strong ground motions at rock sites are more variable than motions at soil sites and the model is not capturing the increased site-to-site variation. The larger rock site bias above 10 Hz suggests a small stable underprediction possibly due to the use of a single smooth rock profile rather than randomizing the profile and using a mean spectrum. The larger variability and bias in the rock site simulations compared to those for the deep soil sites are likely due to a larger variation or wider range in rock site velocity profiles (Silva et al. 1996 [DIRS 110474], Section 5). Typically, the rock site category includes very stiff unweathered to slightly weathered rock outcrop to shallow soil, about 10 to 70 ft of soil overlying rock. Use of a single generic rock site profile likely reflects a poorer representation of the range in rock profiles than a single generic soil profile.

Five earthquakes form the study by Silva et al. (1996 [DIRS 110474]) were modeled. To support the validation of the RVT equivalent-linear site-response model. While this validation does not assess the performance of the RVT linear-equivalent site-response model by itself, validation of the combined RVT point-source/RVT equivalent-linear site-response modeling approaches adds confidence that the site-response component is providing valid results.

7.3.5 Comparison of Equivalent-Linear and Nonlinear Modeling Approaches for the Port Island, Kobe, Japan Vertical Array Site

This section describes the results of the confirmation study that compares the results of 1-D site response analysis using equivalent-linear and nonlinear models for a strong motion vertical array site (Wong and Silva 2004c [DIRS 170446]). The strong motion vertical array at Port Island, Kobe, Japan, experienced liquefaction as a result of the January 17, 1995 Kobe earthquake (**M** 6.9). This site was only 4 km from the surface projection of the rupture (Chung et al. 1996 [DIRS 171465]). The shear strains inferred from the strong motion recordings are the largest available for a vertical array site and exceed the shear strains developed for the Yucca Mountain post-closure design motions.

7.3.5.1 Port Island Vertical Array Site

The Port Island, Kobe, Japan vertical array site was subjected to strong ground shaking (peak horizontal acceleration of 0.3 g) and its soils liquefied during the 1995 **M** 6.9 Kobe earthquake. Soil layer thickness, soil type, depth of the water table, densities, unit weight and shear-wave and compression-wave velocity data are taken from "Liquefaction of Reclaimed Island in Kobe, Japan" (Elgamal et al. 1996 [DIRS 163503]) and are provided in Table 7-20. The vertical array site is characterized by 19m of decomposed granite fill overlying layers of gravels and interbedded sands and clays. The vertical array of three-component accelerometers recorded the earthquake at the surface and at depths of 16, 32 and 83m. Acceleration time histories of the horizontal components at ground surface and 83m-depth are illustrated in Figure 7-45. As noted by Chung et al. (1996 [DIRS 171465]), the surface motions exhibit markedly reduced high frequency motions as compared to the recordings at depth. Surface motions also exhibited amplifications at longer periods. Ground motions recorded at the surface and 83m-depth were modeled. A representative soil boring from Port Island with blow counts and some undrained shear strength values is shown on Figure 7-46 (Chung et al. 1996 [DIRS 171465]). A set of six modulus reduction and damping values used in the SHAKE and RASCALS analyses are provided in Tables 7-21 through 7-26 and these curves are also presented on Figure 7-47 (Wong and Silva, 2004c [DIRS 170446]).

Table 7-20. Soil Model For Port Island Station

Depth (m)	Soil Type	Location of Accelero-meters	Vp (km/s)	Vs (km/s)	ρ (gm/cm^3)	Unit Weight (kcf)	Curve No.*
0 – 2.0	Decomposed Granite Fill^R	PR4 - 0m	0.260	0.170	1.95	0.122	1
2.0 – 5.0			0.330	0.170	1.95	0.122	1
5.0 – 12.6			0.780	0.210	1.95	0.122	1
12.6 – 19.0	Sandy Gravel^R	PR3 – 16M	1.480	0.210	1.95	0.122	2
19.0 – 27.0	Clay		1.180	0.180	1.50	0.094	3
27.0 – 33.0	Sand	PR2 – 32M	1.330	0.245	1.925	0.120	4
33.0 – 50.0	Sandy Gravel and Sand		1.530	0.305	1.925	0.120	4
50.0 – 61.0	Sand		1.610	0.350	1.925	0.120	4
61.0 – 79.0	Clay		1.610	0.303	1.75	0.109	5
79.0 – 82.0	Sandy Gravel		2.000	0.320	1.75	0.109	6

Depth (m)	Soil Type	Location of Accelero-meters	Vp (km/s)	Vs (km/s)	ρ (gm/cm^3)	Unit Weight (kcf)	Curve No.*
82.0 - 85.0	Sandy Gravel	PR1 – 83M	2.000	0.320	1.925	0.120	6

Source: Wong and Silva 2004c [DIRS 170446], page 13

NOTES: ^{R} Reclaimed land
*Curve No.: Modulus Reduction and Damping Curve (see Tables 7-21 through 7-26)
Water Table: 5m

Table 7-21. Dynamic Material Property Curves: Set 1

Shear Strain (%)	Normalized Shear Modulus (G/Gmax)	Material Damping Ratio (%)
0.0001	1.0	1.4
0.0003	0.9	1.6
0.0010	0.8	2.8
0.0032	0.6	5.0
0.0100	0.4	10.0
0.0316	0.3	15.5
0.1000	0.16	21.0
0.3162	0.1	30.0
1.0000	0.05	50.0
1.3162	0.03	50.0

Source: Wong and Silva 2004c [DIRS 170446], page 14

Table 7-22. Dynamic Material Property Curves: Set 2

Shear Strain (%)	Normalized Shear Modulus (G/Gmax)	Material Damping Ratio (%)
0.0001	1.0	1.2
0.0003	1.0	1.2
0.0010	0.99	1.4
0.0032	0.946	2.1
0.0100	0.82	3.6
0.0316	0.608	7.0
0.1000	0.36	12.4
0.3162	0.165	19.1
1.0000	0.06	24.9
1.3162	0.03	28.0

Source: Wong and Silva 2004c [DIRS 170446], page 14

Table 7-23. Dynamic Material Property Curves: Set 3

Shear Strain (%)	Normalized Shear Modulus (G/Gmax)	Material Damping Ratio (%)
0.0001	1.0	1.5
0.0003	1.0	1.5
0.0010	1.0	1.5
0.0032	0.99	1.8
0.0100	0.94	2.2
0.0316	0.82	3.3
0.1000	0.62	6.0
0.3162	0.39	10.3
1.0000	0.16	15.5
1.3162	0.05	24.0

Source: Wong and Silva 2004c [DIRS 170446], page 14

Table 7-24. Dynamic Material Property Curves: Set 4

Shear Strain (%)	Normalized Shear Modulus (G/Gmax)	Material Damping Ratio (%)
0.0001	1.0	1.0
0.0003	1.0	1.0
0.0010	1.0	1.2
0.0032	0.97	1.64
0.0100	0.87	2.8
0.0316	0.68	5.49
0.1000	0.43	10.2
0.3162	0.22	16.5
1.0000	0.09	22.9
1.3162	0.05	27.0

Source: Wong and Silva 2004c [DIRS 170446], page 15

Table 7-25. Dynamic Material Property Curves: Set 5

Shear Strain (%)	Normalized Shear Modulus (G/Gmax)	Material Damping Ratio (%)
0.0001	1.0	1.0
0.0003	1.0	1.0
0.0010	1.0	1.0
0.0032	1.0	1.0
0.0100	0.97	1.2
0.0316	0.9	2.0
0.1000	0.7	4.0
0.3162	0.47	8.0
1.0000	0.25	12.0
1.3162	0.15	18.0

Source: Wong and Silva 2004c [DIRS 170446], page 15

Table 7-26. Dynamic Material Property Curves: Set 6

Shear Strain (%)	Normalized Shear Modulus (G/Gmax)	Material Damping Ratio (%)
0.0001	1.0	0.8
0.0003	1.0	0.9
0.0010	1.0	1.0
0.0032	0.98	1.33
0.0100	0.9	2.2
0.0316	0.74	4.36
0.1000	0.5	8.6
0.3162	0.27	14.61
1.0000	0.12	21.2
1.3162	0.07	25.0

Source: Wong and Silva 2004c [DIRS 170446], page 15

7.3.5.2 Modeling Approaches

The analysis methods chosen for this study are two equivalent-linear models, RASCALS and SHAKE (Section 6.1.1), and two nonlinear models, TESS and SUMDES. A brief discussion of RASCALS, TESS and SUMDES is presented in Section 7.3.2.2. The equivalent-linear model SHAKE is described in Section 6.1.1.

The soil behavior due to cyclic loading is typically modeled using two approaches: equivalent-linear and nonlinear. The two main components of nonlinear analyses are a solution scheme for the wave equation and nonlinear soil model. Nonlinear soil models that have been primarily developed from laboratory test results and utilized in dynamic analyses include the Ramberg-Osgood model, an elasto-plastic model, the hyperbolic model and the Iwan-type model.

7.3.5.3 Validation Process

Input parameter values were selected based on the geotechnical data obtained for the Port Island site. The information is presented in Tables 7-20 through 7-26. While the geotechnical models may not be complete, it was felt that the nature, number, and types of tests performed are those typically available and represented an adequate basis for characterizing the dynamic response of the sites.

The process of conducting the comparative site response analysis involved parameter selection, initial analyses, and then a review of the comparisons of predicted and observed motions. No iterations of input parameters for SHAKE and RASCALS were required. Iterations were allowed for the nonlinear models, whichprovided an opportunity to correct any significant errors in assigning parameter values.

The intent was to perform, to the extent possible, a forward prediction at each site using measured material properties and implementing the analysis in a structured and consistent manner. The results provide a rational basis for evaluating how well the modeling approaches perform.

7.3.5.4 Results for Port Island Site

The results from the analysis using the equivalent-linear and nonlinear codes are summarized below.

7.3.5.4.1 Equivalent Linear Analysis

The results from the equivalent-linear analysis performed using SHAKE and RASCALS are presented on Figures 7-48 and 7-49, respectively. Over the entire frequency range there is an acceptable match to the observed response spectra. At most frequencies, both SHAKE and RASCALS exhibit a slight overprediction. The predicted spectra and time histories are very similar between SHAKE and RASCALS. Not unexpectedly, the high-frequency energy apparent at the onset off the observed motions is not contained in the predicted motions as the strain-compatible velocities are constant in time. The predicted PGA values are summarized in Table 7-27.

Table 7-27. Comparison of Peak Ground Accelerations Predicted Using SHAKE and RASCALS

	North Comp (g)	East Comp (g)
SHAKE	0.371 (18%)	0.362 (30%)
RASCALS	0.398 (26%)	0.332 (19%)
OBSERVED	0.315	0.278

Source: Wong and Silva 2004c [DIRS 170446], page 30

NOTE: (12%) - % difference between the observed and predicted values

7.3.5.4.2 Nonlinear Analysis

The results from the nonlinear analysis performed using TESS and SUMDES are presented on Figures 7-50 and 7-51, respectively. The north component prediction for TESS is a generally good fit to the observed spectra with a slight over-prediction between 7 and 30 Hz. The TESS prediction for the east component is generally good but introduces broad resonances at about 5 and 15 Hz. SUMDES response spectra predictions are generally good for both components. The changing high-frequency character of the time histories is also captured, especially on the north component. The predicted PGA values are summarized in Table 7-28. The predicted time histories for both nonlinear models (TESS and SUMDES) appear to best capture the features in the observed time histories.

Table 7-28. Comparison of Peak Ground Accelerations Predicted Using TESS and SUMDES

	North Comp (g)	East Comp (g)
SUMDES	0.321 (2%)	0.261 (6%)
TESS	0.275 (13%)	0.284(2%)
OBSERVED	0.315	0.278

Source: Wong and Silva 2004c [DIRS 170446], page 30

NOTE: (12%) - % difference between the observed and predicted values

In summary, the equivalent linear-model RASCALS assuming vertically-propagating S-waves models work well for the Port Island data. Both RASCALS and SHAKE adequately predicted the response spectra of both surface horizontal components for a site that liquefied and was only 4 km from the surface projection of the rupture surface of the earthquake. The shear strains for the shallow layers at Port Island exceeded those shear strains achieved in the Yucca Mountain postclosure evaluation (about 0.7%; Table 7-29). This modeling effort validates the use of RASCALS for the high shear strains developed for postclosure. Note that the soil models used in the predictions were developed in a "forward sense", that is iterations in the development of the soil model were not allowed. The equivalent-linear models RASCALS and SHAKE and the non-linear models TESS and SUMDES were all in good agreement with the observed Port Island spectra indicating that all these models work well at high strains of 1%. These comparisons meet the acceptance criteria stated in Section 7.2.5.

7.4 APPLICABILITY OF SITE RESPONSE VALIDATION MODELING APPROACHES TO YUCCA MOUNTAIN

Ideally, validation of the RVT equivalent-linear site-response model for Yucca Mountain would make use of site-specific validation studies for an appropriate range of ground motion levels and site conditions. However, the lack of strong ground motion recorded at Yucca Mountain, necessitates an appeal to validation of the modeling approach carried out at other locations. Successful validation of the modeling approach for a number of different earthquakes and sites, as discussed in Section 7.3, provides the needed confidence that the approach is appropriate for Yucca Mountain and, with the development of appropriate inputs, the Yucca Mountain site response model is also valid.

As described in Section 6.3, ground motions at Yucca Mountain are determined for the emplacement level (Point B) underlying about 300 m (1000 ft) of tuff and for rock and shallow soil (Point E) to deep soil (Point D) sites at the Surface Facilities Area. These sites have stiffnesses that range from soil-like to competent rock.

In developing confidence in the Yucca Mountain site response model based on validation at other locations, one key factor is the level of peak mean shear-strain reached in the site materials. Evaluation of this metric is more appropriate than consideration of initial stiffness or ground motion level in assessing applicability of validation studies to Yucca Mountain. Viewed from the perspective of strain, there is no essential difference between site-response analyses for rock and soil sites.

The most straightforward validation studies discussed in Section 7.3 are EPRI (1993b [DIRS 103320], Appendix 6.B) and the confirmation study using Kobe earthquake recordings. By using control motions from nearby rock sites or from at-depth sensors in a vertical array, ambiguity related to computation of control motions using an additional ground motion model is avoided. The sites modeled range from stiff to soft soil, and one (Gilroy #2) was characterized by a dipping interface that might be associated with 2D effects not explicitly included in the 1D model. In general, the results show that equivalent-linear and nonlinear modeling approaches produce similar ground motions and reasonable agreement to the observed data. For the one case (Treasure Island) in which agreement with the data is poorer, the outcome does not appear to be model dependent, but rather related to the inputs used or site conditions that were not modeled.

At Gilroy #2, the results suggest that, even for sites at which 2D effects are expected, the 1D approach does a good job of modeling the observed ground motions. Overall, the results provide a high level of confidence that the RVT equivalent-linear site-response model is a valid approach.

Shear-strains obtained in the EPRI (1993b [DIRS 103320], Appendix 6.B) validation study and those for the Yucca Mountain ground motion modeling described in Section 6 are summarized in Tables 7-29 and 7-30 as a basis for comparison. Mean peak shear-strains in the Yucca Mountain analyses exceed those for the EPRI (1993b [DIRS 103320], Appendix 6.B) validation study, but are at the same level as the vertical array recordings of the Kobe earthquake at Port Island. The EPRI study together with the Port Island confirmation study provide strong support for the validity of the RVT equivalent-linear site-response modeling approach for application to Yucca Mountain

Table 7-29. Yucca Mountain Peak Predicted Mean Shear-Strains

Frequency of Exceedance (yr-1)	Median Peak Shear-Strain (%)	Condition
$5x10^{-4}$	0.01	Alluvium
10^{-6}	0.25	Tuff
10^{-7}	0.66	Tuff

Source: Wong and Silva 2004a [DIRS 170443], p. 75

Table 7-30. Validation Model Approach and Peak Shear-Strains

Site	Peak Shear-Strain (%)	Condition
Gilroy #2	0.1	Sand/clay
Treasure Island	0.06	Sand/clay
Lotung	0.06	Silt/clayey silt
Port Island	1.00	Sand/gravel

Source: EPRI 1993b [DIRS 103320], Appendix 6.B; Wong and Silva 2004c [DIRS 170446], p. 32

As discussed in Sections 6.1.4 and 6.1.6, 2D and 3D effects, such as topographic amplification are not explicitly addressed in the site response modeling. Consistent with the state-of-the-practice, 2D/3D effects are implicitly included in modeling through use of control motions determined from the PSHA. That is 2D/3D effects including topographic amplification are contained in the aleatory variability about the Point A median attenuation relationships developed by the PSHA ground motion experts (CRWMS M&O 1998a [DIRS 103731], Section 6). U.S. strong motion recording databases (e.g., USGS), which form the bases for the empirical attenuation relationships considered by the experts, include records from sites that have been subjected to 2D and 3D ground motion effects. Approximately 1/3 of the sites in these strong motion databases are rock sites and the remaining 2/3, soil sites. Of the latter, many sites are shallow soil sites located at basin edges where 2D/3D effects on ground motions would be expected. A significant proportion of the earthquake recordings on rock in the strong motion database have probably been impacted by 2D/3D effects due to site locations on topographic features. A few examples include (1) the Corralitos site near Santa Cruz, California, located on a

hillside that recorded the highest peak acceleration in the 1989 Loma Prieta earthquake; (2) the well-known Pacoima Dam abutment site that recorded both the 1971 San Fernando and 1994 Northridge, California, earthquakes; (3) the Tarzana site that also recorded the 1994 Northridge as well as 1987 Whittier Narrows earthquakes; and (4) the Pacoima Kagel Canyon station that recorded the 1992 Landers, California, earthquake. Although it is accepted that 2D/3D effects are probably present at all sites to some extent, validations have clearly indicated that 1D models accommodate the significant and stable features of site response (Silva et al. 1996 [DIRS 110474], Section 7).

The Silva et al. (1996 [DIRS 110474], Section 5) validation study provides confidence that the RVT equivalent-linear site-response modeling approach is valid for use at Yucca Mountain. In this study a combined RVT point-source model was coupled to the RVT equivalent-linear site-response model. Thus, the study does not validate the RVT equivalent-linear approach independently of the RVT point-source approach. However, this study examined a larger suite of earthquakes (16) and sites (503), and included site-response at both soft-rock (159) and soil (344) sites. As discussed in Section 7.3.4, a number of the earthquakes modeled have magnitudes similar to those controlling ground motion hazard at Yucca Mountain and produced nonlinear response at some sites. This validation study thus increases confidence that the RVT equivalent-linear site-response modeling approach is valid for the conditions at Yucca Mountain.

7.5 INDEPENDENT TECHNICAL REVIEW

An additional activity to build confidence in the RVT equivalent-linear site response modeling approach was an independent technical review. The review was carried out on a first draft of Sections 6.1 (Model Description) and 7 (Model Approach Validation) of this report. Drafts of Sections 1 (Purpose) and 6.2 (Model Inputs) were also made available to the reviewers as background material. Reviewers were selected who were independent of the development, checking, and interdisciplinary review of the report. As described in the Technical Work Plan (BSC 2004a [DIRS 171850], Section 2.1.4), the reviewers had expertise in one or more of the following technical areas: probabilistic seismic hazard analyses, ground motion site response, characterization of rock/soil for site response analyses, and use of analysis results. The review team consisted of Dr. Ricardo Dobry (consulting geotechnical engineer), Dr. William Foxall, and Dr. Lawrence Hutchings (both seismologists with the Hazards Mitigation Center at Lawrence Livermore National Laboratory).

The reviewers concluded that the modeling approach "represents the existing state-of-the-art for evaluation of site effects at soil and rock sites, including explicit evaluation of uncertainties" and that "the approach is generally appropriate" (Younker 2003 [DIRS 163519]). They also stated that further validation of the modeling approach for the unique situation at Yucca Mountain needs to be addressed. Issues that the reviewers raised have been addressed both by expanding and strengthening the discussions of the modeling approach and its validation that were in the draft they reviewed and by carrying out the validation confirmation study described in Section 7.3.5.

A general issue raised by the reviewers was that discussion of previous validation activities did not present sufficient detail on the inputs used. This weakness of the draft for independent technical review was rectified in Revision 00 (Section 7.3). Through a clearer discussion of the

previous model validation runs, reviewer concerns about the predictive capability of the model also are addressed. Care was taken in determining inputs to the RVT equivalent-linear model and the nonlinear models such that the validation results are a true test of the models' predictive capabilities.

The reviewers also recommended that justification be strengthened for using a combination of a 1D model and uncertainties in model inputs to simulate ground motions adequately for engineering purposes, neglecting 2D and 3D effects. The introduction to Section 6 contains this expanded discussion. Multi-dimensional effects are accommodated in the uncertainty associated with the control motion that serves as an input to the site response model.

The reviewers suggested that discussion of validation work reported in Silva et al. (1996 [DIRS 110474], Section 5) be focused on earthquake magnitudes and distances that control the seismic hazard at Yucca Mountain. In the original version that they reviewed, modeling results for several earthquakes were highlighted with the intent of focusing on those events with magnitudes similar to those controlling seismic hazard at Yucca Mountain and that exhibited nonlinear site response at some sites. Section 7.3.4 has been expanded to include additional discussion of those specific events and recordings. However, based on the information provided in Silva et al. (1996 [DIRS 110474], Section 5), it is not possible to filter the results to examine model variability and bias for an arbitrary subset of magnitude and distance.

The case in which high strains are produced in site materials was one area for which the reviewers suggested additional validation activities would increase confidence in the RVT equivalent-linear site-response model. The comparison of the RVT-equivalent-linear predictions against the Port Island records (Section 7.1.5) was in response to this recommendation from the reviewers.

The reviewers also pointed out that the RVT equivalent-linear site-response modeling approach has not been validated for Yucca Mountain-specific site conditions. Although strong ground motion data are not available at this time for such a comparison because strong ground motions have not been recorded at Yucca Mountain, comparisons can be made for recorded weak ground motion.

Finally, the reviewers suggested that modifications to model input should be considered. Specifically, they suggested that curves of normalized shear modulus reduction and material damping should be modified to reflect material failure at some level of shear strain above 0.1 percent. While work is underway to address the issue of ground motion saturation at Yucca Mountain (BSC 2004c [DIRS 170137]), this work does not directly address model validation. Rather it aims at developing more realistic model inputs for Yucca Mountain that will lead to more realistic ground motions at annual frequencies of exceedance less than 10^{-5}.

In summary, the independent technical review of the RVT equivalent-linear site response modeling approach concluded that modeling approach is "state-of-the-art" and "generally appropriate" for its intended use. The reviewers raised a number of issues that have been addressed through expanded discussions in this final version of the report. The reviewers also recommended some additional activities that could be undertaken to increase the level of

confidence in the model given the unique conditions at Yucca Mountain. One of these recommendations has been implemented as described in Section 7.3.5.

7.6 MODEL VALIDATION SUMMARY

The major issues involved in the prediction of the effects of site response to strong ground motions include a suitable wave propagation model, the *in situ* strain dependencies of dynamic material properties, and how the effects of material nonlinearities are treated computationally. All three aspects were treated in EPRI (1993b [DIRS 103320], Appendix 6.B) and confirmation study (Section 7.3.5.4) by comparing observed strong ground motions to motions predicted by equivalent-linear and nonlinear approaches at three carefully characterized reference sites. Reasonably comprehensive geotechnical models based in part on laboratory testing were developed for Gilroy #2, Treasure Island, the Lotung, Taiwan LSST, and Port Island, Kobe, Japan sites. The sites possess all of the features that are thought necessary to provide a good validation: recordings of both high- and low-strain ground motions, a dipping interface at least at one site (Gilroy #2), a wide range in material properties from sands and gravels to soft silts and stiff clays, deep (70 ft) and shallow (surface) water tables, and a wide range in stiffness from deep and stiff at Gilroy #2 to shallow and very soft at Lotung.

The equivalent-linear (RASCALS) and nonlinear (DESRA, SUMDES, TESS) analyses used vertically-propagating S-waves. For strong ground motions, and even weak motions at the Lotung LSST site, nonlinear soil response was observed and modeled very well by both the equivalent-linear and nonlinear techniques. Both approaches to model the effects of soil nonlinearity produced equally good comparisons to recorded ground motions for both response spectra and time histories. Analyses at the soil/rock site pair Gilroy #2/Gilroy #1, with a known dipping interface between the sites, showed that 2D or 3D effects were small and not important in modeling the site response.

At reference site Treasure Island, computed motions for the Loma Prieta earthquake using the Yerba Buena recordings as control motions show a broadband and general underprediction of the recorded motions. Either a topographic effect at Yerba Buena Island or a large velocity gradient beneath the level of measured velocities at Treasure Island, or both, may be responsible, but the results do not appear to be dependent on the modeling approach. Until this issue is resolved, uncertainties will remain regarding analyses done with this pair of strong motion recordings.

The general conclusion resulting from these analyses is that conventional 1D site response analyses incorporating equivalent-linear and nonlinear soil behavior based upon careful laboratory testing and with reasonably accurate soil profiles can accurately predict the effects of soils on strong ground motions.

The EPRI (1993a [DIRS 103319], Section 6) validation for the vertical-component modeling approach was based on recordings of the 1989 Loma Prieta earthquake. Vertical response spectra appear to be modeled reasonably well with the 1D linear model. Although validation was limited to only one earthquake, the computed uncertainty of the vertical response spectra was comparable to horizontal component predictions (EPRI 1993a [DIRS 103319], Section 3). Although this model validation approach includes source, path and site response together, the

vertical motion modeling uncertainty was reduced to levels comparable to the horizontal component of motion by using the 1D linear modeling approach on the vertical component.

Further validation of the site response modeling approach is provided by Silva et al. (1996 [DIRS 110474], Section 5). A total of 16 earthquakes were modeled at 503 sites over the fault distance range of about 1 to 177 km (1 to 110 mi) (460 km [290 mi] for Saguenay). Model bias and variabilities were estimated for the 16 study earthquakes over all 503 sites for the RVT point-source model/RVT equivalent-linear site-response model. In general, the bias estimates were low and the variabilities small. The final bias and variability estimates computed for all the earthquakes and over all the sites showed near zero bias for frequencies of about 1 Hz and above. The combined model shows a stable and significant negative bias (overprediction) from about 1 to 0.3 Hz (the approximate low frequency limit of the analyses). The variability estimates are generally uniform at about 0.5 to 0.6 (natural log units) at 1 Hz and above. This is considered low as the majority of the data are for **M** < 6.5 and the sites range in distance out to 177 km (110 mi) (460 km [290 mi] for Saguenay).

The combined RVT point-source/RVT equivalent-linear site-response modeling approach using vertically-propagating S-waves appears to capture the significant and stable features of crustal amplification and site response reflected in strong motion recordings at both soft-rock and deep-soil sites. This is a notable result, as the distances ranged out to 177 km (110 mi) (460 km [290 mi] for Saguenay) and soil column thickness of up to 1,000 ft.

The EPRI (1993a [DIRS 103319]) and Silva et al. (1996 [DIRS 110474]) validations of the equivalent-linear modeling approach demonstrates the appropriateness of the modeling to shear-strains of about 10^{-3}. Modeling of the vertical array motions of the M 6.9 Kobe earthquake recorded at Port Island, Japan (Section 7.3.5), provides additional validation of the equivalent-linear model at strains that exceed the Yucca Mountain post-closure shear-strains (0.7%). These recordings of strong motion in soil were sufficiently strong to induce soil failure. The equivalent linear model predictions of response spectra were judged to provide good agreement with the observed spectra. The nonlinear model predictions of response spectra did not provide any appreciable improvement in predicting response spectra as compared to the equivalent linear predictions. This validation of the RVT equivalent-linear modeling approach at higher ground motions and higher strains increases confidence in the approach.

Validation Summary

The site-response ground motions model has been validated by applying acceptance criteria based on an evaluation of the model's relative importance to the potential performance of the repository system. All validation requirements defined in TWP-MGR-GS-000001 REV 03 ICN 02 (BSC 2004a [DIRS 171850], Section 2.1.4) have been fulfilled. Requirements for confidence building during model development have also been satisfied. The model development activities and post-development validation activities described establish the scientific bases for the site-response ground motion model. Based on this, the site-response ground motion model is considered to be sufficiently accurate and adequate for the intended purpose with the stated limitations and to the level of confidence required by the model's relative importance to the potential performance of the repository system.

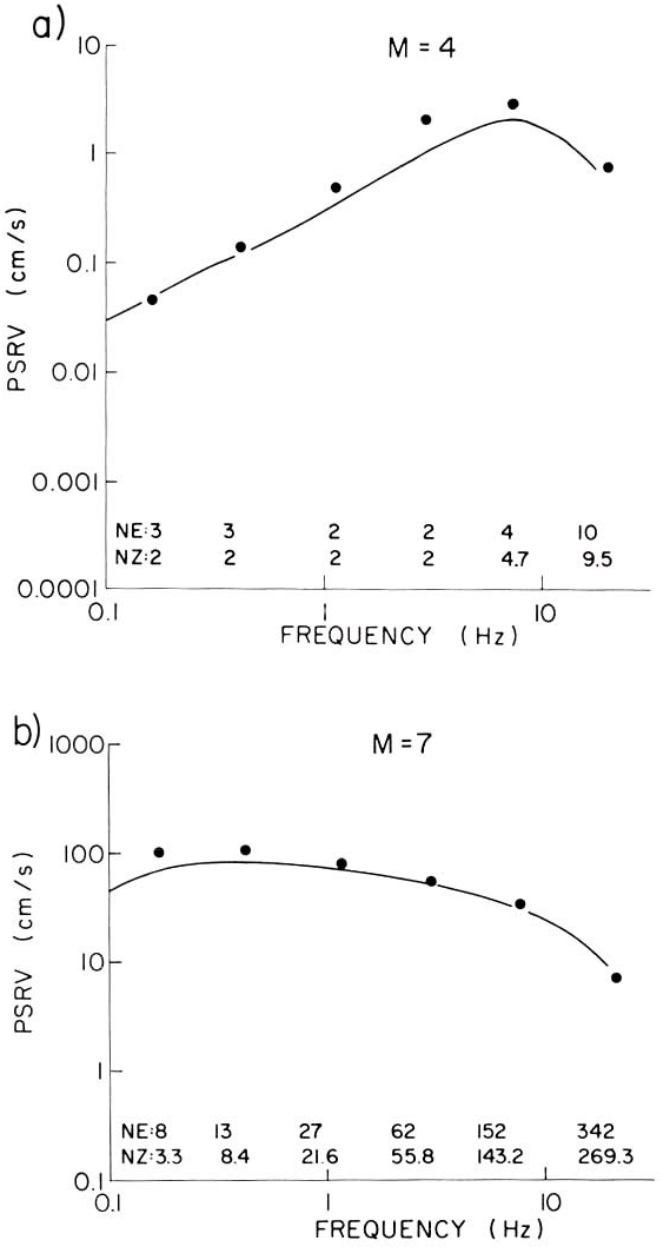

Source: Boore 1983 [DIRS 103317]

Figure 7-1. Predicted 5%-Damped Response Spectra from Time Domain Simulations (Solid Line) and RVT (Dots)

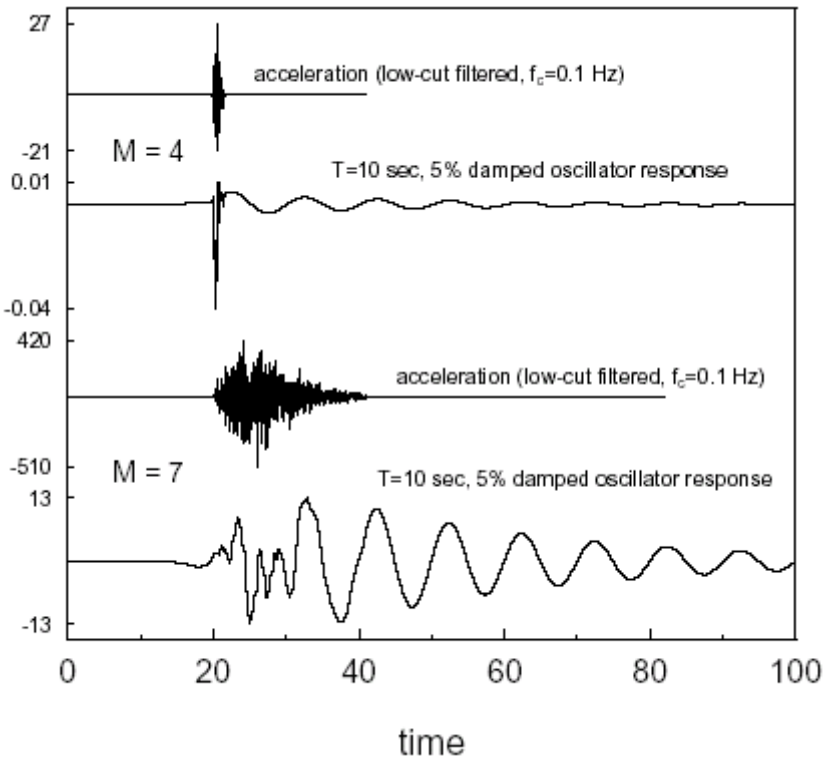

Source: Boore 2003 [DIRS 163706], Figure 19

Figure 7-2. Simulated Acceleration Time Series and Computed Response of 10-Sec, 5%-Damped Oscillator for M 4 and M 7 Earthquakes at a Distance of 10 km

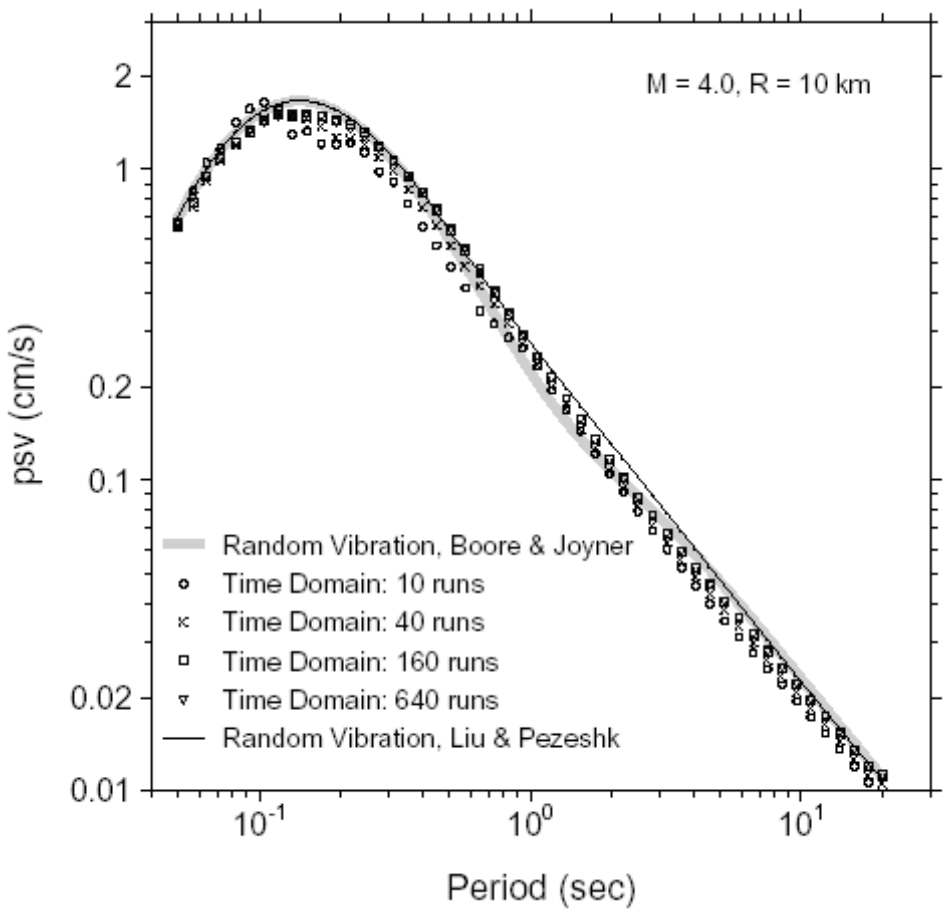

Source: Boore 2003 [DIRS 163706], Figure 20

Figure 7-3. Comparison of Simulations of M 4 at 10 km Using Time-Domain Calculations with Differing Numbers of Simulations Used with RVT Results Using Two Different Modifications (Boore and Joyner [1984] and Liu and Pezeshk [1999])

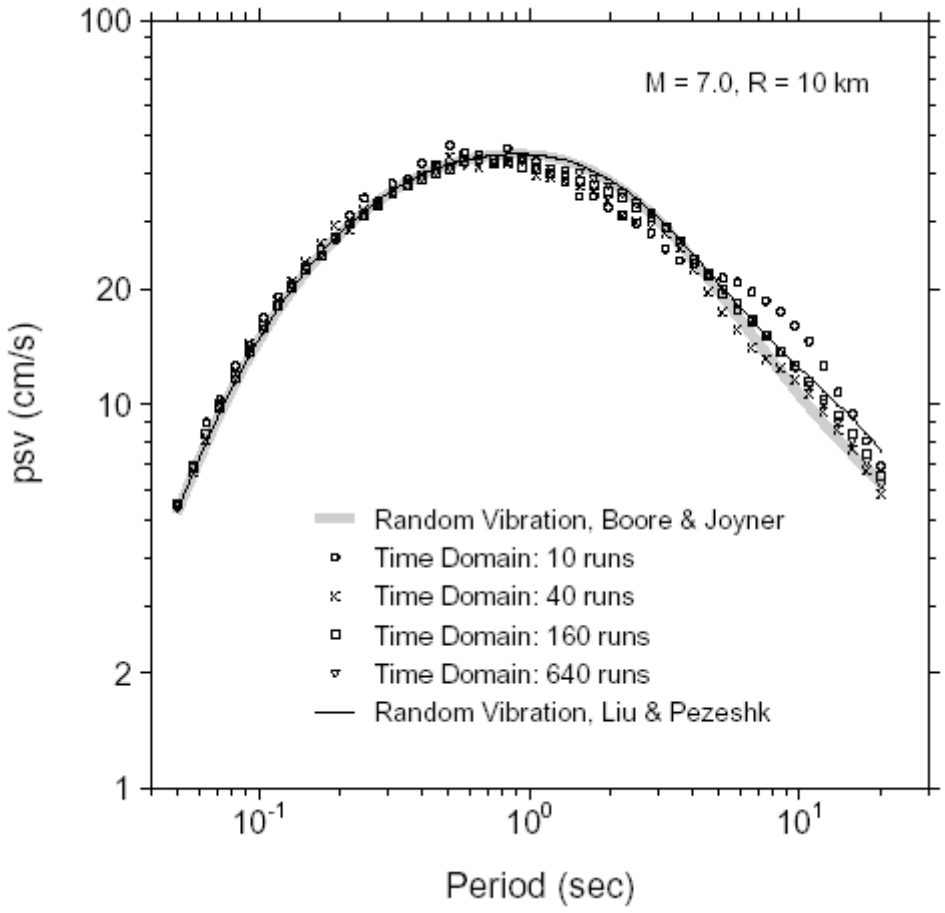

Source: Boore, 2003 [DIRS 163706], Figure 21

Figure 7-4. Comparison of Simulations of M 7 at 10 km Using Time-Domain Calculations with Differing Numbers of Simulations Used with RVT Results Using Two Different Modifications (Boore and Joyner [1984] [DIRS 163174] and Liu and Pezeshk [1999] [DIRS 163995])

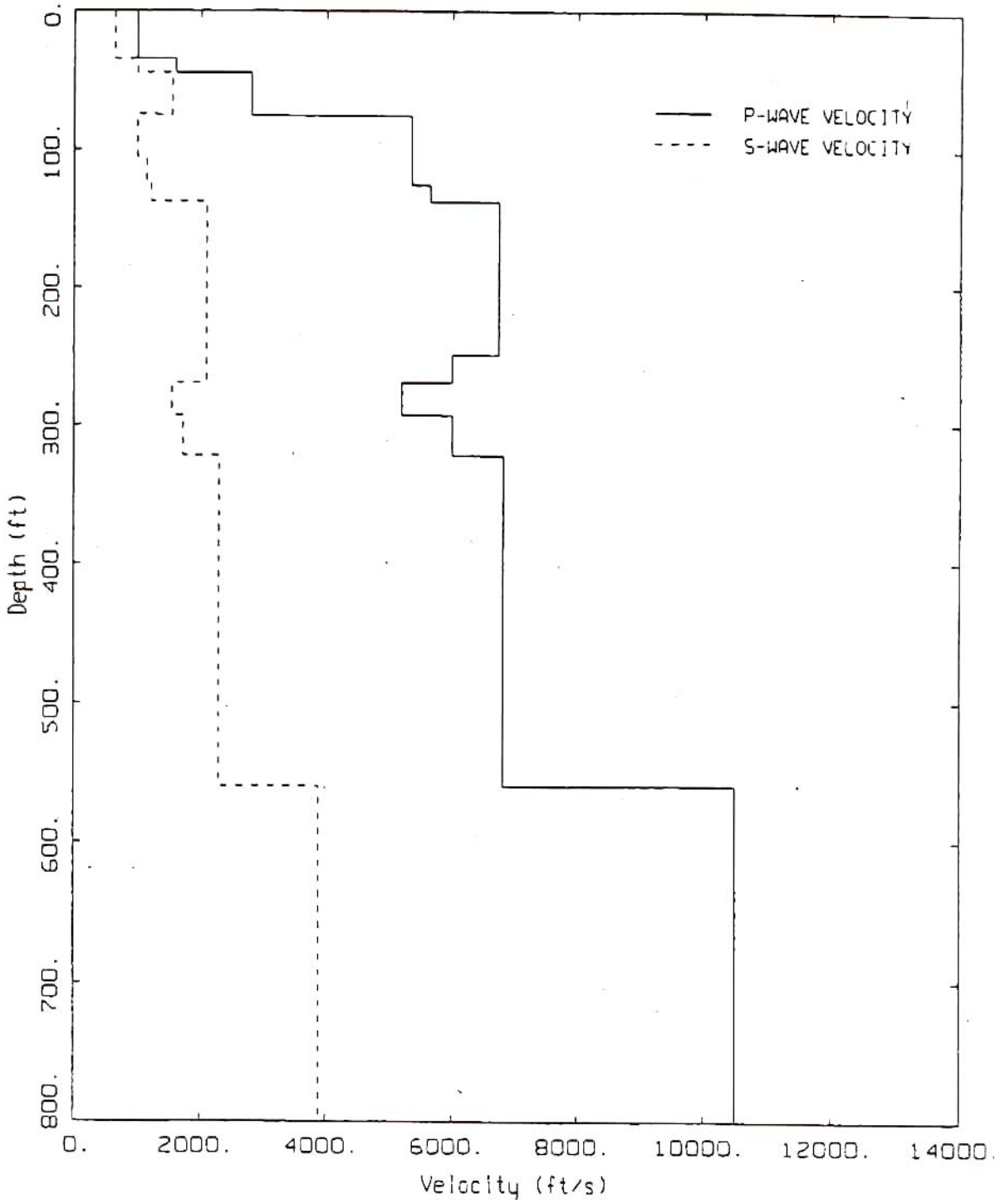

Source: EPRI 1993b [DIRS 103320]; Appendix 6.B, Figure 6.B-1

Figure 7-5. Base Case V_P and V_S Profiles for Reference Site Gilroy #2

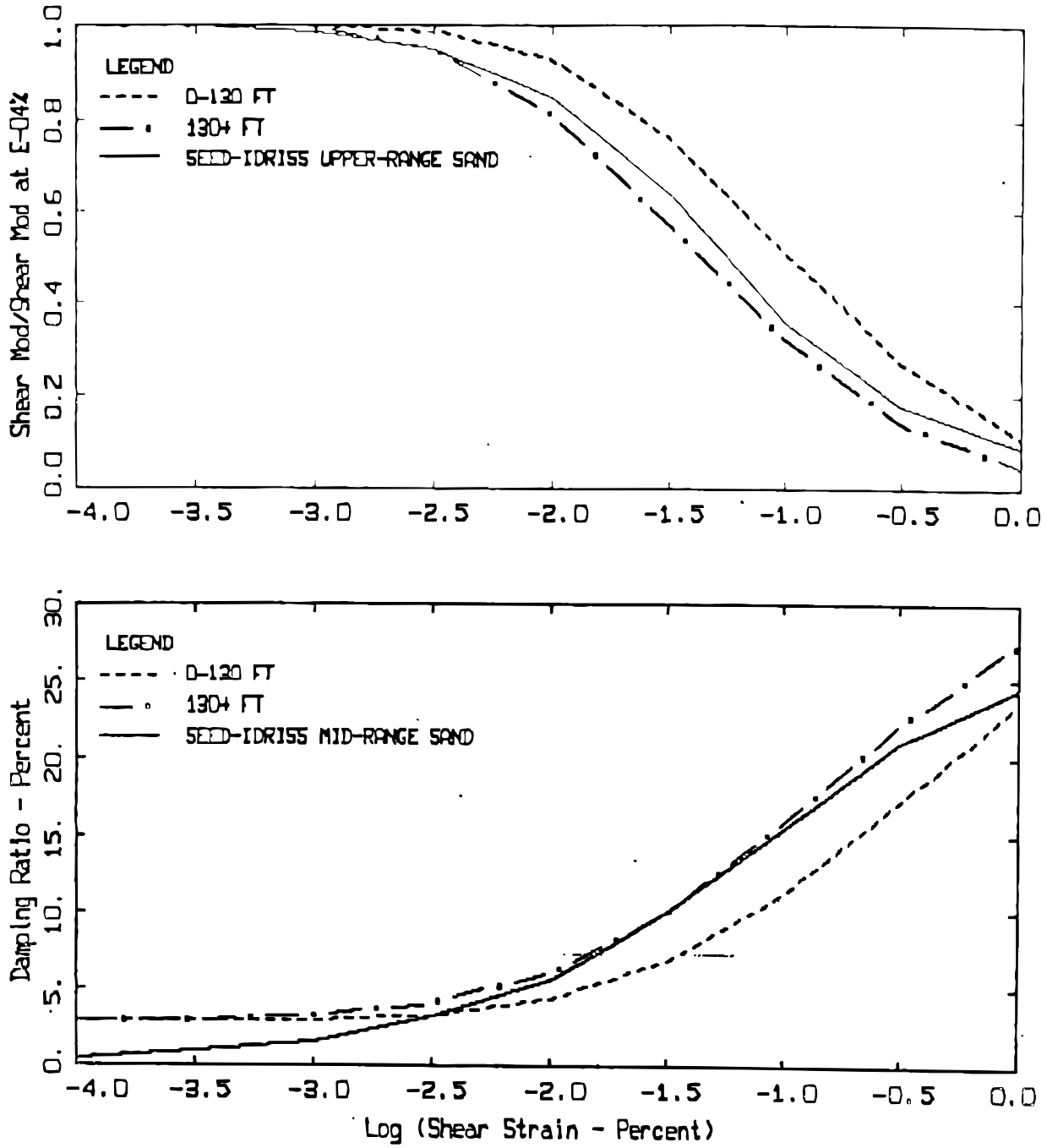

Source: EPRI 1993b [DIRS 103320]; Appendix 6.B, Figure 6.B-3

NOTE: The curves are based on laboratory testing of "undisturbed samples." Typical Seed-Idriss curves are shown for reference.

Figure 7-6. Shear Modulus Reduction and Damping Curves for Reference Site Gilroy #2

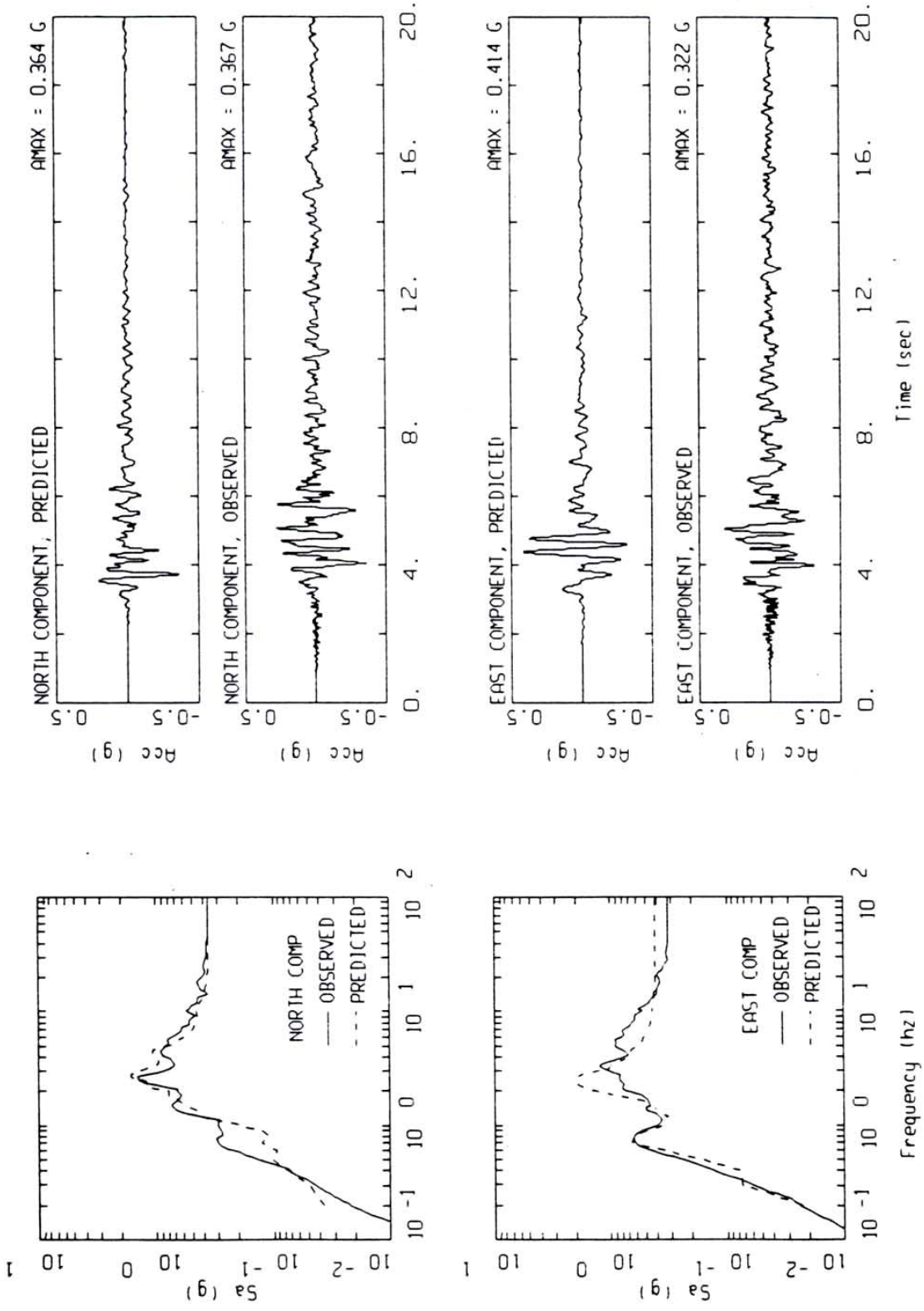

Source: EPRI 1993b [DIRS 103320]; Appendix 6.B, Figure 6.B-13

Figure 7-7. Comparison of Observed and Predicted Time Histories and 5%-Damped Spectral Accelerations for the Loma Prieta Earthquake at Gilroy #2 Using Gilroy #1 Rock Outcrop as Control Motions. RASCAL Equivalent-Linear Analysis

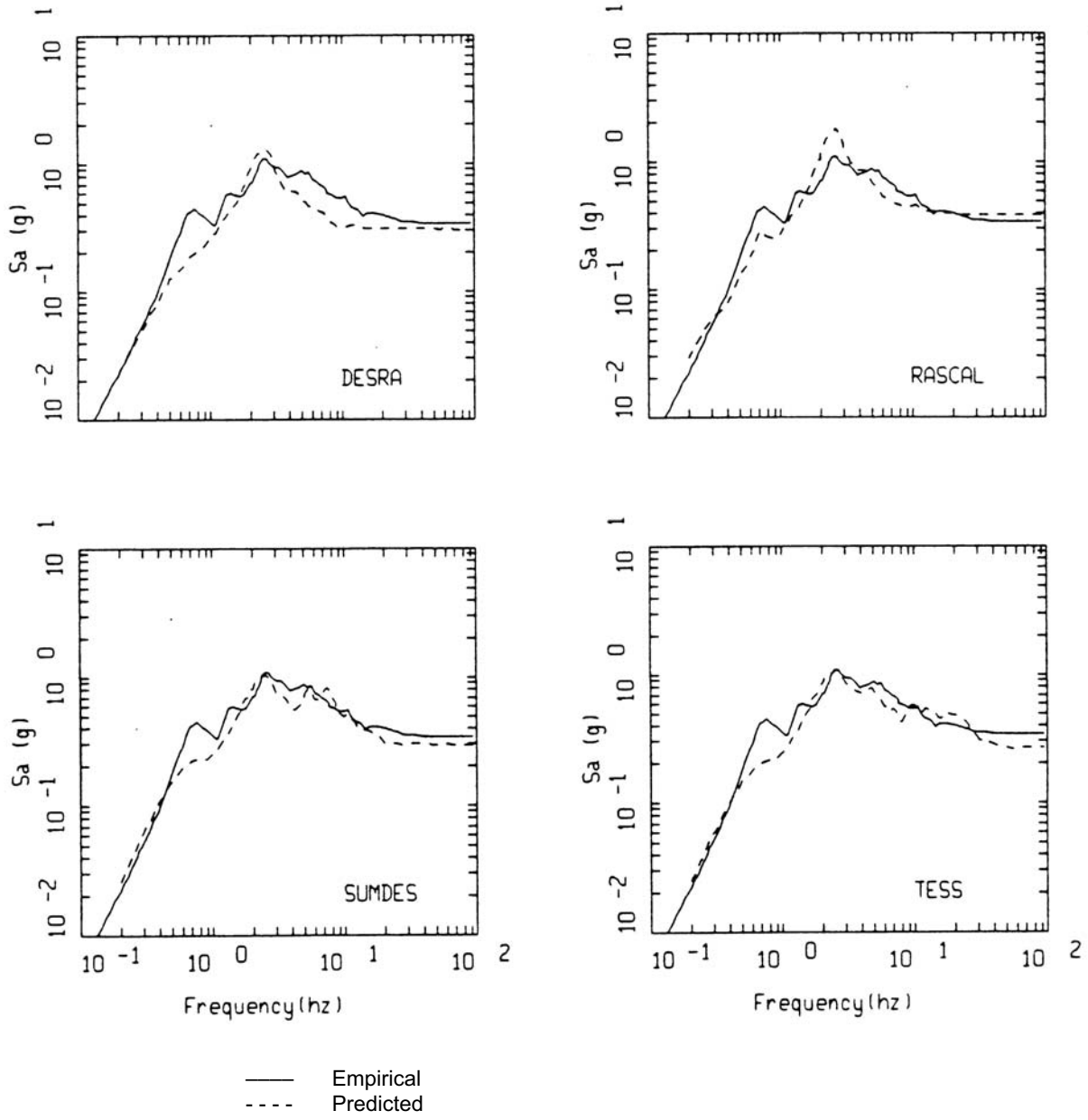

Source: EPRI 1993b [DIRS 103320]; Appendix 6.B, Figure 6.B-17

Figure 7-8. Comparison of Log Average (Horizontal Components) 5%-Damped Spectral Accelerations for the Four Analyses to the Empirical Spectra at Gilroy #2 for the Loma Prieta Earthquake

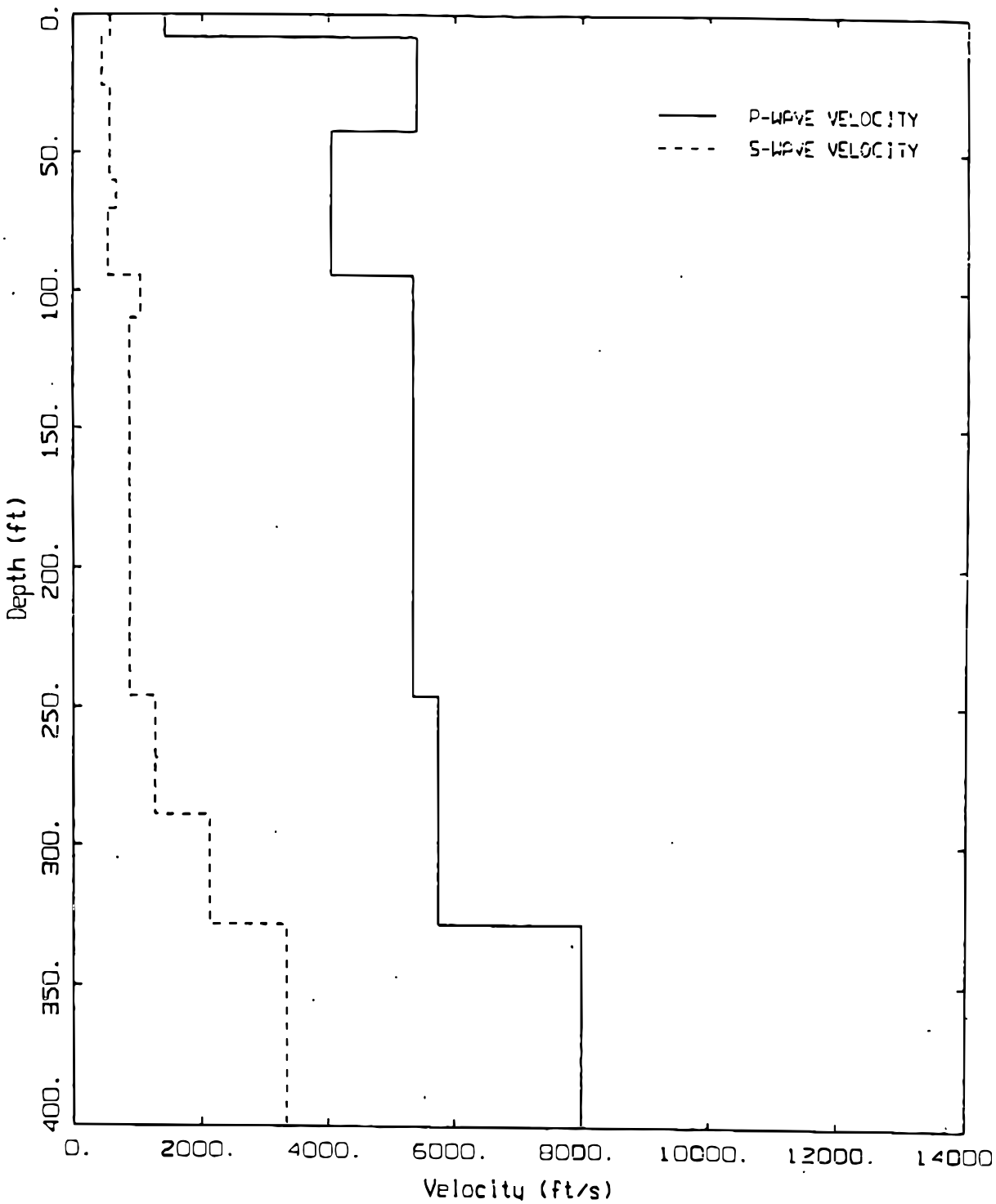

Source: EPRI 1993b [DIRS 103320]; Appendix 6.B, Figure 6.B-4

Figure 7-9. Base Case V_P and V_S Profiles for Reference Site Treasure Island

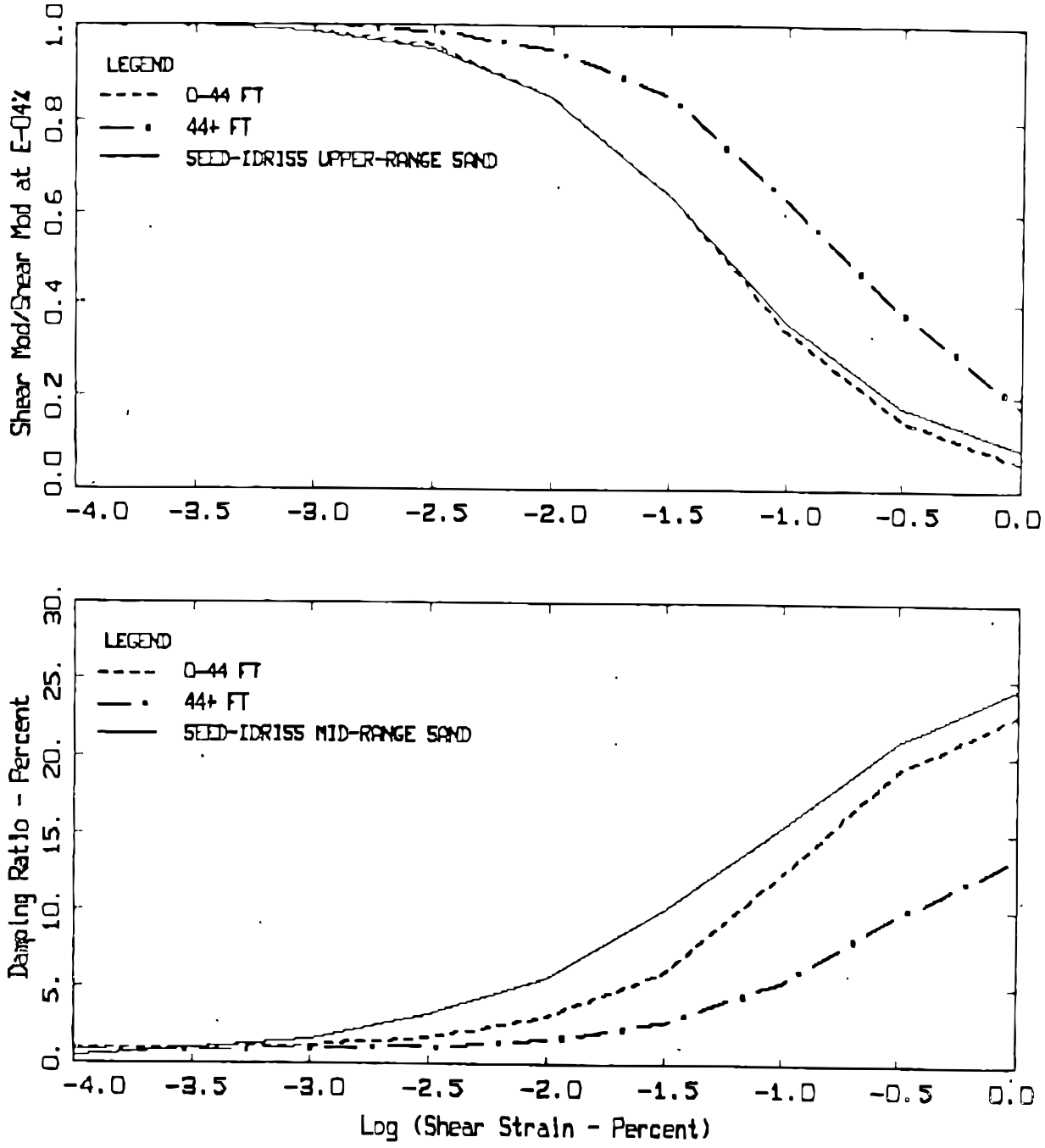

Source: EPRI 1993b [DIRS 103320]; Appendix 6.B, Figure 6.B-6

NOTE: The curves are based on laboratory testing of "undisturbed samples." Typical Seed-Idriss curves are shown for reference.

Figure 7-10. Shear Modulus Reduction and Damping Curves for Reference Site Treasure Island

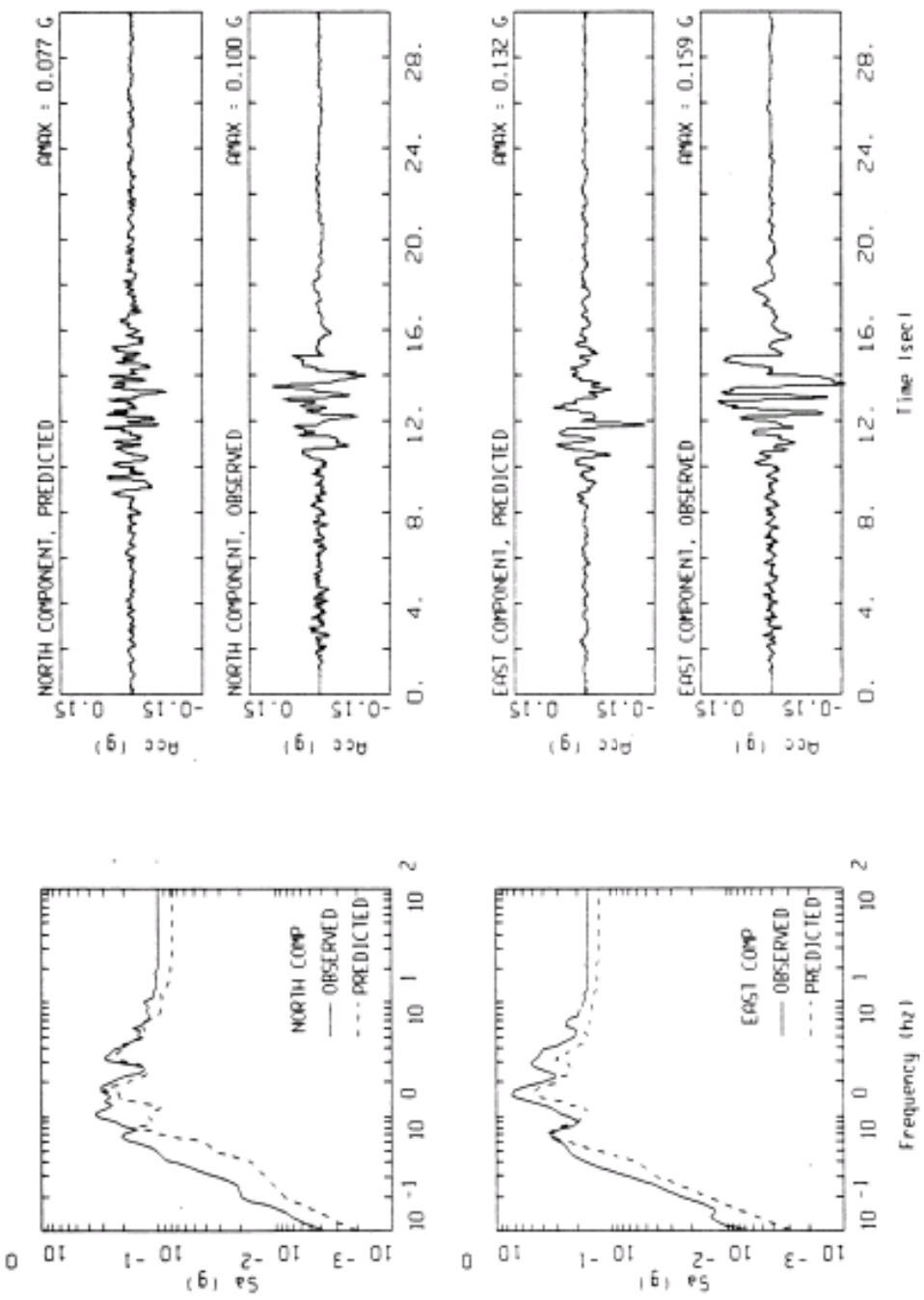

Source: EPRI 1993b [DIRS 103320]; Appendix 6.B, Figure 6.B-20

Figure 7-11. Comparison of Observed and Predicted Time Histories and 5%-Damped Spectral Accelerations for the Loma Prieta Earthquake at Treasure Island Using Yerba Buena Island Rock Outcrop as Control Motions. RASCAL Equivalent-Linear Analysis

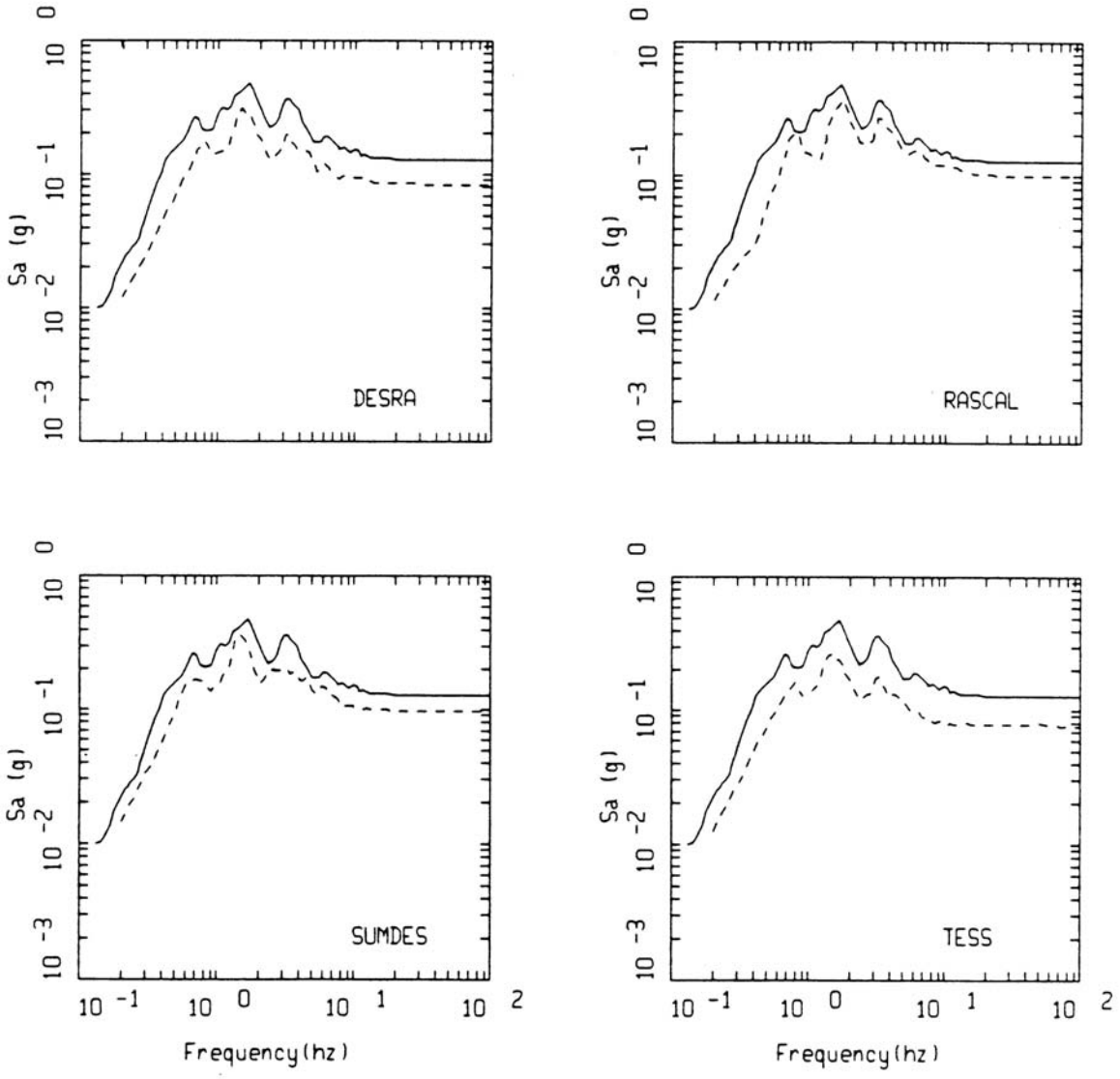

Source: EPRI 1993b [DIRS 103320]; Appendix 6.B, Figure 6.B-24

Figure 7-12. Comparison of Log Average (Horiz ontal Components) 5%-Damped Spectral Accelerations for the Four Analyses to the Empirical Spectra at Treasure Island for the Loma Prieta Earthquake

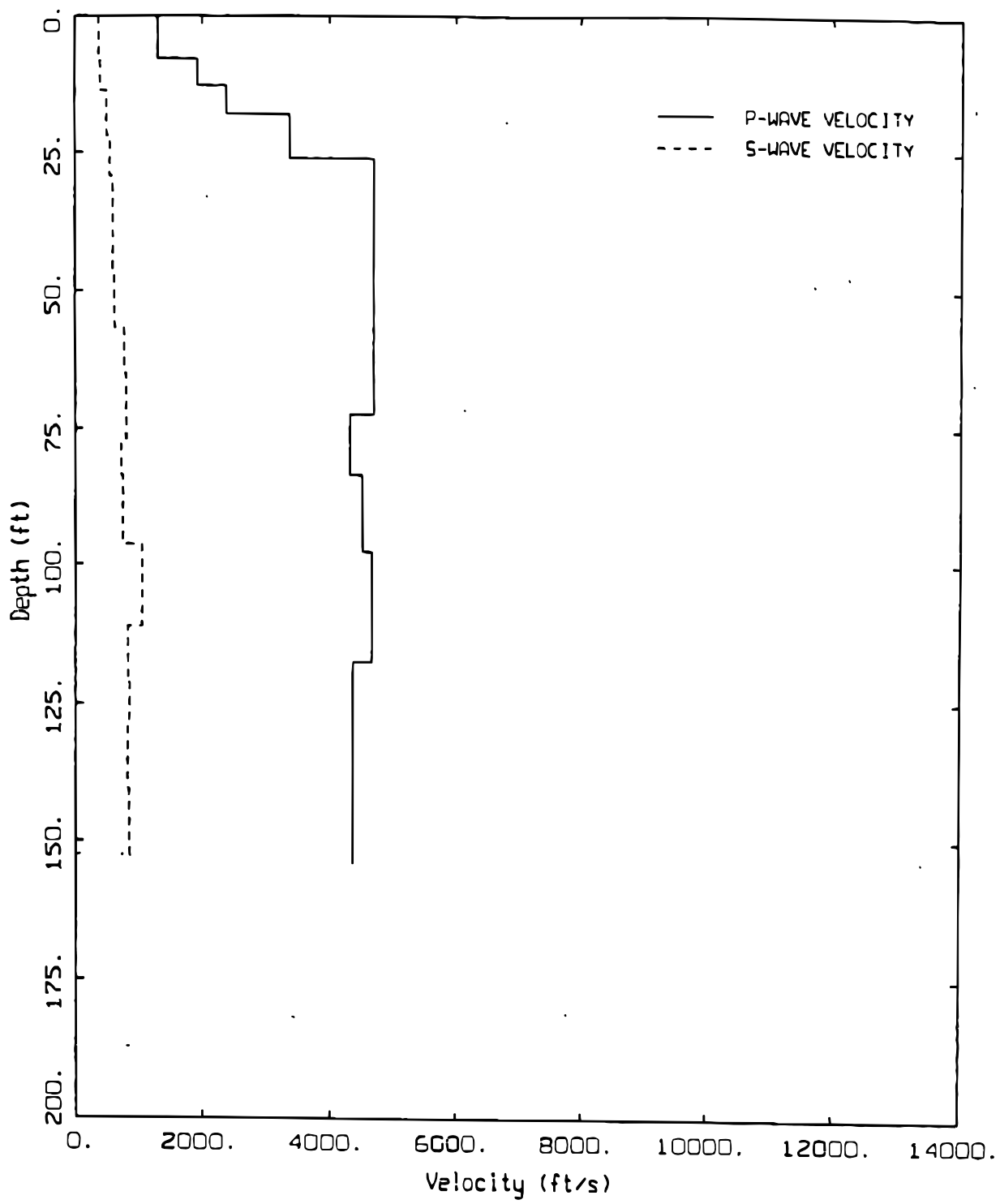

Source: EPRI 1993b [DIRS 103320]; Appendix 6.B, Figure 6.B-7

Figure 7-13. Base Case V_P and V_S Profiles for Reference Site Lotung LSST

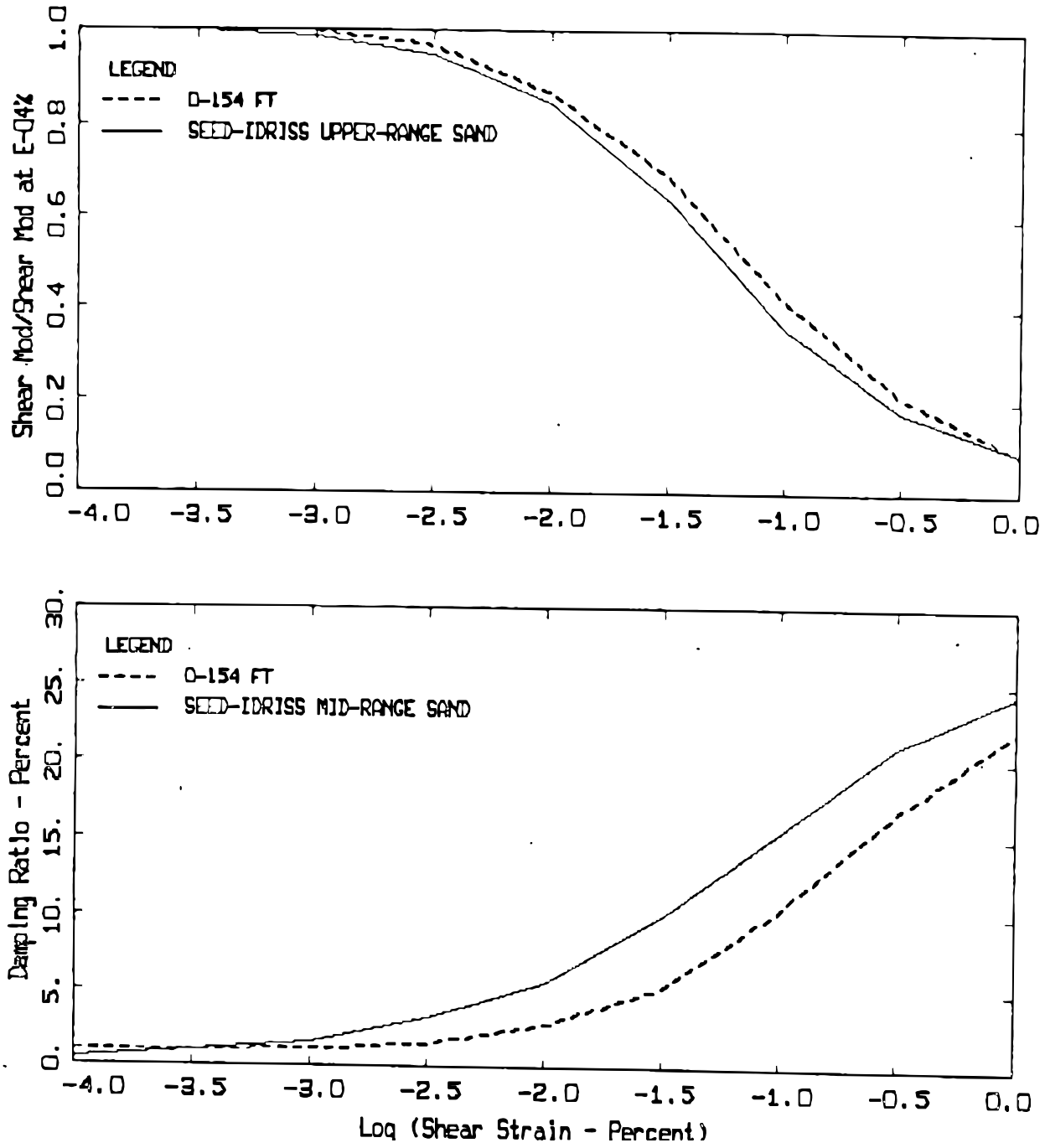

Source: EPRI 1993b [DIRS 103320]; Appendix 6.B, Figure 6.B-8

NOTE: The curves are based on laboratory testing of "undisturbed samples. Typical Seed-Idriss curves are shown for reference.

Figure 7-14. Shear Modulus Reduction and Damping Curves for Reference Site Lotung LSST

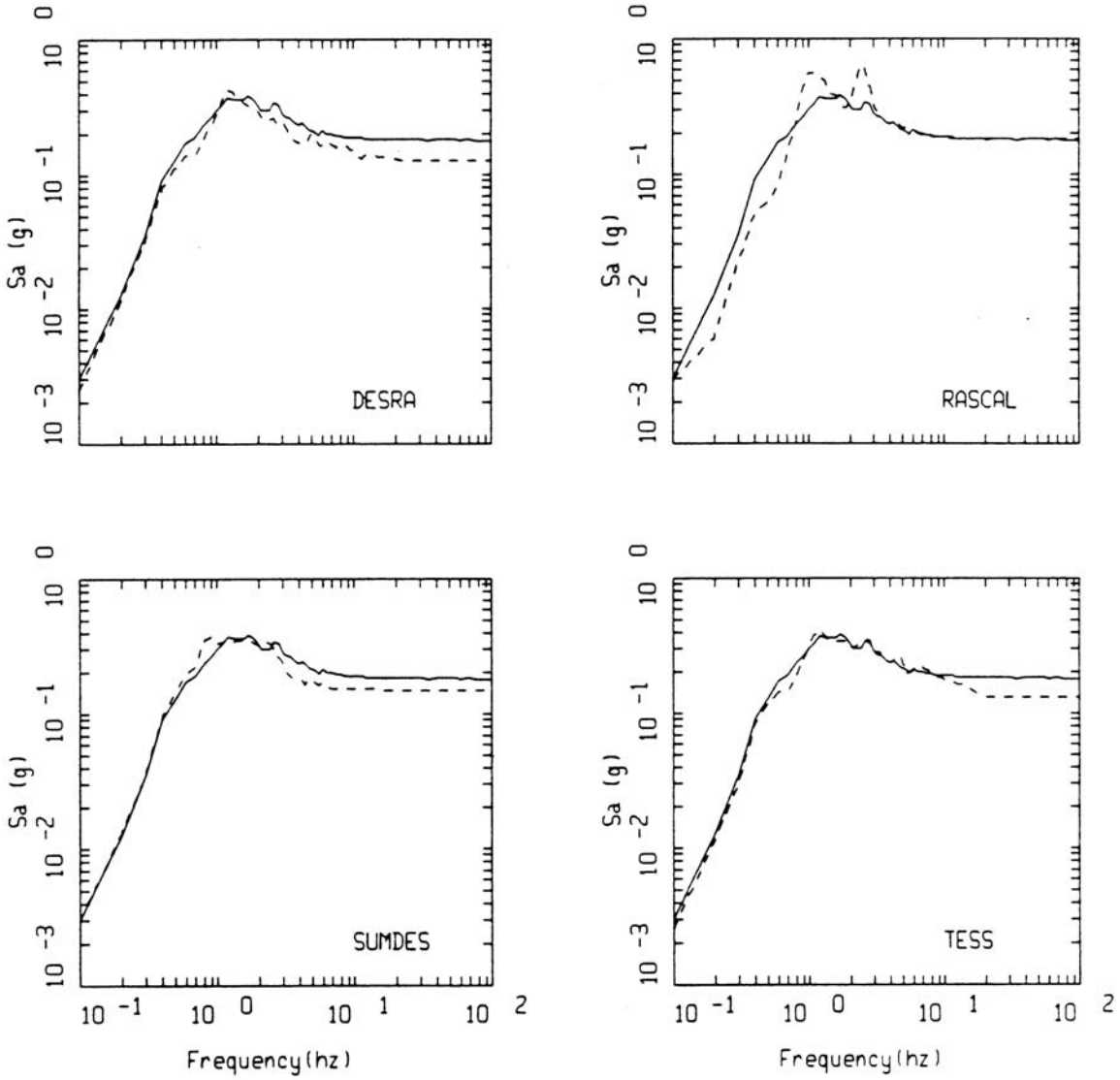

Source: EPRI 1993b [DIRS 103320]; Appendix 6.B, Figure 6.B-68

Figure 7-15. Comparison of Log Average (Horiz ontal Components) 5%-Damped Spectral Accelerations for the Four Analyses to the Empirical Spectra at Lotung for LSST Event 7 Surface Motions

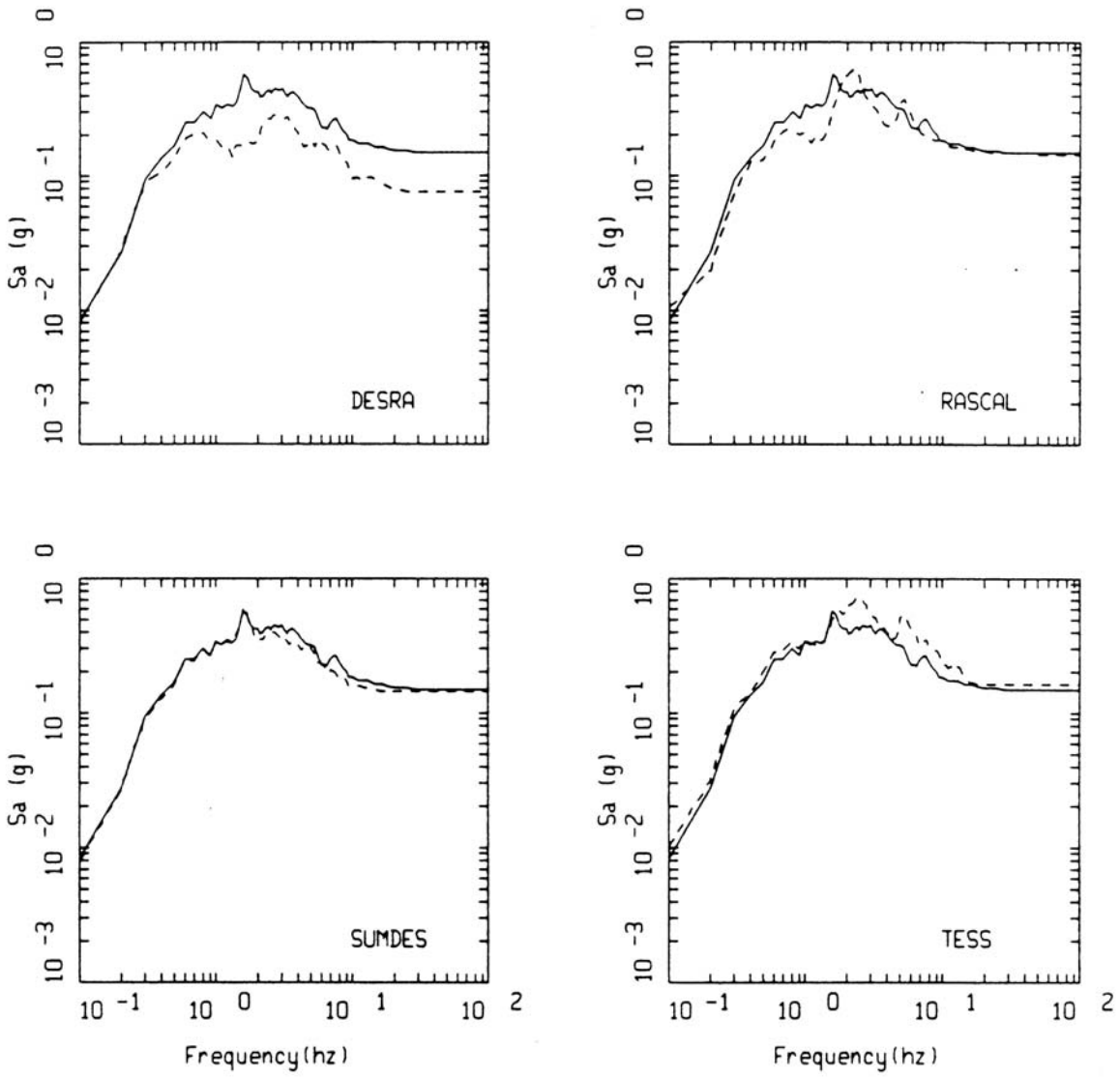

Source: EPRI 1993b [DIRS 103320]; Appendix 6.B, Figure 6.B-72

Figure 7-16. Comparison of Log Average (Horiz ontal Components) 5%-Damped Spectral Accelerations for the Four Analyses to the Empirical Spectra at Lotung for LSST Event 16 Surface Motions

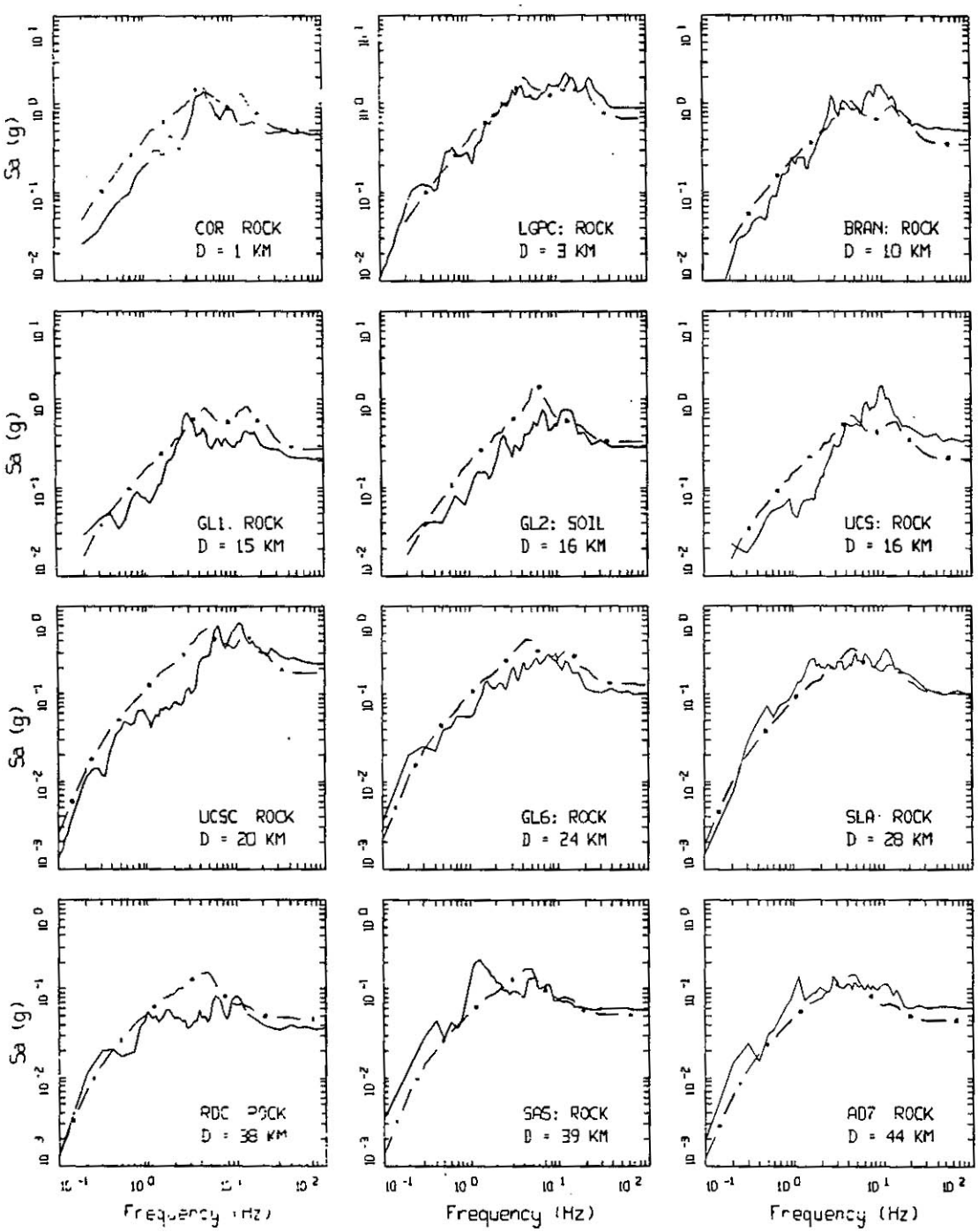

Source: EPRI 1993a [DIRS 103319]; Section 6, Figure 6-42

NOTE: Station names list in Table 7-5.

Figure 7-17a. Comparison of 5%-Damped Vertical-Component Response Spectra for the 1989 Loma Prieta Earthquake

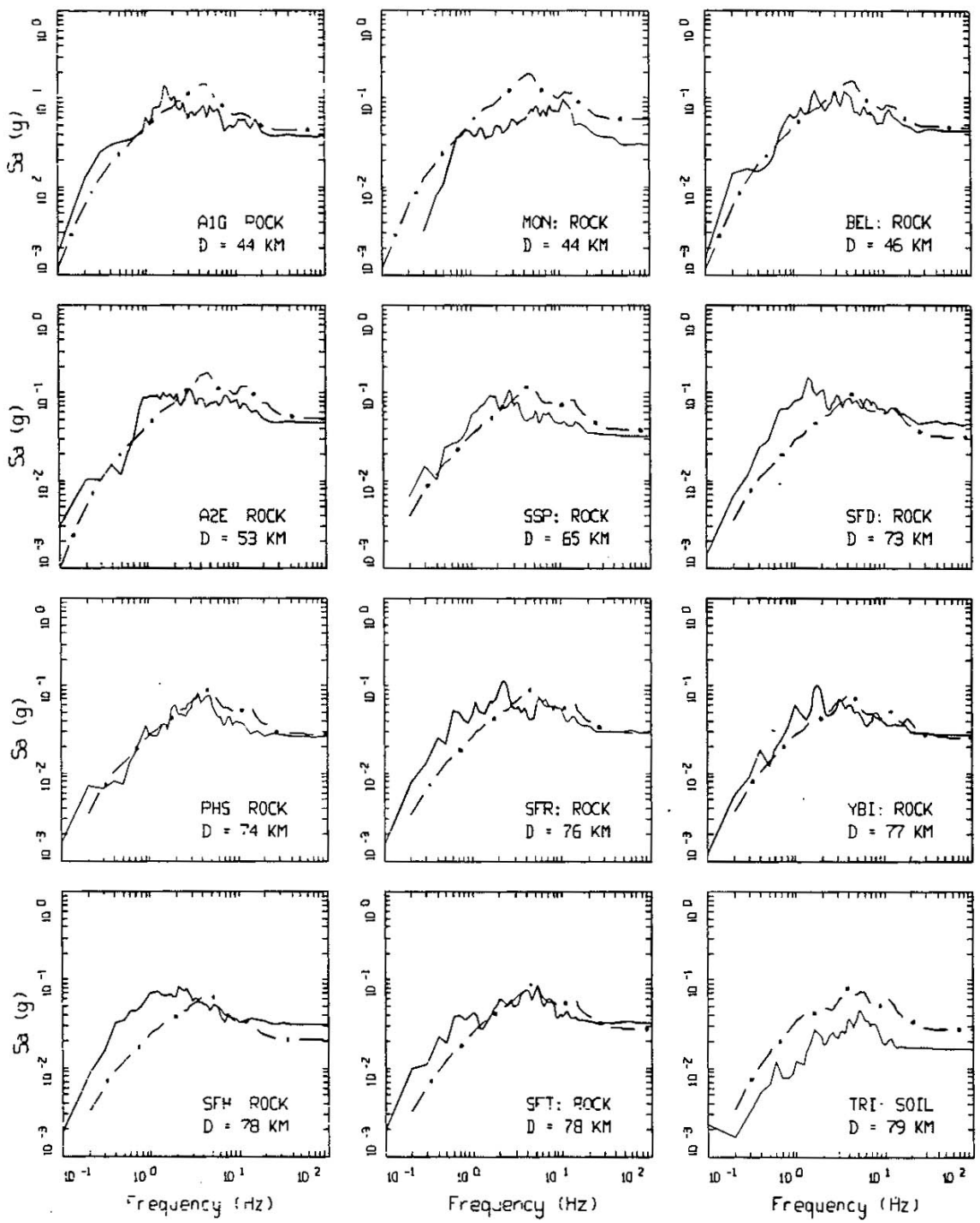

Figure 7-17b. Comparison of 5%-Damped Vertical-Co mponent Response Spectra for the 1989 Loma Prieta Earthquake

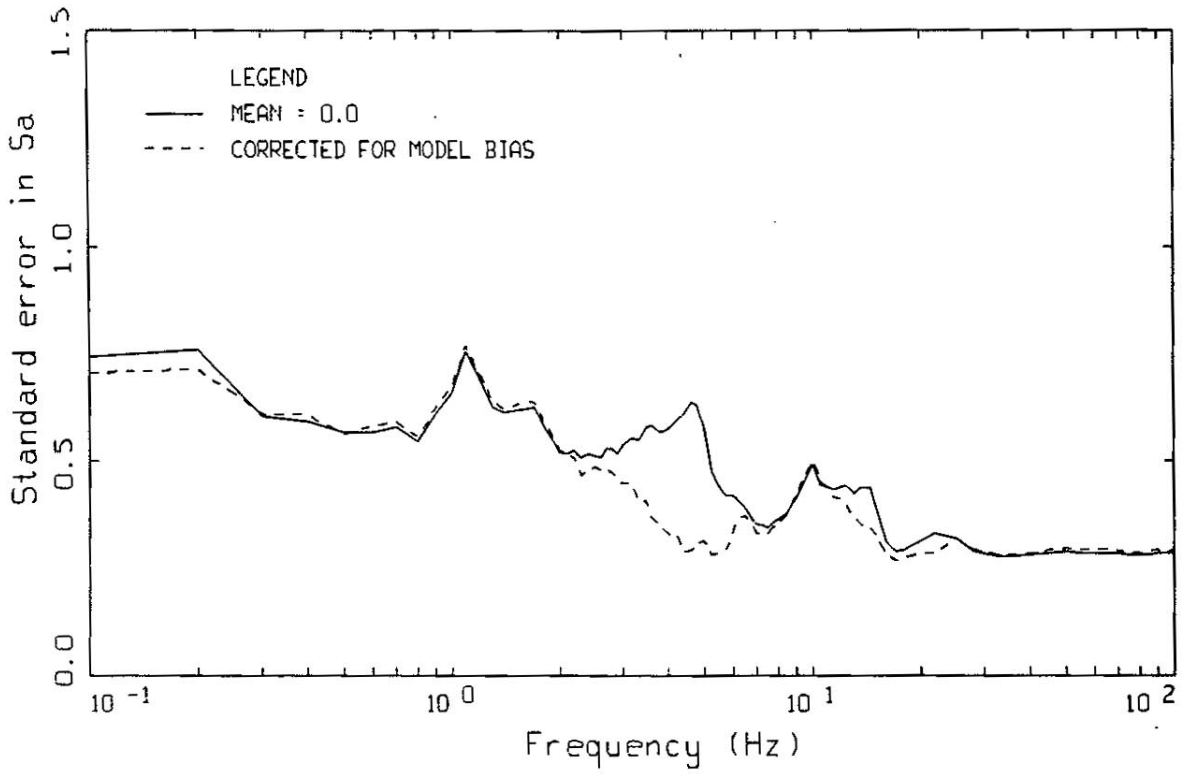

Source: EPRI 1993a [DIRS 103319]; Section 6, Figure 6-43

Figure 7-18. Standard Error (Natural Log) of Modeling Uncertainty Computed for the Loma Prieta Earthquake Using Vertical Motions

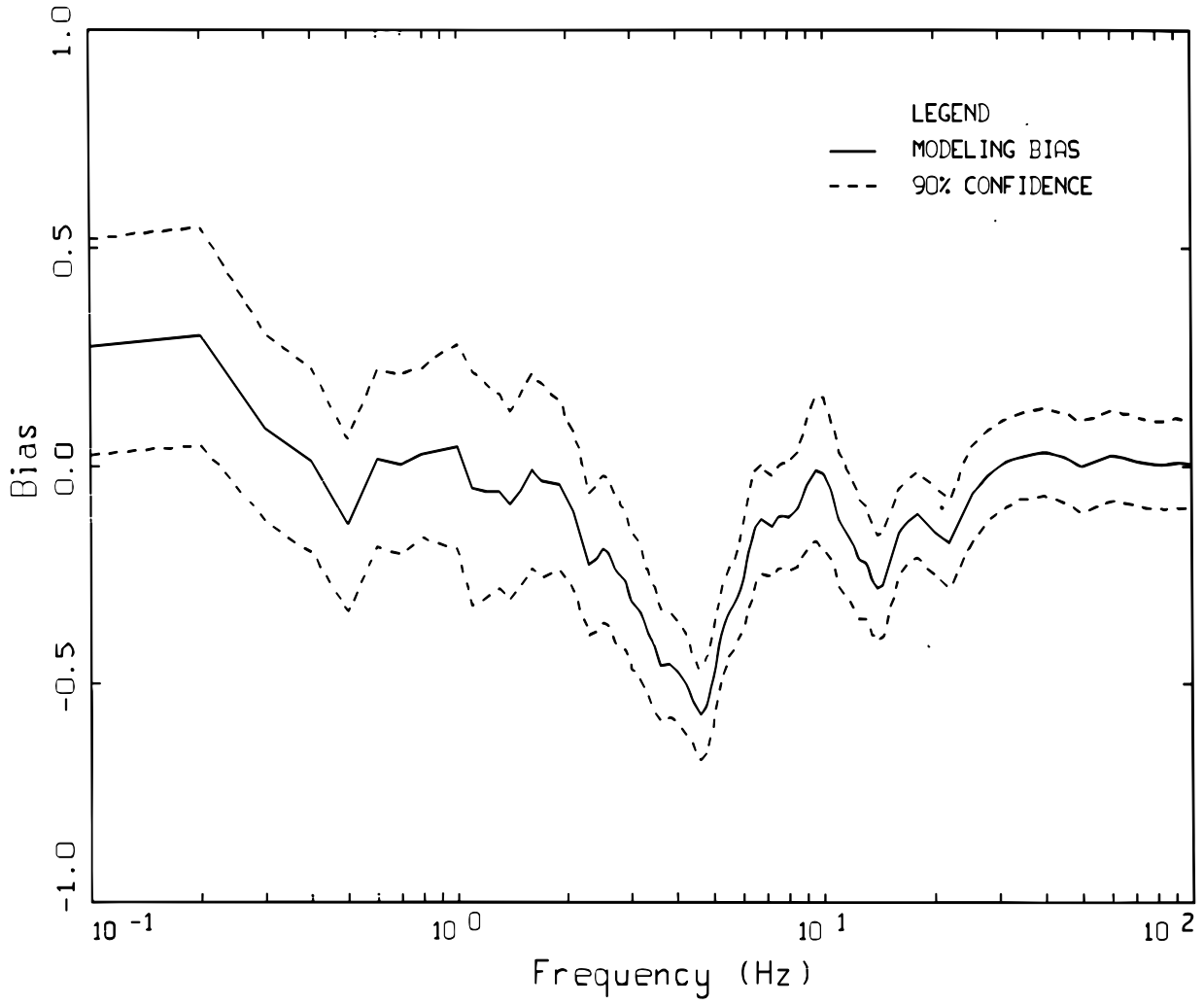

Source: EPRI 1993a [DIRS 103319]; Section 6, Figure 6-44

Figure 7-19. Modeling Bias Computed for the Loma Prieta Earthquake Using Vertical Motions

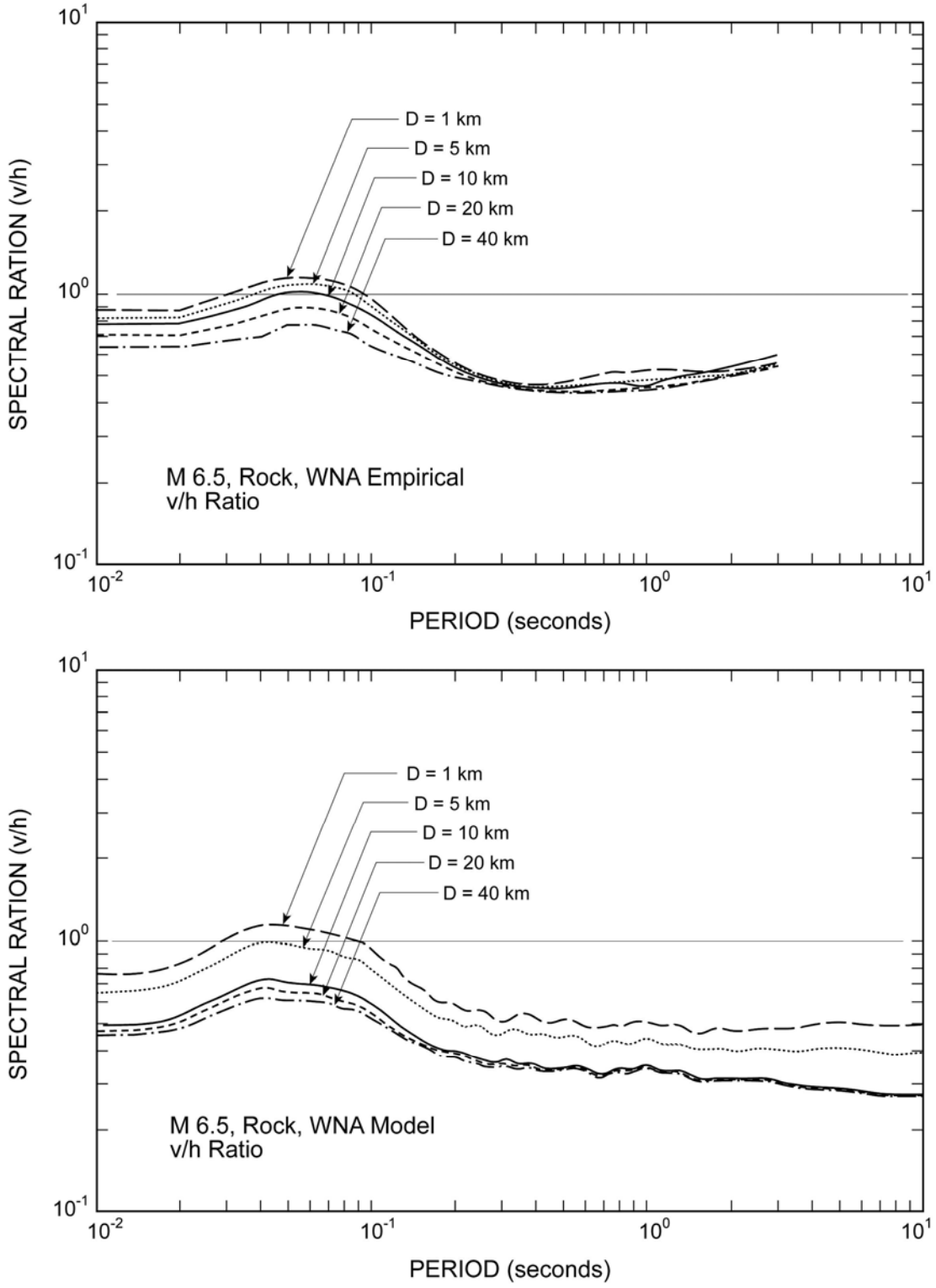

Source: Silva 1997 [DIRS 163747], Figure 29

Figure 7-20. Comparison of Western U.S. Empirical and Modeled Vertical-to-Horizontal Response Spectral Ratios for M 6.5, Rock Sites

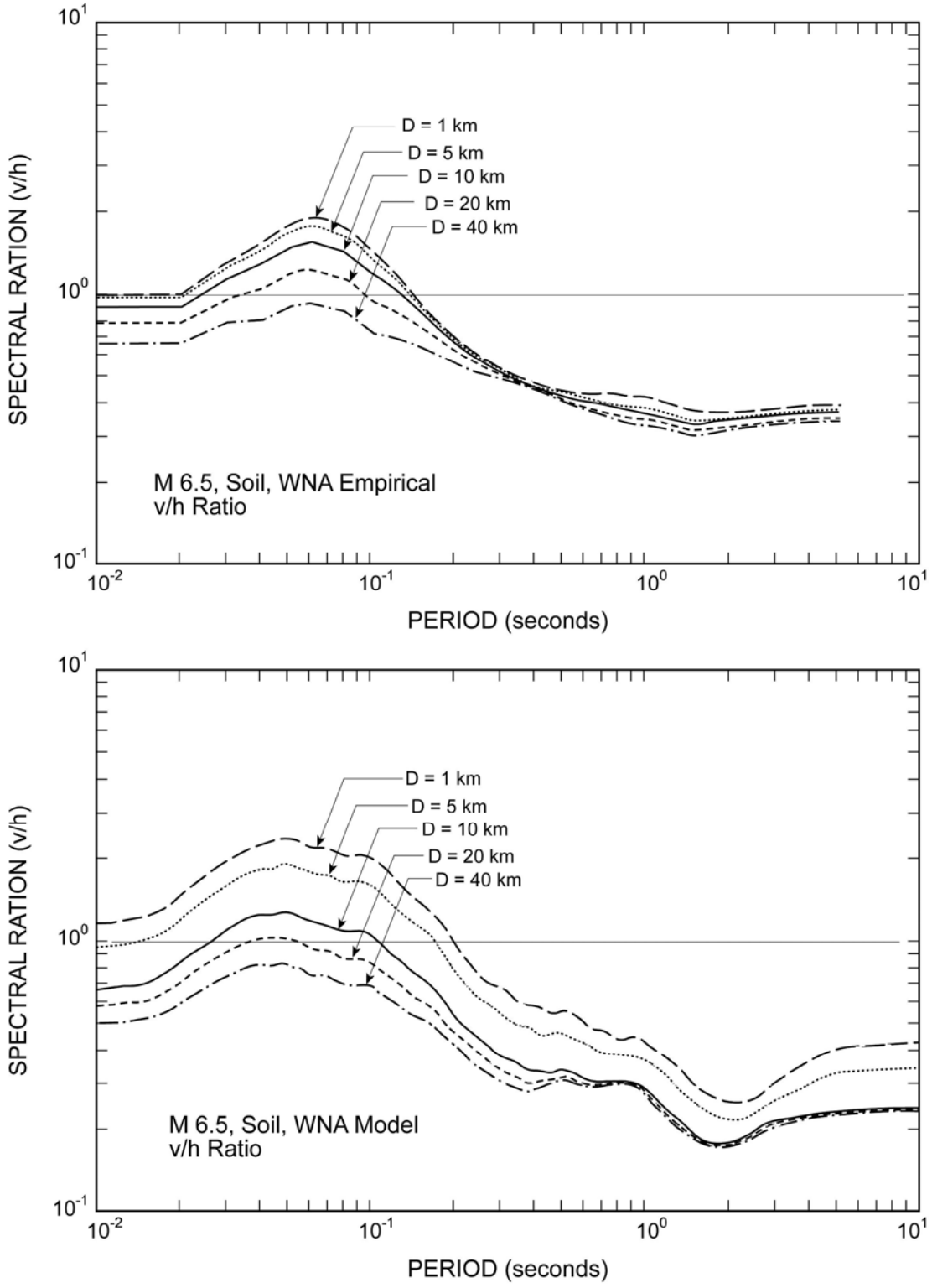

Source: Silva 1997 [DIRS 163747], Figure 30

Figure 7-21. Comparison of Western U.S. Empirical and Modeled Vertical-to-Horizontal Response Spectral Ratios for M 6.5, Soil Sites

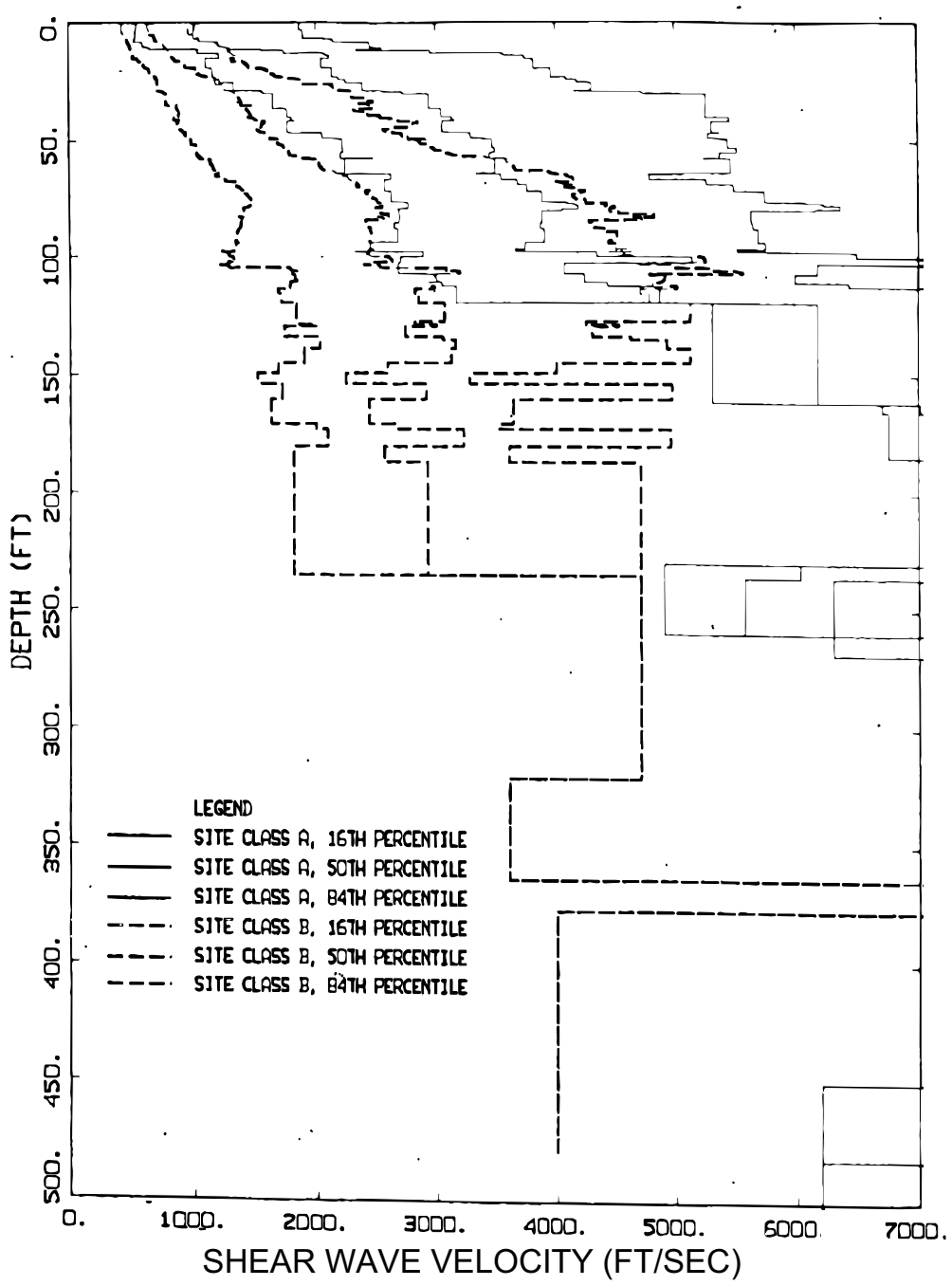

Source: Silva et al. 1996 [DIRS 110474], Figure 3.1a

Figure 7-22a. Velocity Profiles for Geomatrix Site Classes

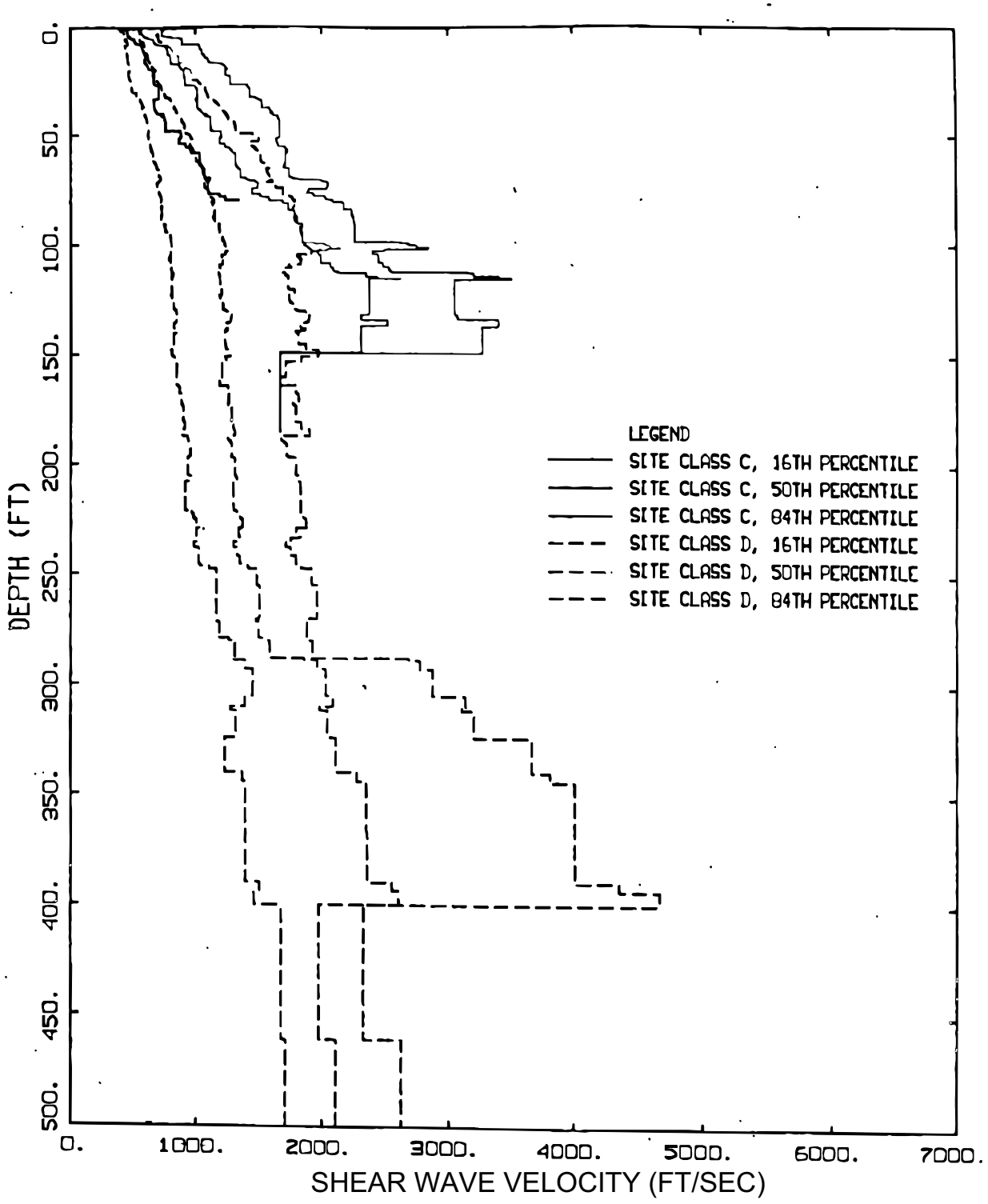

Source: Silva et al. 1996 [DIRS 110474], Figure 3.1b

Figure 7-22b. Velocity Profiles for Geomatrix Site Classes

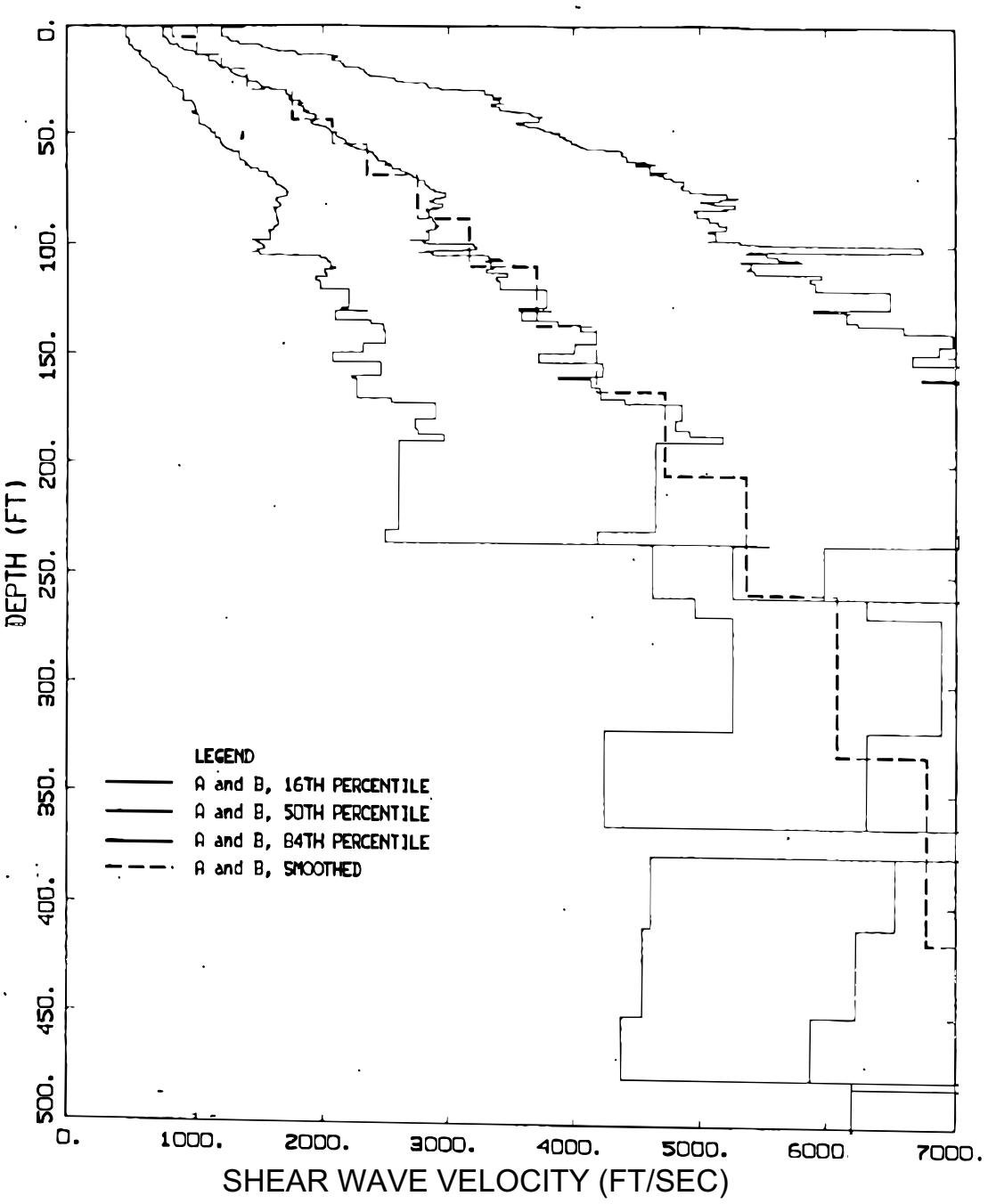

Source: Silva et al. 1996 [DIRS 110474], Figure 3.2

Figure 7-23. Velocity Profiles for Geomatrix Site Classes A and B

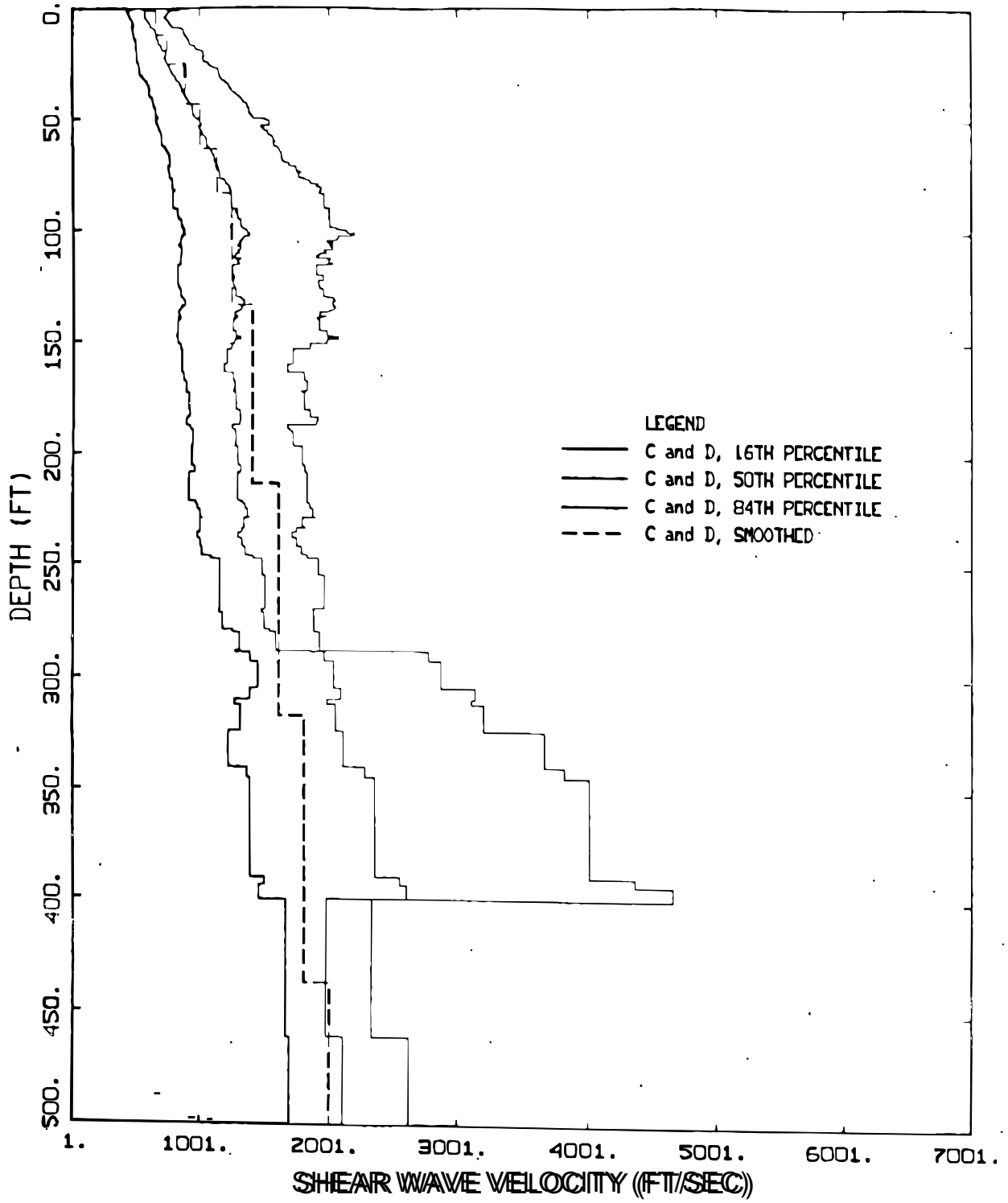

Source: Silva et al. 1996 [DIRS 110474], Figure 3.4

Figure 7-24. Velocity Profiles for Geomatrix Site Classes C and D

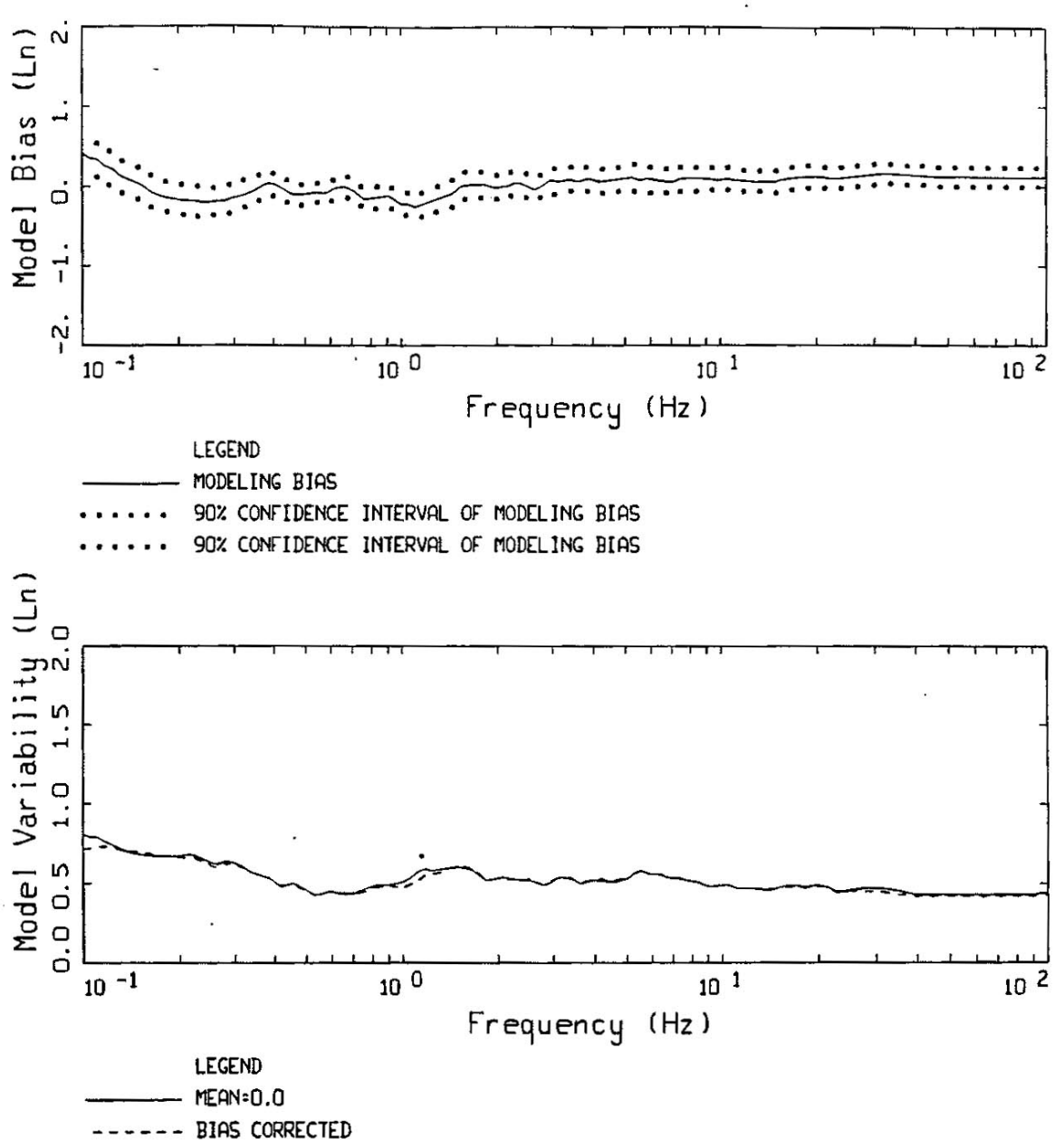

Source: Silva et al. 1996 [DIRS 110474], Figure 5.109

Figure 7-25. Model Bias and Variability for the Imperial Valley Earthquake, All 35 Sites

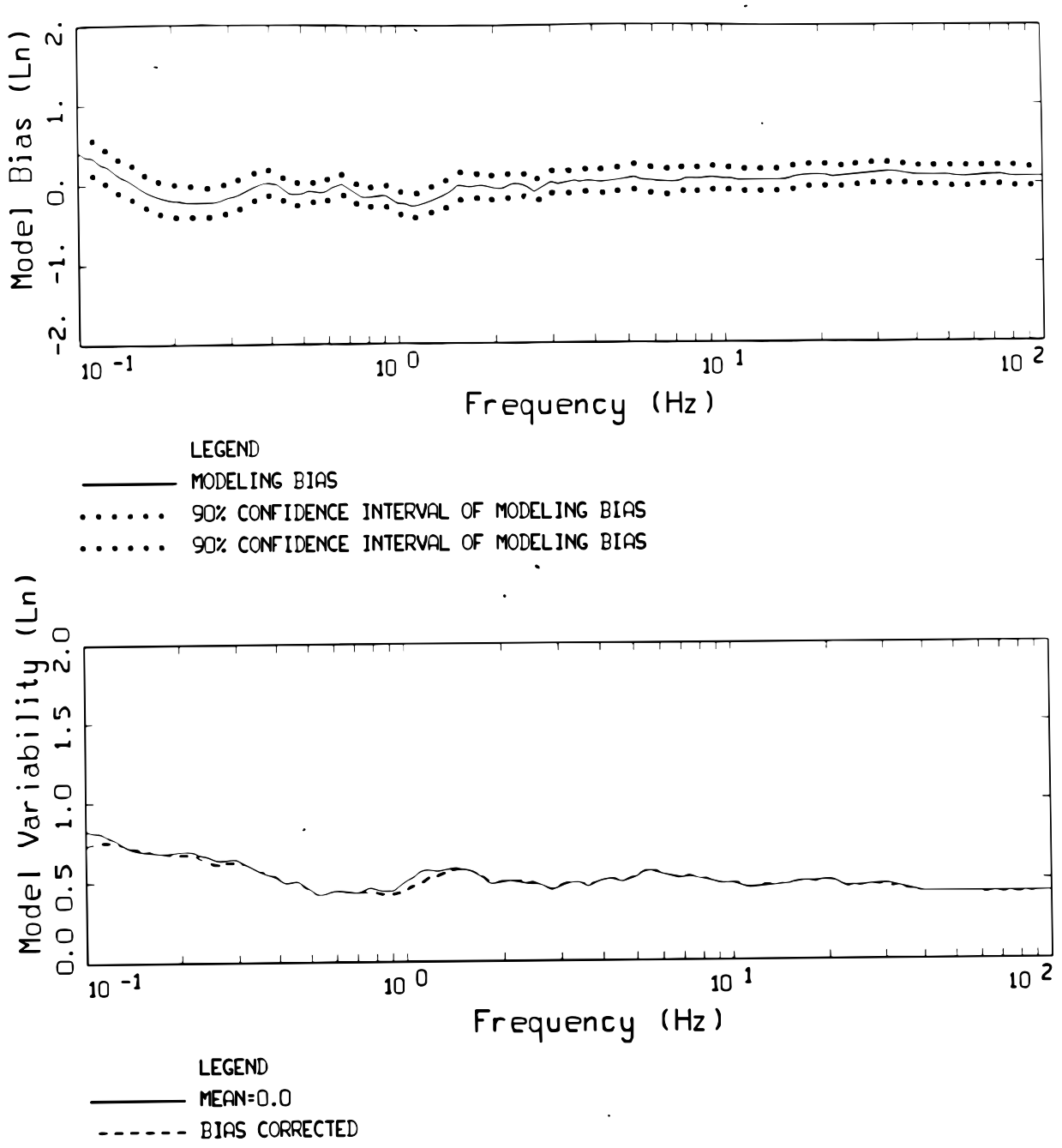

Source: Silva et al. 1996 [DIRS 110474], Figure 5.110

Figure 7-26. Model Bias and Variability for the Imperial Valley Earthquake, 33 Soil Sites

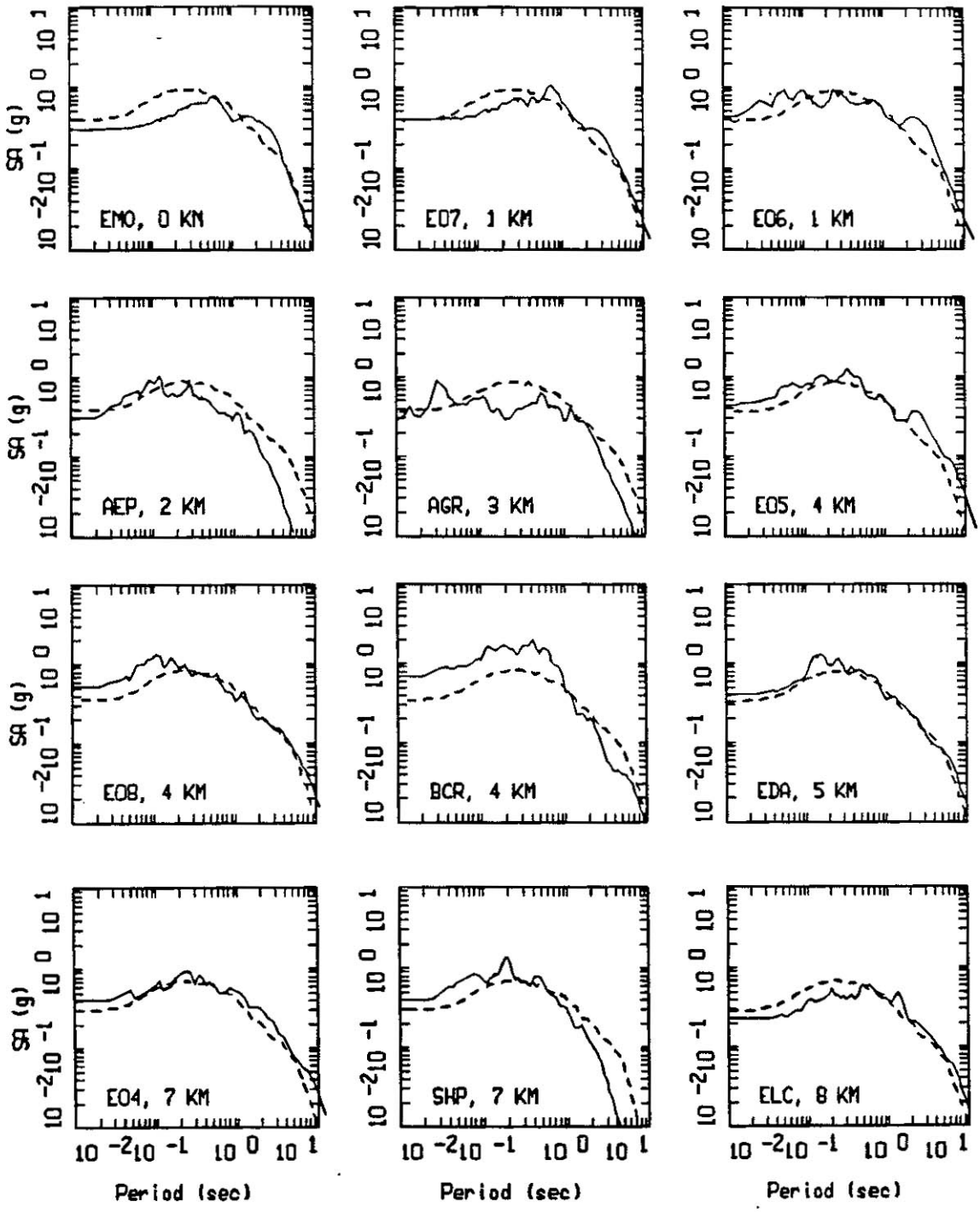

Source: Silva et al. 1996 [DIRS 110474], Figure 5.111

Figure 7-27a. Comparison of Modeled (Dashed) and Observed (Solid) 5%-Damped Acceleration Response Spectra for the Imperial Valley Earthquake, All 35 Sites (1 of 3)

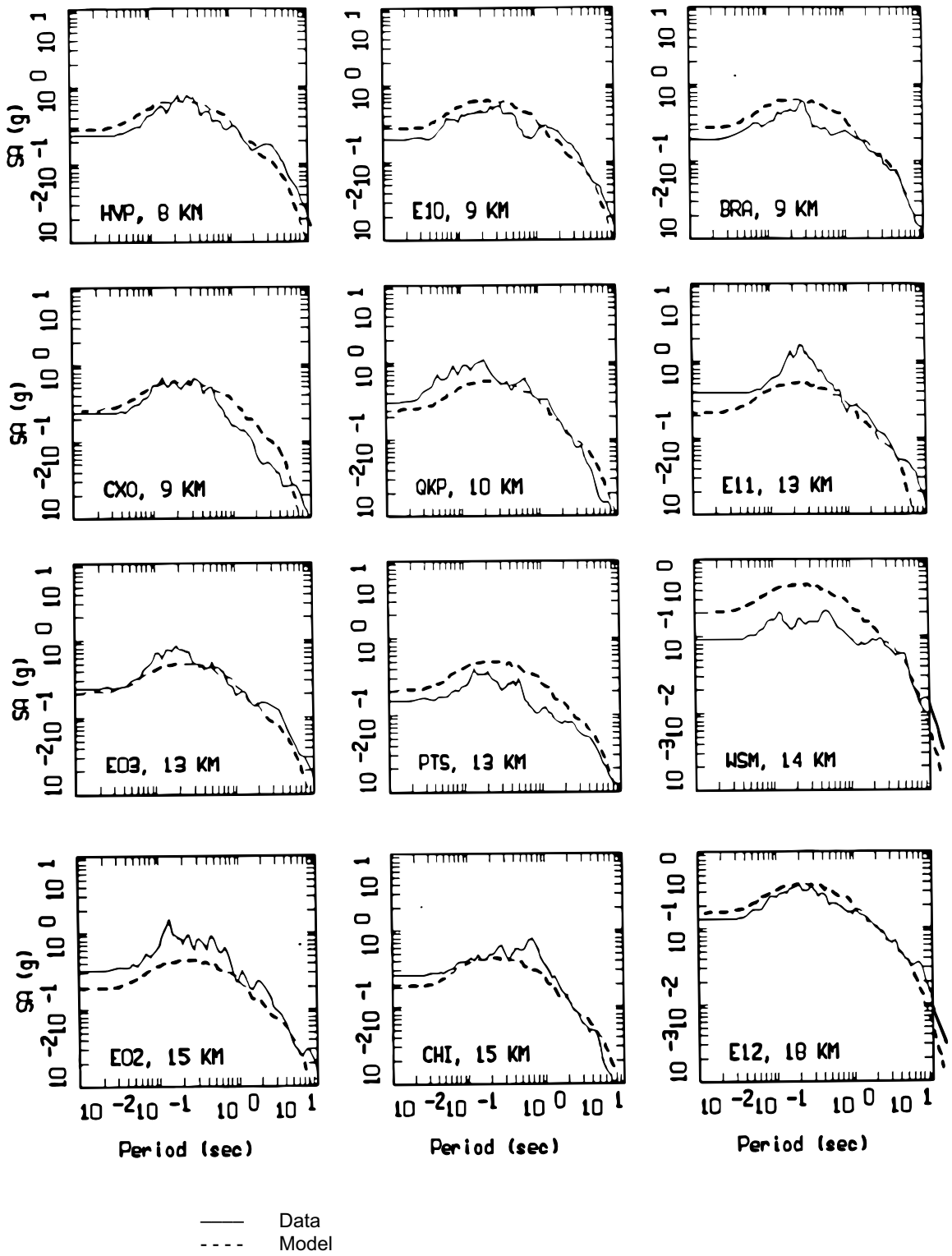

Figure 7-27b. Comparison of Modeled (Dashed) and Observed (Solid) 5%-Damped Acceleration Response Spectra for the Imperial Valley Earthquake, All 35 Sites (2 of 3)

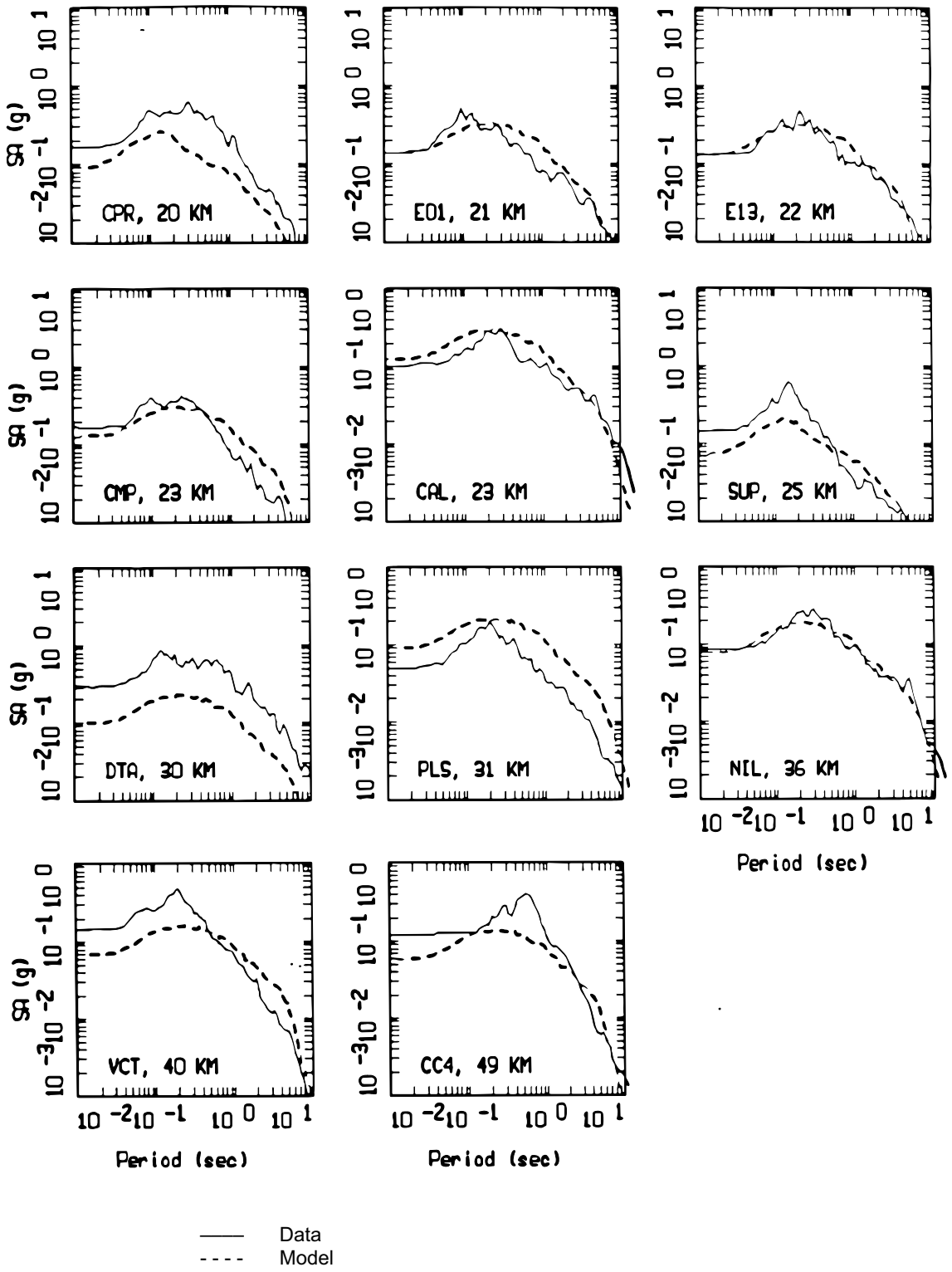

Figure 7-27c. Comparison of Modeled (Dashed) and Observed (Solid) 5%-Damped Acceleration Response Spectra for the Imperial Valley Earthquake, All 35 Sites (3 of 3)

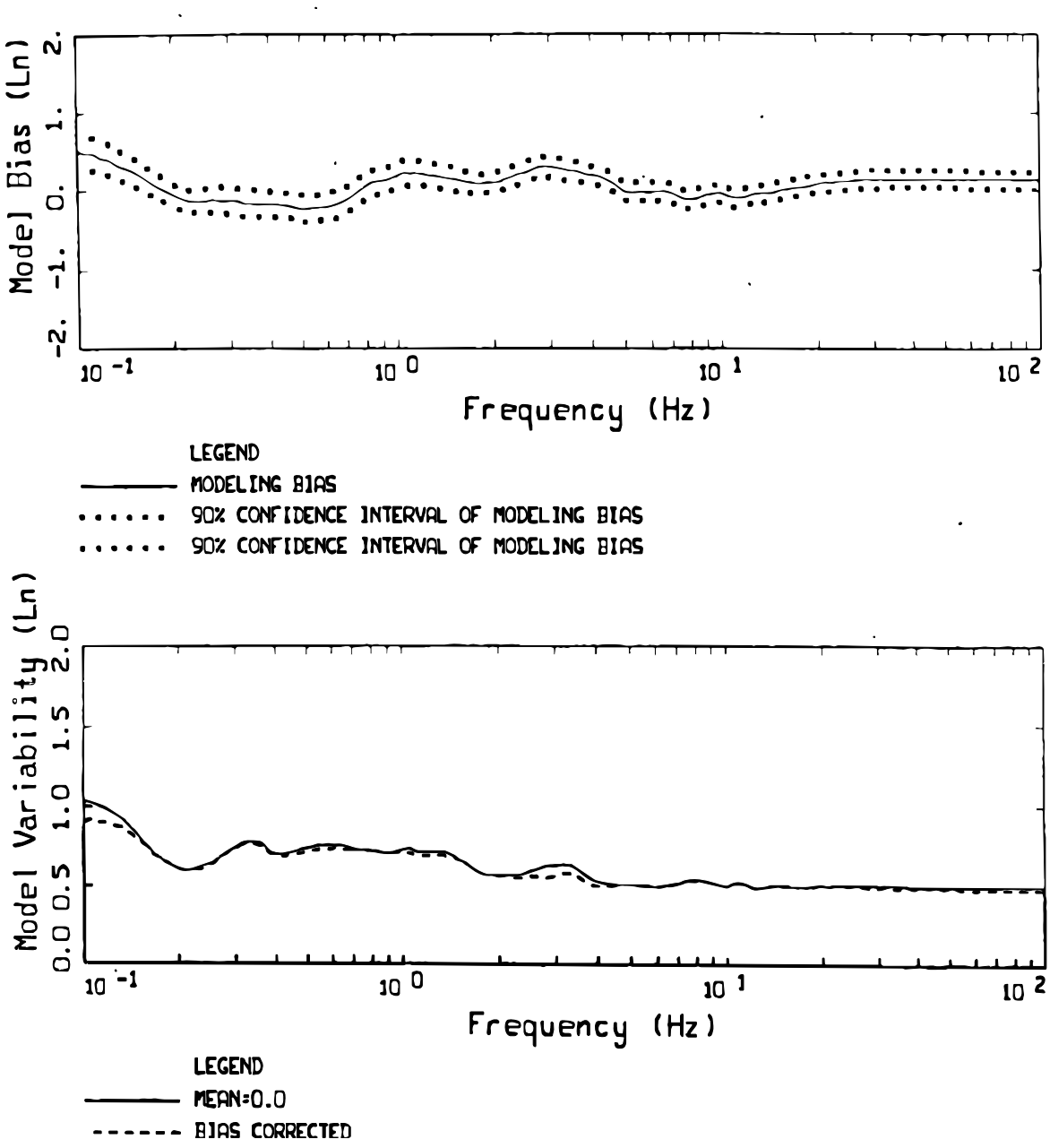

Source: Silva et al. 1996 [DIRS 110474], Figure 5.44

Figure 7-28. Model Bias and Variability for the Loma Prieta Earthquake, All 53 Sites

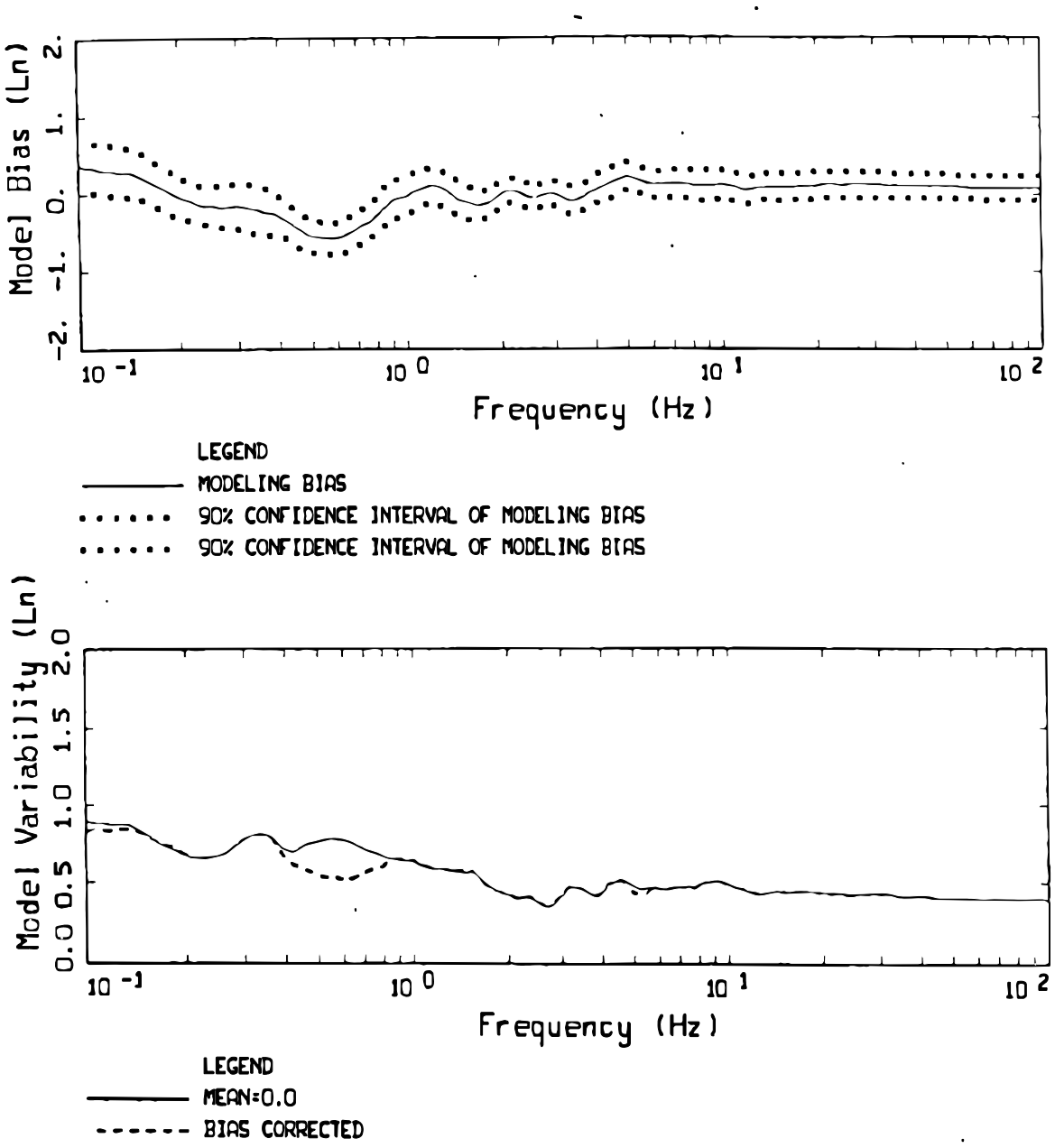

Source: Silva et al. 1996 [DIRS 110474], Figure 5.45

Figure 7-29. Model Bias and Variability for the Loma Prieta Earthquake, 20 Soil Sites

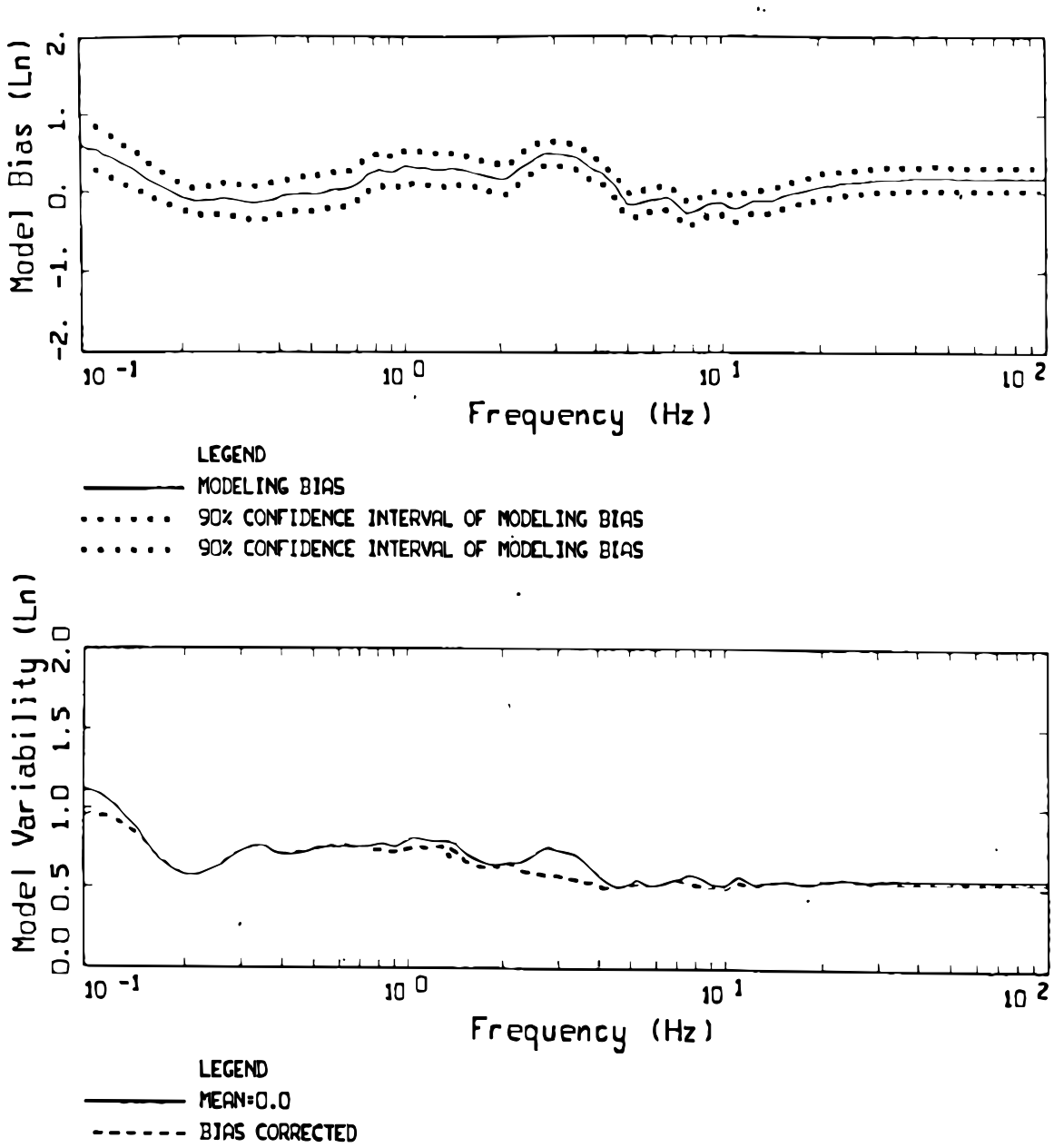

Source: Silva et al. 1996 [DIRS 110474], Figure 5.46

Figure 7-30. Model Bias and Variability for the Loma Prieta Earthquake, 33 Rock Sites

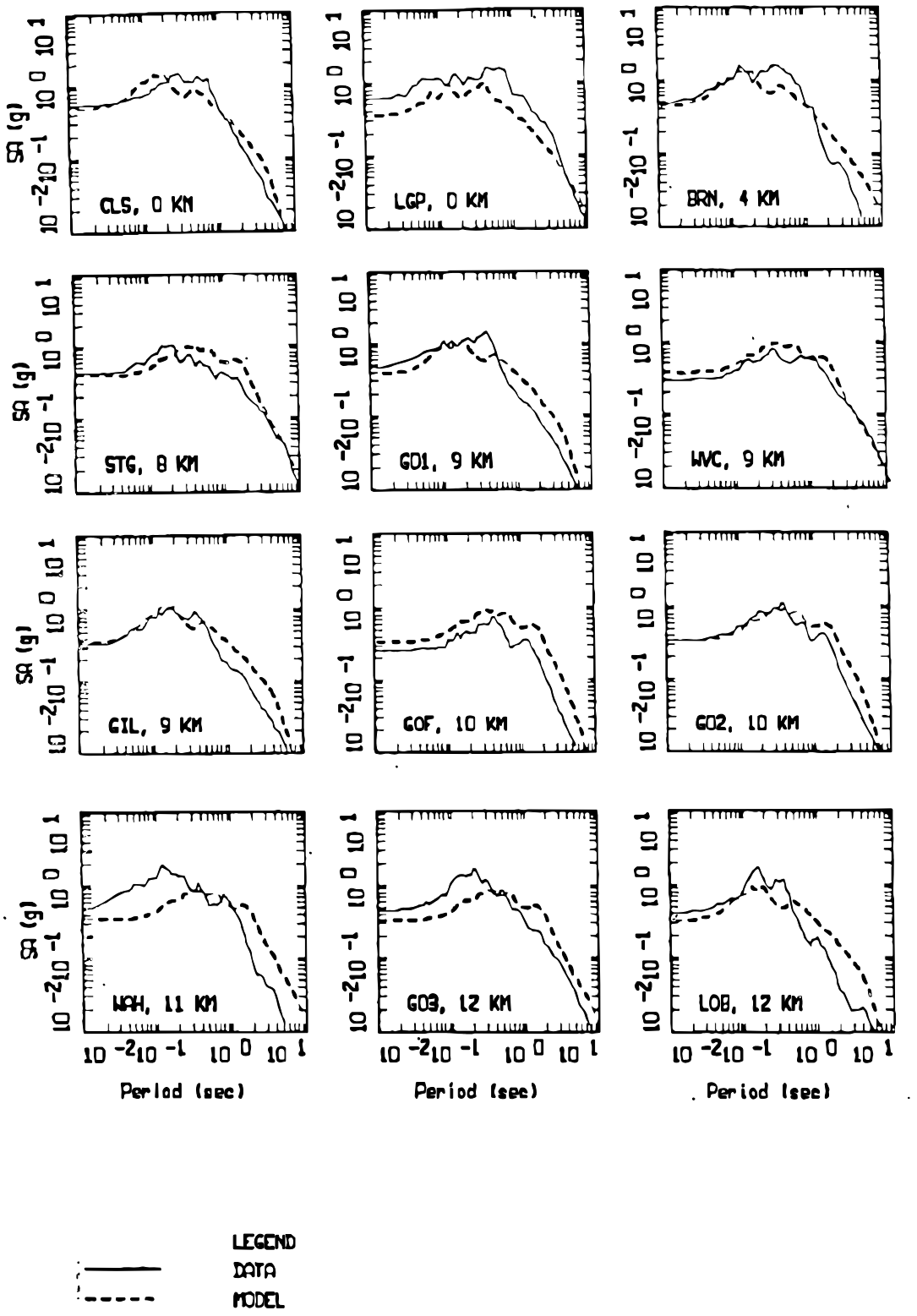

Source: Silva et al. 1996 [DIRS 110474], Figure 5.47

Figure 7-31a. Comparison of Modeled and Observed 5%-Damped Acceleration Response Spectra for the Loma Prieta Earthquake, All 53 Sites (1 of 5)

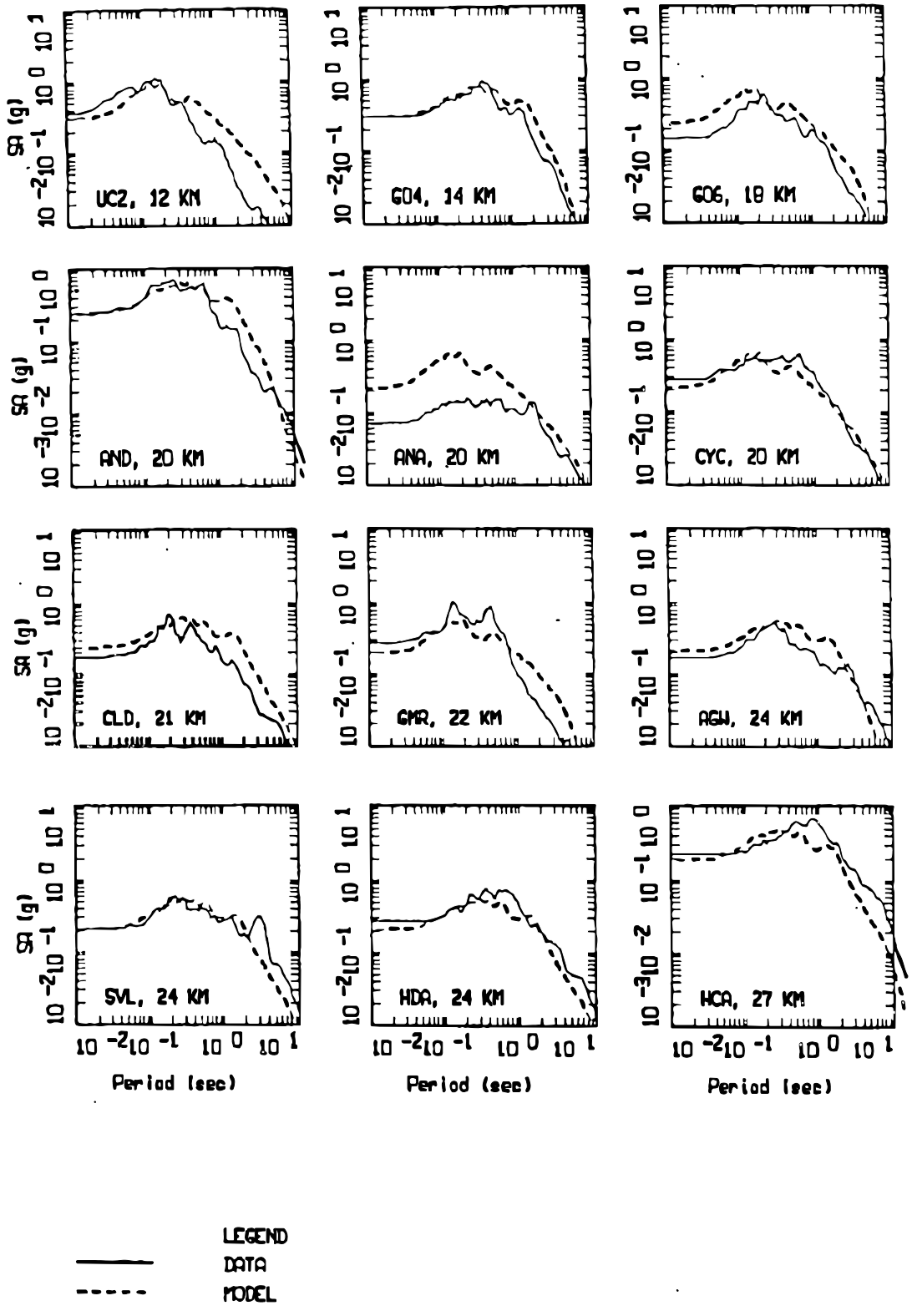

Figure 7-31b. Comparison of Modeled and Observed 5%-Damped Acceleration Response Spectra for the Loma Prieta Earthquake, All 53 Sites (2 of 5)

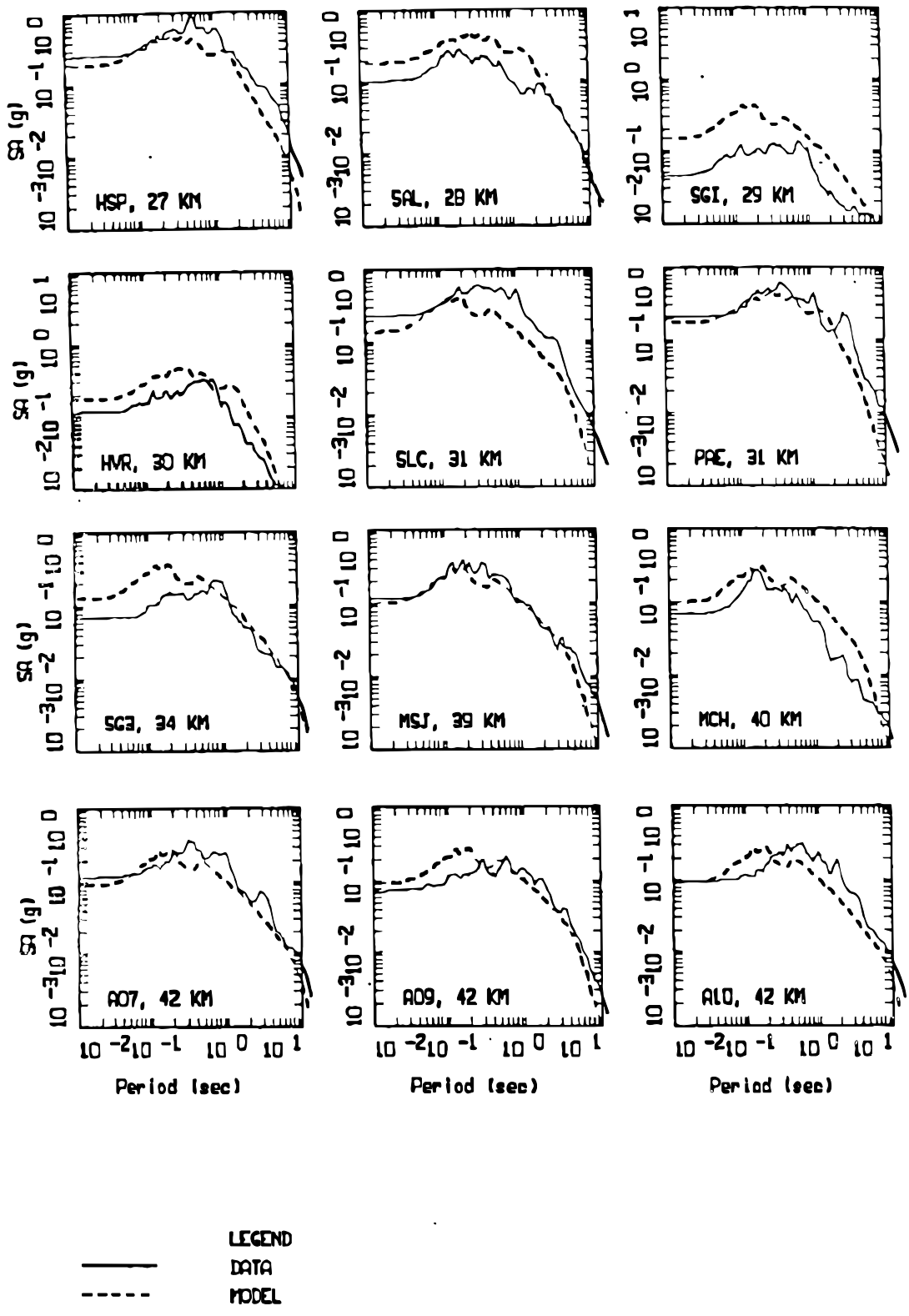

Figure 7-31c. Comparison of Modeled and Observed 5%-Damped Acceleration Response Spectra for the Loma Prieta Earthquake, All 53 Sites (3 of 5)

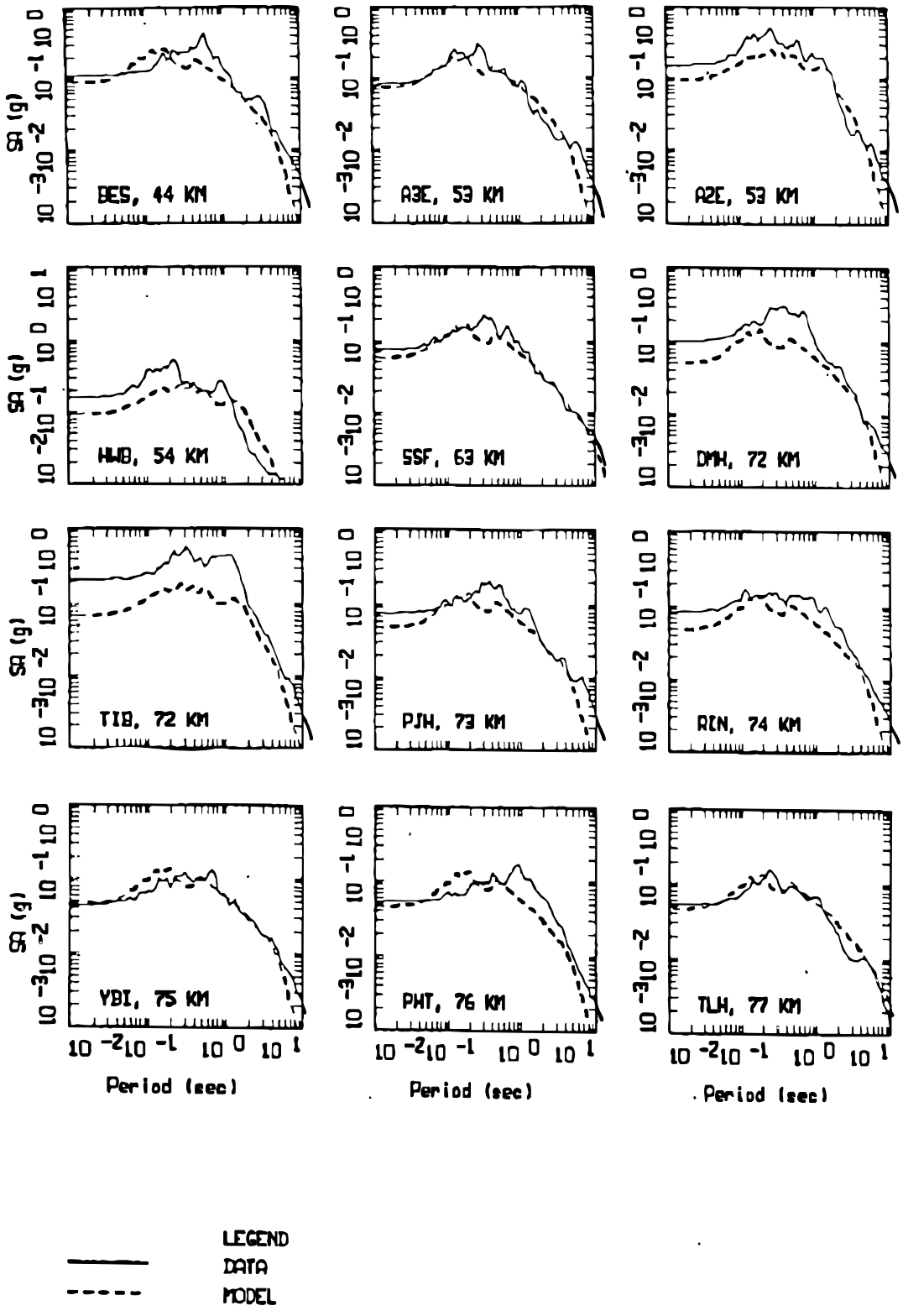

Figure 7-31d. Comparison of Modeled and Observed 5%-Damped Acceleration Response Spectra for the Loma Prieta Earthquake, All 53 Sites (4 of 5)

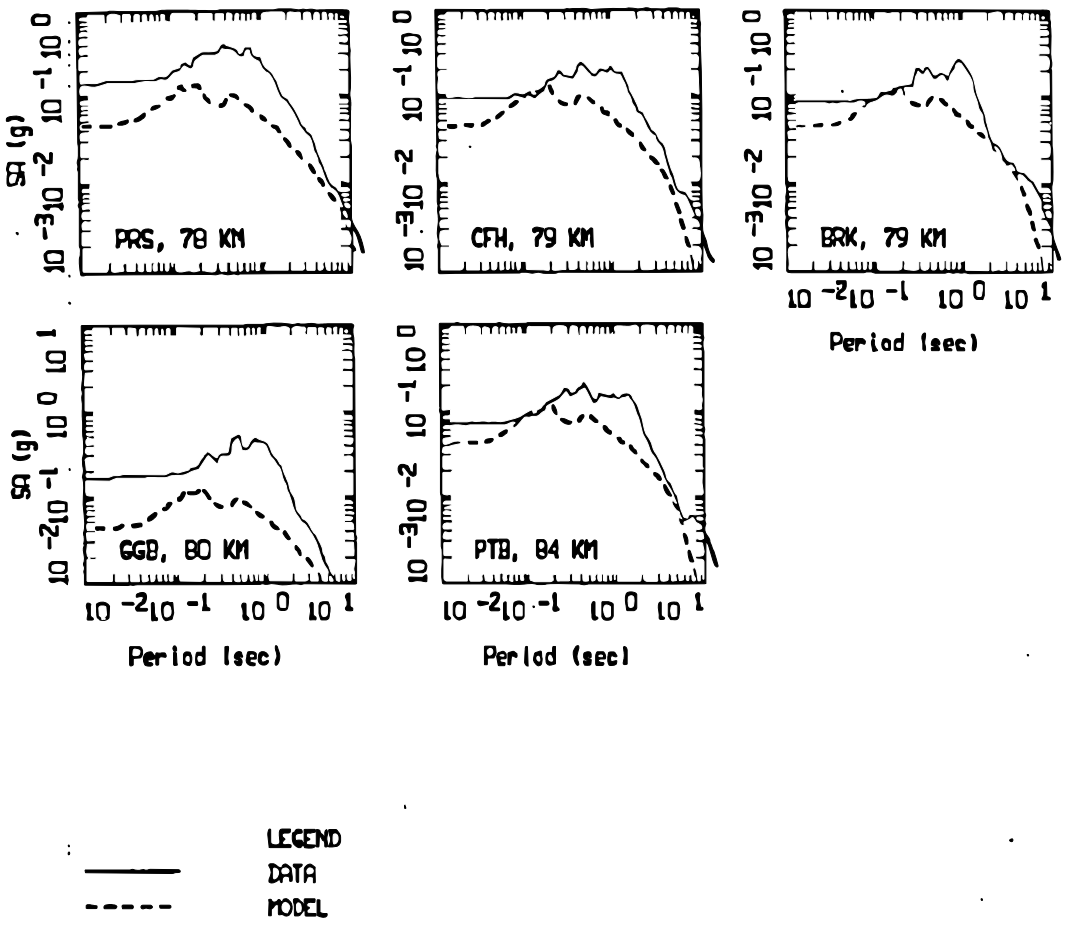

Figure 7-31e. Comparison of Modeled and Observed 5%-Damped Acceleration Response Spectra for the Loma Prieta Earthquake, All 53 Sites (5 of 5)

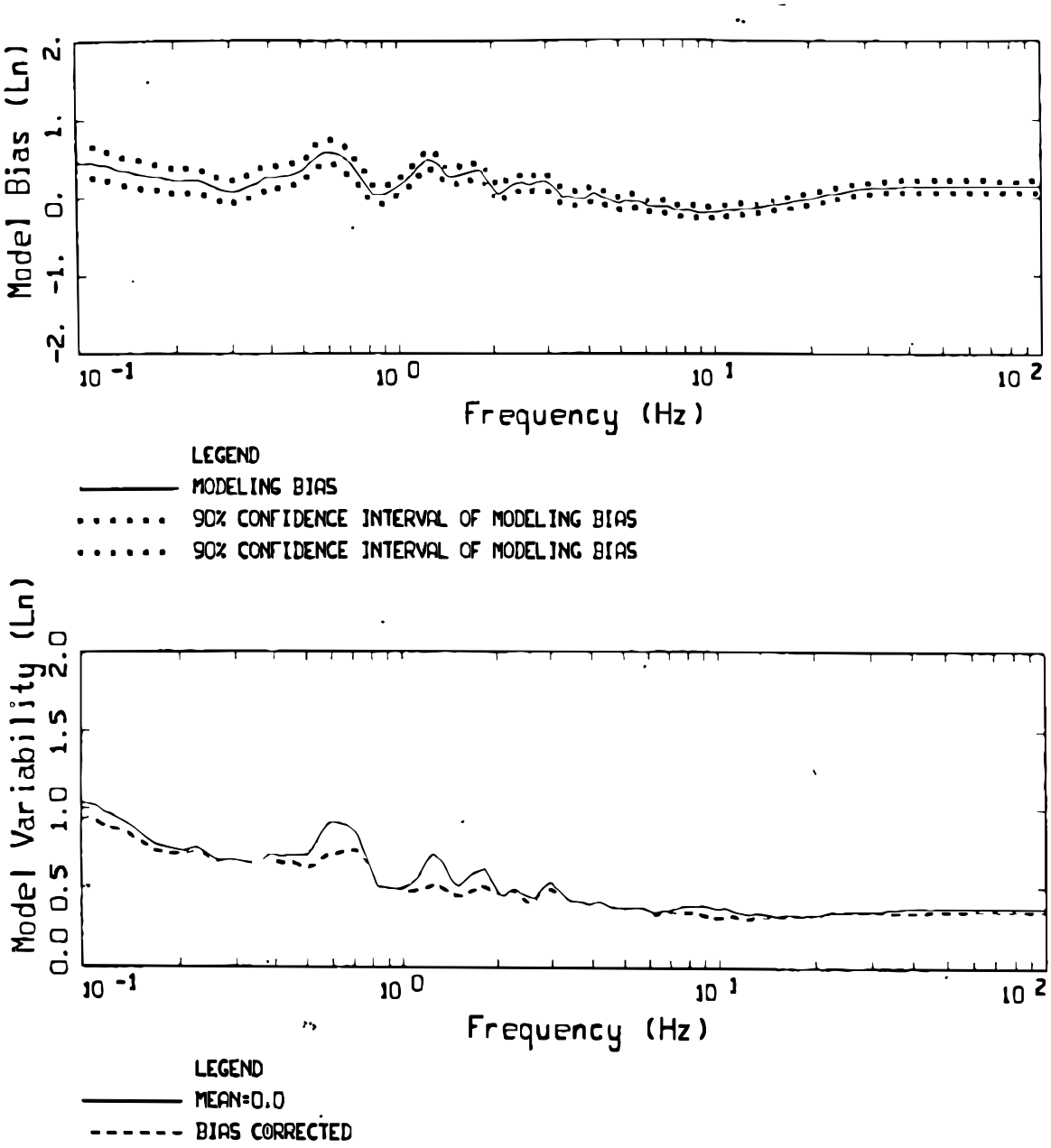

Source: Silva et al. 1996 [DIRS 110474], Figure 5.76

Figure 7-32. Model Bias and Variability for the Landers Earthquake, All 57 Sites

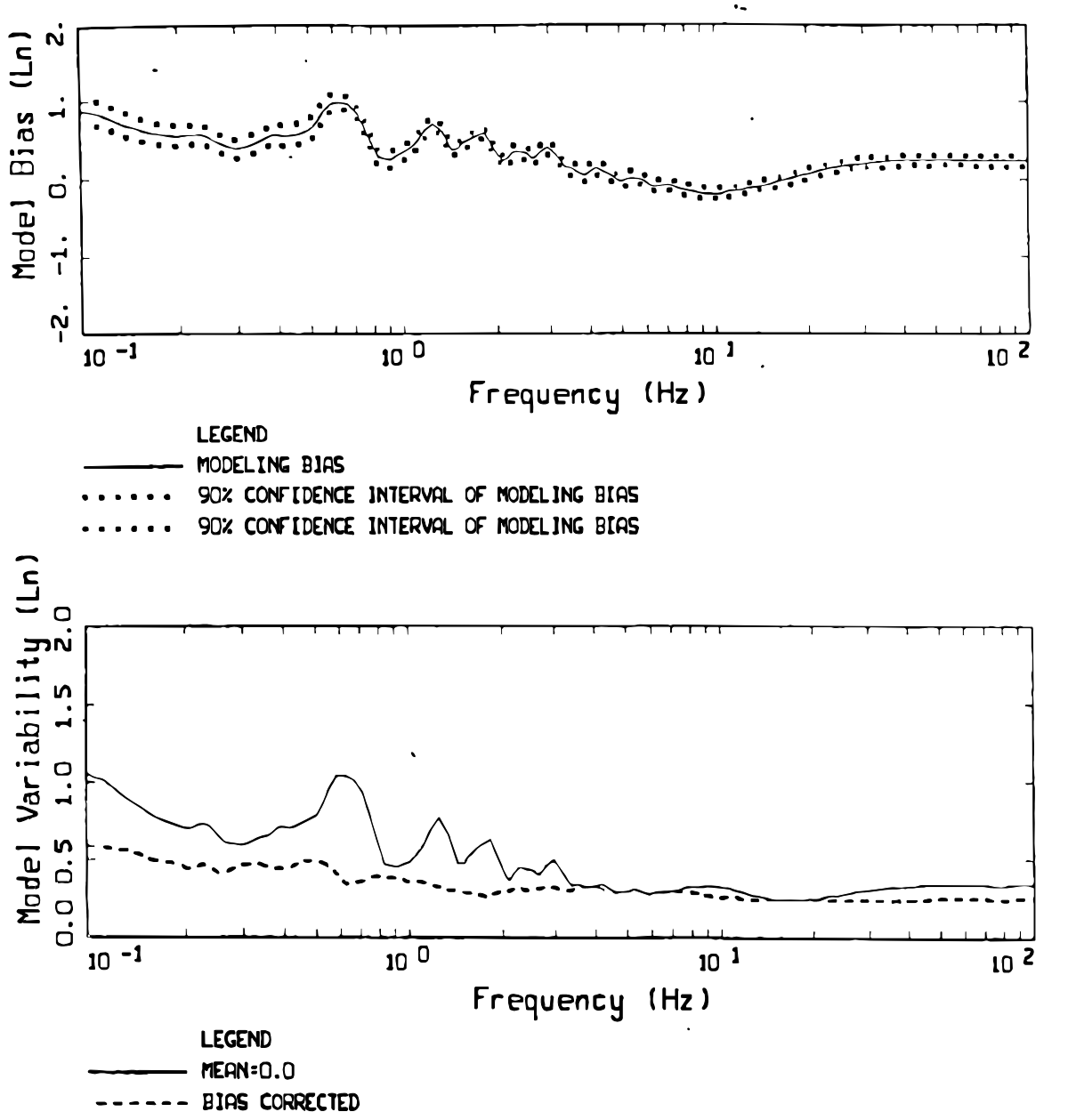

Source: Silva et al. 1996 [DIRS 110474], Figure 5.77

Figure 7-33. Model Bias and Variability for the Landers Earthquake, All 39 Peninsular Range Sites

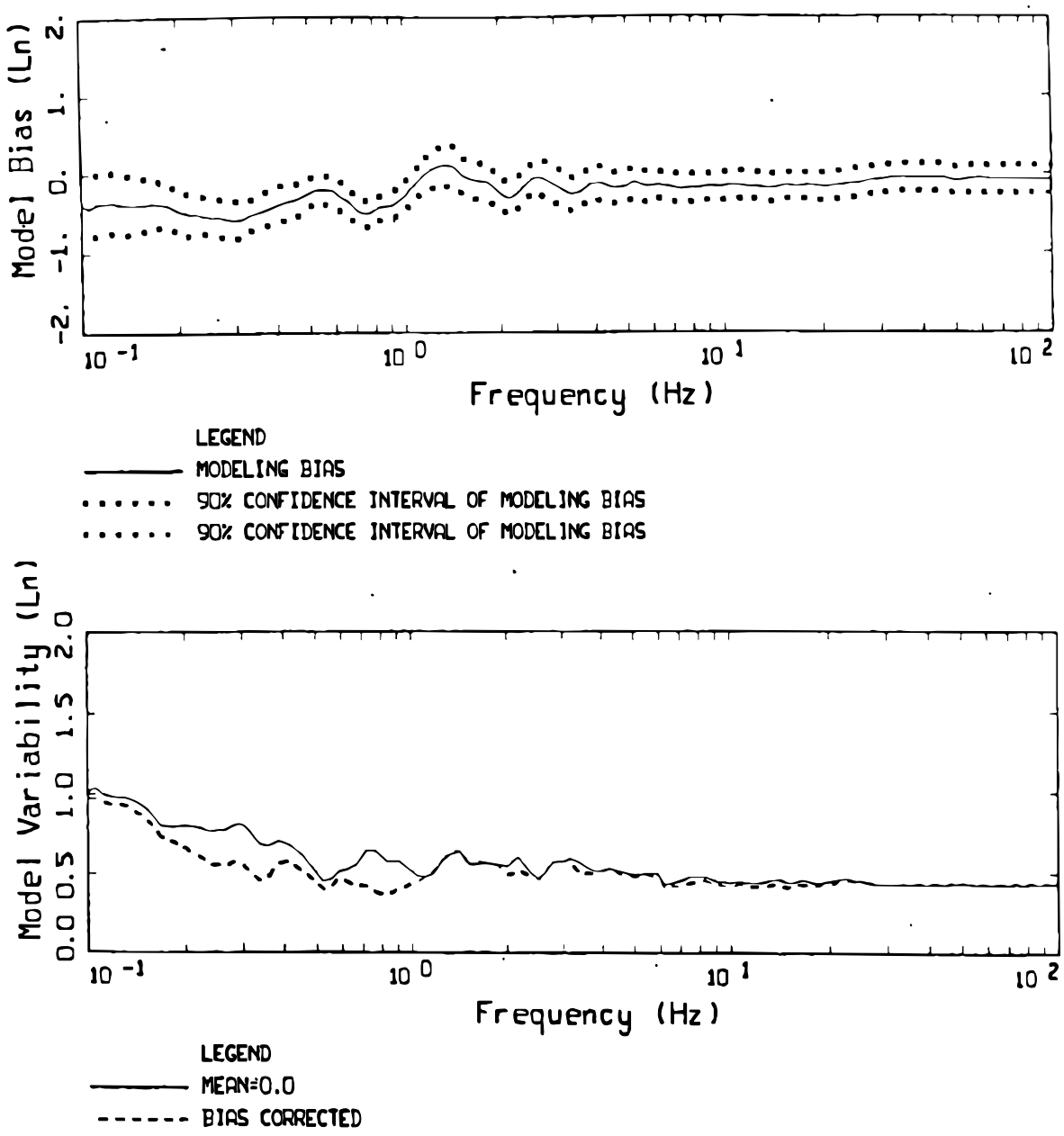

Source: Silva et al. 1996 [DIRS 110474], Figure 5.78

Figure 7-34. Model Bias and Variability for the Landers Earthquake, All 18 Mojave Sites

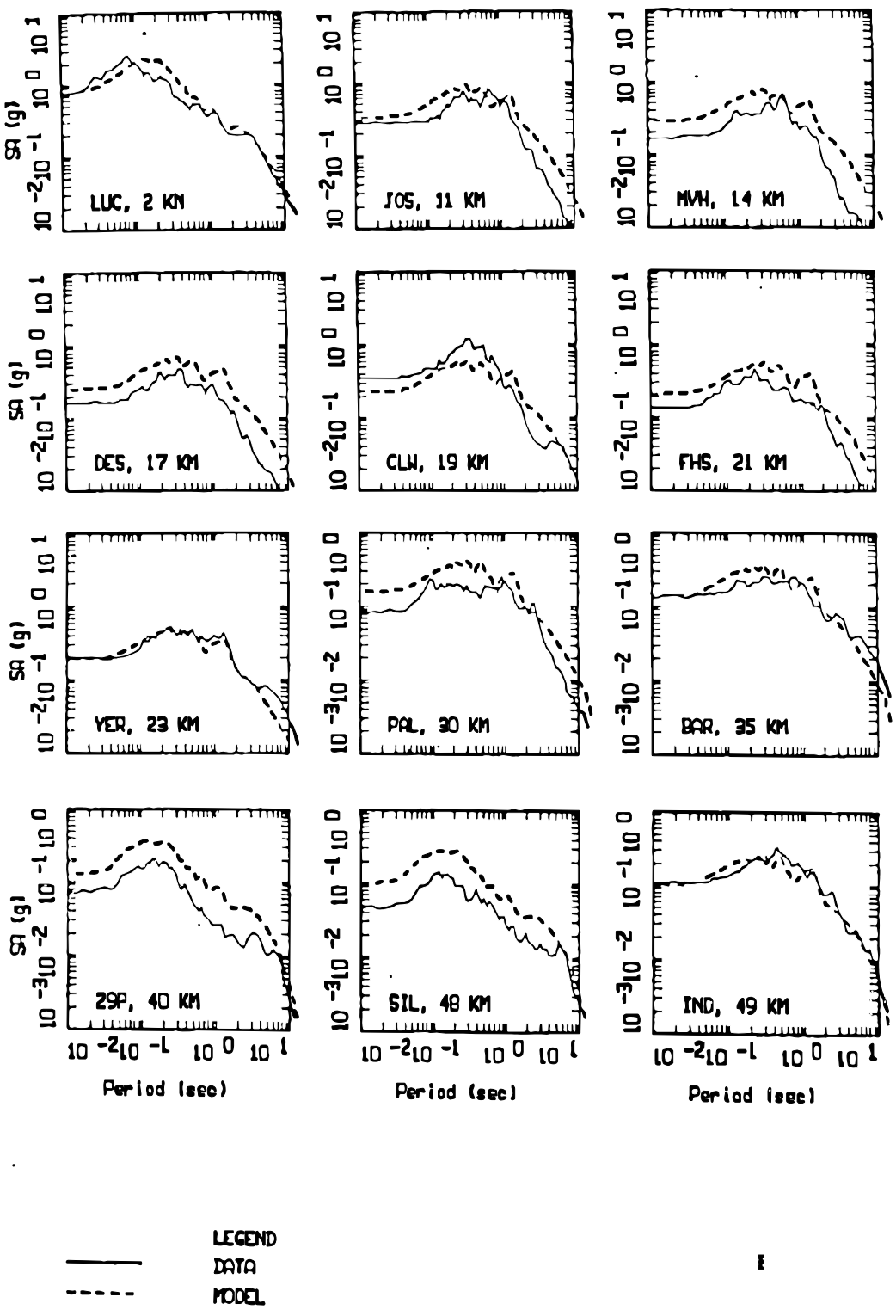

Source: Silva et al. 1996 [DIRS 110474], Figure 5.79

Figure 7-35a. Comparison of Modeled and Observed 5%-Damped Acceleration Response Spectra for the Landers Earthquake, All 57 Sites (1 of 5)

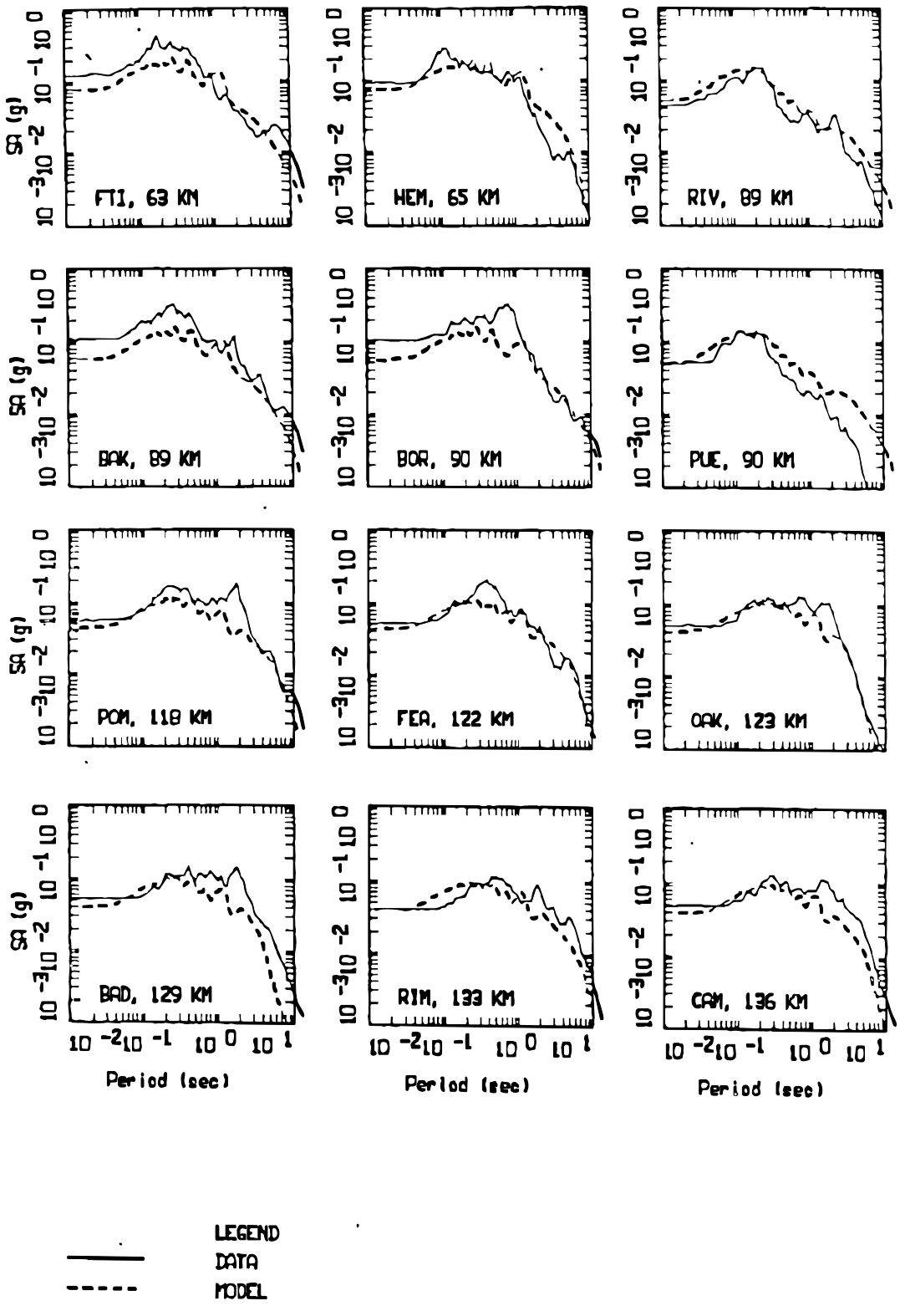

Figure 7-35b. Comparison of Modeled and Observed 5%-Damped Acceleration Response Spectra for the Landers Earthquake, All 57 Sites (2 of 5)

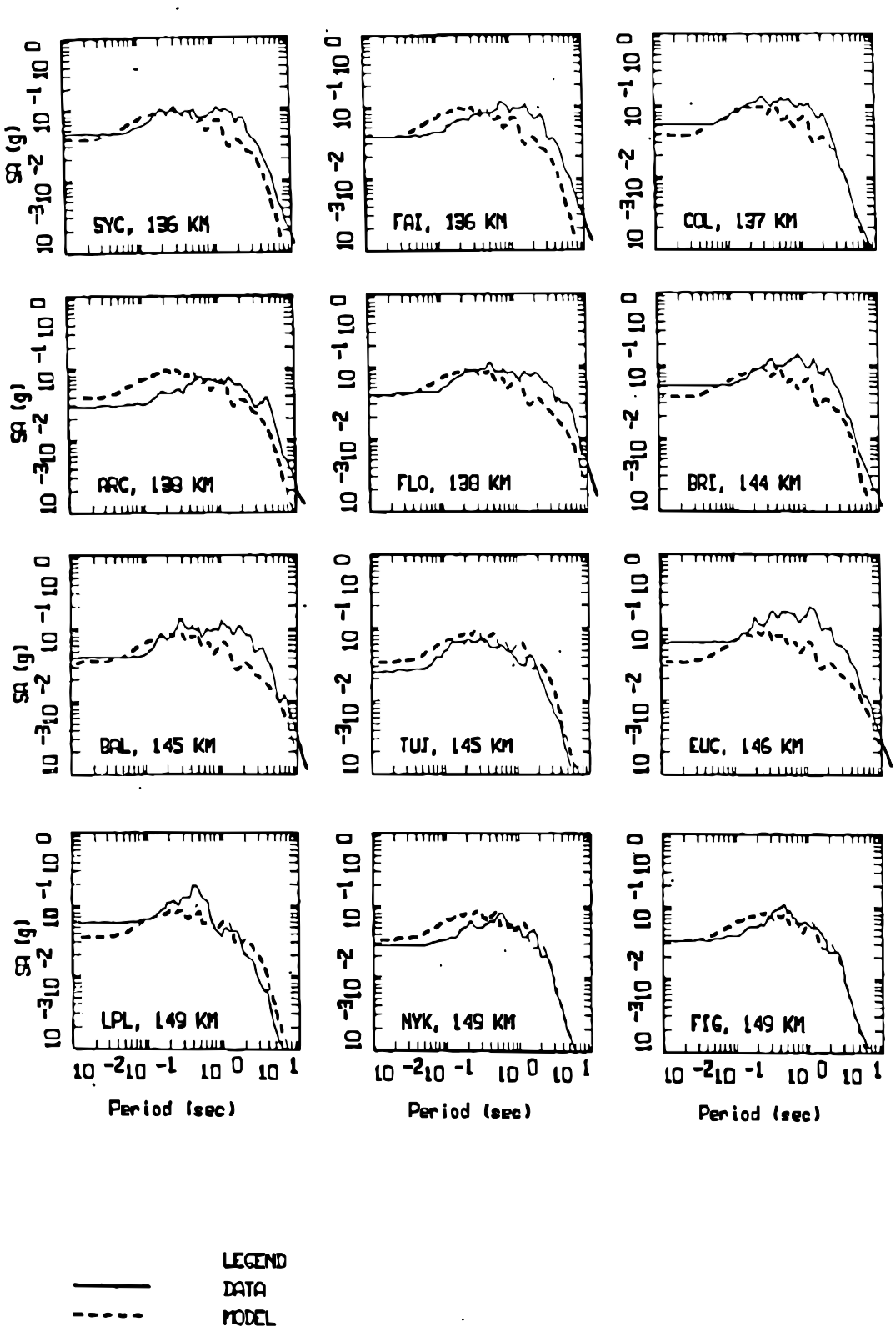

Figure 7-35c. Comparison of Modeled and Observed 5%-Damped Acceleration Response Spectra for the Landers Earthquake, All 57 Sites (3 of 5)

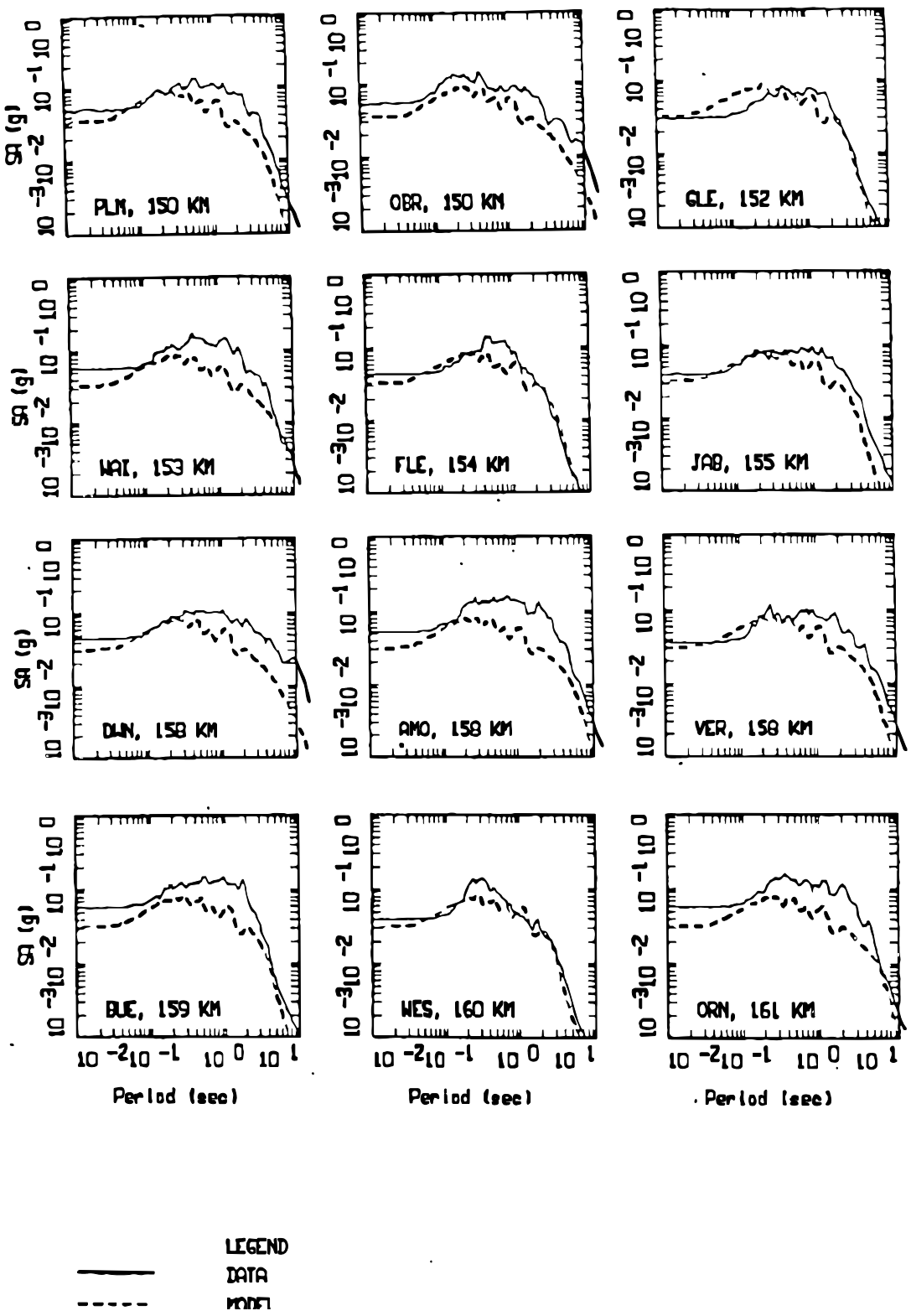

Figure 7-35d. Comparison of Modeled and Observed 5%-Damped Acceleration Response Spectra for the Landers Earthquake, All 57 Sites (4 of 5)

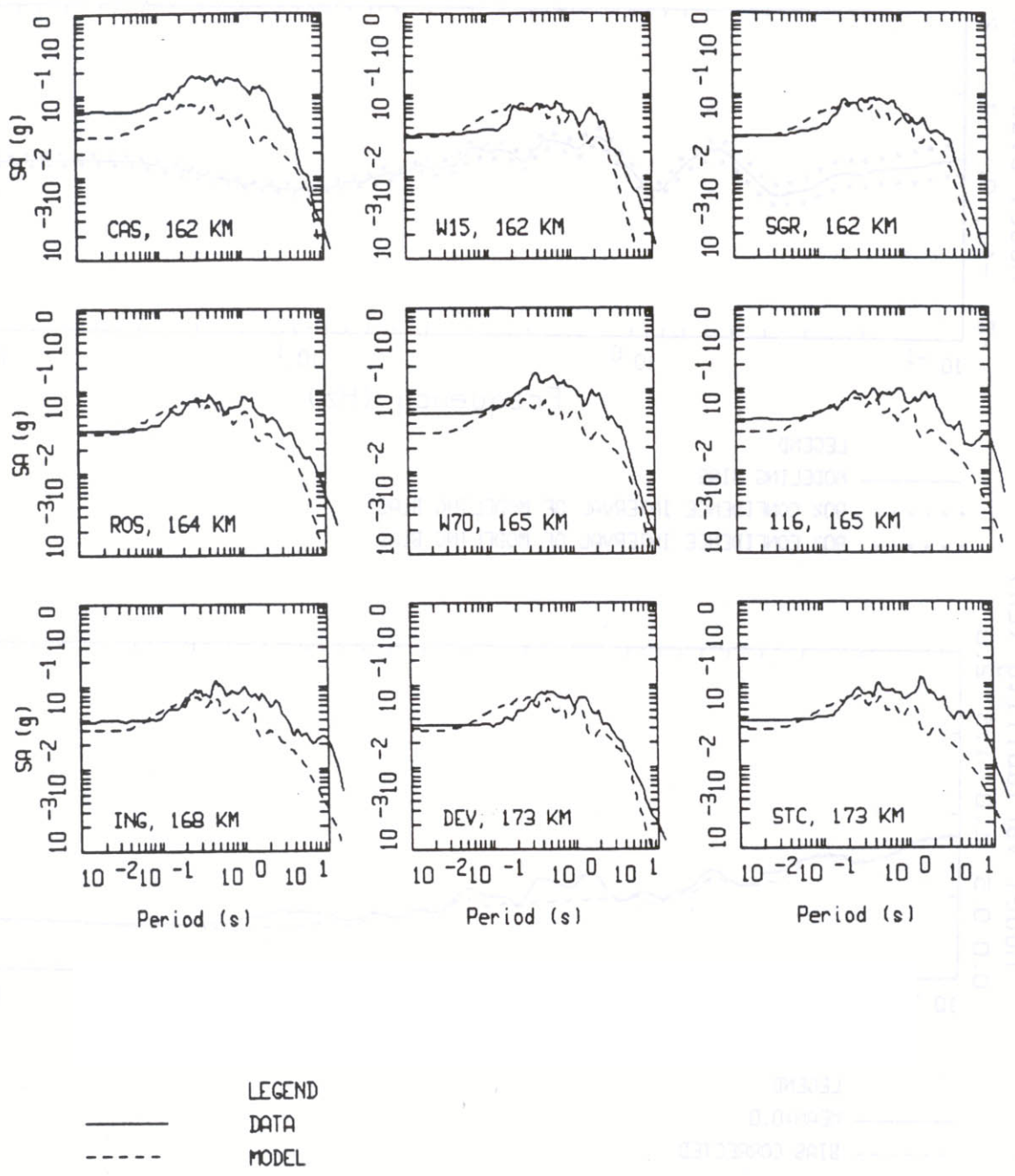

Figure 7-35e. Comparison of Modeled and Observed 5%-Damped Acceleration Response Spectra for the Landers Earthquake, All 57 Sites (5 of 5)

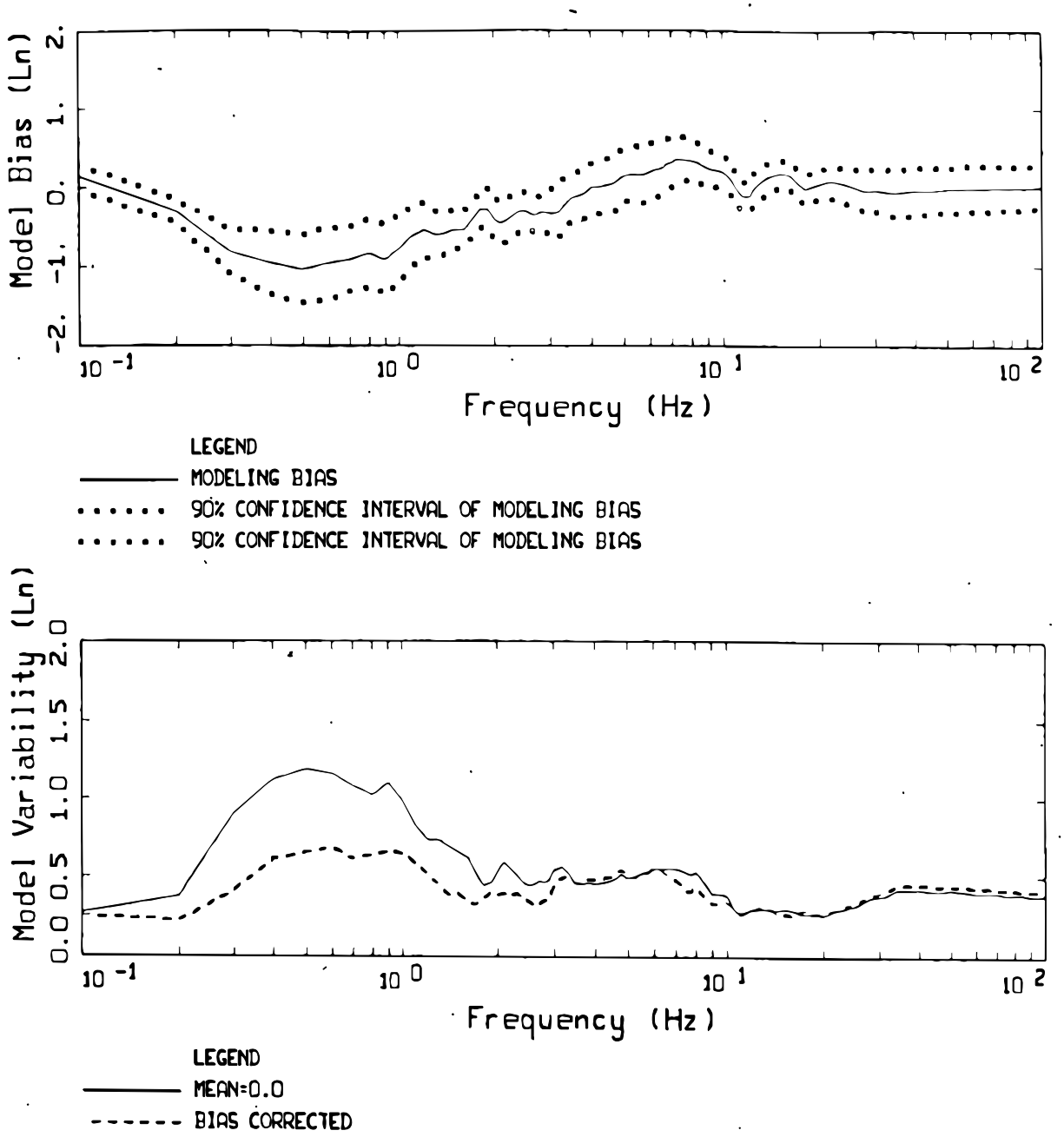

Source: Silva et al. 1996 [DIRS 110474], Figure 5.141

Figure 7-36. Model Bias and Variability for the Little Skull Mountain Earthquake, All 8 Sites

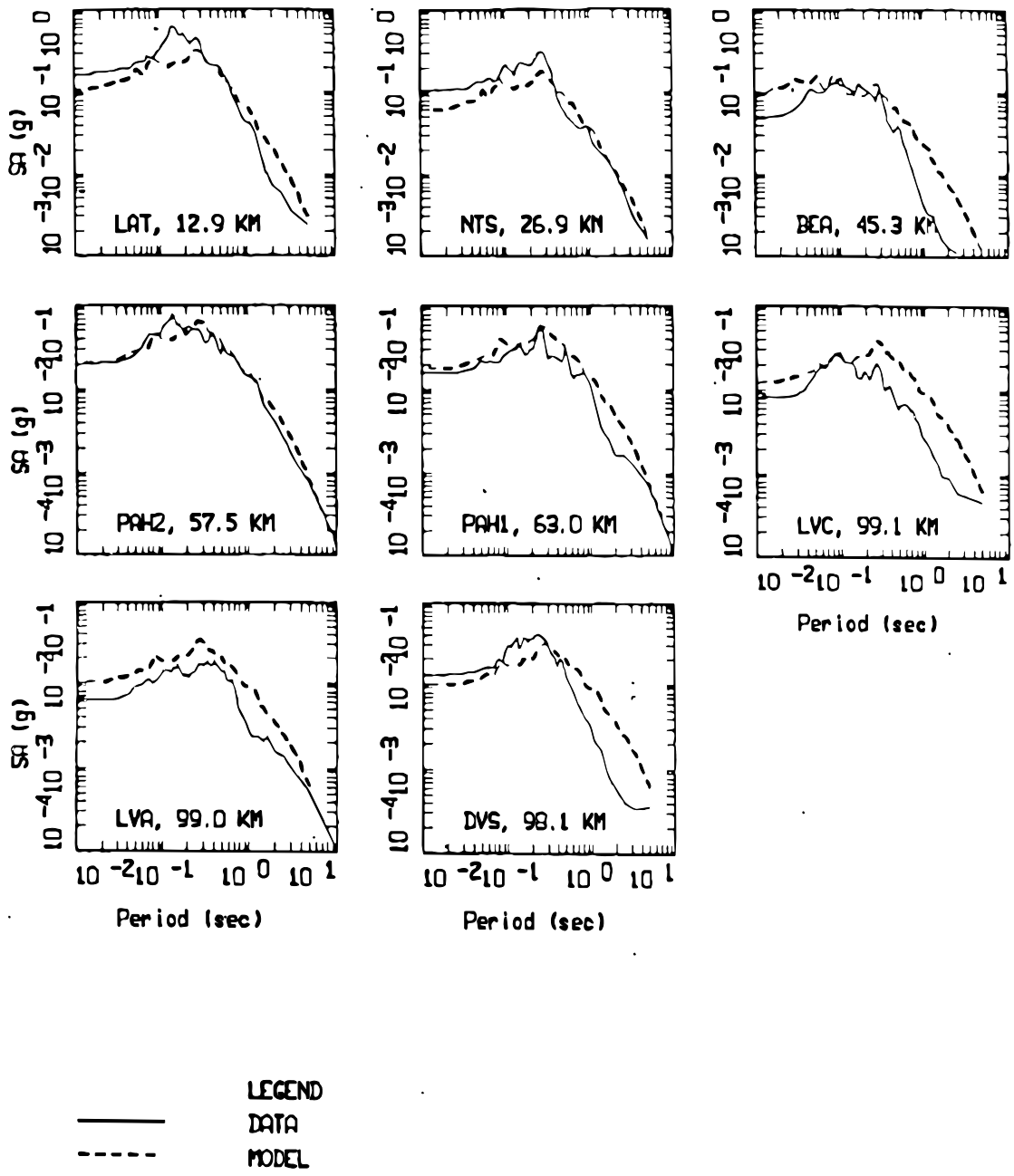

Source: Silva et al. 1996 [DIRS 110474], Figure 5.142

Figure 7-37. Comparison of Modeled and Observed 5%-Damped Acceleration Response Spectra for the Little Skull Mountain Earthquake, All 8 Sites

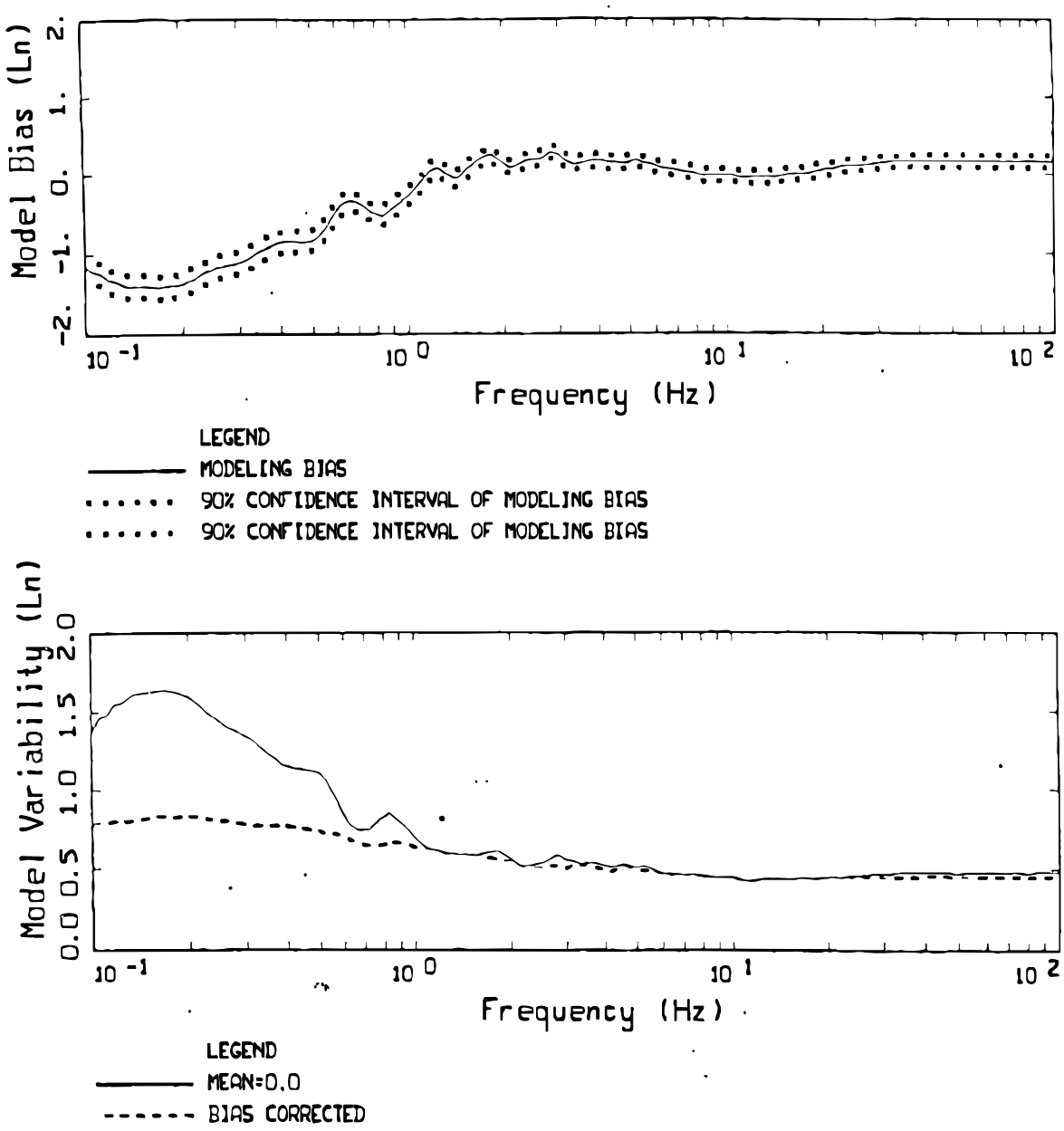

Source: Silva et al. 1996 [DIRS 110474], Figure 5.3

Figure 7-38. Model and Bias Variability for the Northridge Earthquake, All 94 Sites

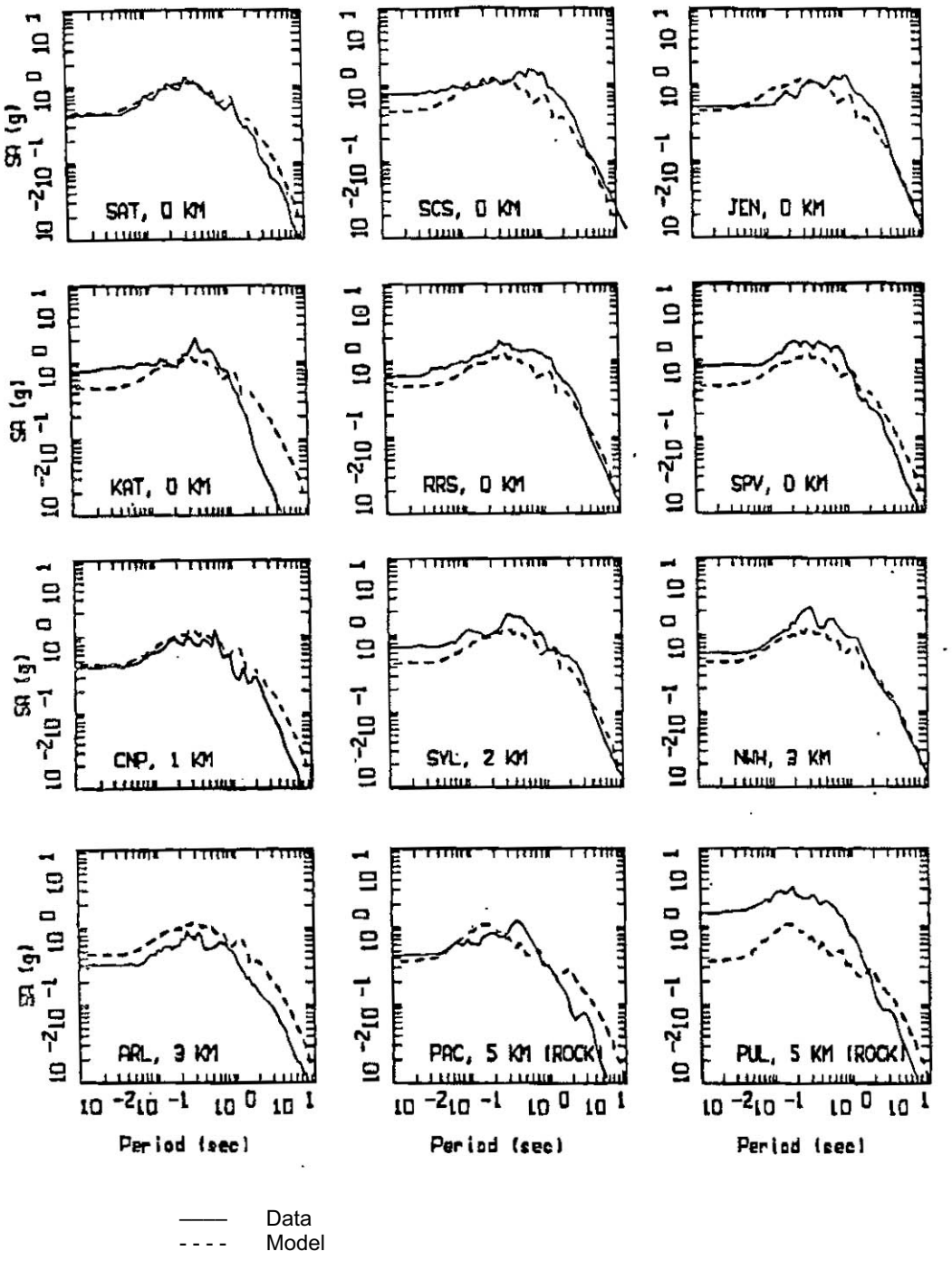

Source: Silva et al. 1996 [DIRS 110474], Figure 5.6

Figure 7-39a. Comparison of Modeled and Observed 5%-Damped Acceleration Response Spectra for the Northridge Earthquake, All 94 Sites (1 of 8)

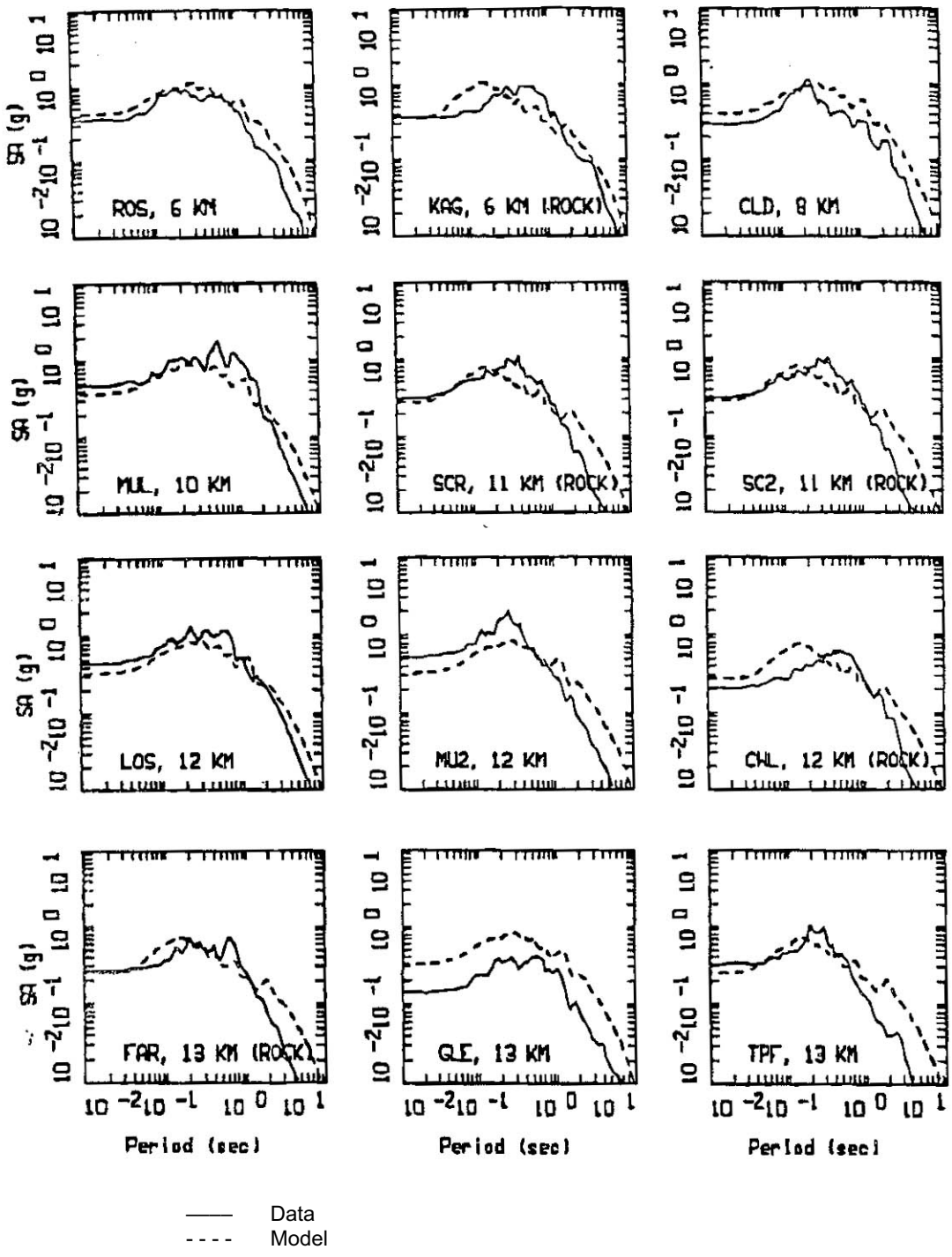

Figure 7-39b. Comparison of Modeled and Observed 5%-Damped Acceleration Response Spectra for the Northridge Earthquake, All 94 Sites (2 of 8)

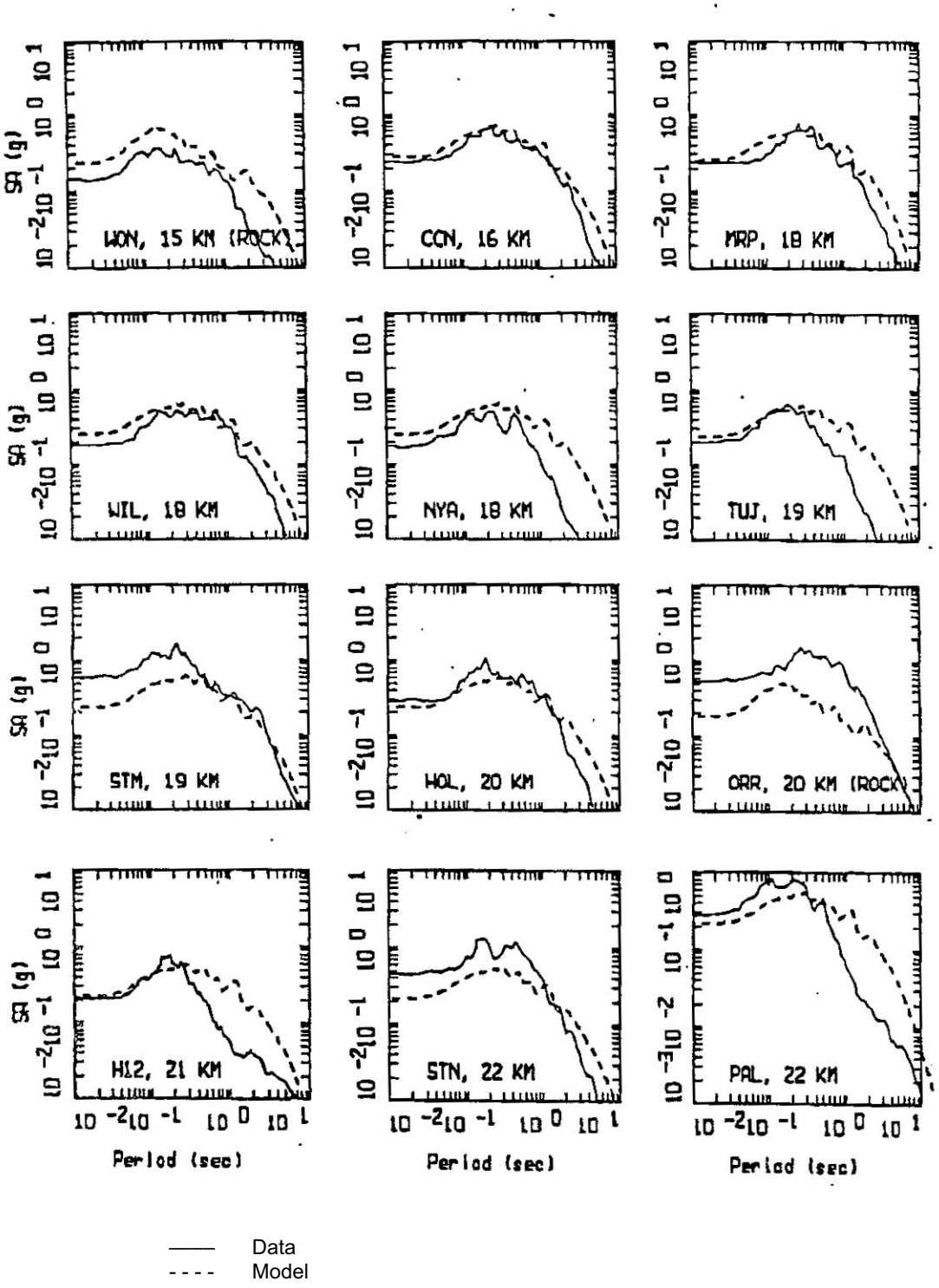

Figure 7-39c. Comparison of Modeled and Observed 5%-Damped Acceleration Response Spectra for the Northridge Earthquake, All 94 Sites (3 of 8)

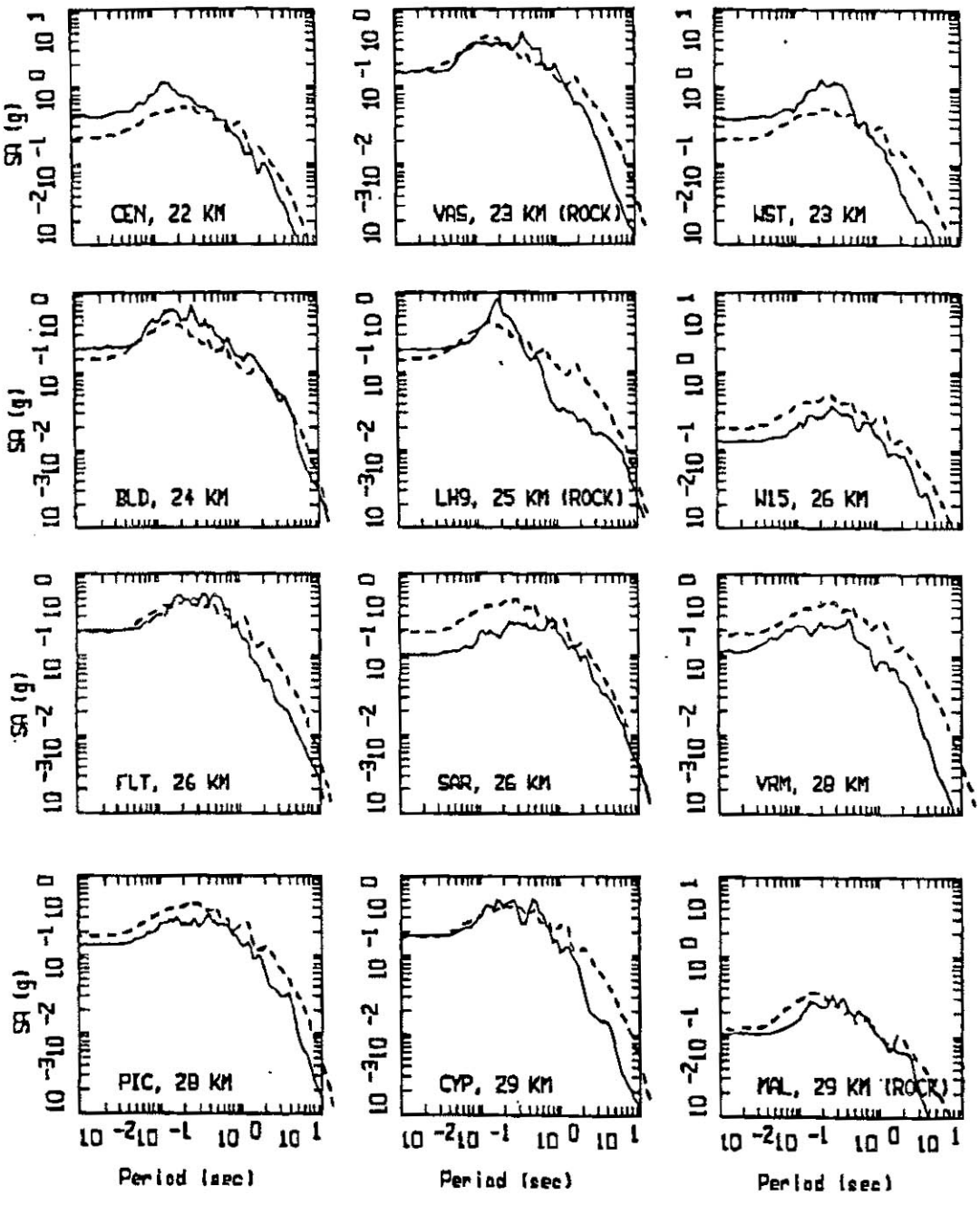

Figure 7-39d. Comparison of Modeled and Observed 5%-Damped Acceleration Response Spectra for the Northridge Earthquake, All 94 Sites (4 of 8)

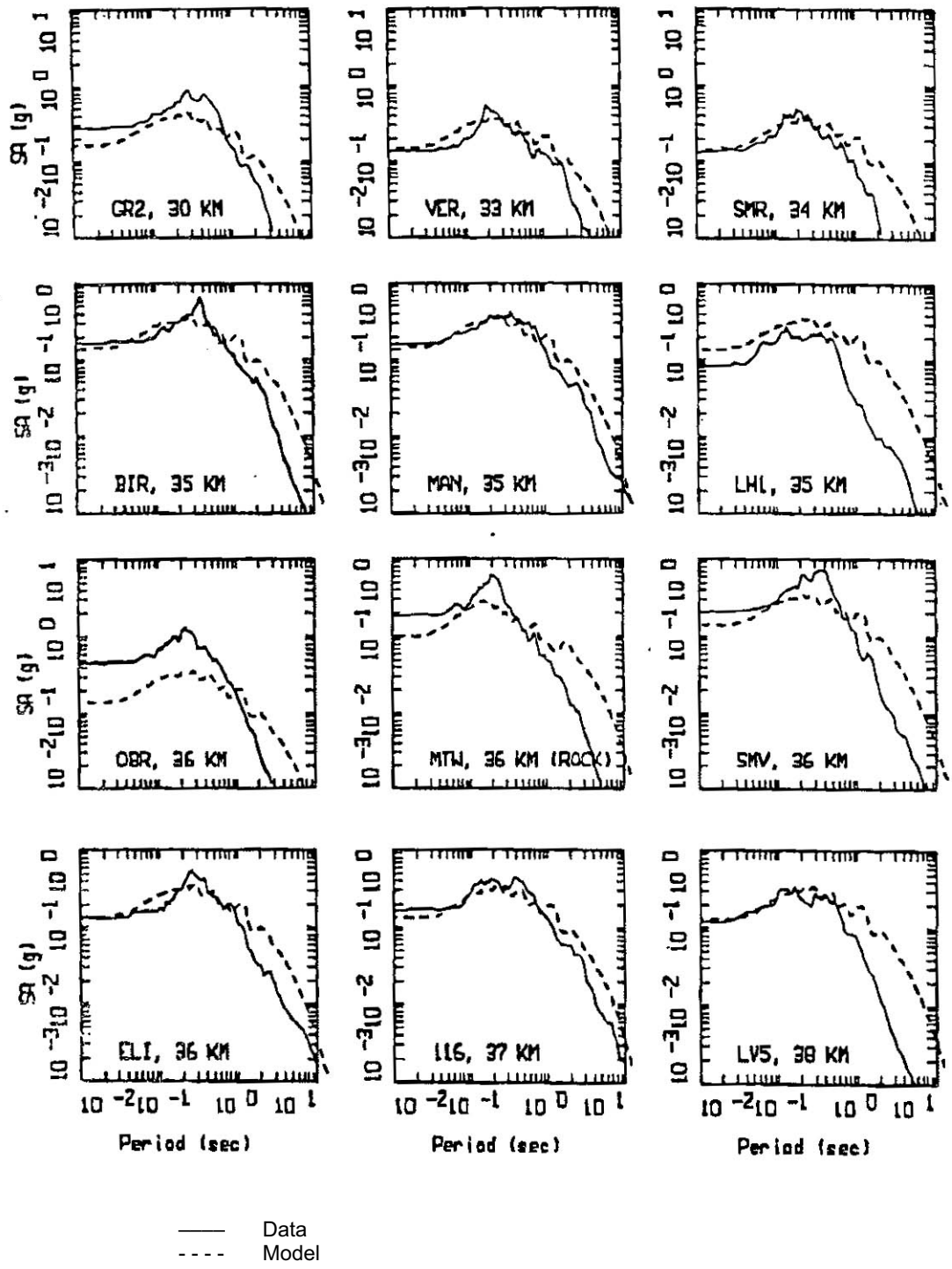

Figure 7-39e. Comparison of Modeled and Observed 5%-Damped Acceleration Response Spectra for the Northridge Earthquake, All 94 Sites (5 of 8)

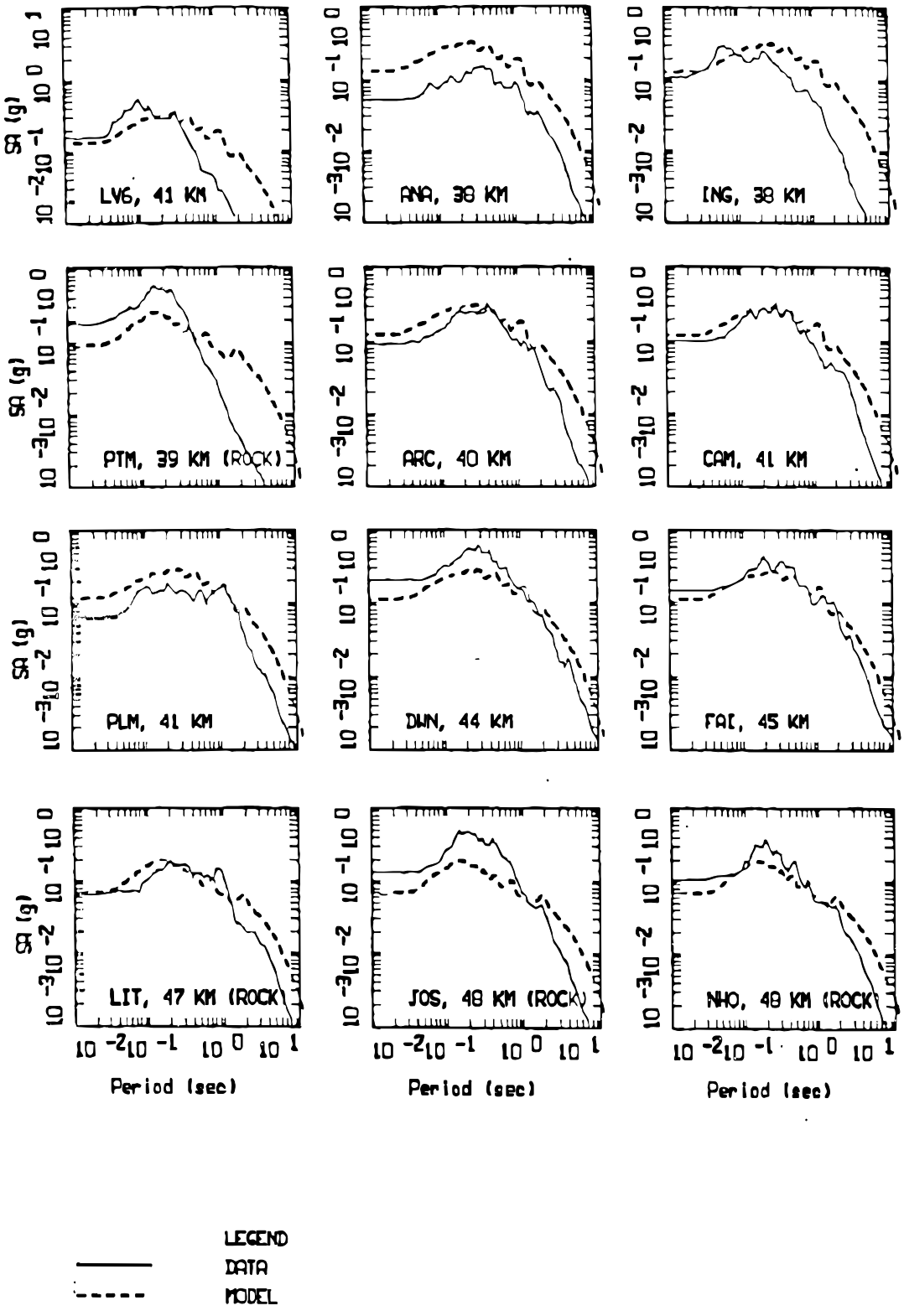

Figure 7-39f. Comparison of Modeled and Observed 5%-Damped Acceleration Response Spectra for the Northridge Earthquake, All 94 Sites (6 of 8)

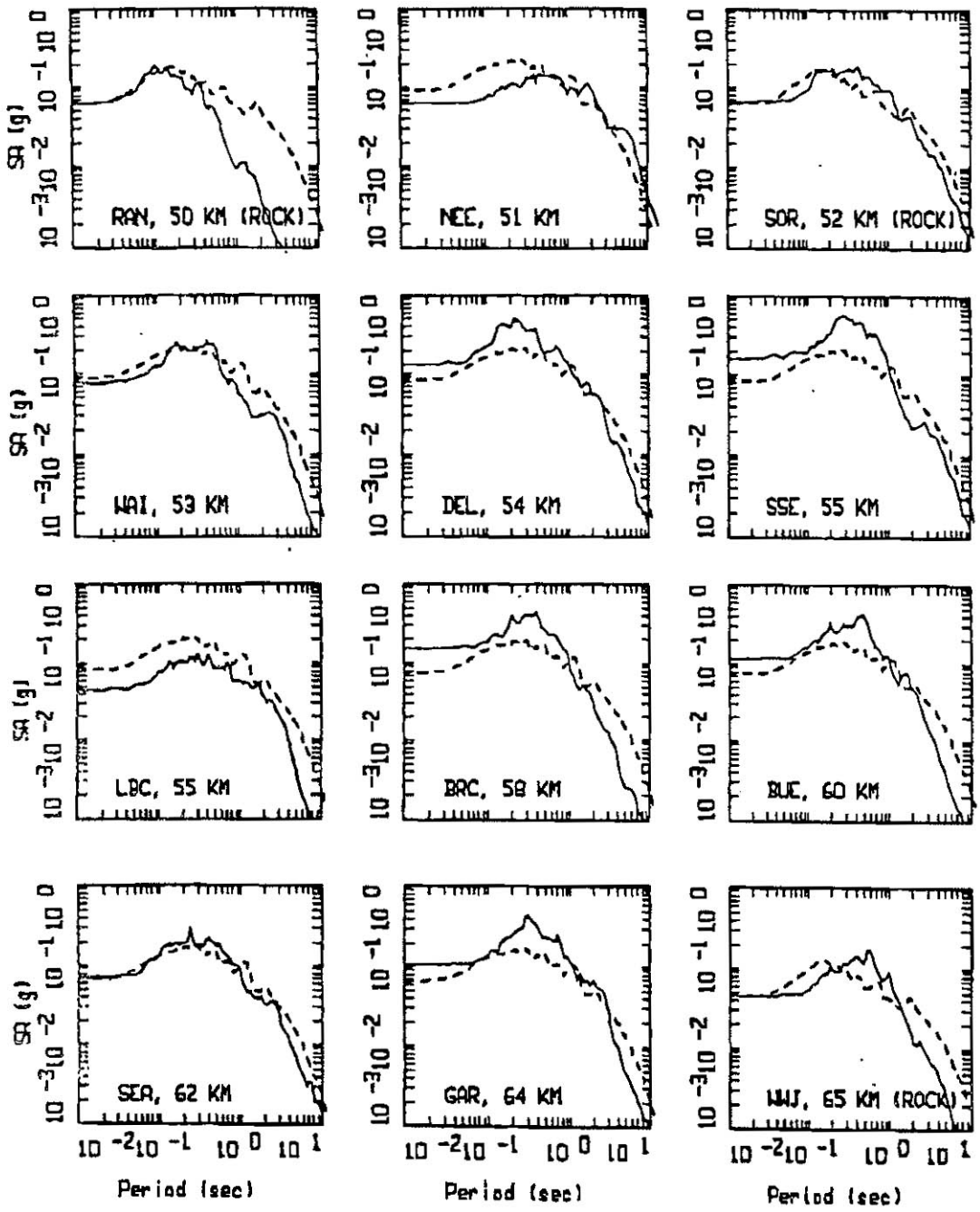

Figure 7-39g. Comparison of Modeled and Observed 5%-Damped Acceleration Response Spectra for the Northridge Earthquake, All 94 Sites (7 of 8)

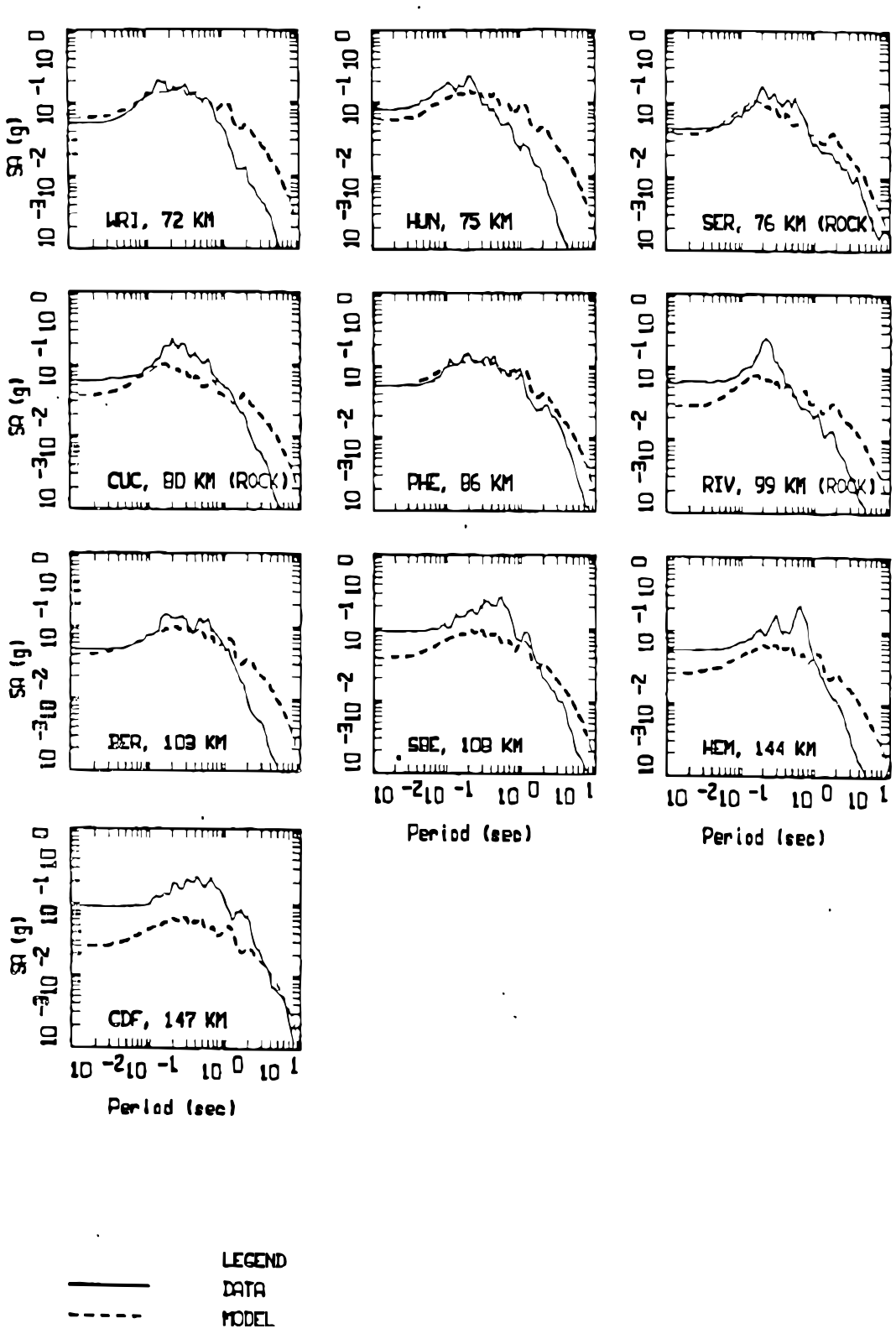

Figure 7-39h. Comparison of Modeled and Observed 5%-Damped Acceleration Response Spectra for the Northridge Earthquake, All 94 Sites (8 of 8)

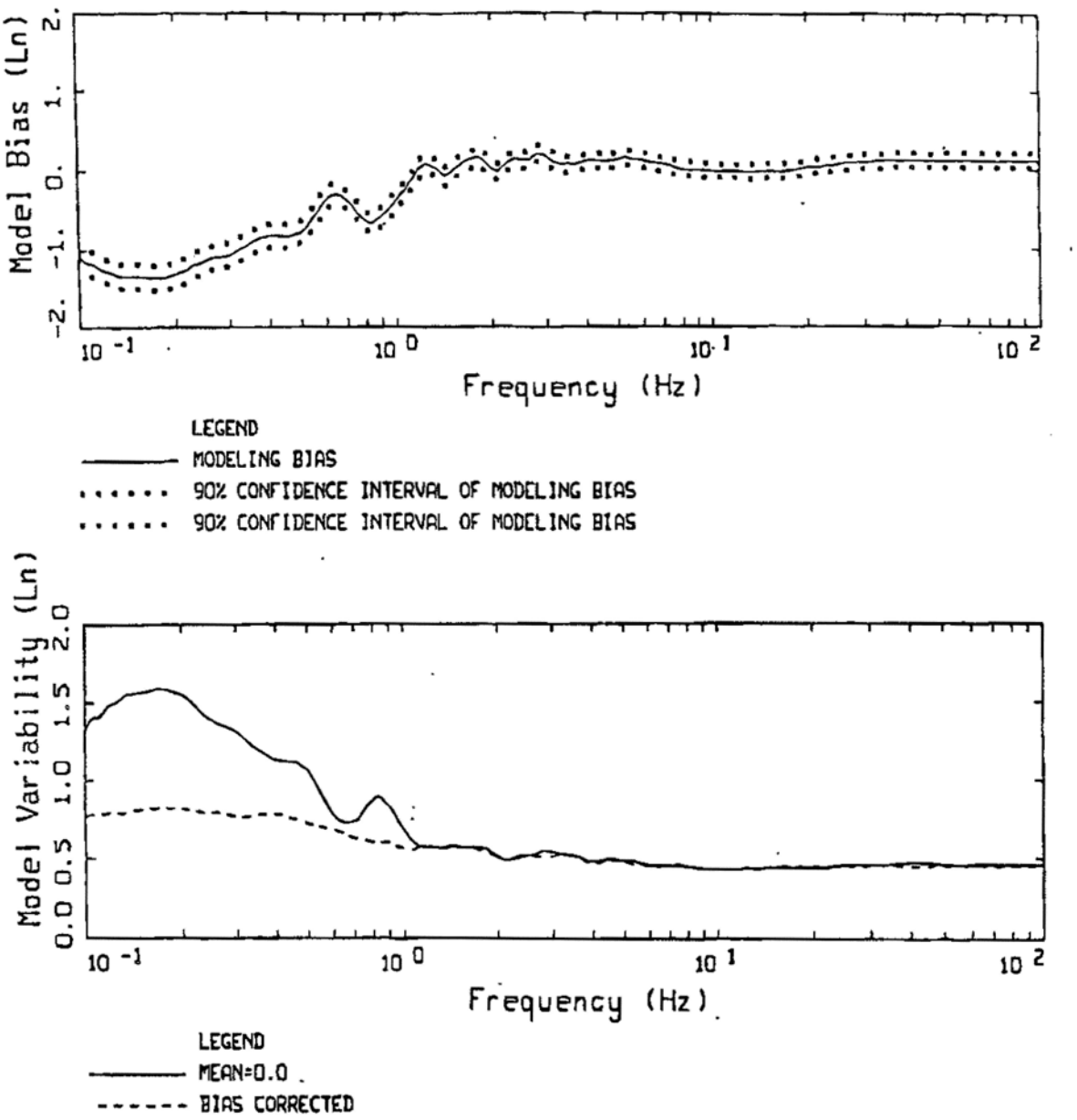

Source: Silva et al. 1996 [DIRS 110474], Figure 5.4

Figure 7-40. Model Bias and Variability for the Northridge Earthquake, 71 Soil Sites

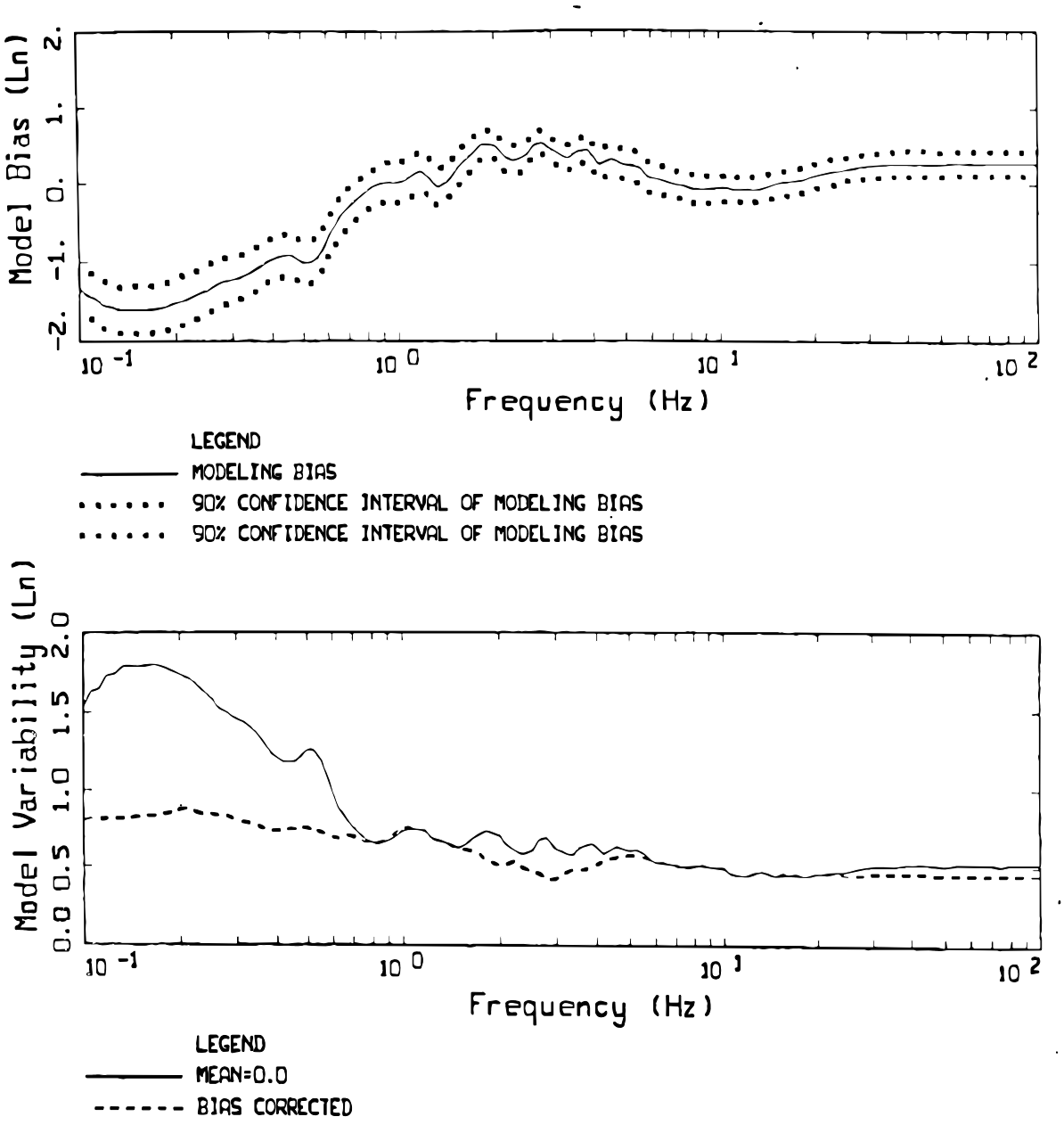

Source: Silva et al. 1996 [DIRS 110474], Figure 5.5

Figure 7-41. Model Bias and Variability for the Northridge Earthquake, 23 Rock Sites

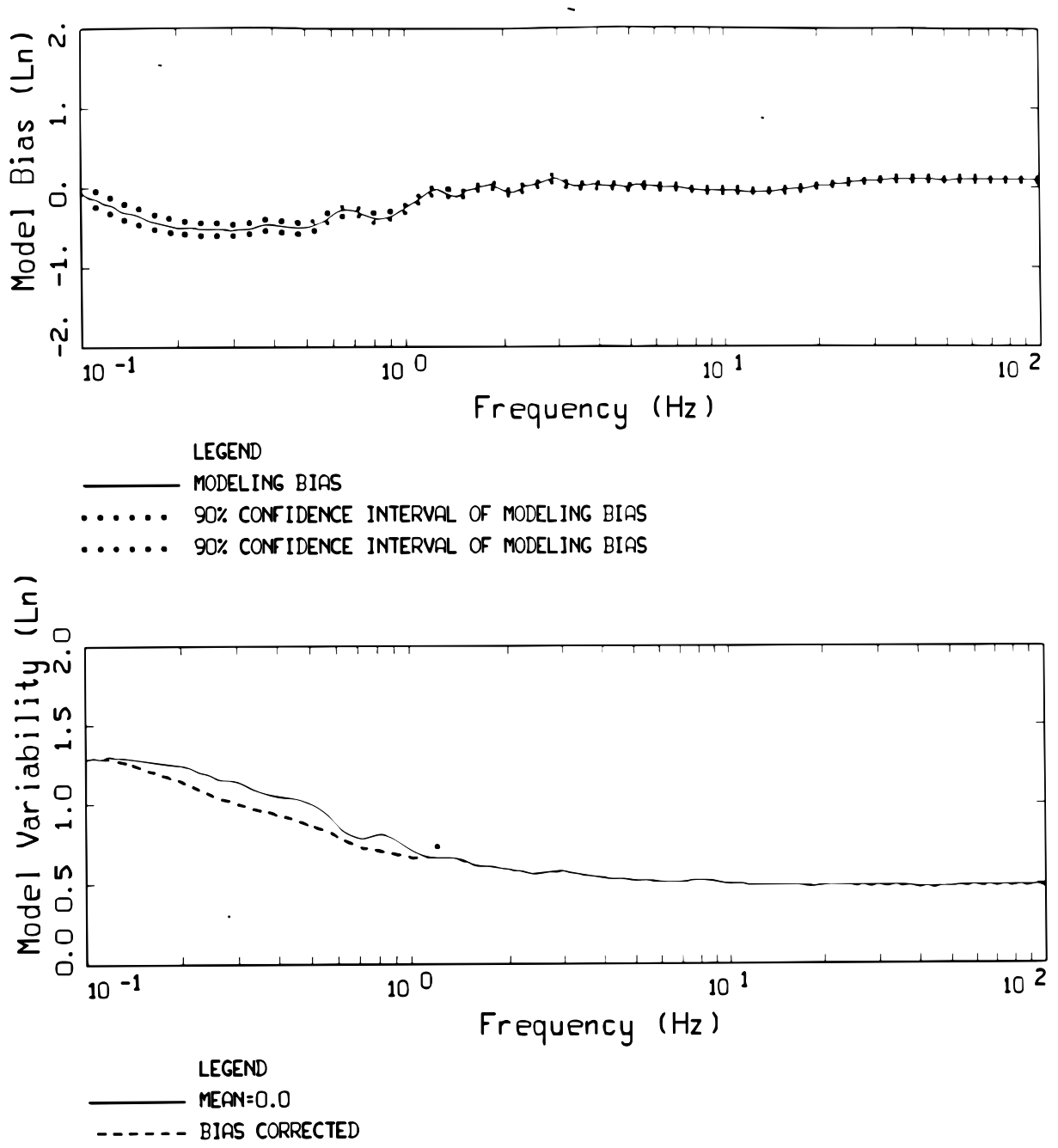

Source: Silva et al. 1996 [DIRS 110474], Figure 5.152

Figure 7-42. Model Bias and Variability for All 16 Earthquakes Studied, All 503 Sites

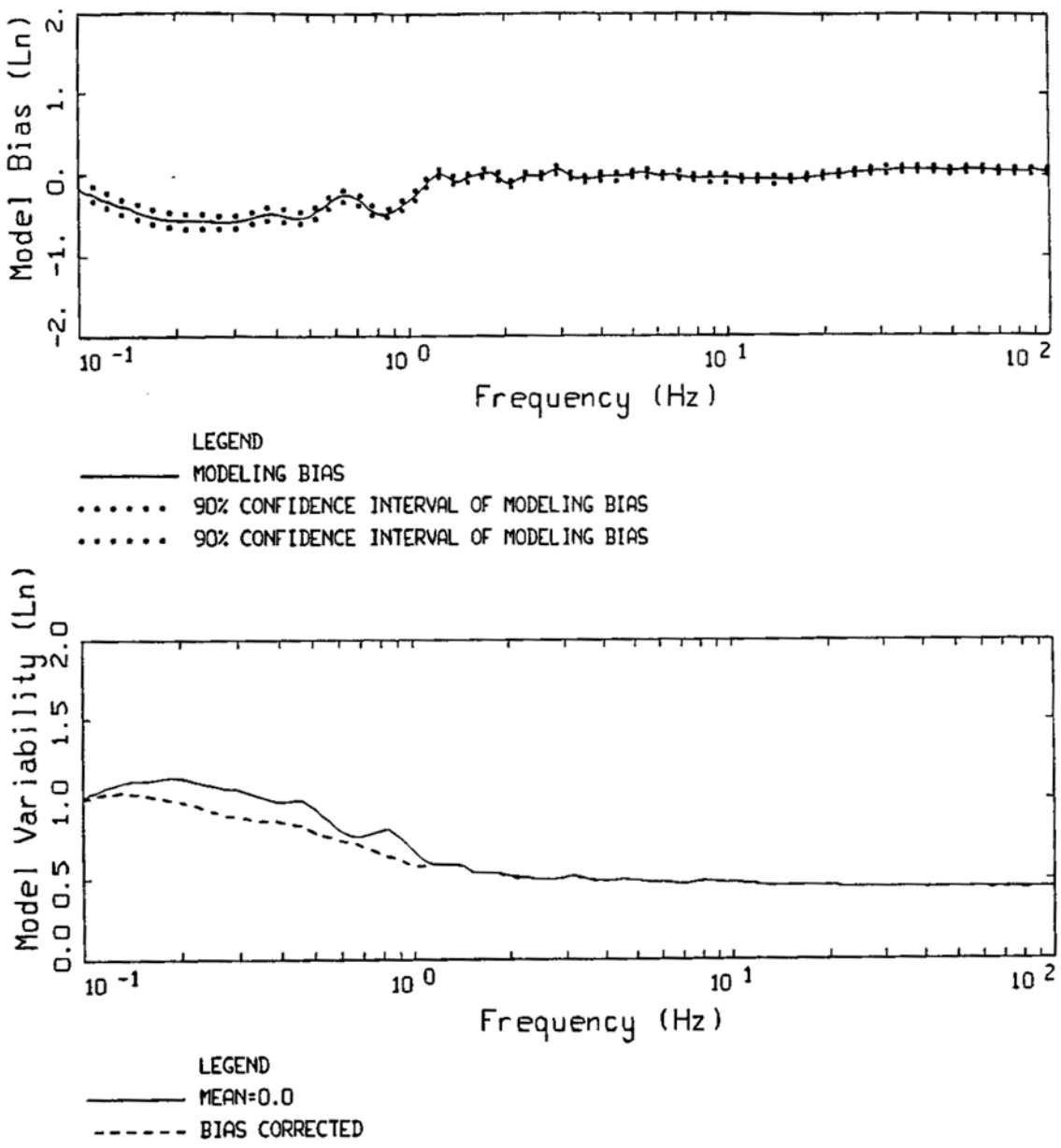

Source: Silva et al. 1996 [DIRS 110474], Figure 5.153

Figure 7-43. Model Bias and Variability for All 16 Earthquakes Studied, All 344 Soil Sites

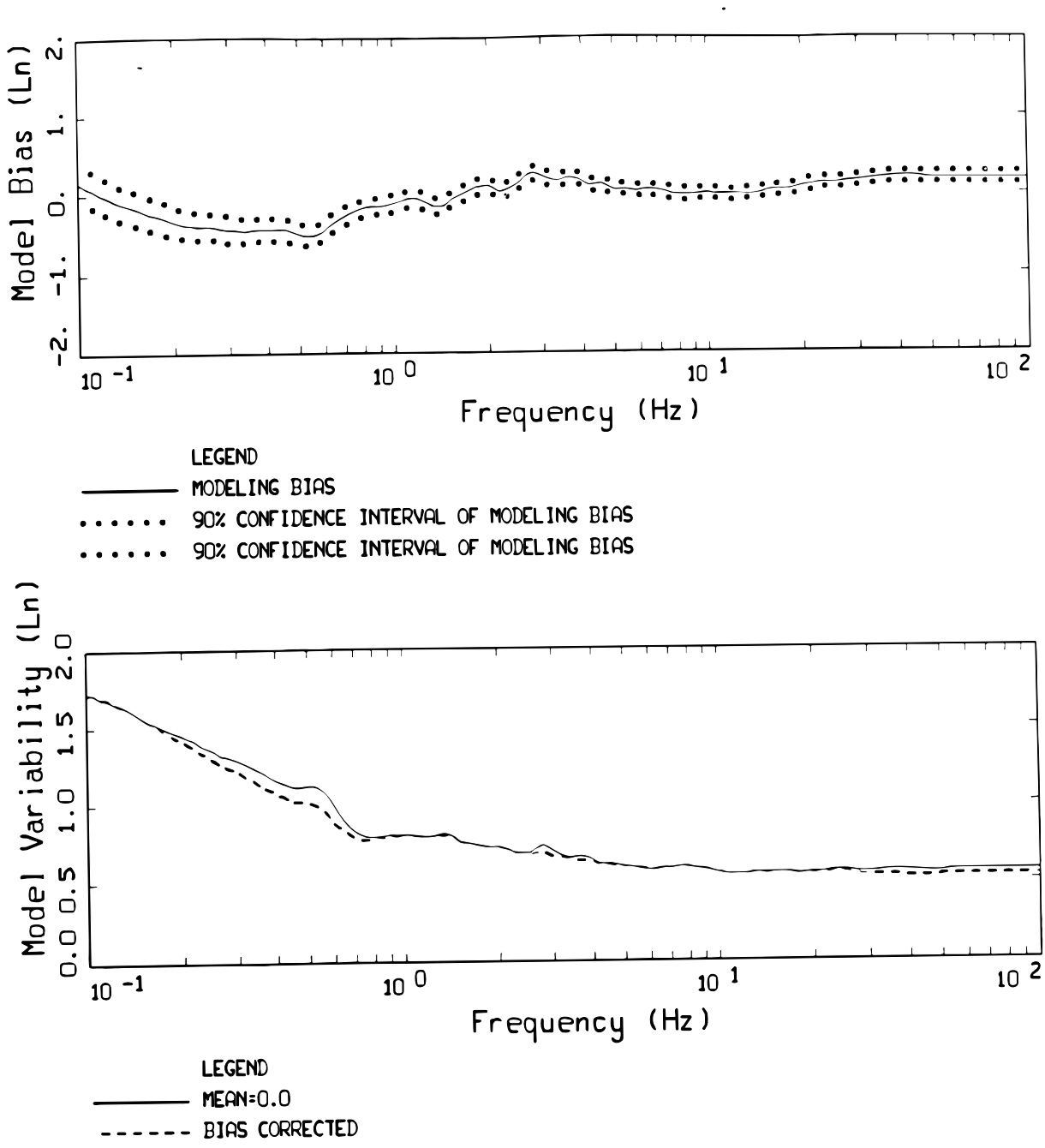

Source: Silva et al. 1996 [DIRS 110474], Figure 5.154

Figure 7-44. Model Bias and Variability for All 16 Earthquakes Studied, All 159 Rock Sites

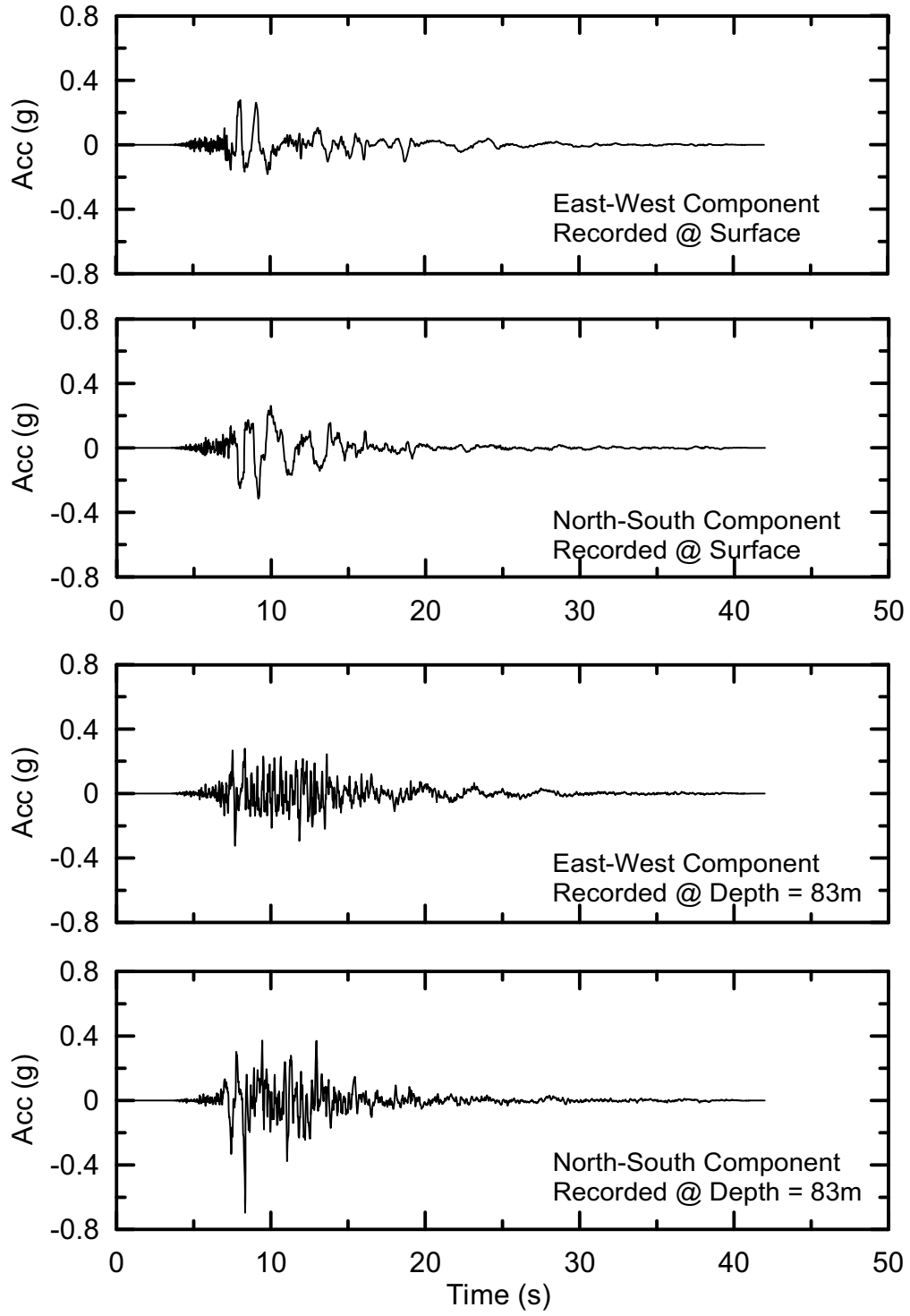

Source: Wong and Silva 2004c [DIRS 170446], page 31

Figure 7-45. Recorded Horizontal Acceleration Time Histories at Port Island at Depths of 0 and 83 m, 1995 Kobe Earthquake

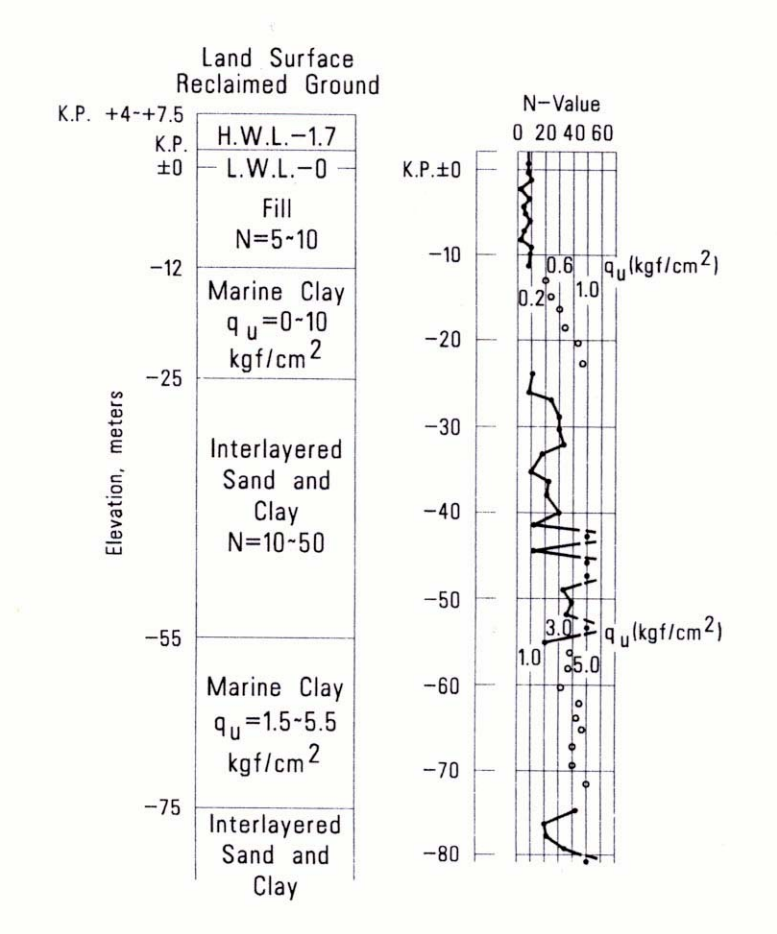

Source: Chung et al. 1996 [DIRS 171465], Figure 2.3.2

Figure 7-46. Representative Soil Boring From Port Island Showing Fill Overlying Natural Soils

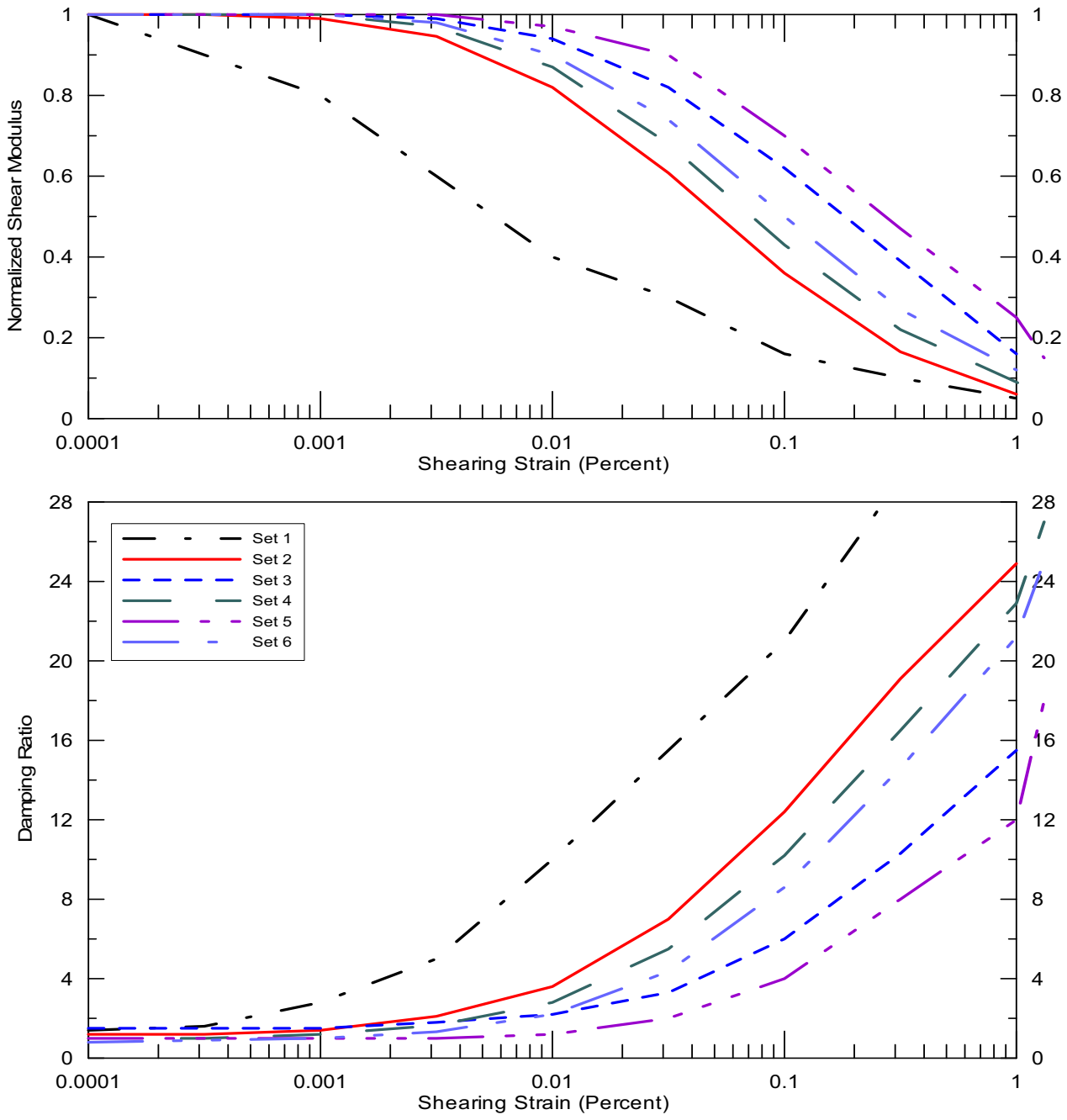

Source: Wong and Silva 2004c [DIRS 170446], page 16

Figure 7-47. Modulus Reduction and Damping Cu rves Used in Equivalent Linear Models Analyses
Set 1 – Decomposed Granite Fill (0-12.6 m);
Set 2 – Sandy Gravel (12.6-19 m);
Set 3 – Clay (19-27 m);
Set 4 – Sand and Sandy Gravel (27-61 m);
Set 5 – Clay (61-79 m);
Set 6 – Sandy Gravel (79-85 m)

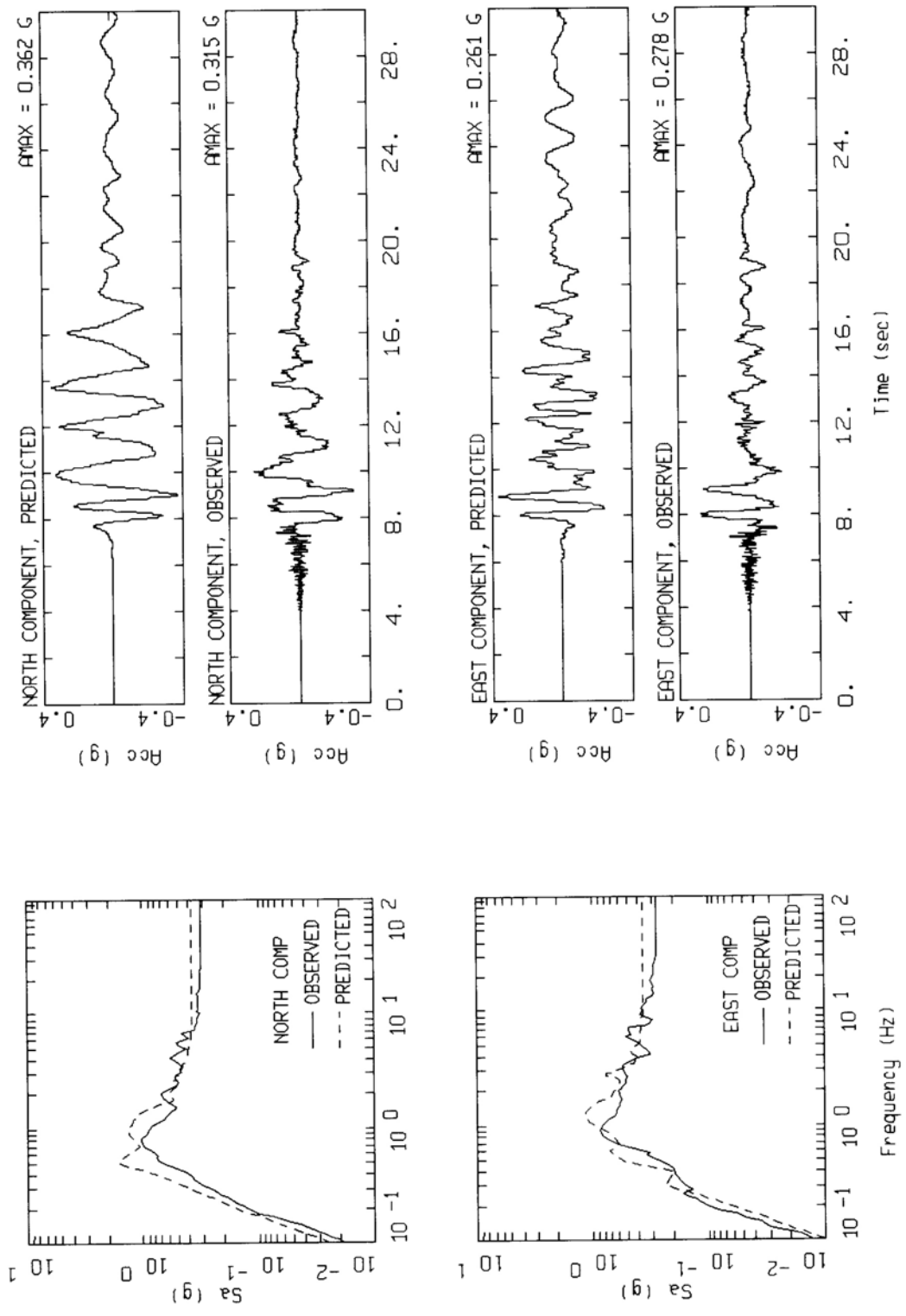

Source: _Wong and Silva 2004d [DIRS 170446], page 20

Figure 7-48. Comparison of Observed and Predicted Motions at Port Island Using SHAKE, Kobe, Port Island Surface

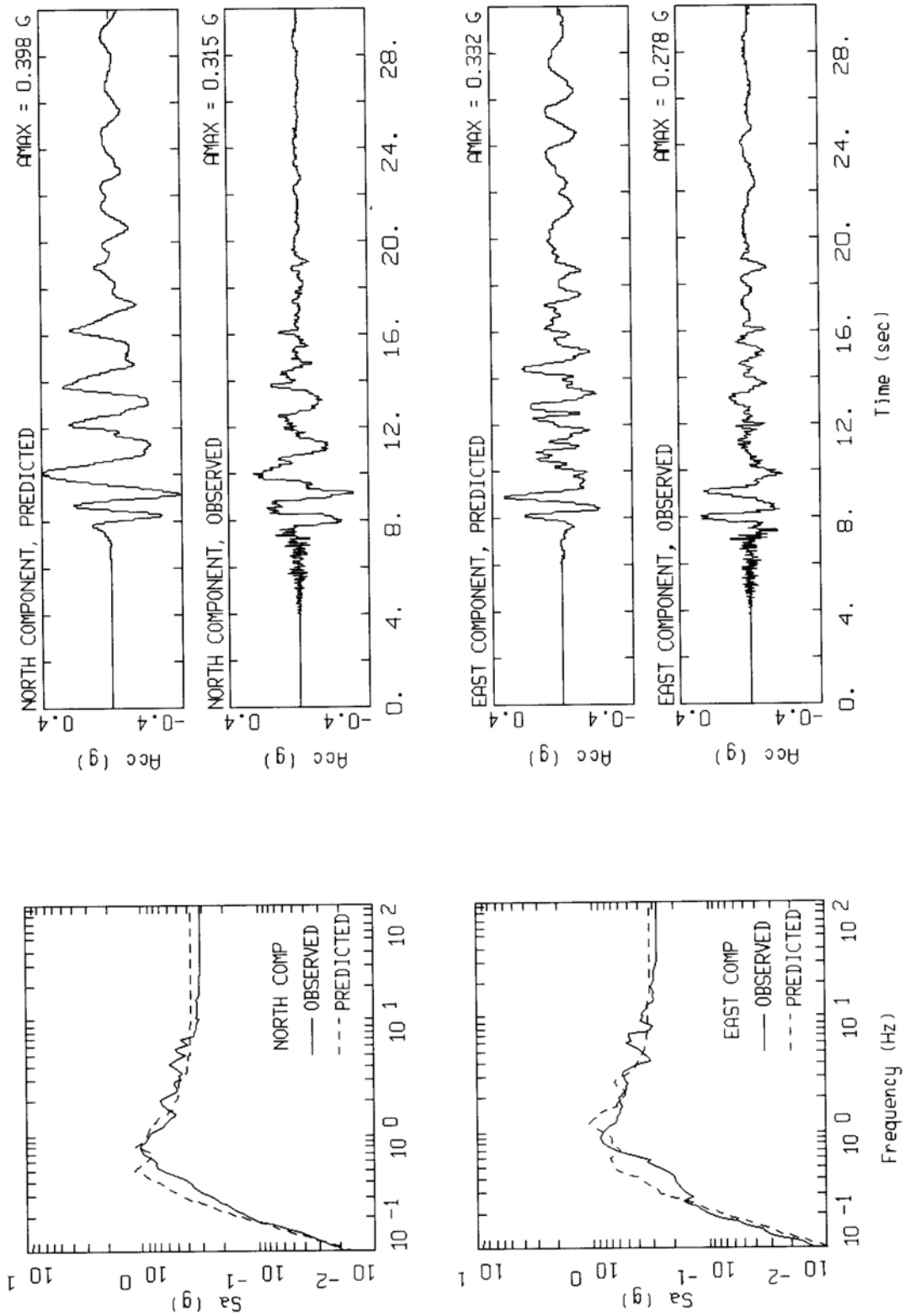

Source: Wong and Silva 2004d [DIRS 170446], page 18

Figure 7-49. Comparison of Observed and Predicted Motions at Port Island Using RASCALS, Kobe, Port Island Surface

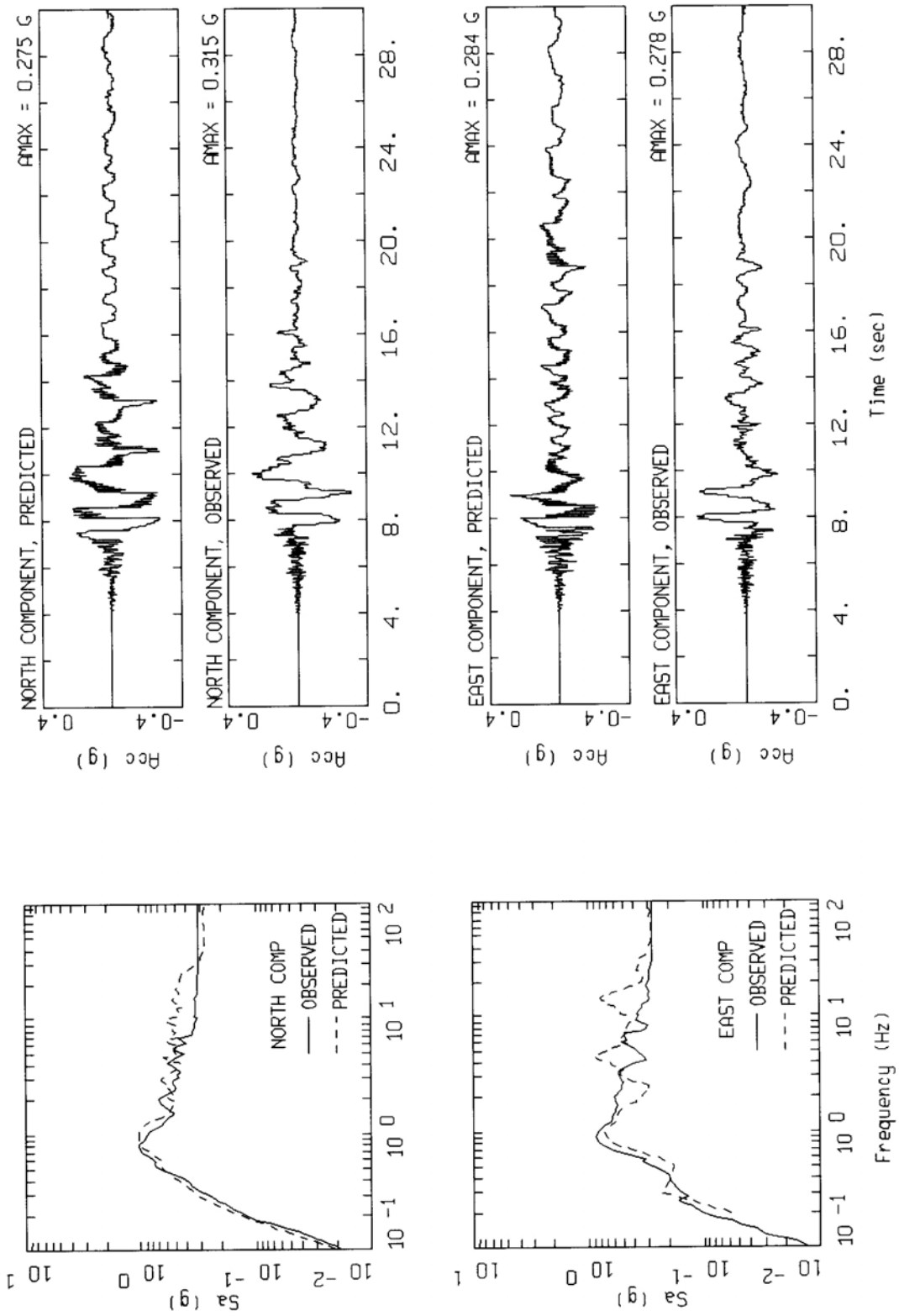

Source: Wong and Silva 2004d [DIRS 170446], page 22

Figure 7-50. Comparison of Observed and Predicted Motions at Port Island Using TESS, Kobe, Port Island Surface

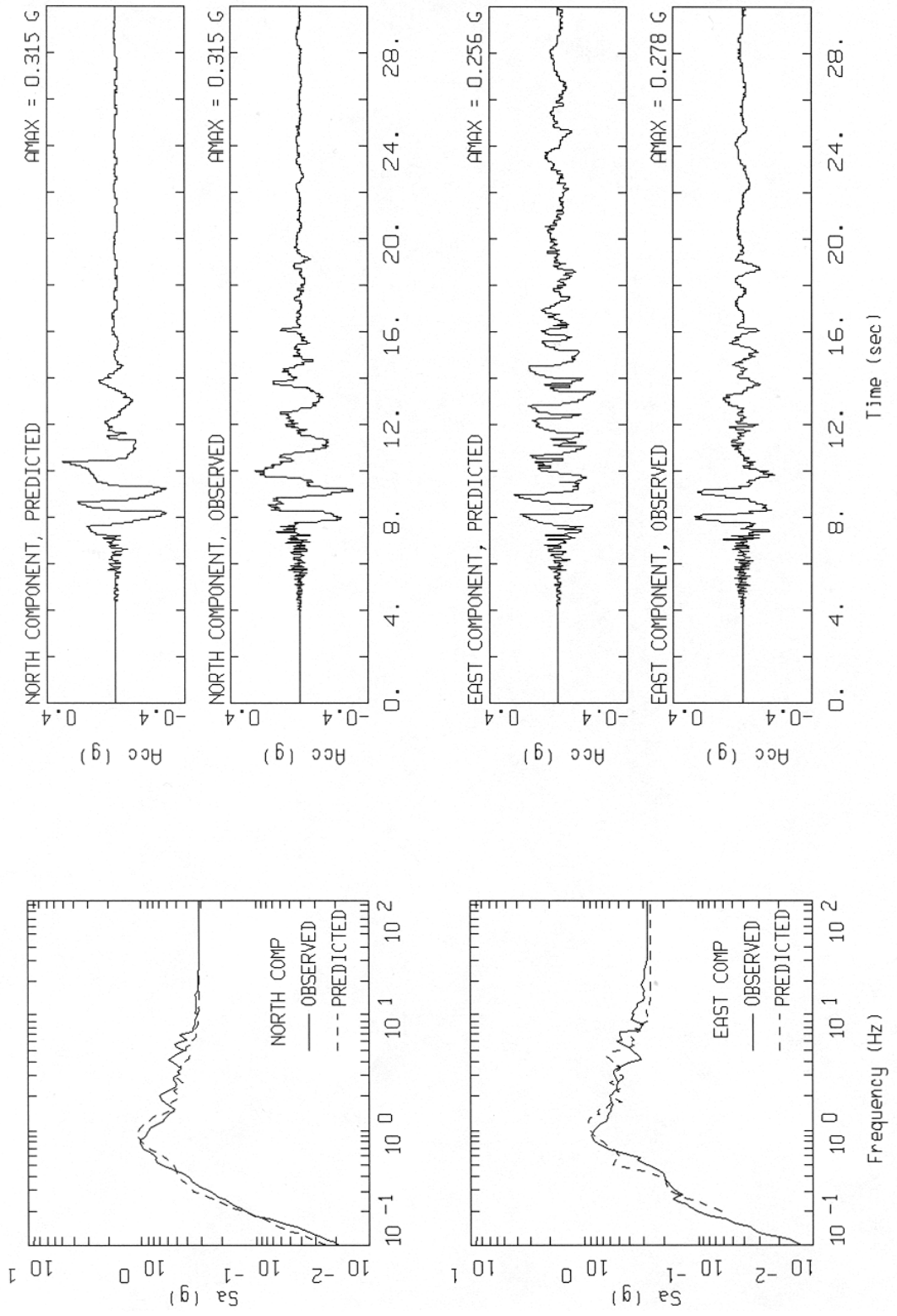

Source: _Wong and Silva 2004d [DIRS 170446], page 29

Figure 7-51. Comparison of Observed and Predicted Motions at Port Island Using SUMDES, Kobe, Port Island Surface

8. CONCLUSIONS

An RVT equivalent-linear site-response model has been used to develop seismic inputs for use in preclosure design analyses and analyses supporting assessment of postclosure performance. The overall modeling activity includes analyses to determine model inputs (Section 6.2). The modeling activity also includes implementation of the model itself to compute preclosure seismic design response spectra and strain-compatible soil properties with annual frequencies of exceedance of 10^{-3}, $5x10^{-4}$, and 10^{-4} (Sections 6.3.1 and 6.3.2). In addition, the model is used to determine peak ground velocities for postclosure analysis with annual frequencies of exceedance of 10^{-4}, 10^{-5}, 10^{-6}, and 10^{-7} (Section 6.3.1). On the basis of these model results, additional analyses were carried out to produce seismic time histories for all annual frequencies of exceedance considered in this report (Section 6.3.2). For preclosure design analyses, five three-component sets of time histories are developed for annual frequencies of exceedance of 10^{-3} and $5x10^{-4}$ and one three-component set is developed for an annual frequency of exceedance of 10^{-4}. These time histories were developed such that their response spectra are a close match to the design response spectra (Sections 6.3.2.1 and 6.3.2.2). For postclosure analyses, several approaches to time history development are followed (Section 6.3.2.3). Characteristics of the suites of postclosure time histories are summarized in Table 8-1. Results from all approaches are considered appropriate for postclosure analyses and reflect various degrees of compromise between achieving goals of matching the emplacement level target spectrum and preserving the observed variability in recorded ground motions.

Table 8-1. Time Histories for Postclosure Assessment

Annual Exceedance Frequency	Number of Time Histories in Suite	Characteristics
10^{-5}	17	Scaled to Point B PGV maintaining intercomponent correlation Spectrally conditioned to Point B spectral shape
10^{-6}	17	All components scaled to Point B PGV No spectral conditioning
10^{-6}	17	Scaled to Point B PGV maintaining intercomponent correlation Spectrally conditioned to Point A spectral shape
10^{-7}	17	Scaled to Point B PGV maintaining intercomponent correlation Spectrally conditioned to Point A spectral shape
10^{-7}	17	Scaled to Point B PGV maintaining intercomponent correlation Spectrally conditioned to Point B spectral shape

Design response spectra and time histories developed for the Surface Facilities Area (Points D and E) are based on site velocity data from that portion of the Waste Handling Building Site Characterization Area that lies southwest of the Exile Hill splay fault. In a sensitivity study, ground motions for the area to the northeast of the Exile Hill fault splay (Point F) were also evaluated on the basis of available data (Section 6.3.5). For horizontal motions the ratio of the Point F response spectrum to the design response spectrum ranges from about 0.9 to 1.0. For

vertical ground motion, the Point F response spectrum exceeds the design response spectrum for frequencies less than about 30 Hz with the response spectral ratio ranging from about 1.0 to 1.15.

This report also describes ground motion inputs associated with potential igneous dike intrusions at Yucca Mountain. A deterministic analysis is carried out based on an assessed range of maximum magnitude earthquakes (**M** 4.8, **M** 5.8, and **M** 6.2) for an igneous dike intrusion and using the site-specific ground motion attenuation results from the PSHA for Yucca Mountain. Acceleration response spectra are documented in Section 6.5. Using median ground motion results from the PSHA, horizontal PGA ranges from 0.14 g for an **M** 4.8 earthquake to 0.39 g for an **M** 6.2 earthquake. If 84th percentile ground motions are used, the corresponding values are 0.28 g and 0.70 g.

Intermediate and final results developed during this modeling activity that have been submitted to the TDMS are summarized in Table 8-2. These data were developed using scientific notebooks and were submitted to the TDMS as they were developed. They are, therefore, not Product Output of this report. Some intermediate results discussed in Section 6.2 were deemed inappropriate for submittal to the TDMS. One data submittal derived from this modeling and analysis work is considered Product Output. That data submittal consists of the input and output files produced during the modeling and analysis activities and is submitted as Model Warehouse Data (DTN TBD).

Table 8-2. Results of Modeling Activity Submitted to the Technical Data Management System

Description	Data Tracking Number	Report Section
Intermediate Results		
Extended Hazard Curves for the PSHA Reference Rock Outcrop (Point A)	MO03061E9PSHA1.000	6.2.2.2
Uniform Hazard Spectra	MO0401MWDRPSHA.000 [DIRS 166962] (10^{-3}, 10^{-4}) MO0208UNHZ5X10.000 [DIRS 163722] ($5x10^{-4}$) MO0308UNHAZ105.000 [DIRS 170425] (10^{-5}) MO0206UNHAZ106.001 [DIRS 163723] (10^{-6}) MO0209UNHAZ107.000 [DIRS 163724] (10^{-7})	6.2.2.3
Reference Earthquakes and Associated Response Spectra	MO0211REDES103.000 [DIRS 170424] (10^{-3}) MO0208UNHZ5X10.000 [DIRS 163722] ($5x10^{-4}$) MO0211DERES104.000 [DIRS 170423] (10^{-4}) MO0308UNHAZ105.000 [DIRS 170425] (10^{-5}) MO0206UNHAZ106.001 [DIRS 163723] (10^{-6}) MO0209UNHAZ107.000 [DIRS 163724] (10^{-7})	6.2.2.4

Description	Data Tracking Number	Report Section
Deaggregation of PSHA Results for Peak Ground Velocity	MO0404PGVAPSHA.000 [DIRS 170436] (10^{-4}) MO0309PGVDEAGG.000 [DIRS 170426] (10^{-5}) MO0208PGVDEAG6.001 [DIRS 164203] (10^{-6}) MO0210PGVD1E07.000 [DIRS 164205] (10^{-7})	6.2.2.4
Deaggregation Earthquakes and Associated Response Spectra	MO0211REDES103.000 [DIRS 170424] (10^{-3}) MO0208UNHZ5X10.000 [DIRS 163722] ($5x10^{-4}$) MO0211DERES104.000 [DIRS 170423] (10^{-4}) MO0308UNHAZ105.000 [DIRS 170425] (10^{-5}) MO0206UNHAZ106.001 [DIRS 163723] (10^{-6}) MO0209UNHAZ107.000 [DIRS 163724] (10^{-7})	6.2.2.5
Velocity (V_P and V_S) profiles for Repository Block tuff	MO0206SASWVSP1.001 [DIRS 163777]	6.2.3.3
Velocity (V_P and V_S) profiles for Surface Facilities Area tuff and alluvium	MO0209VELPRWHB.000 [DIRS 163798]	6.2.3.4
Velocity Correlation Parameters for the Repository Block and the Surface Facilities Area	MO0208VCPRBWHB.000 [DIRS 163801]	6.2.3.6
Normalized Shear Modulus Reduction and Material Damping Curves as a Function of Shear Strain for Tuff, and Alluvium	MO0403SDIAWHBC.003 [DIRS 170434]	6.2.4.3
Final Results		
Response Spectra for the Waste Emplacement Level (Point B)	MO0405SDSTPNTB.001 [DIRS 169851] (10^{-3}) MO0407SDARS104.001 [DIRS 170683]($5x10^{-4}$) MO0306SDSAVDTH.000 [DIRS 164033] (10^{-4}) MO0312SEPRSRLB.019 [DIRS 170427] (10^{-5}) MO04065DSRSPTB.000 [DIRS 170506] (10^{-6})	6.3.1.2, 6.3.1.4
Response Spectra for the Surface Facilities Area (Points D and E)	MO0410SDSDE103.002 [DIRS 172236] (10^{-3}) MO0410SDSTMHIS.005 [DIRS 172237] ($5x10^{-4}$) MO0410WHBDF104.002 [DIRS 172238] (10^{-4})	6.3.1.3
Strain Compatible Soil Properties for the Surface Facilities Area (Points D and E)	MO0404SPCDAMPD.001 [DIRS 169344] (10^{-3}) MO0403SPWHB5E4.005 [DIRS 168376] ($5x10^{-4}$) MO0403SCSPSFAD.001 [DIRS 169342] (10^{-4})	6.3.2.2

Description	Data Tracking Number	Report Section
Peak Ground Velocity for the Waste Emplacement Level (Point B)	MO0404PGVRL104.000 [DIRS 170437] (10^{-4}) MO0401SEPPGVRL.022 [DIRS 169099] (10^{-5}) MO0303DPGVB106.002 [DIRS 162712] (10^{-6}) MO0210PGVPB107.000 [DIRS 162713] (10^{-7})	6.3.1.2.3 6.3.1.4.1 6.3.1.4.2 6.3.1.4.3
Peak Ground Acceleration, Peak Ground Velocity, Strains, and Curvatures as a Function of Depth (Point C to Point B)	MO0408PGAPGVSC.001 [DIRS 171434]	6.3.4.3
Time Histories (1 three-component set) Spectrally Matched to the Target Response Spectrum for the Waste Emplacement Level (Point B)	MO0405SDSTPNTB.001 [DIRS 169851] (10^{-3}) MO0407TMHIS104.003 [DIRS 170599]($5x10^{-4}$) MO0306SDSAVDTH.000 [DIRS 164033] (10^{-4})	6.3.2.1.1 6.3.2.1.2 6.3.2.1.3
Time Histories Spectrally Matched to the Target Response Spectrum for the Surface Facilities Area (Points D and E) 10^{-3}: 5 three-component sets $5x10^{-4}$: 5 three-component sets 10^{-4}: 1 three-component set	MO0410SDSDE103.002 [DIRS 172236] (10^{-3}) MO0410SDSTMHIS.005 [DIRS 172237] ($5x10^{-4}$) MO0410WHBDF104.002 [DIRS 172238] (10^{-4})	6.3.2.2.1 6.3.2.2.2 6.3.2.2.3
Time Histories (17 three-component sets) Scaled to Peak Ground Velocity for the Waste Emplacement Level (Point B)	MO0301TMHIS106.001 [DIRS 161868] (10^{-6})	6.3.2.3.1
Time Histories (17 three-component sets) Weakly Conditioned to the PSHA Reference Rock Outcrop (Point A) Spectrum and Scaled to Peak Ground Velocity for the Waste Emplacement Level (Point B)	MO0403AVDSC106.001 [DIRS 168891] (10^{-6}) MO0403AVTMH107.003 [DIRS 168892] (10^{-7})	6.3.2.3.1 6.3.2.3.2
Time Histories (17 three-component sets) Weakly Conditioned to the Waste Emplacement Level (Point B) Target Spectrum and Scaled to Peak Ground Velocity for the Waste Emplacement Level (Point B)	MO0402AVDTM105.001 [DIRS 168890] (10^{-5}) MO0301TMHSB107.000 [DIRS 164207] (10^{-7})	6.3.2.3.3 6.3.2.3.2

Acceptance Criteria–The work described in this report addresses acceptance criteria from the *Yucca Mountain Review Plan, Final Report* (NRC 2003 [DIRS 163274]). Relevant acceptance criteria are identified in Section 4.2. Table 8-3 lists the acceptance criteria and indicates how they have been addressed.

Table 8-3. Summary of Applicable *Yucca Mountain Review Plan, Final Report* Acceptance Criteria and How They are Addressed in this Report

Yucca Mountain Review Plan, Final Report Acceptance Criteria	Summary of How Acceptance Criteria are Addressed in this Report
Section 1.5.3:	
1. The "General Information" section of the license application contains an adequate description of site characterization activities.	In accordance with part 1 of acceptance criterion 1, this report as a whole provides an overview of the site characterization activity to develop seismic inputs for use in preclosure design and postclosure performance analyses.
2. The "General Information" section of the license applications contains an adequate description of site characterization results.	In accordance with part 1 of acceptance criterion 2, Sections 6.2 and 6.3 address the features and processes that generate seismic ground motions at Yucca Mountain. In accordance with part 2 of acceptance criterion 2, Sections 6.2 and 6.3 also address the seismic ground motions that have the potential to occur in the future at Yucca Mountain.
Section 2.1.1.5.1.3:	
1. Consequence analyses adequately assess normal operations and Category 1 event sequences, as well as factors that allow an event sequence to propagate within the Geologic Repository Operations Area.	In accordance with part 1 of acceptance criterion 1, Sections 6.3.1.2, 6.3.1.3, 6.3.2.1, and 6.3.2.2 provide seismic inputs that represent the seismic hazard for preclosure consequence analyses.
2. Consequence calculations adequately assess the consequences to workers and members of the public from normal operations and Category 1 event sequences.	In accordance with part 1 of acceptance criterion 2, Sections 6.2 and 6.3 provide the technical bases for seismic inputs used in preclosure consequence analyses. In accordance with part 3 of acceptance criterion 2, Sections 6.2 and 6.3 describe the development of site-specific seismic inputs and explains how uncertainties are treated.
3. The Dose to Workers and Members of the Public From Normal Operations and Category 1 Event Sequences is Within the Limits Specified in 10 CFR 63.111(a).	In accordance with part 1 of acceptance criterion 3, Sections 6.2 and 6.3 provide information needed to address seismic hazards in preclosure consequence analyses.
Section 2.1.1.5.2.3	
1. Consequence analyses include Category 2 event sequences as well as factors that allow an event sequence to propagate within the geologic repository operations area.	In accordance with part 1 of acceptance criterion 1, Sections 6.3.1.2, 6.3.1.3, 6.3.2.1, and 6.3.2.2 provide seismic inputs that represent the seismic hazard for preclosure consequence analyses.

Yucca Mountain Review Plan, Final Report Acceptance Criteria	Summary of How Acceptance Criteria are Addressed in this Report
2. Consequence calculations adequately assess the consequences to members of the public from Category 2 event sequences.	In accordance with part 1 of acceptance criterion 2, Sections 6.2 and 6.3 provide the technical bases for seismic inputs used in preclosure consequence analyses. In accordance with part 3 of acceptance criterion 2, Sections 6.2 and 6.3 describe the development of site-specific seismic inputs and explains how uncertainties are treated.
3. The dose to hypothetical members of the public from category 2 event sequences is within the limits specified in 10 CFR 63.111(b)(2).	In accordance with part 1 of acceptance criterion 3, Sections 6.2 and 6.3 provide information needed to address seismic hazards in preclosure consequence analyses.
Section 2.1.1.1.3 *5. The license application contains descriptions of the site geology and seismology adequate to permit evaluation of the preclosure safety analysis and the Geologic Repository Operations Area design.*	In accordance with part 6 of acceptance criterion 5, Sections 6.2 and 6.3 address the characterization of vibratory ground motions for the repository site. By basing seismic inputs on the results of the PSHA for Yucca Mountain, the results take into account uncertainties and randomness in seismic sources and ground motion.
Section 2.1.1.3.3 *1. Technical basis and assumptions for methods for identification of hazards and initiating events are adequate.*	In accordance with part 1 of acceptance criterion 1, Section 6.3 describes how development of seismic inputs is carried out using McGuire et al. (2001 [DIRS 157510]), NRC (1989a [DIRS 165110]), and NRC (1989b [DIRS 165111]). In accordance with part 2 of acceptance criterion 1, Section 6.3 describes exceptions taken to the guidance mentioned with respect to part 1 above and provides the technical basis for exceptions. In accordance with part 3 of acceptance criterion 1, Sections 6.2 and 6.3 describe the development of seismic inputs taking into account site data uncertainty and randomness. In accordance with part 4 of acceptance criterion 1, Section 6.1 describes modeling assumptions and provides their technical basis. Validation of modeling assumptions is described in Section 7.
2. Site data and system information are appropriately used in identification of hazards and initiating events.	In accordance with part 1 of acceptance criterion 2, Section 6.2 describes the use of site-specific data in determining inputs used for modeling and analyses to develop seismic inputs.

Yucca Mountain Review Plan, Final Report Acceptance Criteria	Summary of How Acceptance Criteria are Addressed in this Report
3. Determination of frequency or probability of occurrence of hazards and initiating events is acceptable.	In accordance with part 1 of acceptance criterion 3, Sections 6.2 and 6.3 describe how site-response modeling to develop seismic inputs is carried out such that site-specific seismic inputs are consistent with the hazard level of the control motions. The sections also describe how uncertainty and randomness in input data is incorporated in the process. In accordance with part 3 of acceptance criterion 3, Section 7 describes validation of the random vibration theory-based, equivalent-linear site-response model.
4. Adequate technical bases for the inclusion and exclusion of hazards and initiating events are provided.	In accordance with part 1 of acceptance criterion 4, Sections 6.2 and 6.3 provide the technical basis for seismic inputs that characterize the seismic hazard at Yucca Mountain. Seismic inputs are developed consistent with the available site-specific data. In accordance with part 2 of acceptance criterion 4, Sections 6.2 and 6.3 describe how uncertainties are incorporated into the modeling and analyses carried out to develop seismic inputs.
Section 2.1.1.7.3.2 *1. Geologic repository operations area design methodologies are adequate.*	In accordance with part 4 of acceptance criterion 1, development of seismic inputs take into account McGuire et al. (2001 [DIRS 157510]), NRC (1989a [DIRS 165110]), and NRC (1989b [DIRS 165111]). Exceptions to the guidance and recommendations are documented in Sections 6.2 and 6.3 and their technical basis provided.
Section 2.2.1.2.2.3 *1. Events are adequately defined.*	In accordance with part 1 of acceptance criterion 1, Section 6.2 and 6.3 address development of seismic inputs for various annual frequencies of exceedance. In accordance with part 2 of acceptance criterion 1, Sections 6.2 and 6.3 indicate that the PSHA provides the basis for the control motions used in site response modeling. The PSHA assessments are based on the historical record, paleoseismic studies, and geological analyses. Development of seismic time histories relies on historically recorded strong ground motion data.
2. Probability estimates for future events are supported by appropriate technical bases.	In accordance with part 1 of acceptance criterion 2, Sections 6.2 and 6.3 indicate that the PSHA provides the basis for the control motions used in site response modeling. The PSHA assessments are based on past patterns of seismicity and seismic characteristics for the Yucca Mountain vicinity.

Yucca Mountain Review Plan, Final Report Acceptance Criteria	Summary of How Acceptance Criteria are Addressed in this Report
3. Probability model support is adequate.	In accordance with part 1 of acceptance criterion 3, Section 6.2 describes how control motions for site response modeling are based on the PSHA for Yucca Mountain. The PSHA considered analog data from the Basin and Range province, historical seismicity within 300 km of Yucca Mountain, and tectonic models that were consistent with available data.
4. Probability model parameters have been adequately established.	In accordance with part 1 of acceptance criterion 4, Section 6.2 describes the technical justification for parameter inputs used in ground motion site-response modeling. It describes how those parameter values are determined from available site-specific data.
5. Uncertainty in event probability is adequately evaluated.	In accordance with part 1 of acceptance criterion 5, Sections 6.2 and 6.3 describe how uncertainties and randomness in model input parameters are addressed in the development of seismic inputs for various annual frequencies of exceedance.
Section 2.2.1.3.2.3	
2. Data are sufficient for model justification.	In accordance with part 1 of acceptance criterion 2, Sections 6.2 and 6.3 provide justification for seismic inputs to be used in evaluation of mechanical disruption of engineered barriers. In accordance with part 3 of acceptance criterion 2, Section 6.2 describes how data are used to determine inputs for ground motion site-response modeling.
3. Data uncertainty is characterized and propagated through the model abstraction.	In accordance with part 1 of acceptance criterion 3, Sections 6.2 provides the technical basis for determining inputs to ground motion site-response modeling. The section also, along with Section 6.3, describes how data uncertainties and randomness are addressed. In accordance with part 2 of acceptance criterion 3, Sections 6.1 and Section 7 describe the random vibration theory-based equivalent-linear site-response model and its validation. Determination of input parameter values on the basis of site-specific data is described in Section 6.2. In accordance with part 3 of acceptance criterion 3, Sections 6.2 and 6.3 describe how data uncertainties and randomness are incorporated in the site-response modeling and analyses.

Variability–As defined in this report (Section 6.2.1.1), variability consists of two components: uncertainty and randomness. In the work described here, care has been taken to appropriately address parametric variability. Variability in the ground motions that form input to the model (the control motions) is incorporated into the PSHA results on which the control motions are based (Section 6.2.2.7). Incorporation of this variability results in mean ground motion hazard

values that are very high for low annual frequencies of exceedance. While these uncertainties reflect the scientific community's current understanding of ground motion hazard uncertainty and randomness, they result in large asymmetric uncertainties in ground motion hazard at low annual frequencies of exceedance. As a consequence, ground motion values corresponding to mean annual frequencies of 10^{-6} and lower are unphysically large.

Variability in velocity profiles at Yucca Mountain is addressed in two ways (Section 6.2.3.5). First, for the Repository Block, two base case profiles are used in site-response modeling to account for velocity uncertainty. Different data sets suggest two different velocity profiles, so both are used. Also, professional judgement is used to adjust upward the upper-range base case profile to account for limited spatial coverage by velocity measurements in some portions of the repository outline. For the Surface Facilities Area, consistent with the available data, a single set of V_S and V_P base case profiles is used for tuff, and alluvium. For the Repository Block, model results for the two base case profiles are enveloped.

Second, randomness in velocity across the Yucca Mountain site is accommodated by using multiple random profiles in modeling. Sixty randomized profiles are generated on the basis of each base case profile, consistent with observed randomness and velocity correlation statistics. Model results for the suite of profiles are averaged.

Variability in nonlinear dynamic material properties is treated similarly to that for velocity profiles (Section 6.2.4.5). Uncertainty in the mean curves for normalized shear modulus reduction and material damping is accommodated through the use of two base case curves each for tuff and alluvium. Randomness in dynamic material properties is addressed by using multiple random curves in modeling. As for the velocity profiles, 60 randomized curves are generated for each base case curve. Model results for the suite of randomized curves are averaged. Model results for different base case curves are enveloped.

Within a probabilistic framework, the annual frequency of a given level of ground motion being exceeded is obtained by integrating over all input parameters. The hazard can be deaggregated into a distribution of potential earthquakes with different combinations of magnitude and distance. The range of earthquake magnitudes and distances contributing to ground motion at a particular annual exceedance level is incorporated into the modeling process through the use of deaggregation earthquakes (Section 6.2.2.5). Differences in the nonlinear behavior of site materials related to the different spectral content of different magnitude earthquakes is captured in the modeling by using each deaggregation earthquake as the control motion in a suite of model runs. Modeling results for the deaggregation earthquakes are combined using a weighted average.

The range of magnitude-distance combinations contributing to ground motion hazard at a particular annual exceedance frequency is also addressed in development of ground motion time histories (Section 6.3.2). In analyzing the performance of engineered barrier system items under loading by ground motions with low annual exceedance frequencies (e.g., 10^{-5},10^{-6}, 10^{-7}), it is desirable to use a suite of time histories that reflects the range of magnitudes contributing to the hazard. Thus, recorded strong motion accelerograms that serve as the basis for the suite of developed time histories are selected to reflect a range of magnitudes and distances similar to that determined from the hazard results (Section 6.3.2.3).

While, for some cases, conditioning of the basis accelerograms to reflect either a reference rock outcrop (Point A) or emplacement level (Point B) target spectrum was carried out, only a weak match was imposed (Section 6.3.2.3). This approach represents a compromise between the goals of matching the target spectrum and maintaining the diversity of the observed ground motions.

In developing time histories for postclosure analyses, inter-component randomness is preserved (Section 6.3.2.3). That is, scaling to PGV was done so as to maintain the correlation between the two horizontal components and the vertical components inherent in the original recording. This approach contributes to the large ground motions determined for low annual exceedance frequencies. No bounds were placed on the output of the scaling operation; inter-component correlation observed for the recorded levels of ground motion were taken as appropriate at the higher, scaled levels of ground motion.

Restrictions on Use – There are no restrictions on the use of results from these modeling and analysis activities.

Recommendations – The following recommendation applies to the results of these modeling and analysis activities:

- It is recommended that time history set #15 developed for postclosure analyses (annual frequencies of exceedance of 10^{-5}, 10^{-6}, and 10^{-7}) be used with caution. The strong motion record upon which this time history set is based (recorded at station TCU025 located a distance of 50 km from the Chi-Chi, Taiwan earthquake of **M** 7.6) is anomalous with respect to the western U.S. empirical attenuation relations used by the PSHA ground motion experts in their estimation of the Yucca Mountain ground motions (Section 6.3.2.3.1).

9. INPUTS AND REFERENCES

9.1 DOCUMENTS CITED

164486 Abrahamson, N.A and Shedlock, K.M. 1997. "Overview." *Seismological Research Letters*, 68, (1), 9-23. El Cerrito, California: Seismological Society of America. TIC: 240552.

104205 Abrahamson, N.A. and Silva, W.J. 1997. "Empirical Response Spectral Attenuation Relations for Shallow Crustal Earthquakes." *Seismological Research Letters*, 68, (1), 94-127. El Cerrito, California: Seismological Society of America. TIC: 240553.

150723 Aki, K. and Richards, P.G. 1980. *Quantitative Seismology, Theory and Methods*. Two Volumes. San Francisco, California: W.H. Freeman and Company. TIC: 234297, 243039.

128813 Anderson, J.G. and Hough, S.E. 1984. "A Model for the Shape of the Fourier Amplitude Spectrum of Acceleration at High Frequencies." *Bulletin of the Seismological Society of America,* 74, (5), 1969-1993. El Cerrito, California: Seismological Society of America. TIC: 242440.

163169 Anderson, D.G. and Tang, Y.K. 1989. "Summary of Soil Characterization Program for the Lotung Large-Scale Seismic Experiment." *Proceedings: EPRI/NRC/TPC Workshop on Seismic Soil-Structure Interaction Analysis Techniques Using Data from Lotung, Taiwan held in Palo Alto, California, December 9-11, 1987.* EPRI NP-6154, Volume 1. Pages 4-1 through 4-20. Palo Alto, California: Electric Power Research Institute. TIC: 254750.

148636 ASCE 4-86. 1986. "Seismic Analysis of Safety-Related Nuclear Structures and Commentary on Standard for Seismic Analysis of Safety Related Nuclear Structures." New York, New York: American Society of Civil Engineers. TIC: 238892.

163171 Atkinson, G.M and Silva, W.J. 1997. "An Empirical Study of Earthquake Source Spectra for California Earthquakes." *Bulletin of the Seismological Society of America*, 87, (1), 97-112. El Cerrito, California: Seismological Society of America. TIC: 254822.

105351 Balch, A.H. and Erdemir, C. 1996. *A Nine-Component, Multiple-Offset Vertical Seismic Profile at the UE-25 UZ#16 Borehole, Nevada Test Site, Nye County, Nevada: Taking VSPs to a New Level*. Milestone 3GUPP622M. Denver, Colorado: U.S. Geological Survey. ACC: MOL.19990831.0049.

163172 Benites, R.; Silva, W.J.; and Tucker, B. 1985. "Measurements of Ground Response to Weak Motion in La Molina Valley, Lima, Peru. Correlation with Strong Ground Motion." *Earthquake Notes*, 55, (l), 5. El Cerrito, California: Seismological Society of America, Eastern Section. TIC: 254650.

110221 Benjamin, J.R. and Cornell, C.A. 1970. *Probability, Statistics, and Decision for Civil Engineers.* New York, New York: McGraw-Hill. TIC: 242473.

103317 Boore, D.M. 1983. "Stochastic Simulation of High-Frequency Ground Motions Based on Seismological Models of the Radiated Spectra." *Bulletin of the Seismological Society of America*, 73, (6), 1865-1894. El Cerrito, California: Seismological Society of America. TIC: 245812.

103318 Boore, D.M. 1986. "Short-Period P- and S-Wave Radiation from Large Earthquakes: Implications for Spectral Scaling Relations Spectra." *Bulletin of the Seismological Society of America*, 76, (1) 43-64. El Cerrito, California: Seismological Society of America. TIC: 245811.

163993 Boore, D.M. 2001. "Comparisons of Ground Motion from the 1999 Chi-Chi Earthquake with Empirical Predictions Largely Based on Data from California." *Bulletin of the Seismological Society of America*, 91, (5), 1212-1217. El Cerrito, California: Seismological Society of America. TIC: 254638.

163706 Boore, D.M. 2003. "Simulation of Ground Motion Using the Stochastic Method." *Pure and Applied Geophysics*, 160, (3-4), 635-676. Basel, Switzerland: Birkhäuser Verlag AG. TIC: 254654.

163174 Boore, D.M. and Joyner, W.B. 1984. "A Note on the Use of Random Vibration Theory to Predict Peak Amplitudes of Transient Signals." *Bulletin of the Seismological Society of America*, 74, (5), 2035-2039. El Cerrito, California: Seismological Society of America. TIC: 254639.

163176 Borcherdt, R.D. 1973. "Energy and Plane Waves in Linear Viscoelastic Media." *Journal of Geophysical Research,* 78, (14), 2442–2453. Washington, D.C.: American Geophysical Union. TIC: 254649.

163177 Borcherdt, R.D. and Gibbs, J.F. 1976. "Effects of Local Geologic Conditions in the San Francisco Bay Region on Ground Motions and the Intensities of the 1906 Earthquake." *Bulletin of the Seismological Society of America,* 66, (2), 467–500. El Cerrito, California: Seismological Society of America. TIC: 254640.

163342 Borcherdt, R.D. and Glassmoyer, G. 1992. "On the Characteristics of Local Geology and Their Influence on Ground Motions Generated by the Loma Prieta Earthquake in the San Francisco Bay Region, California." *Bulletin of the Seismological Society of America,* 82, (2), 603-641. El Cerrito, California: Seismological Society of America. TIC: 254641.

159576 Brocoum, S. 2001. "Transmittal of Report Addressing Key Technical Issues (KTI) Structural Deformation and Seismicity (SDS)." Letter from S. Brocoum (DOE/YMSCO) to C.W. Reamer (NRC), October 25, 2001, OL&RC:TCG-0140, with enclosure. ACC: MOL.20020304.0297; MOL.20030714.0094.

103315 Brune, J.N. 1970. "Tectonic Stress and the Spectra of Seismic Shear Waves from Earthquakes." *Journal of Geophysical Research,* 75, (26), 4997-5009. Washington, D.C.: American Geophysical Union. TIC: 220215.

155187 BSC (Bechtel SAIC Company) 2001a. *Ground Control for Emplacement Drifts for SR.* ANL-EBS-GE-000002 REV 00 ICN 01. Las Vegas, Nevada: Bechtel SAIC Company. ACC: MOL.20010627.0028.

157829 BSC (Bechtel SAIC Company) 2002a. *Geotechnical Data for a Potential Waste Handling Building and for Ground Motion Analyses for the Yucca Mountain Site Characterization Project.* ANL-MGR-GE-000003 REV 00. Las Vegas, Nevada: Bechtel SAIC Company. ACC: MOL.20021004.0078.

157756 BSC (Bechtel SAIC Company 2002b. *Design Evolution Study-Underground Layout.* TDR-MGRMG-000003 REV 00. Las Vegas, Nevada: Bechtel SAIC Company. ACC: MOL.20020429.0023.

165937 BSC (Bechtel SAIC Company) 2003a. *Design Peak Ground Velocity for the Repository Level (Point B) at 10^{-6} Annual Exceedance Probability.* Impact Review Action Notice DTN: MO0301DPGVB106.001. Las Vegas, Nevada: Bechtel SAIC Company. ACC: MOL.20030318.0385.

166296 BSC (Bechtel SAIC Company) 2003b. *Total System Performance Assessment-License Application Methods and Approach.* TDR-WIS-PA-000006 REV 00 ICN 01. Las Vegas, Nevada: Bechtel SAIC Company. ACC: DOC.20031215.0001.

170500 BSC (Bechtel SAIC Company) 2003c. *Impact Review Action Notice, Software Problem Report FRISK88*. Las Vegas, Nevada: Bechtel SAIC Company. ACC: MOL.20030929.0188.

166274 BSC (Bechtel SAIC Company) 2003d. *Development of Earthquake Ground Motion Input for Preclosure Seismic Design and Postclosure Performance Assessment of a Geologic Repository at Yucca Mountain, NV*. MDL-MGR-GS-000003 REV 00. Las Vegas, Nevada: Bechtel SAIC Company. ACC: DOC.20031201.0001.

171850 BSC (Bechtel SAIC Company) 2004a. *Development of Seismic Inputs, Preparation of Seismic Topical Reports, and Evaluation of Disruptive Events Features, Events, and Processes.* TWP-MGR-GS-000001 REV 03 ICN 02. Las Vegas, Nevada: Bechtel SAIC Company. ACC: DOC.20040923.0001.

170564 BSC (Bechtel SAIC Company) 2004b. *Preclosure Seismic Design Methodology for a Geologic Repository at Yucca Mountain.* TDR-WHS-MD-000004 REV 01. Las Vegas, Nevada: Bechtel SAIC Company. ACC: DOC.20040827.0011.

170137 BSC (Bechtel SAIC Company) 2004c. *Peak Ground Velocities for Seismic Events at Yucca Mountain, Nevada.* ANL-MGR-GS-000004 REV 000A. Las Vegas, Nevada: Bechtel SAIC Company.

164519 BSC (Bechtel SAIC Company) 2004d. *D&E/PA/C IED Subsurface Facilities.* 800-IED- WIS0-00101-000-00A. Las Vegas, Nevada: Bechtel SAIC Company. ACC: ENG.20040309.0026.

170017 BSC (Bechtel SAIC Company) 2004e. *Features, Event, and Processes: Disruptive Events.* ANL-WIS-MD-000005, Rev. 02. Las Vegas, Nevada: Bechtel SAIC Company.

167083 BSC (Bechtel SAIC Company) 2004f. Structural Calculations of Waste Package Exposed to Vibratory Ground Motion. 000-00C-WIS0-01400-000-00A. Las Vegas, Nevada: Bechtel SAIC Company. ACC: ENG.20040217.0008.

168385 BSC (Bechtel SAIC Company) 2004g. *Additional Structural Calculations of Waste Package Exposed to Vibratory Ground Motion*. 000-00C-WIS0-01700-000-00A. Las Vegas, Nevada: Bechtel SAIC Company. ACC: ENG.20040318.0011.

166107 BSC (Bechtel SAIC Company) 2004h. *Drift Degradation Analysis.* ANL-EBS-MD-000027 REV 03. Las Vegas, Nevada: Bechtel SAIC Company. ACC: DOC.20040915.0010.

169734 BSC (Bechtel SAIC Company) 2004i. *Yucca Mountain Site Description*. TDR-CRW-GS-000001 Rev 02 ICN01. Two volumes. Las Vegas, Nevada: Bechtel SAIC Company. ACC: DOC.20040504.0008.

168030 BSC (Bechtel SAIC Company) 2004j. *Characterize Framework for Seismicity and Structural Deformation at Yucca Mountain, Nevada*. ANL-CRW-GS-000003 REV 00 [Errata 001]. Las Vegas, Nevada: Bechtel SAIC Company. ACC: MOL.20000510.0175; DOC.20040223.0007.

169980 BSC (Bechtel SAIC Company) 2004k. *Characterize Eruptive Processes at Yucca Mountain, Nevada*. ANL-MGR-GS-000002, Rev. 02. Las Vegas, Nevada: Bechtel SAIC Company. ACC: DOC.20041004.0006.

169989 BSC (Bechtel SAIC Company) 2004l. *Characterize Framework for Igneous Activity at Yucca Mountain, Nevada*. ANL-MGR-GS-000001, Rev. 02. Las Vegas, Nevada: Bechtel SAIC Company. ACC: DOC.20041015.0002.

169183 BSC (Bechtel SAIC Company) 2004m. *Seismic Consequence Abstraction.* MDL-WIS-PA-000003, Rev. 01. Las Vegas, Nevada: Bechtel SAIC Company. ACC: DOC.20041025.0004

170029 BSC (Bechtel SAIC Company) 2004n. *Geologic Framework Model (GFM2000).* MDL-NBS-GS-000002 REV 02. Las Vegas, Nevada: Bechtel SAIC Company. ACC: DOC.20040827.0008.

163348 Buchen, P.W. 1971. "Plane Waves in Linear Viscoelastic Media." *Geophysical Journal of the Royal Astronomical Society,* 23, (5), 531-542. Oxford, England: Blackwell Scientific Publications. TIC: 254651.

100106 Buesch, D.C.; Spengler, R.W.; Moyer, T.C.; and Geslin, J.K. 1996. *Proposed Stratigraphic Nomenclature and Macroscopic Identification of Lithostratigraphic Units of the Paintbrush Group Exposed at Yucca Mountain, Nevada*. Open File Report 94-469. Denver, Colorado: U.S. Geological Survey. ACC: MOL.19970205.0061.

163497 Bycroft, G.N. 1980. *El Centro California Differential Ground Motion Array*. Open-File Report 80-919. Menlo Park, California: U.S. Geological Survey. TIC: 254674.

102191 Campbell, K.W. 1981. "Near-Source Attenuation of Peak Horizontal Acceleration." *Bulletin of the Seismological Society of America,* 71, (6), 2039-2070. El Cerrito, California: Seismological Society of America. TIC: 221670.

166275 Canori, G.F. and Leitner, M.M. 2003. *Project Requirements Document*. TER-MGR-MD-000001 REV 02. Las Vegas, Nevada: Bechtel SAIC Company. ACC: DOC.20031222.0006.

163449 Chang, N.Y.; Huang, M.J.; Lien, B.H.; and Chang, F.K. 1986. "EQGEN - A User-Friendly Artificial Earthquake Simulation Program." *Proceedings of the Third U.S. National Conference on Earthquake Engineering, August 24-28, 1986,* Charleston, South Carolina, 1, 439-450. TIC: 209839.

163450 Chang, T.S.; Tang, P.S.; Lee, C.S.; and Hwang, H. 1990. *Evaluation of Liquefaction Potential in Memphis and Shelby County.* Technical Report NCEER-90-0018. Buffalo, New York: National Center for Earthquake Engineering Research. TIC: 254524.

164971 Chávez-García, F.J.; Ramos-Martínez, J.; and Romero-Jiménez, E. 1995. "Surface-Wave Dispersion Analysis in Mexico City." *Bulletin of the Seismological Society of America,* 85, (4), 1116-1126. El Cerrito, California: Seismological Society of America. TIC: 254849.

163451 Chin, B-H. and Aki, K. 1991. "Simultaneous Study of the Source, Path, and Site Effects on Strong Ground Motion During the 1989 Loma Prieta Earthquake: A Preliminary Result on Pervasive Nonlinear Site Effects." *Bulletin of the Seismological Society of America,* 81, (5), 1859-1884. El Cerrito, California: Seismological Society of America. TIC: 254642.

171465 Chung, R.; Ballantyne, D.; Borcherdt, R.; Bucker, I.; Comeau, E.; Cooper, J.; Ha 1996. *The January 17, 1995 Hyogoken-Nanbu (Kobe) Earthquake; Performance of Structures, Lifelines, and Fire Protection Systems.* NIST Special Publication 901. Gaithersburg, Maryland: Building and Fire Research Laboratory National Institute of Standards and Technology. ACC: MOL.20040922.0187.

164683 Clough, R.W. and Penzien, J. 1975. *Dynamics of Structure.* New York, New York: McGraw-Hill. TIC: 254783.

163452 Cooley, J.W. and Tukey, J.W. 1965. "An Algorithm for the Machine Calculation of Complex Fourier Series." *Mathematics of Computation*, 19, (90), 297-301. Providence, Rhode Island: American Mathematical Society. TIC: 254671.

103731 CRWMS M&O 1998a. *Probabilistic Seismic Hazard Analyses for Fault Displacement and Vibratory Ground Motion at Yucca Mountain, Nevada.* Milestone SP32IM3, September 23, 1998. Three volumes. Las Vegas, Nevada: CRWMS M&O. ACC: MOL.19981207.0393.

156499 CRWMS M&O 1998b. *Seismic Design Basis Inputs for a High-Level Waste Repository at Yucca Mountain, Nevada.* B00000000-01727-5700-00018 REV 0. Las Vegas, Nevada: CRWMS M&O. ACC: MOL.19990319.0318.

109209 CRWMS M&O 1999. *Preliminary Geotechnical Investigation for Waste Handling Building, Yucca Mountain Site Characterization Project.* BCB000000-01717-5705-00016 REV 00. Las Vegas, Nevada: CRWMS M&O. ACC: MOL.19990625.0182.

151288 CRWMS M&O 2000. *Preliminary Dynamic Soil-Structure-Interaction Analysis for the Waste Handling Building.* ANL-WHS-ST-000001 REV 00. Las Vegas, Nevada: CRWMS M&O. ACC: MOL.20000504.0313.

163493 Darragh, R.B. and Shakal, A.F. 1991. "The Site Response of Two Rock and Soil Station Pairs to Strong and Weak Ground Motion." *Bulletin of the Seismological Society of America,* 81, (5), 1885-1899. El Cerrito, California: Seismological Society of America. TIC: 254643.

164685 Day, S.M. 1982a. "Three-Dimensional Finite Difference Simulation of Fault Dynamics: Rectangular Faults with Fixed Rupture Velocity." Bulletin of the Seismological Society of America, 72, (3), 705-727. El Cerrito, California: Seismological Society of America. TIC: 254818.

164684 Day, S.M. 1982b. "Three-Dimensional Simulation of Spontaneous Rupture: The Effect of Nonuniform Prestress." Bulletin of the Seismological Society of America, 72, (6), 1881-1902. El Cerrito, California: Seismological Society of America. TIC: 254819.

163496 Dimitriu, P.P.; Papaioannou, C.A.; and Theodulidis, N.P. 1998. "EURO-SEISTEST Strong-Motion Array Near Thessaloniki, Northern Greece: A Study of Site Effects." *Bulletin of the Seismological Society of America,* 88, (3), 862-873. El Cerrito, California: Seismological Society of America. TIC: 254644.

153849 DOE (U.S. Department of Energy) 2001. *Yucca Mountain Science and Engineering Report*. DOE/RW-0539. [Washington, DC]: U.S. Department of Energy, Office of Civilian Radioactive Waste Management. ACC: MOL.20010524.0272.

160065 Dowding, C.H. and Rozen, A. 1978. "Damage to Rock Tunnels from Earthquake Shaking." *Journal of the Geotechnical Engineering Division,* 104, (GT2), 175-192. New York, New York: American Society of Civil Engineers. TIC: 218343.

129364 Durrani, B.A. and Walck, M.C. 1996. *Near-Surface Velocity Modeling at Yucca Mountain Using Borehole and Surface Records from Underground Nuclear, Explosions*. SAND95-1606. Albuquerque, New Mexico: Sandia National Laboratories. ACC: MOL.19970414.0043.

163503 Elgamal, A. W.; Zeghal, M.; and Parra, E. 1996. "Liquefaction of Reclaimed Island in Kobe, Japan." *Journal of Geotechnical Engineering,* 122, (1) 39-49. Reston, Virginia: American Society of Civil Engineers. TIC: 254655.

163669 EPRI (Electric Power Research Institute) 1978. *Study of Nonlinear Effects on One-Dimensional Earthquake Response*. EPRI NP-865. Palo Alto, California: Electric Power Research Institute. TIC: 254753.

163607 EPRI (Electric Power Research Institute) 1981. *Specification of Input Motions for Seismic Analyses of Soil-Structure Systems Within a Nonlinear Analyses Framework.* EPRI NP-2097. Palo Alto, California: Electric Power Research Institute. TIC: 254751.

107489 EPRI (Electric Power Research Institute) 1988. *Soil Response to Earthquake Ground Motion.* EPRI NP-5747. Palo Alto, California: Electric Power Research Institute. TIC: 254577.

103319 EPRI (Electric Power Research Institute) 1993a. *Method and Guidelines for Estimating Earthquake Ground Motion.* Volume 1 of *Guidelines for Determining Design Basis Ground Motion.* EPRI TR-102293. Palo Alto, California: Electric Power Research Institute. TIC: 226495.

103320 EPRI (Electric Power Research Institute) 1993b. *Appendices for Ground Motion Estimation.* Volume 2 of *Guidelines for Determining Design Basis Ground Motion.* EPRI TR-102293. Palo Alto, California: Electric Power Research Institute. TIC: 226495.

163505 Field, E.H.; Jacob, K.H; and Hough, S.E. 1992. "Earthquake Site Response Estimation: A Weak-Motion Case Study." *Bulletin of the Seismological Society of America,* 82, (6), 2283-2307. El Cerrito, California: Seismological Society of America. TIC: 254645.

171474 Fowler, C.M.R. 1990. *The Solid Earth, an Introduction to Global Geophysics.* 1. 472. New York, New York: Press Syndicate of the University of Cambridge. TIC: 256518.

163508 Ganev, T.; Yamazaki, F.; Ishizaki, H.; and Kitazawa, M. 1998. "Response Analysis of the Higashi-Kobe Bridge and Surrounding Soil in the 1995

Hyogoken-Nanbu." *Earthquake and Engineering Structural Dynamics,* 27, (6), 557-576. Hoboken, New Jersey: John Wiley & Sons. TIC: 254828.

163510 Hanks, T.C. and McGuire, R.K. 1981. "The Character of High-Frequency Strong Ground Motion." *Bulletin of the Seismological Society of America*, 71, (6), 2071-2095. El Cerrito, California: Seismological Society of America. TIC: 254646.

157246 Hardin, B.O. and Drnevich, V.P. 1972a. "Shear Modulus and Damping in Soils: Measurement and Parameter Effects." *Journal of the Soil Mechanics and Foundation Division,* 98, (SM6), 603-624. New York, New York: American Society of Civil Engineers. TIC: 251418.

163511 Hardin, B.O. and Drnevich, V.P. 1972b. "Shear Modulus and Damping in Soils: Design Equations and Curves." *Journal of the Soil Mechanics and Foundation Division, 98,* (SM7), 667-692. New York, New York: American Society of Civil Engineers. TIC: 254827.

105106 Harmsen, S.C. 1993. *Seismicity and Focal Mechanisms for the Southern Great Basin of Nevada and California in 1991*. Open-File Report 92-340. Denver, Colorado: U.S. Geological Survey. ACC: NNA.19920629.0129.

151232 Haskell, N.A. [1953]. "The Dispersion of Surface Waves in Multilayered Media." *Bulletin of the Seismological Society of America*, 43, (1), 17-34. Berkeley, California: Seismological Society of America. TIC: 224178.

163513 Haskell, N.A. 1960. "Crustal Reflections of Plane SH Waves." *Journal of Geophysical Research*, 65, (12), 4147-4150. [Washington, D.C.]: American Geophysical Union. TIC: 222421.

163514 Haskell, N.A. 1962. "Crustal Reflection of Plane P and SV Waves." *Journal of Geophysical Research*, 67, (12), 4751-4767. [Washington, D.C.: American Geophysical Union]. TIC: 222422.

163515 Hays, W.W.; Rogers, A.M.; and King, K.W. 1979. "Empirical Data About Local Ground Response." *Proceedings of the 2nd U.S. National Conference on Earthquake Engineering, August 22-24, 1979, Stanford University, Stanford, California.* 223-232. [Berkeley, California]: Earthquake Engineering Research Institute. TIC: 254825.

164686 Hough, S.E. and Anderson, J.G. 1988. "High-Frequency Spectra Observed at Anza, California: Implications for Q Structure." *Bulletin of the Seismological Society of America*, 78, (2), 692-707. [El Cerrito, California]: Seismological Society of America. TIC: 243238.

163516 Hutchings, L.J. and Wu, F. 1990. "Empirical Green's Functions from Small Earthquakes: A Waveform Study of Locally Recorded Aftershocks of the 1971 San Fernando Earthquake." *Journal of Geophysical Research,* 95, (B2), 1187-1214. [Washington, D.C.]: American Geophysical Union. TIC: 254821.

105524 Idriss, I.M. 1993. *Procedures for Selecting Earthquake Ground Motions at Rock Sites (Revised)*. NIST GCR 93-625. Gaithersburg, Maryland: U.S. Department of Commerce, National Institute of Standards and Technology. TIC: 241629.

163520 Idriss, I.M. and Seed, H.B. 1968. "Seismic Response of Horizontal Soil Layers." *Journal of the Soil Mechanics and Foundations Division,* 94, (SM4), 1003-1031. [Ann Arbor, Michigan]: American Society of Civil Engineers, Soil Mechanics and Foundations Division. TIC: 254670.

110379 Iwan, W.D. 1967. "On a Class of Models for the Yielding Behavior of Continuous and Composite Systems." *Journal of Applied Mechanics,* 612-617. New York, New York: American Society of Mechanical Engineers. TIC: 241280.

157248 Joh, S.-H. 1996. *Advances in the Data Interpretation and Analysis Techniques for Spectral-Analysis-of-Surface-Waves (SASW) Measurements*. PhD dissertation. Austin, Texas: University of Texas at Austin. TIC: 252117.

110447 Johnson, L.R. and Silva, W.J. 1981. "The Effects of Unconsolidated Sediments Upon the Ground Motion During Local Earthquakes." *Bulletin of the Seismological Society of America*, 71, (1), 127-142. El Cerrito, California: Seismological Society of America. TIC: 238080.

164134 Joyner, W.B. 2000. "Strong Motion from Surface Waves in Deep Sedimentary Basins." *Bulletin of the Seismological Society of America,* 90, (6B), S95-S112. El Cerrito, California: Seismological Society of America. TIC: 254629.

163521 Joyner, W.B. and Chen, A.T.F. 1975. "Calculation of Nonlinear Ground Response in Earthquakes." *Bulletin of the Seismological Society of America,* 65, (5), 1315-1336. El Cerrito, California: Seismological Society of America. TIC: 254628.

157285 Joyner, W.B.; Warrick, R.E.; and Fumal, T.E. 1981. "The Effect of Quaternary Alluvium on Strong Ground Motion in the Coyote Lake, California Earthquake of 1979." *Bulletin of the Seismological Society of America,* 71, (4), 1333-1349. Berkeley, California: Seismological Society of America. TIC: 251490.

163522 Joyner, W.B.; Warrick, R.E.; and Oliver, A.A. III. 1976. "Analysis of Seismograms from a Downhole Array in Sediments Near San Francisco Bay." *Bulletin of the Seismological Society of America,* 66, (3), 937-958. El Cerrito, California: Seismological Society of America. TIC: 254633.

164981 Kailath, T. 1981. *Lectures on Linear Wiener and Kalman Filtering.* Courses and Lectures, No. 140. New York, New York: Springer-Verlag. TIC: 254816.

164079 Kokusho, T. and Matsumoto, M. 1997. "Nonlinear Site Response during the Hyogoken-Nambu Earthquake Recorded by Vertical Arrays in View of Seismic Zonation Methodology." *Seismic Behavior of Ground and Geotechnical Structures, Proceedings of Discussion Special Technical Session on Earthquake*

Geotechnical Engineering During Fourteenth International Conference on Soil Mechanics and Foundation Engineering, 61-69. Hamburg, Germany, 6-12 September 1997. Sêco e Pinto, P.S., ed. 61-69. Brookfield, Vermont: A.A. Balkema. TIC: 254812.

100909 Kotra, J.P.; Lee, M.P.; Eisenberg, N.A.; and DeWispelare, A.R. 1996. *Branch Technical Position on the Use of Expert Elicitation in the High-Level Radioactive Waste Program*. NUREG-1563. Washington, D.C.: U.S. Nuclear Regulatory Commission. TIC: 226832.

103337 Kramer, S.L. 1996. *Geotechnical Earthquake Engineering.* Prentice-Hall International Series in Civil Engineering and Engineering Mechanics. Hall, W.J., ed. Upper Saddle River, New Jersey: Prentice-Hall. TIC: 243891.

171473 Lay, T. and Wallace, T.C. 1995. *Modern Global Seismology.* 521. San Diego, California: Academic Press, Inc. TIC: 256517.

110451 Lee, R.C.; Maryak, M.E.; and McHood, M.D. 1997. *SRS Seismic Response Analysis and Design Basis Guidelines*. WSRC-TR-97-0085, Rev. 0. Aiken, South Carolina: Westinghouse Savannah River Company. TIC: 242339.

163527 Li, X.S.; Wang, Z.L.; and Shen, C.K. 1992. *SUMDES: A Nonlinear Procedure for Response Analysis of Horizontally-Layered Sites Subjected to Multi-Directional Earthquake Loading*. Davis, California: University of California, Davis, Department of Civil Engineering. TIC: 256676.

163921 Liu, H-L. and Helmberger, D.V. 1985. "The 23:19 aftershock of the 15 October 1979 Imperial Valley Earthquake: More Evidence for an Asperity." *Bulletin of the Seismological Society of America,* 75, (3), 689-708. [El Cerrito, California]: Seismological Society of America. TIC: 254636.

163995 Liu, H-L. and Pezeshk, S. 1999. "An Improvement on the Estimation of Pseudoresponse Spectral Velocity Using RVT Method." *Bulletin of the Seismological Society of America,* 89, (5), 1384-1389. [El Cerrito, California]: Seismological Society of America. TIC: 254635.

163528 Lockett, F.J. 1962. "The Reflection and Refraction of Waves at an Interface Between Viscoelastic Materials." *Journal of the Mechanics and Physics of Solids,* 10, (1), 53-64. New York, New York: Pergamon Press. TIC: 254669.

106330 Majer, E.L.; Feighner, M.; Johnson, L.; Daley, T.; Williams, K.; Karageorgi, E.; and McEvilly, T. 1996a. *Level 4 Milestone Letter Report on Surface Geophysics Synthesis: Data Processing*. Berkeley, California: Lawrence Berkeley National Laboratory. ACC: MOL.19971224.0006.

104685 Majer, E.L.; Feighner, M.; Johnson, L.; Daley, T.; Karageorgi, E.; Lee, K.H.; Williams, K.; and McEvilly, T. 1996b. *Surface Geophysics.* Volume I of *Synthesis of Borehole and Surface Geophysical Studies at Yucca Mountain,*

Nevada and Vicinity. Milestone OB05M. Berkeley, California: Lawrence Berkeley National Laboratory. ACC: MOL.19970610.0150.

163996 McGarr, A. 1984. "Some Applications of Seismic Source Mechanism Studies to Assessing Underground Hazard." *Proceedings of the 1st International Congress on Rockbursts and Seismicity in Mines, Johannesburg, 1982*. Gay, N.C. and Wainwright, E.H., eds. Pages 199-208. Johannesburg, South Africa: South African Institute of Mining and Metallurgy. TIC: 254652.

107483 McGuire, R.K. 1995. "Probabilistic Seismic Hazard Analysis and Design Earthquakes: Closing the Loop.≅ *Bulletin of the Seismological Society of America,* 85, (5), 1275-1284. El Cerrito, California: Seismological Society of America. TIC: 232947.

157510 McGuire, R.K.; Silva, W.J.; and Costantino, C.J. 2001. *Technical Basis for Revision of Regulatory Guidance on Design Ground Motions: Hazard- and Risk-Consistent Ground Motion Spectra Guidelines*. NUREG/CR-6728. Washington, D.C: U.S. Nuclear Regulatory Commission. TIC: 251294.

163799 McGuire, R.K.; Silva, W.J.; and Costantino, C.J. 2002. Technical Basis for Revision of Regulatory Guidance on Design Ground Motions: Development of Hazard- and Risk-Consistent Seismic Spectra for Two Sites. NUREG/CR-6769. Washington, D.C.: U.S. Nuclear Regulatory Commission. TIC: 254478.

164681 Menq, F-Y. 2003. *Dynamic Properties of Sandy and Gravelly Soils.* PhD dissertation. Austin, Texas: University of Texas at Austin. TIC: 254831.

106384 Mooney, W.D., and Schapper, S.G. 1995. "Seismic Refraction Investigations." Chapter 5 of Major Results of Geophysical Investigations at Yucca Mountain and Vicinity, Southern Nevada. Oliver, H.W.; Ponce, D.A.; and Hunter, W.C., eds. Open-File Report 95-74. Menlo Park, California: U.S. Geological Survey. ACC: MOL.19980305.0122.

163608 Murphy, J.R.; Davis, A.H.; and Weaver, N.L. 1971. "Amplification of Seismic Body Waves by Low-Velocity Surface Layers." *Bulletin of the Seismological Society of America,* 61, (1), 109-145. El Cerrito, California: Seismological Society of America. TIC: 254680.

165110 NRC (U.S. Nuclear Regulatory Commission) [1989a]. "Seismic Design Parameters." Revision 2 of Section 3.7.1 of *Standard Review Plan (for the Review of Safety Analysis Reports for Nuclear Power Plants).*. NUREG-0800. Washington, D.C.: U.S. Nuclear Regulatory Commission. ACC: MOL.20030910.0150.

165111 NRC (U.S. Nuclear Regulatory Commission) [1989b]. "Seismic System Analysis." Revision 2 of Section 3.7.2 of *Standard Review Plan (for the Review of Safety Analysis Reports for Nuclear Power Plants).* NUREG-0800.

Washington, D.C.: U.S. Nuclear Regulatory Commission. ACC: MOL.20030910.0151.

163274 NRC (U.S. Nuclear Regulatory Commission) 2003. *Yucca Mountain Review Plan, Final Report.* NUREG-1804, Rev. 2. Washington, D.C.: U.S. Nuclear Regulatory Commission, Office of Nuclear Material Safety and Safeguards. TIC: 254568.

170648 Ou, G., and Herrmann R.B. 1990. "A Statistical Model for Ground Motion Produced by Earthquakes at Local and Regional Distances." *Bulletin of the Seismological Society of America, 80,* (6, Part A), p. 1397-1417. El Cerrito, California: Seismological Society of America. TIC: 256274.

110462 Parzen, E. 1962. *Stochastic Processes.* San Francisco, California: Holden Day. TIC: 208424.

163610 Pitarka, A.S.; Takenaka, H.; and Suetsugu, D.1994. "Modeling Strong Motion in the Ashigara Valley for the 1990 Odawara, Japan, Earthquake." *Bulletin of the Seismological Society of America*, 84, (5), 1327-1335. [El Cerrito, California]: Seismological Society of America. TIC: 254679.

164825 Power, M.S.; Egan, J.A.; Shewbridge, S.; deBecker, J.; and Faris, J.R. 1998. "Analysis of Liquefaction-Induced Damage On Treasure Island." *The Loma Prieta, California, Earthquake of October 17, 1989 - Liquefaction.* Holzer, T.L., ed. U.S. Geological Survey Professional Paper 1551-B. B87-B119. Washington D.C.: U.S. Government Printing Office. TIC: 255058.

145343 Press, W.H.; Flannery, B.P.; Teukolsky, S.A.; and Vetterling, W.T. 1986. *Numerical Recipes, The Art of Scientific Computing.* New York, New York: Cambridge University Press. TIC: 234187

163612 Pyke, R.M. 1979. "Nonlinear Models for Irregular Cyclic Loadings." *Journal of Geotechnical Engineering Division,* 105, (GT6), 715-726. New York, New York: American Society of Civil Engineers. TIC: 254824.

163613 Pyke, R.M. [n.d.]. *TESS, Users' Manual*. Lafayette, California: TAGAsoft Limited. TIC: 256653.

119139 Regulatory Guide 1.165. 1997. *Identification and Characterization of Seismic Sources and Determination of Safe Shutdown Earthquake Ground Motion*. Washington, DC: U.S. Nuclear Regulatory Commission. Readily available.

151402 Regulatory Guide 1.60, Rev. 1. 1973. *Design Response Spectra for Seismic Design of Nuclear Power Plants.* [Washington, D.C.]: U.S. Atomic Energy Commission. TIC: 232770.

163650 Reid, H.F. 1910. "The Influence of the Foundation on the Apparent Intensity." Volume II of *The California Earthquake of April 18, 1906, Report of the State*

Earthquake Investigation Commission. 87. 49-56. Washington, D.C.: Carnegie Institute of Washington. TIC: 254839.

163651 Richart, F.E., Jr. 1975. "Some Effects of Dynamic Soil Properties on Soil-Structure Interaction." *Journal of the Geotechnical Engineering Division,* 101, (GT12), 1197-1240. Reston, VA: American Society of Civil Engineers. TIC: 254668.

163652 Rogers, A.M.; Borcherdt, R.D.; Covington, P.A.; and Perkins, D.M. 1984. "A Comparative Ground Response Study near Los Angeles Using Recordings of Nevada Nuclear Tests and the 1971 San Fernando Earthquake." *Bulletin of the Seismological Society of America,* 74, (5), 1925-1949. [El Cerrito, California]: Seismological Society of America. TIC: 254678.

106702 Rogers, A.M.; Harmsen, S.C.; Corbett, E.J.; Priestly, K.; and dePolo, D. 1991. "The Seismicity of Nevada and Some Adjacent Parts of the Great Basin." Chapter 10 of *The Geology of North America Decade Map.* Volume 1. Boulder, Colorado: Geological Society of America. TIC: 243190.

163653 Rogers, A.M; Tinsley, J.C.; Hays, W.W.; and King, K.W. 1979. "Evaluations of the Relation Between Near-Surface Geological Units and Ground Response in the Vicinity of Long Beach, California." *Bulletin of the Seismological Society of America,* 69, (5), 1603-1622. [El Cerrito, California]: Seismological Society of America. TIC: 254677.

165592 Rollins, K.M.; Mchood, M.D.; Hryciw, R.D.; Homolka, M.; and Shewbridge, S.E. 1994. "Ground Response on Treasure Island." *The Loma Prieta, California, Earthquake of October 17, 1989 - Strong Ground Motion.* Borcherdt, R.D. ed. U.S. Geological Survey Professional Paper 1551-A, A109-A121. Washington, D.C.: U.S. Government Printing Office. TIC: 255057.

104531 Sadigh, K.; Chang, C.-Y.; Egan, J.A.; Makdisi, F.; and Youngs, R.R. 1997. "Attenuation Relationships for Shallow Crustal Earthquakes Based on California Strong Motion Data." *Seismological Research Letters,* 68, (1), 180-189. El Cerrito, California: Seismological Society of America. TIC: 240552.

163654 Satoh, T.; Sato, T.; and Kawase, H. 1995. "Nonlinear Behavior of Soil Sediments Identified by Using Borehole Records Observed at Ashigar Valley, Japan." *Bulletin of the Seismological Society of America, 85, (6),* 1821-1834. [El Cerrito, California]: Seismological Society of America. TIC: 254676.

103323 Schnabel, P.B.; Lysmer, J.; and Seed; H.B. 1972. *SHAKE: A Computer Program for Earthquake Response.* EERC 72-12. Berkeley, California: Earthquake Engineering Research Center, University of California at Berkeley. TIC: 241102.

103270 Schneider, J.F.; Abrahamson, N.A.; and Hanks, T.C. 1996. *Ground Motion Modeling of Scenario Earthquakes at Yucca Mountain, Final Report for Activity 8.3.1.17.3.3.* Volume 1. Denver, Colorado: U.S. Geological Survey. ACC: MOL.19980617.0477.

110467 Schneider, J.F.; Silva, W.J.; and Stark, C.L. 1993. "Ground Motion Model for the 1989 M 6.9 Loma Prieta Earthquake Including Effects of Source, Path and Site." *Earthquake Spectra*, 9, (2), 251-287. Oakland, California: Earthquake Engineering Research Institute. TIC: 241769.

163655 Seed, H.B. and Idriss, I.M. 1969. "The Influence of Soil Conditions on Ground Motions During Earthquakes." *Journal of the Soil Mechanics Foundation Engineering Division,* 95, (SM1), 99-137. [New York, New York]: American Society of Civil Engineers. TIC: 254823.

103324 Seed, H.B. and Idriss, I.M. 1970. *Soil Moduli and Damping Factors for Dynamic Response Analyses.* EERC-70-10. Berkeley, California: Earthquake Engineering Research Center, University of California at Berkeley. TIC: 241070.

163924 Seed, H.B.; Romo, M.P.; Sun, J.I.; Jaime, A.; and Lysmer, J. 1988. "The Mexico Earthquake of September 19, 1985—Relationships Between Soil Conditions and Earthquake Ground Motions." *Earthquake Spectra*, *4*, (4), 687-729. [Oakland, California: Earthquake Engineering Research Institute]. TIC: 254675.

157263 Seed, H.B.; Wong, R.T.; Idriss, I.M.; and Tokimatsu, K. 1986. "Moduli and Damping Factors for Dynamic Analyses of Cohesionless Soils." *Journal of the Geotechnical Engineering*, 112, (11), 1016-1033. New York, New York: American Society of Civil Engineers. TIC: 243355.

103326 Silva, W.J. 1976. "Body Waves in a Layered Anelastic Solid." *Bulletin of the Seismological Society of America*, 66, (5), 1539-1554. El Cerrito, California: Seismological Society of America. TIC: 241277.

163747 Silva, W.J. 1997. "Characteristics of Vertical Strong Ground Motions for Applications to Engineering Design." *Proceedings of the FHWA/NCEER Workshop on the National Representation of Seismic Ground Motion for New and Existing Highway Facilities*, *held at the Park Plaza Hotel, Burlingame, California, May 29-30, 1997.* I.M. Friedland, M.S. Power, and R.L. Mayes, eds. Technical Report NCEER-97-0010, 205-219. Buffalo, New York: National Center for Earthquake Engineering Research. TIC: 254525.

164688 Silva, W. 2003. "'Validation of One-Dimensional Site Response Methodologies' by W. Silva, C. Stark, R. Pyke, I.M. Idriss, and J.R. Humphrey." E-mail from W. Silva (Pacific Engineering) to R. Quittmeyer, October 6, 2003, with attachment. ACC: MOL.20031009.0094.

110474 Silva, W.J.; Abrahamson, N.; Toro, G.; and Costantino, C. 1996. *Description and Validation of the Stochastic Ground Motion Model*. PE&A 94PJ20. El Cerrito, California: Pacific Engineering and Analysis. TIC: 245288.

164081 Silva, W.J.; Costantino, C.; and Iwasaki, Y. 1999. *Assessment of Liquefaction Potential for the 1995 Kobe, Japan Earthquake Including Finite-Source Effects*. Final Report. [Vicksburg, Mississippi]: U.S. Army Corp of Engineers Waterways Experiment Station, Corp of Engineers. ACC: MOL.20030925.0173.

105398 Silva, W.J. and Darragh, R. 1995. *Engineering Characterization of Earthquake Strong Ground Motion Recorded at Rock Sites.* EPRI TR-102262. Palo Alto, California: Electric Power Research Institute. TIC: 245610.

163187 Silva, W.J.; Darragh, R.B.; Green, R.K.; and Turcotte, F.T. 1989. *Estimated Ground Motions for a New Madrid Event.* Miscellaneous Paper GL-89-17. Washington, D.C.: U.S. Army Corps of Engineers. TIC: 254673.

163660 Silva, W.J.; Stark, C.L.; Chiou, S.J.; Green, R.; Stepp, J.C.; Schneider, J.; and Anderson, D. 1990. "Nonlinear Soil Models Based Upon Observations of Strong Ground Motions." *Seismological Research Letters,* 61, (1), 13. Abstract 11B-4. [El Cerrito, California]: Seismological Society of America, Eastern Section. TIC: 254667.

101020 Smith, R.P.; Jackson, S.M.; and Hackett, W.R. 1996. "Paleoseismology and Seismic Hazards Evaluations in Extensional Volcanic Terrains." *Journal of Geophysical Research, 101,* (B3), 6277-6292. Washington, D.C.: American Geophysical Union. TIC: 238265

170607 Smith, R. B., and Bruhn, R. L. 1984. "Intraplate extensional tectonics of the eastern Basin-Range; inferences on structural style from seismic reflection data, regional tectonics, and thermal-mechanical models of brittle-ductile deformation." *Journal of Geophysical Research, 89,* (7), pp 5733-5762. [Washington, D.C.]: American Geophysical Union. TIC: 223264

158656 Stepp, J.C.; Wong, I.; Whitney, J.; Quittmeyer, R.; Abrahamson, N.; Toro, G.; Youngs, R.; Coppersmith, K.; Savy, J.; and Sullivan, T. 2001. "Probabilistic Seismic Hazard Analyses for Ground Motions and Fault Displacement at Yucca Mountain, Nevada." *Earthquake Spectra, 17,* (1), 113-151. [Oakland, California: Earthquake Engineering Research Institute]. TIC: 250931.

107635 Stokoe, K.; Darendeli, M.B.; and Moulin, B.S. 1998. *Laboratory Evaluation of the Dynamic Properties of Intact Tuff Specimens from the Yucca Mountain Site*. Geotechnical Engineering Report GR98-1. Austin, Texas: University of Texas at Austin. ACC: MOL.19990827.0153.

170521 Stokoe, K.H.; Rosenblad, B.L.; Wong, I.G.; Bay, J.A.; Thomas, P.A.; and Silva, W.J. 2004. "Deep V_S Profiling Along the Top of Yucca Mountain Using a Vibroseis Source and Surface Waves." *13th World Conference on Earthquake Engineering,*

Vancouver, B.C., Canada, August 1-6, 2004. Paper No. 538, Ottawa, Ontario, Canada: Canadian Society of Earthquake Engineering. TIC: 256632.

164689 Stokoe, K.H., II and Valle, C. 2003. *Dynamic Laboratory Tests: Naturally Cemented Sand from Capitol Aggregates Site, Austin, Texas.* Summary Report: GR-03-5. Austin, Texas: University of Texas at Austin, College of Engineering. TIC: 254998.

157265 Stokoe, K.H., II; Wright, S.G.; Bay, J.A.; and Roesset, J.M. 1994. "Characterization of Geotechnical Sites by SASW Method." *Volume Prepared by ISSMFE Technical Committee # 10 for XIII ICSMFE, 1994, New Delhi, India.* Woods, R.D., ed. New York, New York: International Science Publisher. TIC: 251421.

163661 Streeter, V.L.; Wylie, E.B.; and Richart, F.E. Jr. 1974. " Soil Motion Computations by Characteristics Method." *Journal of the Geotechnical Engineering Division,* 100, (GT3), 247-263. New York, New York: America Society of Civil Engineers. TIC: 254814.

163182 Su, F.; Aki, K.; Teng, T.; Zeng, Y.; Koyanagi, S.; and Mayeda, K. 1992. "The Relation Between Site Amplification Factor and Surficial Geology in Central California." *Bulletin of the Seismological Society of America,* 82, (2), 580-602. [El Cerrito, California]: Seismological Society of America. TIC: 254672.

100087 Su, F.; Anderson, J.G.; Brune, J.N.; and Zeng, Y. 1996. "A Comparison of Direct S-Wave and Coda-Wave Site Amplification Determined from Aftershocks of the Little Skull Mountain Earthquake." *Bulletin of the Seismological Society of America*, 86, (4), 1006-1018. El Cerrito, California: Seismological Society of America. TIC: 236585.

163663 Taylor, P.W. and Larkin, T.J. 1978. "Seismic Site Response of Nonlinear Soil Media." *Journal of the Geotechnical Engineering Division,* 104, (GT3), 369-383. New York, New York: American Society of Civil Engineers. TIC: 254813.

163720 Toro, G.R. 2003. PSHA Calculations for Annual Exceedance Probabilities as Low as 1E-9. Scientific Notebook SN-M&O-SCI-038-V1. ACC: MOL.20030723.0324; MOL.20030723.0325; MOL.20030723.0326; MOL.20030723.0327.

172034 Toro, G.R. 2004. PSHA Calculations for Annual Exceedance Probabilities as Low as 1E-9 [partial submittal]. Scientific Notebook SN-M&O-SCI-038-V2. Pages 1-90. ACC: MOL.20040816.0180; MOL.20041025.0043; MOL.20040816.0181; MOL.20040816.0182; MOL.20040816.0183; MOL.20040816.0184; MOL.20040816.0185; MOL.20040816.0186; MOL.20040816.0187; MOL.20040816.0188; MOL.20040816.0189; MOL.20040816.0190; MOL.20040816.0191; MOL.20040816.0192; MOL.20040816.0193; MOL.20040816.0194; MOL.20040816.0195; MOL.20040816.0196; MOL.20040816.0197; MOL.20040816.0198;

MOL.20040816.0199; MOL.20040816.0200; MOL.20040816.0201; MOL.20040816.0202; MOL.20040816.0203; MOL.20040816.0204; MOL.20040816.0205; MOL.20040816.0206; MOL.20040816.0207; MOL.20040816.0208; MOL.20040816.0209; MOL.20040816.0210; MOL.20040816.0211; MOL.20040816.0212; MOL.20040816.0213; MOL.20040816.0214; MOL.20040816.0215; MOL.20040816.0216; MOL.20040816.0217; MOL.20040816.0218; MOL.20040816.0219; MOL.20040816.0220; MOL.20040816.0221; MOL.20040816.0222; MOL.20040816.0223; MOL.20040816.0224; MOL.20040816.0225; MOL.20040816.0226; MOL.20040816.0227; MOL.20040816.0228; MOL.20040816.0229; MOL.20040816.0230; MOL.20040816.0231; MOL.20040816.0232; MOL.20040816.0233; MOL.20040816.0234; MOL.20040816.0235; MOL.20040816.0236; MOL.20040816.0237; MOL.20040816.0238; MOL.20041025.0044; MOL.20041025.0045; MOL.20041025.0046; MOL.20041025.0047; MOL.20041025.0048; MOL.20041025.0049; MOL.20041025.0050; MOL.20041025.0051; MOL.20041025.0052; MOL.20041025.0053; MOL.20041025.0054; MOL.20041025.0055; MOL.20041025.0056.

163181 Tucker, B.E. and King, J.L. 1984. "Dependence of Sediment-Filled Valley Response on the Input Amplitude and the Valley Properties." *Bulletin of the Seismological Society of America,* 74, (1), 153-165. [El Cerrito, California]: Seismological Society of America. TIC: 254682.

163890 Van Hoff, D.J. 1993. *Evaluation of the Dynamic Properties of Artificially Cemented Sand at Low Confining Pressures.* Master's thesis. Austin, Texas: University of Texas at Austin. TIC: 254684.

170522 von Seggern, D. 2004. *Borehole Accelerometer Array Observations Near the North Portal of the ESF*. TR-04-001. Las Vegas, Nevada: University and Community College. System of Nevada. ACC: MOL.20040819.0022.

164084 Wald, D.J. and Heaton, T.H. 1994a. *A Dislocation Model of the 1994 Northridge, California, Earthquake Determined from Strong Ground Motions*. Open-File Report 94-278. Pasadena, California: U.S. Geological Survey. TIC: 254820.

164085 Wald, D.J. and Heaton, T.H. 1994b. "Spatial and Temporal Distribution of Slip for the 1992 Landers, California, Earthquake." *Bulletin of the Seismological Society of America,* 84, (3), 668-691. [El Cerrito, California: Seismological Society of America]. TIC: 254815.

164086 Wald, D.J.; Helmberger, D.V.; and Heaton, T.H. 1991. "Rupture Model of the 1989 Loma Prieta Earthquake for the Inversion of Strong-Motion and Broadband and Teleseismic Data." *Bulletin of the Seismological Society of America,* 81, (5), 1540-1572. [El Cerrito, California: Seismological Society of America]. TIC: 254817.

107201 Wells, D.L. and Coppersmith, K.J. 1994. "New Empirical Relationships Among Magnitude, Rupture Length, Rupture Width, Rupture Area, and Surface Displacement." *Bulletin of the Seismological Society of America, 84,* (4), 974-1002. El Cerrito, California: Seismological Society of America. TIC: 226273

163926 Wesnousky, S.G. 1986. "Earthquakes, Quaternary Faults, and Seismic Hazard in California." *Journal of Geophysical Research*, 91, (B12), 12,587-12,631. [Washington, D.C.]: American Geophysical Union. TIC: 241686.

163671 Wiggins, J.H., Jr. 1964. "Effect of Site Conditions on Earthquake Intensity." *Journal of the Structural Division,* 90, (ST2), 279-313. [New York, New York]: American Society of Civil Engineers. TIC: 254666.

105550 Wong, I.; Kelson, K.; Olig, S.; Kolbe, T.; Hemphill-Haley, M.; Bott, J.; Green, R.; Kanakari, H.; Sawyer, J.; Silva, W.; Stark, C.; Haraden, C.; Fenton, C.; Unruh, J.; Gardner, J.; Reneau, S.; and House, L. 1995. *Seismic Hazards Evaluation of the Los Alamos National Laboratory*. Volume 1. Oakland, California: Woodward-Clyde Federal Services. TIC: 247191.

163201 Wong, I. and Silva, W., 2003. Development of Seismic Design Ground Motion Inputs. Scientific Notebook SN-M&O-SCI-037-V1. ACC: MOL.20030324.0235.

170443 Wong, I. and Silva, W., 2004a. Development of Seismic Design Ground Motion Inputs. Scientific Notebook SN-M&O-SCI-037-V2. Pages 1-60 Pages 61-143. ACC: MOL.20040914.0069.

170444 Wong, I. and Silva, W., 2004b. Development of Seismic Design Ground Motion Inputs. Scientific Notebook SN-M&O-SCI-037-V3. Pages 1-77 Pages 72-125. ACC: MOL.20031027.0158; MOL.20040918.0004.

170446 Wong, I. and Silva, W., 2004c. Ground Motion Site Response Model Confirmation Studies. Scientific Notebook SN-M&O-SCI-046-V1. ACC: MOL.20040914.0168.

172075 Wong, I. and Silva, W., 2004d. Development of Seismic Design Ground Motion Inputs [partial submittal]. Scientific Notebook SN-M&O-SCI-037-V4. Pages 1-62. ACC: MOL.20040918.0002; MOL.20041029.0033.

163848 Wong, I.G. and Toro, G.R. 2003. Statistical Analysis of Velocity Profiles at the Repository Block and at the Potential Site of the Waste Handling Building. Scientific Notebook SN-M&O-SCI-036-V1. ACC: MOL.20030723.0322; MOL.20030723.0323.

170544 Wong. I.; Olig, S.; Dober, M.; Silva, W.; Wright, D.; Thomas, P.; Gregor, N.; Sanford, A.; Lin, K.; and Love, D. 2004. "Earthquake Scenario and Probabilistic Ground-Shaking Hazard Maps for the Albuquerque-Belen-Santa Fe, New Mexico, corridor." *New Mexico Geology,* 26, (1), 3-33. Albuquerque, New Mexico: New Mexico Bureau Geology and Mineral Resources. TIC: 256271.

163672 Wood, H.O. 1908. "Distribution of Apparent Intensity in San Francisco." Volume I of *The California Earthquake of April 18, 1906, Report of the State Earthquake Investigation Commission,* 220-245. Washington, DC: Carnegie Institute of Washington. TIC: 254840.

163519 Younker, J. 2003. "Independent Technical Review of the RVT-Based Equivalent Linear Site Response Model by R. Dobry, W. Foxall, and L. Hutchings." E-mail from J. Younker to R. Quittmeyer, August 29, 2003, with attachment. ACC: MOL.20031014.0163; MOL.20030602.0392.

100521 YMP (Yucca Mountain Site Characterization Project). 1997a. *Preclosure Seismic Design Methodology for a Geologic Repository at Yucca Mountain*. Topical Report YMP/TR-003-NP, Rev. 2. Las Vegas, Nevada: Yucca Mountain Site Characterization Office. ACC: MOL.19971009.0412.

100522 YMP (Yucca Mountain Site Characterization Project). 1997b. *Methodology to Assess Fault Displacement and Vibratory Ground Motion Hazards at Yucca Mountain*. Topical Report YMP/TR-002-NP, Rev. 1. Las Vegas, Nevada: Yucca Mountain Site Characterization Office. ACC: MOL.19971016.0777.

154817 YMP (Yucca Mountain Site Characterization Project) 2001. *Q-List.* YMP/90-55Q, Rev. 7. Las Vegas, Nevada: Yucca Mountain Site Characterization Office. ACC: MOL.20010409.0366.

9.2 STATUTES AND REGULATIONS

126059 10 CFR 60. 1999. *Energy: Disposal of High-Level Radioactive Wastes in Geologic Repositories*. Readily available.

156605 10 CFR 63. *Energy: Disposal of High-Level Radioactive Wastes in a Geologic Repository at Yucca Mountain, Nevada*. Readily available.

9.3 DATA

158242 GS020483114233.004. Geotechnical Field and Laboratory Test Results from Waste Handling Building Foundation Investigation. Submittal date: 04/15/2002.

159542 GS020783114233.005. Gradation Analysis Test Results and Graphical Plots from Tests Performed on Materials Excavated from In-Situ Density Test Locations in Test Pits from the Waste Handling Building Foundation Investigations. Submittal date: 07/23/2002.

164561 GS030783114233.001. Geotechnical Borehole Logs for the Waste Handling Building, Yucca Mountain Project, Nevada Test Site, Nevada, Version 7/16/03. Submittal date: 07/23/2003.

152631 GS990908314224.010. Geology of the ECRB Cross Drift: Graphical Data. Submittal date: 09/14/1999.

170768 LA0407DK831811.001. Physical Parameters of Basaltic Magma and Eruption Phenomena. Submittal date: 07/15/2004

164559 LB0306VSP95DAT.001. Processed VSP and Velocity Survey Data: UZ#16, NRG-6, WT-2, RF-4, RF-7A,SD-12, G-2, G-4. Submittal date: 06/25/2003.

149092 MO0004MWDRIFM3.002. Results of the Yucca Mountain Probabilistic Seismic Hazard Analysis (PSHA). Submittal date: 04/14/2000.

153777 MO0012MWDGFM02.002. Geologic Framework Model (FGM2000). Submittal date: 12/18/2000.

157295 MO0110DVDBOREH.000. Downhole Velocity Data from Boreholes RF-13 and RF-17. Submittal date: 10/17/2001.

158076 MO0110SASWVDYM.000. SASW Velocity Data from the Top of Yucca Mountain. Submittal date: 10/02/2001.

157969 MO0110SASWWHBS.000. SASW Velocity Data from the Waste Handling Building Site Characterization Area. Submittal date: 10/02/2001.

157296 MO0111DVDWHBSC.001. Downhole Velocity Data at the Waste Handling Building Site Characterization Area. Submittal date: 11/08/2001.

158078 MO0202DVDWHBSC.002. Downhole Velocity Data from the Top of Yucca Mountain. Submittal date: 02/11/2002.

158082 MO0203DHRSSWHB.001. Dynamic Laboratory Test Data for Rock and Soil Samples from the Waste Handling Building Site Characterization Area. Submittal date: 03/19/2002.

158084 MO0203SEPSASWD.000. SASW Velocity Data from the Top of Yucca Mountain. Submittal date: 03/28/2002.

159744 MO0204RIB00130.000. Rock Bulk Density (Dry). Submittal date: 04/03/2002.

158086 MO0204SEISDWHB.001. Suspension Seismic Data for Borehole UE-25 RF#13 at the Waste Handling Building Site Characterization Area. Submittal date: 04/08/2002.

158088 MO0204SEPBSWHB.001. Borehole Suspension Data for Waste Handling Building Site Characterization Area. Submittal date: 04/10/2002.

158125 MO0204SEPGAMDM.000. Statistical Analysis of Gamma-Gamma Density Measurements by Lithostratigraphic Unit. Submittal date: 04/22/2002.

159081 MO0206SASWROCK.000. SASW Velocity Data from Rock Sites on the Crest of Yucca Mountain and in the ESF. Submittal date: 06/19/2002.

163777 MO0206SASWVSP1.001. Velocity Profiles for the Repository Block. Submittal date: 06/03/2002.

163723 MO0206UNHAZ106.001. Uniform Hazard, Reference Event and Deaggregation Event Spectra at 10^{-6} Annual Exceedance Frequency Based on the Probabilistic Seismic Hazard Analyses for Yucca Mountain. Submittal date: 06/03/2002.

164203 MO0208PGVDEAG6.001. PGV Deaggregation at 10^{-6} Annual Exceedance Frequency. Submittal date: 08/19/2002.

163722 MO0208UNHZ5X10.000. Uniform Hazard, Reference Event and Deaggregation Event Spectra at $5x10^{-4}$ Annual Exceedance Frequency Based on the Results of the Probabilistic Seismic Hazard Analyses for Yucca Mountain. Submittal date: 08/06/2002.

163801 MO0208VCPRBWHB.000. Velocity Correlation Parameters for the Yucca Mountain Repository Block and Waste Handling Building Site. Submittal date: 08/20/2002.

163724 MO0209UNHAZ107.000. Uniform Hazard, Reference Event and Deaggregation Event Spectra at 10^{-7} Annual Exceedance Frequency Based on the Results of the Probabilistic Seismic Hazard Analyses for Yucca Mountain. Submittal date: 09/25/2002.

163798 MO0209VELPRWHB.000. Velocity Profiles for the Waste Handling Building Site Characterization Area. Submittal date: 09/23/2002.

164205 MO0210PGVD1E07.000. PGV Deaggregation at 10^{-7} Annual Exceedance Frequency. Submittal date: 10/10/2002.

162713 MO0210PGVPB107.000. Design Peak Ground Velocity for the Repository Level (Point B) at 10^{-7} Annual Exceedance Probability. Submittal date: 10/17/2002.

170423 MO0211DERES104.000. Reference Event and Deaggregation Event Spectra at 10^{-4} Annual Exceedance Frequency Based on the Results of the Probabilistic Seismic Hazard Analyses for Yucca Mountain. Submittal date: 11/04/2002.

170424 MO0211REDES103.000. Reference Event and Deaggregation Event Spectra at 10^{-3} Annual Exceedance Frequency Based on the Results of the Probabilistic Seismic Hazard Analyses for Yucca Mountain. Submittal date: 11/04/2002.

165935 MO0301DPGVB106.001. Design Peak Ground Velocity For The Repository Level (Point B) At 10^{-6} Annual Exceedance Probability. Submittal date: 01/22/2003.

161868 MO0301TMHIS106.001. Acceleration, Velocity, and Displacement Time Histories for the Repository Level at 10^{-6} Annual Exceedance Frequency. Submittal date: 01/28/2003.

164207 MO0301TMHSB107.000. Time Histories Spectrally Conditioned To Point B For The Repository Level At 10^{-7} Annual Exceedance Frequency. Submittal date: 01/20/2003.

162712 MO0303DPGVB106.002. Design Peak Ground Velocity for the Repository Level (Point B) at 10^{-6} Annual Exceedance Probability. Submittal date: 03/10/2003.

163721 MO03061E9PSHA1.000. Spectral Acceleration and Velocity Hazard Curves Extended to 1E-9 Based on the Results of the PSHA for Yucca Mountain. Submittal date: 06/09/2003.

164033 MO0306SDSAVDTH.000. Seismic Design Spectra and Acceleration, Velocity, and Displacement Time Histories for the Emplacement Level at 10^{-4} Annual Exceedance Frequency. Submittal date: 06/26/2003.

170425 MO0308UNHAZ105.000. Uniform Hazard, Reference Event and Deaggregation Event Spectra at 10^{-5} Annual Exceedance Frequency Based on the Results of the Probabilistic Seismic Hazard Analyses for Yucca Mountain. Submittal date: 08/06/2003.

170426 MO0309PGVDEAGG.000. PGV Deaggregation at 10^{-5} Annual Exceedance Frequency. Submittal date: 09/09/2003.

170427 MO0312SEPRSRLB.019. 5% Damped Response Spectra for the Emplacement Level (Point B) at 10^{-5} Annual Exceedance Frequency. Submittal date: 02/18/2003.

166962 MO0401MWDRPSHA.000. Results of the Yucca Mountain Probabilistic Seismic Hazard Analysis (PSHA). Submittal date: 01/21/2004.

169099 MO0401SEPPGVRL.022. Preliminary Seismic Design Peak Ground Velocity for the Repository Level (Point B) for 10-5 Annual Exceedance Probability. Submittal date: 01/26/2004.

168890 MO0402AVDTM105.001. Acceleration, Velocity, and Displacement Time Histories for the Repository Level at 10^{-5} Annual Exceedance Frequency. Submittal date: 02/09/2004.

168891 MO0403AVDSC106.001. Acceleration, Velocity, and Displacement Time Histories for the Repository Level at 10^{-6} Annual Exceedance Frequency. Submittal Date: 03/22/2004.

168892 MO0403AVTMH107.003. Acceleration, Velocity, and Displacement Time Histories for the Repository Level at 10-7 Annual Exceedance Frequency. Submittal date: 03/22/2004

169342 MO0403SCSPSFAD.001. Strain Compatible Soil Properties for the Surface Facilities Area (Point D) at 10^{-4} Annual Exceedance Frequency. Submittal date: 03/15/2004.

170434 MO0403SDIAWHBC.003. Normalized Shear Modulus and Material Damping Versus Shearing Strain Curves for Rock, Alluvium, and Engineered Fill for Seismic Input Analyses. Submittal date: 03/26/2004.

168376 MO0403SPWHB5E4.005. Strain Compatible Soil Properties for the Surface Facilities Area (Point D) at 5E-4 Annual Exceedance Frequency. Submittal date: 03/15/2004.

170436 MO0404PGVAPSHA.000. Peak Ground Velocity (PGV) for Point A From the PSHA at 10^{-4} Annual Exceedance Frequency. Submittal date: 04/14/2004.

170437 MO0404PGVRL104.000. Peak Ground Velocity for the Repository Level (Point B) at 10^{-4} Annual Exceedance Frequency. Submittal date: 04/23/2004.

169344 MO0404SPCDAMPD.001. Strain Compatible Soil Properties for the Surface Facilities Area (Point D) at 10^{-3} Annual Exceedance Frequency. Submittal date: 04/19/2004.

169851 MO0405SDSTPNTB.001. Seismic Design Spectra (5% Damped) and Time Histories for the Emplacement Level (Point B) at 10^{-3} Annual Exceedance Frequency. Submittal date: 05/03/2004.

170506 MO04065DSRSPTB.000. 5% Damped Response Spectra for the Emplacement Level (Point B) at 10^{-6} Annual Exceedance Frequency. Submittal date: 06/29/2004. Imaging in process.

170683 MO0407SDARS104.001. Seismic Design Spectra (5% Damped) for the Emplacement Level (Point B) at $5x10^{-4}$ Annual Exceedance Frequency. Submittal date: 07/14/2004.

170760 MO0407SEPFEPLA.000. LA FEP List. Submittal date: 07/20/2004.

170599 MO0407TMHIS104.003. Acceleration, Velocity, and Displacement Time Histories for the Emplacement Level (Point B) at $5X10^{-4}$ Annual Exceedance Frequency. Submittal date: 07/15/2004.

171434 MO0408PGAPGVSC.001. Peak Ground Acceleration, Peak Ground Velocity, Strains and Curvatures as a Function of Depth for Yucca Mountain Corresponding to 1E-3, 5E-4, and 1E-4 Annual Exceedance Frequency. Submittal date: 08/18/2004

172236 MO0410SDSDE103.002. Seismic Design Spectra and Time Histories for the Surface Facilities Area (Point D/E) at 10^{-3} Annual Exceedance Frequency. Submittal date: 11/02/2004.

172218 MO0410SDSEHFSF.002. Response Spectra for the Surface Facilities Area North of Exile Hill Fault Splay (Point F) at 5E-4 Annual Exceedance Frequency. Submittal date: 10/08/2004.

172237 MO0410SDSTMHIS.005. Seismic Design Spectra and Acceleration, Velocity, and Displacement Time Histories for the Waste Handling Building Site Characterization Area (Points D and E Less than 20 Ft of Soil) for $5x10^{-4}$ Annual Exceedance Frequency. Submittal date: 02/09/2004.

172238 MO0410WHBDF104.002. Seismic Design Spectra and Time Histories for the Surface Facilities Area (Point D/E) at 10^{-4} Annual Exceedance Frequency. Submittal date: 11/02/2004.

103792 MO9905LABDYNRS.000. Laboratory Dynamic Rock/Soil Testing UE-25 RF #13. Submittal date: 05/06/1999.

150042 SNL01A05059301.002. Thermal Conductivity Data from USW NRG-6 Drillhole Samples from Depth of 28.8 ft. to 987.0 ft. Submittal date: 07/15/1994.

109002 SNL01A05059301.005. Laboratory Thermal Conductivity Data for Boreholes UE25 NRG-4, NRG-5; USW NRG-6 and NRG-7/7A. Submittal date: 02/07/1996.

108415 SNL02030193001.004. Mechanical Properties Data for Drillhole USW NRG-6 Samples from Depth 462.3 ft. to 1085.0 ft. Submittal date: 08/05/1993.

108416 SNL02030193001.012. Mechanical Properties Data for Drillhole UE25 NRG-5 Samples from Depth 847.2 ft. to 896.5 ft. Submittal date: 12/02/1993.

108431 SNL02030193001.019. Mechanical Properties Data for Drillhole USW NRG-7/7A Samples from Depth 507.4 ft. to 881.0 ft. Submittal date: 06/29/1994.

108432 SNL02030193001.020. Mechanical Properties Data for Drillhole USW NRG-7/7A Samples from Depth 554.7 ft. to 1450.1 ft. Submittal date: 07/25/1994.

108433 SNL02030193001.021. Mechanical Properties Data (Ultrasonic Velocities, Static Elastic Properties, Triaxial Strength, Dry Bulk Density & Porosity) for Drillhole USW NRG-7/7A Samples from Depth 345.0 ft. to 1408.6 ft. Submittal date: 02/16/1995.

9.4 SOFTWARE

167994 Dynamic Graphics 2000. *Software Code: EARTHVISION*. Version 5.1. SGI/IRIX 6.5. 10174-5.1-00.

163293 Pacific Engineering and Analysis 2002a. *Software Code: BASE4.* Version 4.0. PC, DOS 6.22. 10940-4.0-00.

163295 Pacific Engineering and Analysis 2002b. *Software Code: CORBB.* Version 1.0. PC, DOS 6.22. 10941-1.0-00.

163304 Pacific Engineering and Analysis 2002c. *Software Code: INTEG1.* Version 1.0. PC, DOS 6.22. 10943-1.0-00.

163305 Pacific Engineering and Analysis 2002d. *Software Code: INTERPOL.* Version 1.0. PC, DOS 6.22. 10944-1.0-00.

163308 Pacific Engineering and Analysis 2002e. *Software Code: LOGNORM.* Version 1.0. PC, DOS 6.22. 10384-1.0-00.

163309 Pacific Engineering and Analysis 2002f. *Software Code: MAXMIN.* Version 1.0. PC, DOS 6.22. 10945-1.0-00.

163313 Pacific Engineering and Analysis 2002g. *Software Code: NORM.* Version 1.01. PC, DOS 6.22. 10386-1.01-00.

163314 Pacific Engineering and Analysis 2002h. *Software Code: PARINP.* Version 1.1. PC, DOS 6.22. 10387-1.1-00.

163315 Pacific Engineering and Analysis 2002i. *Software Code: RANPAR.* Version 2.0. PC, DOS 6.22. 10486-2.0-00.

163367 Pacific Engineering and Analysis 2002j. *Software Code: RASCALP.* Version 2.01. PC, DOS 6.22. 10388-2.01-00.

163316 Pacific Engineering and Analysis 2002k. *Software Code: RASCALP.* Version 2.02. PC, DOS 6.22. 10388-2.02-00.

163317 Pacific Engineering and Analysis 2002l. *Software Code: RASCALS.* Version 5.4. PC, DOS 6.22. 10389-5.4-00.

163319 Pacific Engineering and Analysis 2002m. *Software Code: SCALE1.* Version 1.0. PC, DOS 6.22. 10946-1.0-00.

163320 Pacific Engineering and Analysis 2002n. *Software Code: SMRATIO.* Version 1.0. PC, DOS 6.22. 10917-1.0-00.

163322 Pacific Engineering and Analysis 2002o. *Software Code: SPMEAN.* Version 1.0. PC, DOS 6.22. 10918-1.0-00.

163325 Pacific Engineering and Analysis 2002p. *Software Code: VELAVG.* Version 1.0. PC, DOS 6.22. 10390-1.0-00.

163326 Pacific Engineering and Analysis 2002q. *Software Code: XYMULT.* Version 1.0. PC, DOS 6.22. 10919-1.0-00.

163303 Pacific Engineering and Analysis 2003a. *Software Code: DUR.* Version 1.0. PC, DOS 6.22. 10942-1.0-00.

163318 Pacific Engineering and Analysis 2003b. *Software Code: REPLOT.* Version 1.0. PC, DOS 6.22. 10949-1.0-00.

163321 Pacific Engineering and Analysis 2003c. *Software Code: SPCTLR.* Version 1.0. PC, DOS 6.22. 10947-1.0-00.

170442 Pacific Engineering and Analysis 2003d. *Software Code: RANPAR.* Version 2.1. PC, DOS 6.22. 10486-2.1-00.

170313 Pacific Engineering and Analysis 2004. *Software Code: LOGNORM.* Version 1.01. PC, DOS 6.22. 10384-1.01-00.

163365 Risk Engineering, Inc. 2000a. *Software Code: FRISK88.* Version 2.0. HP-735, HP-UX 10.01. 10139-2.0-00.

163312 Risk Engineering, Inc. 2000d. *Software Code: MRE88*. Version 1.0. HP-735. HP-UX 10.01. 10140-1.0-00.

163361 Risk Engineering, Inc. 2000b. *Software Code: POST88.* Version 1.0. HP-735, HP-UX 10.01. 10136-1.0-00.

163362 Risk Engineering, Inc. 2000c. *Software Code: PREP88.* Version 1.0. HP-735, HP-UX 10.01. 10138-1.0-00.

163294 Risk Engineering, Inc. 2002a. *Software Code: CMB_FRAC.* Version 2.0. HP-735, HP-UX 10.01. 10464-2.0-00.

163302 Risk Engineering, Inc. 2002b. *Software Code: DESIGN_EVENTS.* Version 1.0. PC, DOS 6.22. 10362-1.0-00.

163307 Risk Engineering, Inc. 2002c. *Software Code: LAYERING.* Version 1.0. PC, Windows 98. 10648-1.0-00.

163310 Risk Engineering, Inc. 2002d. *Software Code: MEAN.* Version 1.1. HP-735, HP-UX 10.01. 10463-1.1-00.

163323 Risk Engineering, Inc. 2002e. *Software Code: VEL_SIMUL.* Version 1.0. PC, Windows 98. 10647-1.0-00.

163324 Risk Engineering, Inc. 2002f. *Software Code: VEL_STAT.* Version 1.0. PC, Windows 98. 10646-1.0-00.

APPENDIX I

DOCUMENTATION OF THE USE OF COMMERCIAL-OFF-THE-SHELF SOFTWARE PROGRAMS

Appendix I consists of a CD-Rom that contains documentation of the use of commercial-off-the-self software programs.

INTENTIONALLY LEFT BLANK

APPENDIX II

ACCELERATION, VELOCITY, AND DISPLACEMENT TIME HISTORIES

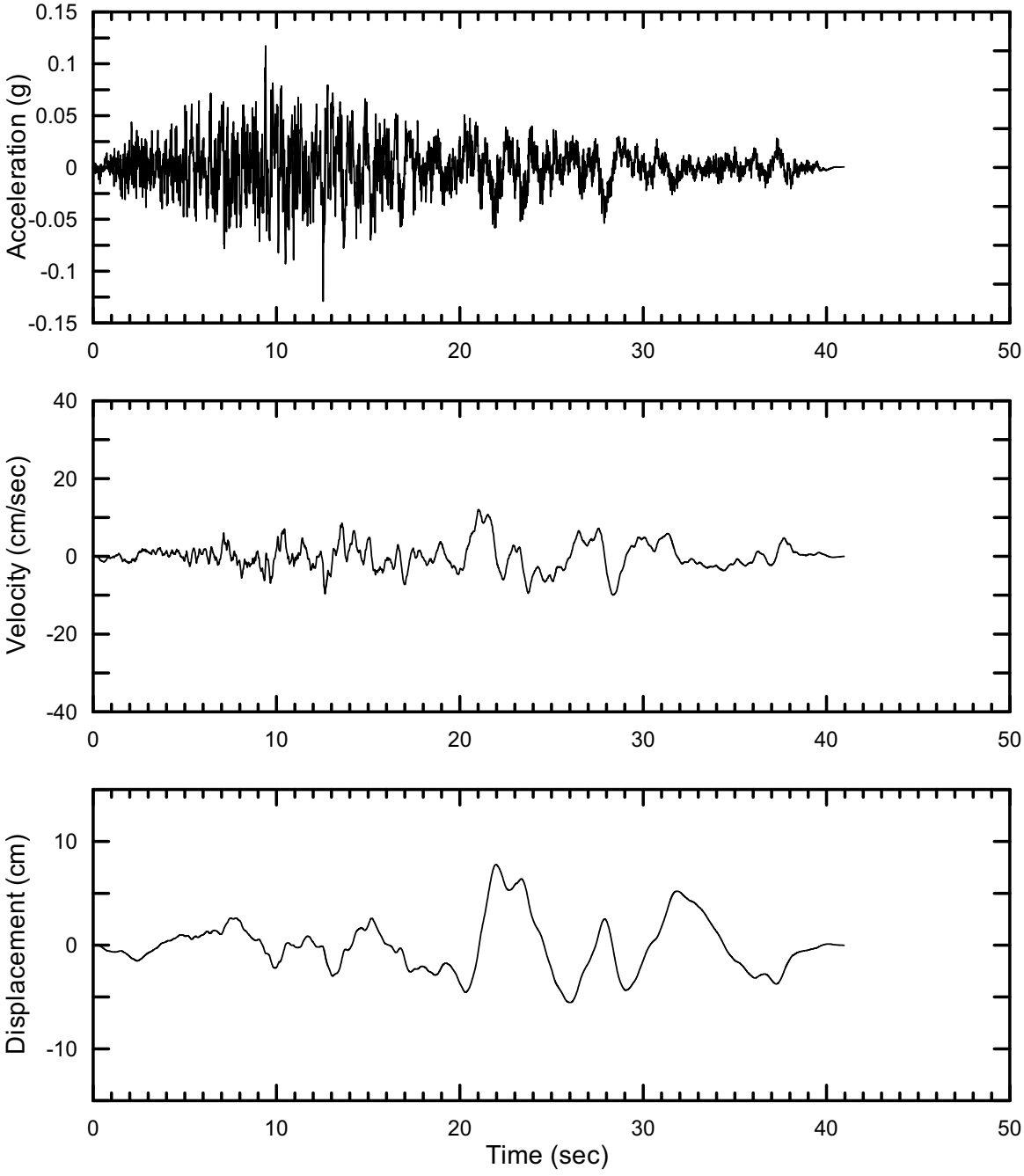

DTN: MO0405SDSTPNTB.001 [DIRS 169851]

Figure II-1. Point B Horizontal-1 Time Histories at an Annual Exceedance Probability of 10^{-3}

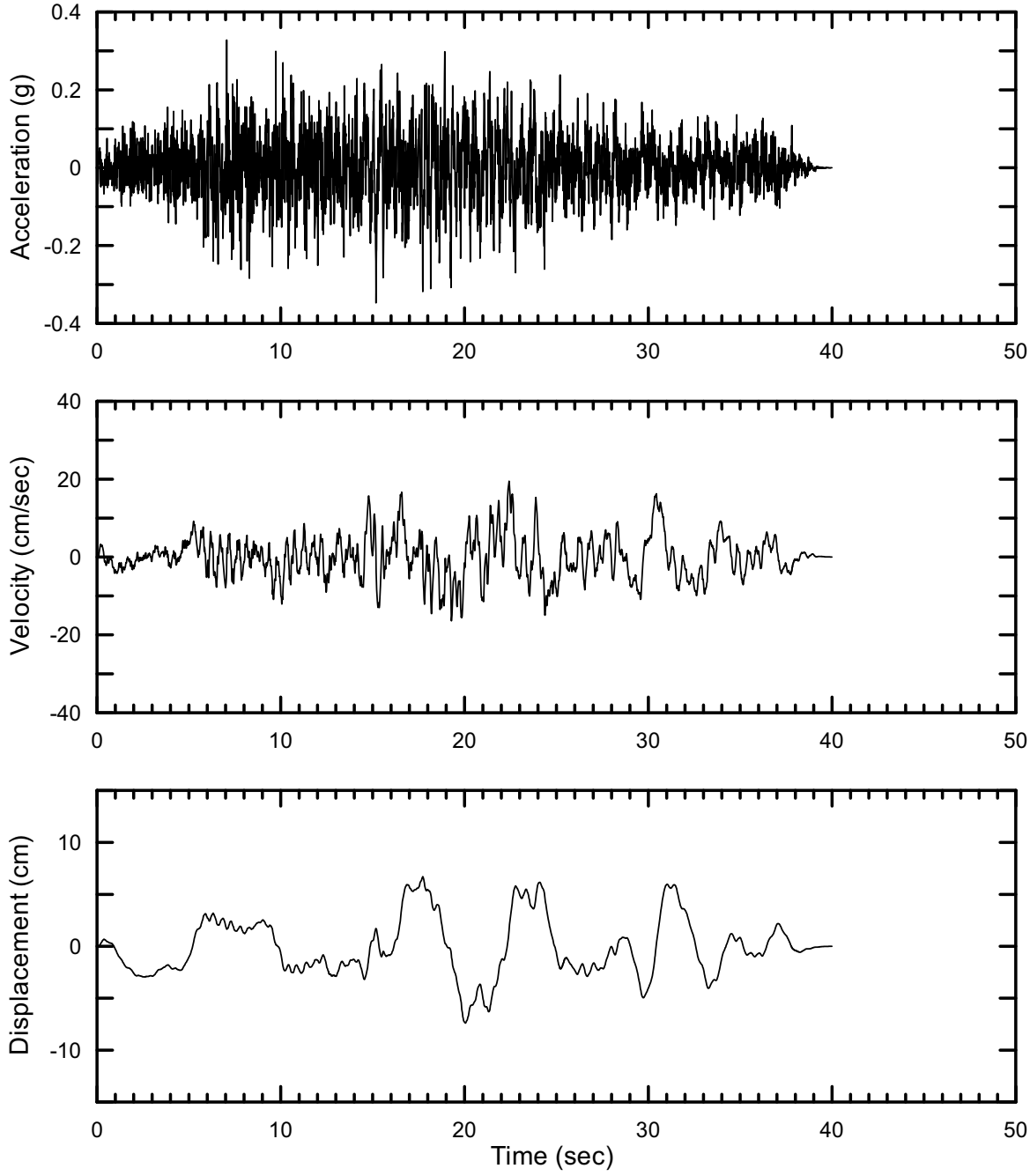

DTN: MO0405SDSTPNTB.001 [DIRS 169851]

Figure II-2. Point B Horizontal-2 Time Histories at an Annual Exceedance Probability of 10^{-3}

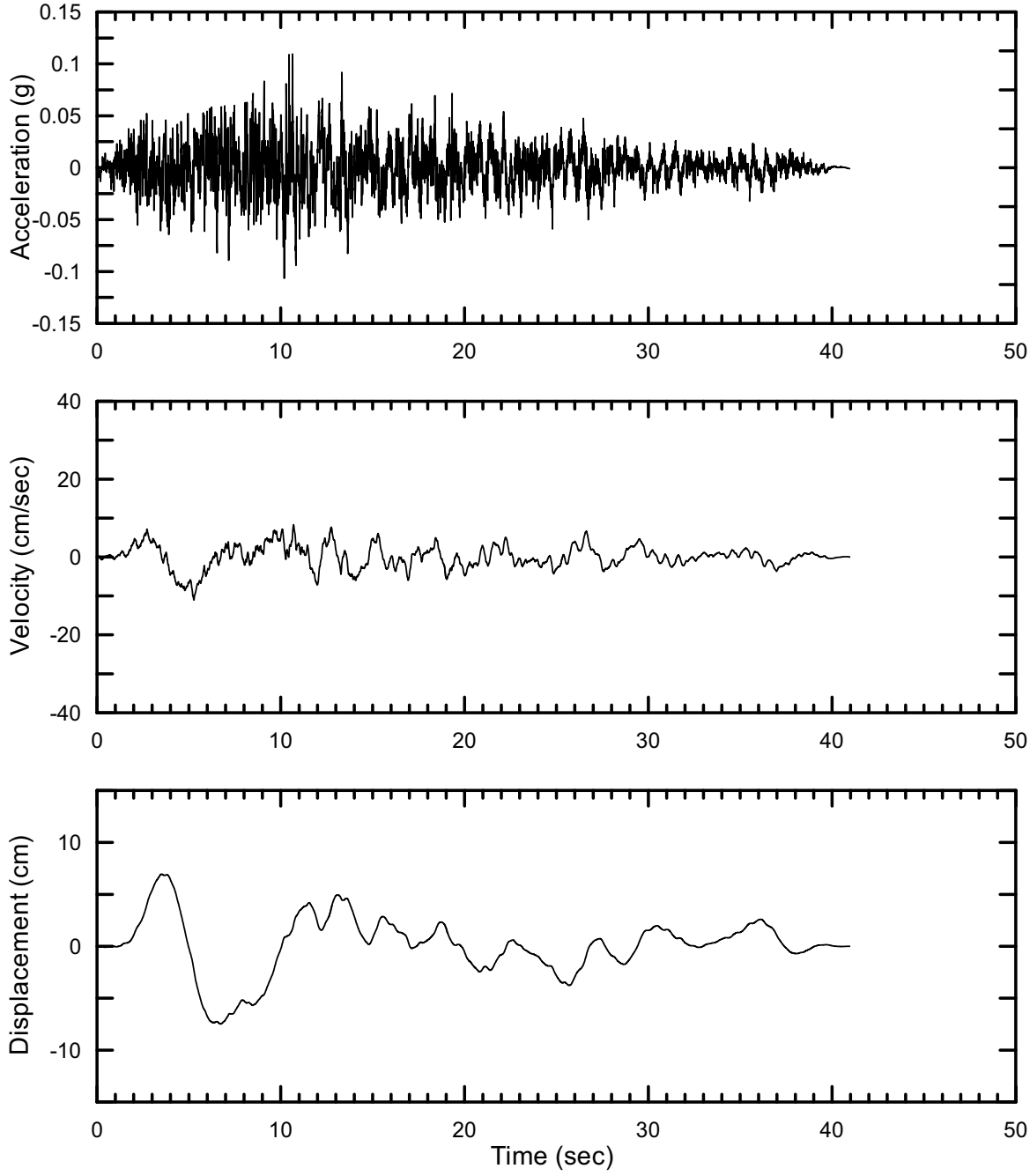

DTN: MO0405SDSTPNTB.001 [DIRS 169851]

Figure II-3. Point B Vertical Time Histories at an Annual Exceedance Probability of 10^{-3}

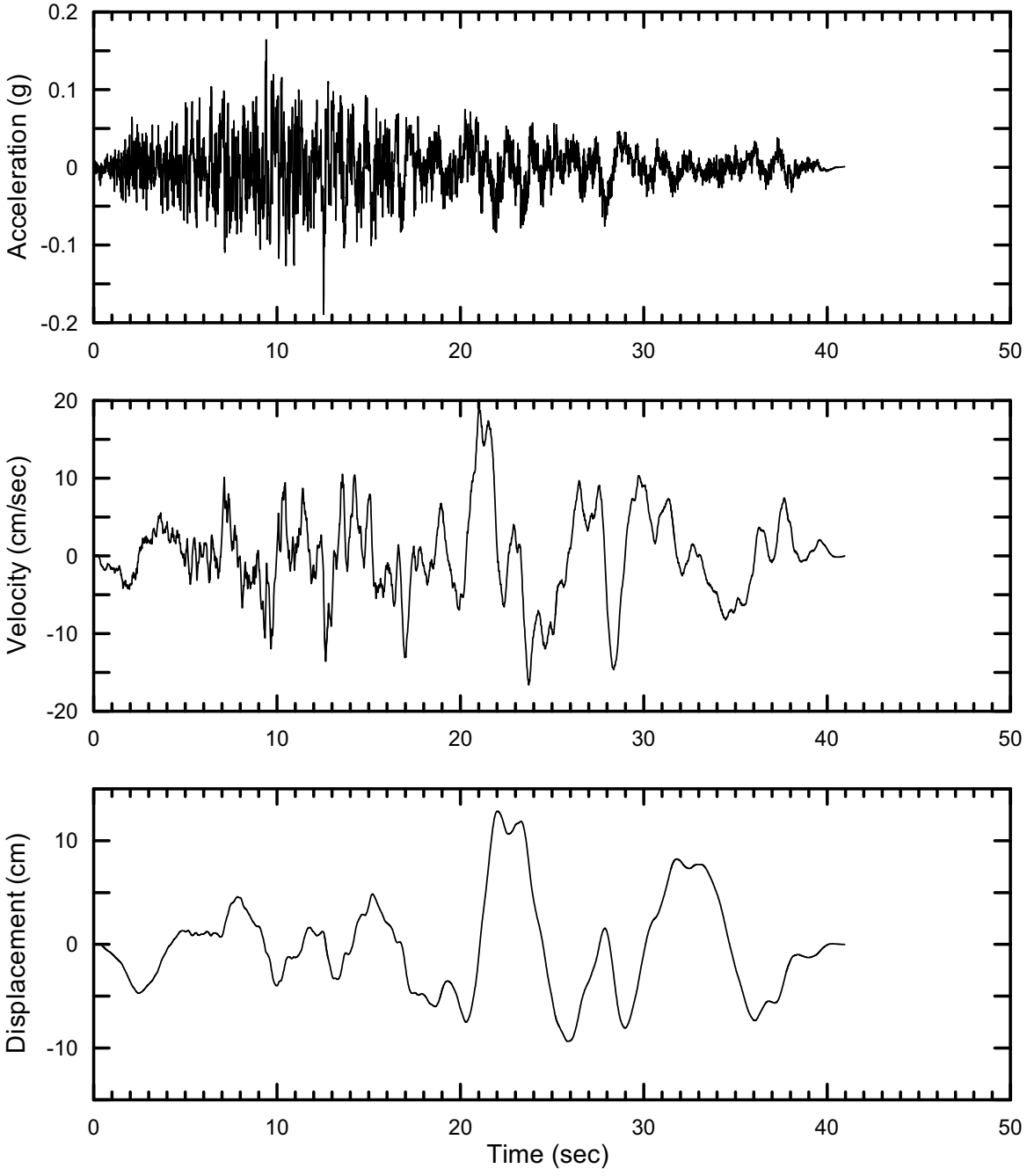

DTN: MO0407TMHIS104.003 [DIRS 170599]

Figure II-4. Point B Horizontal-1 Time Histories at an Annual Exceedance Probability of 5×10^{-4}

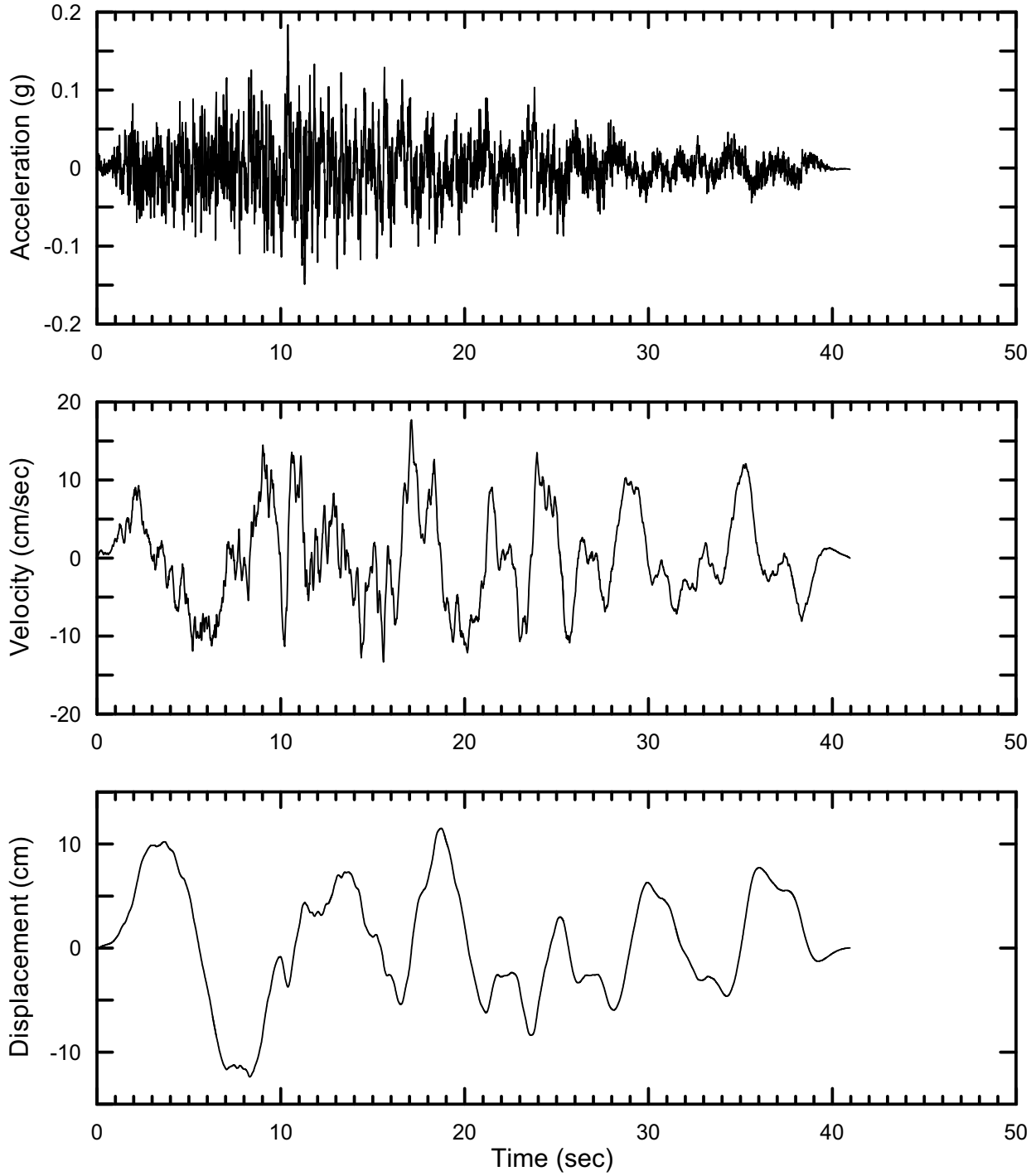

DTN: MO0407TMHIS104.003 [DIRS 170599]

Figure II-5. Point B Horizontal-2 Time Histories at an Annual Exceedance Probability of 5×10^{-4}

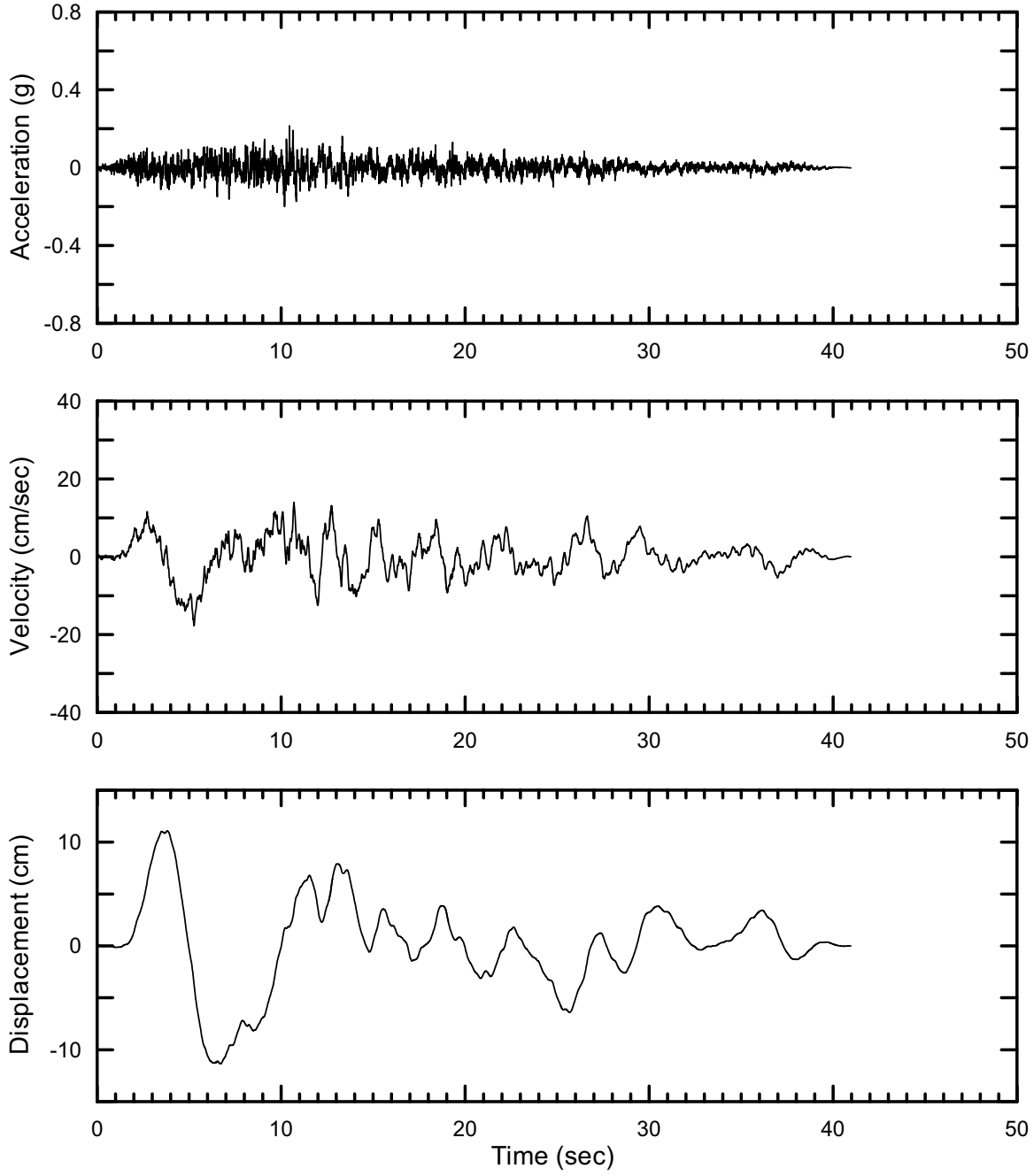

DTN: MO0407TMHIS104.003 [DIRS 170599]

Figure II-6. Point B Vertical Time Histories at an Annual Exceedance Probability of 5×10^{-4}

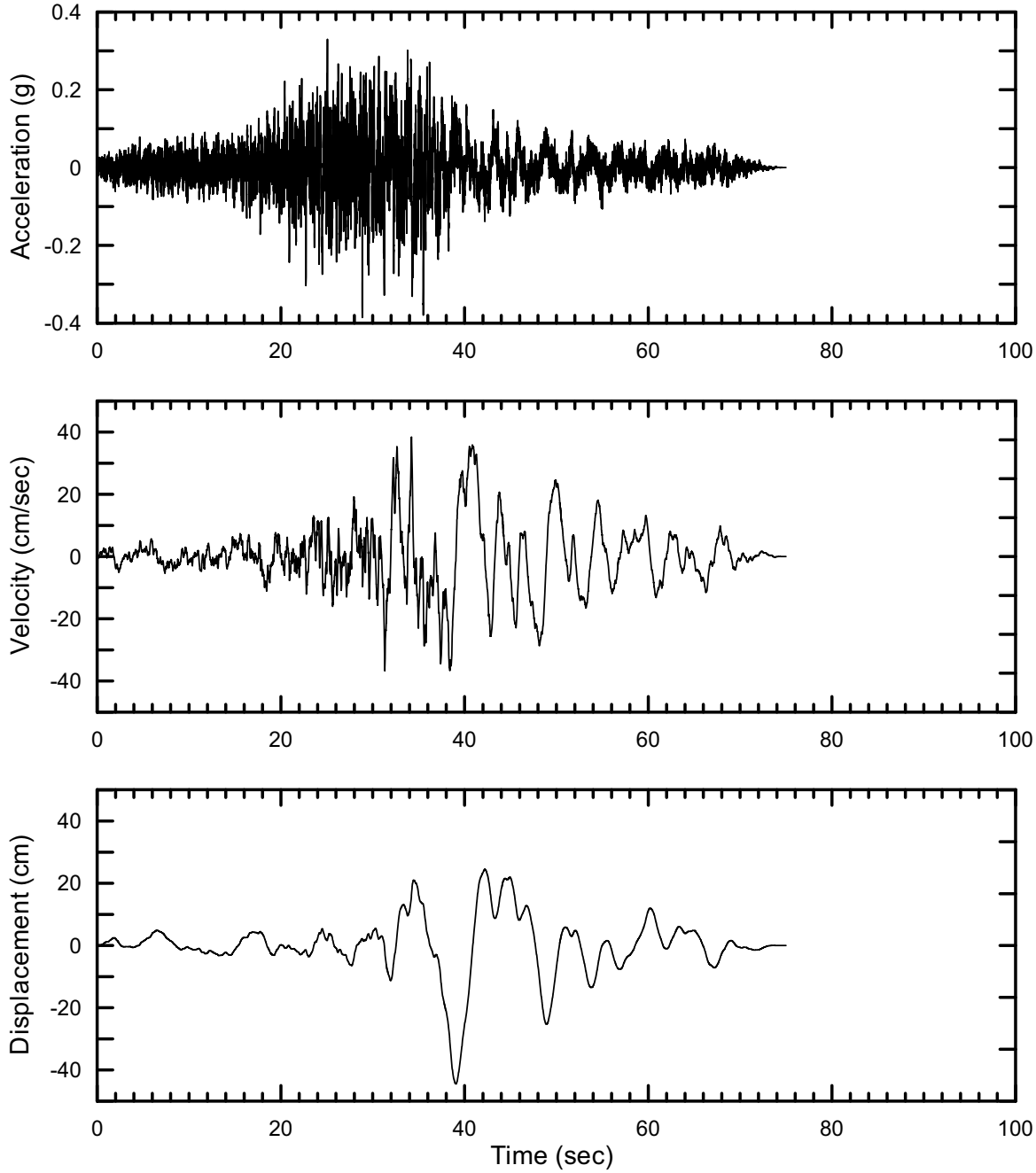

DTN: MO0306SDSAVDTH.000 [DIRS 164033]

Figure II-7. Point B Horizontal-1 Time Histories at an Annual Exceedance Probability of 10^{-4}

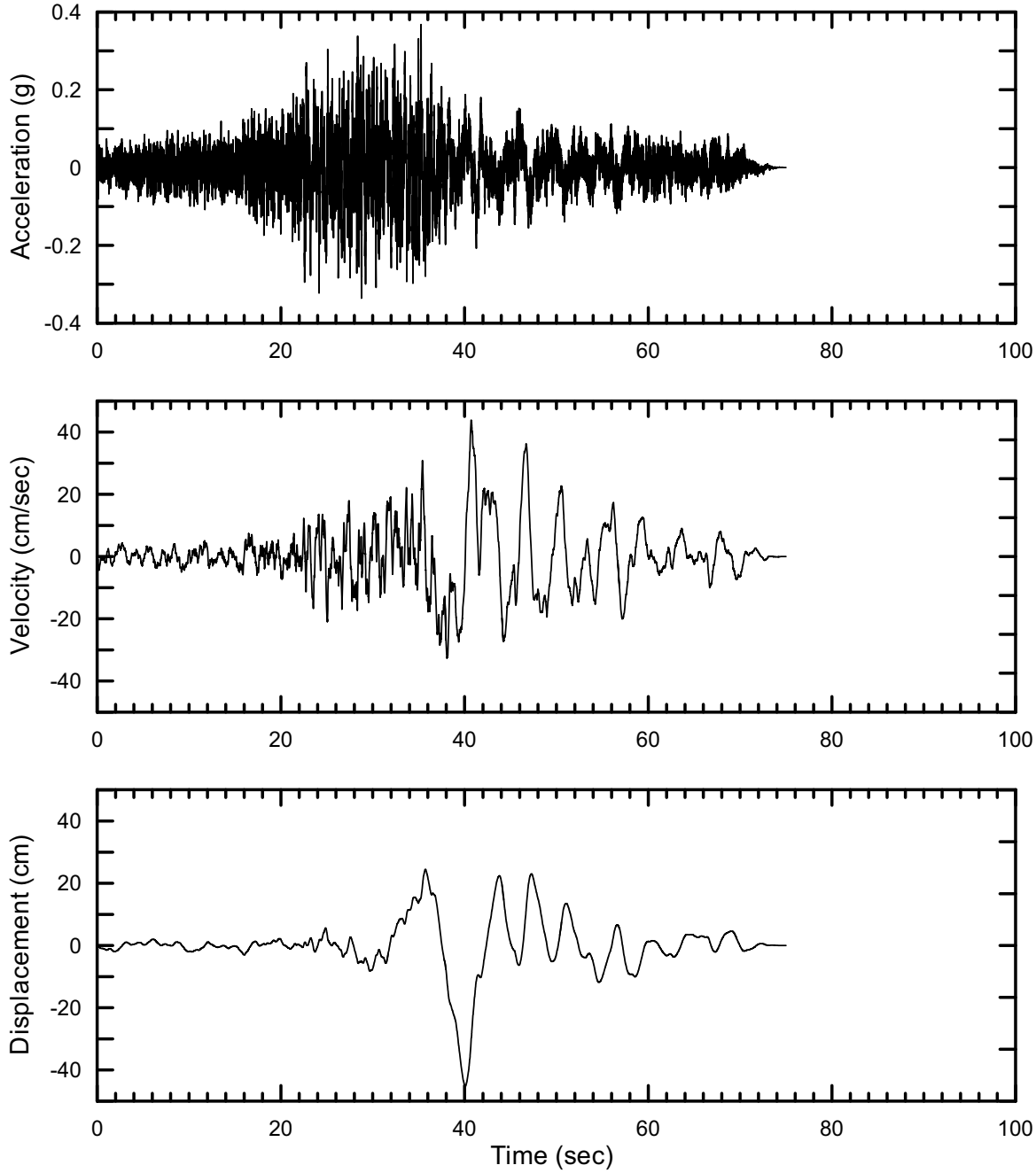

DTN: MO0306SDSAVDTH.000 [DIRS 164033]

Figure II-8. Point B Horizontal-2 Time Histories at an Annual Exceedance Probability of 10^{-4}

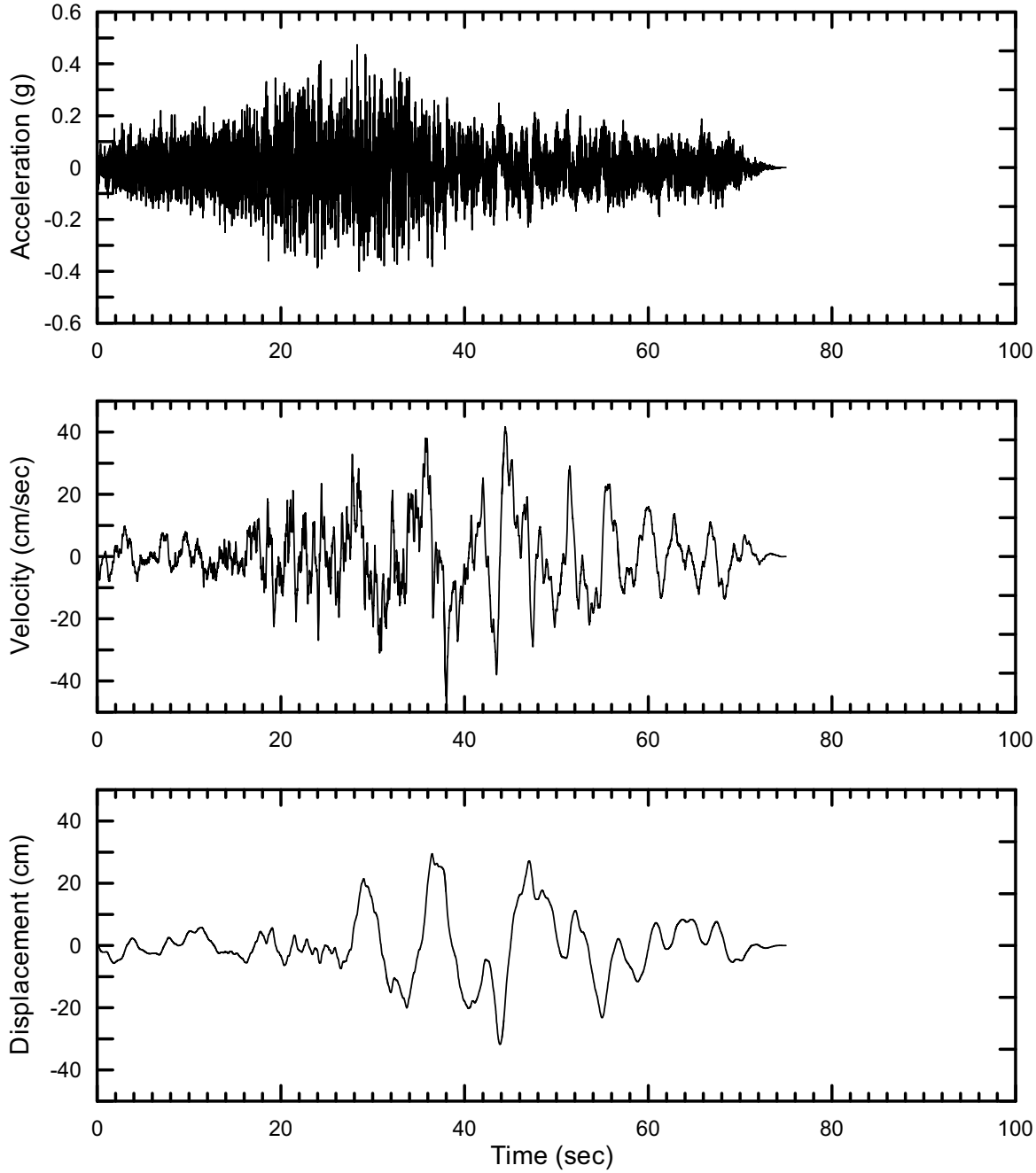

DTN: MO0306SDSAVDTH.000 [DIRS 164033]

Figure II-9. Point B Vertical Time Histories at an Annual Exceedance Probability of 10^{-4}

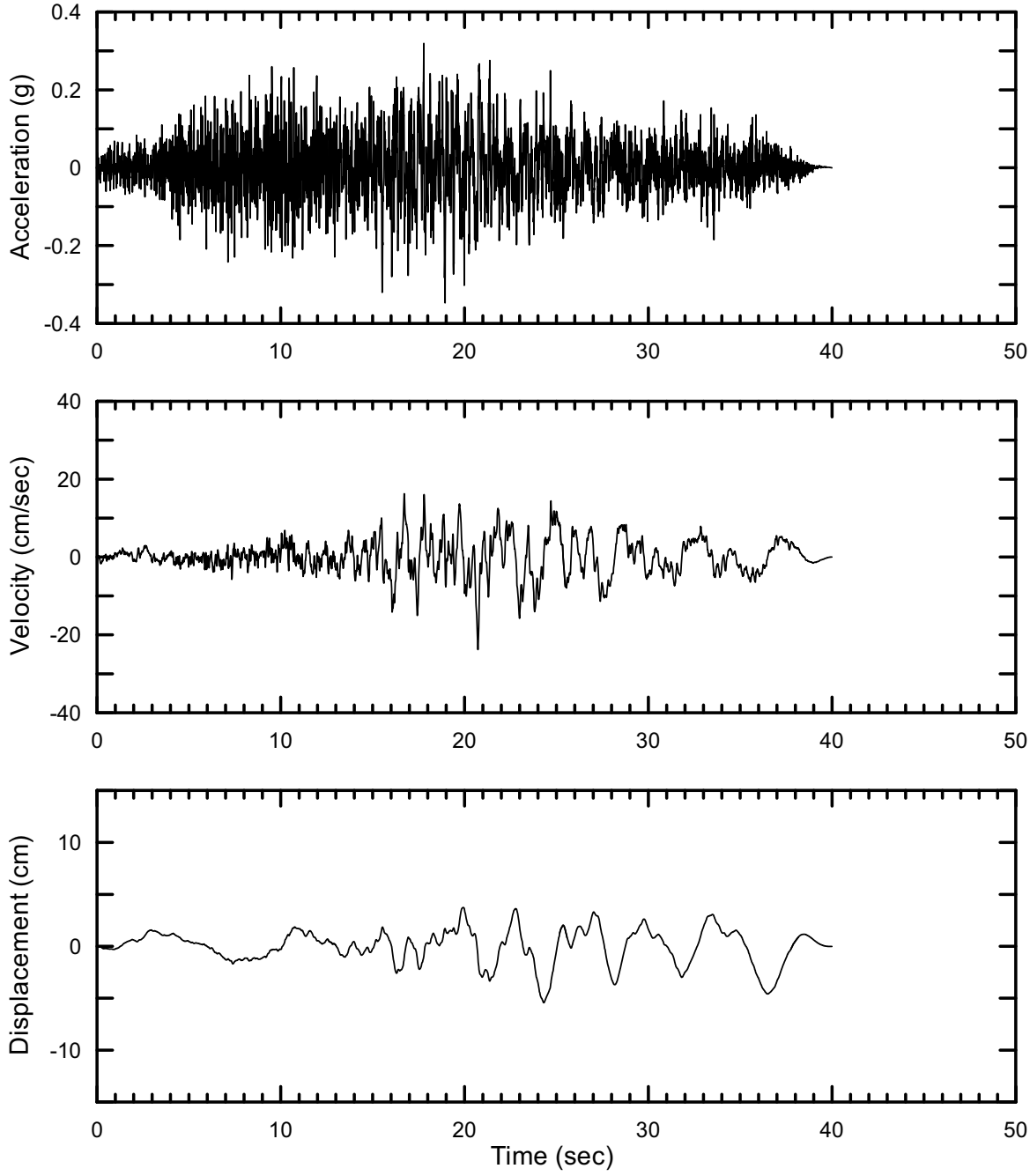

DTN: MO0410SDSDE103.002 [DIRS 172236]

Figure II-10. Point D/E Horizontal-1 Time Histories at an Annual Exceedance Probability of 10^{-3}, Set #1

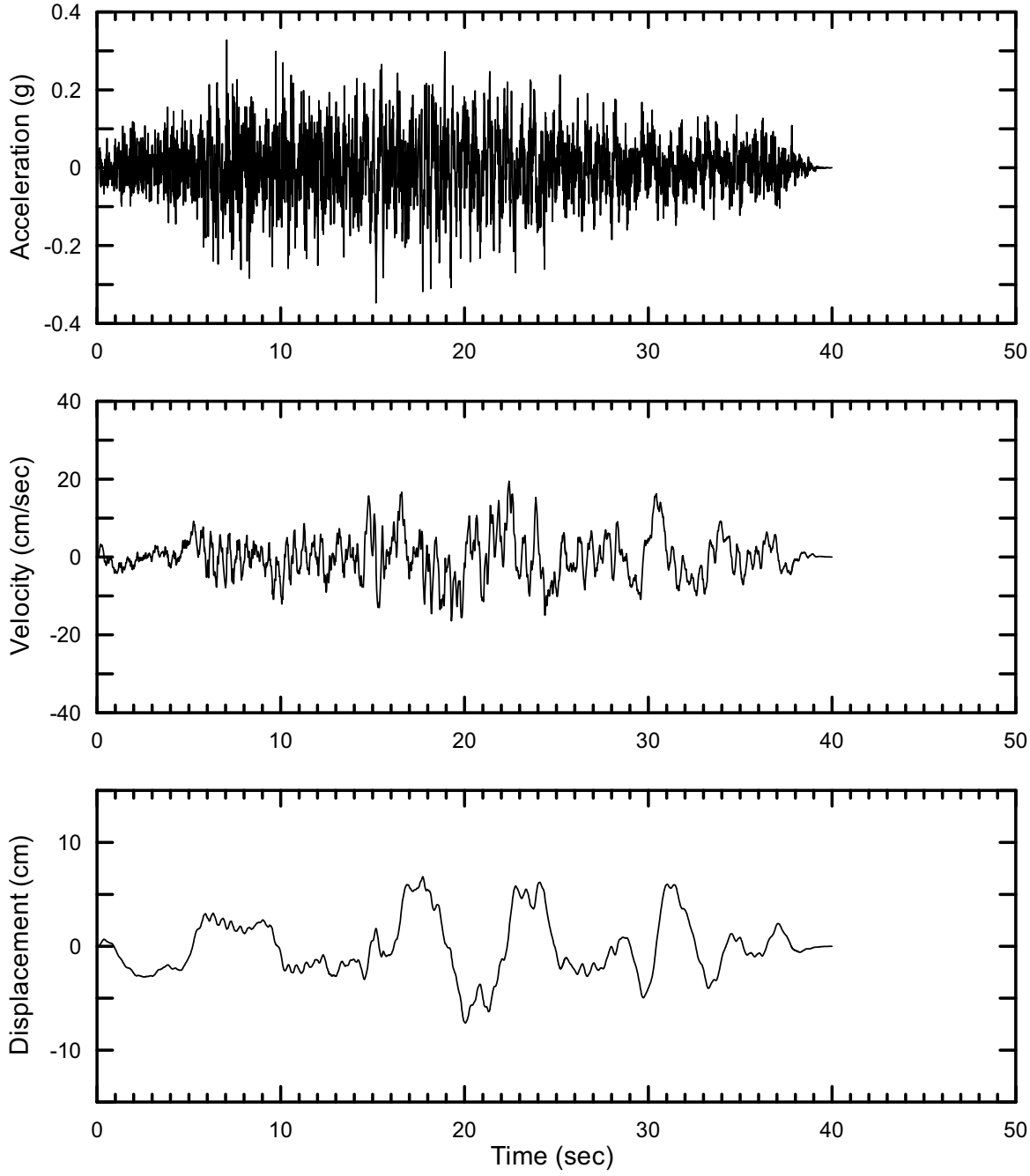

DTN: MO0410SDSDE103.002 [DIRS 172236]

Figure II-11. Point D/E Horizontal-2 Time Histories at an Annual Exceedance Probability of 10^{-3}, Set #1

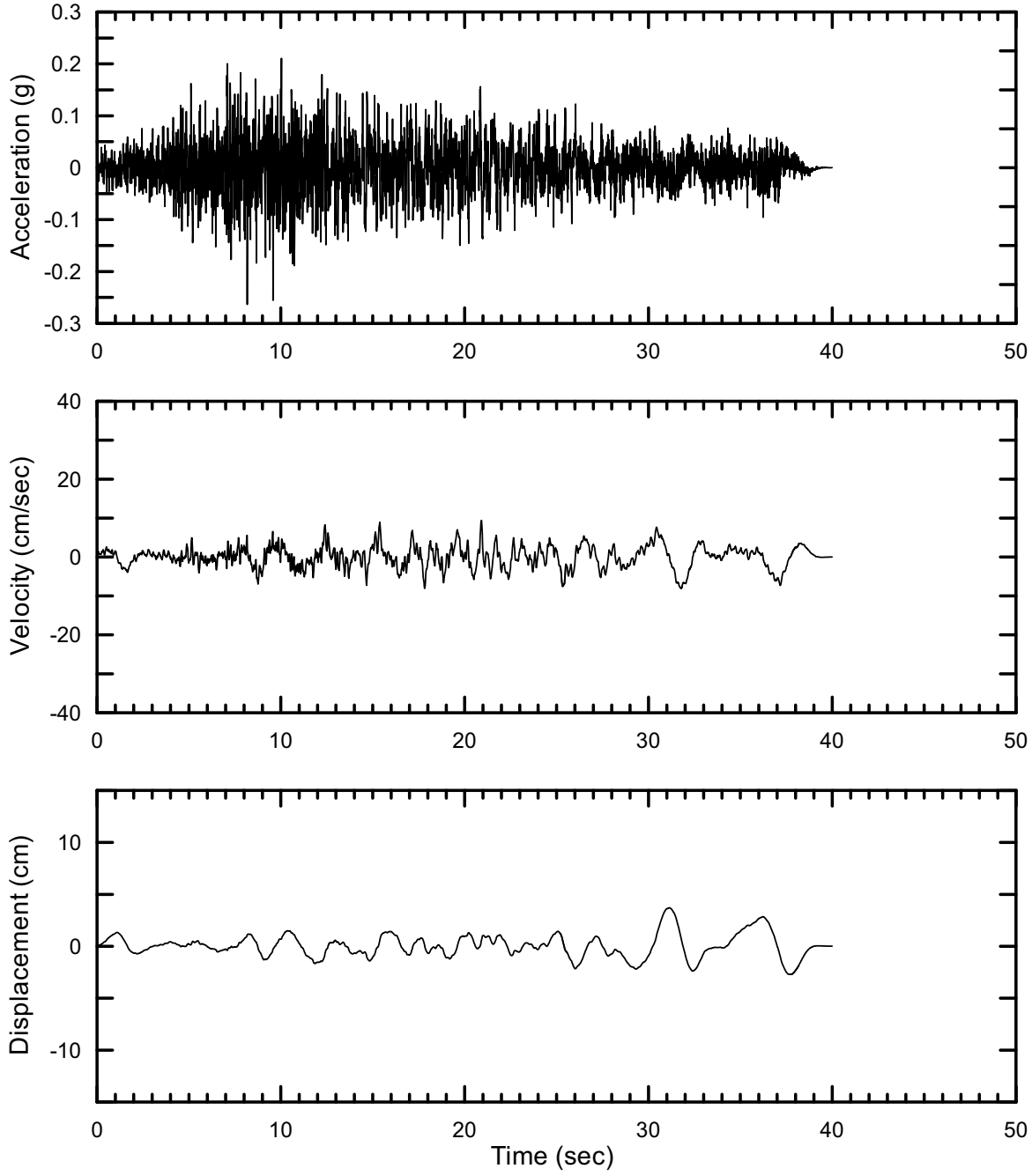

DTN: MO0410SDSDE103.002 [DIRS 172236]

Figure II-12. Point D/E Vertical Time Histories at an Annual Exceedance Probability of 10^{-3}, Set #1

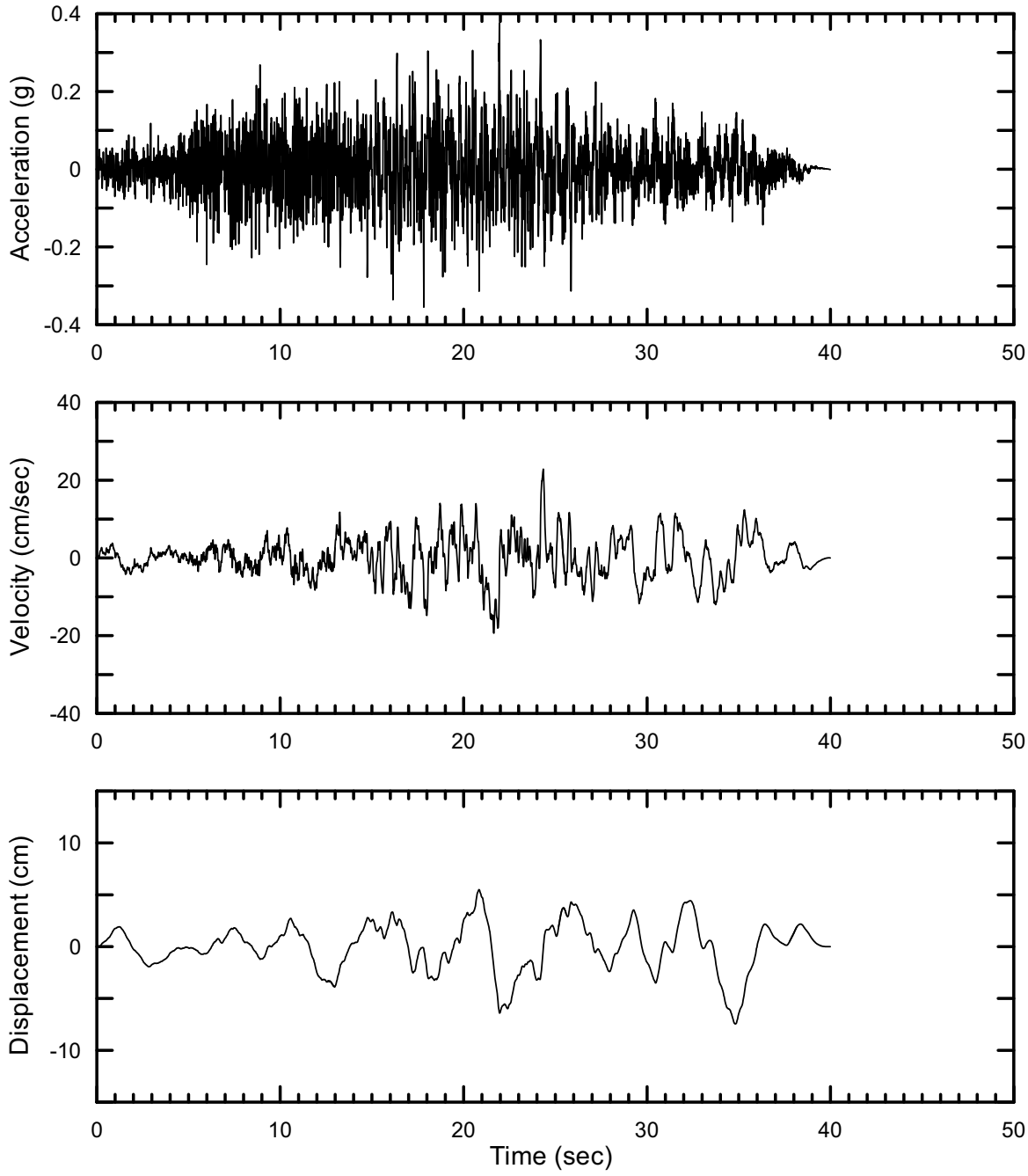

DTN: MO0410SDSDE103.002 [DIRS 172236]

Figure II-13. Point D/E Horizontal-1 Time Histories at an Annual Exceedance Probability of 10^{-3}, Set #2

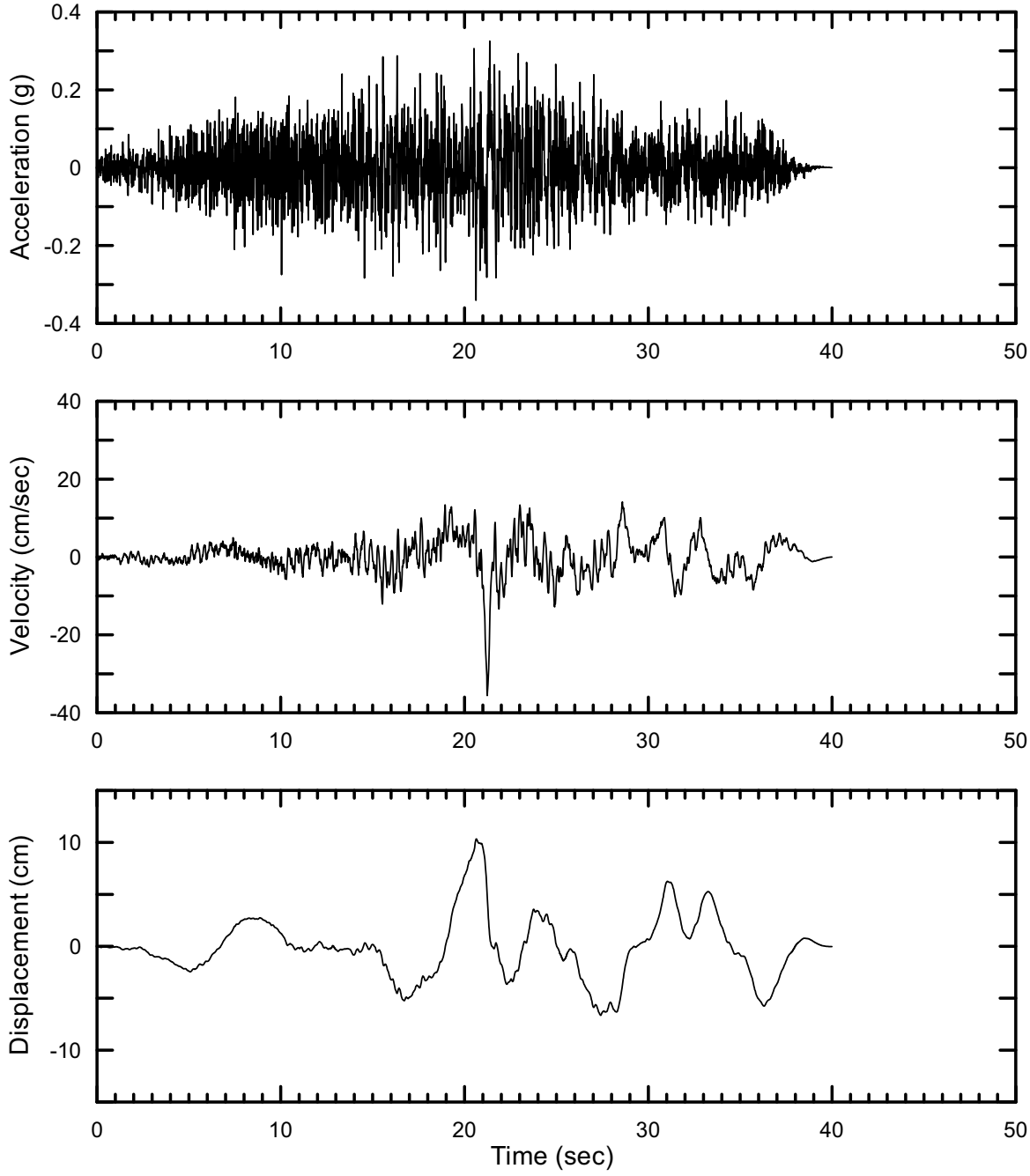

DTN: MO0410SDSDE103.002 [DIRS 172236]

Figure II-14. Point D/E Horizontal-2 Time Histories at an Annual Exceedance Probability of 10^{-3}, Set #2

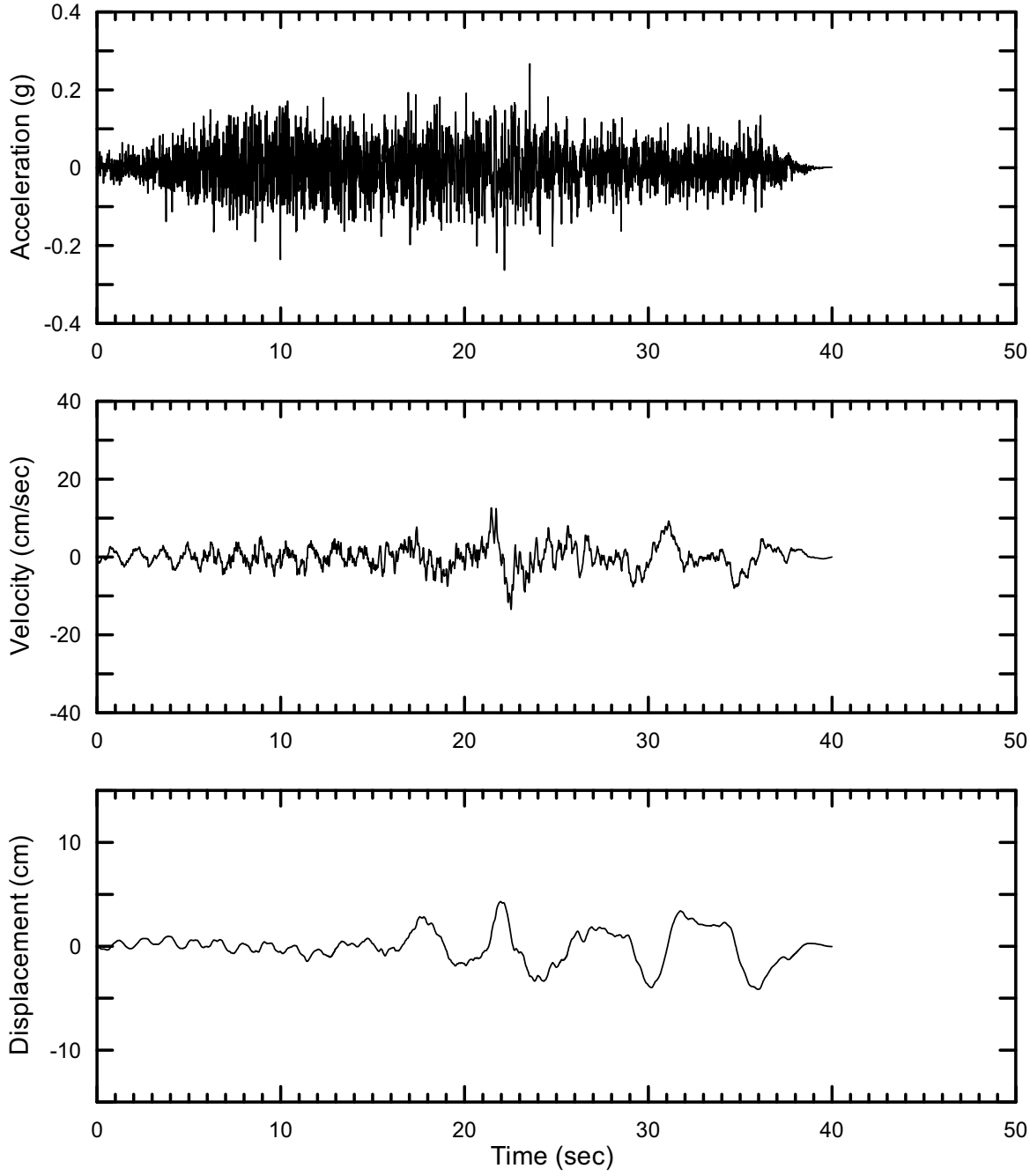

DTN: MO0410SDSDE103.002 [DIRS 172236]

Figure II-15. Point D/E Vertical Time Histories at an Annual Exceedance Probability of 10^{-3}, Set #2

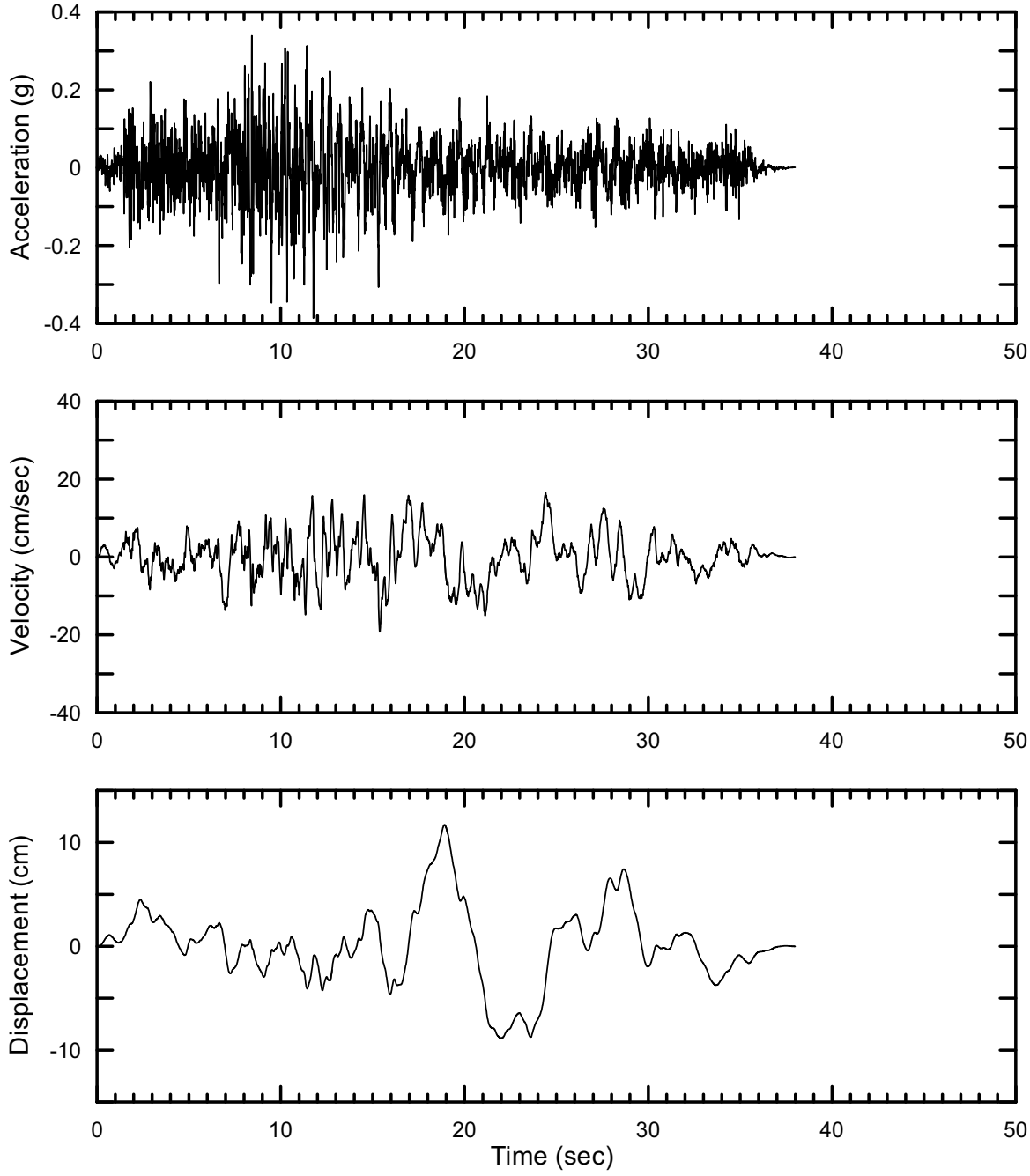

DTN: MO0410SDSDE103.002 [DIRS 172236]

Figure II-16. Point D/E Horizontal-1 Time Histories at an Annual Exceedance Probability of 10^{-3}, Set #3

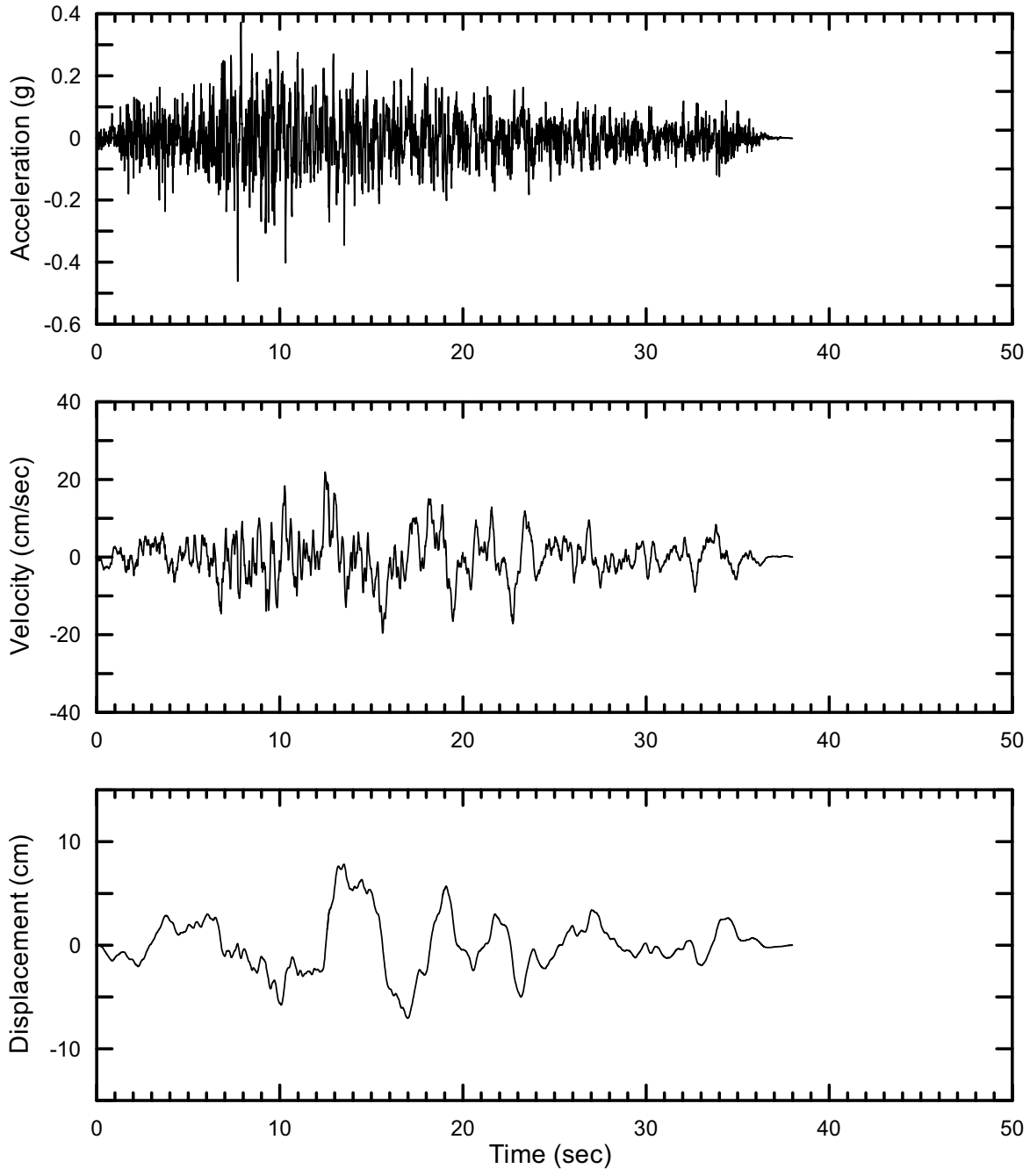

DTN: MO0410SDSDE103.002 [DIRS 172236]

Figure II-17. Point D/E Horizontal-2 Time Histories at an Annual Exceedance Probability of 10^{-3}, Set #3

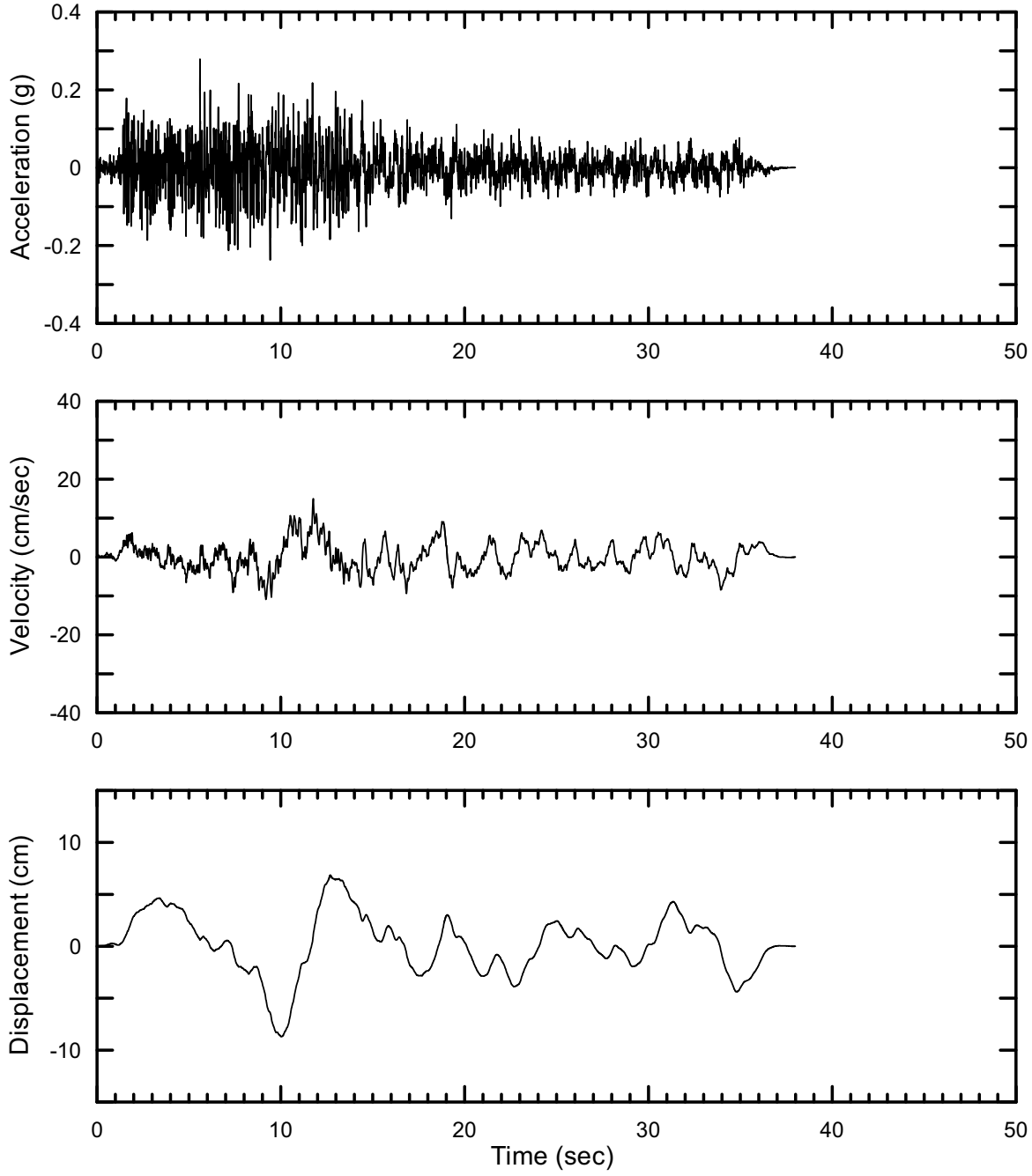

DTN: MO0410SDSDE103.002 [DIRS 172236]

Figure II-18. Point D/E Vertical Time Histories at an Annual Exceedance Probability of 10^{-3}, Set #3

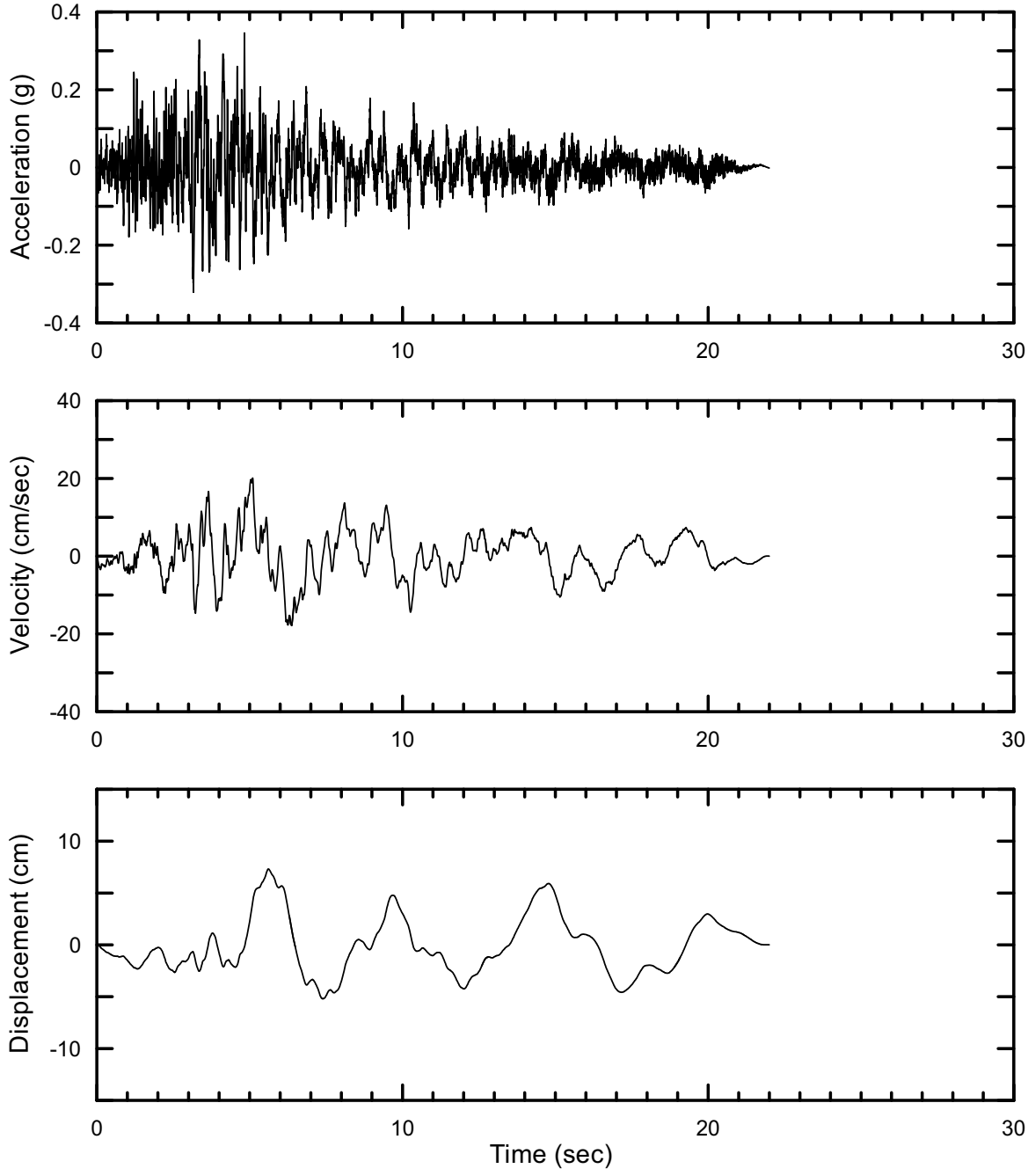

DTN: MO0410SDSDE103.002 [DIRS 172236]

Figure II-19. Point D/E Horizontal-1 Time Histories at an Annual Exceedance Probability of 10^{-3}, Set #4

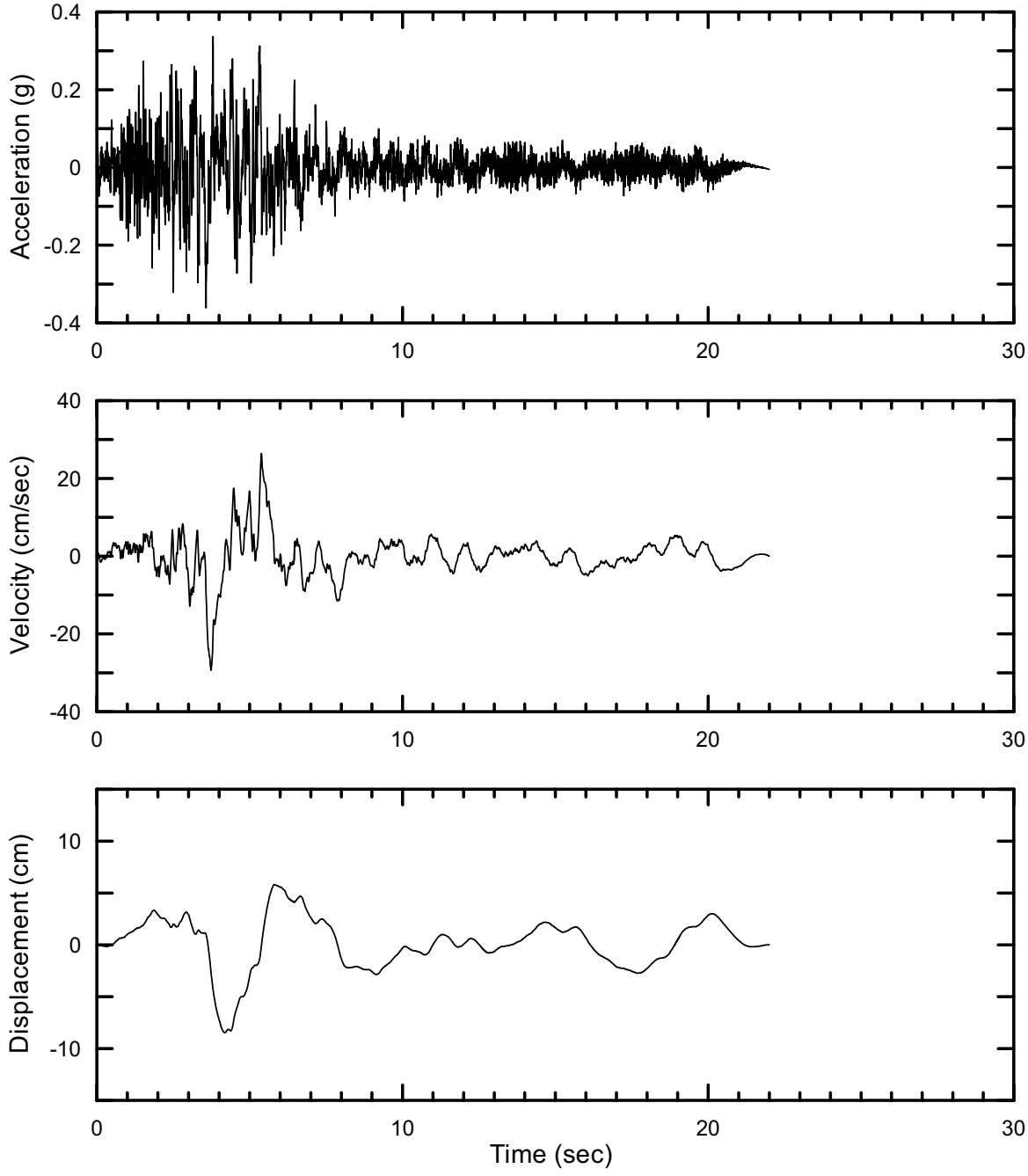

DTN: MO0410SDSDE103.002 [DIRS 172236]

Figure II-20. Point D/E Horizontal-2 Time Histories at an Annual Exceedance Probability of 10^{-3}, Set #4

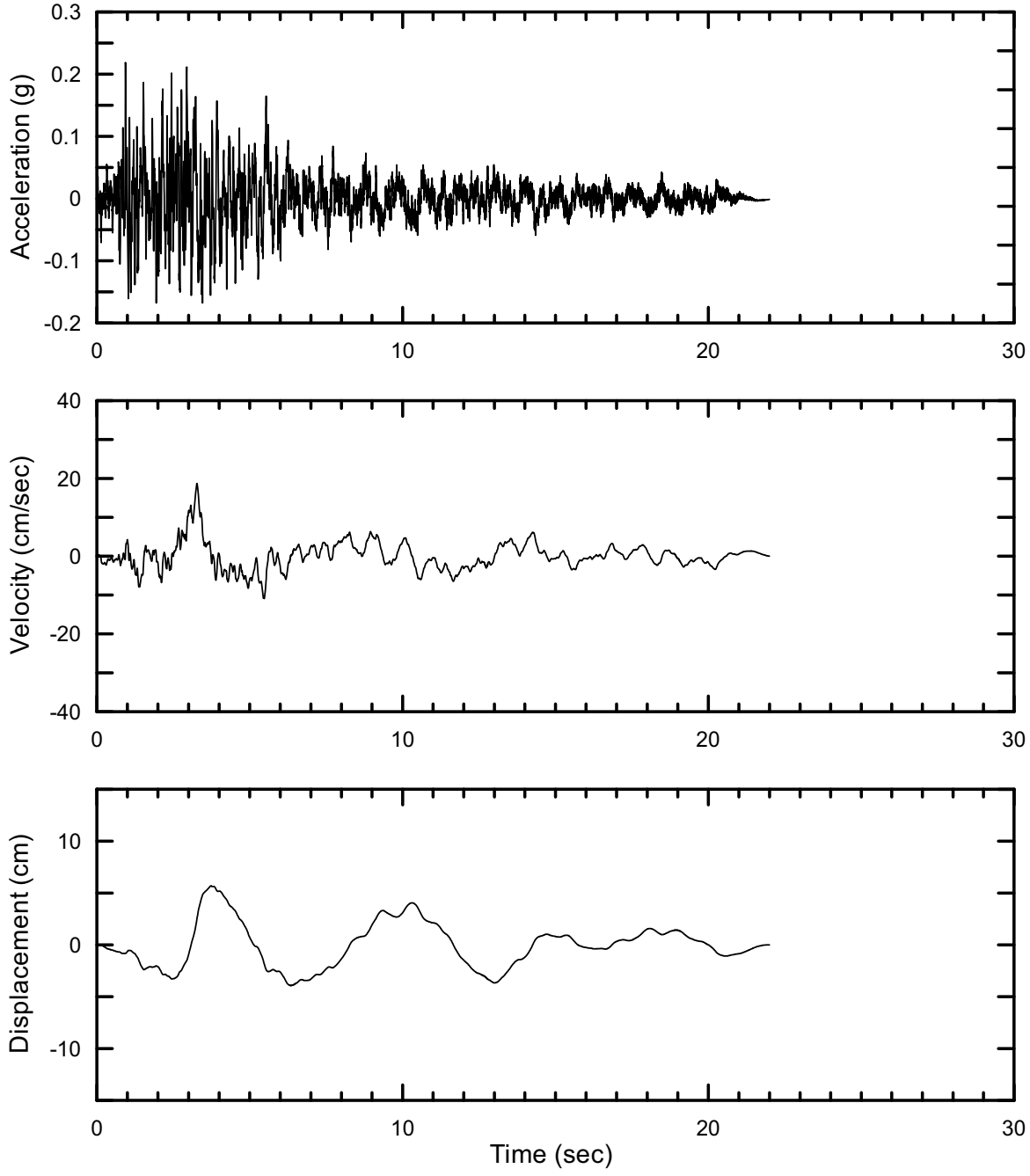

DTN: MO0410SDSDE103.002 [DIRS 172236]

Figure II-21. Point D/E Vertical Time Histories at an Annual Exceedance Probability of 10^{-3}, Set #4

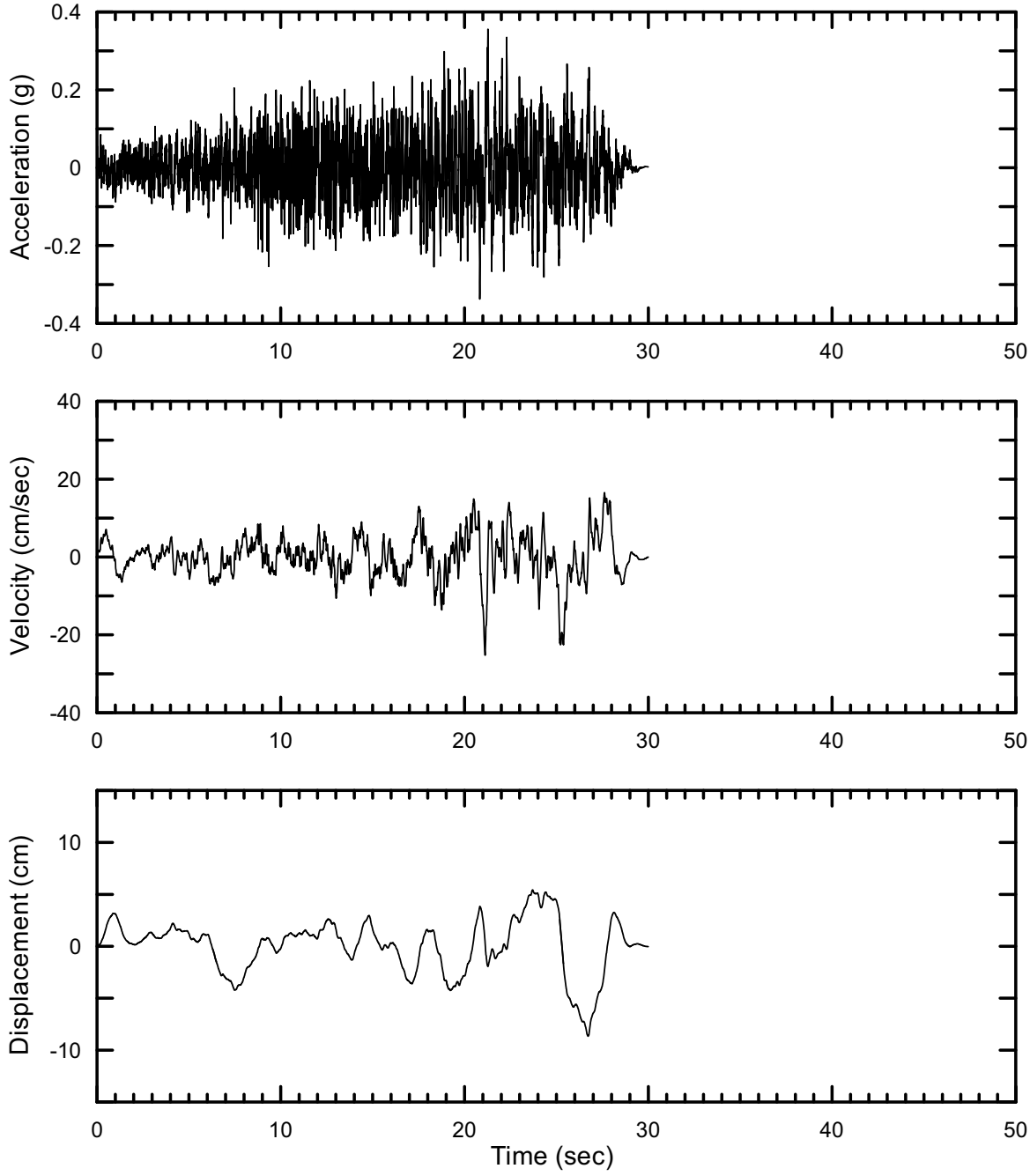

DTN: MO0410SDSDE103.002 [DIRS 172236]

Figure II-22. Point D/E Horizontal-1 Time Histories at an Annual Exceedance Probability of 10^{-3}, Set #5

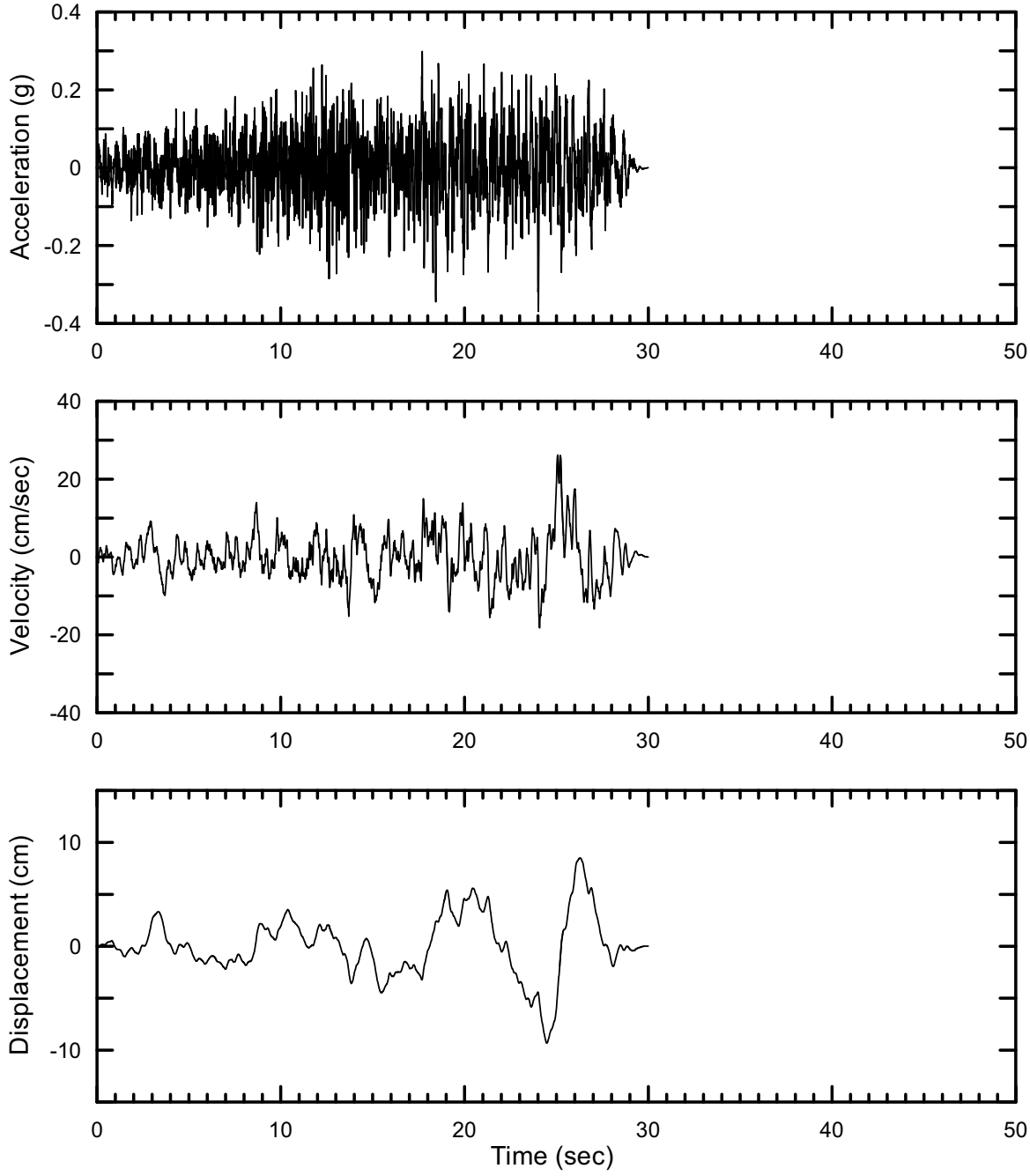

DTN: MO0410SDSDE103.002 [DIRS 172236]

Figure II-23. Point D/E Horizontal-2 Time Histories at an Annual Exceedance Probability of 10^{-3}, Set #5

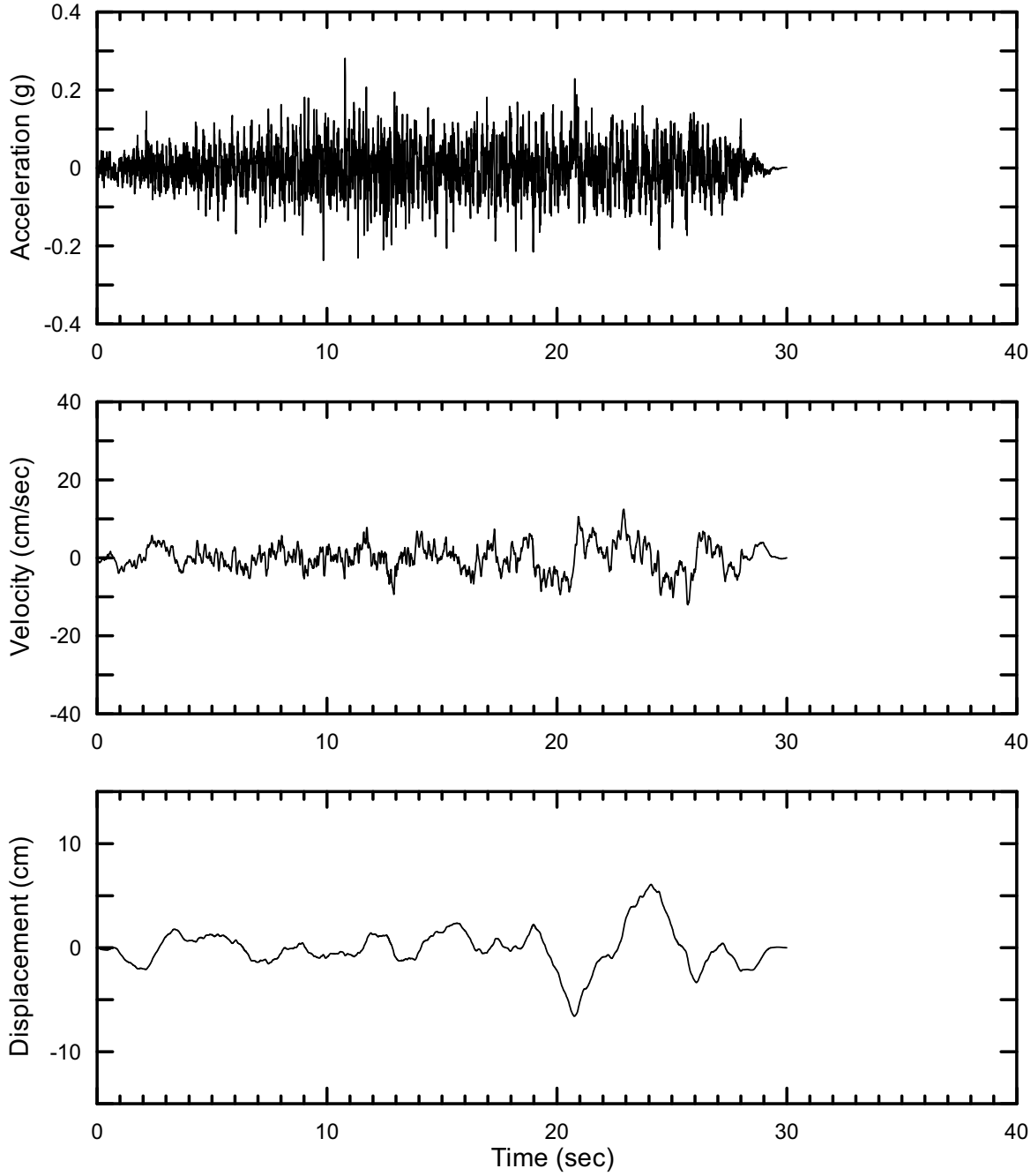

DTN: MO0410SDSDE103.002 [DIRS 172236]

Figure II-24. Point D/E Vertical Time Histories at an Annual Exceedance Probability of 10^{-3}, Set #5

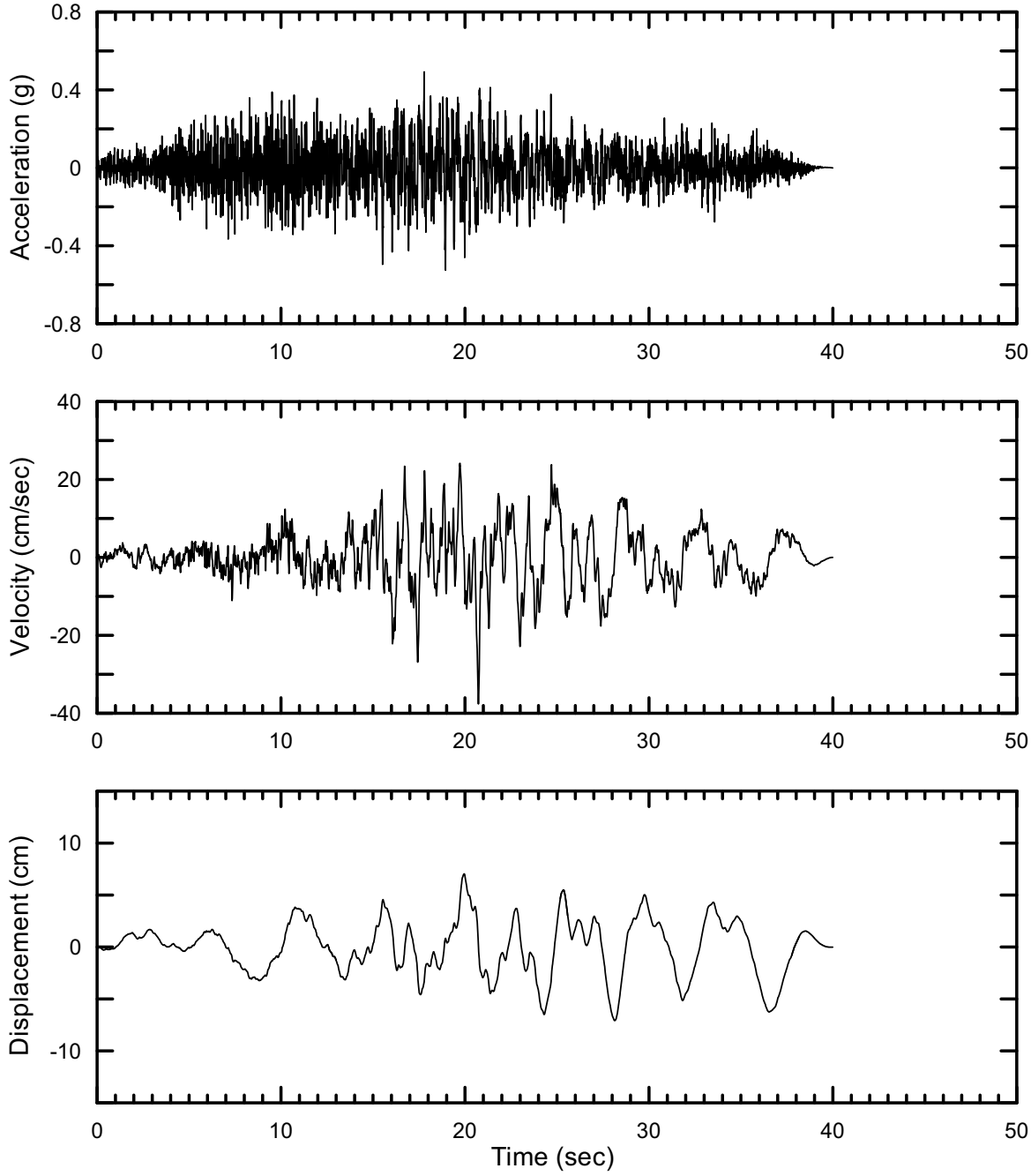

DTN: MO0410SDSTMHIS.005 [DIRS 172237]

Figure II-25. Point D/E Horizontal-1 Ti me Histories at an Annual Exceedance Probability of 5×10^{-4}, Set #1

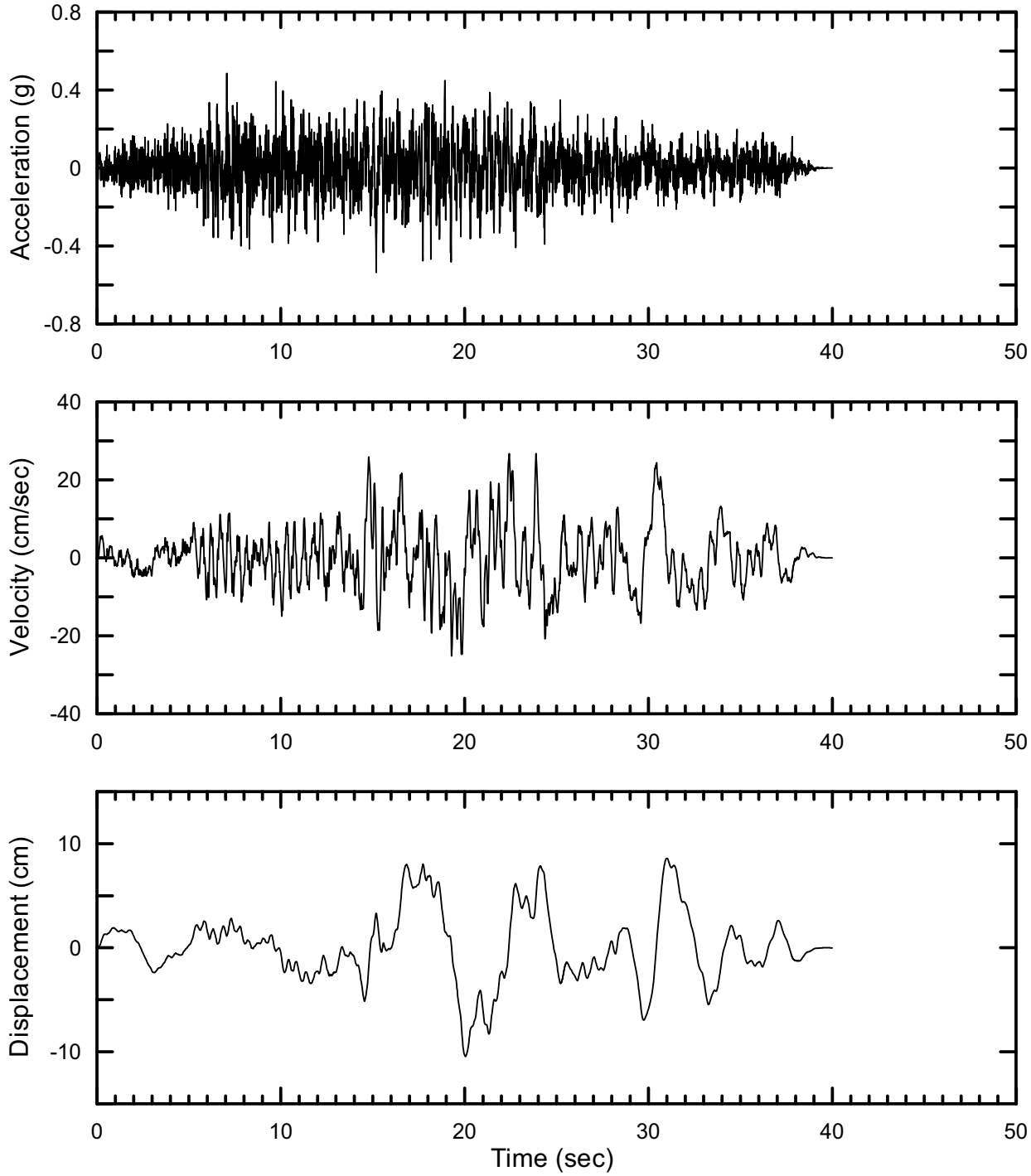

DTN: MO0410SDSTMHIS.005 [DIRS 172237]

Figure II-26. Point D/E Horizontal-2 Ti me Histories at an Annual Exceedance Probability of 5×10^{-4}, Set #1

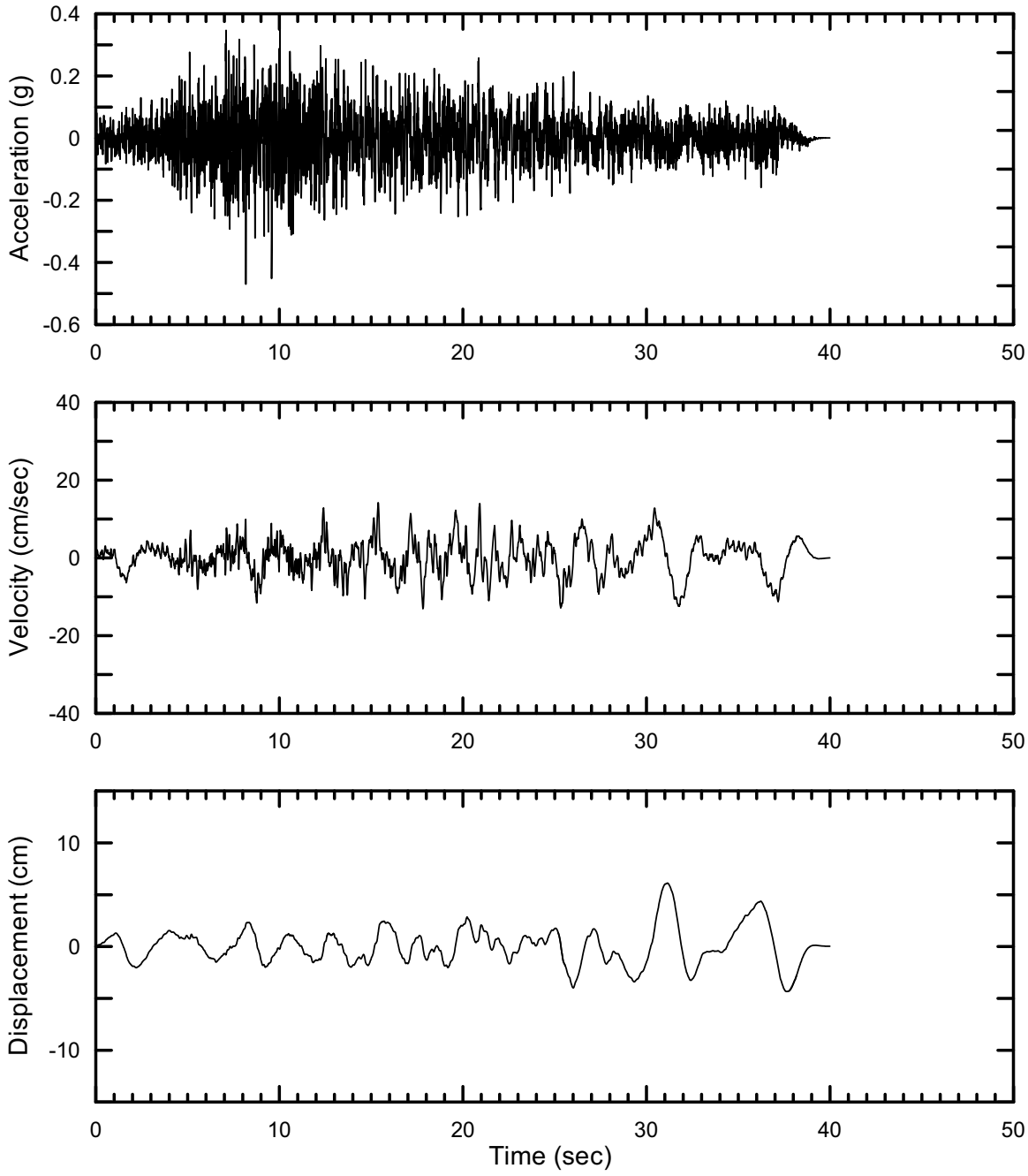

DTN: MO0410SDSTMHIS.005 [DIRS 172237]

Figure II-27. Point D/E Vertical Time Histories at an Annual Exceedance Probability of 5×10^{-4}, Set #1

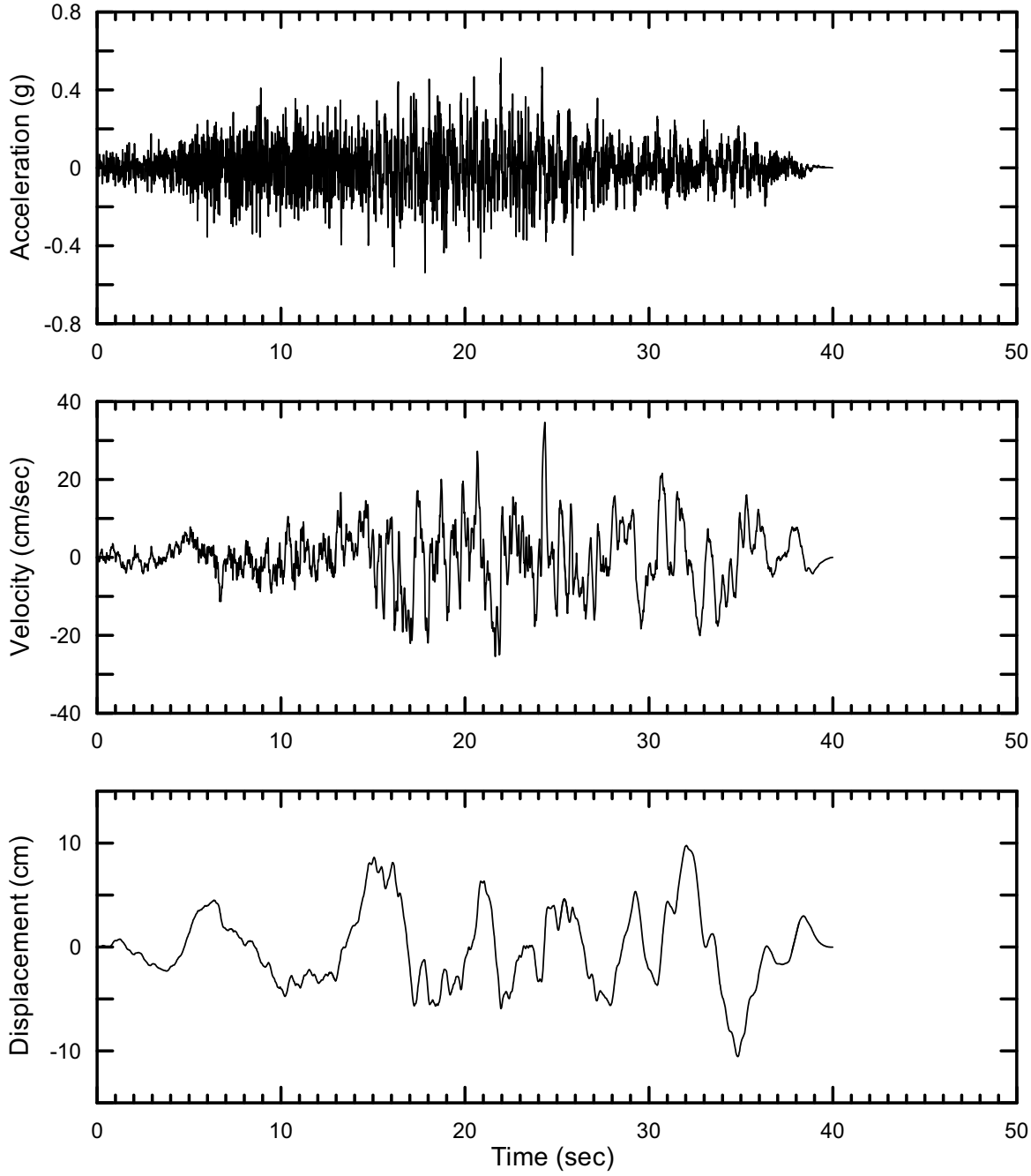

DTN: MO0410SDSTMHIS.005 [DIRS 172237]

Figure II-28. Point D/E Horizontal-1 Ti me Histories at an Annual Exceedance Probability of 5×10^{-4}, Set #2

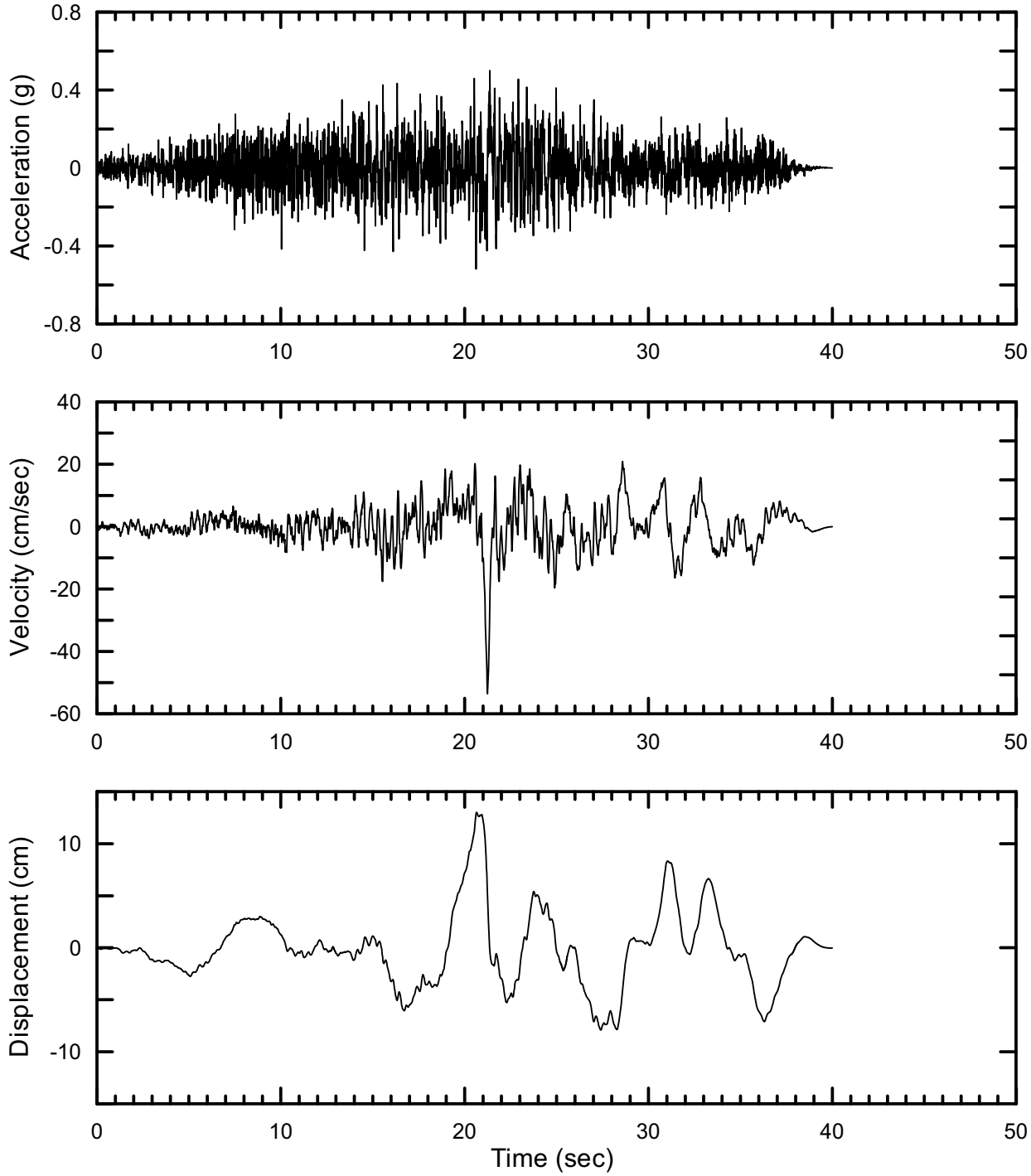

DTN: MO0410SDSTMHIS.005 [DIRS 172237]

Figure II-29. Point D/E Horizontal-2 Ti me Histories at an Annual Exceedance Probability of 5×10^{-4}, Set #2

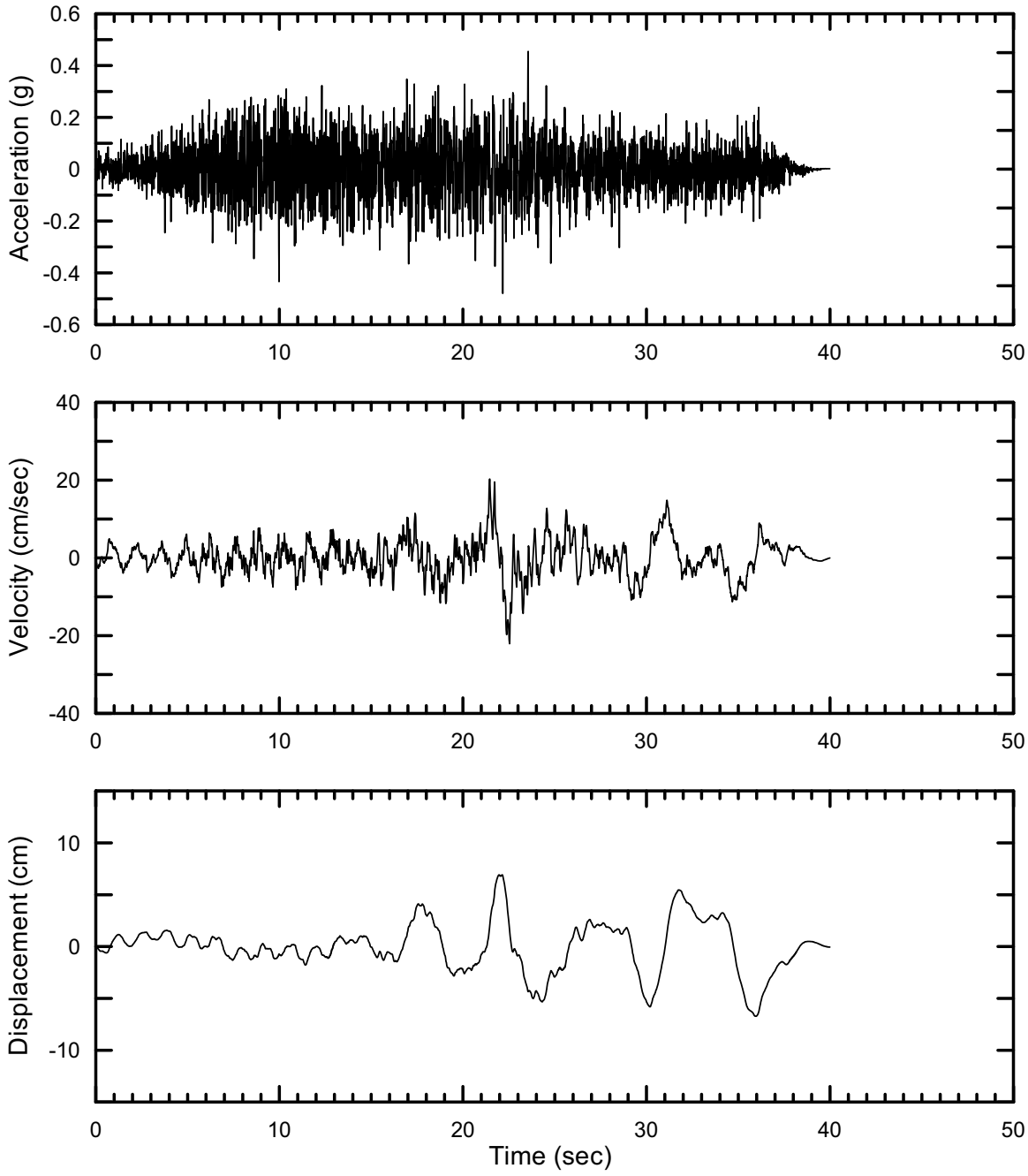

DTN: MO0410SDSTMHIS.005 [DIRS 172237]

Figure II-30. Point D/E Vertical Time Histories at an Annual Exceedance Probability of 5×10^{-4}, Set #2

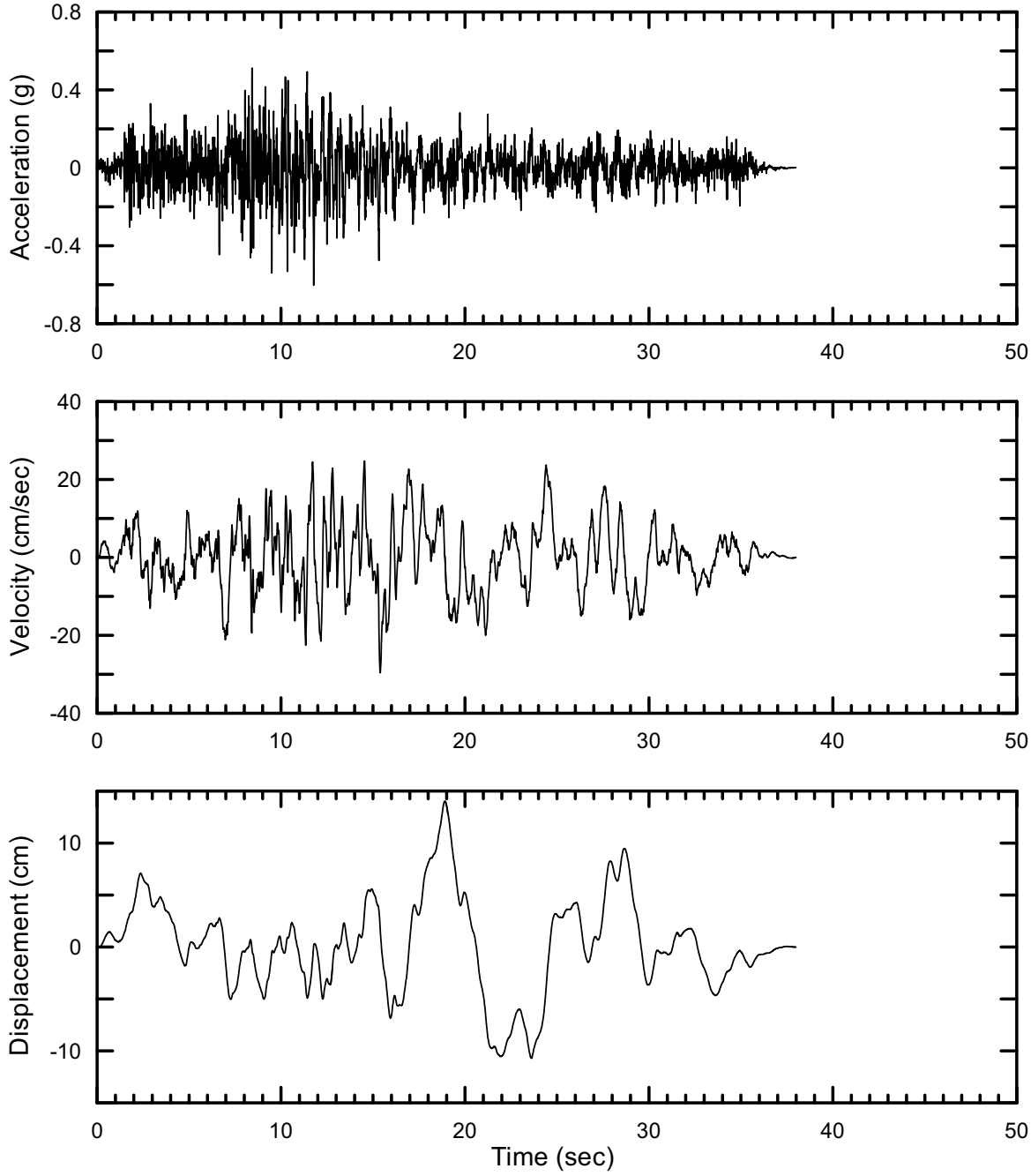

DTN: MO0410SDSTMHIS.005 [DIRS 172237]

Figure II-31. Point D/E Horizontal-1 Ti me Histories at an Annual Exceedance Probability of 5×10^{-4}, Set #3

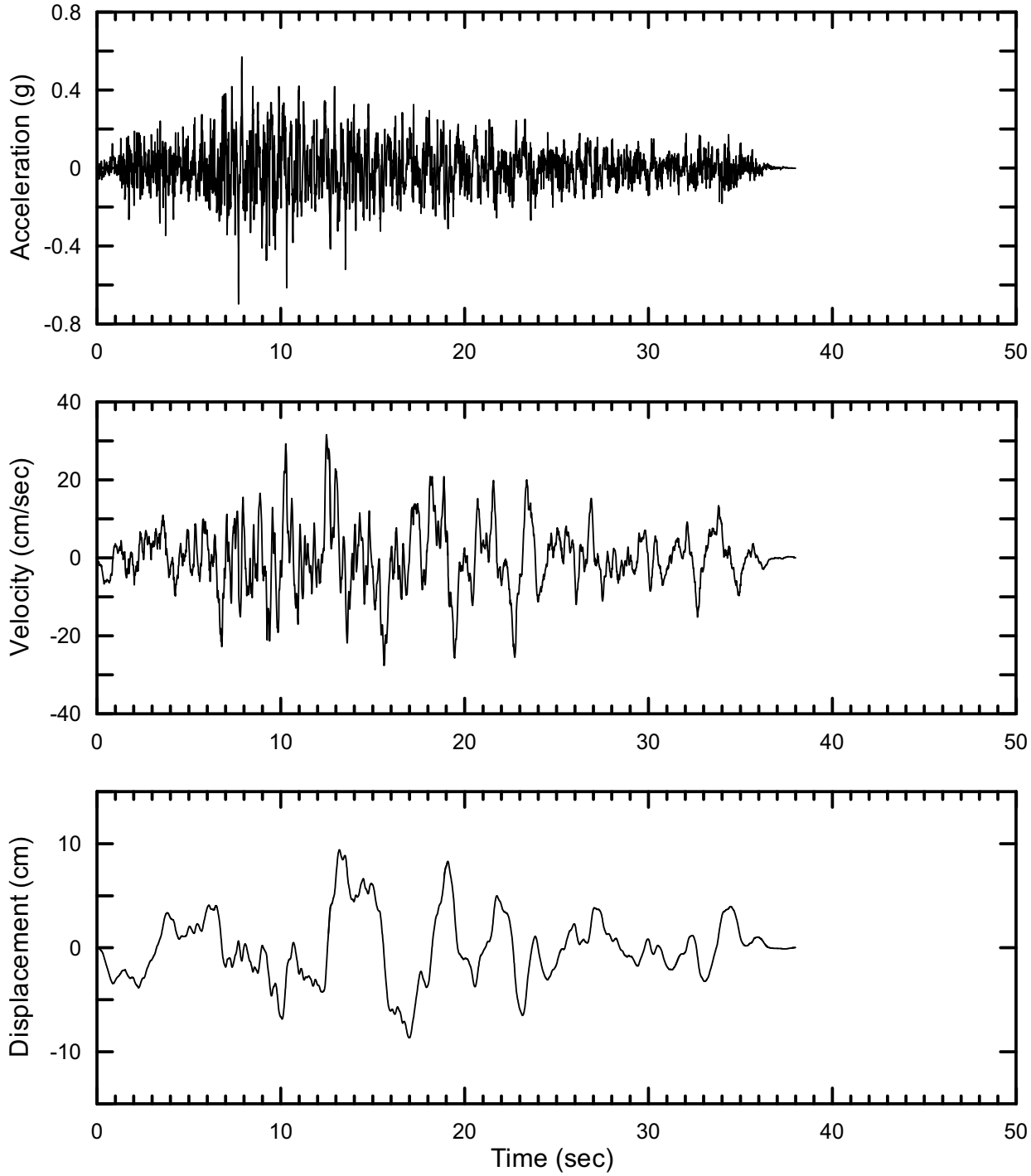

DTN: MO0410SDSTMHIS.005 [DIRS 172237]

Figure II-32. Point D/E Horizontal-2 Ti me Histories at an Annual Exceedance Probability of 5×10^{-4}, Set #3

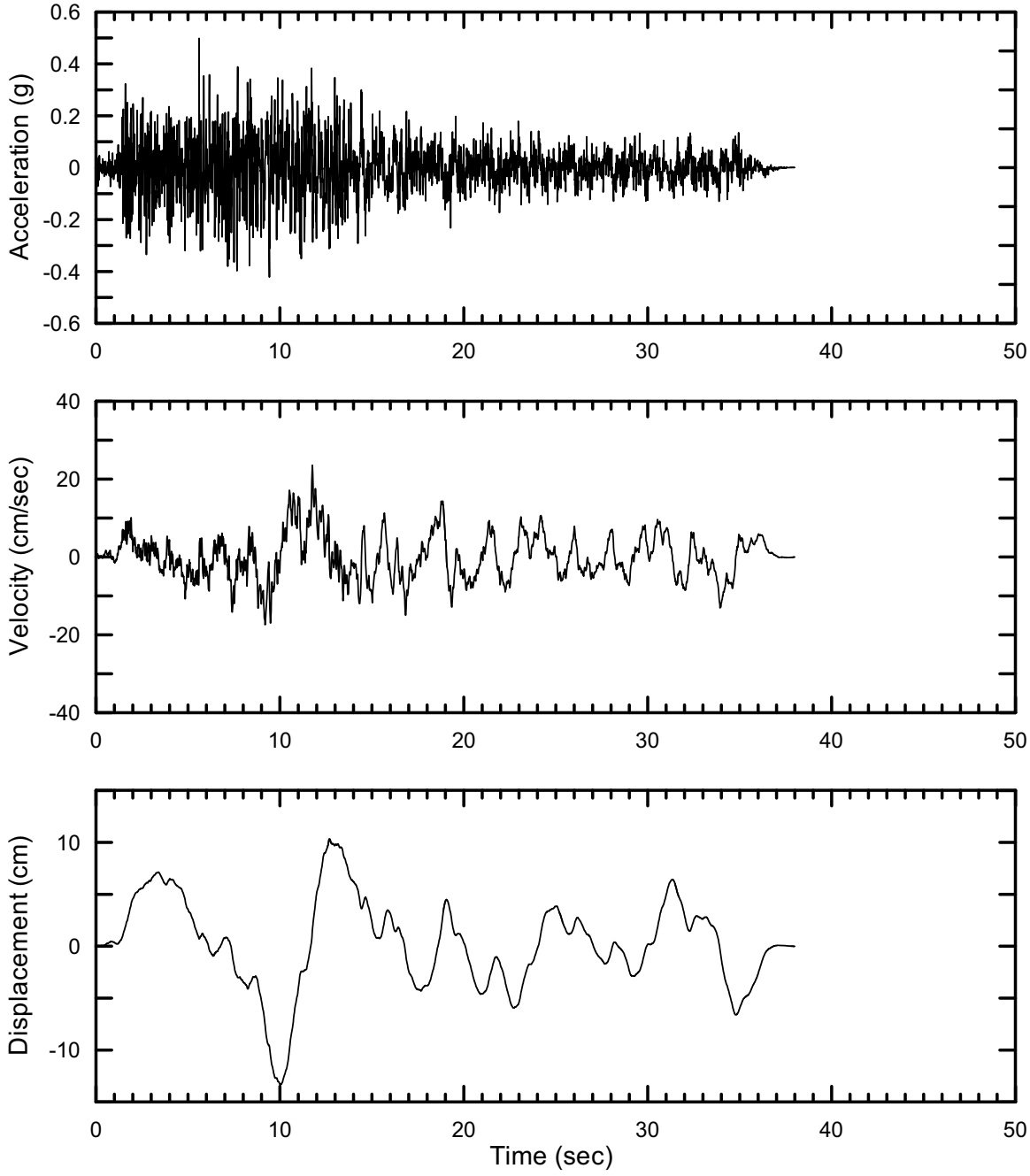

DTN: MO0410SDSTMHIS.005 [DIRS 172237]

Figure II-33. Point D/E Vertical Time Histories at an Annual Exceedance Probability of 5×10^{-4}, Set #3

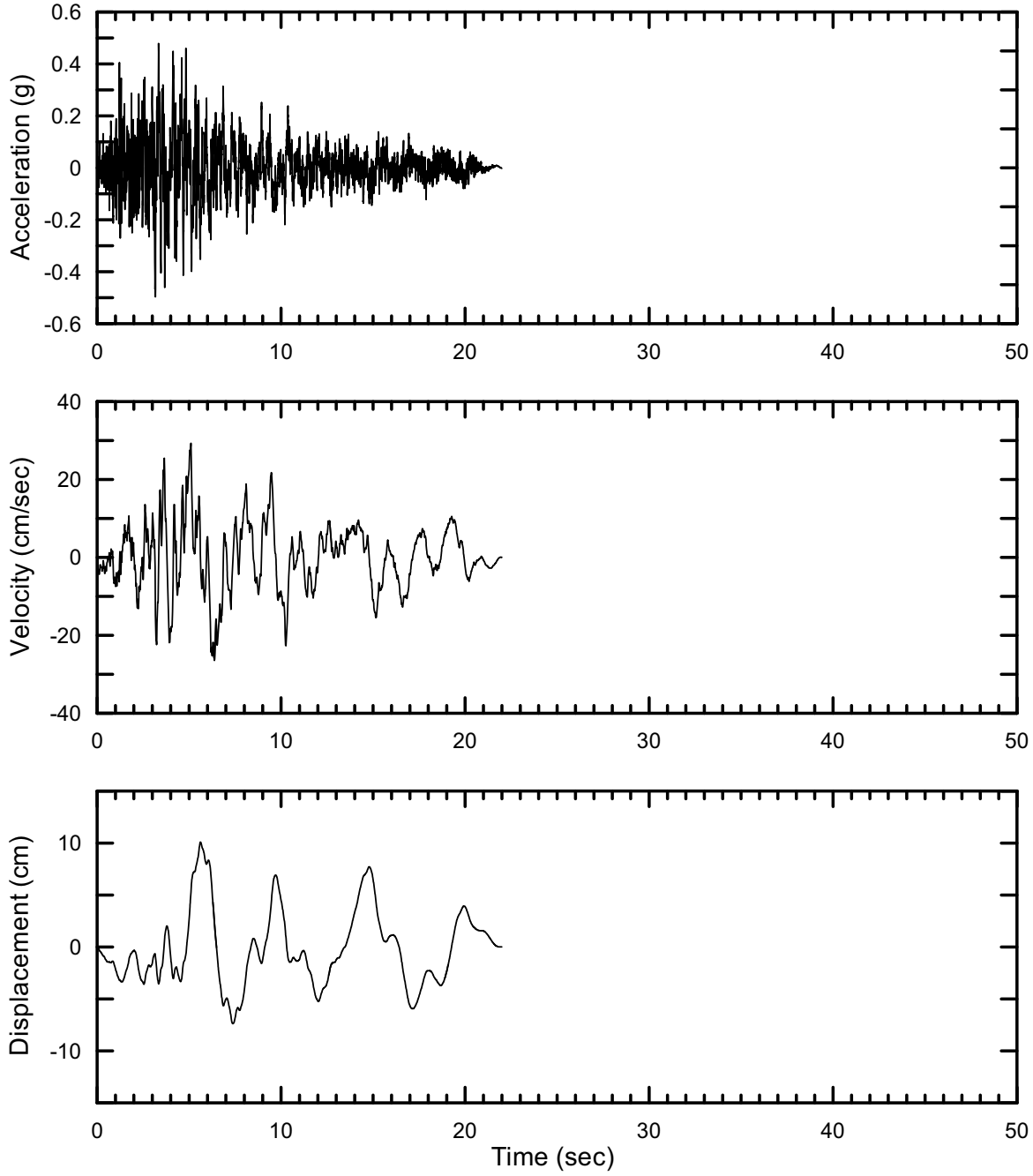

DTN: MO0410SDSTMHIS.005 [DIRS 172237]

Figure II-34. Point D/E Horizontal-1 Ti me Histories at an Annual Exceedance Probability of $5x10^{-4}$, Set #4

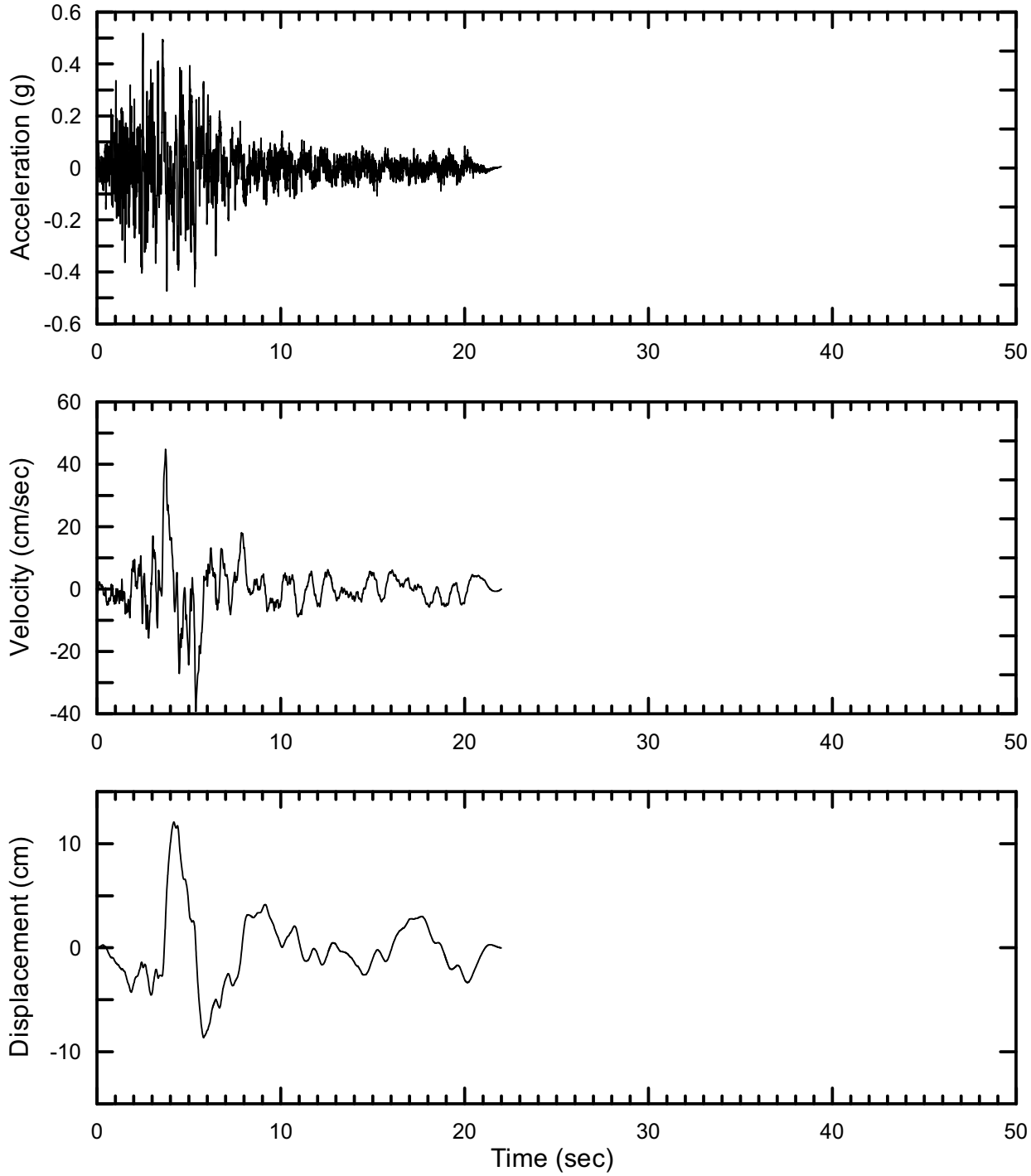

DTN: MO0410SDSTMHIS.005 [DIRS 172237]

Figure II-35. Point D/E Horizontal-2 Ti me Histories at an Annual Exceedance Probability of 5×10^{-4}, Set #4

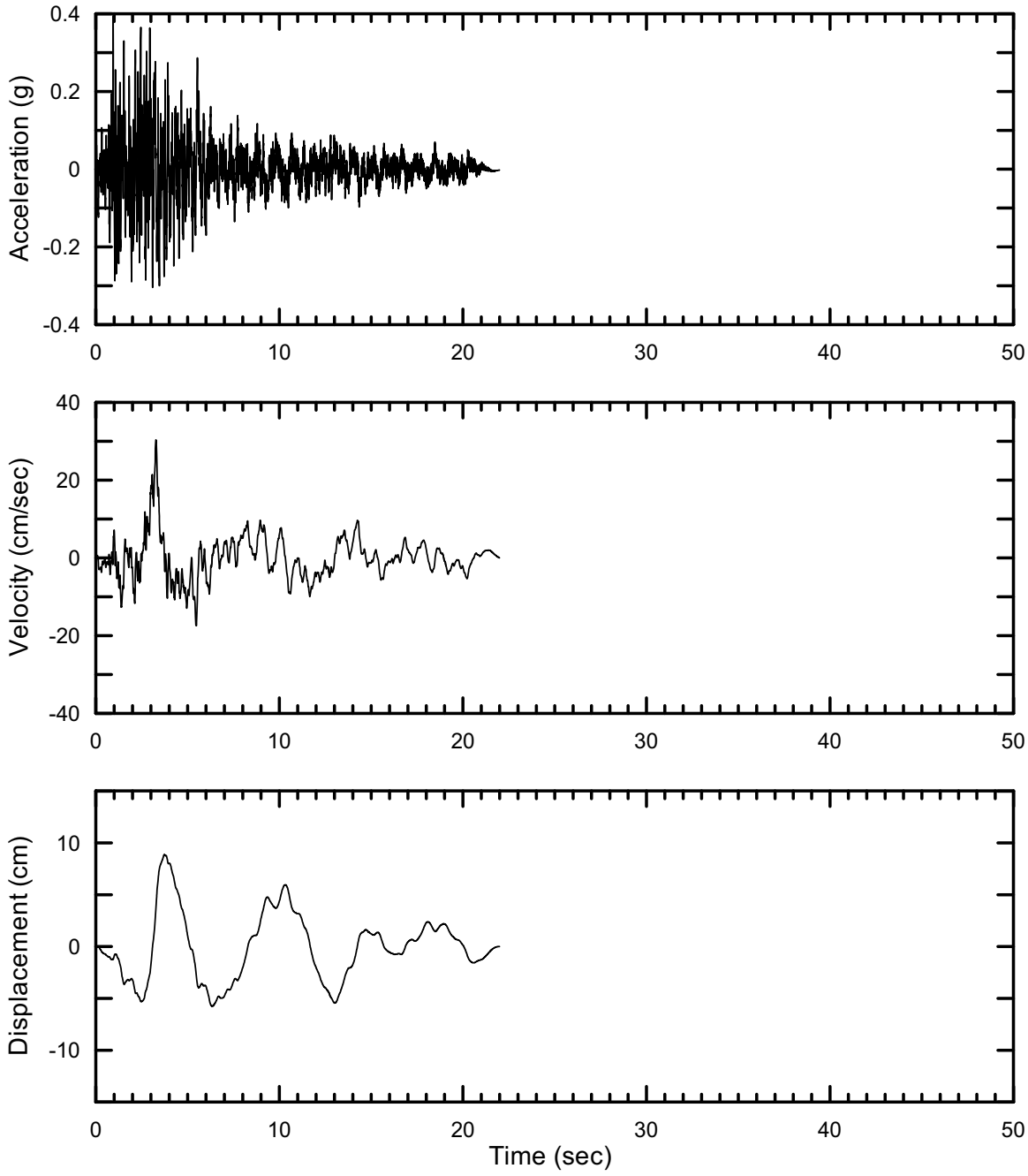

DTN: MO0410SDSTMHIS.005 [DIRS 172237]

Figure II-36. Point D/E Vertical Time Histories at an Annual Exceedance Probability of 5×10^{-4}, Set #4

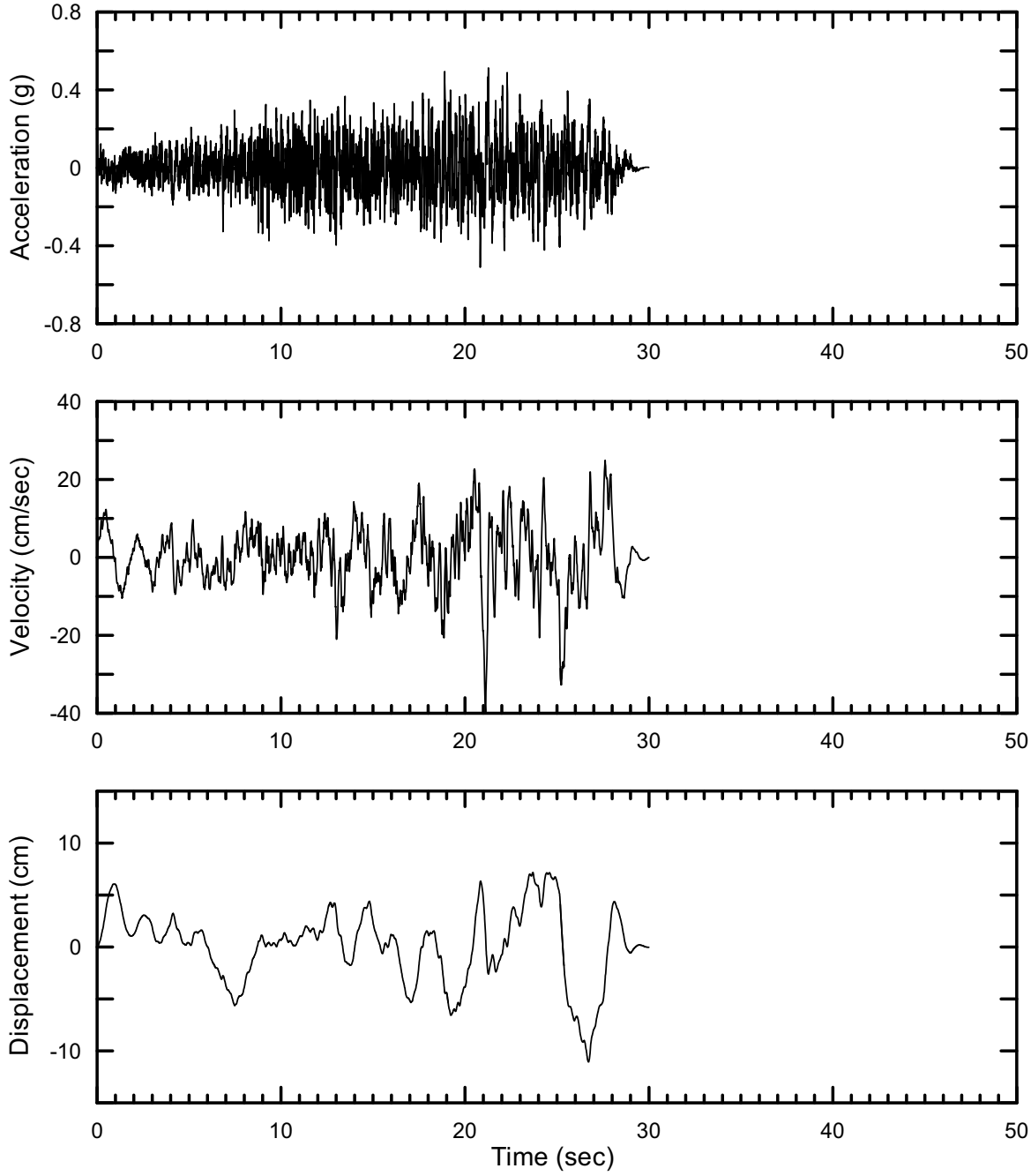

DTN: MO0410SDSTMHIS.005 [DIRS 172237]

Figure II-37. Point D/E Horizontal-1 Ti me Histories at an Annual Exceedance Probability of 5×10^{-4}, Set #5

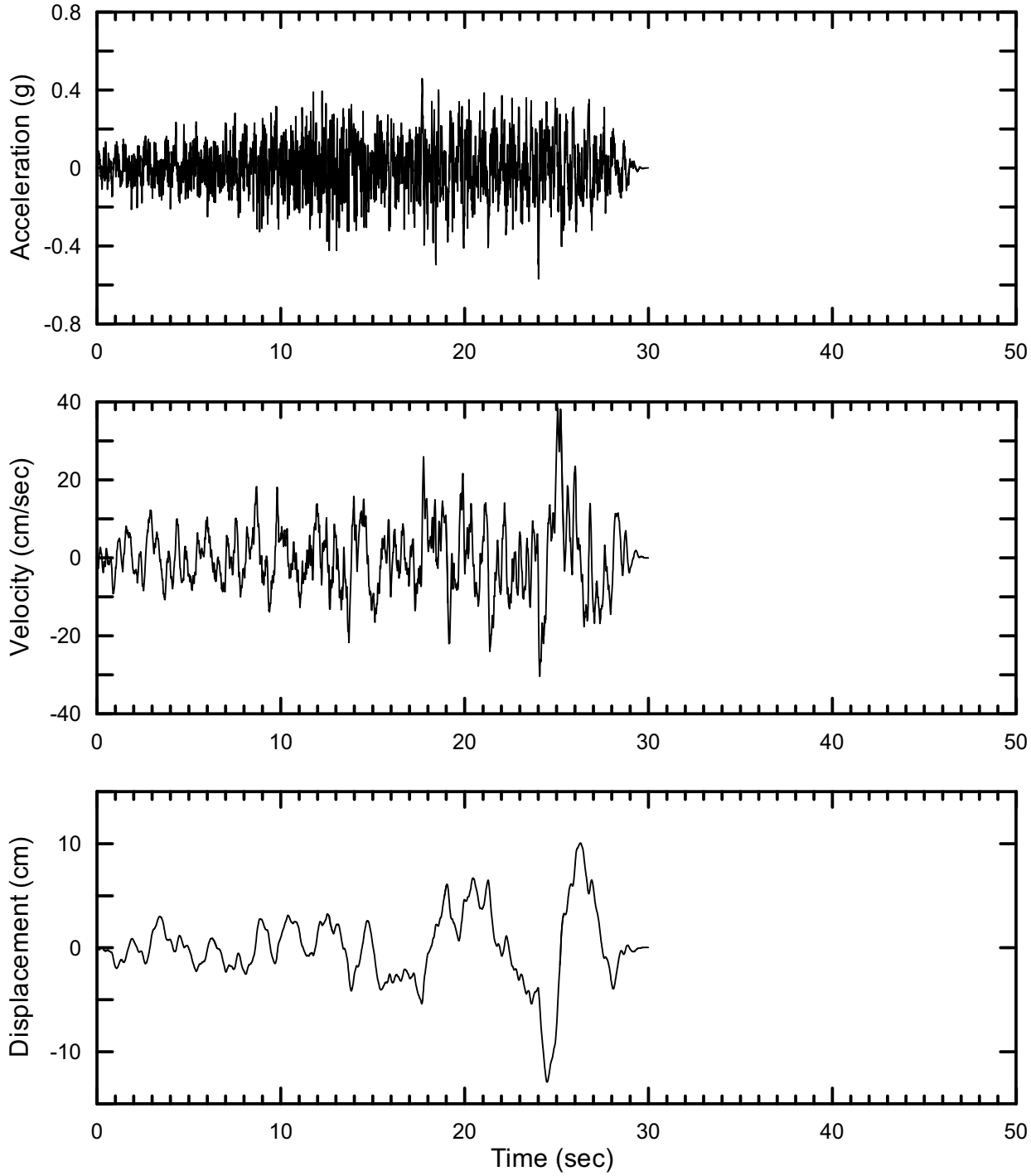

DTN: MO0410SDSTMHIS.005 [DIRS 172237]

Figure II-38. Point D/E Horizontal-2 Ti me Histories at an Annual Exceedance Probability of 5×10^{-4}, Set #5

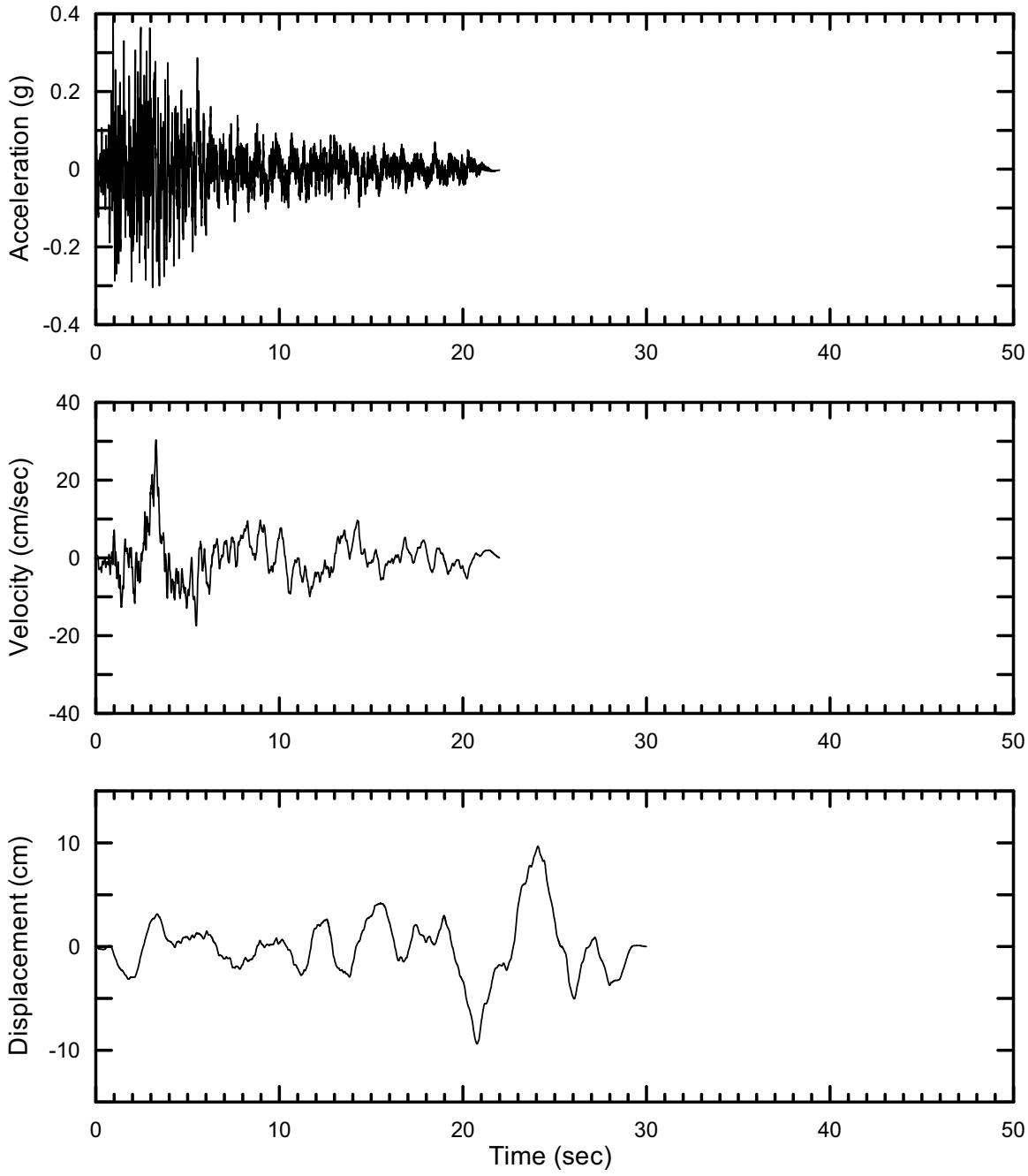

DTN: MO0410SDSTMHIS.005 [DIRS 172237]

Figure II-39. Point D/E Vertical Time Histories at an Annual Exceedance Probability of 5×10^{-4}, Set #5

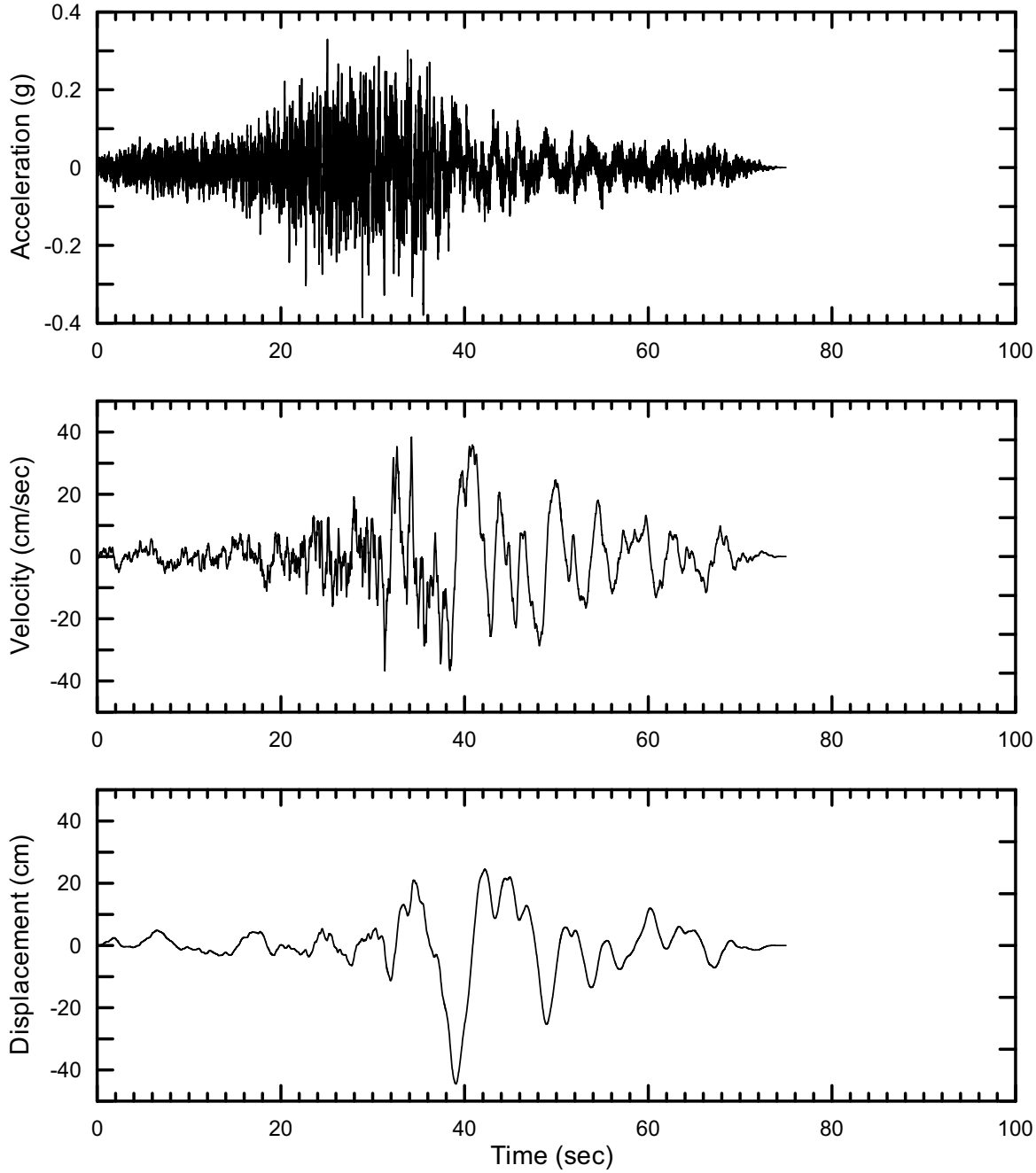

DTN: MO0410WHBDF104.002 [DIRS 172238]

Figure II-40. Point D/E Horizontal-1 Time Histories at an Annual Exceedance Probability of 10^{-4}

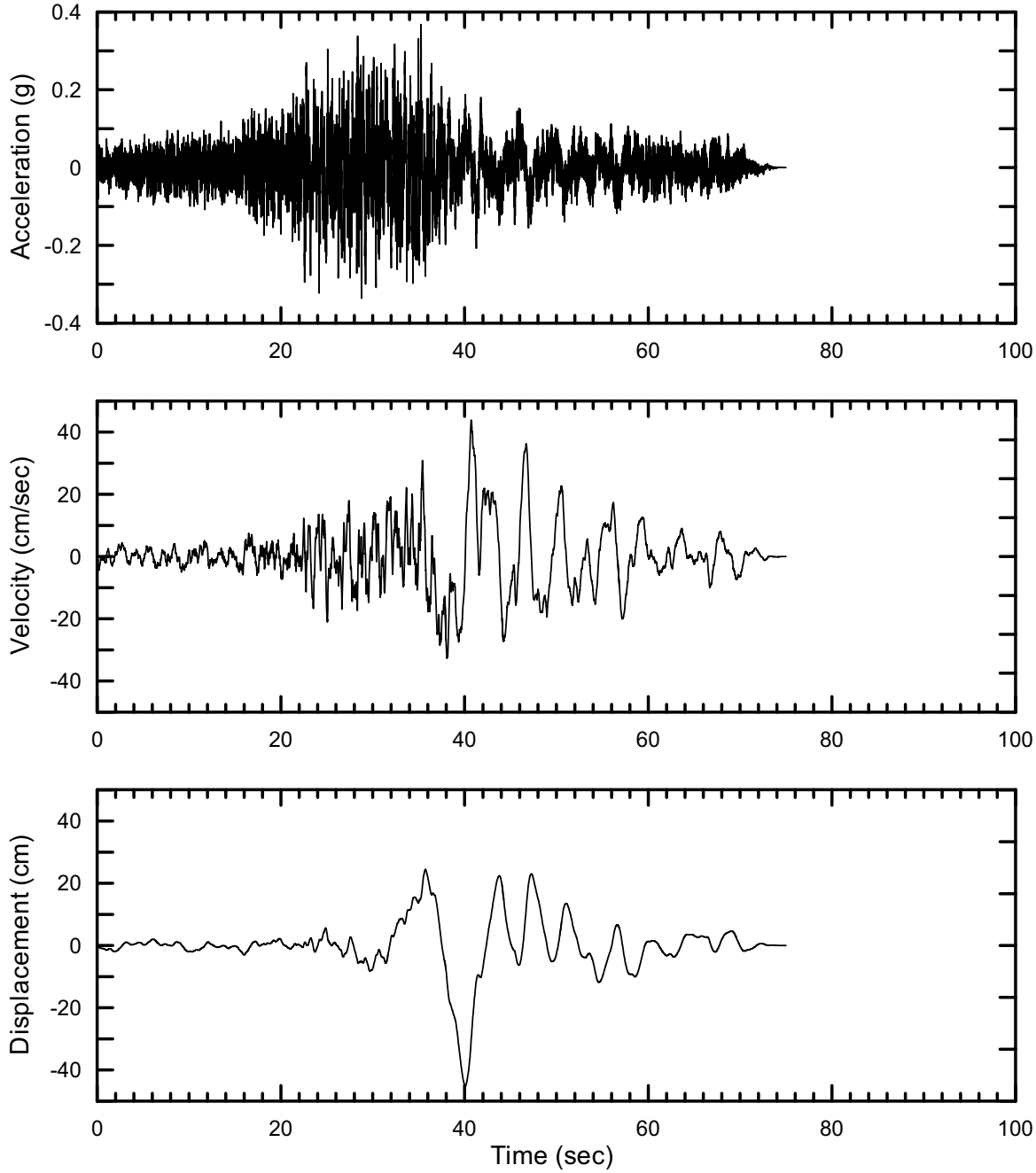

DTN: MO0410WHBDF104.002 [DIRS 172238]

Figure II-41. Point D/E Horizontal-2 Time Histories at an Annual Exceedance Probability of 10^{-4}

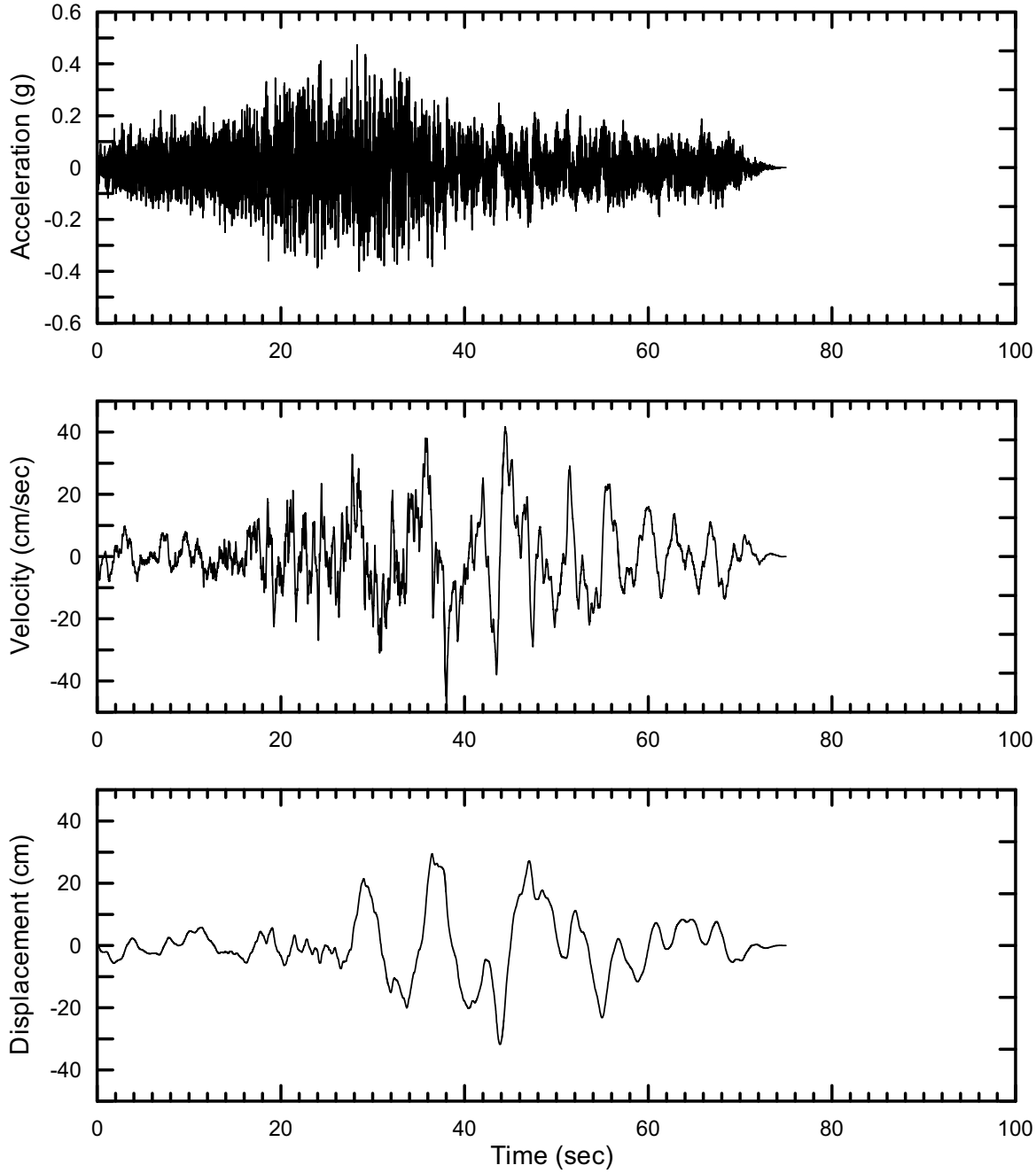

DTN: MO0410WHBDF104.002 [DIRS 172238]

Figure II-42. Point D/E Vertical Time Histories at an Annual Exceedance Probability of 10^{-4}

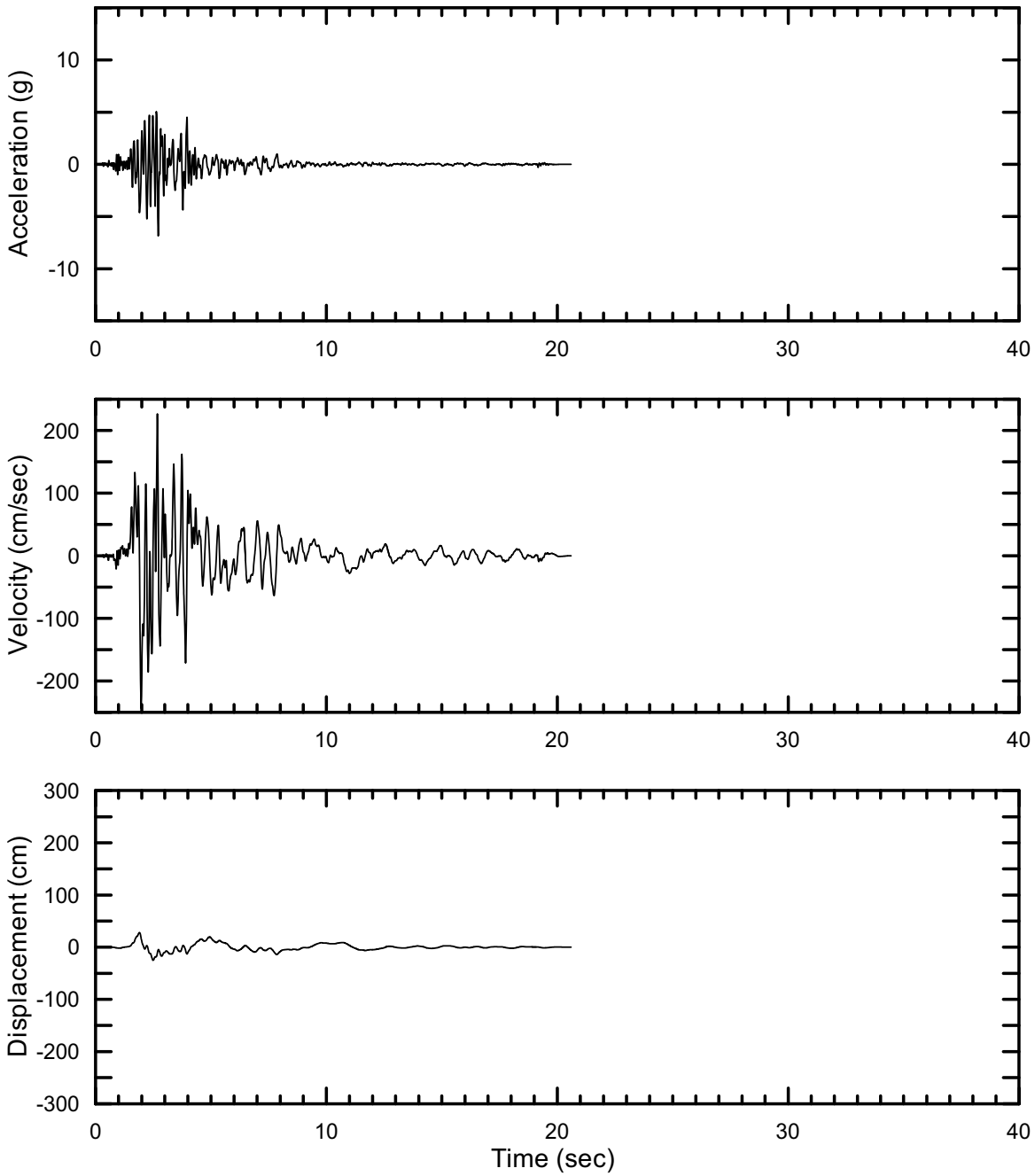

DTN: MO0301TMHIS106.001 [DIRS 161868]

Figure II-43. Point B Horizontal-1 Time Histories (PGV Scaled) at an Annual Exceedance Probability of 10^{-6}, Set #1

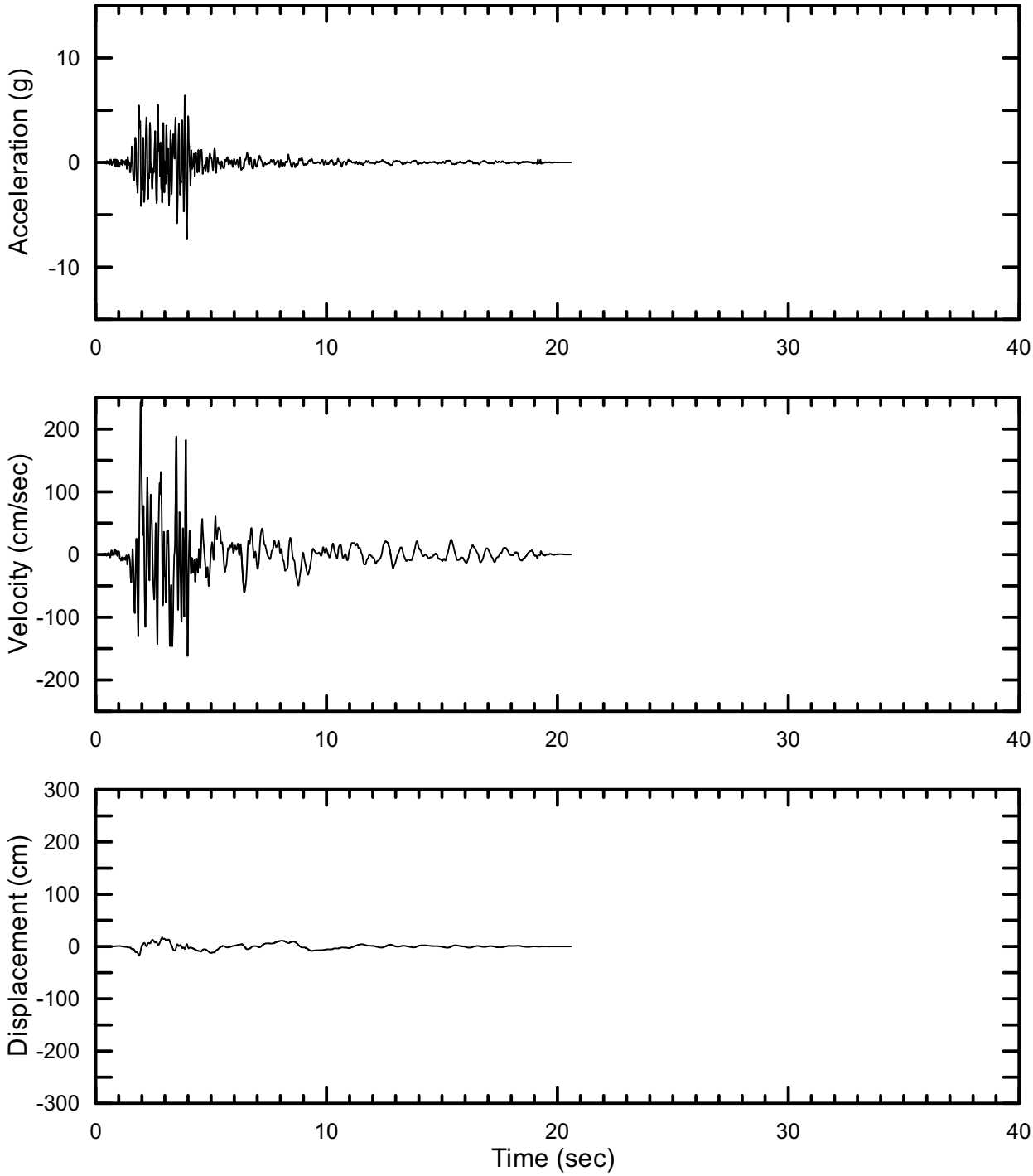

DTN: MO0301TMHIS106.001 [DIRS 161868]

Figure II-44. Point B Horizontal-2 Time Histories (PGV Scaled) at an Annual Exceedance Probability of 10^{-6}, Set #1

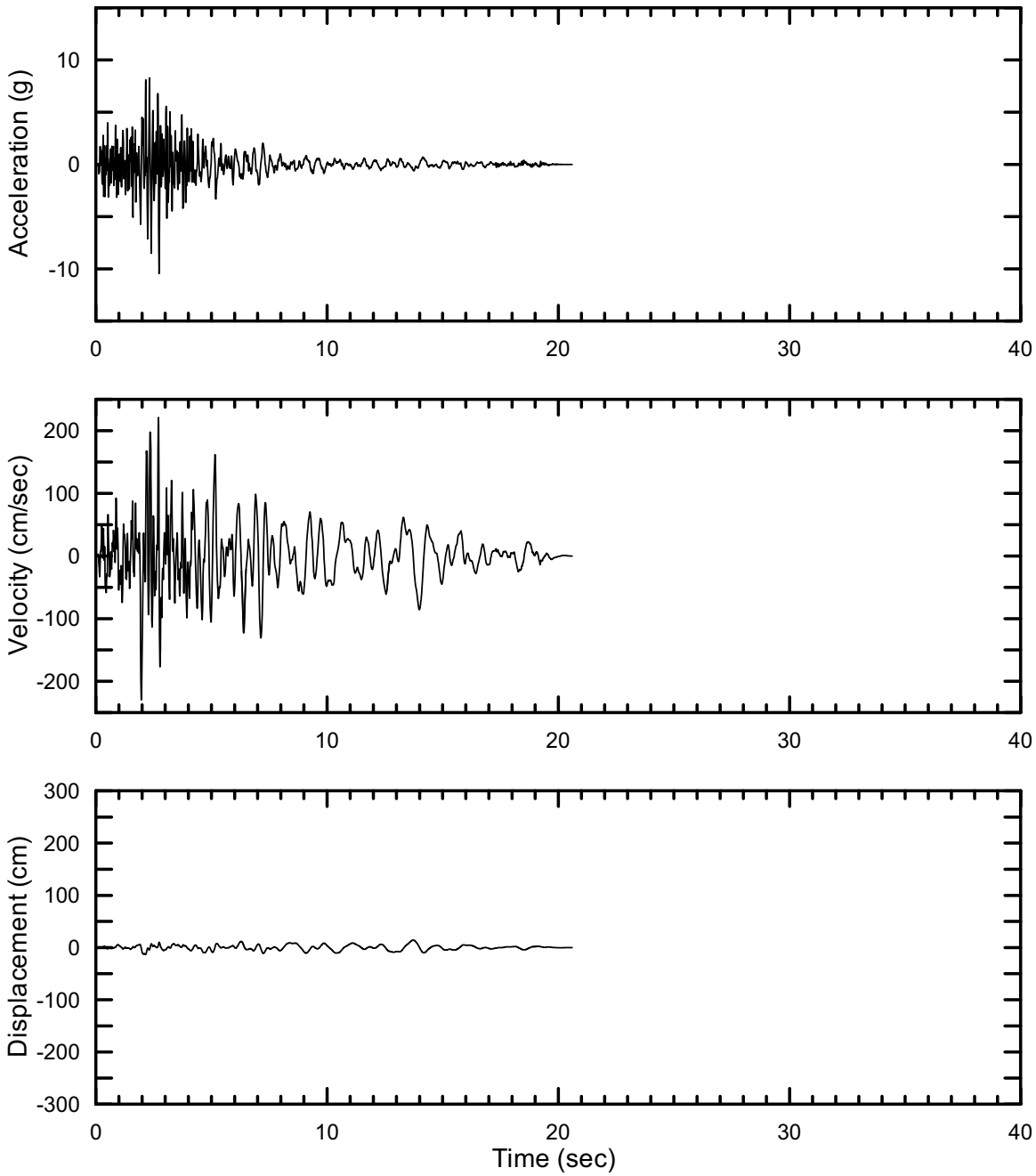

DTN: MO0301TMHIS106.001 [DIRS 161868]

Figure II-45. Point B Vertical Time Histories (PGV Scaled) at an Annual Exceedance Probability of 10^{-6}, Set #1

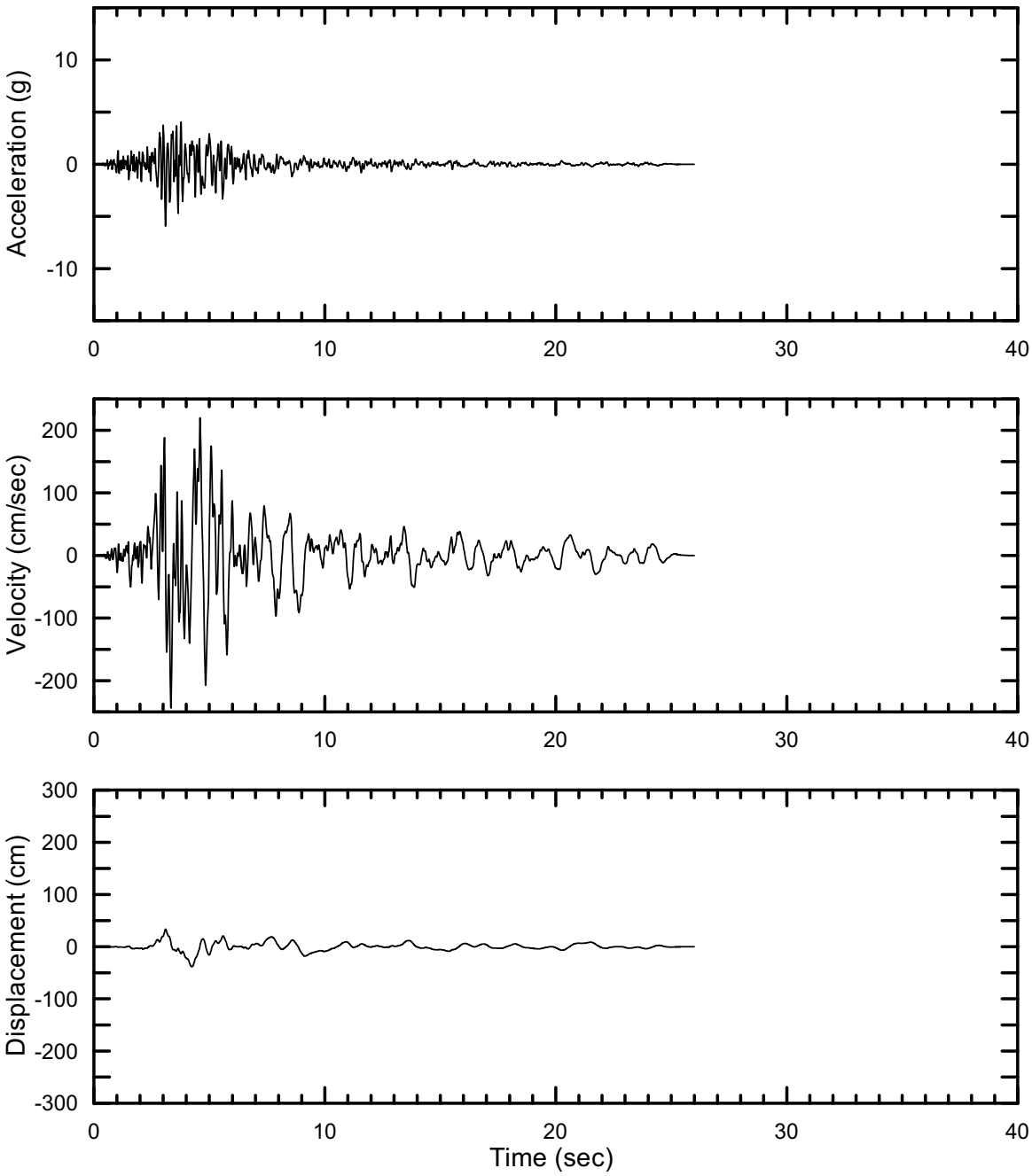

DTN: MO0301TMHIS106.001 [DIRS 161868]

Figure II-46. Point B Horizontal-1 Time Histories (PGV Scaled) at an Annual Exceedance Probability of 10^{-6}, Set #2

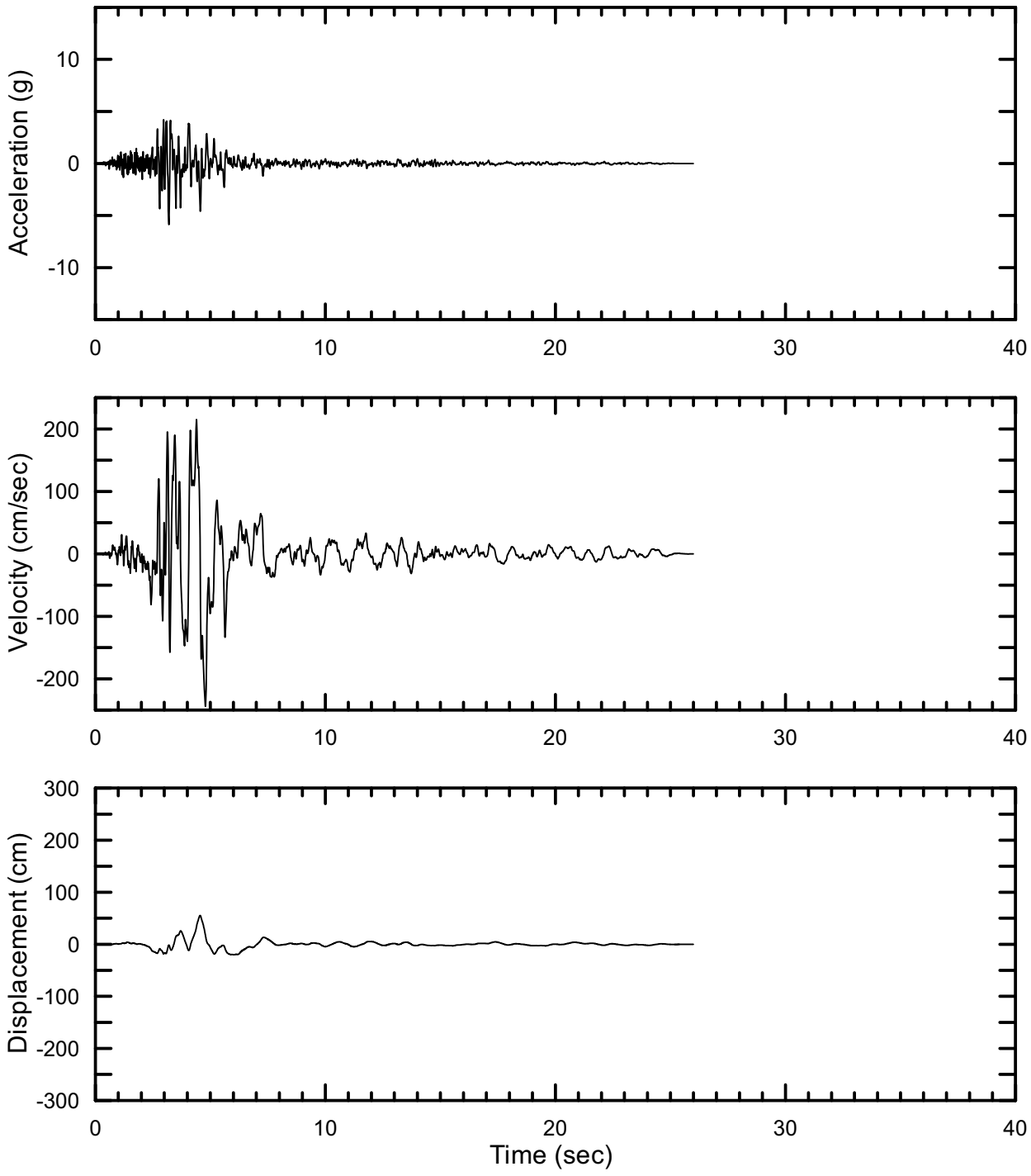

DTN: MO0301TMHIS106.001 [DIRS 161868]

Figure II-47. Point B Horizontal-2 Time Histories (PGV Scaled) at an Annual Exceedance Probability of 10^{-6}, Set #2

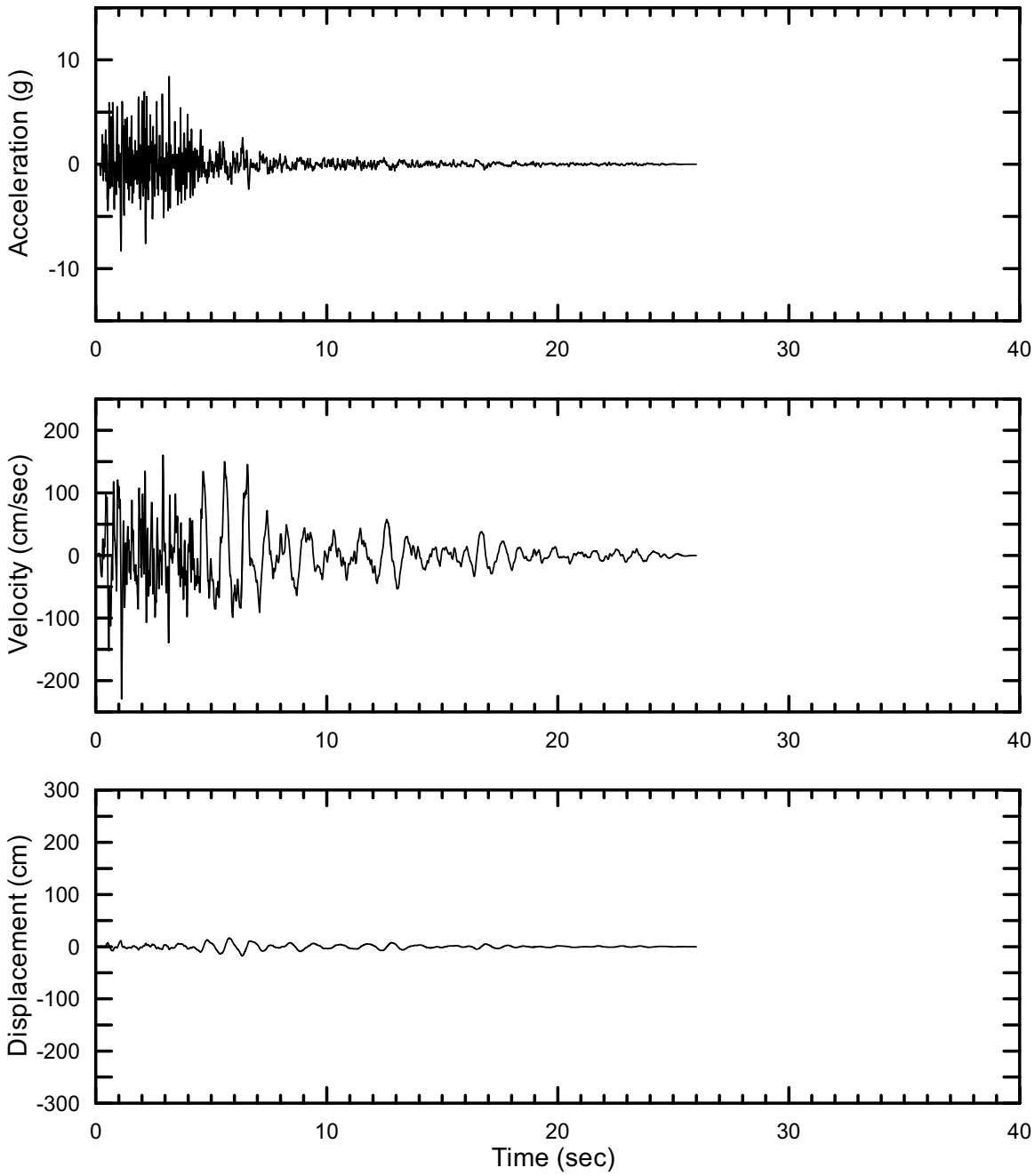

DTN: MO0301TMHIS106.001 [DIRS 161868]

Figure II-48. Point B Vertical Time Histories (PGV Scaled) at an Annual Exceedance Probability of 10^{-6}, Set #2

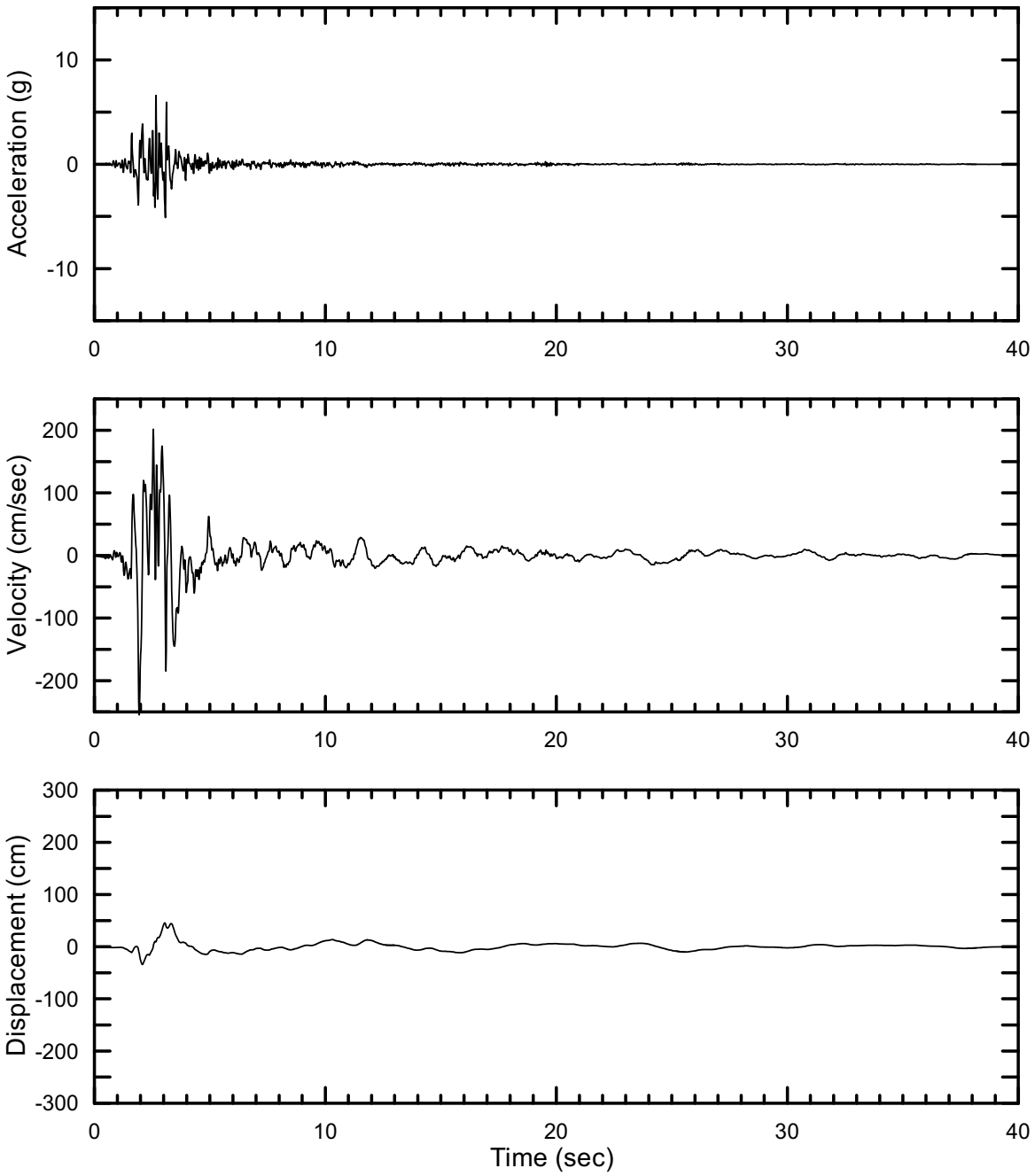

DTN: MO0301TMHIS106.001 [DIRS 161868]

Figure II-49. Point B Horizontal-1 Time Histories (PGV Scaled) at an Annual Exceedance Probability of 10^{-6}, Set #3

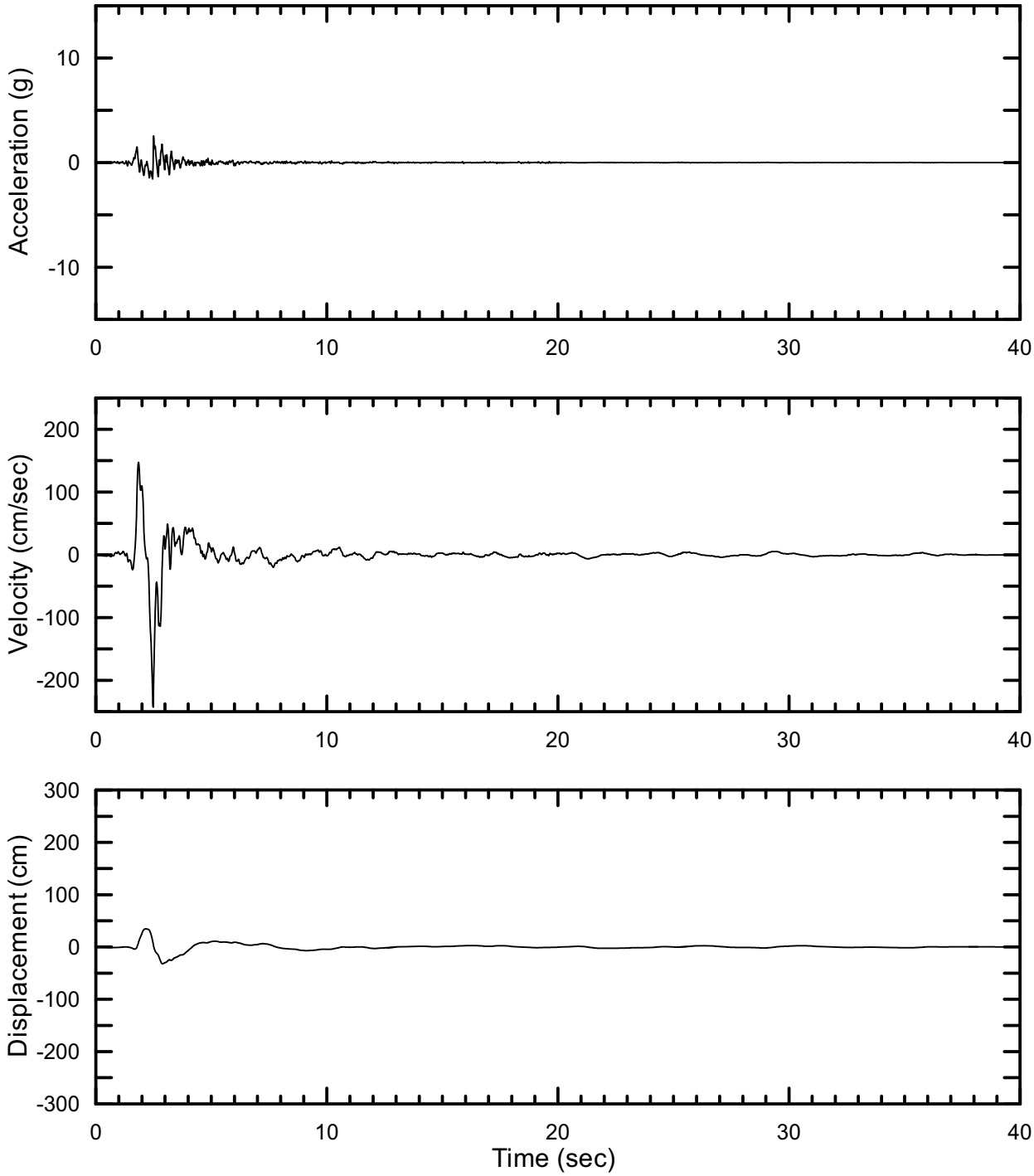

DTN: MO0301TMHIS106.001 [DIRS 161868]

Figure II-50. Point B Horizontal-2 Time Histories (PGV Scaled) at an Annual Exceedance Probability of 10^{-6}, Set #3

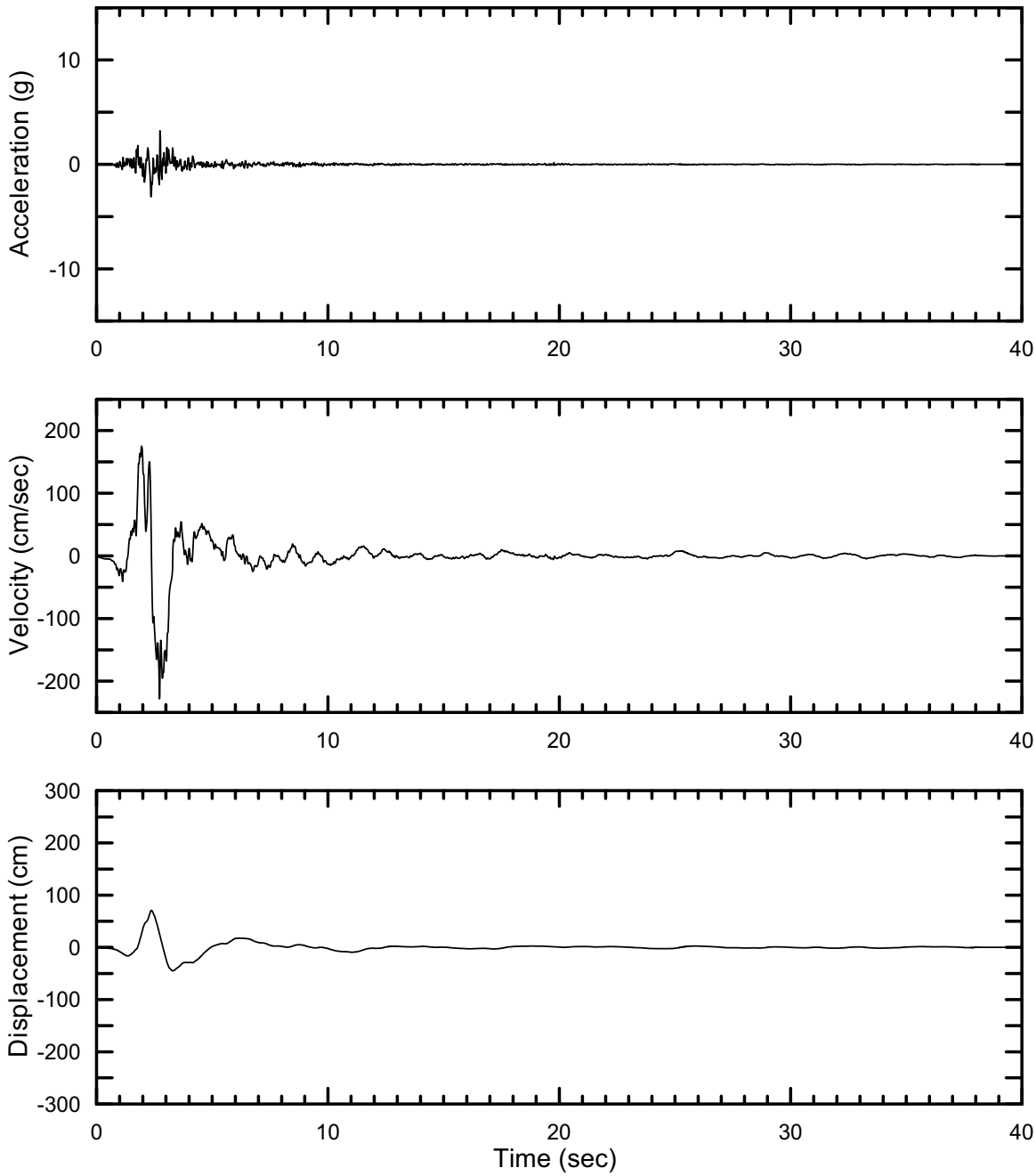

DTN: MO0301TMHIS106.001 [DIRS 161868]

Figure II-51. Point B Vertical Time Histories (PGV Scaled) at an Annual Exceedance Probability of 10^{-6}, Set #3

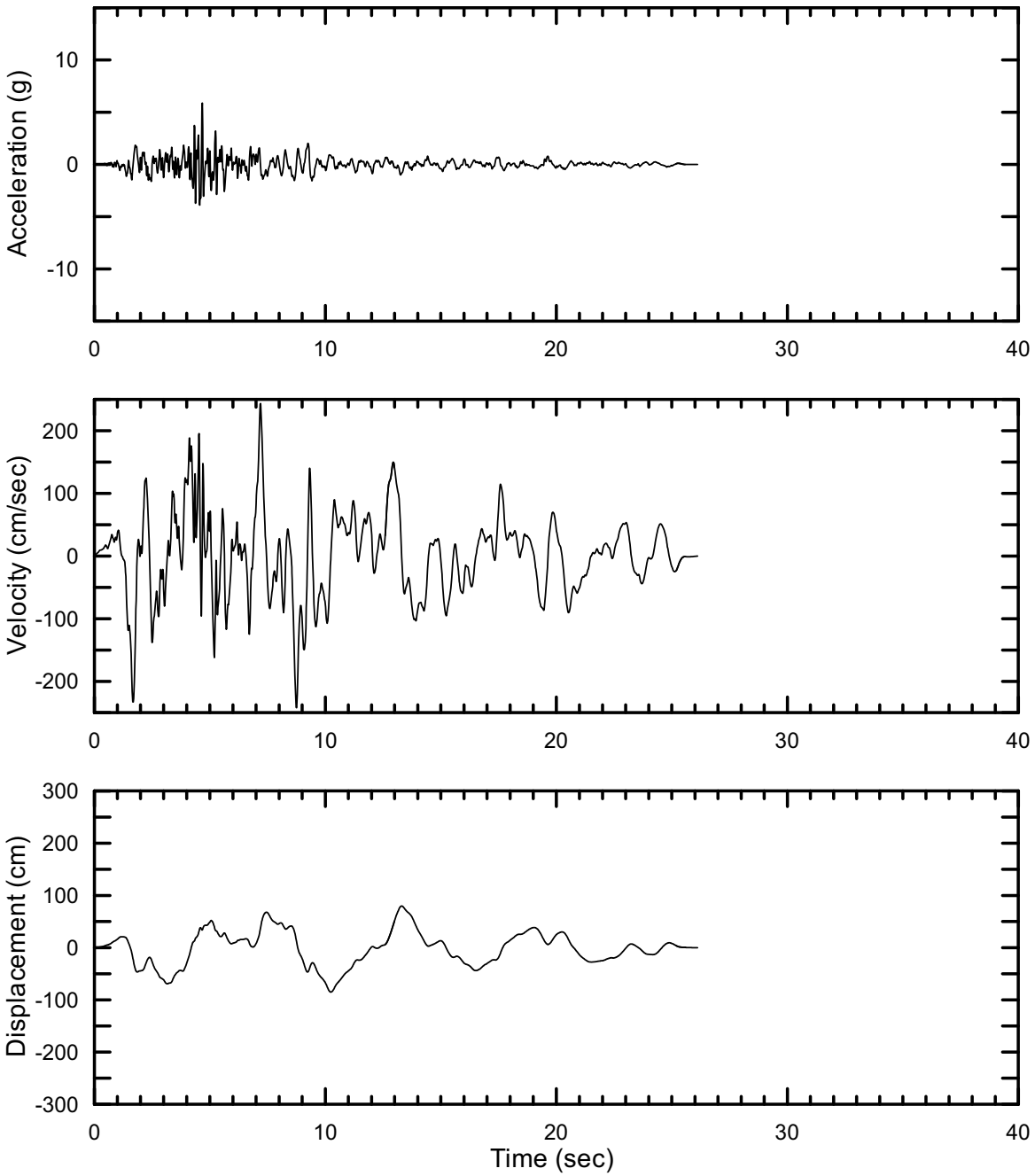

DTN: MO0301TMHIS106.001 [DIRS 161868]

Figure II-52. Point B Horizontal-1 Time Histories (PGV Scaled) at an Annual Exceedance Probability of 10^{-6}, Set #4

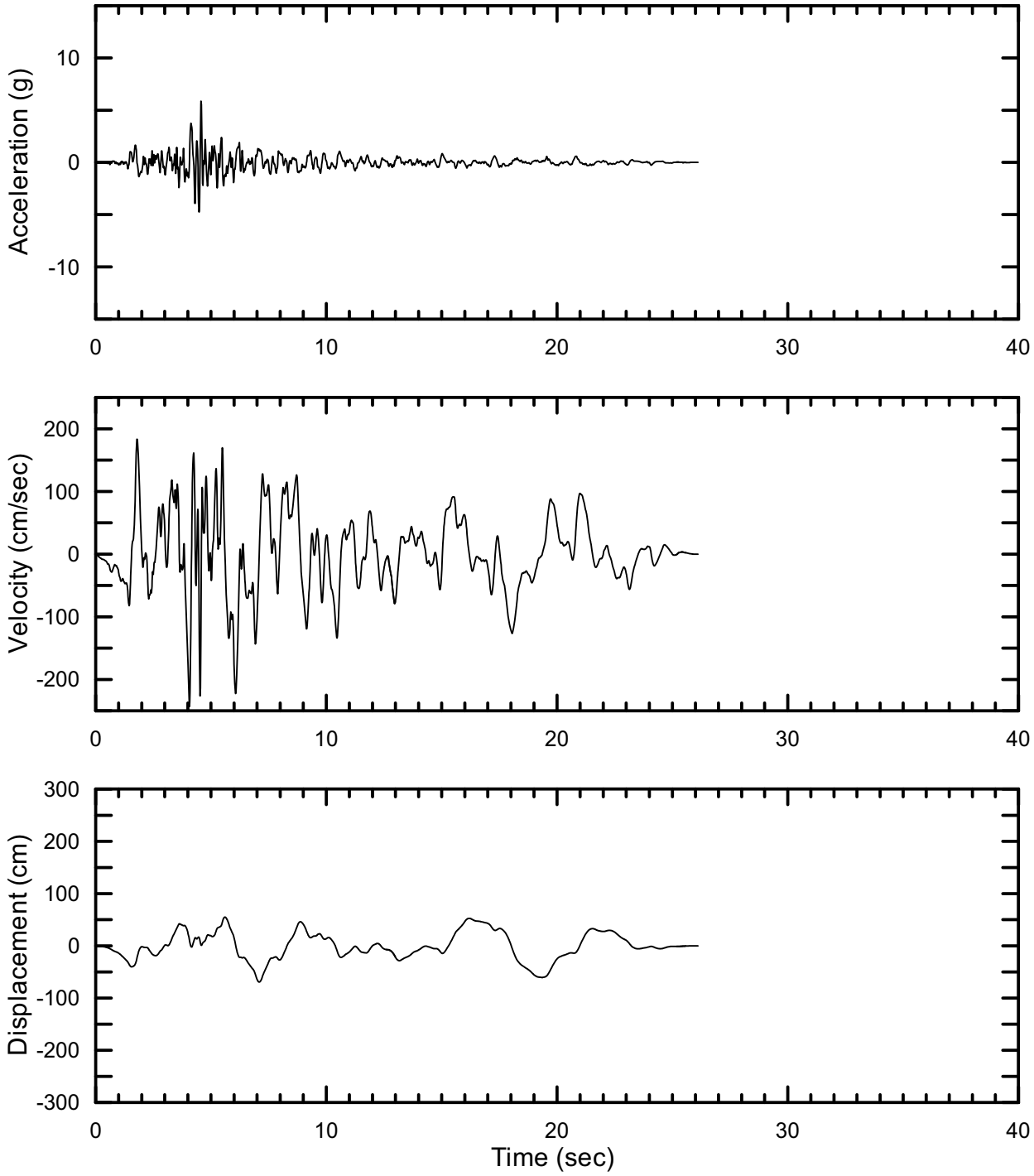

DTN: MO0301TMHIS106.001 [DIRS 161868]

Figure II-53. Point B Horizontal-2 Time Histories (PGV Scaled) at an Annual Exceedance Probability of 10^{-6}, Set #4

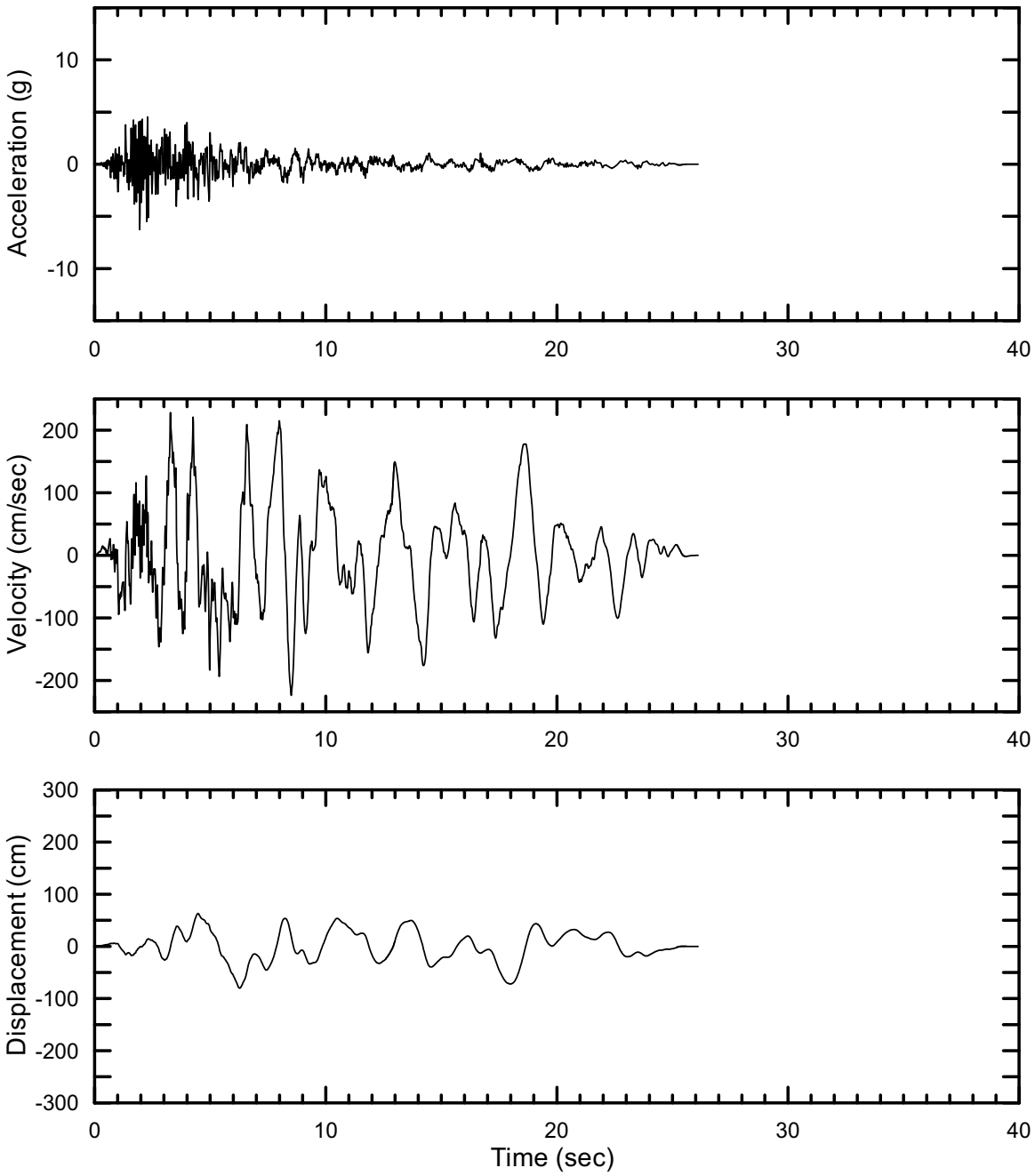

DTN: MO0301TMHIS106.001 [DIRS 161868]

Figure II-54. Point B Vertical Time Histories (PGV Scaled) at an Annual Exceedance Probability of 10^{-6}, Set #4

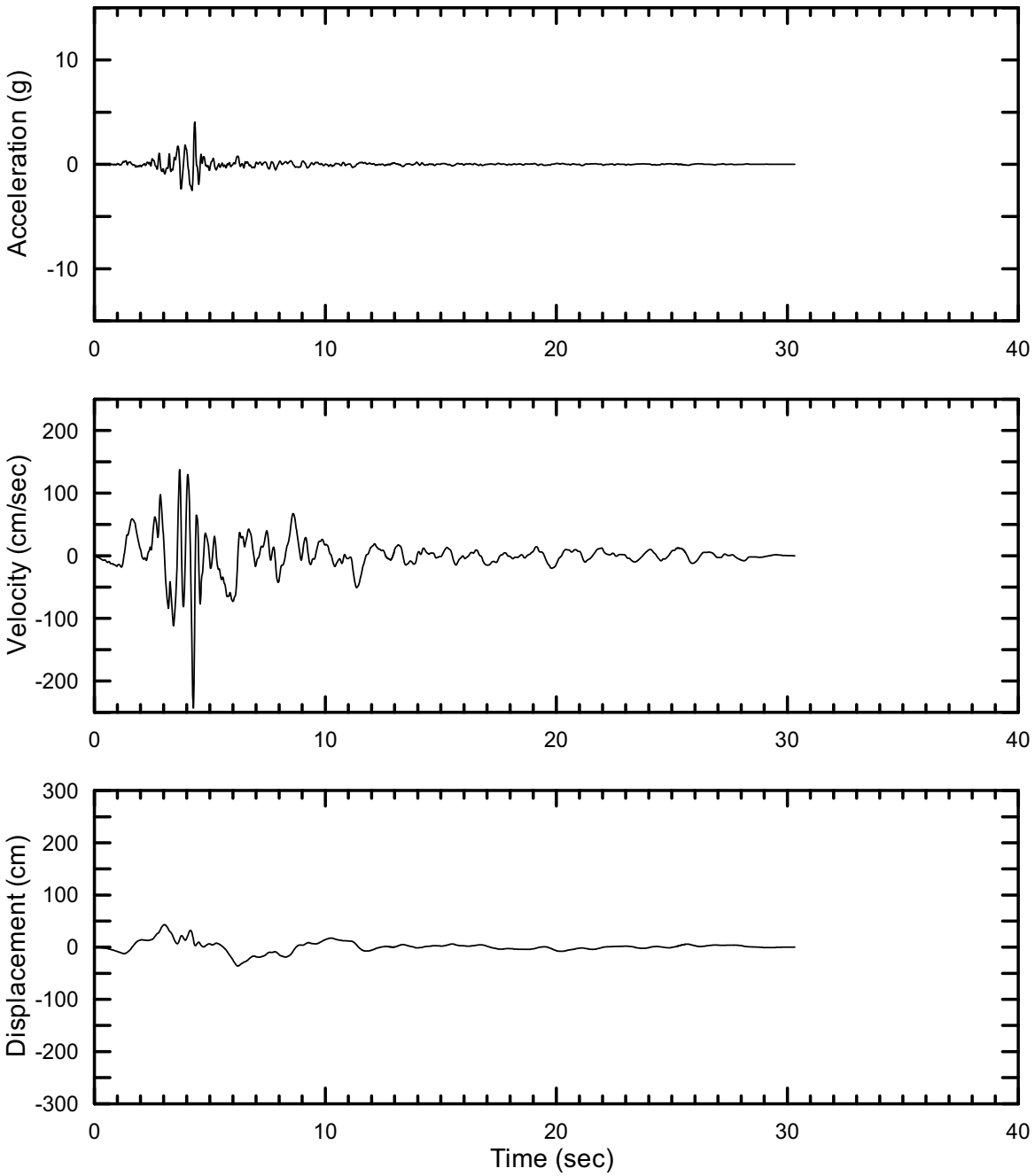

DTN: MO0301TMHIS106.001 [DIRS 161868]

Figure II-55. Point B Horizontal-1 Time Histories (PGV Scaled) at an Annual Exceedance Probability of 10^{-6}, Set #5

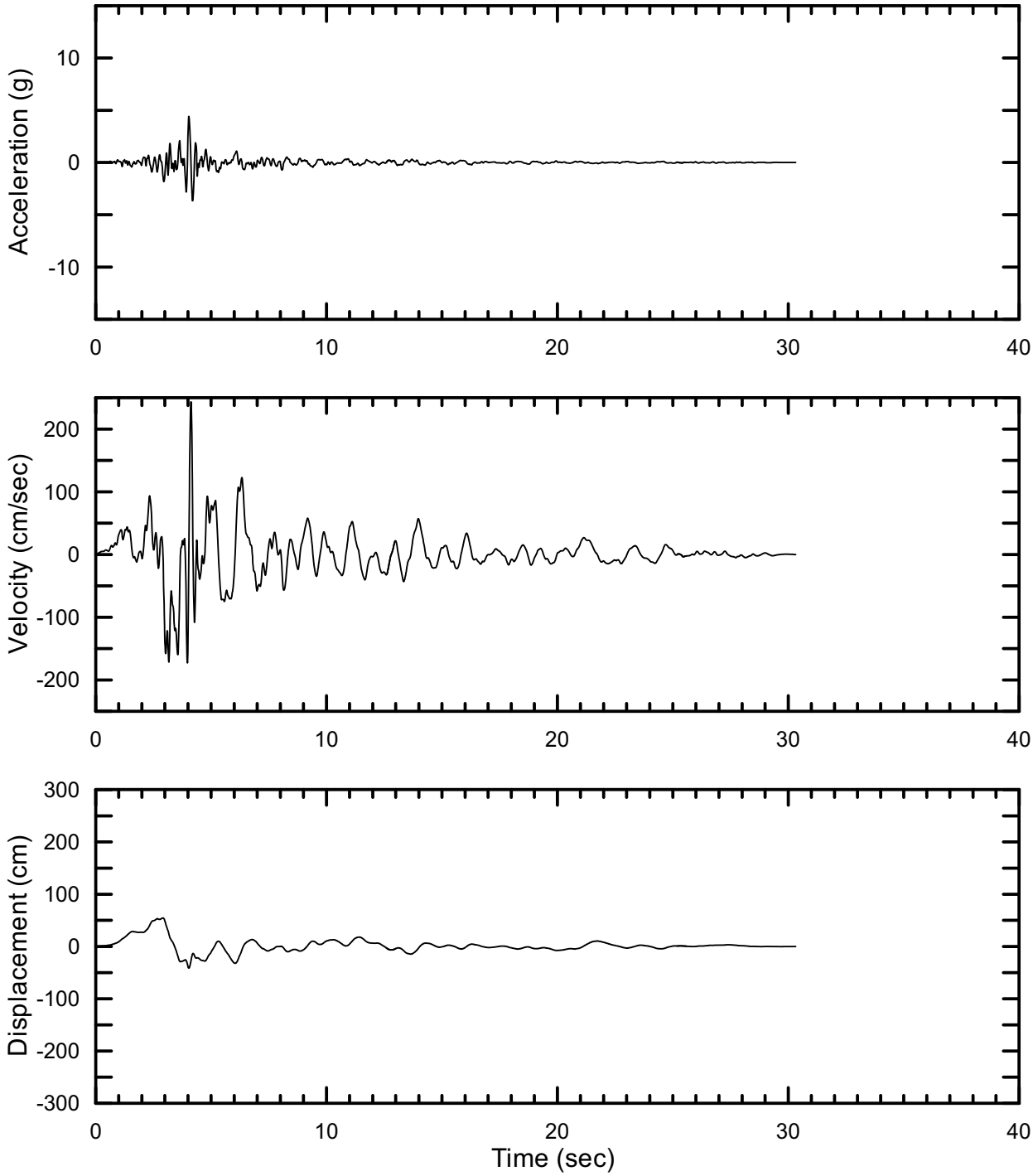

DTN: MO0301TMHIS106.001 [DIRS 161868]

Figure II-56. Point B Horizontal-2 Time Histories (PGV Scaled) at an Annual Exceedance Probability of 10^{-6}, Set #5

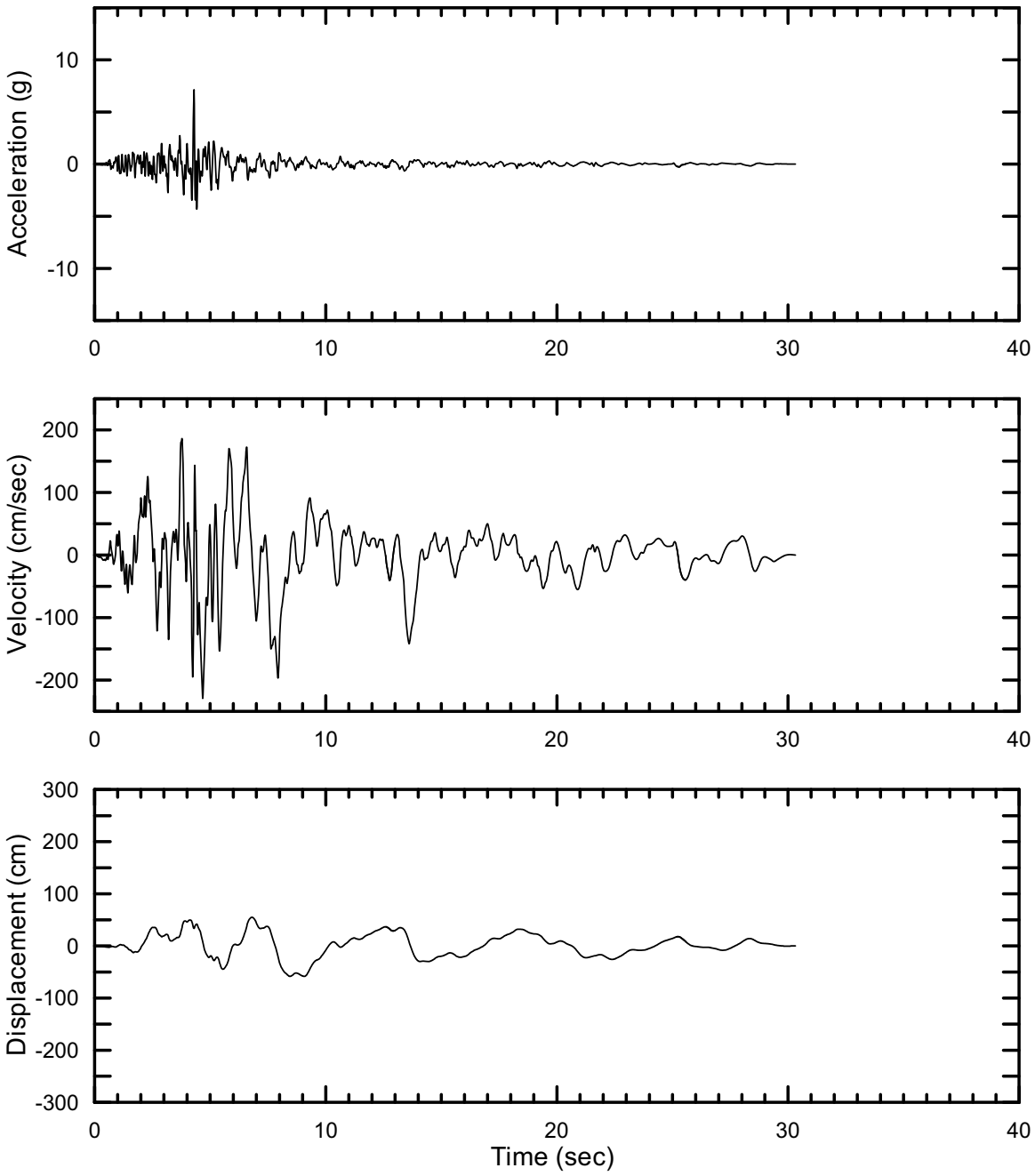

DTN: MO0301TMHIS106.001 [DIRS 161868]

Figure II-57. Point B Vertical Time Histories (PGV Scaled) at an Annual Exceedance Probability of 10^{-6}, Set #5

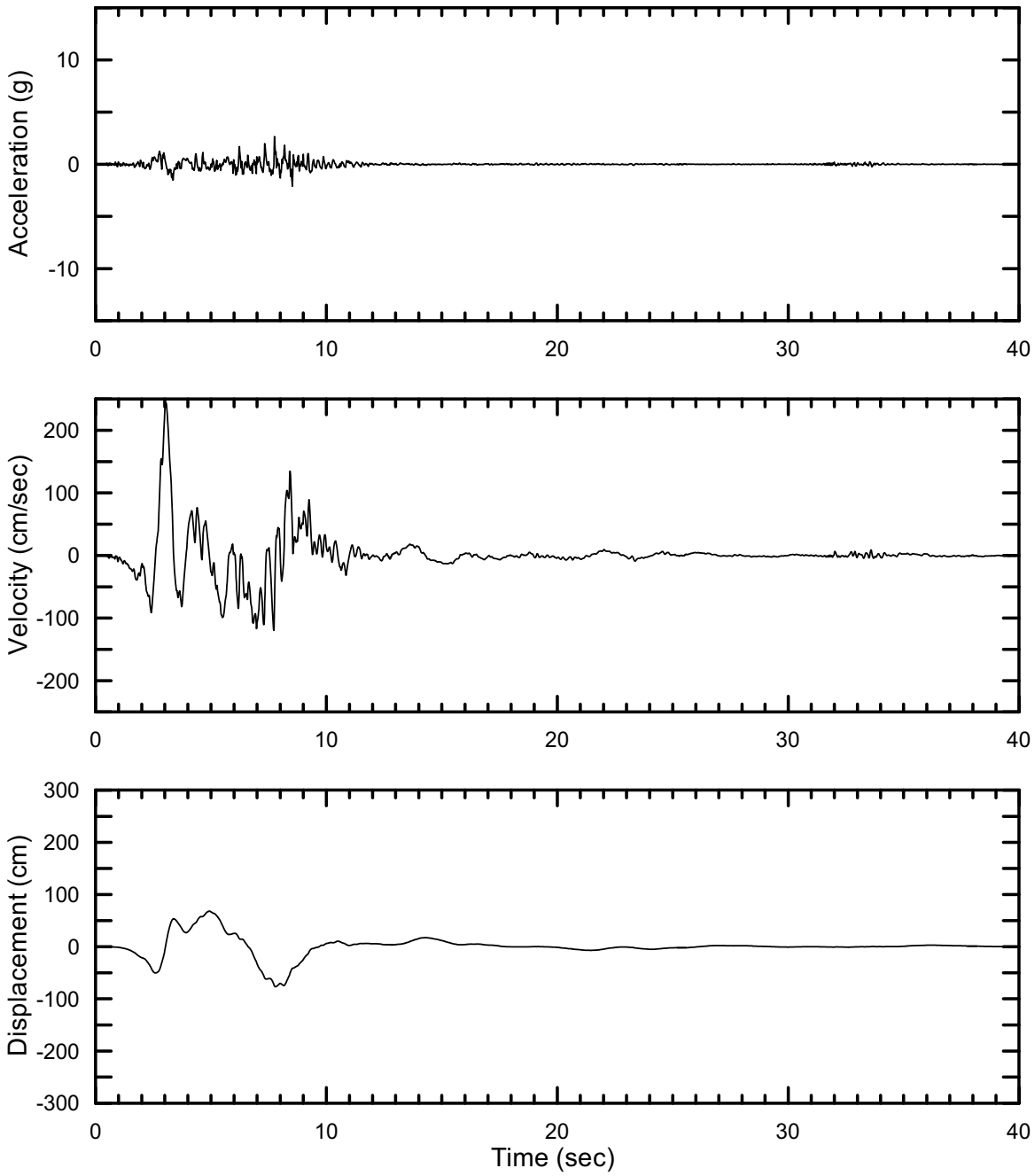

DTN: MO0301TMHIS106.001 [DIRS 161868]

Figure II-58. Point B Horizontal-1 Time Histories (PGV Scaled) at an Annual Exceedance Probability of 10^{-6}, Set #6

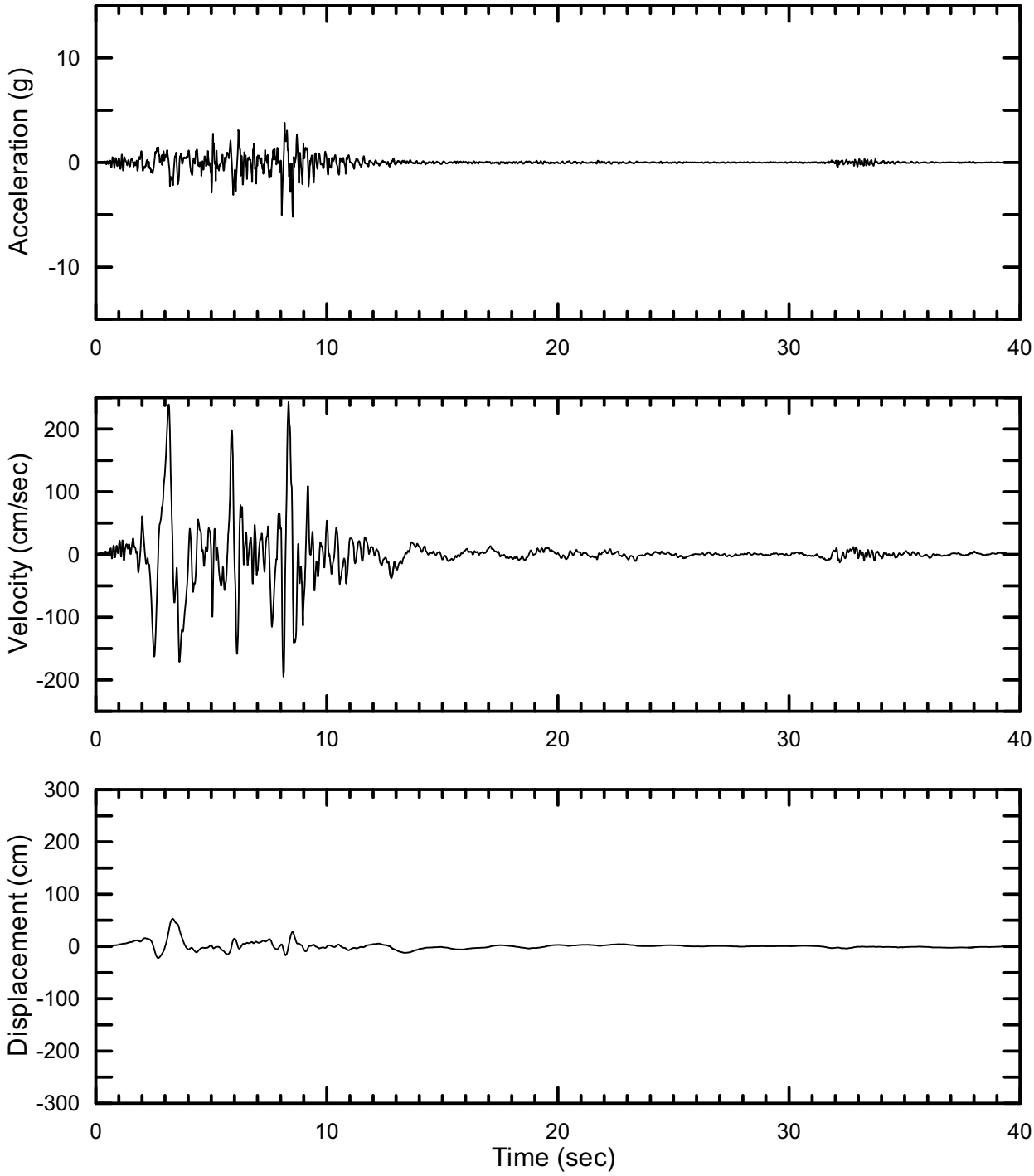

DTN: MO0301TMHIS106.001 [DIRS 161868]

Figure II-59. Point B Horizontal-2 Time Histories (PGV Scaled) at an Annual Exceedance Probability of 10^{-6}, Set #6

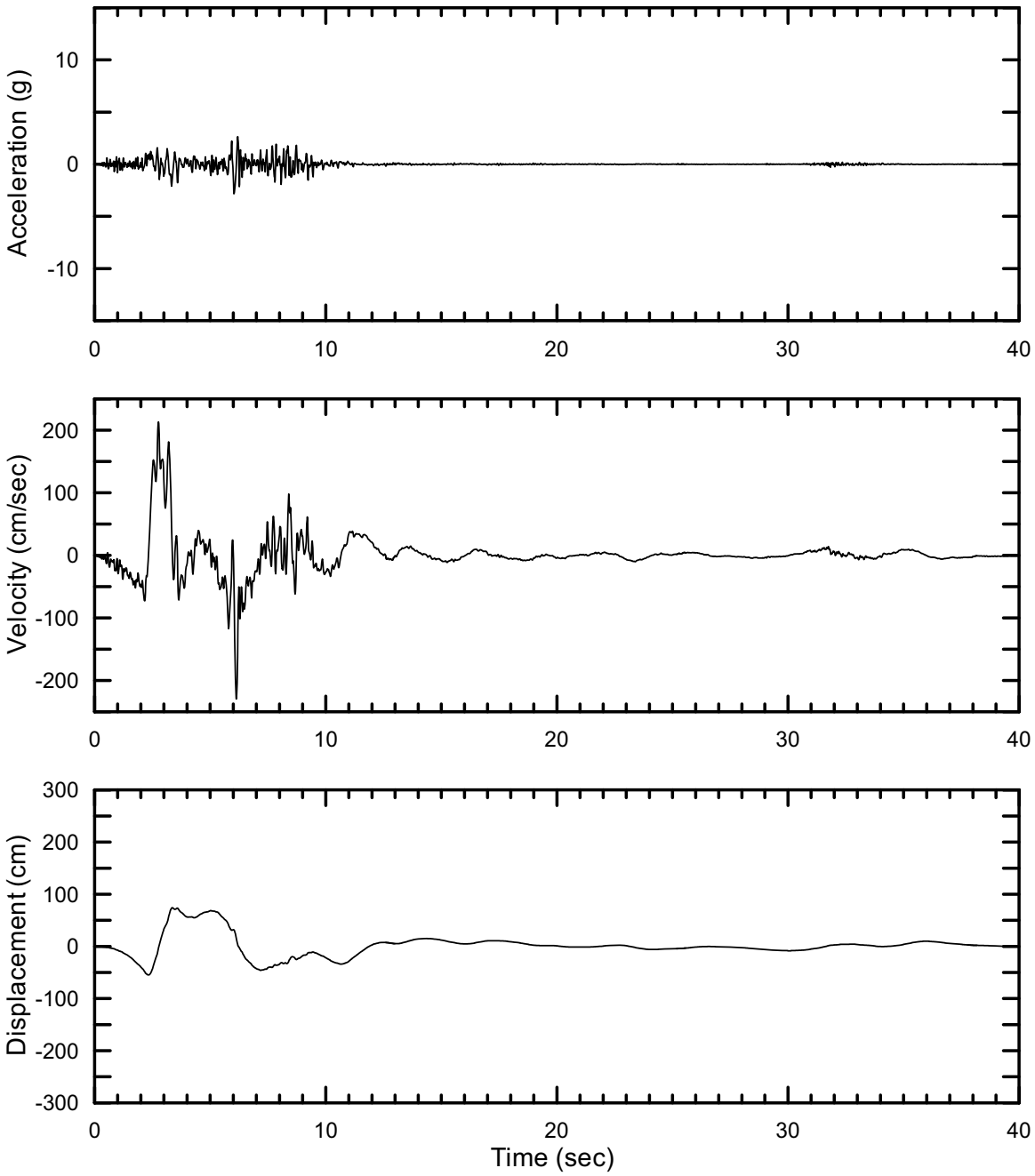

DTN: MO0301TMHIS106.001 [DIRS 161868]

Figure II-60. Point B Vertical Time Histories (PGV Scaled) at an Annual Exceedance Probability of 10^{-6}, Set #6

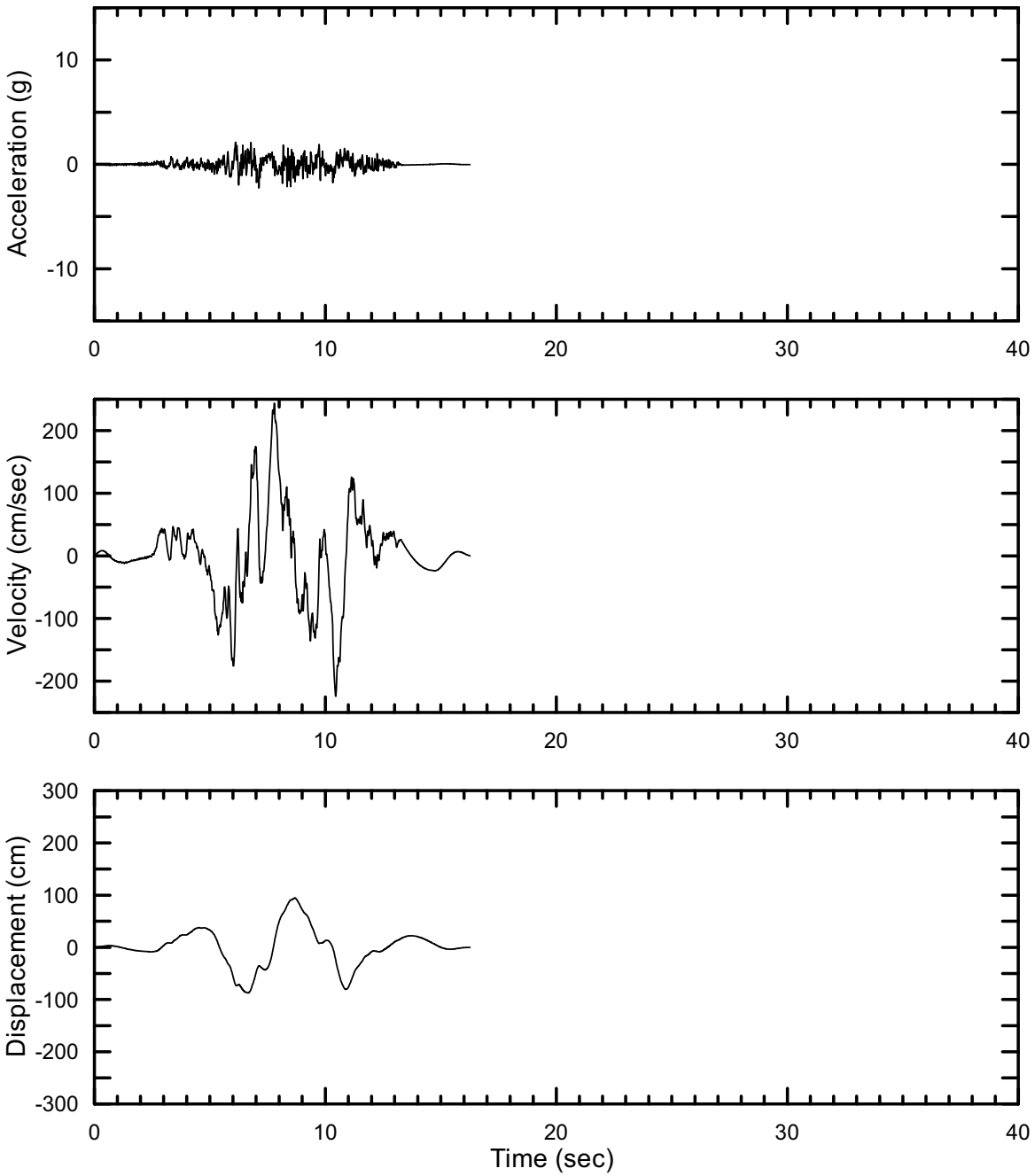

DTN: MO0301TMHIS106.001 [DIRS 161868]

Figure II-61. Point B Horizontal-1 Time Histories (PGV Scaled) at an Annual Exceedance Probability of 10^{-6}, Set #7

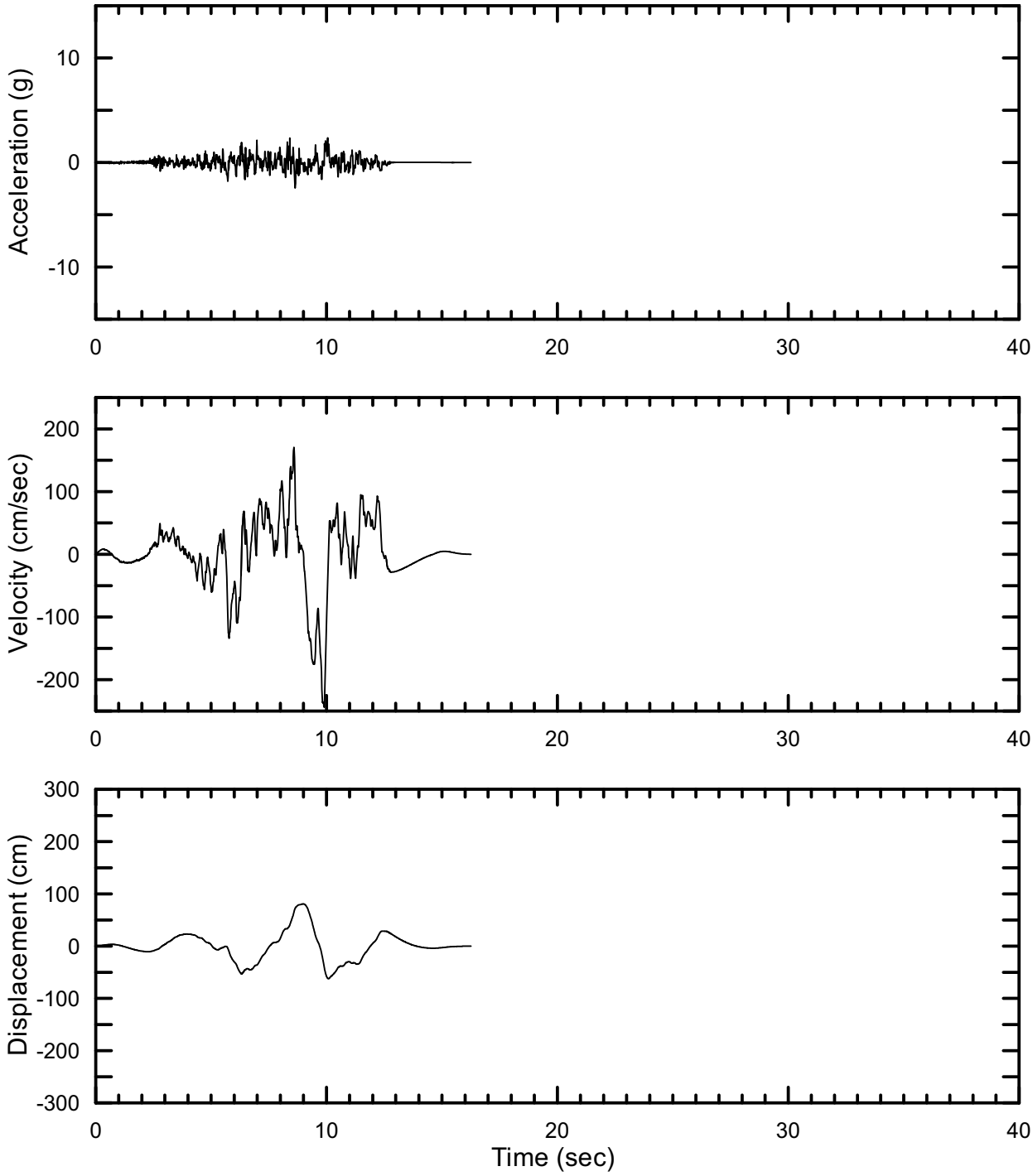

DTN: MO0301TMHIS106.001 [DIRS 161868]

Figure II-62. Point B Horizontal-2 Time Histories (PGV Scaled) at an Annual Exceedance Probability of 10^{-6}, Set #7

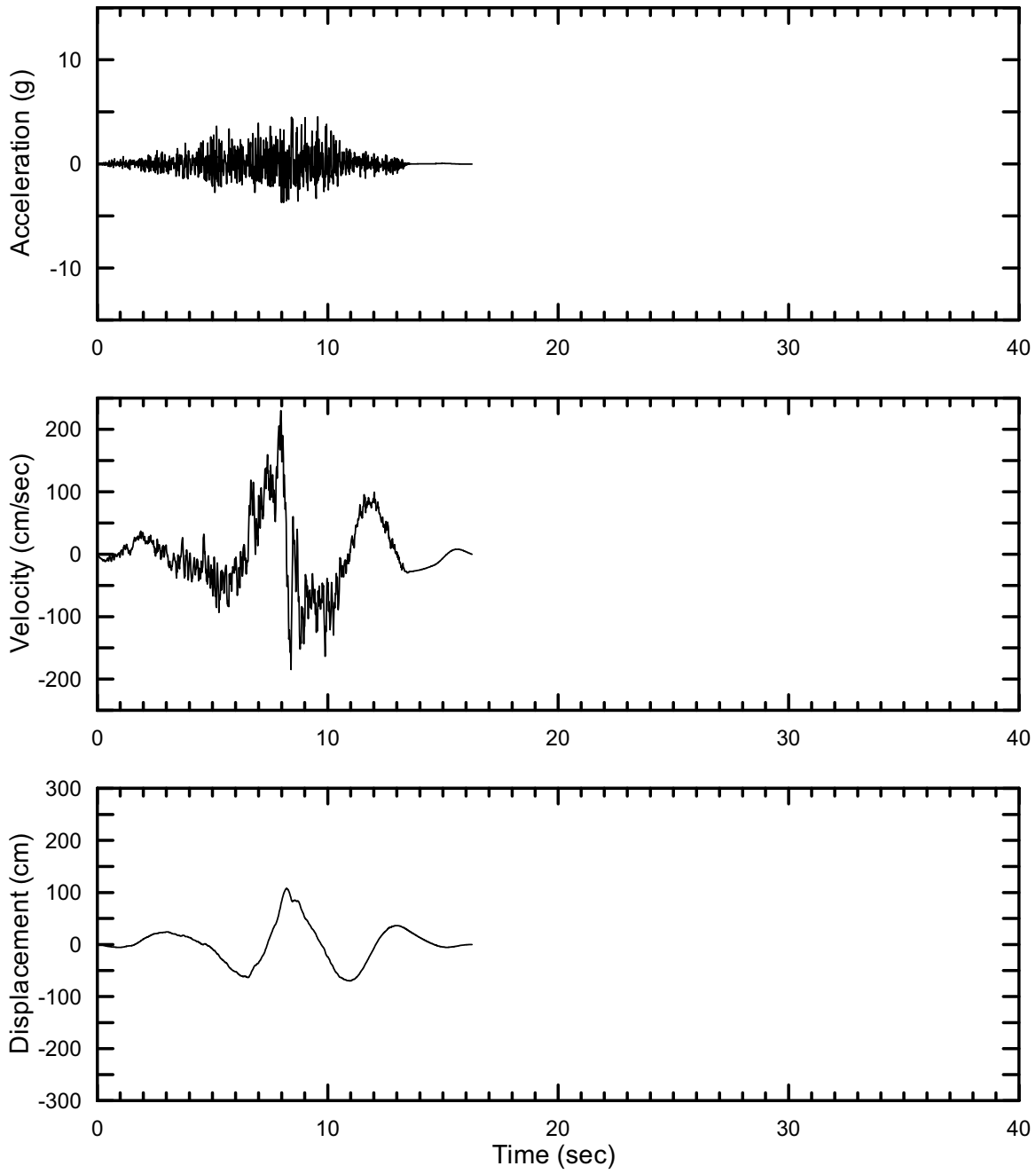

DTN: MO0301TMHIS106.001 [DIRS 161868]

Figure II-63. Point B Vertical Time Histories (PGV Scaled) at an Annual Exceedance Probability of 10^{-6}, Set #7

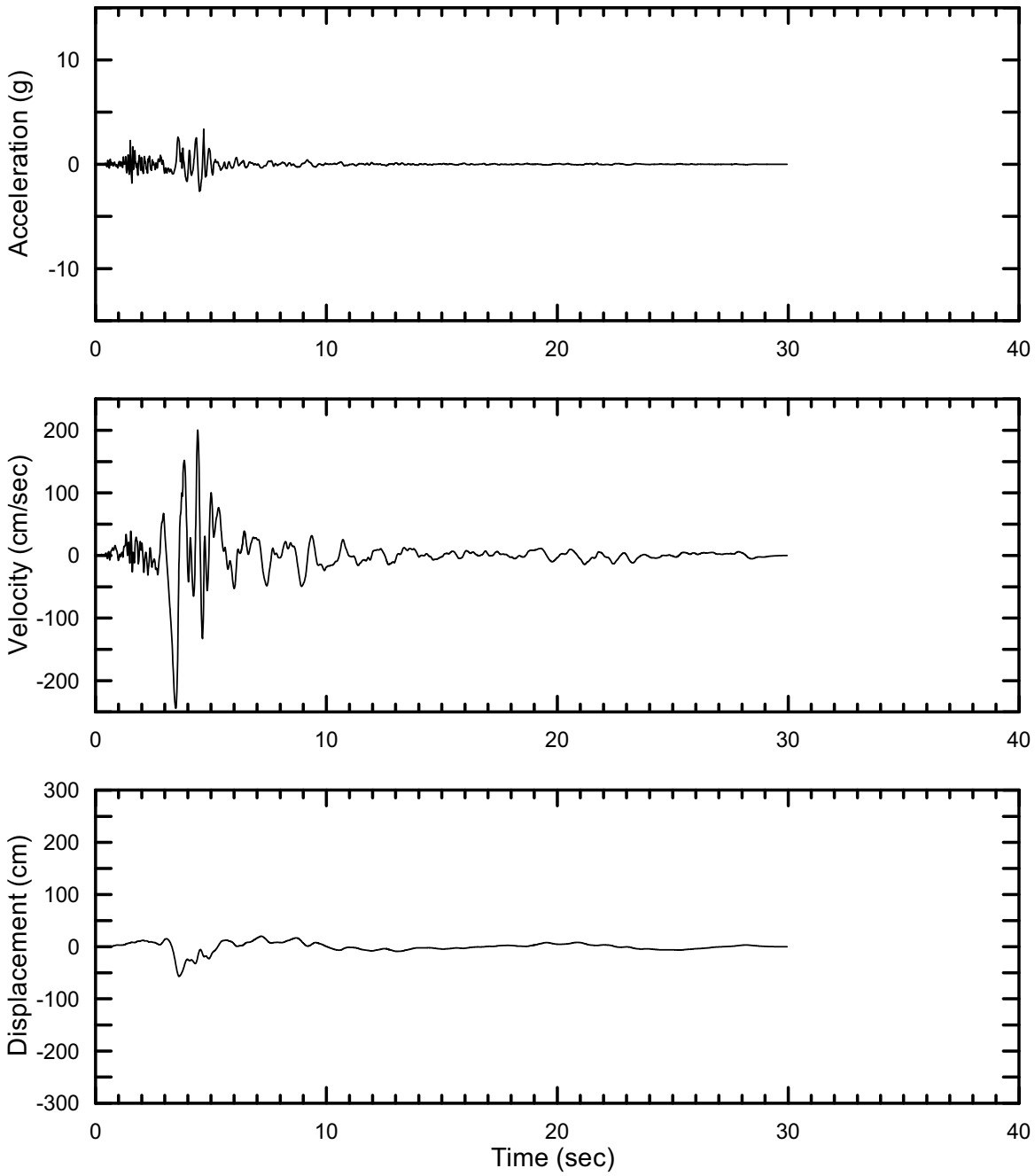

DTN: MO0301TMHIS106.001 [DIRS 161868]

Figure II-64. Point B Horizontal-1 Time Histories (PGV Scaled) at an Annual Exceedance Probability of 10^{-6}, Set #8

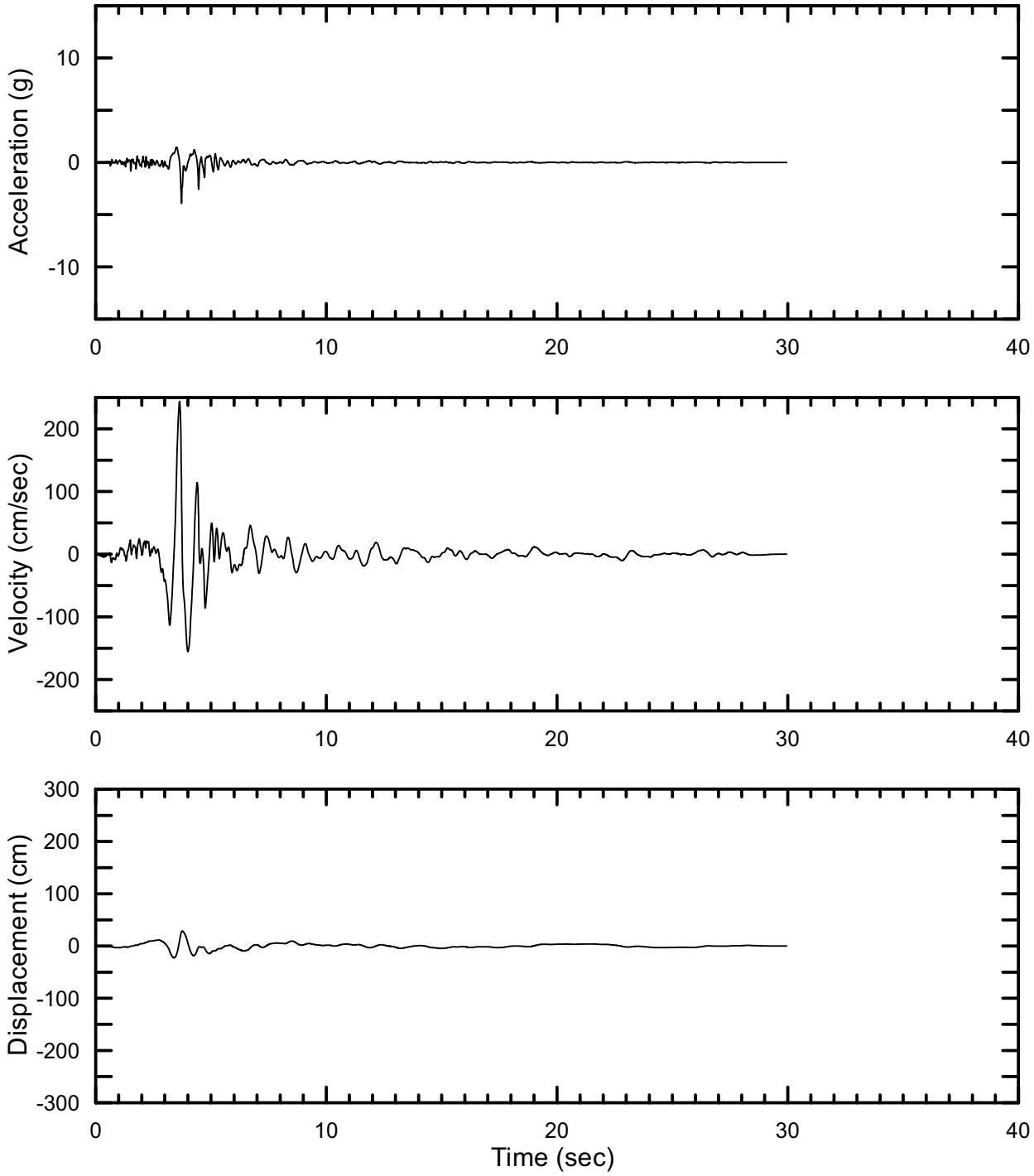

DTN: MO0301TMHIS106.001 [DIRS 161868]

Figure II-65. Point B Horizontal-2 Time Histories (PGV Scaled) at an Annual Exceedance Probability of 10^{-6}, Set #8

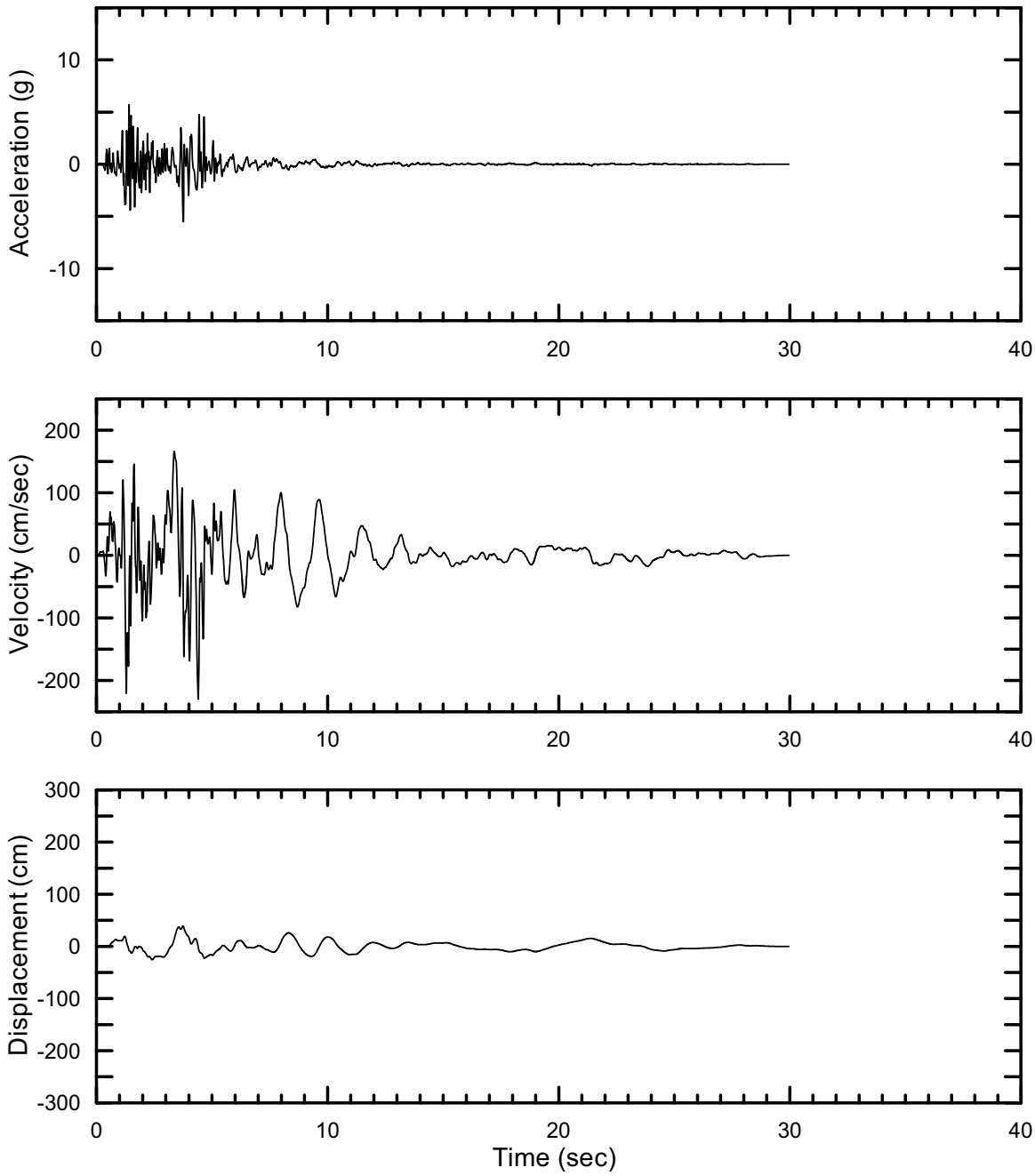

DTN: MO0301TMHIS106.001 [DIRS 161868]

Figure II-66. Point B Vertical Time Histories (PGV Scaled) at an Annual Exceedance Probability of 10^{-6}, Set #8

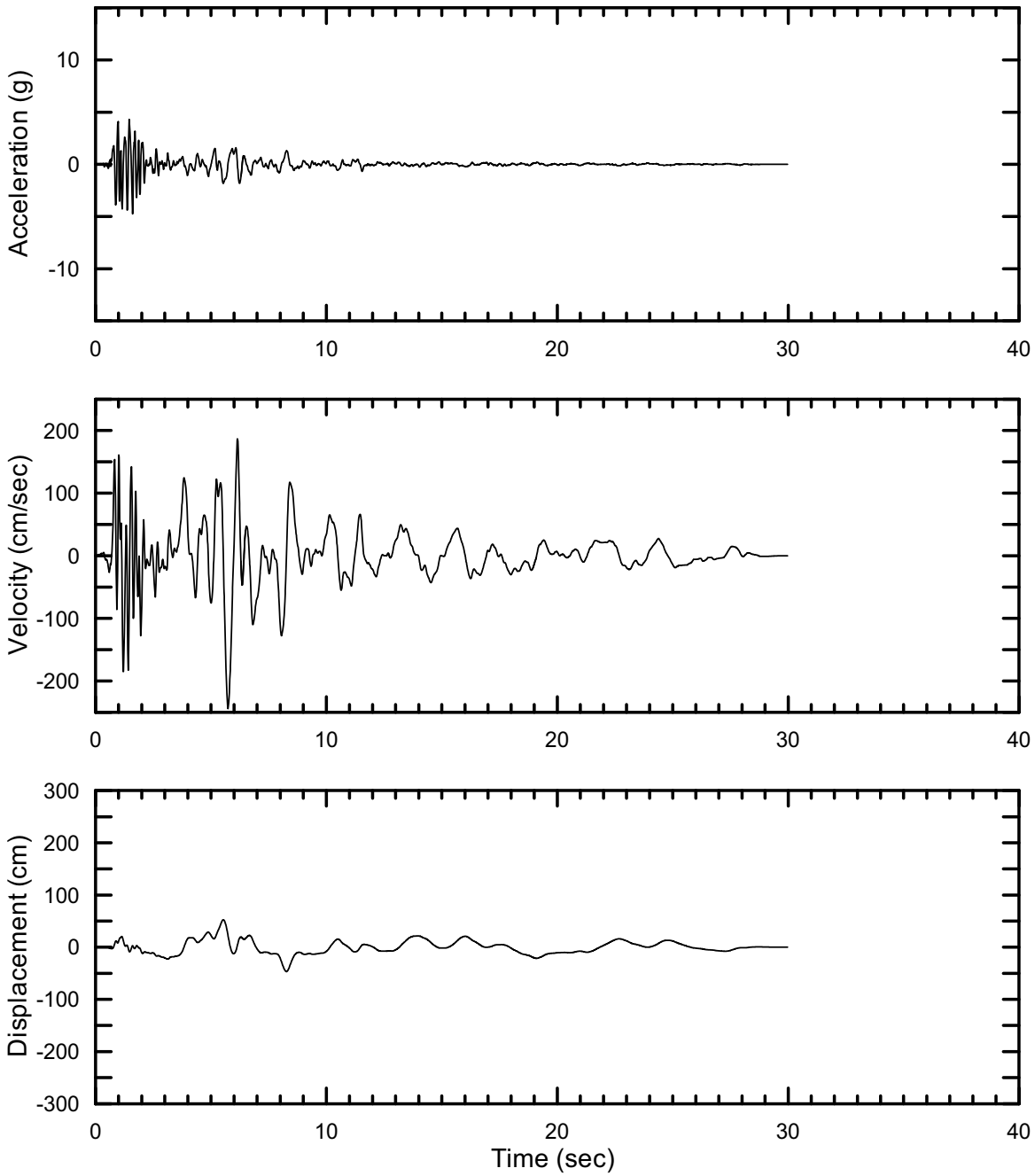

DTN: MO0301TMHIS106.001 [DIRS 161868]

Figure II-67. Point B Horizontal-1 Time Histories (PGV Scaled) at an Annual Exceedance Probability of 10^{-6}, Set #9

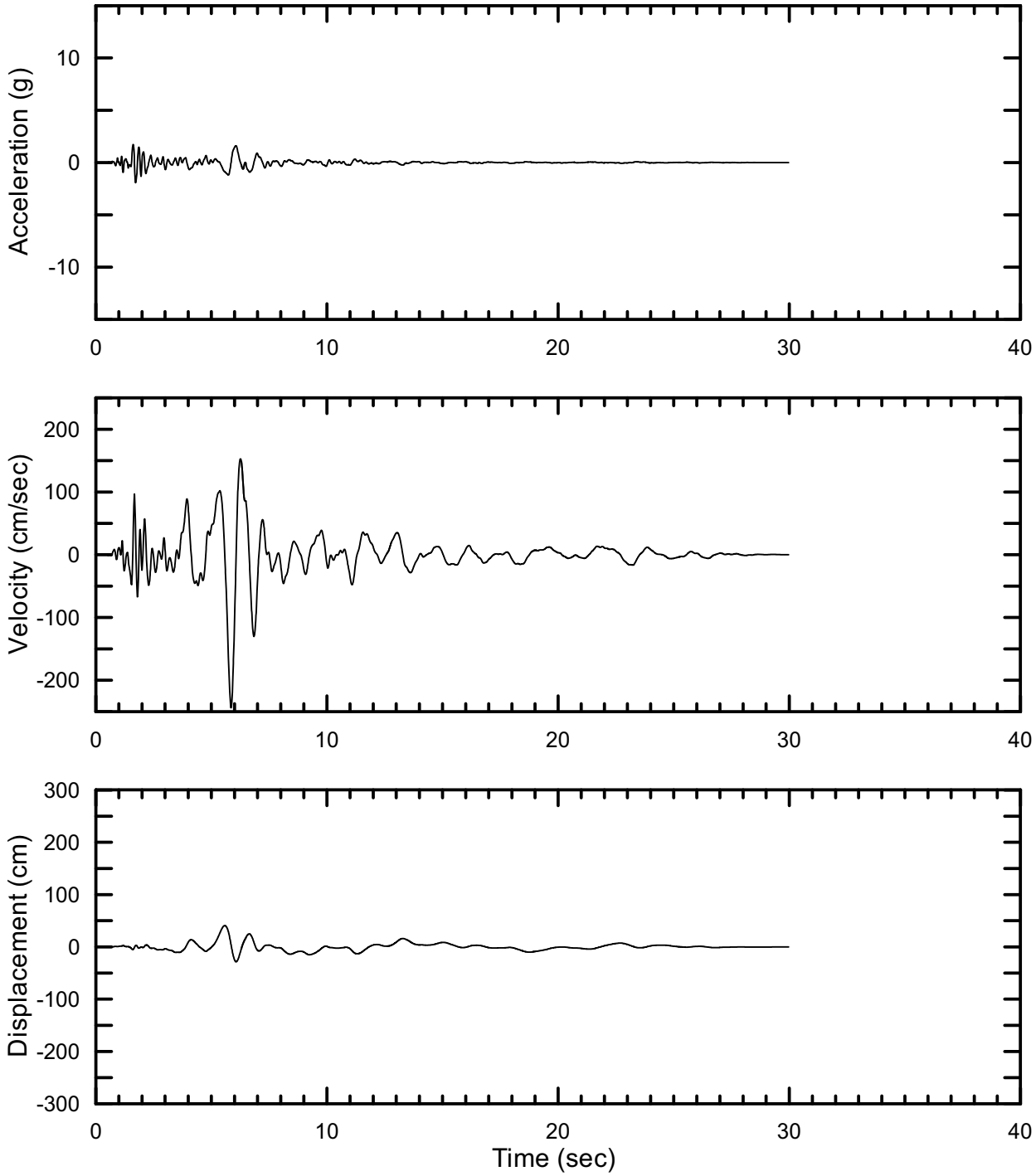

DTN: MO0301TMHIS106.001 [DIRS 161868]

Figure II-68. Point B Horizontal-2 Time Histories (PGV Scaled) at an Annual Exceedance Probability of 10^{-6}, Set #9

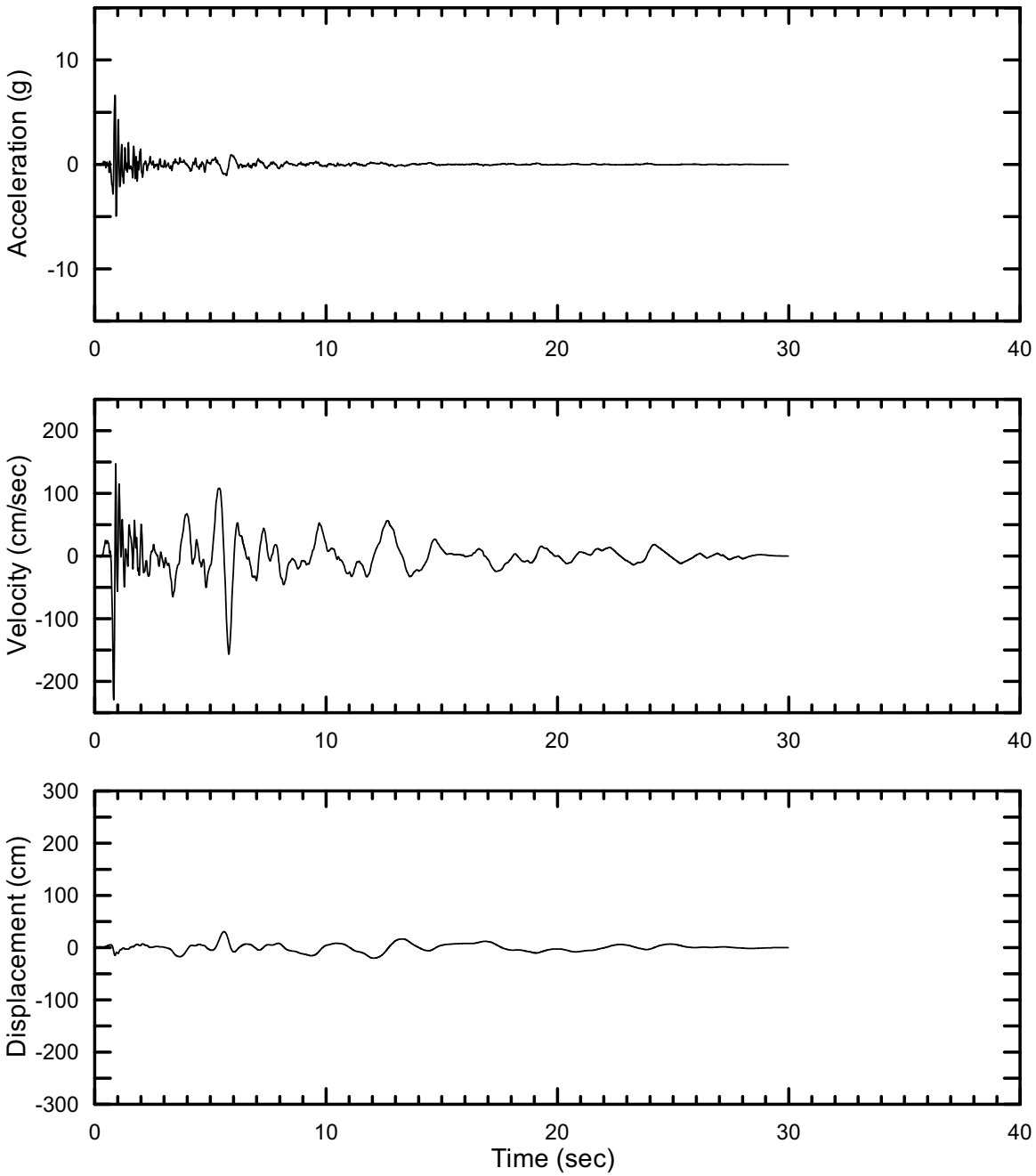

DTN: MO0301TMHIS106.001 [DIRS 161868]

Figure II-69. Point B Vertical Time Histories (PGV Scaled) at an Annual Exceedance Probability of 10^{-6}, Set #9

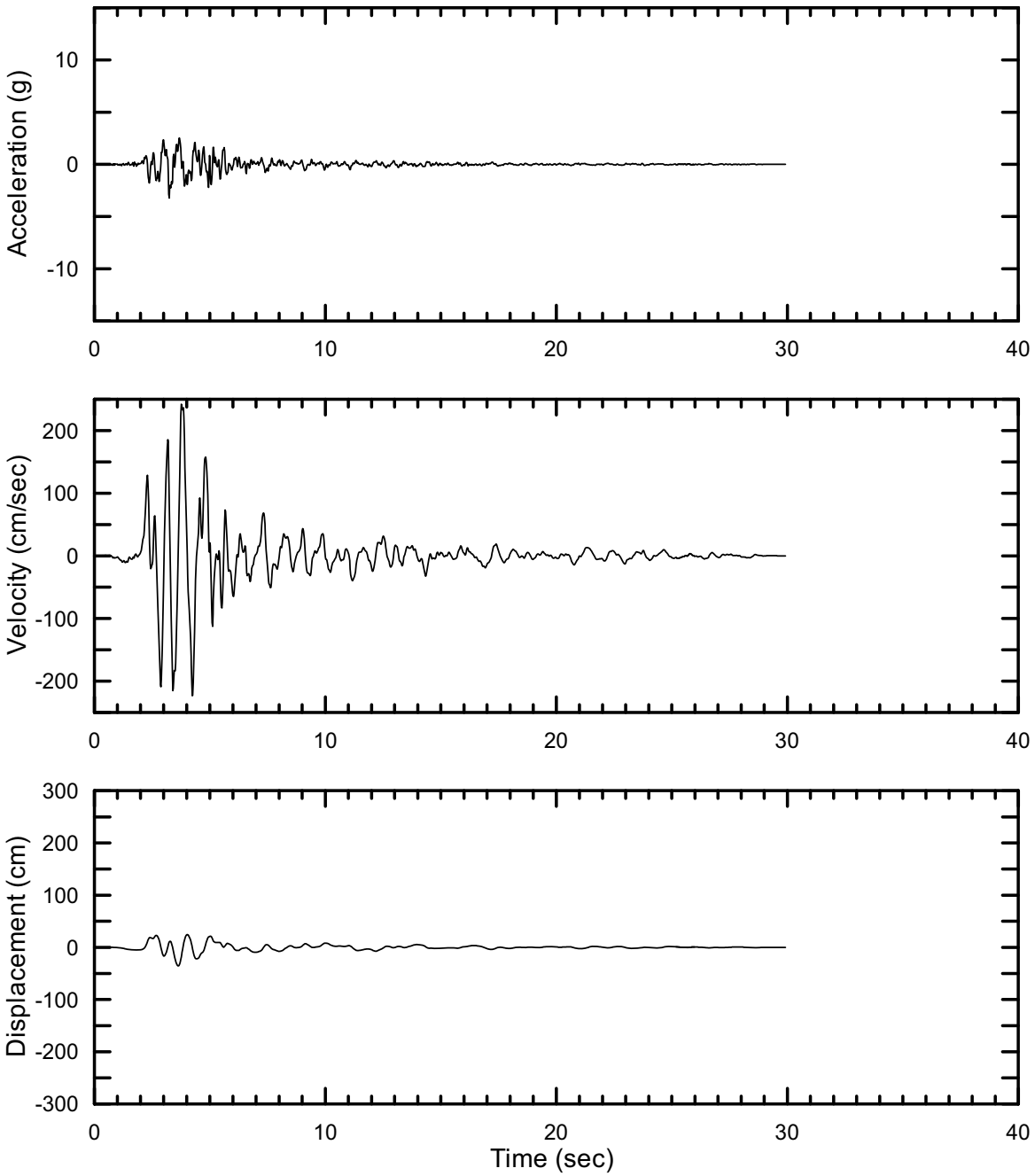

DTN: MO0301TMHIS106.001 [DIRS 161868]

Figure II-70. Point B Horizontal-1 Time Histories (PGV Scaled) at an Annual Exceedance Probability of 10^{-6}, Set #10

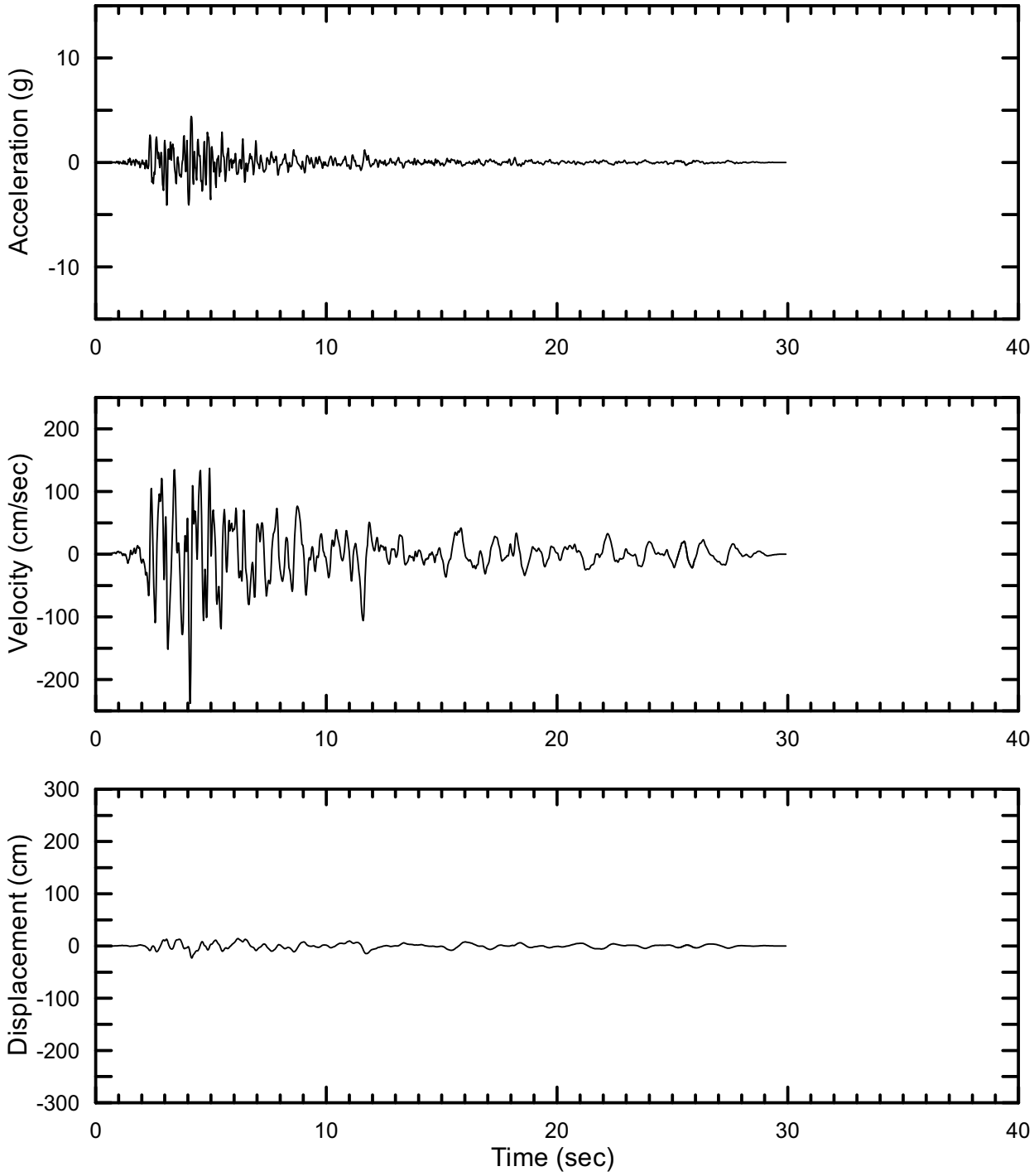

DTN: MO0301TMHIS106.001 [DIRS 161868]

Figure II-71. Point B Horizontal-2 Time Histories (PGV Scaled) at an Annual Exceedance Probability of 10^{-6}, Set #10

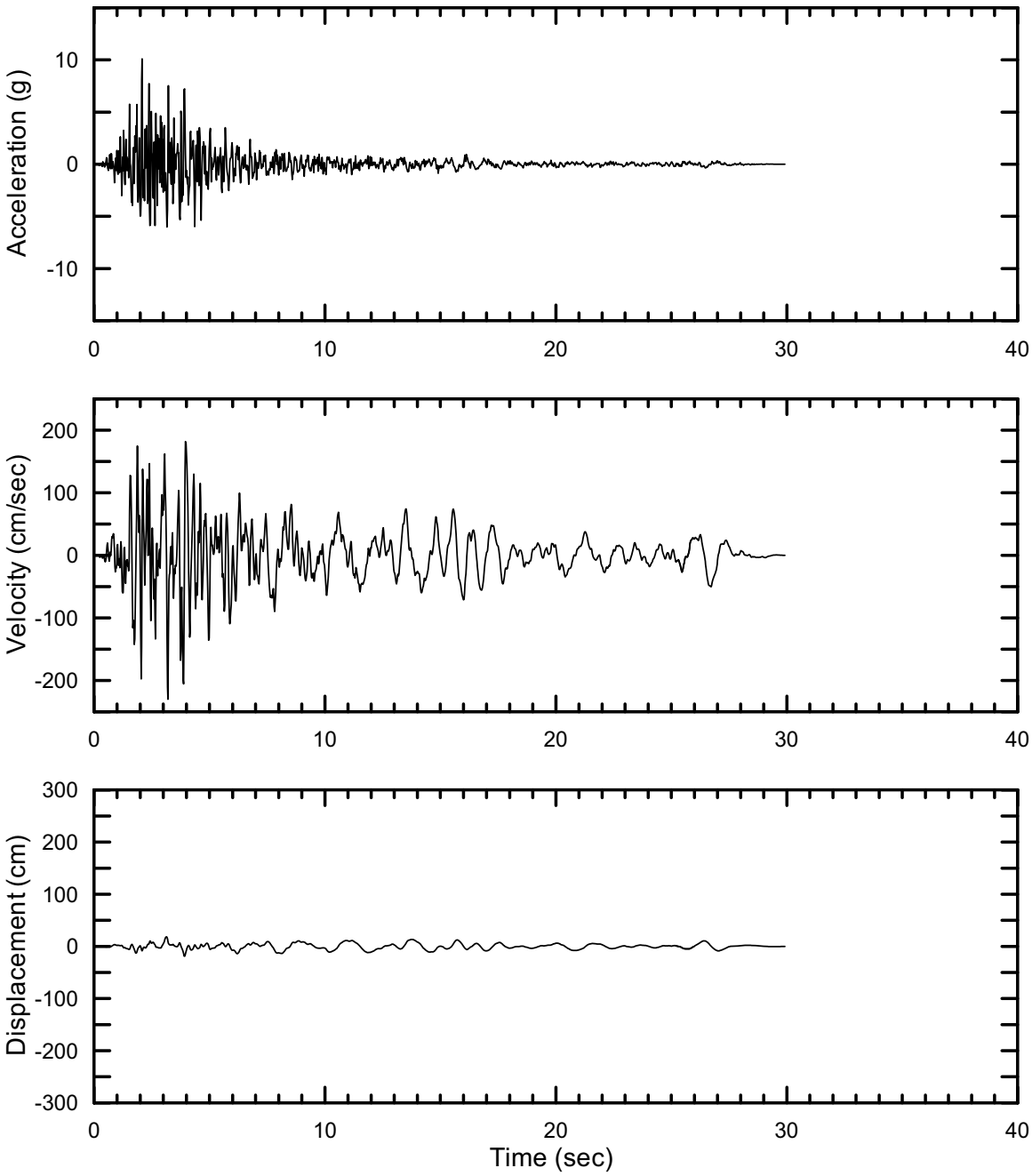

DTN: MO0301TMHIS106.001 [DIRS 161868]

Figure II-72. Point B Vertical Time Histories (PGV Scaled) at an Annual Exceedance Probability of 10^{-6}, Set #10

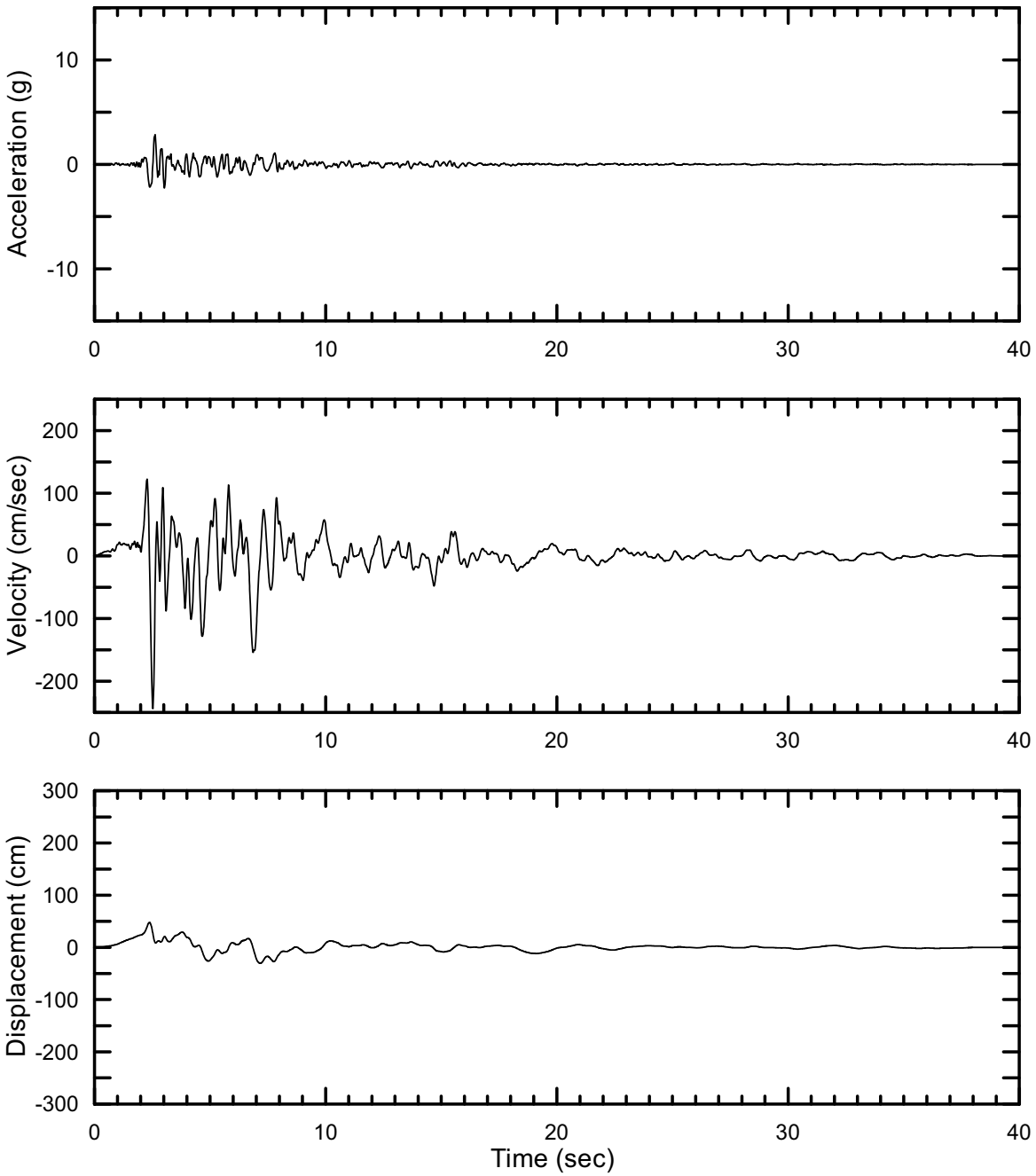

DTN: MO0301TMHIS106.001 [DIRS 161868]

Figure II-73. Point B Horizontal-1 Time Histories (PGV Scaled) at an Annual Exceedance Probability of 10^{-6}, Set #11

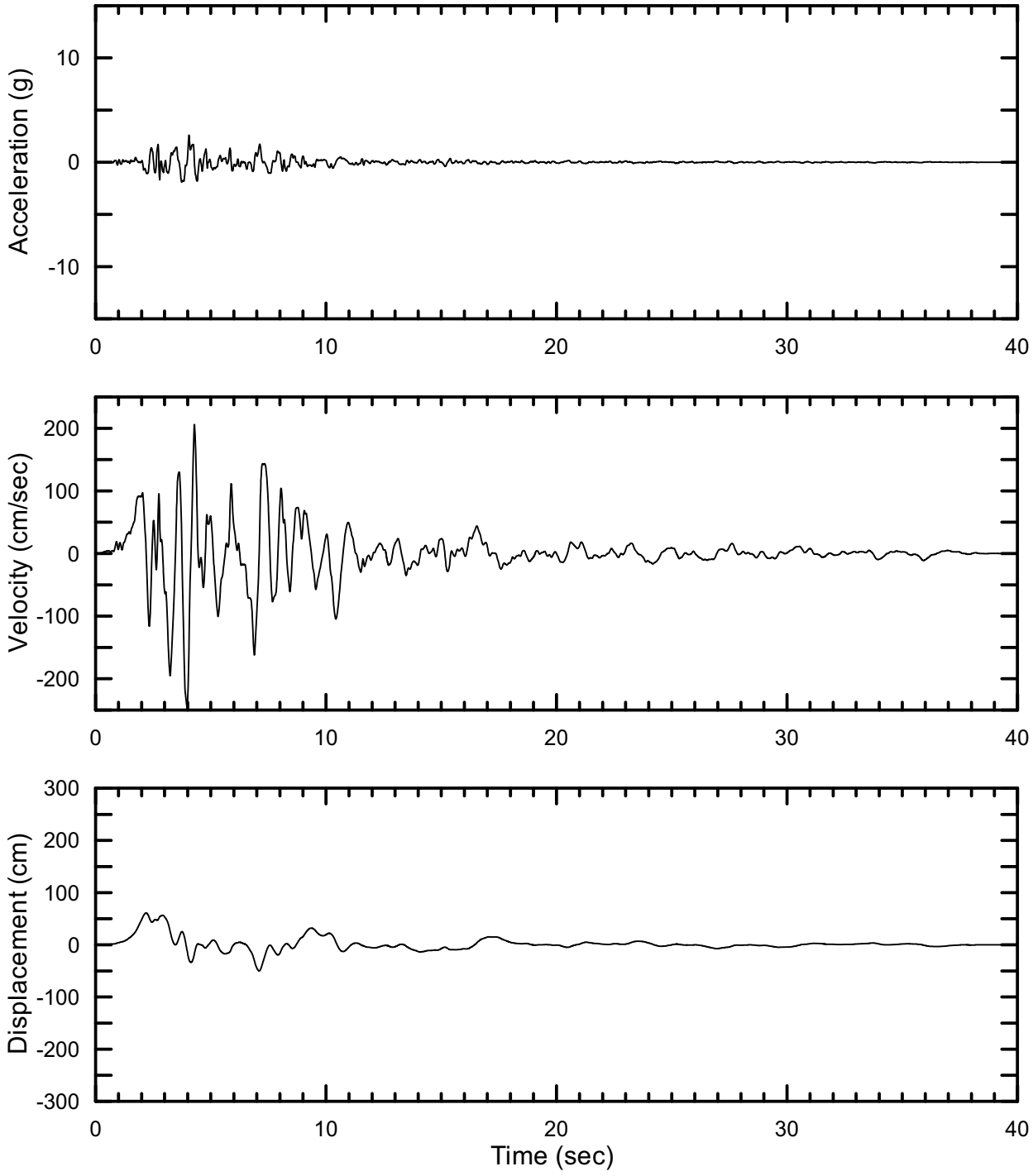

DTN: MO0301TMHIS106.001 [DIRS 161868]

Figure II-74. Point B Horizontal-2 Time Histories (PGV Scaled) at an Annual Exceedance Probability of 10^{-6}, Set #11

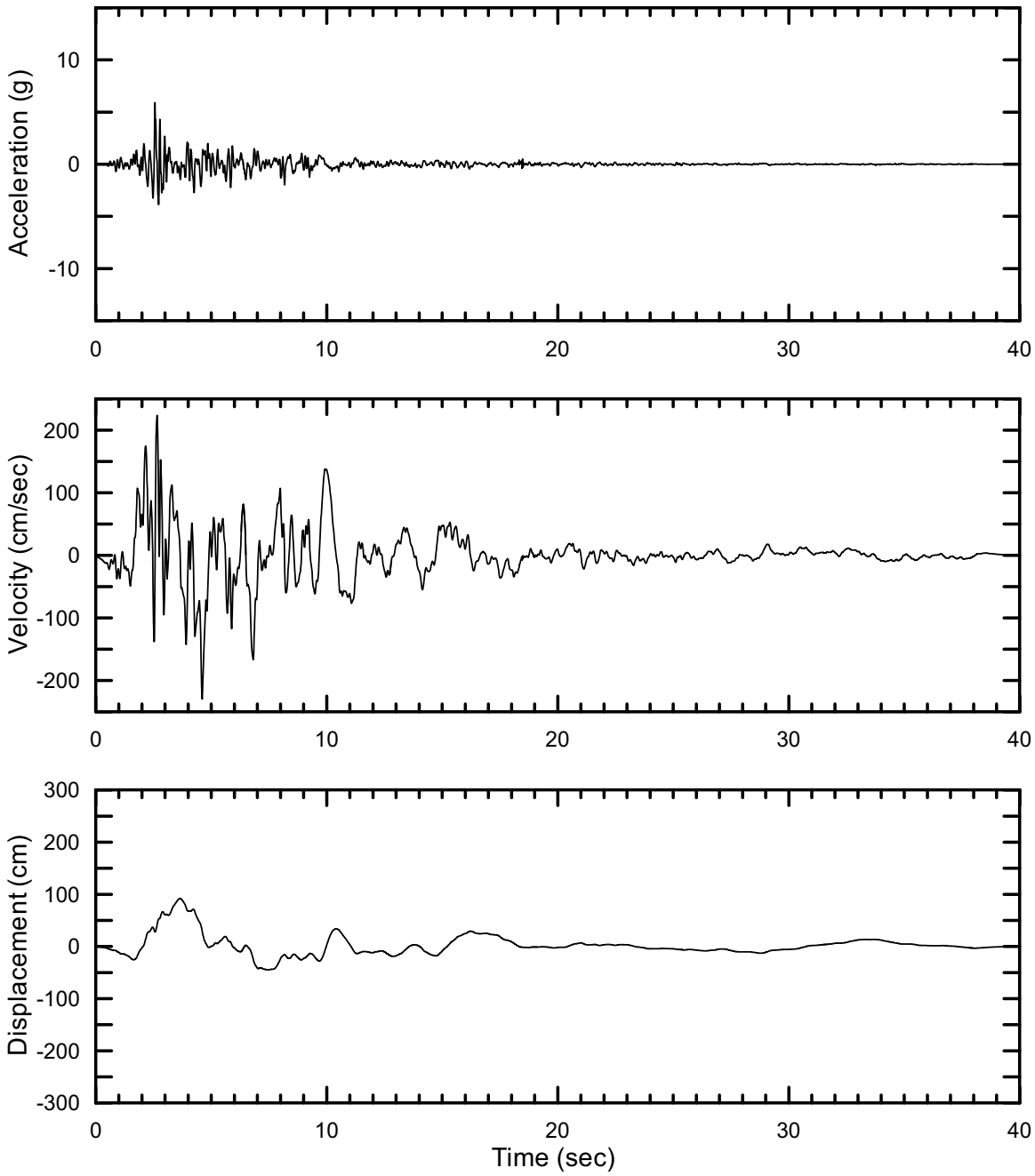

DTN: MO0301TMHIS106.001 [DIRS 161868]

Figure II-75. Point B Vertical Time Histories (PGV Scaled) at an Annual Exceedance Probability of 10^{-6}, Set #11

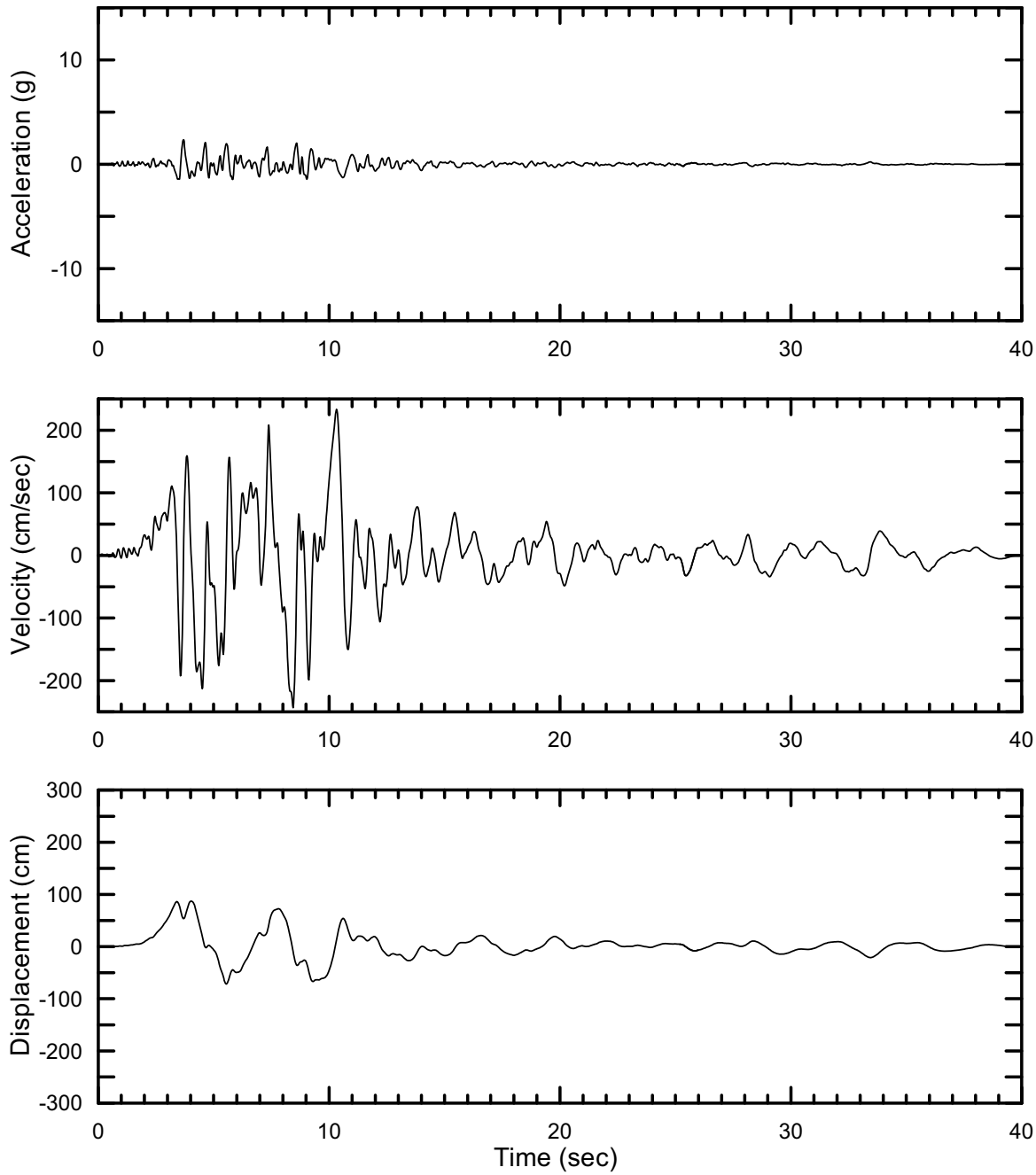

DTN: MO0301TMHIS106.001 [DIRS 161868]

Figure II-76. Point B Horizontal-1 Time Histories (PGV Scaled) at an Annual Exceedance Probability of 10^{-6}, Set #12

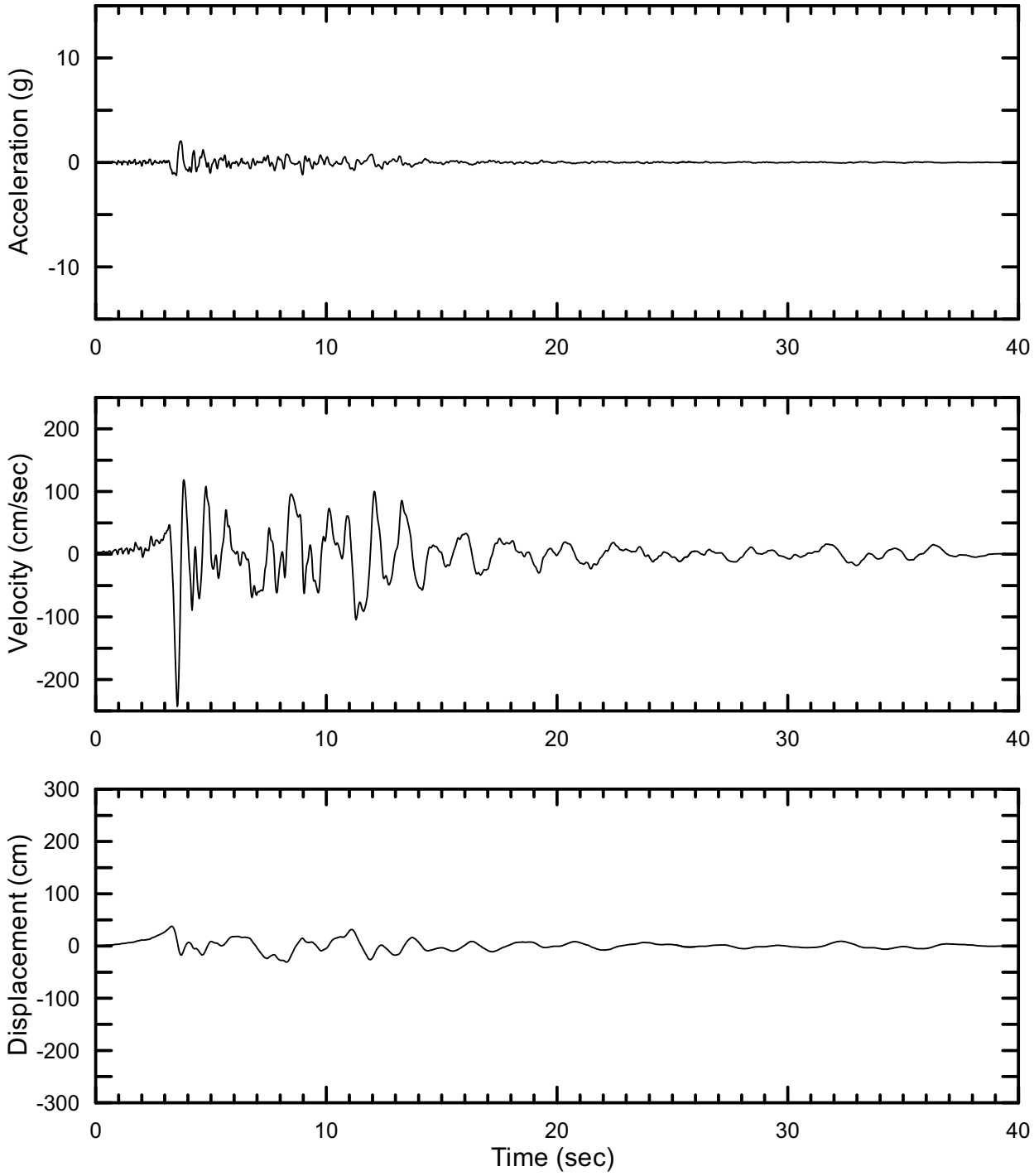

DTN: MO0301TMHIS106.001 [DIRS 161868]

Figure II-77. Point B Horizontal-2 Time Histories (PGV Scaled) at an Annual Exceedance Probability of 10^{-6}, Set #12

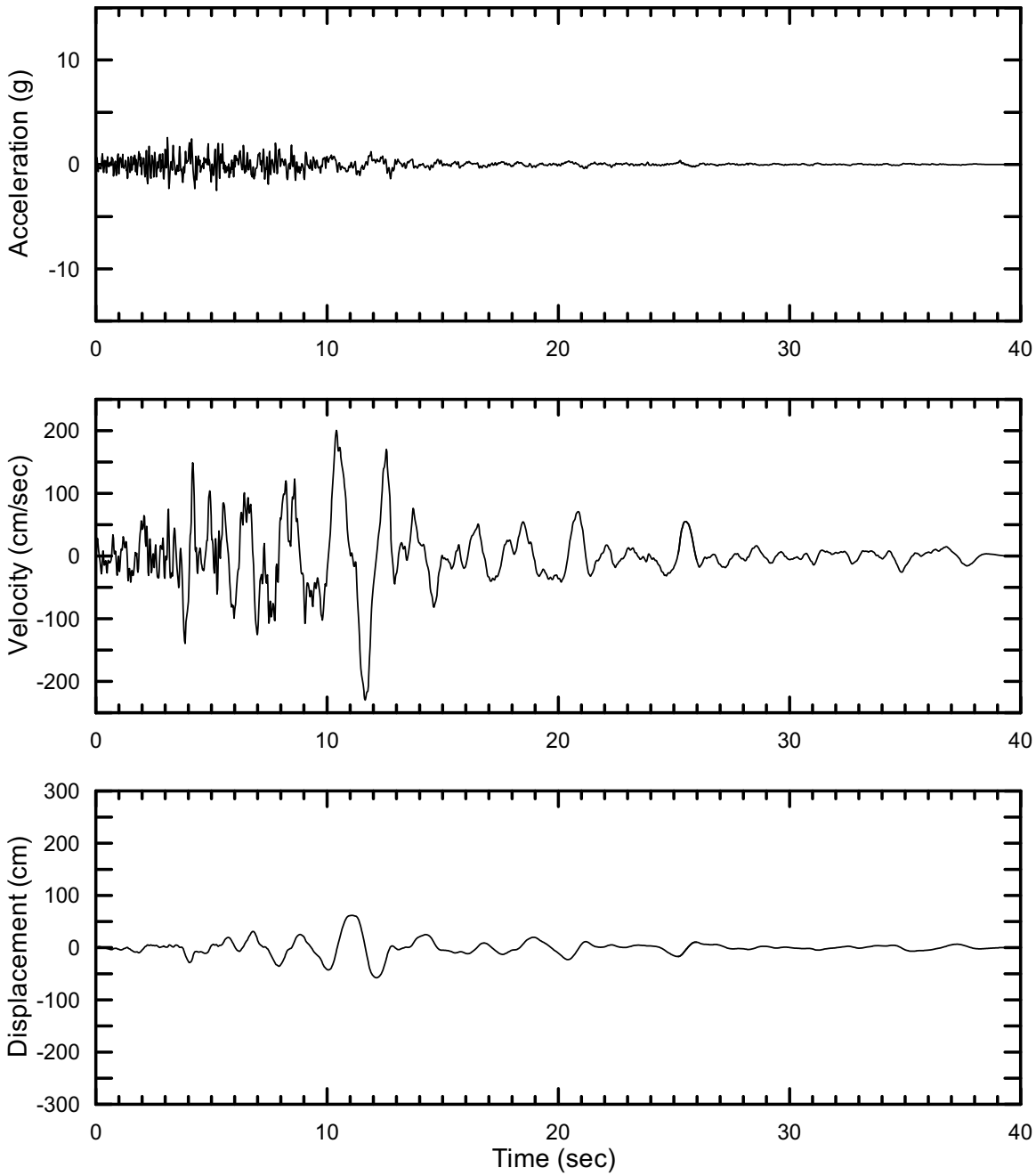

DTN: MO0301TMHIS106.001 [DIRS 161868]

Figure II-78. Point B Vertical Time Histories (PGV Scaled) at an Annual Exceedance Probability of 10^{-6}, Set #12

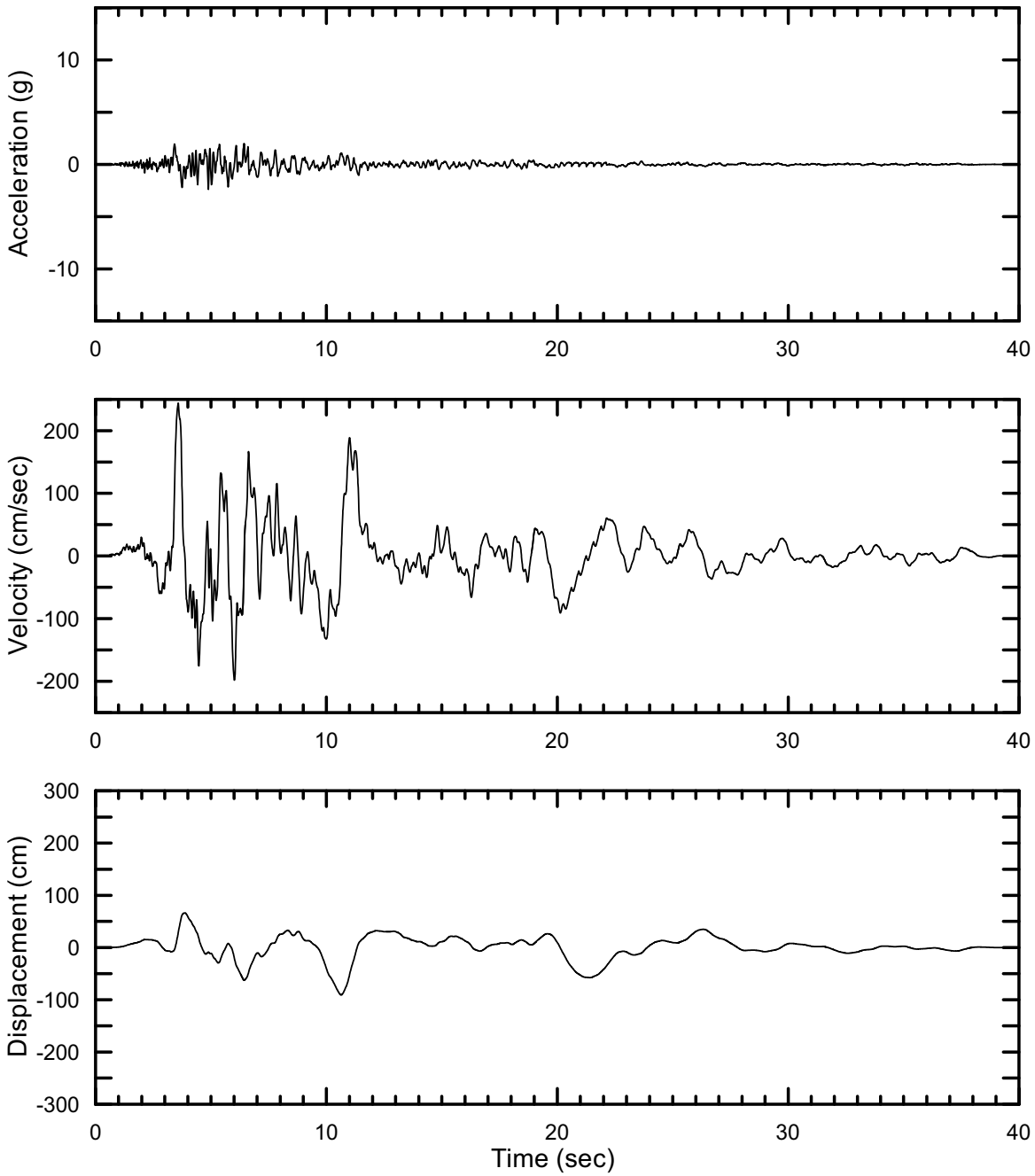

DTN: MO0301TMHIS106.001 [DIRS 161868]

Figure II-79. Point B Horizontal-1 Time Histories (PGV Scaled) at an Annual Exceedance Probability of 10^{-6}, Set #13

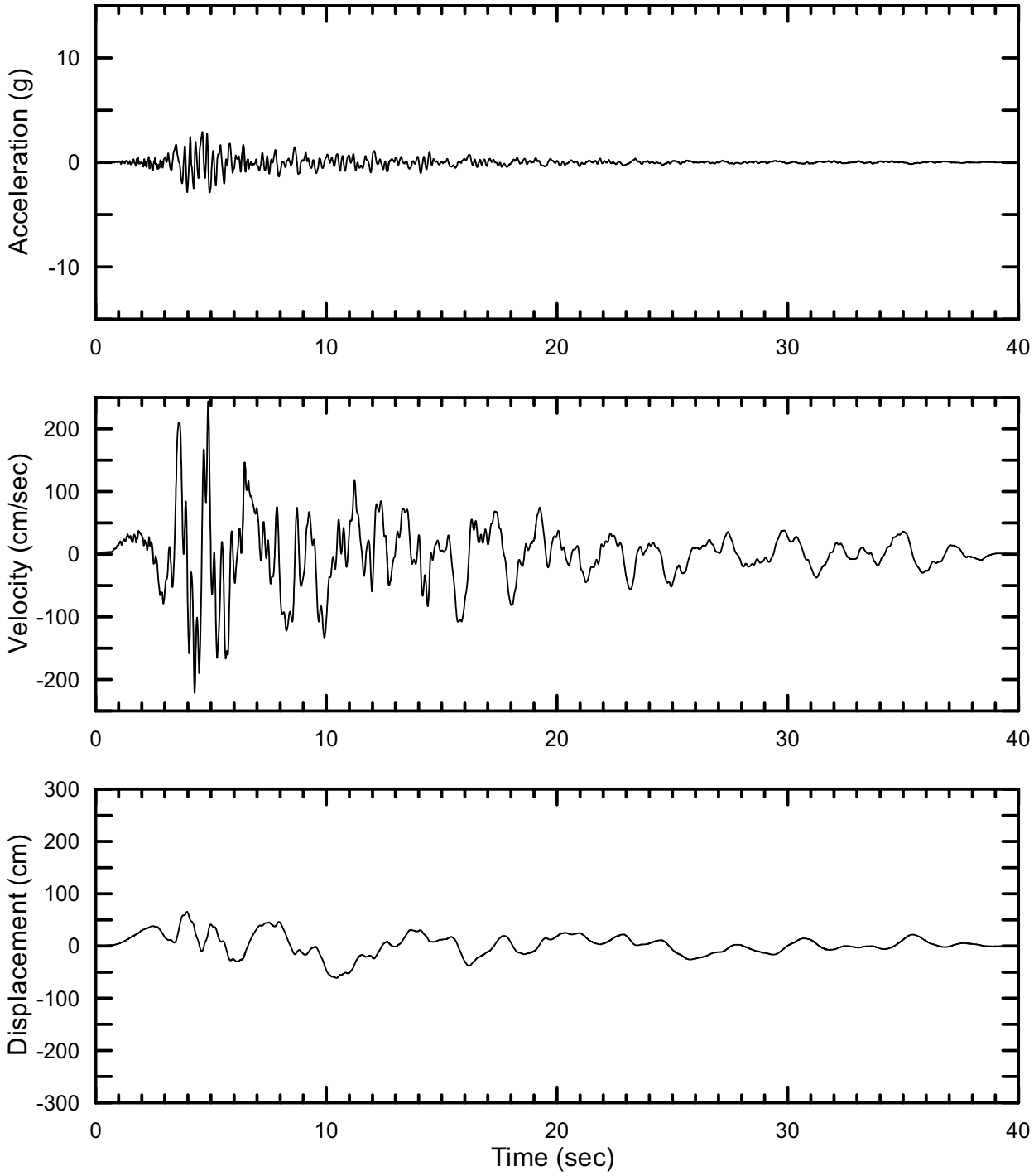

DTN: MO0301TMHIS106.001 [DIRS 161868]

Figure II-80. Point B Horizontal-2 Time Histories (PGV Scaled) at an Annual Exceedance Probability of 10^{-6}, Set #13

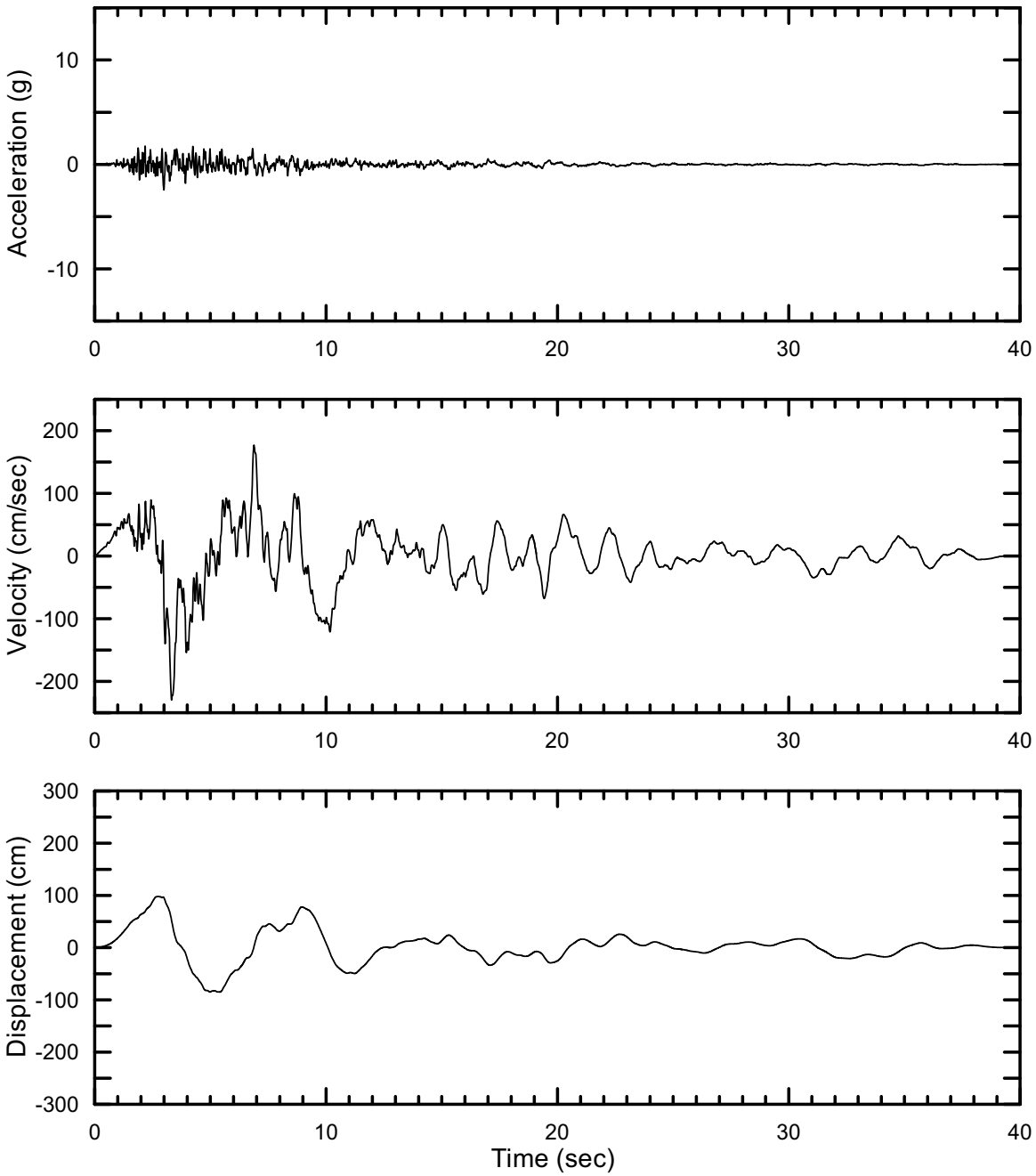

DTN: MO0301TMHIS106.001 [DIRS 161868]

Figure II-81. Point B Vertical Time Histories (PGV Scaled) at an Annual Exceedance Probability of 10^{-6}, Set #13

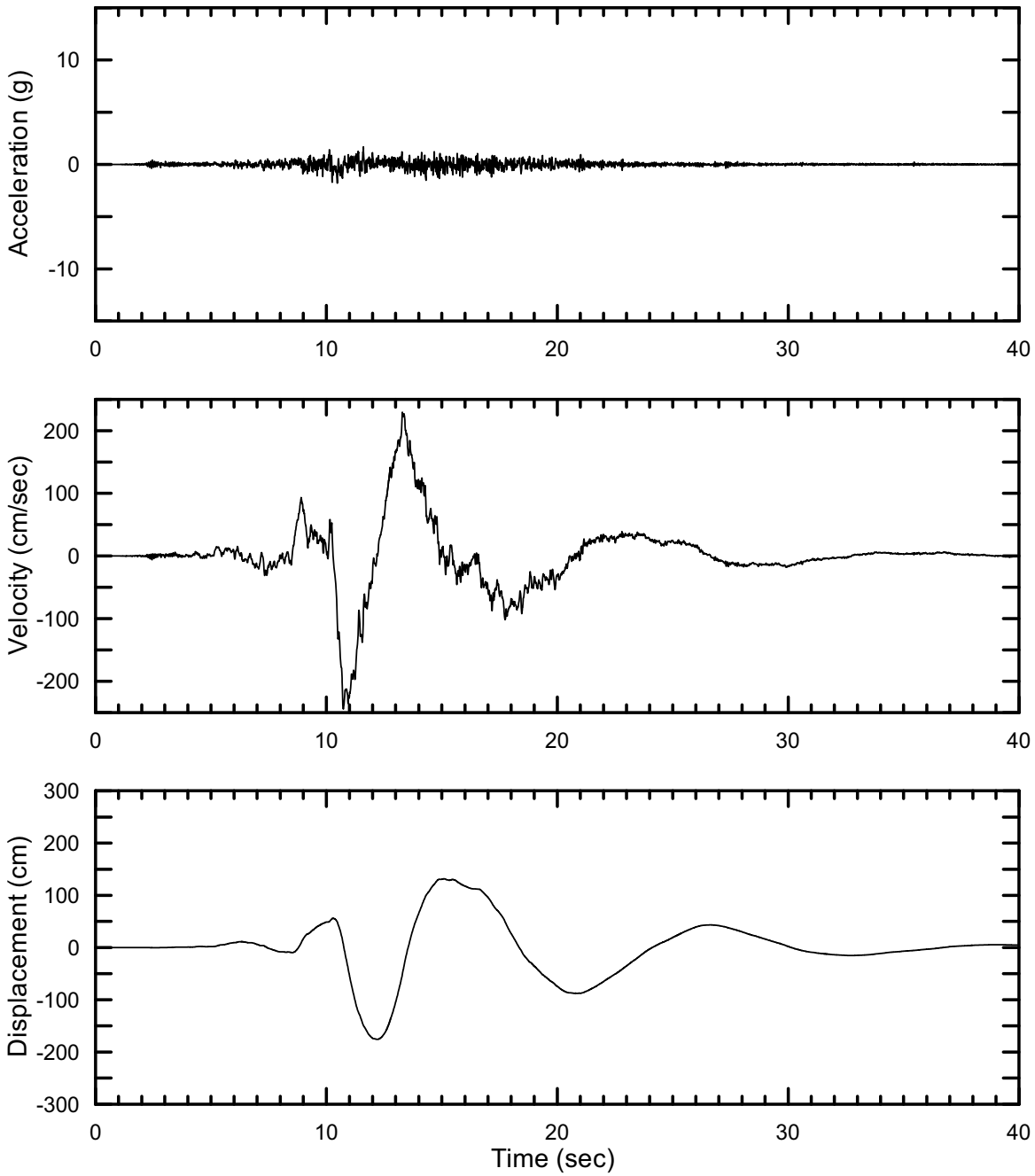

DTN: MO0301TMHIS106.001 [DIRS 161868]

Figure II-82. Point B Horizontal-1 Time Histories (PGV Scaled) at an Annual Exceedance Probability of 10^{-6}, Set #14

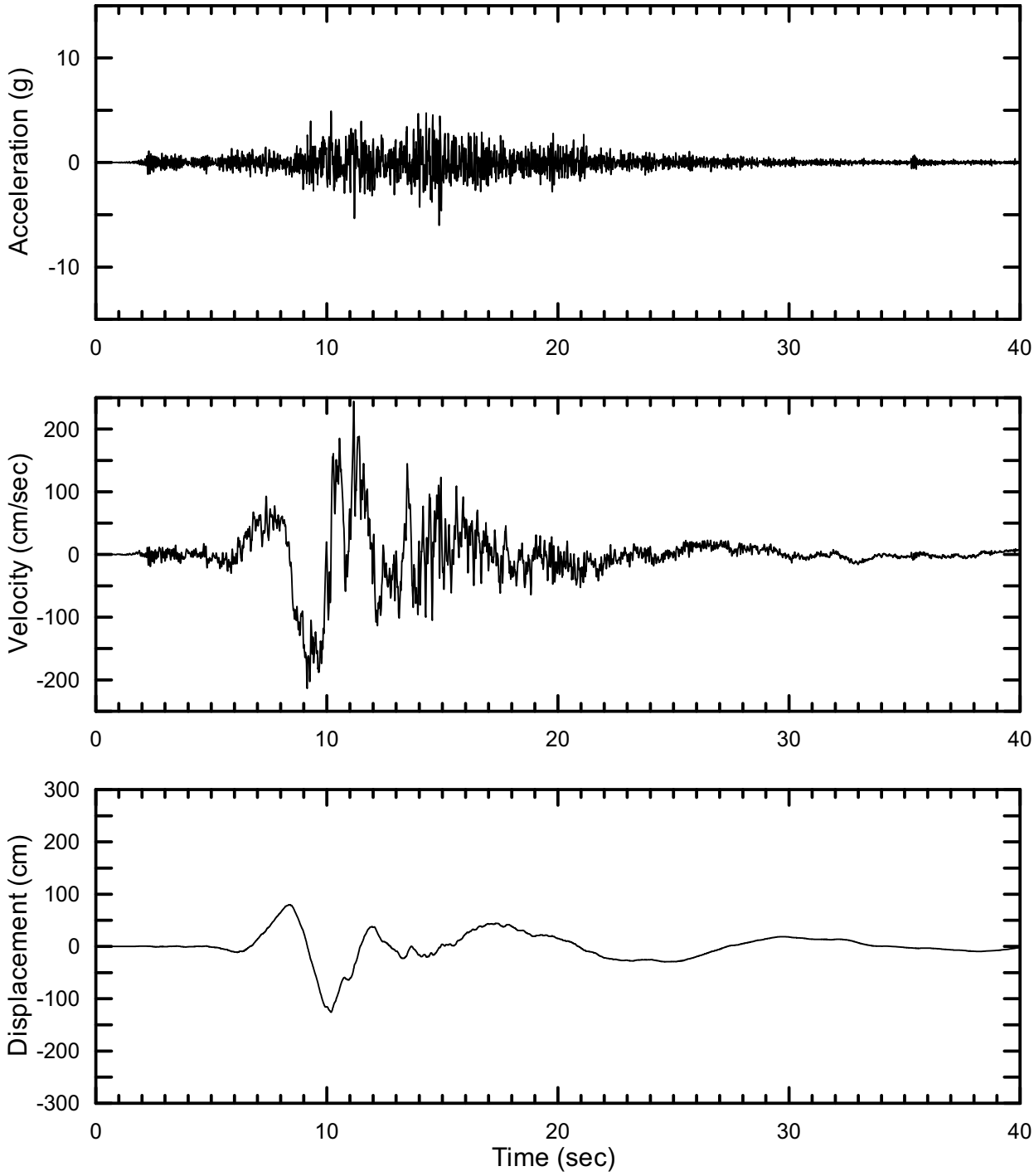

DTN: MO0301TMHIS106.001 [DIRS 161868]

Figure II-83. Point B Horizontal-2 Time Histories (PGV Scaled) at an Annual Exceedance Probability of 10^{-6}, Set #14

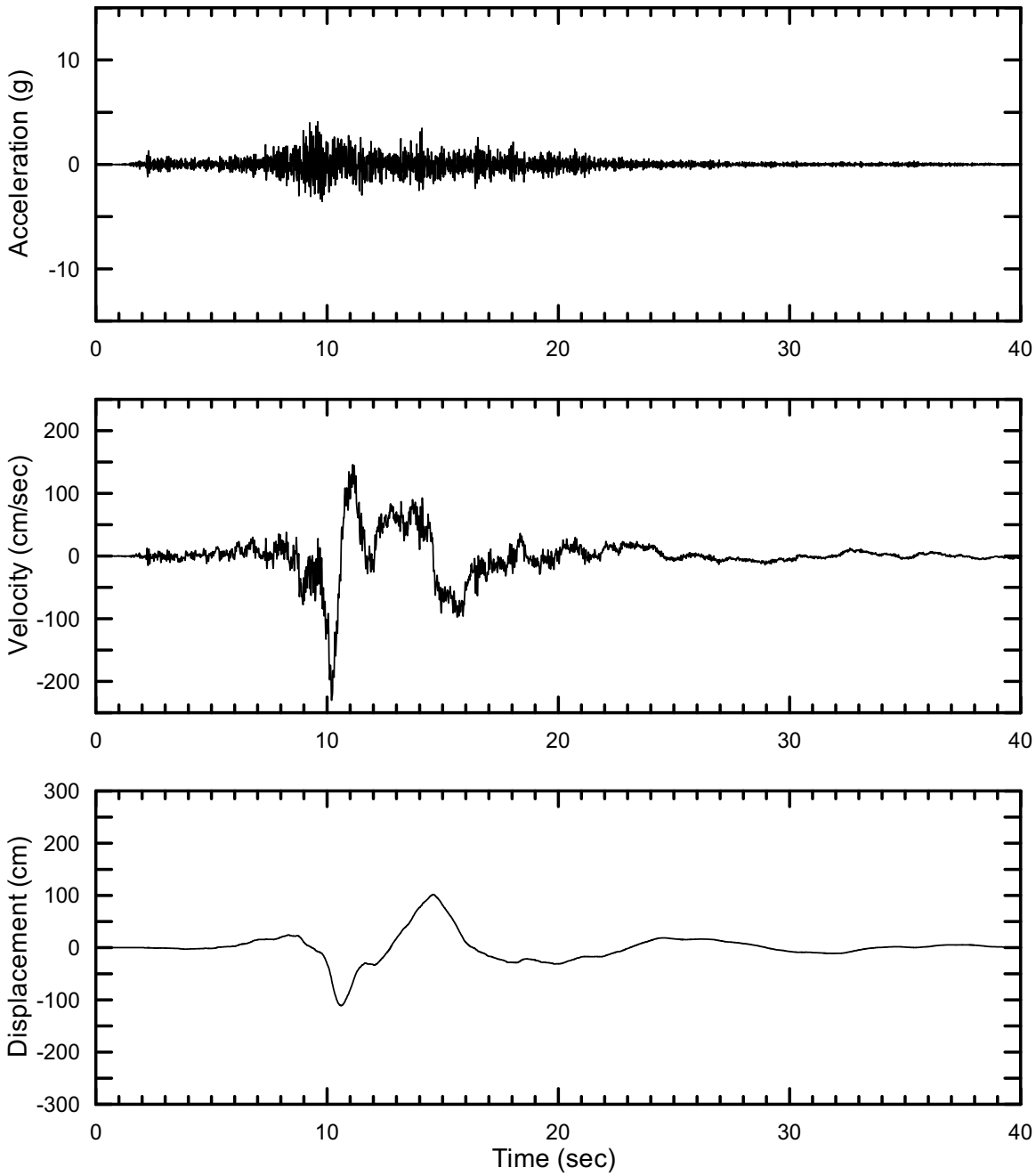

DTN: MO0301TMHIS106.001 [DIRS 161868]

Figure II-84. Point B Vertical Time Histories (PGV Scaled) at an Annual Exceedance Probability of 10^{-6}, Set #14

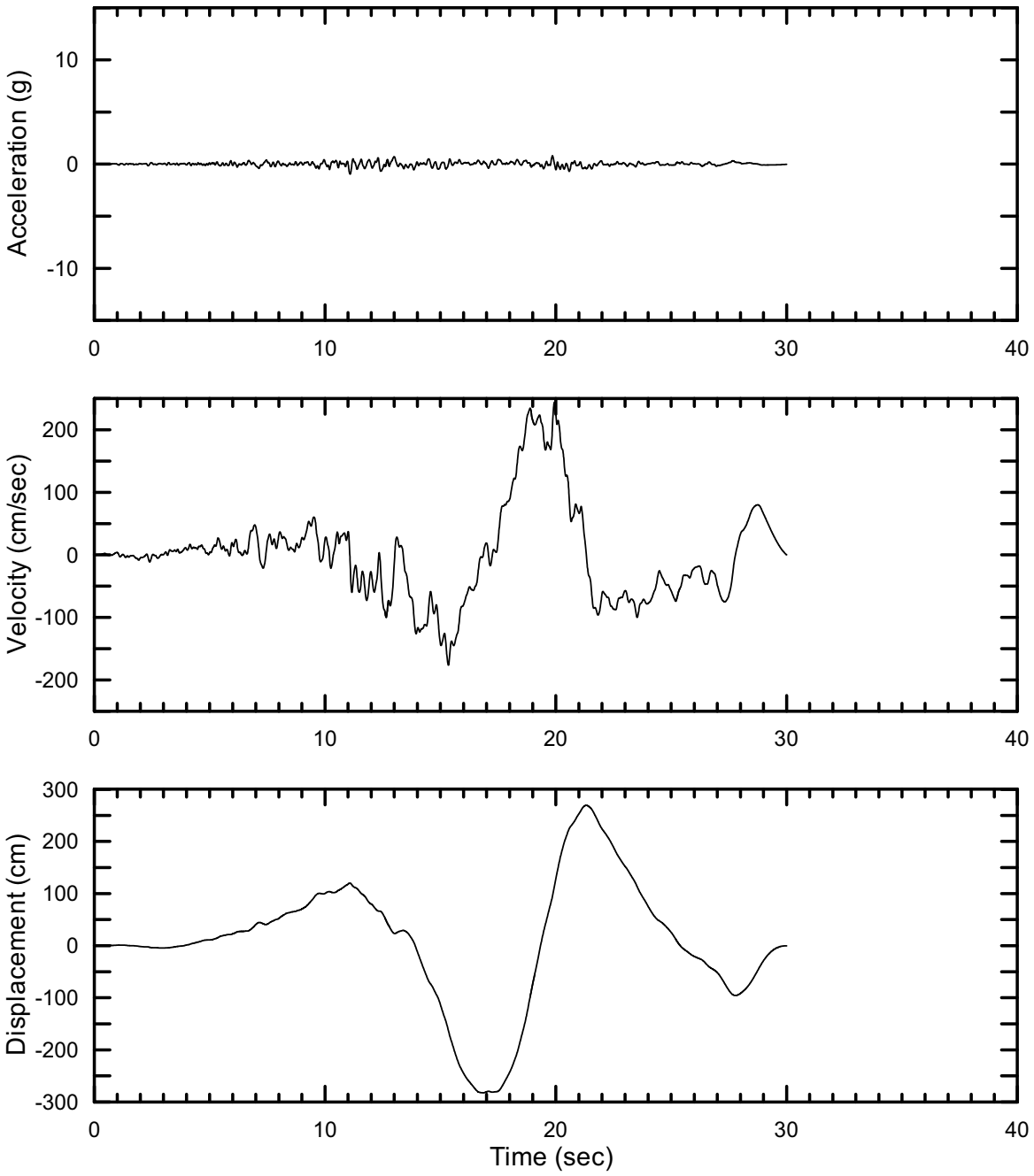

DTN: MO0301TMHIS106.001 [DIRS 161868]

Figure II-85. Point B Horizontal-1 Time Histories (PGV Scaled) at an Annual Exceedance Probability of 10^{-6}, Set #15

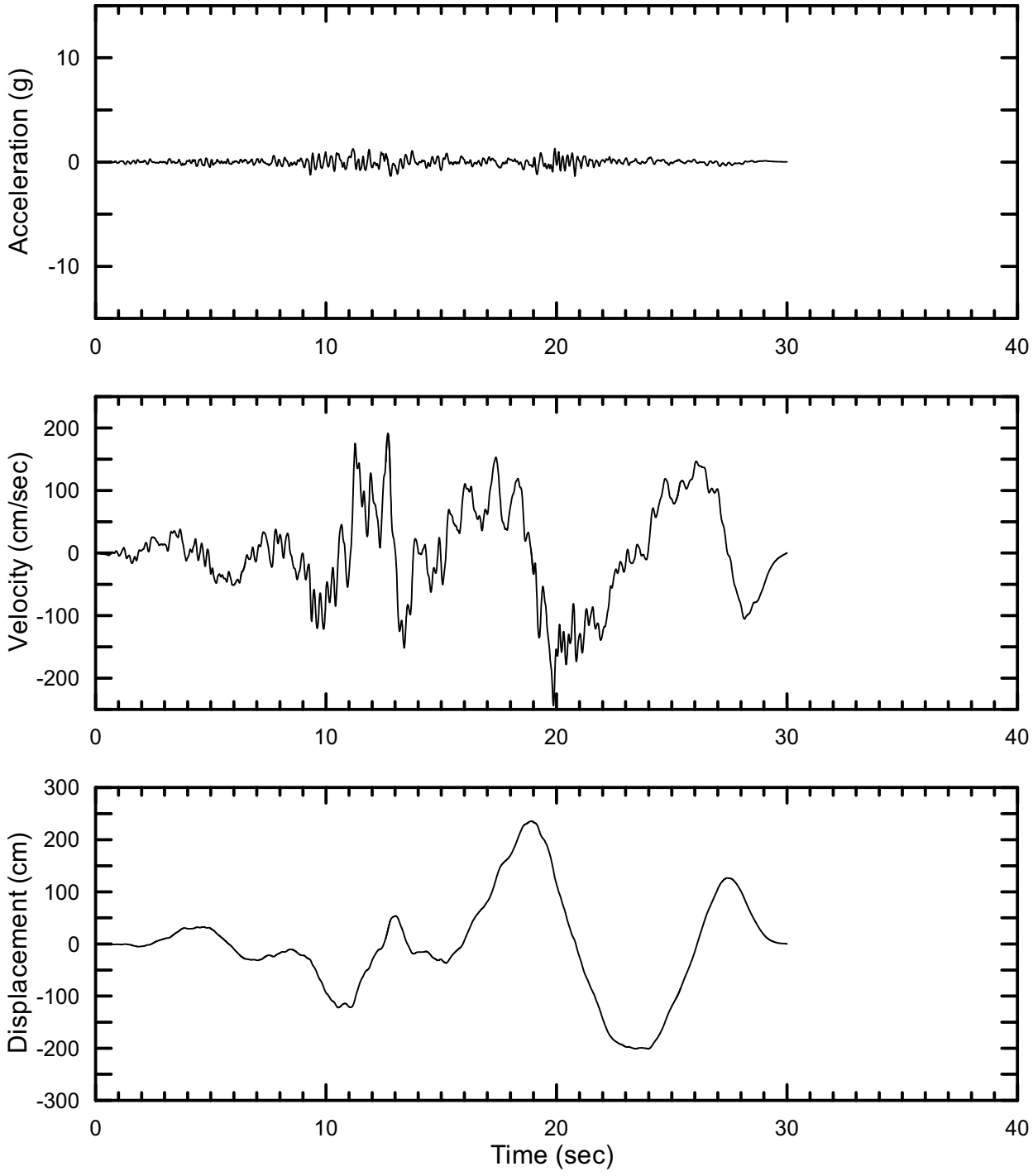

DTN: MO0301TMHIS106.001 [DIRS 161868]

Figure II-86. Point B Horizontal-2 Time Histories (PGV Scaled) at an Annual Exceedance Probability of 10^{-6}, Set #15

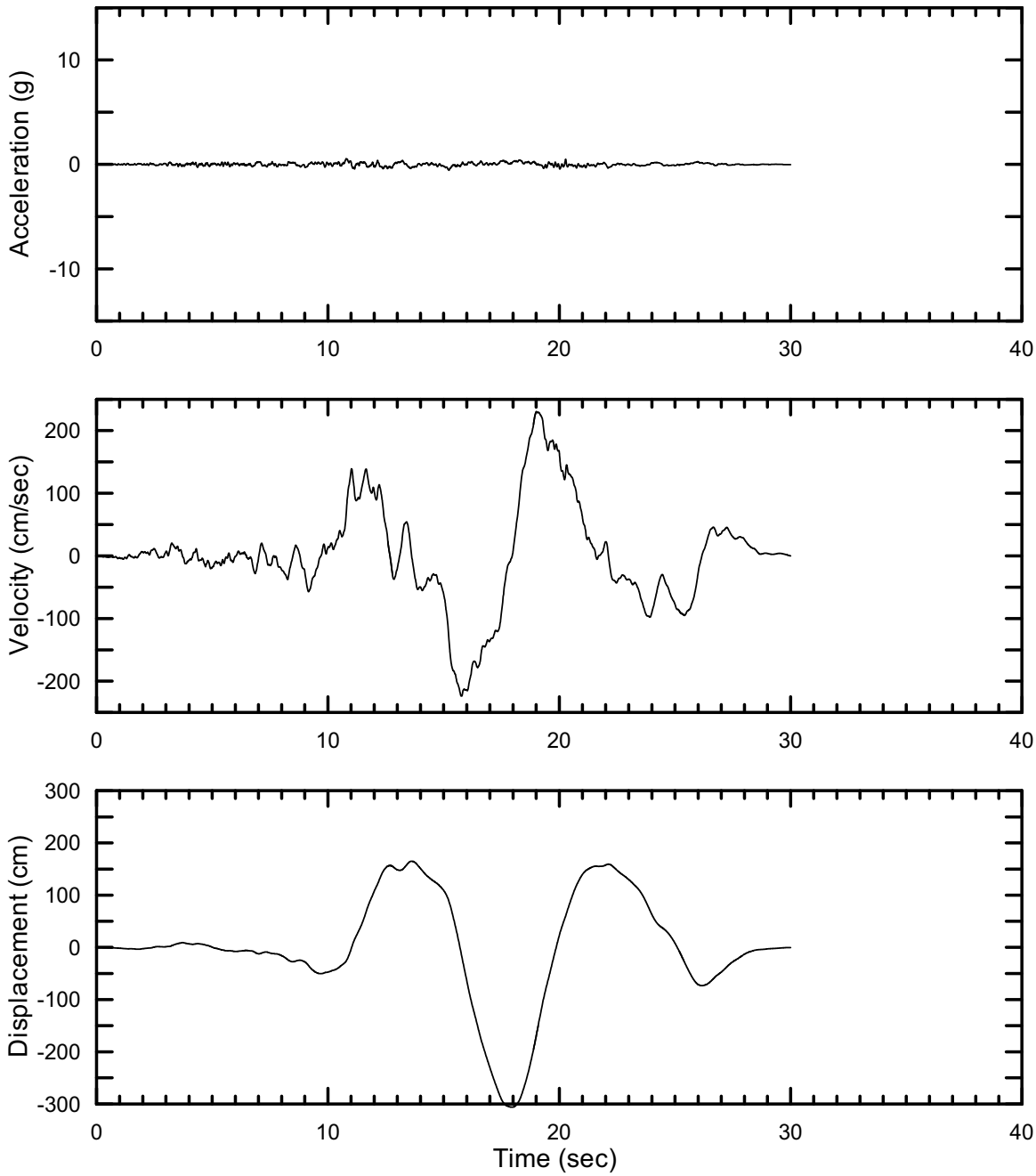

DTN: MO0301TMHIS106.001 [DIRS 161868]

Figure II-87. Point B Vertical Time Histories (PGV Scaled) at an Annual Exceedance Probability of 10^{-6}, Set #15

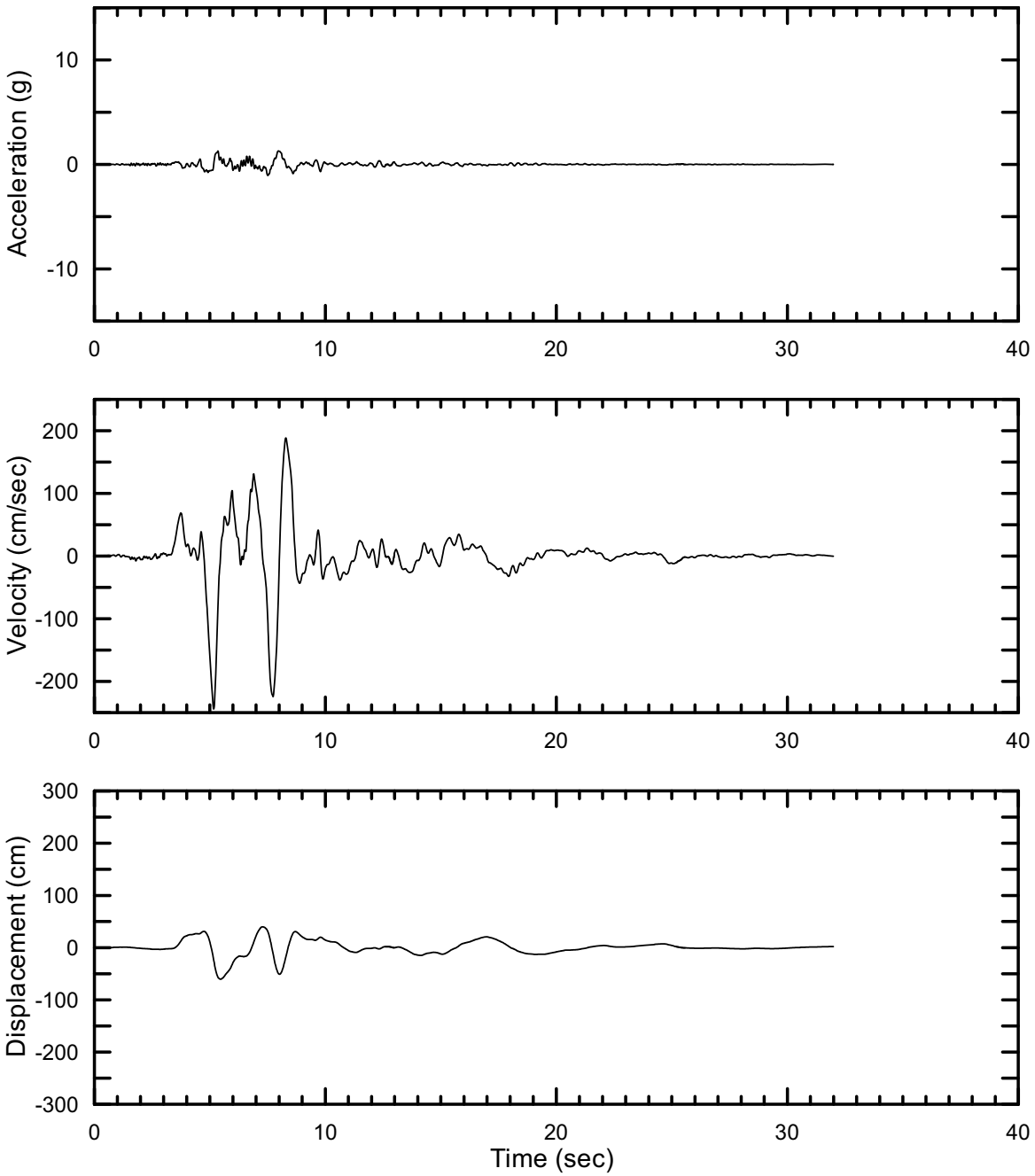

DTN: MO0301TMHIS106.001 [DIRS 161868]

Figure II-88. Point B Horizontal-1 Time Histories (PGV Scaled) at an Annual Exceedance Probability of 10^{-6}, Set #16

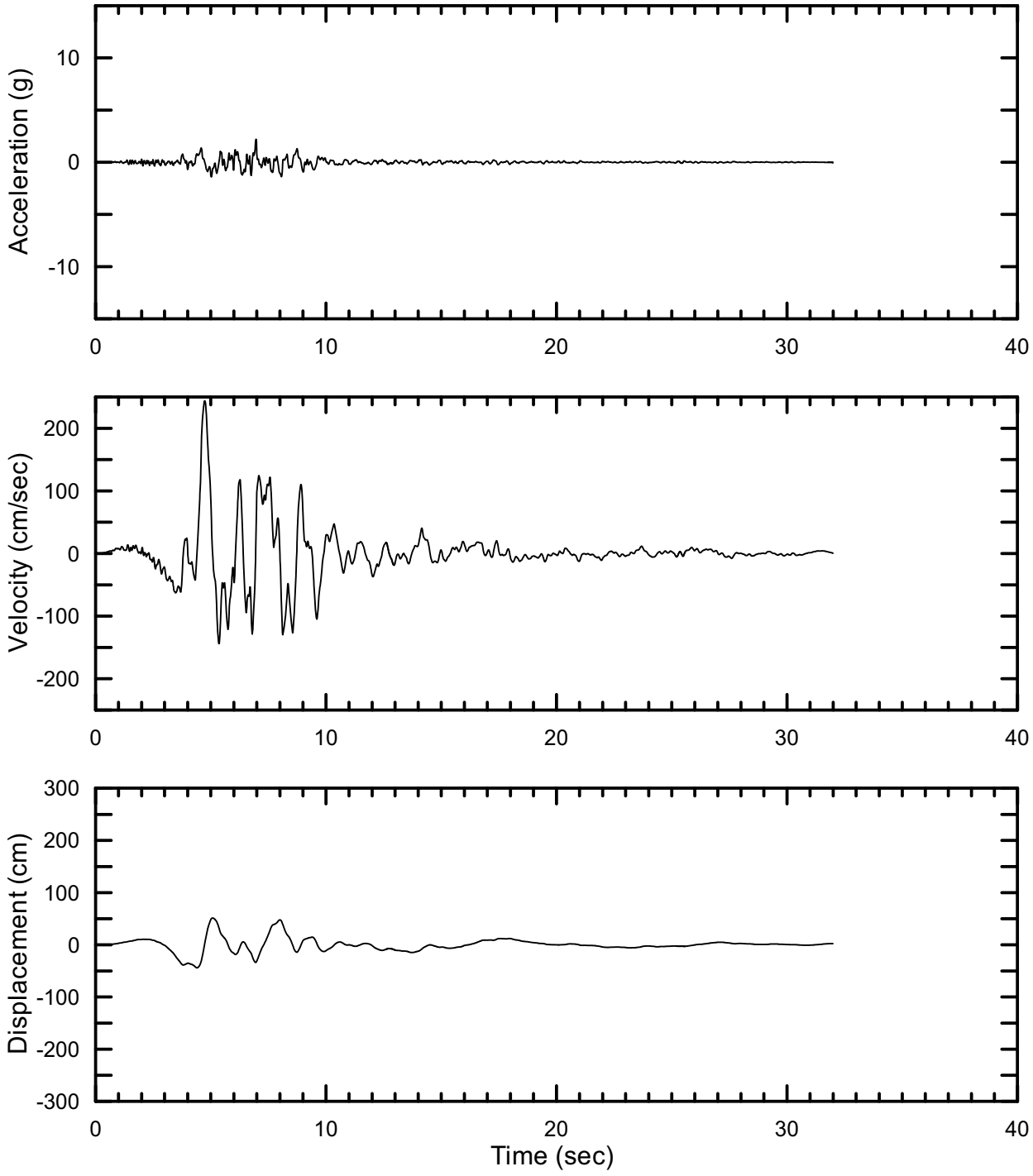

DTN: MO0301TMHIS106.001 [DIRS 161868]

Figure II-89. Point B Horizontal-2 Time Histories (PGV Scaled) at an Annual Exceedance Probability of 10^{-6}, Set #16

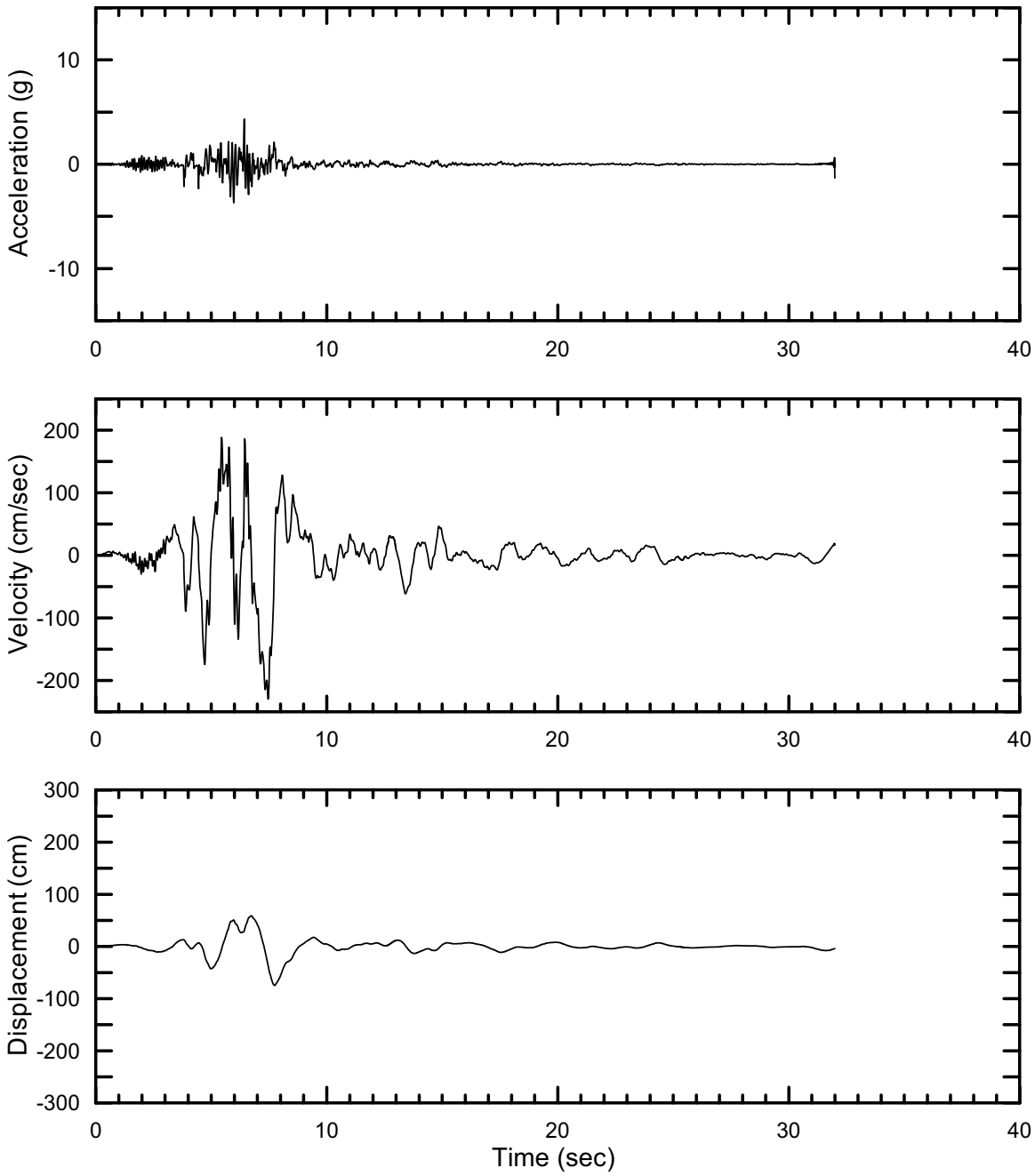

DTN: MO0301TMHIS106.001 [DIRS 161868]

Figure II-90. Point B Vertical Time Histories (PGV Scaled) at an Annual Exceedance Probability of 10^{-6}, Set #16

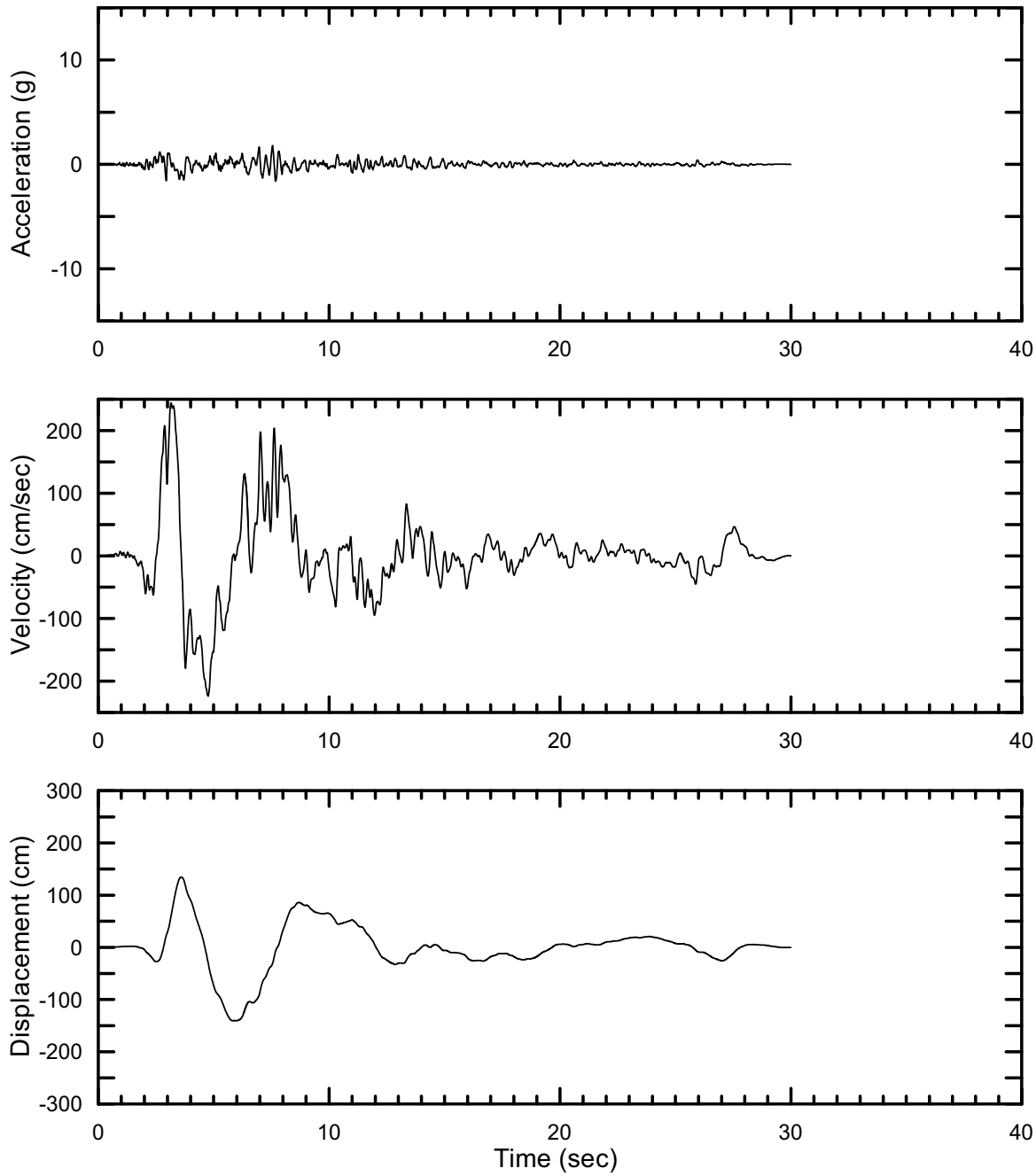

DTN: MO0301TMHIS106.001 [DIRS 161868]

Figure II-91. Point B Horizontal-1 Time Histories (PGV Scaled) at an Annual Exceedance Probability of 10^{-6}, Set #17

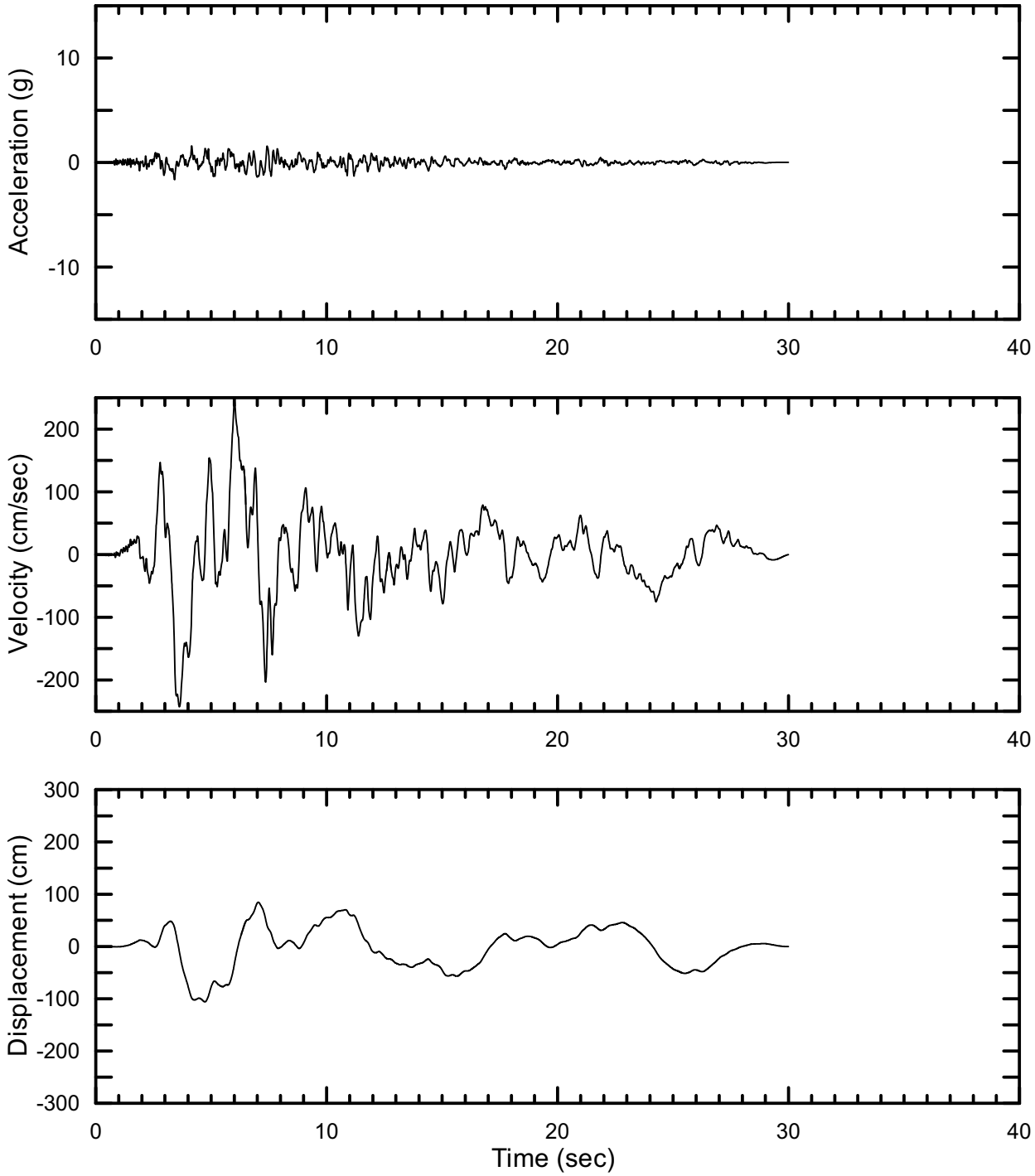

DTN: MO0301TMHIS106.001 [DIRS 161868]

Figure II-92. Point B Horizontal-2 Time Histories (PGV Scaled) at an Annual Exceedance Probability of 10^{-6}, Set #17

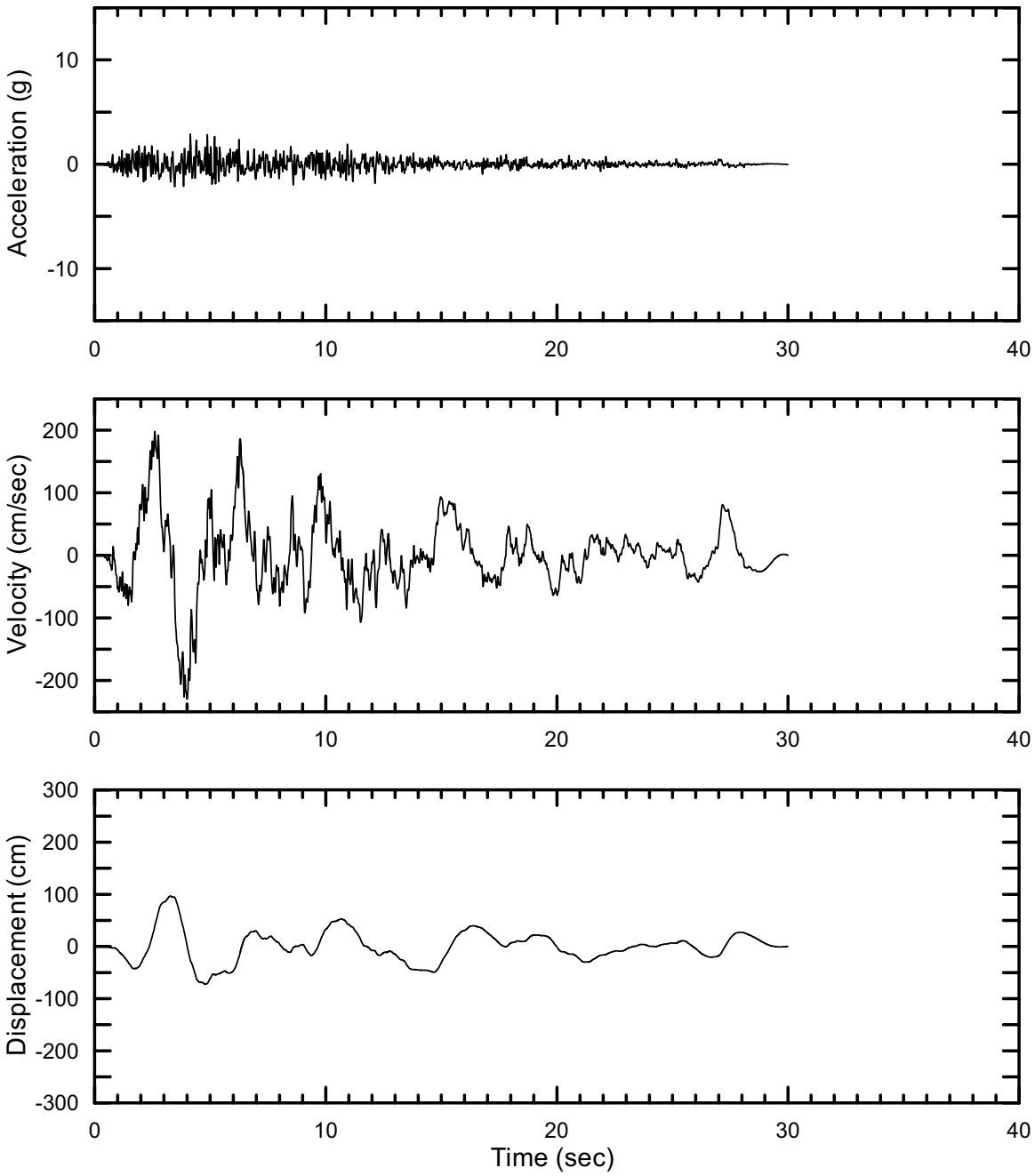

DTN: MO0301TMHIS106.001 [DIRS 161868]

Figure II-93. Point B Vertical Time Histories (PGV Scaled) at an Annual Exceedance Probability of 10^{-6}, Set #17

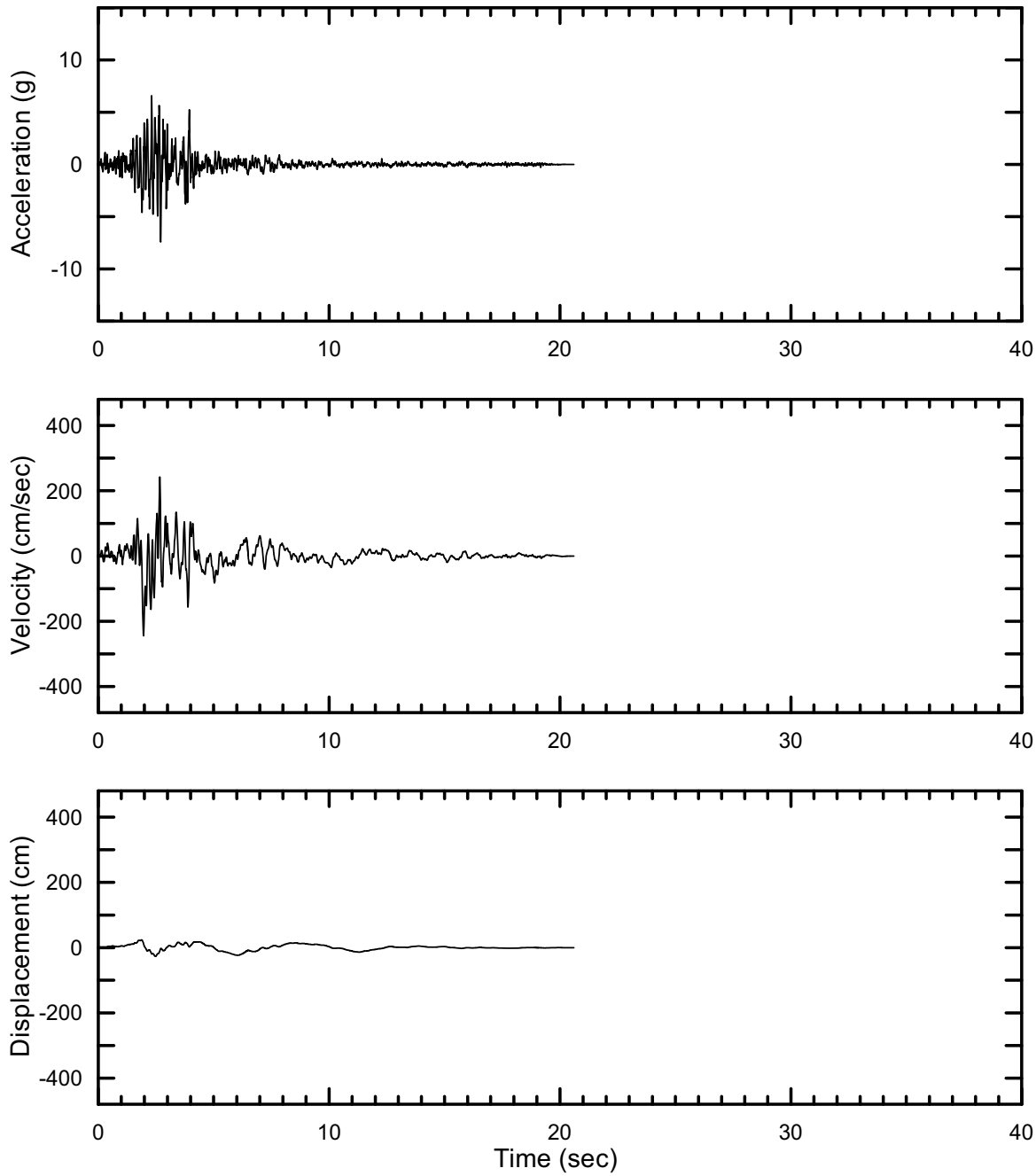

DTN: MO0403AVDSC106.001 [DIRS 168891]

Figure II-94. Point B Horizontal-1 Spectrally Conditioned to Point A Time Histories at an Annual Exceedance Probability of 10^{-6}, Set #1

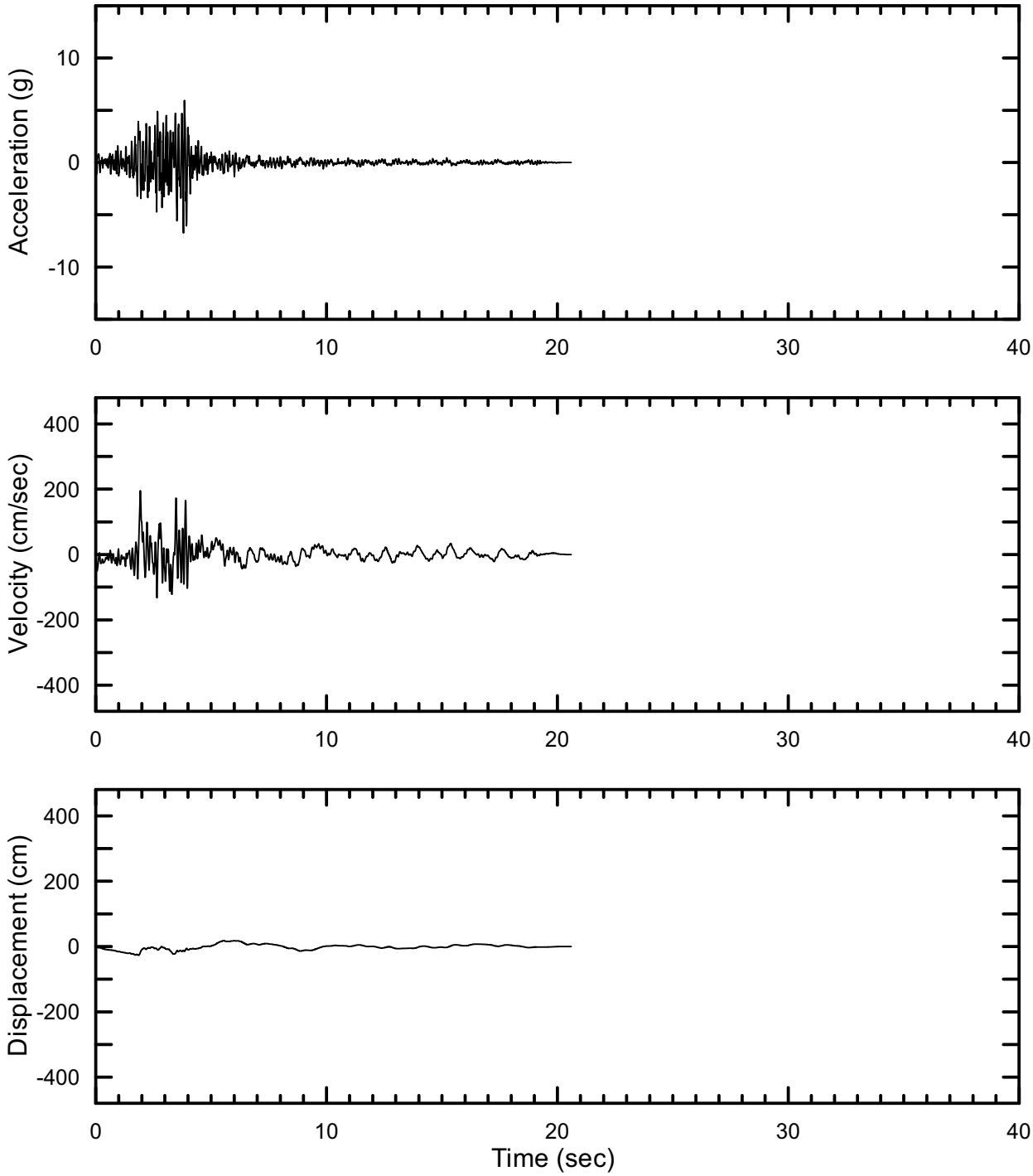

DTN: MO0403AVDSC106.001 [DIRS 168891]

Figure II-95. Point B Horizontal-2 Spectrally Conditioned to Point A Time Histories at an Annual Exceedance Probability of 10^{-6}, Set #1

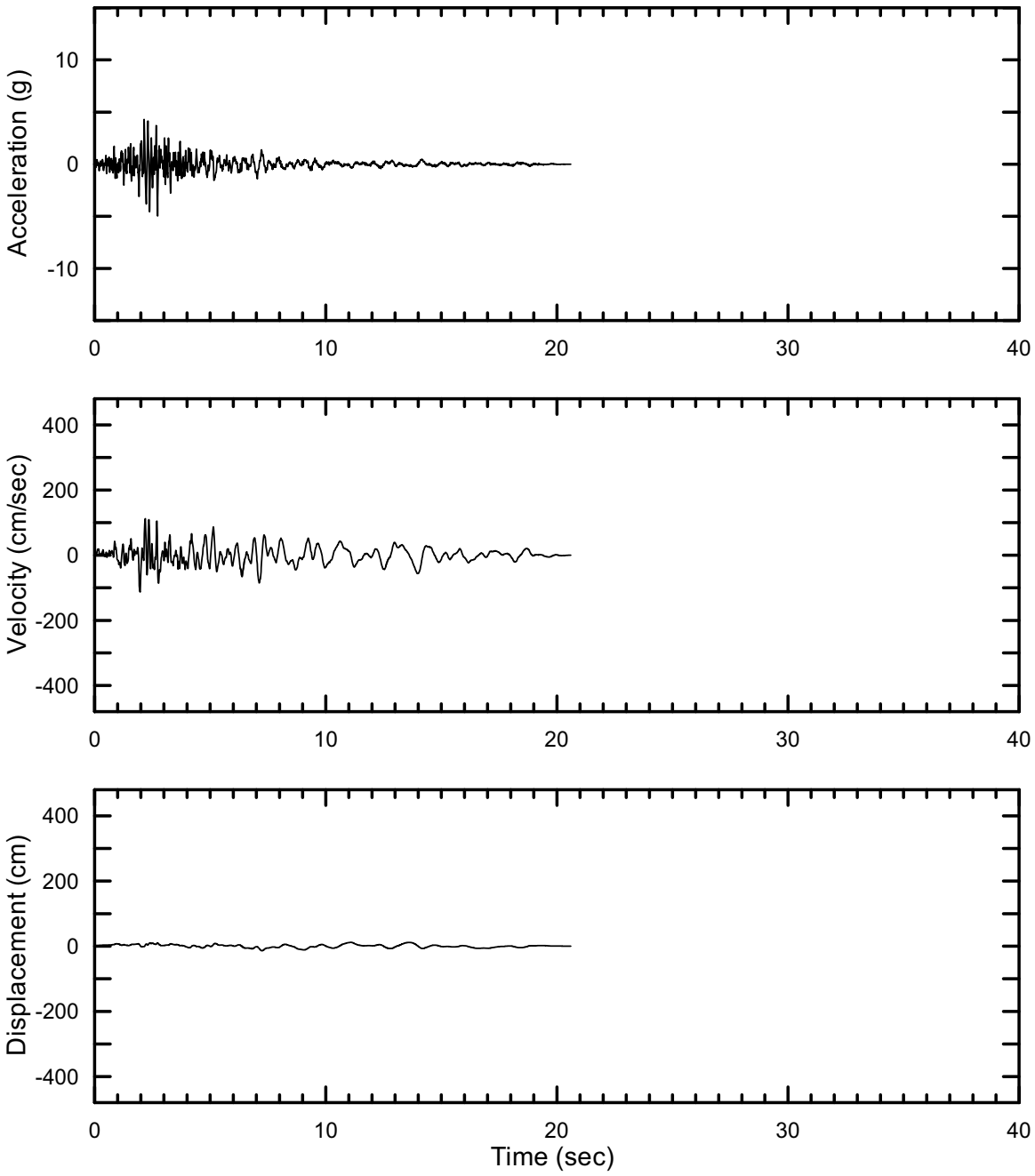

DTN: MO0403AVDSC106.001 [DIRS 168891]

Figure II-96. Point B Vertical Spectrally Conditioned to Point A Time Histories at an Annual Exceedance Probability of 10^{-6}, Set #1

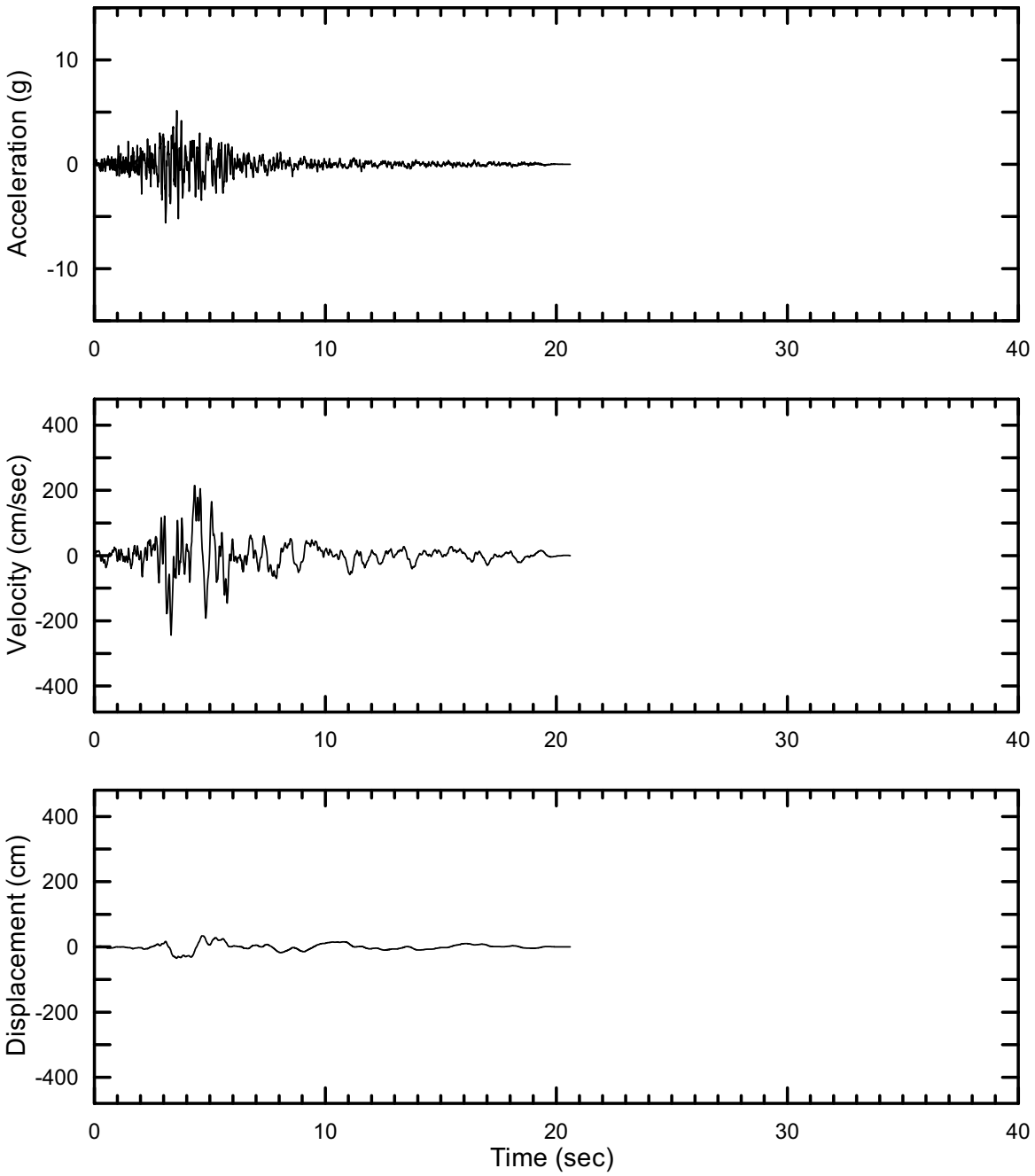

DTN: MO0403AVDSC106.001 [DIRS 168891]

Figure II-97. Point B Horizontal-1 Spectrally Conditioned to Point A Time Histories at an Annual Exceedance Probability of 10^{-6}, Set #2

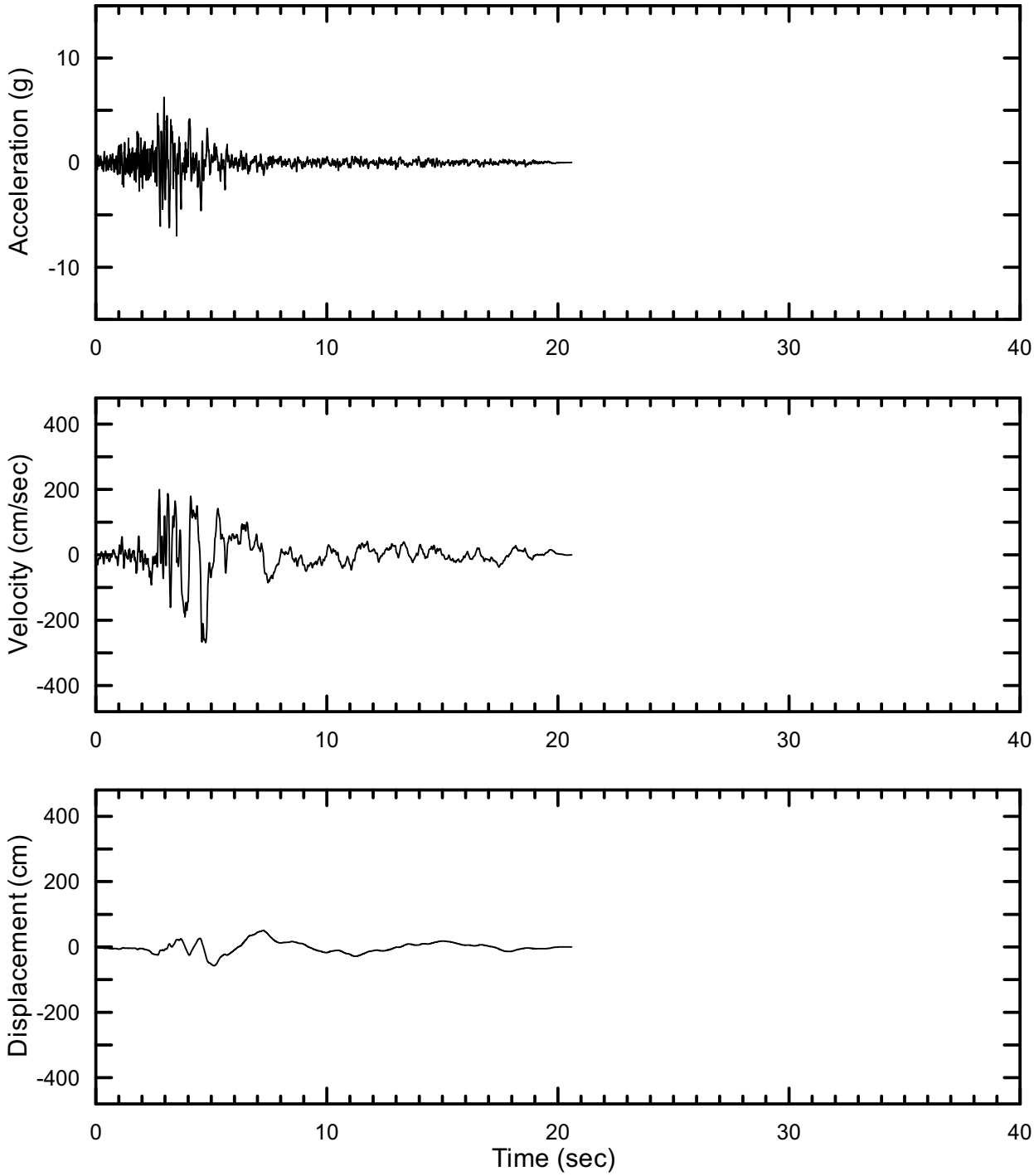

DTN: MO0403AVDSC106.001 [DIRS 168891]

Figure II-98. Point B Horizontal-2 Spectrally Conditioned to Point A Time Histories at an Annual Exceedance Probability of 10^{-6}, Set #2

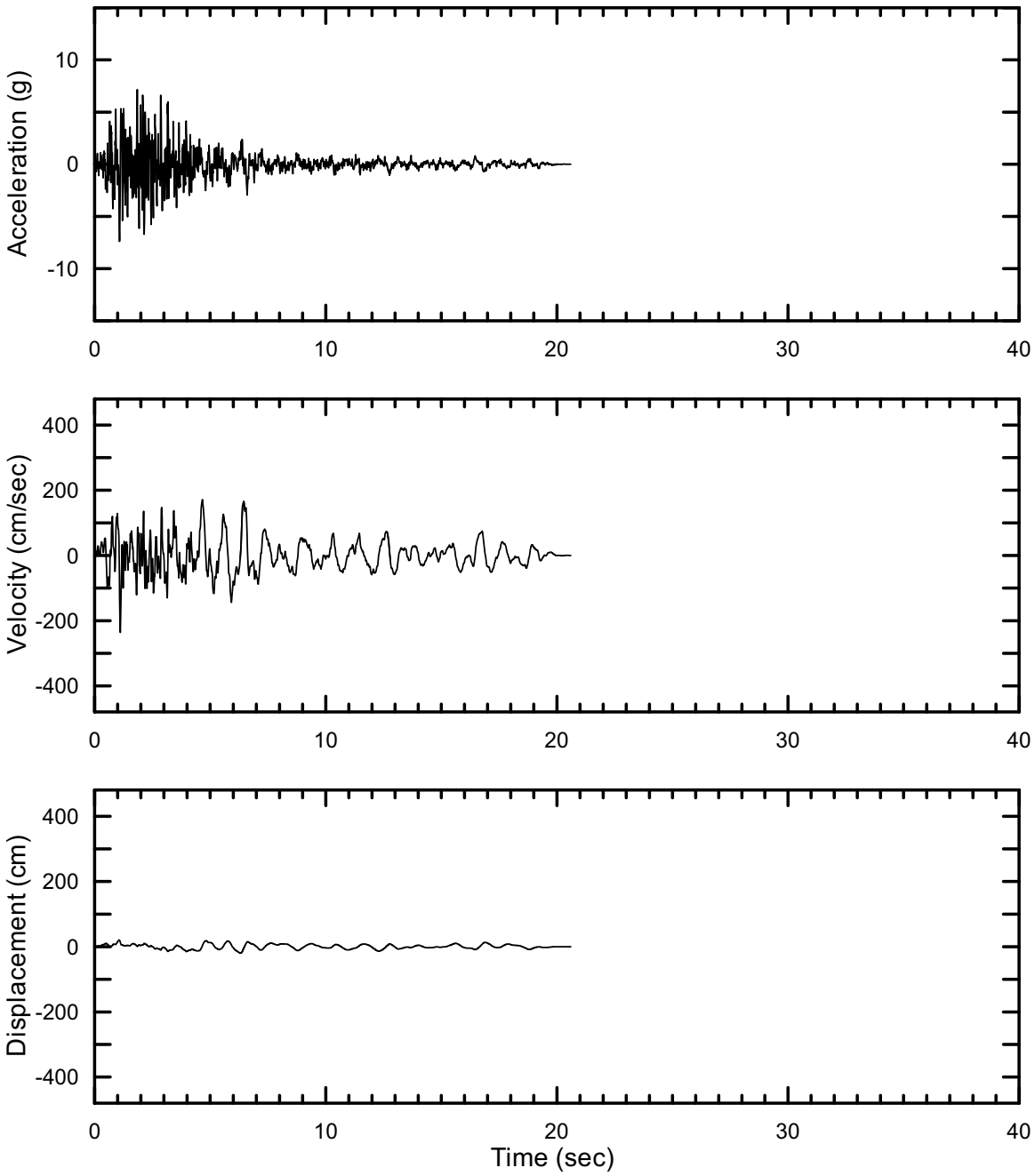

DTN: MO0403AVDSC106.001 [DIRS 168891]

Figure II-99. Point B Vertical Spectrally Conditioned to Point A Time Histories at an Annual Exceedance Probability of 10^{-6}, Set #2

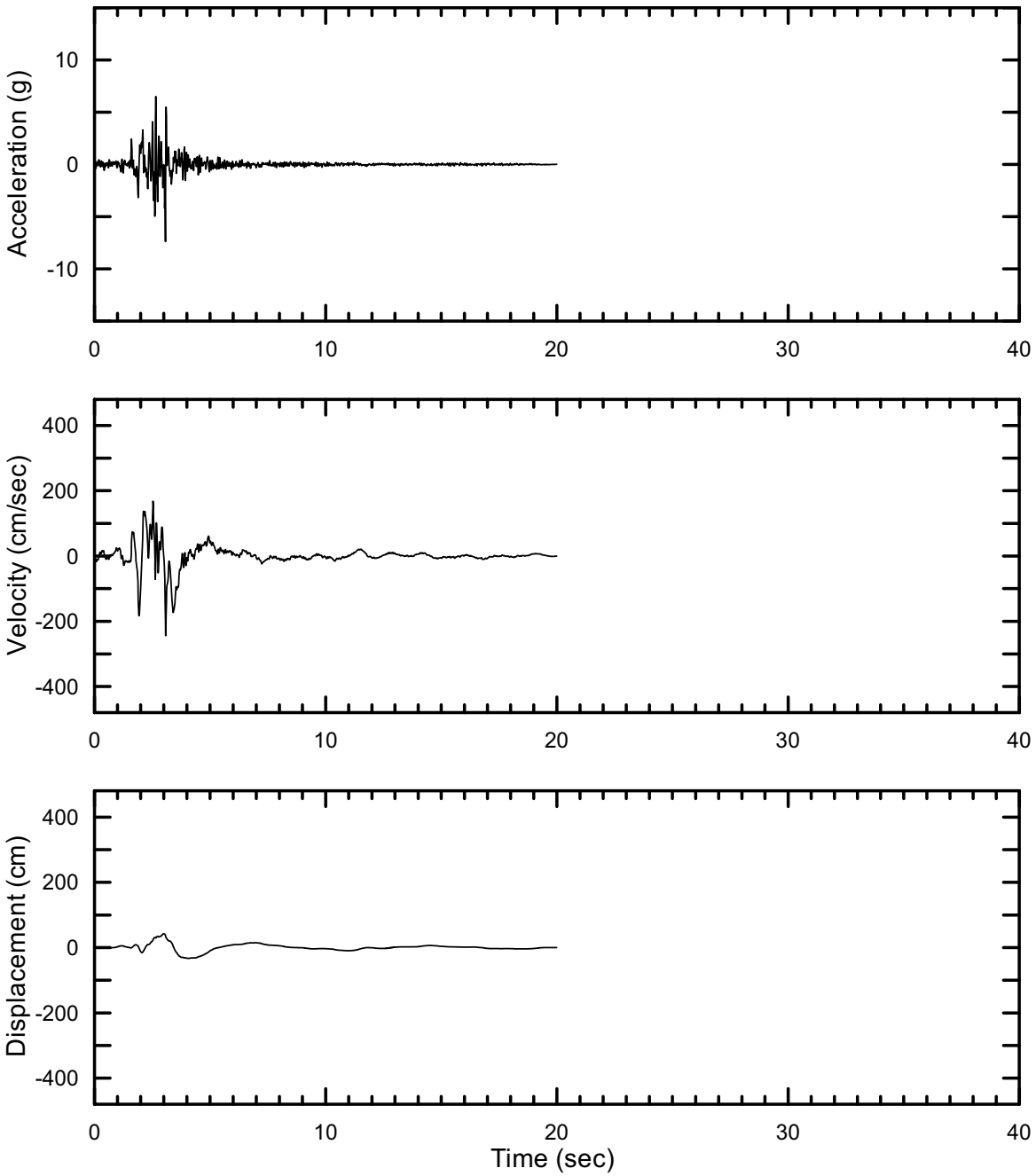

DTN: MO0403AVDSC106.001 [DIRS 168891]

Figure II-100. Point B Horizontal-1 Spectrally Conditioned to Point A Time Histories at an Annual Exceedance Probability of 10^{-6}, Set #3

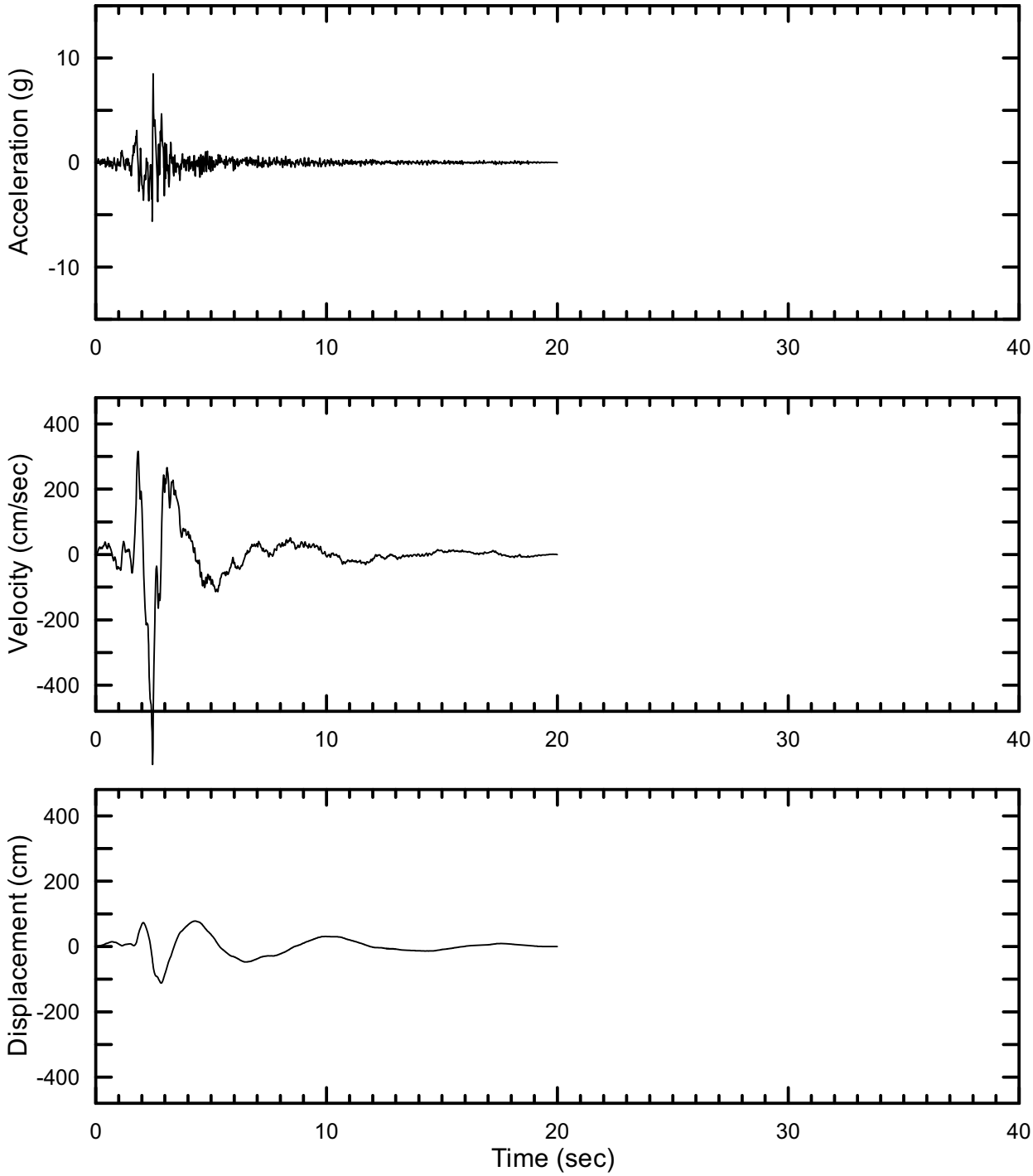

DTN: MO0403AVDSC106.001 [DIRS 168891]

Figure II-101. Point B Horizontal-2 Spectrally Conditioned to Point A Time Histories at an Annual Exceedance Probability of 10^{-6}, Set #3

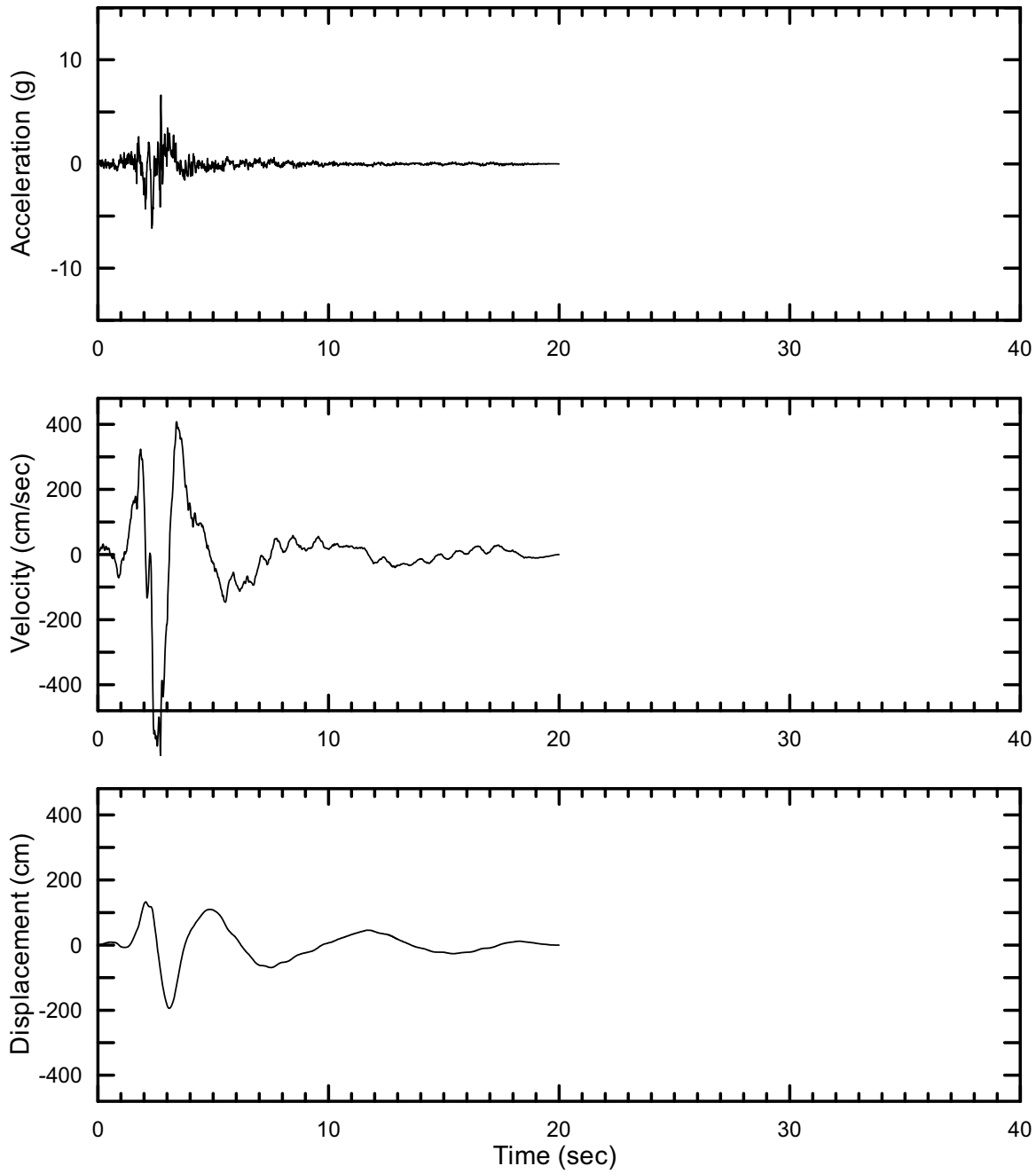

DTN: MO0403AVDSC106.001 [DIRS 168891]

Figure II-102. Point B Vertical Spectrally Conditioned to Point A Time Histories at an Annual Exceedance Probability of 10^{-6}, Set #3

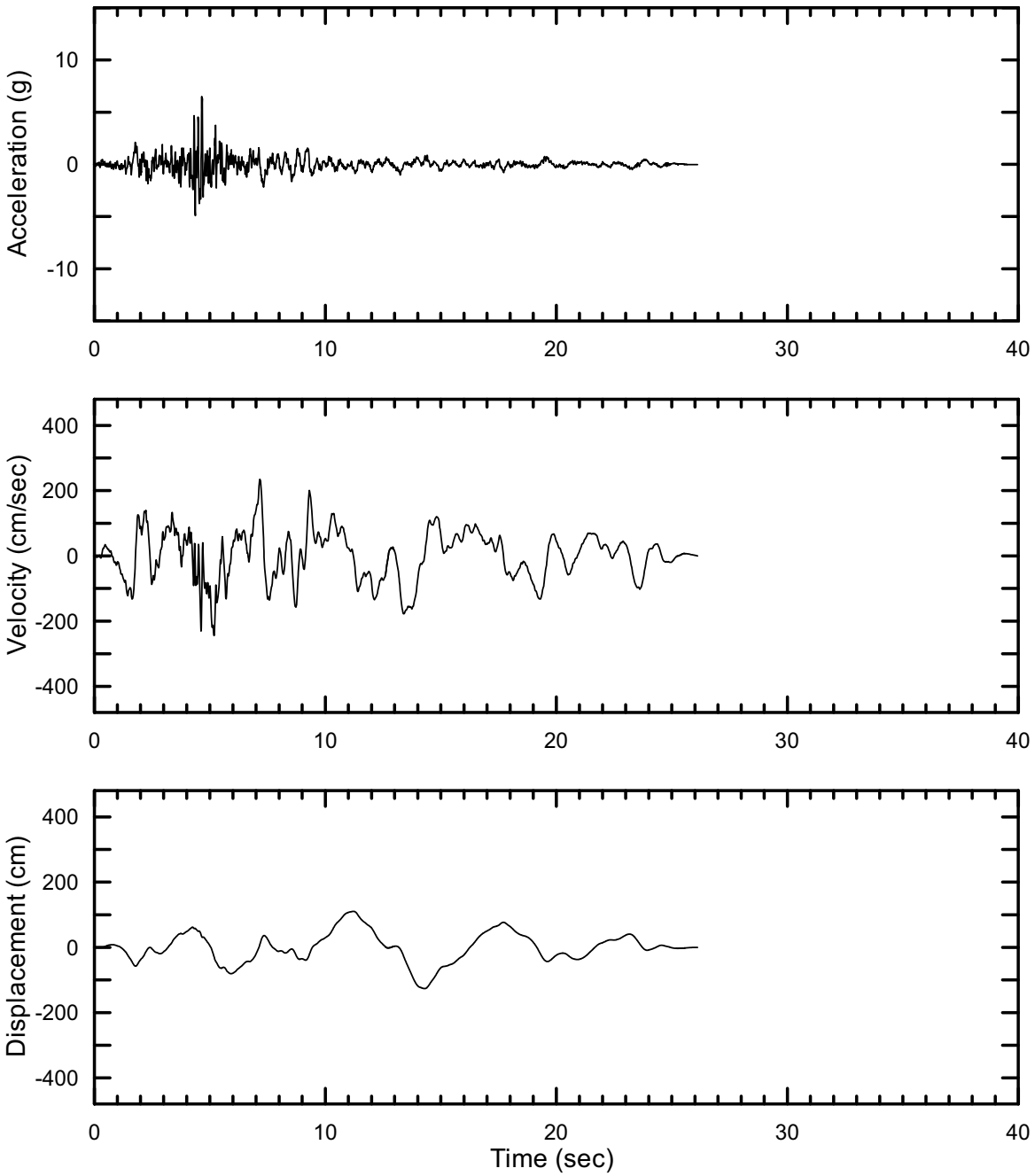

DTN: MO0403AVDSC106.001 [DIRS 168891]

Figure II-103. Point B Horizontal-1 Spectrally Conditioned to Point A Time Histories at an Annual Exceedance Probability of 10^{-6}, Set #4

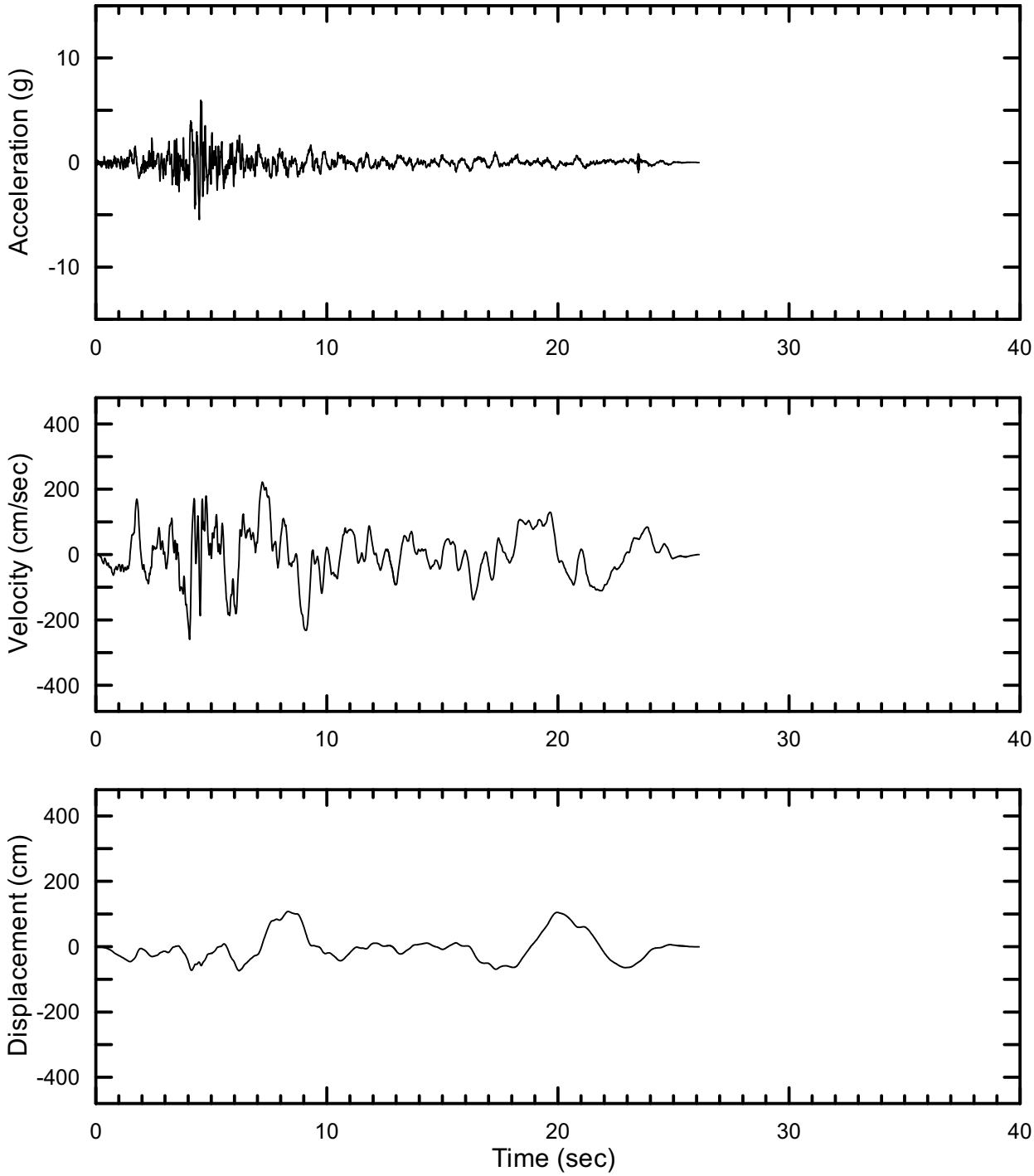

DTN: MO0403AVDSC106.001 [DIRS 168891]

Figure II-104. Point B Horizontal-2 Spectrally Conditioned to Point A Time Histories at an Annual Exceedance Probability of 10^{-6}, Set #4

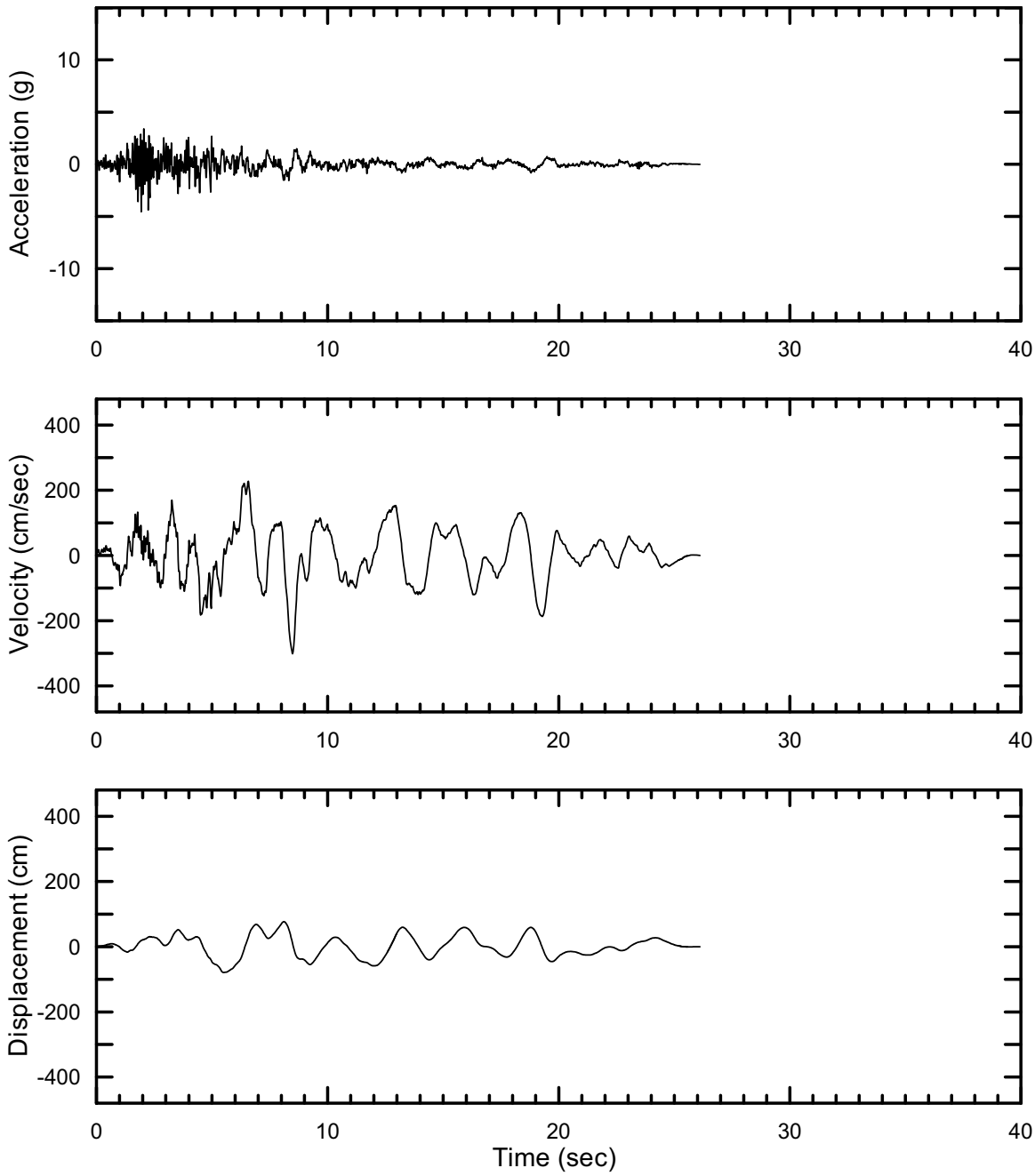

DTN: MO0403AVDSC106.001 [DIRS 168891]

Figure II-105. Point B Vertical Spectrally Conditioned to Point A Time Histories at an Annual Exceedance Probability of 10^{-6}, Set #4

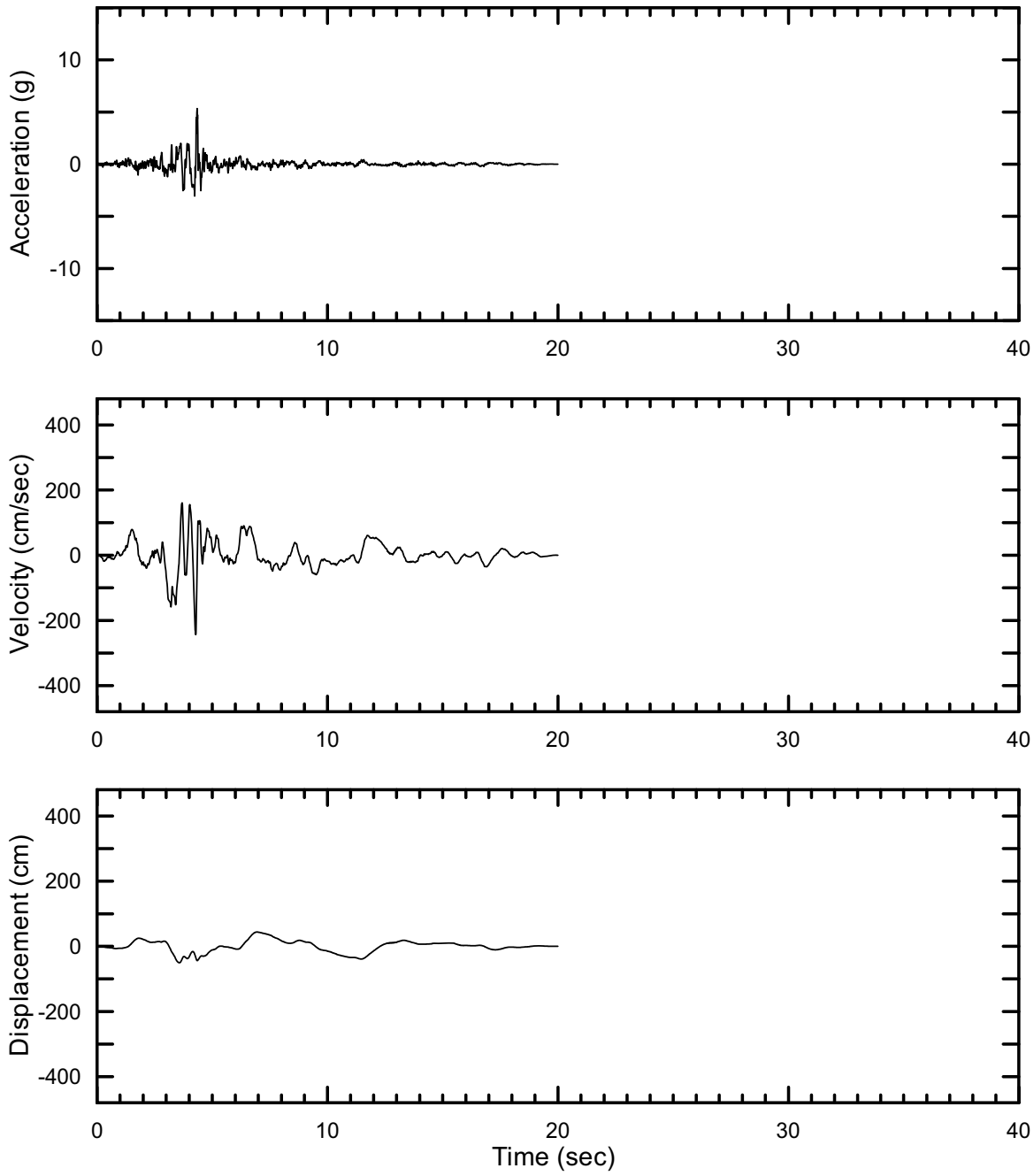

DTN: MO0212AVDSC106.000

Figure II-106. Point B Horizontal-1 Spectrally Conditioned to Point A Time Histories at an Annual Exceedance Probability of 10^{-6}, Set #5

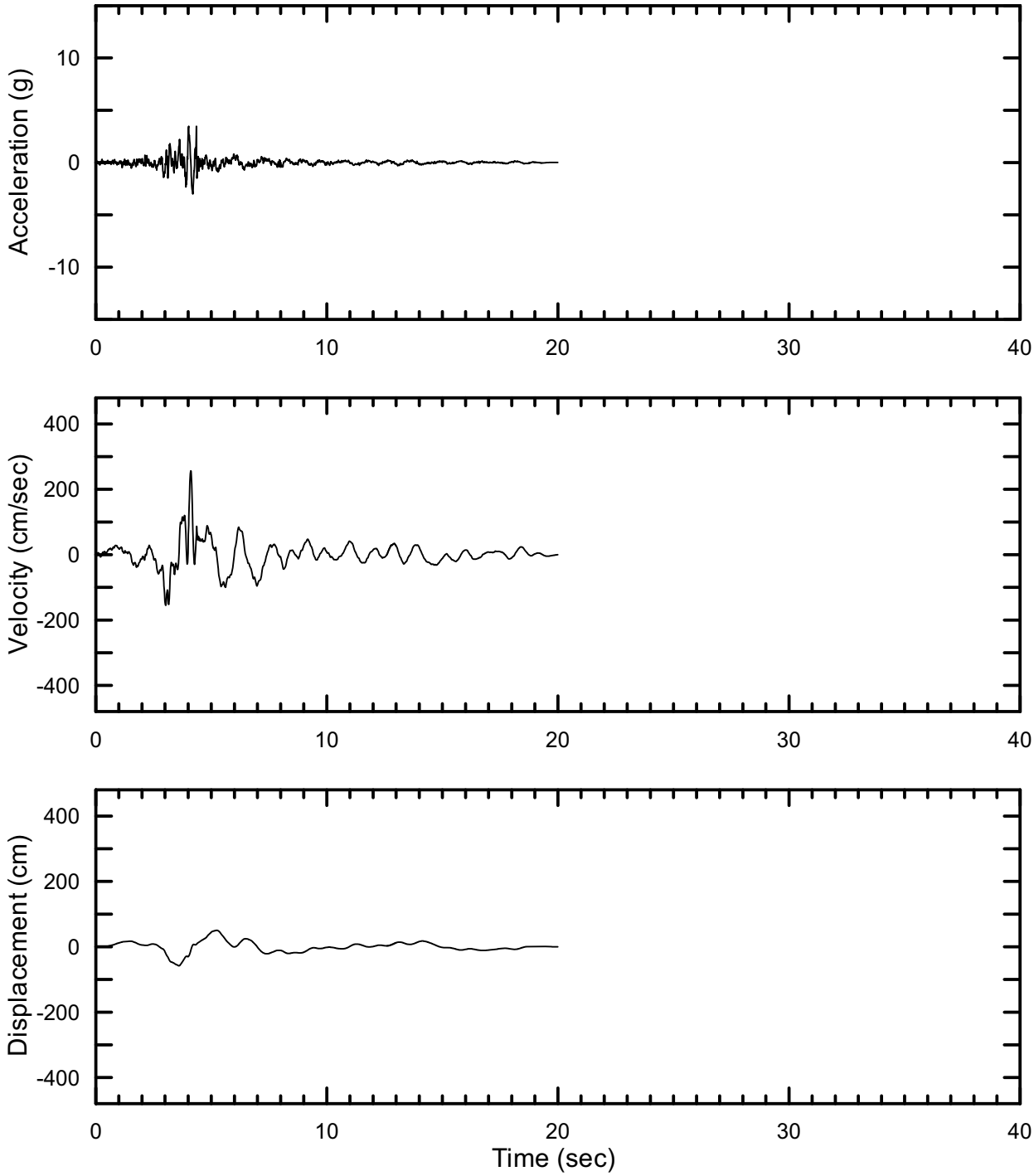

DTN: MO0403AVDSC106.001 [DIRS 168891]

Figure II-107. Point B Horizontal-2 Spectrally Conditioned to Point A Time Histories at an Annual Exceedance Probability of 10^{-6}, Set #5

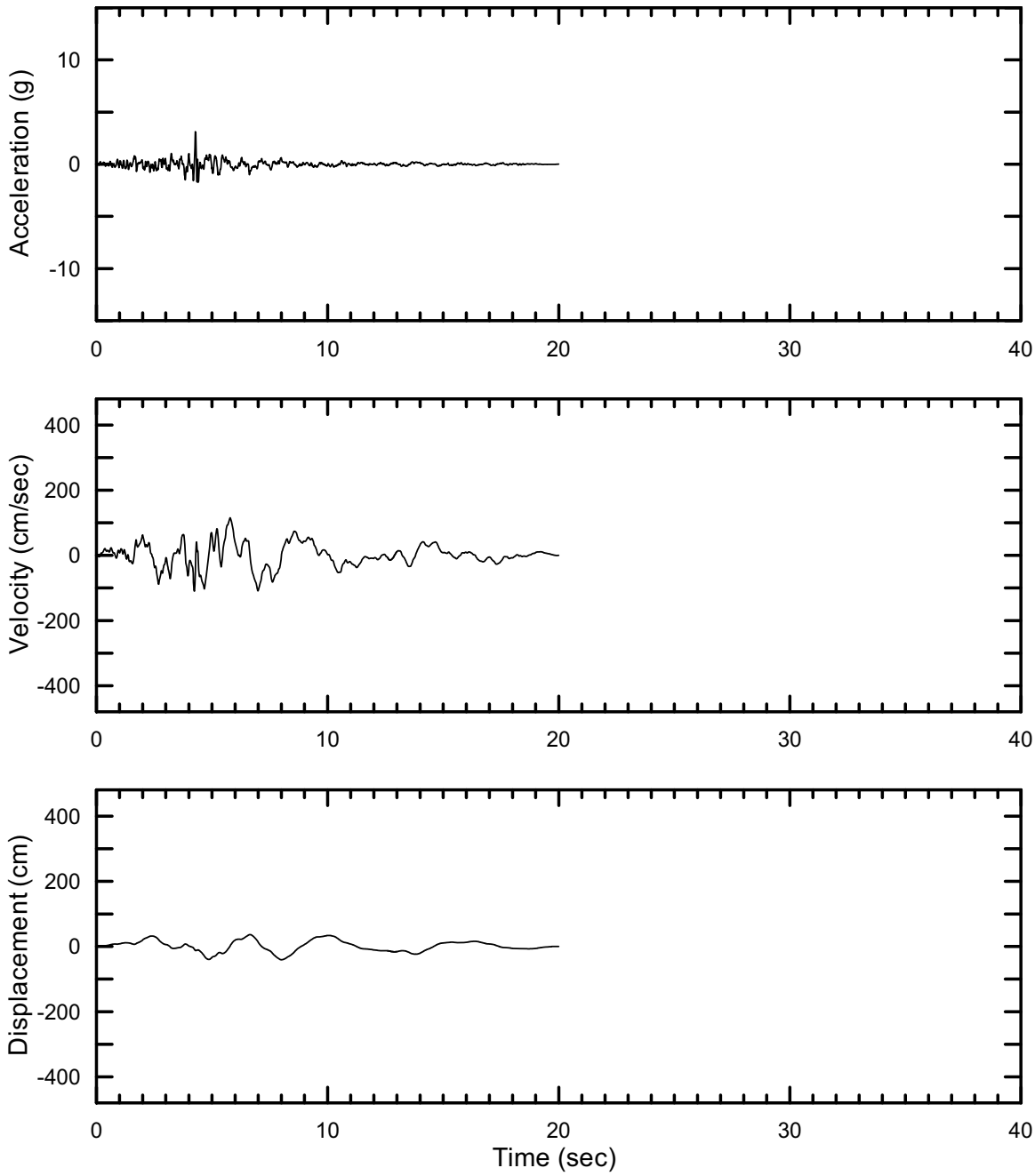

DTN: MO0403AVDSC106.001 [DIRS 168891]

Figure II-108. Point B Vertical Spectrally Conditioned to Point A Time Histories at an Annual Exceedance Probability of 10^{-6}, Set #5

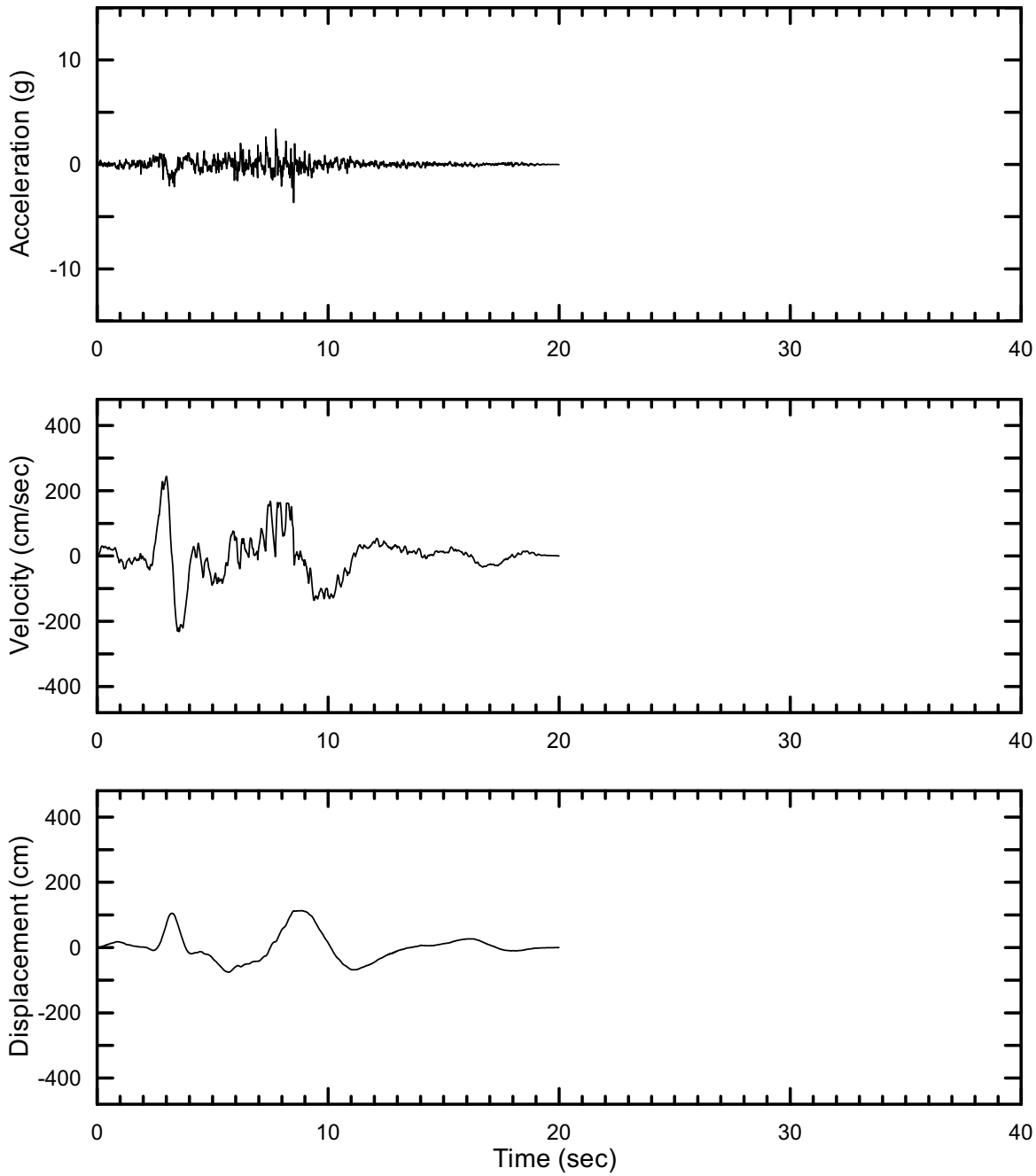

DTN: MO0403AVDSC106.001 [DIRS 168891]

Figure II-109. Point B Horizontal-1 Spectrally Conditioned to Point A Time Histories at an Annual Exceedance Probability of 10^{-6}, Set #6

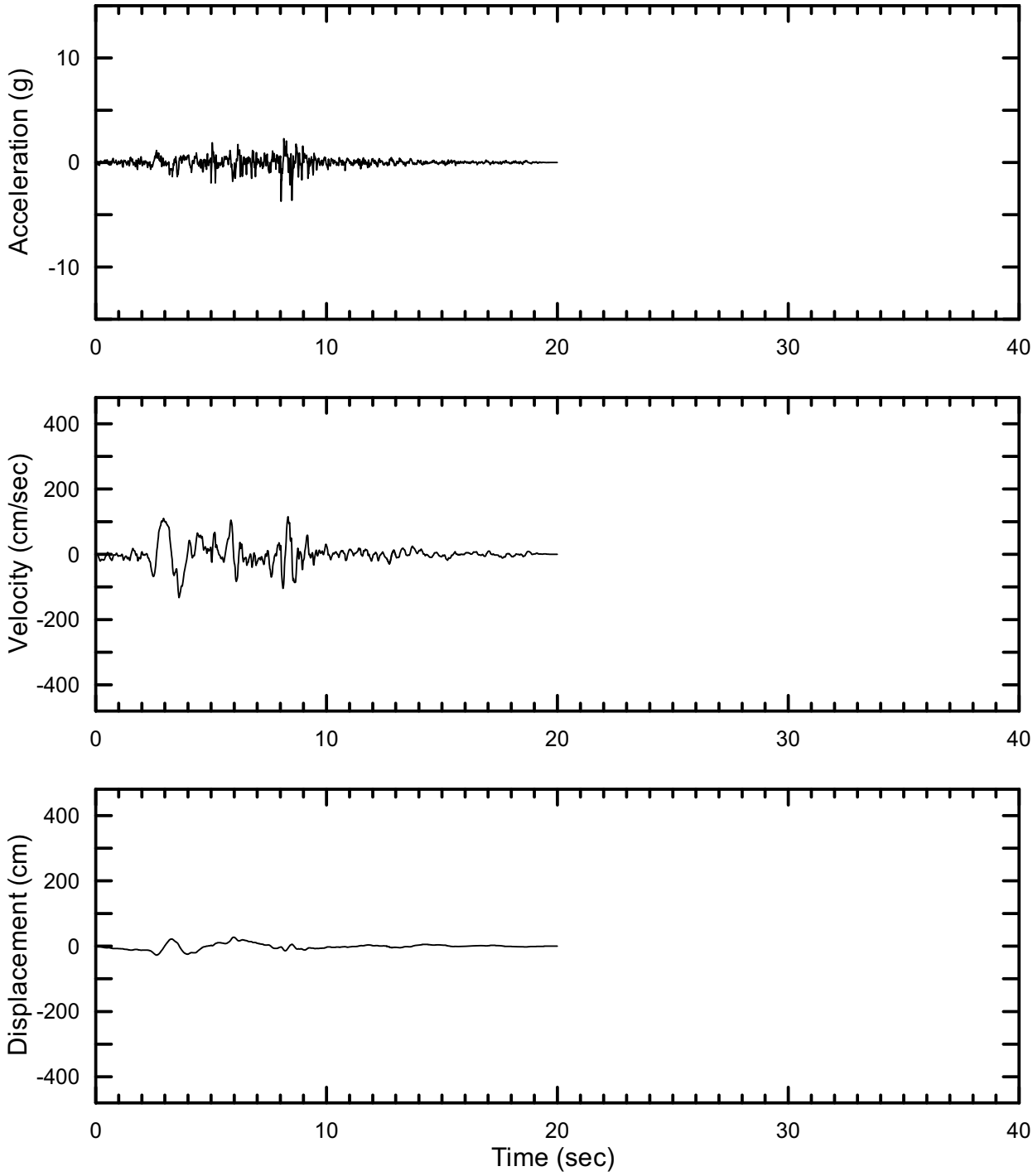

DTN: MO0403AVDSC106.001 [DIRS 168891]

Figure II-110. Point B Horizontal-2 Spectrally Conditioned to Point A Time Histories at an Annual Exceedance Probability of 10^{-6}, Set #6

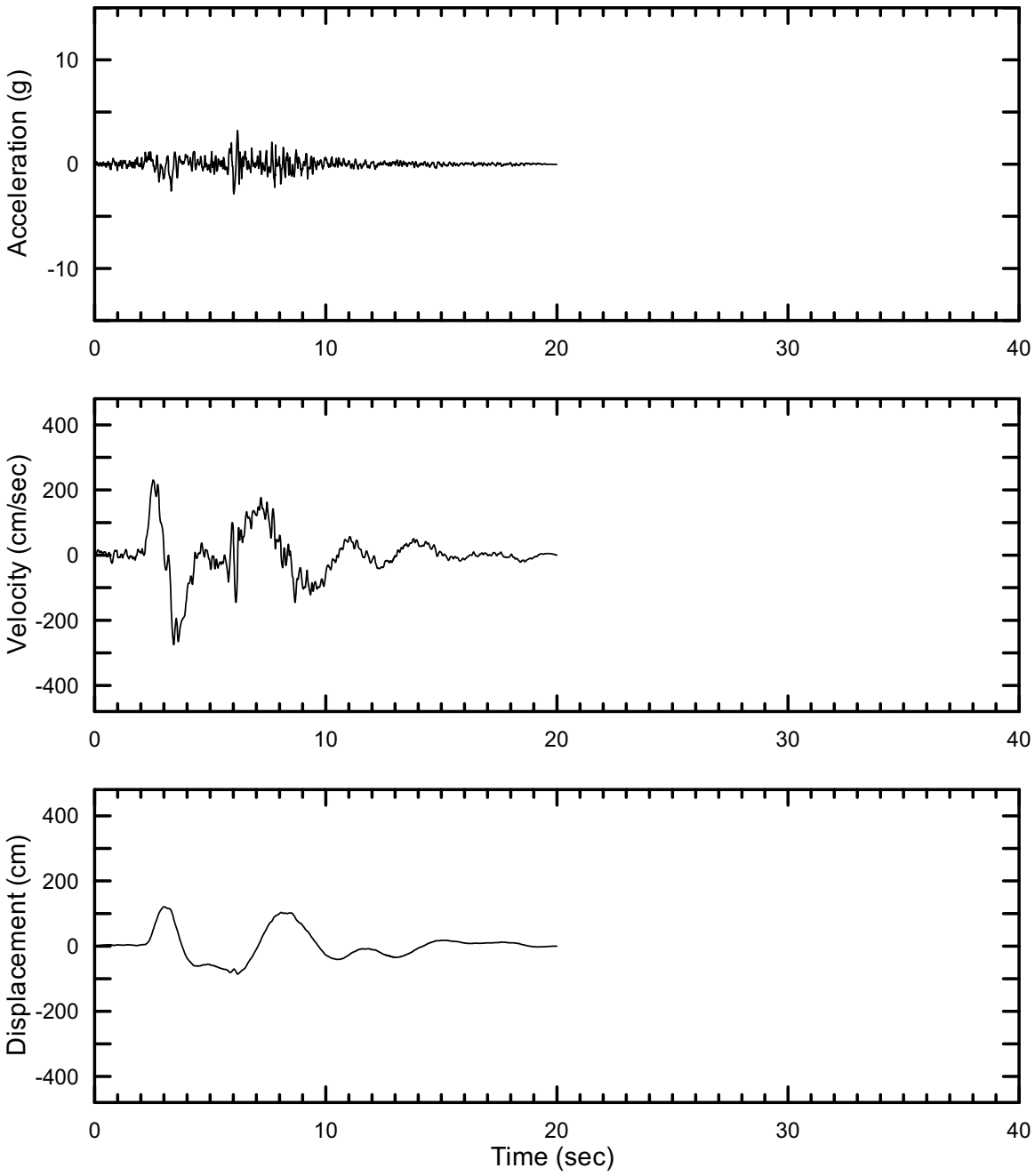

DTN: MO0403AVDSC106.001 [DIRS 168891]

Figure II-111. Point B Vertical Spectrally Conditioned to Point A Time Histories at an Annual Exceedance Probability of 10^{-6}, Set #6

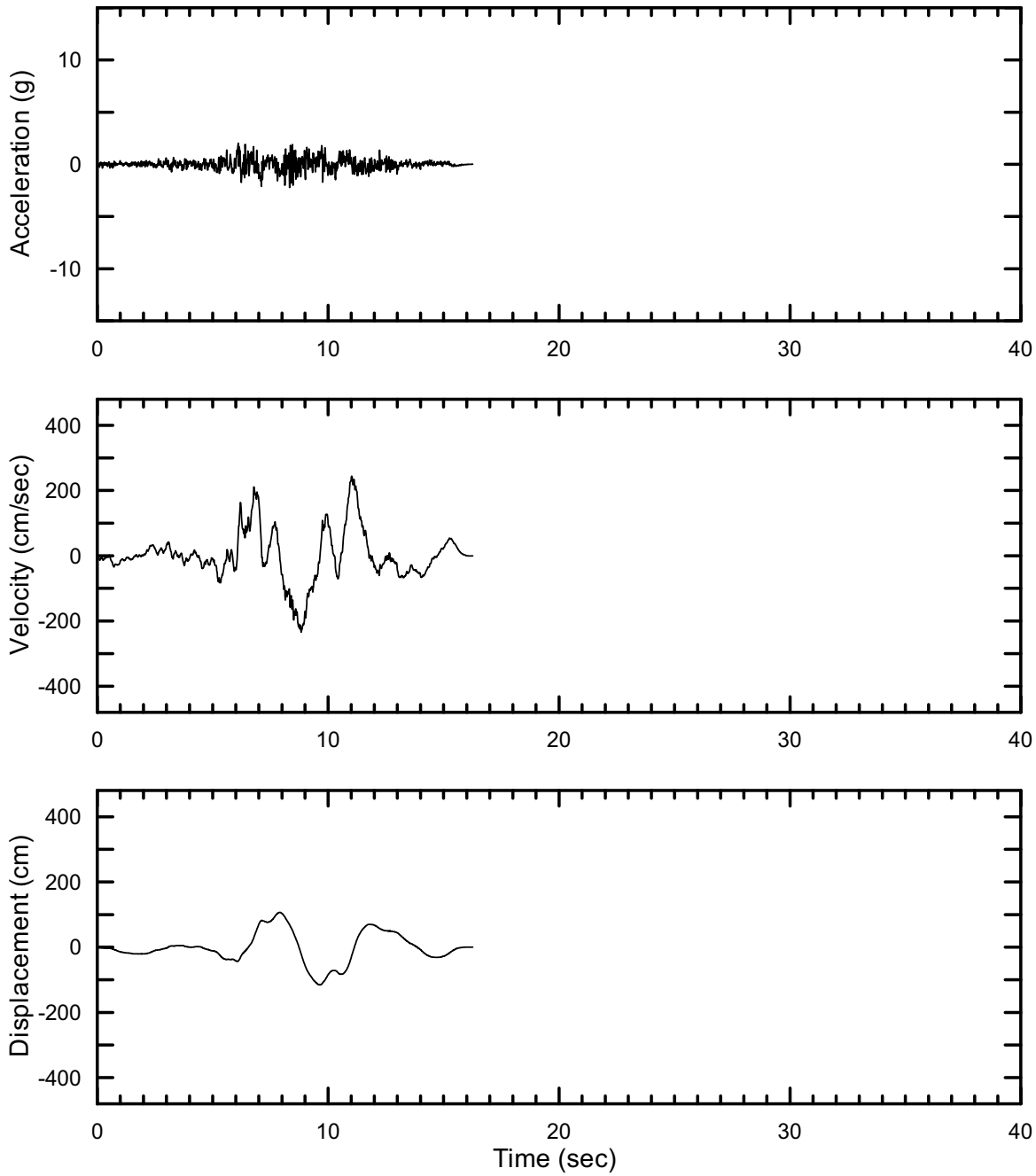

DTN: MO0403AVDSC106.001 [DIRS 168891]

Figure II-112. Point B Horizontal-1 Spectrally Conditioned to Point A Time Histories at an Annual Exceedance Probability of 10^{-6}, Set #7

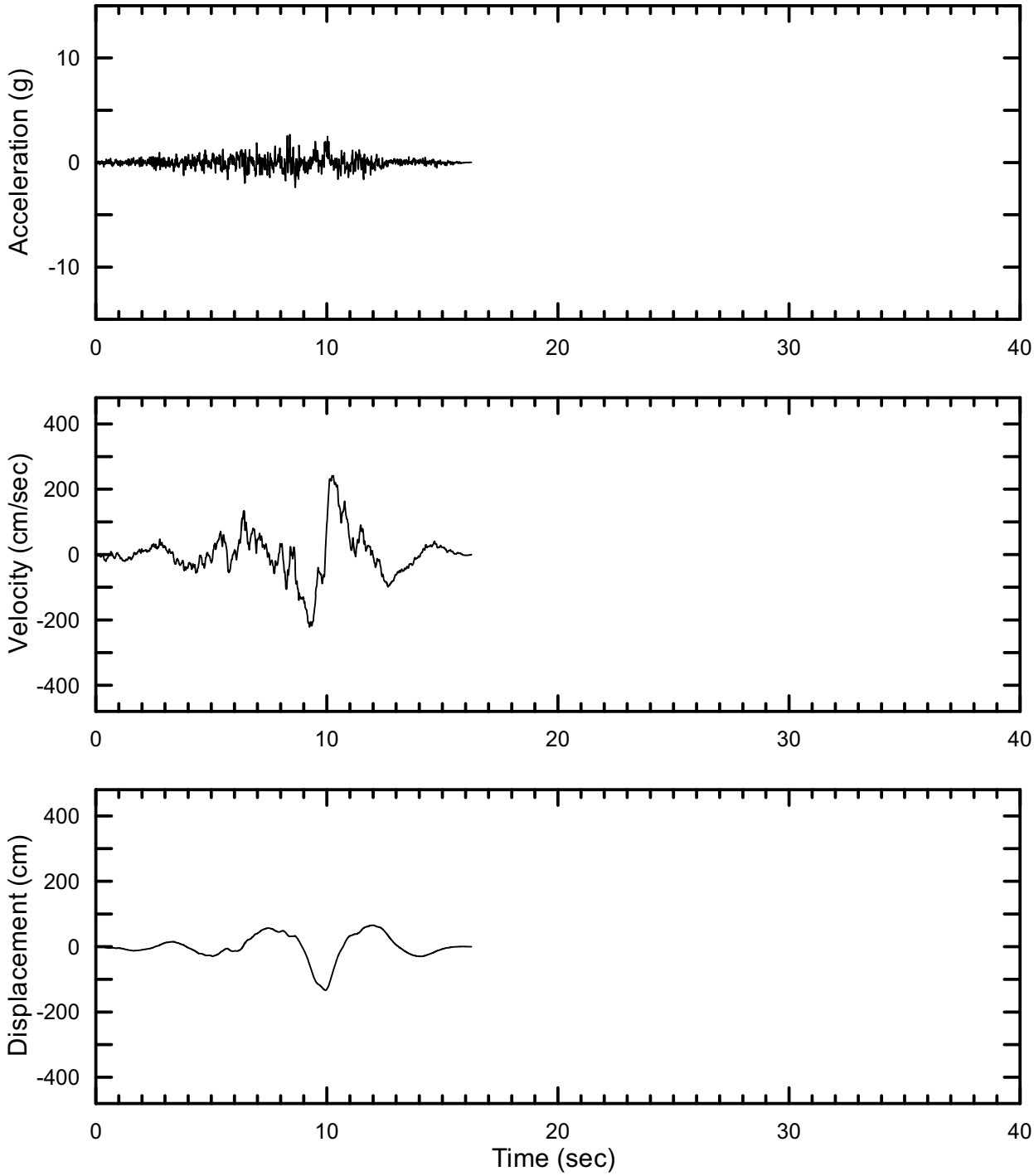

DTN: MO0403AVDSC106.001 [DIRS 168891]

Figure II-113. Point B Horizontal-2 Spectrally Conditioned to Point A Time Histories at an Annual Exceedance Probability of 10^{-6}, Set #7

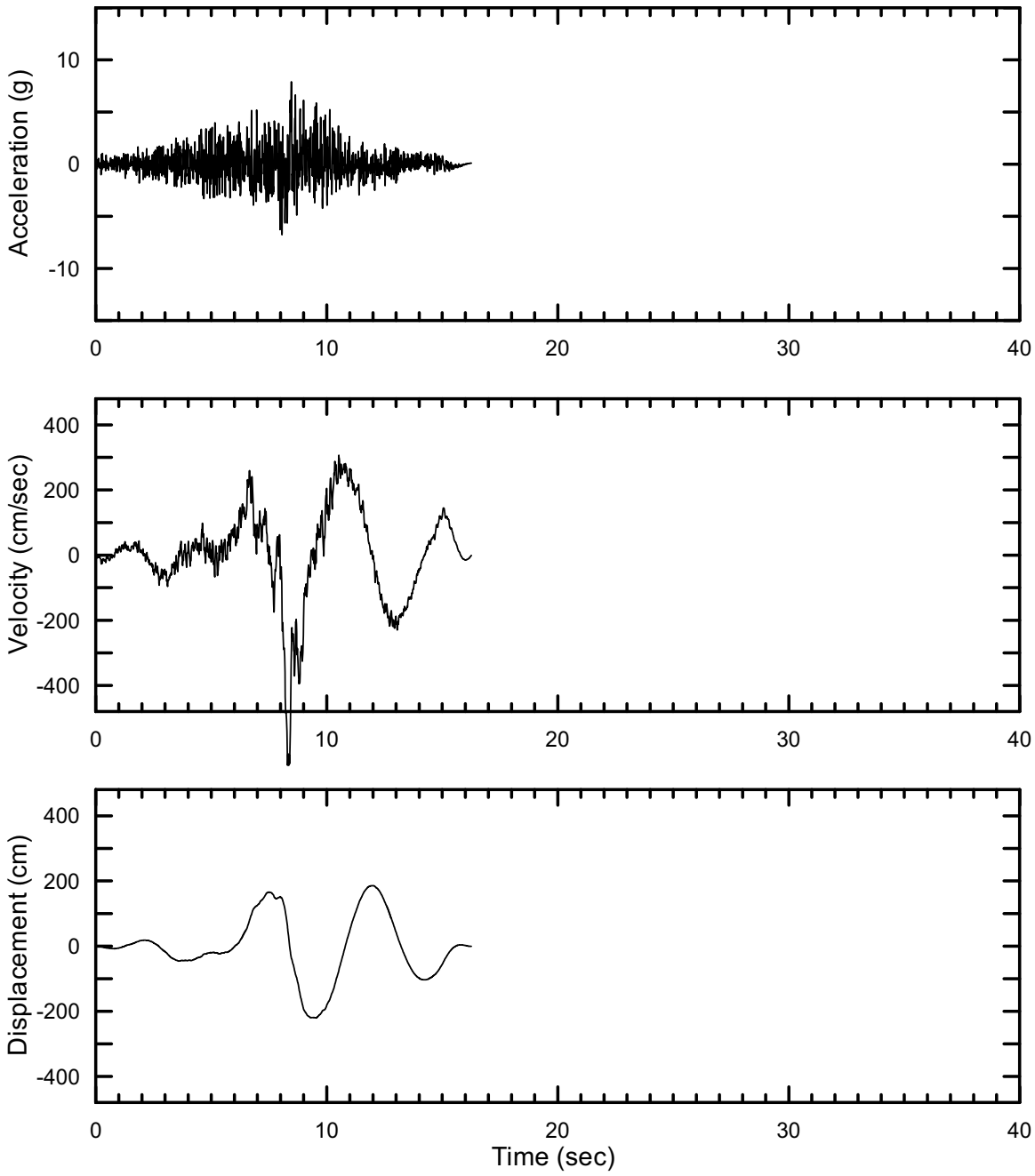

DTN: MO0403AVDSC106.001 [DIRS 168891]

Figure II-114. Point B Vertical Spectrally Conditioned to Point A Time Histories at an Annual Exceedance Probability of 10^{-6}, Set #7

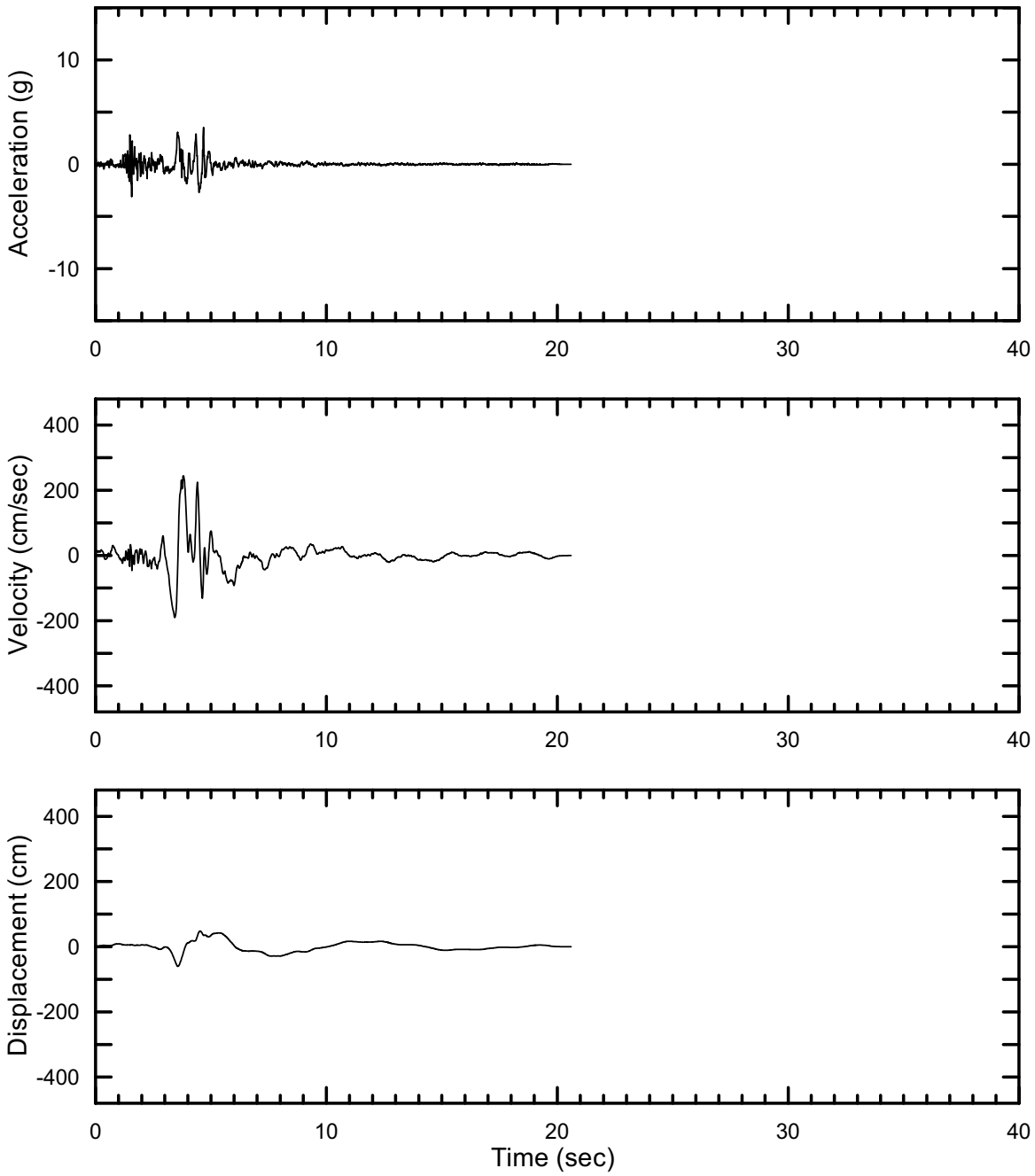

DTN: MO0403AVDSC106.001 [DIRS 168891]

Figure II-115. Point B Horizontal-1 Spectrally Conditioned to Point A Time Histories at an Annual Exceedance Probability of 10^{-6}, Set #8

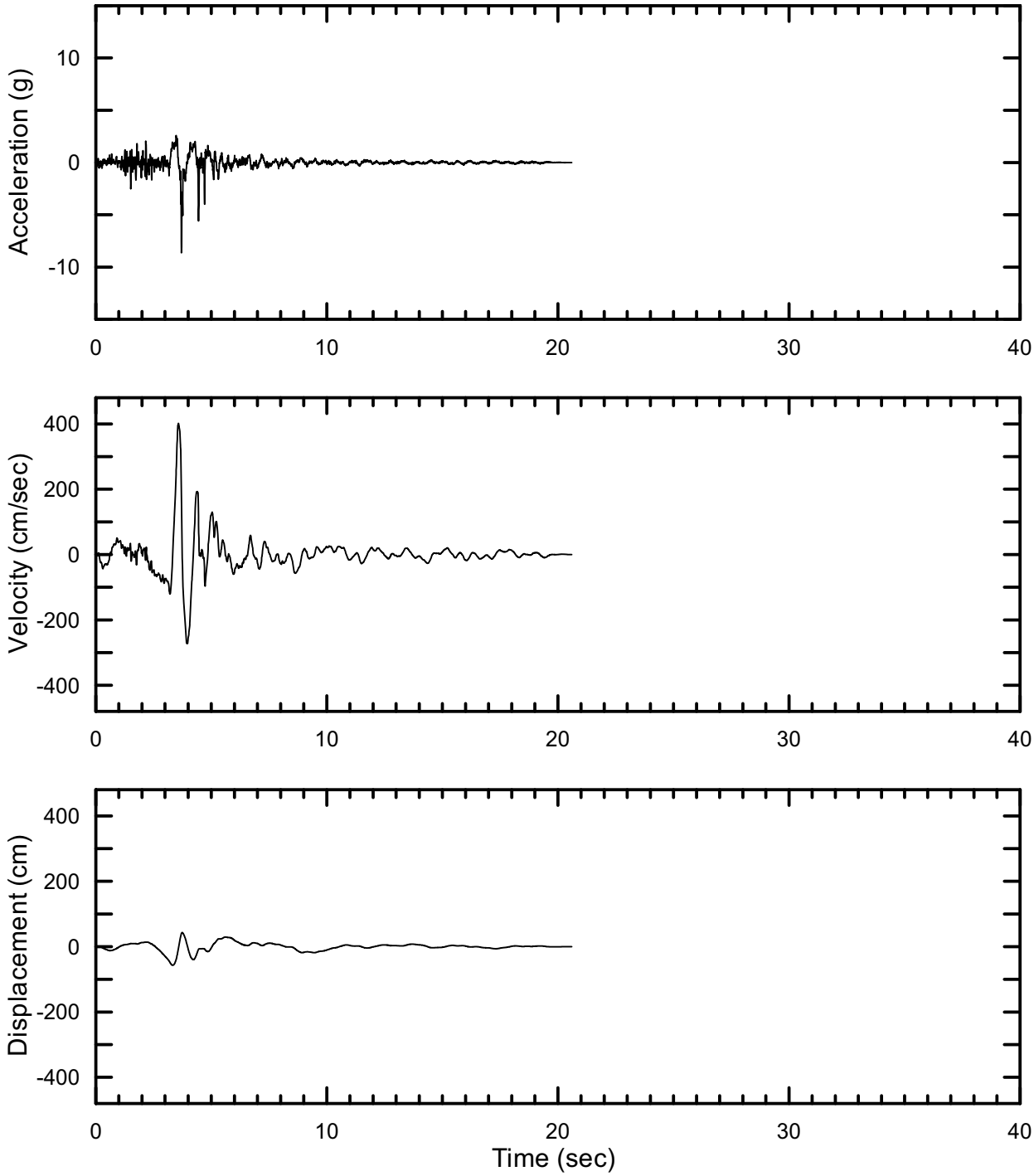

DTN: MO0403AVDSC106.001 [DIRS 168891]

Figure II-116. Point B Horizontal-2 Spectrally Conditioned to Point A Time Histories at an Annual Exceedance Probability of 10^{-6}, Set #8

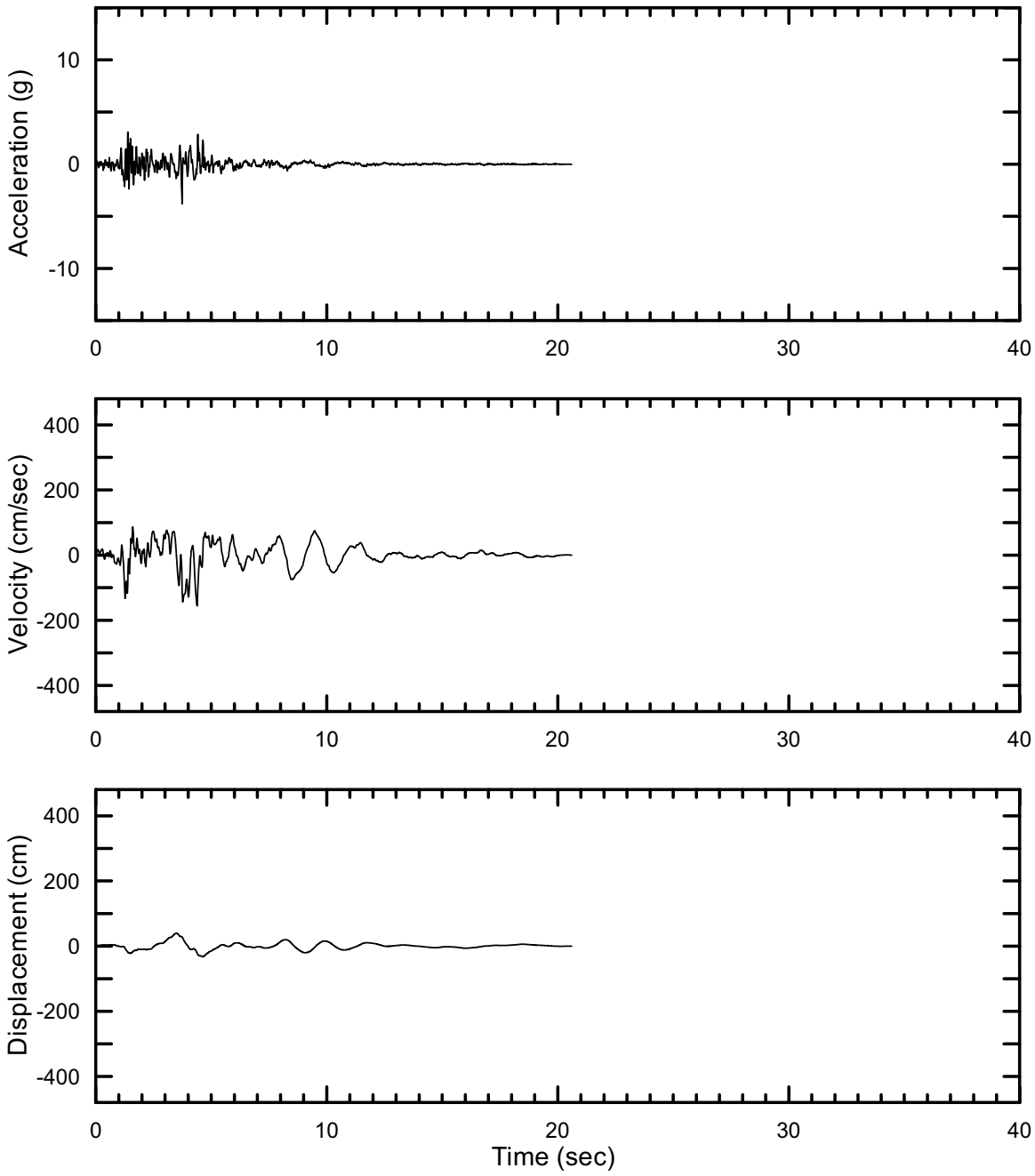

DTN: MO0403AVDSC106.001 [DIRS 168891]

Figure II-117. Point B Vertical Spectrally Conditioned to Point A Time Histories at an Annual Exceedance Probability of 10^{-6}, Set #8

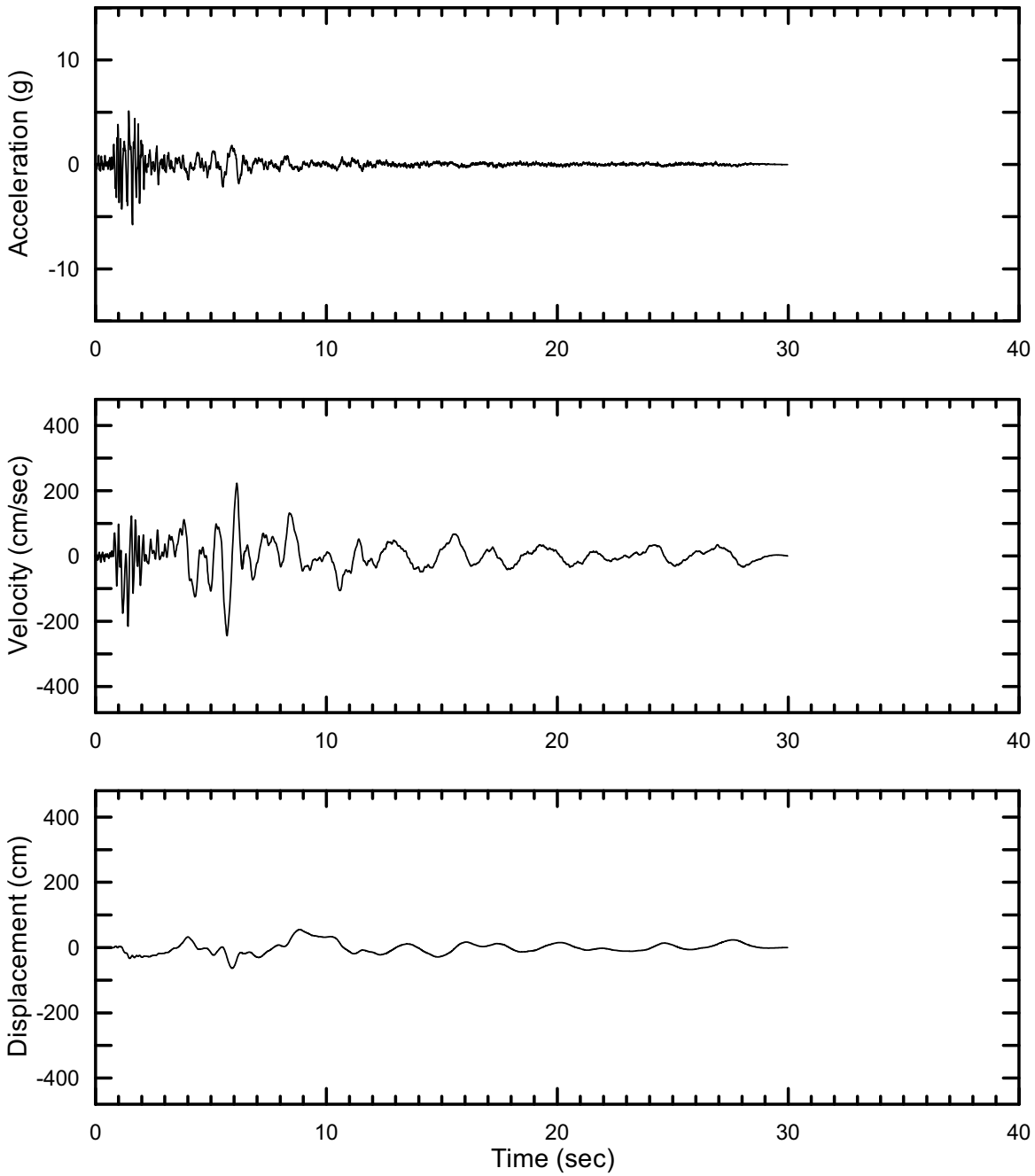

DTN: MO0403AVDSC106.001 [DIRS 168891]

Figure II-118. Point B Horizontal-1 Spectrally Conditioned to Point A Time Histories at an Annual Exceedance Probability of 10^{-6}, Set #9

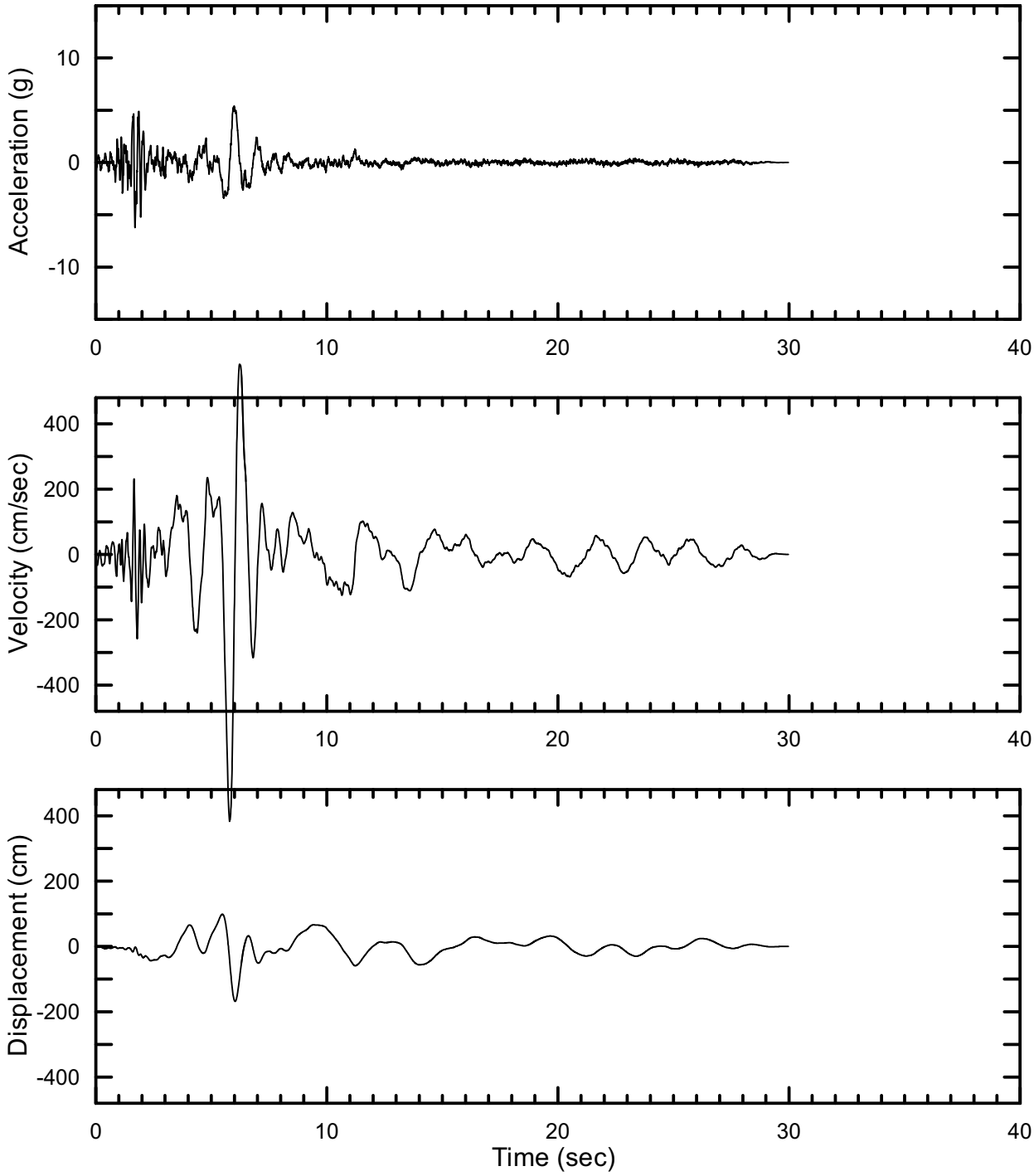

DTN: MO0403AVDSC106.001 [DIRS 168891]

Figure II-119. Point B Horizontal-2 Spectrally Conditioned to Point A Time Histories at an Annual Exceedance Probability of 10^{-6}, Set #9

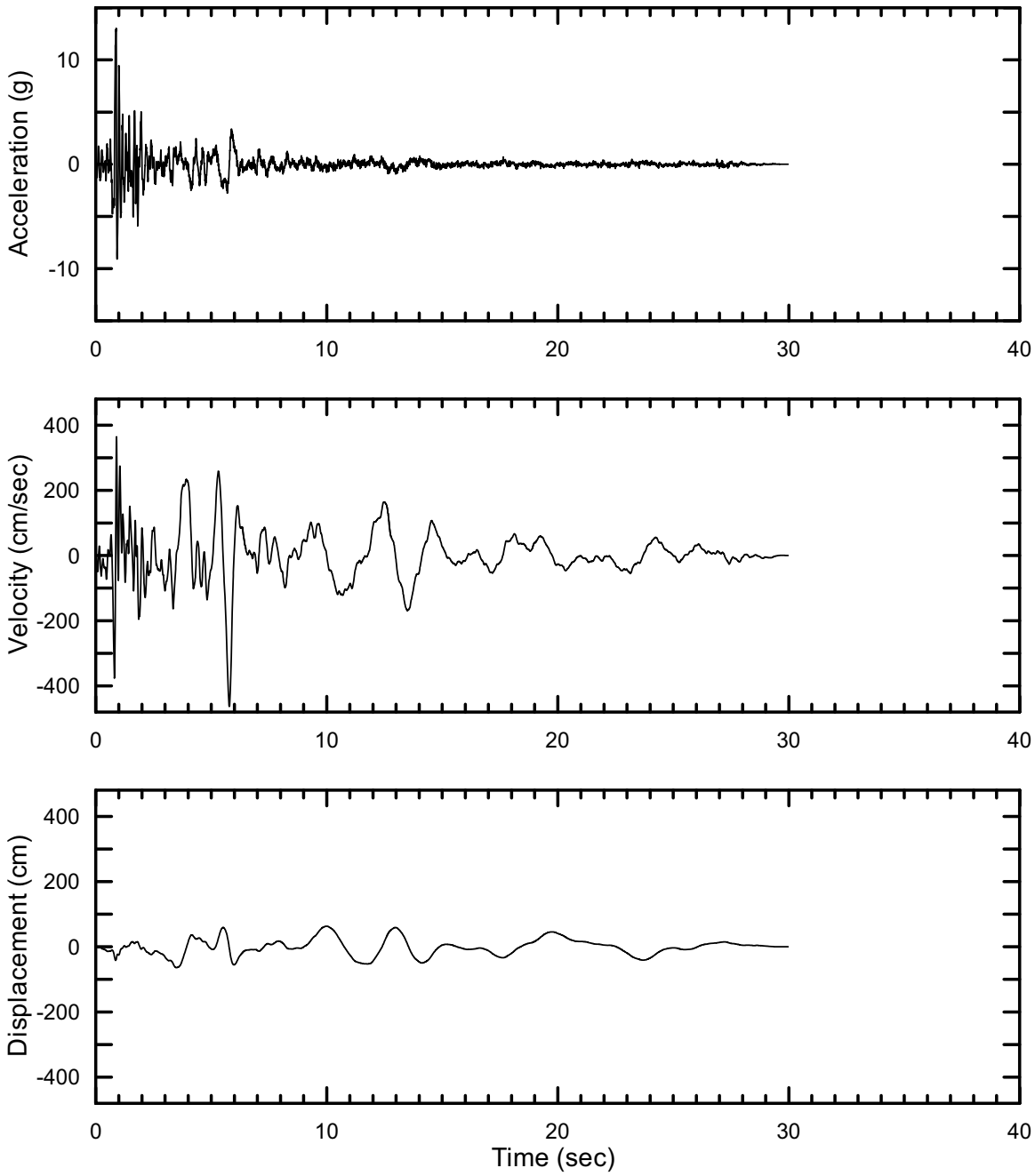

DTN: MO0403AVDSC106.001 [DIRS 168891]

Figure II-120. Point B Vertical Spectrally Conditioned to Point A Time Histories at an Annual Exceedance Probability of 10^{-6}, Set #9

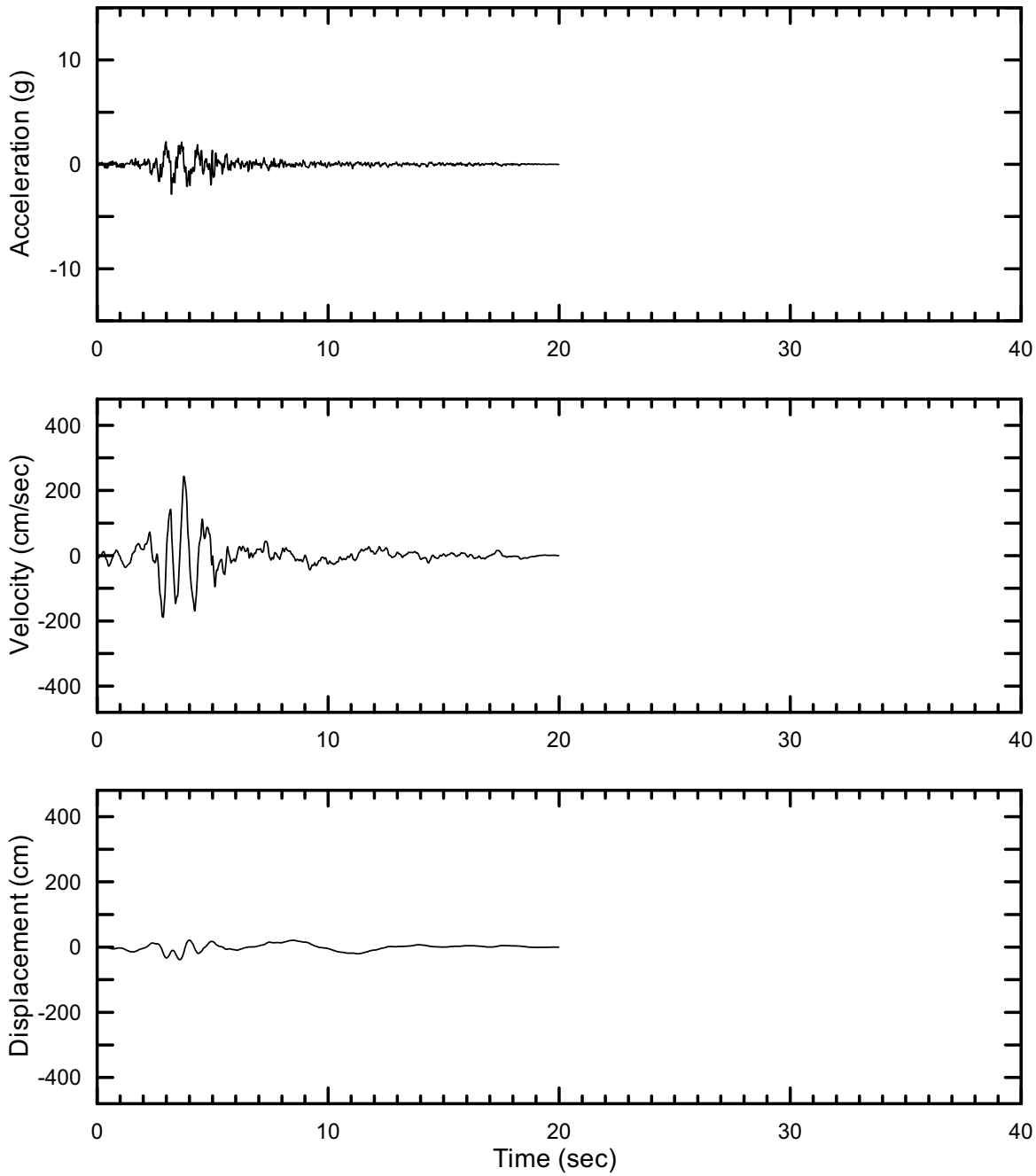

DTN: MO0403AVDSC106.001 [DIRS 168891]

Figure II-121. Point B Horizontal-1 Spectrally Conditioned to Point A Time Histories at an Annual Exceedance Probability of 10^{-6}, Set #10

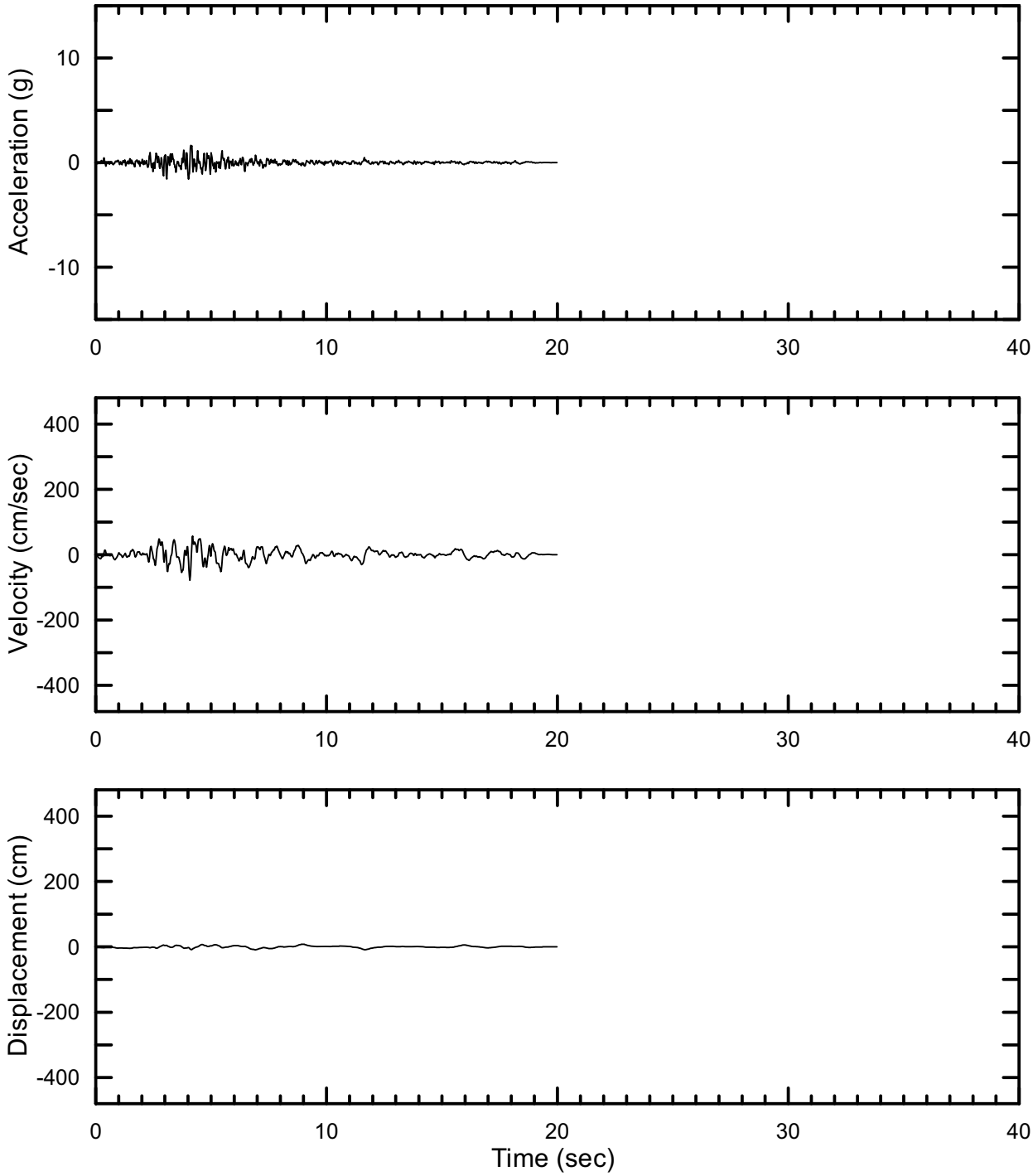

DTN: MO0403AVDSC106.001 [DIRS 168891]

Figure II-122. Point B Horizontal-2 Spectrally Conditioned to Point A Time Histories at an Annual Exceedance Probability of 10^{-6}, Set #10

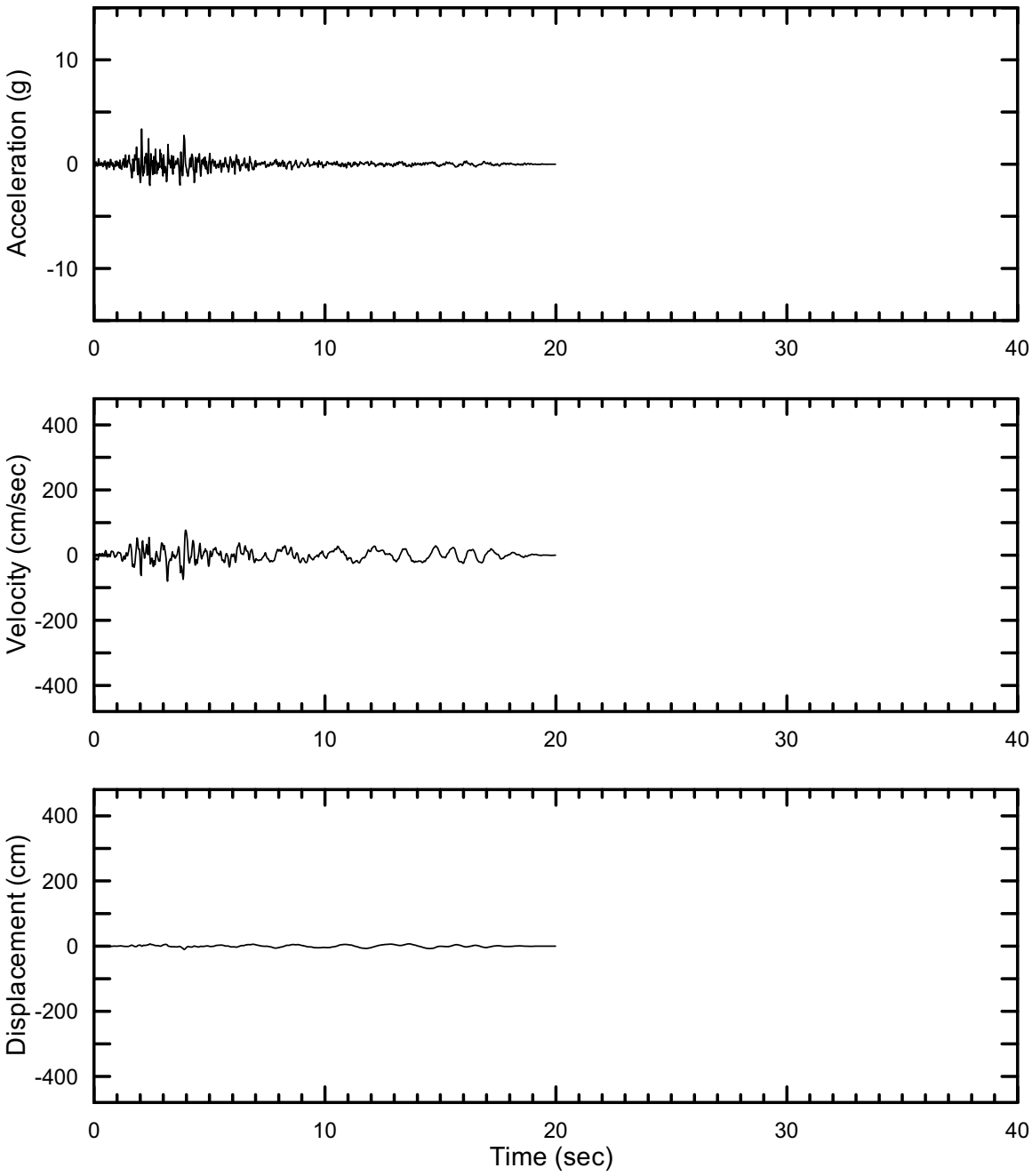

DTN: MO0403AVDSC106.001 [DIRS 168891]

Figure II-123. Point B Vertical Spectrally Conditioned to Point A Time Histories at an Annual Exceedance Probability of 10^{-6}, Set #10

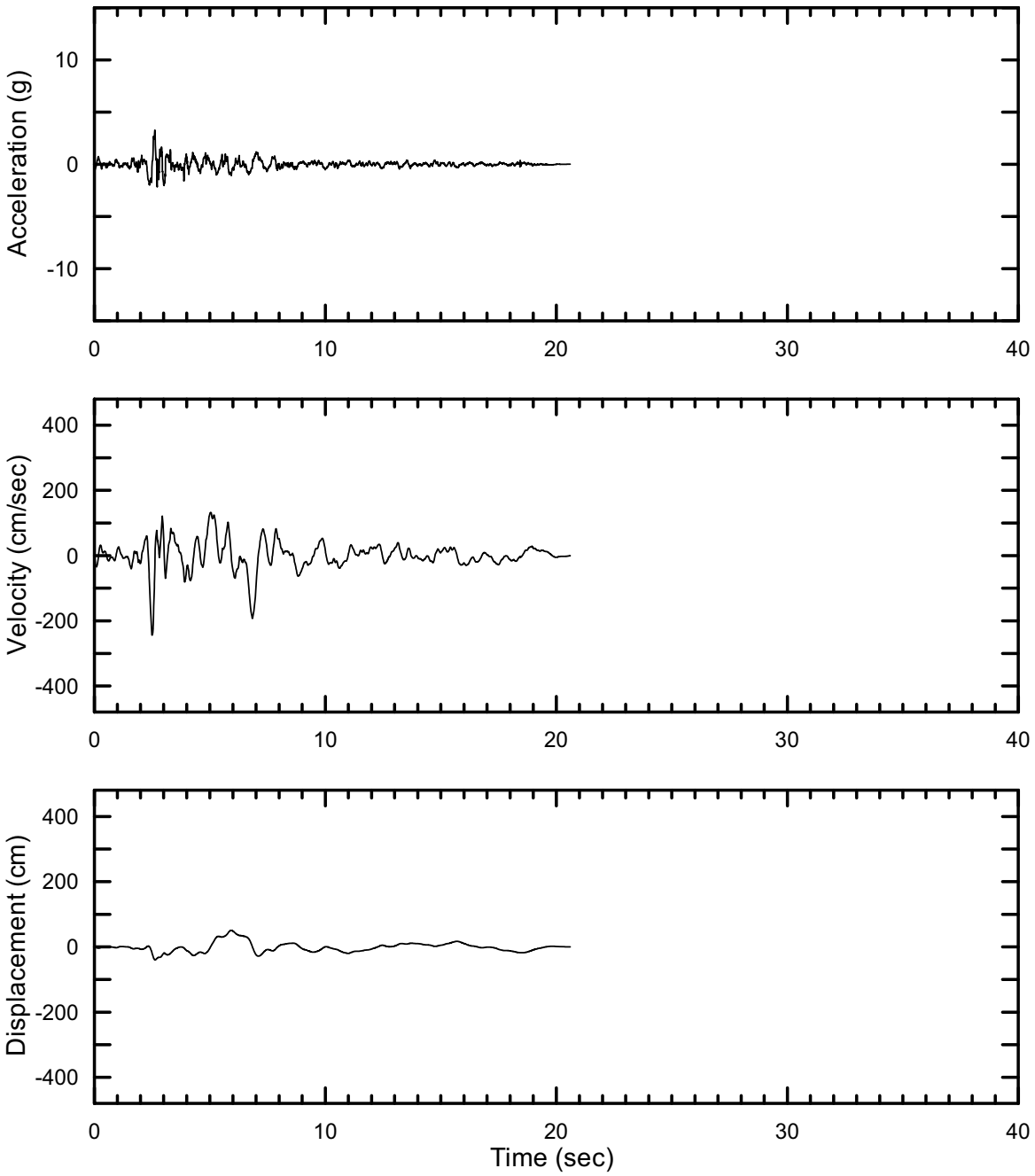

DTN: MO0403AVDSC106.001 [DIRS 168891]

Figure II-124. Point B Horizontal-1 Spectrally Conditioned to Point A Time Histories at an Annual Exceedance Probability of 10^{-6}, Set #11

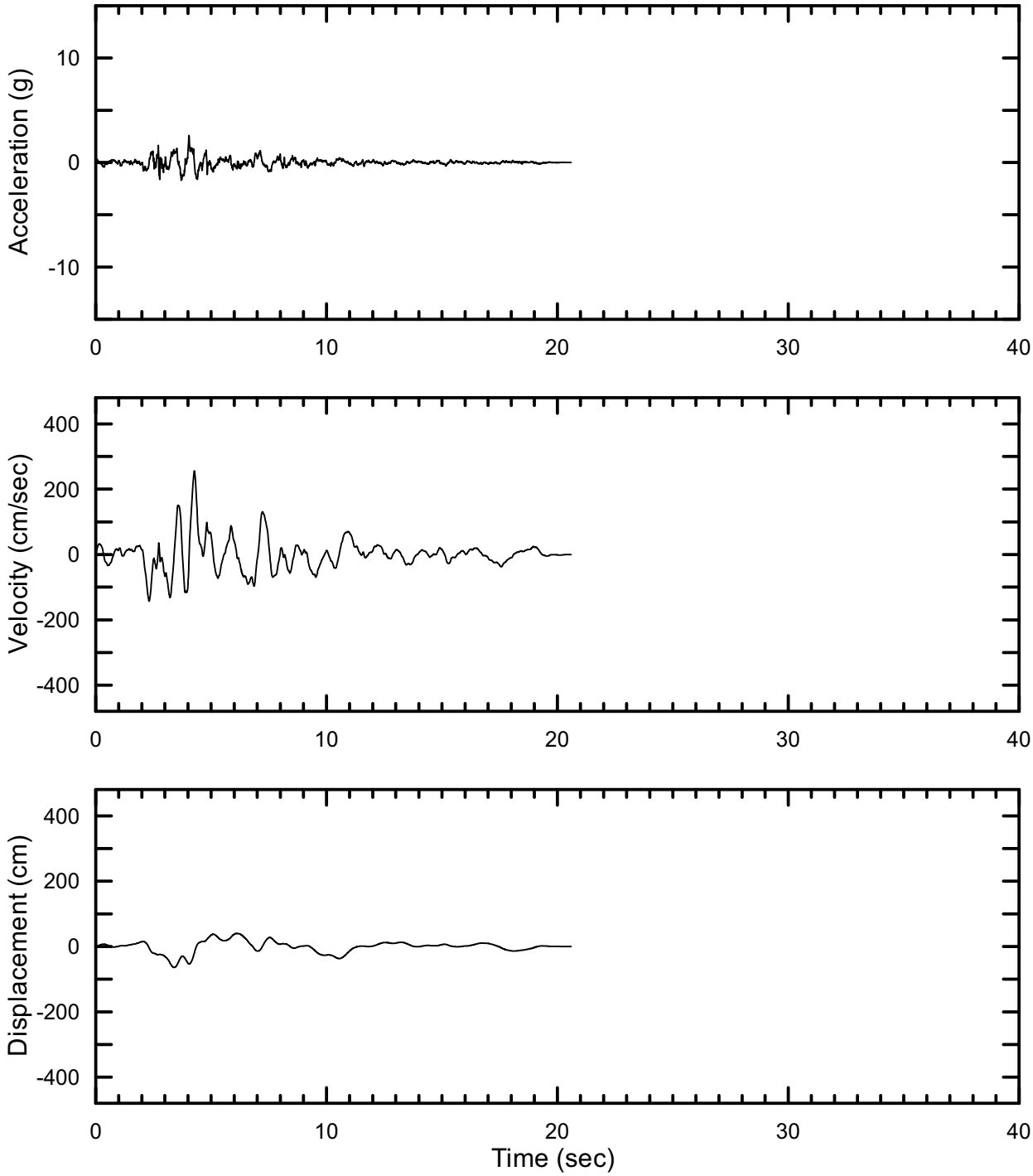

DTN: MO0403AVDSC106.001 [DIRS 168891]

Figure II-125. Point B Horizontal-2 Spectrally Conditioned to Point A Time Histories at an Annual Exceedance Probability of 10^{-6}, Set #11

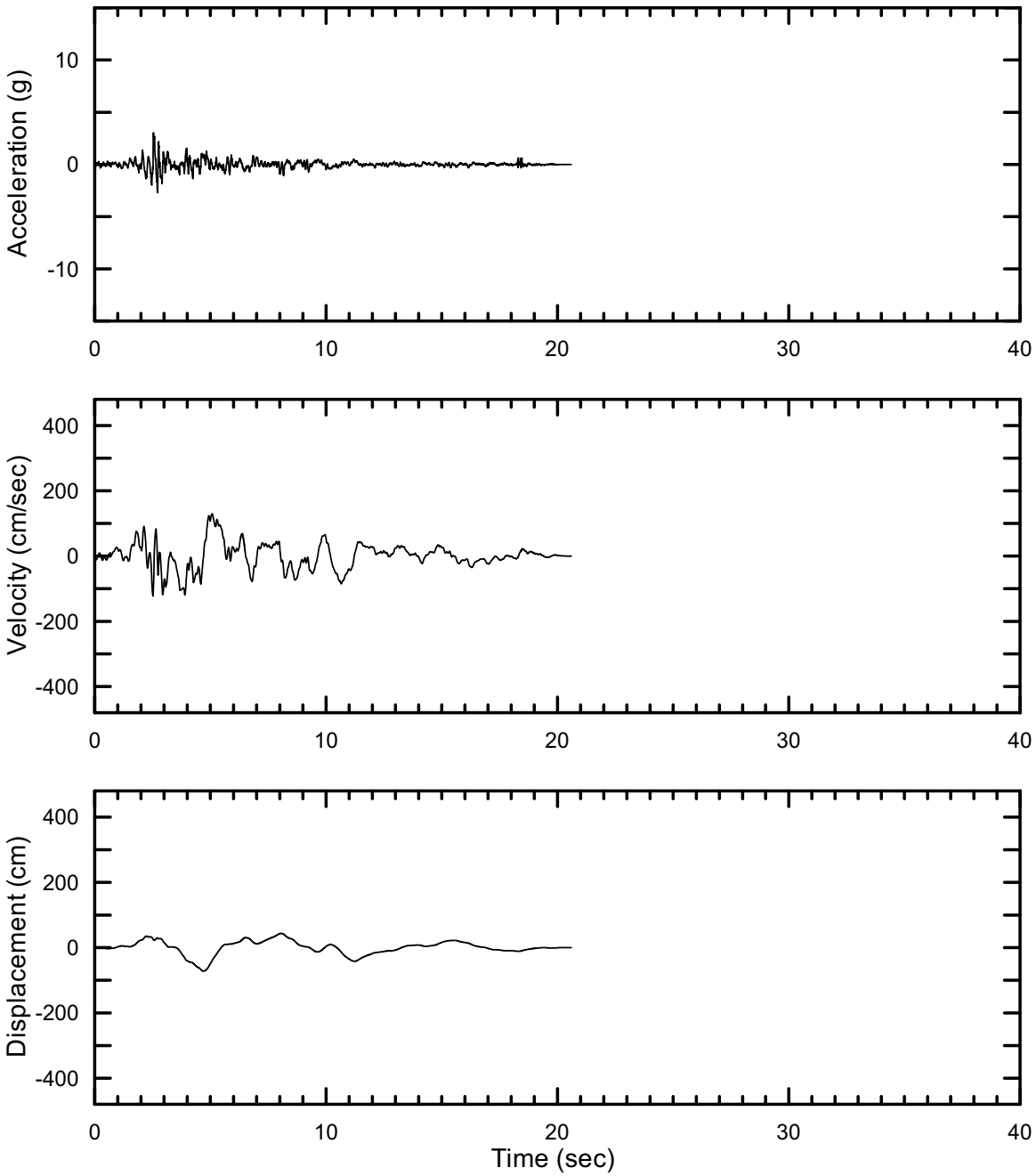

DTN: MO0403AVDSC106.001 [DIRS 168891]

Figure II-126. Point B Vertical Spectrally Conditioned to Point A Time Histories at an Annual Exceedance Probability of 10^{-6}, Set #11

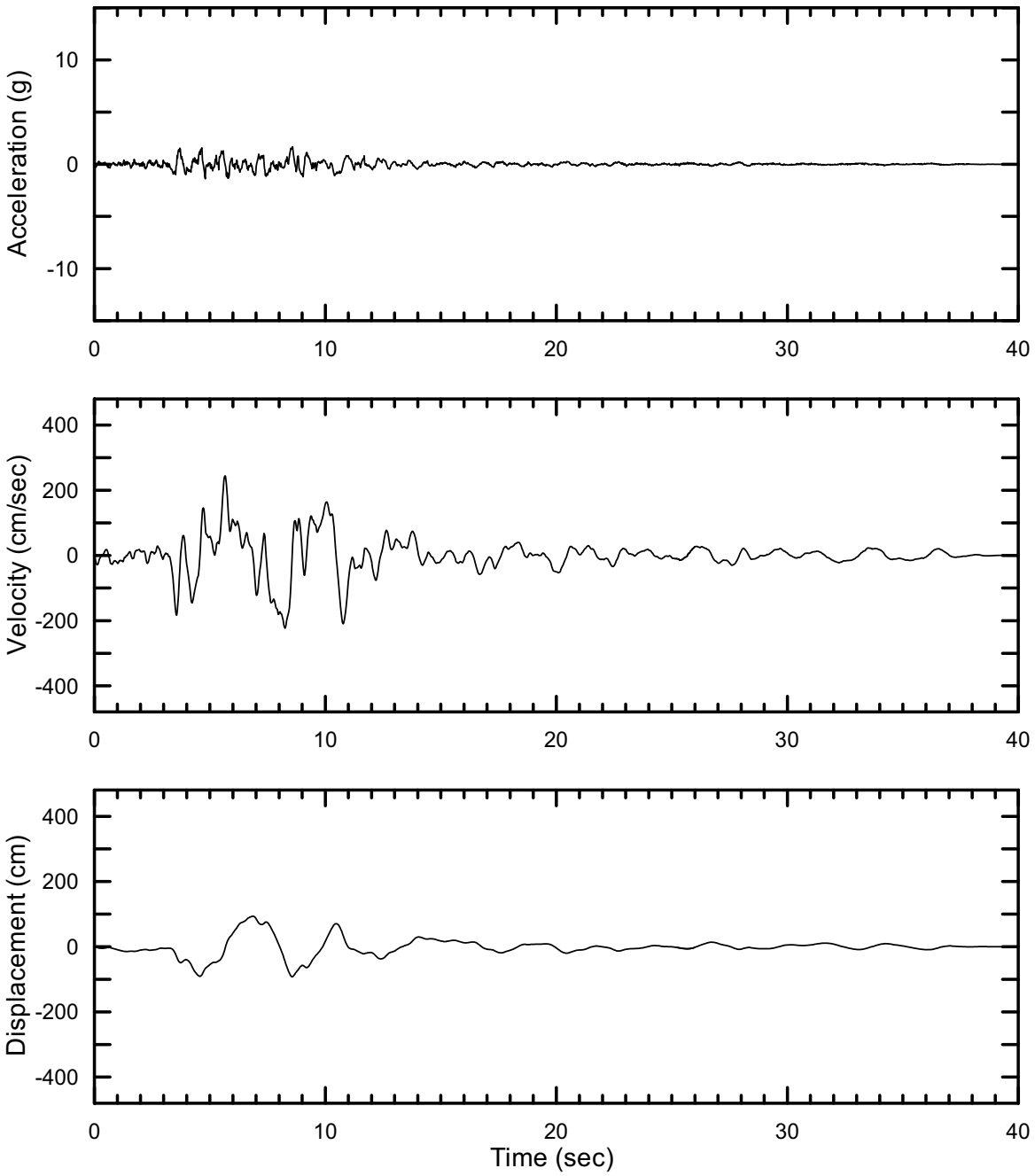

DTN: MO0403AVDSC106.001 [DIRS 168891]

Figure II-127. Point B Horizontal-1 Spectrally Conditioned to Point A Time Histories at an Annual Exceedance Probability of 10^{-6}, Set #12

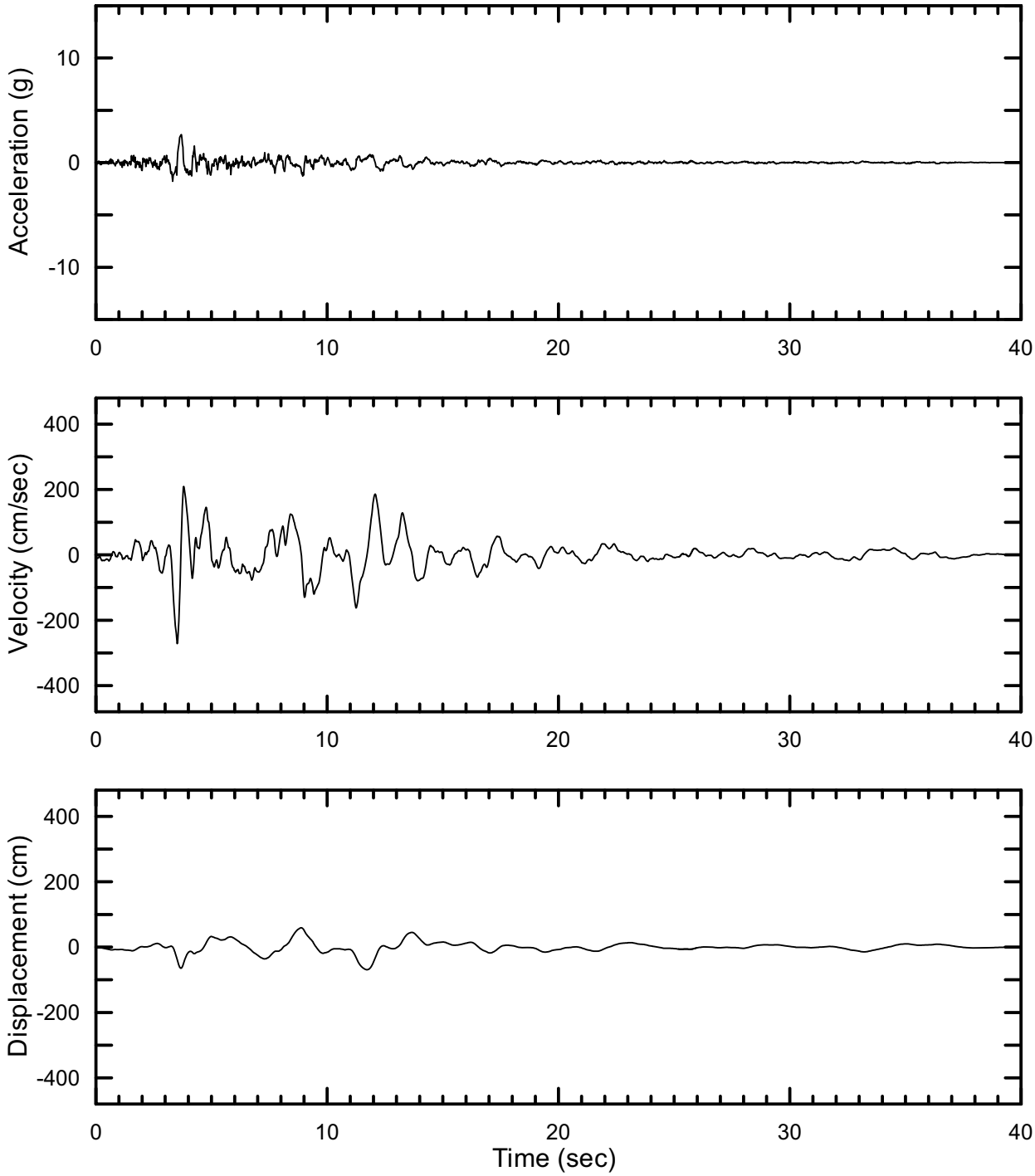

DTN: MO0403AVDSC106.001 [DIRS 168891]

Figure II-128. Point B Horizontal-2 Spectrally Conditioned to Point A Time Histories at an Annual Exceedance Probability of 10^{-6}, Set #12

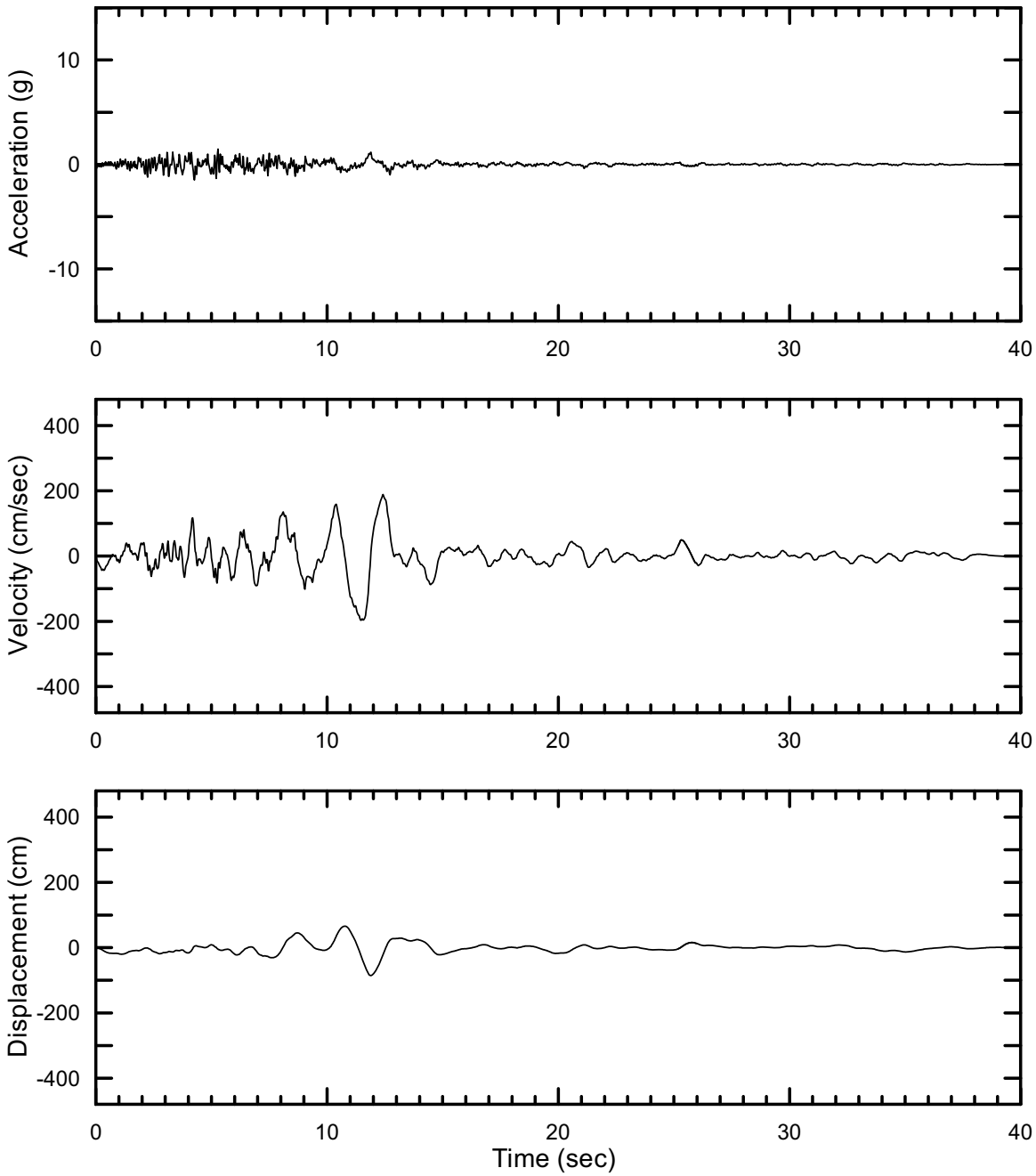

DTN: MO0403AVDSC106.001 [DIRS 168891]

Figure II-129. Point B Vertical Spectrally Conditioned to Point A Time Histories at an Annual Exceedance Probability of 10^{-6}, Set #12

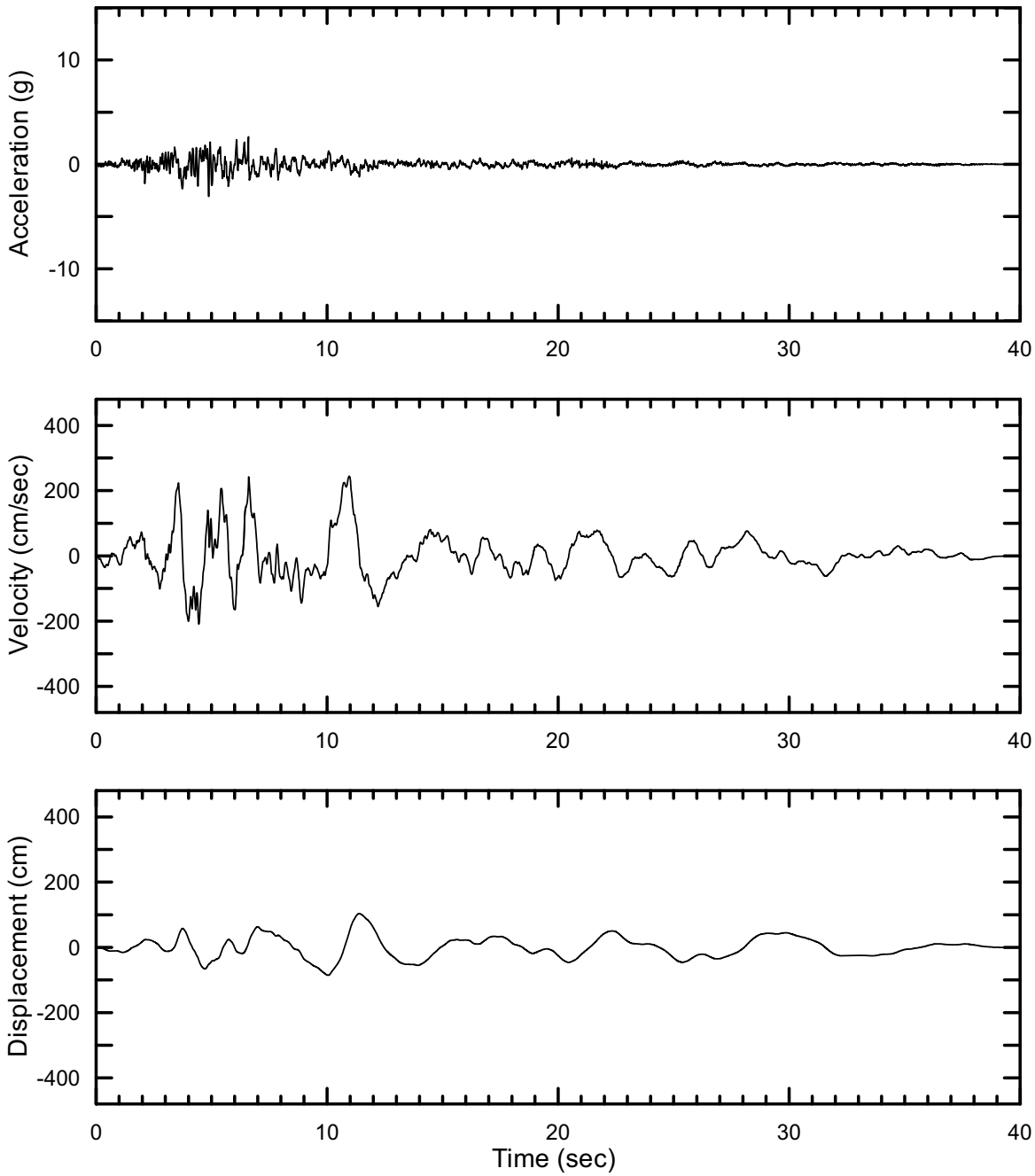

DTN: MO0403AVDSC106.001 [DIRS 168891]

Figure II-130. Point B Horizontal-1 Spectrally Conditioned to Point A Time Histories at an Annual Exceedance Probability of 10^{-6}, Set #13

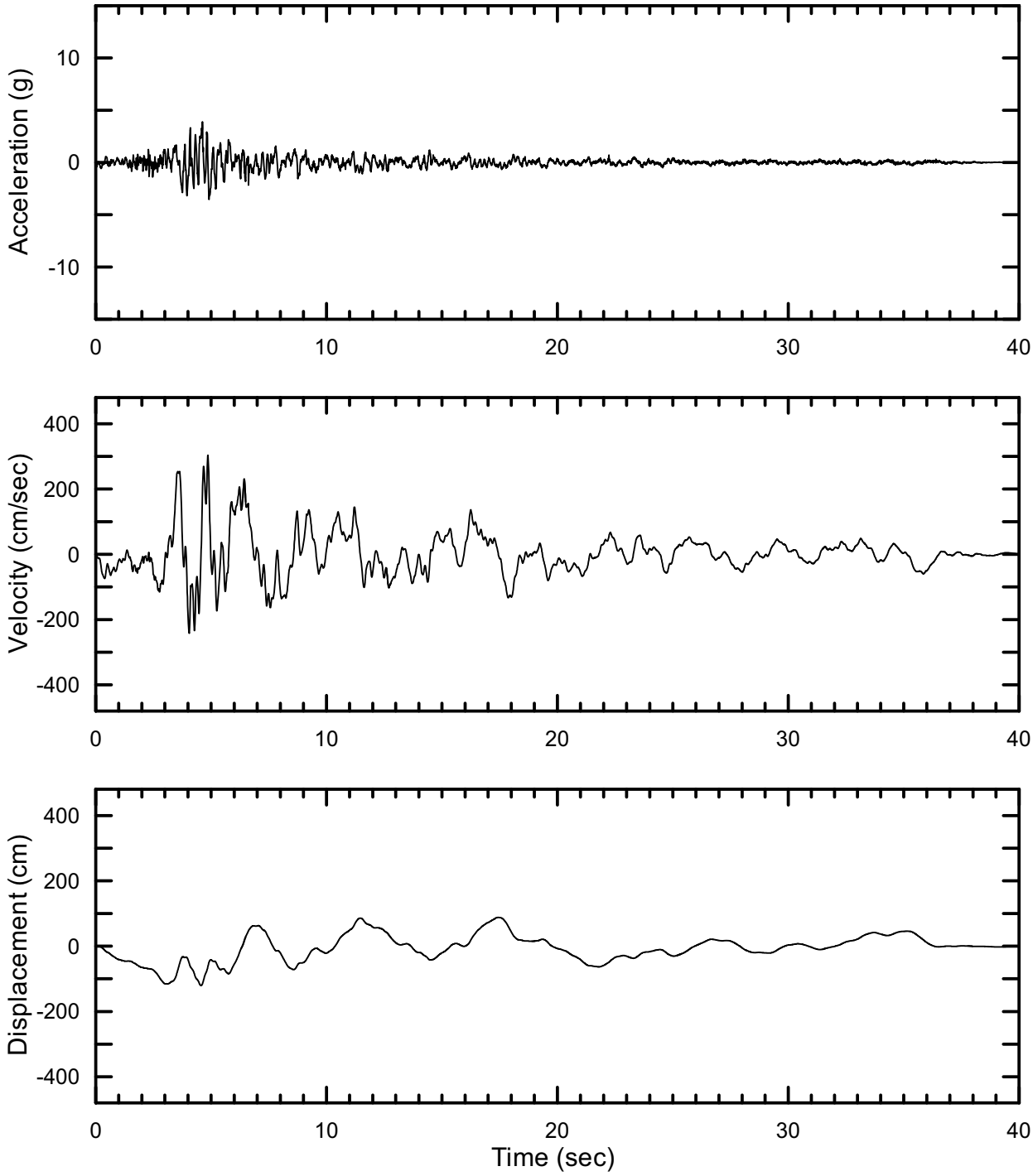

DTN: MO0403AVDSC106.001 [DIRS 168891]

Figure II-131. Point B Horizontal-2 Spectrally Conditioned to Point A Time Histories at an Annual Exceedance Probability of 10^{-6}, Set #13

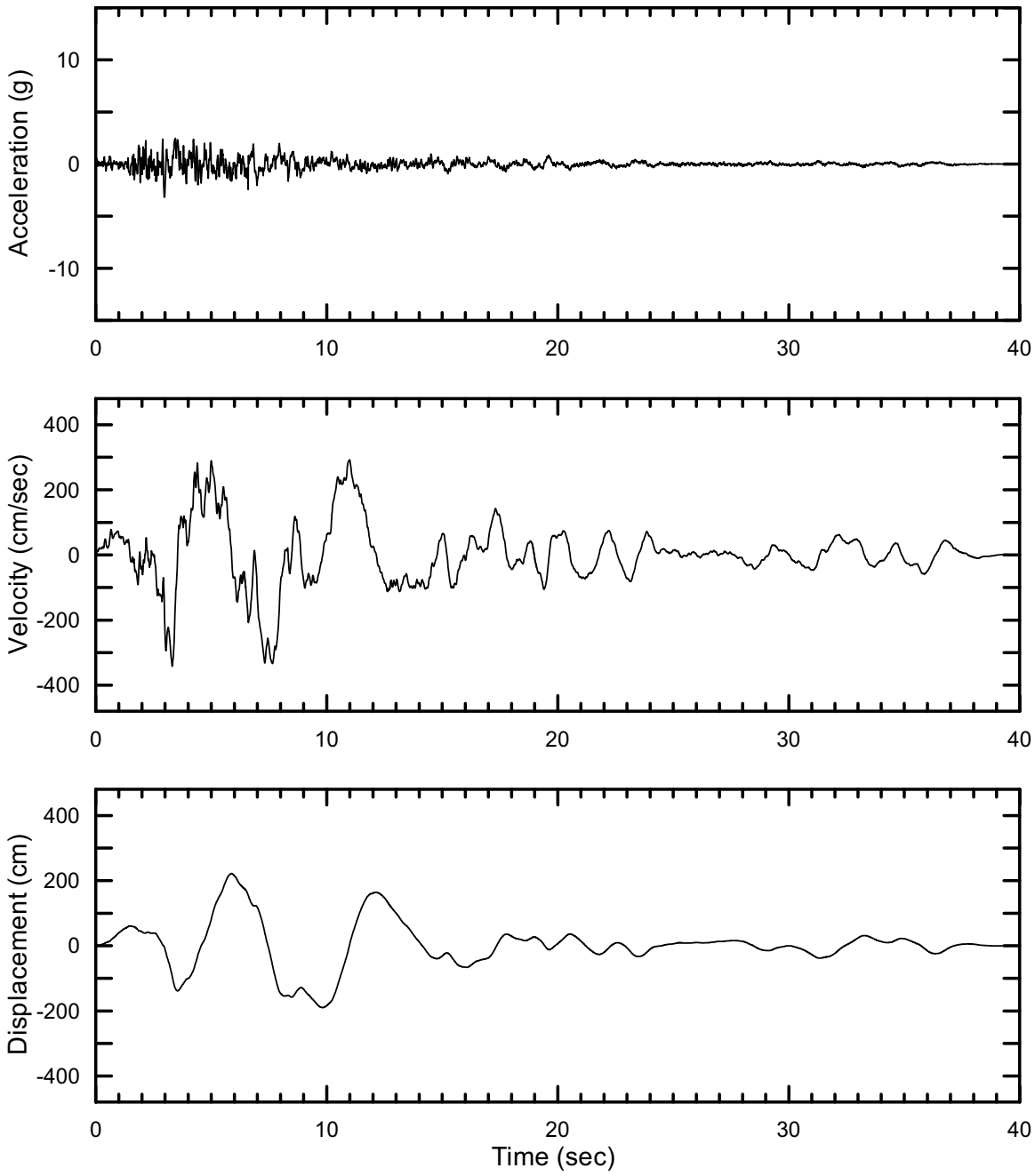

DTN: MO0403AVDSC106.001 [DIRS 168891]

Figure II-132. Point B Vertical Spectrally Conditioned to Point A Time Histories at an Annual Exceedance Probability of 10^{-6}, Set #13

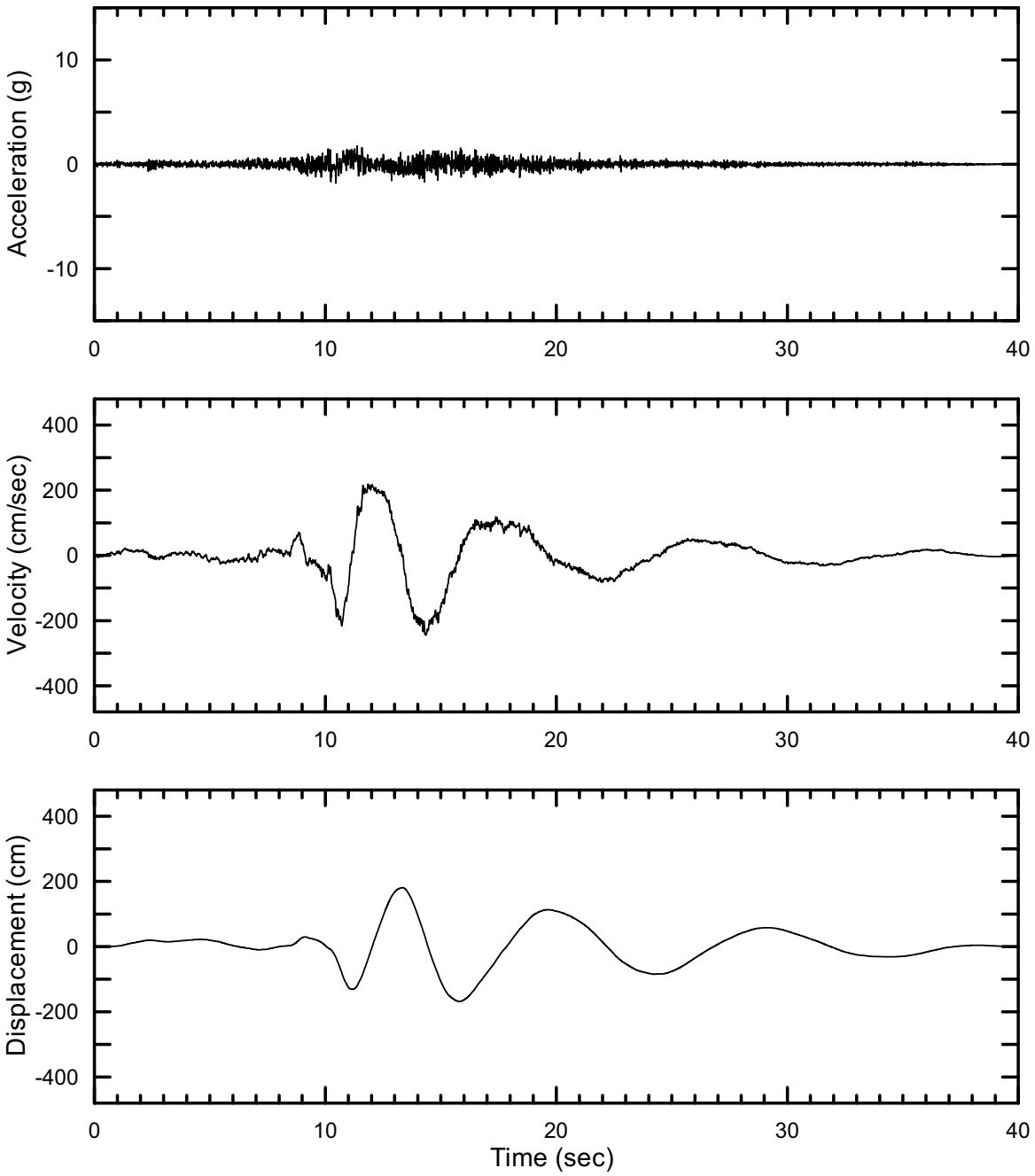

DTN: MO0403AVDSC106.001 [DIRS 168891]

Figure II-133. Point B Horizontal-1 Spectrally Conditioned to Point A Time Histories at an Annual Exceedance Probability of 10^{-6}, Set #14

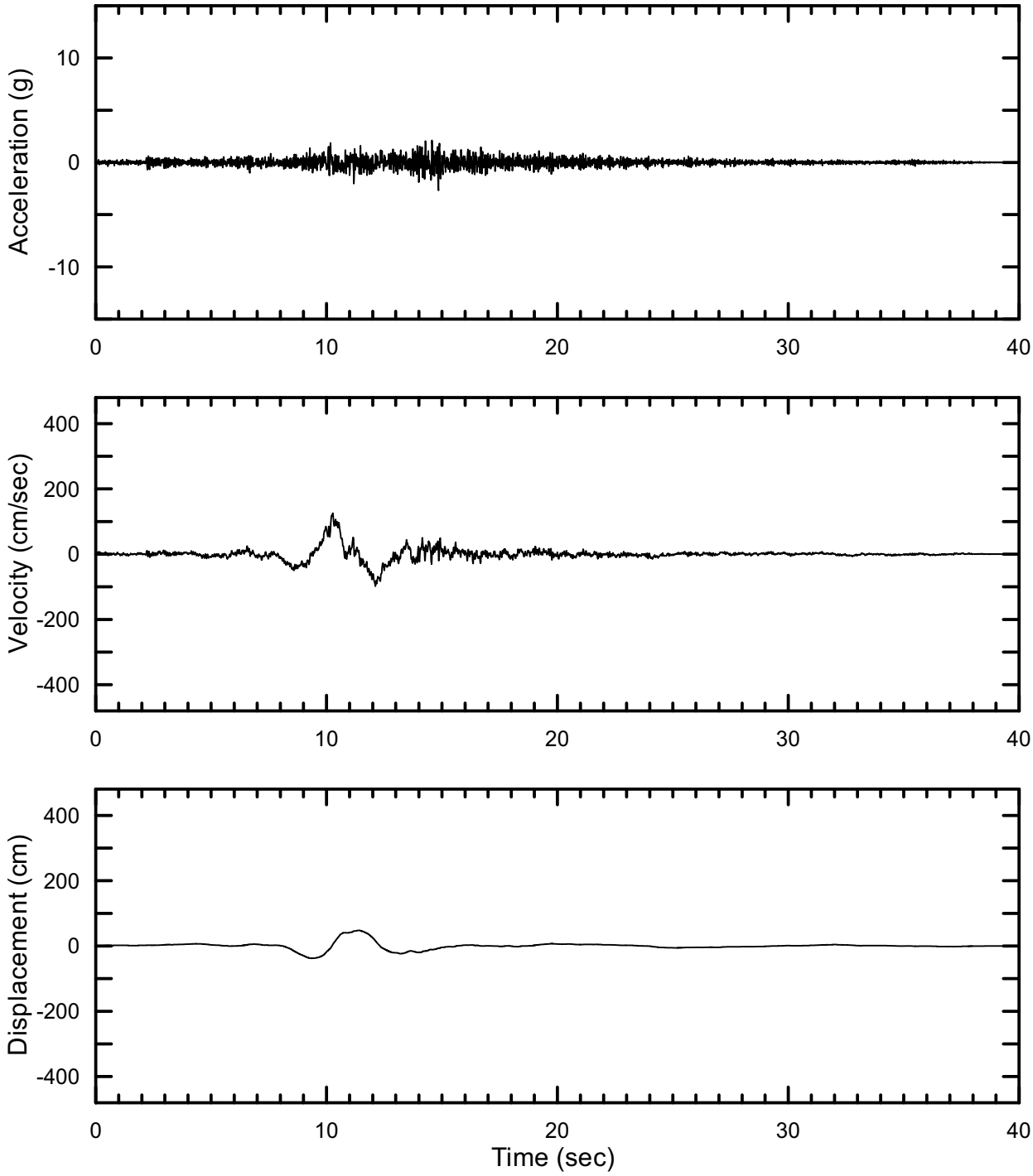

DTN: MO0403AVDSC106.001 [DIRS 168891]

Figure II-134. Point B Horizontal-2 Spectrally Conditioned to Point A Time Histories at an Annual Exceedance Probability of 10^{-6}, Set #14

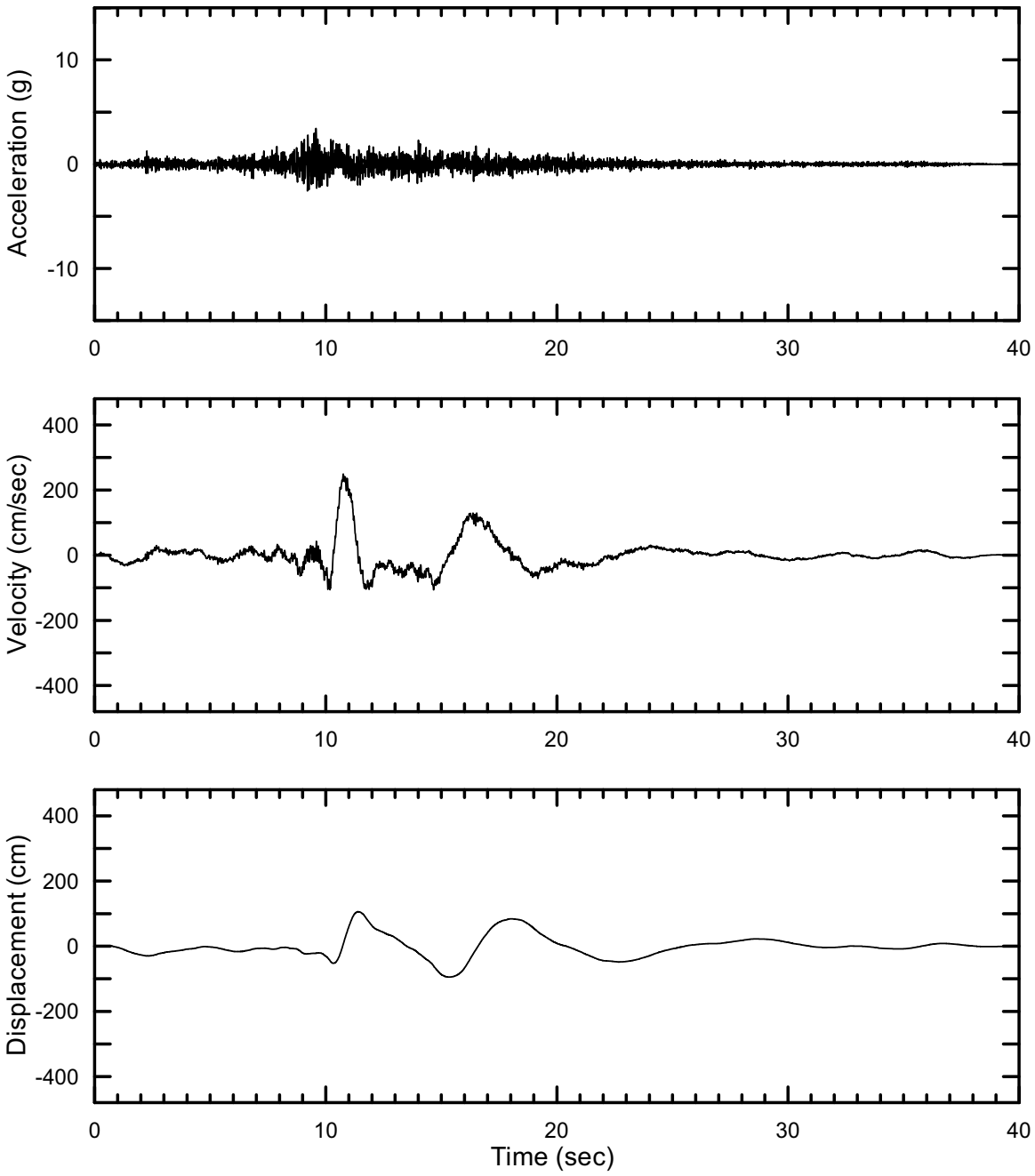

DTN: MO0403AVDSC106.001 [DIRS 168891]

Figure II-135. Point B Vertical Spectrally Conditioned to Point A Time Histories at an Annual Exceedance Probability of 10^{-6}, Set #14

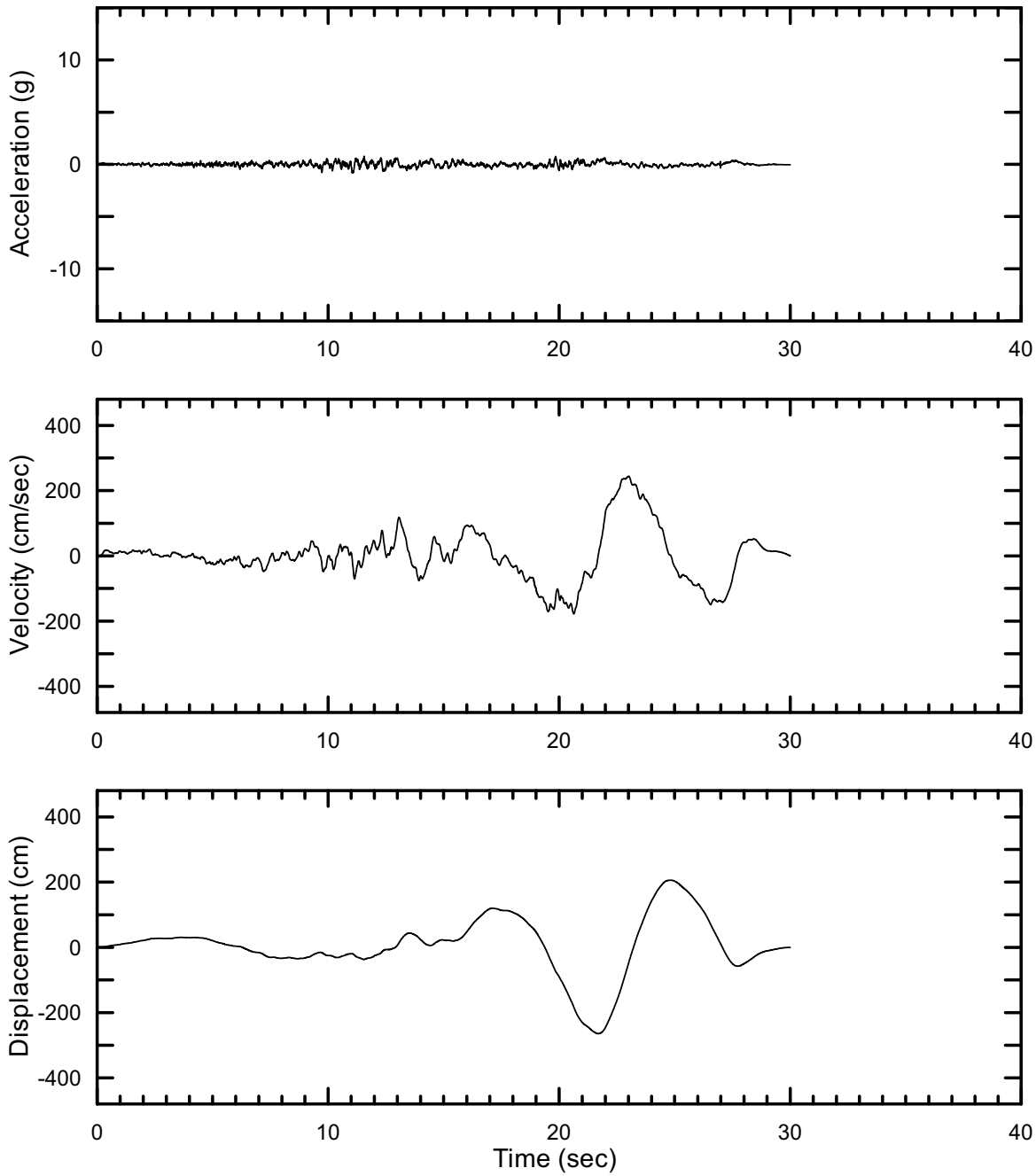

DTN: MO0403AVDSC106.001 [DIRS 168891]

Figure II-136. Point B Horizontal-1 Spectrally Conditioned to Point A Time Histories at an Annual Exceedance Probability of 10^{-6}, Set #15

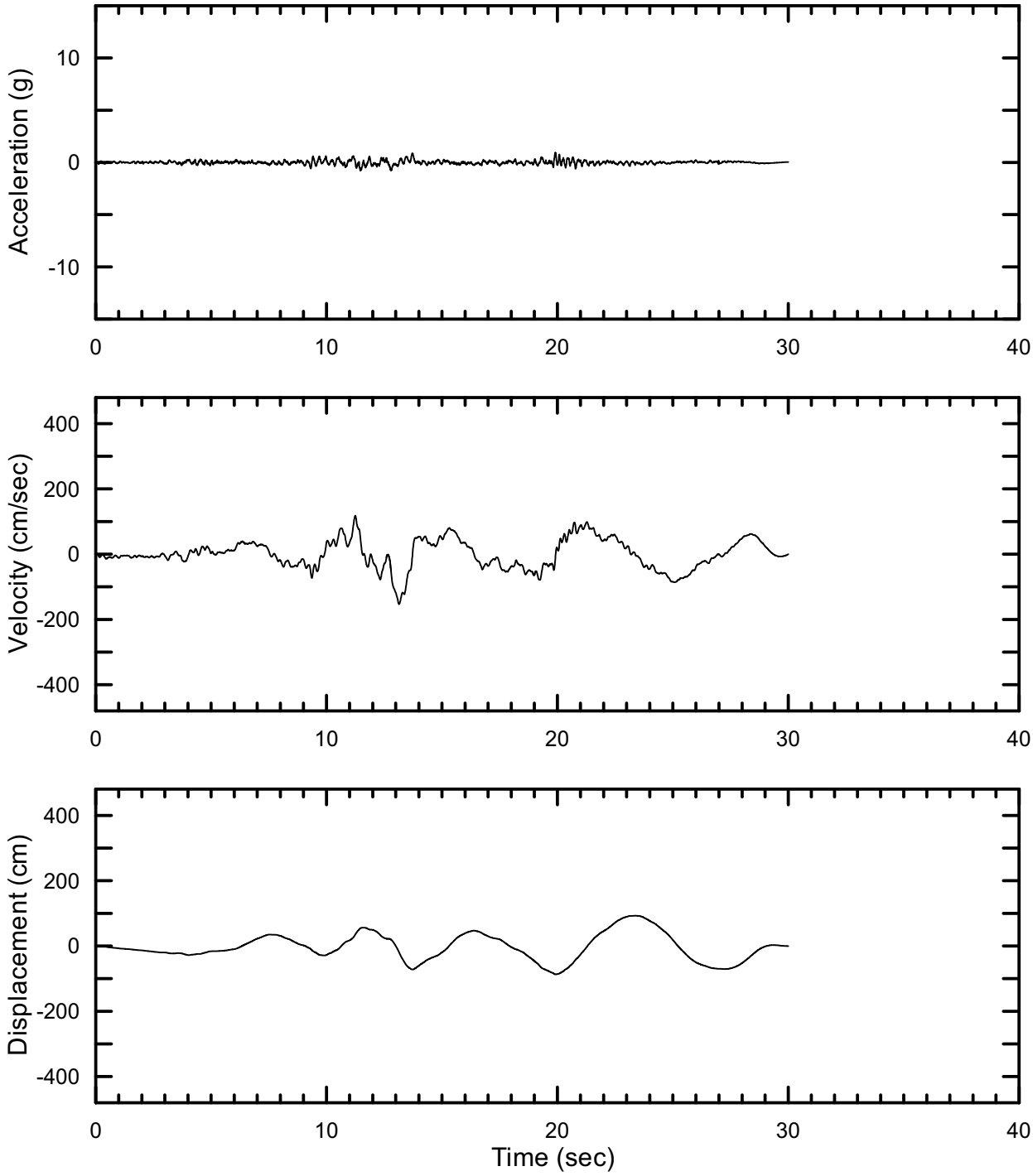

DTN: MO0403AVDSC106.001 [DIRS 168891]

Figure II-137. Point B Horizontal-2 Spectrally Conditioned to Point A Time Histories at an Annual Exceedance Probability of 10^{-6}, Set #15

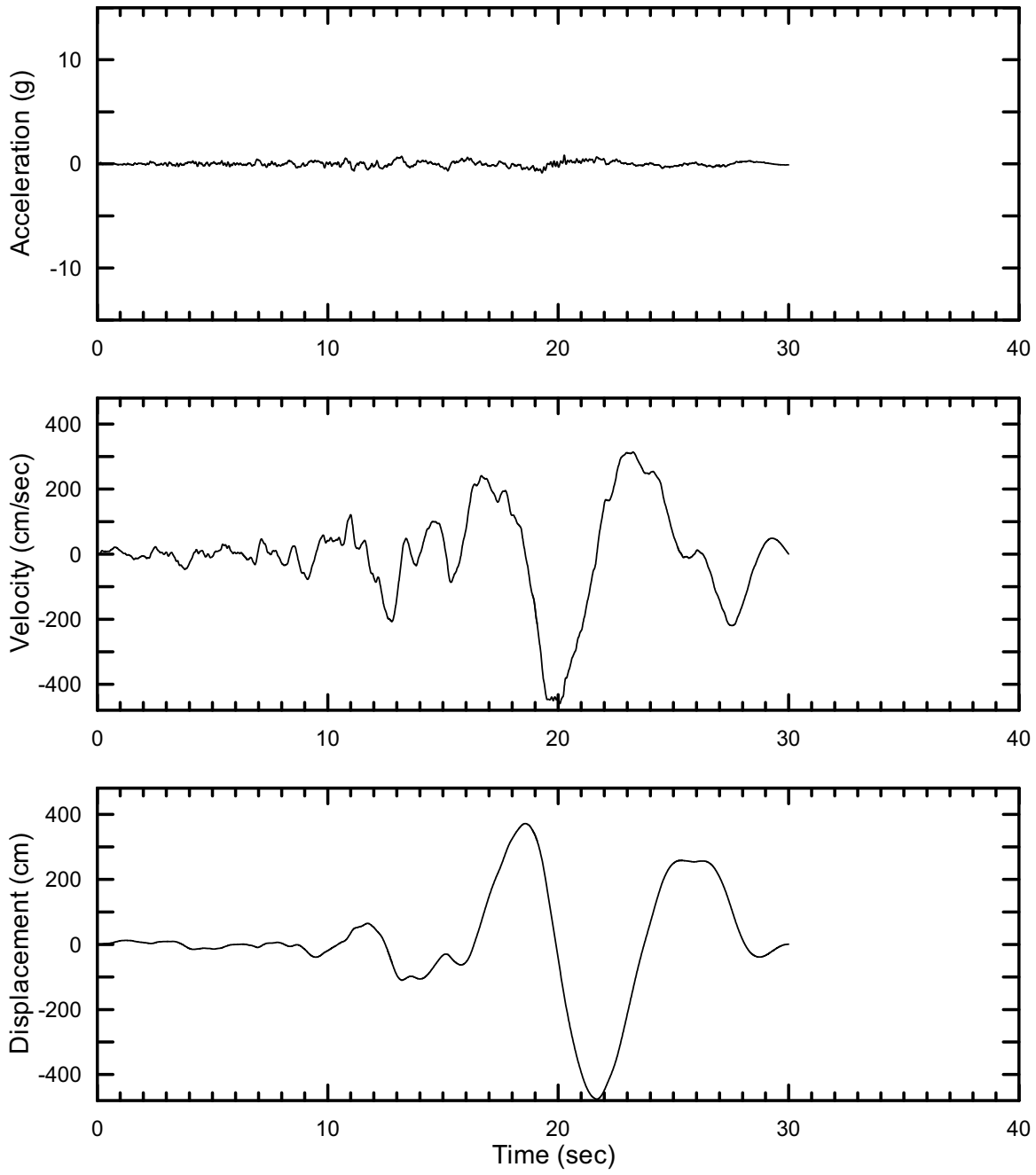

DTN: MO0403AVDSC106.001 [DIRS 168891]

Figure II-138. Point B Vertical Spectrally Conditioned to Point A Time Histories at an Annual Exceedance Probability of 10^{-6}, Set #15

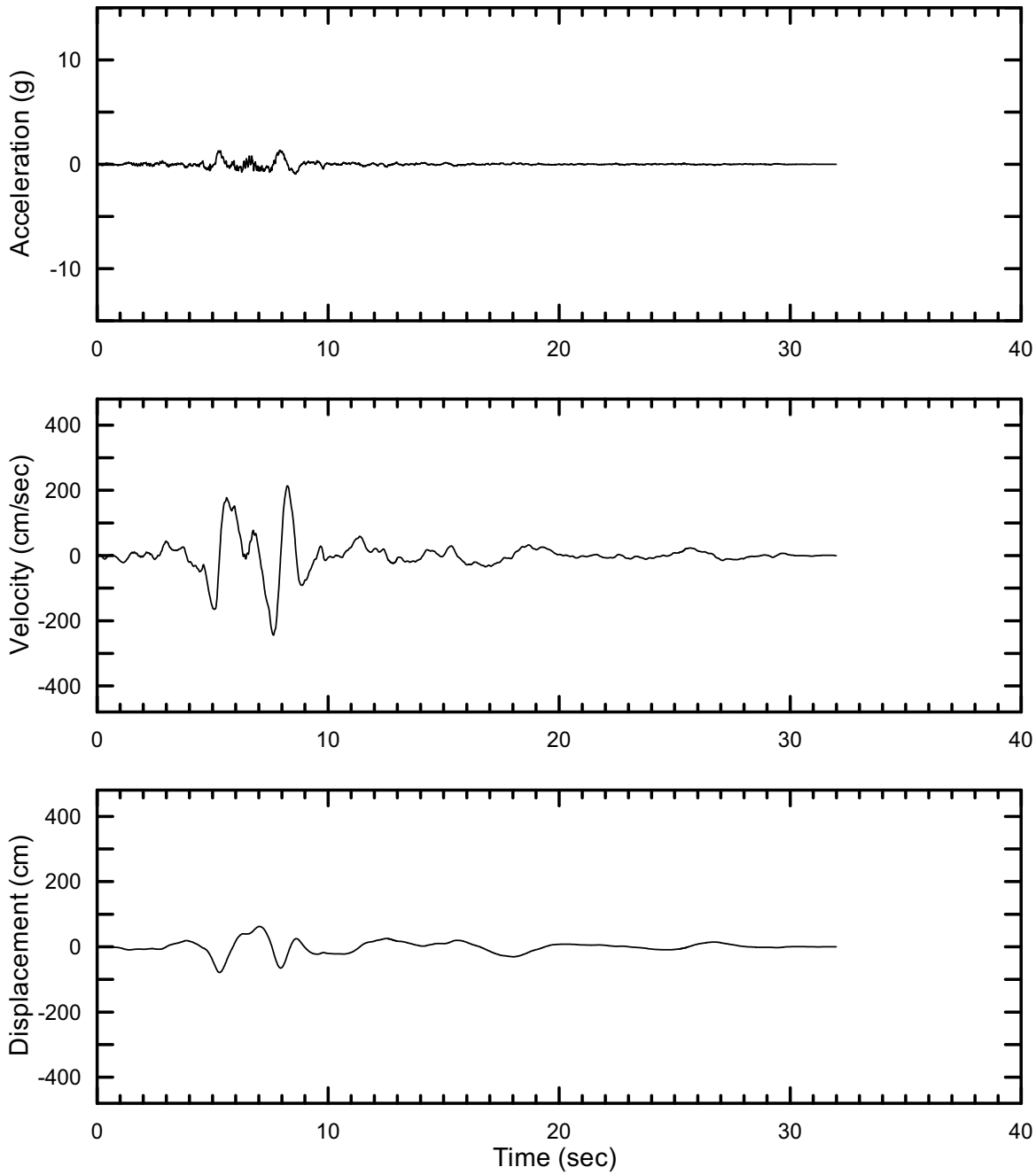

DTN: MO0403AVDSC106.001 [DIRS 168891]

Figure II-139. Point B Horizontal-1 Spectrally Conditioned to Point A Time Histories at an Annual Exceedance Probability of 10^{-6}, Set #16

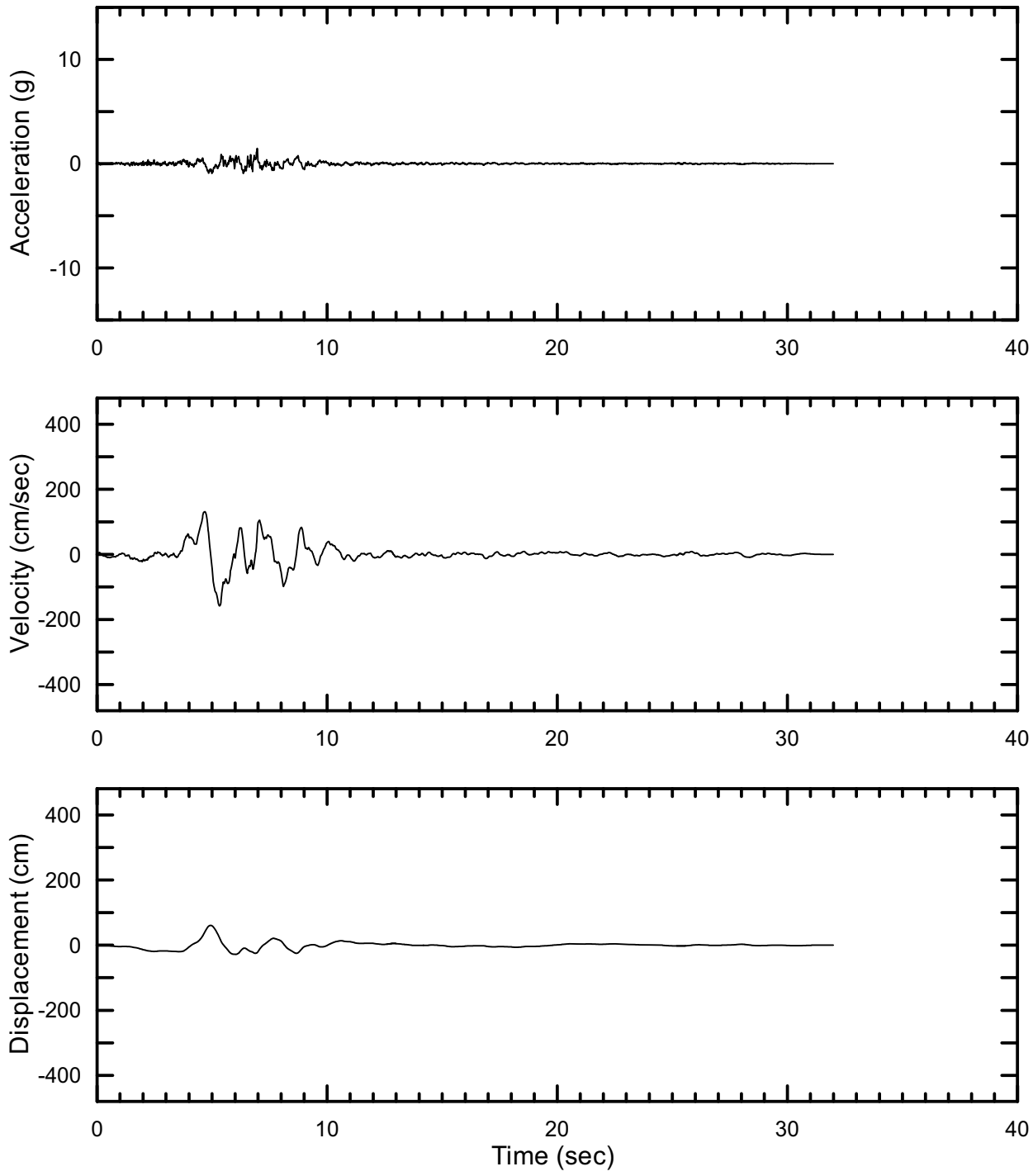

DTN: MO0403AVDSC106.001 [DIRS 168891]

Figure II-140. Point B Horizontal-2 Spectrally Conditioned to Point A Time Histories at an Annual Exceedance Probability of 10^{-6}, Set #16

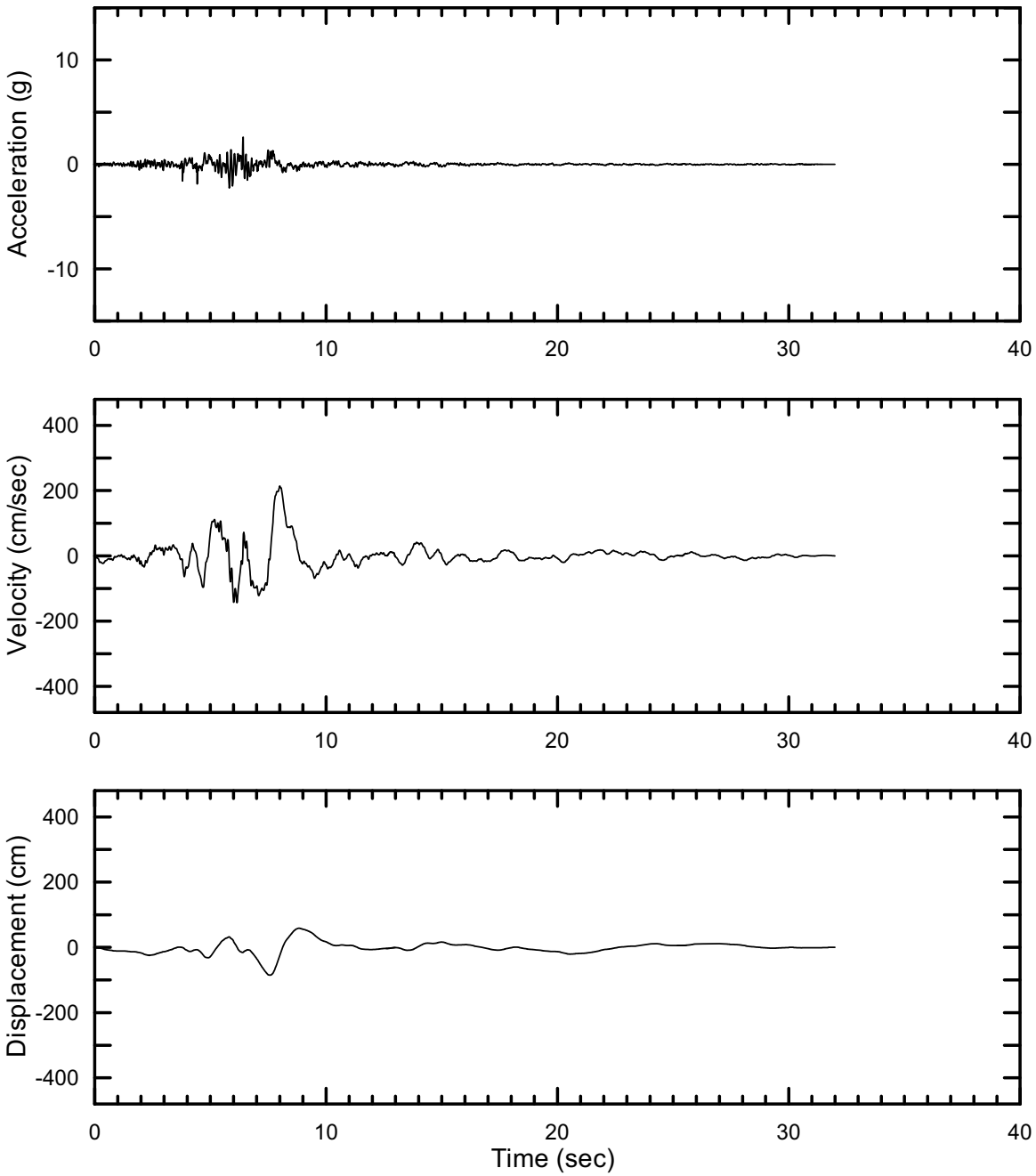

DTN: MO0403AVDSC106.001 [DIRS 168891]

Figure II-141. Point B Vertical Spectrally Conditioned to Point A Time Histories at an Annual Exceedance Probability of 10^{-6}, Set #16

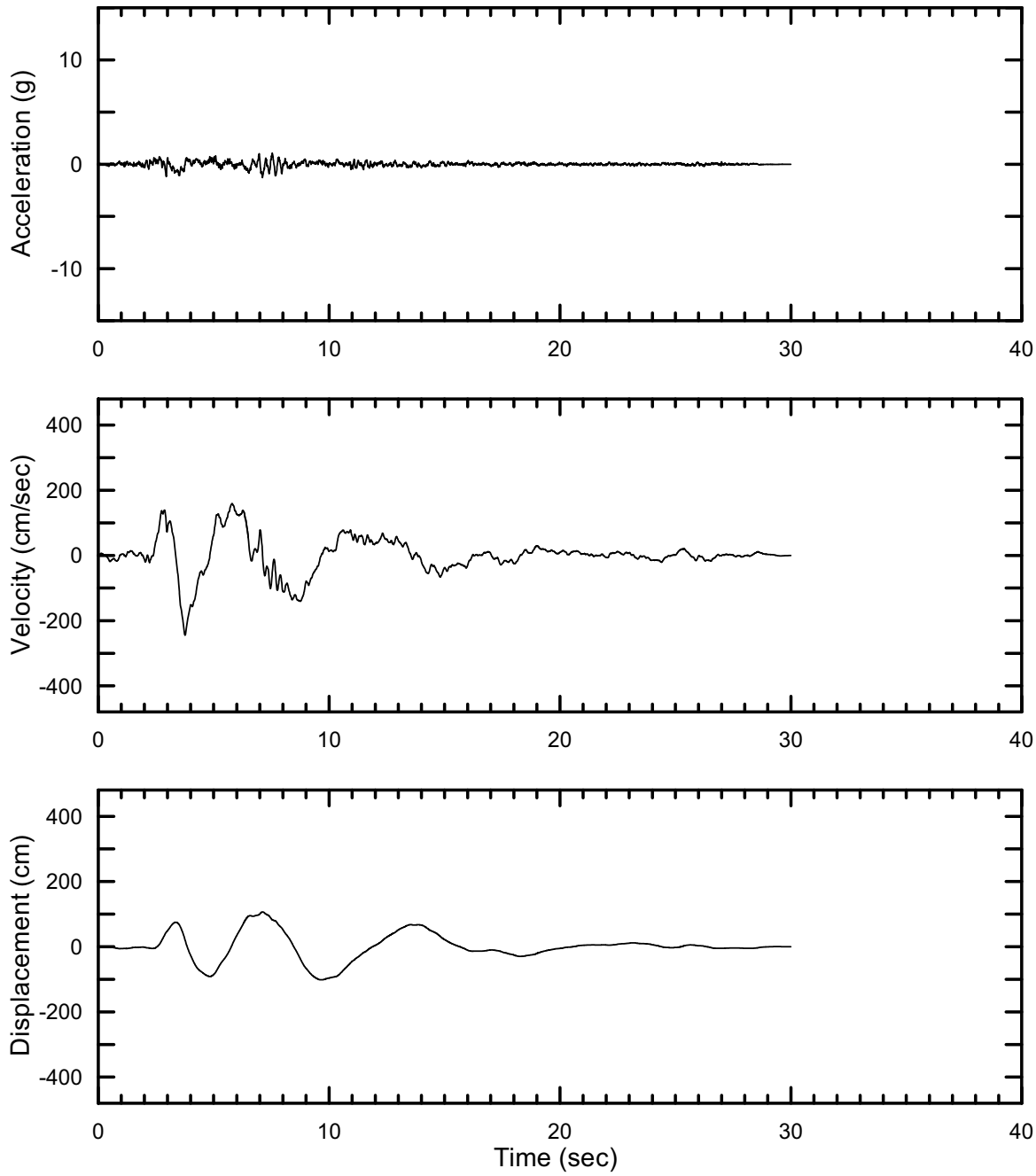

DTN: MO0403AVDSC106.001 [DIRS 168891]

Figure II-142. Point B Horizontal-1 Spectrally Conditioned to Point A Time Histories at an Annual Exceedance Probability of 10^{-6}, Set #17

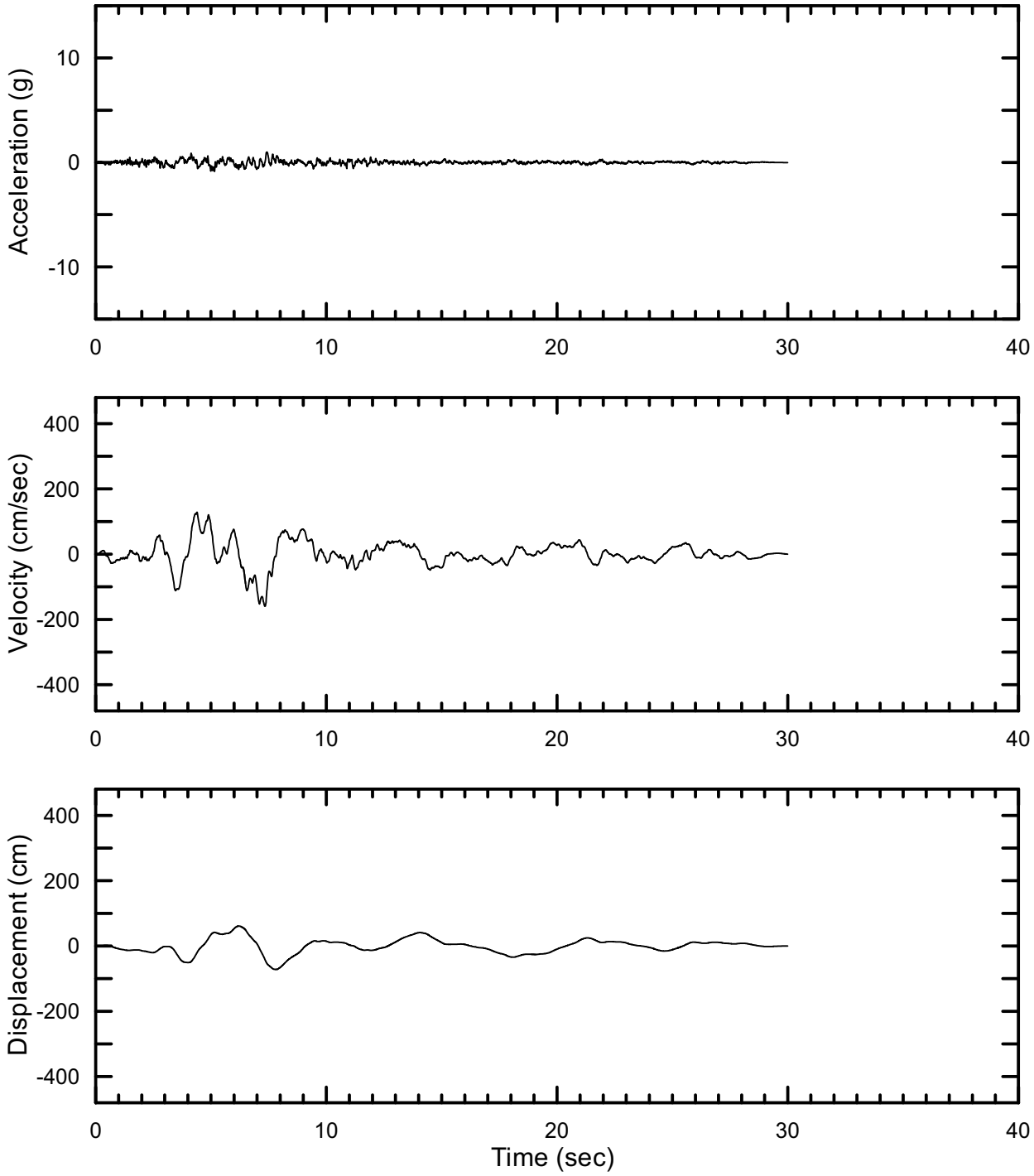

DTN: MO0403AVDSC106.001 [DIRS 168891]

Figure II-143. Point B Horizontal-2 Spectrally Conditioned to Point A Time Histories at an Annual Exceedance Probability of 10^{-6}, Set #17

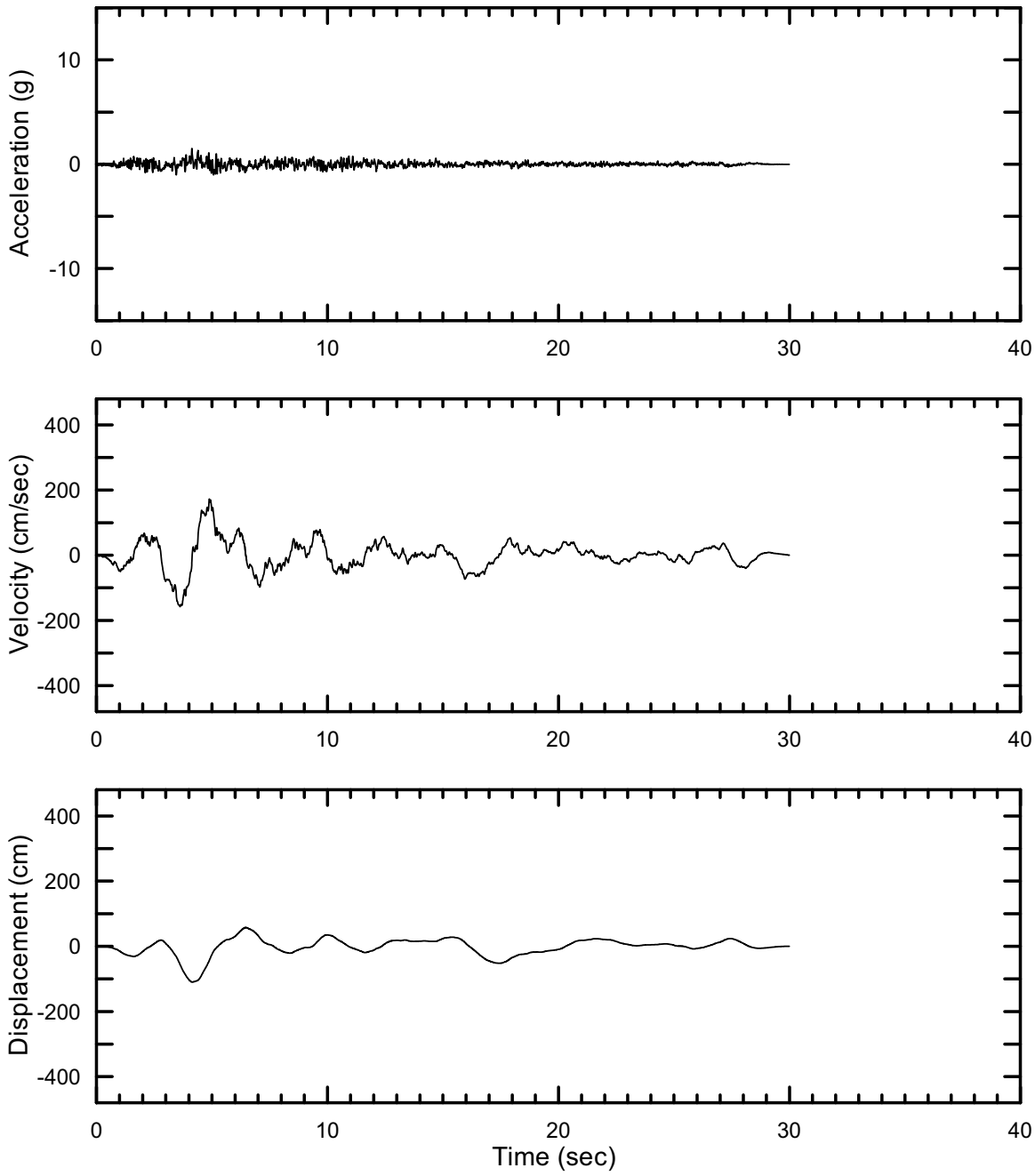

DTN: MO0403AVDSC106.001 [DIRS 168891]

Figure II-144. Point B Vertical Spectrally Conditioned to Point A Time Histories at an Annual Exceedance Probability of 10^{-6}, Set #17

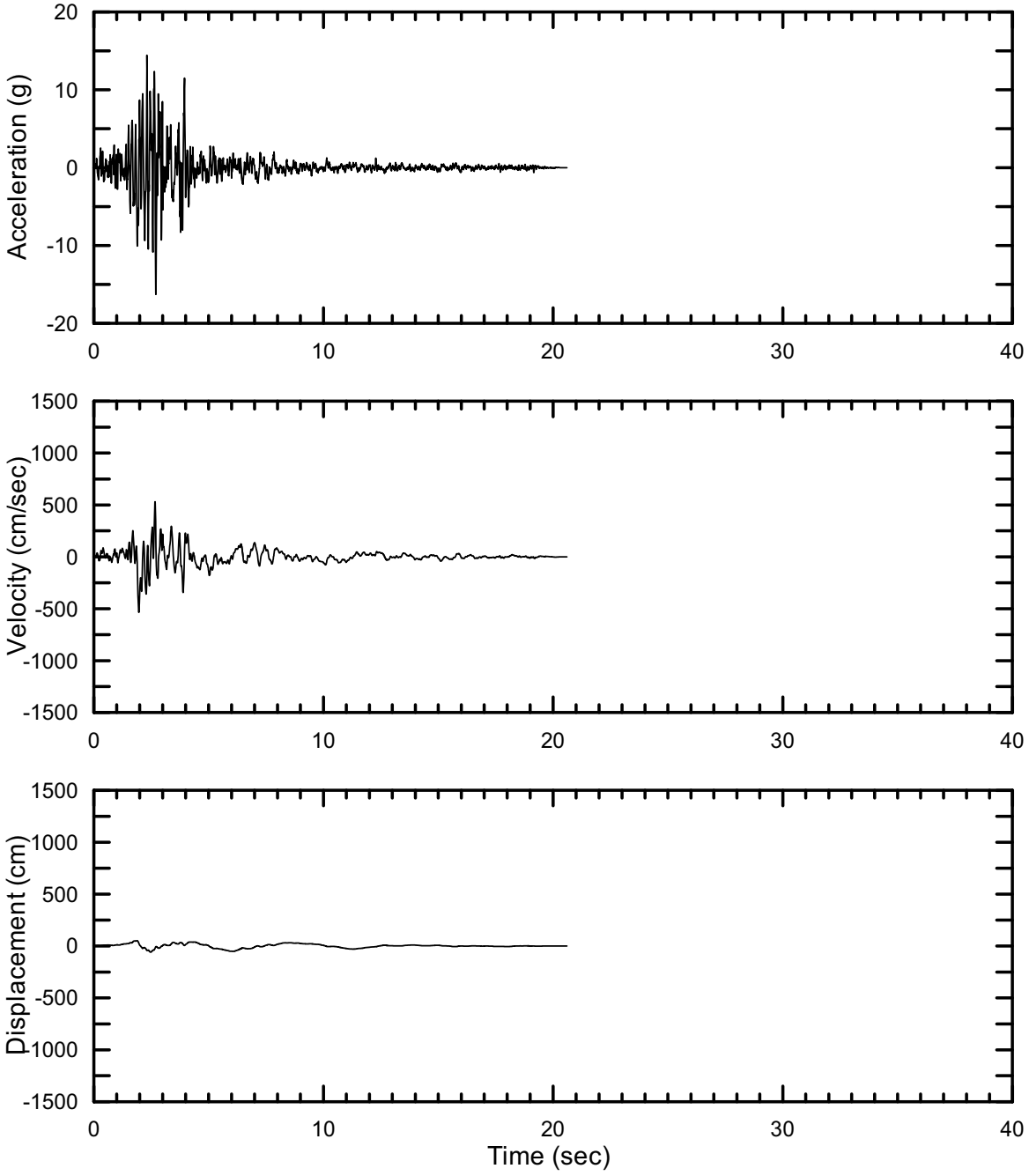

DTN: MO0403AVTMH107.003 [DIRS 168892]

Figure II-145. Point B Horizontal-1 Ti me Histories at an Annual Exceedance Probability of 10^{-7}, Set #1

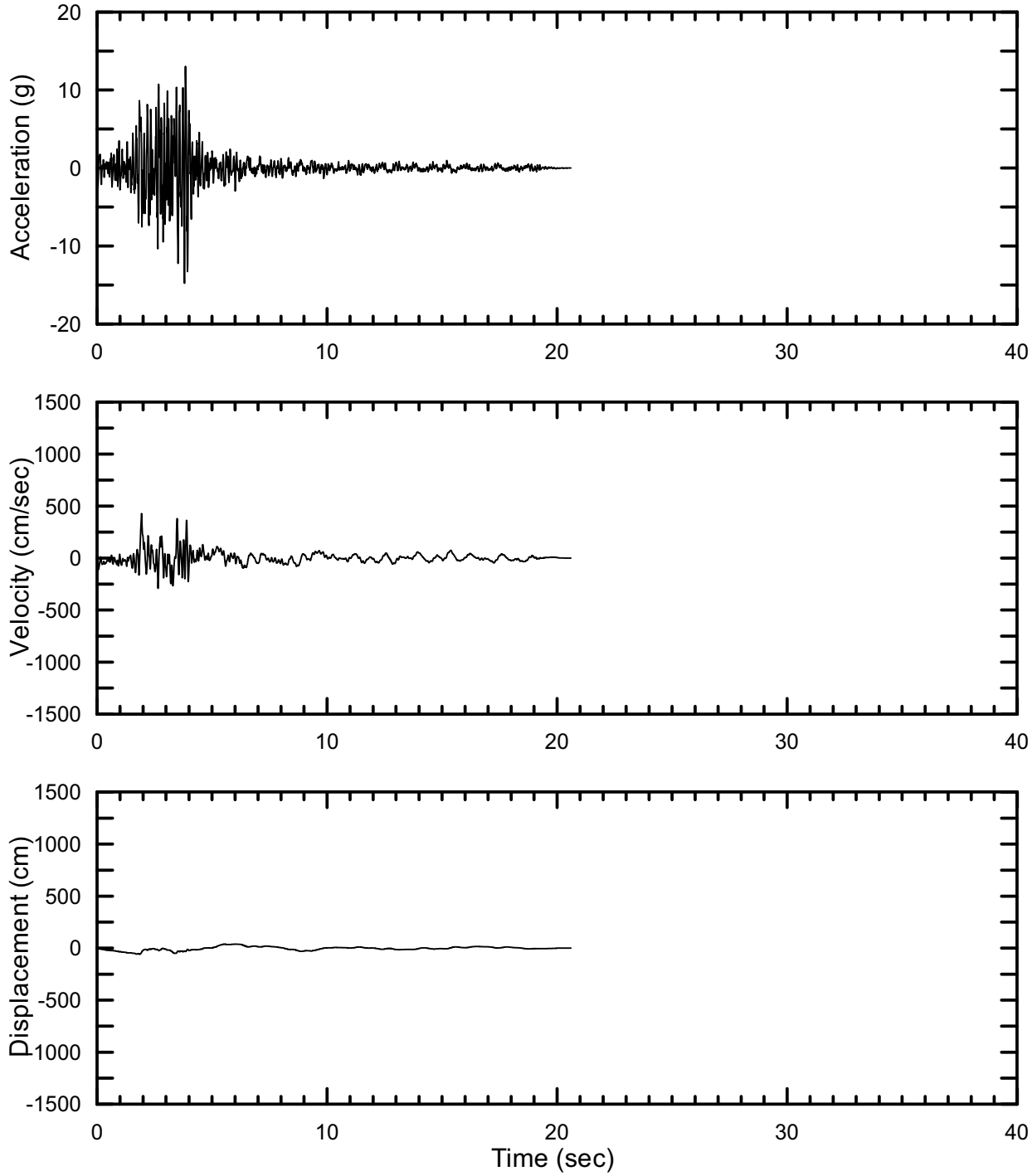

DTN: MO0403AVTMH107.003 [DIRS 168892]

Figure II-146. Point B Horizontal-2 Ti me Histories at an Annual Exceedance Probability of 10^{-7}, Set #1

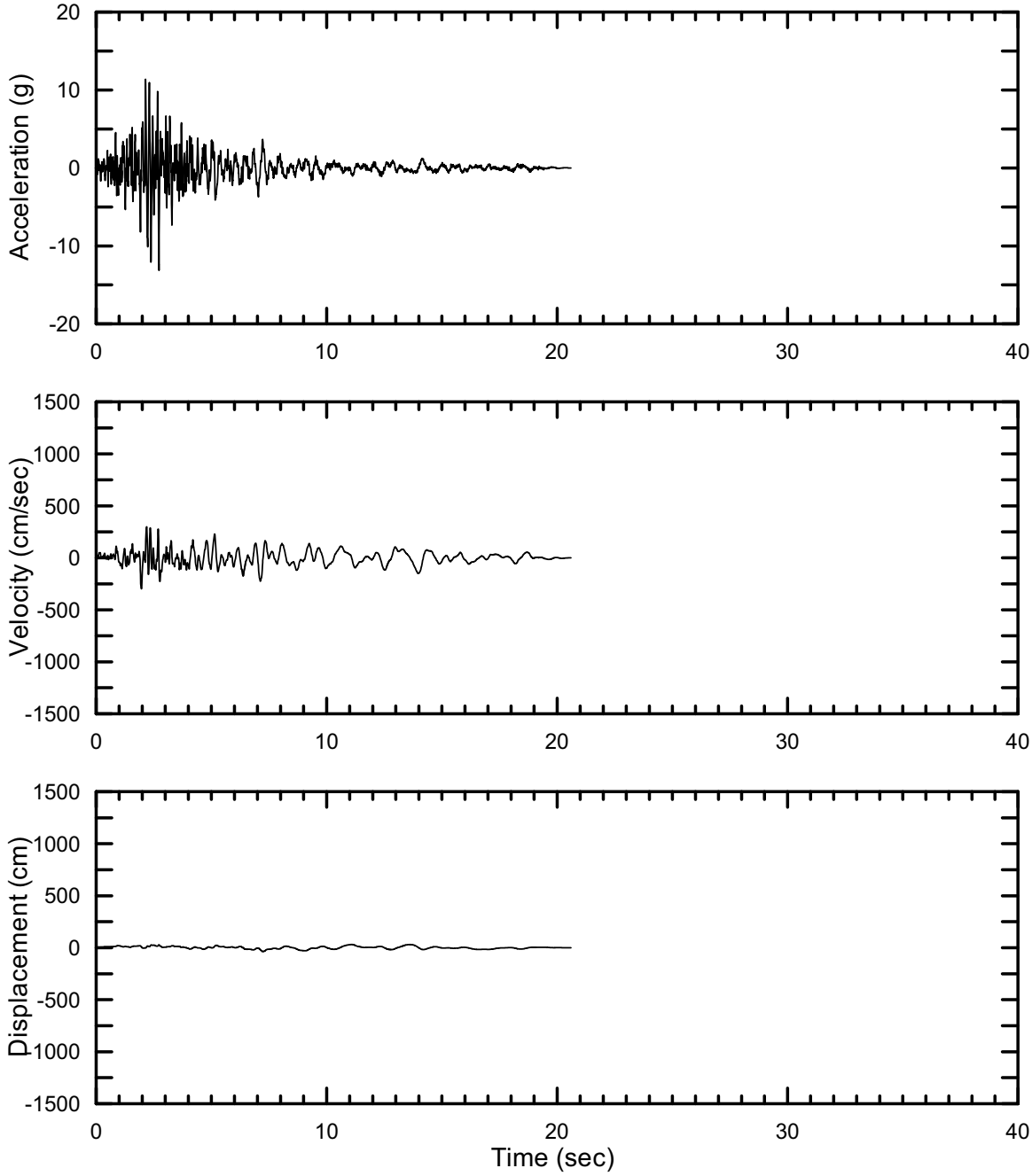

DTN: MO0403AVTMH107.003 [DIRS 168892]

Figure II-147. Point B Vertical Time Histories at an Annual Exceedance Probability of 10^{-7}, Set #1

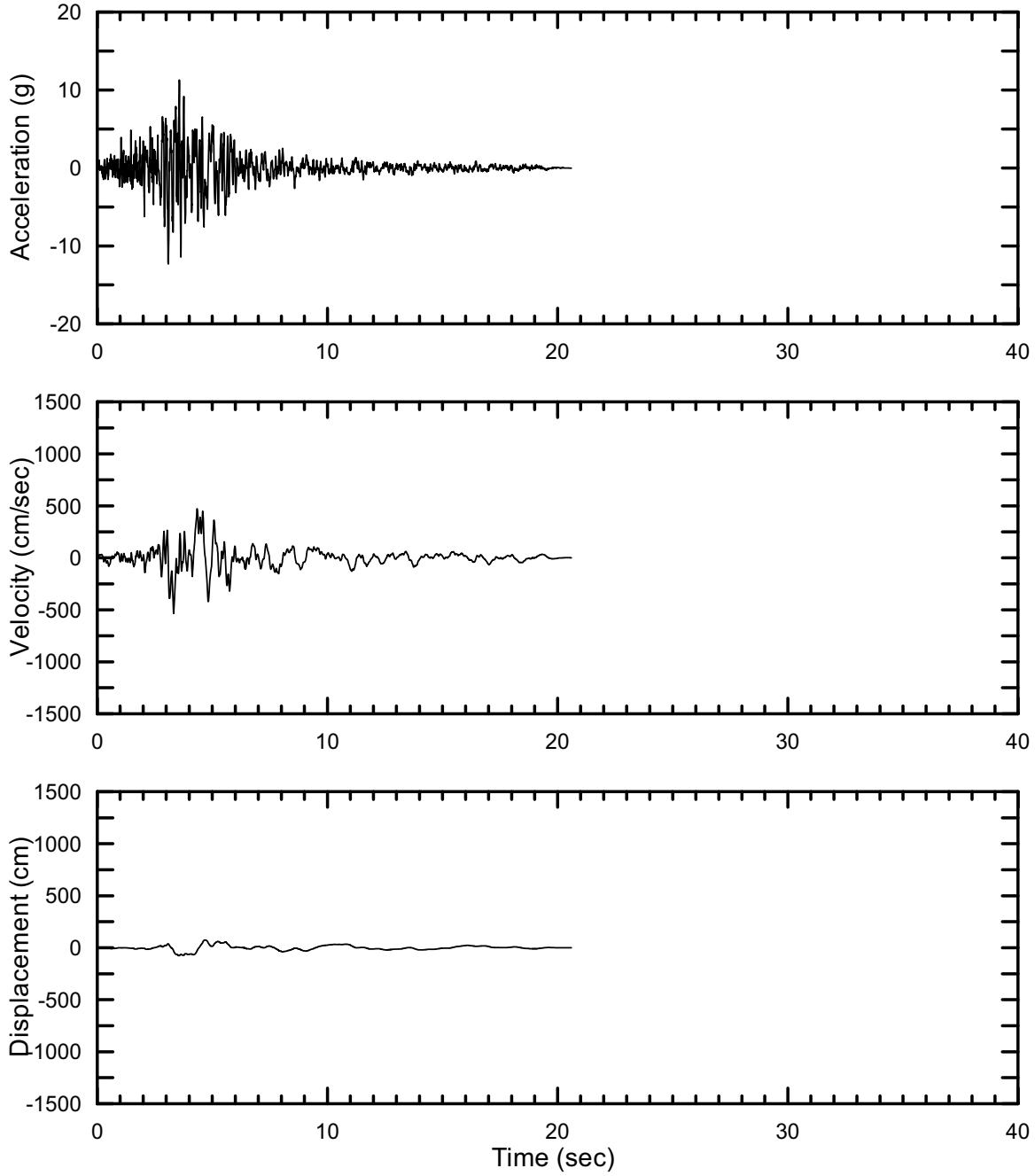

DTN: MO0403AVTMH107.003 [DIRS 168892]

Figure II-148. Point B Horizontal-1 Ti me Histories at an Annual Exceedance Probability of 10^{-7}, Set #2

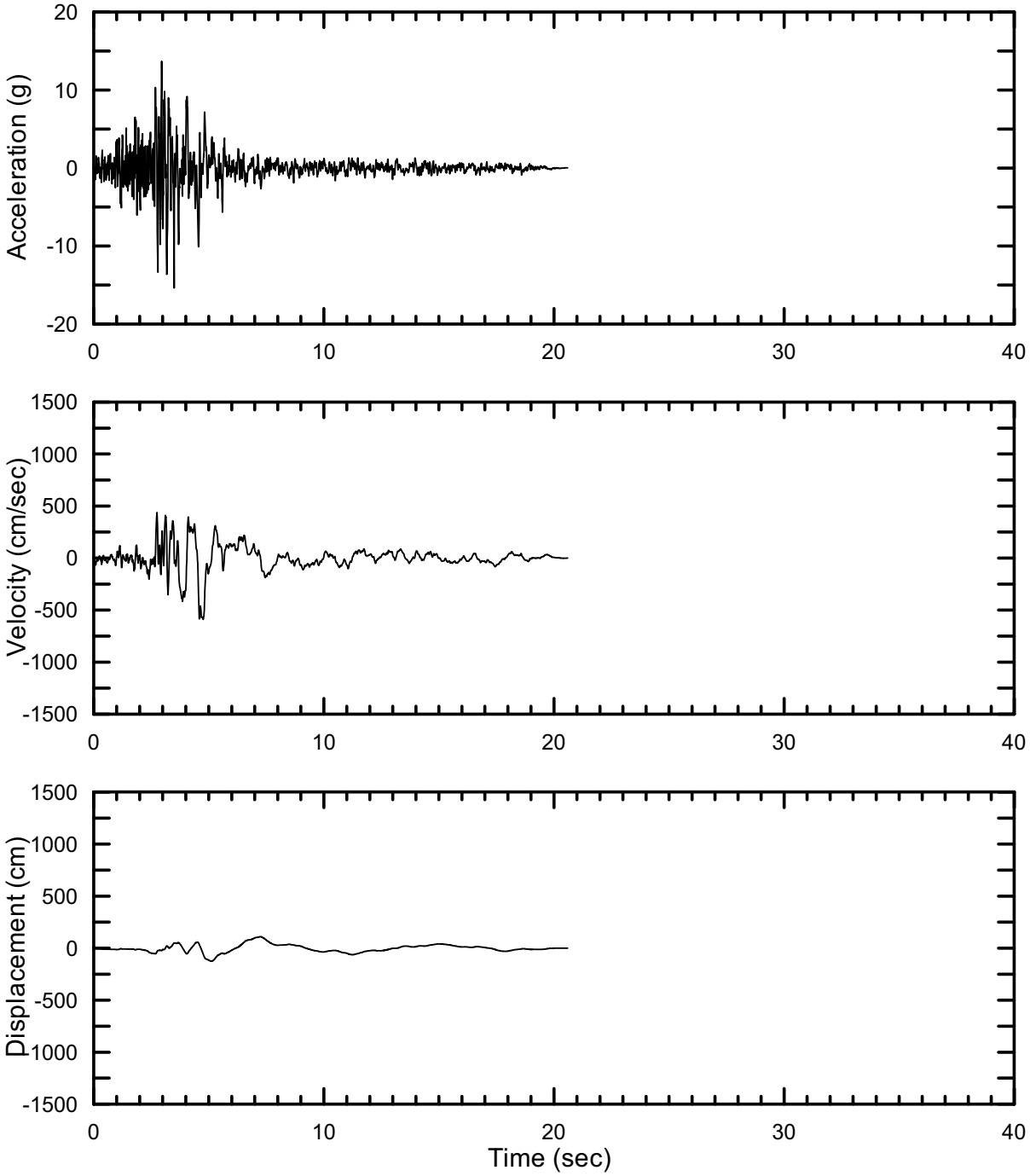

DTN: MO0403AVTMH107.003 [DIRS 168892]

Figure II-149. Point D Horizontal-2 Time Histories at an Annual Exceedance Probability of 10^{-7}, Set #2

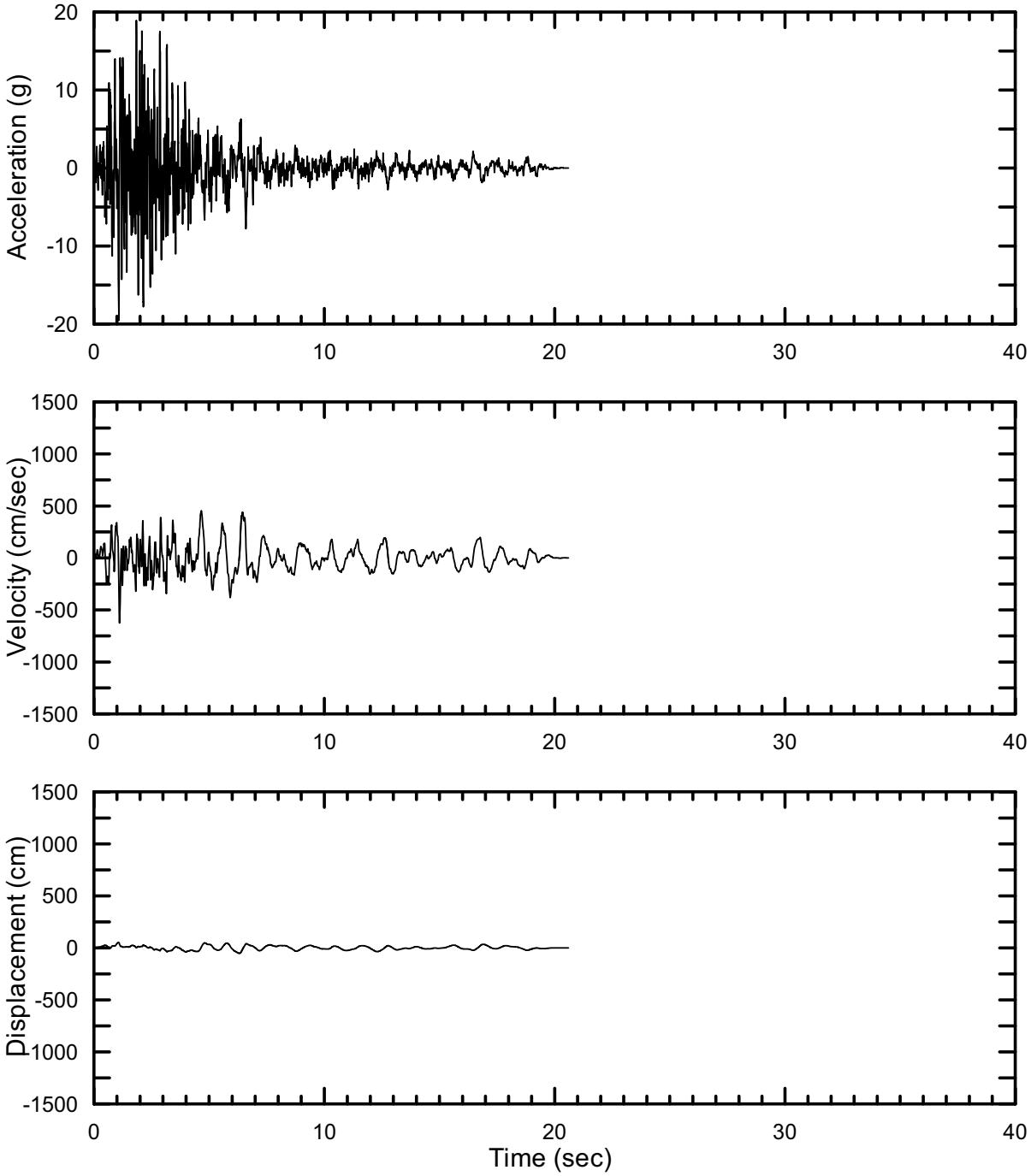

DTN: MO0403AVTMH107.003 [DIRS 168892]

Figure II-150. Point B Vertical Time Histories at an Annual Exceedance Probability of 10^{-7}, Set #2

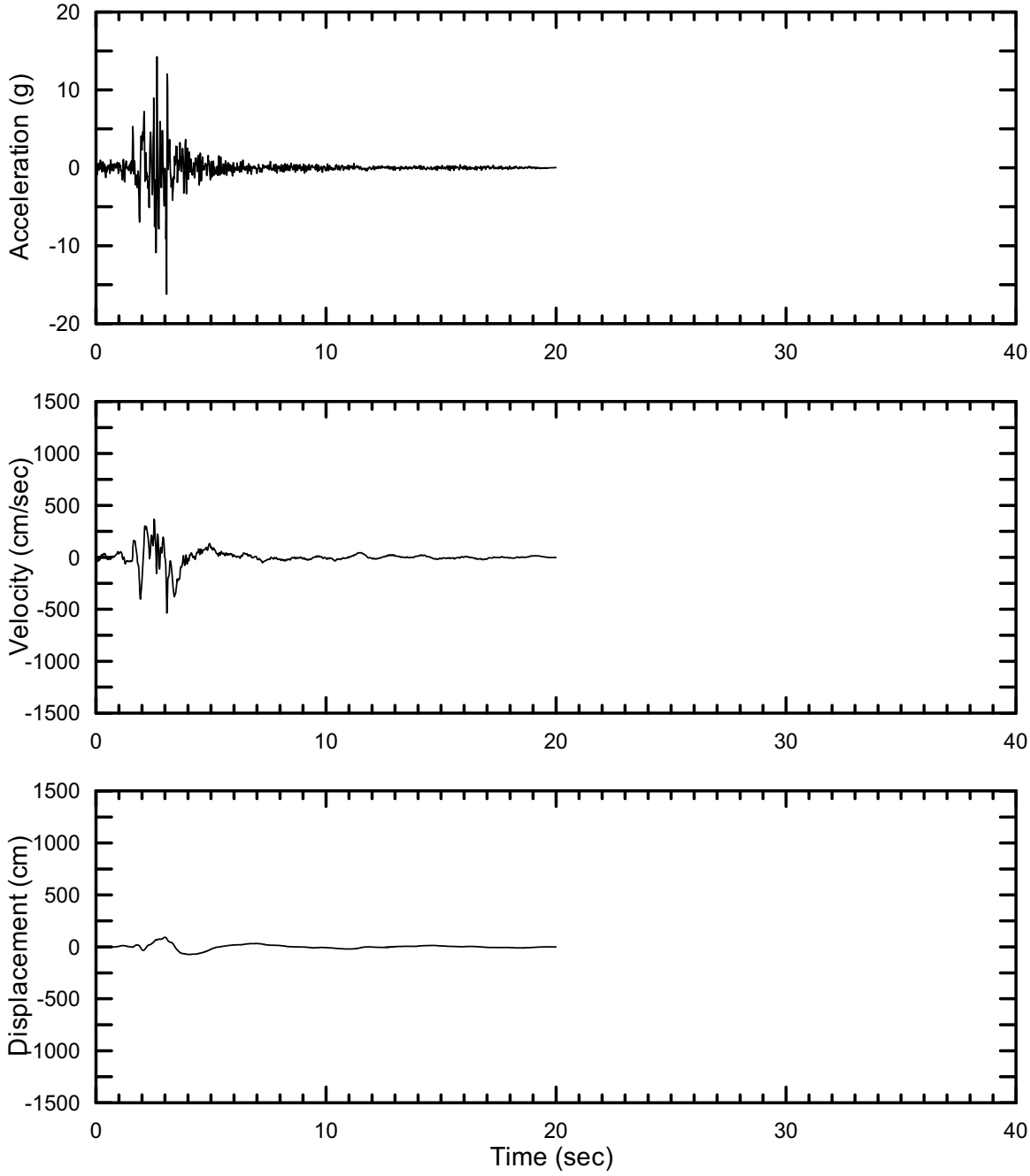

DTN: MO0403AVTMH107.003 [DIRS 168892]

Figure II-151. Point B Horizontal-1 Ti me Histories at an Annual Exceedance Probability of 10^{-7}, Set #3

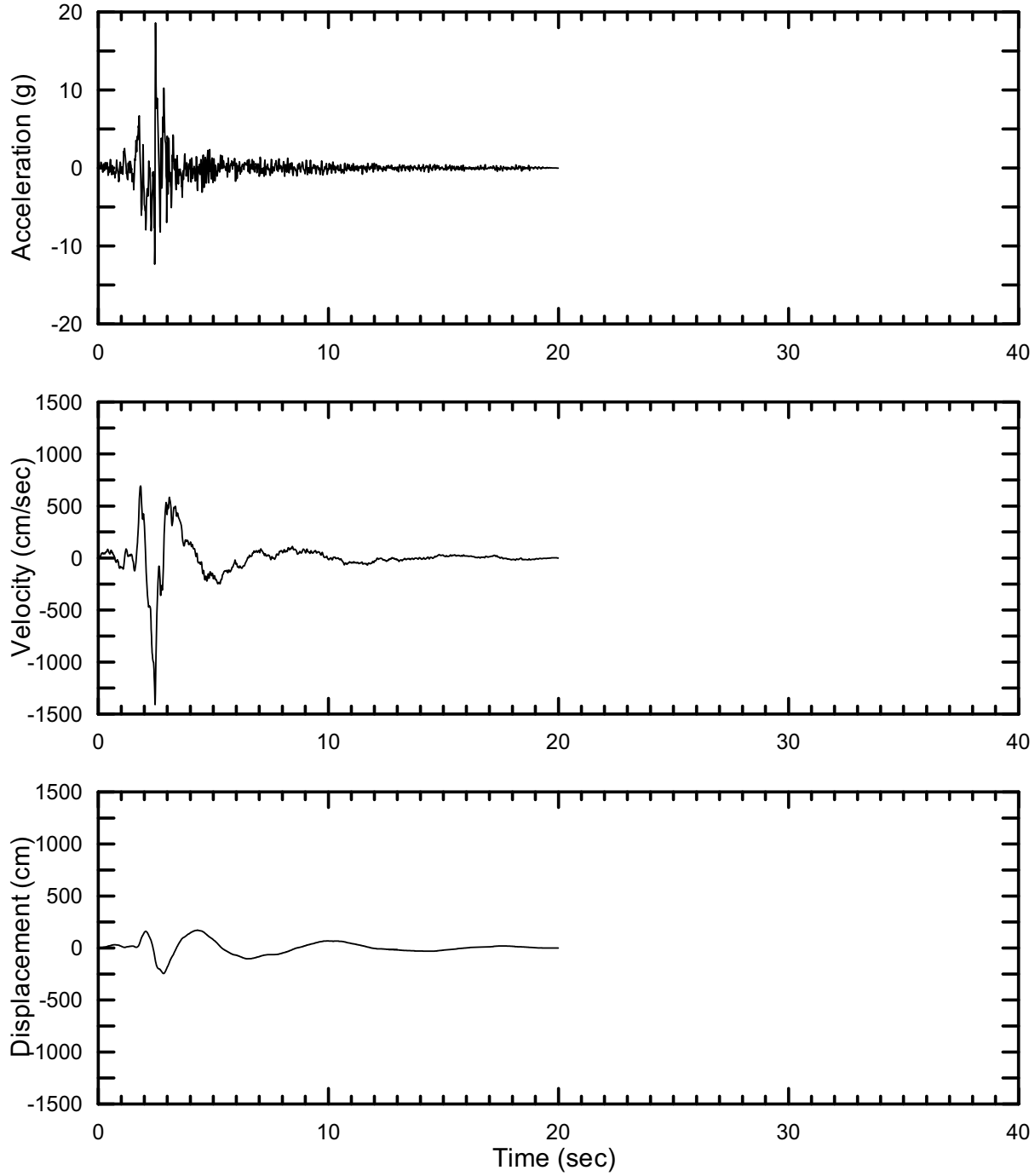

DTN: MO0403AVTMH107.003 [DIRS 168892]

Figure II-152. Point B Horizontal-2 Ti me Histories at an Annual Exceedance Probability of 10^{-7}, Set #3

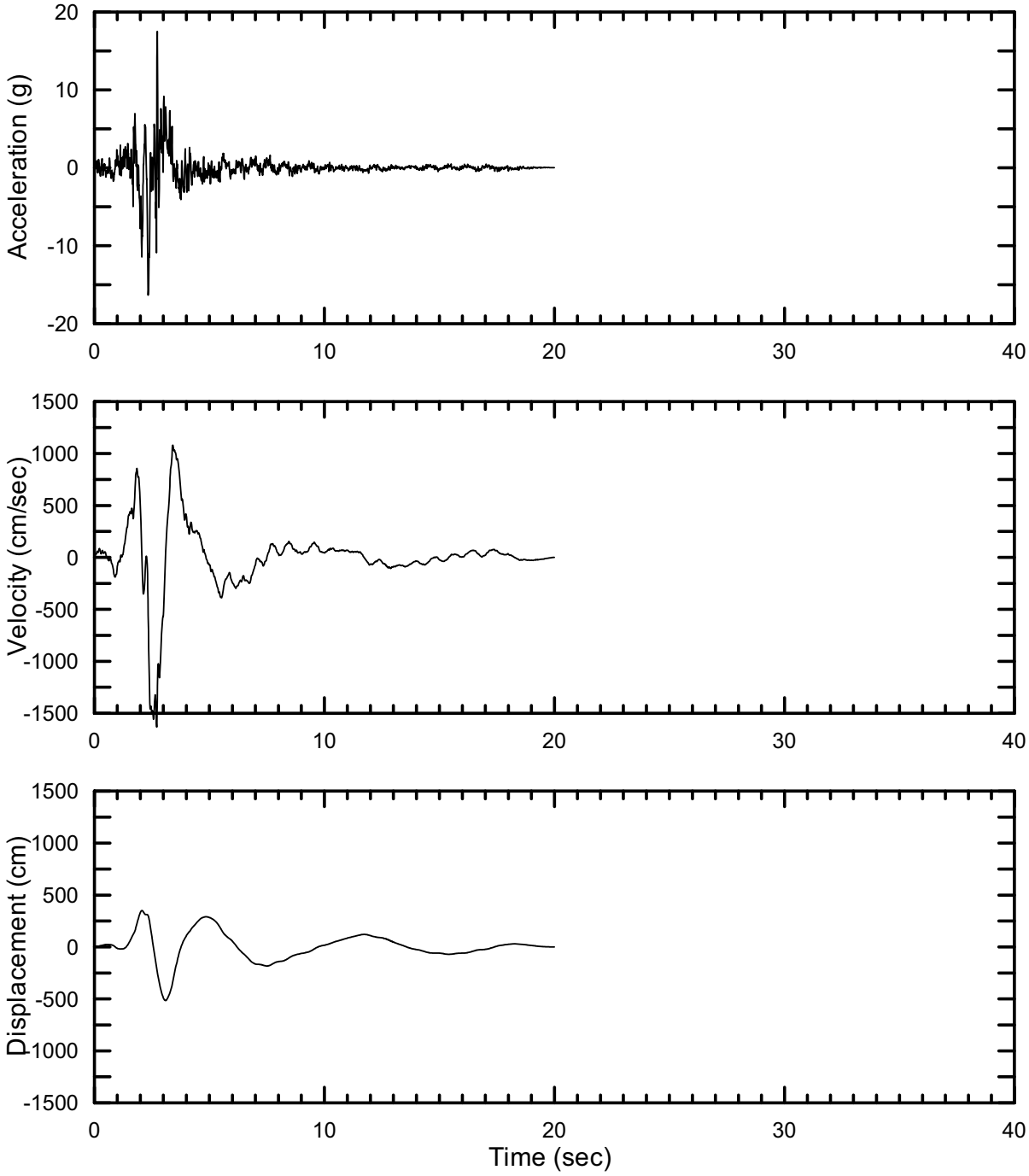

DTN: MO0403AVTMH107.003 [DIRS 168892]

Figure II-153. Point B Vertical Time Histories at an Annual Exceedance Probability of 10^{-7}, Set #3

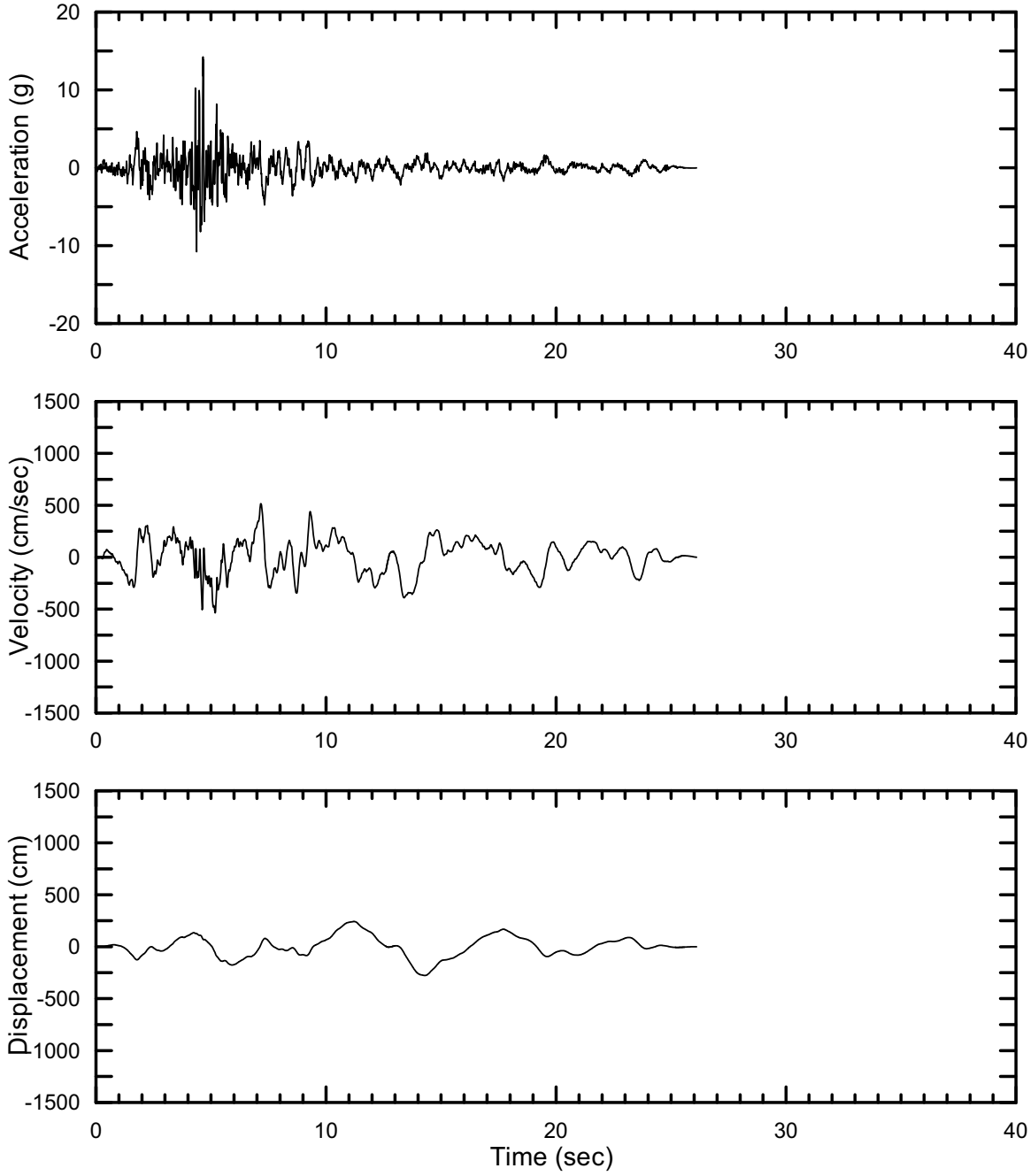

DTN: MO0403AVTMH107.003 [DIRS 168892]

Figure II-154. Point B Horizontal-1 Ti me Histories at an Annual Exceedance Probability of 10^{-7}, Set #4

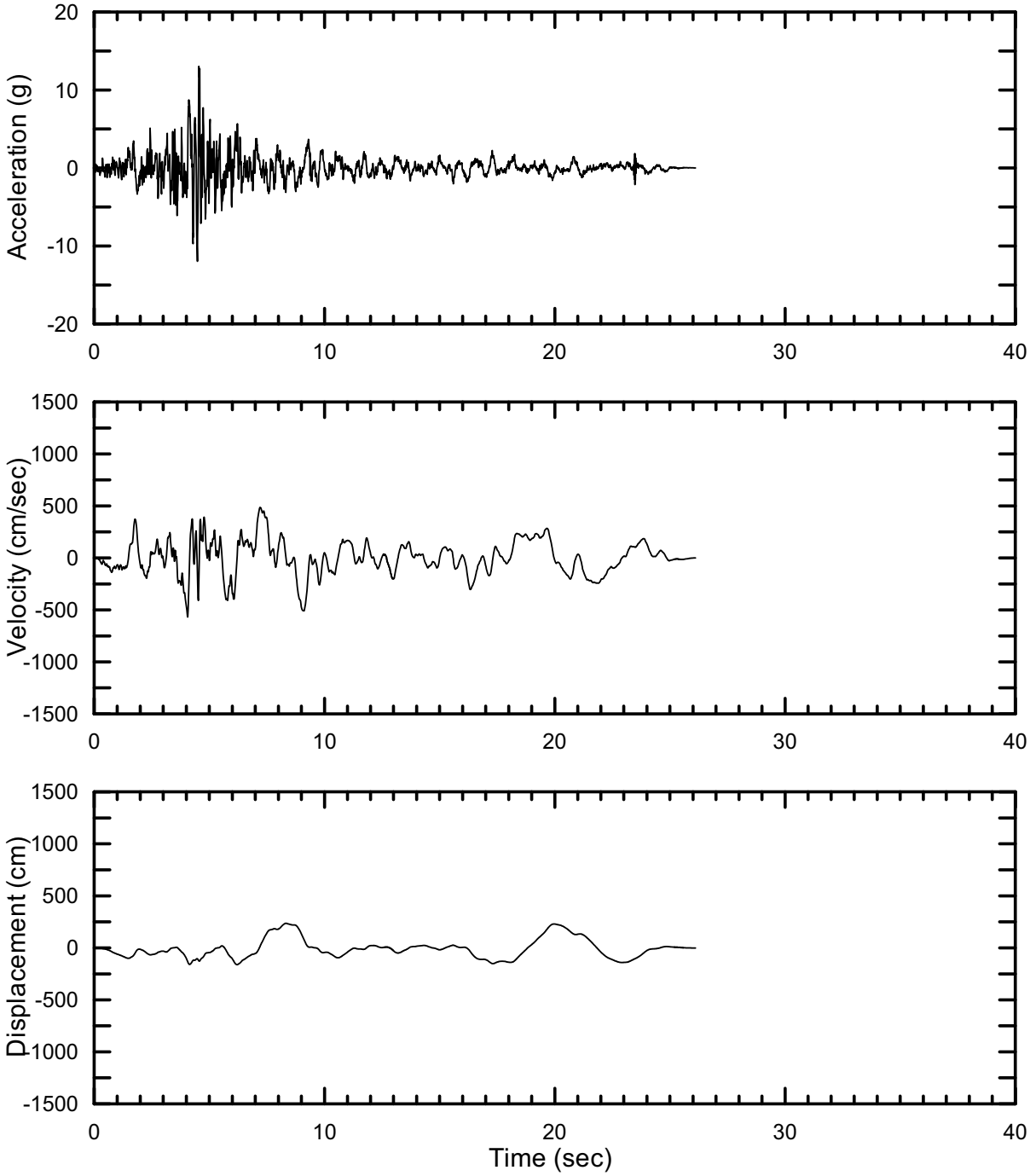

DTN: MO0403AVTMH107.003 [DIRS 168892]

Figure II-155. Point B Horizontal-2 Ti me Histories at an Annual Exceedance Probability of 10^{-7}, Set #4

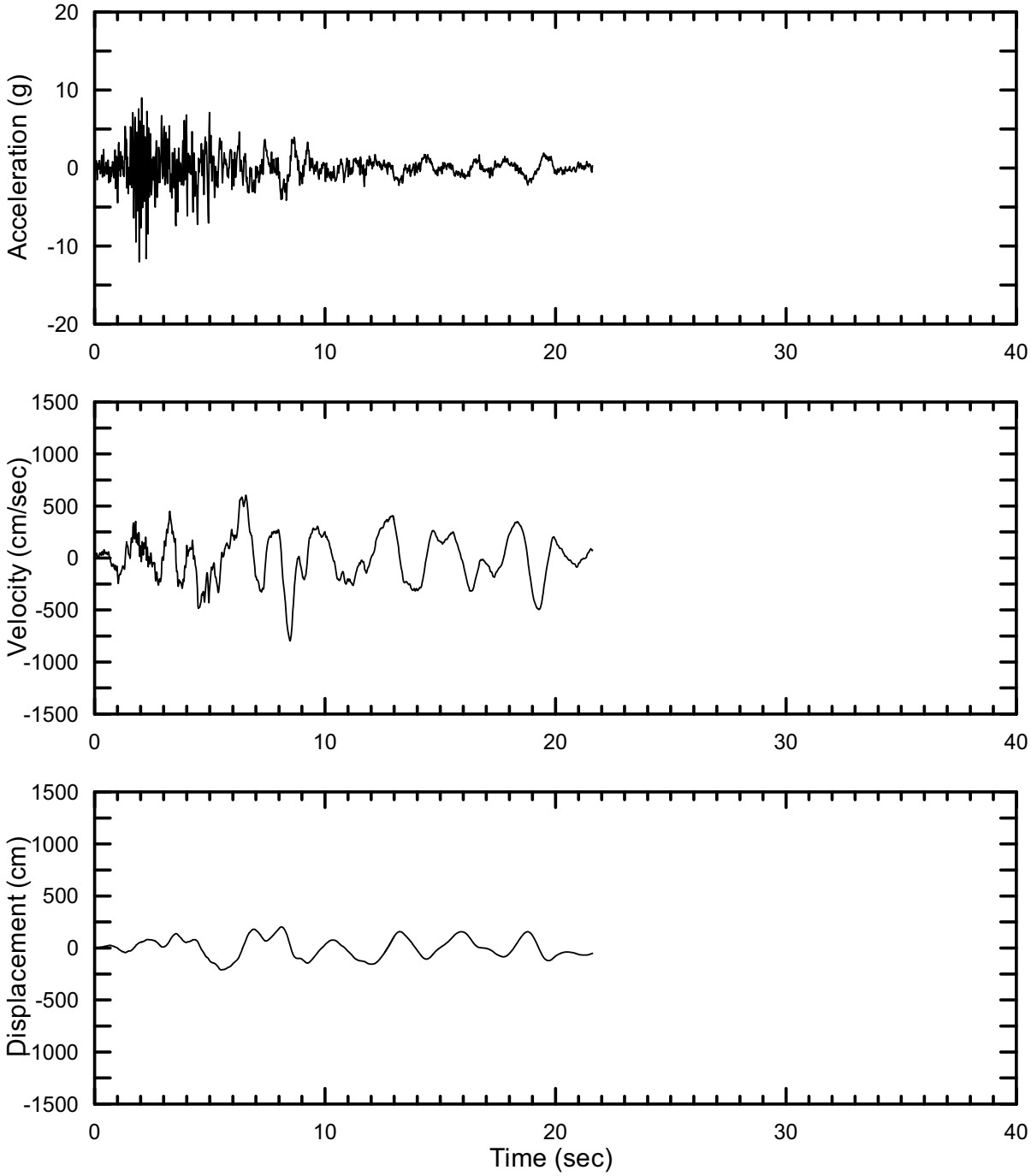

DTN: MO0403AVTMH107.003 [DIRS 168892]

Figure II-156. Point B Vertical Time Histories at an Annual Exceedance Probability of 10^{-7}, Set #4

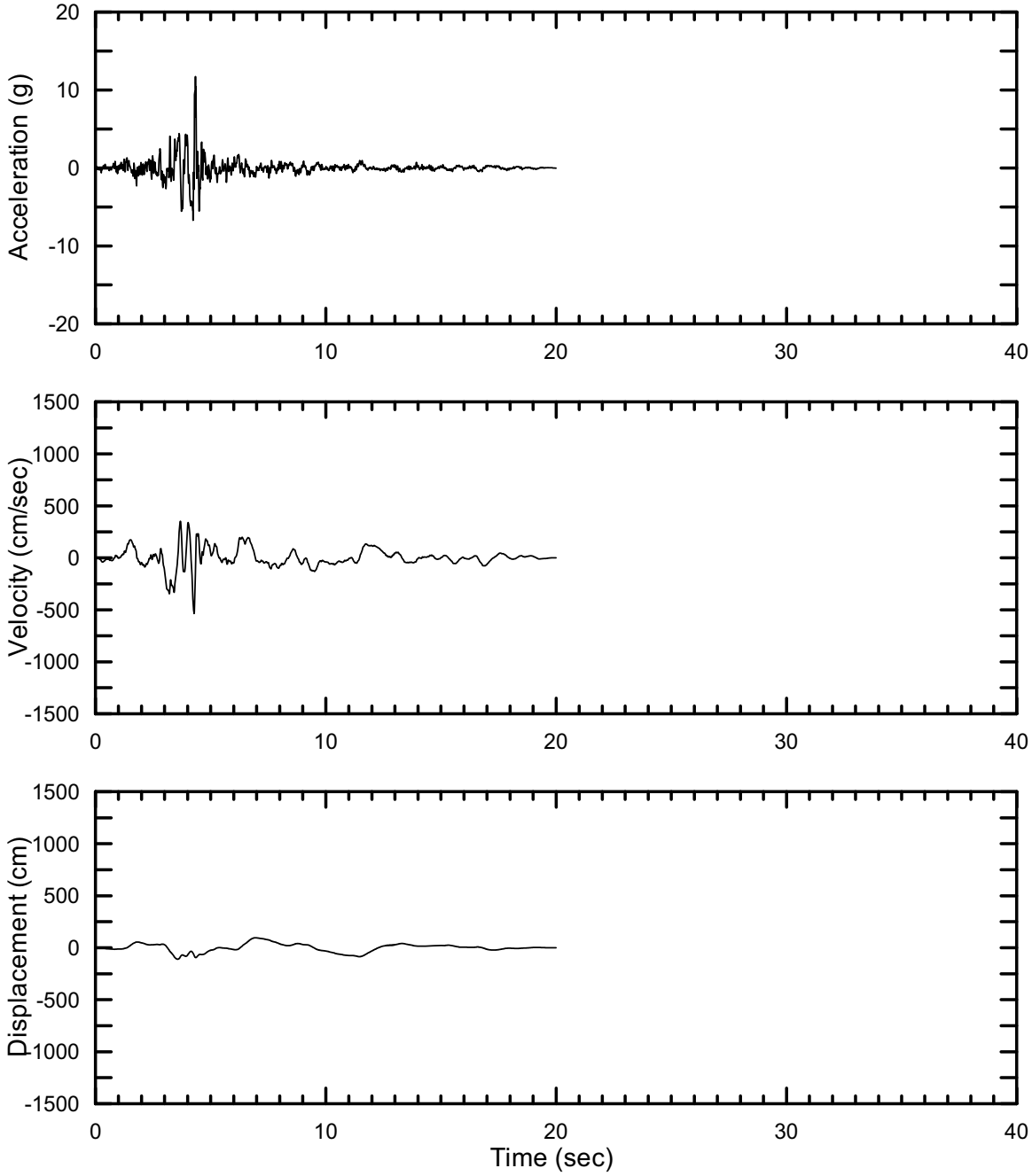

DTN: MO0403AVTMH107.003 [DIRS 168892]

Figure II-157. Point B Horizontal-1 Ti me Histories at an Annual Exceedance Probability of 10^{-7}, Set #5

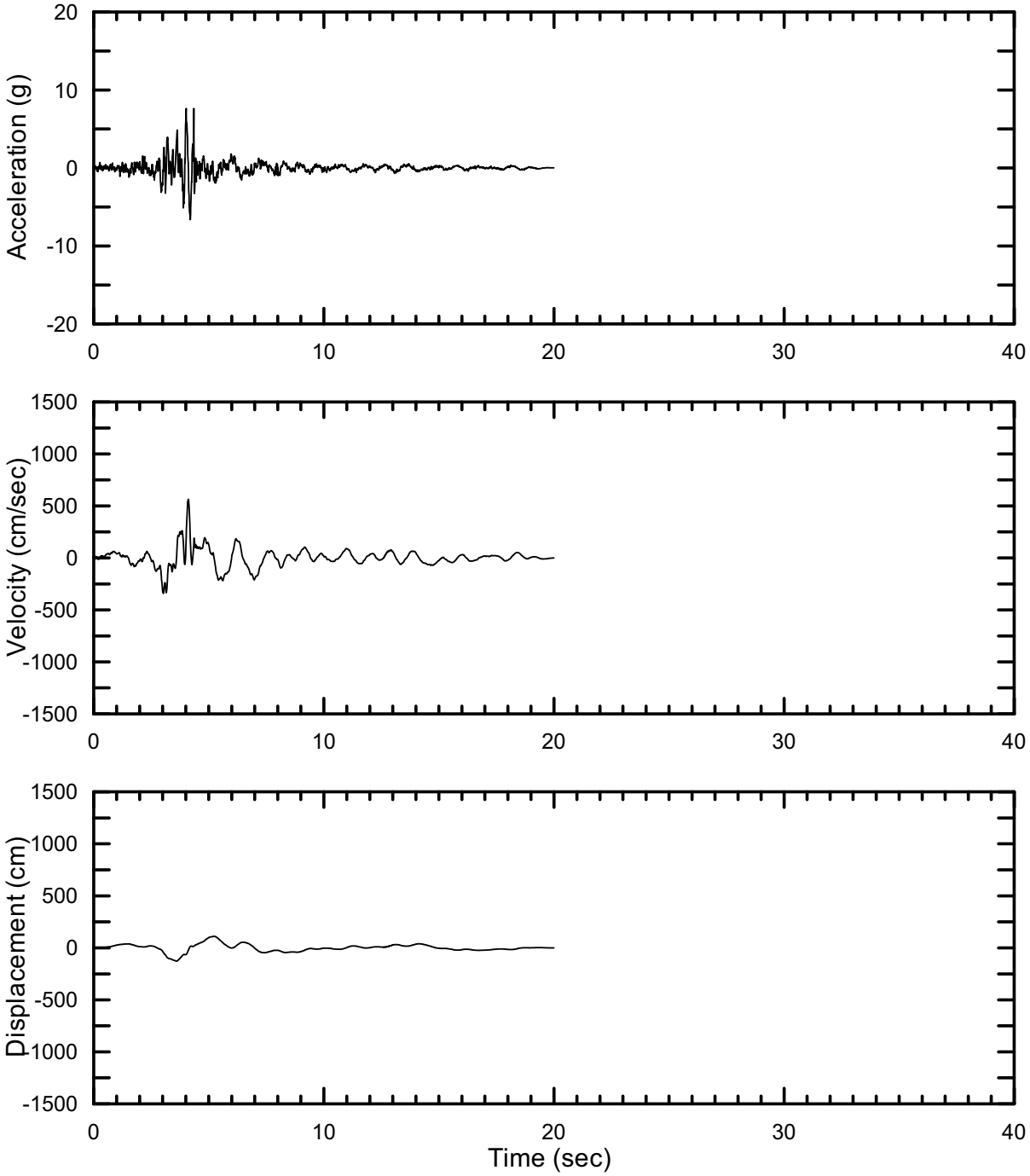

DTN: MO0403AVTMH107.003 [DIRS 168892]

Figure II-158. Point B Horizontal-2 Ti me Histories at an Annual Exceedance Probability of 10^{-7}, Set #5

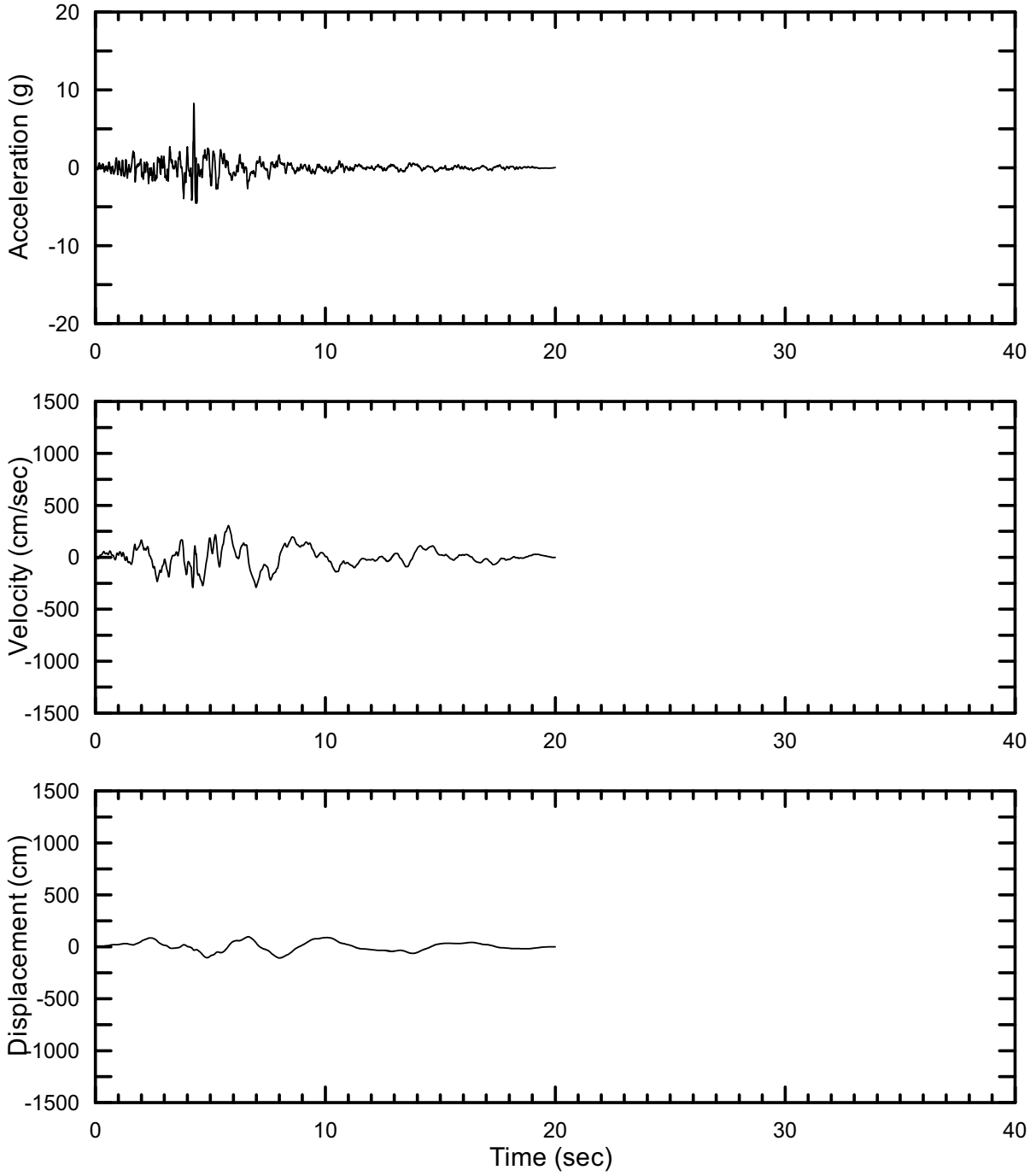

DTN: MO0403AVTMH107.003 [DIRS 168892]

Figure II-159. Point B Vertical Time Histories at an Annual Exceedance Probability of 10^{-7}, Set #5

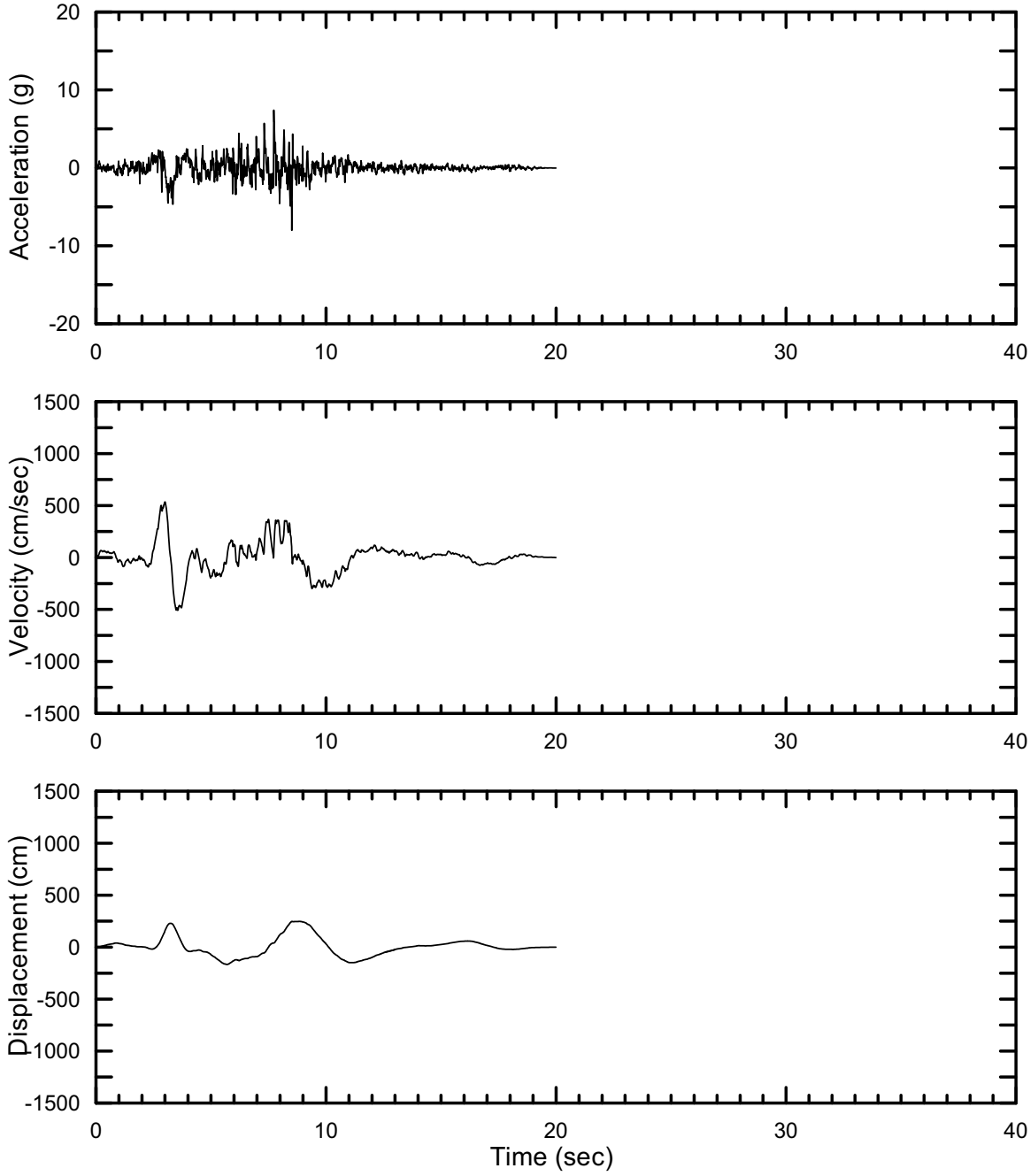

DTN: MO0403AVTMH107.003 [DIRS 168892]

Figure II-160. Point B Horizontal-1 Ti me Histories at an Annual Exceedance Probability of 10^{-7}, Set #6

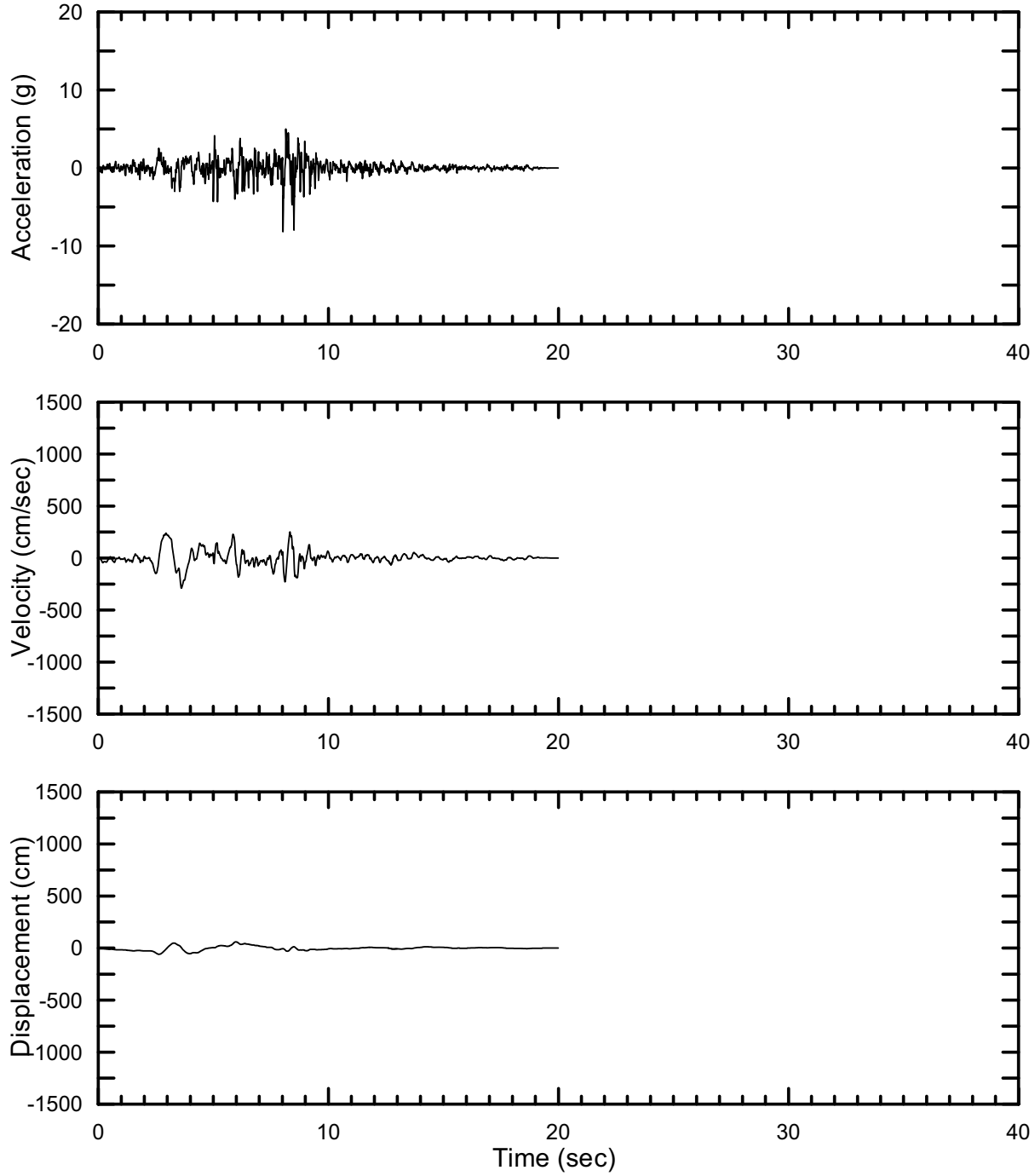

DTN: MO0403AVTMH107.003 [DIRS 168892]

Figure II-161. Point B Horizontal-2 Ti me Histories at an Annual Exceedance Probability of 10^{-7}, Set #6

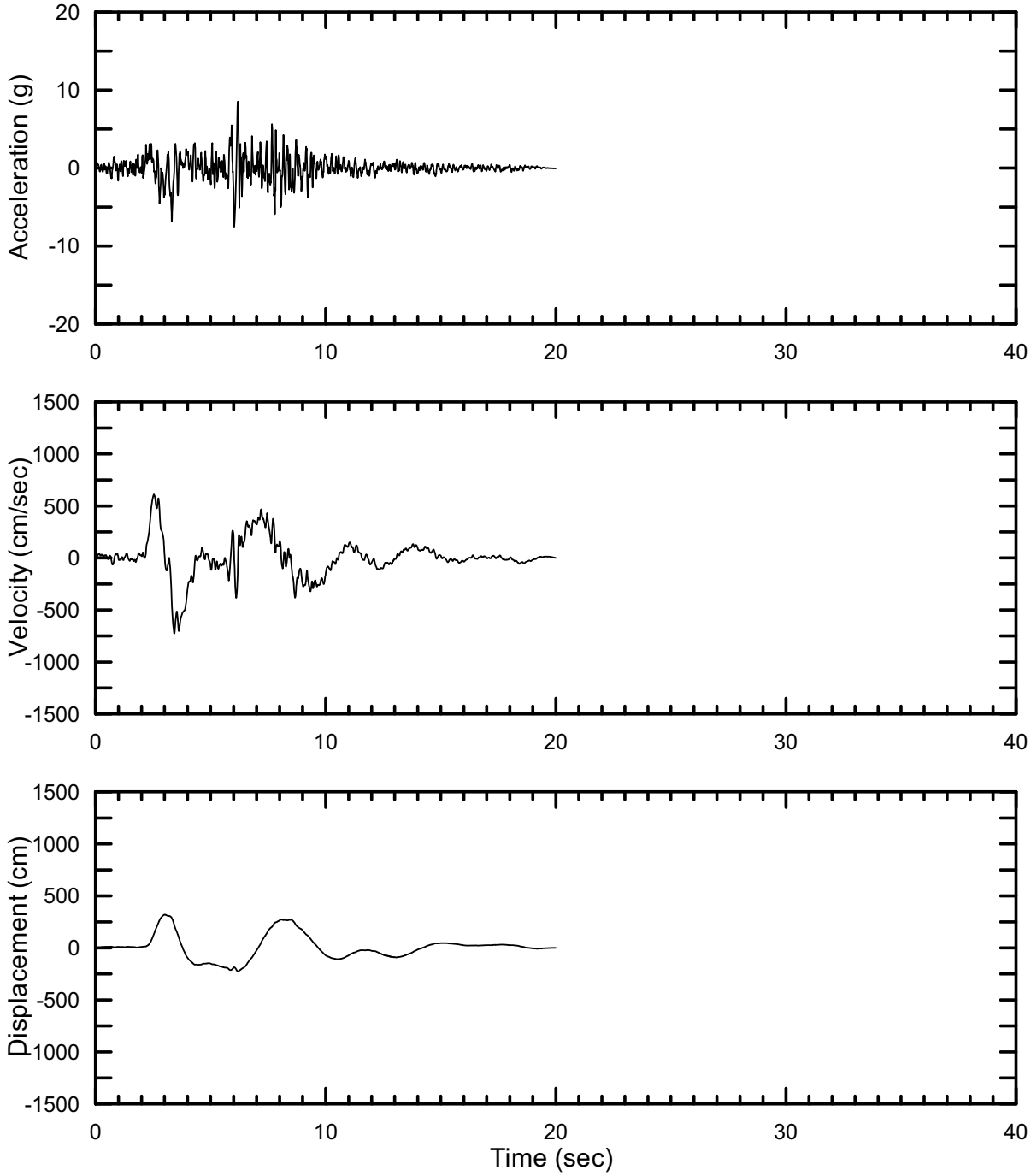

DTN: MO0403AVTMH107.003 [DIRS 168892]

Figure II-162. Point B Vertical Time Histories at an Annual Exceedance Probability of 10^{-7}, Set #6

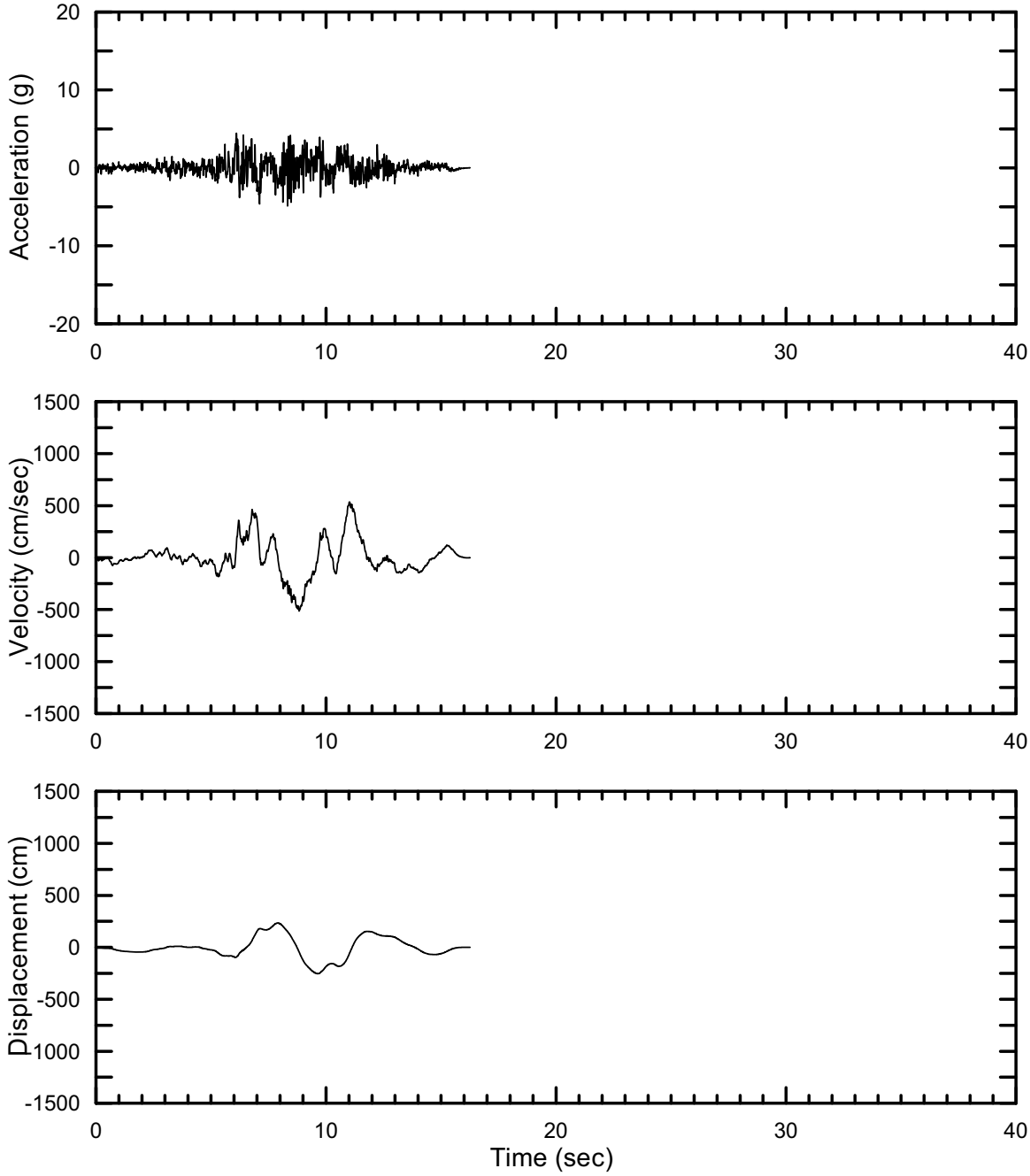

DTN: MO0403AVTMH107.003 [DIRS 168892]

Figure II-163. Point B Horizontal-1 Ti me Histories at an Annual Exceedance Probability of 10^{-7}, Set #7

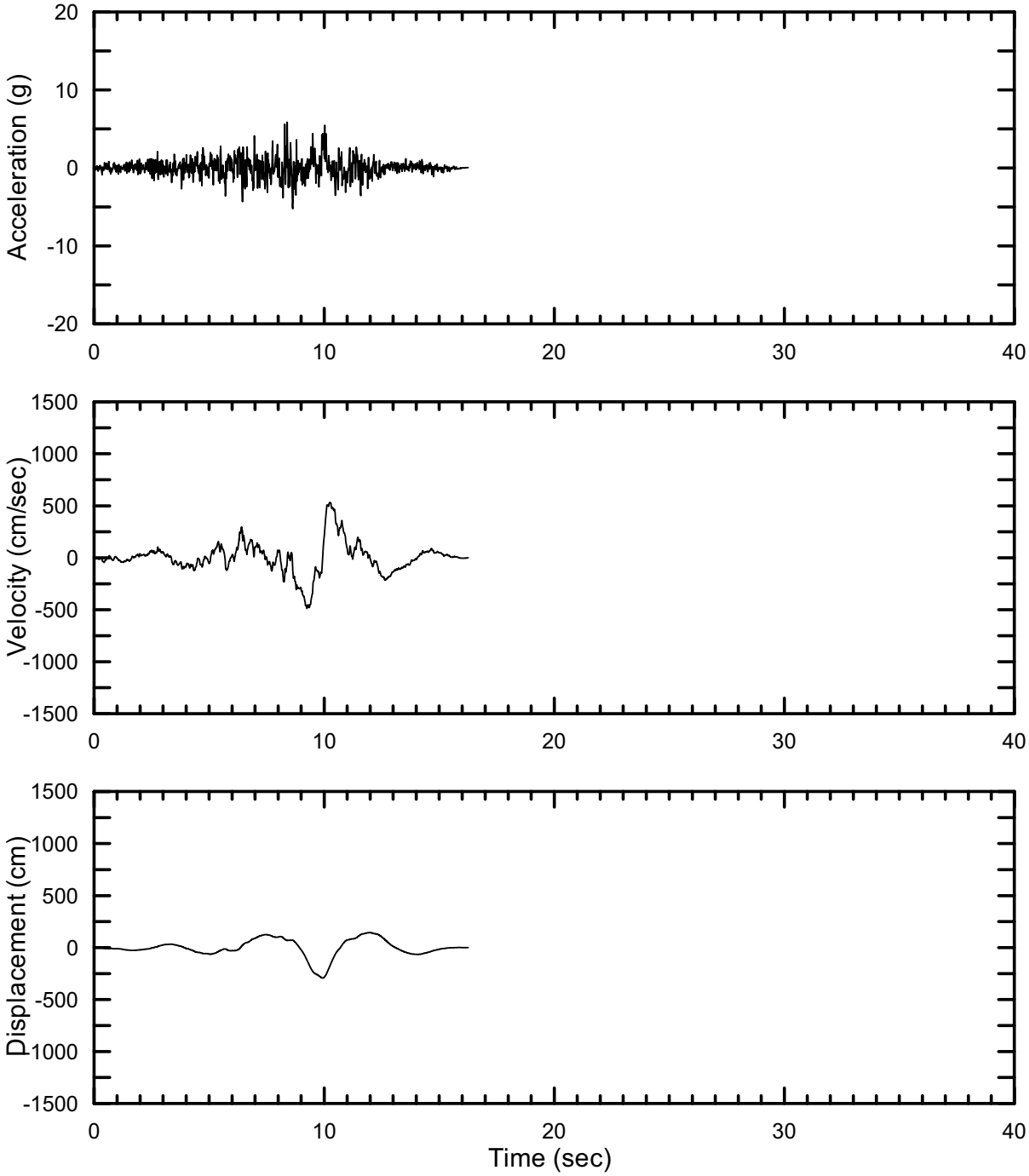

DTN: MO0403AVTMH107.003 [DIRS 168892]

Figure II-164. Point B Horizontal-2 Ti me Histories at an Annual Exceedance Probability of 10^{-7}, Set #7

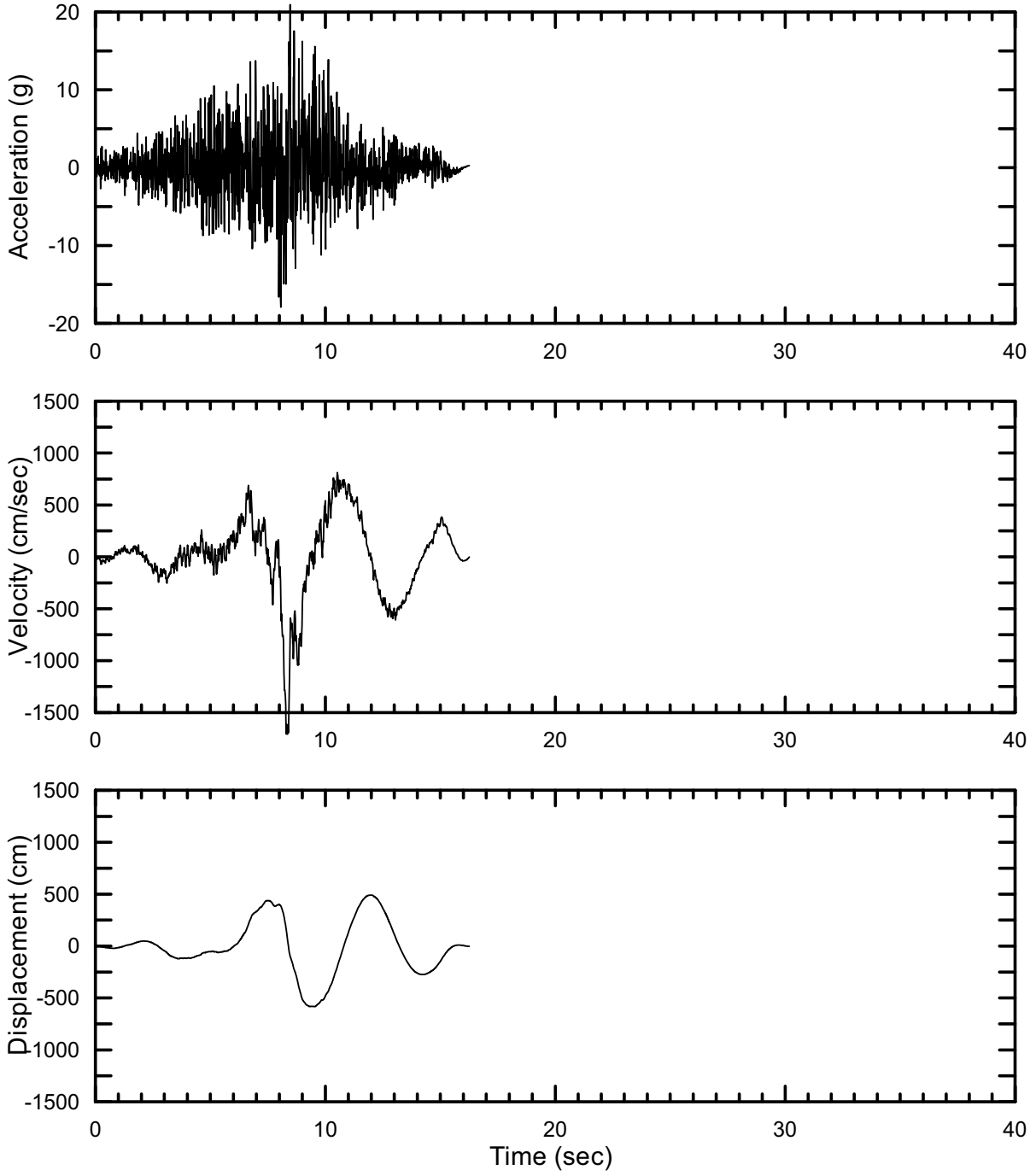

DTN: MO0403AVTMH107.003 [DIRS 168892]

Figure II-165. Point B Vertical Time Histories at an Annual Exceedance Probability of 10^{-7}, Set #7

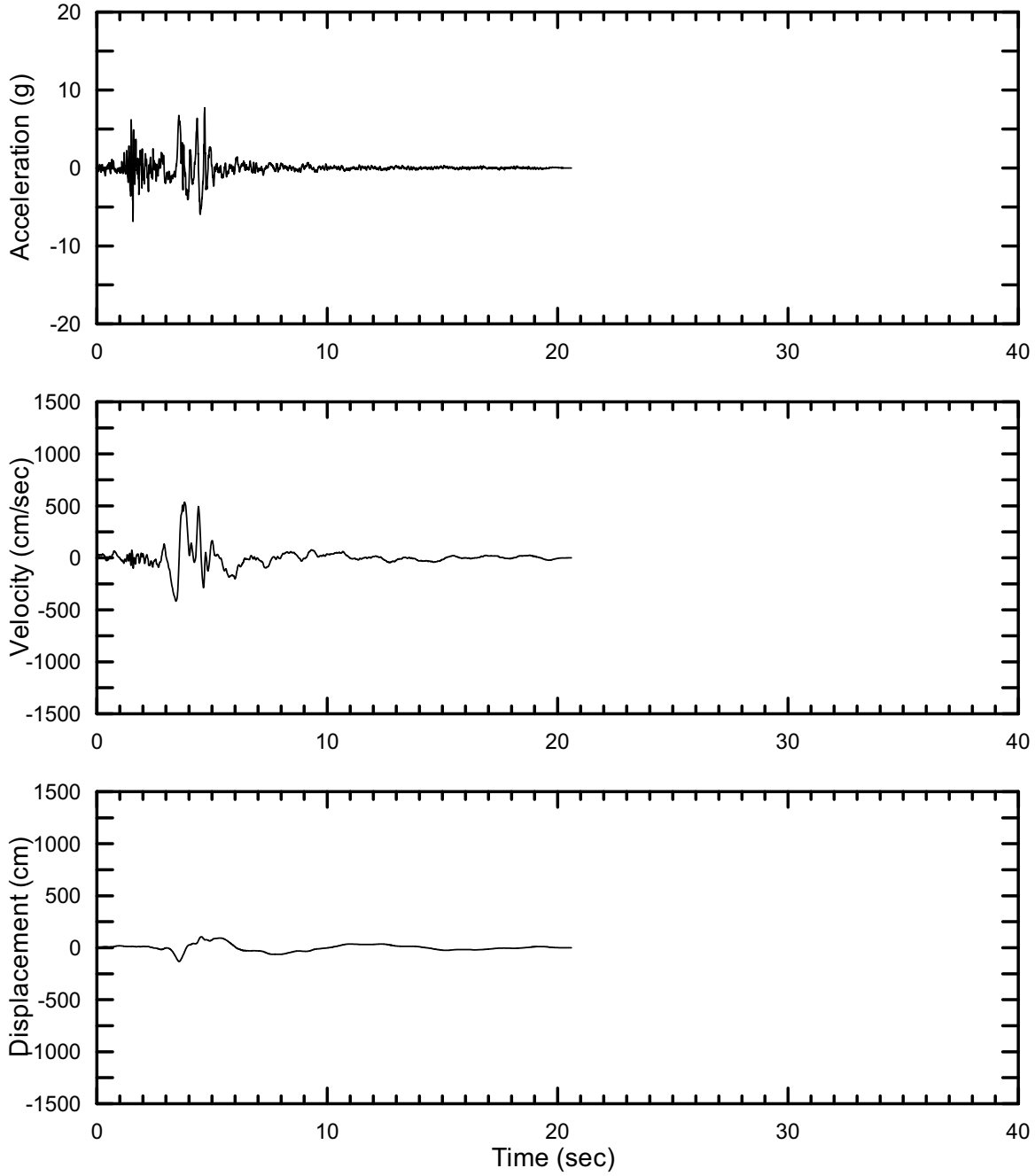

DTN: MO0403AVTMH107.003 [DIRS 168892]

Figure II-166. Point B Horizontal-1 Ti me Histories at an Annual Exceedance Probability of 10^{-7}, Set #8

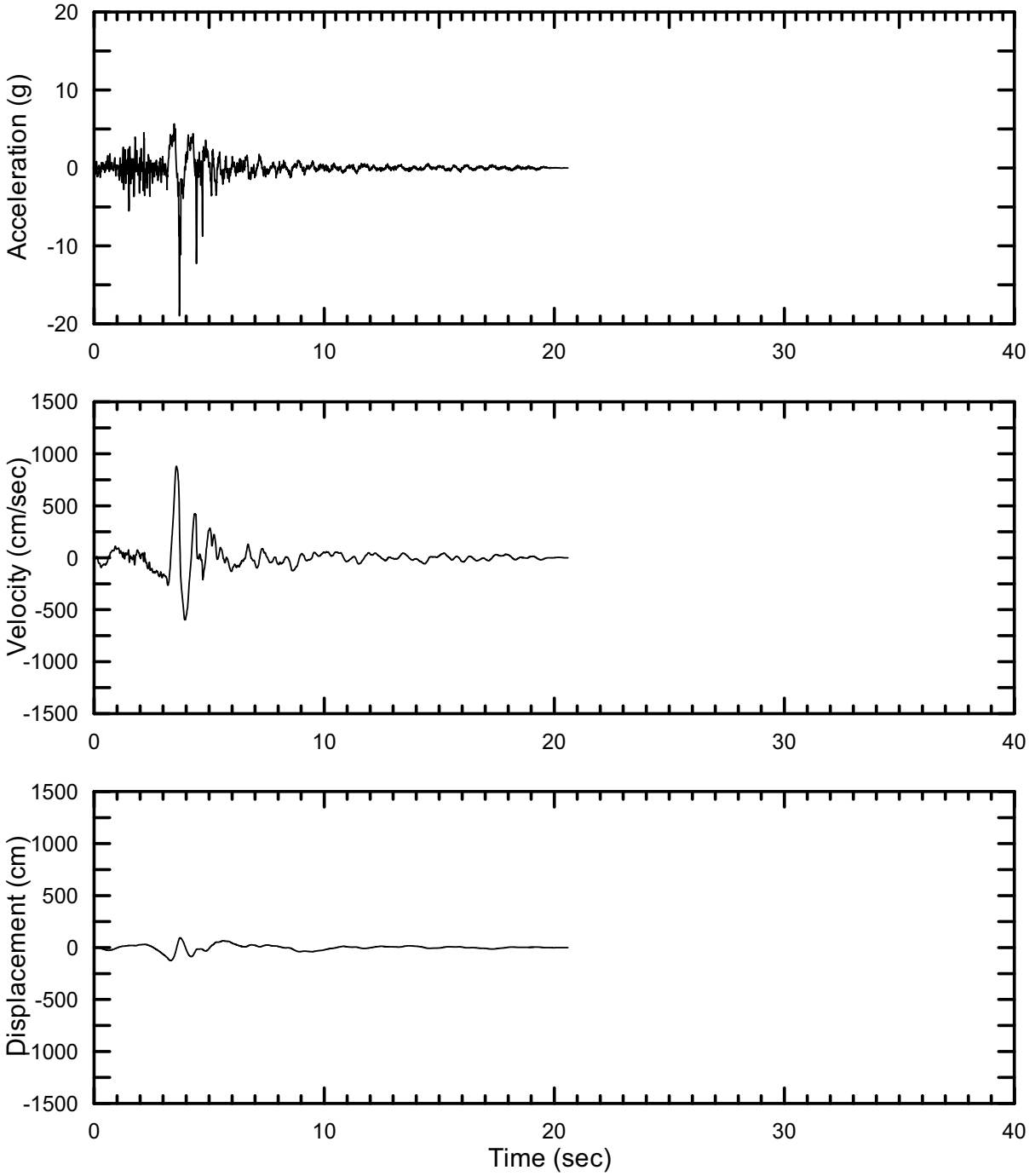

DTN: MO0403AVTMH107.003 [DIRS 168892]

Figure II-167. Point B Horizontal-2 Ti me Histories at an Annual Exceedance Probability of 10^{-7}, Set #8

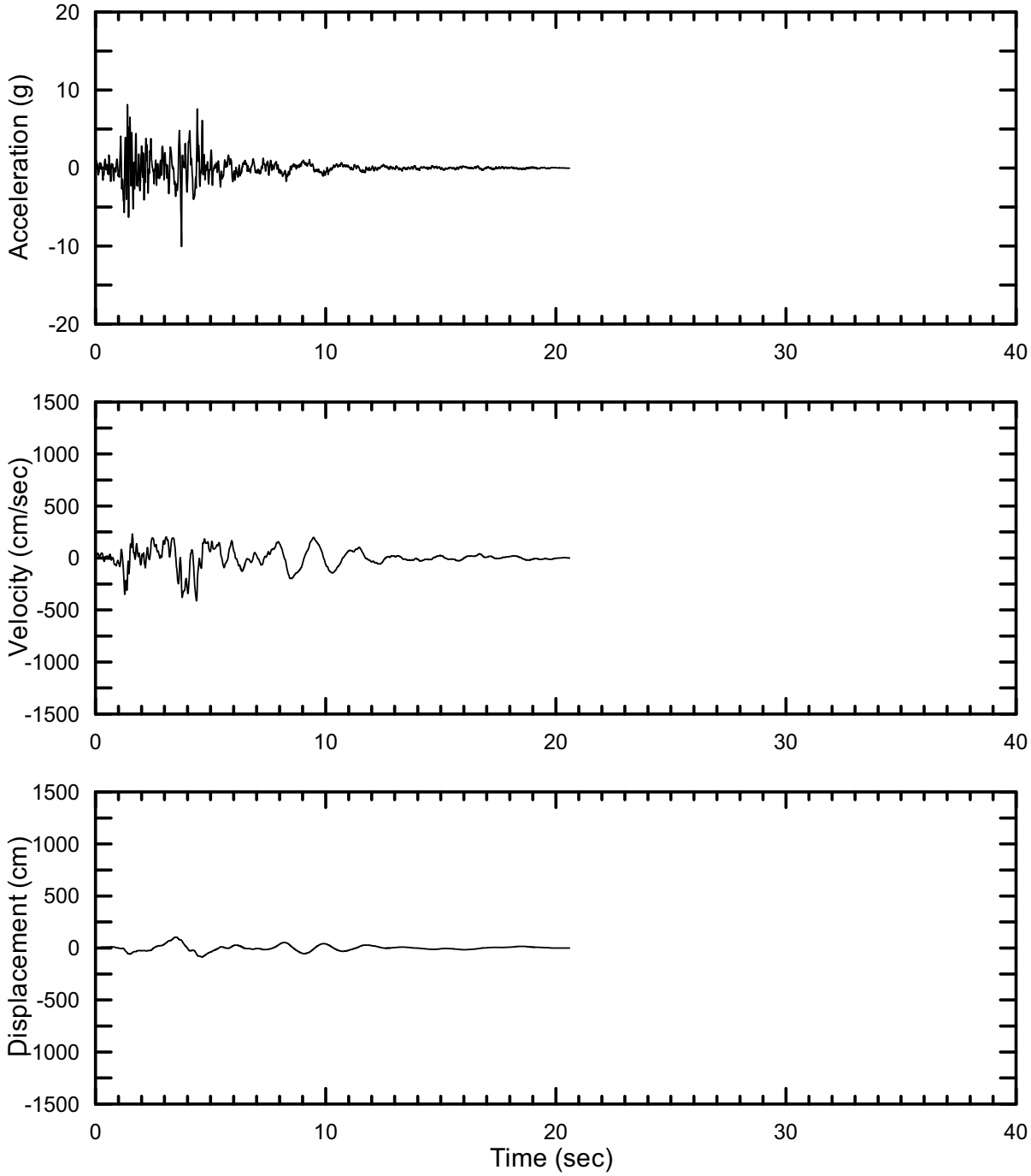

DTN: MO0403AVTMH107.003 [DIRS 168892]

Figure II-168. Point B Vertical Time Histories at an Annual Exceedance Probability of 10^{-7}, Set #8

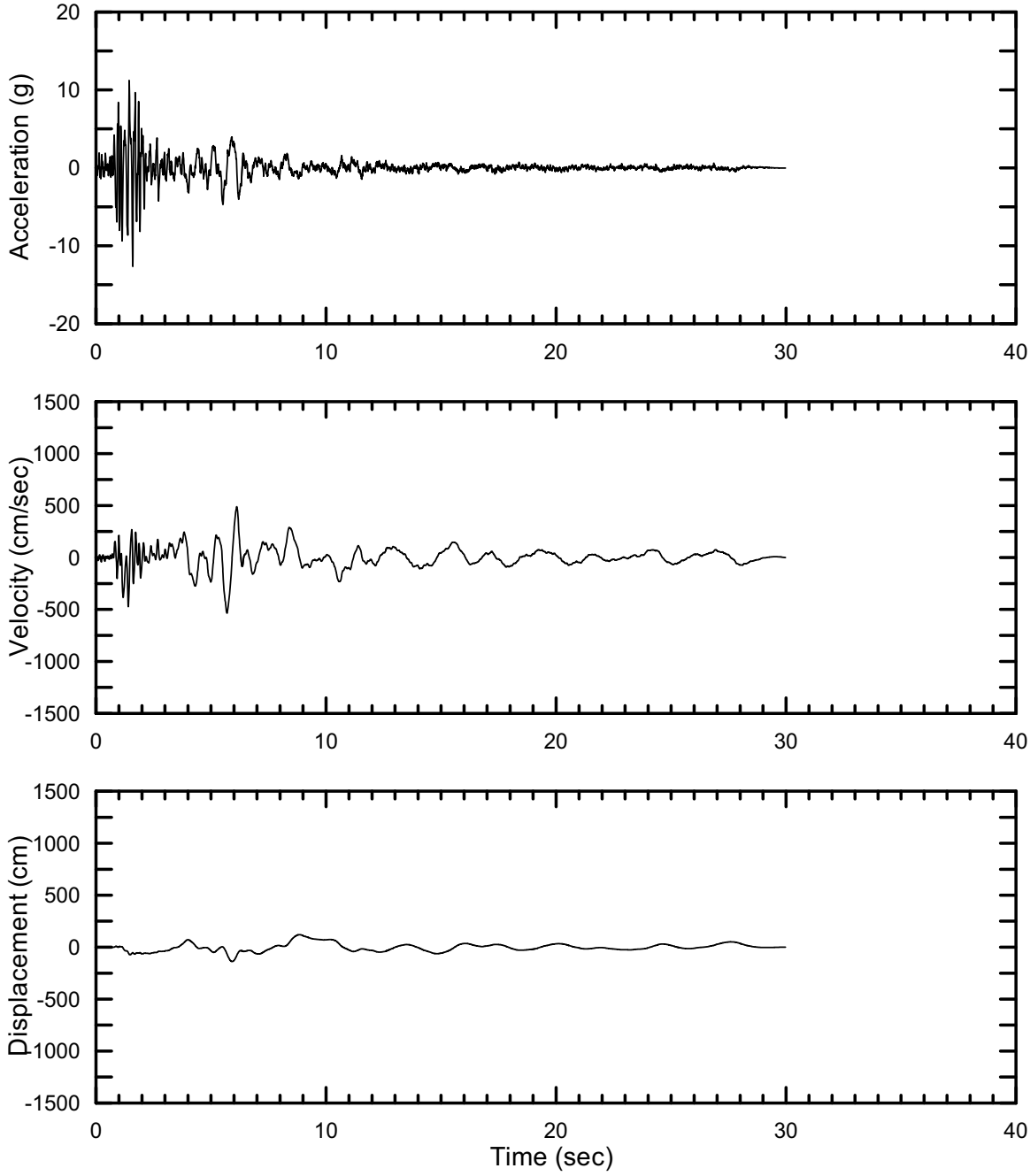

DTN: MO0403AVTMH107.003 [DIRS 168892]

Figure II-169. Point B Horizontal-1 Ti me Histories at an Annual Exceedance Probability of 10^{-7}, Set #9

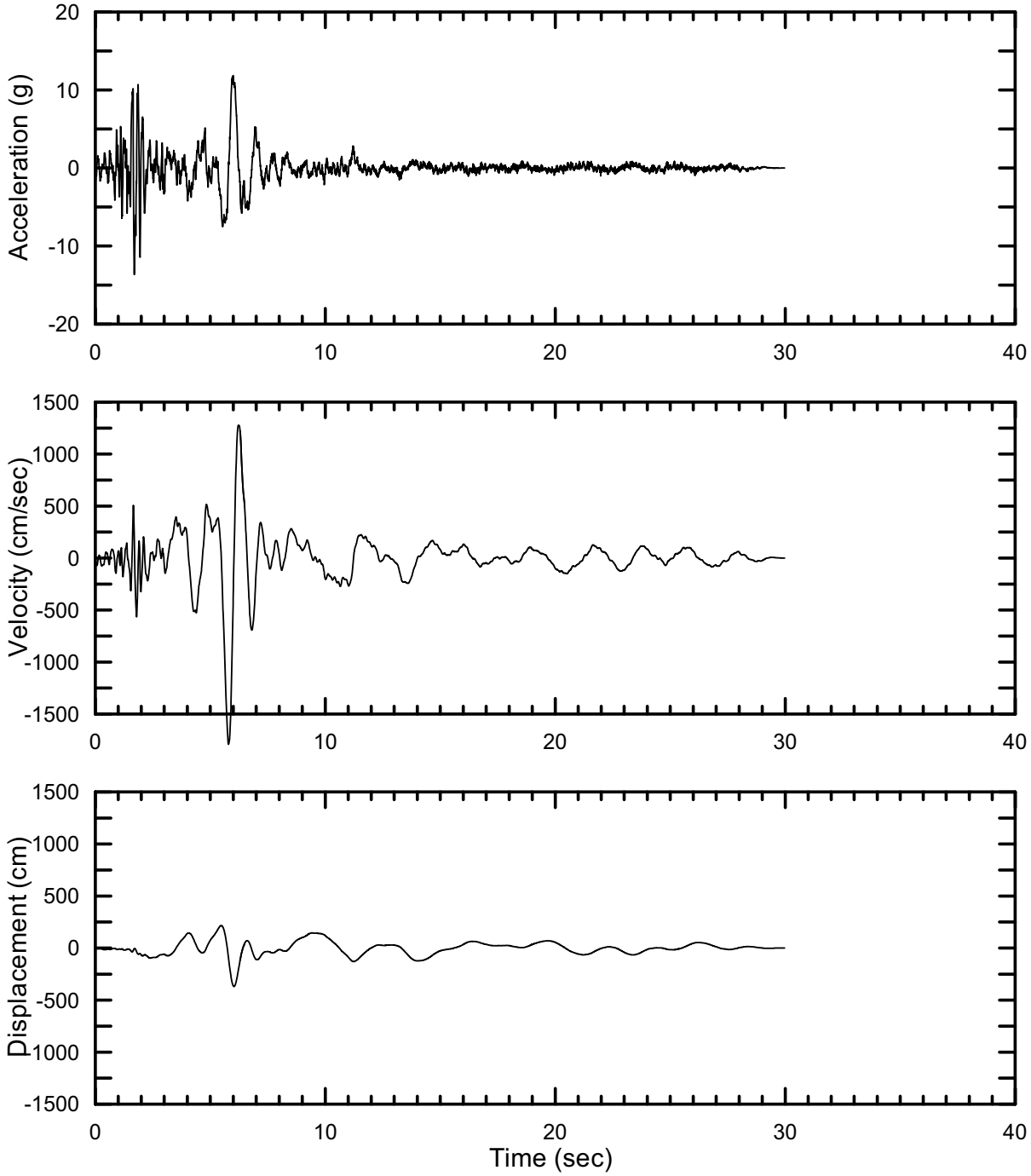

DTN: MO0403AVTMH107.003 [DIRS 168892]

Figure II-170. Point B Horizontal-2 Ti me Histories at an Annual Exceedance Probability of 10^{-7}, Set #9

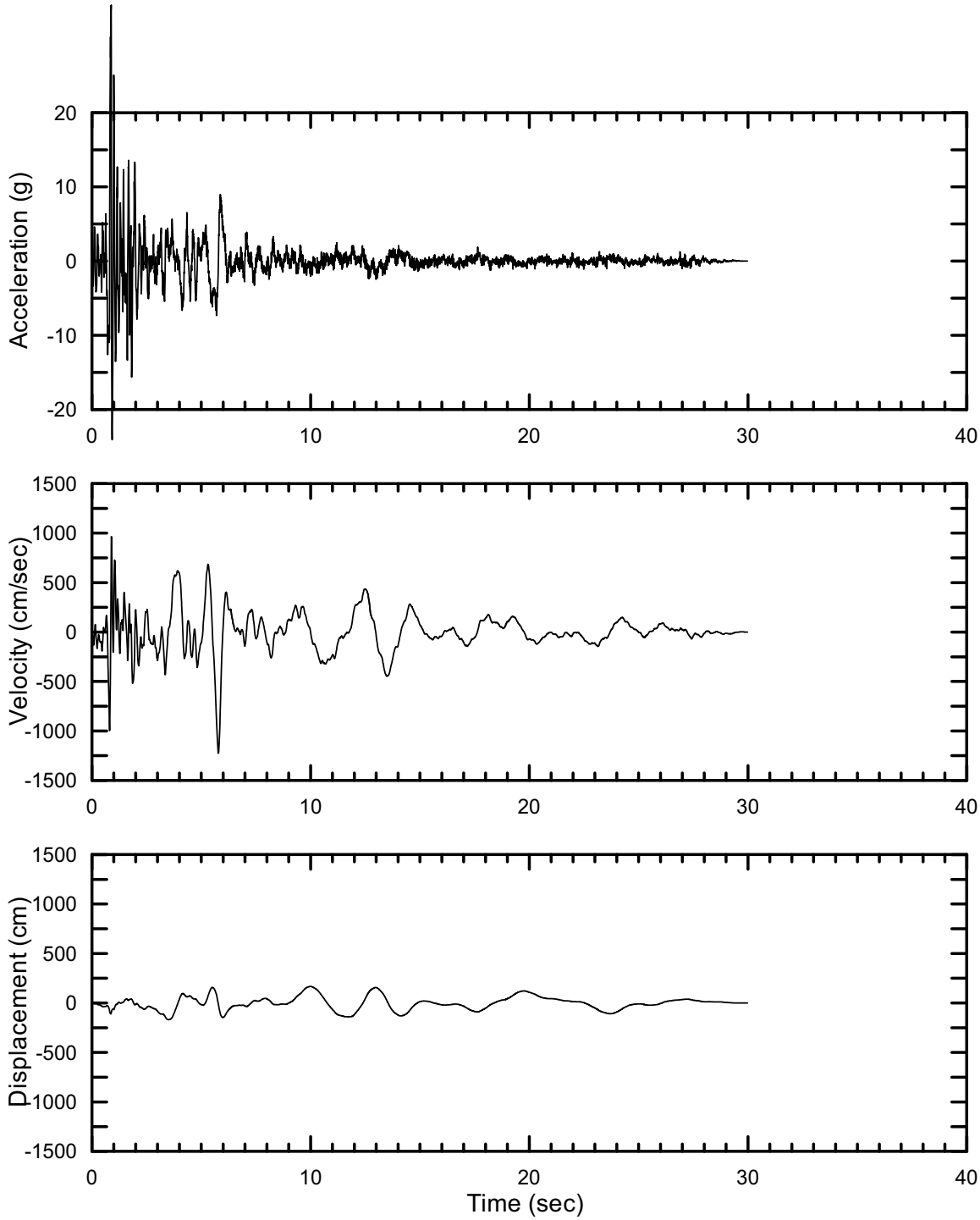

DTN: MO0403AVTMH107.003 [DIRS 168892]

Figure II-171. Point B Vertical Time Histories at an Annual Exceedance Probability of 10^{-7}, Set #9

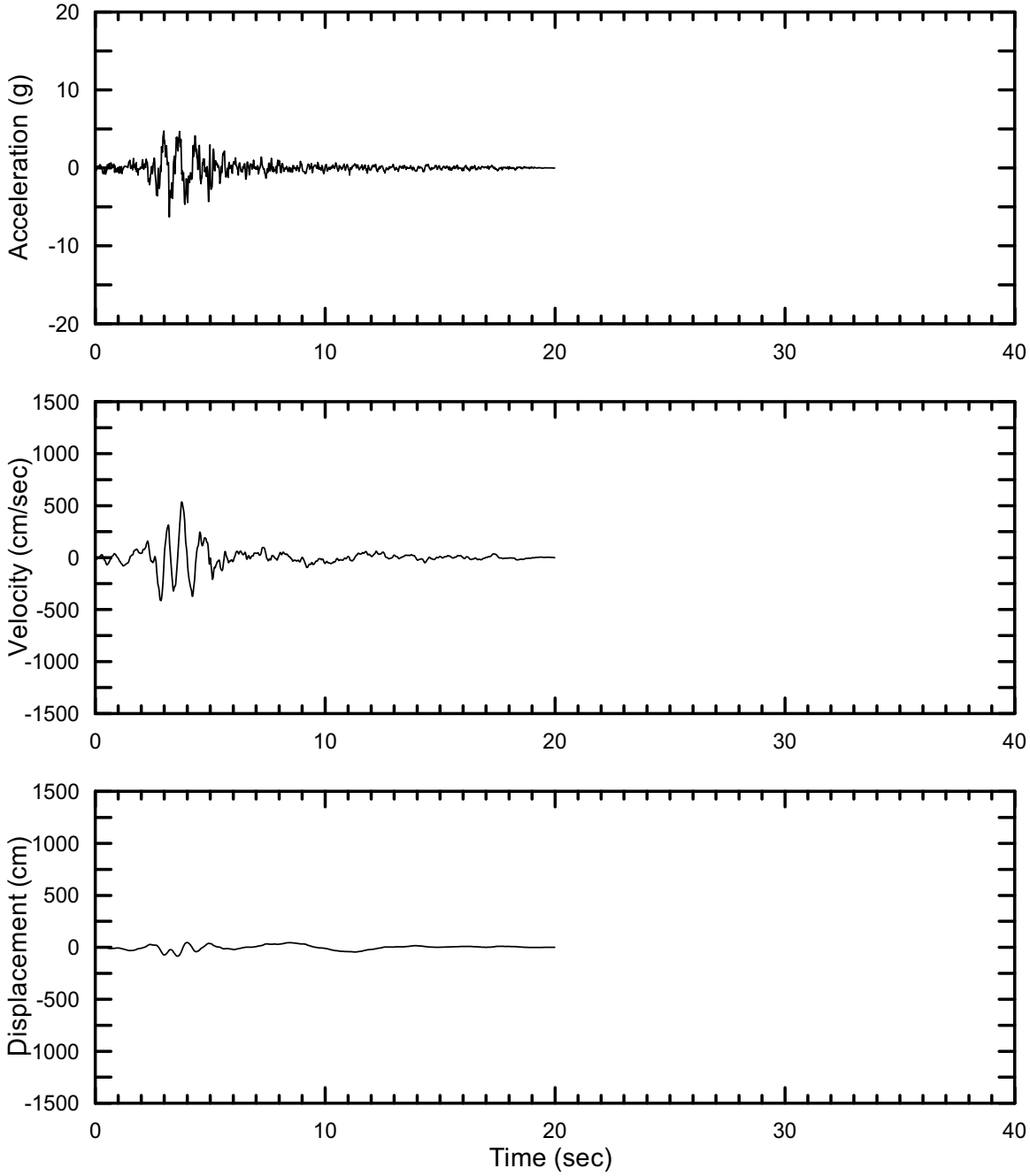

DTN: MO0403AVTMH107.003 [DIRS 168892]

Figure II-172. Point B Horizontal-1 Ti me Histories at an Annual Exceedance Probability of 10^{-7}, Set #10

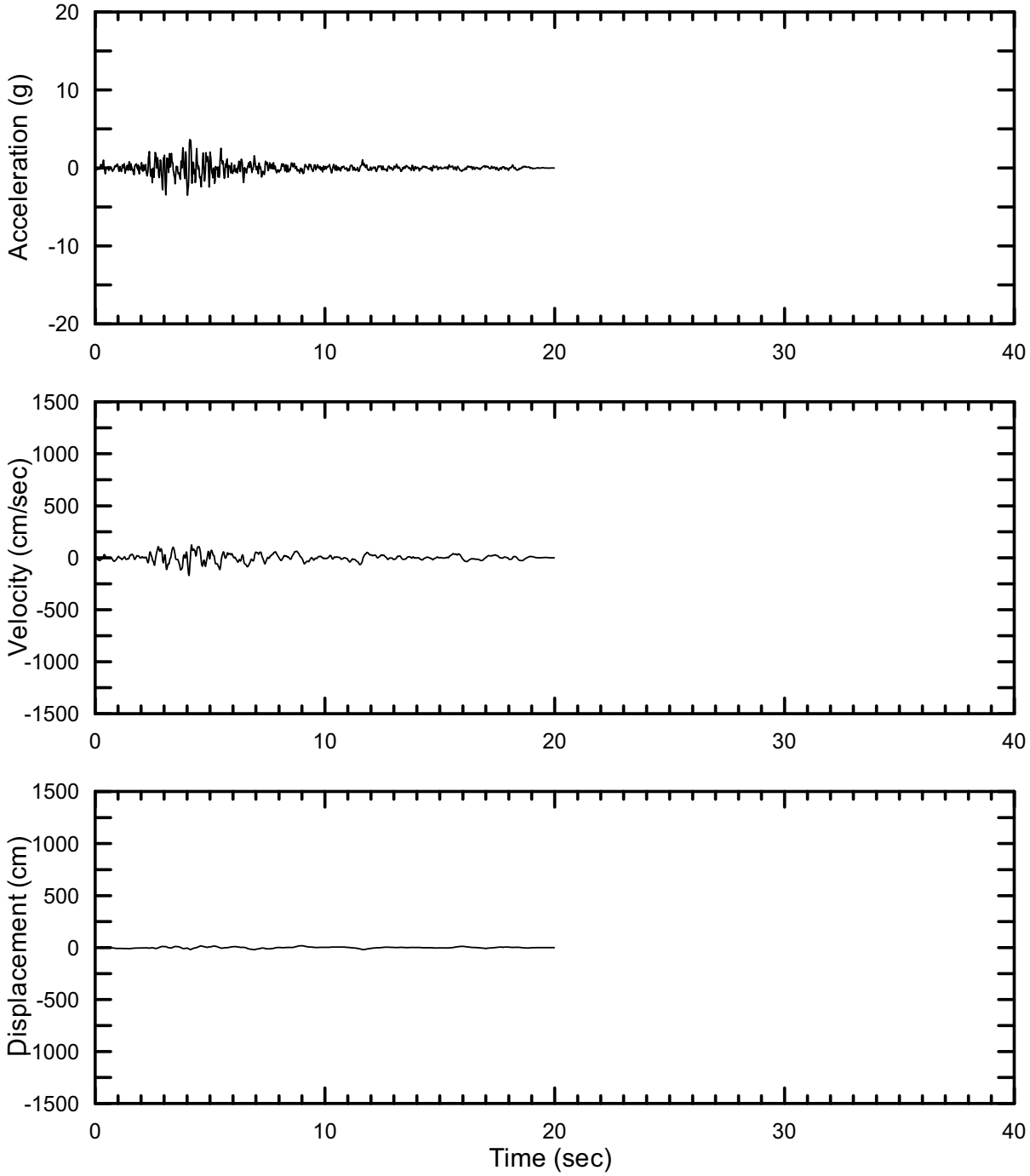

DTN: MO0403AVTMH107.003 [DIRS 168892]

Figure II-173. Point B Horizontal-2 Time Histories at an Annual Exceedance Probability of 10^{-7}, Set #10

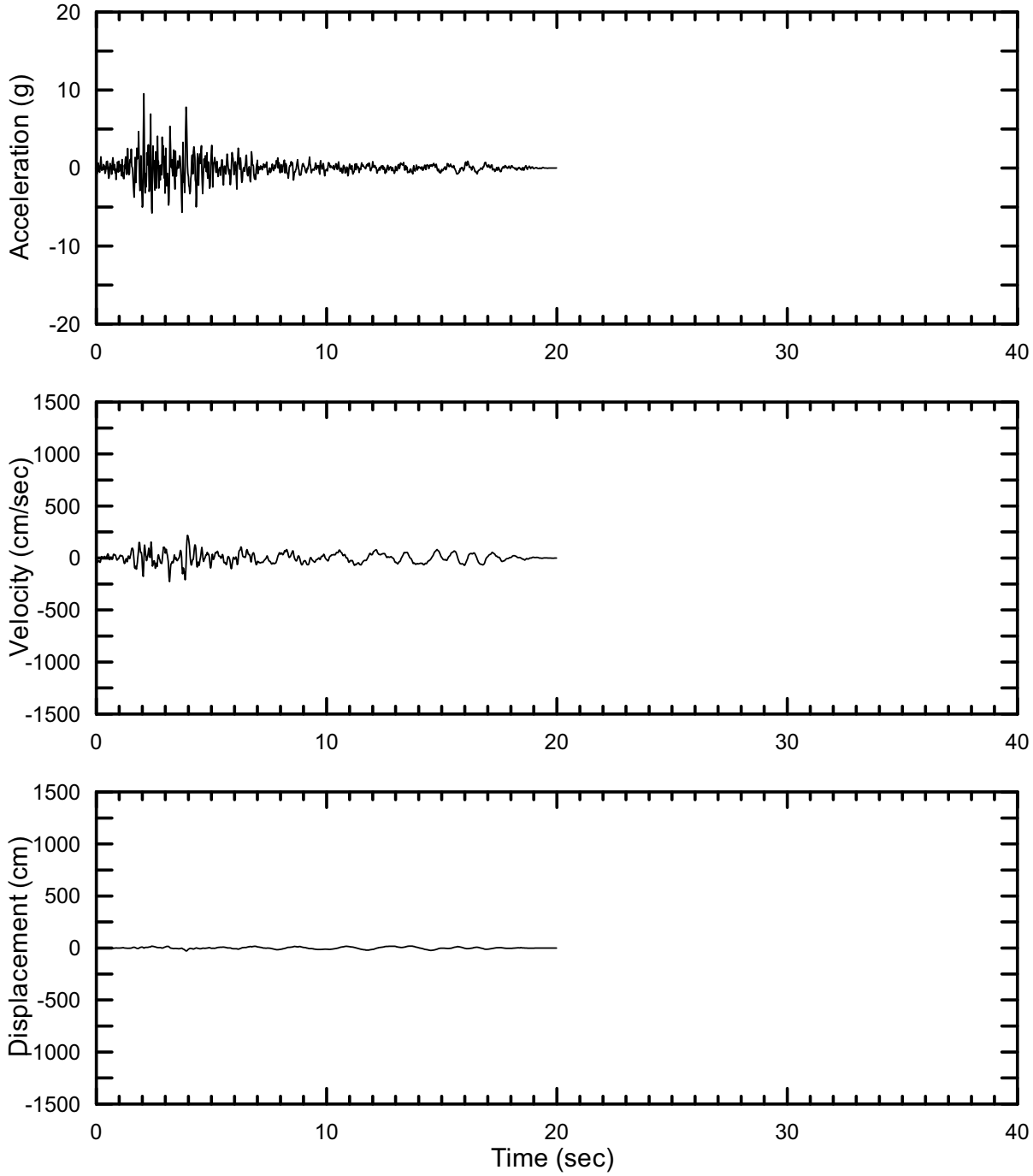

DTN: MO0403AVTMH107.003 [DIRS 168892]

Figure II-174. Point B Vertical Time Histories at an Annual Exceedance Probability of 10^{-7}, Set #10

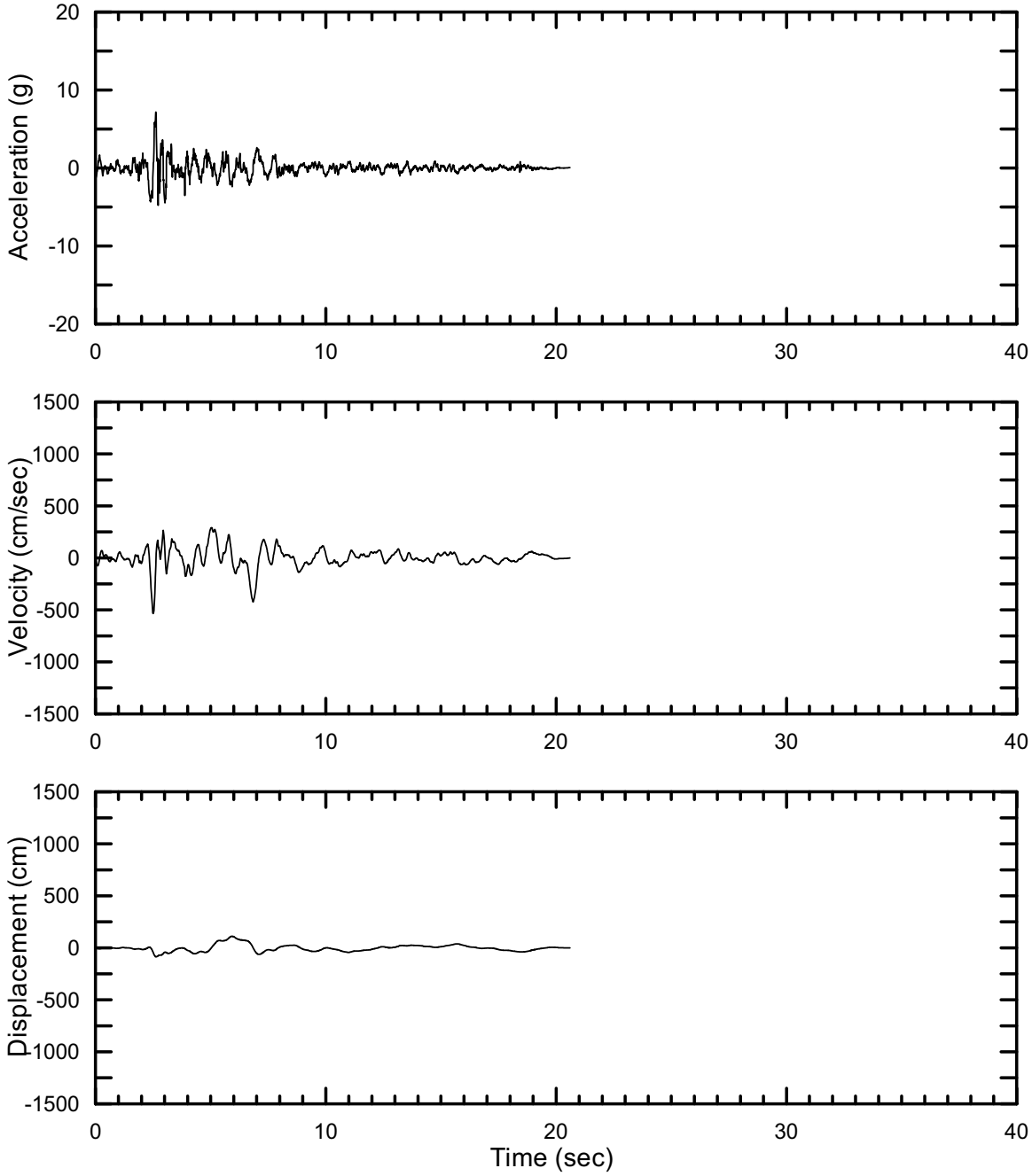

DTN: MO0403AVTMH107.003 [DIRS 168892]

Figure II-175. Point B Horizontal-1 Ti me Histories at an Annual Exceedance Probability of 10^{-7}, Set #11

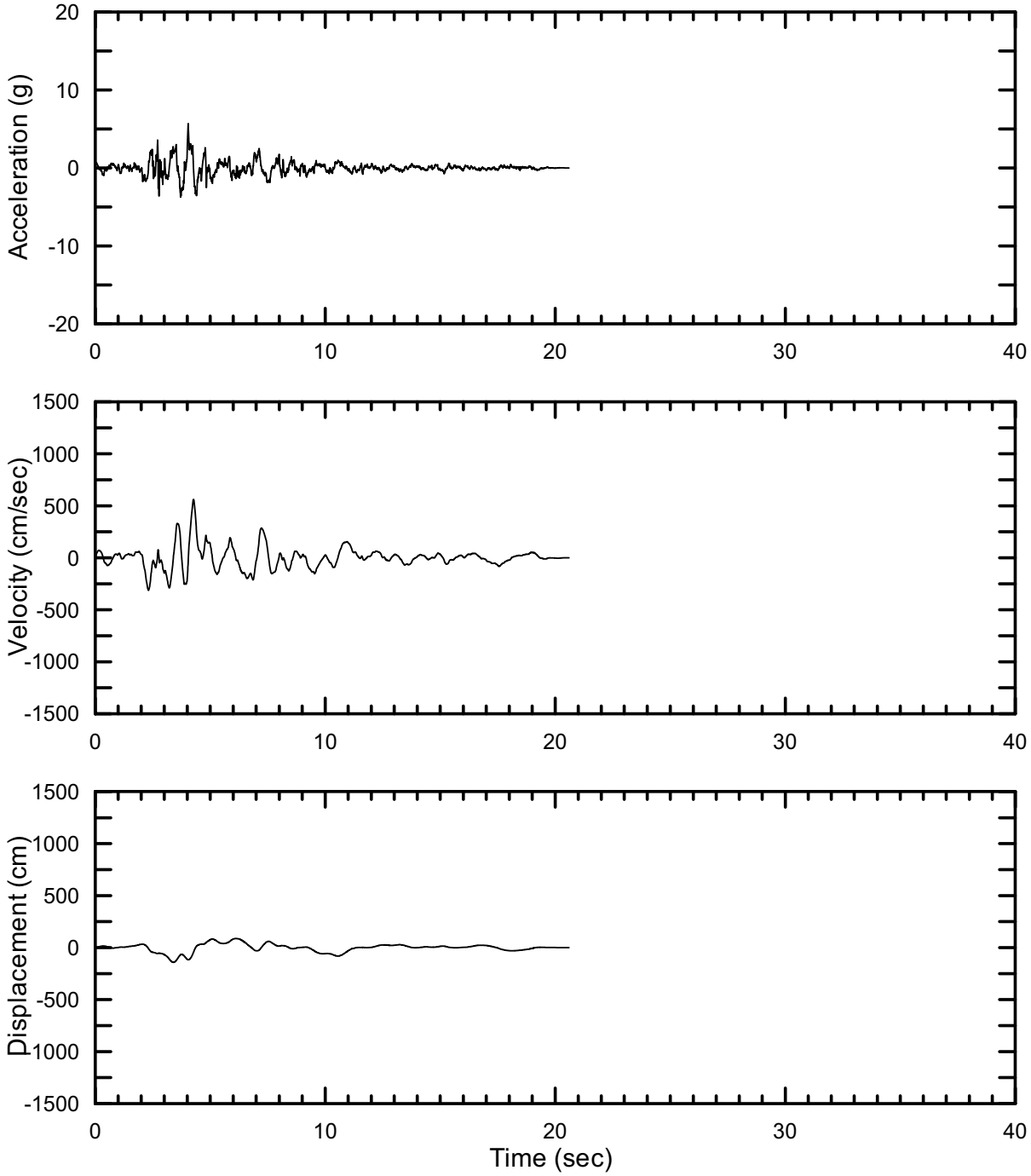

DTN: MO0403AVTMH107.003 [DIRS 168892]

Figure II-176. Point B Horizontal-2 Ti me Histories at an Annual Exceedance Probability of 10^{-7}, Set #11

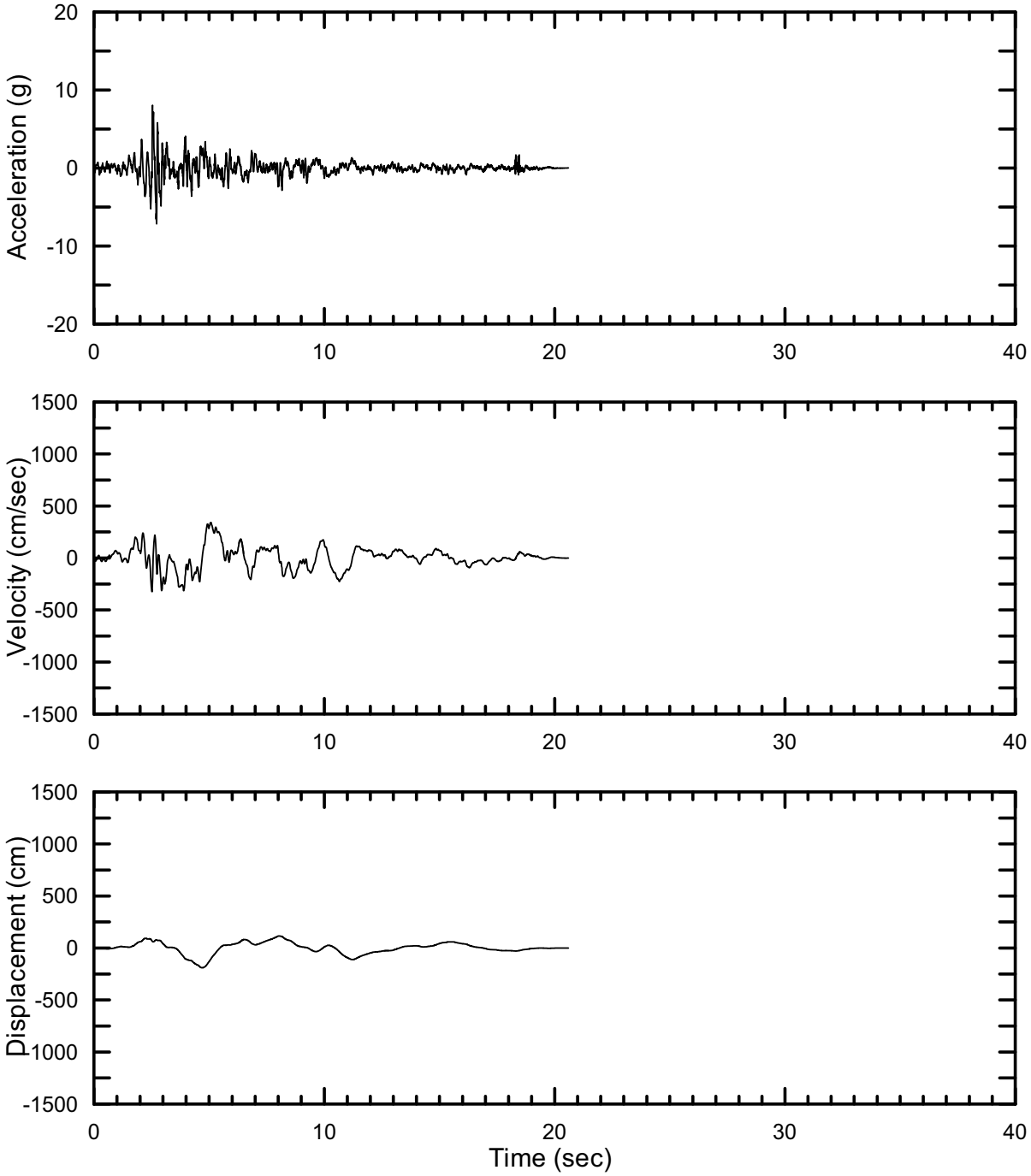

DTN: MO0403AVTMH107.003 [DIRS 168892]

Figure II-177. Point B Vertical Time Histories at an Annual Exceedance Probability of 10^{-7}, Set #11

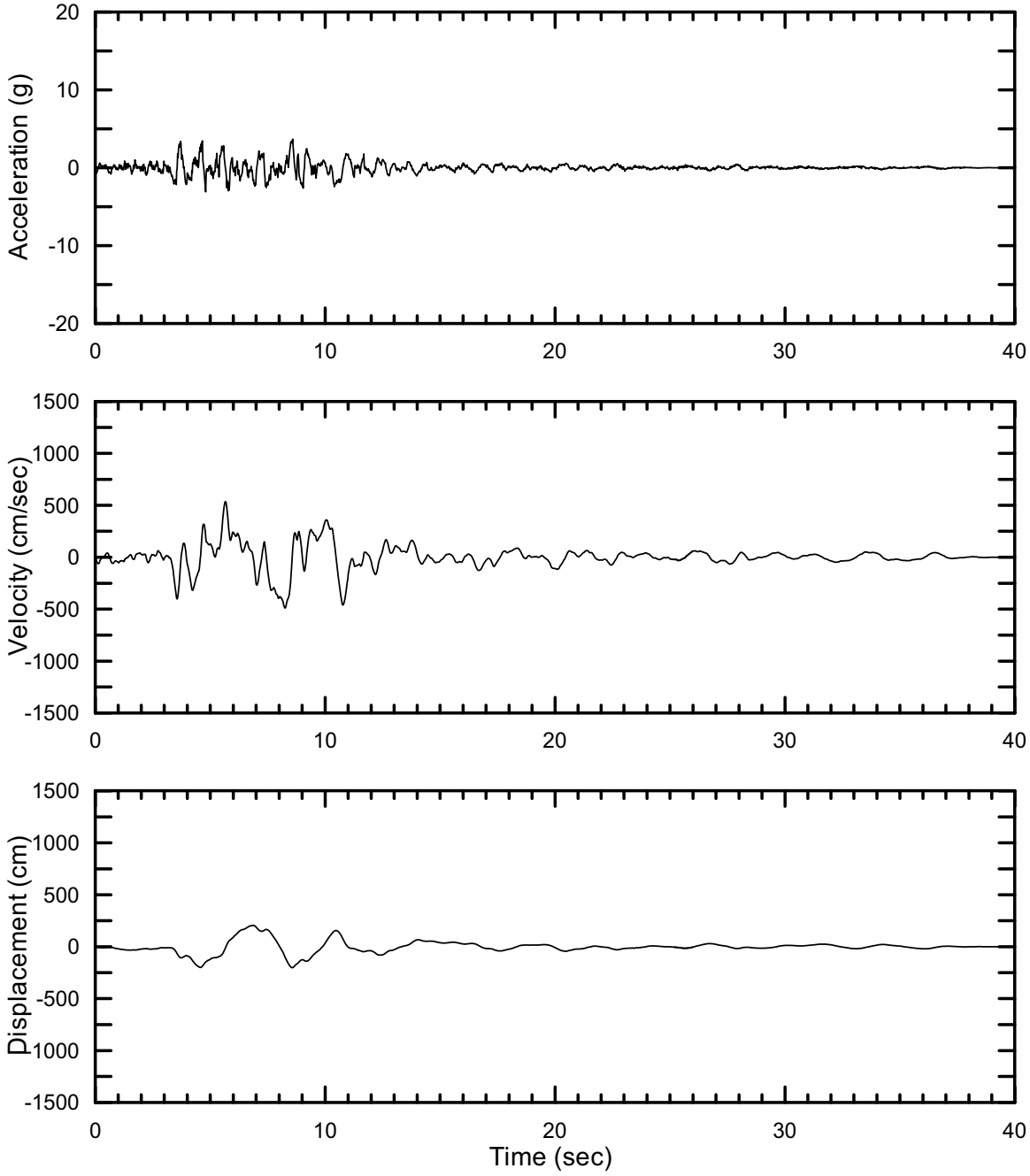

DTN: MO0403AVTMH107.003 [DIRS 168892]

Figure II-178. Point B Horizontal-1 Ti me Histories at an Annual Exceedance Probability of 10^{-7}, Set #12

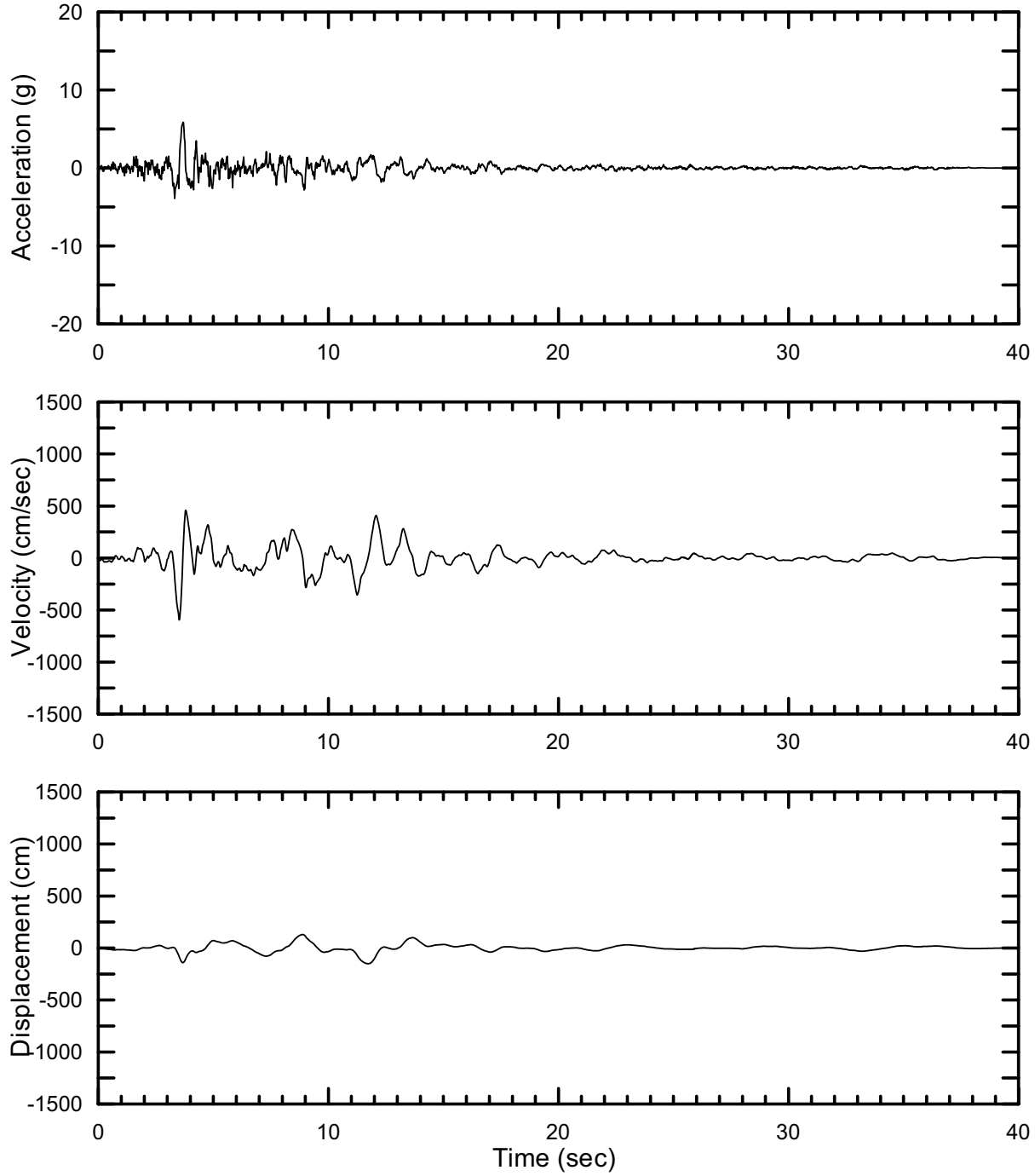

DTN: MO0403AVTMH107.003 [DIRS 168892]

Figure II-179. Point B Horizontal-2 Ti me Histories at an Annual Exceedance Probability of 10^{-7}, Set #12

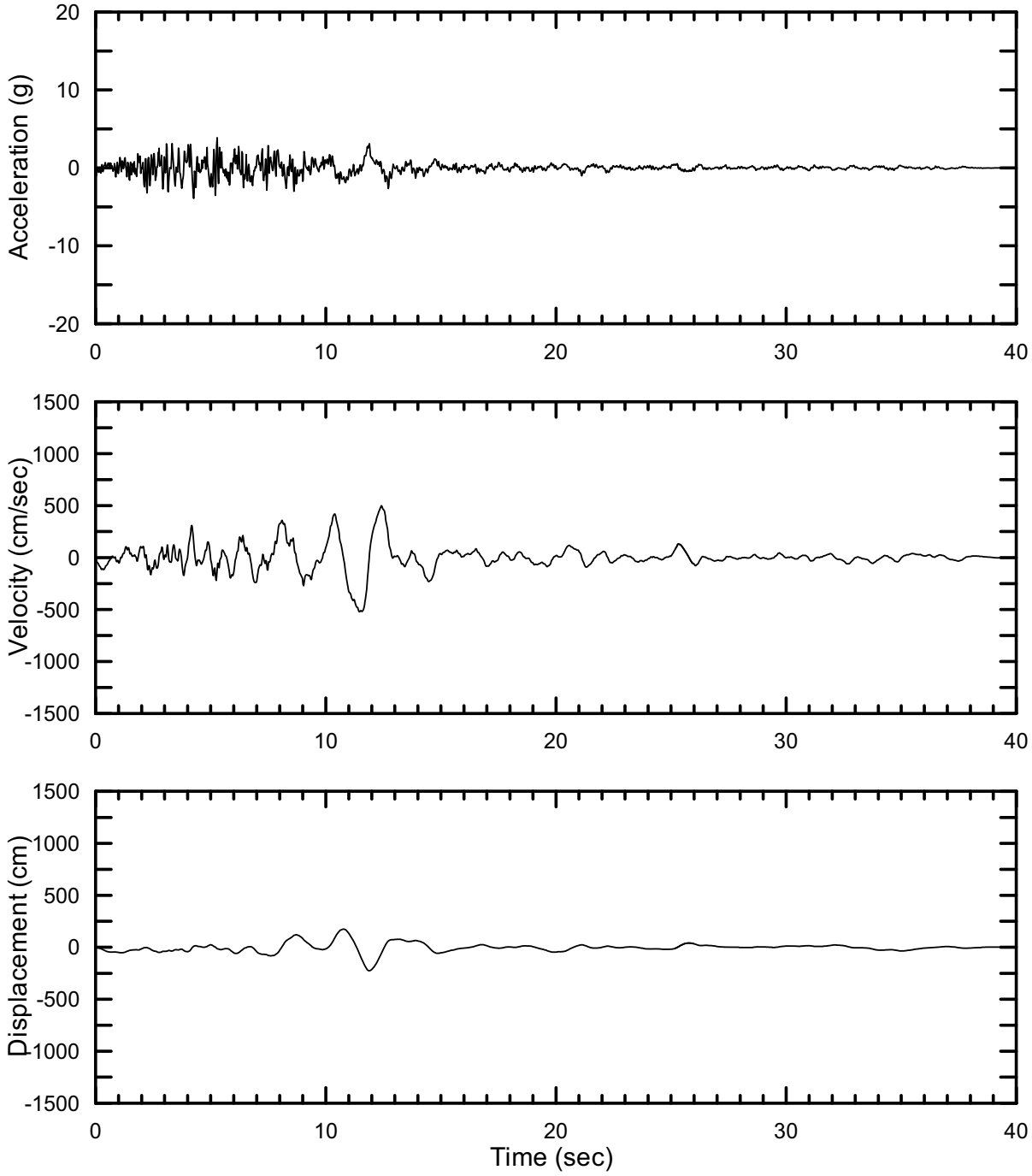

DTN: MO0403AVTMH107.003 [DIRS 168892]

Figure II-180. Point B Vertical Time Histories at an Annual Exceedance Probability of 10^{-7}, Set #12

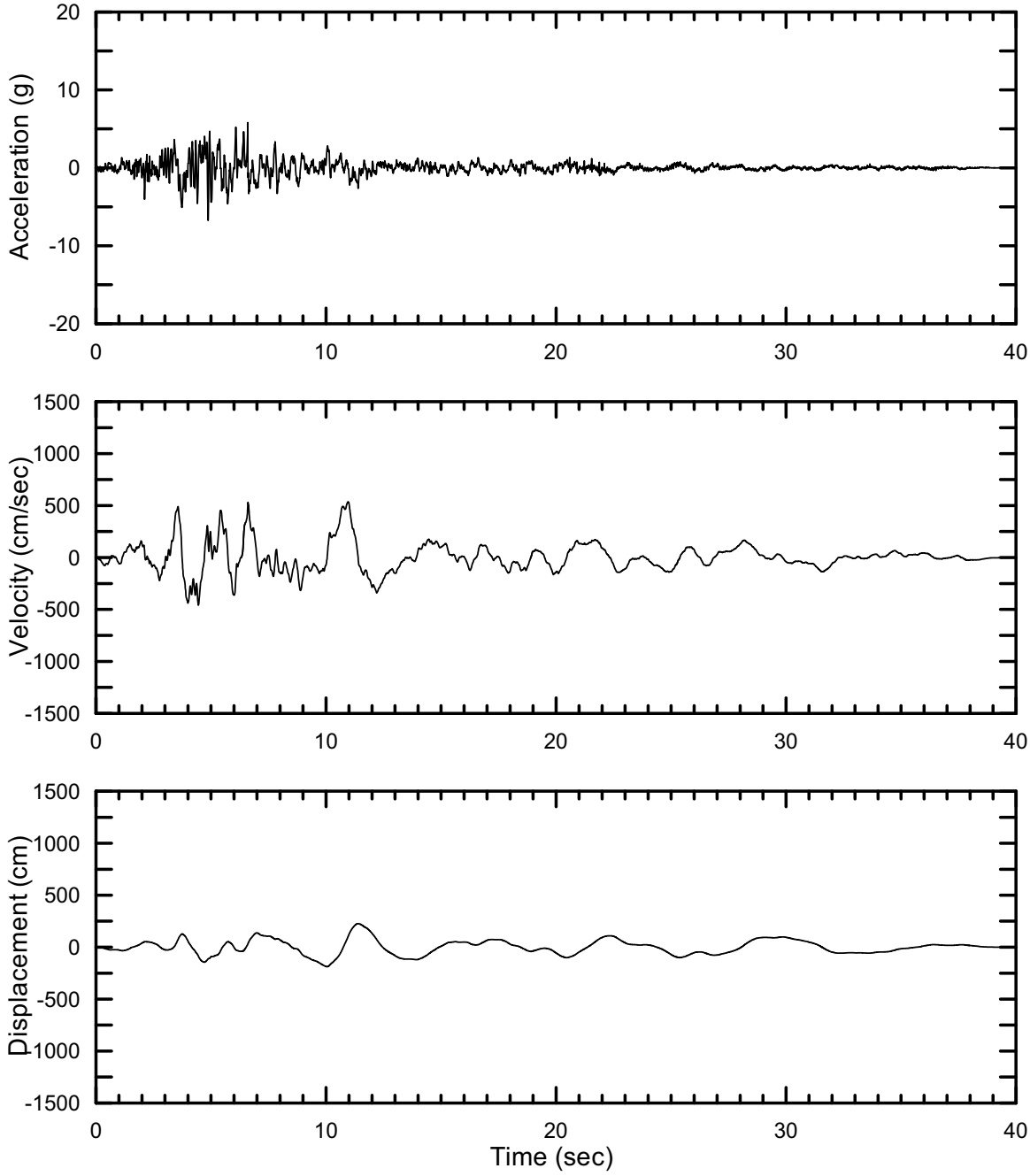

DTN: MO0403AVTMH107.003 [DIRS 168892]

Figure II-181. Point B Horizontal-1 Ti me Histories at an Annual Exceedance Probability of 10^{-7}, Set #13

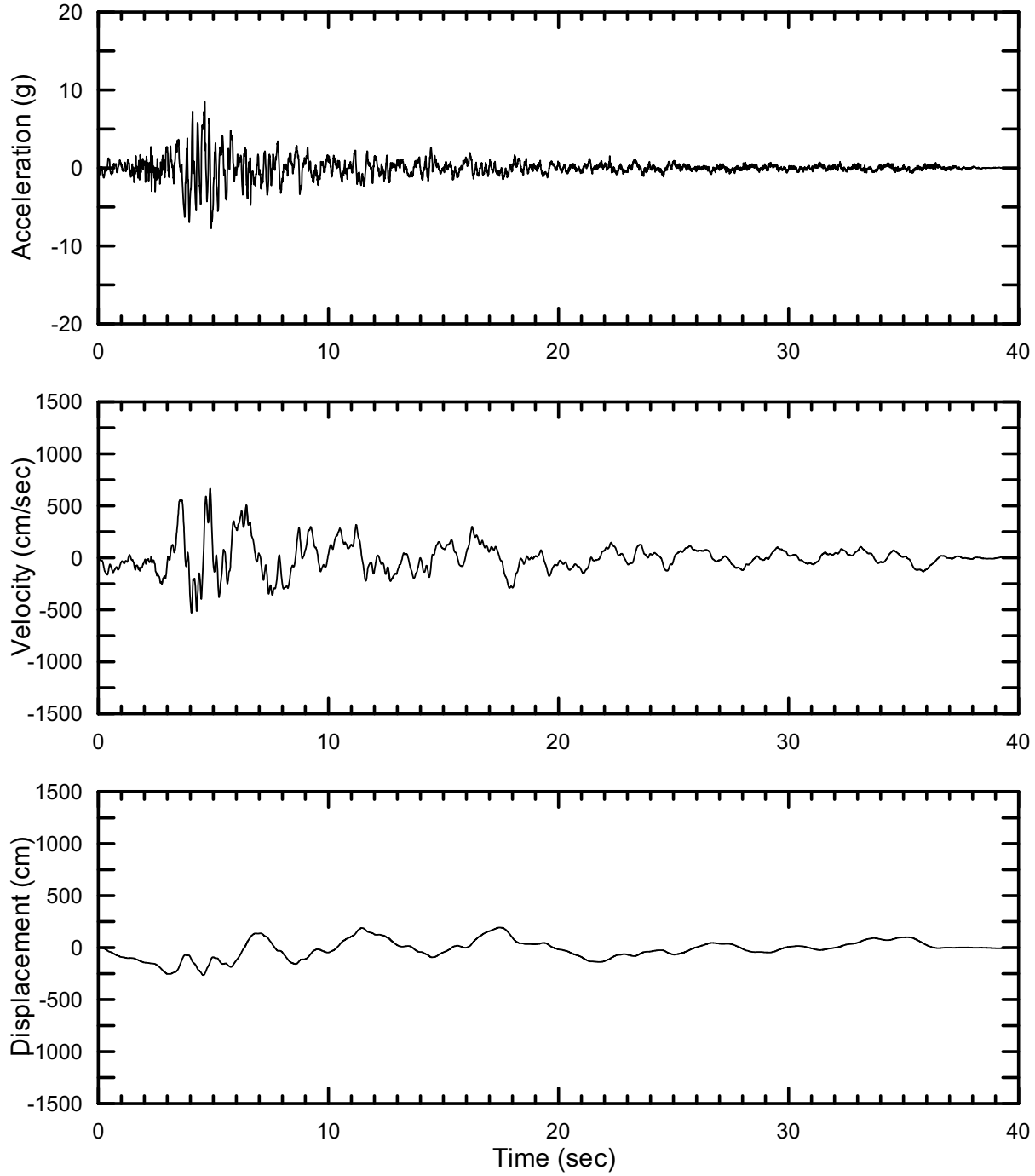

DTN: MO0403AVTMH107.003 [DIRS 168892]

Figure II-182. Point B Horizontal-2 Ti me Histories at an Annual Exceedance Probability of 10^{-7}, Set #13

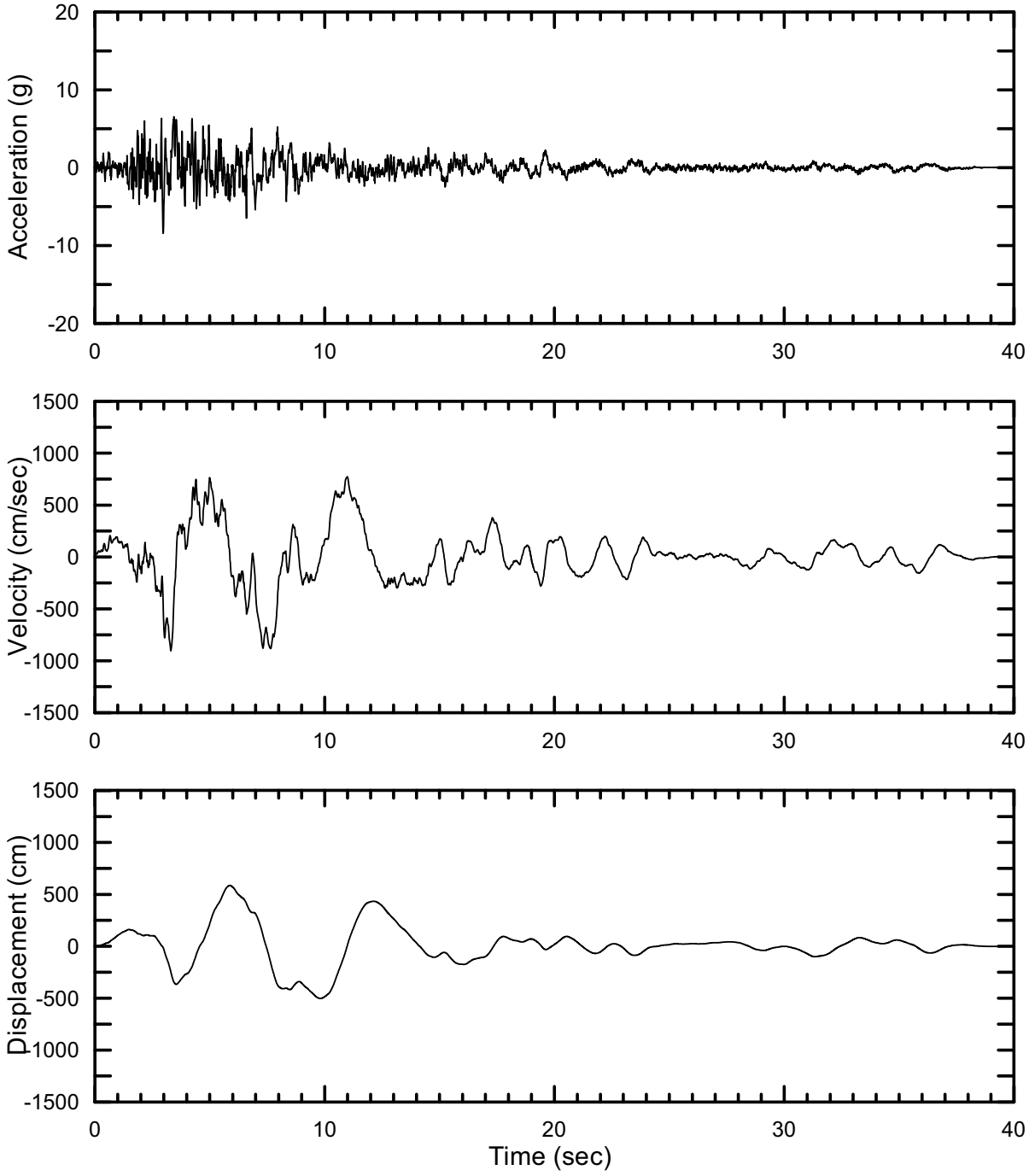

DTN: MO0403AVTMH107.003 [DIRS 168892]

Figure II-183. Point B Vertical Time Histories at an Annual Exceedance Probability of 10^{-7}, Set #13

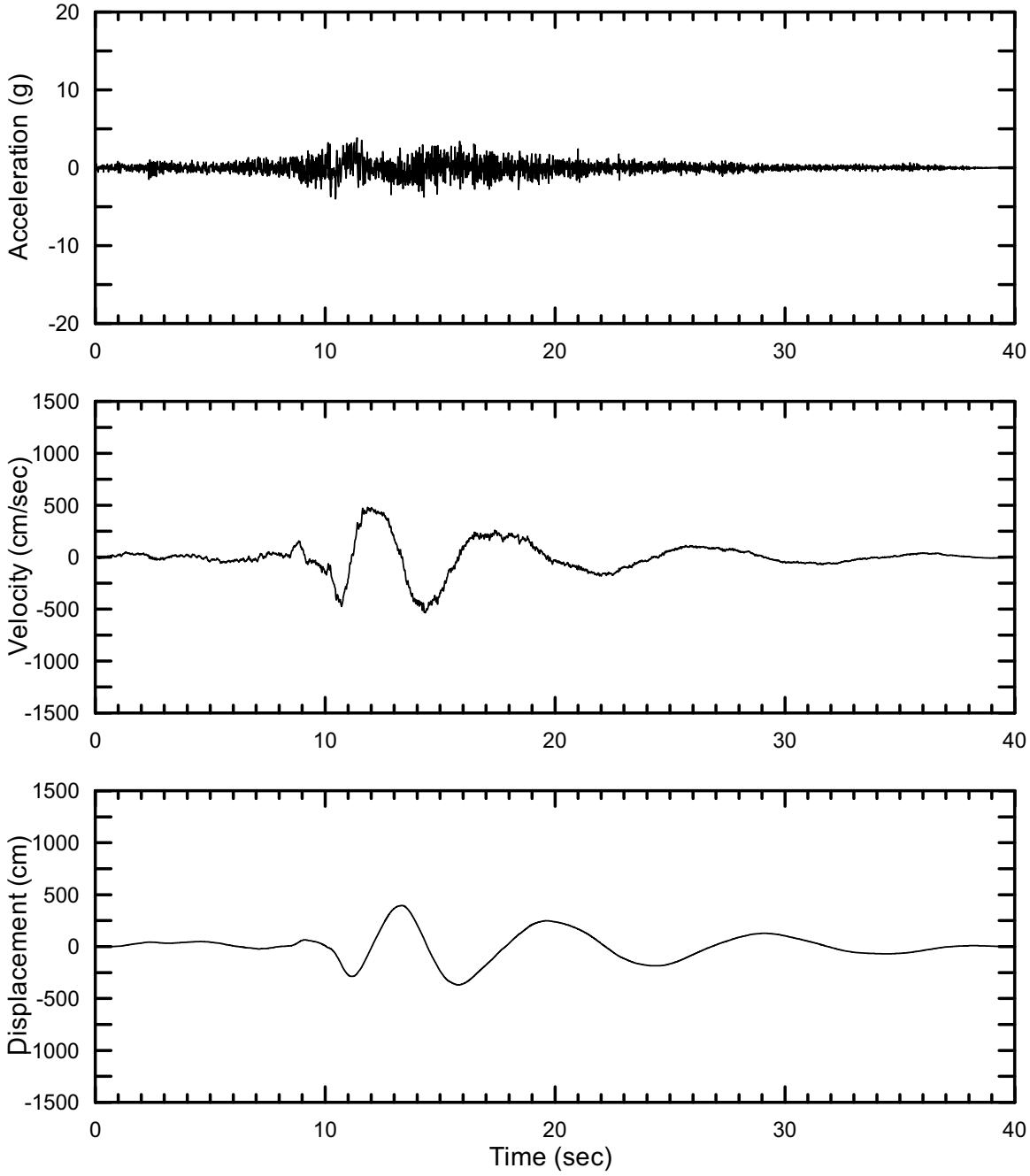

DTN: MO0403AVTMH107.003 [DIRS 168892]

Figure II-184. Point B Horizontal-1 Ti me Histories at an Annual Exceedance Probability of 10^{-7}, Set #14

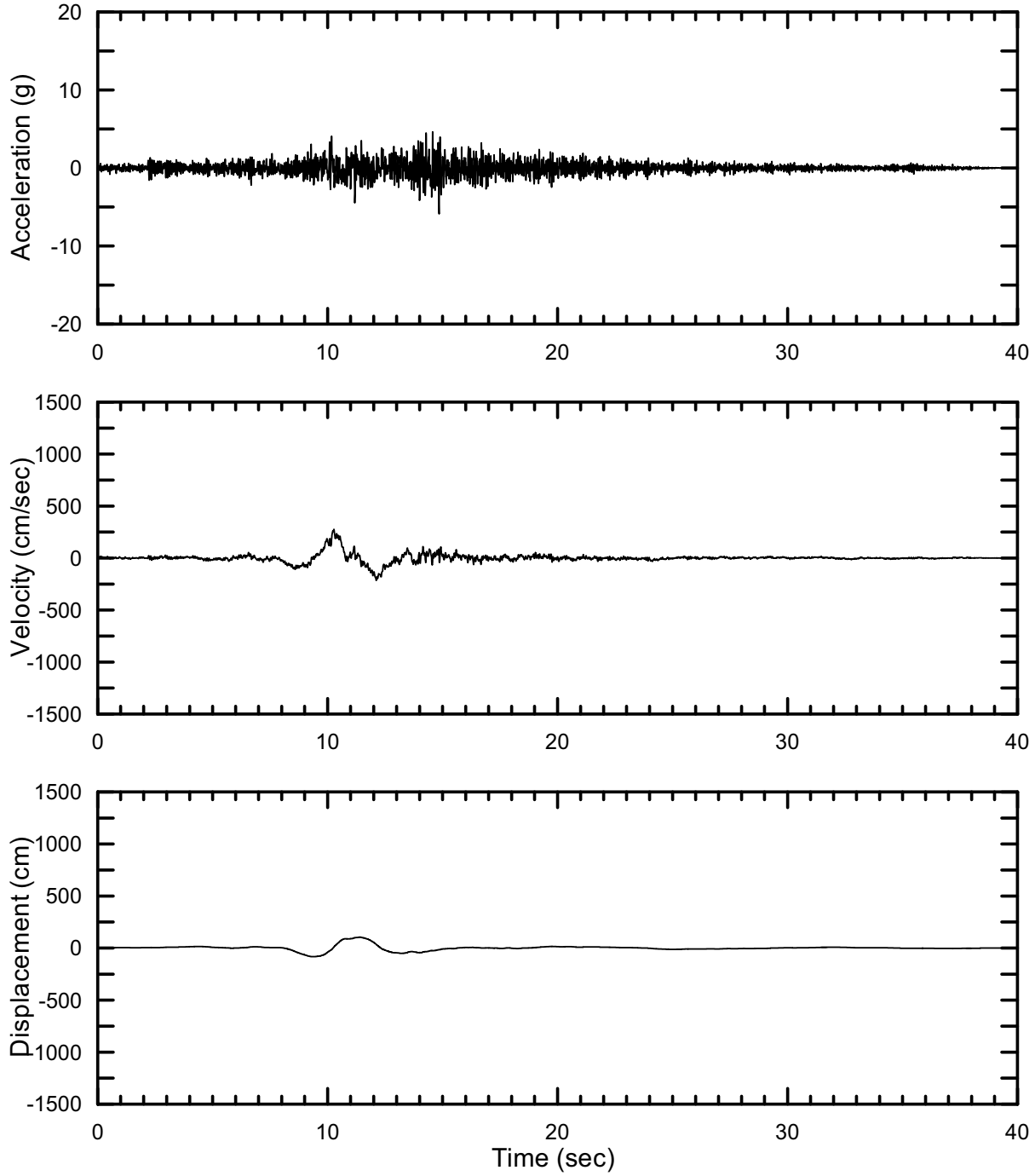

DTN: MO0403AVTMH107.003 [DIRS 168892]

Figure II-185. Point B Horizontal-2 Ti me Histories at an Annual Exceedance Probability of 10^{-7}, Set #14

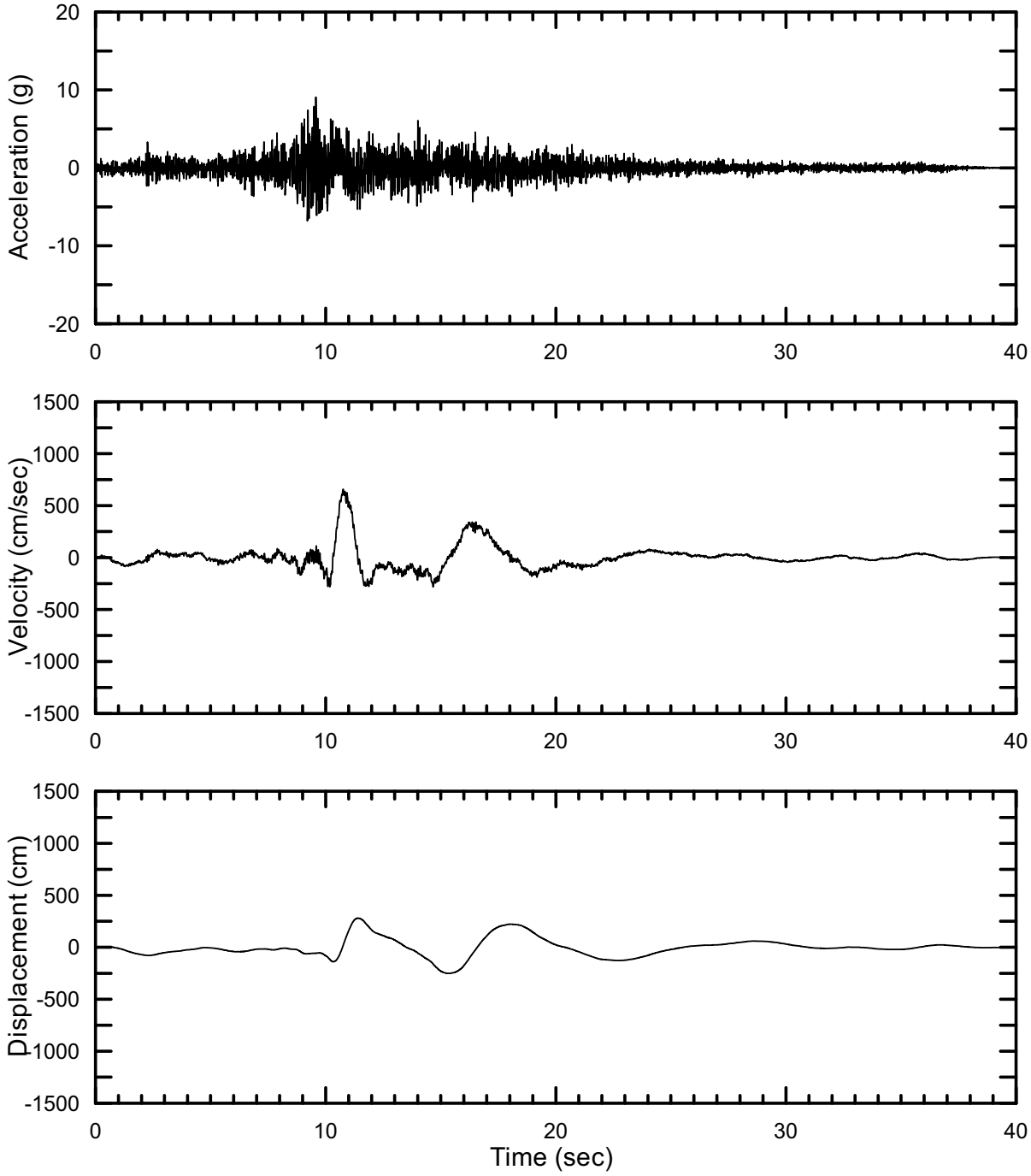

DTN: MO0403AVTMH107.003 [DIRS 168892]

Figure II-186. Point B Vertical Time Histories at an Annual Exceedance Probability of 10^{-7}, Set #14

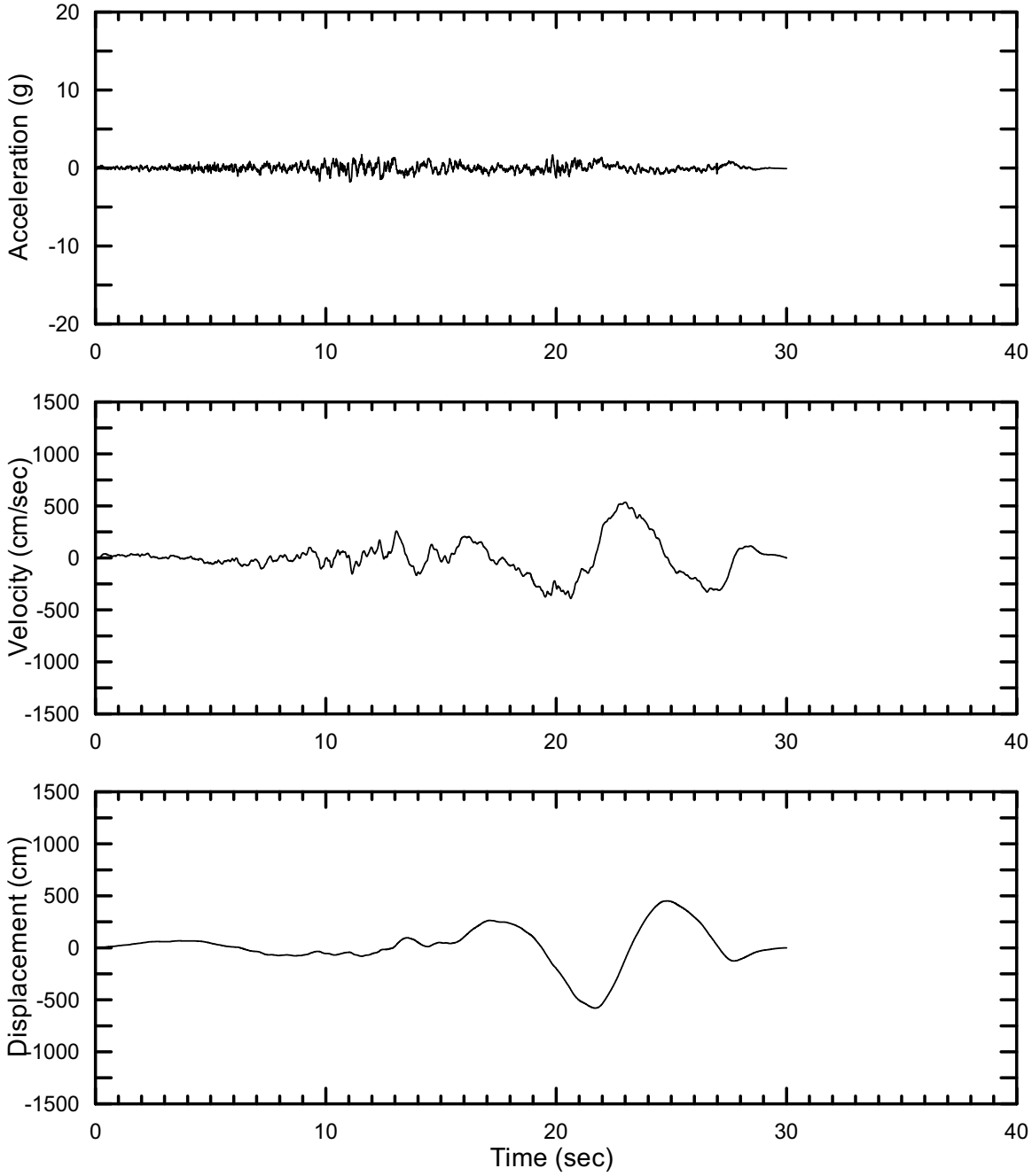

DTN: MO0403AVTMH107.003 [DIRS 168892]

Figure II-187. Point B Horizontal-1 Ti me Histories at an Annual Exceedance Probability of 10^{-7}, Set #15

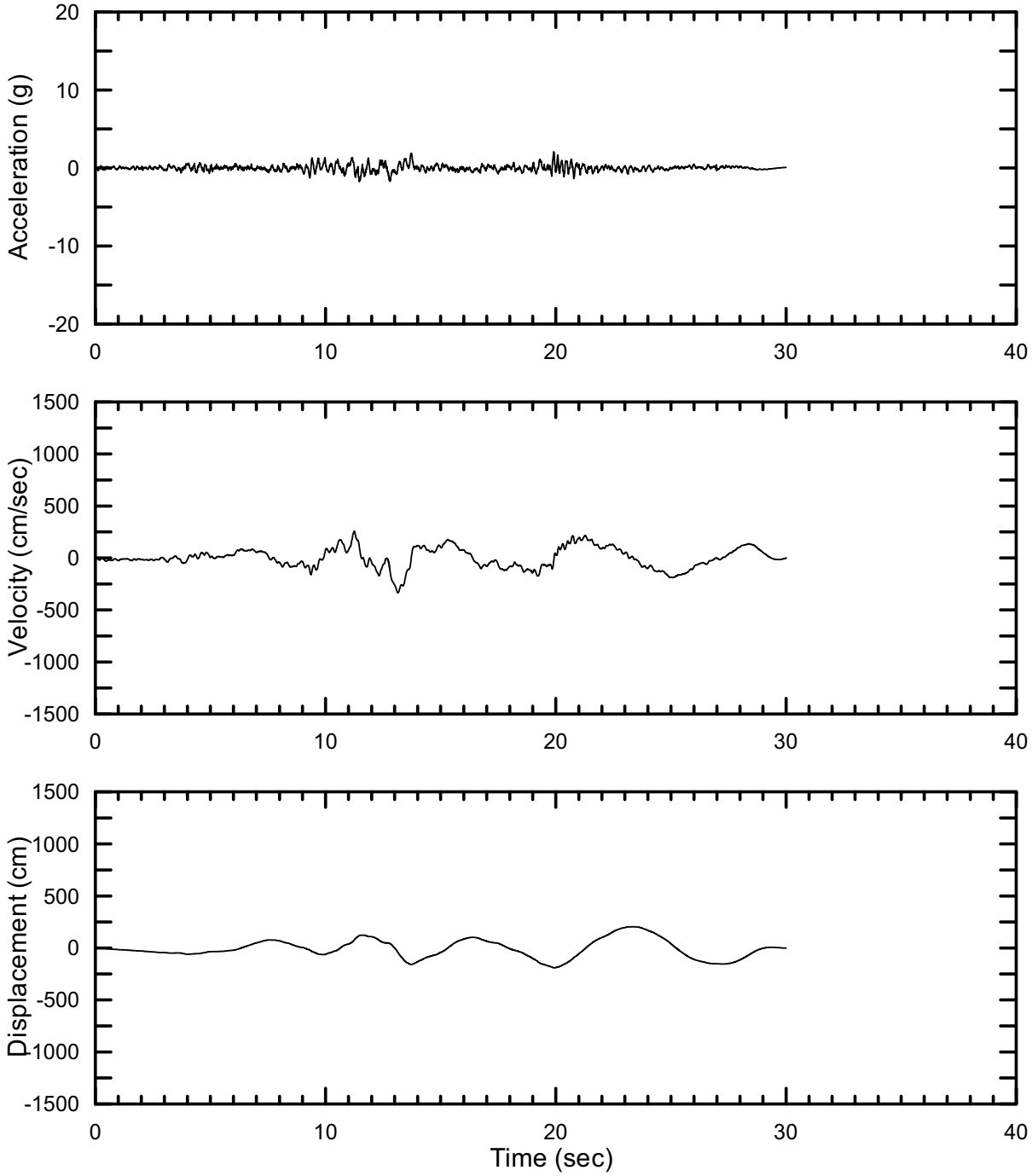

DTN: MO0403AVTMH107.003 [DIRS 168892]

Figure II-188. Point B Horizontal-2 Ti me Histories at an Annual Exceedance Probability of 10^{-7}, Set #15

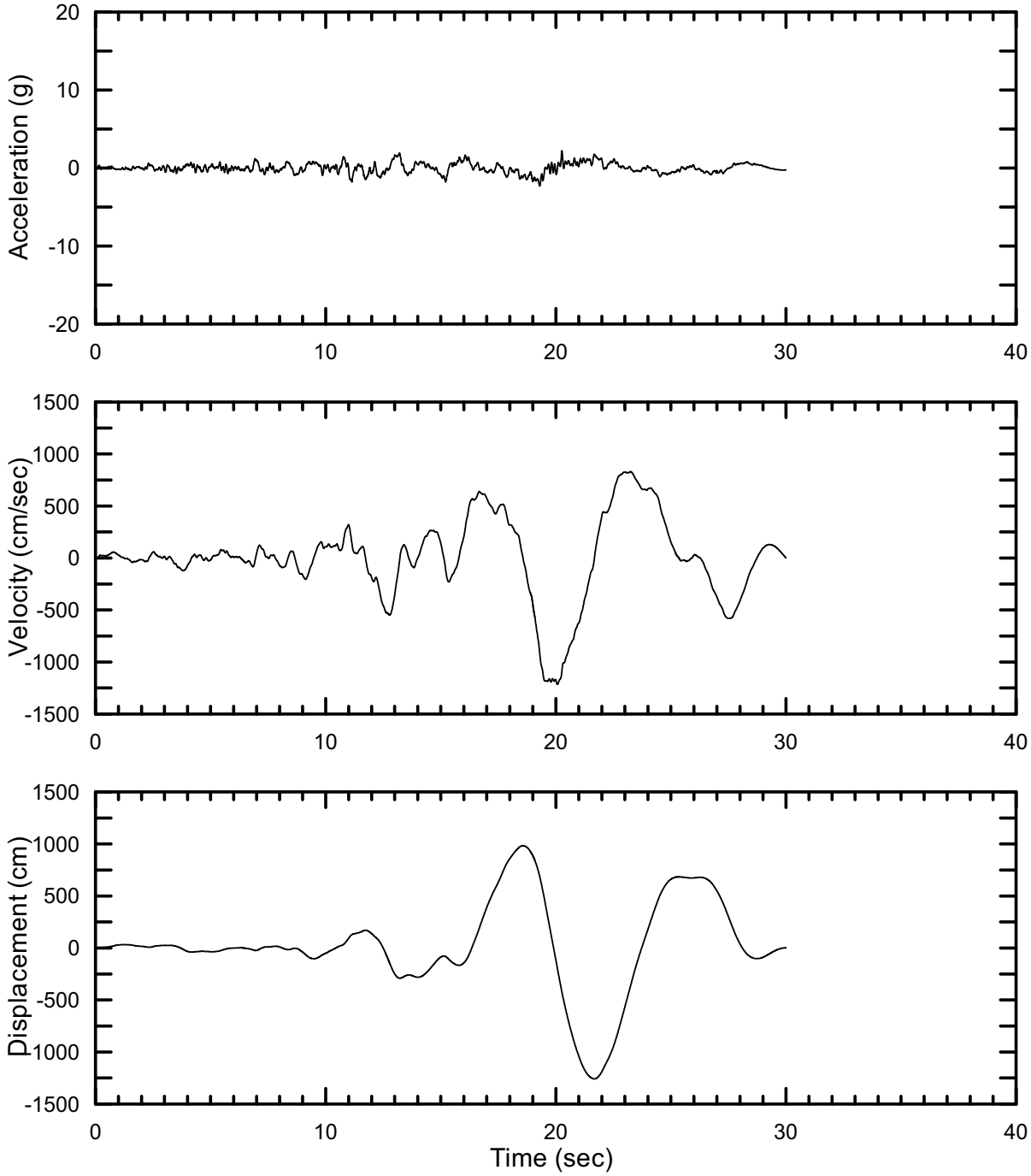

DTN: MO0403AVTMH107.003 [DIRS 168892]

Figure II-189. Point B Vertical Time Histories at an Annual Exceedance Probability of 10^{-7}, Set #15

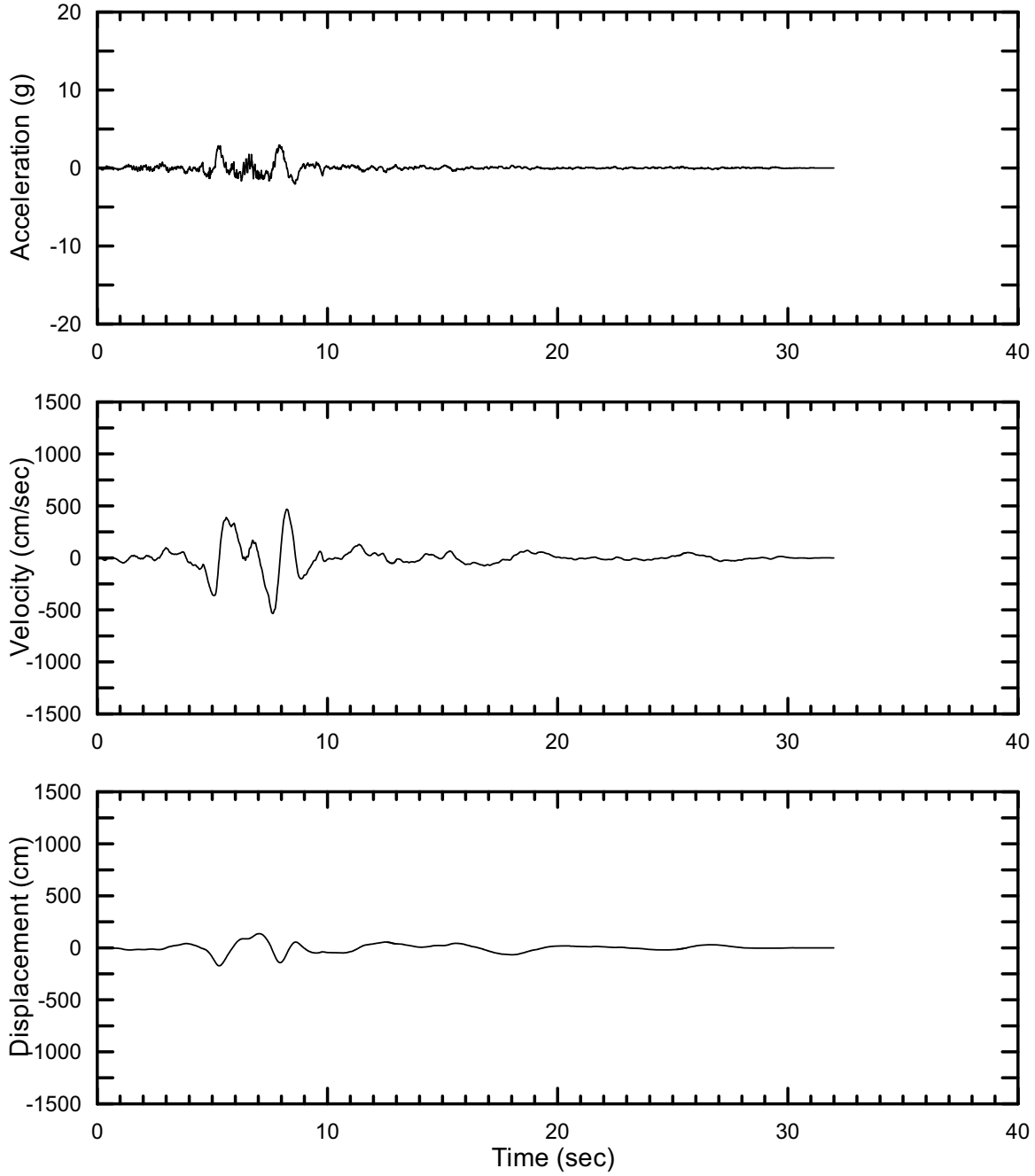

DTN: MO0403AVTMH107.003 [DIRS 168892]

Figure II-190. Point B Horizontal-1 Ti me Histories at an Annual Exceedance Probability of 10^{-7}, Set #16

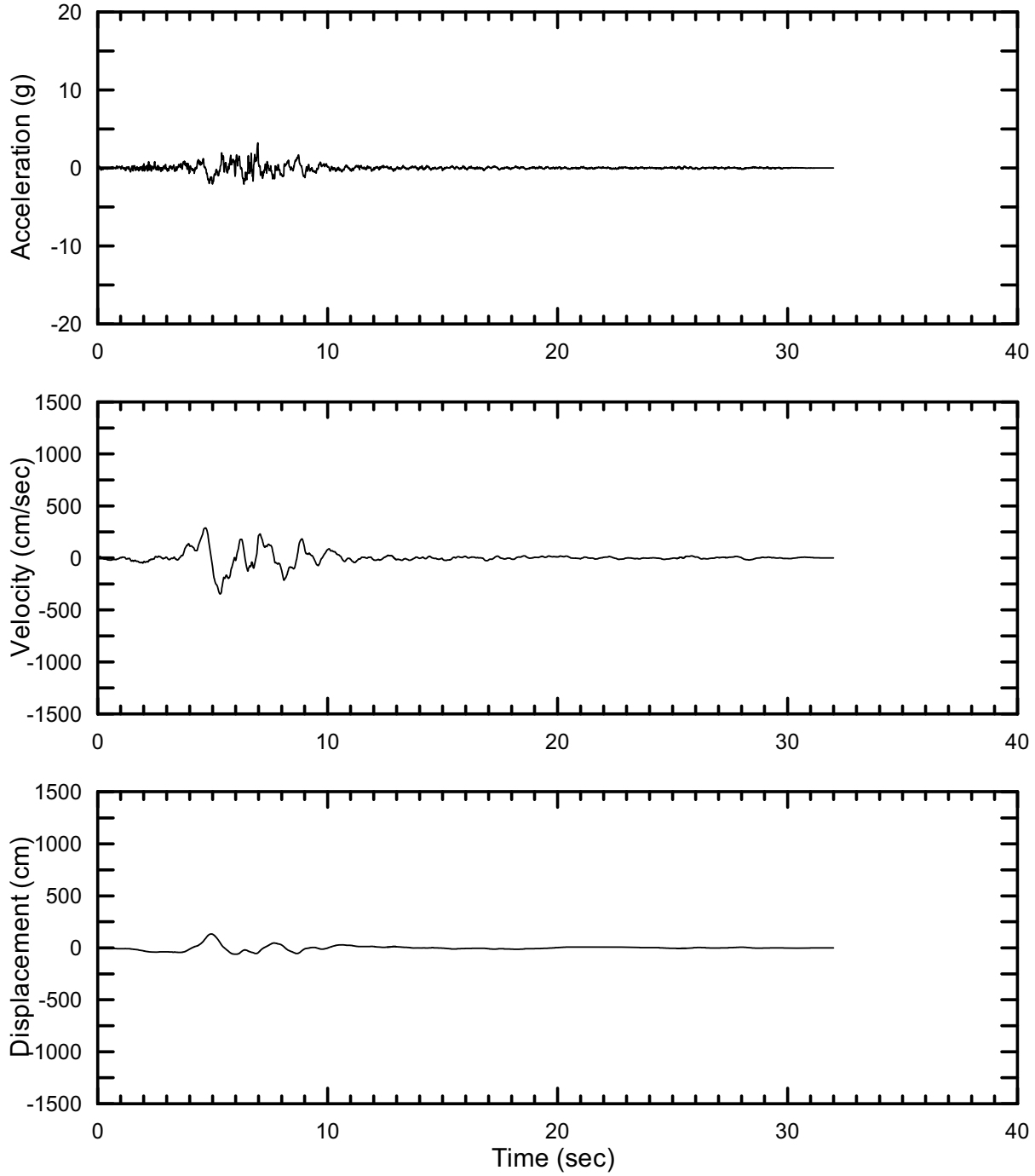

DTN: MO0403AVTMH107.003 [DIRS 168892]

Figure II-191. Point B Horizontal-2 Ti me Histories at an Annual Exceedance Probability of 10^{-7}, Set #16

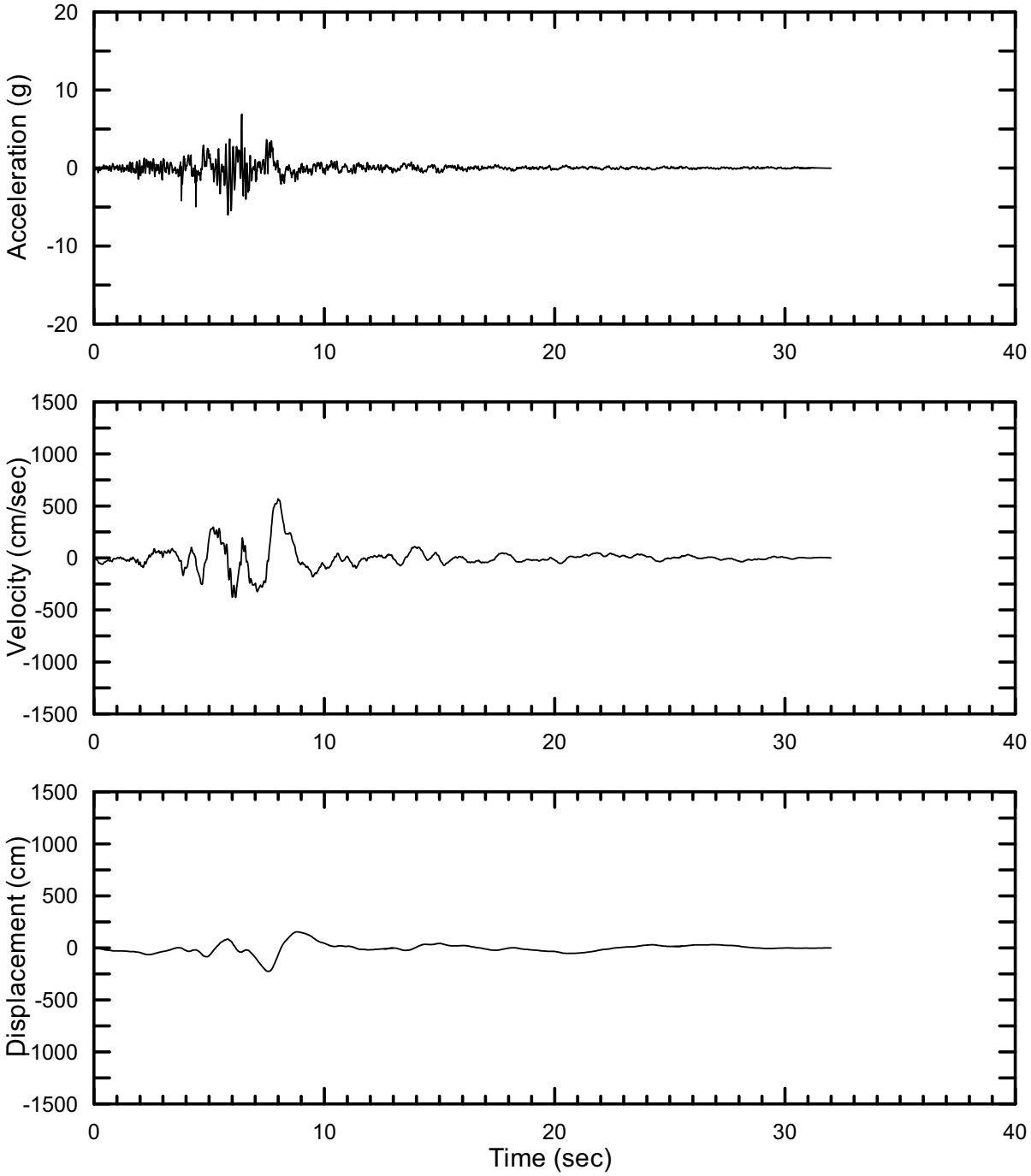

DTN: MO0403AVTMH107.003 [DIRS 168892]

Figure II-192. Point B Vertical Time Histories at an Annual Exceedance Probability of 10^{-7}, Set #16

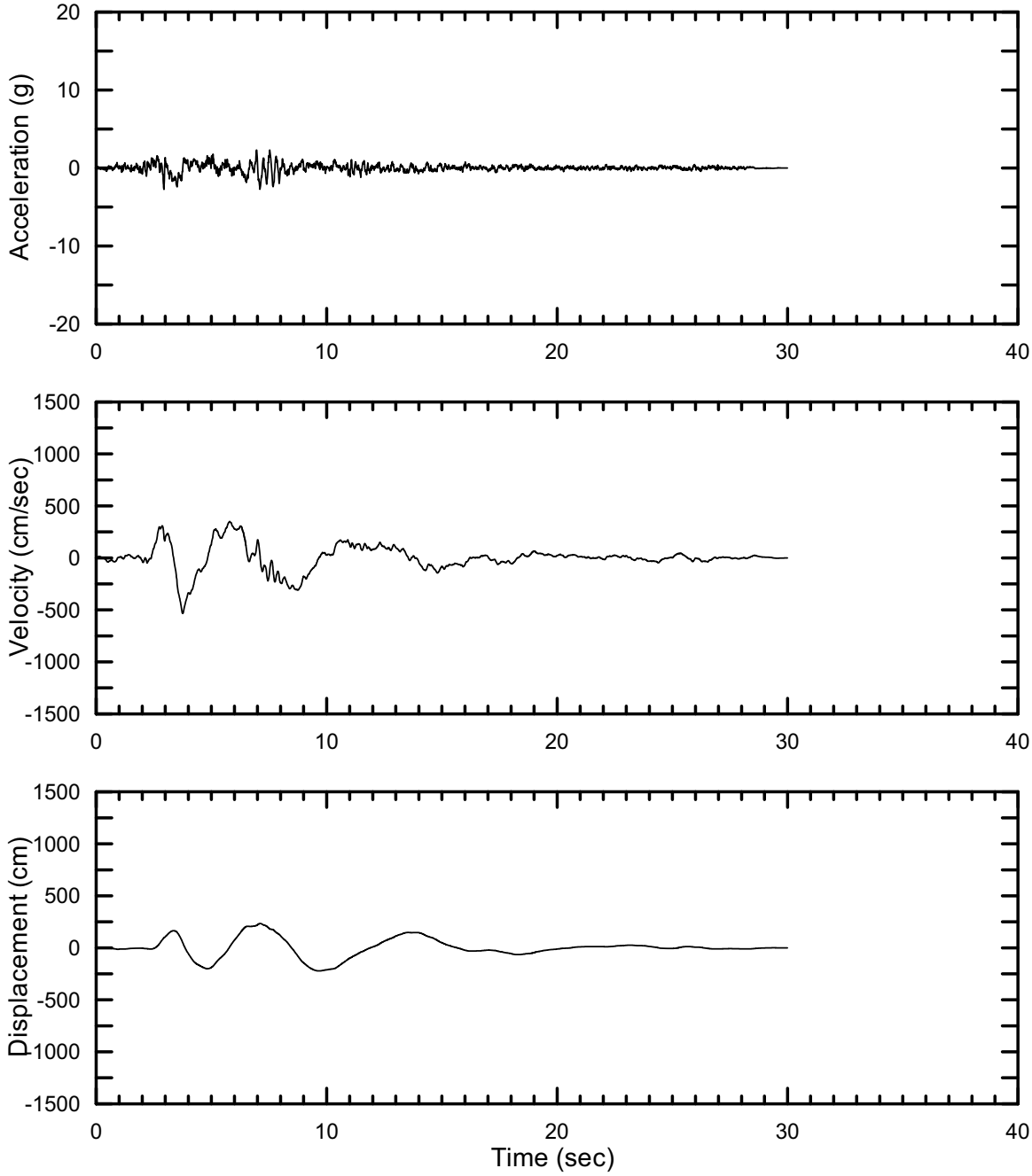

DTN: MO0403AVTMH107.003 [DIRS 168892]

Figure II-193. Point B Horizontal-1 Ti me Histories at an Annual Exceedance Probability of 10^{-7}, Set #17

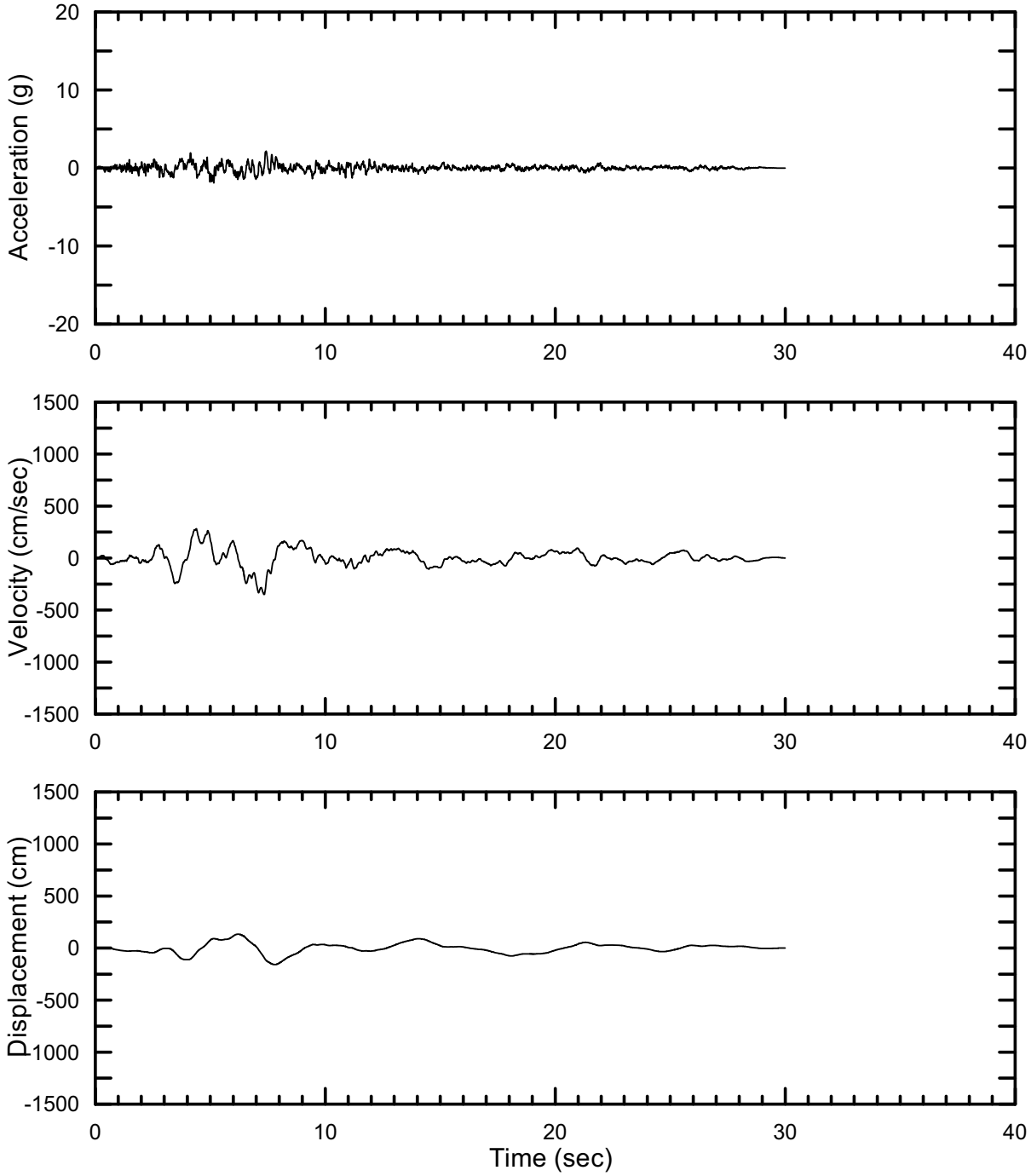

DTN: MO0403AVTMH107.003 [DIRS 168892]

Figure II-194. Point B Horizontal-2 Ti me Histories at an Annual Exceedance Probability of 10^{-7}, Set #17

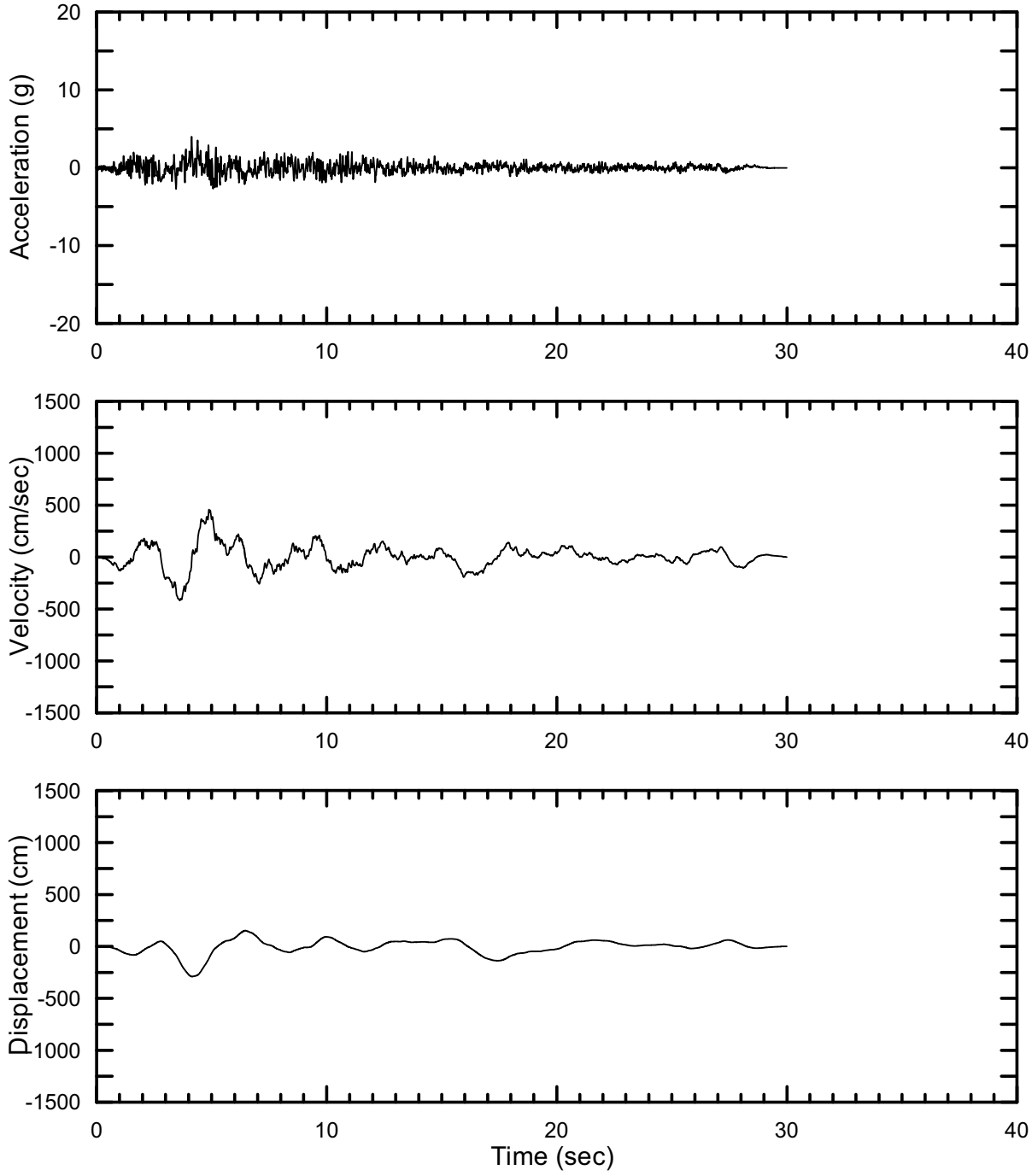

DTN: MO0403AVTMH107.003 [DIRS 168892]

Figure II-195. Point B Vertical Time Histories at an Annual Exceedance Probability of 10^{-7}, Set #17

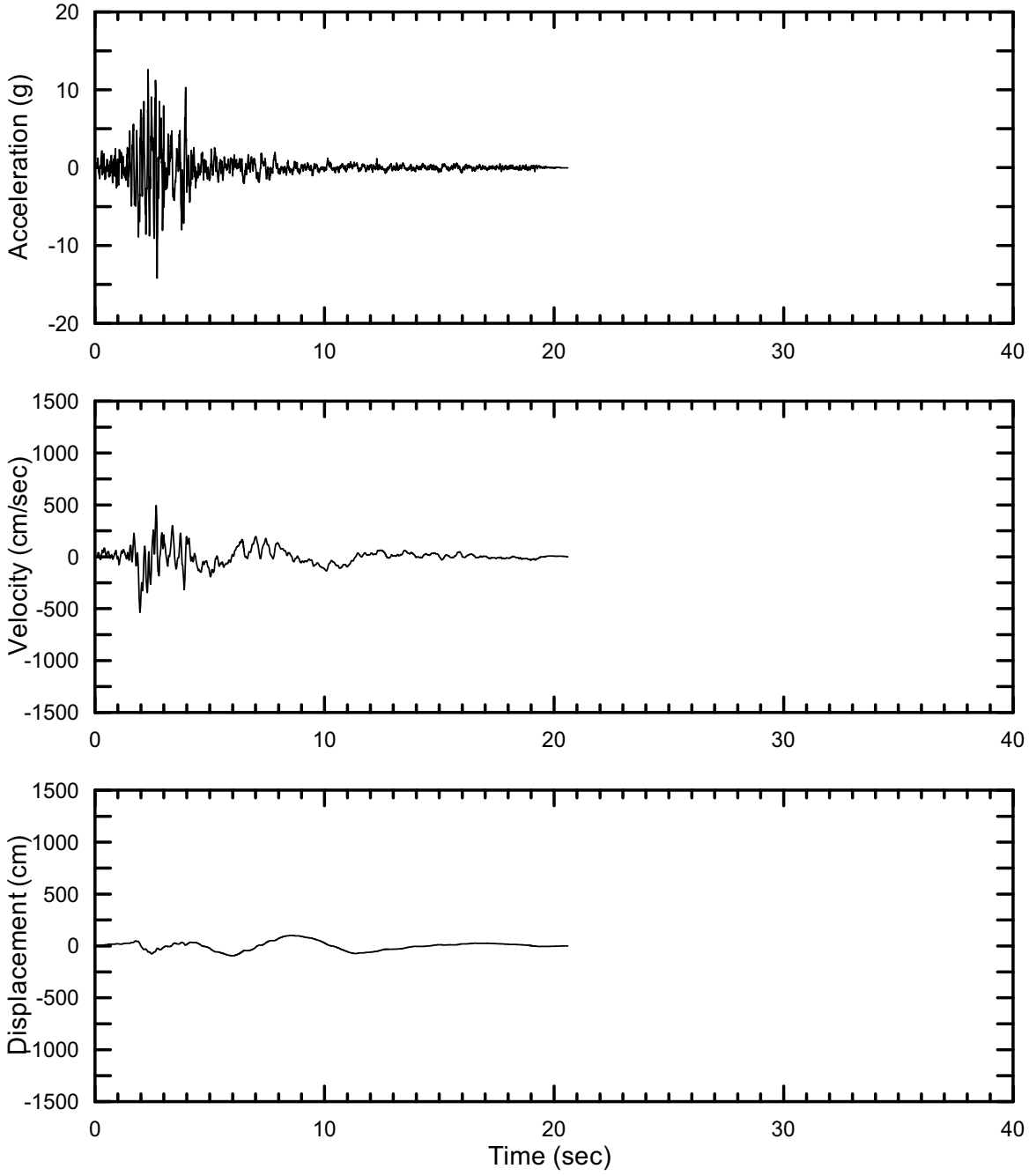

DTN: MO0301TMHSB107.000 [DIRS 164207]

Figure II-196. Point B Horizontal-1 Spectrally Conditioned to Point B Time Histories at an Annual Exceedance Probability of 10^{-7}, Set #1

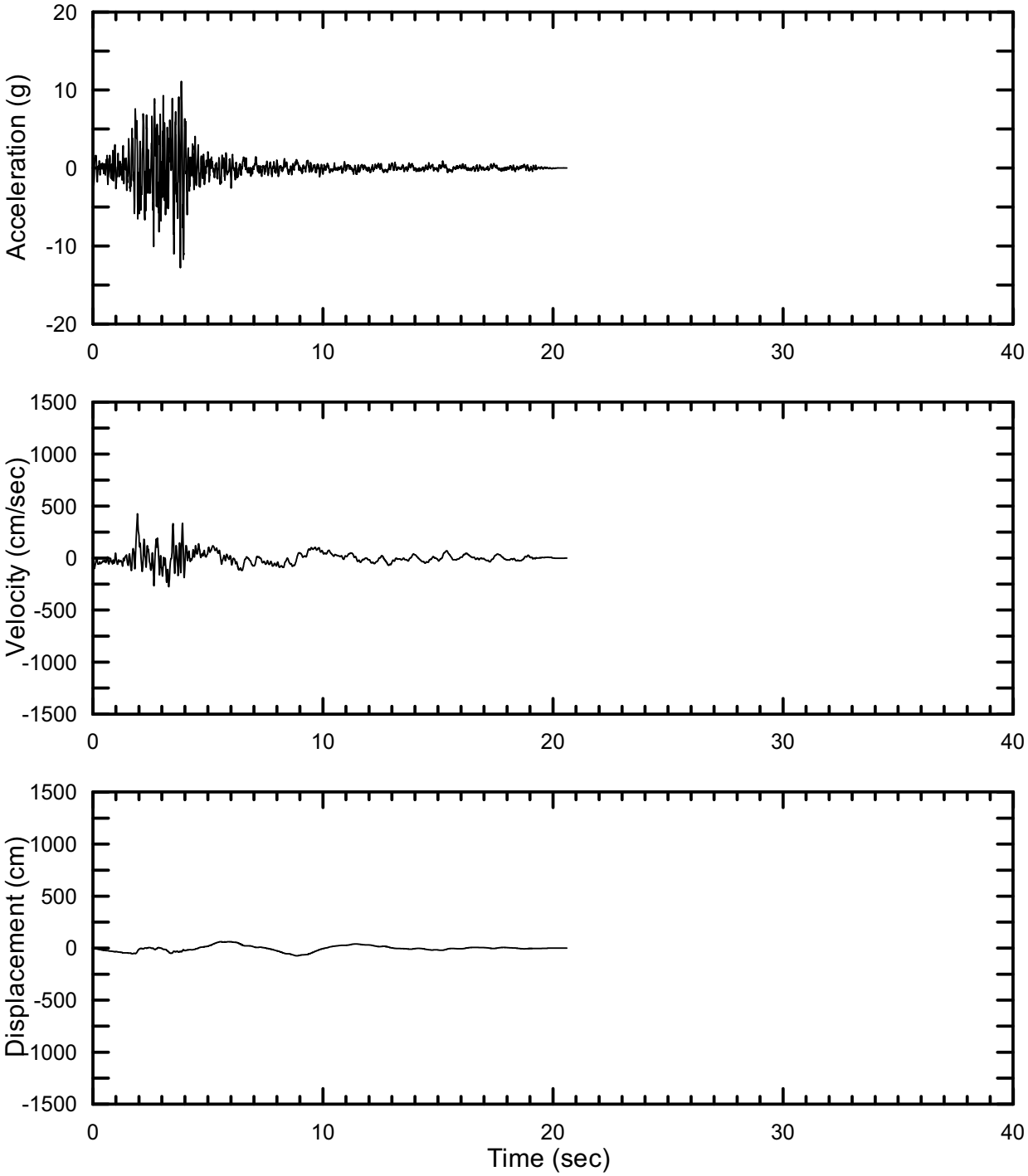

DTN: MO0301TMHSB107.000 [DIRS 164207]

Figure II-197. Point B Horizontal-2 Spectrally Conditioned to Point B Time Histories at an Annual Exceedance Probability of 10^{-7}, Set #1

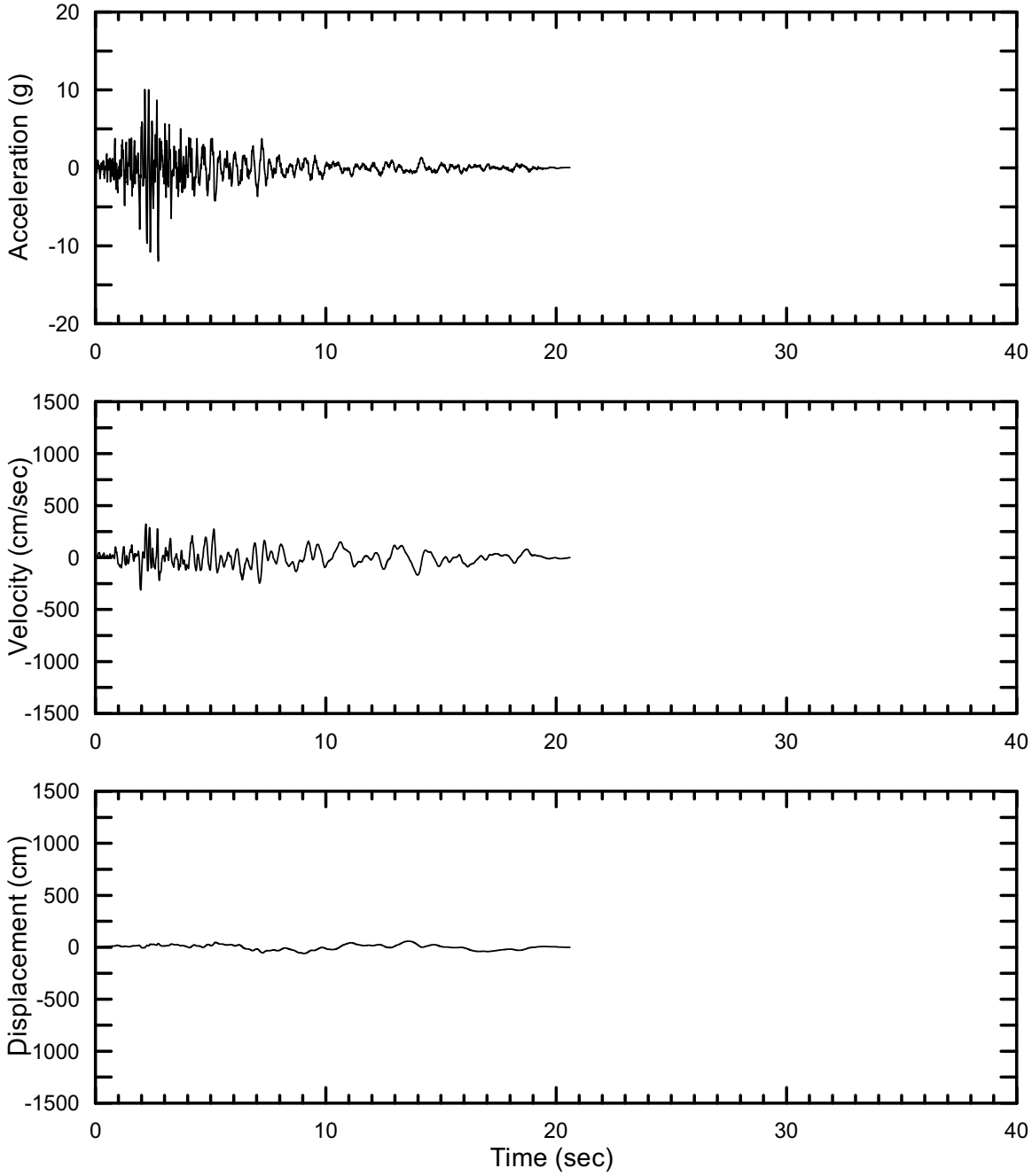

DTN: MO0301TMHSB107.000 [DIRS 164207]

Figure II-198. Point B Vertical Spectrally Conditioned to Point B Time Histories at an Annual Exceedance Probability of 10^{-7}, Set #1

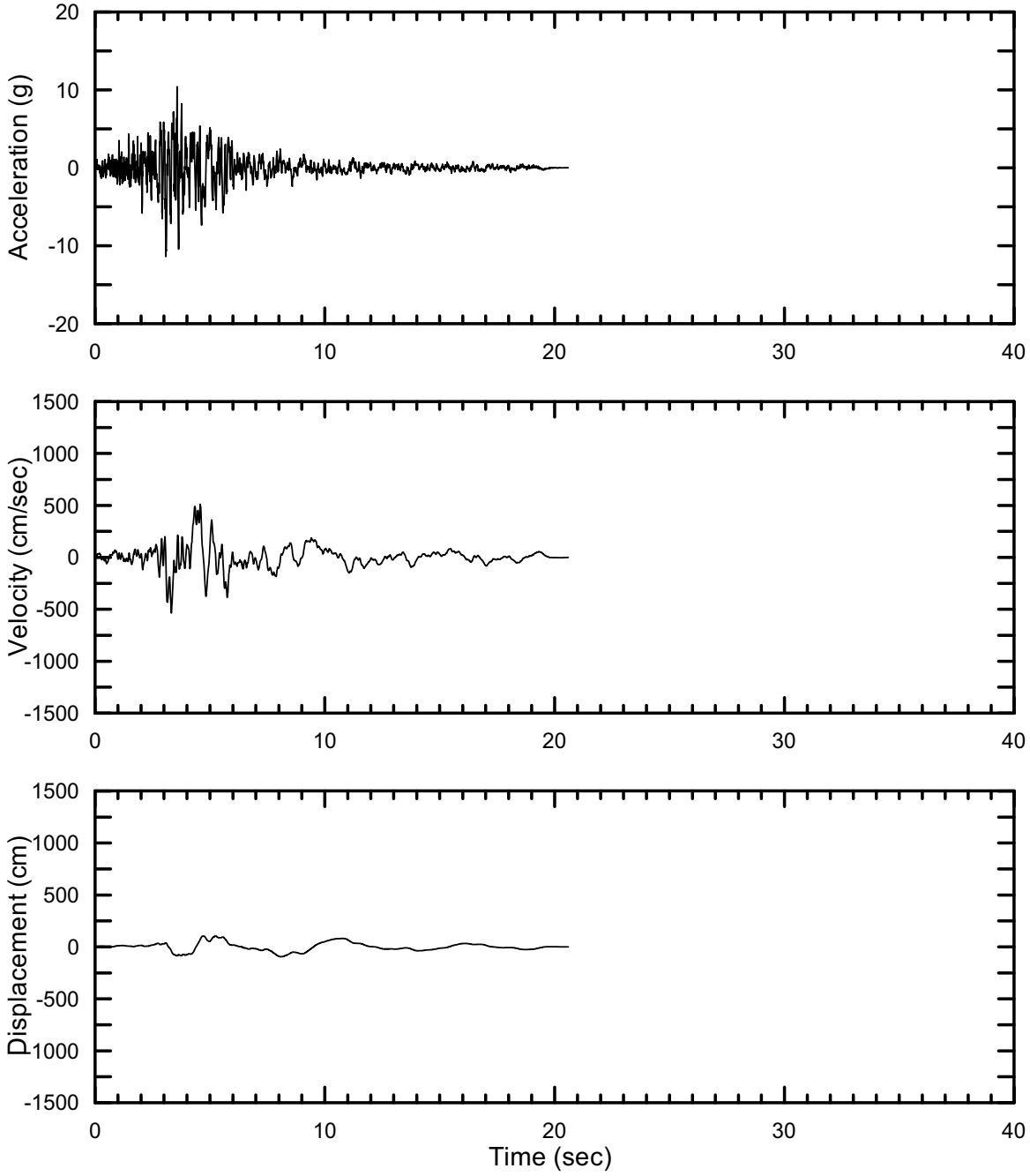

DTN: MO0301TMHSB107.000 [DIRS 164207]

Figure II-199. Point B Horizontal-1 Spectrally Conditioned to Point B Time Histories at an Annual Exceedance Probability of 10^{-7}, Set #2

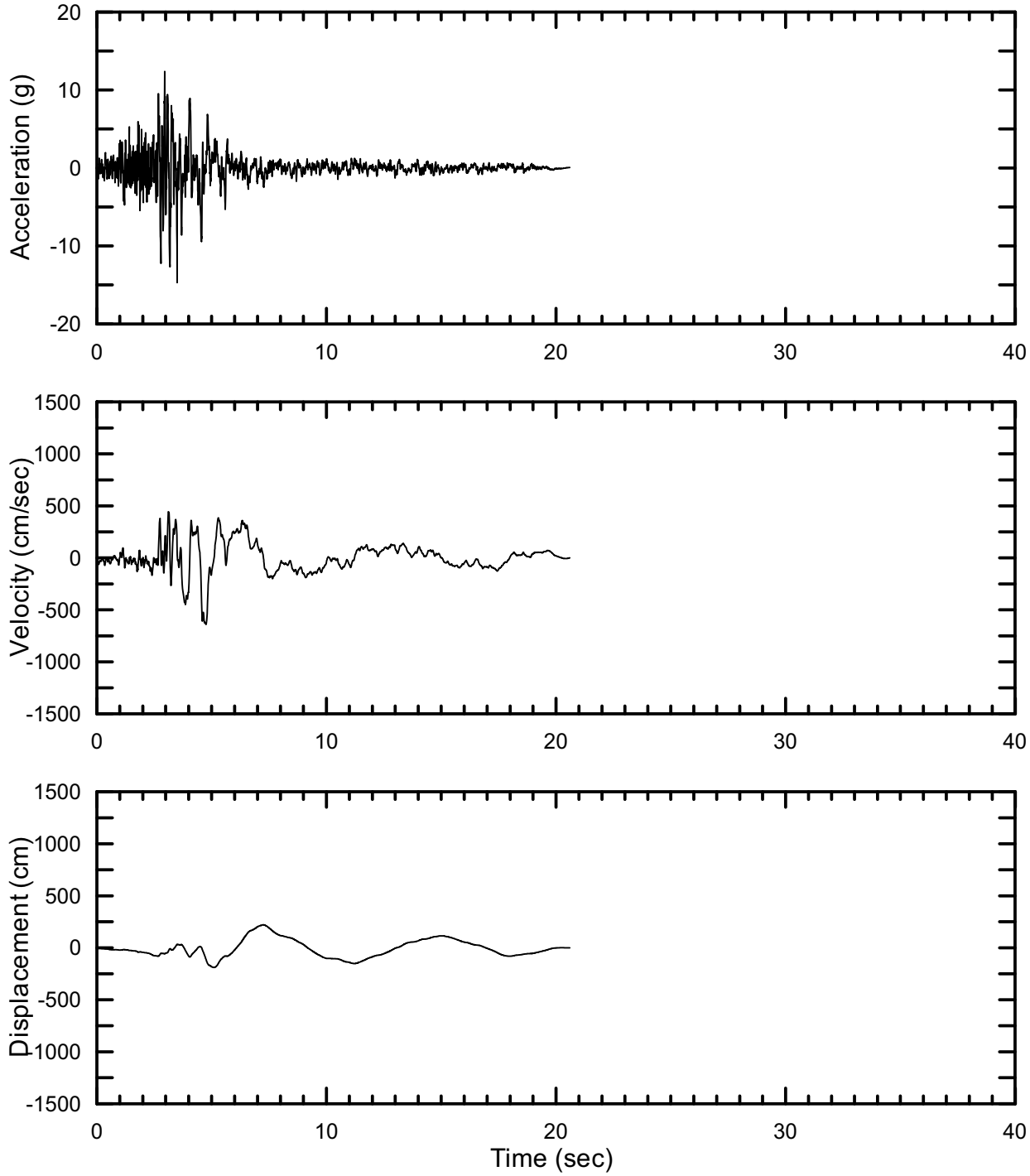

DTN: MO0301TMHSB107.000 [DIRS 164207]

Figure II-200. Point D Horizontal-2 Spectrally Conditioned to Point B Time Histories at an Annual Exceedance Probability of 10^{-7}, Set #2

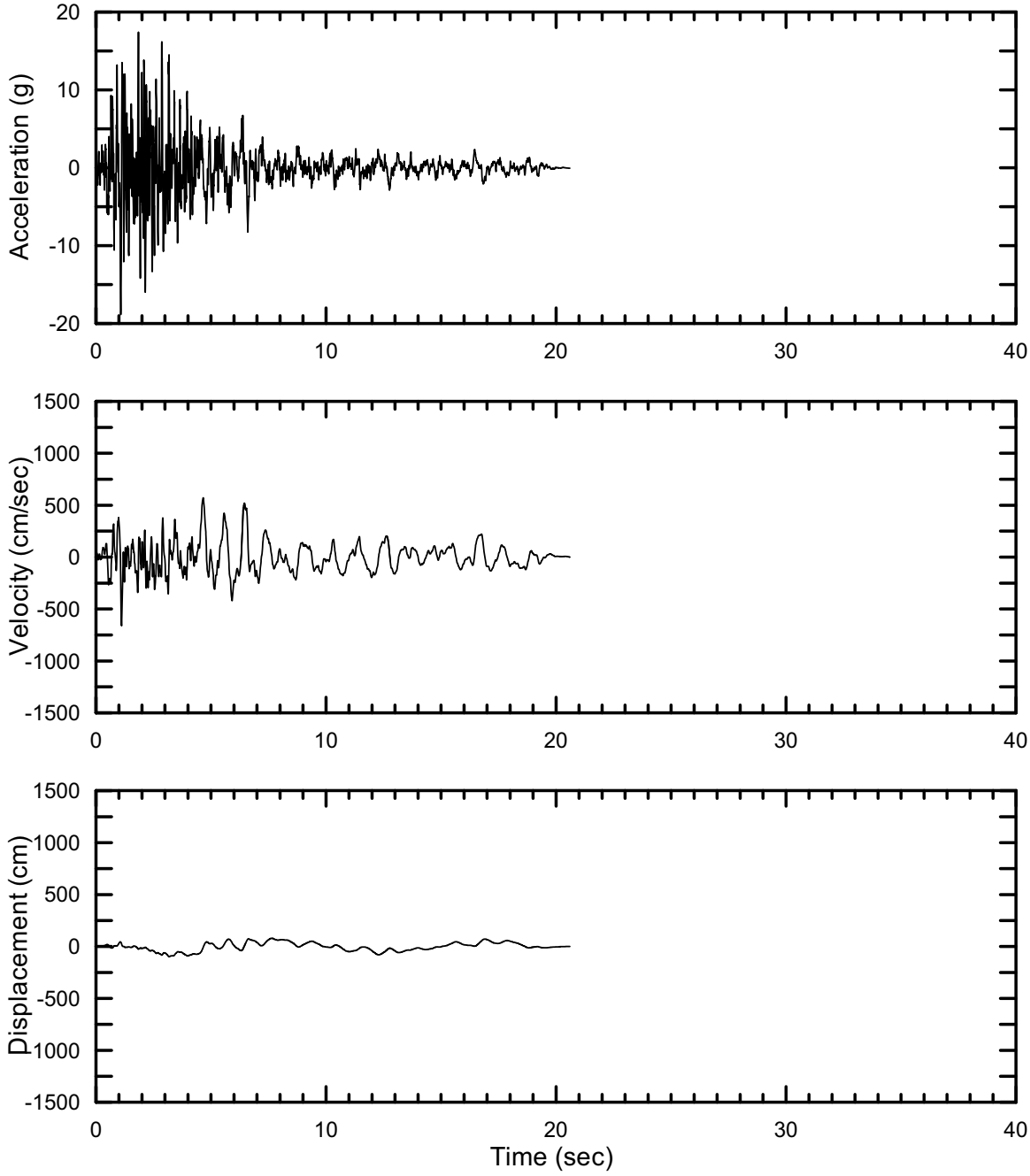

DTN: MO0301TMHSB107.000 [DIRS 164207]

Figure II-201. Point B Vertical Spectrally Conditioned to Point B Time Histories at an Annual Exceedance Probability of 10^{-7}, Set #2

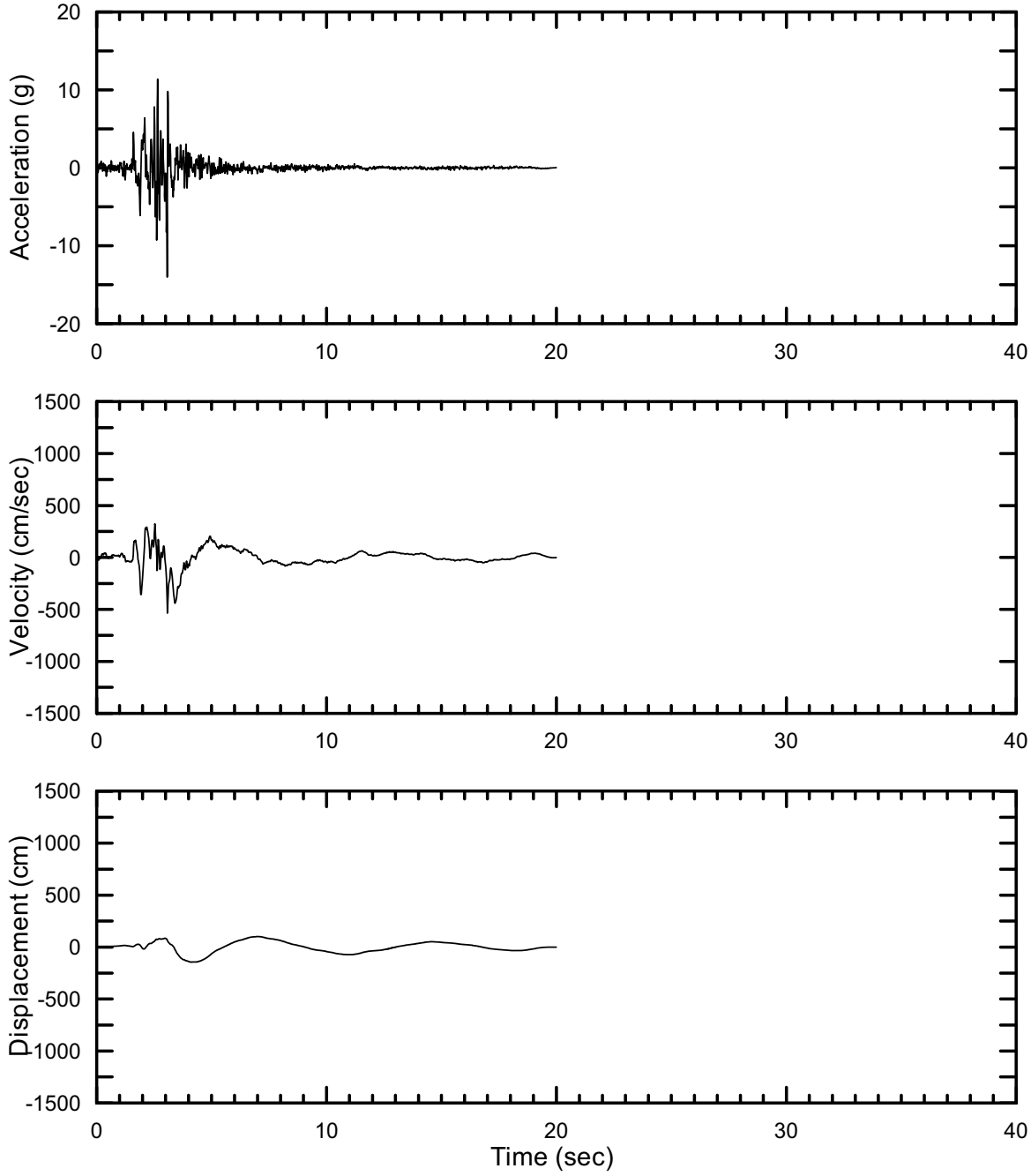

DTN: MO0301TMHSB107.000 [DIRS 164207]

Figure II-202. Point B Horizontal-1 Spectrally Conditioned to Point B Time Histories at an Annual Exceedance Probability of 10^{-7}, Set #3

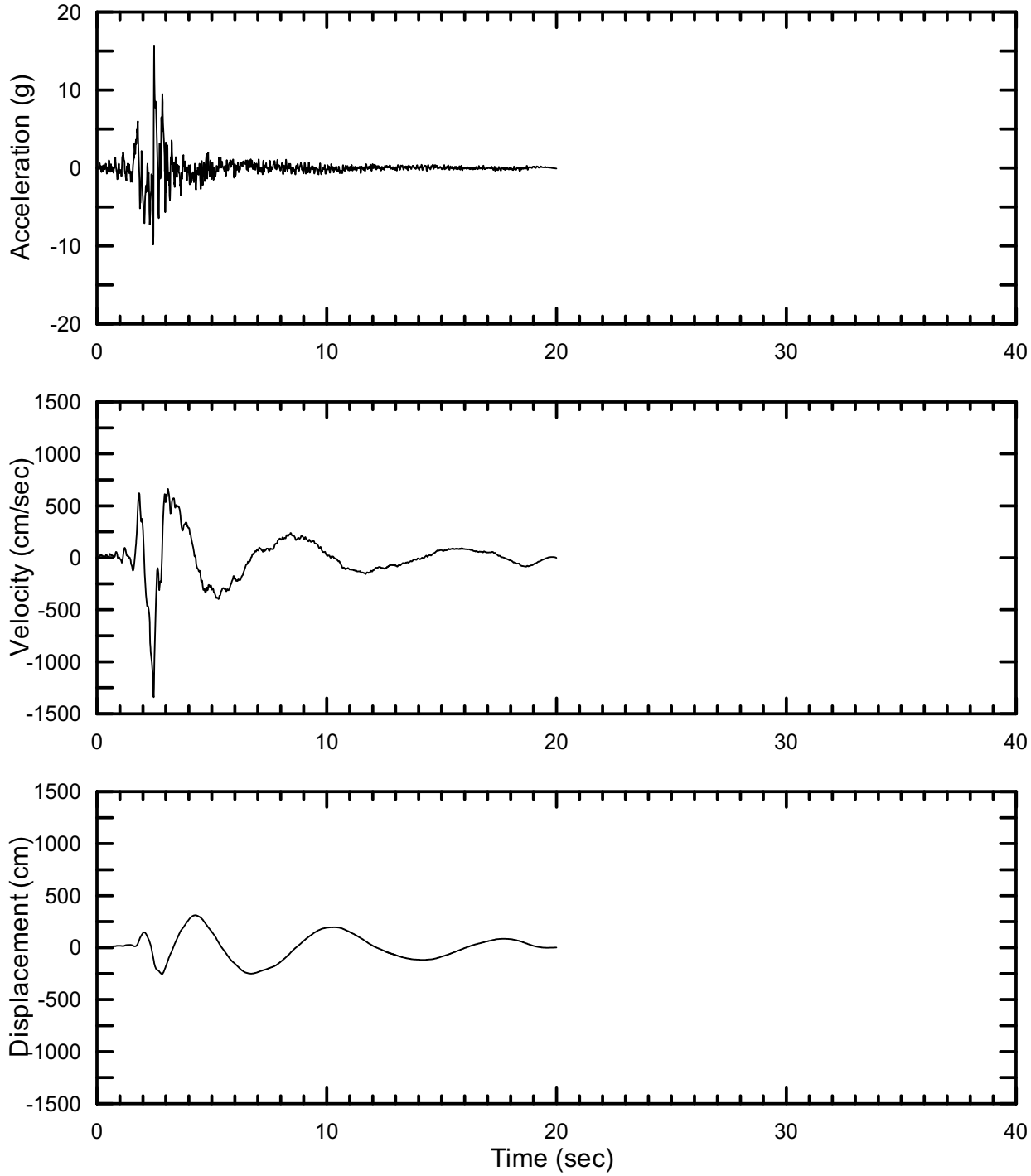

DTN: MO0301TMHSB107.000 [DIRS 164207]

Figure II-203. Point B Horizontal-2 Spectrally Conditioned to Point B Time Histories at an Annual Exceedance Probability of 10^{-7}, Set #3

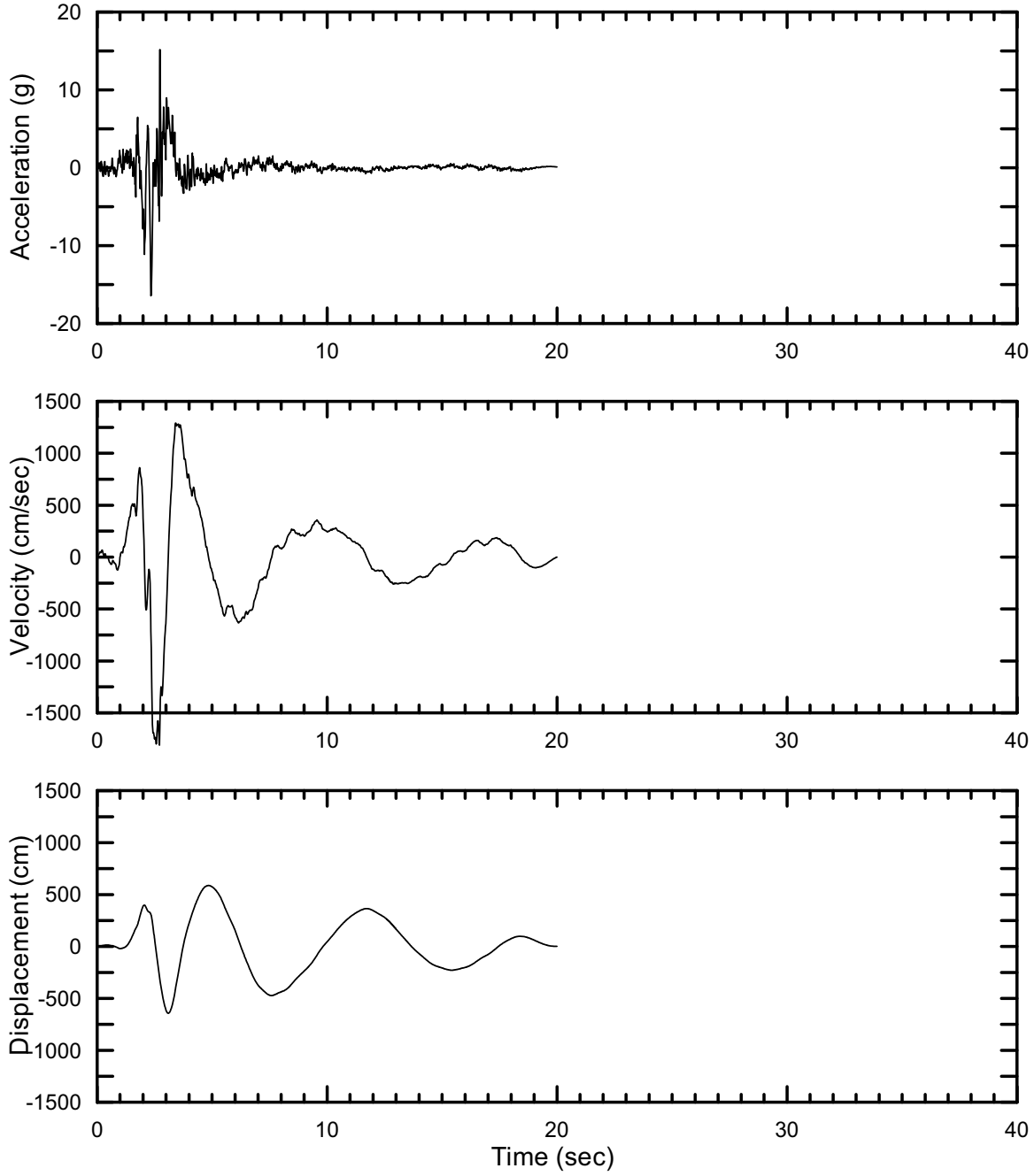

DTN: MO0301TMHSB107.000 [DIRS 164207]

Figure II-204. Point B Vertical Spectrally Conditioned to Point B Time Histories at an Annual Exceedance Probability of 10^{-7}, Set #3

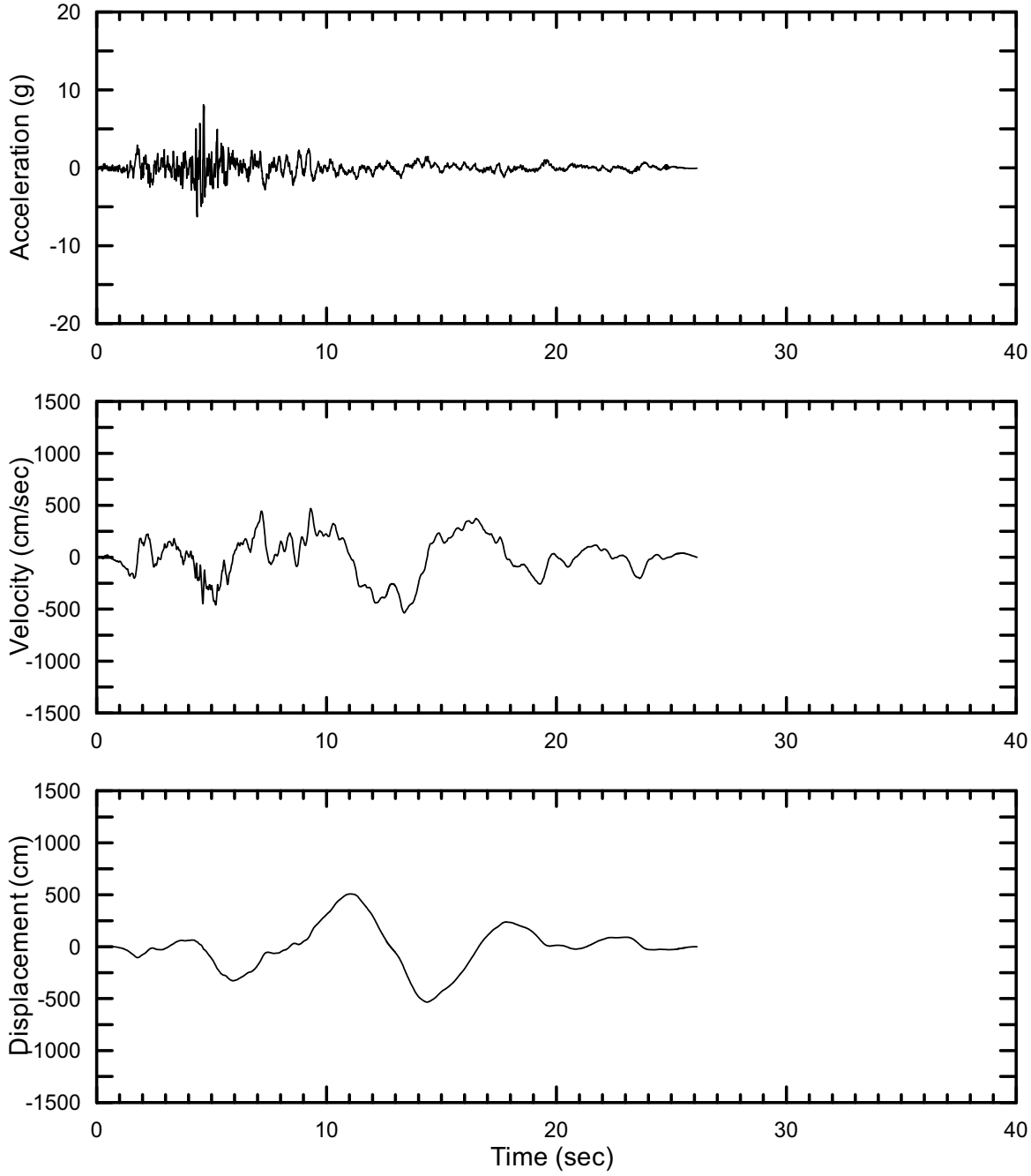

DTN: MO0301TMHSB107.000 [DIRS 164207]

Figure II-205. Point B Horizontal-1 to Point B Time Histories at an Annual Exceedance Probability of 10^{-7}, Set #4

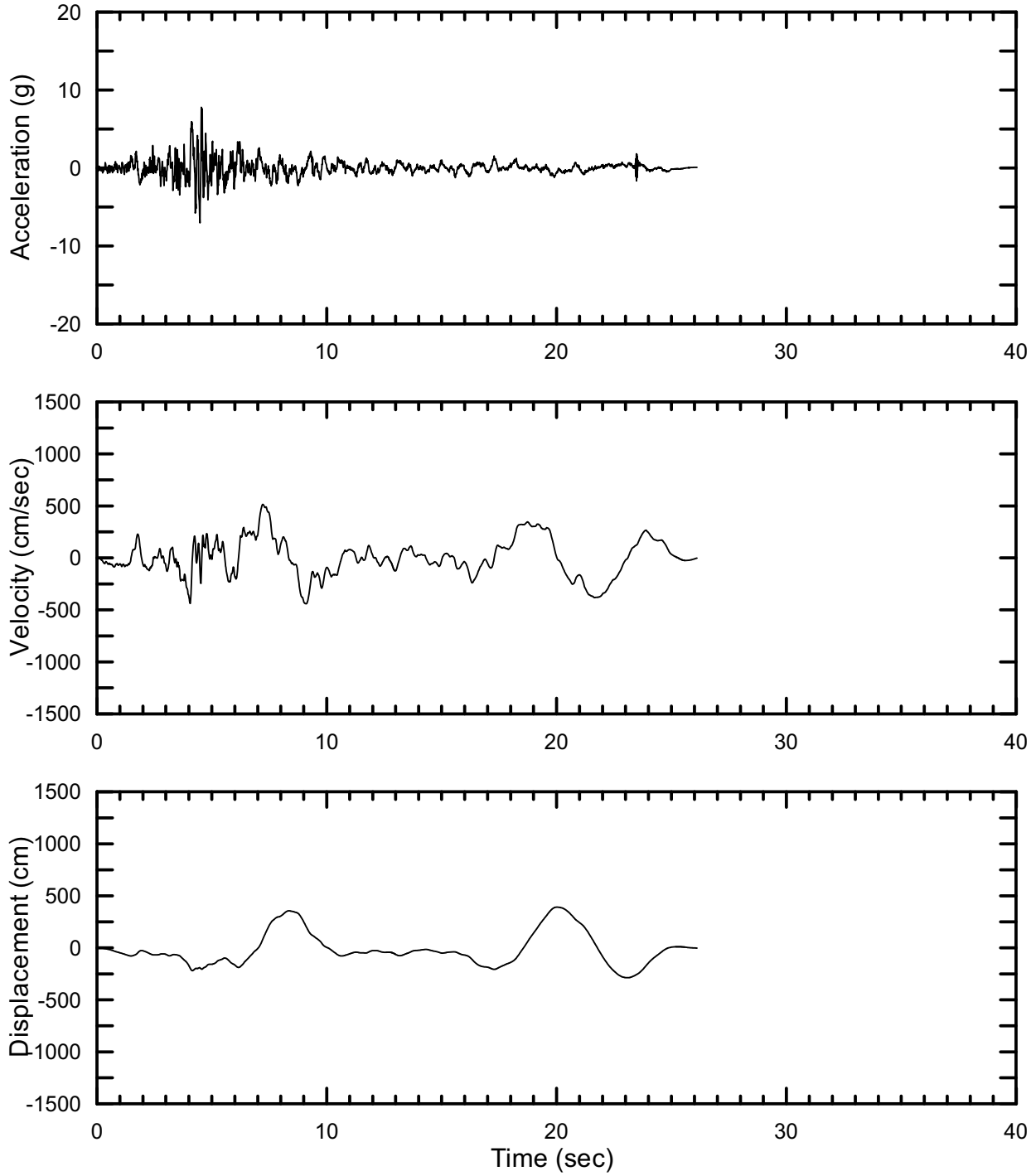

DTN: MO0301TMHSB107.000 [DIRS 164207]

Figure II-206. Point B Horizontal-2 Spectrally Conditioned to Point B Time Histories at an Annual Exceedance Probability of 10^{-7}, Set #4

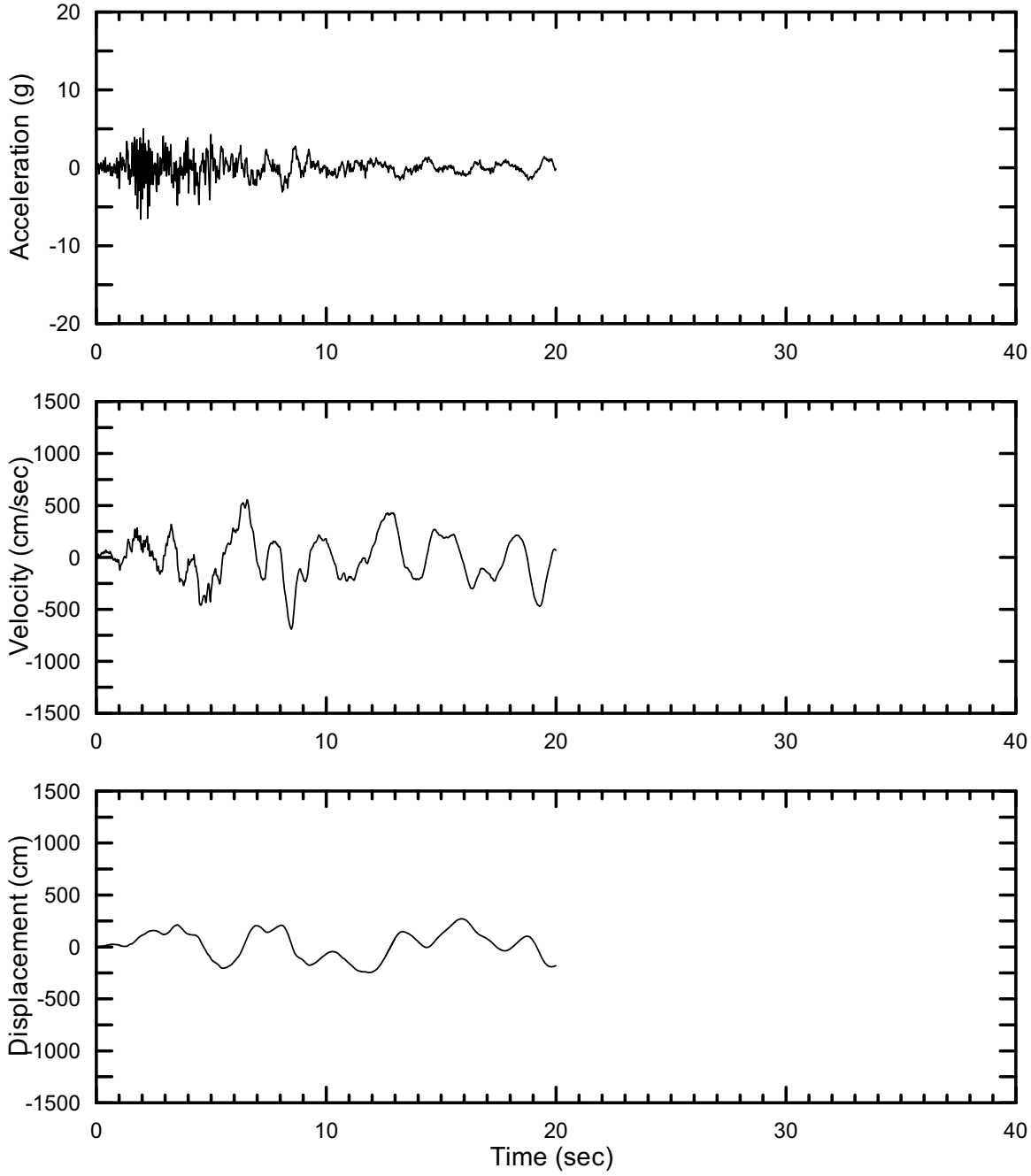

DTN: MO0301TMHSB107.000 [DIRS 164207]

Figure II-207. Point B Vertical Spectrally Conditioned to Point B Time Histories at an Annual Exceedance Probability of 10^{-7}, Set #4

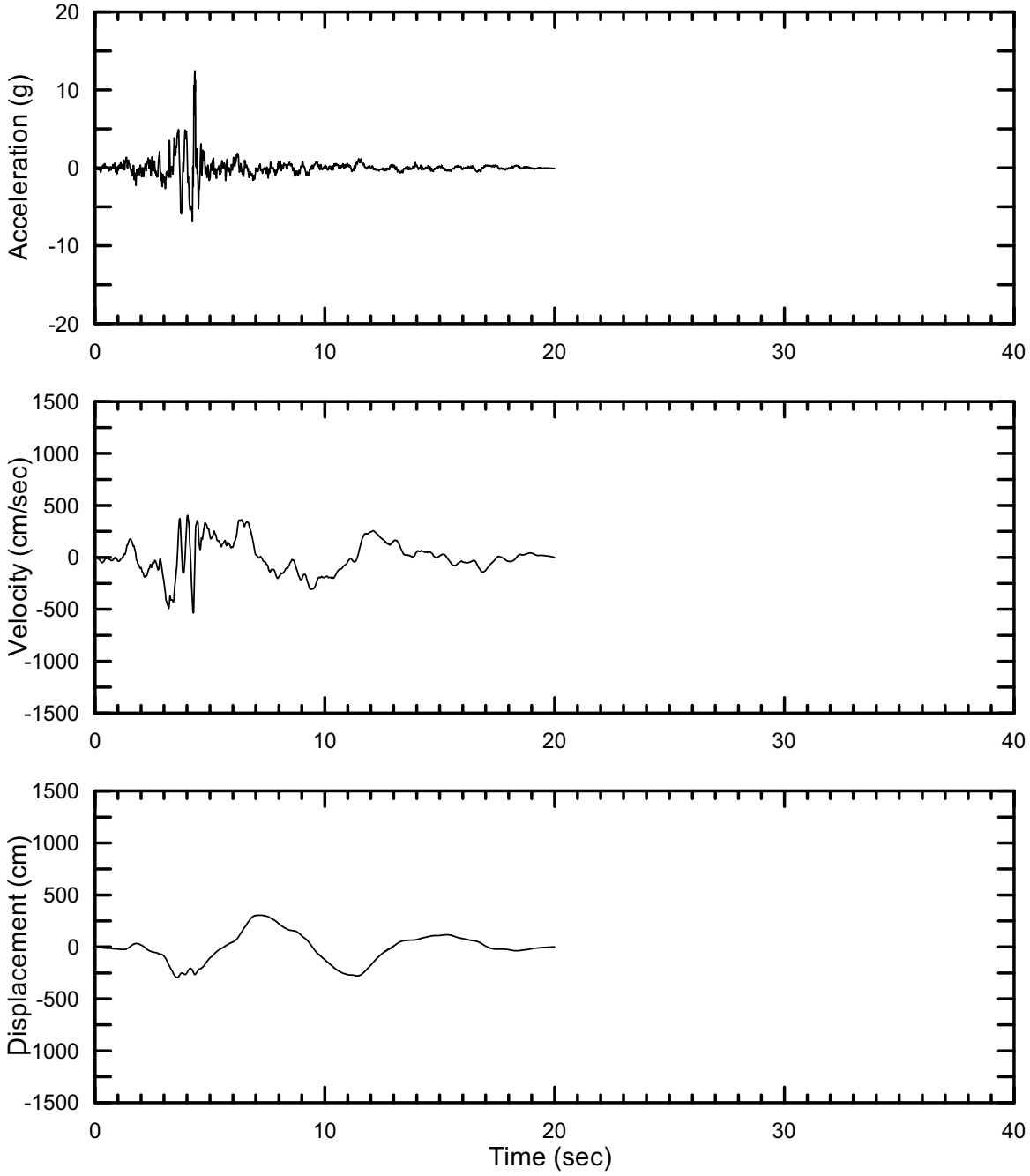

DTN: MO0301TMHSB107.000 [DIRS 164207]

Figure II-208. Point B Horizontal-1 Spectrally Conditioned to Point B Time Histories at an Annual Exceedance Probability of 10^{-7}, Set #5

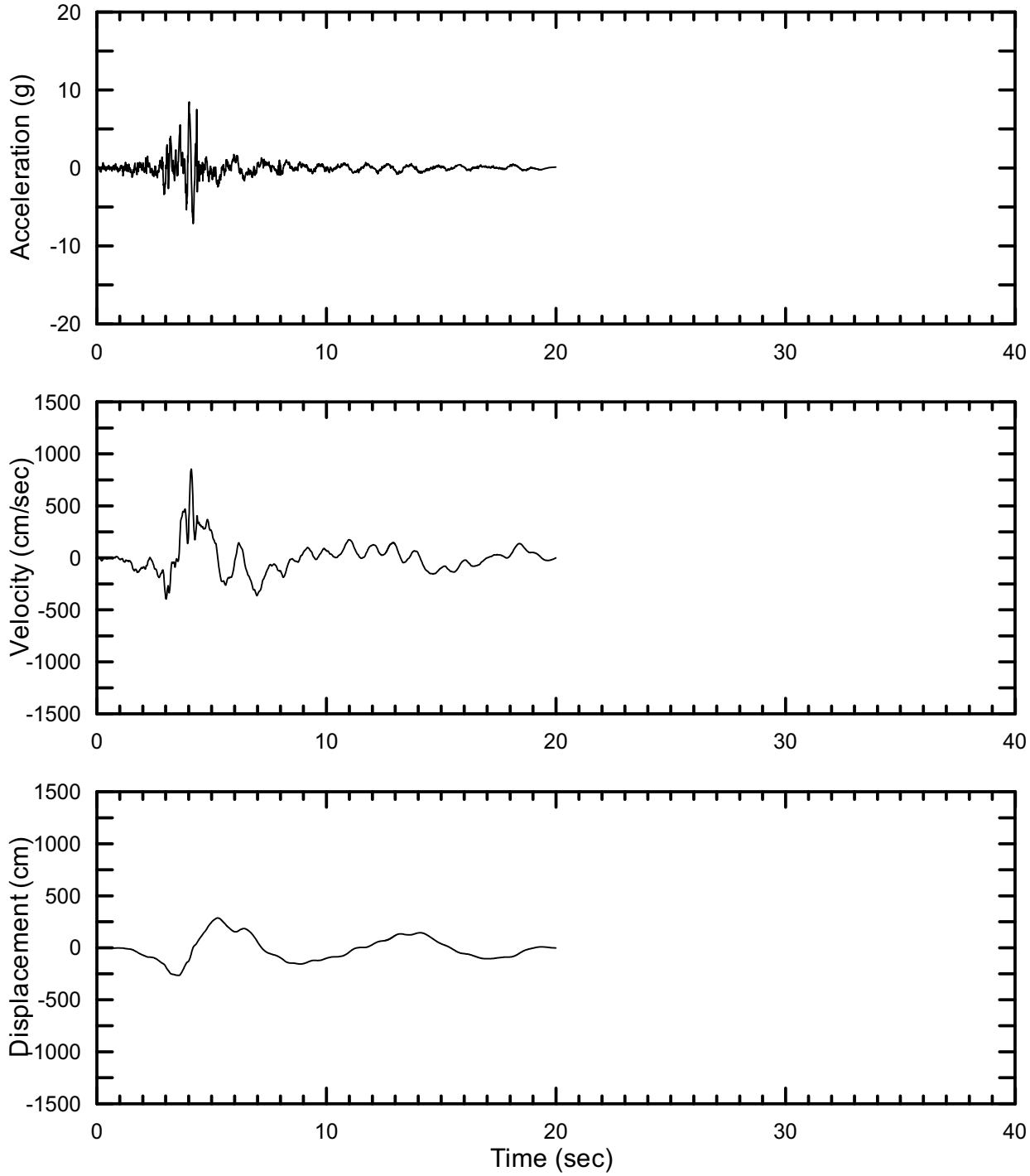

DTN: MO0301TMHSB107.000 [DIRS 164207]

Figure II-209. Point B Horizontal-2 Spectrally Conditioned to Point B Time Histories at an Annual Exceedance Probability of 10^{-7}, Set #5

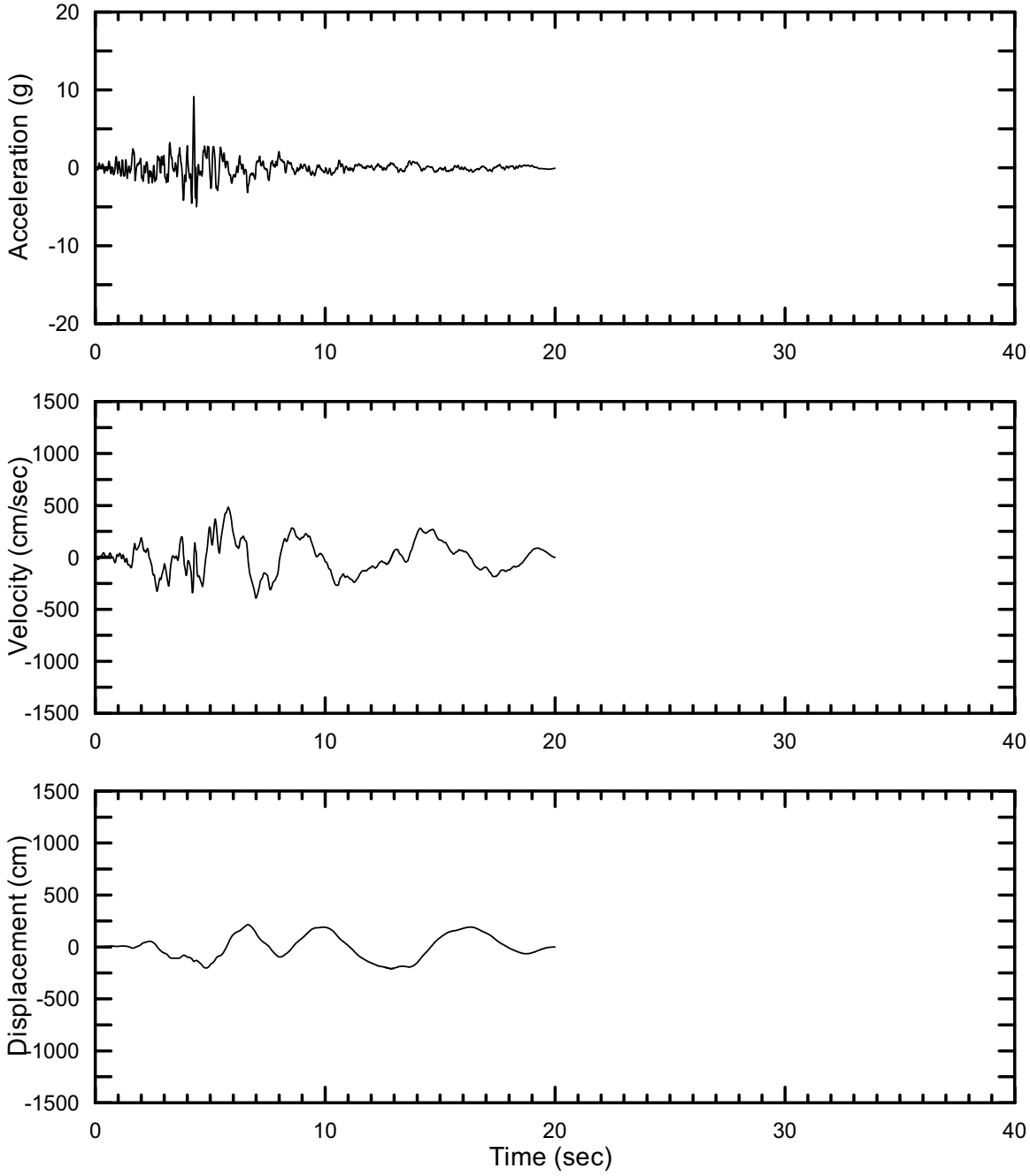

DTN: MO0301TMHSB107.000 [DIRS 164207]

Figure II-210. Point B Vertical Spectrally Conditioned to Point B Time Histories at an Annual Exceedance Probability of 10^{-7}, Set #5

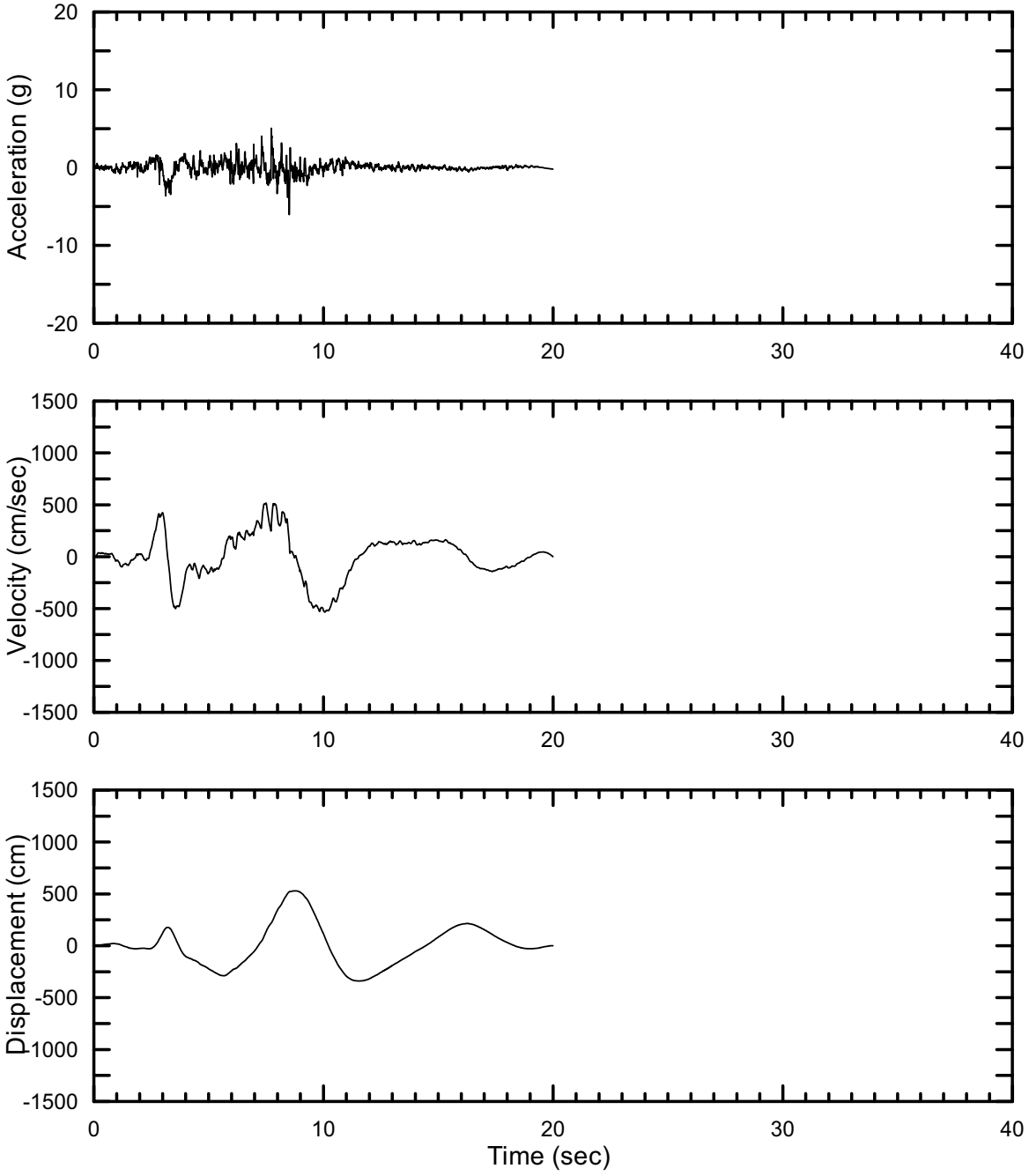

DTN: MO0301TMHSB107.000 [DIRS 164207]

Figure II-211. Point B Horizontal-1 Spectrally Conditioned to Point B Time Histories at an Annual Exceedance Probability of 10^{-7}, Set #6

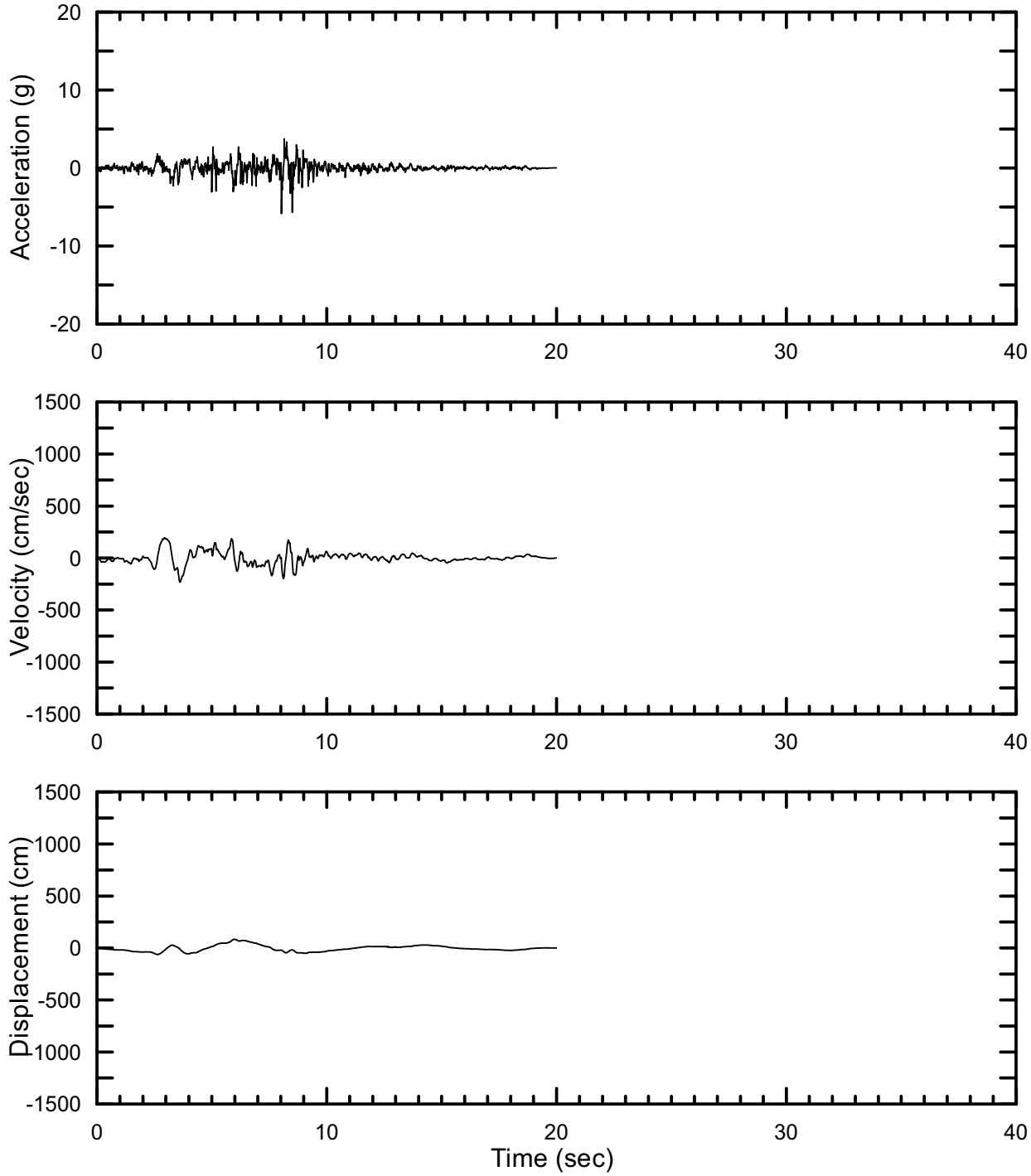

DTN: MO0301TMHSB107.000 [DIRS 164207]

Figure II-212. Point B Horizontal-2 Spectrally Conditioned to Point B Time Histories at an Annual Exceedance Probability of 10^{-7}, Set #6

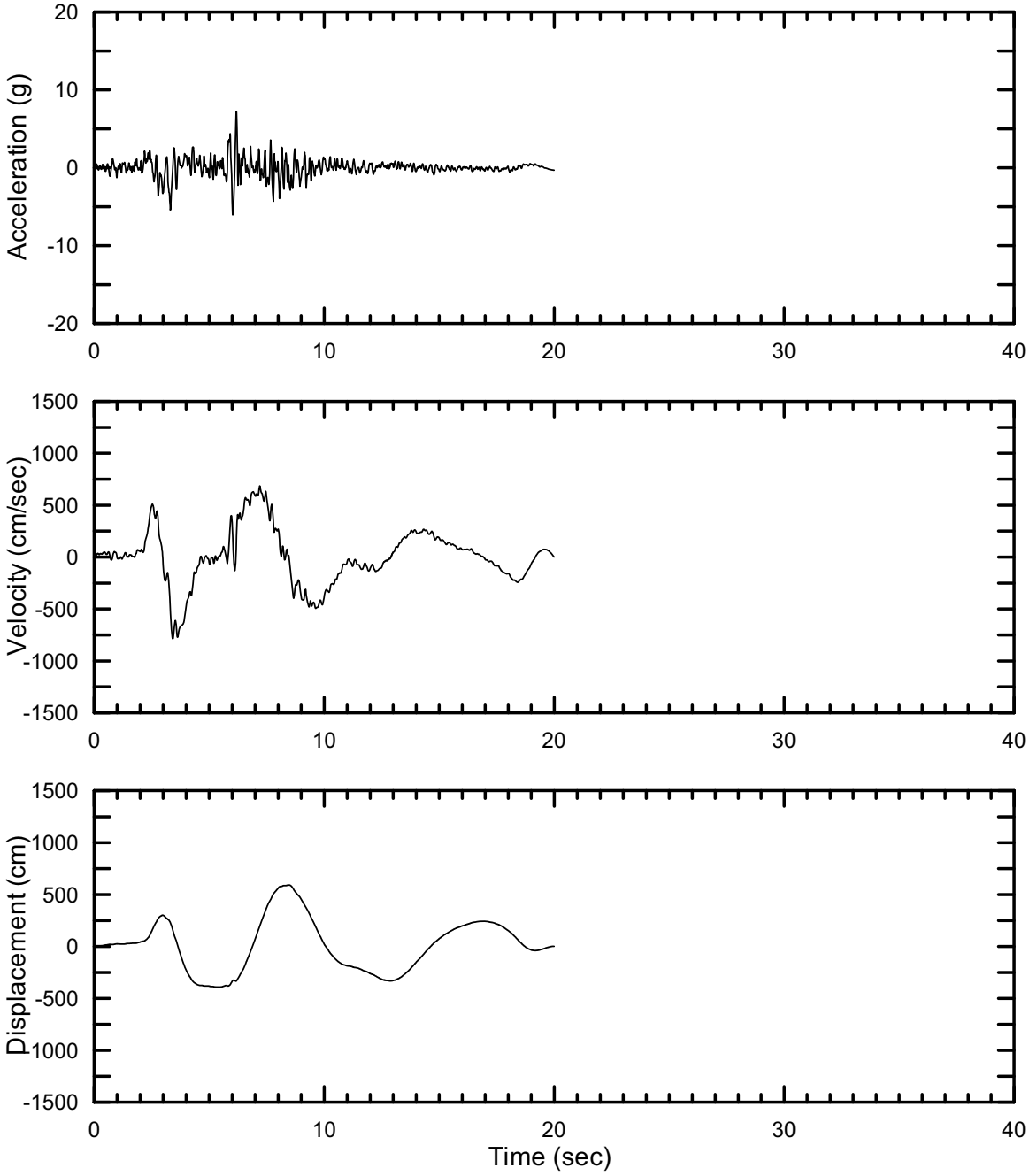

DTN: MO0301TMHSB107.000 [DIRS 164207]

Figure II-213. Point B Vertical Spectrally Conditioned to Point B Time Histories at an Annual Exceedance Probability of 10^{-7}, Set #6

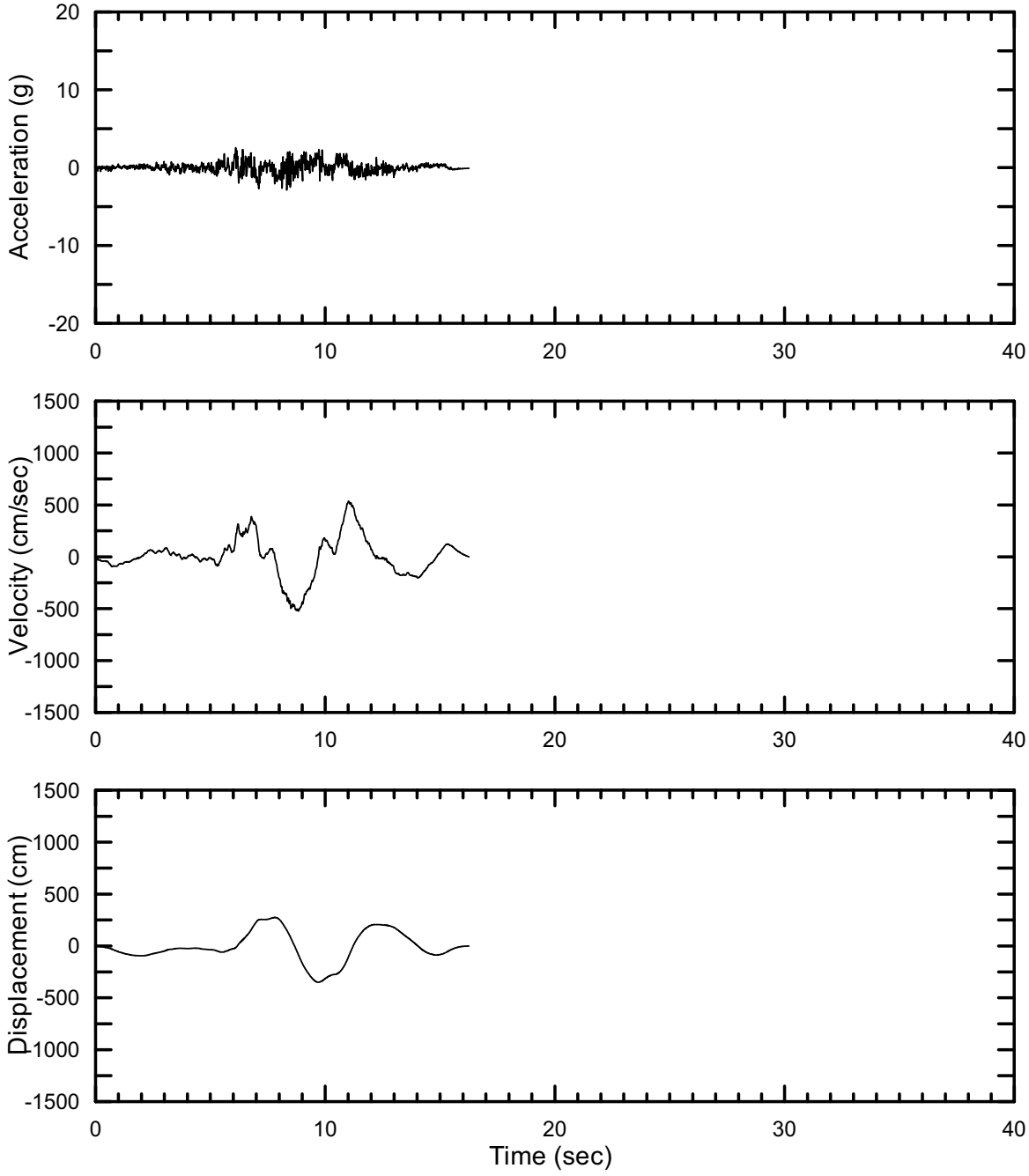

DTN: MO0301TMHSB107.000 [DIRS 164207]

Figure II-214. Point B Horizontal-1 Spectrally Conditioned to Point B Time Histories at an Annual Exceedance Probability of 10^{-7}, Set #7

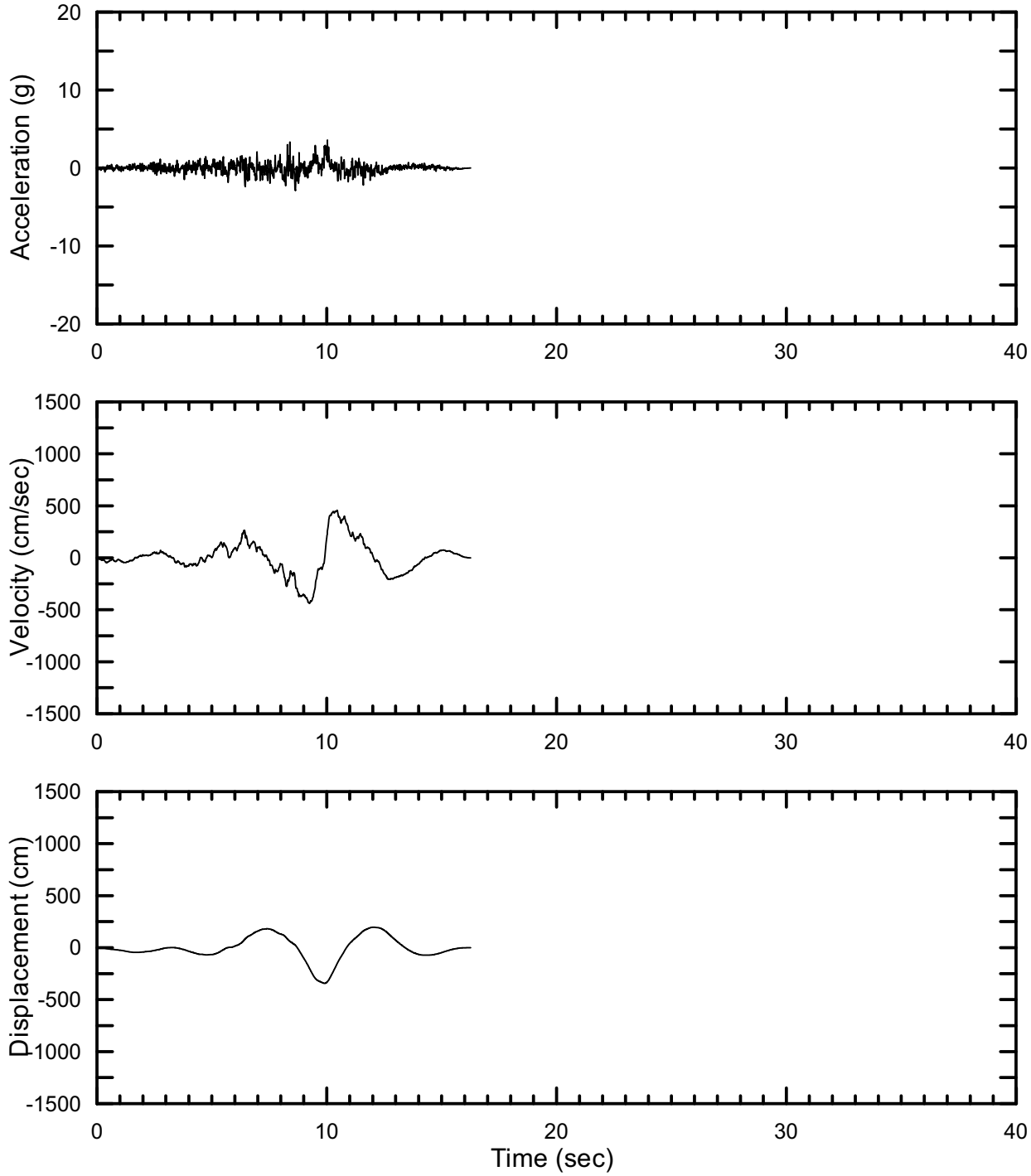

DTN: MO0301TMHSB107.000 [DIRS 164207]

Figure II-215. Point B Horizontal-2 Spectrally Conditioned to Point B Time Histories at an Annual Exceedance Probability of 10^{-7}, Set #7

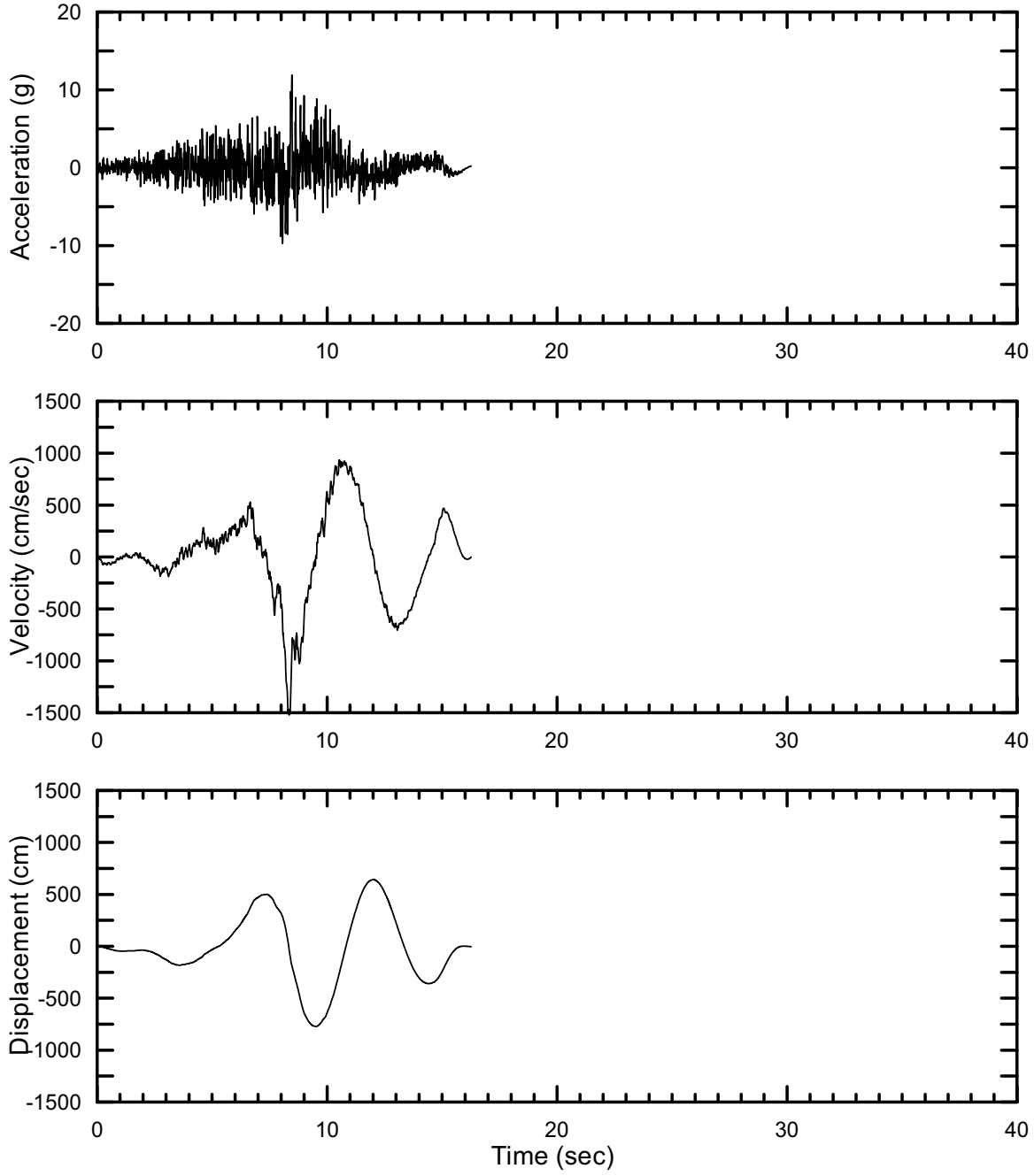

DTN: MO0301TMHSB107.000 [DIRS 164207]

Figure II-216. Point B Vertical Spectrally Conditioned to Point B Time Histories at an Annual Exceedance Probability of 10^{-7}, Set #7

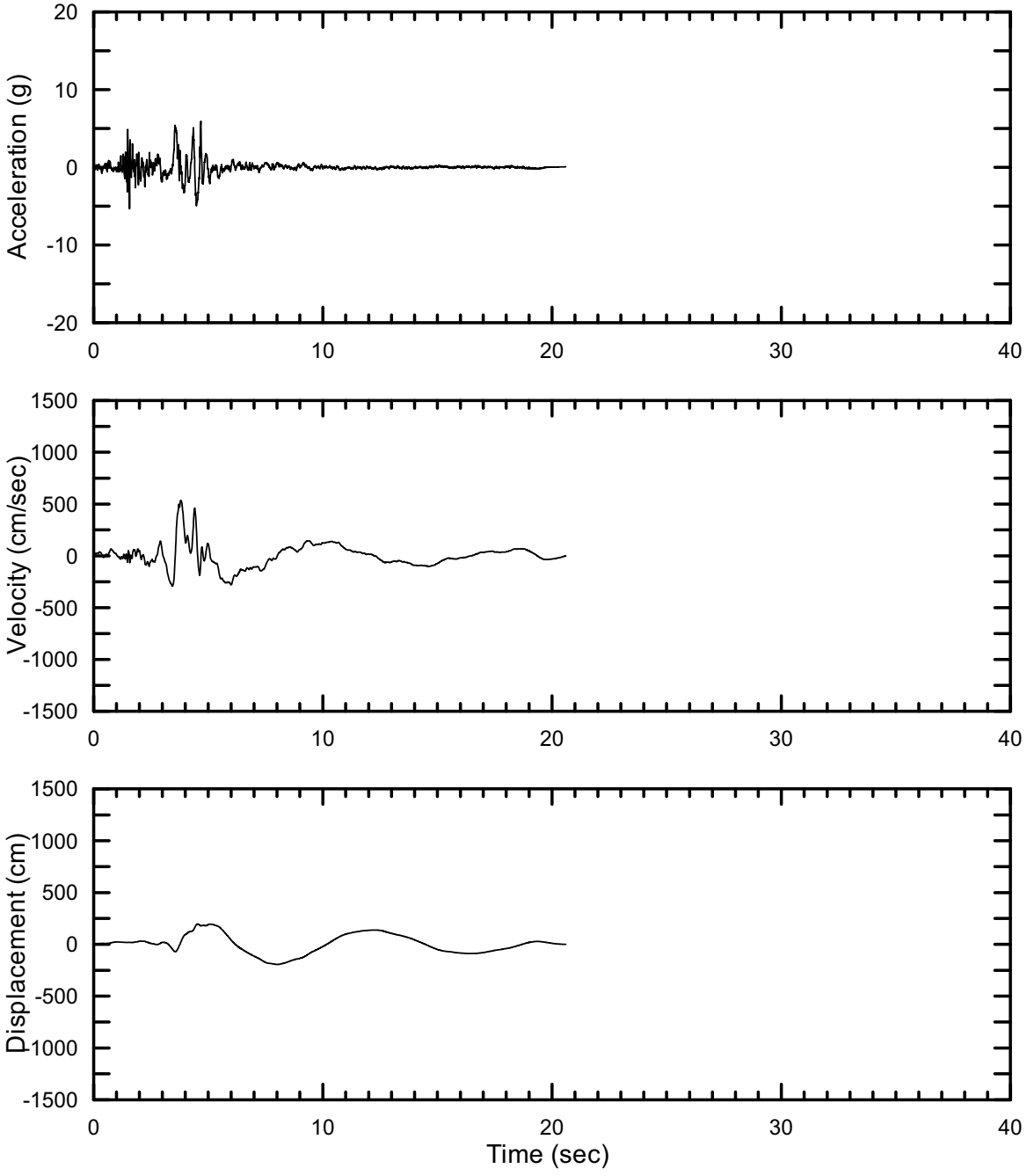

DTN: MO0301TMHSB107.000 [DIRS 164207]

Figure II-217. Point B Horizontal-1 Spectrally Conditioned to Point B Time Histories at an Annual Exceedance Probability of 10^{-7}, Set #8

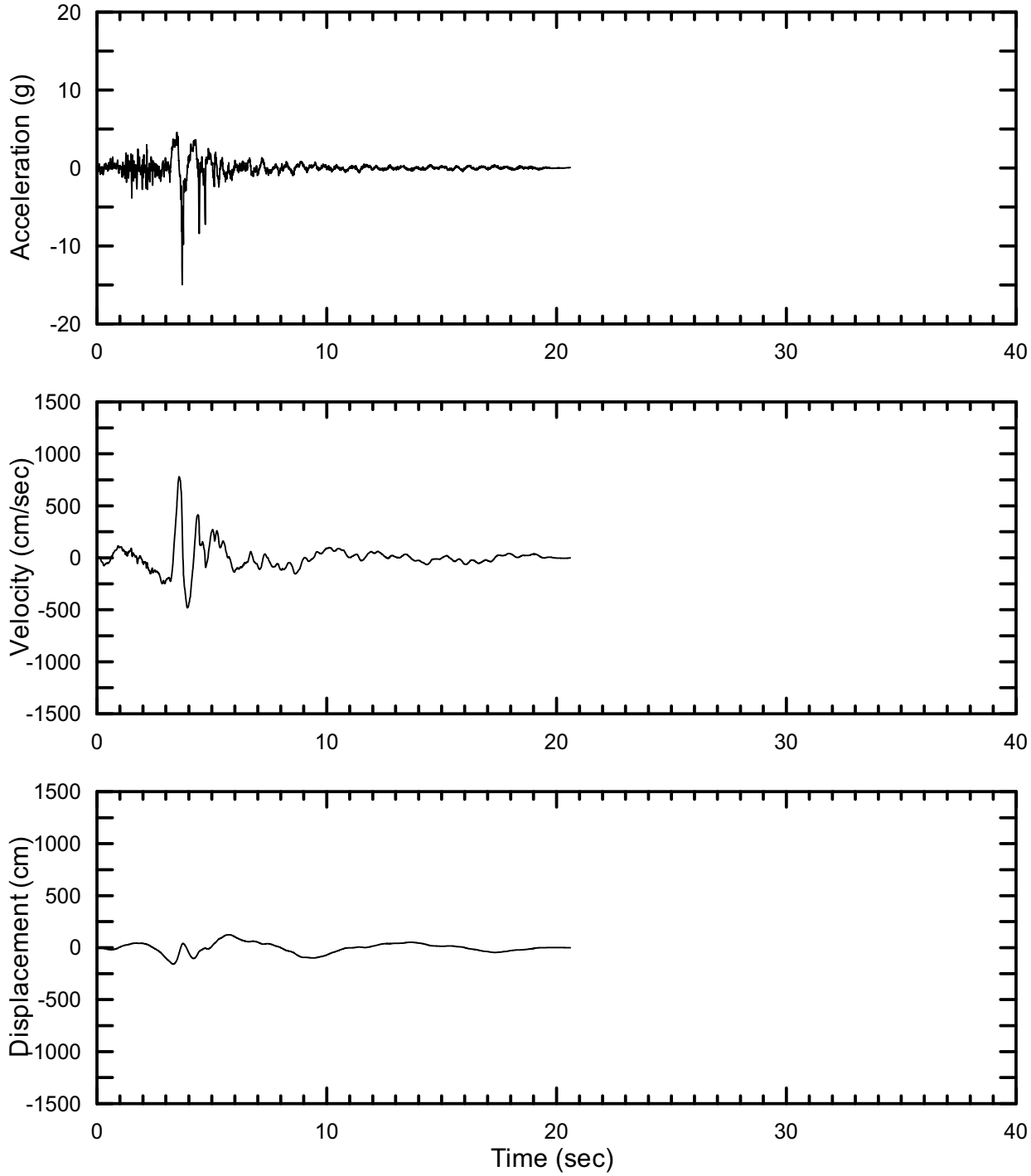

DTN: MO0301TMHSB107.000 [DIRS 164207]

Figure II-218. Point B Horizontal-2 Spectrally Conditioned to Point B Time Histories at an Annual Exceedance Probability of 10^{-7}, Set #8

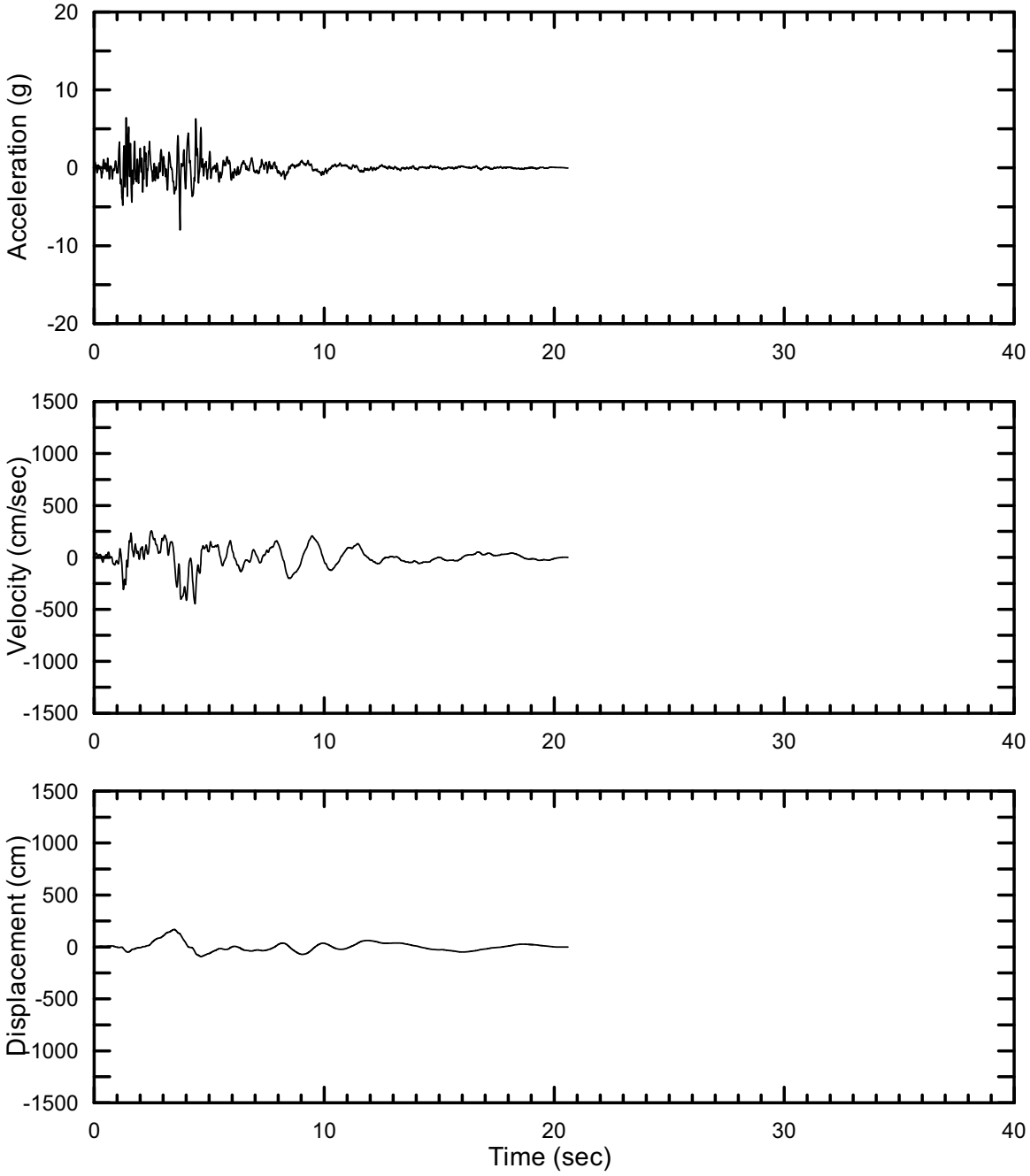

DTN: MO0301TMHSB107.000 [DIRS 164207]

Figure II-219. Point B Vertical Spectrally Conditioned to Point B Time Histories at an Annual Exceedance Probability of 10^{-7}, Set #8

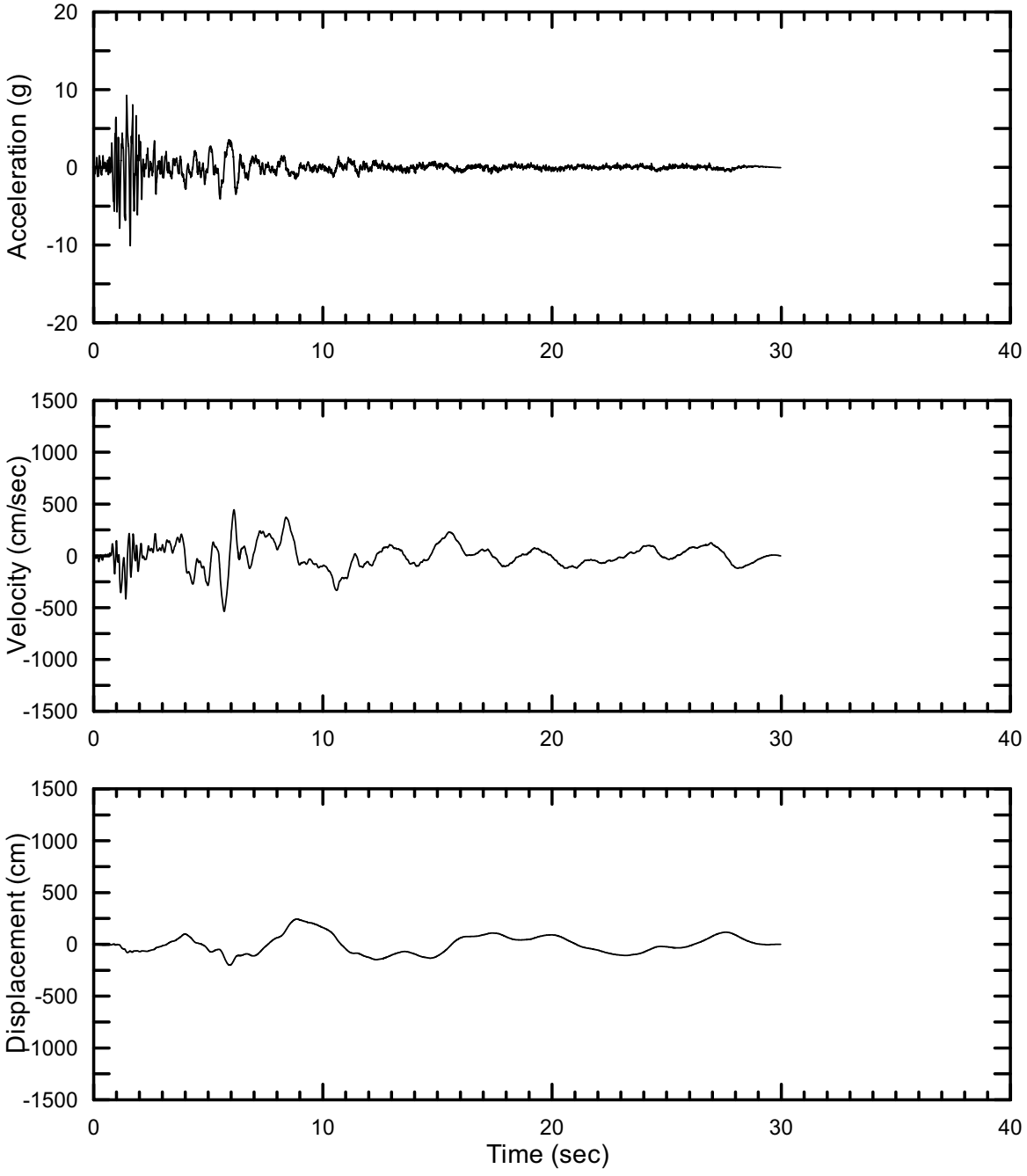

DTN: MO0301TMHSB107.000 [DIRS 164207]

Figure II-220. Point B Horizontal-1 Spectrally Conditioned to Point B Time Histories at an Annual Exceedance Probability of 10^{-7}, Set #9

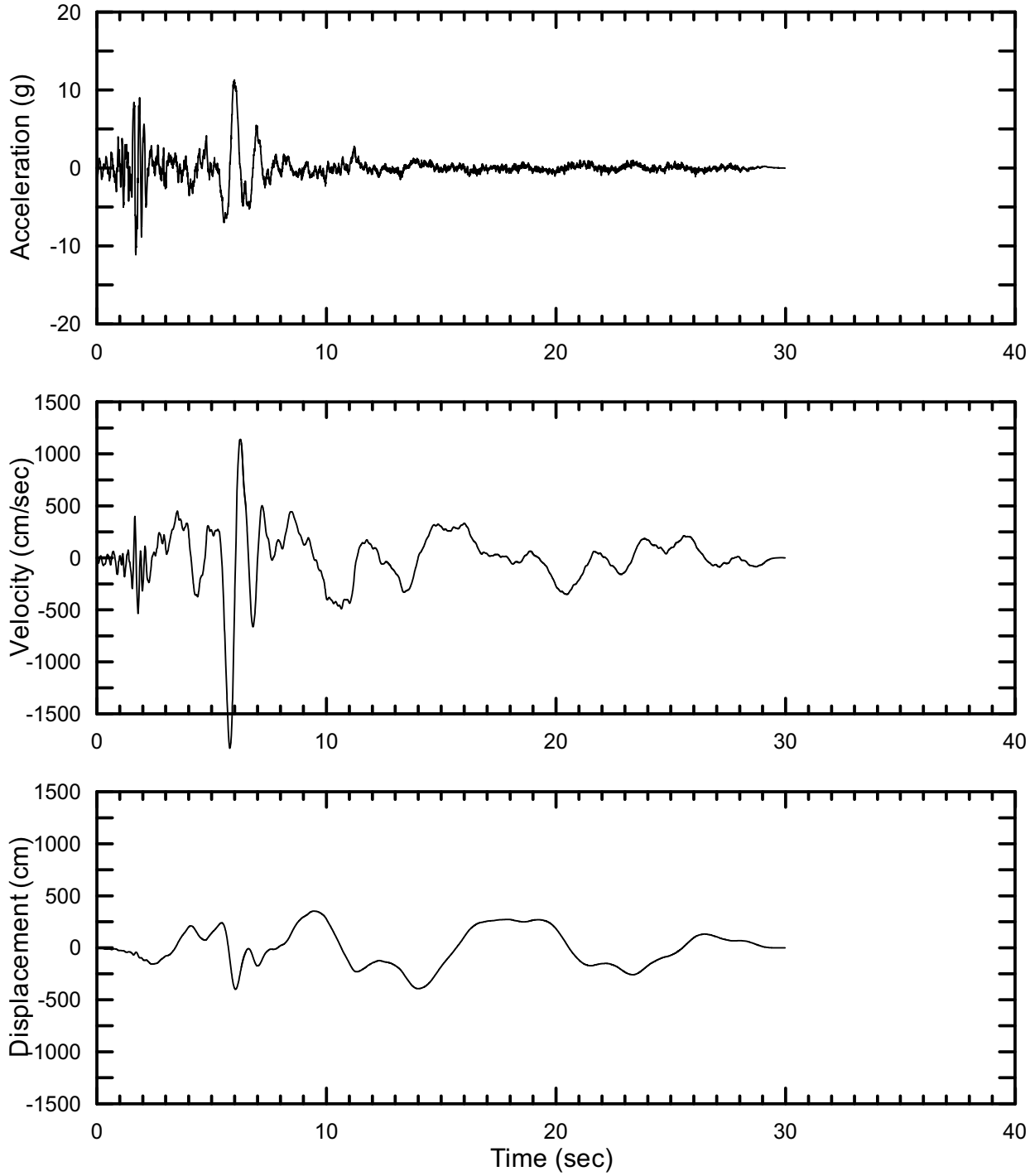

DTN: MO0301TMHSB107.000 [DIRS 164207]

Figure II-221. Point B Horizontal-2 Spectrally Conditioned to Point B Time Histories at an Annual Exceedance Probability of 10^{-7}, Set #9

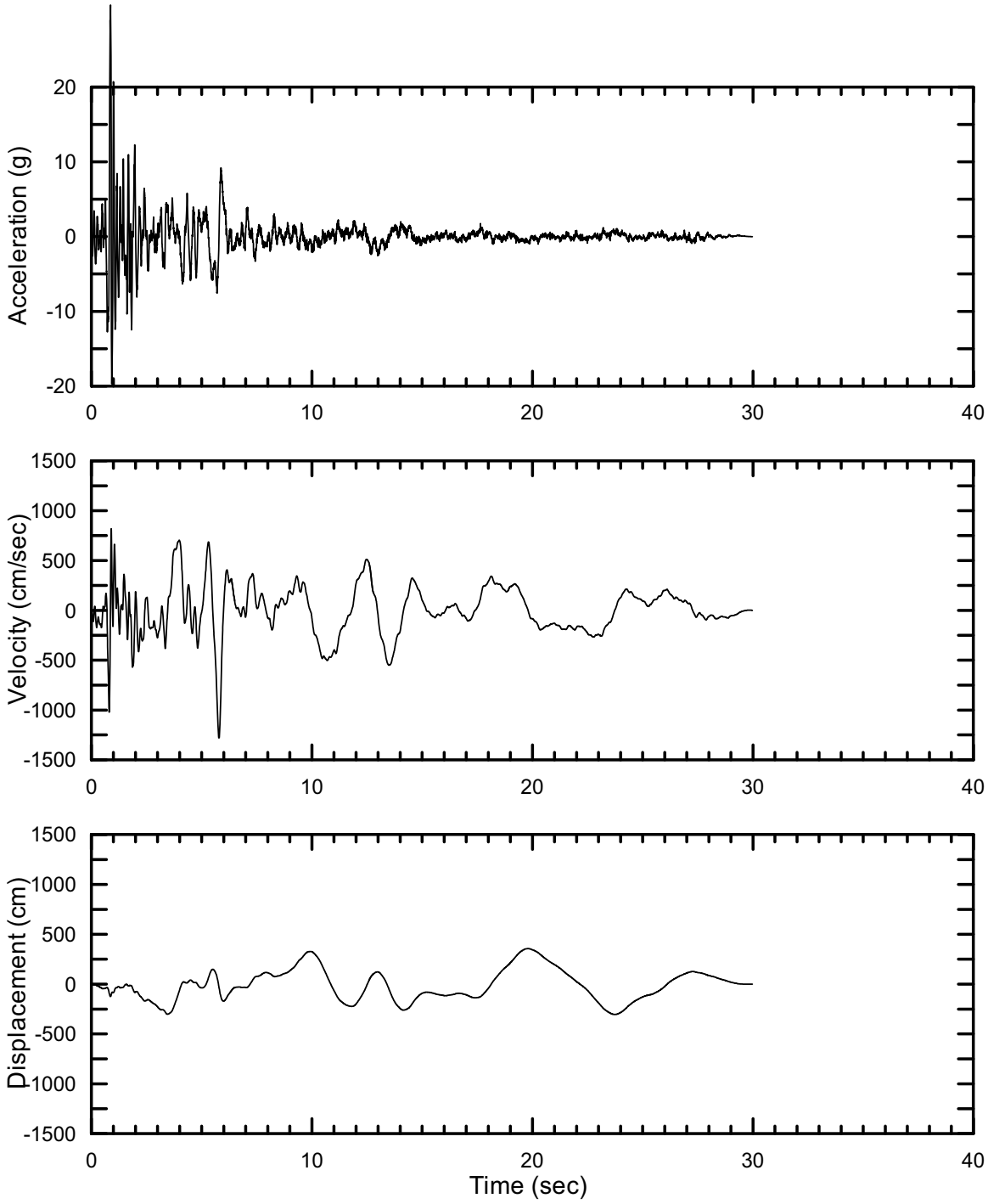

DTN: MO0301TMHSB107.000 [DIRS 164207]

Figure II-222. Point B Vertical Spectrally Conditioned to Point B Time Histories at an Annual Exceedance Probability of 10^{-7}, Set #9

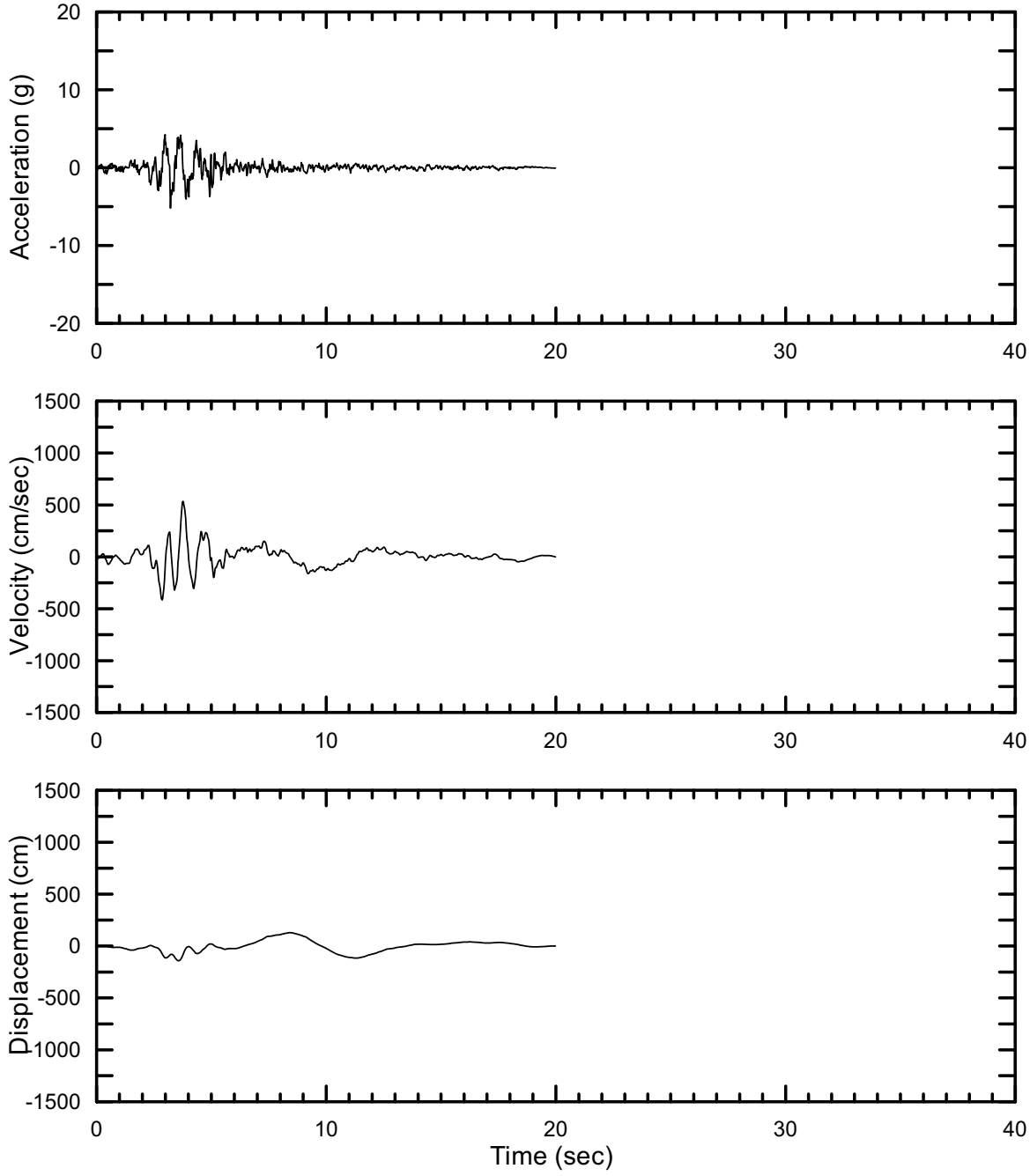

DTN: MO0301TMHSB107.000 [DIRS 164207]

Figure II-223. Point B Horizontal-1 Spectrally Conditioned to Point B Time Histories at an Annual Exceedance Probability of 10^{-7}, Set #10

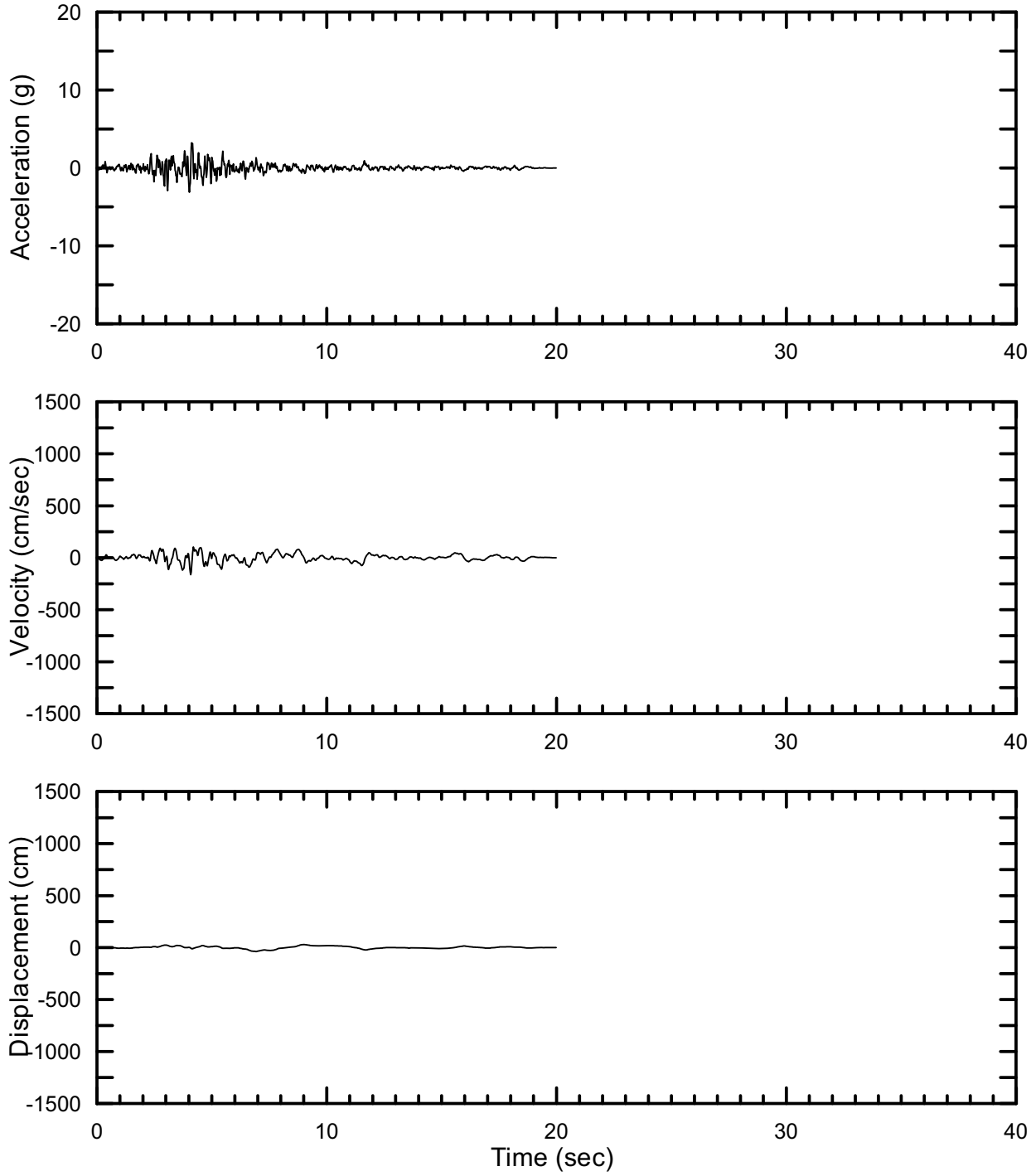

DTN: MO0301TMHSB107.000 [DIRS 164207]

Figure II-224. Point B Horizontal-2 Spectrally Conditioned to Point B Time Histories at an Annual Exceedance Probability of 10^{-7}, Set #10

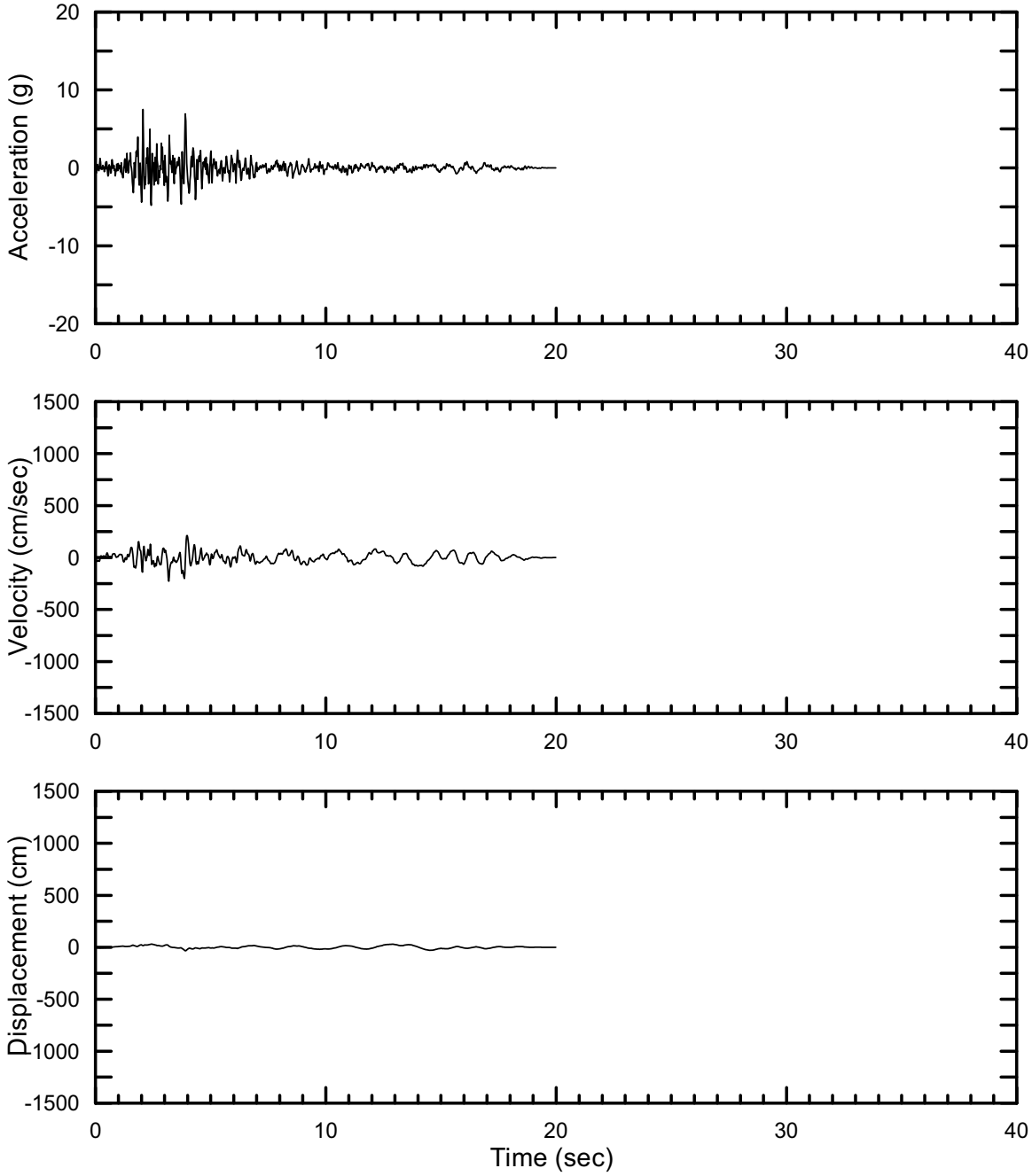

DTN: MO0301TMHSB107.000 [DIRS 164207]

Figure II-225. Point B Vertical Spectrally Conditioned to Point B Time Histories at an Annual Exceedance Probability of 10^{-7}, Set #10

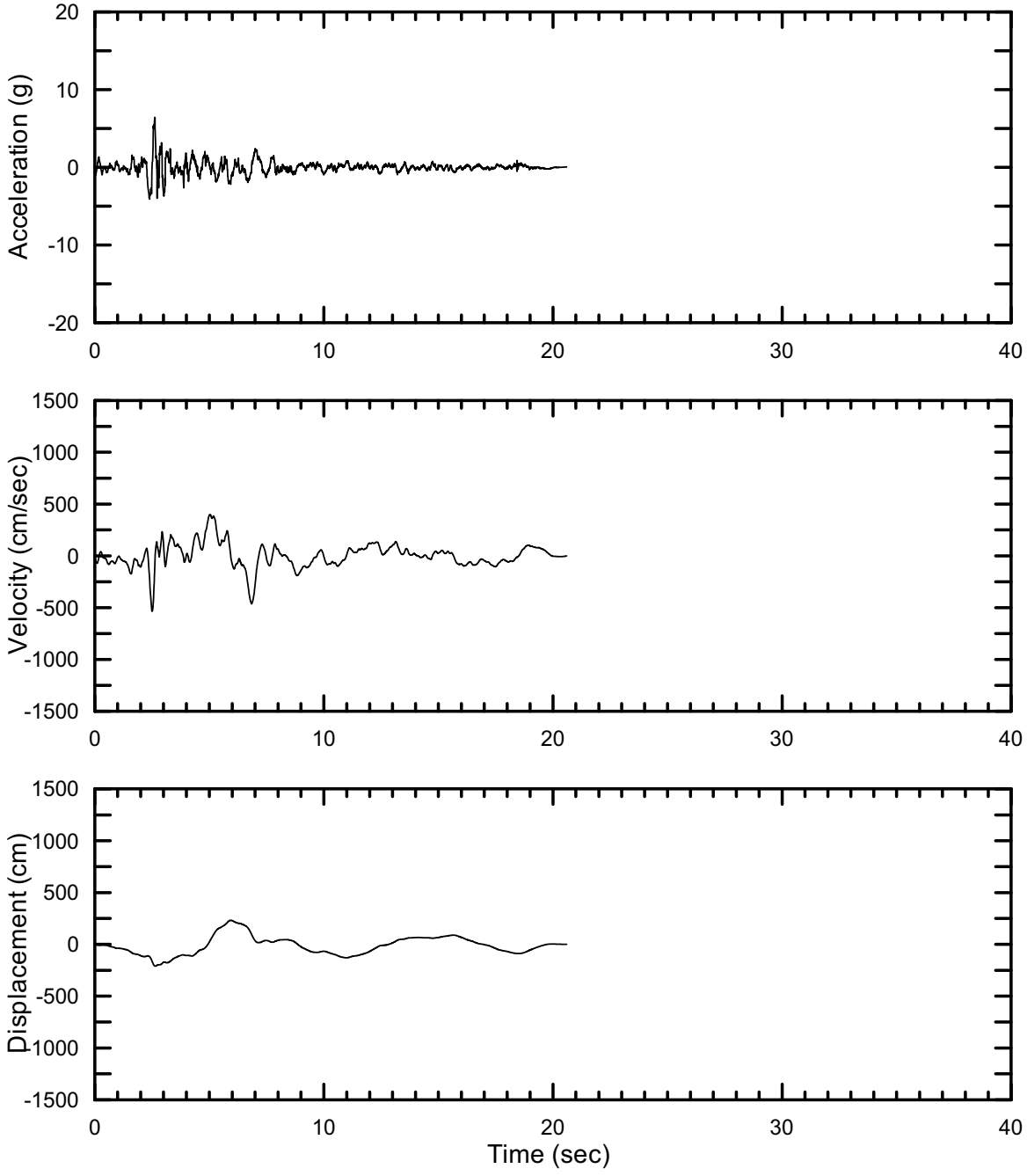

DTN: MO0301TMHSB107.000 [DIRS 164207]

Figure II-226. Point B Horizontal-1 Spectrally Conditioned to Point B Time Histories at an Annual Exceedance Probability of 10^{-7}, Set #11

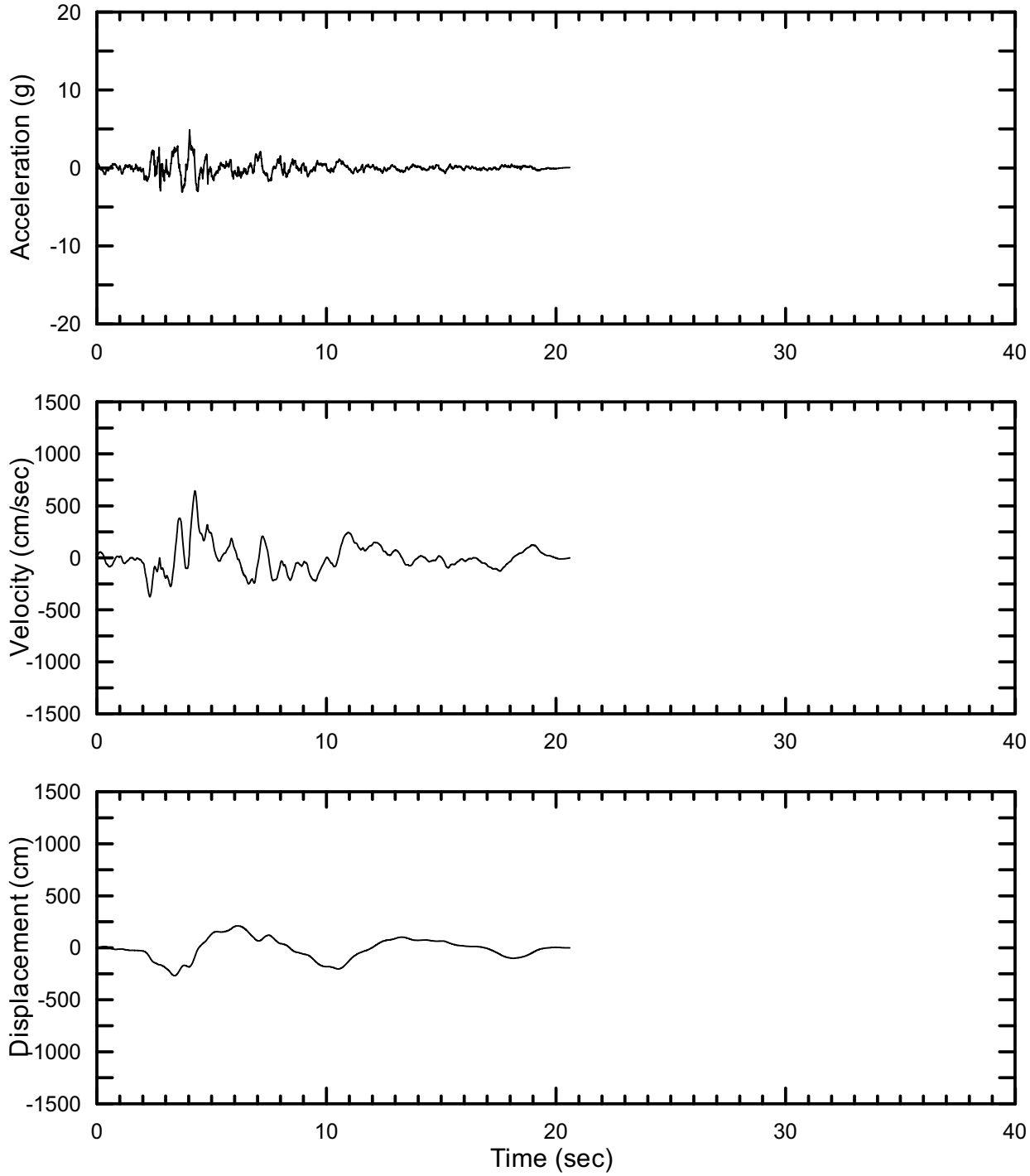

DTN: MO0301TMHSB107.000 [DIRS 164207]

Figure II-227. Point B Horizontal-2 Spectrally Conditioned to Point B Time Histories at an Annual Exceedance Probability of 10^{-7}, Set #11

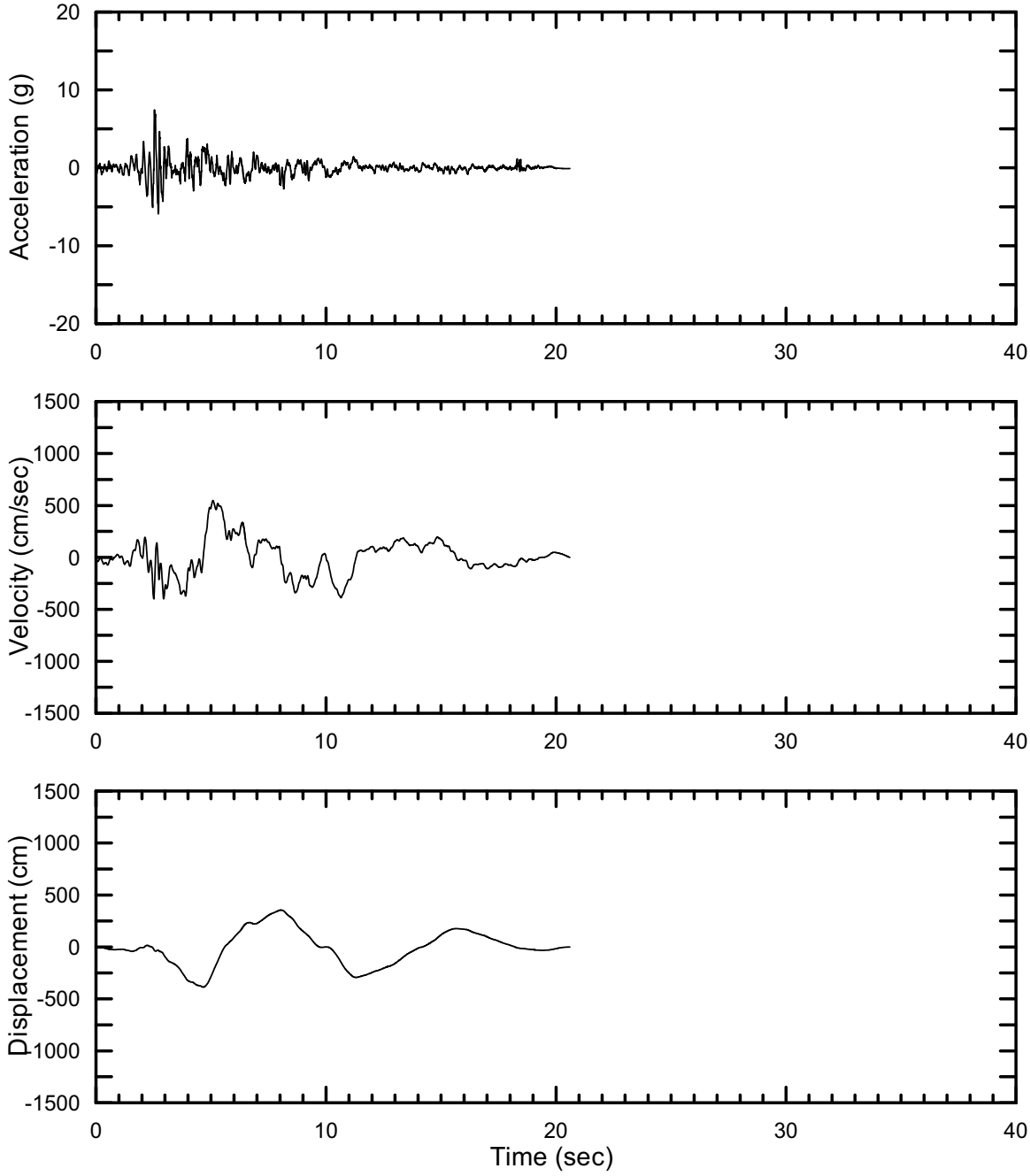

DTN: MO0301TMHSB107.000 [DIRS 164207]

Figure II-228. Point B Vertical Spectrally Conditioned to Point B Time Histories at an Annual Exceedance Probability of 10^{-7}, Set #11

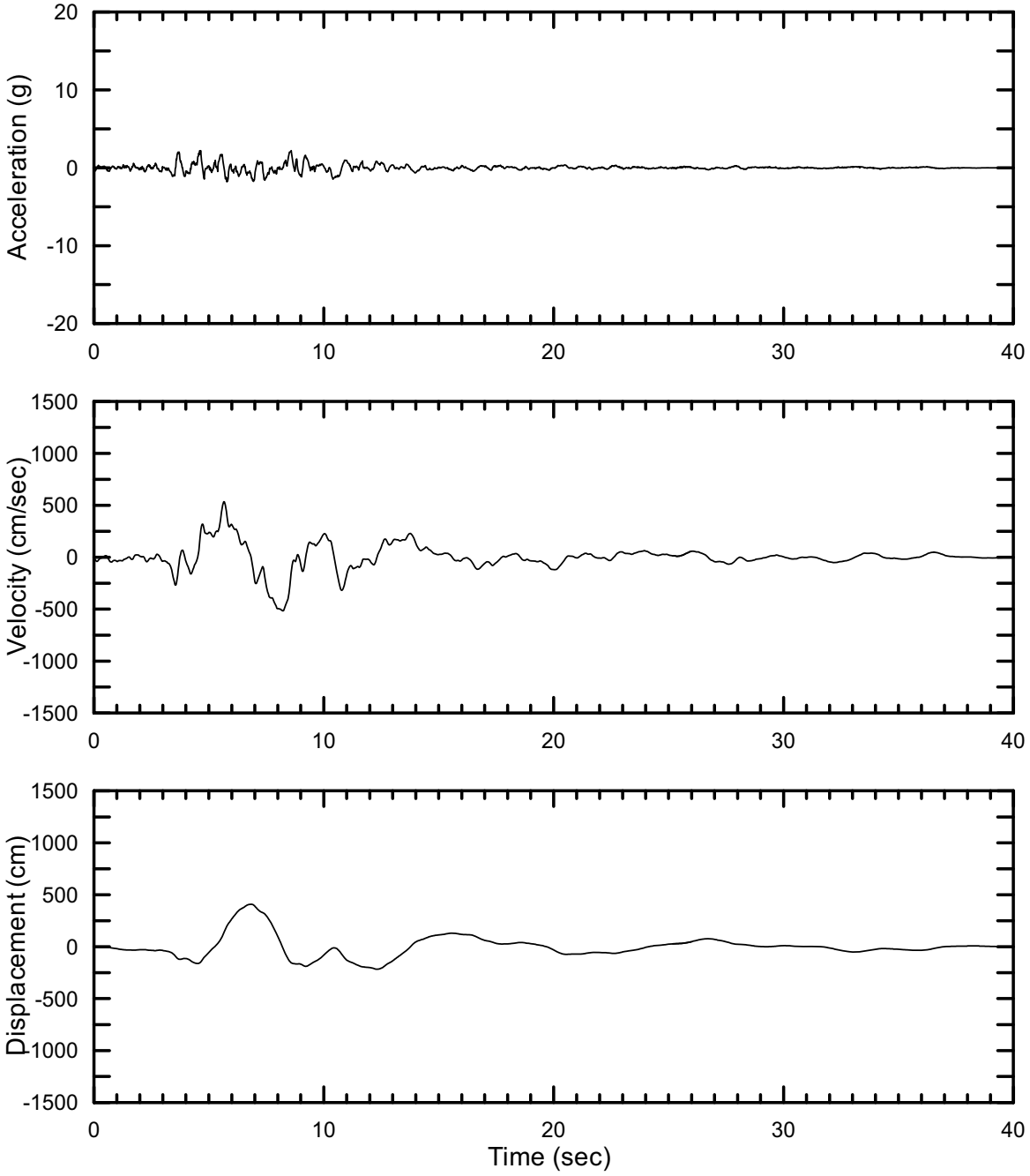

DTN: MO0301TMHSB107.000 [DIRS 164207]

Figure II-229. Point B Horizontal-1 Spectrally Conditioned to Point B Time Histories at an Annual Exceedance Probability of 10^{-7}, Set #12

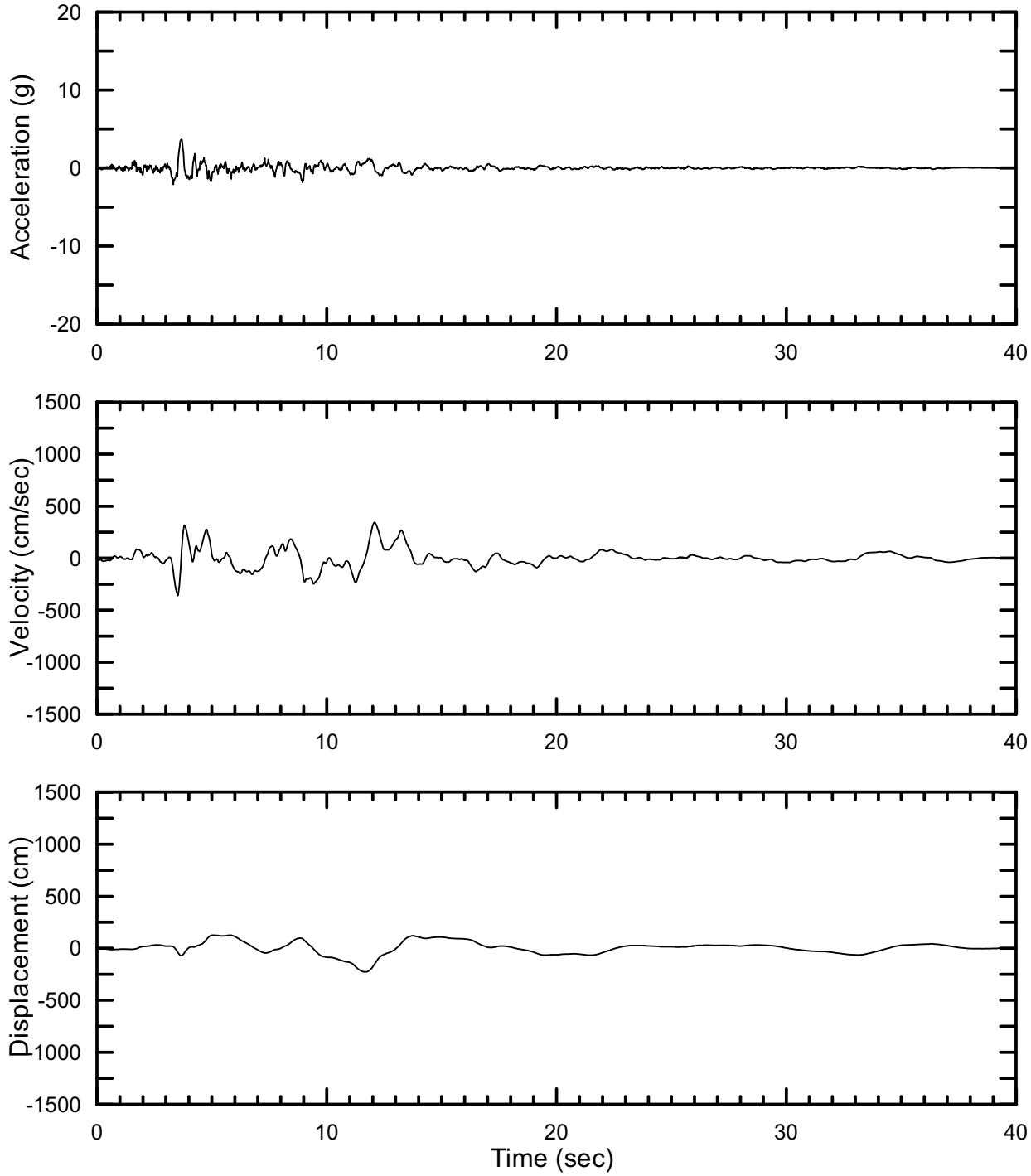

DTN: MO0301TMHSB107.000 [DIRS 164207]

Figure II-230. Point B Horizontal-2 Spectrally Conditioned to Point B Time Histories at an Annual Exceedance Probability of 10^{-7}, Set #12

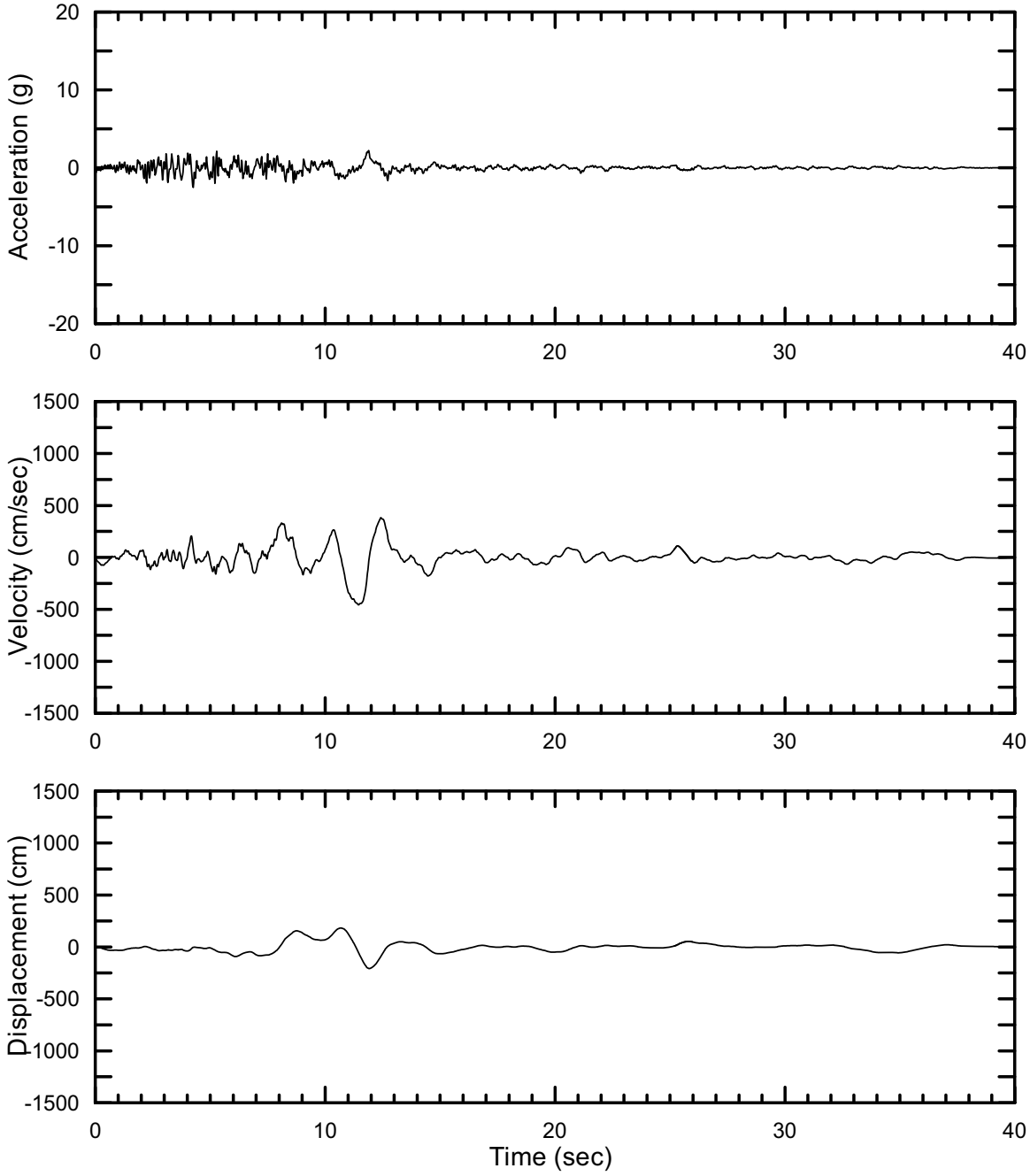

DTN: MO0301TMHSB107.000 [DIRS 164207]

Figure II-231. Point B Vertical Spectrally Conditioned to Point B Time Histories at an Annual Exceedance Probability of 10^{-7}, Set #12

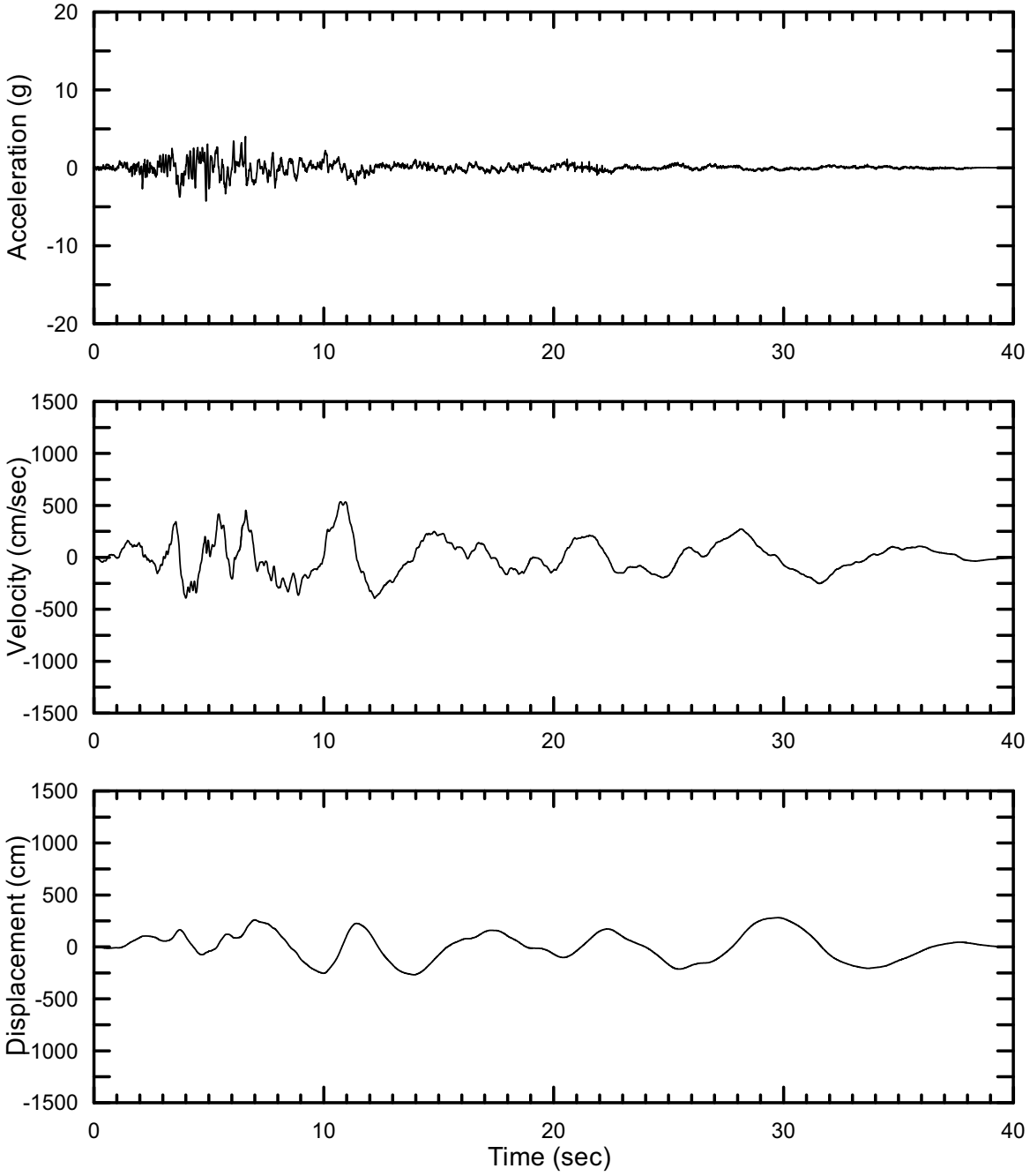

DTN: MO0301TMHSB107.000 [DIRS 164207]

Figure II-232. Point B Horizontal-1 Spectrally Conditioned to Point B Time Histories at an Annual Exceedance Probability of 10^{-7}, Set #13

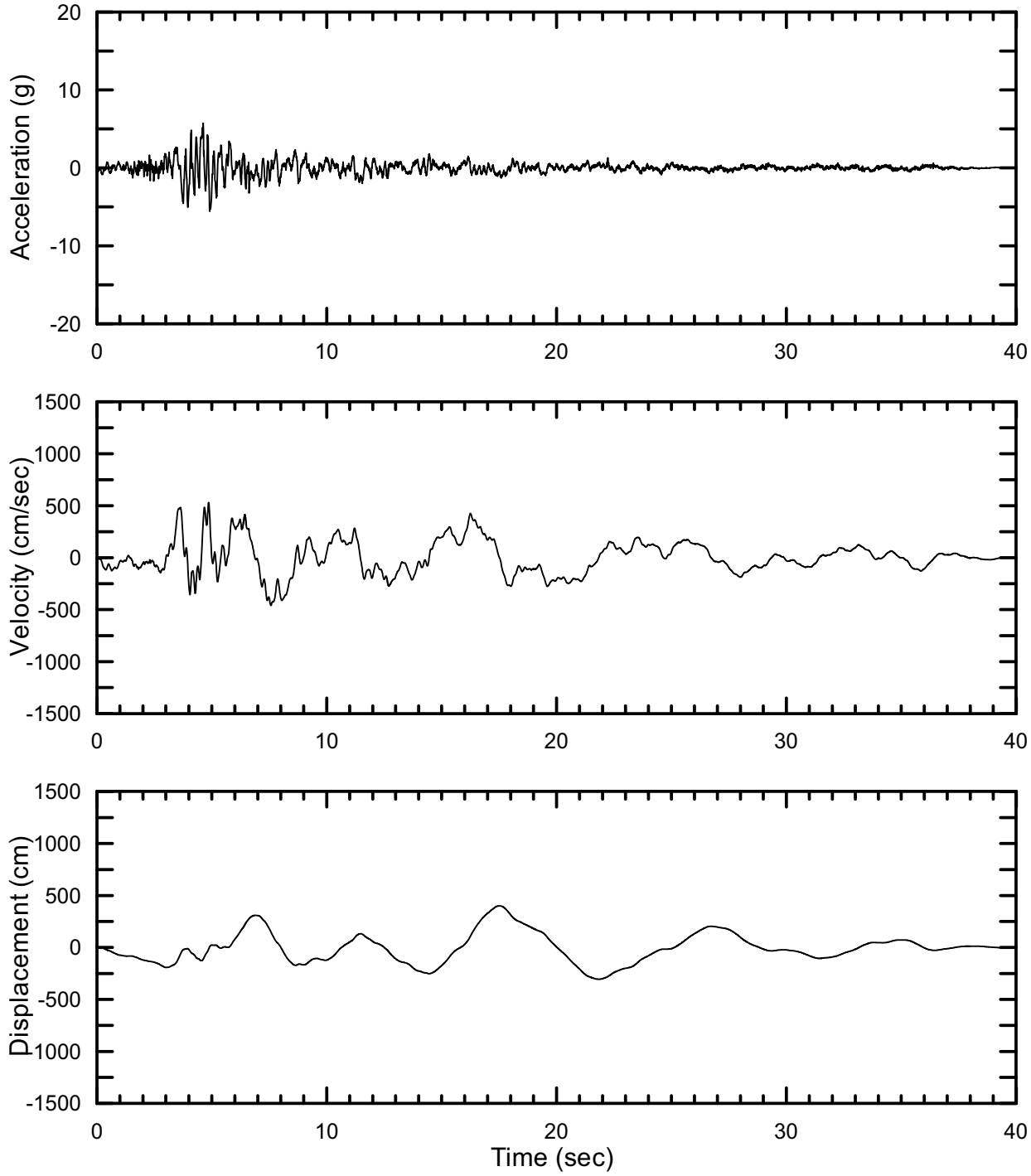

DTN: MO0301TMHSB107.000 [DIRS 164207]

Figure II-233. Point B Horizontal-2 Spectrally Conditioned to Point B Time Histories at an Annual Exceedance Probability of 10^{-7}, Set #13

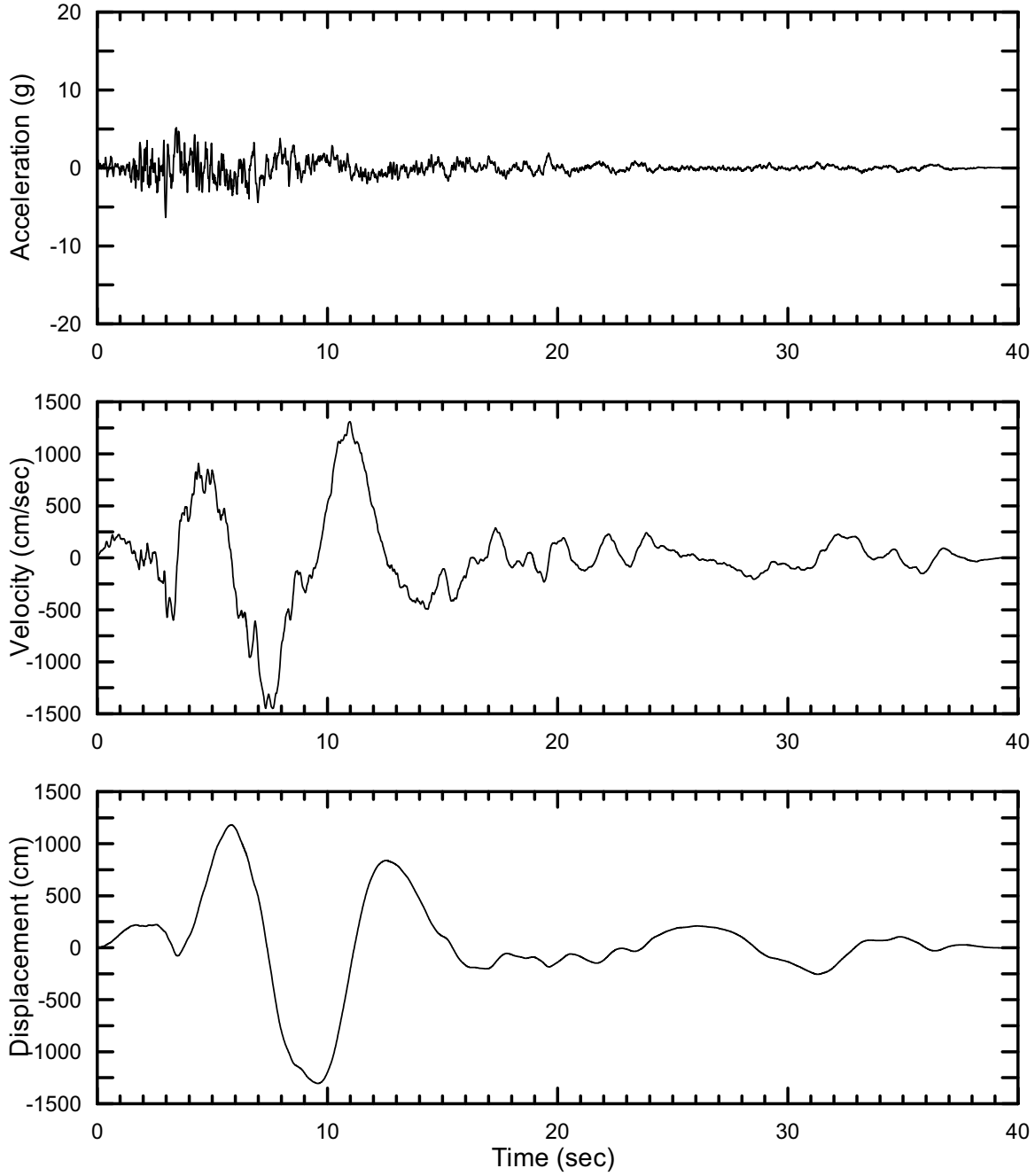

DTN: MO0301TMHSB107.000 [DIRS 164207]

Figure II-234. Point B Vertical Spectrally Conditioned to Point B Time Histories at an Annual Exceedance Probability of 10^{-7}, Set #13

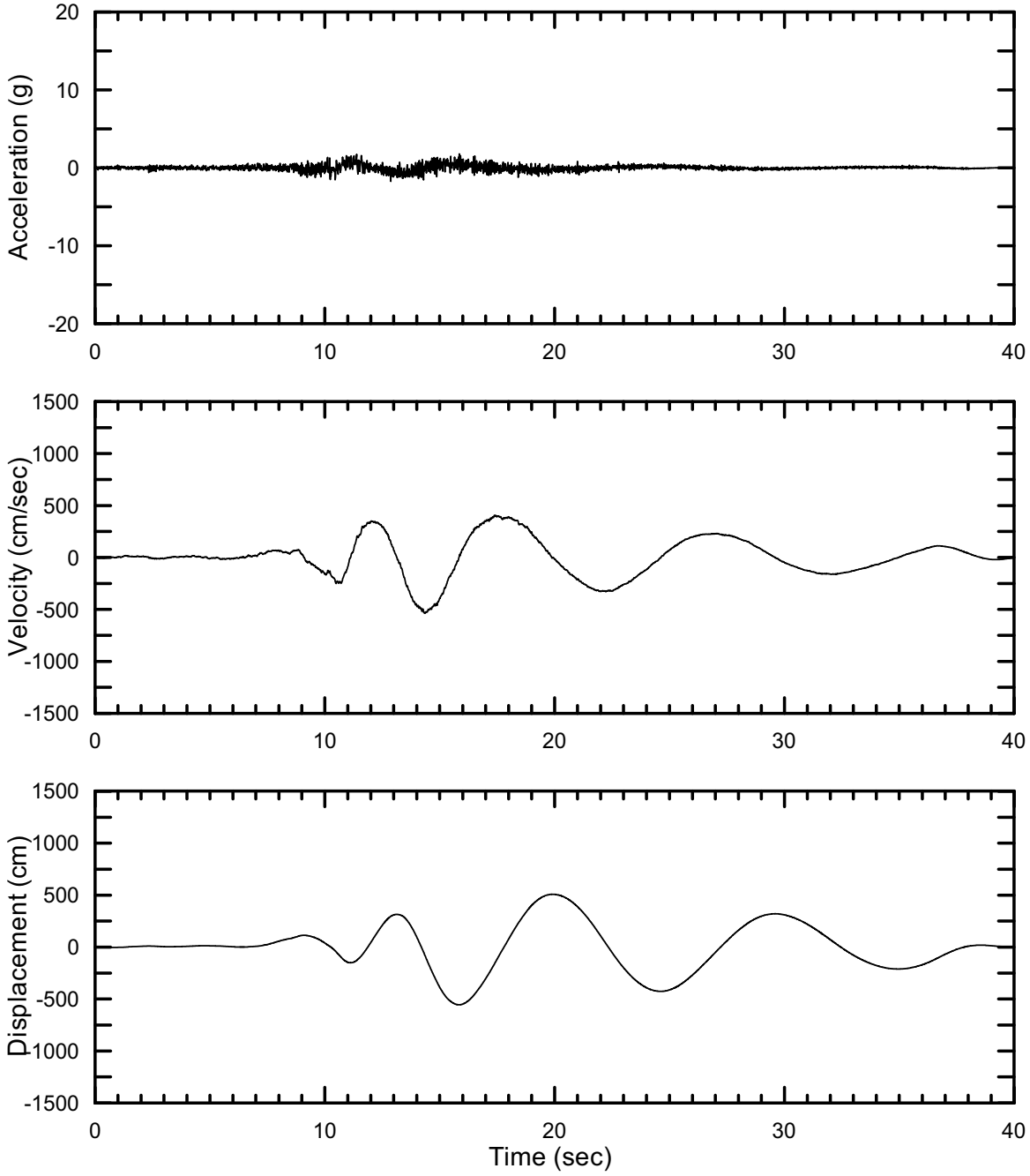

DTN: MO0301TMHSB107.000 [DIRS 164207]

Figure II-235. Point B Horizontal-1 Spectrally Conditioned to Point B Time Histories at an Annual Exceedance Probability of 10^{-7}, Set #14

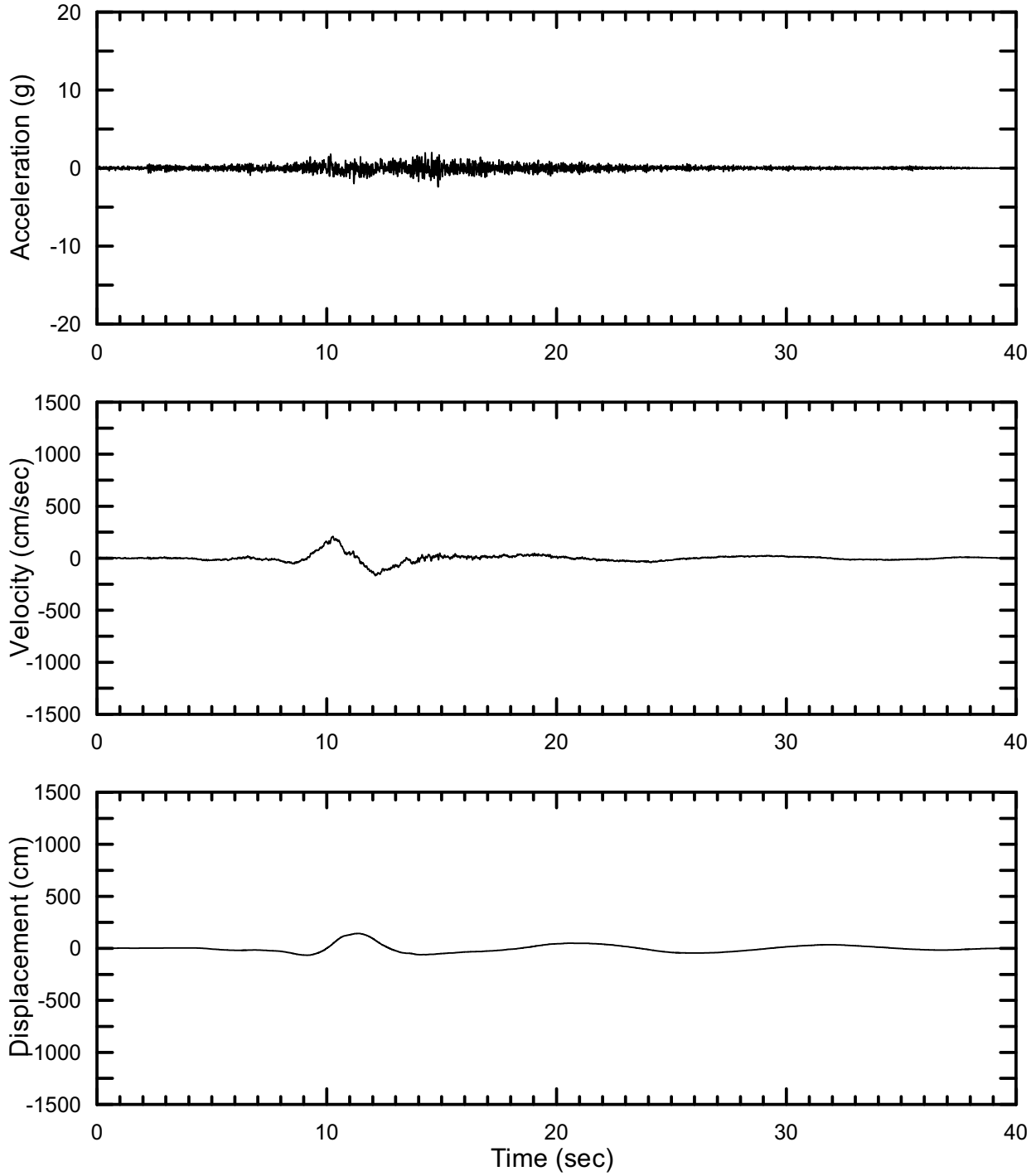

DTN: MO0301TMHSB107.000 [DIRS 164207]

Figure II-236. Point B Horizontal-2 Spectrally Conditioned to Point B Time Histories at an Annual Exceedance Probability of 10^{-7}, Set #14

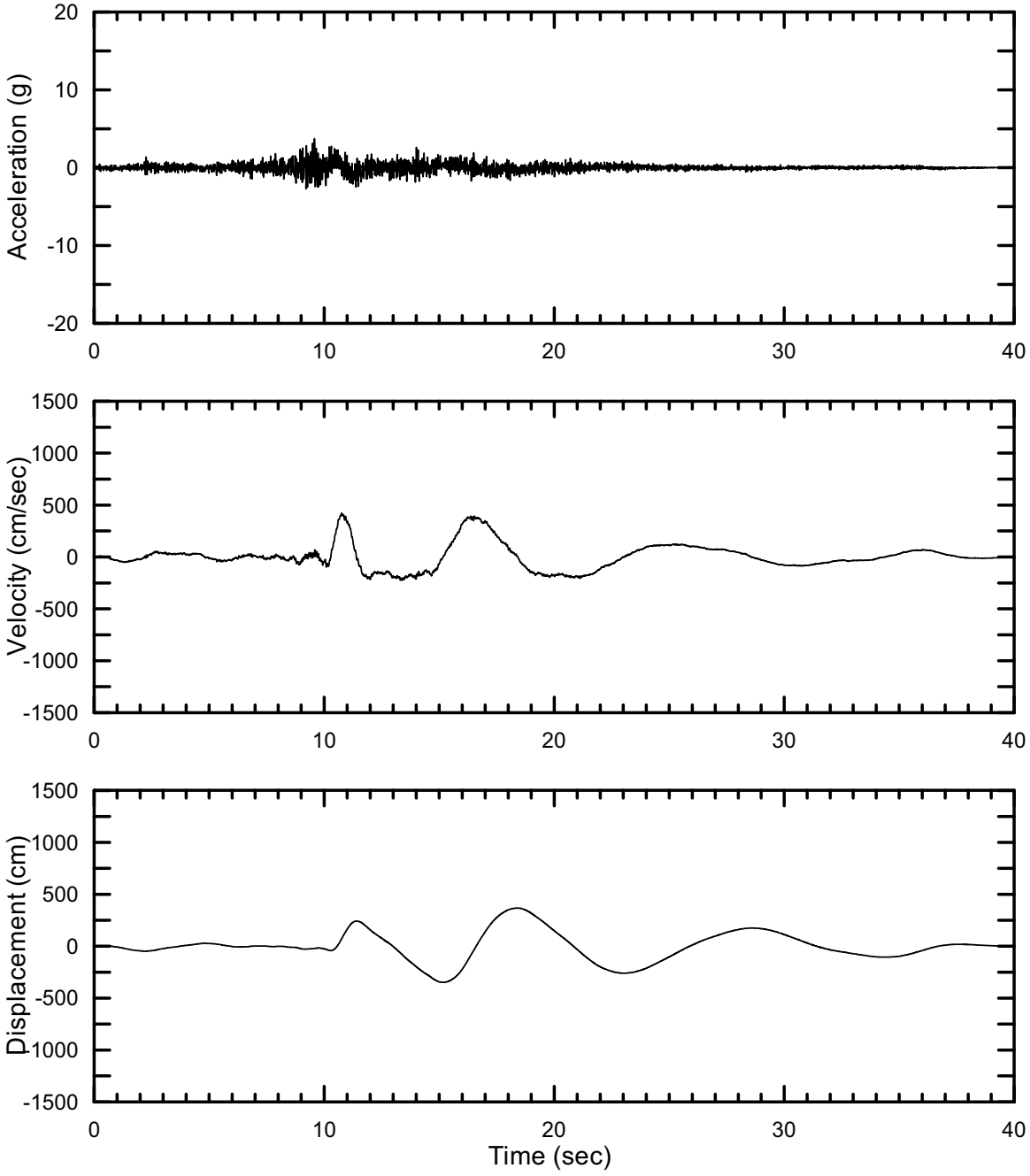

DTN: MO0301TMHSB107.000 [DIRS 164207]

Figure II-237. Point B Vertical Spectrally Conditioned to Point B Time Histories at an Annual Exceedance Probability of 10^{-7}, Set #14

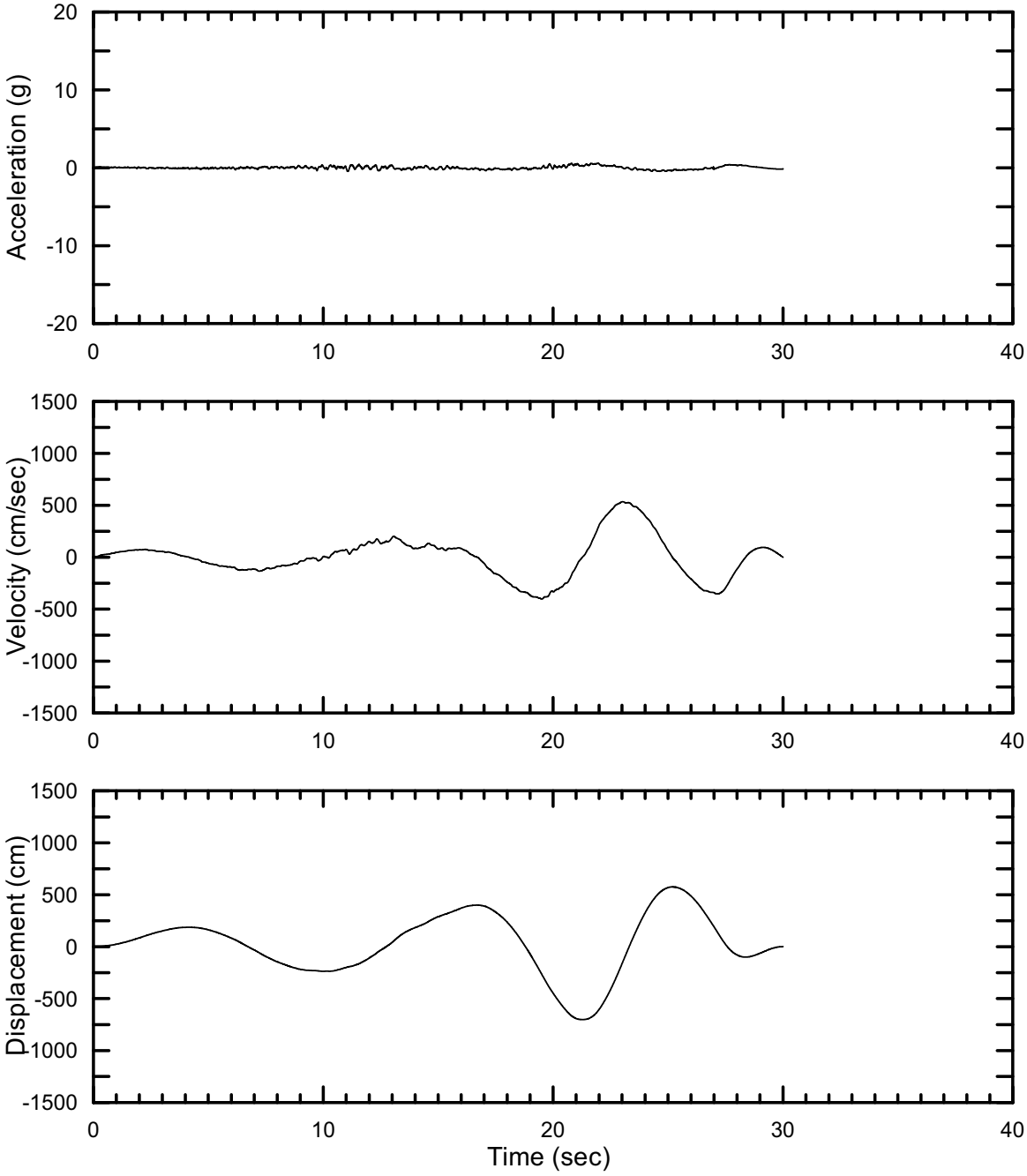

DTN: MO0301TMHSB107.000 [DIRS 164207]

Figure II-238. Point B Horizontal-1 Spectrally Conditioned to Point B Time Histories at an Annual Exceedance Probability of 10^{-7}, Set #15

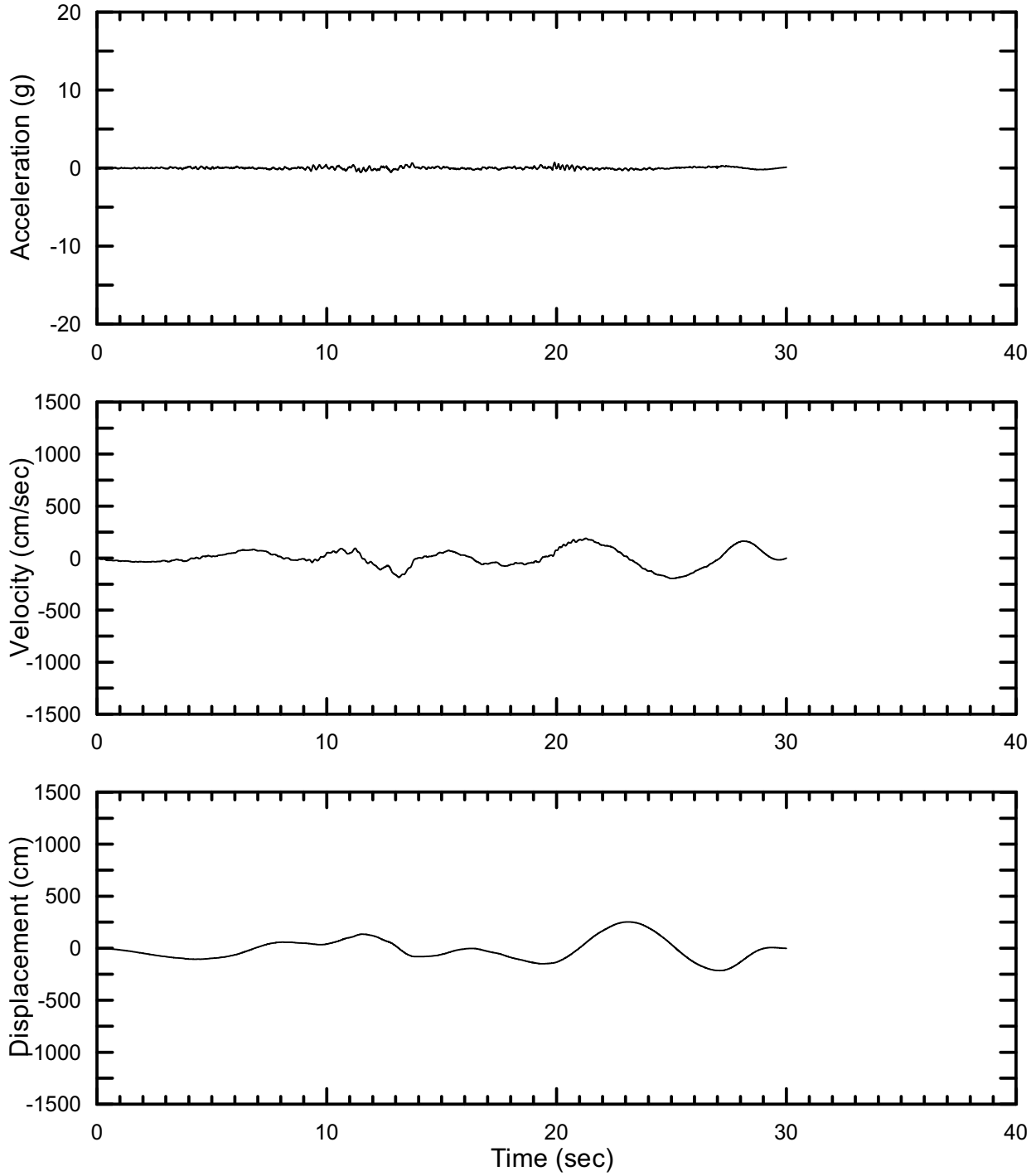

DTN: MO0301TMHSB107.000 [DIRS 164207]

Figure II-239. Point B Horizontal-2 Spectrally Conditioned to Point B Time Histories at an Annual Exceedance Probability of 10^{-7}, Set #15

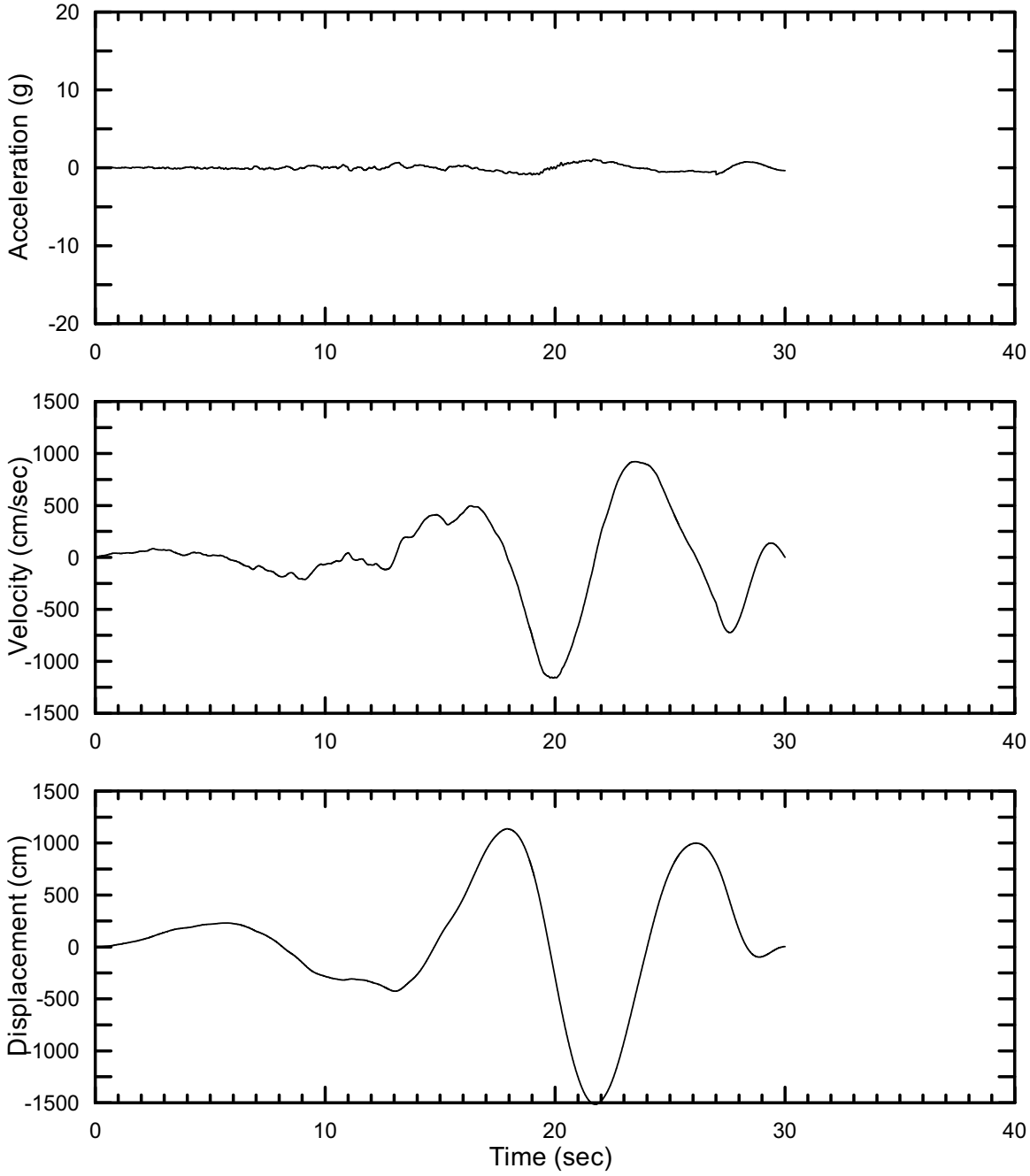

DTN: MO0301TMHSB107.000 [DIRS 164207]

Figure II-240. Point B Vertical Spectrally Conditioned to Point B Time Histories at an Annual Exceedance Probability of 10^{-7}, Set #15

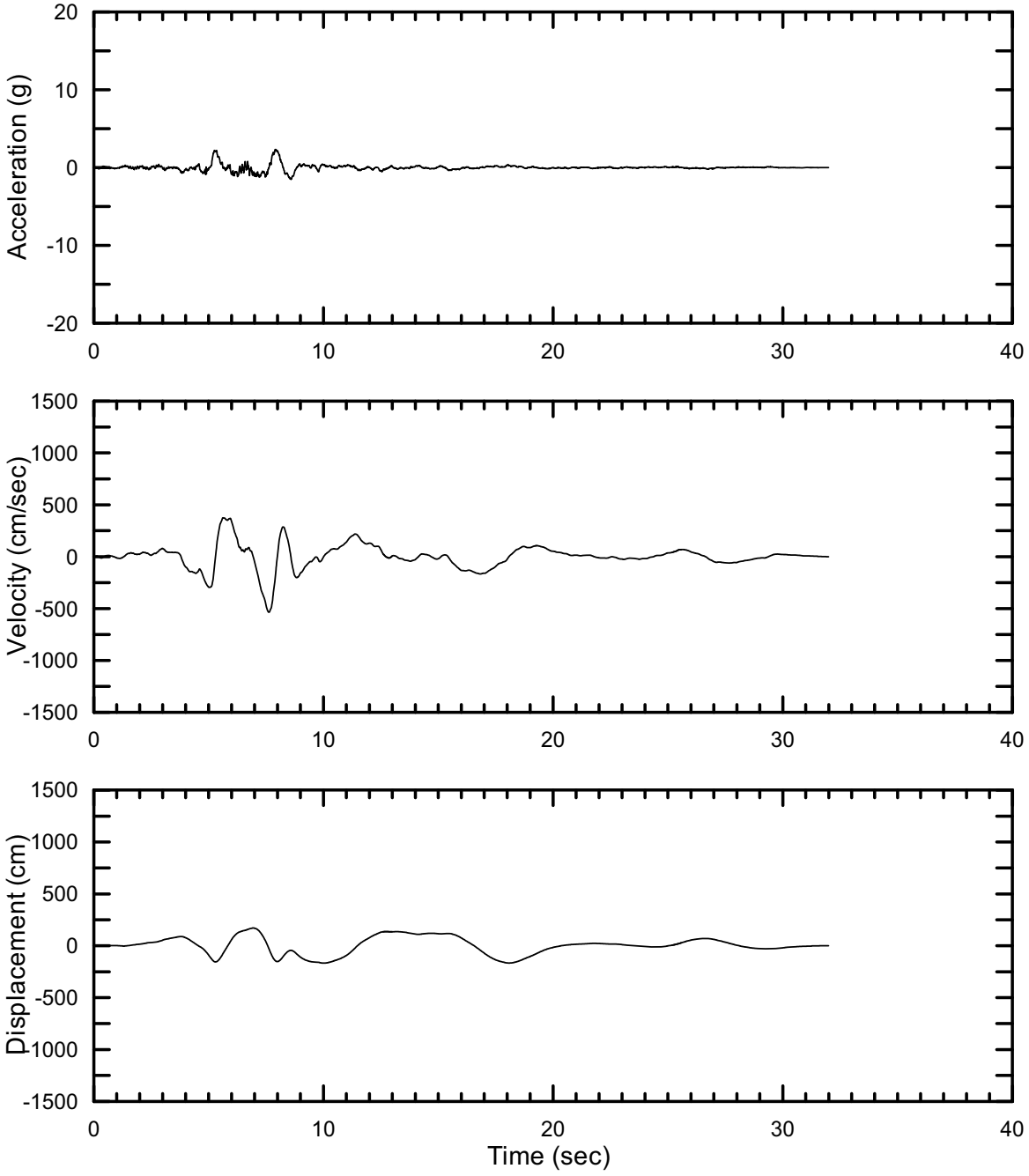

DTN: MO0301TMHSB107.000 [DIRS 164207]

Figure II-241. Point B Horizontal-1 Spectrally Conditioned to Point B Time Histories at an Annual Exceedance Probability of 10^{-7}, Set #16

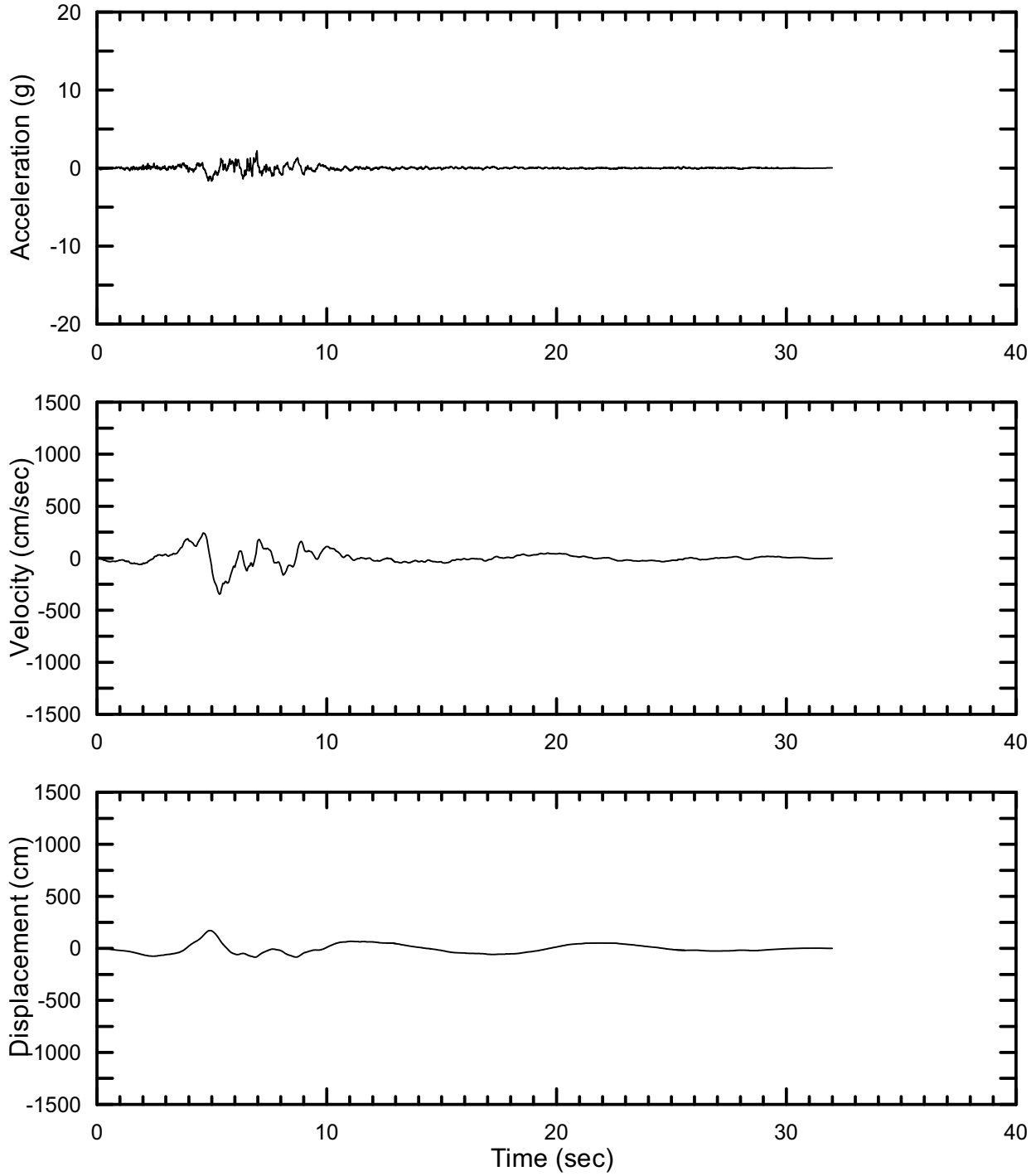

DTN: MO0301TMHSB107.000 [DIRS 164207]

Figure II-242. Point B Horizontal-2 Spectrally Conditioned to Point B Time Histories at an Annual Exceedance Probability of 10^{-7}, Set #16

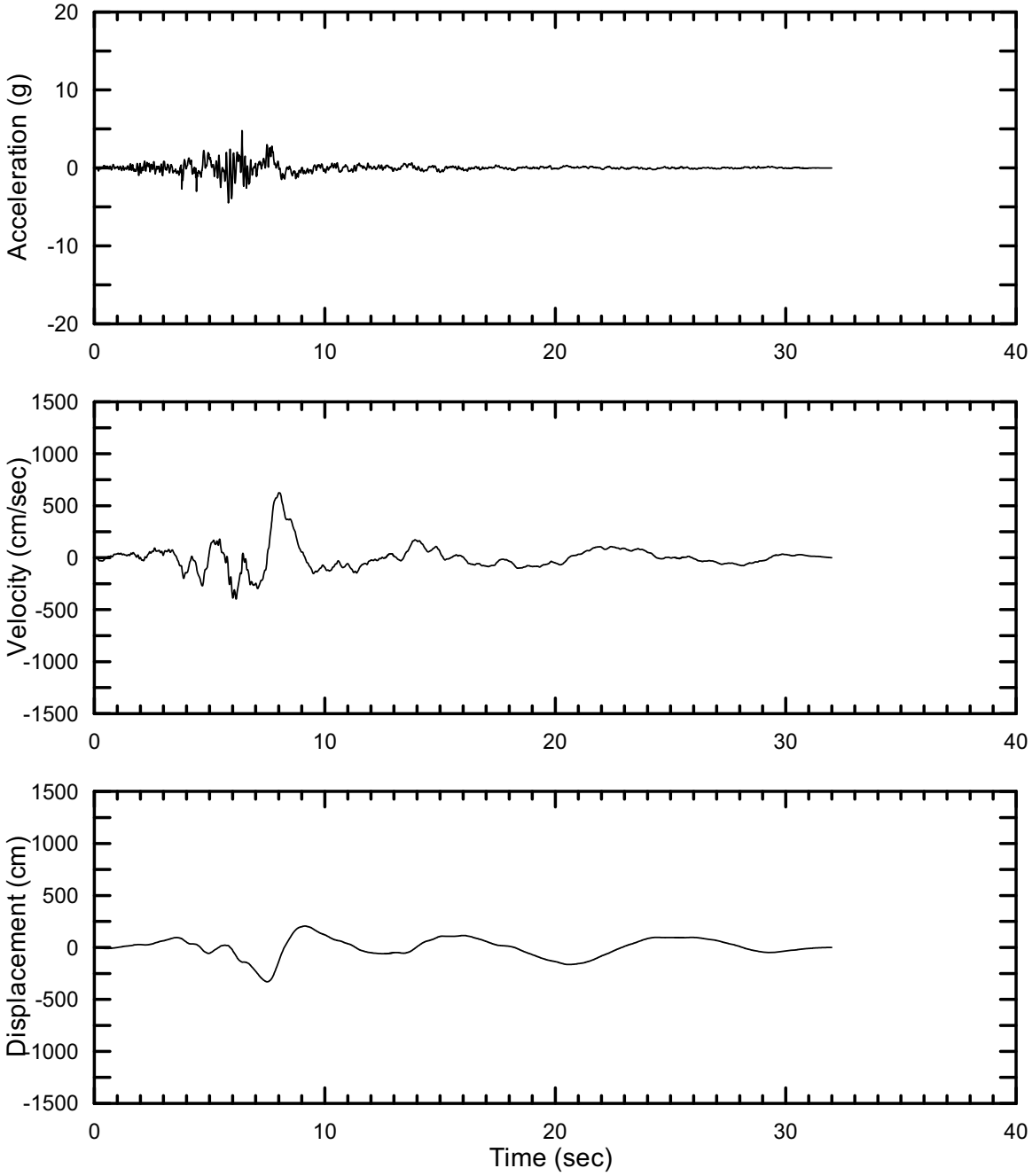

DTN: MO0301TMHSB107.000 [DIRS 164207]

Figure II-243. Point B Vertical Spectrally Conditioned to Point B Time Histories at an Annual Exceedance Probability of 10^{-7}, Set #16

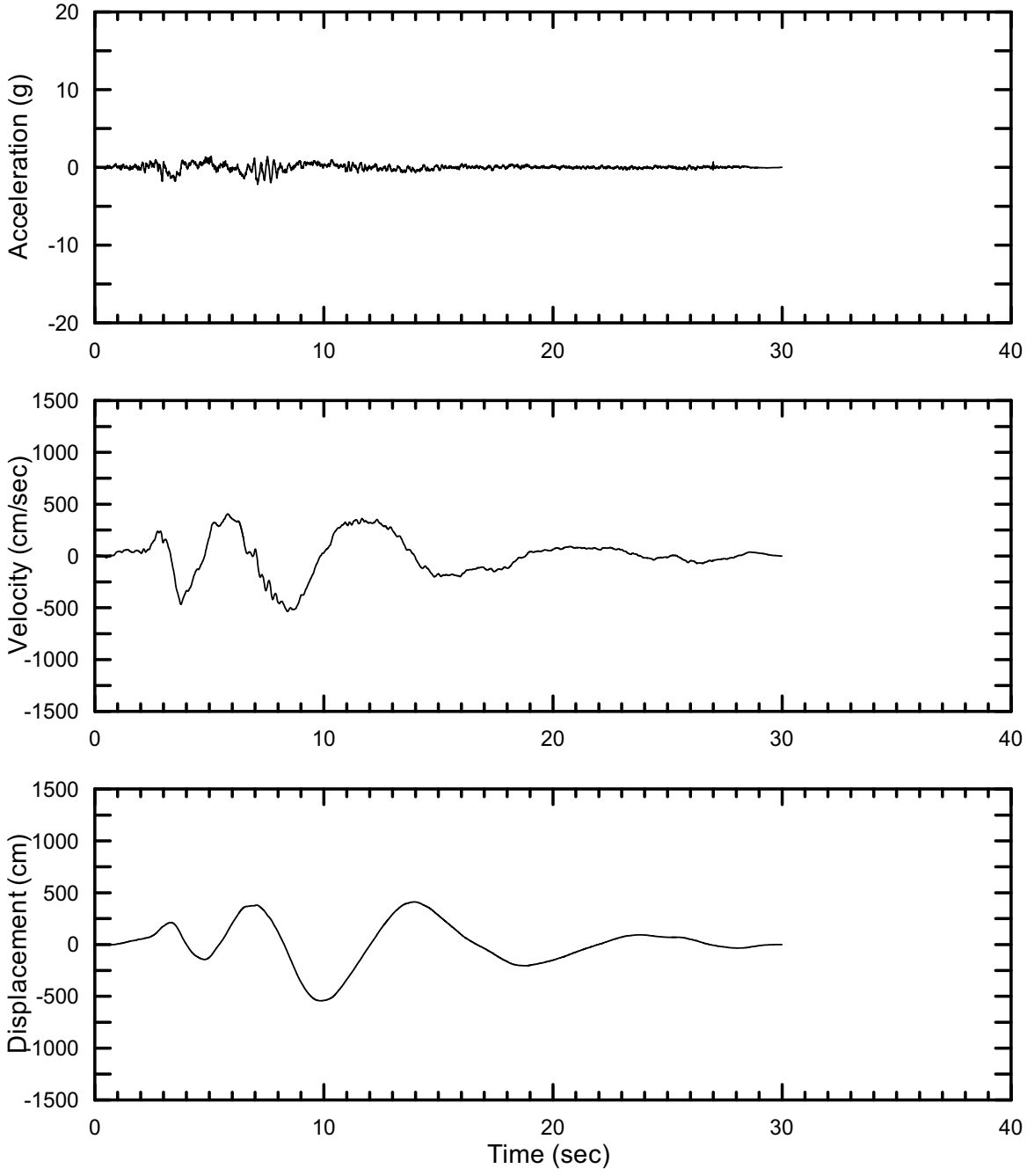

DTN: MO0301TMHSB107.000 [DIRS 164207]

Figure II-244. Point B Horizontal-1 Spectrally Conditioned to Point B Time Histories at an Annual Exceedance Probability of 10^{-7}, Set #17

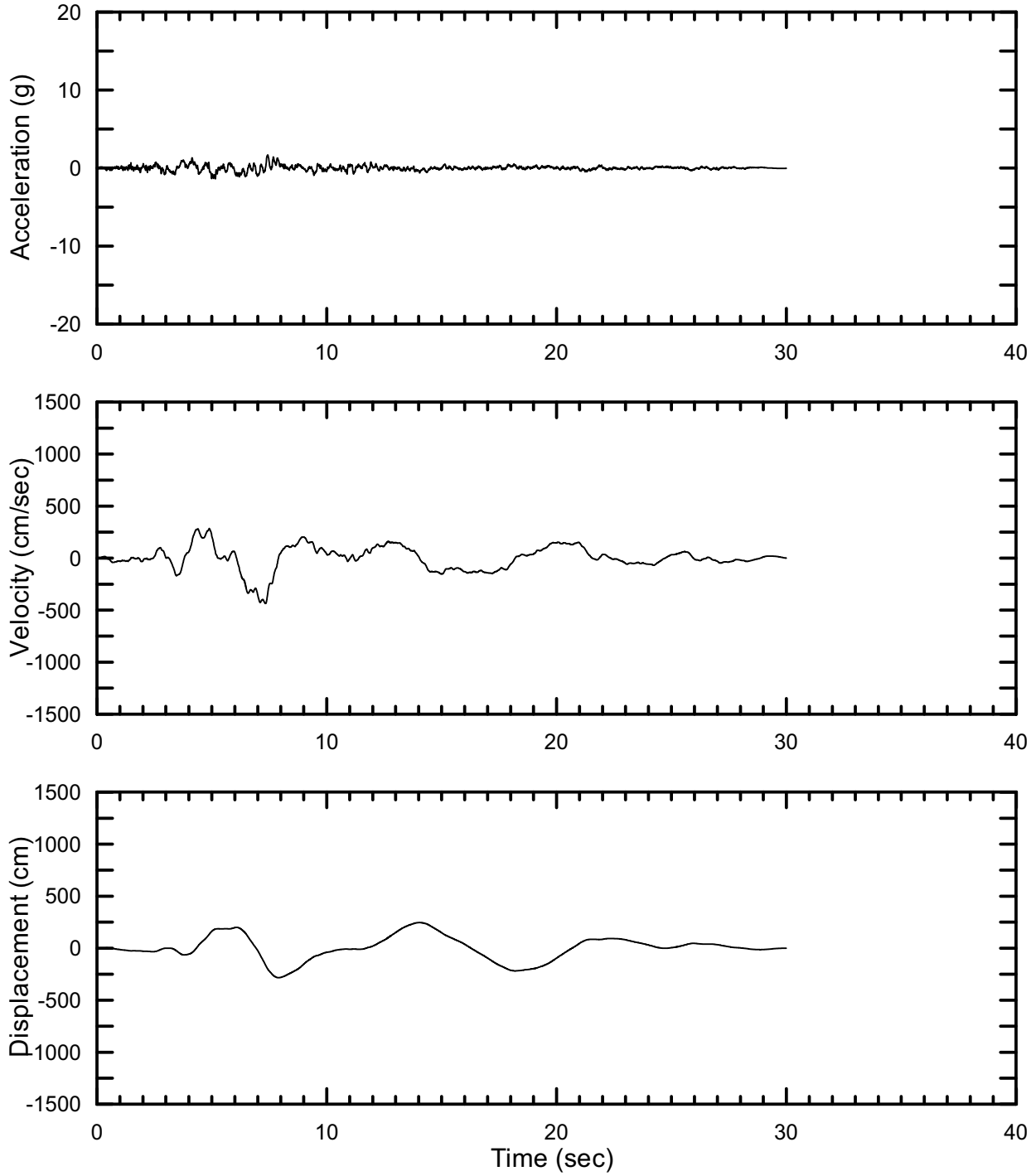

DTN: MO0301TMHSB107.000 [DIRS 164207]

Figure II-245. Point B Horizontal-2 Spectrally Conditioned to Point B Time Histories at an Annual Exceedance Probability of 10^{-7}, Set #17

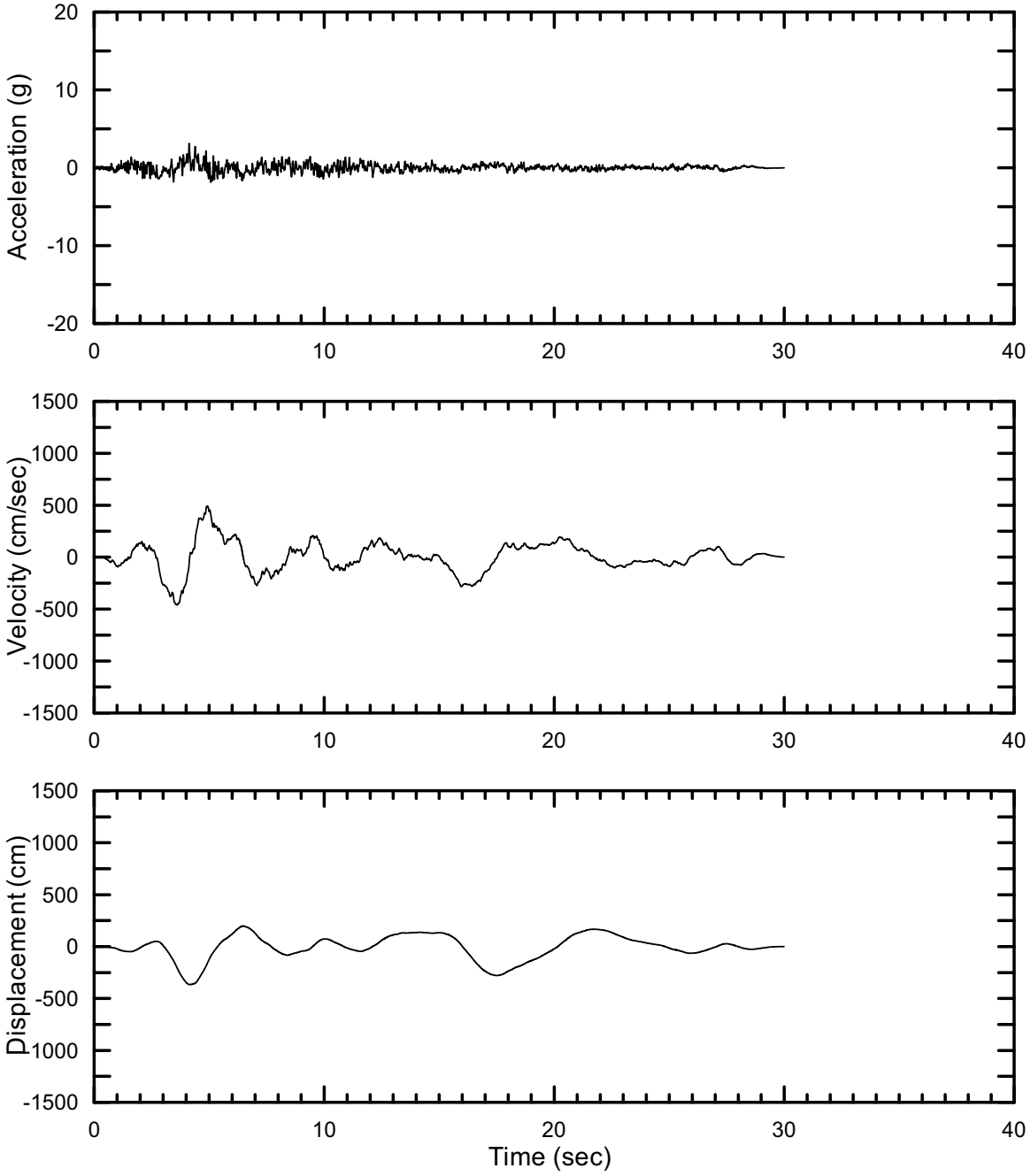

DTN: MO0301TMHSB107.000 [DIRS 164207]

Figure II-246. Point B Vertical Spectrally Conditioned to Point B Time Histories at an Annual Exceedance Probability of 10^{-7}, Set #17

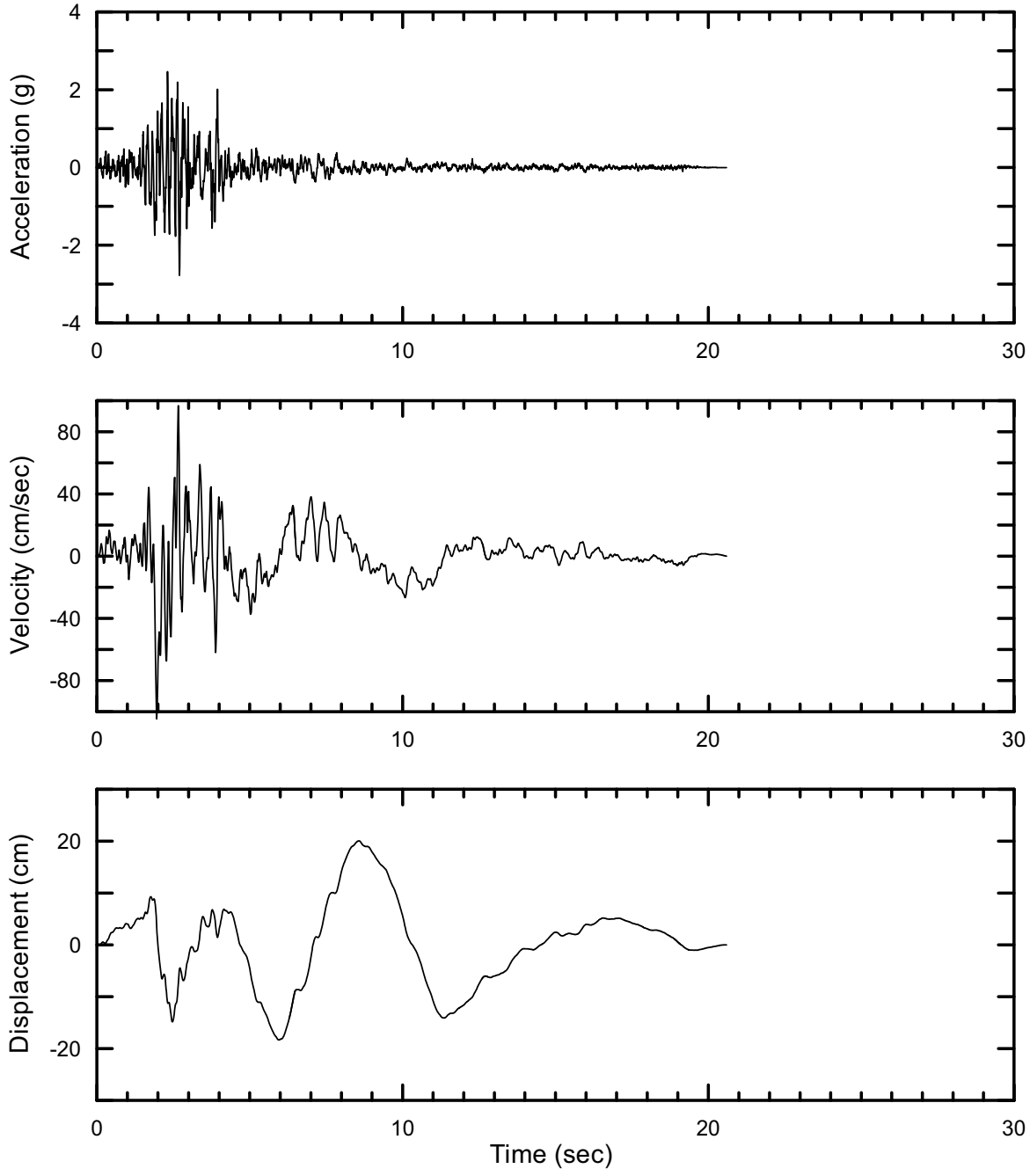

DTN: MO0402AVDTM105.001 [DIRS 168890]

Figure II-247. Point B Horizontal-1 Time Histories at an Annual Exceedance Probability of 10^{-5}, Set #1

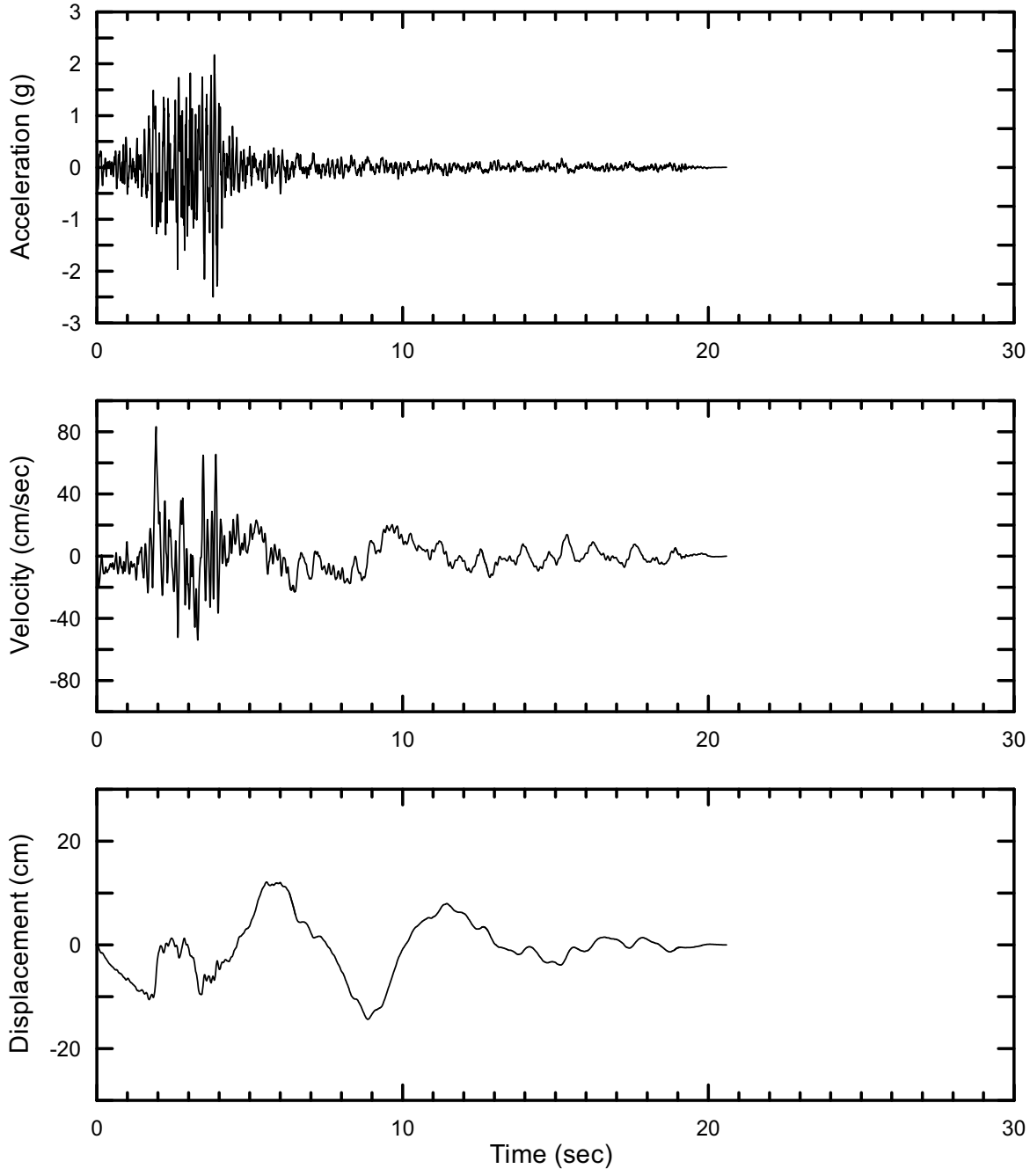

DTN: MO0402AVDTM105.001 [DIRS 168890]

Figure II-248. Point B Horizontal-2 Time Histories at an Annual Exceedance Probability of 10^{-5}, Set #1

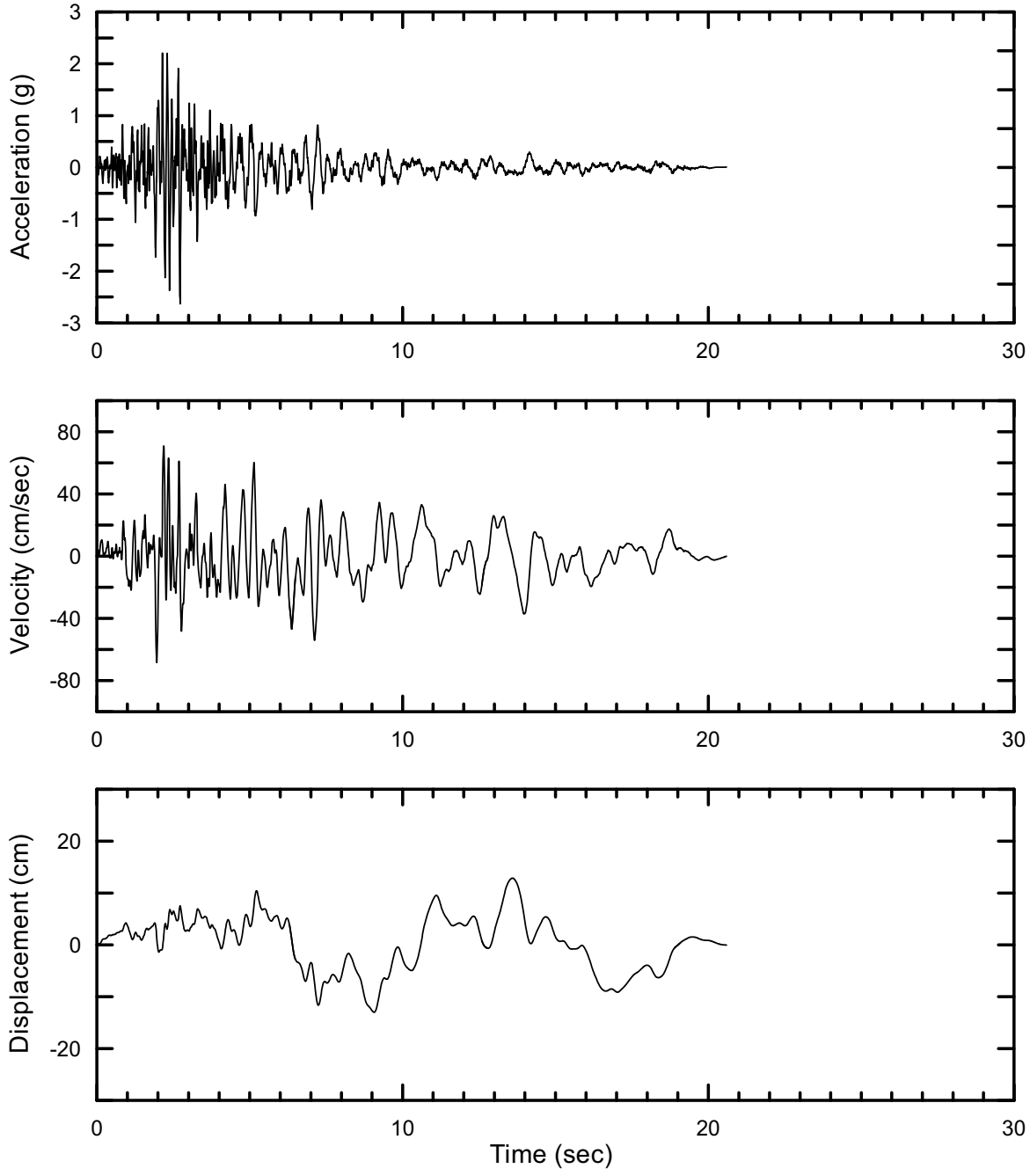

DTN: MO0402AVDTM105.001 [DIRS 168890]

Figure II-249. Point B Vertical Time Histories at an Annual Exceedance Probability of 10^{-5}, Set #1

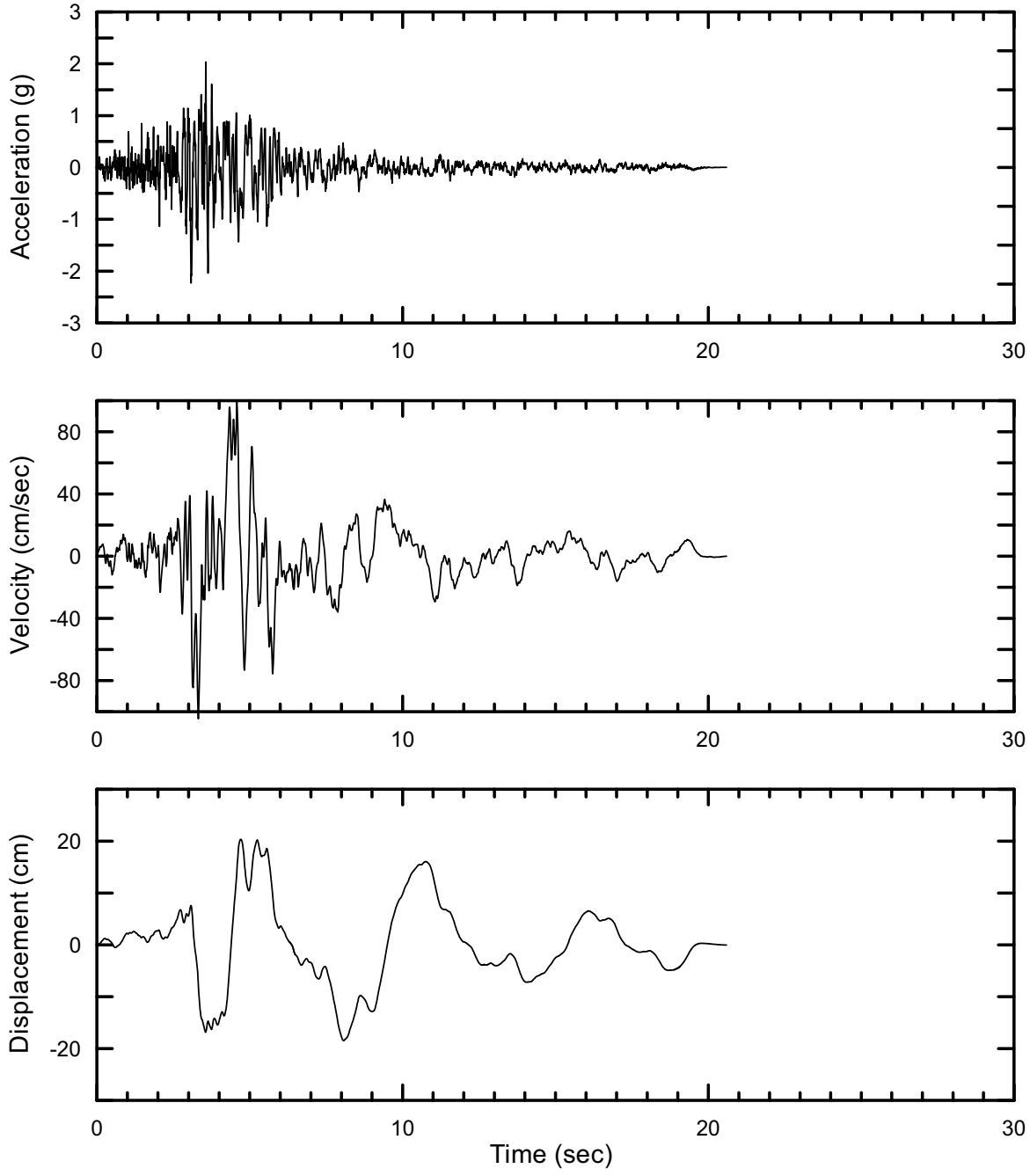

DTN: MO0402AVDTM105.001 [DIRS 168890]

Figure II-250. Point B Horizontal-1 Time Histories at an Annual Exceedance Probability of 10^{-5}, Set #2

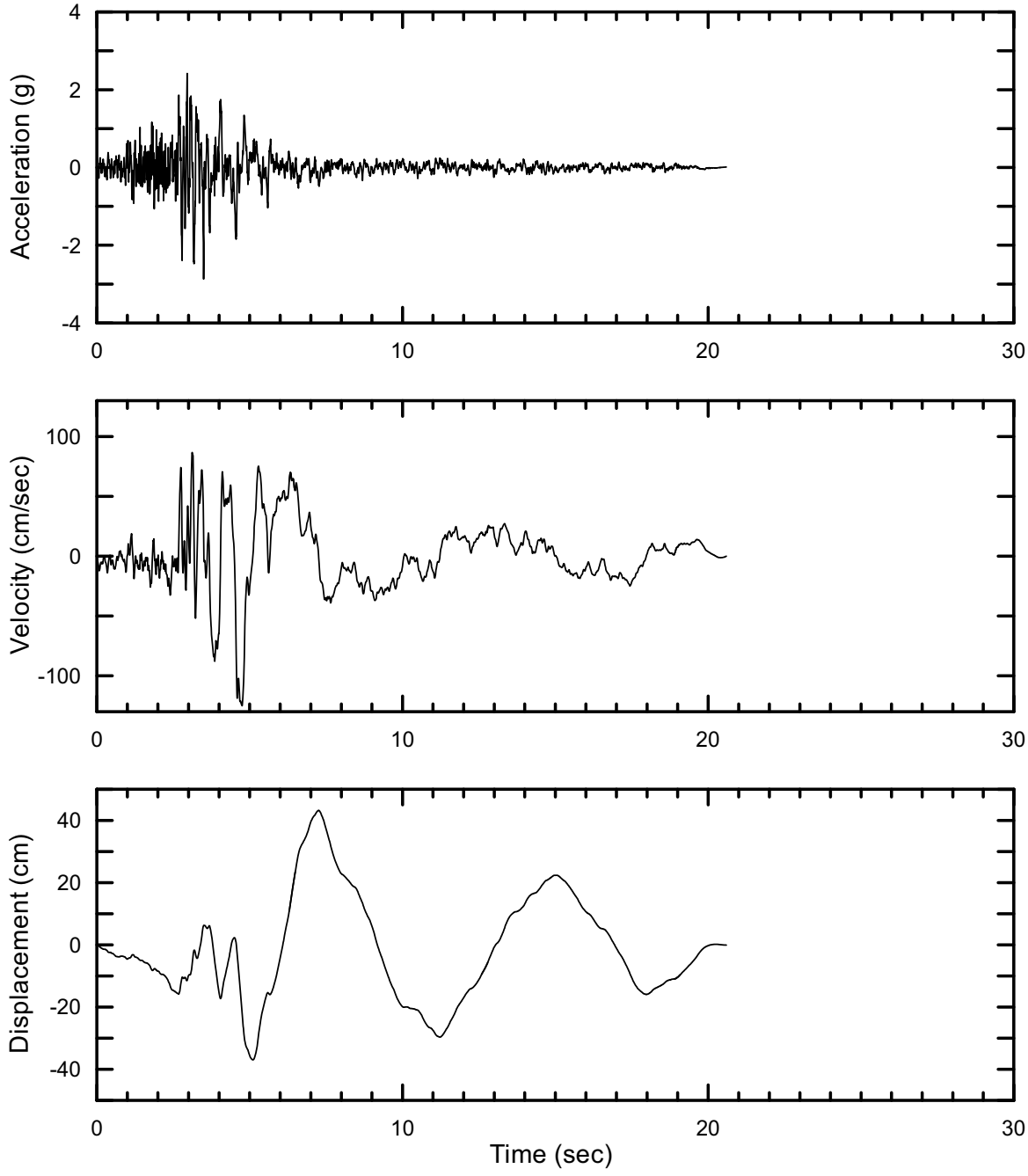

DTN: MO0402AVDTM105.001 [DIRS 168890]

Figure II-251. Point B Horizontal-2 Time Histories at an Annual Exceedance Probability of 10^{-5}, Set #2

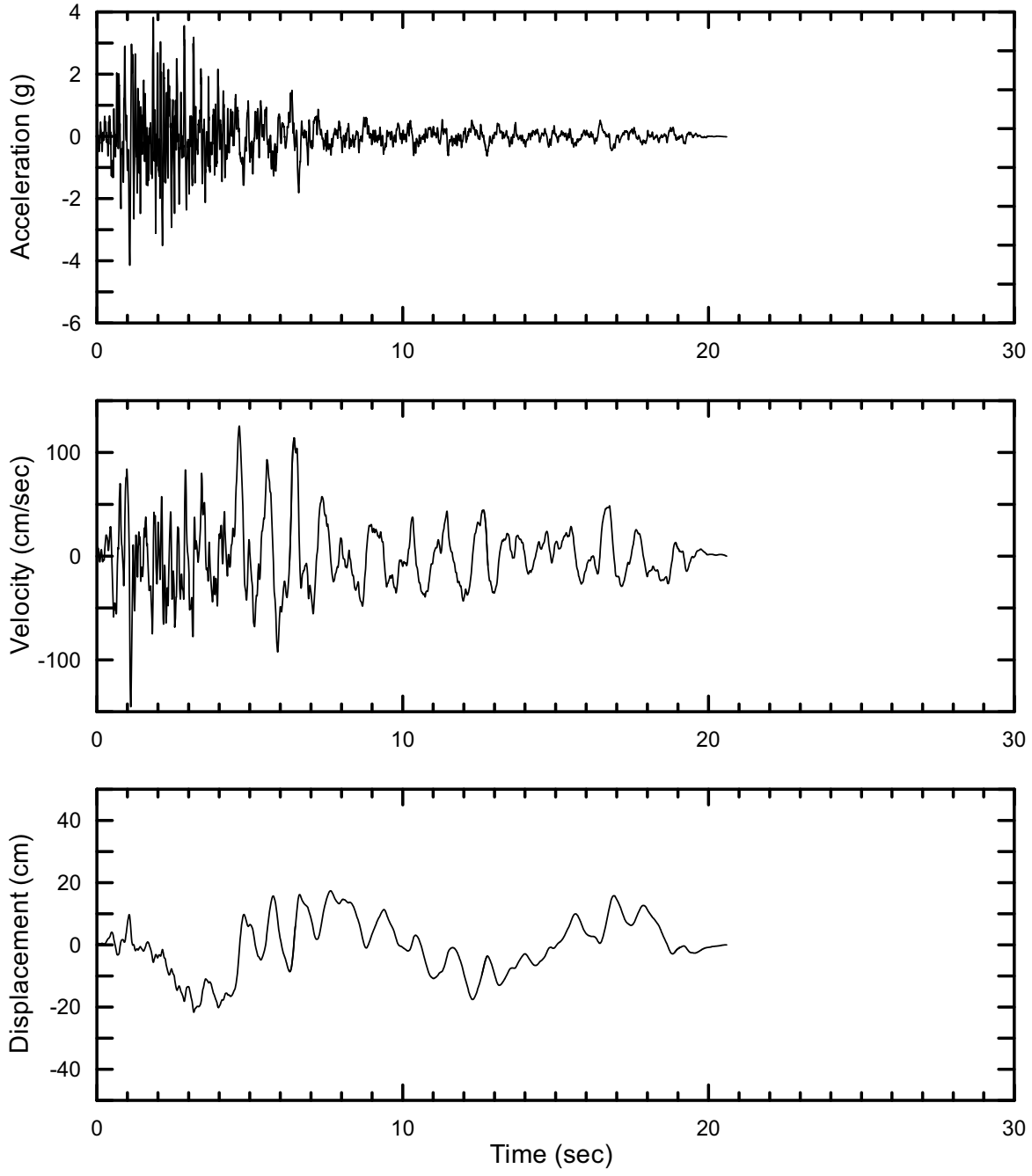

DTN: MO0402AVDTM105.001 [DIRS 168890]

Figure II-252. Point B Vertical Time Histories at an Annual Exceedance Probability of 10^{-5}, Set #2

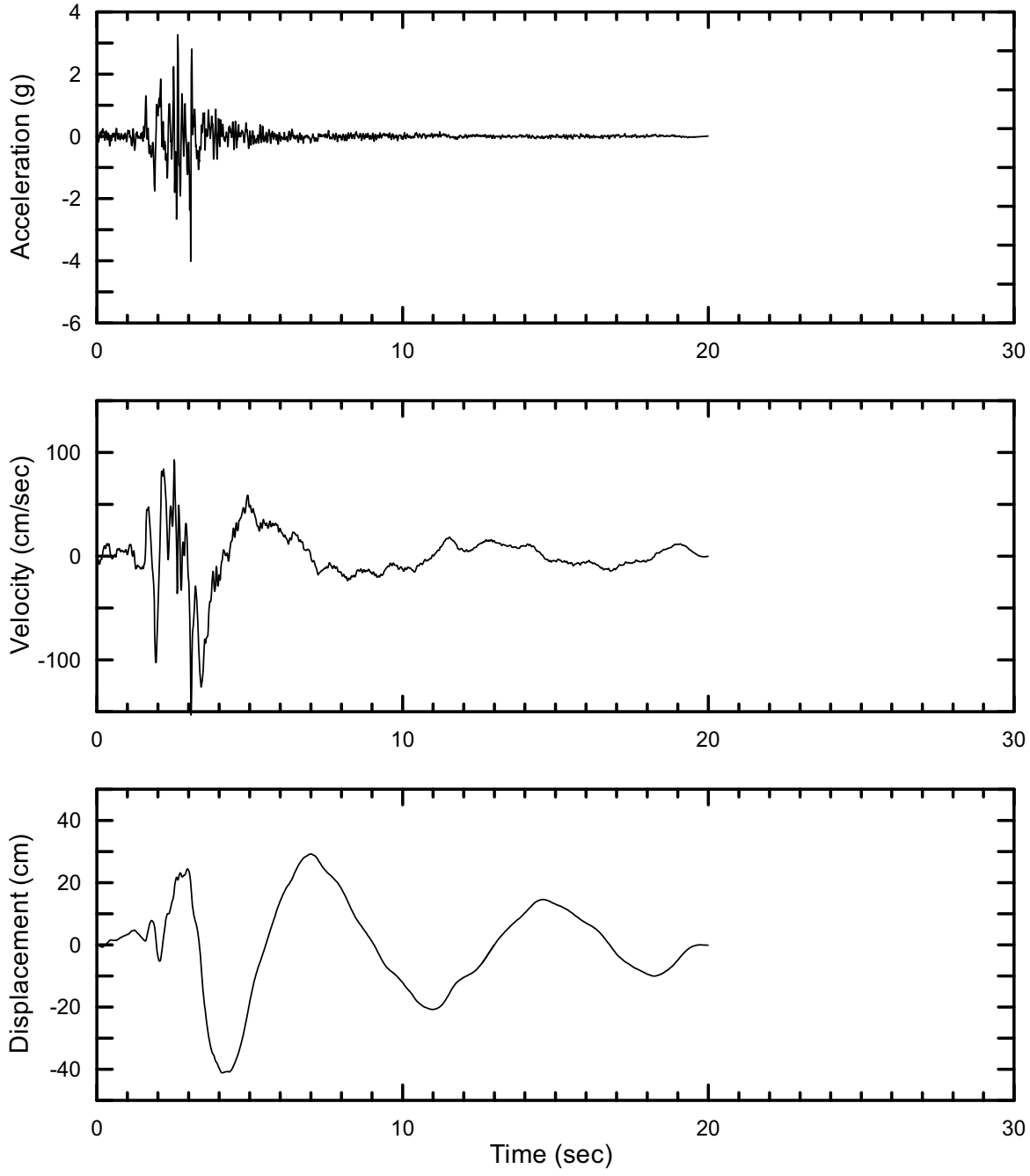

DTN: MO0402AVDTM105.001 [DIRS 168890]

Figure II-253. Point B Horizontal-1 Time Histories at an Annual Exceedance Probability of 10^{-5}, Set #3

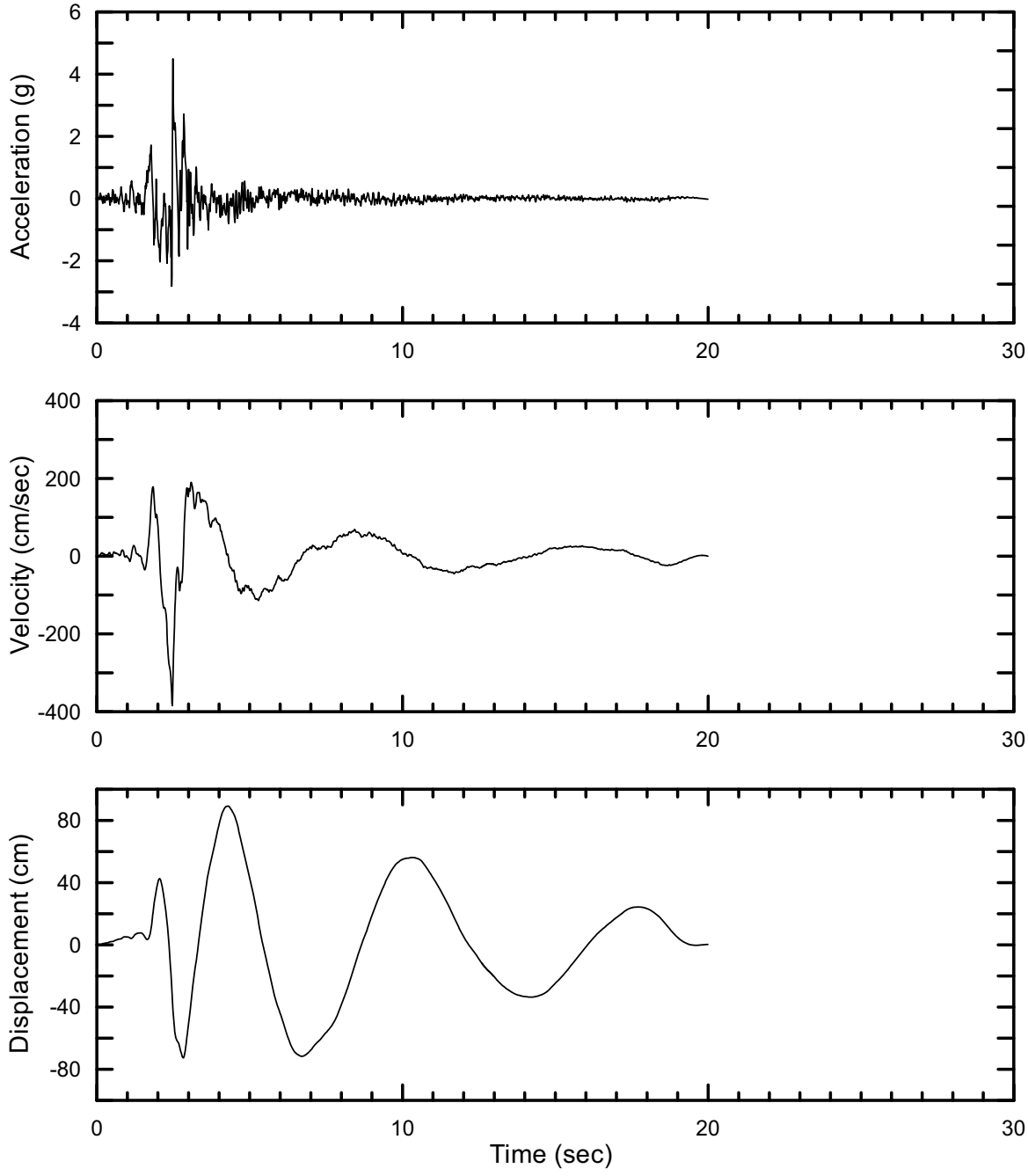

DTN: MO0402AVDTM105.001 [DIRS 168890]

Figure II-254. Point B Horizontal-2 Time Histories at an Annual Exceedance Probability of 10^{-5}, Set #3

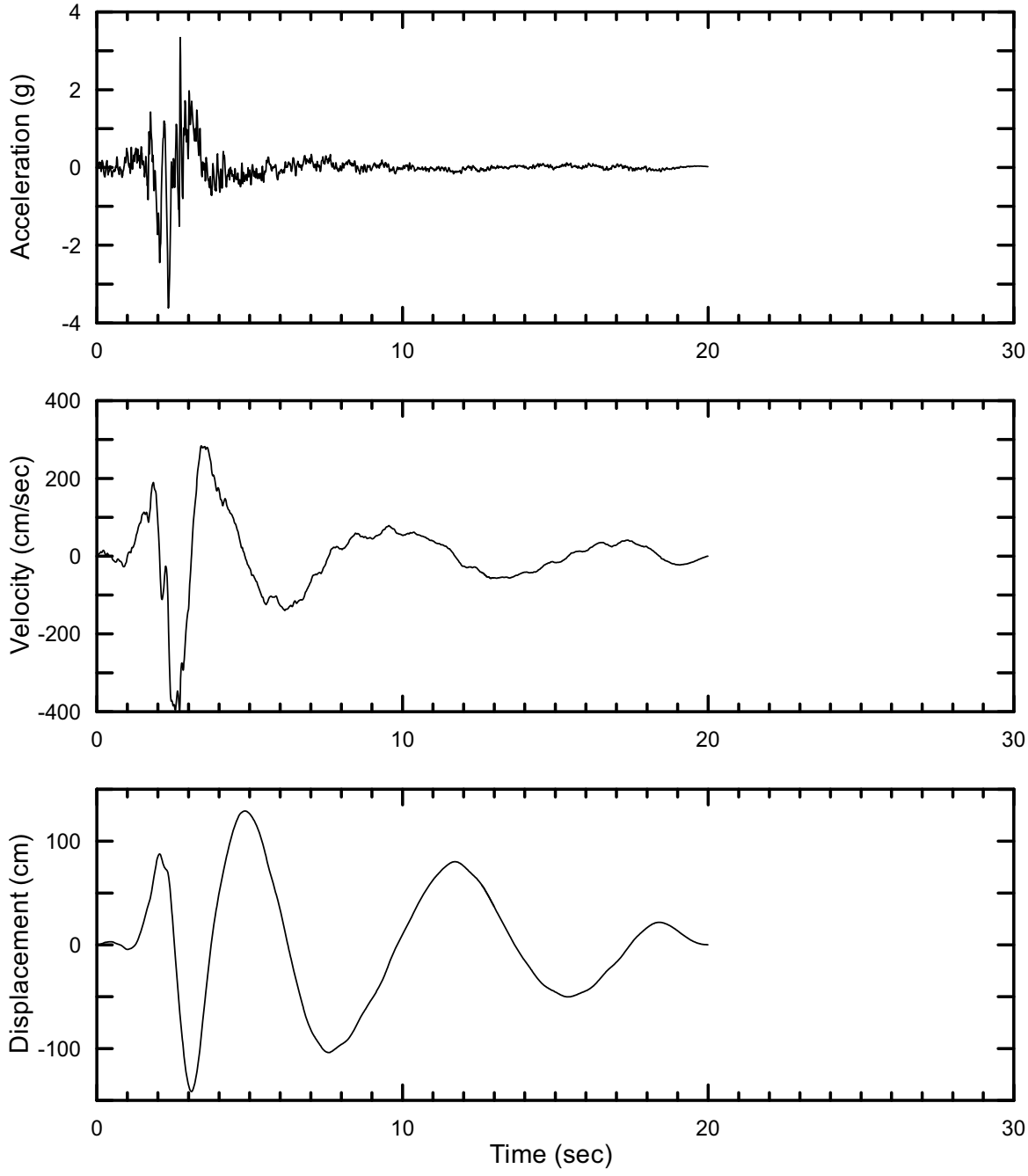

DTN: MO0402AVDTM105.001 [DIRS 168890]

Figure II-255. Point B Vertical Time Histories at an Annual Exceedance Probability of 10^{-5}, Set #3

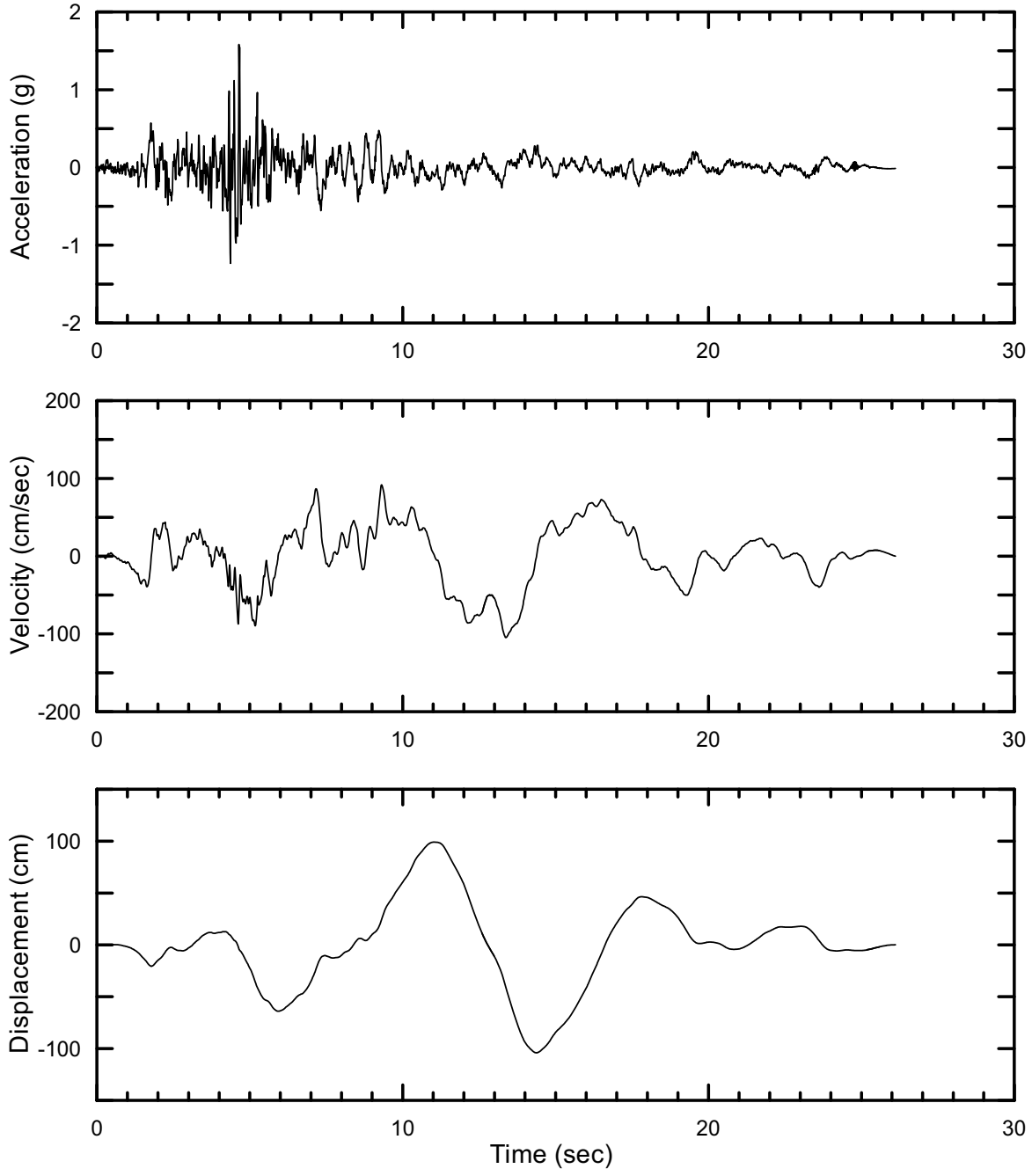

DTN: MO0402AVDTM105.001 [DIRS 168890]

Figure II-256. Point B Horizontal-1 Time Histories at an Annual Exceedance Probability of 10^{-5}, Set #4

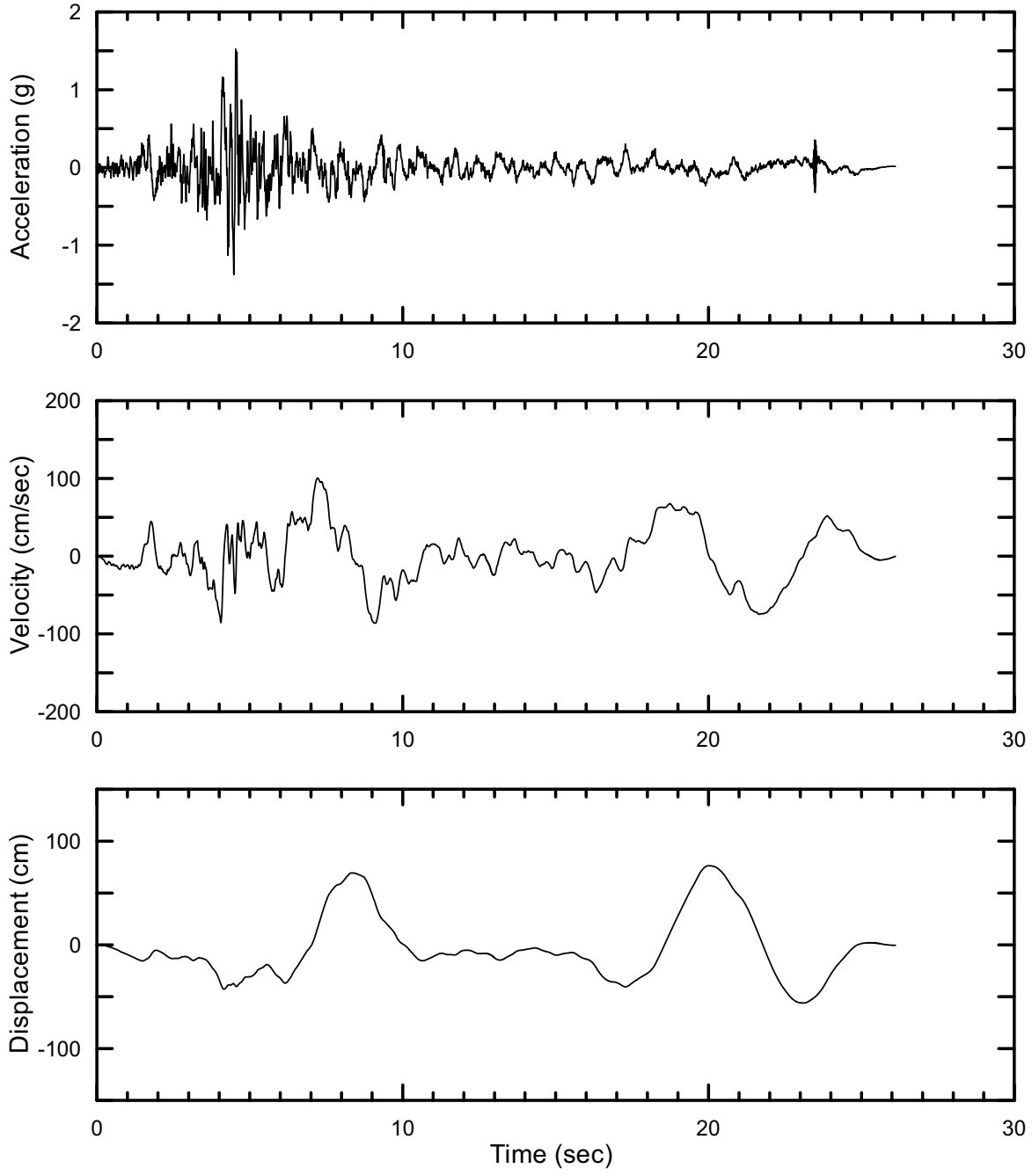

DTN: MO0402AVDTM105.001 [DIRS 168890]

Figure II-257. Point B Horizontal-2 Time Histories at an Annual Exceedance Probability of 10^{-5}, Set #4

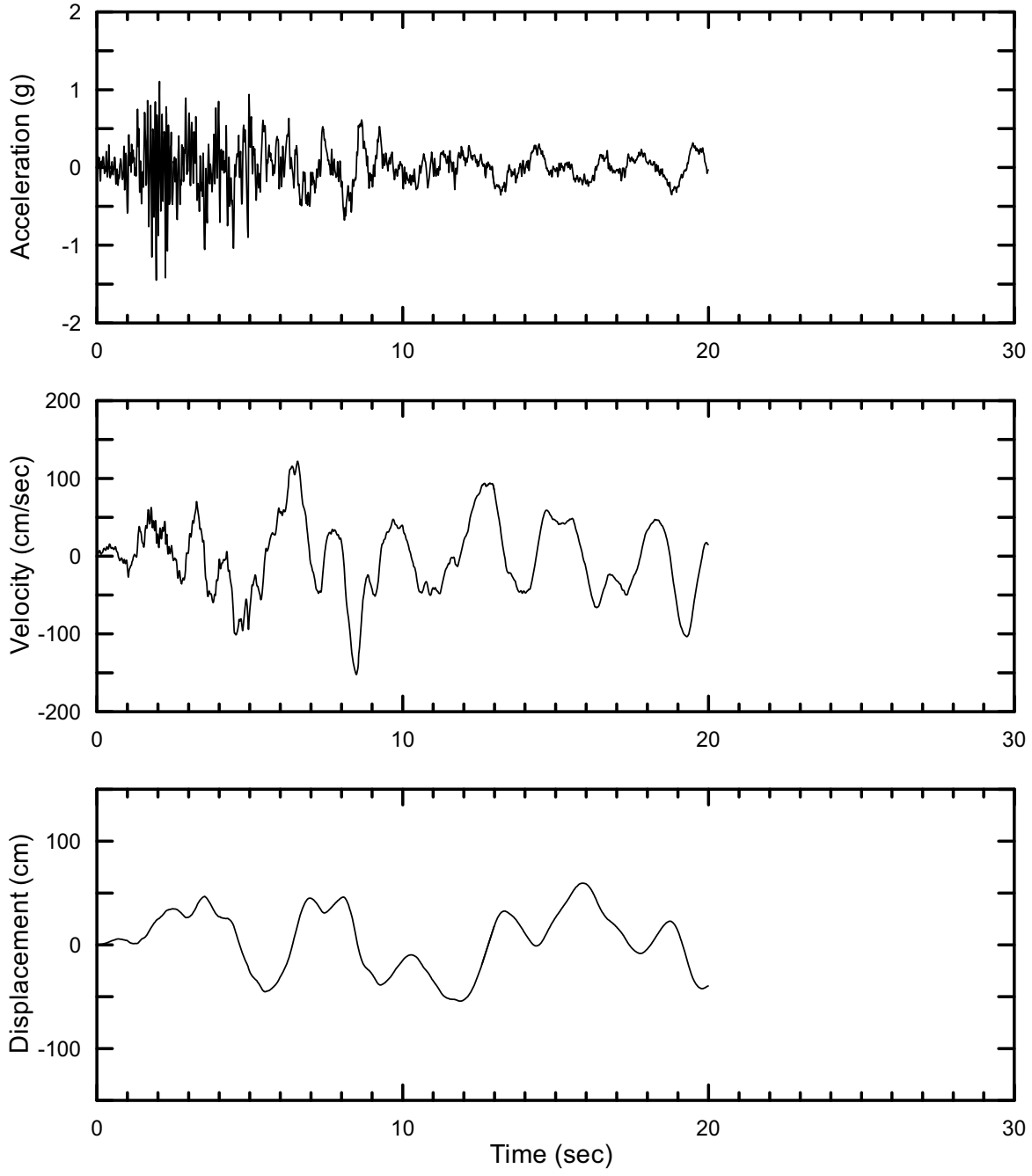

DTN: MO0402AVDTM105.001 [DIRS 168890]

Figure II-258. Point B Vertical Time Histories at an Annual Exceedance Probability of 10^{-5}, Set #4

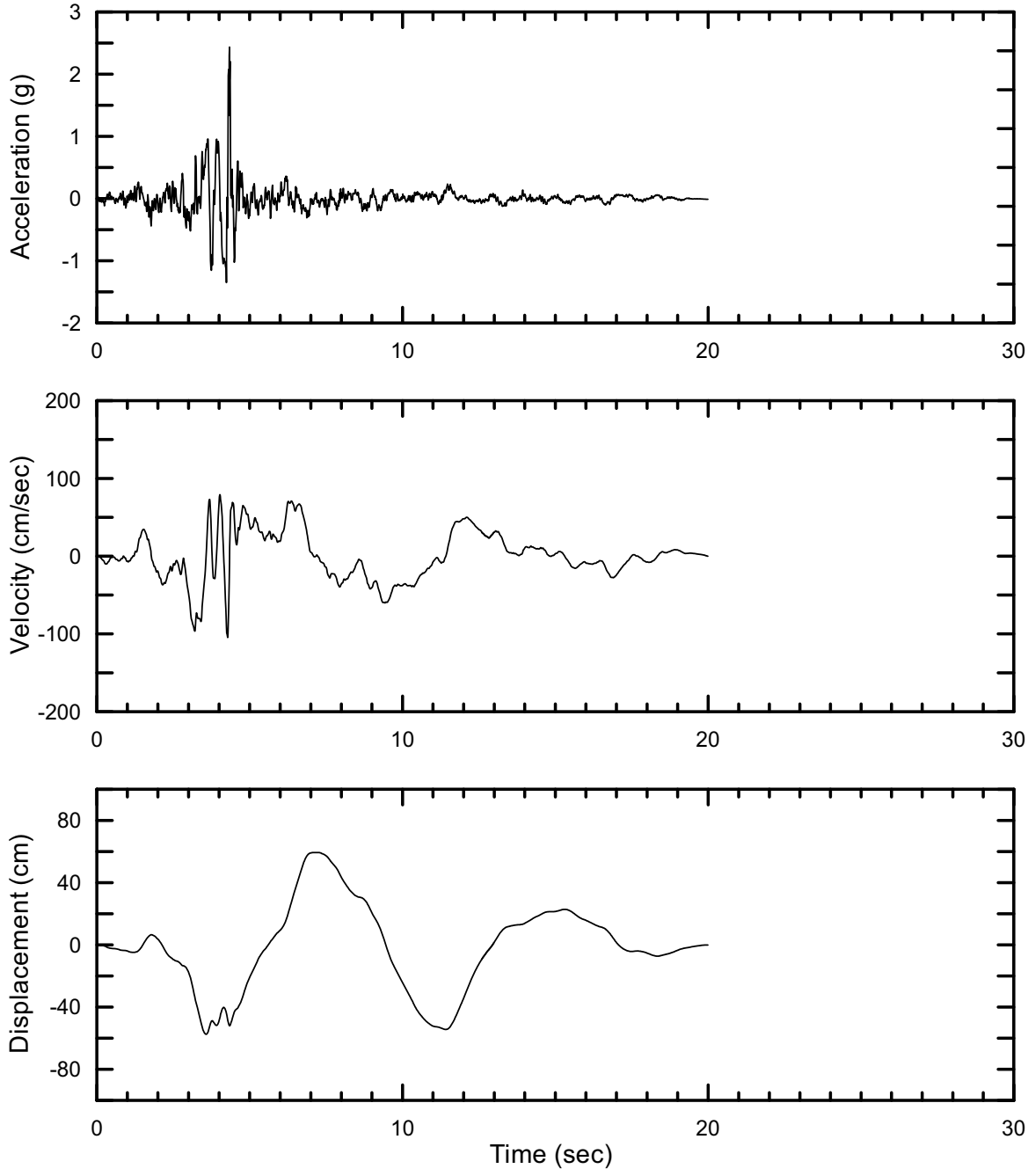

DTN: MO0402AVDTM105.001 [DIRS 168890]

Figure II-259. Point B Horizontal-1 Time Histories at an Annual Exceedance Probability of 10^{-5}, Set #5

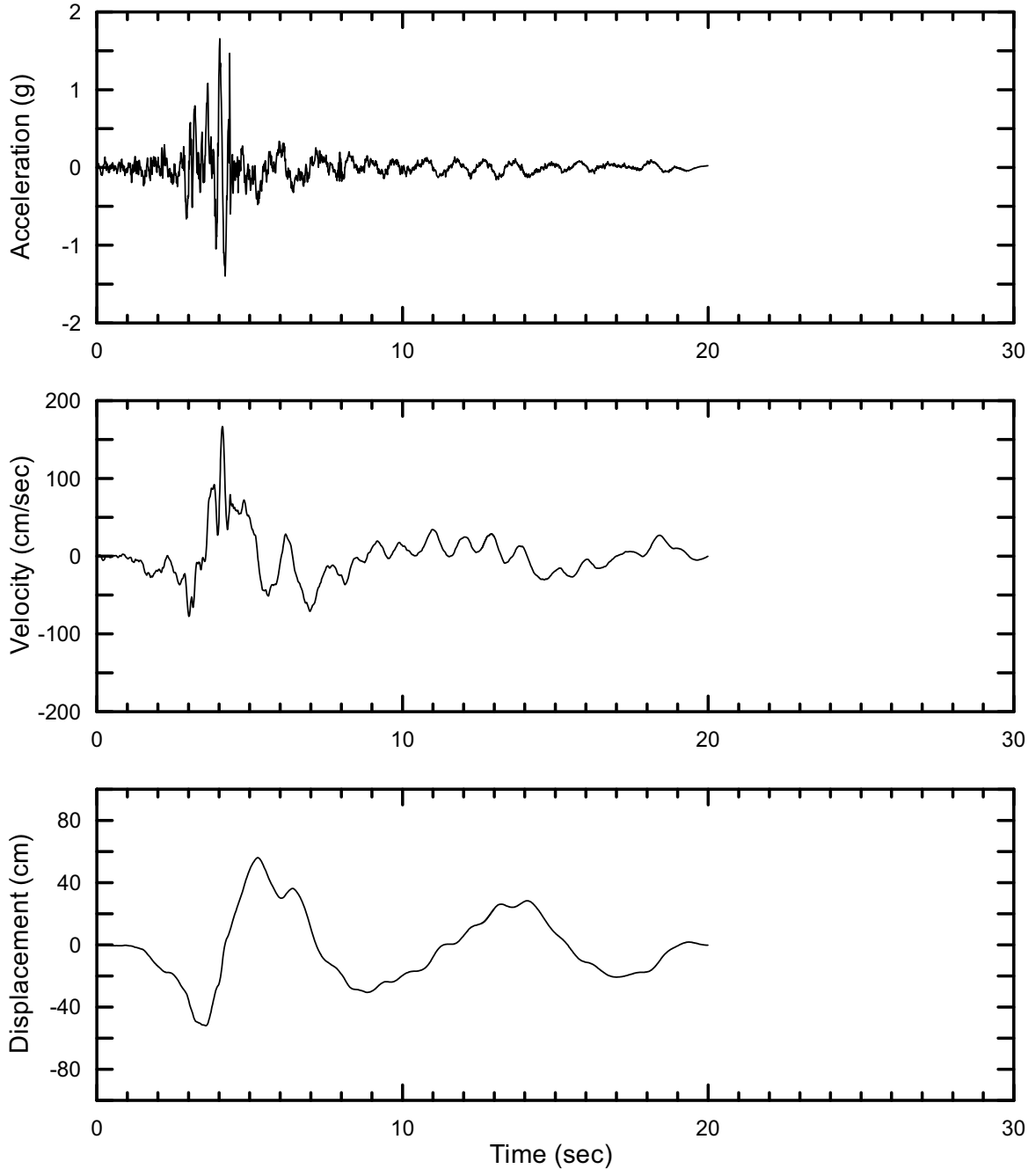

DTN: MO0402AVDTM105.001 [DIRS 168890]

Figure II-260. Point B Horizontal-2 Time Histories at an Annual Exceedance Probability of 10^{-5}, Set #5

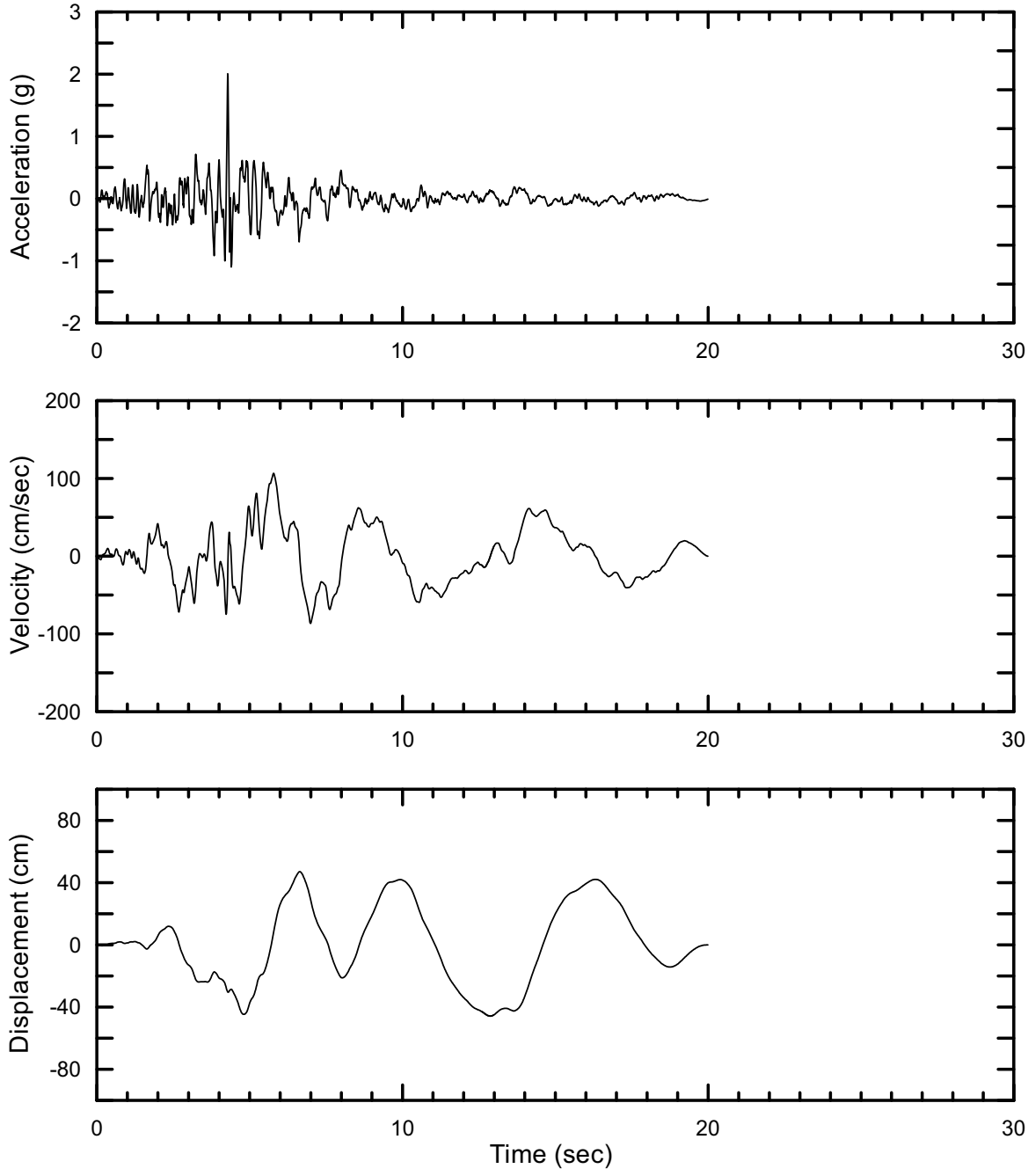

DTN: MO0402AVDTM105.001 [DIRS 168890]

Figure II-261. Point B Vertical Time Histories at an Annual Exceedance Probability of 10^{-5}, Set #5

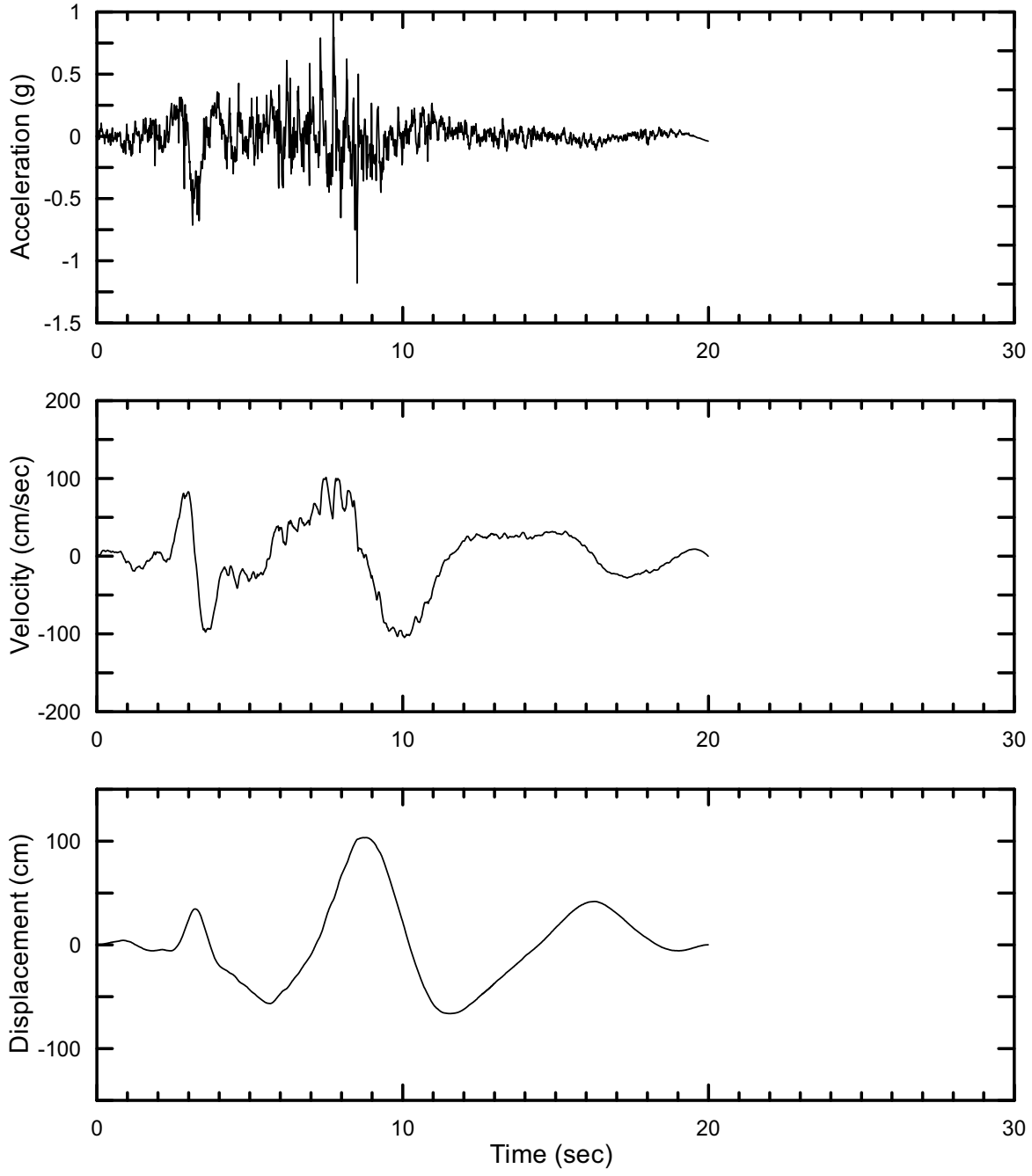

DTN: MO0402AVDTM105.001 [DIRS 168890]

Figure II-262. Point B Horizontal-1 Time Histories at an Annual Exceedance Probability of 10^{-5}, Set #6

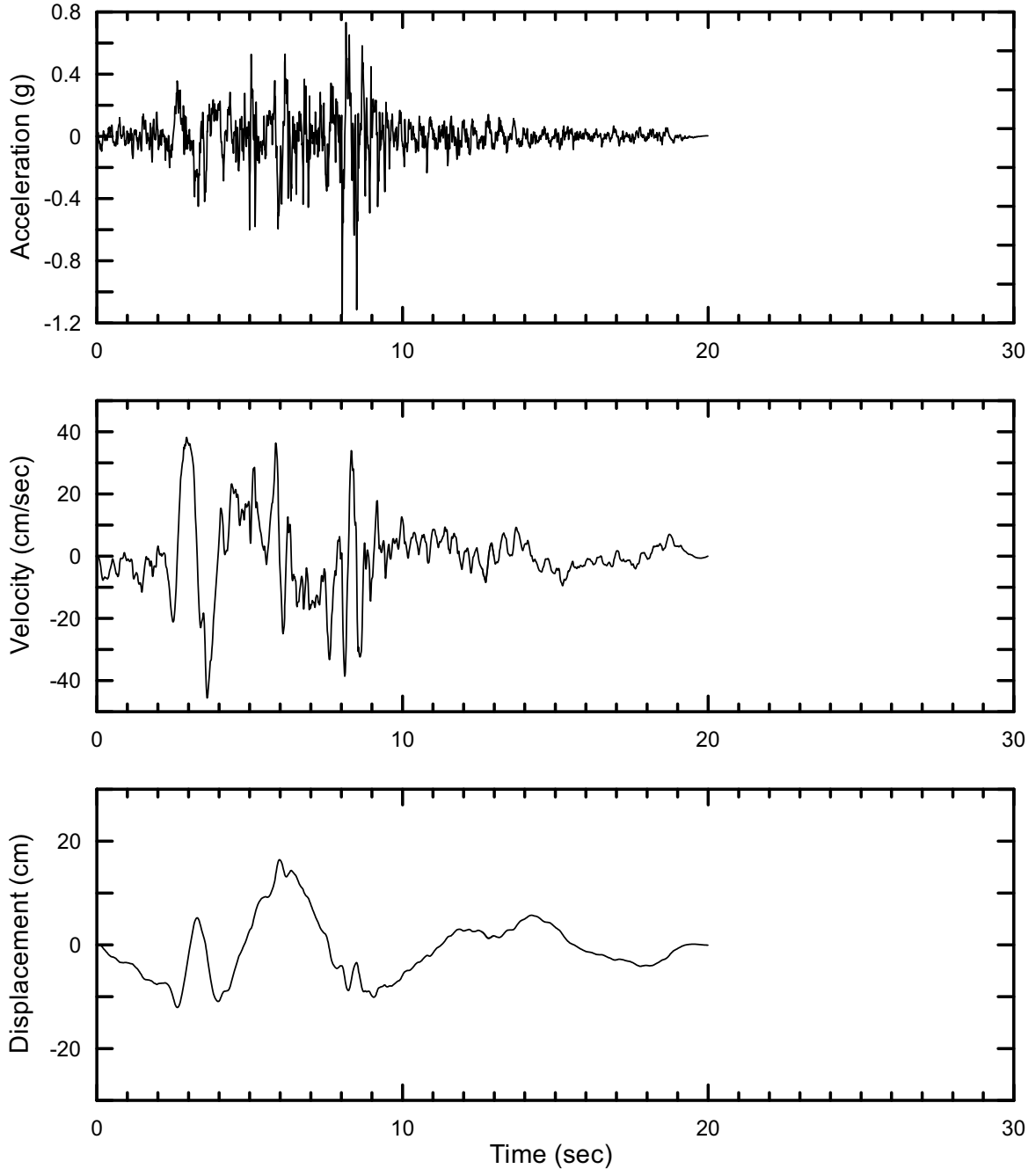

DTN: MO0402AVDTM105.001 [DIRS 168890]

Figure II-263. Point B Horizontal-2 Time Histories at an Annual Exceedance Probability of 10^{-5}, Set #6

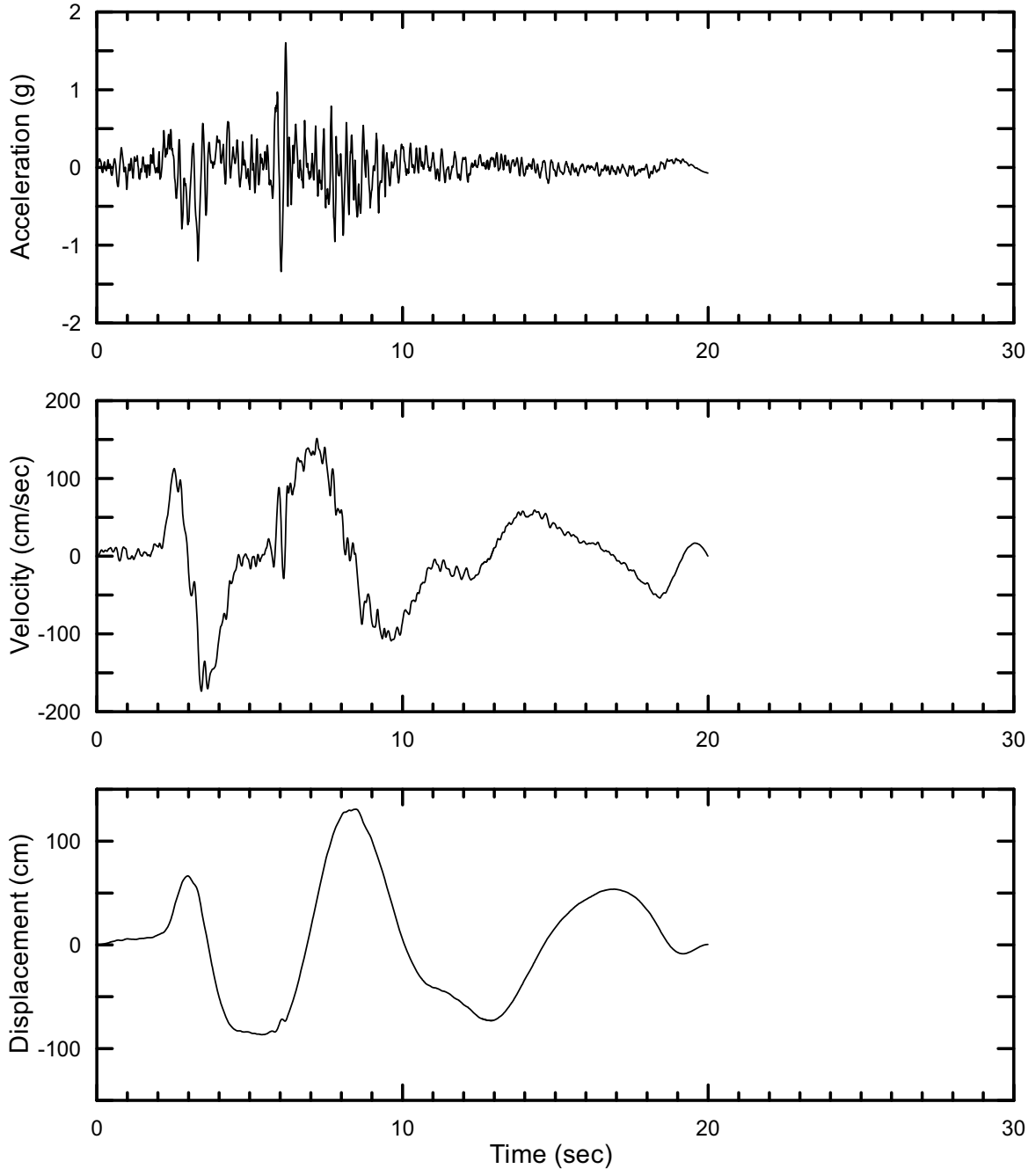

DTN: MO0402AVDTM105.001 [DIRS 168890]

Figure II-264. Point B Vertical Time Histories at an Annual Exceedance Probability of 10^{-5}, Set #6

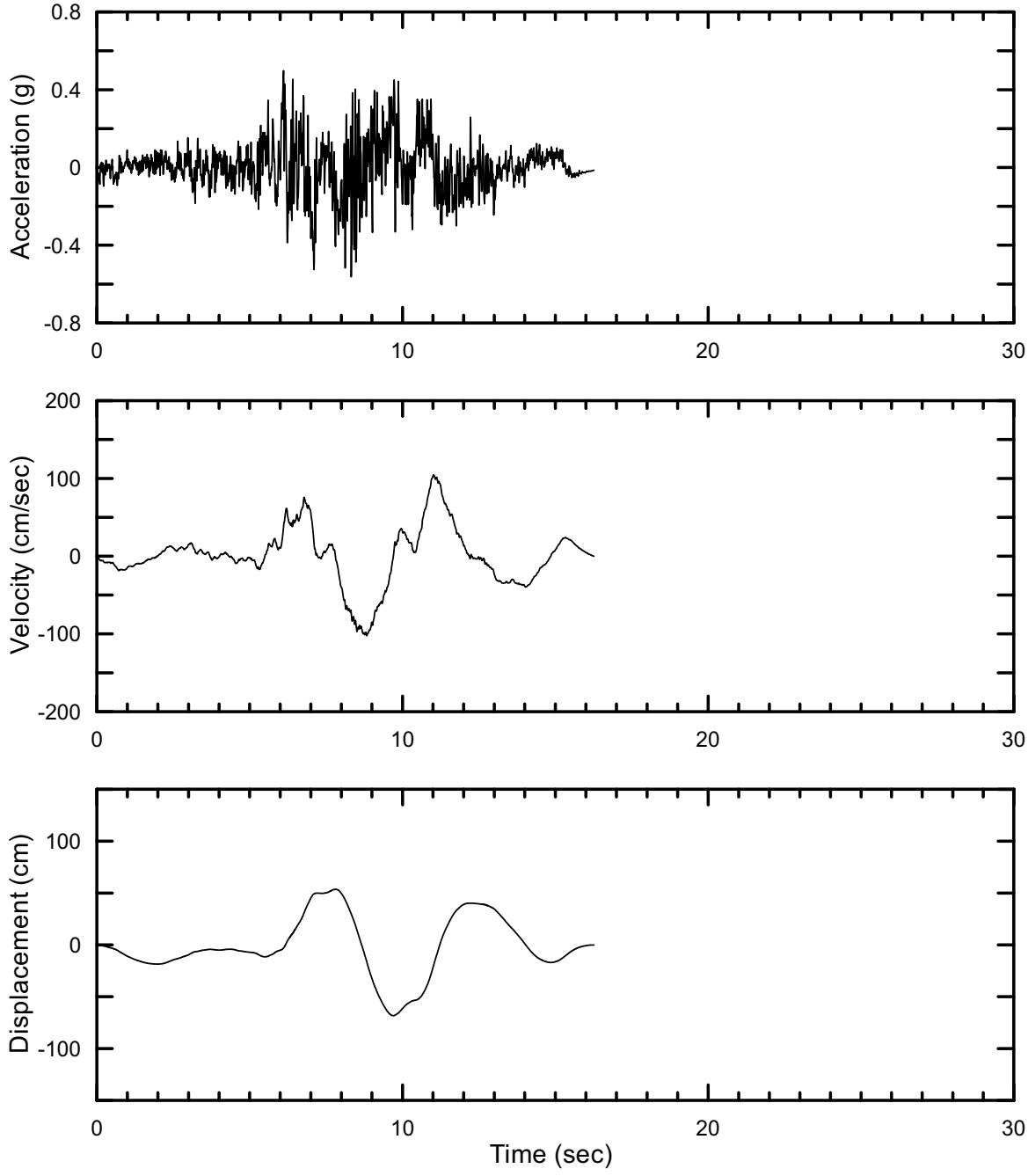

DTN: MO0402AVDTM105.001 [DIRS 168890]

Figure II-265. Point B Horizontal-1 Time Histories at an Annual Exceedance Probability of 10^{-5}, Set #7

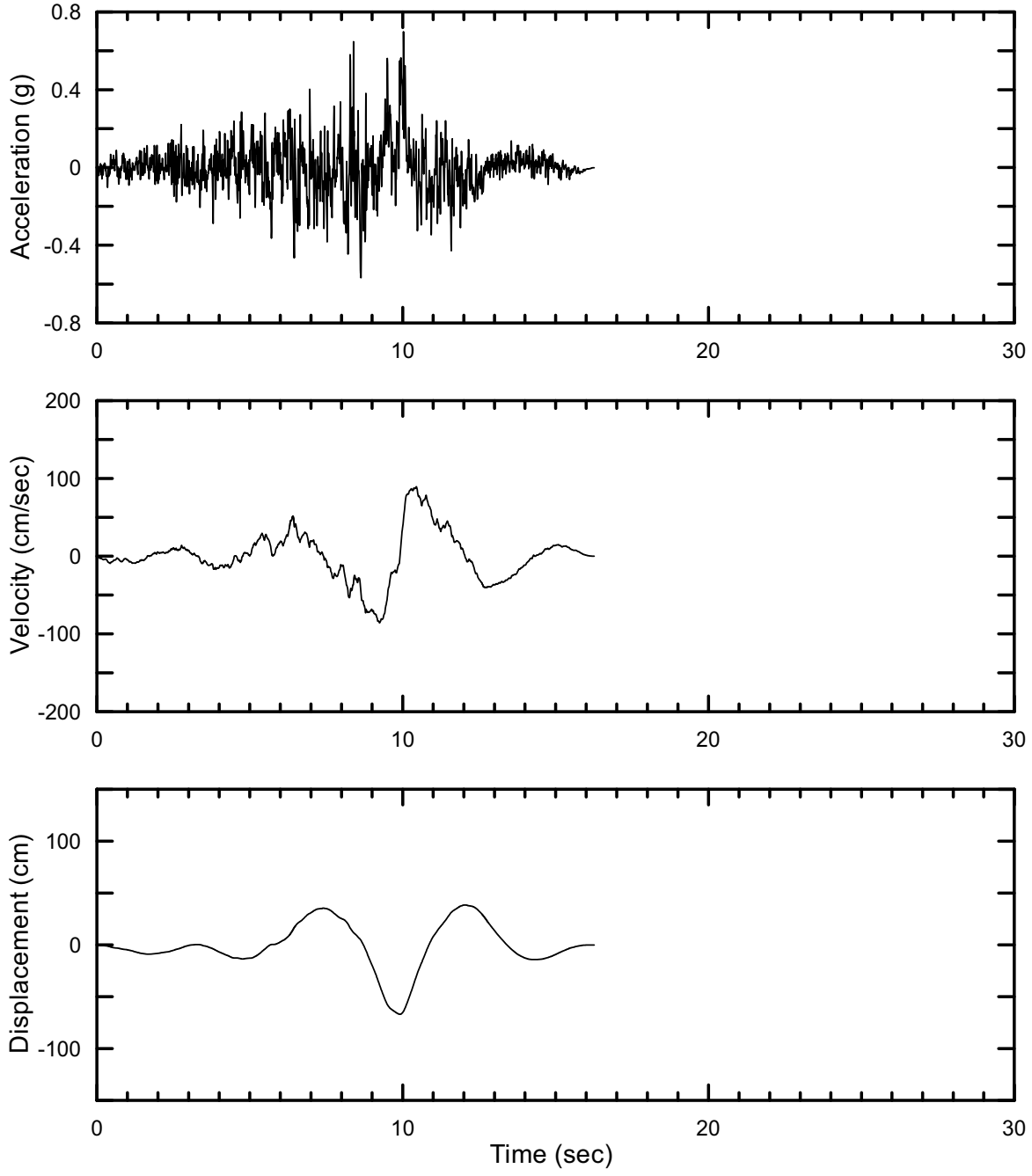

DTN: MO0402AVDTM105.001 [DIRS 168890]

Figure II-266. Point B Horizontal-2 Time Histories at an Annual Exceedance Probability of 10^{-5}, Set #7

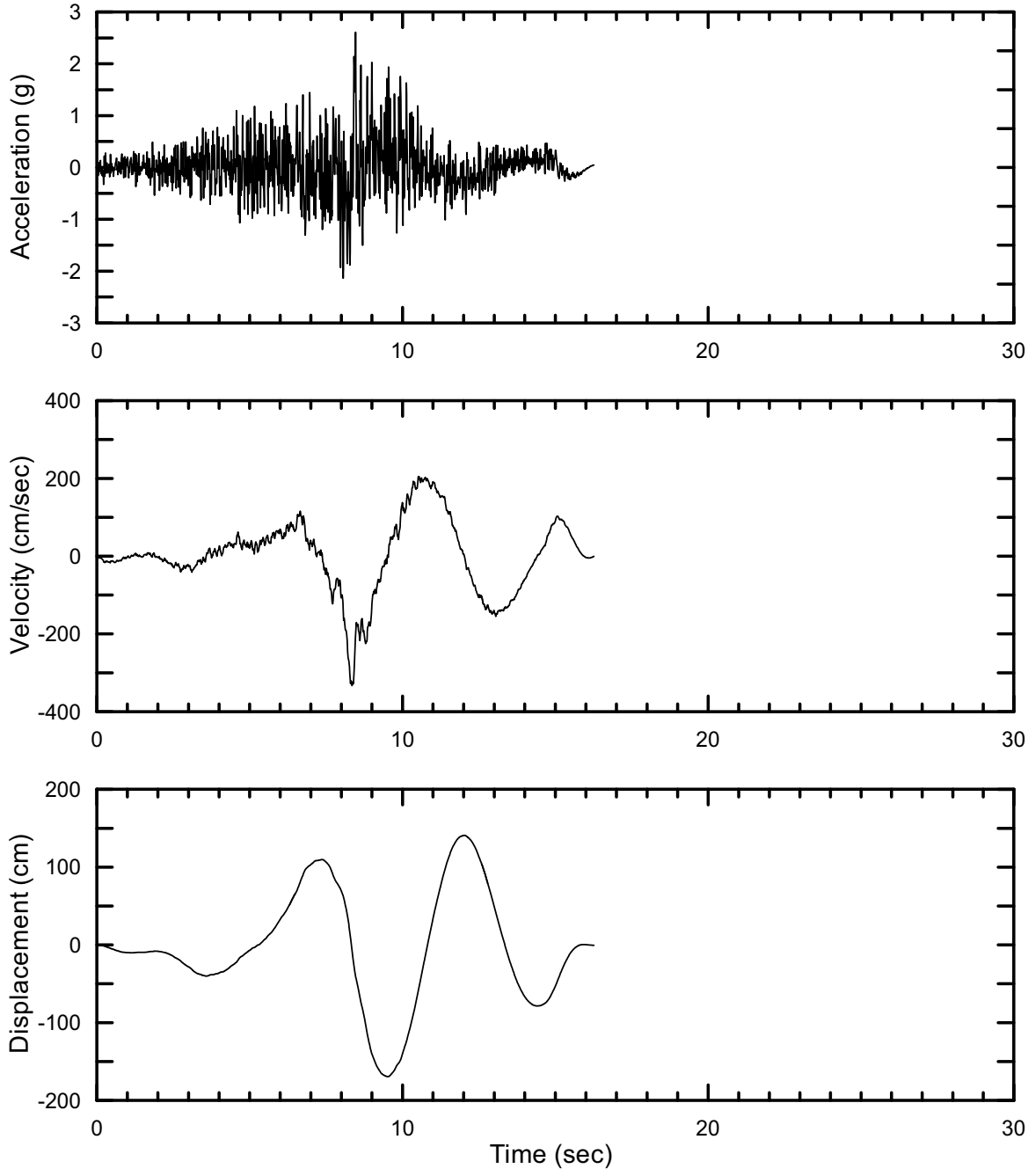

DTN: MO0402AVDTM105.001 [DIRS 168890]

Figure II-267. Point B Vertical Time Histories at an Annual Exceedance Probability of 10^{-5}, Set #7

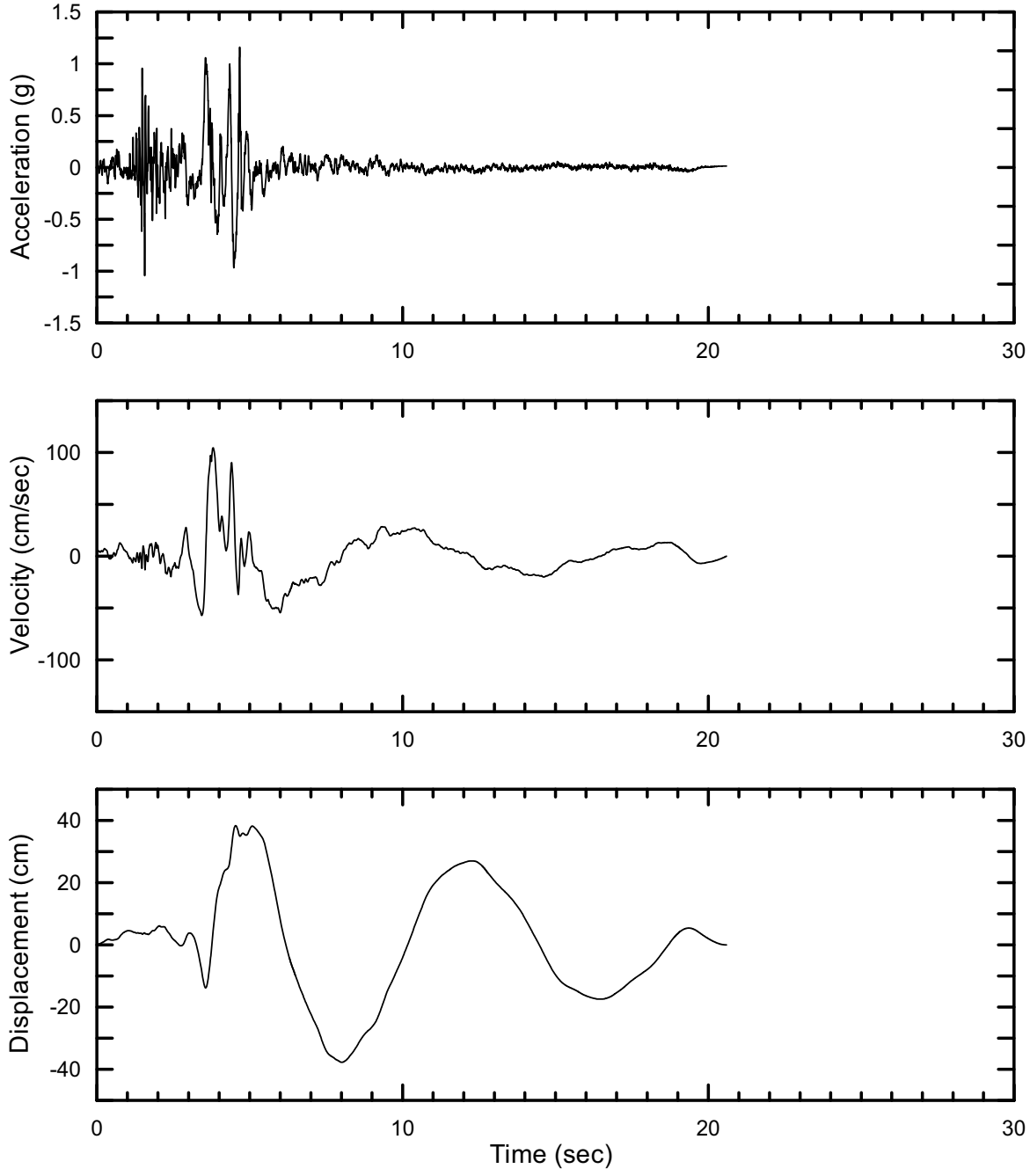

DTN: MO0402AVDTM105.001 [DIRS 168890]

Figure II-268. Point B Horizontal-1 Time Histories at an Annual Exceedance Probability of 10^{-5}, Set #8

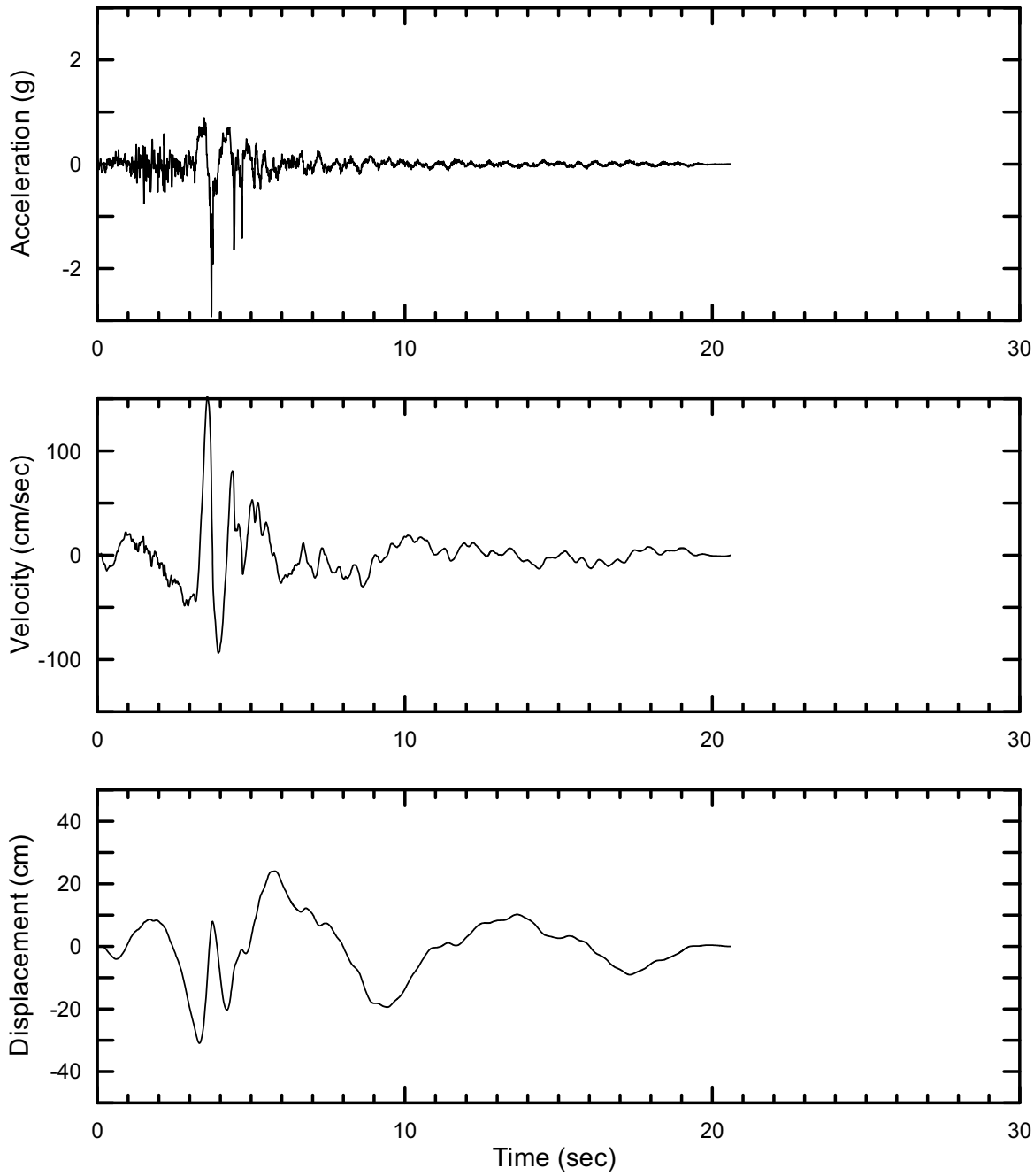

DTN: MO0402AVDTM105.001 [DIRS 168890]

Figure II-269. Point B Horizontal-2 Time Histories at an Annual Exceedance Probability of 10^{-5}, Set #8

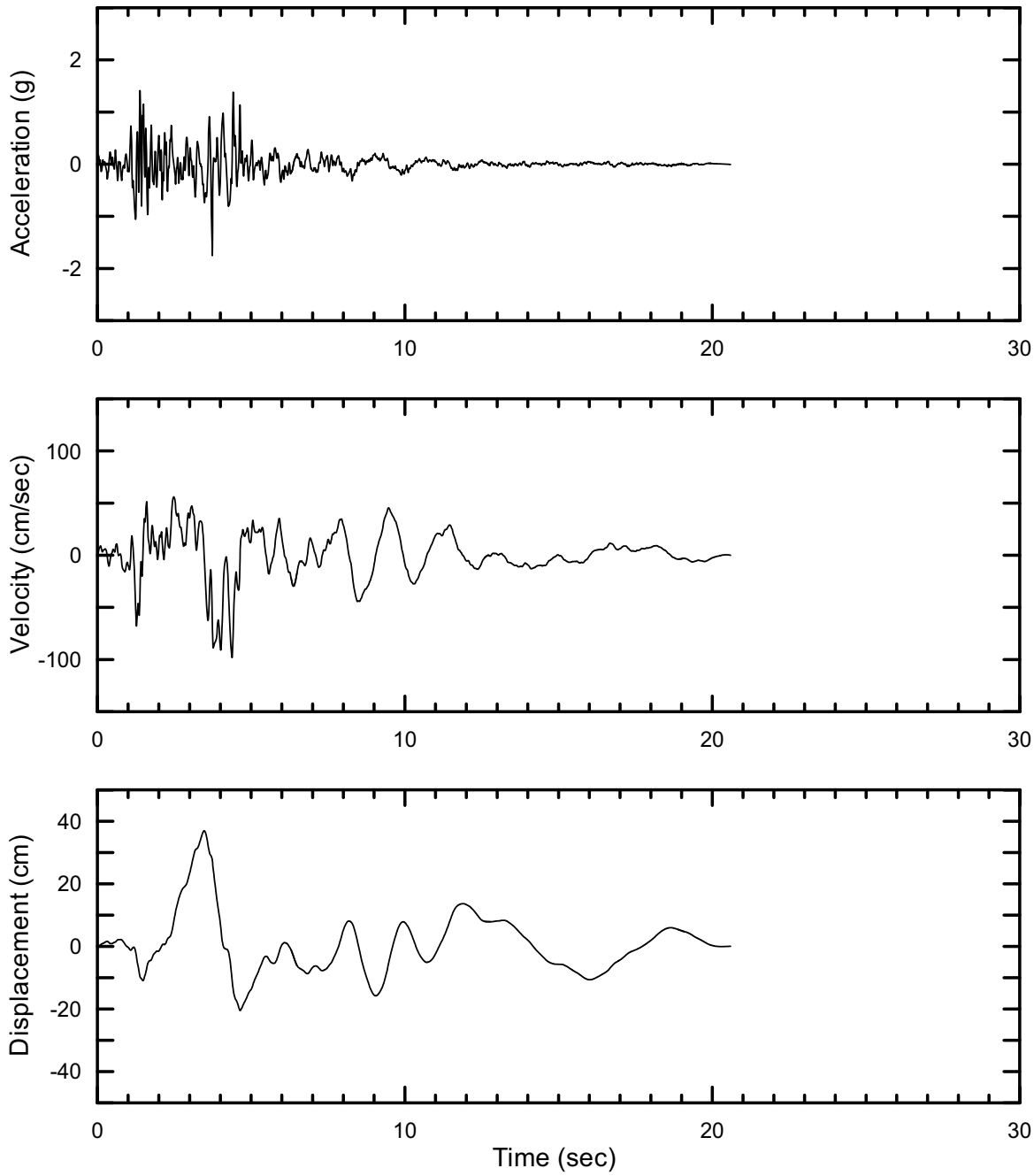

DTN: MO0402AVDTM105.001 [DIRS 168890]

Figure II-270. Point B Vertical Time Histories at an Annual Exceedance Probability of 10^{-5}, Set #8

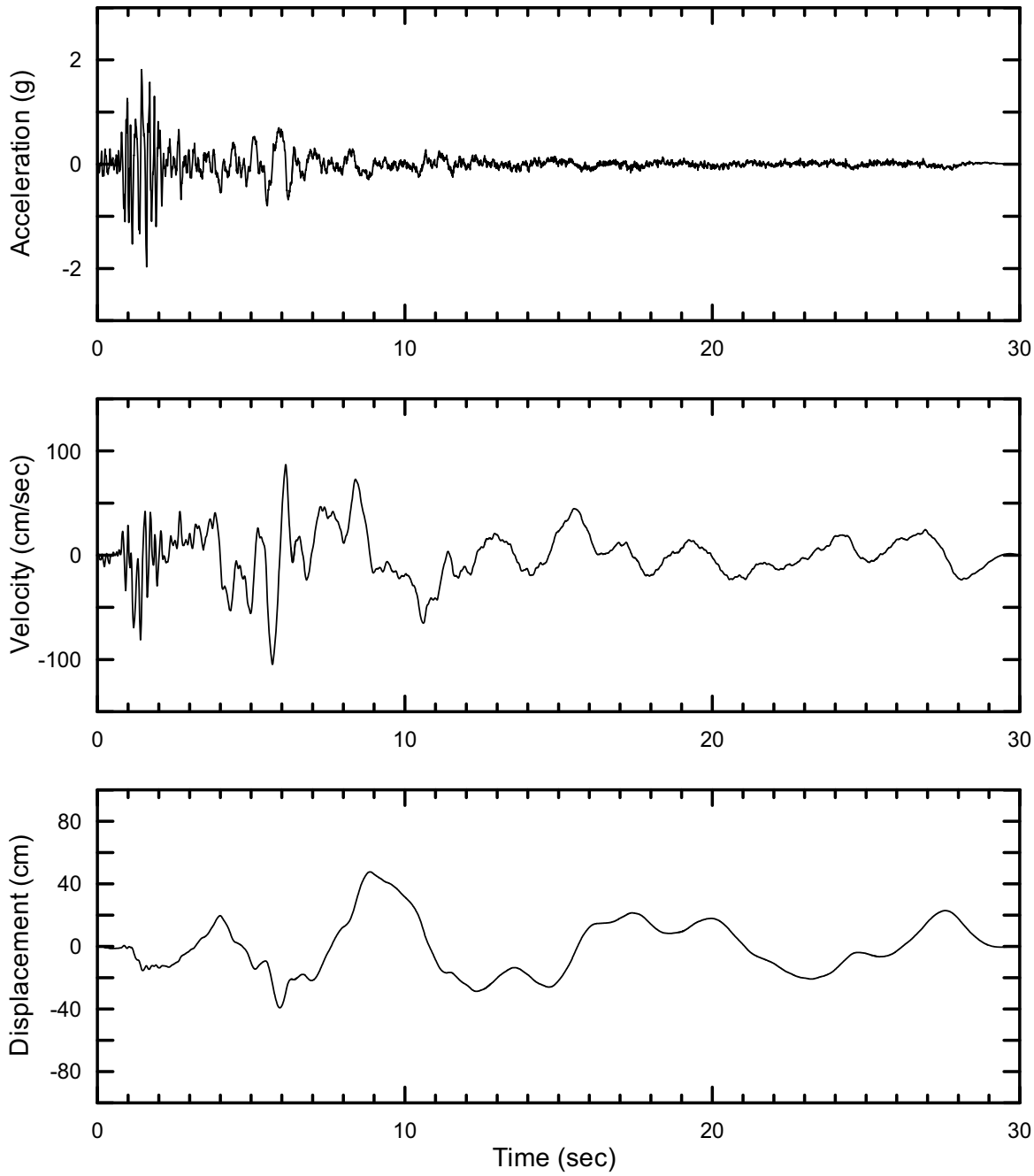

DTN: MO0402AVDTM105.001 [DIRS 168890]

Figure II-271. Point B Horizontal-1 Time Histories at an Annual Exceedance Probability of 10^{-5}, Set #9

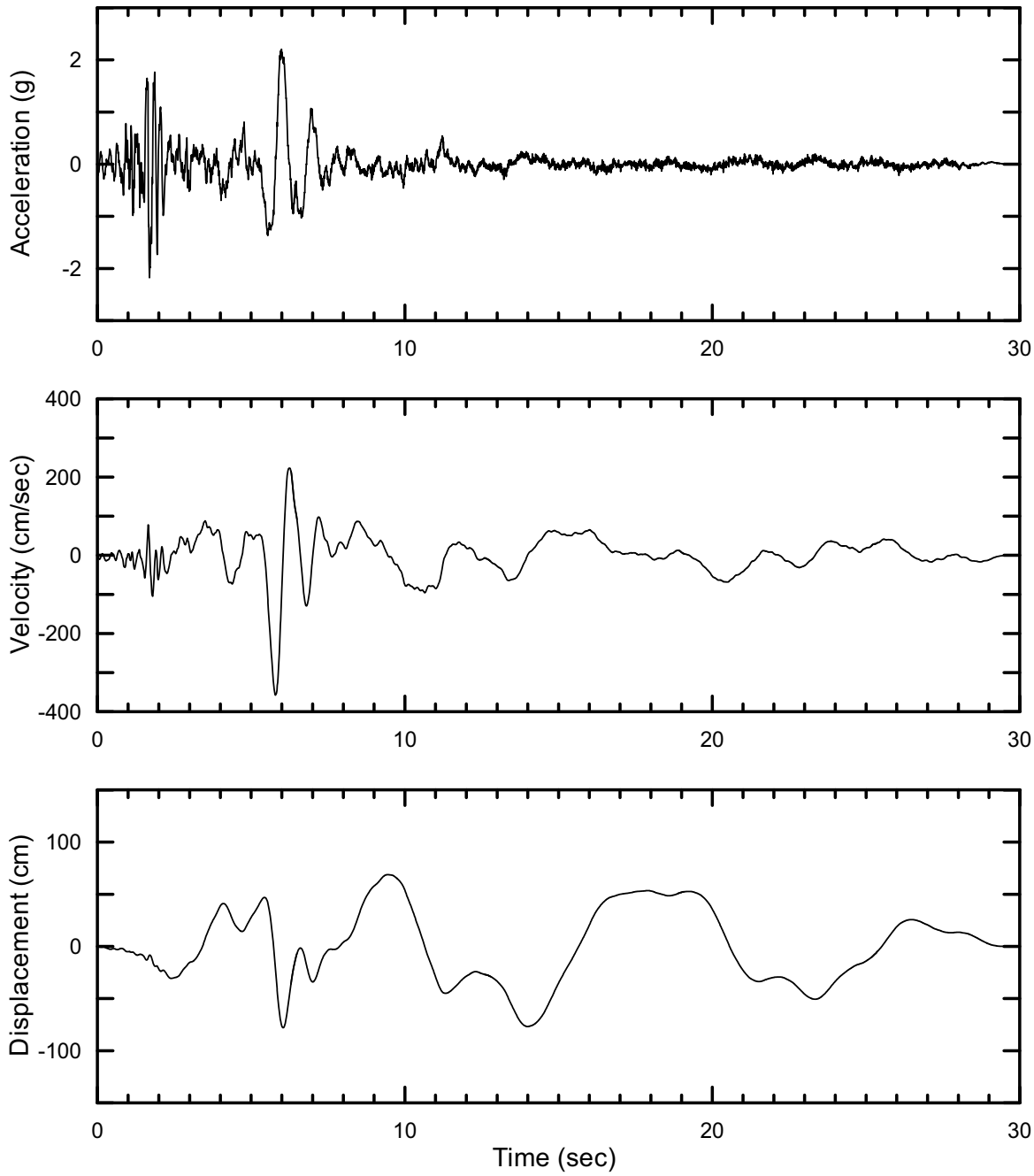

DTN: MO0402AVDTM105.001 [DIRS 168890]

Figure II-272. Point B Horizontal-2 Time Histories at an Annual Exceedance Probability of 10^{-5}, Set #9

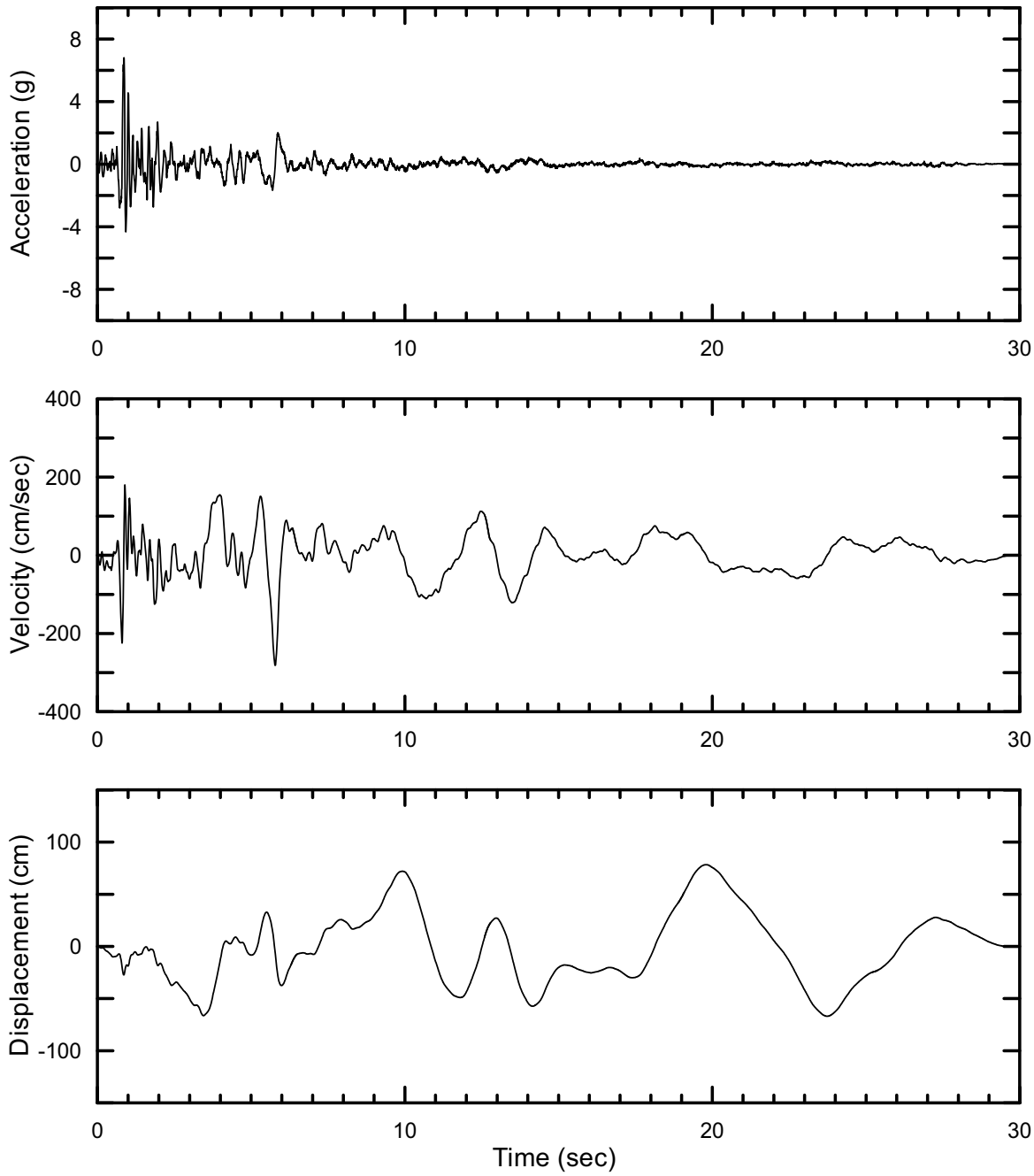

DTN: MO0402AVDTM105.001 [DIRS 168890]

Figure II-273. Point B Vertical Time Histories at an Annual Exceedance Probability of 10^{-5}, Set #9

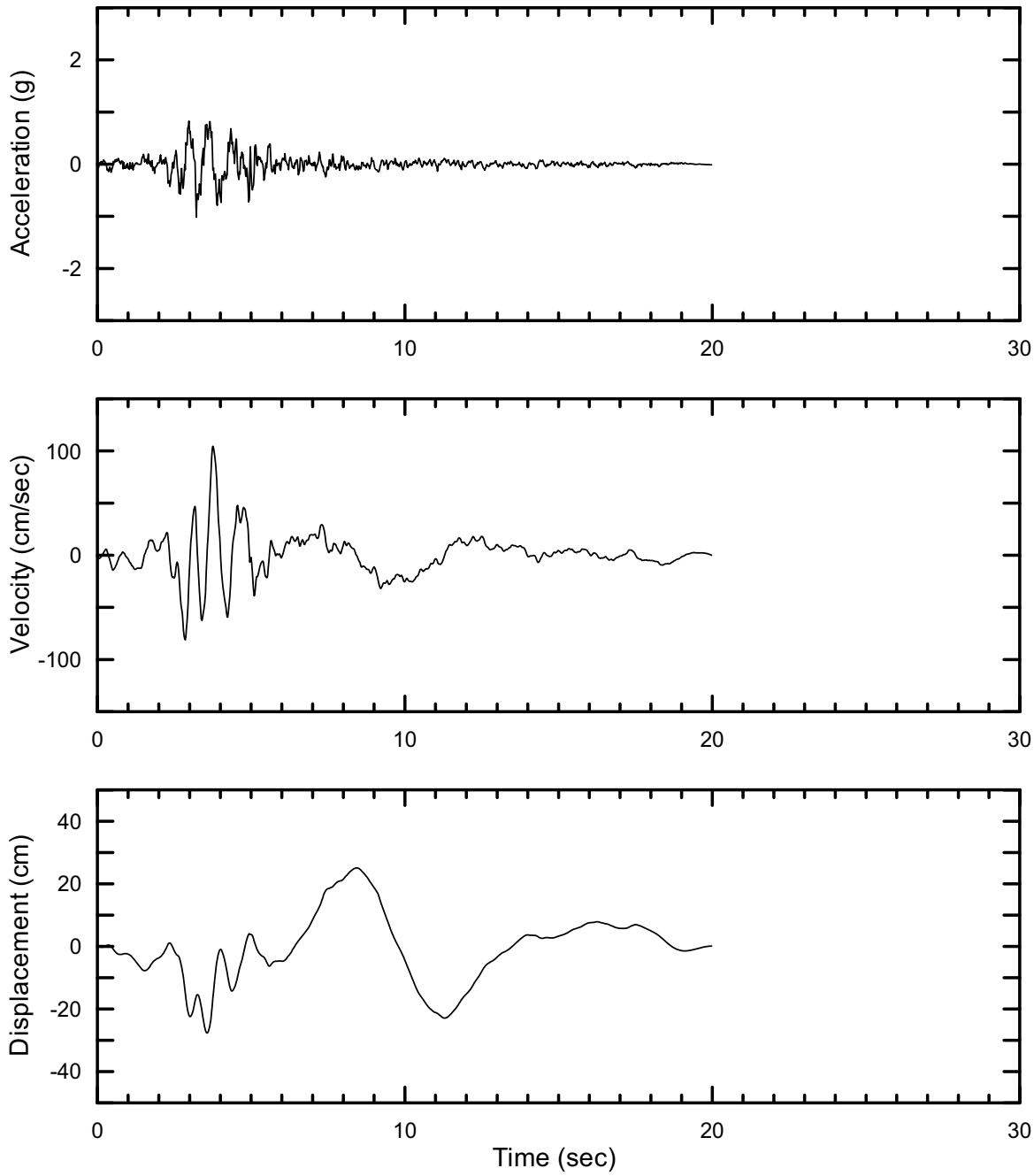

DTN: MO0402AVDTM105.001 [DIRS 168890]

Figure II-274. Point B Horizontal-1 Time Histories at an Annual Exceedance Probability of 10^{-5}, Set #10

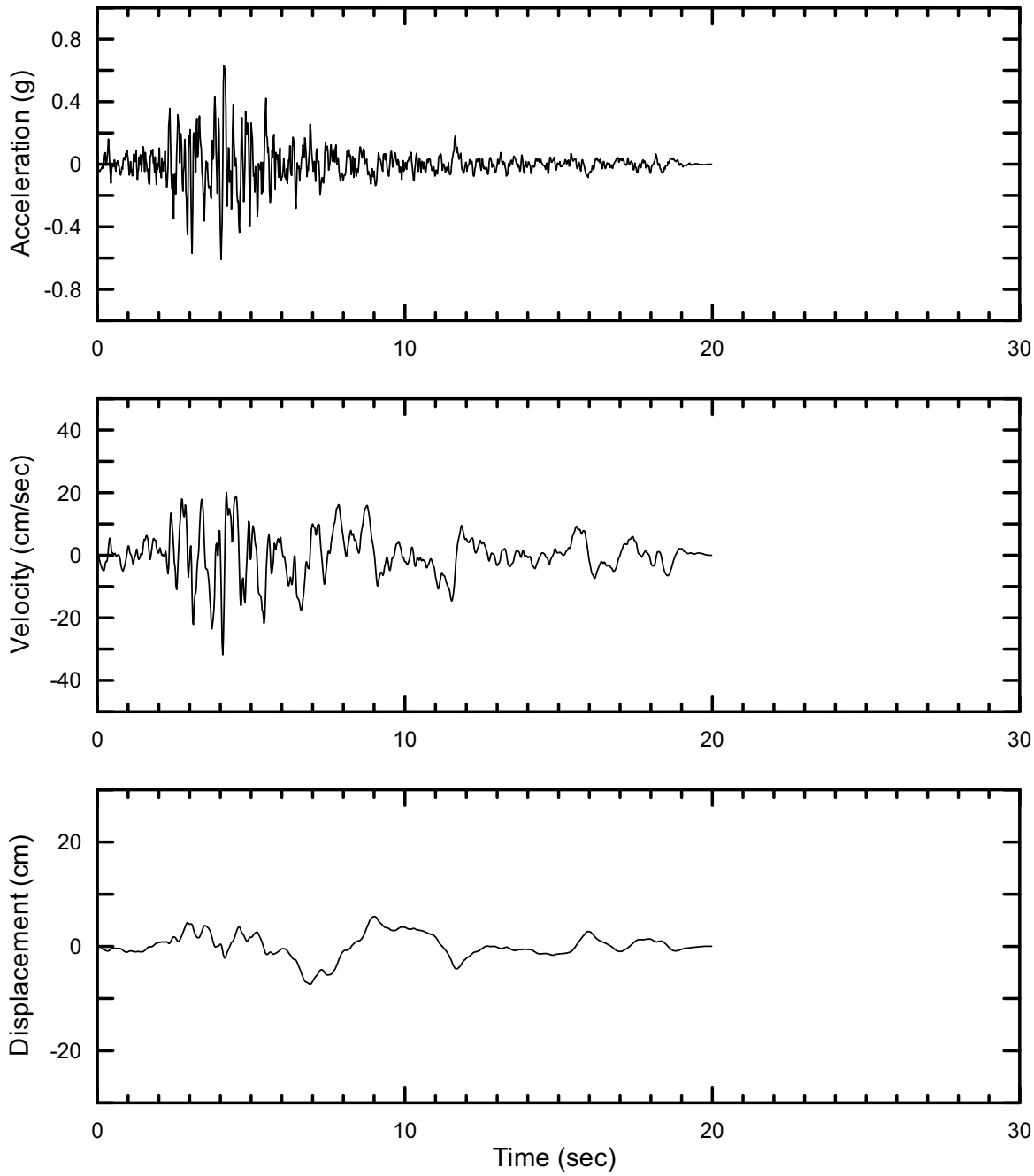

DTN: MO0402AVDTM105.001 [DIRS 168890]

Figure II-275. Point B Horizontal-2 Time Histories at an Annual Exceedance Probability of 10^{-5}, Set #10

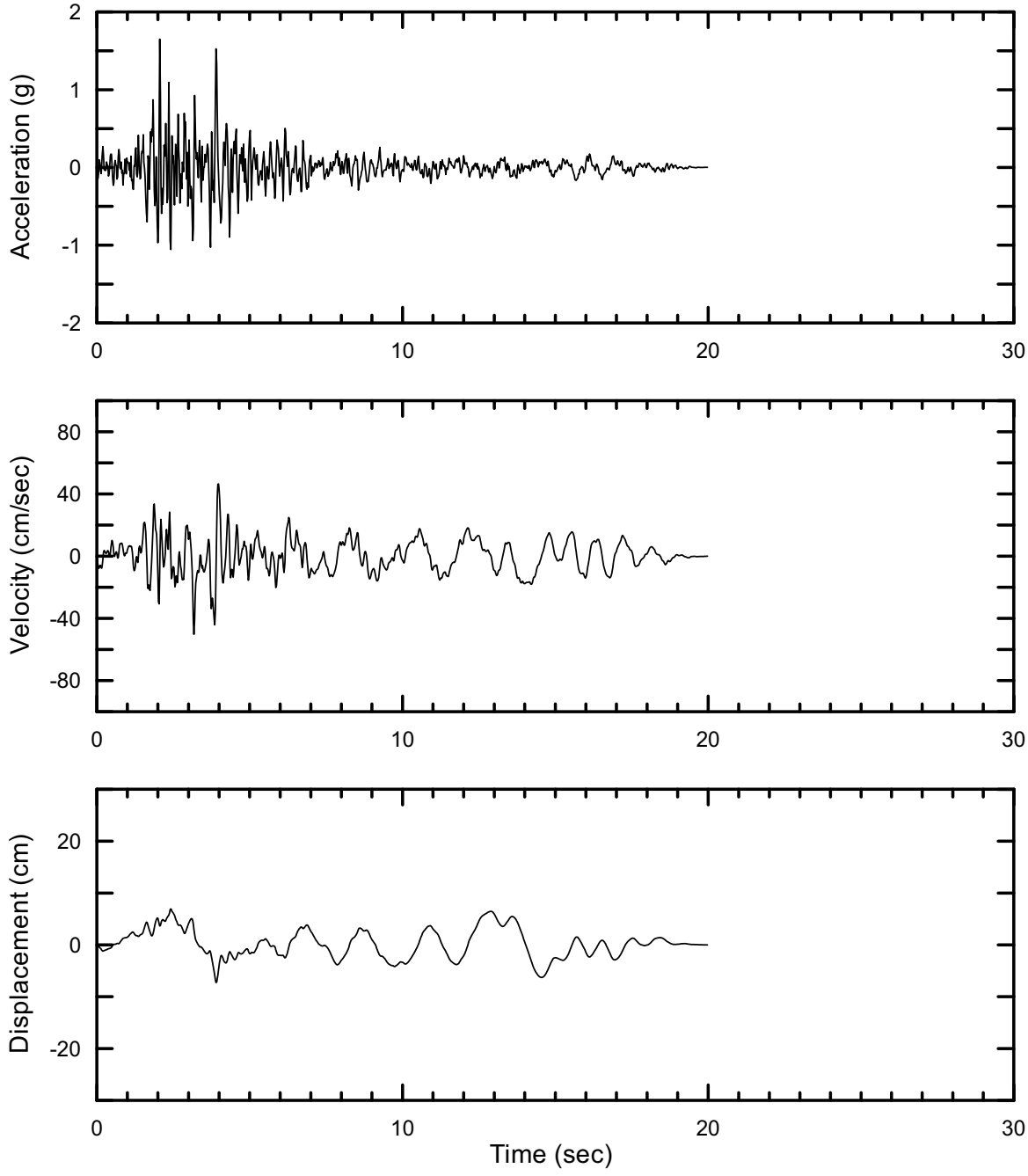

DTN: MO0402AVDTM105.001 [DIRS 168890]

Figure II-276. Point B Vertical Time Histories at an Annual Exceedance Probability of 10^{-5}, Set #10

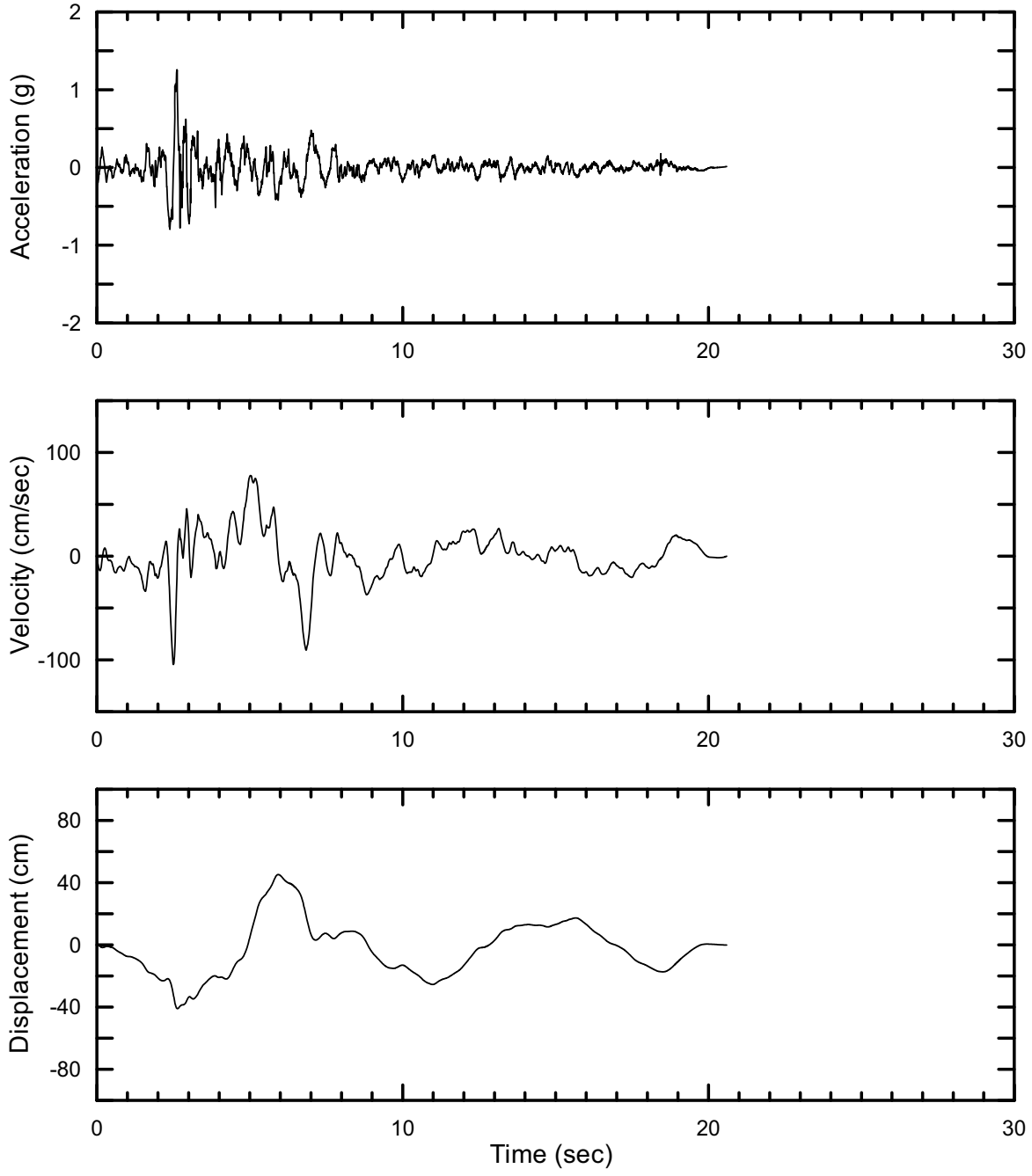

DTN: MO0402AVDTM105.001 [DIRS 168890]

Figure II-277. Point B Horizontal-1 Time Histories at an Annual Exceedance Probability of 10^{-5}, Set #11

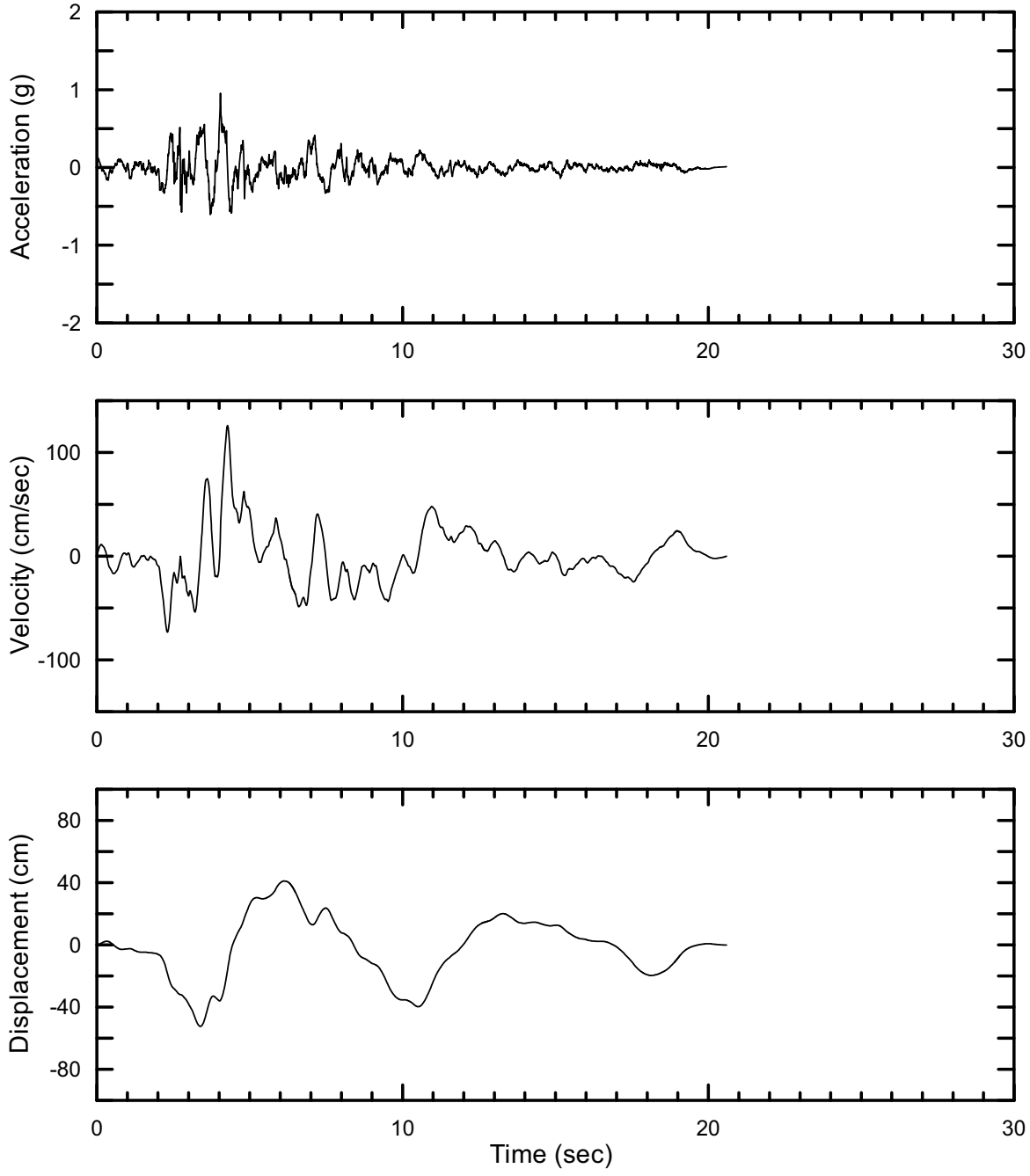

DTN: MO0402AVDTM105.001 [DIRS 168890]

Figure II-278. Point B Horizontal-2 Time Histories at an Annual Exceedance Probability of 10^{-5}, Set #11

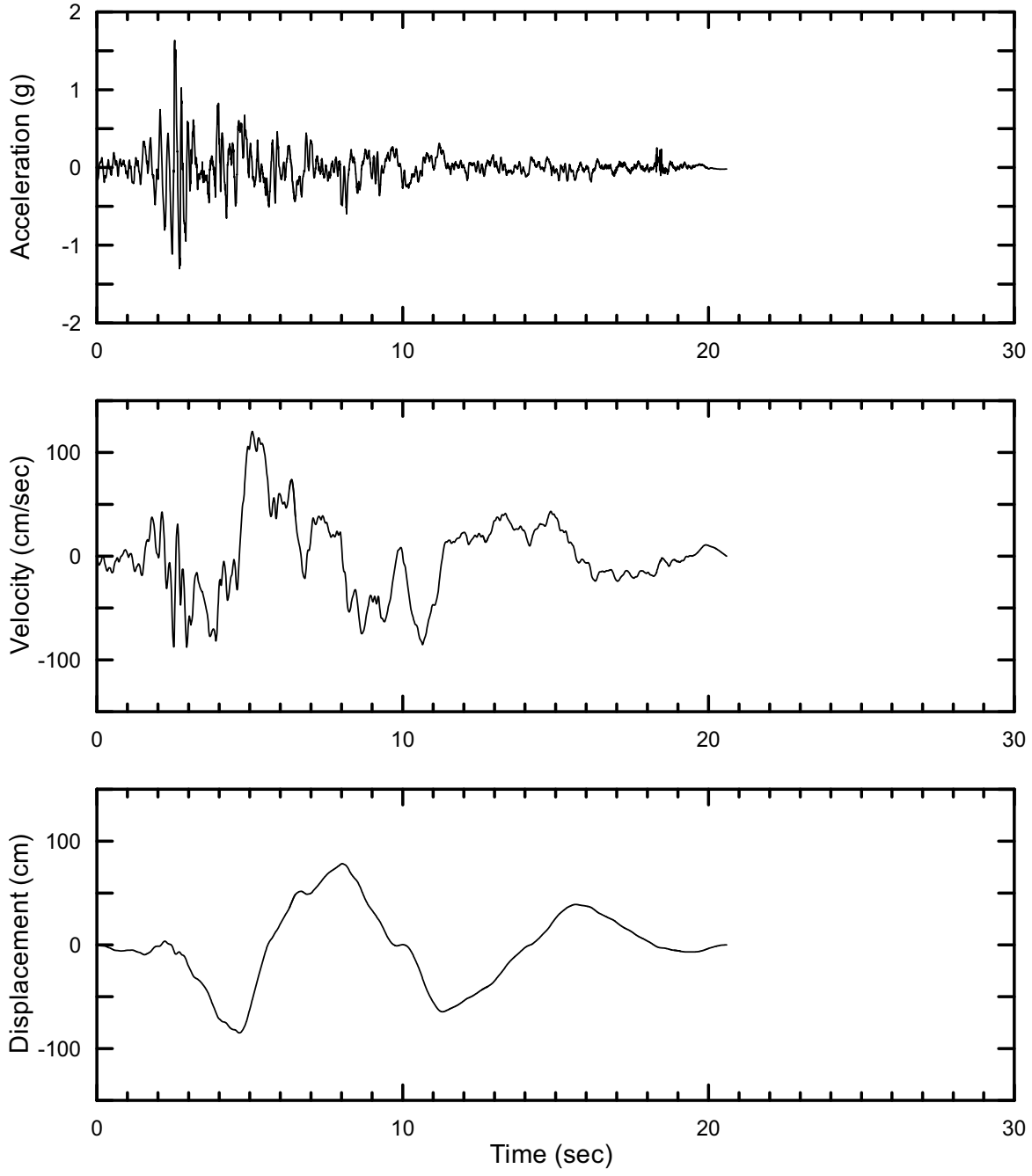

DTN: MO0402AVDTM105.001 [DIRS 168890]

Figure II-279. Point B Vertical Time Histories at an Annual Exceedance Probability of 10^{-5}, Set #11

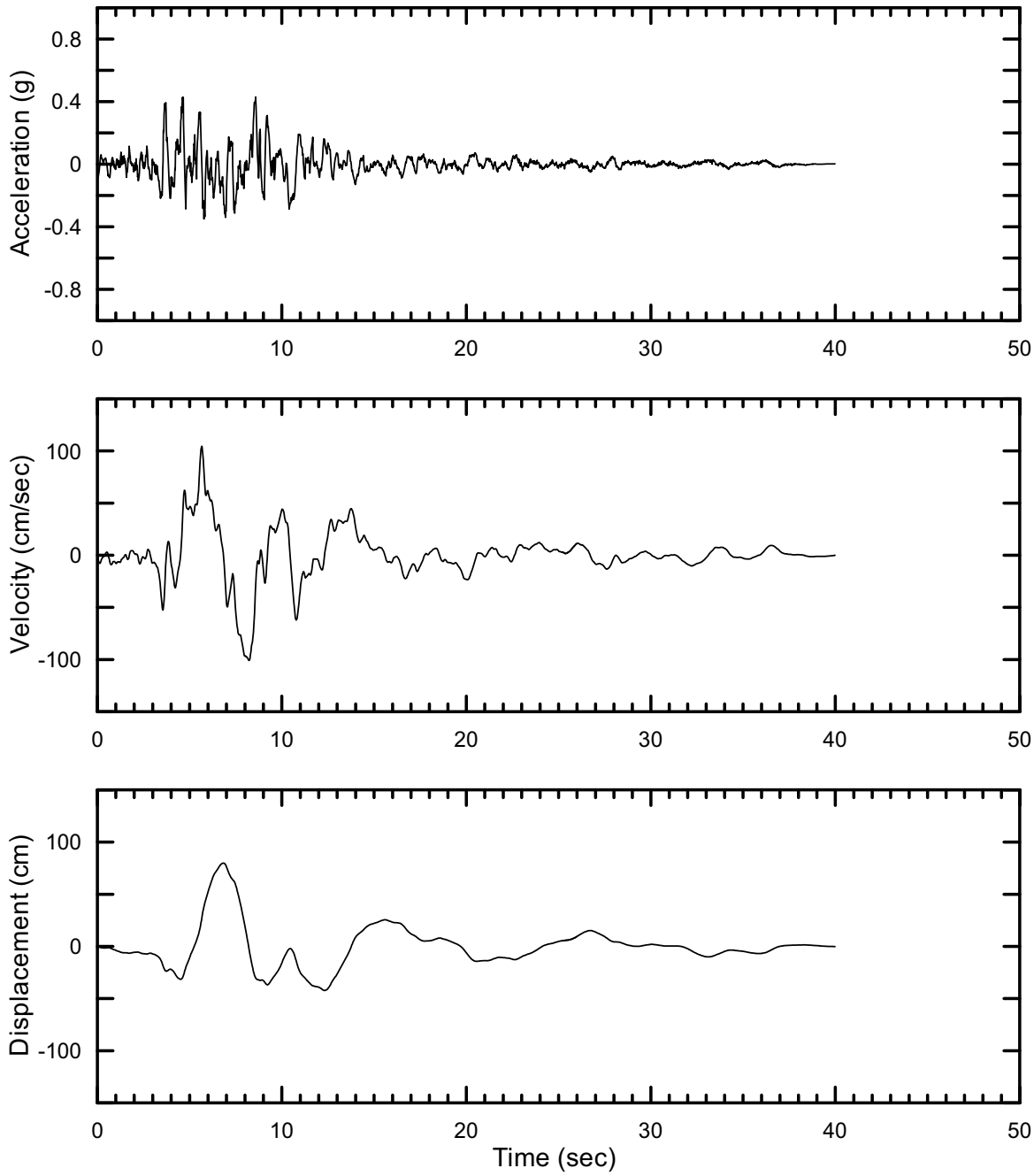

DTN: MO0402AVDTM105.001 [DIRS 168890]

Figure II-280. Point B Horizontal-1 Time Histories at an Annual Exceedance Probability of 10^{-5}, Set #12

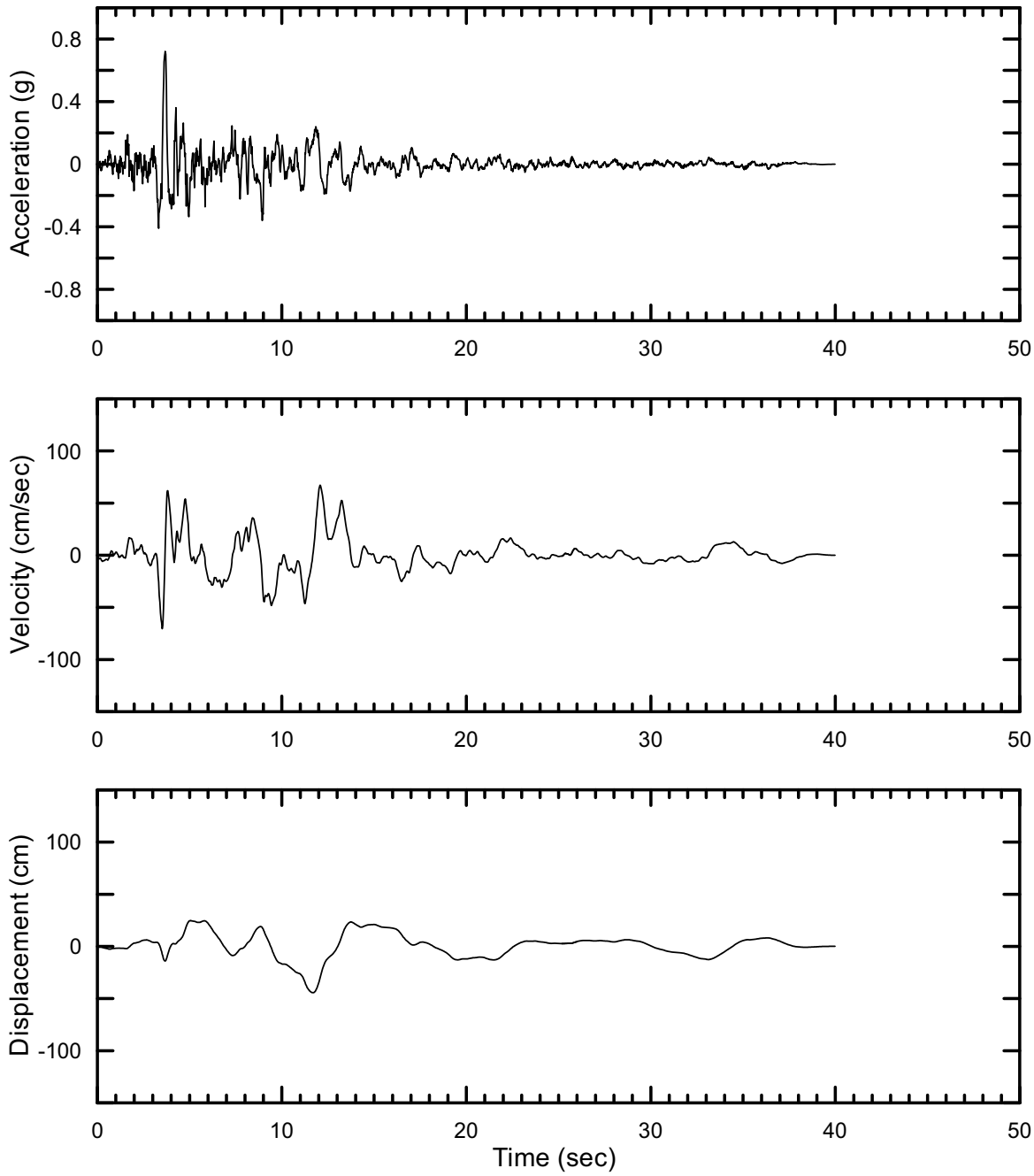

DTN: MO0402AVDTM105.001 [DIRS 168890]

Figure II-281. Point B Horizontal-2 Time Histories at an Annual Exceedance Probability of 10^{-5}, Set #12

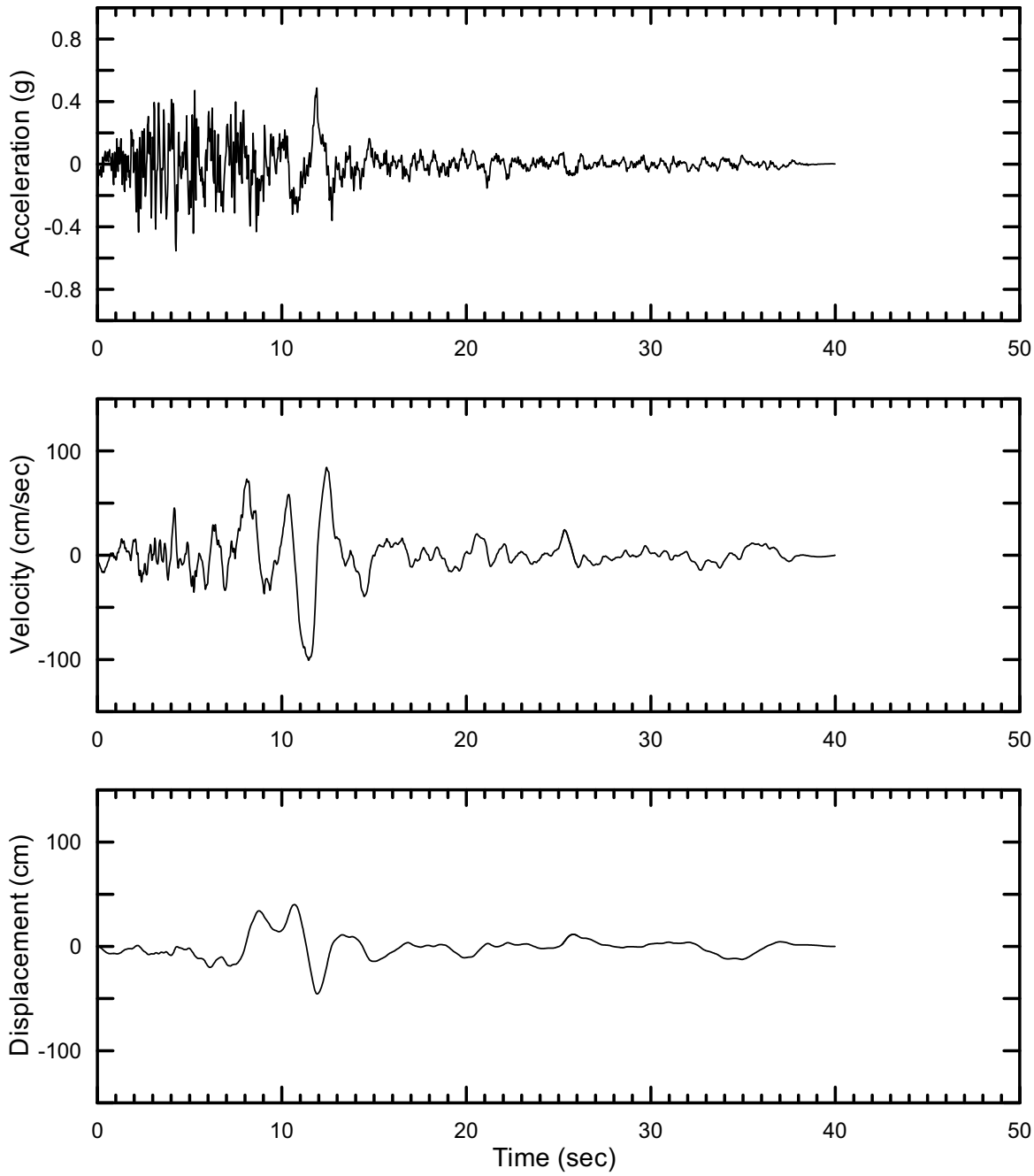

DTN: MO0402AVDTM105.001 [DIRS 168890]

Figure II-282. Point B Vertical Time Histories at an Annual Exceedance Probability of 10^{-5}, Set #12

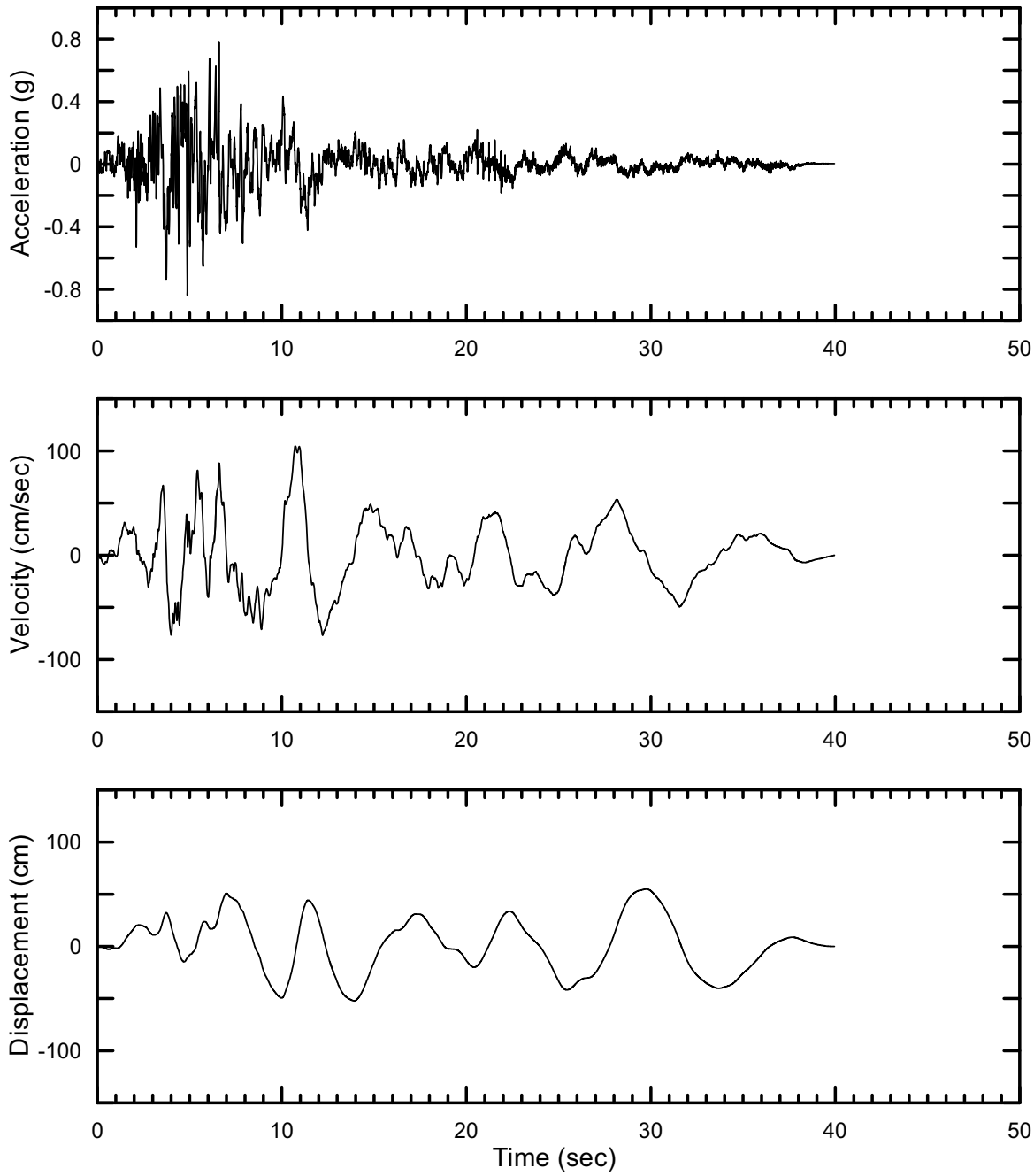

DTN: MO0402AVDTM105.001 [DIRS 168890]

Figure II-283. Point B Horizontal-1 Time Histories at an Annual Exceedance Probability of 10^{-5}, Set #13

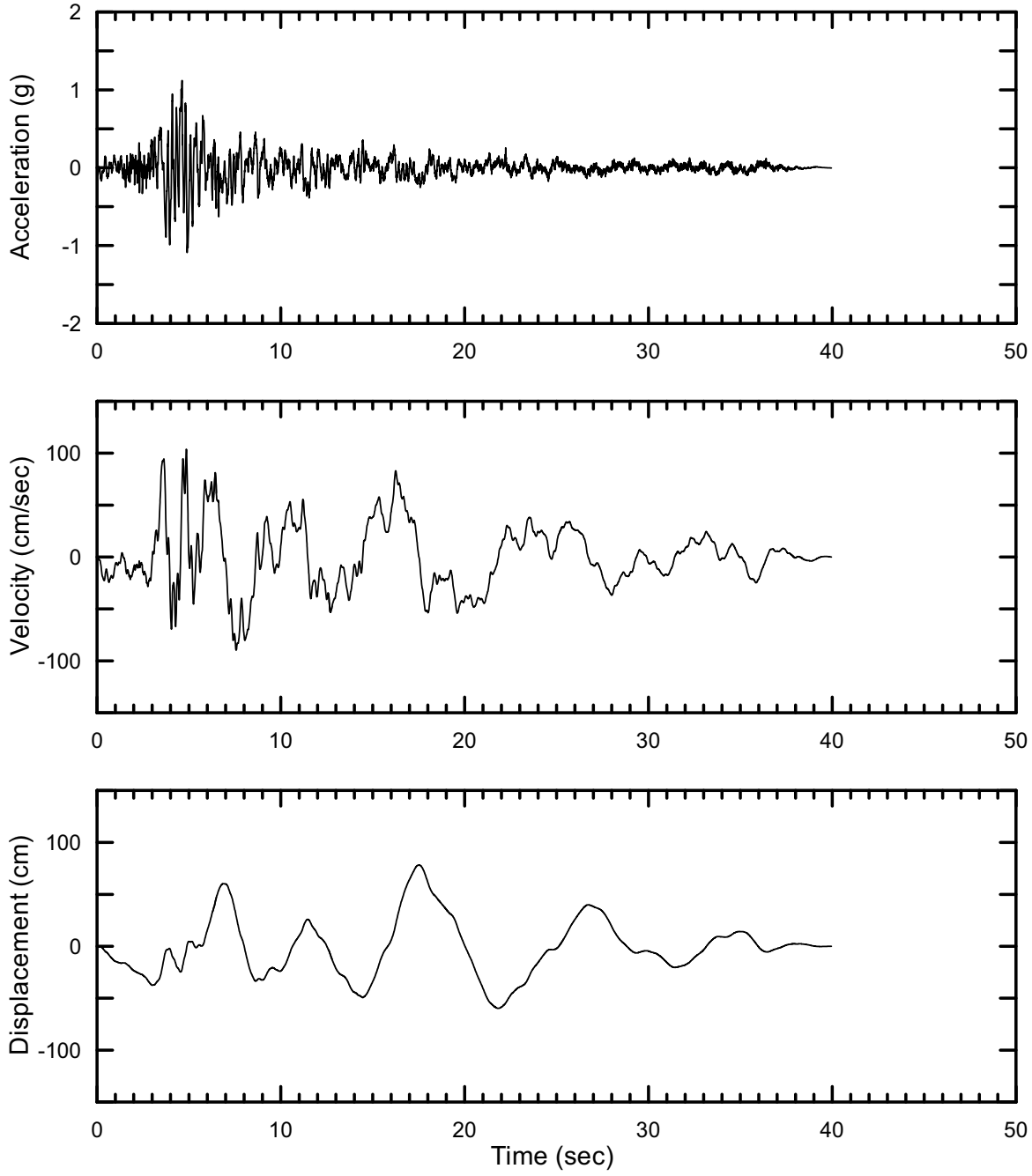

DTN: MO0402AVDTM105.001 [DIRS 168890]

Figure II-284. Point B Horizontal-2 Time Histories at an Annual Exceedance Probability of 10^{-5}, Set #13

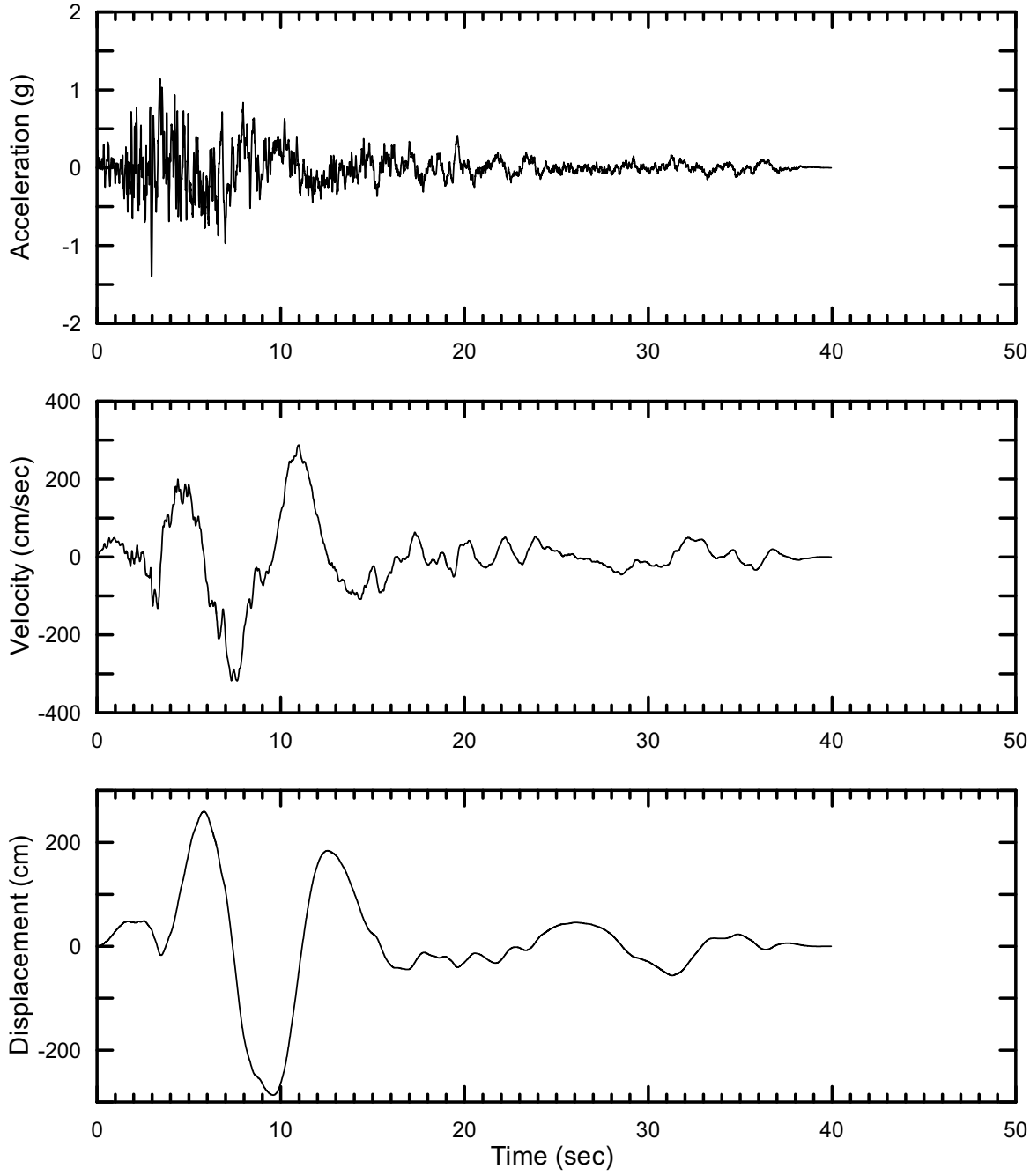

DTN: MO0402AVDTM105.001 [DIRS 168890]

Figure II-285. Point B Vertical Time Histories at an Annual Exceedance Probability of 10^{-5}, Set #13

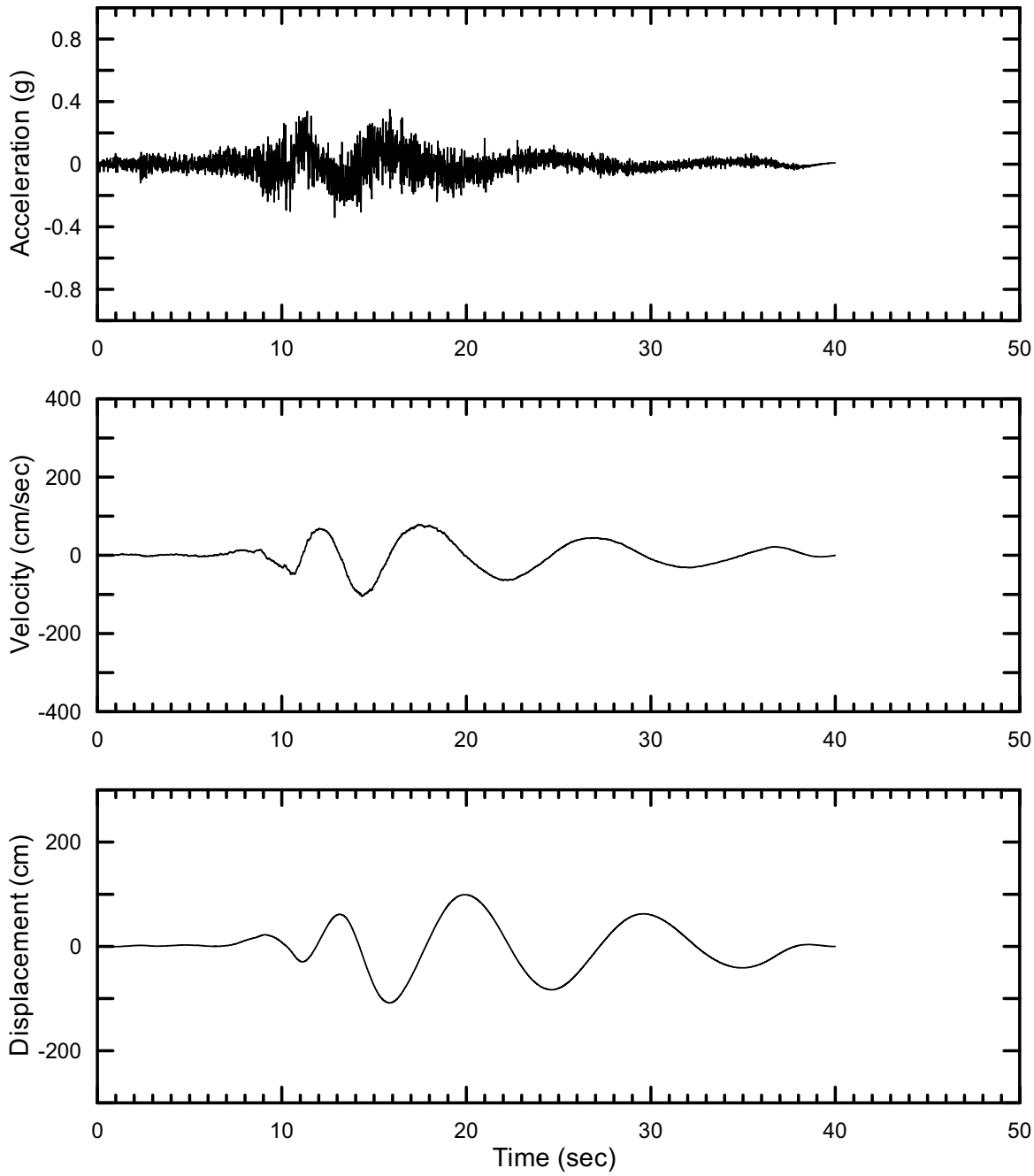

DTN: MO0402AVDTM105.001 [DIRS 168890]

Figure II-286. Point B Horizontal-1 Time Histories at an Annual Exceedance Probability of 10^{-5}, Set #14

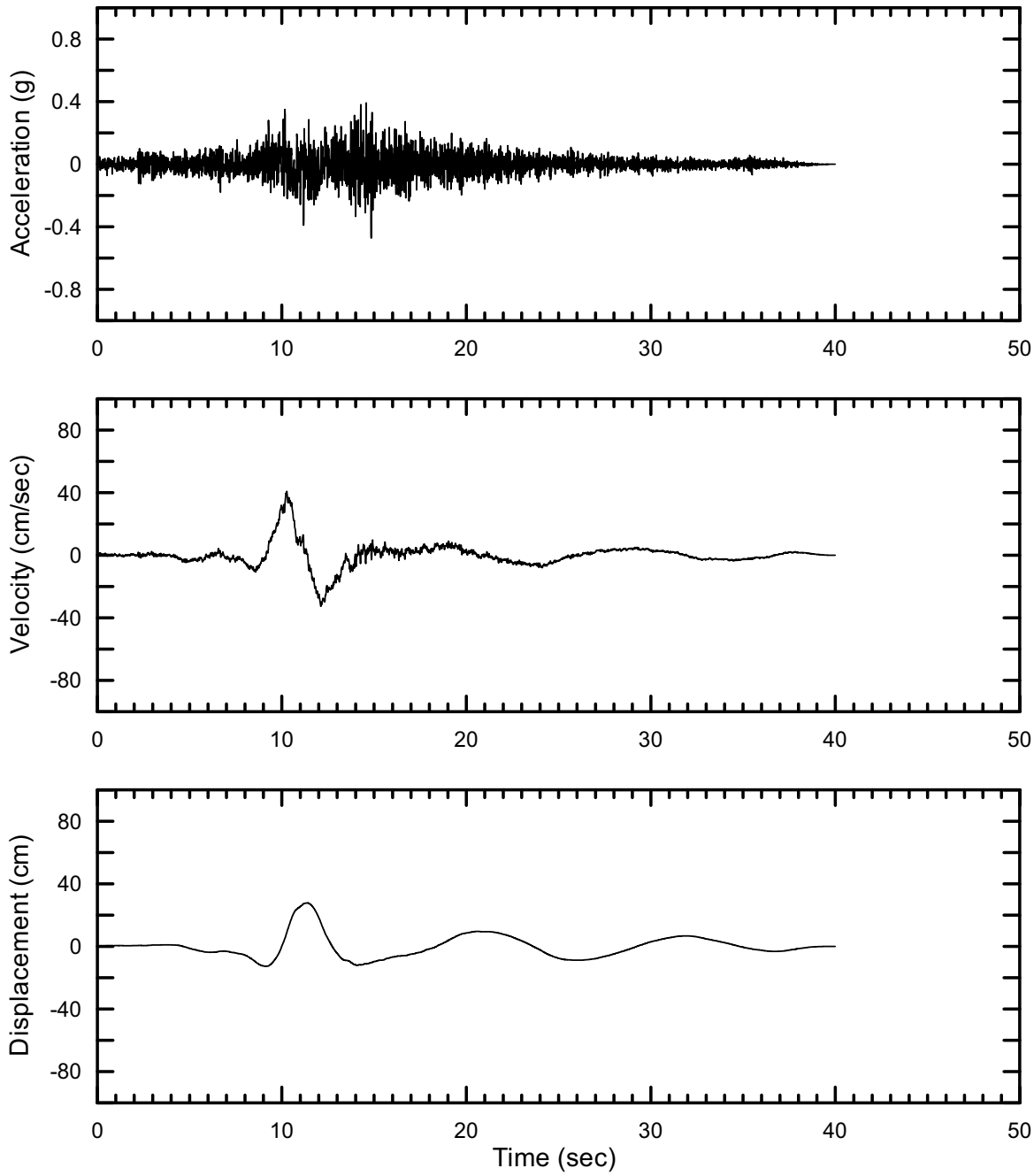

DTN: MO0402AVDTM105.001 [DIRS 168890]

Figure II-287. Point B Horizontal-2 Time Histories at an Annual Exceedance Probability of 10^{-5}, Set #14

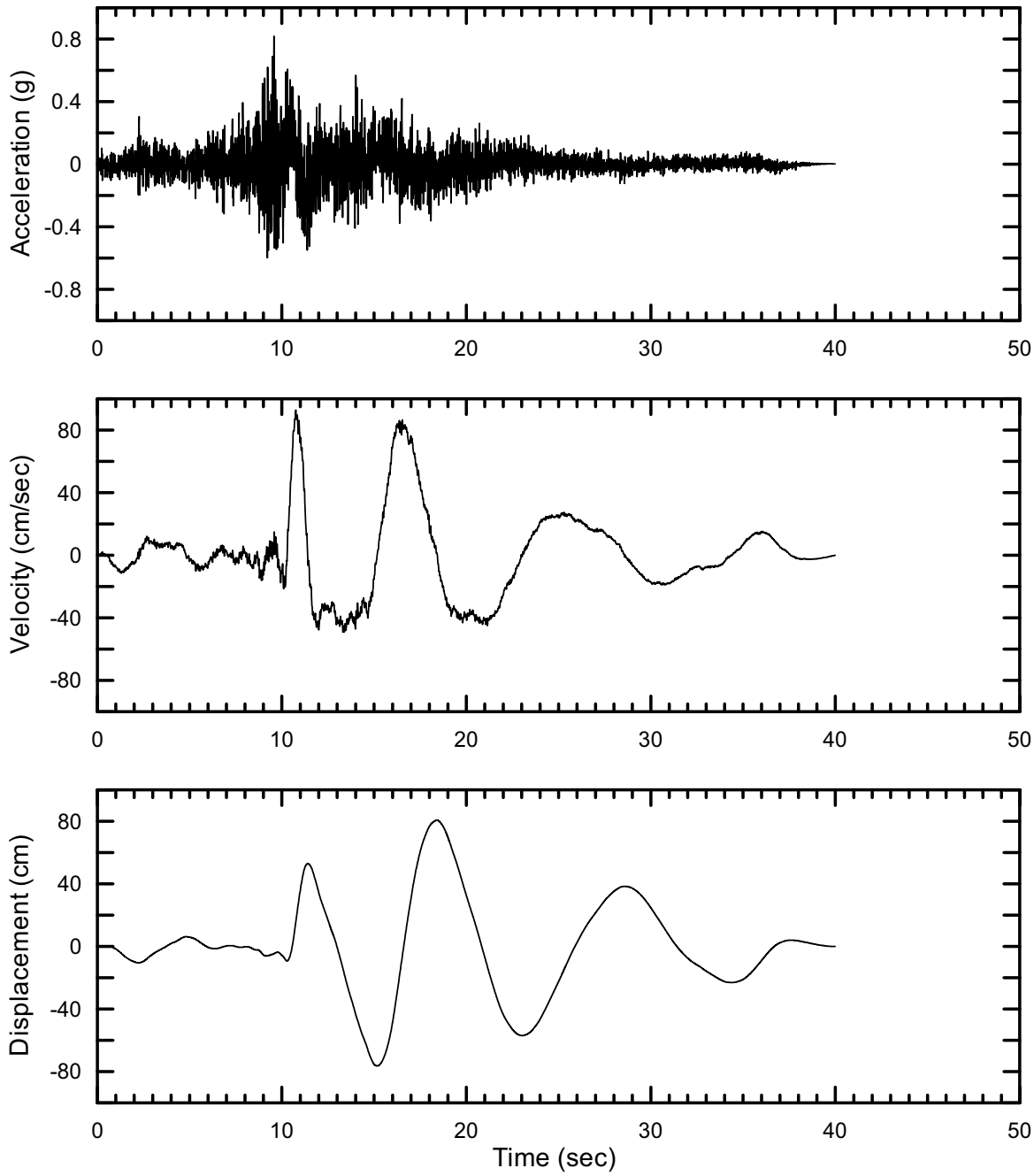

DTN: MO0402AVDTM105.001 [DIRS 168890]

Figure II-288. Point B Vertical Time Histories at an Annual Exceedance Probability of 10^{-5}, Set #14

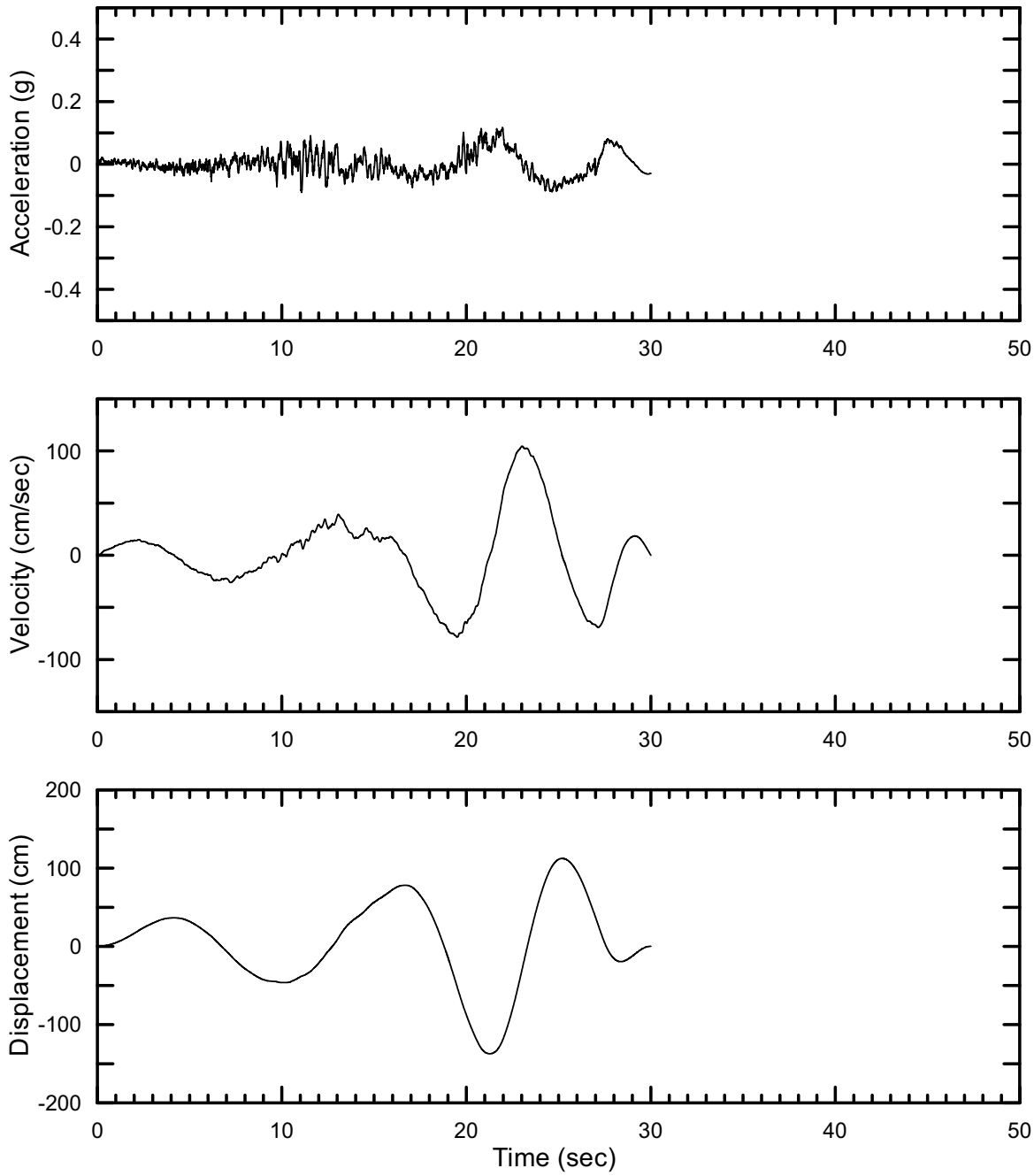

DTN: MO0402AVDTM105.001 [DIRS 168890]

Figure II-289. Point B Horizontal-1 Time Histories at an Annual Exceedance Probability of 10^{-5}, Set #15

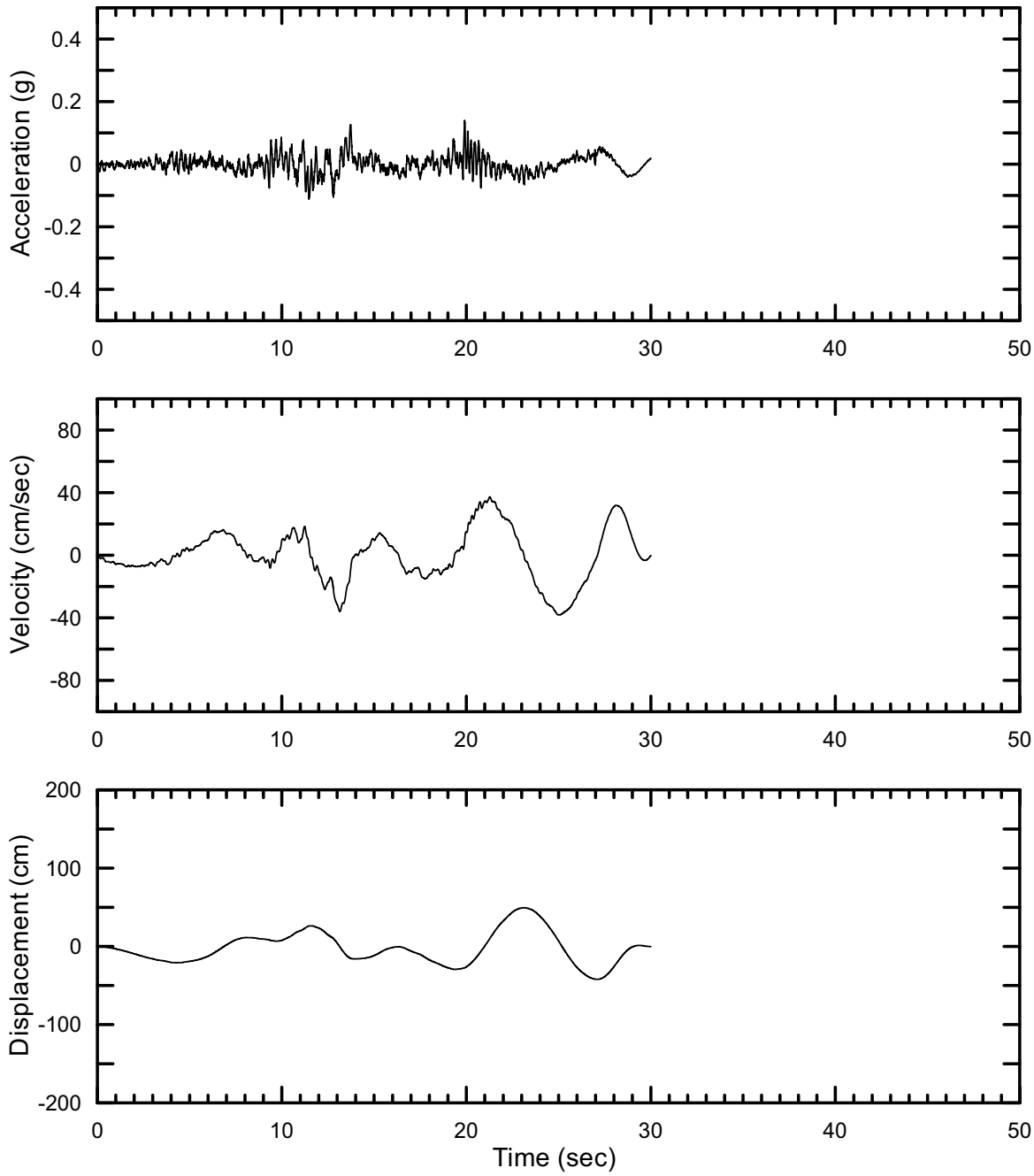

DTN: MO0402AVDTM105.001 [DIRS 168890]

Figure II-290. Point B Horizontal-2 Time Histories at an Annual Exceedance Probability of 10^{-5}, Set #15

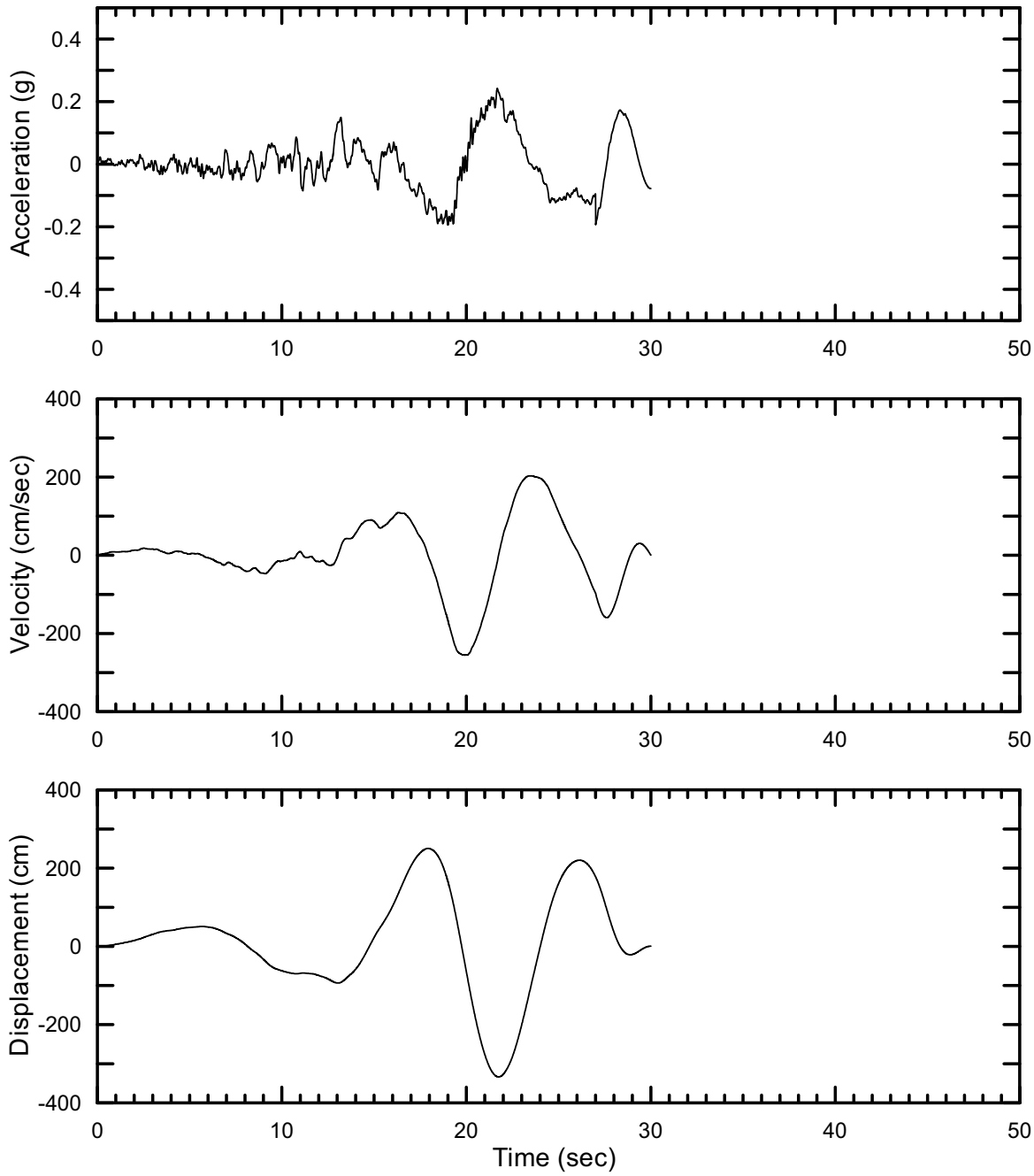

DTN: MO0402AVDTM105.001 [DIRS 168890]

Figure II-291. Point B Vertical Time Histories at an Annual Exceedance Probability of 10^{-5}, Set #15

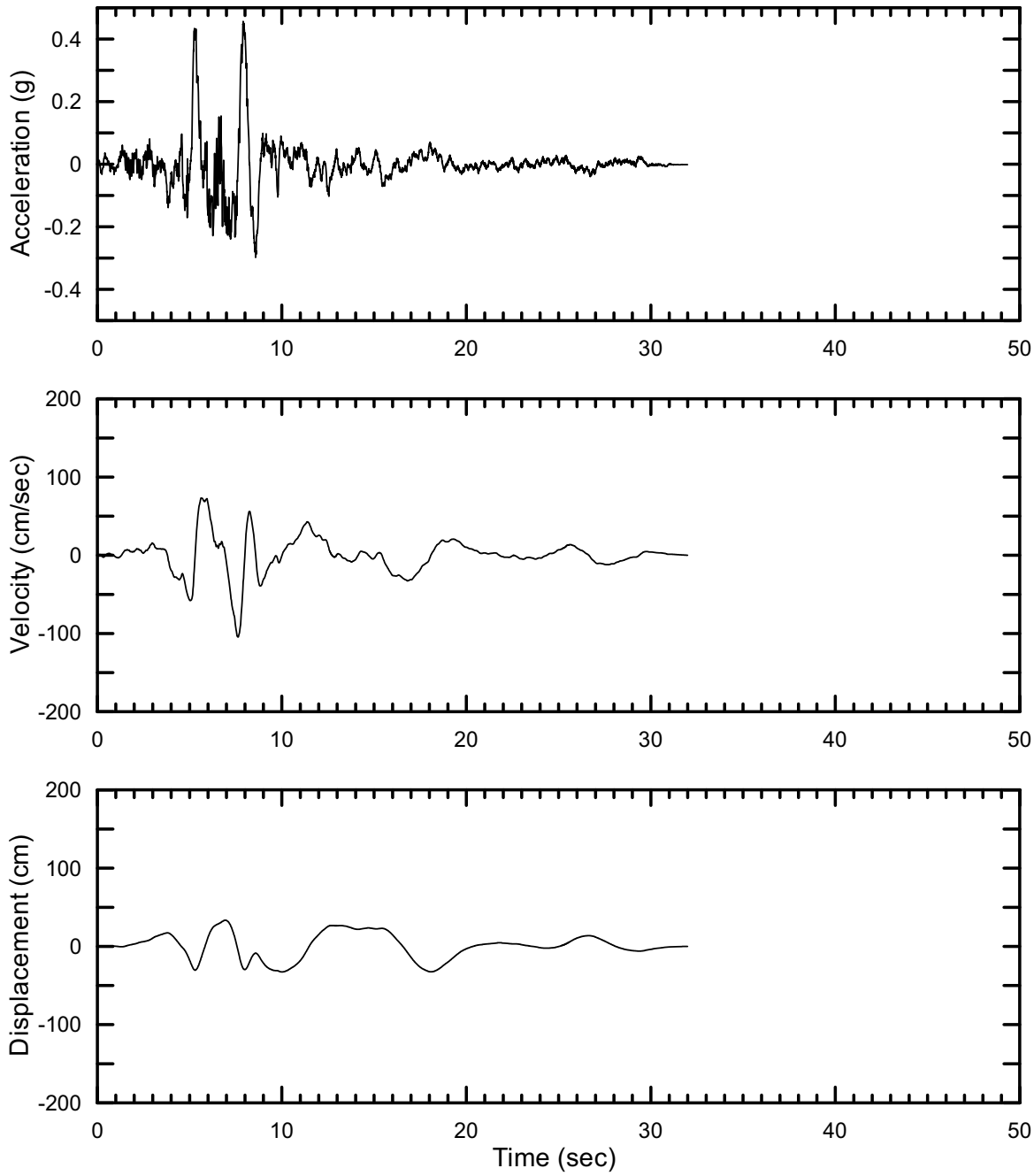

DTN: MO0402AVDTM105.001 [DIRS 168890]

Figure II-292. Point B Horizontal-1 Time Histories at an Annual Exceedance Probability of 10^{-5}, Set #16

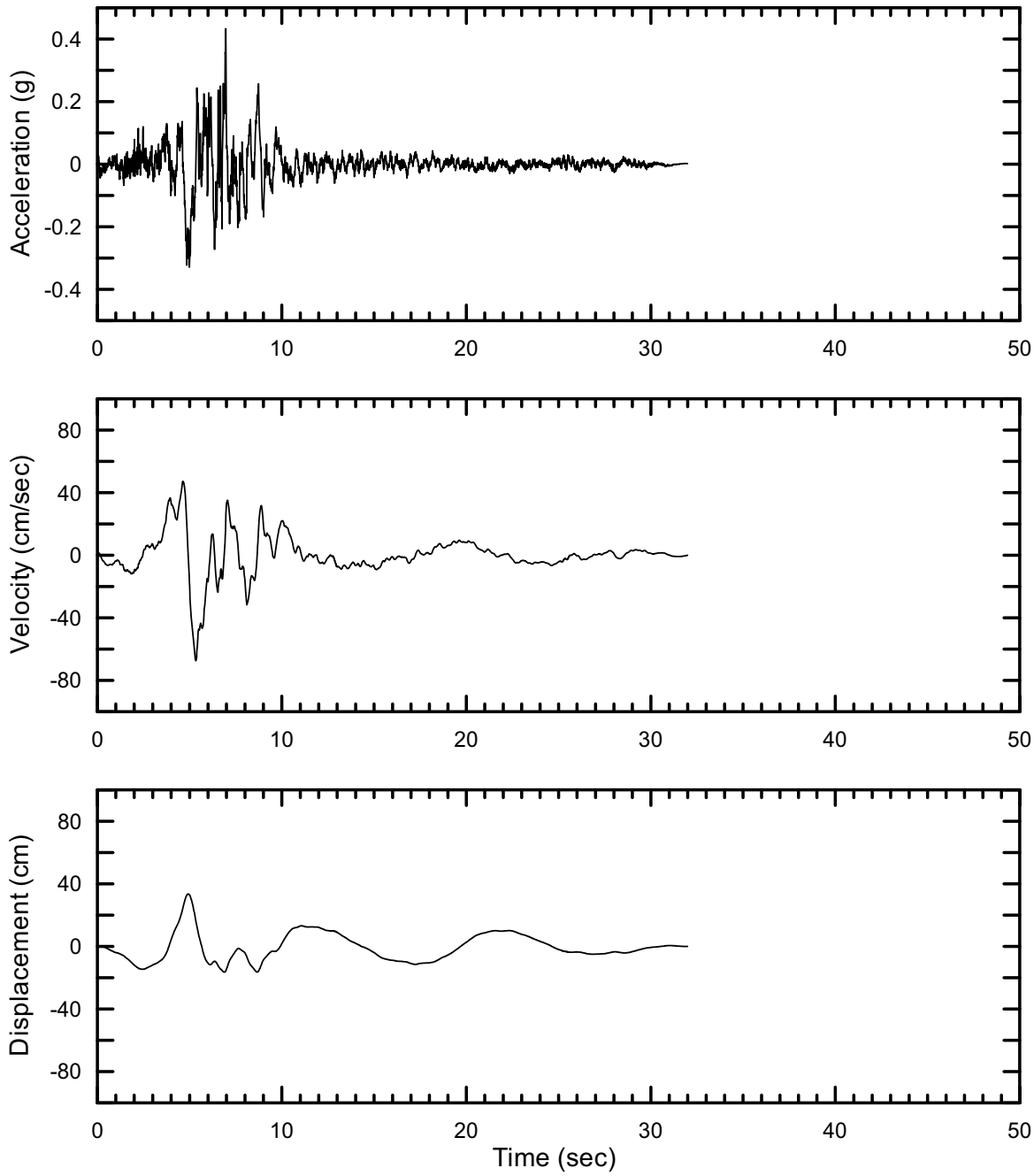

DTN: MO0402AVDTM105.001 [DIRS 168890]

Figure II-293. Point B Horizontal-2 Time Histories at an Annual Exceedance Probability of 10^{-5}, Set #16

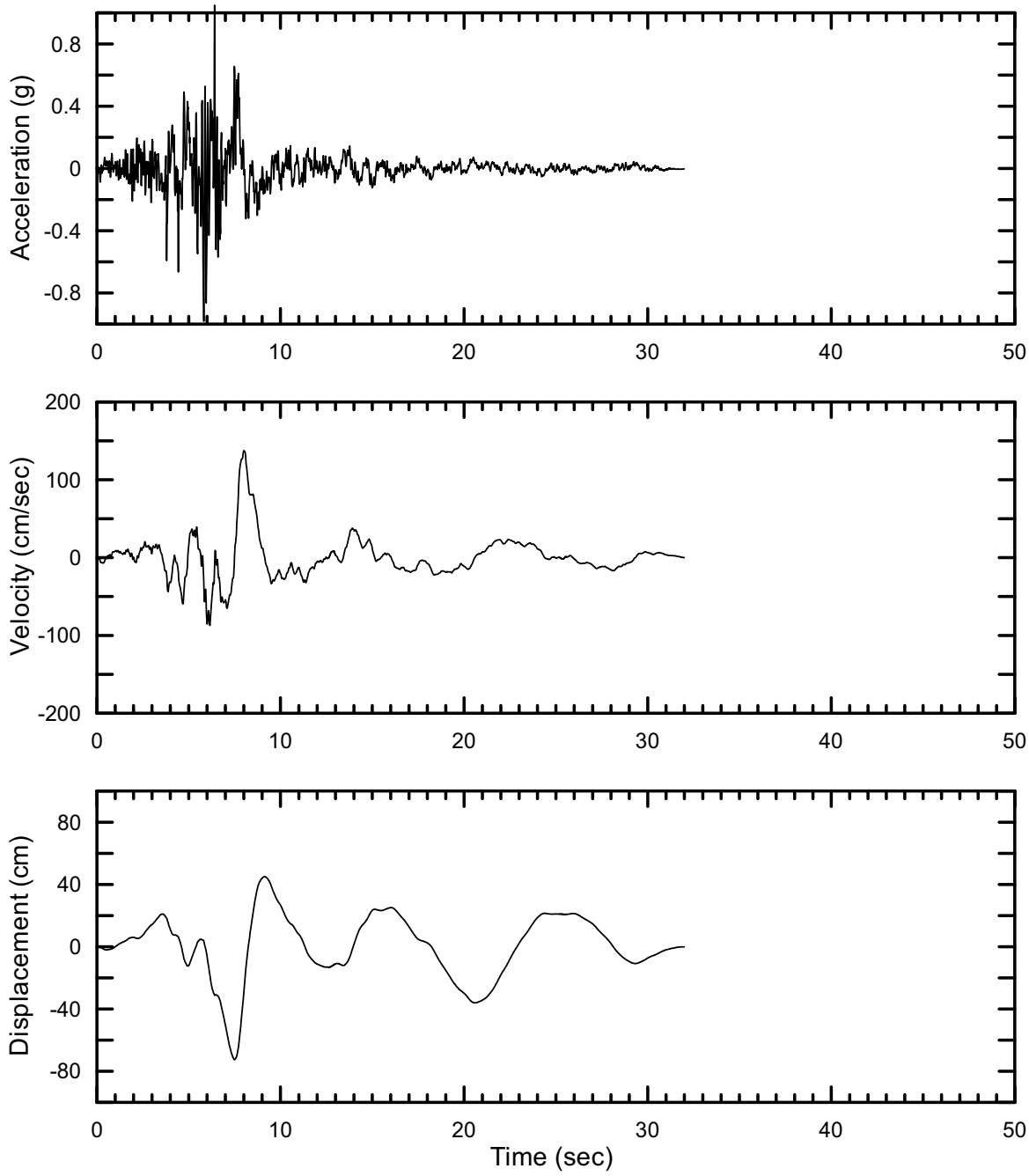

DTN: MO0402AVDTM105.001 [DIRS 168890]

Figure II-294. Point B Vertical Time Histories at an Annual Exceedance Probability of 10^{-5}, Set #16

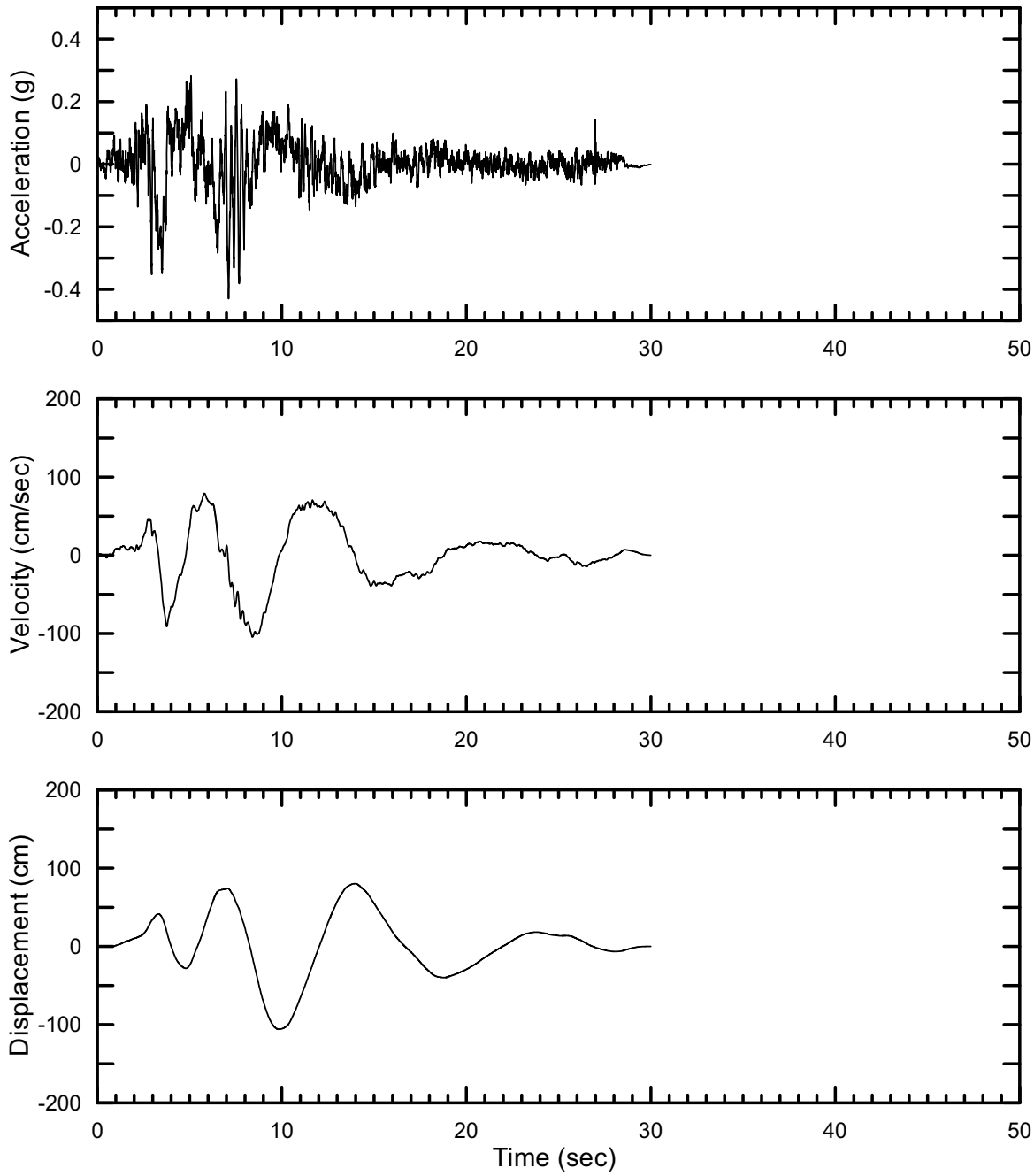

DTN: MO0402AVDTM105.001 [DIRS 168890]

Figure II-295. Point B Horizontal-1 Time Histories at an Annual Exceedance Probability of 10^{-5}, Set #17

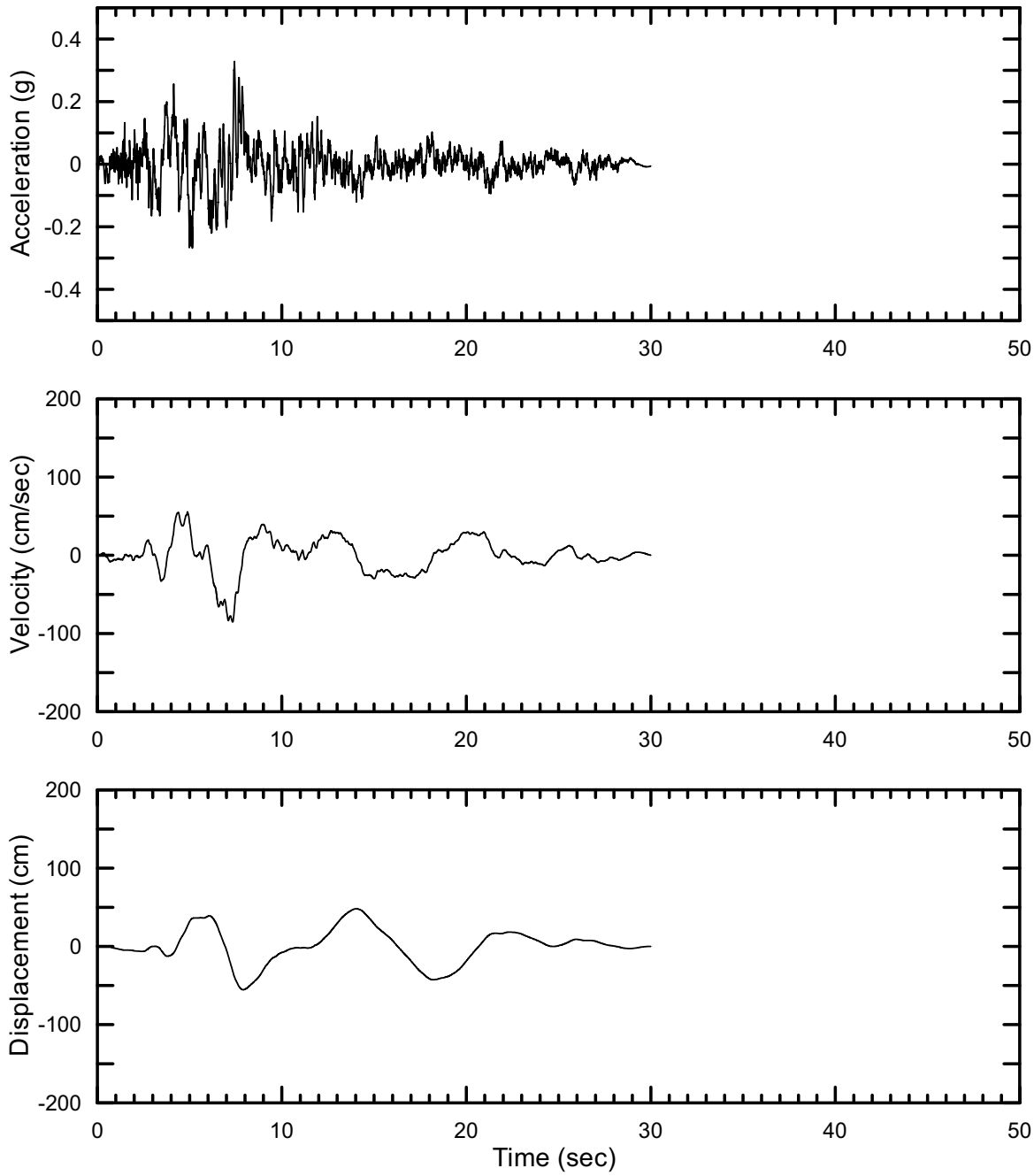

DTN: MO0402AVDTM105.001 [DIRS 168890]

Figure II-296. Point B Horizontal-2 Time Histories at an Annual Exceedance Probability of 10^{-5}, Set #17

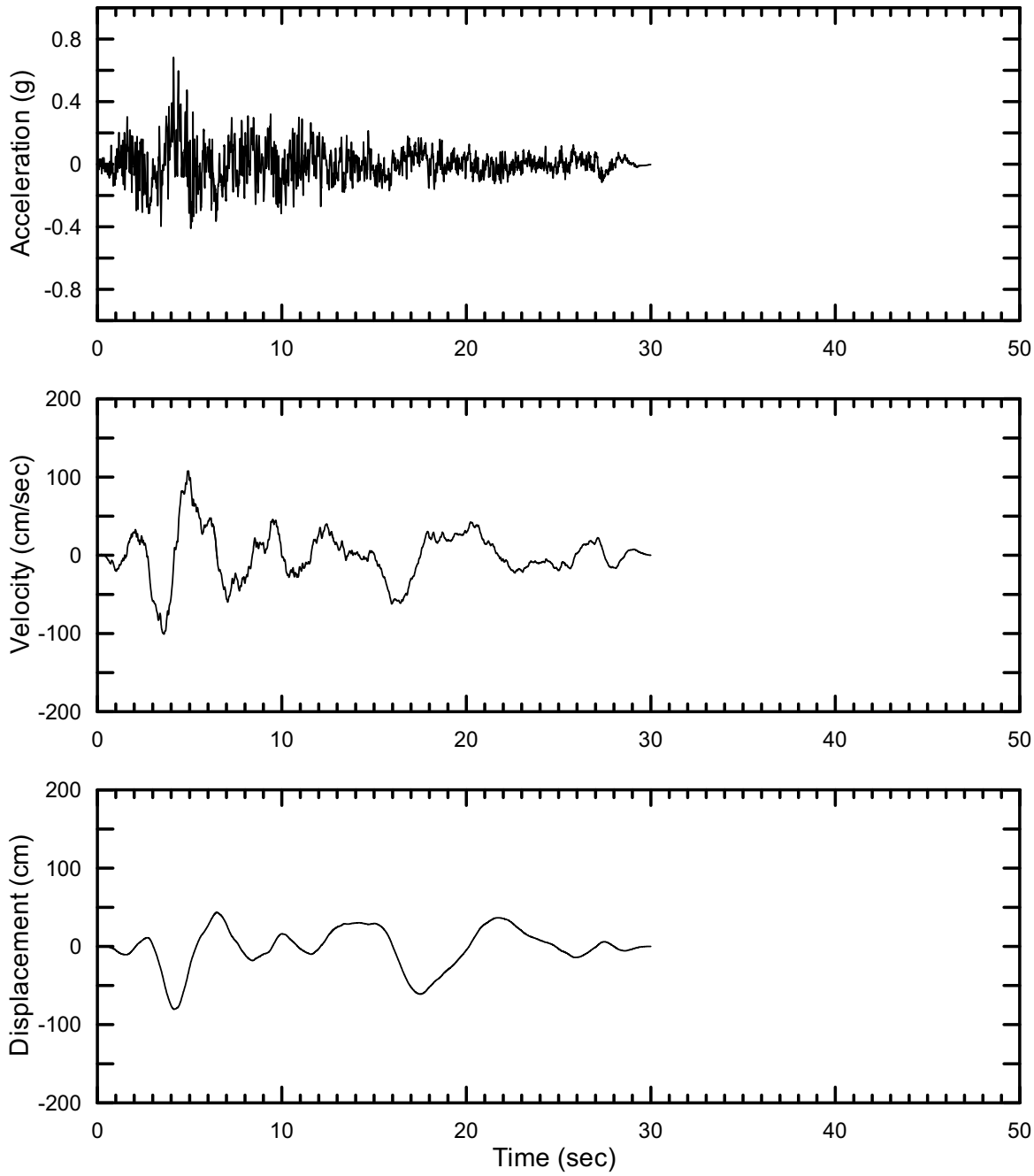

DTN: MO0402AVDTM105.001 [DIRS 168890]

Figure II-297. Point B Vertical Time Histories at an Annual Exceedance Probability of 10^{-5}, Set #17

INTENTIONALLY LEFT BLANK